Distribution Agreement

Distribution Agreement In presenting this thesis or dissertation as a partial fulfillment of the requirements for an advanced degree from Emory University, I hereby grant to Emory University and its agents the non-exclusive license to archive, make accessible, and display my thesis or dissertation in whole or in part in all forms of media, now or hereafter known, including display on the world wide web. I understand that I may select some access restrictions as part of the online submission of this thesis or dissertation. I retain all ownership rights to the copyright of the thesis or dissertation. I also retain the right to use in future works (such as articles or books) all or part of this thesis or dissertation.

Signature:

_____ _____

Date

Controlling Carbenes: Stories of Diruthenium, Dirhodium, and Photoinduced Carbene Transformations

By

Joshua K. Sailer

Doctor of Philosophy

Chemistry

_____
Huw M. L. Davies, Ph.D.
Advisor

_____
Simon B. Blakey, Ph.D.
Committee Member

_____
Frank E. McDonald, Ph.D.
Committee Member

Accepted:

_____
Kimberly Jacob Arriola, Ph.D., M.P.H
Dean of the James T. Laney School of Graduate Studies

_____
Date

Controlling Carbenes: Stories of Diruthenium, Dirhodium, and Photoinduced Carbene Transformations

By

Joshua K. Sailer

B.S., University of North Carolina at Charlotte, 2019

Advisor: Huw M. L. Davies, Ph.D.

An abstract of
A dissertation submitted to the Faculty of the
James T. Laney School of Graduate Studies of Emory University
in partial fulfillment of the requirements for the degree of
Doctor of Philosophy
in Chemistry,
2025

Abstract

Controlling Carbenes: Stories of Diruthenium, Dirhodium, and Photoinduced Carbene Transformations

By

Joshua K. Sailer

Carbene intermediates are a valuable synthetic tool in organic chemistry. These highly reactive species are capable of a wide variety of transformations, most notably via metallo-carbene intermediates. Dirhodium tetracarboxylate catalysts are capable of rendering cyclopropanation and C–H insertion reactions in a highly selective manner, enabling the synthesis of valuable scaffolds. However, while this is a powerful catalytic system, using rhodium offers a sustainability issue due to the high price. Herein, the development of an alternative metal for carbene transfer reactions has been developed and optimized. Additionally, two novel methodologies for synthesis of strained rings have been developed using carbenes, showcasing the powerful capabilities of these reactive intermediates.

Chapter 1: This chapter will give an overview of carbenes as reactive intermediates. Singlet and triplet carbenes are discussed, along with dirhodium tetracarboxylate complexes, with a brief survey of reactions that these complexes catalyzed. Then, some drawbacks and limitations of the dirhodium systems will be discussed along with the introduction to the solutions developed in later chapters of this dissertation.

Chapter 2: This chapter will discuss the optimization of alternative metals in the tetracarboxylate bimetallic core for cyclopropanation using aryldiazoacetate compounds. Ruthenium is shown to be the optimal metal, and a large scope of olefin cyclopropanation is disclosed. Computational studies help elucidate some of the key differences between the two metal centers.

Chapter 3: This section elaborates on the diruthenium catalysts for C–H functionalization of a variety of alkanes using aryldiazoacetates as carbene precursors. General reactivity trends for the ruthenium complexes are developed by testing substrates with differing sites of C–H insertion. A direct comparison is made with the dirhodium analogues highlighting the similarities and differences between the two catalyst systems.

Chapter 4: The chapter will explore the development of a cyclopropanation reaction of exocyclic olefins to afford chiral spiro[2.n]cyclopropanes using dirhodium catalysts. Several classes of exocyclic olefins are explored, with high levels of diastereoselectivity and enantioselectivity achieved.

Chapter 5: The final chapter will discuss a novel synthesis of 2-substituted bicyclo[1.1.1]pentanes via triplet carbene addition to the strained C–C bond of bicyclo[1.1.0]butane. This methodology affords rapid access to a challenging synthetic scaffold to reach, highlighting the power of carbene intermediates to afford privaliged motifs.

Controlling Carbenes: Stories of Diruthenium, Dirhodium, and Photoinduced Carbene Transformations

By

Joshua K. Sailer

B.S., University of North Carolina at Charlotte, 2019

Advisor: Huw M. L. Davies, Ph.D

A dissertation submitted to the Faculty of the
James T. Laney School of Graduate Studies of Emory University
in partial fulfillment of the requirements for the degree of
Doctor of Philosophy
in Chemistry,
2025

Acknowledgments

Dr. Huw Davies: I have learned so much from your mentorship over the past five years. I am forever grateful for the opportunity you have given me to work in your lab, and for the freedom you give to explore new ideas. Thank you for all that you have helped me achieve in the lab, and for always being supportive of me and my family, through whatever was happening.

Dr. Simon Blakey and Dr. Frank McDonald: Your input and feedback throughout my academic career has been invaluable. From teaching courses to asking challenging questions during my milestones, both of you have helped me to become a better chemist. I am grateful to have both of you on my committee. Thank you for all your help during my time here at Emory.

Dr. Michael Walter and Dr. Richard Jew: To my undergraduate research and academic advisors: Both of you had a profound impact on my chemistry journey. I can confidently say that without your guidance and input, I would not be a chemist, and that would be a very sad thing. Thank you for the direction you helped me move forward in.

Dr. Jack Sharland: Your ‘tough love’ was tough at first, but it helped me progress as a chemist quickly when I needed it the most. I learned so much from your mentorship during our overlap in lab. Thank you for the time and effort you put forward in that mentorship. One day I hope to get a beer with you, but I’ll probably be too busy.

Dr. Yannick Boni: I did not meet you in person for the first six months of being in the Davies lab because of Covid, but your presence was always felt in the mighty Bay #4. I’m grateful that I got to work in the hood next to yours. Your kindness and willingness to help even when you were busy made a lasting impact on me and the way I want to treat my mentees. Thank you for being a great mentor and a great bay partner.

Brockton Keen, William Tracy, Terrence-Thang Nguyen, and Jasper Luo: To my fellow cohort members – each of you have played an instrumental role on my time in the

Davies lab. I am grateful for each of you. Brock and Will, thanks for being great office mates – even when I am a little cranky. Terrence, thanks for all the chemicals I borrowed from you, and for recommending the best boba in town. Jasper, thanks for all the laughs and making the lab a little more colorful and artistic.

Duc Ly: Duc, I am so grateful that you joined our lab and that you moved into Bay 4. I have learned so much from you, even though I am two years ahead of you. You are truly the best chemist I have ever met. I will miss being able to work with you, brainstorm new ideas, and watch Ronaldo play during the summers. I'm excited to see what you do with your career – I know it's going to be great.

Other Davies Lab Members: During my time in the Davies lab, I was able to work with so many great chemists, who I have learned so much from. Aaron, Bo, Mazie, Yassir – Thanks for being a welcoming lab and helping me during those early years where I didn't know what I was doing. Ziyi, Kristen, Takeru, and Kagiso – you are a great group of chemists, I am excited to see the massive amounts of chemistry you all will complete with your time in the Davies lab. Feng Zhai and Christian Bettencourt – Thanks for being great postdocs in the lab. You both have taught the lab so much, we are all better chemists because of it.

Emory Chemistry Community: So many people in the Emory community have played an integral role on my time here. People like Steve and Michelle, who always had coffee down in the stockroom. Drs. John Bacsa, Fred Strobel, and Bing Wang who helped me characterize challenging complexes. Rio and Alan, for making the CCHF and CIC something that helped me become a better chemist and a better professional. The Blakey lab, for letting me use the constant chiller. I would not have been able to complete the BCP project without this, so thank you for your willingness to letting me use it. And all of the other graduate students in the chemistry department. Thank you all for your help and support along the way.

Atlanta Community: When Sarah and I moved to Atlanta, we knew no one. Moving in the middle of the Pandemic, it was challenging to find a community. Now, as we prepare to move away, there are so many people who we will miss dearly. Joe and Lily Goble, Marcel Bouchard, Ryan Fykes, Drew and Emma Hughes, Rob and Jayde Sequerth, Mary-Ellen Mitchell – you made Atlanta start feeling like home and are making leaving even harder than moving here. Thank you for all of the great times we have had. Thank you for the endless support, listening to the qualms of grad school, and asking about what I do, even if it didn't make a ton of sense to you. I will miss all of you greatly and look forward to sharing our next meal together.

Jefferson Park Neighbors: Brenda, Lowell, Jim, Zack – You all were such an amazing blessing that we didn't even know we needed. Having neighbors as good as you all will be one of the lasting memories of our time in Atlanta. Thank you so much for always being willing to sit out on the lawn and talk until the owls come out. We will miss you, especially on Halloween.

Sarah's Side of the Family: To the family I gained 6 years ago, thank you for your constant and endless support. Thank you also for your trust – I'm sure there was some disappointment when we told you we were moving 7 hours away just a year after getting married. I'm grateful you always supported us through this decision, never making us feel alone. I specifically want to thank Sarah's mom, Cathy. Thank you for all the help you have given us over the past 6 years. You have helped us more than you know – from answering our nurse questions, to supporting us through bringing Dottie home, knowing you are always one phone call away gave us security that made this journey possible. I am grateful we will be moving closer so that you don't have to make that drive (or battle the Atlanta airport) anymore. Thank you for all that you have done for us and continue to do for us.

My Side of the Family: To the family I've had since birth – I could never put into words my thankfulness for all the love and support you all have given me and Sarah over the past 5 years. To my siblings, Michelle and Nathan, Nick and Brittany, John and Lucy – I

look up to all of you so much. Thank you for being so supportive of me and Sarah during this journey. To Mom and Dad, I truly cannot thank you enough for everything. Growing up, both of you lit a passion for science in me even before I really knew it. Because of your support, I have been able to achieve this dream. Thank you so much for all of that you have given us during graduate school. We truly are so grateful, and we can't wait to be living closer to you, and for Dottie to have lots of Nana and Papa time. I love you both.

Sarah: Where to even being? My wife and best friend, we have been through it all during out time in Atlanta. Truly, it has been the most challenging and yet rewarding experience we could have had – I could not have done this without you. Your constant support through frustration and stress, worry and sadness, you never stopped believing in me. You helped me see the bigger picture when I got bogged down by experiments. You celebrated my achievements and comforted me during failure. You sacrificed, and continue to sacrifice, *so* much for me to achieve this dream. From the bottom of my heart, thank you. I love you and will always love you.

This Dissertation is Dedicated to:

My Wife, Sarah

Who I would be lost without.

and

My Daughter, Dorothy

That you will grow up to live
in awe and wonder of our beautiful world.

Table of Contents

List of Figures

Chapter 1

Chapter 2

Chapter 3

Chapter 4

Chapter 5

List of Tables

Chapter 2

Chapter 3

Chapter 4

Chapter 5

List of Schemes

Chapter 1

Chapter 2

Chapter 3

Chapter 4

Chapter 5

List of Abbreviations

RI: Reactive Intermediates

TMS: Trimethylsilyl

TMSOTf: Trimethylsilyl trifluoromethanesulfonate

PC: Photocatalyst

OAc: Acetato

DOSP: ((4-dodecylphenyl)sulfonyl)-prolinato

PTAD: 2-((3S,5S,7S)-adamantan-1-yl)-2-(1,3-dioxoisoindolin-2-yl)acetate

TPCP: Triphenylcyclopropane carboxylate

TPPTTL: *tetra*-phenylphthalimido-tert leucinato

DCC: Dicyclohexylcarbodiimide

Troc: Trichloroethyl ester

Equiv: Equivalents

r.r.: Regiomeric ratio

d.r.: Diastereomic ratio

ee: Enantiomeric excess

HFIP: 1,1,1,3,3,3-hexafluoroisopropanol

esp: α,α,α′,α′-tetramethyl-1,3-benzenedipropionate

TON: Turn-over number

PhCl: Chlorobenzene

DCM: Dichloromethane

4 Å MS: 4 Angstrom molecular sieves

MeCN: Acetonitrile

N/a: Not available

HR-MR: High Resolution-Mass Spectroscopy

$NaBAr^F$: Sodium tetrakis[3,5-bis(trifluoromethyl)-phenyl]borate

PES: Potential energy surface

kcal/mol: Kilocalories per mole

TCPTTL: tetra-chlorophthalimido-tert leucinato

h: Hour

Maj: Major

Min: Minor

THF: Tetrahydrofuran

TFT: Trifluorotoluene

SCP: Spiro[2.n]cyclopropane

Her-2: Human epidermal growth factor receptor-2-sheddase

Boc: *tert*-butoxycarbonyl

Ts: Tosyl

Oct: Octanoate

KR: Kinetic Resolution

NMR: Nuclear magnetic resonance

BCP: Bicyclo[1.1.1]pentane

CYP450: Cytochrome P450

BCB: Bicyclo[1.1.0]pentane

TEnT: Triplet energy transfer

ISC: Intersystem Crossing

EDA: 2-ethyldiazoacetate

nm: Nanometer

$Ir(ppy)_3$: Tris(2-phenylpyridine)iridium

TX: Thioxanthone

HNMR: Proton nuclear magnetic resonance

CNMR: Carbon nuclear magnetic resonance

FNMR: Fluorine nuclear magnetic resonance

MHz: Megahertz

ppm: Parts per million

$CDCl_3$: Deuterated chloroform

UV: Ultraviolet

CAM: Cerium ammonium molybdate

APCI: Atmospheric-pressure chemical ionization

ESI: Electrospray ionization

mp: melting point

FT-IR: Fourier transform infrared spectroscopy

HPLC: High-performance liquid chromatography

UHPLC: Ultra-High-Performance Liquid Chromatography

RT: Retention time

SFC: Supercritical fluid chromatography

CO_2: Carbon dioxide

COSY: Homonuclear Correlation Spectroscopy

Chapter 1. An Introduction to Carbenes and Dirhodium Tetracarboxylate Catalysis

1.1 Introduction

Organic chemists attempt to control reactions, and particularly, reactive intermediates (RIs), to enable the desired product to be formed. An intermediate is a transient chemical species that exists for some finite length of time in a stepwise reaction pathway.[1] There are many types of reactive intermediates that can be generated with ease using common synthetic methods. Some carbon-based RIs known to organic chemists include carbocations and carbanions, arynes, radicals, and carbenes. These intermediates have provided chemists with countless methodologies for making new molecules. However, a key consideration for these intermediates is how to control them – controlling the intermediate dictates the utility it will have. Carbocations have captured the minds of organic chemists since the late 1800s, and still do today, with much applicability to the general community with carbocation chemistry. Work from the Jacobsen, Maulide, and List groups have all harnessed this intermediate for development of novel synthetic methodologies (Scheme 1.1A).[2-4] Aryne chemistry has recently seen a resurgence, with the first reported isolation of indolynes recently reported from the Roberts group (Scheme 1.1B).[5, 6] Radical chemistry has seen a reemergence in popularity over the past 15 years due to photoredox and metallo-photoredox catalysis.[7, 8] Additionally, efforts towards selective trapping of radicals have been shown by the MacMillan group, using the 'radical-sorting' mechanism to tame these otherwise highly reactive intermediates for selective coupling reactions (Scheme 1.1C).[9-12]

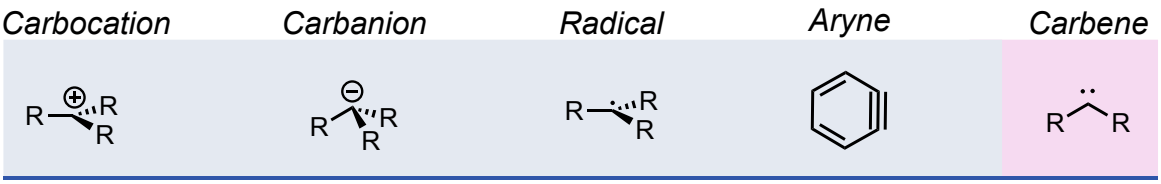

A. Carbocation Chemistry

Jacobsen et. al.

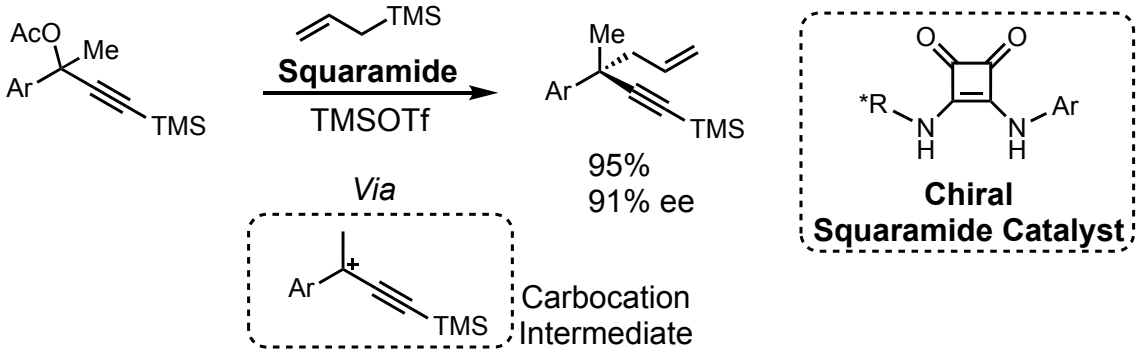

B. Aryne Intermediates

Roberts et. al.

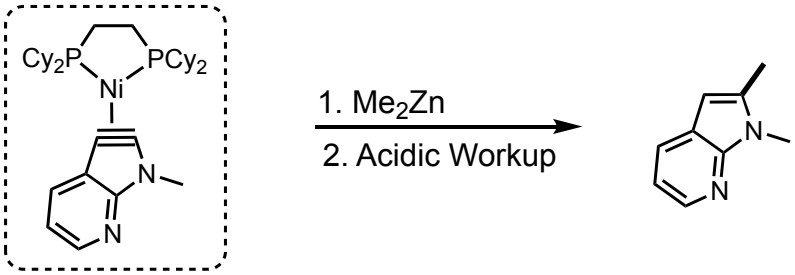

First Reported Indolyne

C. Radical Methodology

Macmillan et. al.

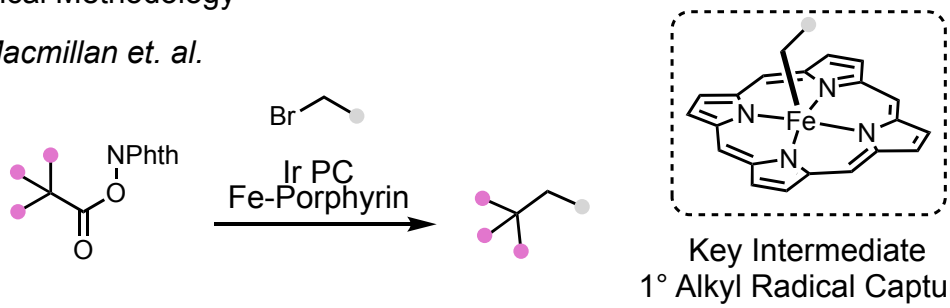

Scheme 1.1 Common reactive intermediates. Recent advances in taming a) carbocations, b) arynes, and c) radicals.

While most often not isolable, organic chemists have developed methods to trap otherwise transient radicals for highly useful reactions. As seen with many of these examples, a common way chemists think about controlling these reactive intermediates is by use of transition metal catalysis. These metals can often stabilize the intermediate, making a stable complex with what would otherwise be an uncontrollable species. One such intermediate that has captured the interest of the organic chemistry community is the carbene.

1.2 Electronic Structure of Carbenes

A carbene is a divalent carbon with two non-bonding electrons.[13] These electrons can exist in two distinct spin states – the singlet state, where both electrons reside in the same orbital, and the triplet state, where the electrons occupy two separate orbitals. The two paired electrons share an orbital within the molecular plane. This orbital is stabilized due to the adoption of the s character from the σ orbital on the carbon. With both electrons in the hybridized orbital, singlet carbenes also bear an empty p-orbital. On the other hand, triplet carbenes have one electron in each p-orbital (Figure 1.1).

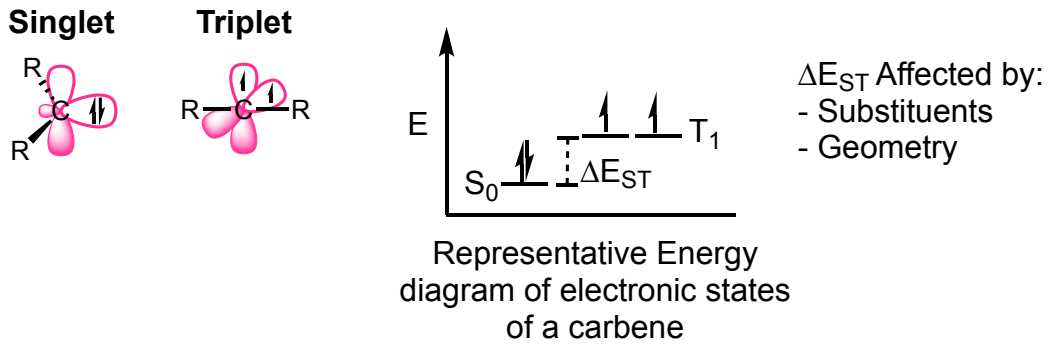

Figure 1.1 Possible spin states of carbenes with representative energy diagram

The simplest carbene to visualize this phenomenon is methylene. Generated most often from diazomethane, this transient species is a model to understanding the principles of the carbene. Methylene adopts a bent geometry, with the two hydrogens out of the plane from one another. As mentioned above, this induces one of the two degenerate p-orbitals to adopt more s-character, becoming stabilized. Intuitively, this would indicate that methylene would exist in the singlet (S_0) ground state. However, spectroscopic studies have shown that methylene exists in the triplet state, highlighting the singlet-triplet energy gap.[14, 15] For free-carbenes, this gap is often very small, being highly affected by both the substituents on the carbene itself as well as the geometry that the intermediate adopts.

1.3 Generation of Carbenes

Carbenes are generated through a variety of means, using materials known as carbene precursors.[16-19] These compounds are primed with a leaving group which, under certain conditions, can undergo alpha-elimination, extrusion of the leaving group, or rearrangement, revealing a carbene. The most ubiquitous intermediate to generate carbenes are diazo compounds.[20] These compounds can generate carbenes through the extrusion of nitrogen gas, offering an incredible entropic driving force for carbene formation. However, while this makes carbene formation a generally facile process, diazo compounds are notoriously hazardous to work with due to their high energy of decomposition.[21] Even with these considerations, diazo compounds have long been used as an invaluable tool for the synthetic organic chemist.

Diazo compounds can be divided into three primary categories which can guide the reactivity and selectivity of the resultant carbene (Figure 1.2).[22] The first class of are known as acceptor-only carbenes. These occur when the carbene is alpha to an electron

withdrawing group. Common withdrawing groups for acceptor-only carbenes include cyano,[23] trifluoromethyl,[24] and nitro,[25] with the most common being the ester group.[20] Ethyl diazo acetate has long been utilized as a readily available carbene precursor for a plethora of organic transformations. Acceptor-only carbenes are known to be highly reactive, unable to achieve good selectivity in many of the reactions they are known for. The second class of diazo compounds are donor carbenes.[26] These are classified with having an electron-donating group alpha to the carbene. This type of carbene is often highly unstable, only found in transient conditions, and prone to carbene dimerization. A happy medium was found when donor/acceptor carbenes were discovered.[27]

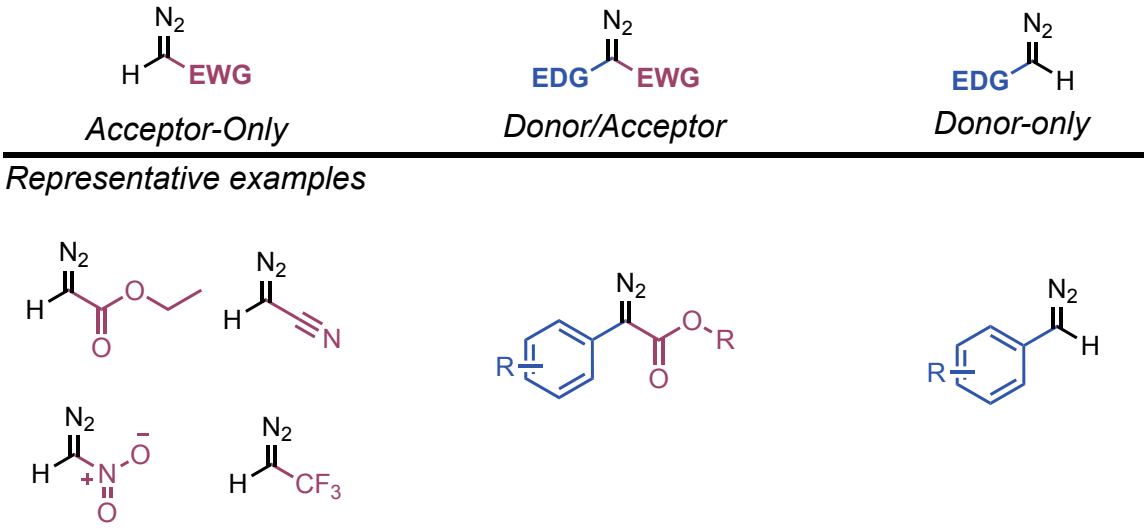

Figure 1.2 Different classes of diazo compounds

Having both an electron-donating and withdrawing group, donor/acceptor carbenes have high reactivity due to the electron-withdrawing group yet are stabilized by the electron-donating group. The donating group can attenuate the reactivity by stabilizing the empty

p-orbital on the carbene. This allows for higher levels of selectivity to be obtained, while also still maintaining the high reactivity profile due to the acceptor-carbene.

Free carbenes, a carbene not stabilized by any transition metal, can be generated by thermal or photochemical means and can undergo a range of carbene insertion reactions.[28-31] While typically used in their singlet state, free carbenes are also able to exist in their triplet state. This most commonly occurs with the sensitization of the diazo compound, either through direct sensitization, in which the carbene exists in an equilibrium between its triplet and singlet state, or via an energy transfer photocatalyst. Triplet carbenes are diradical in nature, with two singly occupied orbitals. This can lead to a variety of unique transformations that differ in reactivity from the singlet carbene reactivity. Chapter 5 of this dissertation will explore in more depth photogenerated triplet carbenes from diazo compounds and the development of a novel synthetic methodology using these intermediates.

1.4 Reactions of Carbenes

The most common way to decompose diazo compounds is through transition metal catalysis to form metallo-carbene intermediates. Metals such as Cu,[32] Co,[33] Ag,[34] Au,[35, 36] Pd,[37, 38] Ru,[39, 40] and Rh[22, 41] have all been reported to decompose diazo compounds to generate metallo-carbene intermediates and catalyze a variety of organic transformations. Metallo-carbenes are often able to be controlled by the ligand design around the metal center, allowing for highly selective reactions to occur.[32, 42, 43] This paradigm is the key way that chemists think about controlling the reactive carbene intermediates. One catalyst system which has enjoyed much success in metallo-carbene insertion reactions are dirhodium tetracarboxylate complexes.

1.5 Dirhodium metallo-carbene complexes

The simplest dirhodium tetracarboxylate is dirhodium tetraacetate. This complex gives us a representative example of the unique paddlewheel structure in which more complex dirhodium complexes are derived. The paddlewheel structure adopts what is also known as a lantern structure, with each carboxylate ligand bound to both rhodium atoms, with a central rhodium–rhodium bond along the central axis of the complex.[44]

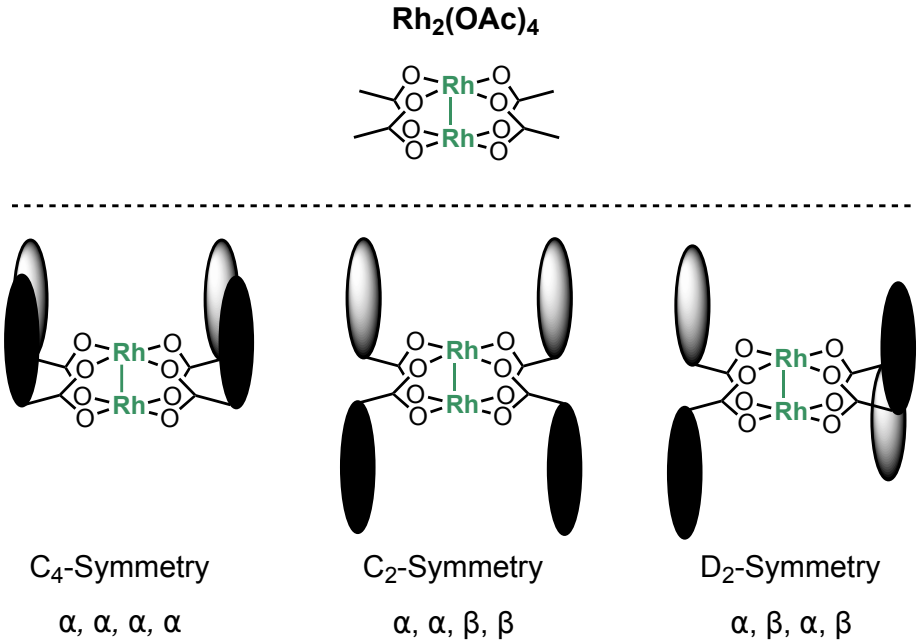

Figure 1.3 The structure of dirhodium tetracarboxylate catalysts

These complexes can undergo a ligand exchange with a variety of chiral carboxylic acids, enabling the synthesis of elaborate paddlewheel complexes. The structure of the complexes can vary drastically depending on the ligand environment around the dirhodium core, leading to higher symmetry complexes than the ligands themselves (Figure 1.3). For example, if the four carboxylate ligands are in an all up *α, α, α, α*, orientation the complex will have C_4-symmetry. D_2-symmetry is observed for catalysts

with an *α, β, α, β* geometry, while *α, α, β, β* orientation leads to C_2-symmetry. The ligand orientation has a significant impact on the selectivity of the subsequent reaction.

1.6 Dirhodium tetracarboxylate catalyzed Carbene Transfer Reactions

The Davies group has relied heavily on this concept for the past 40 years, reporting a plethora of carboxylate dirhodium complexes.[45-50] These complexes have all been shown to generate metallo-carbene intermediates from the corresponding aryl diazoacetate compounds, with excellent reactivity towards cyclopropanation and C–H insertion carbene transfer reactions.[45, 51-53] The general mechanism of a carbene transfer reaction follows a concerted asynchronous pathway (Scheme 1.2).[54-57] First, approach of the diazo compound towards the open coordination site of one of the rhodium atoms allows for the extrusion of nitrogen to form the metallo-carbene intermediate. Then, the substrate approaches, engaging the carbene in either a [2+1] cycloaddition or C–H insertion step for olefin cyclopropanation or C–H functionalization, respectively.

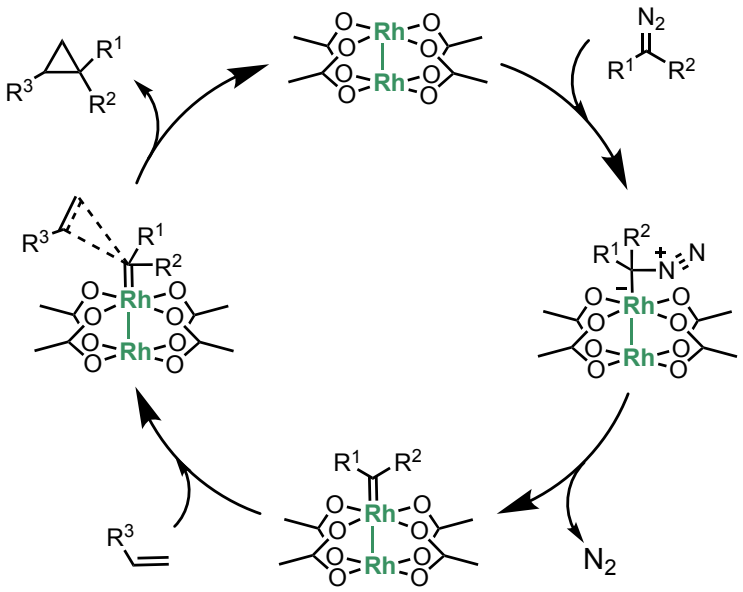

Scheme 1.2 Mechanism of carbene insertion reactions, specifically cyclopropanation

The mechanism is concerted but proceeds in an asynchronous manner.

The choice of ligand has a profound impact on the result of the reaction, allowing for one to select specific catalysts for a specific reaction. To this end a 'toolbox' of catalysts have been developed, each with their own specific uses for selective cyclopropanation or C–H functionalization (Scheme 1.3A). The C–H functionalization of *p*-cymene showcases this feature nicely due to the internal competition between the primary and tertiary C–H bonds (Scheme 1.3B).

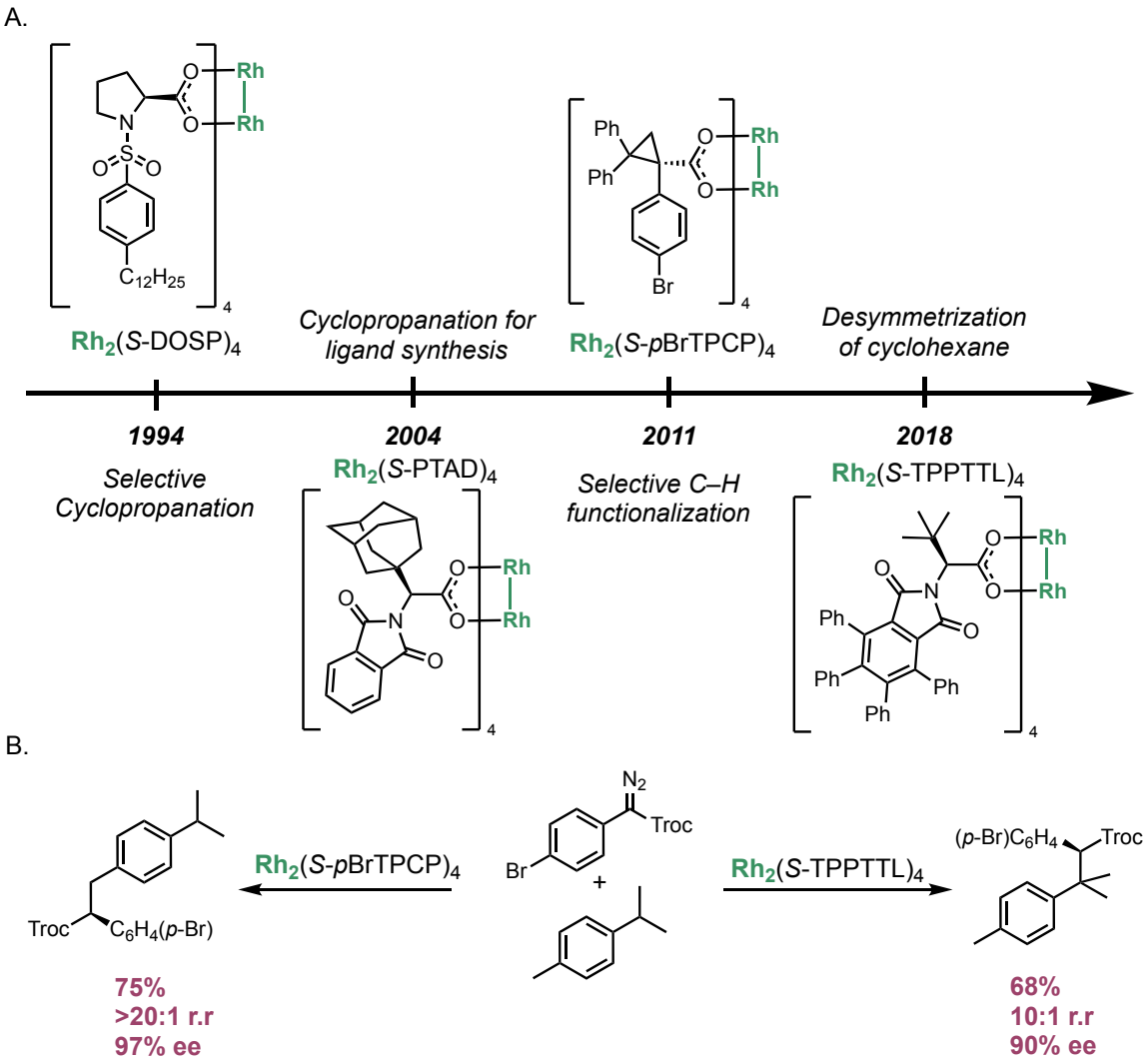

Scheme 1.3 A) Timeline of dirhodium tetracarboxylate catalysts, B) example of selective C–H functionalization using different catalysts.

Rh_2(*S*-TPPTTL)$_4$, a catalyst first disclosed in 2018, gives selective insertion into the tertiary C–H bond in a 10:1 ratio. However, simply by changing the catalyst to Rh_2(*S*-*p*BrTPCP)$_4$, a more sterically demanding ligand, the selectivity is switched entirely to favor the primary C–H insertion in >20:1 regioselectivity.

Taking advantage of the substrate interaction with the catalyst wall has led to a variety of novel transformations for dirhodium catalysts.[58-60] Rh_2(*S*-TPPTTL)$_4$, derived from *tert*-leucine phthalamido-carboxylic acid, adopts a C_4-geometry, with the ligands being in the all-α position. This leads to one face of the catalyst being open, with a bowl-shape being formed by the ligands around the axial site of one of the rhodium atoms. The ligand has been designed to block the other face of the catalyst with sterically bulky *tert*-butyl groups, forcing the metallo-carbene to be generated inside of the bowl of the catalyst. Because of this bowl-shaped structure of the catalyst, the ligand wall can impact the selectivity by interacting with the substrate approach to the carbene. This catalyst was developed in 2018 for the desymmetrization of cyclohexane derivatives.[58] Using aryldiazoacetates, the catalyst was able to selectively functionalize the C3 position of *tert*-butylcyclohexane in >20:1 regioselectivity, with high d.r. (10:1) and ee (95%). The key interaction is contributed to the wall of the catalyst interfering with bulky *tert*-butyl group of the substrate. This forces the substrate to adopt a position within the bowl where the C3 C–H bond is preferentially functionalized by the metallo-carbene intermediate. Chapter 4 of this dissertation will expound on this bowl-effect in the development of selective cyclopropanation of exocyclic olefins for generation of spirocyclopropanes.

1.7 Drawbacks and Solutions to Dirhodium Tetracarboxylate Chemistry

While the dirhodium tetracarboxylate complexes have enjoyed a myriad of success in carbene transfer reactions, the fact that rhodium is a precious heavy metal can be seen as a drawback due to price and sustainability (Figure 1.4). Two solutions can be identified to mitigate this problem, namely the exploration of dirhodium catalysts in low-catalyst loading for both cyclopropanation and C–H functionalization and the use of alternative metals in the tetracarboxylate core. The Davies lab has recently investigated efforts toward low catalyst loading for carbene transfer reactions.[57, 61] In 2019, our lab reported on the cyclopropropanation of activated olefins using low-catalyst loading with Rh_2(*S*-*p*PhTPCP)$_4$, achieving a catalyst loading of 0.0025 mol%. This was achieved using dimethyl carbonate as solvent enabling the high enantioselectivity to be maintained. Additionally, the Davies lab reported on ultra-low catalyst loading for C–H functionalization using the bowl-shaped catalyst Rh_2(*S*-TPPTTL)$_4$ along with an additive dicyclohexanecarbodiimide (DCC). Serendipitously discovered, it was found that adding 1.0 mol% of DCC enabled catalyst loadings as low as 0.0005 mol% for the C–H functionalization of cyclohexane. These examples show how dirhodium tetracarboxylate catalysts can be made practical by changing the reaction conditions or introducing an additive to the reaction.

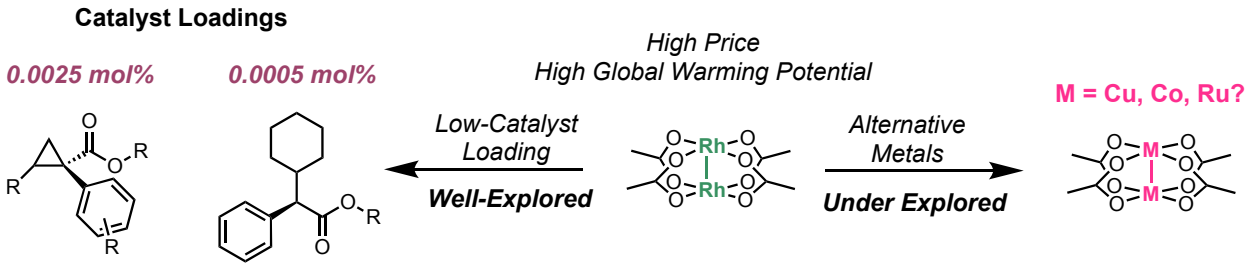

Figure 1.4 Potential solutions to the problem of rhodium

The second solution to mitigate the cost of rhodium is to use a different metal entirely. Investigations into using alternative metals in the tetracarboxylate complexes for carbene transfer reactions will be the topic of Chapter 2 and 3 of this dissertation.

1.8 Conclusion

In summary, carbenes are a powerful reactive intermediate used by organic chemists for a plethora of synthetic transformations. Both singlet and triplet carbenes have synthetic utility, even though the result of the reaction can change drastically based on the spin-state of the intermediate. Using transition metal catalysts is a key way in which organic chemists think about controlling the reactivity of carbenes, with dirhodium tetracarboxylate complexes being the premier catalytic systems for aryl diazoacetate carbene precursors. The Davies group has been pioneering this field for the past 40 years, having generated a catalysts 'toolbox' in which we can select specific catalysts for specific carbene transfer reactions we want to achieve. Subsequent chapters of this dissertation will aim to take on the challenges still unsolved with dirhodium tetracarboxylate catalysis, as well as advance the field of controlling carbenes for developing synthetic methodology.

1.9 References

1. Wentrup, C., *Reactive Molecules*. John Wiley & Sons, Inc: 1984.
2. Wendlandt, A. E.; Vangal, P.; Jacobsen, E. N., Quaternary stereocentres via an enantioconvergent catalytic SN1 reaction. *Nature* **2018,** *556* (7702), 447-451.
3. Grant, P. S.; Vavrík, M.; Porte, V.; Meyrelles, R.; Maulide, N., Remote proton elimination: C–H activation enabled by distal acidification. *Science* **2024,** *384* (6697), 815-820.
4. Properzi, R.; Kaib, P. S. J.; Leutzsch, M.; Pupo, G.; Mitra, R.; De, C. K.; Song, L.; Schreiner, P. R.; List, B., Catalytic enantiocontrol over a non-classical carbocation. *Nat. Chem.* **2020,** *12* (12), 1174-1179.
5. Humke, J. N.; Belli, R. G.; Plasek, E. E.; Kargbo, S. S.; Ansel, A. Q.; Roberts, C. C., Nickel binding enables isolation and reactivity of previously inaccessible 7-aza-2,3-indolynes. *Science* **2024,** *384* (6694), 408-414.
6. Gavin, J. T.; Anderson, L. W.; Roberts, C. C., Aryne Aminohalogenation Using Protic Amines Enabled by Halogen Transfer. *Org. Lett.* **2024,** *26* (36), 7530-7534.
7. Chan, A. Y.; Perry, I. B.; Bissonnette, N. B.; Buksh, B. F.; Edwards, G. A.; Frye, L. I.; Garry, O. L.; Lavagnino, M. N.; Li, B. X.; Liang, Y.; Mao, E.; Millet, A.; Oakley, J. V.; Reed, N. L.; Sakai, H. A.; Seath, C. P.; MacMillan, D. W. C., Metallaphotoredox: The Merger of Photoredox and Transition Metal Catalysis. *Chem. Rev.* **2022,** *122* (2), 1485-1542.
8. Zuo, Z.; Ahneman, D. T.; Chu, L.; Terrett, J. A.; Doyle, A. G.; MacMillan, D. W. C., Merging photoredox with nickel catalysis: Coupling of α-carboxyl sp3-carbons with aryl halides. *Science* **2014,** *345* (6195), 437-440.
9. Liu, W.; Lavagnino, M. N.; Gould, C. A.; Alcázar, J.; MacMillan, D. W. C., A biomimetic SH2 cross-coupling mechanism for quaternary sp3-carbon formation. *Science* **2021,** *374* (6572), 1258-1263.
10. Yamaguchi, Y.; Hirata, Y.; Higashida, K.; Yoshino, T.; Matsunaga, S., Cobalt/Photoredox Dual-Catalyzed Cross-Radical Coupling of Alkenes via Hydrogen Atom Transfer and Homolytic Substitution. *Org. Lett.* **2024,** *26* (23), 4893-4897.
11. Zhang, Y.; Li, K.-D.; Huang, H.-M., Bimolecular Homolytic Substitution (SH2) at a Transition Metal. *ChemCatChem* **2024,** *16* (21), e202400955.
12. Chen, R.; Intermaggio, N. E.; Xie, J.; Rossi-Ashton, J. A.; Gould, C. A.; Martin, R. T.; Alcázar, J.; MacMillan, D. W. C., Alcohol-alcohol cross-coupling enabled by SH2 radical sorting. *Science* **2024,** *383* (6689), 1350-1357.
13. Kirmse, W., *Carbene Chemistry*. Academic Press, Inc: 1971; Vol. 1, p 598.
14. Lengel, R. K.; Zare, R. N., Experimental determination of the singlet-triplet splitting in methylene. *J. Am. Chem. Soc.* **1978,** *100* (24), 7495-7499.
15. Hayden, C. C.; Neumark, D. M.; Shobatake, K.; Sparks, R. K.; Lee, Y. T., Methylene singlet–triplet energy splitting by molecular beam photodissociation of ketene. *The Journal of Chemical Physics* **1982,** *76* (7), 3607-3613.
16. Jia, M.; Ma, S., New Approaches to the Synthesis of Metal Carbenes. *Angew. Chem. Int. Ed.* **2016,** *55* (32), 9134-9166.
17. Anderson, T. E.; Thamattoor, D. M.; Phillips, D. L., Formation of 3-Oxa- and 3-Thiacyclohexyne from Ring Expansion of Heterocyclic Alkylidene Carbenes: A Mechanistic Study. *Org. Lett.* **2023,** *25* (9), 1364-1369.

18. Rosenberg, M. G.; Schrievers, T.; Brinker, U. H., Competitive 1,2-C Atom Shifts in the Strained Carbene Spiro[3.3]hept-1-ylidene Explained by Distinct Ring-Puckered Conformers. *J. Org. Chem.* **2016,** *81* (24), 12388-12400.
19. Zhang, L.; DeMuynck, B. M.; Paneque, A. N.; Rutherford, J. E.; Nagib, D. A., Carbene reactivity from alkyl and aryl aldehydes. *Science* **2022,** *377* (6606), 649-654.
20. Wang, J., Diazo compounds: Recent applications in synthetic organic chemistry and beyond. *Tetrahedron Lett.* **2022,** *108*, 154135.
21. Green, S. P.; Wheelhouse, K. M.; Payne, A. D.; Hallett, J. P.; Miller, P. W.; Bull, J. A., Thermal Stability and Explosive Hazard Assessment of Diazo Compounds and Diazo Transfer Reagents. *Org. Process Res. Dev.* **2020,** *24* (1), 67-84.
22. Davies, H. M. L., Finding Opportunities from Surprises and Failures. Development of Rhodium-Stabilized Donor/Acceptor Carbenes and Their Application to Catalyst-Controlled C–H Functionalization. *J. Org. Chem.* **2019,** *84* (20), 12722-12745.
23. Xiao, M.-Y.; Zheng, M.-M.; Peng, X.; Xue, X.-S.; Zhang, F.-G.; Ma, J.-A., Catalytic Direct Construction of Cyano-tetrazoles. *Org. Lett.* **2020,** *22* (19), 7762-7767.
24. Mertens, L.; Hock, K. J.; Koenigs, R. M., Fluoroalkyl-Substituted Diazomethanes and Their Application in a General Synthesis of Pyrazoles and Pyrazolines. *Chem. Eur. J.* **2016,** *22* (28), 9542-9545.
25. So, S. S.; Mattson, A. E., Urea Activation of α-Nitrodiazoesters: An Organocatalytic Approach to N–H Insertion Reactions. *J. Am. Chem. Soc.* **2012,** *134* (21), 8798-8801.
26. Zhu, D.; Chen, L.; Fan, H.; Yao, Q.; Zhu, S., Recent progress on donor and donor–donor carbenes. *Chem. Soc. Rev.* **2020,** *49* (3), 908-950.
27. Davies, H. M. L.; Clark, T. J.; Church, L. A., Stereoselective cyclopropanations with vinylcarbenoids. *Tetrahedron Lett.* **1989,** *30* (38), 5057-5060.
28. Chen, P.; Nan, J.; Hu, Y.; Kang, Y.; Wang, B.; Ma, Y.; Szostak, M., Metal-free tandem carbene N–H insertions and C–C bond cleavages. *Chem. Sci.* **2021,** *12* (2), 803-811.
29. Hansen, S. R.; Spangler, J. E.; Hansen, J. H.; Davies, H. M. L., Metal-Free N–H Insertions of Donor/Acceptor Carbenes. *Org. Lett.* **2012,** *14* (17), 4626-4629.
30. Gomes, L. F. R.; Veiros, L. F.; Maulide, N.; Afonso, C. A. M., Diazo- and Transition-Metal-Free C□H Insertion: A Direct Synthesis of β-Lactams. *Chem. Eur. J.* **2015,** *21* (4), 1449-1453.
31. Arunprasath, D.; Sekar, G., A Transition-Metal-Free and Base-Mediated Carbene Insertion into Sulfur-Sulfur and Selenium-Selenium Bonds: An Easy Access to Thio- and Selenoacetals. *Adv. Synth. Catal.* **2017,** *359* (4), 698-708.
32. Zhao, X.; Zhang, Y.; Wang, J., Recent developments in copper-catalyzed reactions of diazo compounds. *Chem. Commun.* **2012,** *48* (82), 10162-10173.
33. Wang, X.; Peter Zhang, X., Catalytic Radical Approach for Selective Carbene Transfers via Cobalt(II)-Based Metalloradical Catalysis. In *Transition Metal-Catalyzed Carbene Transformations*, 2022; pp 25-66.
34. Álvarez, M.; Molina, F.; Pérez, P. J., Carbene-Controlled Regioselective Functionalization of Linear Alkanes under Silver Catalysis. *J. Am. Chem. Soc.* **2022,** *144* (51), 23275-23279.

35. Li, D.-Y.; Fang, W.; Wei, Y.; Shi, M., C(sp3)−H Functionalizations Promoted by the Gold Carbene Generated from Vinylidenecyclopropanes. *Chem. Eur. J.* **2016,** *22* (50), 18080-18084.
36. Huang, T.; Shao, Y.; Tang, S.; Sun, J., Gold-catalyzed tandem reaction of o-alkynylphenols with diazo compounds: access to 2,3-disubstituted benzofurans. *Org. Biomol. Chem.* **2023,** *21* (28), 5752-5756.
37. Zhang, Z.; Kvasovs, N.; Dubrovina, A.; Gevorgyan, V., Visible Light Induced Brønsted Acid Assisted Pd-Catalyzed Alkyl Heck Reaction of Diazo Compounds and N-Tosylhydrazones. *Angew. Chem. Int. Ed.* **2022,** *61* (1), e202110924.
38. Li, S.; Tong, W.-Y.; Zhou, Q.; Yu, X.; Shi, J.-L.; Li, S.-S.; Qu, S.; Wang, J., Palladium-Catalyzed Oxidative Coupling of Dibenzosiloles with α-Diazo Esters: Formal Replacement of the Silyl Group with Carbenes. *Organometallics* **2023,** *42* (8), 660-671.
39. Maas, G., Ruthenium-catalysed carbenoid cyclopropanation reactions with diazo compounds. *Chem. Soc. Rev.* **2004,** *33* (3), 183-190.
40. Choi, M. K.-W.; Yu, W.-Y.; Che, C.-M., Ruthenium-Catalyzed Stereoselective Intramolecular Carbenoid C−H Insertion for β- and γ-Lactam Formations by Decomposition of α-Diazoacetamides. *Org. Lett.* **2005,** *7* (6), 1081-1084.
41. Doraghi, F.; Baghershahi, P.; Ghasemi, M.; Mahdavi, M.; Al-Harrasi, A., Rhodium-catalyzed transformations of diazo compounds via a carbene-based strategy: recent advances. *RCS Adv.* **2024,** *14* (53), 39337-39352.
42. Davies, H. M. L.; Morton, D., Guiding principles for site selective and stereoselective intermolecular C–H functionalization by donor/acceptor rhodium carbenes. *Chem. Soc. Rev.* **2011,** *40* (4), 1857-1869.
43. Zi, W.; Dean Toste, F., Recent advances in enantioselective gold catalysis. *Chem. Soc. Rev.* **2016,** *45* (16), 4567-4589.
44. Cotton, F. A., DeBoer, B. G., LaPrade, M. D., Pipal, J. R., Ucko, D. A., The crystal and molecular structures of dichromium tetraacetate dihydrate and dirhodium tetraacetate dihydrate. *Acta Crystallographica* **1971**, 1664-1671.
45. Davies, H. M. L.; Bruzinski, P. R.; Lake, D. H.; Kong, N.; Fall, M. J., Asymmetric Cyclopropanations by Rhodium(II) N-(Arylsulfonyl)prolinate Catalyzed Decomposition of Vinyldiazomethanes in the Presence of Alkenes. Practical Enantioselective Synthesis of the Four Stereoisomers of 2-Phenylcyclopropan-1-amino Acid. *J. Am. Chem. Soc.* **1996,** *118* (29), 6897-6907.
46. Reddy, R. P.; Lee, G. H.; Davies, H. M. L., Dirhodium Tetracarboxylate Derived from Adamantylglycine as a Chiral Catalyst for Carbenoid Reactions. *Org. Lett.* **2006,** *8* (16), 3437-3440.
47. Qin, C.; Boyarskikh, V.; Hansen, J. H.; Hardcastle, K. I.; Musaev, D. G.; Davies, H. M. L., D2-Symmetric Dirhodium Catalyst Derived from a 1,2,2-Triarylcyclopropanecarboxylate Ligand: Design, Synthesis and Application. *J. Am. Chem. Soc.* **2011,** *133* (47), 19198-19204.
48. Liao, K.; Liu, W.; Niemeyer, Z. L.; Ren, Z.; Bacsa, J.; Musaev, D. G.; Sigman, M. S.; Davies, H. M. L., Site-Selective Carbene-Induced C–H Functionalization Catalyzed by Dirhodium Tetrakis(triarylcyclopropanecarboxylate) Complexes. *ACS Catal.* **2018,** *8* (1), 678-682.
49. Liao, K.; Yang, Y.-F.; Li, Y.; Sanders, J. N.; Houk, K. N.; Musaev, D. G.; Davies, H. M. L., Design of catalysts for site-selective and enantioselective

functionalization of non-activated primary C–H bonds. *Nat. Chem.* **2018,** *10* (10), 1048-1055.
50. Garlets, Z. J.; Boni, Y. T.; Sharland, J. C.; Kirby, R. P.; Fu, J.; Bacsa, J.; Davies, H. M. L., Design, Synthesis, and Evaluation of Extended C4–Symmetric Dirhodium Tetracarboxylate Catalysts. *ACS Catal.* **2022,** *12* (17), 10841-10848.
51. Davies, H. M. L.; Hansen, T., Asymmetric Intermolecular Carbenoid C−H Insertions Catalyzed by Rhodium(II) (S)-N-(p-Dodecylphenyl)sulfonylprolinate. *J. Am. Chem. Soc.* **1997,** *119* (38), 9075-9076.
52. Davies, H. M. L.; Hansen, T.; Churchill, M. R., Catalytic Asymmetric C−H Activation of Alkanes and Tetrahydrofuran. *J. Am. Chem. Soc.* **2000,** *122* (13), 3063-3070.
53. Davies, H. M. L.; Beckwith, R. E. J., Catalytic Enantioselective C−H Activation by Means of Metal−Carbenoid-Induced C−H Insertion. *Chem. Rev.* **2003,** *103* (8), 2861-2904.
54. P. Doyle, M.; Liu, Y.; Ratnikov, M., Catalytic, Asymmetric, Intramolecular Carbon–Hydrogen Insertion. In *Organic Reactions*, 2013; pp 1-132.
55. Wong, F. M.; Wang, J.; Hengge, A. C.; Wu, W., Mechanism of Rhodium-Catalyzed Carbene Formation from Diazo Compounds. *Org. Lett.* **2007,** *9* (9), 1663-1665.
56. Davies, H. M. L.; Pelphrey, P. M., Intermolecular C–H Insertions of Carbenoids. In *Organic Reactions*, 2011; pp 75-212.
57. Wei, B.; Sharland, J. C.; Lin, P.; Wilkerson-Hill, S. M.; Fullilove, F. A.; McKinnon, S.; Blackmond, D. G.; Davies, H. M. L., In Situ Kinetic Studies of Rh(II)-Catalyzed Asymmetric Cyclopropanation with Low Catalyst Loadings. *ACS Catal.* **2020,** *10* (2), 1161-1170.
58. Fu, J.; Ren, Z.; Bacsa, J.; Musaev, D. G.; Davies, H. M. L., Desymmetrization of cyclohexanes by site- and stereoselective C–H functionalization. *Nature* **2018,** *564* (7736), 395-399.
59. Ly, D.; Bacsa, J.; Davies, H. M. L., Rhodium(II)-Catalyzed Asymmetric Cyclopropanation and Desymmetrization of [2.2]Paracyclophanes. *ACS Catal.* **2024,** *14* (9), 6423-6431.
60. Nguyen, T.-T. H.; Bosse, A. T.; Ly, D.; Suarez, C. A.; Fu, J.; Shimabukuro, K.; Musaev, D. G.; Davies, H. M. L., Diaryldiazoketones as Effective Carbene Sources for Highly Selective Rh(II)-Catalyzed Intermolecular C–H Functionalization. *J. Am. Chem. Soc.* **2024,** *146* (12), 8447-8455.
61. Wei, B.; Sharland, J. C.; Blackmond, D. G.; Musaev, D. G.; Davies, H. M. L., In Situ Kinetic Studies of Rh(II)-Catalyzed C–H Functionalization to Achieve High Catalyst Turnover Numbers. *ACS Catal.* **2022,** *12* (21), 13400-1341

Chapter 2. Development of Diruthenium (II,III) Tetracarboxylate Catalysts for Cyclopropanation using Aryldiazoacetates as Carbene Precursors

2.1 Introduction

Transition metal catalyzed organic transformations are the bedrock of modern synthetic methodology. In particular, asymmetric catalysis provides valuable chiral scaffolds important for drug discovery,[1-3] allowing for new chemical space to be explored to combat disease. Cyclopropanes are a valuable motif in drug development and library generation.[4-6] This constrained three membered ring offers a conformationally ridged scaffold, enabling the direct placement of substituents in particular chemical environments. Chiral dirhodium tetracarboxylate complexes have been the premier catalytic system for the synthesis of chiral cyclopropanes in the last 30 years.[7-10] Using donor/acceptor diazo compounds as carbene precursors, these chiral catalysts have been shown to generate novel cyclopropane scaffolds in up to >99% ee through a carbene transfer reaction.[11]

The Davies group has been on the forefront of these investigations since the early days of dirhodium catalysis.[12] With the development of the dirhodium catalyst toolbox, a range of cyclopropanation reactions can be performed depending on the desired outcome of the reaction. In 2019, the dirhodium catalyst Rh_2(*S*-*p*-PhTPCP)$_4$ was shown to catalyze the cyclopropanation of styrene derivatives using only 0.001 mol% catalyst loading (Scheme 2.1A).[13] This type of cyclopropanation was used by Bristol Meyer Squibb in the synthesis of Beclabuvir, a Hepatitis C drug.[14] Additionally, Rh_2(*S*-TPPTTL)$_4$ was used by

Abbvie in the 100g synthesis of a key intermediate for a drug development campaign combatting Cystic Fibrosis (Scheme 2.1B).[15] However, high market volatility and limited supply raise concerns over the practicality of using rhodium-derived catalysts, especially on large scale.[16]

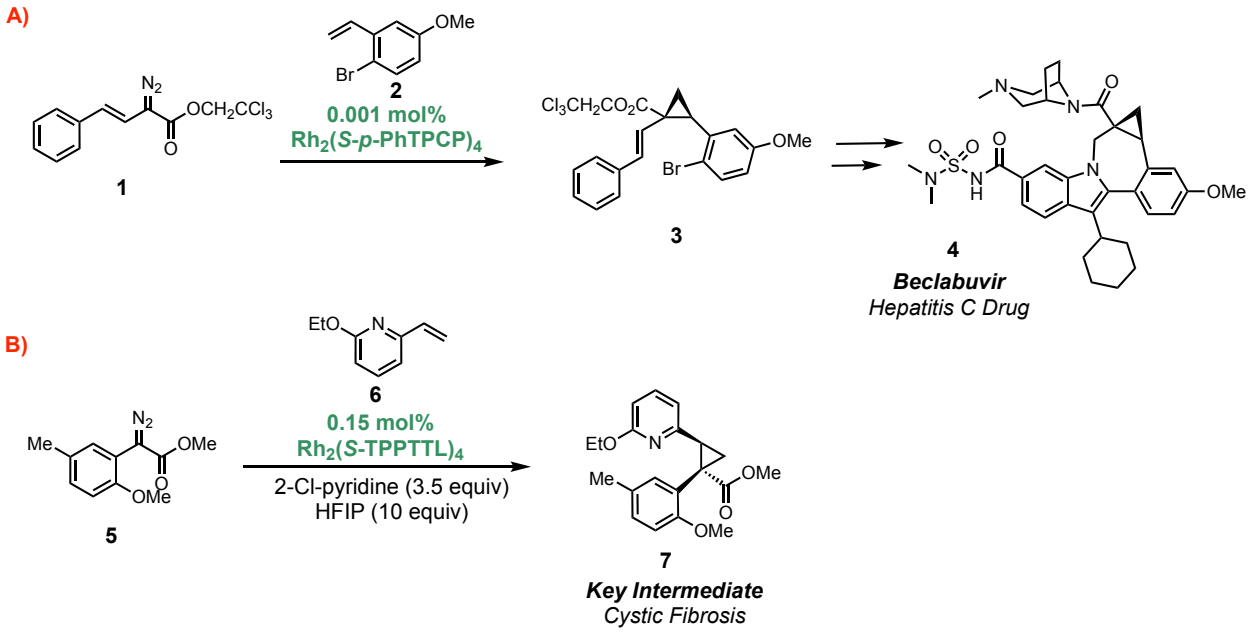

Scheme 2.1 Use of dirhodium catalysts for the synthesis of A) Key intermediate for the synthesis of Hepatitis C drug Beclabuvir and B) Key intermediate for a Cystic Fibrosis drug discovery campaign

Rhodium is not the only metal which has been used in carbene-transfer cyclopropanation with the tetracarboxylate scaffold. While the dirhodium complexes have had the most success with carbene chemistry, other catalysts with cheaper core metals have been developed, with varying degrees of success for catalytic activity. For example, in 2019 Berry and coworkers reported the synthesis of achiral molybdenum and chromium paddlewheel tetracarboxylate complexes (Scheme 2.2A).[17] These complexes, however, proved to be inactive as carbene transfer catalysts. Using cobalt in the same ligand

system did prove to be an active catalyst for styrene cyclopropanation using donor/acceptor diazo compounds however, low catalytic turnover and only moderate yield diminished the impact of these results. Several chiral tetracarboxylate catalysts with alternative metals have been reported, forming highly symmetrical structures which are thought to induce the high selectivity seen for the dirhodium analogues. While a number of mono-copper complexes have been reported for the decomposition of donor/acceptor diazo compounds[18-20], chiral dicopper complexes have not been shown to have catalytic activity.[21, 22]

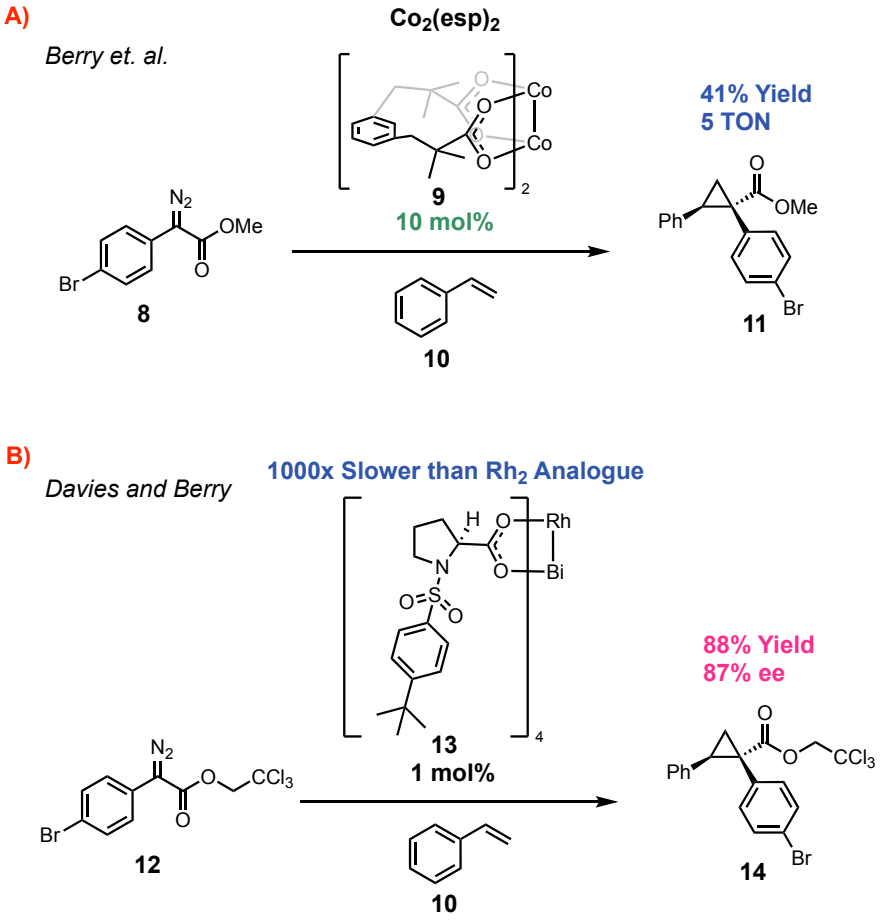

Scheme 2.2 Previously reported alternatives to dirhodium paddlewheel complexes A) achiral dicobalt complexes and B) a rhodium-bismuth chiral catalyst for asymmetric cyclopropanation.

A rhodium/bismuth bimetallic catalyst has been shown to be active in both cyclopropanation and C–H insertion reactions using donor/acceptor diazo compounds (Scheme 2.2B).[23] These catalysts are able to generate the products in high yield and selectivity but are roughly 1000 times slower than the dirhodium counterpart. In 2020, Miyazawa and coworkers reported a diruthenium paddlewheel complex which was capable of undergoing carbene transfer reactions for cyclopropanation of activated olefins (Scheme 2.3).[24] Instead of using a diazo as the carbene precursor, they utilized iodonium ylide **15**. They showed this to be a much more reactive carbene precursor than the diazo malonate (**16**) for the ruthenium system. However, being confined to using the iodonium ylide as the carbene precursor significantly reduced the scope of their reaction.

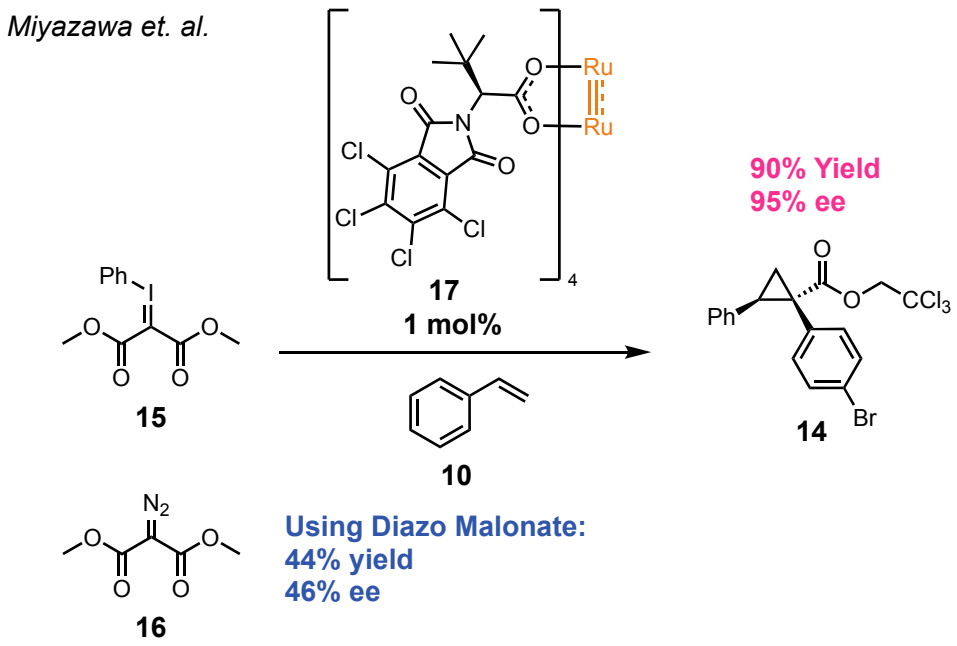

Scheme 2.3 Diruthenium catalyzed cyclopropanation using iodonium ylides as carbene precursor.

These reports inspired us to study whether dicopper, dicobalt, or diruthenium tetracarboxylate catalysts could act as a replacement for rhodium in the cyclopropanation reaction using donor/acceptor diazo compounds. Copper and cobalt are both first-row transition metals that are readily available, making them an attractive alternative for rhodium. While ruthenium is a rare-earth metal, the price is roughly 100 times lower than that of rhodium (Figure 2.1A), with a significantly lower global warming potential associated with its production (Figure 2.1B).[16, 25]

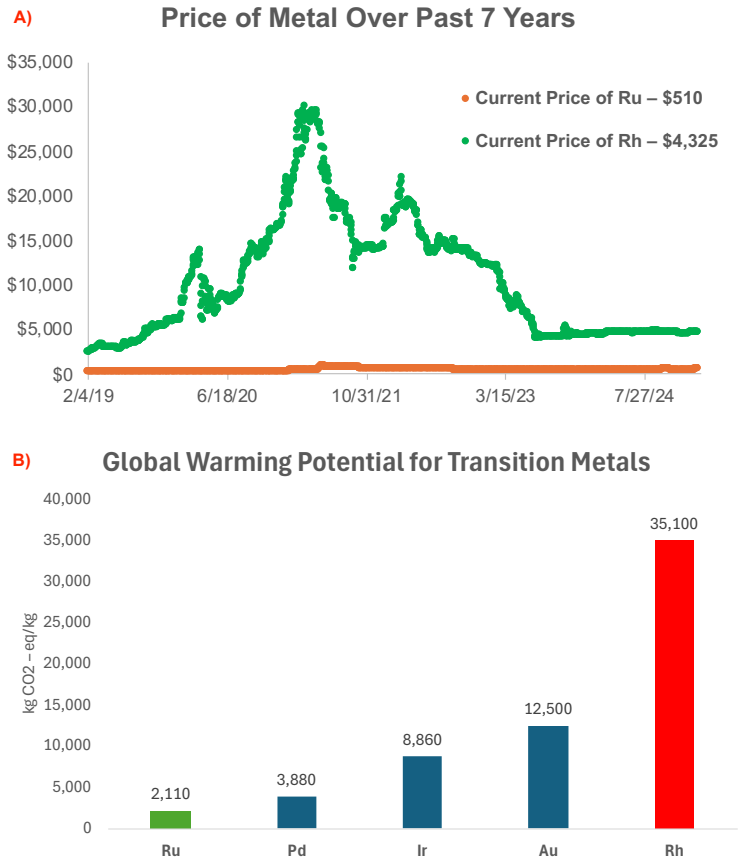

Figure 2.1 A) Graph showing the price of rhodium and ruthenium over the past 7 years[16] and B) chart showing the global warming potential for a variety of precious metals.[25]

The desire to find a cheaper alternative to rhodium has been a long-standing challenge for the Davies group. In 2021, Dr. Jack Sharland in the Davies lab conducted a thorough investigation into replacing rhodium with copper.[26] He successfully synthesized Cu_2(*S*-TPPTTL)$_4$ (**19**) using the standard ligand exchange procedure (Scheme 2.4). This catalyst was found to be stable to chromatography, and upon recrystallization from acetonitrile afforded the desired dicopper catalyst. Analyzing the X-ray crystal structure, showed the same C_4-symmetric bowl shape structure imparted by the self-assembly of four tetracarboxylate ligands observed in the dirhodium analogues. Additionally, the two axial sites of the dicopper complex were occupied with acetonitrile solvent molecules.

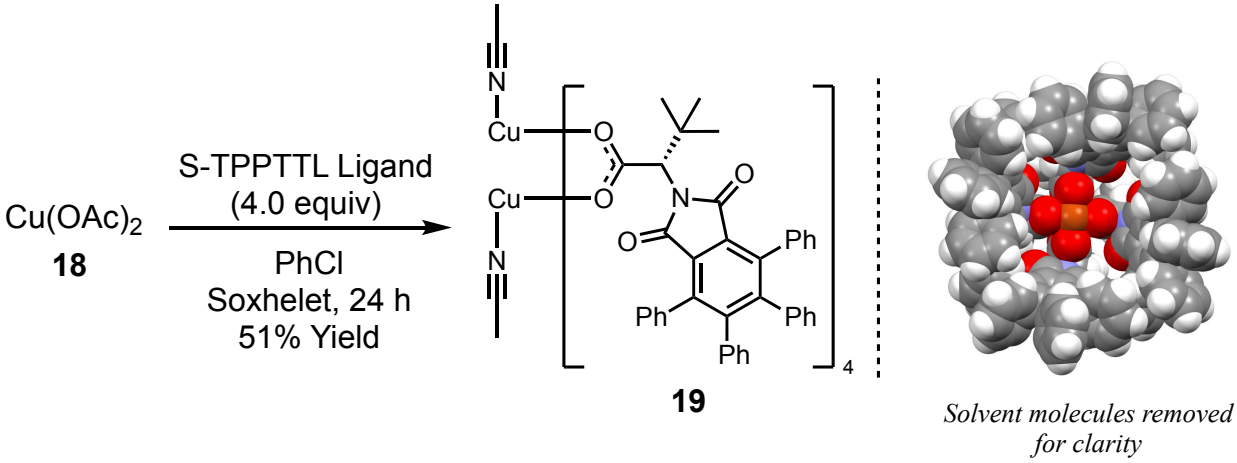

Scheme 2.4 Synthesis of Cu2(S-TPPTTL)4•2ACN and the X-ray crystal structure

With the synthesis and characterization of the dicopper complex completed, the catalytic activity in the cyclopropanation of styrene using a donor/acceptor diazo compound **12** as the carbene precursor was tested (Table 2.1). Dr. Jack Sharland found the catalyst to be

inactive at 25 °C, unable to decompose the diazo. Heating the reaction to 40 °C saw resurrection of the catalytic activity, providing the product in a 73% yield.

Table 2.1 Cu_2(*S*-TPPTTL)$_4$-catalyzed cyclopropanation

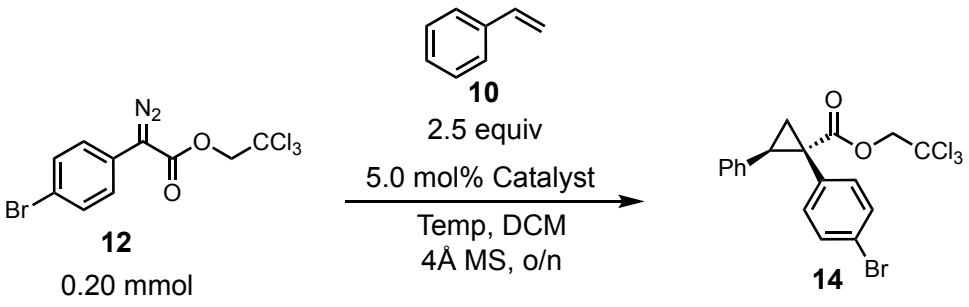

Entry	Catalyst	Temp (°C)	Yield (%)	ee (%)
1	Cu_2(*S*-TPPTTL)$_4$•2MeCN	25	0	N/a
2	Cu_2(*S*-TPPTTL)$_4$•2MeCN	40	73	<5
3	Cu_2(*S*-TPPTTL)$_4$	25	95	<5

However, the isolated product was essentially racemic, suggesting that heating the mixture caused decomposition of the chiral dicopper complex itself, resulting in an achiral catalytic environment. To mitigate this, the dicopper complex was subjected to high vacuum in attempts to remove the coordinating solvent molecules hypothesized to be inhibiting the catalytic activity. After several days, a noticeable change in color of the complex was observed and this material was subjected to the cyclopropanation reaction. This time, the reaction at 25 °C gave the **14** in 93% yield, but the enantioselectivity was still <5%, indicating the high symmetry complex was not stable under these reaction conditions. Because of these results, Dr. Sharland turned towards computation to help explain these phenomena.

Dr. Djamaladdin Musaev calculated the transition state of metallo-carbene formation. A key finding indicated that when the metallo-carbene intermediate is formed, the oxygen-copper bonds on one of the copper centers begin to elongate, significantly distorting the tetracarboxylate scaffold (Figure 2.2). The calculated distances for the Cu–O bond for $Cu_2(OAc)_4$ was found to be approximately 1.97 Å. When the metallo-carbene intermediate is formed, these same bonds increase to 2.23 Å, showing that the chiral scaffold begins to fall off the dicopper core, yielding a competent, yet racemic reaction.

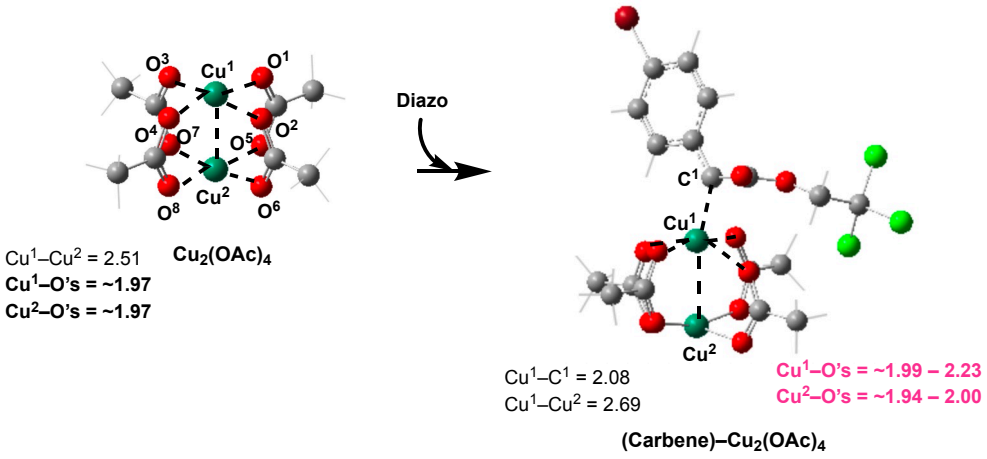

Figure 2.2 Computational findings of labile carboxylate ligands upon metallo-carbene formation.

With the dicopper system shown to be inadequate to produce an asymmetric reaction, our attention turned towards both cobalt and ruthenium. With both the desire for a cheaper and more environmentally friendly metal center, as well as the literature precedent for these metals to be viable replacements for rhodium in the tetracarboxylate scaffold, we began our investigation on the synthesis and application for cyclopropanation using donor/acceptor diazo compounds using these alternative metal centers.

2.2 Results and Discussion

The study began with investigations into replacing rhodium with cobalt. Our lab has a longstanding collaboration with the Berry group, who are specialists in inorganic synthesis of tetracarboxylate scaffolds, and particularly cobalt complexes. We collaborated with them to synthesize Co_2(*S*-TPPTTL)$_4$, which we would subsequently test in the cyclopropanation reaction. Dr. Caleb Harris carried out the synthesis of this material which resulted in a magenta-colored powder. While this material was characterized via HR-MS, giving the Co_2(*S*-TPPTTL)$_4^+$ ion, as well as IR spectroscopy, the material was unable to be analyzed by NMR due to the paramagnetic nature of the complex. Additionally, the material was never successfully crystalized, rendering full structural assignment not possible. Nevertheless, the material was pushed forward to test the catalytic activity. The material was found to be active at both 25°C and 40 °C yielding **14** in good yield. However, the enantioselectivity was found to be quite low (Table 2.2).

Table 2.2 'Co2(S-TPPTTL)$_4$'-Catalyzed cyclopropanation

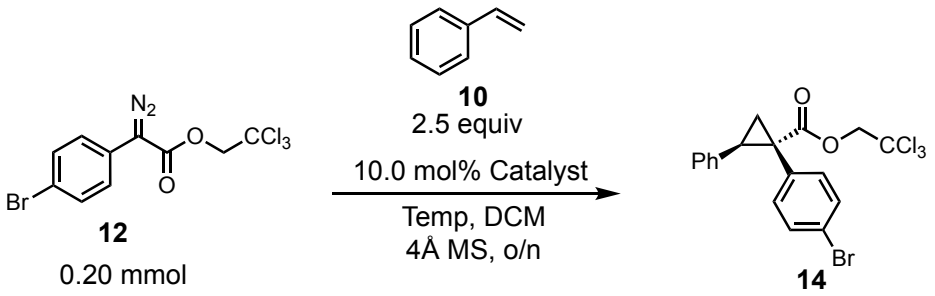

Entry	Catalyst	Temp (°C)	Yield (%)	ee (%)
1	'Co_2(*S*-TPPTTL)$_4$'	25	73	8
2	'Co_2(*S*-TPPTTL)$_4$'	40	66	12

Again, turning to computation to help rationalize these results, Dr. Djamaladdin Musaev found that the carbene-carbon in the metallo-carbene intermediate contained a radical character with a 0.75 |e| unpaired spin (Figure 2.3). This indicates that the carbene is acting as a triplet carbene rather than a singlet carbene.

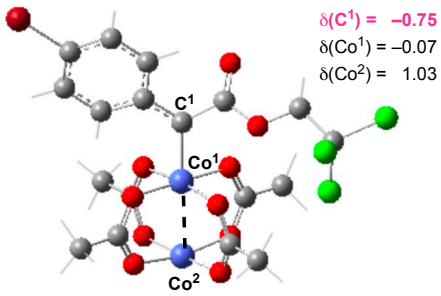

(Carbene)–$Co_2(OAc)_4$

Figure 2.3 Computational results showing radical character on the carbene carbon.

Triplet carbenes have a distinct reactivity profile, operating under a stepwise process for cyclopropanation. While triplet carbene cobalt catalyst have been previously reported,[27] the tetracarboxylate catalysts are not optimized to perform under this reaction mechanism, contributing to the low enantioselectivity observed. While it would be most attractive to use a first-row transition metal as a replacement for the dirhodium core for this catalytic system, these studies show that copper and cobalt are not viable options.

Finally, we turned to using ruthenium as the core of the tetracarboxylate complex. We began with the synthesis of Ru_2(*S*-TPPTTL)$_4$Cl from $Ru_2(OAc)_4$Cl and the carboxylic acid ligand (Scheme 2.5). The ligand exchange proceeded smoothly, furnishing **20-Cl** in 83% yield. Due to the success of this ligand exchange, four other novel diruthenium

paddlewheel complexes (**21-24-Cl**) were synthesized, using the same procedure. Due to the non-integer spin multiplicity inherent to the diruthenium complexes,[28] characterization

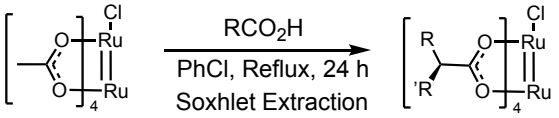

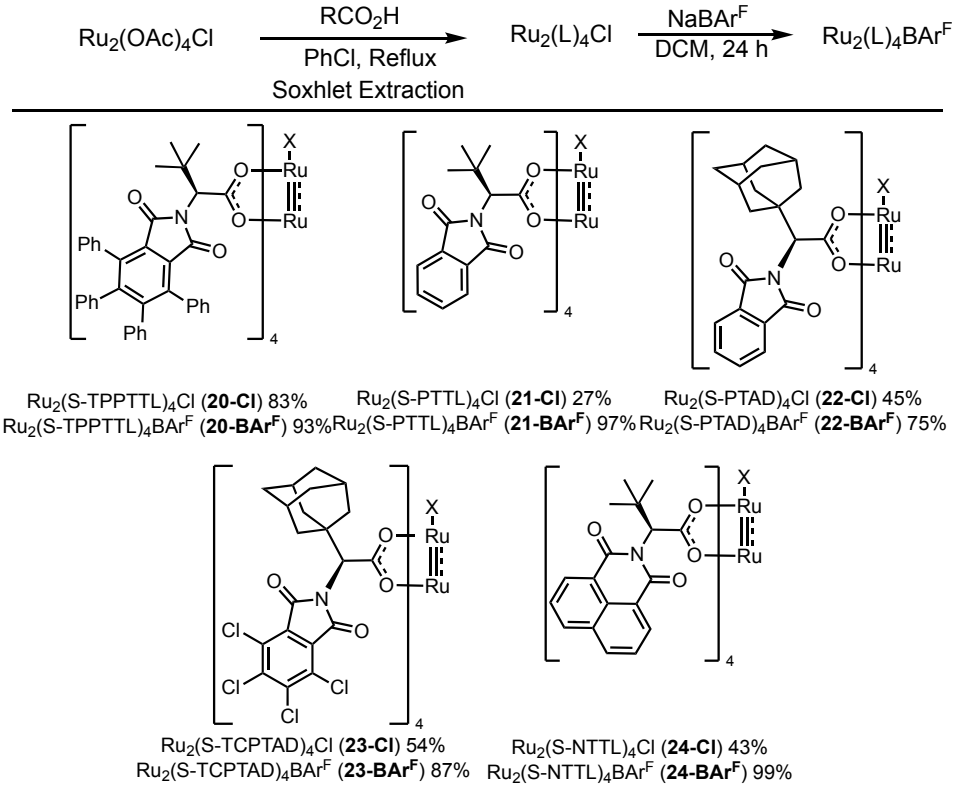

Scheme 2.5 Synthesis of diruthenium complexes

of these catalysts by NMR is not possible due to the paramagnetic nature. However, characterization by both HR-MS and X-ray crystallography unequivocally confirmed the identity of the novel complexes. Analyzing the X-ray structure of these complexes more closely reveals several interesting features (Figure 2.4). First, for all five of the catalysts,

the ligand geometry is essentially equivalent to the dirhodium analogues, with the ligands self-assembling into C_4-symmetric bowl-shaped structures. The second interesting feature is the position of the axial chloride coordinating ligand. Because the diruthenium complex is a mixed valent Ru_2(II,III) species, it bears a cationic charge associated with the ruthenium metals, requiring an anionic axial ligand. While the axial chloride ligand is there simply because of the ruthenium precursor used in the ligand exchange, we were surprised to see coordination to different faces based on the different catalysts. For example, the chloride ligand is bound to the face of the catalyst outside of the bowl for three of the catalysts, Ru_2(*S*-TPPTTL)$_4$Cl, Ru_2(*S*-PTAD)$_4$, and Ru_2(*S*-NTTL)$_4$Cl, while it is bound within the bowl for Ru_2(*S*-PTTL)$_4$Cl and Ru_2(*S*-TCPTAD)$_4$Cl (Figure 2.4A). If the chloride ligand remained bound to the axial site within the bowl of the catalyst during the catalytic reaction, the reaction yield may be significantly impacted. However, if the chloride ligand proved to be labile, it could disassociate from the metal center in solution, leaving the axial site free for metallo-carbene formation and the subsequent [2+1] cycloaddition to furnish the desired cyclopropane. One way to mitigate this possible inhibition is performing an anion exchange with a non-coordinating anion. All of the chloride catalysts were subjected to the anion exchange using sodium tetrakis[3,5-bis(trifluoromethyl)-phenyl]borate (NaBAr^F). Ru_2(*S*-TPPTTL)$_4$BAr^F was crystalized and the structure was compared to the rhodium analogue. Interestingly, the large BAr^F anion sits nicely on top of the bowl generated from the chiral ligands (Figure 2.4B). However, deleting the BAr^F anion from the structure shows that the anion does not actually alter the C_4-symmetric structure at all, with both the BAr^F catalyst and the Cl catalyst looking identical.

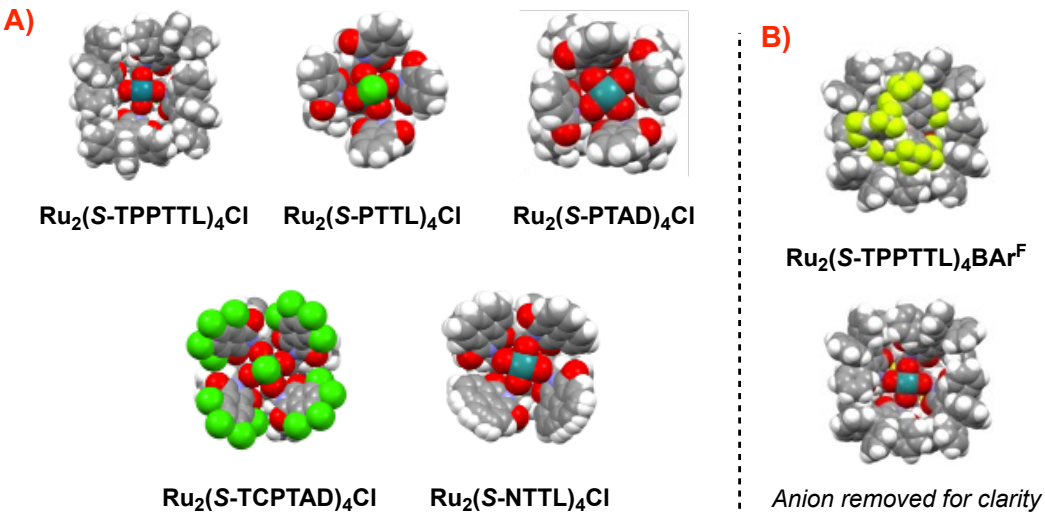

Figure 2.4 A) X-ray crystal structures of the 5 novel diruthenium catalysts and B) X-ray crystal structure of Ru2(S-TPPTTL)4BArF

With the five novel diruthenium paddlewheel complexes synthesized and characterized, their catalytic competence was tested in the cyclopropanation reaction of styrene with diazo compound **12** (Table 2.3). To our delight, all the catalysts were found to be catalytically active using 1.0 mol% catalyst loading at room temperature, giving **14** from 57-85% yield. All the reactions gave only one diastereomer, with low to good levels of enantioinduction. The most selective catalyst was Ru_2(*S*-TPPTTL)$_4$BAr^F, giving **14** in 70% yield and 82% ee (Table 2.3, entry 6). Interestingly, this was the only catalyst bearing the BAr^F anion that gave better enantioselectivity than the chloride catalyst. Additionally, the two catalysts in which the chloride was seen bound to the open face of the catalyst gave similar results to the catalysts with the chloride bound to the back face, indicating that chloride dissociation is a facile process during the reaction (Table 2.3, entries 2 and 4).

Table 2.3 Diruthenium catalyst screen for cyclopropanation with aryldiazoaceate as carbene precursor

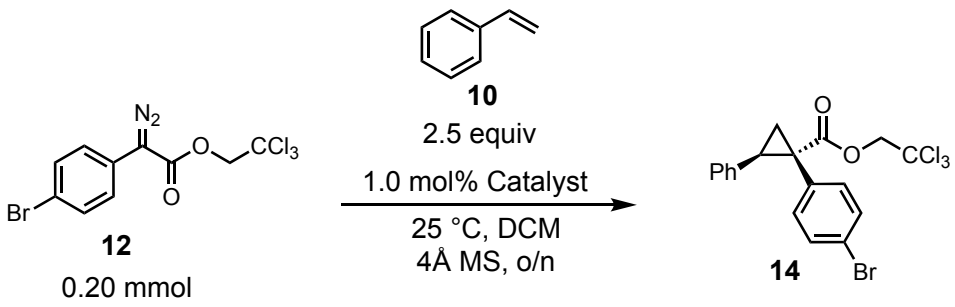

Entry	Catalyst	Yield (%)	e.e. %
1	Ru_2(S-TPPTTL)$_4$Cl	66	77
2	Ru_2(S-PTTL)$_4$Cl	67	-60
3	Ru_2(S-PTAD)$_4$Cl	67	-61
4	Ru_2(S-TCPTAD)$_4$Cl	77	65
5	Ru_2(S-NTTL)$_4$Cl	85	50
6	**Ru_2(S-TPPTTL)$_4$BAr^F**	**70**	**82**
7	Ru_2(S-PTTL)$_4$BAr^F	67	-46
8	Ru_2(S-PTAD)$_4$BAr^F	57	-55
9	Ru_2(S-TCPTAD)$_4$BAr^F	60	39
10	Ru_2(S-NTTL)$_4$BAr^F	71	20

A scope of the reaction was performed using the optimal catalyst, Ru_2(*S*-TPPTTL)$_4$BAr^F (Table 2.4). This was chosen due to this catalyst giving the highest enantioselectivity. The reaction of the standard diazo compound with a broad variety of olefin substrates formed cyclopropanes **25**-**59** with moderate to high enantioselectivity. Styryl derivatives with *para*-substituents were tolerated nicely (**25-31**), with *para*-methyl styrene giving product **28** in the highest enantioselectivity for the activated olefins at 92% ee. Alkyl olefins generally gave higher enantioselectivity (**32**-**35**), except for product **34**,

Table 2.4 Scope of Ru2(S-TPPTTL)4-Catalyzed cyclopropanation reaction.

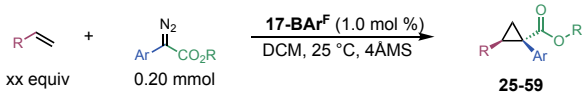

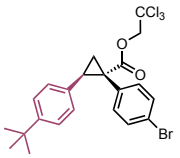 **25** 65%, 80% ee[a]	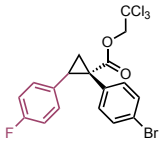 **26** 68%, 78% ee[a]	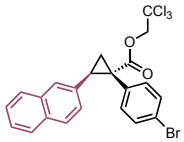 **27** 66%, 76% ee[a]	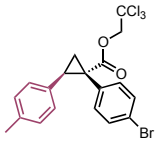 **28** 74%, 92% ee[a]	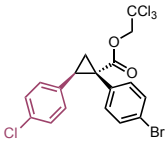 **29** 76%, 82% ee[a]	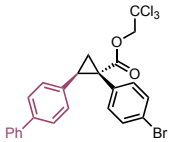 **30** 49%, 80% ee[a]
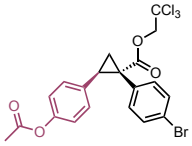 **31** 55%, 76% ee[a]	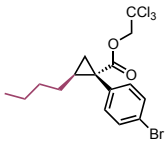 **32** 80%, 92% ee[a]	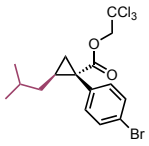 **33** 79%, 94% ee[a]	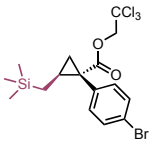 **34** 88%, 92% ee[b]	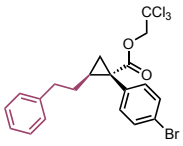 **34** 54%, 74% ee[b]	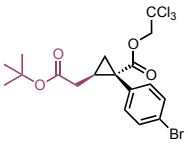 **35** 21%, 92% ee[b]
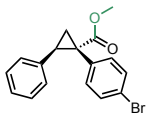 **36** 60%, 66% ee[a]	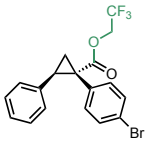 **37** 65%, 80% ee[a]	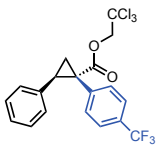 **38** 85%, 76% ee[a]	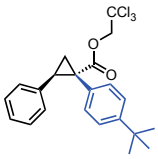 **39** 84%, 70% ee[a]	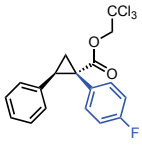 **40** 76%, 80% ee[a]	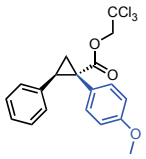 **41** 61%, 80% ee[a]
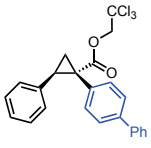 **42** 89%, 82% ee[a]	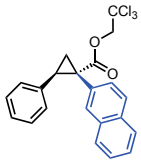 **43** 76%, 90% ee[a]	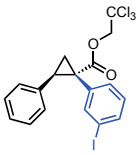 **44** 80%, 58% ee[a]	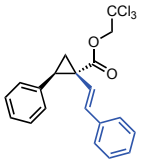 **45** 50%, 44% ee[a]	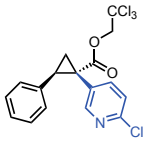 **46** 39%[c], 44% ee[a]	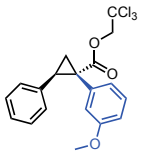 **47** 39%[c], 64% ee[a]
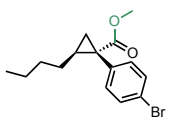 **48** 41%, 58% ee[b]	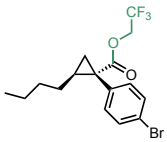 **49** 71%, 90% ee[b]	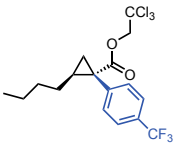 **50** 74%, 80% ee[b]	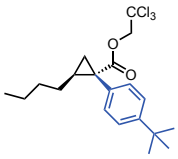 **51** 78%, 76% ee[b]	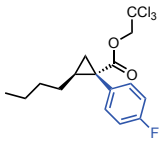 **52** 56%, 92% ee[b]	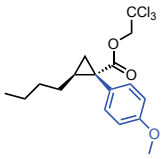 **53** 57%, 52% ee[b]
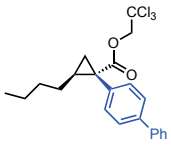 **54** 76%, 80% ee[b]	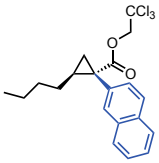 **55** 81%, 94% ee[b]	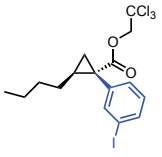 **56** 63%, 78% ee[b]	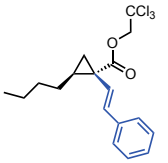 **57** 67%[c], 84% ee[b]	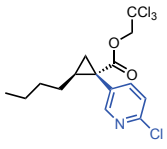 **58** 54%[c], 76% ee[b]	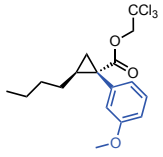 **59** 54%, 76% ee[b]

[a]Reaction run using 2.5 equiv of trap. [b]Reactions run using 10 equiv of trap.

giving the cyclopropane in 74% ee. The diastereoselectivity was high for most of the substrates except for allyl-trimethylsilane, forming **34** in only 11:1 d.r. A scope of aryldiazoacetate compounds was also explored using both styrene and 1-hexene as the trap, forming products **36**-**47** and **48-59**, respectively. Switching the ester group from trichloroethyl to methyl ester resulted in lower levels of asymmetric inductions for both **36** (66% ee) and **48** (58% ee). However, using trifluoroethyl ester (**37** and **49**) gave almost analogous results with the trichloroethyl derivatives. In general, the reactions with 1-hexene gave products with slightly higher enantioselectivity than the reactions with styrene as the trap, with the only two diazo compounds not following this trend being the *para*-methoxy and *para*-phenyl aryldiazoaceate compounds, giving **41** and **42** in 80% and 82% ee for styrene, respectively, and **53** and **54** in 52% and 80% for 1-hexene, respectively. The diazo compound which gave the highest enantioselectivity for both traps was 2,2,2-trichlrooethyl-2-diazo-2-(napthalene-2-yl)acetate, which gave products **43** and **55** in 90% ee and 94% ee, respectively.

With the scope of both the 1-hexene and styrene traps and the aryldiazoaceate explored, we moved to understanding the kinetics of the reaction using a ReactIR. This is a common technique for investigating the kinetics of reaction, especially using diazo compounds due to the significant IR stretching vibration of the diazo at ~2100 cm^{-1}. Previously, diazo decomposition has been shown to be directly correlated with product generation, enabling an excellent way to monitor the rate of the reaction. In 2019, a thorough kinetics study of dirhodium cyclopropanation of styrene was conducted using aryldiazoacetate compounds.[13] In this study it was found that styrene has an inhibitory

effect on the catalytic cycle due to π-coordination to the axial site of the rhodium complex. This concerned us considering the cationic nature of the diruthenium catalyst causes

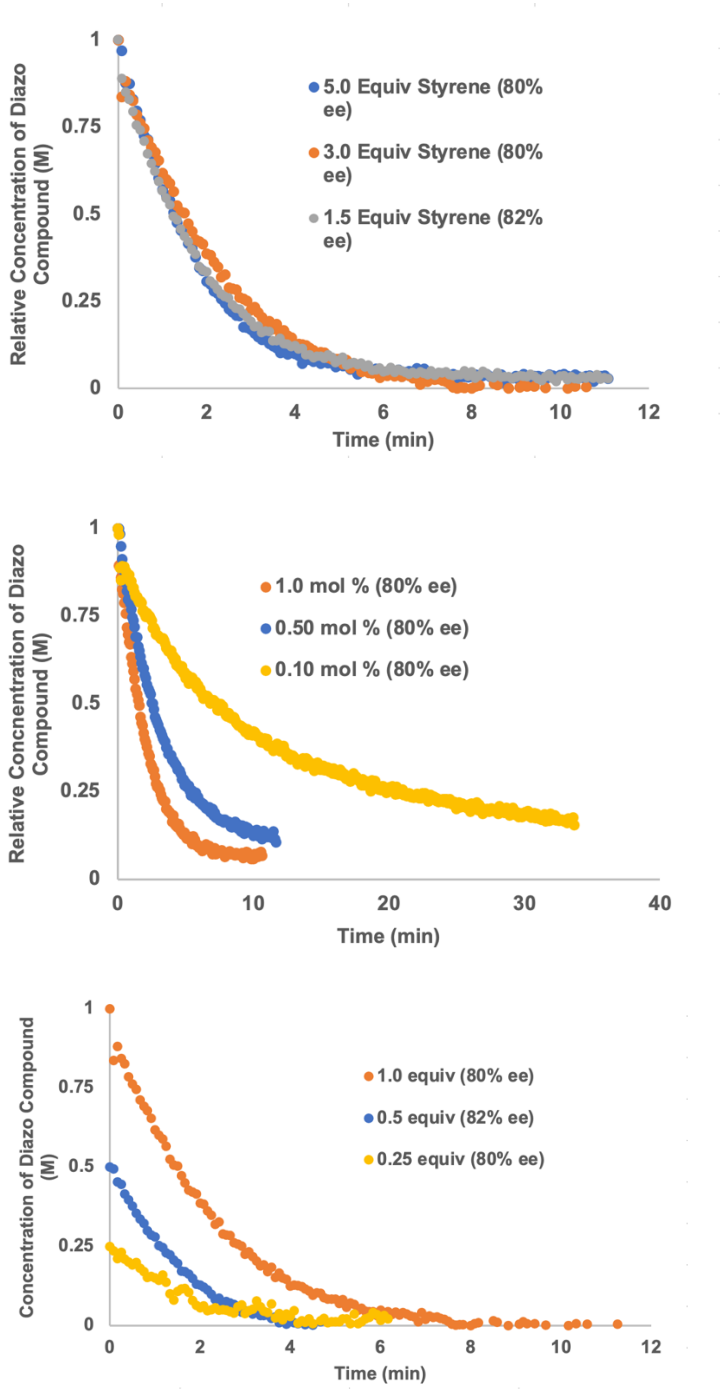

Figure 2.5 Kinetic profiles of reaction progress kinetic analysis studies with A) styrene equivalence dependence, B) Catalyst loading screen, and C) Diazo dependence.

it to be more Lewis acidic. However, conducting a varying equivalents screen with styrene under React IR monitoring showed that styrene has no effect on the rate of the reaction (Figure 2.5A). The reactions were finished in roughly 10 minutes using 1.0 mol% catalyst loading. This is a key difference between the rhodium and ruthenium analogues as the rhodium catalysts can finish the reaction under the same conditions in just 15 s. Next, the catalyst loading was varied to understand the capabilities for low loading with the ruthenium complexes (Figure 2.5B). Going down to 0.1 mol% catalyst loading showed a significantly decreased rate, with the reaction finishing in roughly 40 minutes. Finally, the dependency of aryldiazoaceate was established as first order with respect to diazo concentration (Figure 2.5C).

To understand the rate differences observed between the ruthenium and rhodium reactions we again turned to computation. These studies, again performed by Dr. Musaev, focused on three representative metal complexes: $Ru_2(OAc)_4Cl$, $Ru_2(OAc)_4^+$, and $Rh_2(OAc)_4$. These computational studies were caried out at the [B3LYP-D3(BJ)] + PCM(in DCM) level of theory. The ground state of $Ru_2(OAc)_4Cl$ was found to be the quartet state with a low-spin Ru(II)-Ru(III) core, in line with both previously reported data[28] and the experimentally observed paramagnetism. The potential energy surface (PES) of the reaction with the three model complexes was then calculated (Figure 2.6). It was found that the free energy barrier for formation of the metallo-carbene generation for both $Ru_2(OAc)_4^+$ and $Rh_2(OAc)_4$ was nearly identical, with calculated values of 12.0 kcal/mol and 11.5 kcal/mol, respectively, relative to the catalyst and diazo compound. The calculated values for the chloride complex, however, tell a different story. The activation barrier for carbene formation for this complex was found to be 19.3 kcal/mol, roughly 7

kcal/mol higher than that of the cationic complex. To fully understand the effect of the chloride ion on the energetics of the reaction, the dissociation of the chloride from the $Ru_2(OAc)_4^+$ complex was calculated. This was found to require 19.3 kcal/mol. However, since the experimental reactions have an explicit solvent, it is rational to assume the $Ru_2(OAc)_4^+ \bullet Cl^-$ compound form a solvated complex, lowering the activation barrier of chloride dissociation.

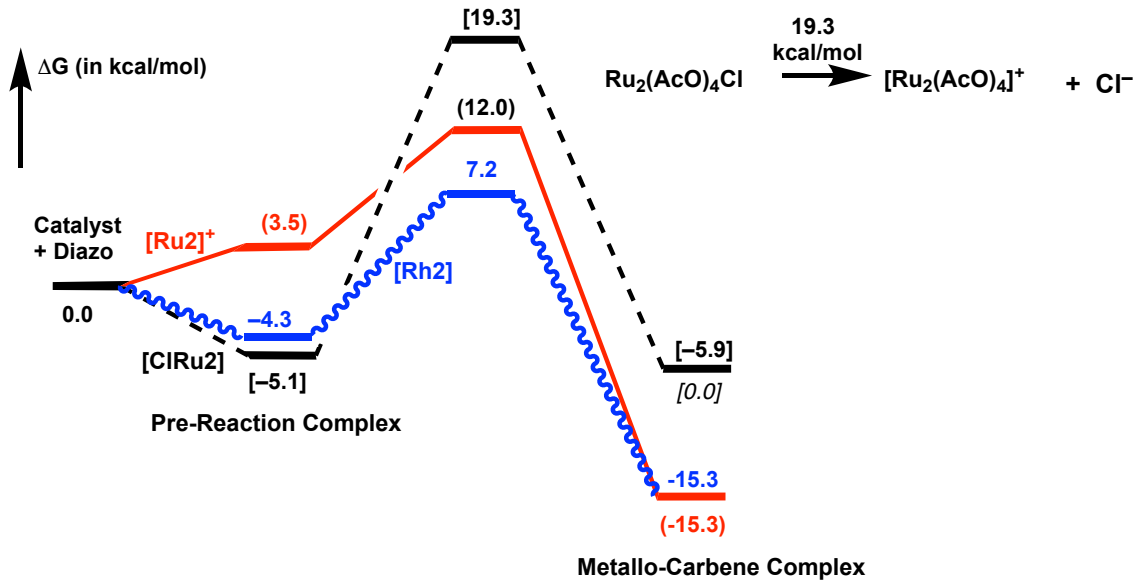

Figure 2.6 Calculated reaction coordinate for Ru2(OAc)4+ (in red), Ru2(OAc)4Cl (in black), and Rh2(OAc)4 (in blue).

Thus, in reality, the activation barrier for dissociation of the chloride can be assumed to be <19.3 kcal/mol. Additionally, this logic can be applied to the BAr^F analogues, as this large non-coordinating anion will have less of an attraction to the cationic complex. This rationalizes why the BAr^F analogues are qualitatively seen to have a much faster rate of reaction than the chloride analogue, but still slower than the rhodium analogues.

2.3 Conclusion

In summary, Co and Ru have been tested as a replacement for rhodium in tetracarboxylate paddlewheel complexes for the cyclopropanation of olefins using donor/acceptor diazo compounds. It was shown that while the Co complexes can be formed and give appreciable yields of the cyclopropane product, the enantioselectivity is lacking, casting doubt on its viability for use as a replacement for rhodium. These experimental results were rationalized by using computation to help understand why the enantioselectivity was low. However, five novel diruthenium paddlewheel complexes were synthesized, characterized, and applied to the cyclopropanation of activated and unactivated olefins using aryldiazoacetates as carbene precursor. One catalyst, Ru_2(*S*-TPPTTL)$_4$BAr^F, was shown to generate cyclopropanes in good yield and moderate to high enantioselectivity for the cyclopropanation, giving up to 94% ee in some cases. Unactivated terminal alkenes proved to be the best substrates, with the selectivity generally being higher than that of activated olefins. These studies show the potential for ruthenium to be a replacement for rhodium in tetracarboxylate-catalyzed carbene cyclopropanation using aryldiazoacetates.

2.4 Distribution of Credit

Dr. Caleb Harris from the Berry Lab synthesized the Co_2(*S*-TPPTTL)$_4$ material. Dr. Djamaladdin Musaev conducted the computational studies.

2.5 References

1. Brooks, W. H.; Guida, W. C.; Daniel, K. G., The Significance of Chirality in Drug Design and Development. *Curr. Top. Med. Chem.* **2011,** *11* (7), 760-770.
2. Senkuttuvan, N.; Komarasamy, B.; Krishnamoorthy, R.; Sarkar, S.; Dhanasekaran, S.; Anaikutti, P., The significance of chirality in contemporary drug discovery-a mini review. *RCS Adv.* **2024,** *14* (45), 33429-33448.
3. Ceramella, J.; Iacopetta, D.; Franchini, A.; De Luca, M.; Saturnino, C.; Andreu, I.; Sinicropi, M. S.; Catalano, A. A Look at the Importance of Chirality in Drug Activity: Some Significative Examples *Applied Sciences* [Online], 2022.
4. Talele, T. T., The "Cyclopropyl Fragment" is a Versatile Player that Frequently Appears in Preclinical/Clinical Drug Molecules. *J. Med. Chem.* **2016,** *59* (19), 8712-8756.
5. Marson, C. M., New and unusual scaffolds in medicinal chemistry. *Chem. Soc. Rev.* **2011,** *40* (11), 5514-5533.
6. Časar, Z., Synthetic Approaches to Contemporary Drugs that Contain the Cyclopropyl Moiety. *Synthesis* **2020,** *52* (09), 1315-1345.
7. Sun, X.; Gu, P.; Qin, J.; Su, Y., Rhodium-catalysed diastereo- and enantio-selective cyclopropanation of α-boryl styrenes. *Chem. Commun.* **2020,** *56* (82), 12379-12382.
8. Tran, U. P. N.; Hommelsheim, R.; Yang, Z.; Empel, C.; Hock, K. J.; Nguyen, T. V.; Koenigs, R. M., Catalytic Synthesis of Trifluoromethyl Cyclopropenes and Oligo-Cyclopropenes. *Chem. Eur. J.* **2020,** *26* (6), 1254-1257.
9. Pons, A.; Delion, L.; Poisson, T.; Charette, A. B.; Jubault, P., Asymmetric Synthesis of Fluoro, Fluoromethyl, Difluoromethyl, and Trifluoromethylcyclopropanes. *Acc. Chem. Res.* **2021,** *54* (14), 2969-2990.
10. Chen, L.; Minh Thi Le, T.; Bouillon, J.-P.; Poisson, T.; Jubault, P., Catalytic Enantioselective Synthesis of Functionalized Cyclopropanes from α-Substituted Allyl Sulfones with Donor-Acceptor or Diacceptor Diazo Reagents. *Chem. Eur. J.* **2022,** *28* (42), e202201254.
11. Davies, H. M. L., Finding Opportunities from Surprises and Failures. Development of Rhodium-Stabilized Donor/Acceptor Carbenes and Their Application to Catalyst-Controlled C–H Functionalization. *J. Org. Chem.* **2019,** *84* (20), 12722-12745.
12. Davies, H. M. L.; Bruzinski, P. R.; Lake, D. H.; Kong, N.; Fall, M. J., Asymmetric Cyclopropanations by Rhodium(II) N-(Arylsulfonyl)prolinate Catalyzed Decomposition of Vinyldiazomethanes in the Presence of Alkenes. Practical Enantioselective Synthesis of the Four Stereoisomers of 2-Phenylcyclopropan-1-amino Acid. *J. Am. Chem. Soc.* **1996,** *118* (29), 6897-6907.
13. Wei, B.; Sharland, J. C.; Lin, P.; Wilkerson-Hill, S. M.; Fullilove, F. A.; McKinnon, S.; Blackmond, D. G.; Davies, H. M. L., In Situ Kinetic Studies of Rh(II)-Catalyzed Asymmetric Cyclopropanation with Low Catalyst Loadings. *ACS Catal.* **2020,** *10* (2), 1161-1170.
14. Bien, J.; Davulcu, A.; DelMonte, A. J.; Fraunhoffer, K. J.; Gao, Z.; Hang, C.; Hsiao, Y.; Hu, W.; Katipally, K.; Littke, A.; Pedro, A.; Qiu, Y.; Sandoval, M.; Schild, R.; Soltani, M.; Tedesco, A.; Vanyo, D.; Vemishetti, P.; Waltermire, R. E., The First Kilogram Synthesis of Beclabuvir, an HCV NS5B Polymerase Inhibitor. *Org. Process Res. Dev.* **2018,** *22* (10), 1393-1408.

15. Lathrop, S. P.; Mlinar, L. B.; Manjrekar, O. N.; Zhou, Y.; Harper, K. C.; Sacia, E. R.; Higgins, M.; Bogdan, A. R.; Wang, Z.; Richter, S. M.; Gong, W.; Voight, E. A.; Henle, J.; Diwan, M.; Kallemeyn, J. M.; Sharland, J. C.; Wei, B.; Davies, H. M. L., Continuous Process to Safely Manufacture an Aryldiazoacetate and Its Direct Use in a Dirhodium-Catalyzed Enantioselective Cyclopropanation. *Org. Process Res. Dev.* **2023,** *27* (1), 90-104.
16. https://www.dailymetalprice.com/rhodium.html (accessed 02-25-2025).
17. Pakula, R. J.; Martinez, A. M.; Noten, E. A.; Harris, C. F.; Berry, J. F., New chromium, molybdenum, and cobalt complexes of the chelating esp ligand. *Polyhedron* **2019,** *161*, 93-103.
18. Zhao, X.; Zhang, Y.; Wang, J., Recent developments in copper-catalyzed reactions of diazo compounds. *Chem. Commun.* **2012,** *48* (82), 10162-10173.
19. Zhu, S.-F.; Xu, B.; Wang, G.-P.; Zhou, Q.-L., Well-Defined Binuclear Chiral Spiro Copper Catalysts for Enantioselective N–H Insertion. *J. Am. Chem. Soc.* **2012,** *134* (1), 436-442.
20. Wang, Q.; Liu, A.; Wang, Y.; Ni, C.; Hu, J., Copper-Mediated Cross-Coupling of Diazo Compounds with Sulfinates. *Org. Lett.* **2021,** *23* (17), 6919-6924.
21. DeAngelis, A.; Boruta, D. T.; Lubin, J.-B.; Plampin, I. I. I. J. N.; Yap, G. P. A.; Fox, J. M., The chiral crown conformation in paddlewheel complexes. *Chem. Commun.* **2010,** *46* (25), 4541-4543.
22. Reger, D. L.; Horger, J. J.; Debreczeni, A.; Smith, M. D., Syntheses and Characterization of Copper(II) Carboxylate Dimers Formed from Enantiopure Ligands Containing a Strong π···π Stacking Synthon: Enantioselective Single-Crystal to Single-Crystal Gas/Solid-Mediated Transformations. *Inorg. Chem.* **2011,** *50* (20), 10225-10240.
23. Ren, Z.; Sunderland, T. L.; Tortoreto, C.; Yang, T.; Berry, J. F.; Musaev, D. G.; Davies, H. M. L., Comparison of Reactivity and Enantioselectivity between Chiral Bimetallic Catalysts: Bismuth–Rhodium- and Dirhodium-Catalyzed Carbene Chemistry. *ACS Catal.* **2018,** *8* (11), 10676-10682.
24. Miyazawa, T.; Suzuki, T.; Kumagai, Y.; Takizawa, K.; Kikuchi, T.; Kato, S.; Onoda, A.; Hayashi, T.; Kamei, Y.; Kamiyama, F.; Anada, M.; Kojima, M.; Yoshino, T.; Matsunaga, S., Chiral paddle-wheel diruthenium complexes for asymmetric catalysis. *Nat. Catal.* **2020,** *3* (10), 851-858.
25. Nuss, P.; Eckelman, M. J., Life Cycle Assessment of Metals: A Scientific Synthesis. *PLOS ONE* **2014,** *9* (7), e101298.
26. Sailer, J. K.; Sharland, J. C.; Bacsa, J.; Harris, C. F.; Berry, J. F.; Musaev, D. G.; Davies, H. M. L., Diruthenium Tetracarboxylate-Catalyzed Enantioselective Cyclopropanation with Aryldiazoacetates. *Organometallics* **2023,** *42* (15), 2122-2133.
27. Wang, X.; Peter Zhang, X., Catalytic Radical Approach for Selective Carbene Transfers via Cobalt(II)-Based Metalloradical Catalysis. In *Transition Metal-Catalyzed Carbene Transformations*, 2022; pp 25-66.
28. Norman, J. G., Jr.; Renzoni, G. E.; Case, D. A., Electronic structure of Ru2(O2CR)4+ and Rh2(O2CR)4+ complexes. *J. Am. Chem. Soc.* **1979,** *101* (18), 5256-5267.

Chapter 3. Comparison of Diruthenium and Dirhodium Tetracarboxylate Catalyzed C–H Functionalization with Aryldiazoaceate compounds

3.1 Introduction

While dirhodium tetracarboxylate complexes are exceptional catalysts for cyclopropanation of olefins using diazo compounds, their true specialty lies within the realm of C–H functionalization chemistry.[1] Selective C–H functionalization has seen an influx of interest from the organic chemistry community over the past 30 years,[2-5] even broaching the challenging field of total synthesis.[6, 7] These methodologies allow one to quickly add complexity to an otherwise inert molecule or moiety. Playing on the subtle differences between C–H bonds allow chemists to view organic synthesis through a new lens. As previously mentioned, the Davies lab has developed a plethora of chiral dirhodium complexes capable of catalyzing the C–H functionalization of a variety of C–H bonds.[8-12] Depending on the features the C–H bond bears, a particular dirhodium catalyst can selectively insert into each bond, enabling reactions with excellent regio- diastereo- and enantioselectivity. However, as laid out in Chapter 2, the use of rhodium in the bimetallic core of the paddlewheel complex is not attractive due to the high price and global warming potential of the metal.[13, 14] While using rhodium at ultra-low catalyst loadings can potentially mitigate this problem,[15] turning towards other metals to replace rhodium in the tetracarboxylate complexes offers a viable solution.

Currently, dirhodium complexes are not the only catalyst that can perform C–H functionalization reactions, albeit many other catalysts cannot render the reaction selective.[16-19] One system that has enjoyed some success for selective C–H functionalization is the rhodium-bismuth tetracarboxylate catalyst mentioned in Chapter

2.[20] While this catalyst matches the reactivity and selectivity of the dirhodium analogue nicely, the rate of the reaction is significantly slower, hampering the capabilities for this system to garner much attention. In 2022, Fürstner reported on the synthesis and application of a rhodium-bismuth catalyst, capable of selectively functionalizing activated methyl groups.[21] Recently, diruthenium paddlewheel complexes have been reported in carbene transfer for cyclopropanation[22, 23] (Scheme 3.1a) and C–H amination reactions (Scheme 3.1b).[24]

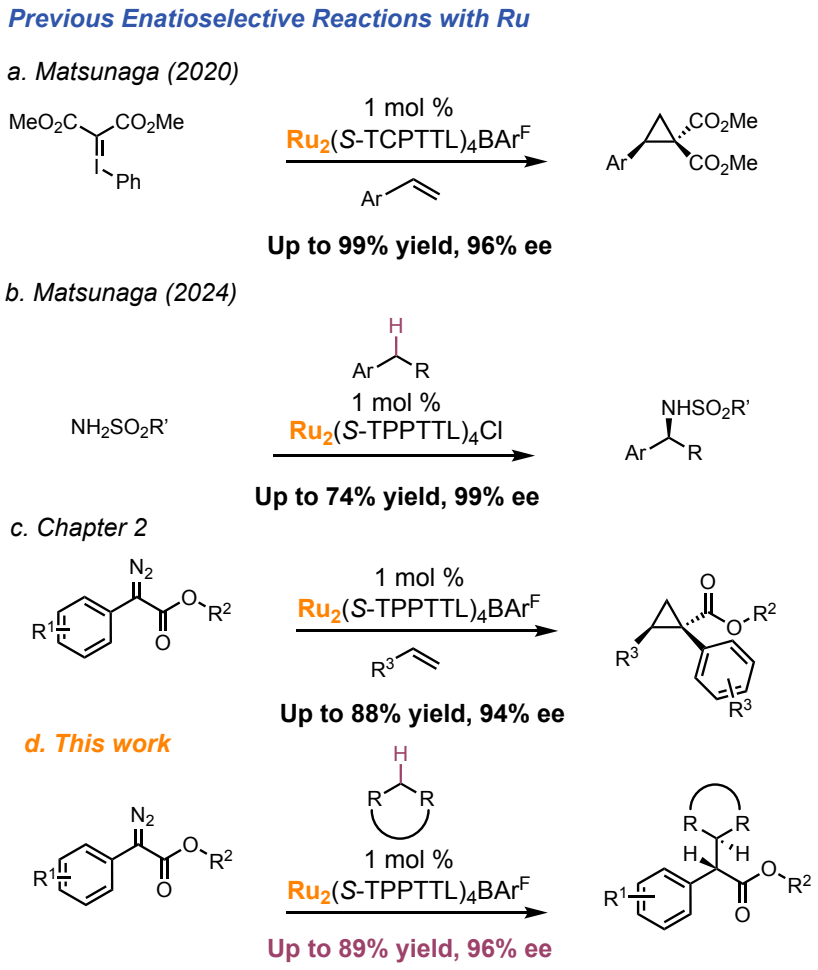

Scheme 3.1 Diruthenium-catalyzed a) selective cyclopropanation using iodonium ylides, b) selective C–H amination, c) work presented in previous chapter d) work presented in this chapter - selective C–H functionalization

However, one notable reaction missing from the diruthenium playbook is the C–H functionalization through a carbene insertion reaction. With the success seen in the cyclopropanation study using aryldiazoacetates in the previous chapter (Scheme 3.1c), we hypothesized that the diruthenium catalysts would be able to catalyze C–H functionalization reactions with high yield and selectivity. Thus, a study was performed on the comparison of diruthenium and dirhodium catalysts in selective C–H functionalization reactions using aryldiazoacetates as carbene precursor (Scheme 3.1d).

3.2 Results and Discussion

While the five diruthenium catalysts synthesized for the cyclopropanation study are a good representation of the dirhodium toolbox developed, it does not include the bulky triarylcyclopropane carboxylate (TPCP) catalysts which enable selective primary C–H bond insertion reactions, thus our efforts began with the synthesis of this ruthenium complex.

When subjected to the standard ligand exchange procedure in refluxing chlorobenzene, no desired product was obtained due to the degradation of the cyclopropyl ligand. After some optimization of the reaction conditions, *tert*-butylacetate was identified to be the optimal solvent, yielding the desired diruthenium complex **3** in 16% yield after several chromatographic purification and recrystallization from a 3:1 mixture of hexanes/chloroform (Scheme 3.2).

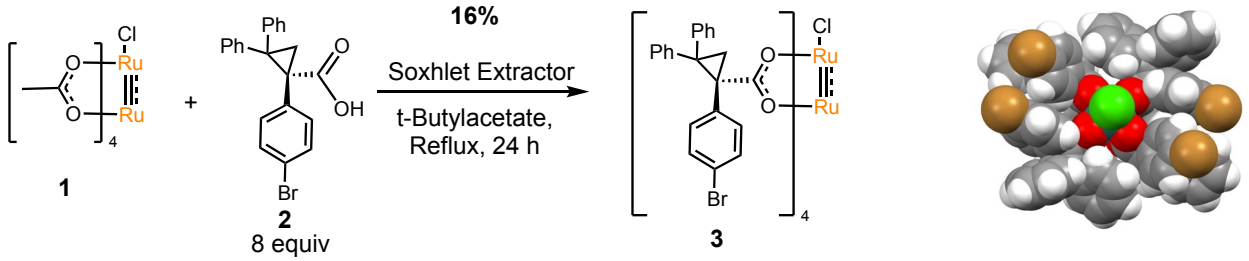

Scheme 3.2 Synthesis of Ru2(S-pBrTPCP)4Cl catalyst

X-ray crystallographic analysis revealed a C_2-symmetric structure, nearly analogues to the dirhodium analogue.[25] With this synthesis in hand, we moved forward with the six diruthenium and dirhodium analogues (Figure 3.1) for testing in C–H functionalization reactions.

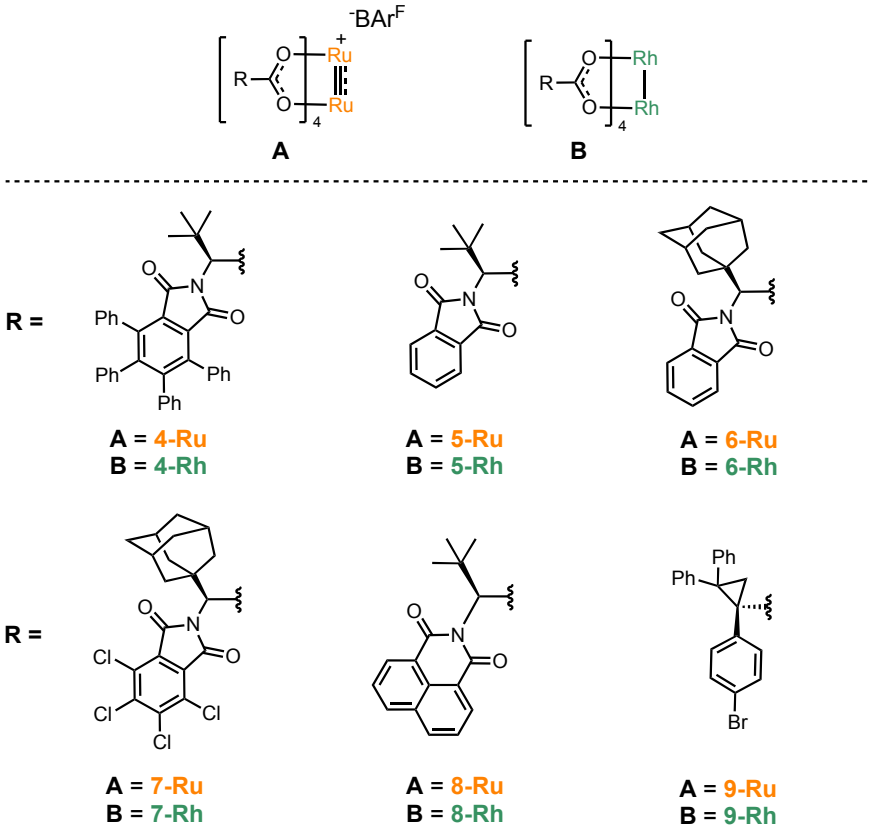

Figure 3.1 Structure of six ruthenium and rhodium paddlewheel complexes

We first wanted to gain an understanding of how the selectivity of these catalyst compare to that of their dirhodium analogues, thus we performed a catalyst screen with both sets of catalysts using *p*-cymene (**11**) and 4-isopropylethylbenzene (**14**), two substrates that offer interesting internal selectivity competitions.

Beginning with *p*-cymene, a substrate that tests the preference between primary and tertiary C–H functionalization, in reaction with 2,2,2-trichlrooethyl-(*p*Brphenyl)diazoaceate (**10**), we saw that the ruthenium catalyst **5-Ru–8-Ru** had a strong preference for primary functionalization, with all of the catalysts giving a >20:1 r.r (Table 3.1a).

Table 3.1 Catalyst screen with p-cymene

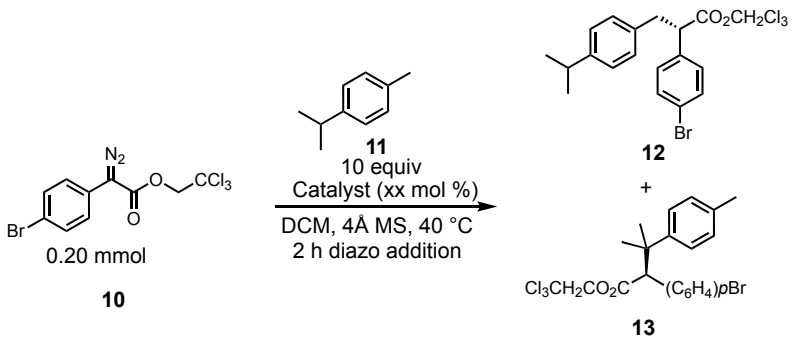

a.

Entry	Catalyst[a]	r.r.: **12:13**	Yield (%)[b]	ee **12** (%)
1	**4-Ru**	6:1	20	-34
2	**5-Ru**	>20:1	77	76
3	**6-Ru**	>20:1	73	86
4	**7-Ru**	>20:1	62	-50
5	**8-Ru**	>20:1	75	-42
6	**9-Ru**	3.6:1	8	60

b.

Entry	Catalyst[c]	r.r.: **12:13**	Yield (%)[b]	ee **12** (%)
1	**4-Rh**	1:5	74	66
2	**5-Rh**	1.9:1	74	-88
3	**6-Rh**	2:1	69	-90
4	**7-Rh**	1:2.5	76	38
5	**8-Rh**	1:1.2	23	-62
6	**9-Rh**	>20:1	79	94

[a]Reactions run with 5.0 mol% catalyst loading. [b]Combined yields. [c]Reactions run using 1.0 mol% catalyst loading Negative value for the ee indicates that the opposite enantiomer to the drawn structure is preferentially formed.

This was in stark contrast with the dirhodium analogues, which did not see a selectivity preference using any of these catalysts (Table 3.1b). Interestingly, Rh_2(TPPTTL)$_4$ had a mild preference for tertiary insertion of roughly 5:1 r.r. (Table 3.1b, entry 1), while the ruthenium analogue switched this selectivity preference to favor the primary insertion with a ratio of 6:1 (Table 3.1a, entry 1). The newly synthesized ruthenium catalyst, **9-Ru**, performed poorly, with both the yield and regioselectivity suffering greatly compared to that of the rhodium analogue, a catalyst designed specifically for primary functionalization (Table 3.1a-b, entries 6). Interestingly, in some cases the diruthenium catalysts preferentially generated the opposite enantiomer to the one formed with the dirhodium catalysts.

The next substrate that was tested was 4-isopropylethylbenzene (**14**) (Table 3.2). Like *p*-cymene, this substrate offers an interesting competition between C–H bonds, whereas in this case it is testing the preference for secondary or tertiary insertion. A catalyst screen was performed using both systems, again using 5.0 mol% and 1.0 mol% for the ruthenium and rhodium catalysts, respectively. The diruthenium systems again gave excellent regioselectivity, this time in preference for the secondary over tertiary bond, with four of the six catalysts giving >20:1 r.r (Table 3.2a). The dirhodium catalysts matched the preferred site of insertion with the diruthenium results, however, in most cases the preference was not as strong (Table 3.2b). Again, the newly synthesized diruthenium catalyst Ru_2(*S*-*p*BrTPCP)$_4$BAr^F (**9-Ru**) performed poorly, giving the lowest r.r. and yield out of all the ruthenium catalysts, and rendering the product as essentially a racemate (Table 3.2a, entry 6). Comparing the diastereoselectivity for the secondary insertion product between both metal system showed that the diruthenium catalysts were

generally outperformed by the rhodium analogues, a trend seen across nearly all substrates tested. However, Ru_2(*S*-TPPTTL)$_4$BAr^F could give product **15a-b** in 94% ee for the both diastereomers (Table 3.2a, entry 1), highlighting the ability for the ruthenium complexes to be efficient asymmetric catalysts. Some of the diruthenium catalysts again gave the opposite enantiomer to that of the dirhodium analogues.

Table 3.2 Catalyst screen with 4-isopropylethyltoluene

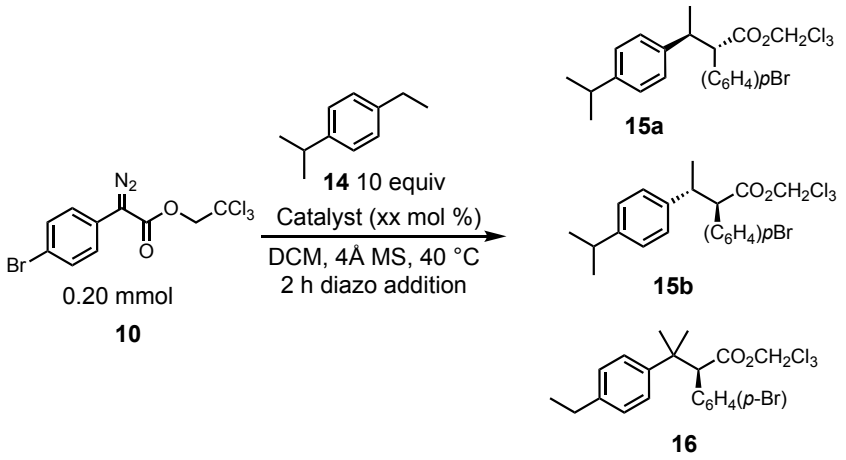

a.

Entry	Catalyst[a]	r.r.: **15:16**	Yield (%)[b]	d.r.	ee **15a** (%)	ee **15b** (%)
1	**4-Ru**	>20:1	54	3.6:1	94	94
2	**5-Ru**	11.8:1	48	3.8:1	30	13
3	**6-Ru**	>20:1	55	3.4:1	-42	-16
4	**7-Ru**	>20:1	52	4.2:1	72	30
5	**8-Ru**	>20:1	46	4.4:1	20	54
6	**9-Ru**	10:1	33	4.8:1	1	0

b.

Entry	Catalyst[c]	r.r.: **15:16**	Yield (%)[b]	d.r.	ee **15a** (%)	ee **15b** (%)
1	**4-Rh**	6.5:1	50	12:1	94	58
2	**5-Rh**	16:1	72	4.7:1	-80	-59
3	**6-Rh**	16:1	48	3.6:1	-76	-54
4	**7-Rh**	9.5:1	59	5:1	78	44
5	**8-Rh**	10:1	59	4.5:1	-36	14
6	**9-Rh**	>20:1	63	2.7:1	36	58

[a]Reactions run with 5.0 mol% catalyst loading. [b]Combined yields. [c]Reactions run using 1.0 mol% catalyst loading. Negative value for the ee indicates that the opposite enantiomer to the drawn structure is preferentially formed.

While the benzylic substrates offered an interesting study into the preference of reaction for the diruthenium catalysts, a particular area which the dirhodium catalysts shine is in the functionalization of unactivated alkanes. Thus, a final catalyst screen was performed, using cyclohexane as the substrate (Table 3.3). In this case, only 1.0 mol% catalyst loading was needed for the diruthenium catalysts too perform a competent reaction. Ruthenium catalysts **4-8-Ru** gave high yields and low to excellent enantioselectivity (Table 3.3a, entries 1-5), with **9-Ru** unable to generate the product at all. The rhodium catalysts matched the ruthenium results closely (Table 3.3b), apart from Rh_2(*S*-*p*BrTPCP)$_4$ (**9-Rh**) giving a competent reaction. Ru_2(*S*-TPPTTL)$_4$BAr^F (**4-Ru**) gave the product in 76% yield and 95% ee (Table 3.3a, entry 1). Because of these excellent results, this catalyst was chosen to explore a scope of alkane substrates in direct comparison with the dirhodium analogue (Table 3.4).

Table 3.3 C–H functionalization of cyclohexane with a) diruthenium catalysts and b) dirhodium catalysts.

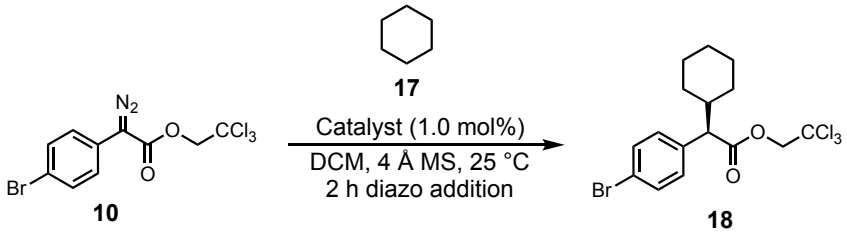

a.

Entry	Catalyst	Yield (%)	ee (%)
1	**4-Ru**	76	95
2	**5-Ru**	73	-59
3	**6-Ru**	70	-65
4	**7-Ru**	70	60
5	**8-Ru**	80	7
6[a]	**9-Ru**	nr	-

b.

Entry	Catalyst	Yield (%)	ee (%)
1	**4-Rh**	75	94
2	**5-Rh**	54	-66
3	**6-Rh**	64	-64
4	**7-Rh**	69	80
5	**8-Rh**	62	8
6	**9-Rh**	59	68

Negative value for the ee indicates that the opposite enantiomer to the drawn structure is preferentially formed.

Beginning with a series of cycloalkane derivatives showed the ruthenium catalyst could furnish functionalized products **19-22** in high yield and asymmetric induction (90-96% ee), matching the rhodium analogue nicely. Reaction with adamantane gave the tertiary insertion product **22** cleanly in an 81% yield and 92%

Table 3.4 Substrate scope in C–H functionalization reaction.

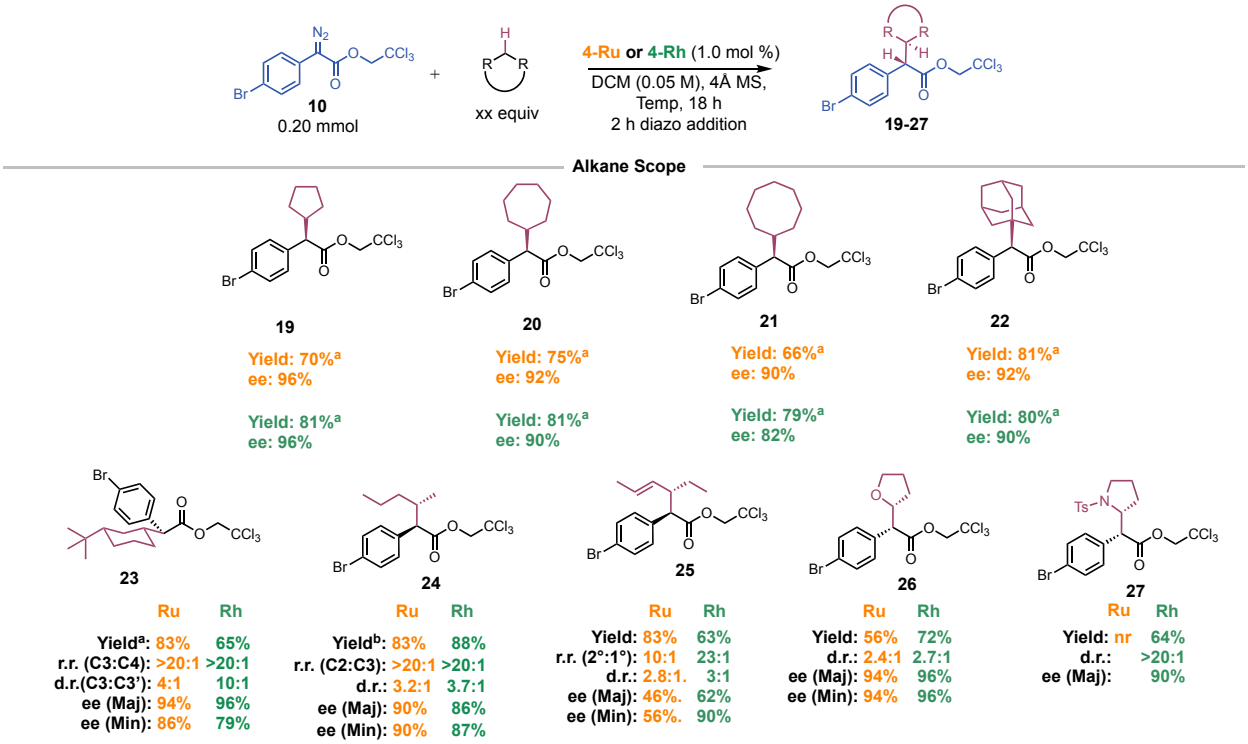

[a]Reactions run at 25 °C. [b]Reactions run neat under refluxing conditions

ee. This result matches previously reported reactions with aryldiazoaceates showing preference for tertiary insertion over secondary. Next, substrates with challenging selectivity preferences were tested with **4-Ru**. One substrate which **4-Rh** was initially reported to functionalize selectively is *tert*-butylcyclohexane. This rhodium catalyst was shown to desymmetrize the cyclohexane ring, selectively functionalizing the C3 C–H bond

in high yield, enantioselectivity, and diastereoselectivity.[26] We wondered whether the diruthenium analogue would match the dirhodium result, thus we subjected the catalyst to the reaction conditions. Pleasingly, **4-Ru** gave an excellent reaction, with **23** being formed in 84% yield, with a >20:1 r.r., and high asymmetric induction. The diastereoselectivity of the reaction between the two catalysts differed, with the diruthenium and dirhodium catalysts giving 4:1 and 10:1 d.r., respectively. The next substrate tested was pentane, a challenging substrate for C–H functionalization reactions. Typically, the C2 C–H bond can be functionalized selectively when using a sterically bulky dirhodium catalyst,[10] thus we were curious to see for which bond the ruthenium and rhodium catalysts would have a preference. Gratifyingly, both catalysts performed very well, giving **24** in nearly identical results, with high site selectivity of >20:1 for the C2 carbon and high levels of asymmetric induction (86-90% ee). Next, *trans*-2-hexene was tested under the reaction conditions. Bulky dirhodium catalysts have previously been shown to selectively functionalized the primary C–H bond in this primary or secondary competition.[27] While, the TPPTTL ligand is generally thought to be a more open catalyst,[28] our initial competition studies with **4-Ru** have shown a preference for more sterically accessible sites, thus we were curious to see what the results of the reaction would be. Indeed, when *trans*-2-hexene was subjected to the two catalysts, a major preference for the secondary insertion product was seen. However, while the dirhodium analogue gave **25** in 23:1 r.r., the diruthenium catalyst gave it in only 10:1, showing a greater preference for less sterically accessible sites. Finally, wanting to explore the scope of tolerated substrates, we tested two heterocyclic compounds with both catalysts. Generally, the dirhodium catalysts have a broad tolerance towards heteroatoms, however there was

question whether this feature would apply to the diruthenium analogues due to the higher Lewis acidity from the cationic complex. Testing tetrahydrofuran as the substrate under the standard reaction conditions with the dirhodium catalyst gave **26** in a 72% yield, with high asymmetric induction (96% ee for both diastereomers), but low d.r. (2.7:1). Using the diruthenium catalysts under these reaction conditions, however, gave a sluggish reaction, unable to complete the decomposition of diazo. This problem was mitigated by heating the reaction to 60 °C in trifluorotoluene (TFT), giving **26** in 56% yield, with high asymmetric induction (94% ee), and low d.r. (2.4:1). These results show the need for harsher conditions for the diruthenium catalyst to functionalize heterocyclic compounds, presumably due to the competitive coordinating of Lewis basic sites at the axial position of the paddlewheel complex. This effect is even more pronounced in the reaction with *N*-tosyl-pyrrolidine, where no product was observed for the diruthenium catalyzed reaction and undecomposed diazo compound was recovered, even under the 60 °C conditions. The dirhodium catalyst furnished **27** in 64% yield, with >20:1 d.r., and 90% ee. These reactions highlight the similarities and differences of the two catalytic systems, with the diruthenium complex capable of reaching the high levels of regioselectivity and asymmetric induction seen for the dirhodium complexes, but often unable to match the diastereoselectivity and even the reactivity achievable with **4**-**Rh**.

With the substrate scope explored, a scope of aryldiazoacetate compounds were tested in the reaction with cyclohexane (Table 3.5). A range of C–H functionalized products (**28**-**35**) were furnished in good yield (65-88%) and high enantioselectivity (86-99% ee), except for the reaction with *p*-methoxy aryldiazoaceate, which gave product **34** in 50% yield and only 28% ee. The generation of products **32**-**35**, containing electron-

donating aryl substituents on the diazo compound, needed to be run in refluxing cyclohexane for appreciable yields to be observed. Thus, the lower enantioselectivity seen for **34** could be rationalized through the possibility of a thermal background reaction, rendering the racemic product.

Table 3.5 Scope of Aryldiazoacetate in the C–H functionalization reaction

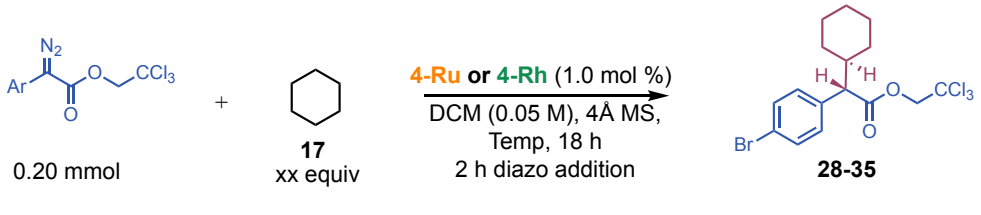

Diazo Scope

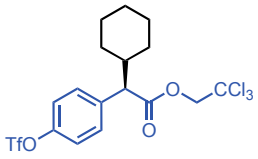

28

Ru Yield: 82%[a] ee: 86%

Rh Yield: 86%[a] ee: 82%

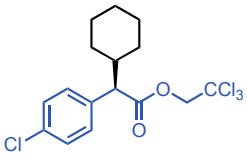

29

Ru Yield: 79%[a] ee: 96%

Rh Yield: 60%[a] ee: 97%

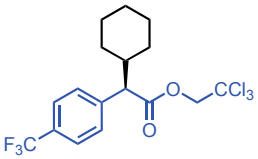

30

Ru Yield: 70%[a] ee: 90%

Rh Yield: 59%[a] ee: 90%

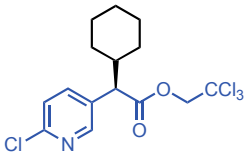

31

Ru Yield: 65%[a] ee: 96%

Rh Yield: 61%[a] ee: 98%

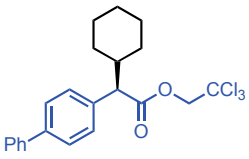

32

Ru Yield: 74%[b] ee: 92%

Rh Yield: 75%[b] ee: 92%

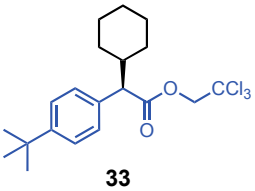

33

Ru Yield: 88%[b] ee: 90%

Rh Yield: 80%[b] ee: 94%

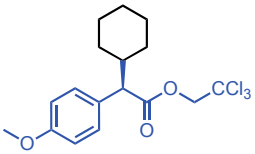

34

Ru Yield: 50%[b] ee: 28%

Rh Yield: 69%[b] ee: 92%

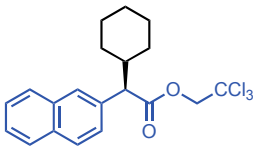

35

Ru Yield: 75%[a] ee: 99%

Rh Yield: 83%[a] ee: 97%

[a]Reactions run at 15 °C. [b]Reactions run in refluxing cyclohexane.

A serendipitous discovery was made when the reaction scope was being explored with alkenylcyclohexane derivatives. For the dirhodium catalyst, the reaction with

allylcyclohexane has previously been reported to give exclusive cyclopropanation,[29] owing to the fact that cyclopropanation is known to be orders of magnitude faster than C–H insertion for dirhodium complexes.[30] However, when running this reaction with the diruthenium analogue, we found it gave a higher propensity for C–H insertion than that of its rhodium counterpart, giving a 71:29 ratio of products **37:38** (Scheme 3.3).

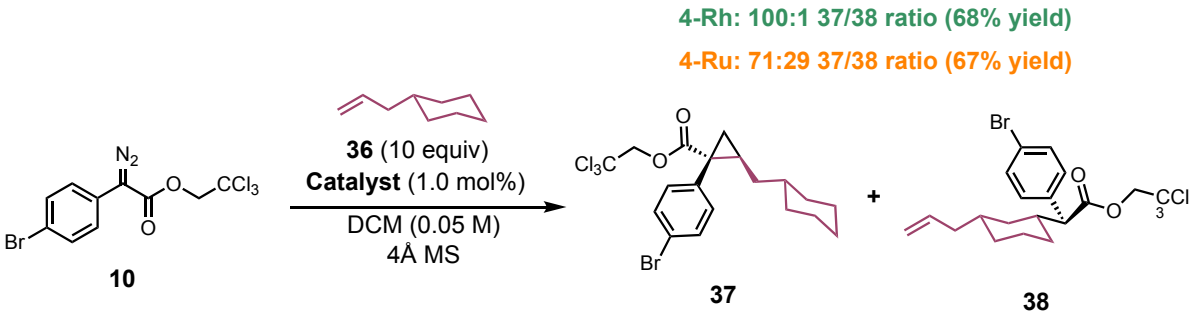

Scheme 3.3 Reaction with allylcyclohexane giving unusual selectivity preference for C–H insertion

Wanting to explore this result further, a series of competition reactions were conducted using cyclohexane (10 equiv) and 1-hexene (2 equiv) as the two carbene traps (Table 3.6). Interestingly, while the dirhodium catalyst gave an unselective mixture of products, often slightly favoring the cyclopropane product, the diruthenium analogues were selective for the C–H functionalized product in a range from 9-19:1. These results show that ruthenium has a greater propensity for C–H functionalization over cyclopropanation.

Table 3.6 Competition reactions for C–H insertion vs cyclopropanation reactions

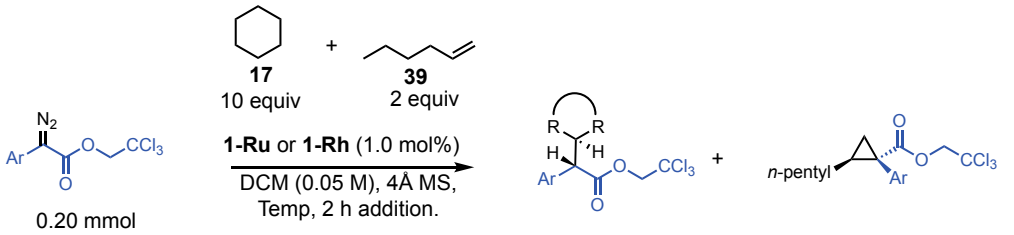

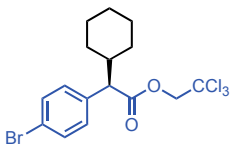

18

	Ru	Rh
CH:CP:	14.5:1	1:1.2
Yield:	72%	60%
ee:	86%	92%

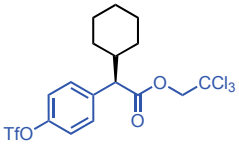

28

	Ru	Rh
CH:CP:	16:1	1:2.4
Yield:	74%	55%
ee:	88%	92%

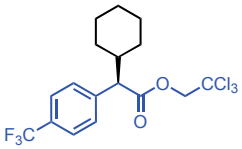

30

	Ru	Rh
CH:CP:	9.4:1	1:1.3
Yield:	76%	60%
ee:	78%	90%

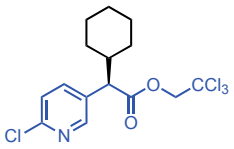

31

	Ru	Rh
CH:CP:	19:1	1:1.5
Yield:	70%	58%
ee:	92%	99%

3.3 Conclusion

In summary, a diruthenium tetracarboxylate catalyzed C–H functionalization reaction using aryldiazoaceate as carbene precursors has been discovered. Six diruthenium catalysts were shown to be capable of functionalization of benzylic C–H bonds, with the ruthenium catalysts being more selective for the most accessible C–H bond while the dirhodium analogues gave little selectivity for either site. Additionally, five of the ruthenium catalysts were found to readily functionalize cyclohexane, showcasing the ability for insertion into unactivated C–H bonds. Ru_2(*S*-TPPTTL)$_4$BAr^F was found to be the premier catalyst and a substrate scope was explored in direct comparison to its dirhodium analogue. The ruthenium catalyst was shown to match the dirhodium analogues nicely for yield, regioselectivity, and enantioselectivity, but are generally lacking regarding diastereoselectivity. Additionally, Lewis basic functional groups are less tolerated by the ruthenium system. Finally, unique reactivity was found for the ruthenium

complexes, being more prone to C–H insertion over cyclopropanation. This novel reactivity, as well as high selectivity seen for the C–H functionalization reactions demonstrate the possible utility for the diruthenium catalysts in some C–H insertion reactions.

3.4 References

1. Davies, H. M. L.; Morton, D., Guiding principles for site selective and stereoselective intermolecular C–H functionalization by donor/acceptor rhodium carbenes. *Chem. Soc. Rev.* **2011,** *40* (4), 1857-1869.
2. Davies, H. M. L.; Du Bois, J.; Yu, J.-Q., C–H Functionalization in organic synthesis. *Chem. Soc. Rev.* **2011,** *40* (4), 1855-1856.
3. Neufeldt, S. R.; Sanford, M. S., Controlling Site Selectivity in Palladium-Catalyzed C–H Bond Functionalization. *Acc. Chem. Res.* **2012,** *45* (6), 936-946.
4. Davies, H. M. L.; Liao, K., Dirhodium tetracarboxylates as catalysts for selective intermolecular C–H functionalization. *Nat. Rev. Chem* **2019,** *3* (6), 347-360.
5. Zhang, J.; Lu, X.; Shen, C.; Xu, L.; Ding, L.; Zhong, G., Recent advances in chelation-assisted site- and stereoselective alkenyl C–H functionalization. *Chem. Soc. Rev.* **2021,** *50* (5), 3263-3314.
6. Gutekunst, W. R.; Baran, P. S., C–H functionalization logic in total synthesis. *Chem. Soc. Rev.* **2011,** *40* (4), 1976-1991.
7. Wencel-Delord, J.; Glorius, F., C–H bond activation enables the rapid construction and late-stage diversification of functional molecules. *Nat. Chem.* **2013,** *5* (5), 369-375.
8. Davies, H. M. L.; Hansen, T., Asymmetric Intermolecular Carbenoid C−H Insertions Catalyzed by Rhodium(II) (S)-N-(p-Dodecylphenyl)sulfonylprolinate. *J. Am. Chem. Soc.* **1997,** *119* (38), 9075-9076.
9. Qin, C.; Davies, H. M., Role of sterically demanding chiral dirhodium catalysts in site-selective C-H functionalization of activated primary C-H bonds. *J. Am. Chem. Soc.* **2014,** *136* (27), 9792-6.
10. Liao, K.; Negretti, S.; Musaev, D. G.; Bacsa, J.; Davies, H. M. L., Site-selective and stereoselective functionalization of unactivated C–H bonds. *Nature* **2016,** *533* (7602), 230-234.
11. Liao, K.; Pickel, T. C.; Boyarskikh, V.; Bacsa, J.; Musaev, D. G.; Davies, H. M. L., Site-selective and stereoselective functionalization of non-activated tertiary C–H bonds. *Nature* **2017,** *551* (7682), 609-613.
12. Liao, K.; Yang, Y.-F.; Li, Y.; Sanders, J. N.; Houk, K. N.; Musaev, D. G.; Davies, H. M. L., Design of catalysts for site-selective and enantioselective functionalization of non-activated primary C–H bonds. *Nat. Chem.* **2018,** *10* (10), 1048-1055.
13. Nuss, P.; Eckelman, M. J., Life Cycle Assessment of Metals: A Scientific Synthesis. *PLOS ONE* **2014,** *9* (7), e101298.
14. https://www.dailymetalprice.com/rhodium.html (accessed 02-25-2025).
15. Wei, B.; Sharland, J. C.; Blackmond, D. G.; Musaev, D. G.; Davies, H. M. L., In Situ Kinetic Studies of Rh(II)-Catalyzed C–H Functionalization to Achieve High Catalyst Turnover Numbers. *ACS Catal.* **2022,** *12* (21), 13400-13410.
16. Martínez-Laguna, J.; Altarejos, J.; Fuentes, M. Á.; Sciortino, G.; Maseras, F.; Carreras, J.; Caballero, A.; Pérez, P. J., Alkanes C1–C6 C–H Bond Activation via a Barrierless Potential Energy Path: Trifluoromethyl Carbenes Enhance Primary C–H Bond Functionalization. *J. Am. Chem. Soc.* **2024,** *146* (49), 34014-34022.

17. Álvarez, M.; Molina, F.; Pérez, P. J., Carbene-Controlled Regioselective Functionalization of Linear Alkanes under Silver Catalysis. *J. Am. Chem. Soc.* **2022,** *144* (51), 23275-23279.
18. Amemiya, E.; Zheng, S.-L.; Betley, T. A., C–H Insertion from Isolable Copper Benzylidenes. *J. Am. Chem. Soc.* **2024,** *146* (44), 30653-30661.
19. Li, D.-Y.; Fang, W.; Wei, Y.; Shi, M., C(sp3)−H Functionalizations Promoted by the Gold Carbene Generated from Vinylidenecyclopropanes. *Chem. Eur. J.* **2016,** *22* (50), 18080-18084.
20. Ren, Z.; Sunderland, T. L.; Tortoreto, C.; Yang, T.; Berry, J. F.; Musaev, D. G.; Davies, H. M. L., Comparison of Reactivity and Enantioselectivity between Chiral Bimetallic Catalysts: Bismuth–Rhodium- and Dirhodium-Catalyzed Carbene Chemistry. *ACS Catal.* **2018,** *8* (11), 10676-10682.
21. Buchsteiner, M.; Singha, S.; Decaens, J.; Fürstner, A., Chiral Bismuth-Rhodium Paddlewheel Complexes Empowered by London Dispersion: The C−H Functionalization Nexus. *Angew. Chem. Int. Ed.* **2022,** *61* (45), e202212546.
22. Miyazawa, T.; Suzuki, T.; Kumagai, Y.; Takizawa, K.; Kikuchi, T.; Kato, S.; Onoda, A.; Hayashi, T.; Kamei, Y.; Kamiyama, F.; Anada, M.; Kojima, M.; Yoshino, T.; Matsunaga, S., Chiral paddle-wheel diruthenium complexes for asymmetric catalysis. *Nat. Catal.* **2020,** *3* (10), 851-858.
23. Sailer, J. K.; Sharland, J. C.; Bacsa, J.; Harris, C. F.; Berry, J. F.; Musaev, D. G.; Davies, H. M. L., Diruthenium Tetracarboxylate-Catalyzed Enantioselective Cyclopropanation with Aryldiazoacetates. *Organometallics* **2023,** *42* (15), 2122-2133.
24. Makino, K.; Mori, K.; Kiryu, S.; Miyazawa, T.; Kumagai, Y.; Higashida, K.; Kojima, M.; Yoshino, T.; Matsunaga, S., Enantioselective Intermolecular Benzylic C–H Amination under Chiral Paddle-Wheel Diruthenium Catalysis. *ACS Catal.* **2025,** *15* (1), 523-528.
25. Qin, C.; Boyarskikh, V.; Hansen, J. H.; Hardcastle, K. I.; Musaev, D. G.; Davies, H. M. L., D2-Symmetric Dirhodium Catalyst Derived from a 1,2,2-Triarylcyclopropanecarboxylate Ligand: Design, Synthesis and Application. *J. Am. Chem. Soc.* **2011,** *133* (47), 19198-19204.
26. Fu, J.; Ren, Z.; Bacsa, J.; Musaev, D. G.; Davies, H. M. L., Desymmetrization of cyclohexanes by site- and stereoselective C–H functionalization. *Nature* **2018,** *564* (7736), 395-399.
27. Falcone, N. A.; Bosse, A. T.; Park, H.; Yu, J.-Q.; Davies, H. M. L.; Sorensen, E. J., A C–H Functionalization Strategy Enables an Enantioselective Formal Synthesis of (−)-Aflatoxin B2. *Org. Lett.* **2021,** *23* (24), 9393-9397.
28. Garlets, Z. J.; Boni, Y. T.; Sharland, J. C.; Kirby, R. P.; Fu, J.; Bacsa, J.; Davies, H. M. L., Design, Synthesis, and Evaluation of Extended C4–Symmetric Dirhodium Tetracarboxylate Catalysts. *ACS Catal.* **2022,** *12* (17), 10841-10848.
29. Sharland, J. C.; Dunstan, D.; Majumdar, D.; Gao, J.; Tan, K.; Malik, H. A.; Davies, H. M. L., Hexafluoroisopropanol for the Selective Deactivation of Poisonous Nucleophiles Enabling Catalytic Asymmetric Cyclopropanation of Complex Molecules. *ACS Catal.* **2022,** *12* (20), 12530-12542.
30. Davies, H. M. L.; Hansen, T.; Churchill, M. R., Catalytic Asymmetric C−H Activation of Alkanes and Tetrahydrofuran. *J. Am. Chem. Soc.* **2000,** *122* (13), 3063-3070.

Chapter 4. Dirhodium Catalyzed Spiro[2.n]cyclopropanation of Exocyclic Olefins

4.1 Introduction

Cyclopropanes are a common structural motif in many natural products, as well as many pharmaceutically relevant scaffolds due to their ability to place substituents in a defined chemical space.[1-6] These three membered rings have a high degree of rigidity, allowing for careful design of scaffolds for specific functional group placement, often leading to higher potency and better pharmacokinetics for the drug scaffold (Figure 4.1).

Natural Products

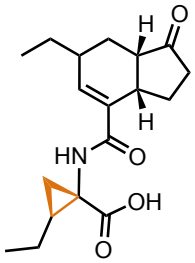

Coronatine

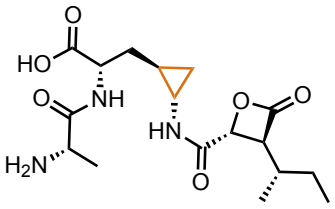

Belactosin A

Pharmacuetical Drug Molecules

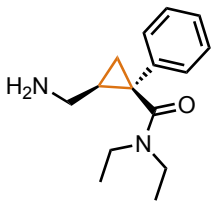

Levimilnacipran

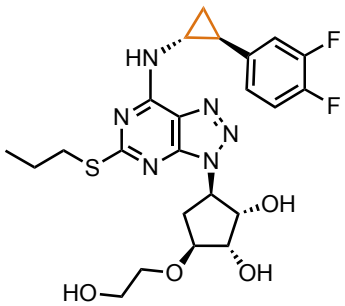

Ticagrelor

Figure 4.1 Natural products and pharmaceutically relevant scaffolds containing cyclopropanes

Most pharmaceutically relevant cyclopropane scaffolds are either mono substituted or 1,2-disusbstitued motifs. However, due to the increased demand for 'escaping flatland', more interest has been drawn towards spiro[2.n]cyclopropanes (SCPs).[7-10] Several drug candidates containing SCP scaffolds have been reported.

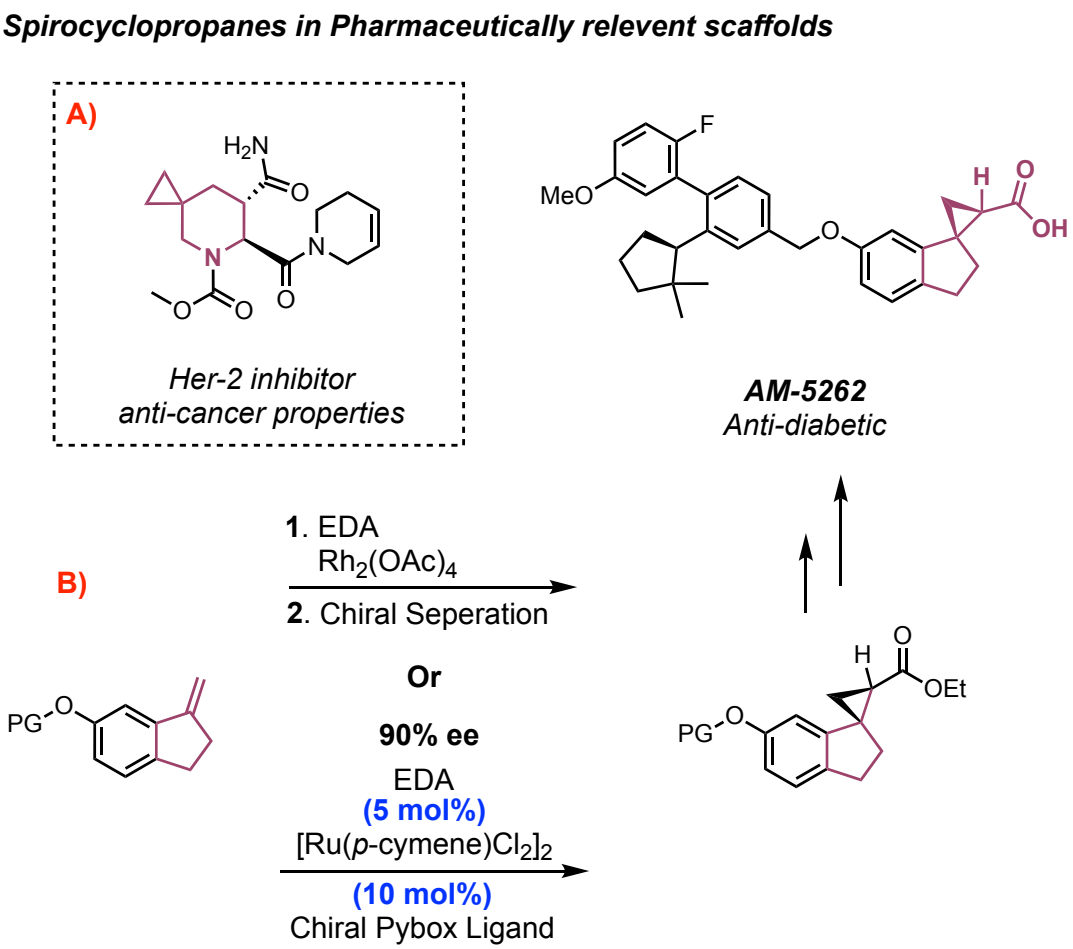

Scheme 4.1 Spiro[2.1.]cyclopropanes in pharmaceutically relevant compounds. A) Her-2 inhibitor shown to have anti-tumor properties. B) SAR campaign at Amgen resulted in SPC giving higher potency than lead compound.

In 2007, Incyte disclosed a potent and orally available Human Epidermal Growth Factor Receptor-2 Sheddase (Her-2) inhibitor for cancer treatment containing a

spiro[2.1]cyclopropane (Scheme 4.1A).[11] The SCP was constructed by reaction of diazomethane and $Pd(OAc)_2$ with an exocyclic olefin, affording the spirocyclic motif. In 2013, Amgen embarked on a structure-activity relationship campaign for a drug candidate for Type II diabetes (Scheme 4.1B).[12] They found that rigidifying the 'head' of the molecule by installing a spiro[2.4]cyclopropane improved the pharmacokinetics and overall selectivity of the drug candidate. The initial route to access the desired cyclopropane motif relied on the use of the achiral dirhodium catalyst $Rh_2(OAc)_4$ with ethyl diazoacetate, furnishing a mixture of four diastereomers needing chiral resolution to isolate each one individually. Once the desired confirmer was identified, the asymmetric synthesis was completed by using a chiral ruthenium catalyst. However, high catalyst loading for this step highlights the need for novel asymmetric methodology to furnish chiral SPCs.

Chiral cyclopropanes have garnered much attention from the synthetic community, leading to many unique methodologies to generate them such as through reactive ylides[13], radical[14-17], biocatalytic,[18, 19] and asymmetric transition-metal catalysis[20, 21] approaches. Additionally, methods towards the synthesis of spiro[2.n]cyclopropanes have emerged using transition metal catalysis (Scheme 4.2A),[22, 23] Simons-Smith conditions,[24] reactive ylides (Scheme 4.2B),[25] and organocatalysis (Scheme 4.2C).[26] While high selectivity can be achieved in some cases,[23, 25, 26] a general methodology to furnish asymmetric sprio[2.n]cyclopropanes is lacking.

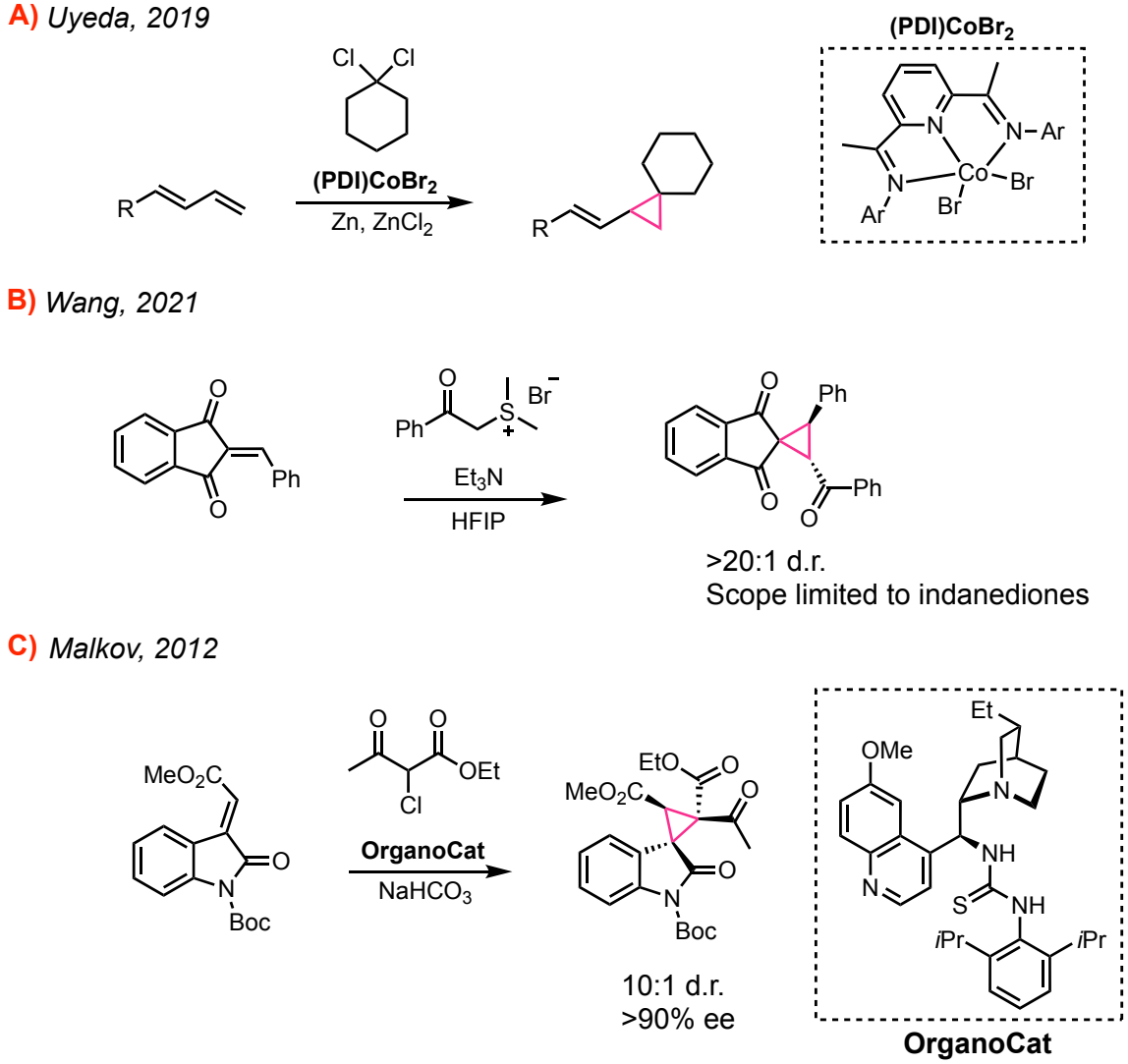

Scheme 4.2 Synthesis of spirocyclopropanes by A) transition-metal catalysis, B) reactive ylides, and C) organocatalysis.

One prominent way to deliver asymmetric cyclopropanes is through using chiral dirhodium tetracarboxylate catalysts using donor/acceptor diazo compounds as carbene precursor. A key advantage to using these dirhodium catalysts is not only the high enantioselectivity, but also the high diastereoselectivity which these complexes impart. Using the dirhodium catalyst toolbox developed in the Davies lab, several of these methods have been adopted for the synthesis of pharmaceutically relevant scaffolds, as

discussed in Chapter 1.[27-29] These catalysts are a prime candidate to furnish SPCs due to the success seen by the dirhodium catalyst for cyclopropanation. However, while methods to cyclopropanate 1,1-diphenylethylene were reported in 2000 using dirhodium catalysts, application of these catalysts to other 1,1-disubstitued olefins has been underexplored (Figure 4.2A).[30]

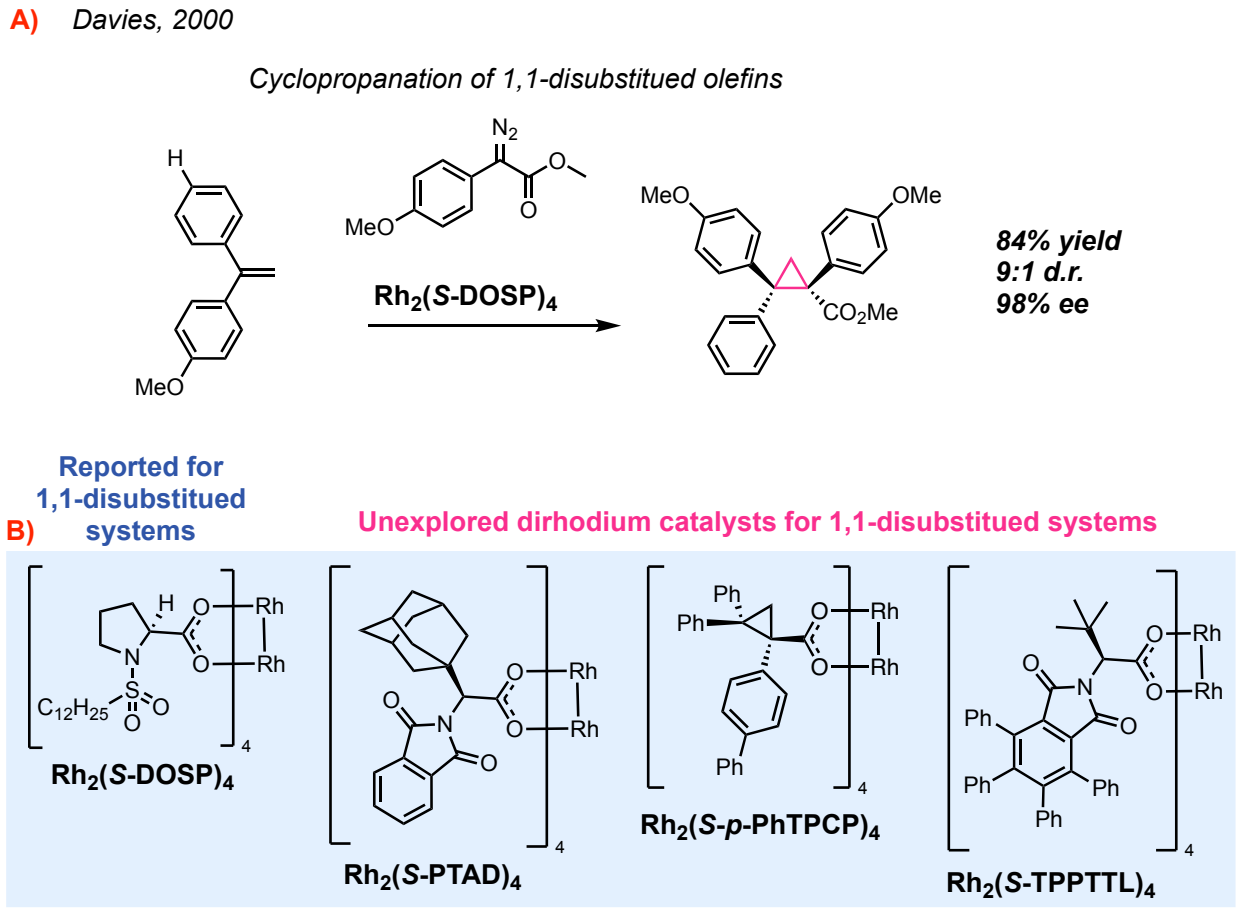

Figure 4.2 Previously reported dirhodium catalyzed cyclopropanation with 1,1-disubstitued olefins.

This chapter focuses on the cyclopropanation of 1,1-disubstitued olefins for the synthesis of novel spiro[2.n]cyclopropane scaffolds using the Davies lab dirhodium toolbox with aryldiazoacetates (Figure 4.2B). Four distinct classes of compounds have

been used as substrates in the cyclopropanation reactions: symmetrical azacyclomethylidenes, azacyclomethylidenes and cycloalkylidenes which generate diastereomers, and racemic cycloalkylidnenes for kinetic resolution. Several of these substrates would be considered challenging due to the differentiating functionality being distal from the site of reaction at the olefin. Thus, these substrates would challenge how the wall of the catalysts can influence the result of the reaction via secondary substrate/wall interactions. Using the dirhodium catalyst toolbox, these reactions were able to be rendered asymmetric, revealing novel SCP scaffolds which will have impact on drug discovery in an underexplored chemical space.

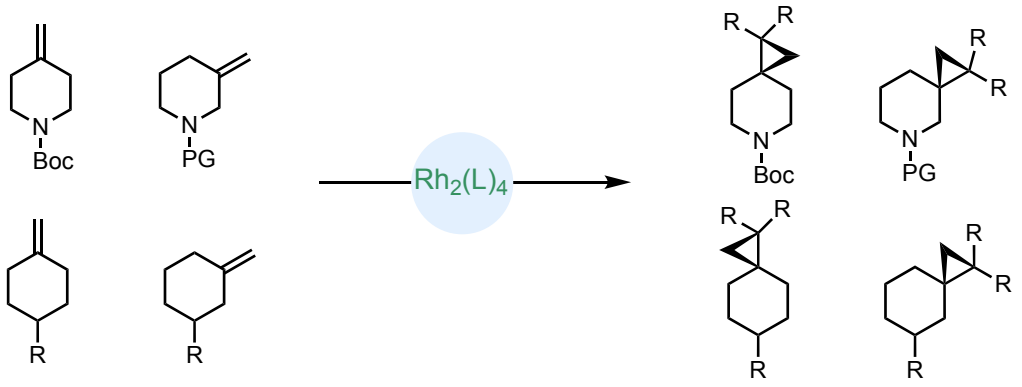

Figure 4.3 The focus of this study using four distinct classes of substrates to synthesize novel spiro[2.1.]cyclopropane products

4.2 Results and Discussion

This study began with the cyclopropanation of symmetrical aza-cyclomethylidenes to generate novel spirocyclic compounds in high asymmetric induction (Table 4.1). Using Rh_2(*S*-*p*-PhTPCP)4, the previously optimized catalyst for cyclopropanation,[27] the reactions proceeded smoothly, with high levels of enantioselectivity seen for all

substrates. Reaction with 3-methylenazetidine gave product **2** in 80% yield with 94% ee, while increasing the ring size to 4-methylenepipereidine gave **3** in slightly higher ee of 96%. Two interesting products were furnished when the cyclopropanation of spirocyclic compounds azaspiro[3.3]heptane and azaspiro[3.5]nonane was carried out, furnishing products **4** and **5** in good yield and high asymmetric induction.

Table 4.1 Scope of symmetrical azacyclomethylidenes

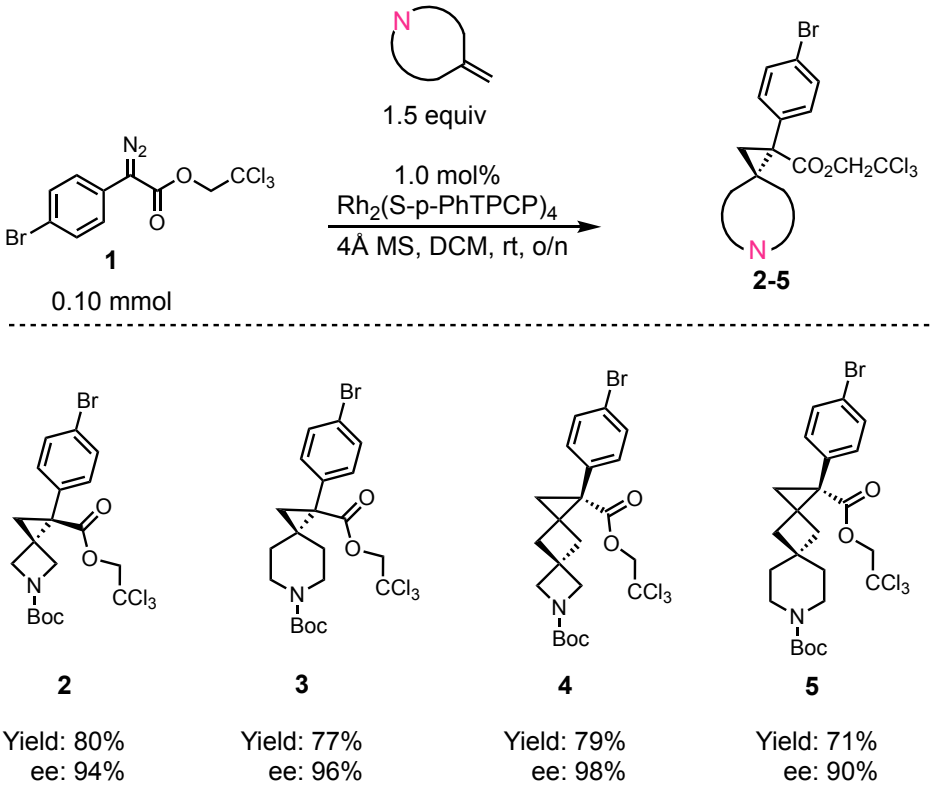

With these initial studies conducted, this methodology was applied to systems that would challenge the selectivity of the catalyst. Thus, a catalyst screen was conducted using *N*-Boc-3-methylenepiperidine (**6**), a substrate capable of producing four distinct diastereomers in the reaction with an aryldiazoacetate (Table 4.2). Beginning with the

optimal catalyst for the symmetrical azasirocyclopropanation, the diastereomeric ratio was quite good from the outset, generating product **8** in 11:1 d.r., with high levels of enantioinduction (Table 4.2, Entry 1). Screening other dirhodium catalysts showed that this catalyst indeed gave the best result, with three other catalysts giving low levels of diastereoselectivity. Not satisfied with only 11:1 d.r., the Boc group was replaced with a tosyl group, hypothesizing that the bulkier protecting group would have a larger steric clash with the wall of the catalyst, inducing a higher level of selectivity. Using Rh_2(*S*-TPPTTL)$_4$ gave **9** in slightly higher d.r. than with *N*-Boc protection, albeit still quite low. Gratifyingly, using Rh_2(*S*-*p*PhTPCP)$_4$ in the cyclopropanation reaction of **7** gave **9** in 80% yield, >20:1 d.r., and 99% ee.

Table 4.2 Catalyst screen for unsymmetrical azacyclomethylidene substrates

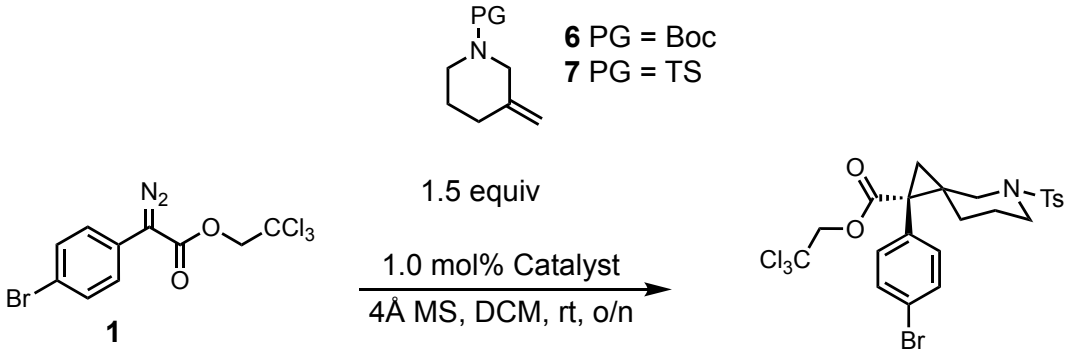

Entry	PG	Catalyst	Yield (%)	d.r.	ee (%)
1	Boc	Rh_2(S-pPhTPCP)$_4$	86	11:1	99
2	Boc	Rh_2(S-TPPTTL)$_4$	61	2.4:1	79
3	Boc	Rh_2(*S*-DOSP)$_4$	59	1:1	10
4	Boc	Rh_2(*S*-PTAD)$_4$	81	1.4:1	86
5	Tosyl	Rh_2(*S*-TPPTTL)$_4$	72	4:1	70
6	Tosyl	Rh_2(S-pPhTPCP)$_4$	80	>20:1	99

With these optimized conditions in hand, a range of aryldiazoaceate compounds were tested in the cyclopropanation reaction with **7** (Table 4.3). First, several *para* substituents were tested to understand the effect of substitution of the phenyl ring. Electron-withdrawing groups on the aryl ring were found to be compatible, with *para*-trifluoromethyl, -methylcarboxylate, and -nitro giving products **10-12** in high yield, d.r., and ee. Electron donating groups phenyl and methoxy gave products **13** and **14** with high selectivity as well, with both products being furnished in >20:1 diastereomeric ratio. Product **15** showed it to be unnecessary to have any substituent on the phenyl ring, with the unsubstituted aryldiazoaceate giving 91% yield, 20:1 d.r., and 98% ee. Walking the substituent around the ring, *meta*-substituted aryldiazoacetates worked nicely, albeit with a slight decrease in diastereoselectivity, with *meta*-methyl and *meta*-bromo substituents giving **16** and **17** in 17:1 and 13:1 d.r., respectively, but with high enantioselectivity. 3,5-dibromo substitution continued the downward trend for selectivity, with **18** only being formed in a 6:1 ratio. Continuing with the scope of the reaction, a styryldiazoacetate derivative gave product **19** in 60% yield, 15:1 d.r., and 78% ee. This reaction gives an interesting product for further diversification due to the oxidizable styryl group. Moving into heteroaryldiazoacetate compounds, products **20** and **21** containing a benzodioxole and dihydrobenzofuran group, respectively, gave good yields and 99% ee for both reactions, with a 19:1 and 12:1 d.r., respectively. Nitrogen-containing heterocyclic products were furnished, with a 3-methylisoxazole (**22**) and 2-chloropyridine (**23**) heteroaryl groups giving high ee and good to excellent d.r. These examples demonstrate the capability for dirhodium catalysts to generate heterocyclic scaffolds which are commonly used in drug discovery. Swapping the tosyl group for a *p*-nosyl protecting group

gave **24** in 79% yield, >20:1 d.r., and 98% ee, at a 1.0 mmol scale. The product was nicely crystallizable from slow evaporation of solvent, allowing for the absolute configuration to be assigned. Finally, using the 5-membered *N*-tosyl-3-methylenepyrrolidine in the reaction gave product **25** in 85% yield and 98% ee, with a 7:1 diastereomeric ratio, highlighting the expanded generality of this methodology to include substrates beyond the piperidine scaffold.

Table 4.3 Scope of aryldiazoaceate compound in the spirocyclopropanation reaction.

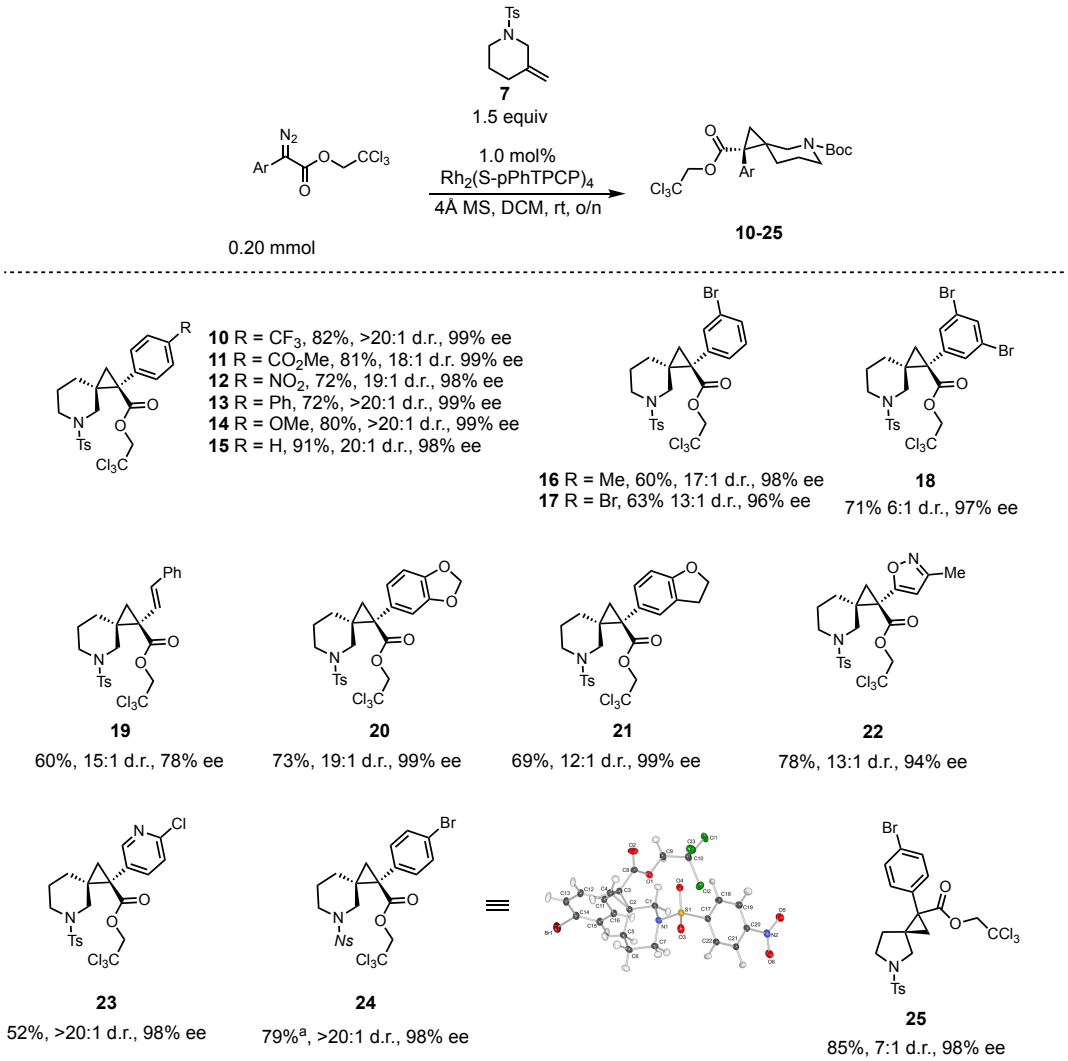

[a]Reaction run at 1.0 mmol scale.

With the azacyclomethylidenes heavily explored, our attention turned towards cycloalkylidenes. Beginning again with a catalyst screen, (4-methylencyclohexyl)benzene (**26**) was used as the standard substrate to achieve selective spirocyclopropanation in reaction with aryldiazoaceate **1** (Table 4.4). For this substrate, Rh_2(*S*-TPPTTL)$_4$ was found to give **27** in the highest diastereomeric ratio of 19:1, with Rh_2(*S*-*p*-PhTPCP)$_4$ giving only 13:1. Of note is the reaction with the achiral rhodium catalyst Rh_2(esp)$_2$ (Table 4, entry 5). This is a sterically open catalyst with an achiral ligand however, it still gives the product in a 11:1 d.r., demonstrating the inherent substrate preference for cyclopropanation of one face over the other.

Table 4.4 Catalyst screen for cycloalkylidenes substrates

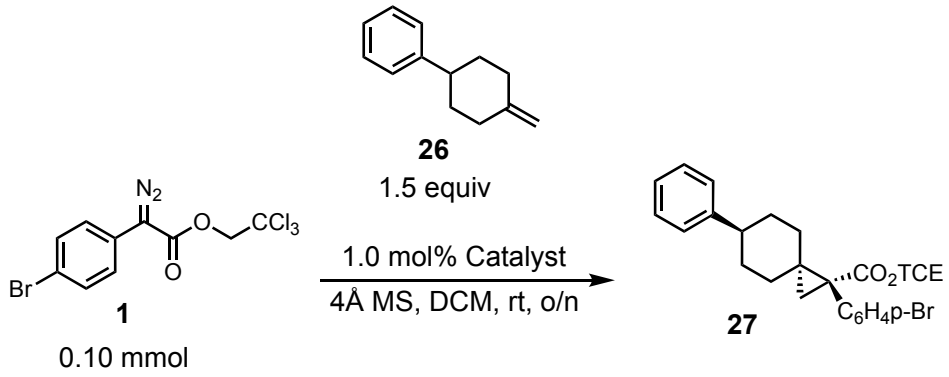

Entry	Catalyst	Yield (%)	d.r.	ee (%)
1	Rh_2(*S*-TPPTTL)$_4$	67	19:1	92
2	Rh_2(*S*-*p*PhTPCP)$_4$	87	13:1	96
3	Rh_2(*S*-DOSP)$_4$	87	10.5:1	30
4	Rh_2(*S*-PTAD)$_4$	83	14:1	-74
5	Rh_2(esp)$_4$	82	11:1	0

With the catalyst screen complete, we turned towards other substrates with challenging facial selectivity (Table 4.5). Continuing with the cyclohexyl scaffold, 4-*tert*-butylcyclohexylmethylene was subjected to the reaction conditions, giving **28** in 71% yield and 92% ee, with a >20:1 d.r. However, the racemic catalyst again gave high d.r. (>20:1), indicating the inherent substrate preference for substituted cyclohexane derivatives. Moving to 1,3-disubstuted cyclobutane substrates told a different story. Using 3-arylated methylene cyclobutane under the standard reaction conditions gave product **29** in a much lower d.r. of only 2.9:1 with the optimal catalyst. Due to the high planarity of the substrate, it is challenging for the catalyst to differentiate between to two faces of the substrate, leading to a low ratio of diastereomers.

Table 4.5 Substrates with facial selectivity

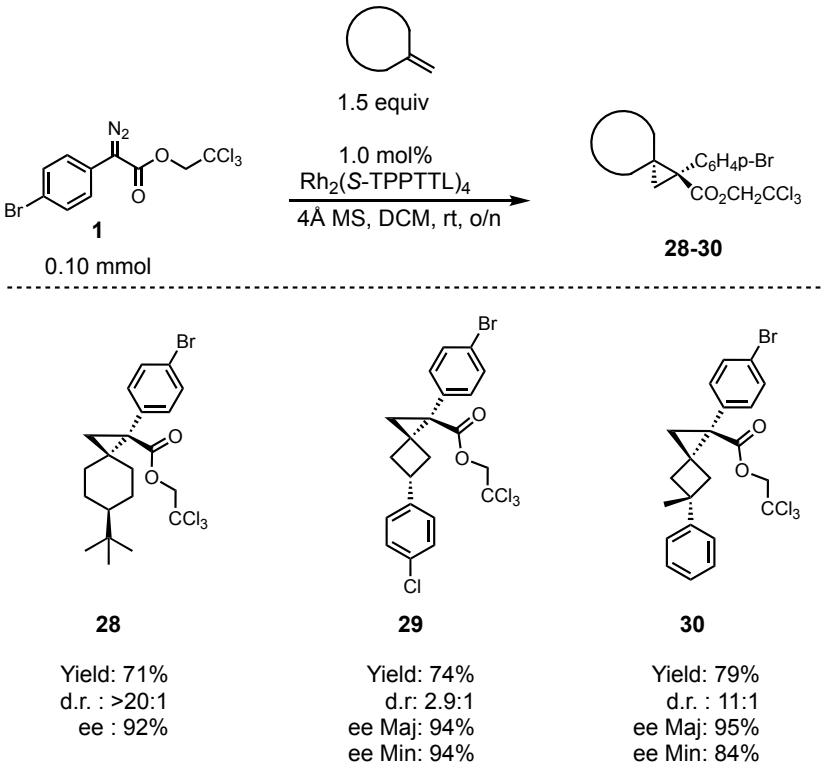

However, when adding a methyl substituent to generate a 1,1-disusbtitued methylenecyclobutane derivative, **30** was delivered in 11:1 d.r., with 79% yield and 95% ee for the major diastereomer. Both Rh_2(*S*-*p*-PhTPCP)$_4$ and the achiral Rh_2(Oct)$_4$ gave a 5:1 d.r., highlighting the ability for Rh_2(*S*-TPPTTL)$_4$ to have catalyst control of the reaction. The methyl substituent offers a more sterically demanding environment, forcing the carbene cyclopropanation to occur on the trans face of the olefin (Figure 4.4). In the case of **29**, the substrate does not have this steric demand, with only a hydrogen occupying one of the faces. Thus, the carbene cyclopropanation is not heavily favored for one side over the other, resulting in a low d.r.

Computationally Optimized Geometry

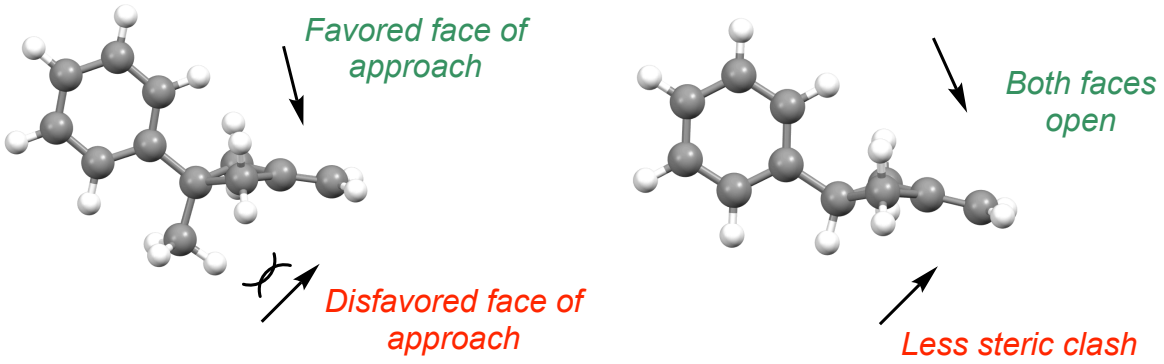

Figure 4.4 Rationale for diastereoselectivity using geometry optimized structures

Finally, racemic cycloalkylidenes were tested for the possibility of kinetic resolution. We began with racemic (3-methylencyclohexyl)benzene in reaction with **1** and Rh_2(*S*-TPPTTL)$_4$ (Table 4.6). The reaction gave **31** in an 81% yield, however, four diastereomers were seen in the crude NMR analysis showing poor kinetic resolution and proving to be an intractable mixture. Wondering whether adding more steric bulk to the phenyl ring

would increase the substate/catalyst interactions improving the selectivity of the reaction, *p*-chloro and a 3,5-di-*tert*-butylphenyl substrates were subjected to the reaction.

Table 4.6 Kinetic resolution of racemic cyclohexylalkylidenes.

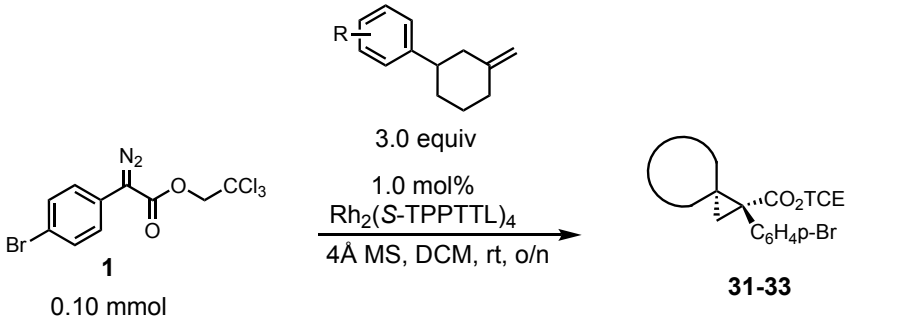

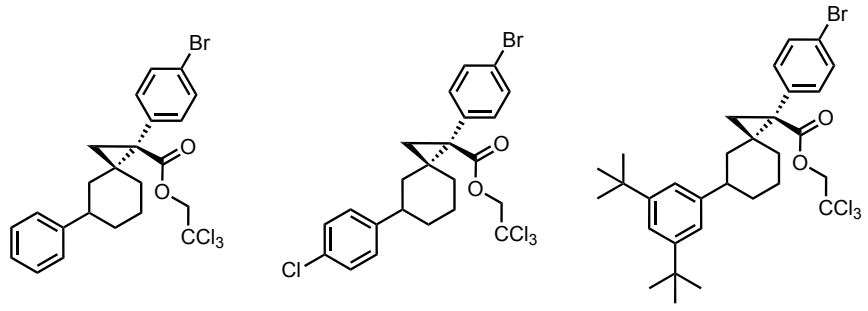

31	**32**	**33**
Yield: 81%	Yield: 82%	Yield: 62%
d.r.: 34:6.5:5:1	d.r.: 21:6:4.5:1	d.r. : 16:1
ee[a]: not determined	ee[a]: not determined	ee: 92%

[a]ee not determined because signals could not be resolved

Unsurprisingly, the *p*-Cl substituent saw little change between the parent unsubstituted substrate, giving **32** with an intractable mixture of diastereomers. Gratifyingly, the 3,5-disubstituted phenyl substrate gave **33** as a mixture of only two products, in a 16:1 d.r., with a 93% enantioselectivity, indicating high kinetic resolution was capable under this rhodium catalyst. Using Rh_2(*S*-*p*-PhTPCP)$_4$ gave **33** in a 5:1 d.r., with an 82% enantioselectivity, indicating the need for a large catalyst wall to enable high kinetic

resolution for this substrate. Increasing the steric bulk of the substrate is thought to increase the substrate/wall interaction, favoring one substrate approach, contributing to the selectivity of the catalyst. The smaller substrates may not have the strong substrate/wall interactions, causing the selectivity of the reactions to suffer, as seen by the poor d.r. for **32** and **33**.

4.3 Conclusion

In summary, a dirhodium cyclopropanation study of exocyclicmethylene substrates has been completed to generate a variety of spiro[2.n]cyclopropane products. Both symmetrical and unsymmetrical substrates have been shown to be compatible with this methodology, giving high asymmetric induction. Additionally, unsymmetrical substrates capable of producing diastereomers have been shown to be highly diastereoselective using Rh_2(*S*-*p*-PhTPCP)$_4$ as catalyst, with a large scope of aryldiazoacetate compounds shown in reaction with a 3-methylenepipereidine substrate, leading to novel chiral scaffolds. Additionally, using Rh_2(*S*-TPPTTL)$_4$ as catalyst enabled facial selectivity for cycloalkylidene substrates, achieving catalyst control via substrate/wall interactions. Finally, this methodology was applied to the kinetic resolution of racemic 3-phenylmethylenecyclohexane derivatives, showing that KR could be achieved when using substrates with sterically bulky phenyl groups. This methodology has generated novel chiral spirocyclic scaffolds, difficult to obtain through other means, important for novel drug discovery and development.

4.4 Distribution of Credit

This work was conceived by both myself and Duc Ly. Initial screening with N-boc-3-methylepiperidine and 4-phenylmetheylencyclohexane were conducted by Duc Ly. The diazo compound scope was conduct by myself, Duc Ly, and Andrew Wang. Starting material synthesis was conducted by both myself and Duc Ly.

4.5 References

1. Bonnaud, B.; Cousse, H.; Mouzin, G.; Briley, M.; Stenger, A.; Fauran, F.; Couzinier, J. P., 1-Aryl-2-(aminomethyl)cyclopropanecarboxylic acid derivatives. A new series of potential antidepressants. *J. Med. Chem.* **1987,** *30* (2), 318-325.
2. Springthorpe, B.; Bailey, A.; Barton, P.; Birkinshaw, T. N.; Bonnert, R. V.; Brown, R. C.; Chapman, D.; Dixon, J.; Guile, S. D.; Humphries, R. G.; Hunt, S. F.; Ince, F.; Ingall, A. H.; Kirk, I. P.; Leeson, P. D.; Leff, P.; Lewis, R. J.; Martin, B. P.; McGinnity, D. F.; Mortimore, M. P.; Paine, S. W.; Pairaudeau, G.; Patel, A.; Rigby, A. J.; Riley, R. J.; Teobald, B. J.; Tomlinson, W.; Webborn, P. J. H.; Willis, P. A., From ATP to AZD6140: The discovery of an orally active reversible P2Y12 receptor antagonist for the prevention of thrombosis. *Bioorganic & Medicinal Chemistry Letters* **2007,** *17* (21), 6013-6018.
3. Auclair, A. L.; Martel, J. C.; Assié, M. B.; Bardin, L.; Heusler, P.; Cussac, D.; Marien, M.; Newman-Tancredi, A.; O'Connor, J. A.; Depoortère, R., Levomilnacipran (F2695), a norepinephrine-preferring SNRI: Profile in vitro and in models of depression and anxiety. *Neuropharmacology* **2013,** *70*, 338-347.
4. Talele, T. T., The “Cyclopropyl Fragment” is a Versatile Player that Frequently Appears in Preclinical/Clinical Drug Molecules. *J. Med. Chem.* **2016,** *59* (19), 8712-8756.
5. Littleson, M. M.; Baker, C. M.; Dalençon, A. J.; Frye, E. C.; Jamieson, C.; Kennedy, A. R.; Ling, K. B.; McLachlan, M. M.; Montgomery, M. G.; Russell, C. J.; Watson, A. J. B., Scalable total synthesis and comprehensive structure–activity relationship studies of the phytotoxin coronatine. *Nature Communications* **2018,** *9* (1), 1105.
6. Ma, S.; Mandalapu, D.; Wang, S.; Zhang, Q., Biosynthesis of cyclopropane in natural products. *Natural Product Reports* **2022,** *39* (5), 926-945.
7. Lovering, F.; Bikker, J.; Humblet, C., Escape from Flatland: Increasing Saturation as an Approach to Improving Clinical Success. *J. Med. Chem.* **2009,** *52* (21), 6752-6756.
8. Martin, M. W. Z., Mary-Margaret; Mente, Scot; Dinsmore, Christopher; Wang, Zhongguo; Zheng, Xiaozhang Inhibiting Fatty Acid Synthase (FASN). EP3636637A1, 2020.
9. Carreira, E. M.; Fessard, T. C., Four-Membered Ring-Containing Spirocycles: Synthetic Strategies and Opportunities. *Chem. Rev.* **2014,** *114* (16), 8257-8322.
10. Ding, A.; Meazza, M.; Guo, H.; Yang, J. W.; Rios, R., New development in the enantioselective synthesis of spiro compounds. *Chem. Soc. Rev.* **2018,** *47* (15), 5946-5996.
11. Yao, W.; Zhuo, J.; Burns, D. M.; Xu, M.; Zhang, C.; Li, Y.-L.; Qian, D.-Q.; He, C.; Weng, L.; Shi, E.; Lin, Q.; Agrios, C.; Burn, T. C.; Caulder, E.; Covington, M. B.; Fridman, J. S.; Friedman, S.; Katiyar, K.; Hollis, G.; Li, Y.; Liu, C.; Liu, X.; Marando, C. A.; Newton, R.; Pan, M.; Scherle, P.; Taylor, N.; Vaddi, K.; Wasserman, Z. R.; Wynn, R.; Yeleswaram, S.; Jalluri, R.; Bower, M.; Zhou, B.-B.; Metcalf, B., Discovery of a Potent, Selective, and Orally Active Human Epidermal Growth Factor Receptor-2 Sheddase Inhibitor for the Treatment of Cancer. *J. Med. Chem.* **2007,** *50* (4), 603-606.

12. Wang, Y.; Liu, J.; Dransfield, P. J.; Zhu, L.; Wang, Z.; Du, X.; Jiao, X.; Su, Y.; Li, A.-r.; Brown, S. P.; Kasparian, A.; Vimolratana, M.; Yu, M.; Pattaropong, V.; Houze, J. B.; Swaminath, G.; Tran, T.; Nguyen, K.; Guo, Q.; Zhang, J.; Zhuang, R.; Li, F.; Miao, L.; Bartberger, M. D.; Correll, T. L.; Chow, D.; Wong, S.; Luo, J.; Lin, D. C. H.; Medina, J. C., Discovery and Optimization of Potent GPR40 Full Agonists Containing Tricyclic Spirocycles. *ACS Medicinal Chemistry Letters* **2013,** *4* (6), 551-555.
13. Wang, H.-X.; Li, W.-P.; Zhang, M.-M.; Xie, M.-S.; Qu, G.-R.; Guo, H.-M., Synthesis of chiral pyrimidine-substituted diester D–A cyclopropanes via asymmetric cyclopropanation of phenyliodonium ylides. *Chem. Commun.* **2020,** *56* (78), 11649-11652.
14. Lee, W.-C. C.; Wang, D.-S.; Zhang, C.; Xie, J.; Li, B.; Zhang, X. P., Asymmetric radical cyclopropanation of dehydroaminocarboxylates: Stereoselective synthesis of cyclopropyl α-amino acids. *Chem* **2021,** *7* (6), 1588-1601.
15. Wang, X.; Ke, J.; Zhu, Y.; Deb, A.; Xu, Y.; Zhang, X. P., Asymmetric Radical Process for General Synthesis of Chiral Heteroaryl Cyclopropanes. *J. Am. Chem. Soc.* **2021,** *143* (29), 11121-11129.
16. Gao, Z.; Liu, L.; Liu, J.-R.; Wang, W.; Yang, N.-Y.; Tao, L.; Li, Z.-L.; Gu, Q.-S.; Liu, X.-Y., Copper-catalysed synthesis of chiral alkynyl cyclopropanes using enantioconvergent radical cross-coupling of cyclopropyl halides with terminal alkynes. *Nature Synthesis* **2025,** *4* (1), 84-96.
17. Wang, X.; Shi, Z.; Xu, M.; Lin, X.; Wang, Z., Asymmetric Radical Cyclopropanation of α,β-Unsaturated Amides with α-Boryl and α-Silyl Dibromomethanes via Cr(II)-Based Metalloradical Catalysis. *J. Am. Chem. Soc.* **2025**.
18. Bajaj, P.; Sreenilayam, G.; Tyagi, V.; Fasan, R., Gram-Scale Synthesis of Chiral Cyclopropane-Containing Drugs and Drug Precursors with Engineered Myoglobin Catalysts Featuring Complementary Stereoselectivity. *Angew. Chem. Int. Ed.* **2016,** *55* (52), 16110-16114.
19. Nam, D.; Steck, V.; Potenzino, R. J.; Fasan, R., A Diverse Library of Chiral Cyclopropane Scaffolds via Chemoenzymatic Assembly and Diversification of Cyclopropyl Ketones. *J. Am. Chem. Soc.* **2021,** *143* (5), 2221-2231.
20. Cao, L.-Y.; Wang, J.-L.; Wang, K.; Wu, J.-B.; Wang, D.-K.; Peng, J.-M.; Bai, J.; Zhuo, C.-X., Catalytic Asymmetric Deoxygenative Cyclopropanation Reactions by a Chiral Salen-Mo Catalyst. *J. Am. Chem. Soc.* **2023,** *145* (5), 2765-2772.
21. Li, S.; Zhang, D.; Purushothaman, A.; Lv, H.; Shilpa, S.; Sunoj, R. B.; Li, X.; Zhang, X., Chemo-, regio- and enantioselective hydroformylation of trisubstituted cyclopropenes: access to chiral quaternary cyclopropanes. *Nature Communications* **2024,** *15* (1), 6377.
22. Werth, J.; Berger, K.; Uyeda, C., Cobalt Catalyzed Reductive Spirocyclopropanation Reactions. *Adv. Synth. Catal.* **2020,** *362* (2), 348-352.
23. Wang, H.; Li, Y.; Huang, L.; Xu, H.; Jiao, Y.; Zhou, Z.; Tang, Z.; Fang, F.; Zhang, X.; Ding, K.; Yi, W.; Liu, H.; Wu, X.; Zhou, Y., The synthesis of spirocyclopropane skeletons enabled by Rh(III)-catalyzed enantioselective C–H activation/[4 + 2] annulation. *Chem Catalysis* **2023,** *3* (12), 100822.
24. Ramazanov, I. R.; Kadikova, R. N.; Zosim, T. y. P.; Dzhemilev, U. M.; de Meijere, A., Synthesis of Spiro[2.2]pentanes and Spiro[2.3]hexanes Employing the Me3Al/CH2I2 Reagent. *Eur. J. Org. Chem.* **2017,** *2017* (47), 7060-7067.

25. Huang, J.; Sun, S.; Ma, P.; Wang, J.; Lee, K.; Xing, Y.; Wu, Y.; Wang, G., Highly diastereoselective spiro-cyclopropanation of 2-arylidene-1,3-indanediones and dimethylsulfonium ylides. *New J. Chem.* **2021,** *45* (40), 18776-18780.
26. Noole, A.; Sucman, N. S.; Kabeshov, M. A.; Kanger, T.; Macaev, F. Z.; Malkov, A. V., Highly Enantio- and Diastereoselective Generation of Two Quaternary Centers in Spirocyclopropanation of Oxindole Derivatives. *Chem. Eur. J.* **2012,** *18* (47), 14929-14933.
27. Wei, B.; Sharland, J. C.; Lin, P.; Wilkerson-Hill, S. M.; Fullilove, F. A.; McKinnon, S.; Blackmond, D. G.; Davies, H. M. L., In Situ Kinetic Studies of Rh(II)-Catalyzed Asymmetric Cyclopropanation with Low Catalyst Loadings. *ACS Catal.* **2020,** *10* (2), 1161-1170.
28. Sharland, J. C.; Wei, B.; Hardee, D. J.; Hodges, T. R.; Gong, W.; Voight, E. A.; Davies, H. M. L., Asymmetric synthesis of pharmaceutically relevant 1-aryl-2-heteroaryl- and 1,2-diheteroarylcyclopropane-1-carboxylates. *Chem. Sci.* **2021,** *12* (33), 11181-11190.
29. Lathrop, S. P.; Mlinar, L. B.; Manjrekar, O. N.; Zhou, Y.; Harper, K. C.; Sacia, E. R.; Higgins, M.; Bogdan, A. R.; Wang, Z.; Richter, S. M.; Gong, W.; Voight, E. A.; Henle, J.; Diwan, M.; Kallemeyn, J. M.; Sharland, J. C.; Wei, B.; Davies, H. M. L., Continuous Process to Safely Manufacture an Aryldiazoacetate and Its Direct Use in a Dirhodium-Catalyzed Enantioselective Cyclopropanation. *Org. Process Res. Dev.* **2022**.
30. Davies, H. M. L.; Nagashima, T.; Klino, J. L., Stereoselectivity of Methyl Aryldiazoacetate Cyclopropanations of 1,1-Diarylethylene. Asymmetric Synthesis of a Cyclopropyl Analogue of Tamoxifen. *Org. Lett.* **2000,** *2* (6), 823-826.

Chapter 5. Synthesis of 2-Substituted Bicyclo[1.1.1]pentanes via Triplet Carbene insertion into Bicyclo[1.1.0]butanes

5.1 Introduction

Bicyclo[1.1.1]pentanes (BCPs) have become a highly sought after scaffold in recent years due to their bio-isosteric properties as replacements for substituted benzene rings. In an effort to 'escape from flatland',[1] *para*-substituted benzene rings have been replaced with 1,3-disubstituted BCPs in some common drug scaffolds in order to increase the pharmacological properties of these drugs.[2] In particular, increasing more C(sp^3) character often improves pharmacological properties of these target molecules, thus, developing facile methods to make BCP building blocks is an important area of research. Additionally, replacing the arene moieties with saturated isosteres lends the molecule to be more stable towards CYP450 metabolism. In 2012, Pfizer reported the substitution of a fluroaryl group with a BCP isostere in Avagacestat, a lead compound for treating Alzheimer Disease (Figure 5.1A).[3] This change increased cell permeability and solubility with little to no change in the efficacy compared to the original compound.

1,3-disubstitued BCPs are the most common substitution pattern, with many available synthetic routes to access these moieties. Most synthetic routes begin with [1.1.1]propellane. A variety of both polar and radical methods have been developed to synthesize the 1,3-disubstitued BCPs starting from the highly strained propellane compound.[4-6] However, a much more challenging scaffold to construct is the 1,2-disubstituted or 1,2,3-trisubstituted BCPs. This substitution pattern has been shown to be a possible bioisostere for *ortho*- or *meta*-substituted benzene rings, extending this

valuable motif into an important chemical space (Figure 5.1B). While methods exist for this synthesis, they are often hampered by long synthetic sequences, use of harsh reagents, or limited scope.[7-11]

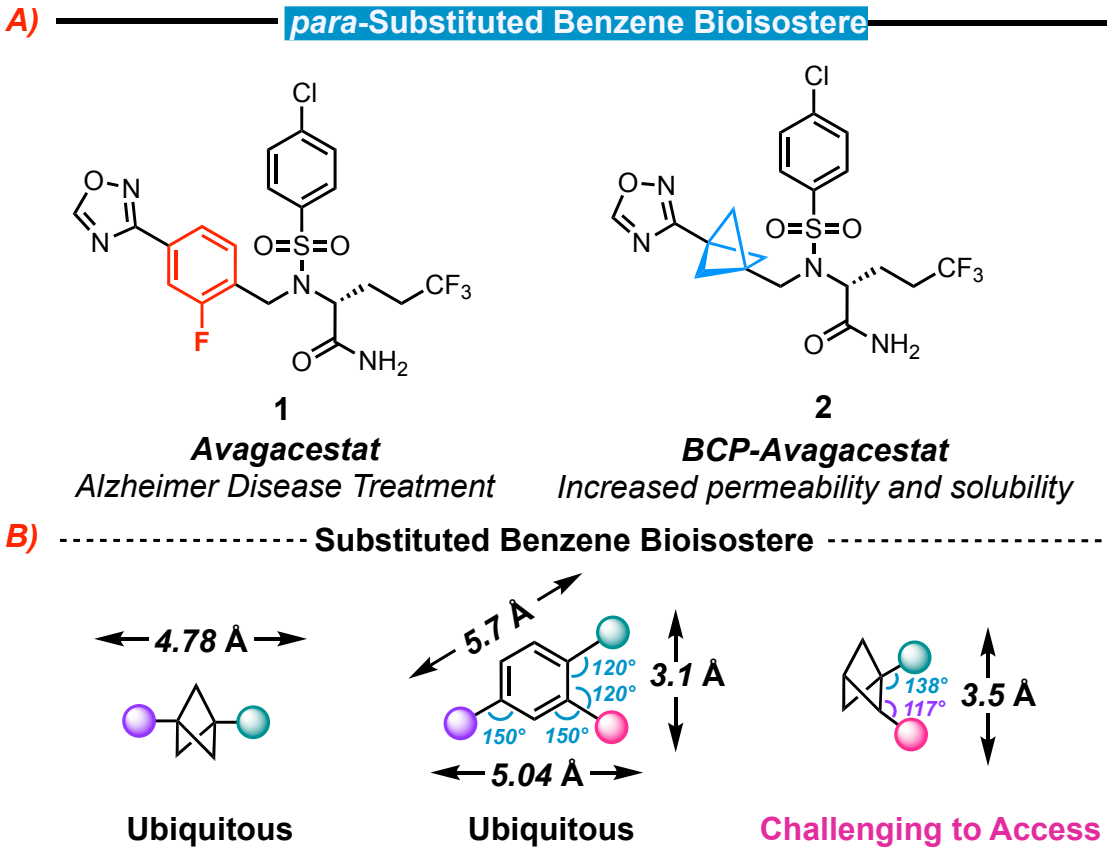

Figure 5.1 A) Example of para-substituted benzene bioisostere in pharmaceutically relevant scaffolds, B) Similarity of distance and geometry of substituents of BCPs and benzene ring.

Recently, Baran developed a route to access 1,2-disusbtitued BCPs (Scheme 5.1). However, the route is lengthy, low yielding, and requires the use of harsh reagents, showcasing the need for simpler methods to be developed.[12] The MacMillan lab turned towards a radical approach, accessing 2-bromo substituents on the BCP core.[13] This enabled a metallophotoredox cross-coupling method to install aromatic and

heteoaromatic substituents at the 2-position of the BCP. In 2025, the Tan group reported the enantioselective synthesis of 2-substitued BCPs, employing a nitrogen deletion strategy.[14] Lewis acid catalyzed imine addition across a bicyclo[1.1.0.]butane (BCB) afforded enantioenriched aza-bicycloheptanes, followed by deprotection and nitrogen deletion furnished the 2-substituted BCPs with high enantioretention.

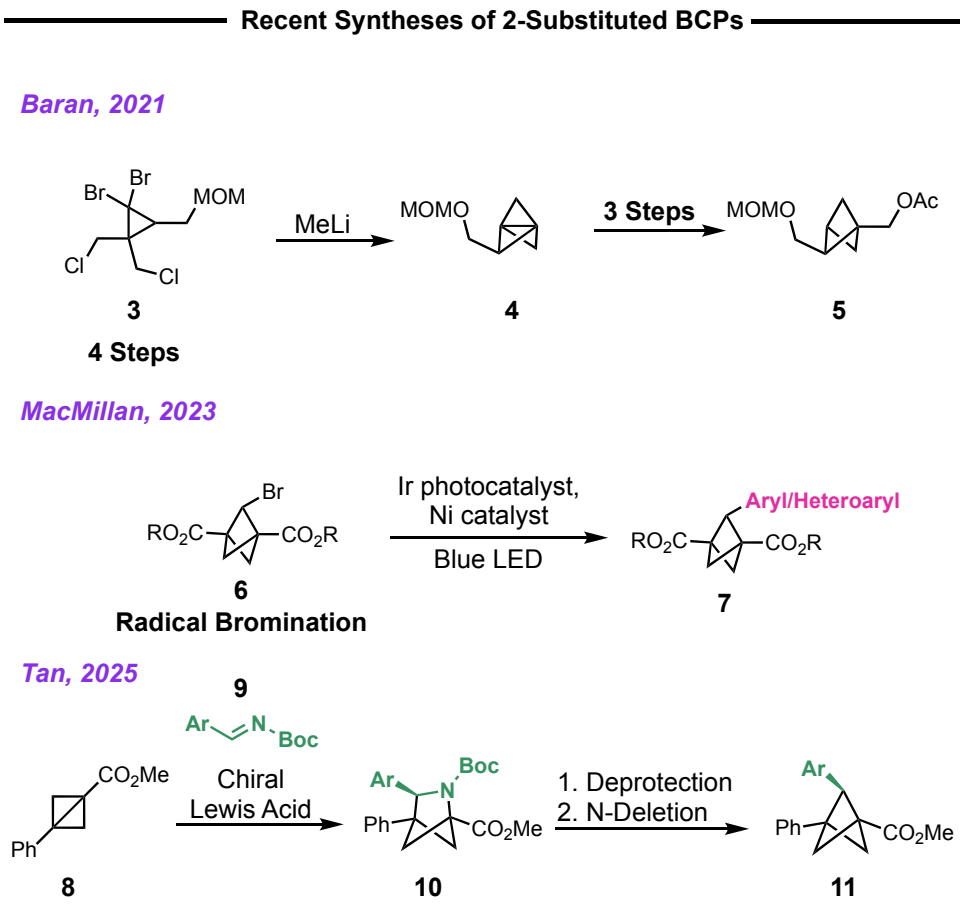

Scheme 5.1 Previous synthetic methods to access 2-substituted BCPs.

Like the Tan group, a plethora of new synthetic methodologies have emerged harnessing the strain-release energy of the bridging C–C bond in BCBs. Recently, the Davies lab has reported the facile synthesis of BCBs using dirhodium catalyzed

cyclization of diazo compounds (Scheme 5.2A).[15] This offered quick access to a valuable building block, capable of undergoing a range of transformations. Many bicyclic products can be generated through use of 1, 2, or 3-carbon synthons to form bicyclo[1.1.1]pentanes, -[2.1.1]hexanes, and -[3.1.1]heptanes, respectively.[16-22] However, by far the most challenging is the synthesis of BCPs. A general strategy to achieve this goal is employing a carbene to undergo a [2+1] cycloaddition, inserting into the strained C–C bond. However, this strategy is often limited to the highly electrophlic dihalocarbenes, installing useful, albeit limited functionality into the BCB. Recently, the Ma, Mykhailiuk, and Davies labs have elaborated this strategy to generate 2,2-difluoro-functionalized BCP products (Scheme 5.2B).[15, 23-25]

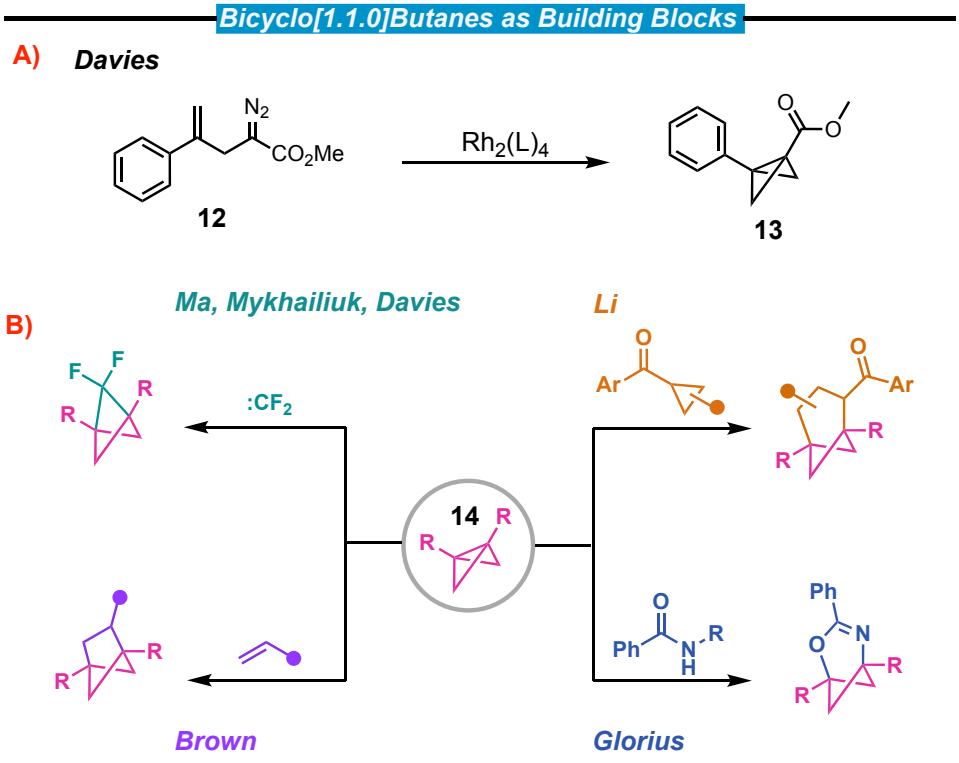

Scheme 5.2 Bicyclo[1.1.1]butanes, A) Facile synthesis of BCBs from dirhodium catalyzed cyclization, B) Reactions of BCBs generating a variety of bicyclic scaffolds.

While both Mykhailiuk and Davies use TMS-CF_3 with NaI to generate difluorocarbene, Ma used trimethylsilyl 2-fluorosulfonyl-2,2-difluoroacetate as the carbene precursor. A shift towards radical functionalization has become prominent upon reports from Glorius, Brown, and Li (Scheme 5.2B).[16, 18, 21, 26] Through either triplet energy transfer to the BCB, photoredox methods, or boryl radical-mediated cascade reactions, the resulting radicals can be trapped by a plethora of radical acceptors including activated olefins, cyclobutanones, and phenols to generate a variety of bicyclic scaffolds. However, to date the only conditions capable of generating the BCP scaffolds are with dihalocarbenes, highlighting the need for further development in this area.

As our lab has a long-standing interest in dirhodium carbenes, these intermediates would be the obvious choice to insert more complex functionality into BCBs to generate 2-substituted BCPs. However, reports are not promising, as only highly electron-deficient carbenes can insert into the C–C bond.[27] Inspired by the recent advent of photoinduced triplet carbene reactivity, we wondered whether switching the mode of carbene reactivity from singlet carbene to triplet carbene would enable radical addition into the BCB, furnishing 2-substituted BCPs.

Photoinduced carbene reactions have become a prominent means for synthetic transformations. In 2018, the Davies group disclosed the blue-light induced photolysis of aryldiazoacetates, generating the free singlet carbene which subsequently undergoes cyclopropanation or X–H insertion (Figure 5.2A).[28] Later in the same year, the He and Zhou groups reported the blue-light promoted coupling of aryldiazoacetates with diazoesters to afford *E*-alkenes (Figure 5.2B).[29] The following year the Koenigs group

reported blue-light photolysis of aryldiazoacetates for cyclopropenation of alkynes and Doyle-Kirmse rearrangement of sulfides (Figure 5.2C).[30]

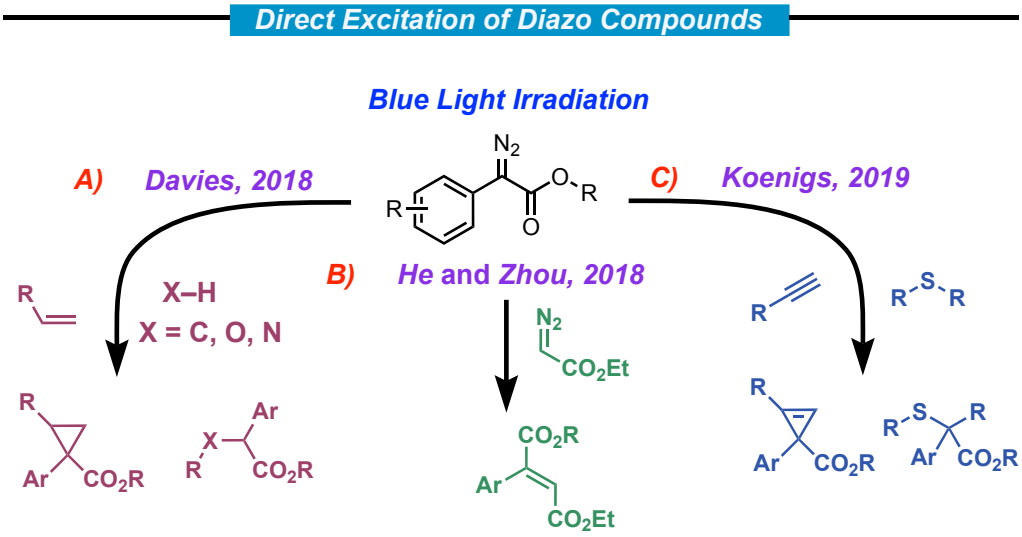

Figure 5.2 : Recent literature examples of direct blue light excitation of diazo compounds for reactions with A) olefins and X–H insertion, B) ethyldiazoacetate, and C) alkynes and sulfides.

These examples use direct sensitization of the diazo compound to induce carbene formation. Since these initial reports, blue-light photolysis of diazo compounds has seen an increase in popularity within the scientific community.[31, 32] While most reports focused on reactions of free singlet carbenes, photosensitized triplet carbenes have drawn interest as well. Photosensitization, also known as triplet energy transfer (TEnT), is the process of excitation of a substrate from a catalyst in its triplet excited state (Figure 5.3A). A photocatalyst will absorb a photon and be promoted to its singlet excited state. Then, relaxation by intersystem crossing will occur to generate the triplet excited state, which is long-lived for most photocatalysts, enabling bimolecular reactions to occur. Finally, the photocatalyst will undergo energy transfer to a substrate with a triplet energy lower than

that of the excited photocatalyst, promoting the substrate into its triplet excited state while relaxing back down to its singlet ground state.

Triplet carbenes are relatively underexplored as compared to singlet carbenes. Typically generated through TEnT catalysis from the corresponding diazo precursor, triplet carbenes have a distinct reactivity profile compared to their singlet counterparts due to the inherent radical character of these intermediates, allowing for one-electron type reactions to occur (Figure 5.3B).

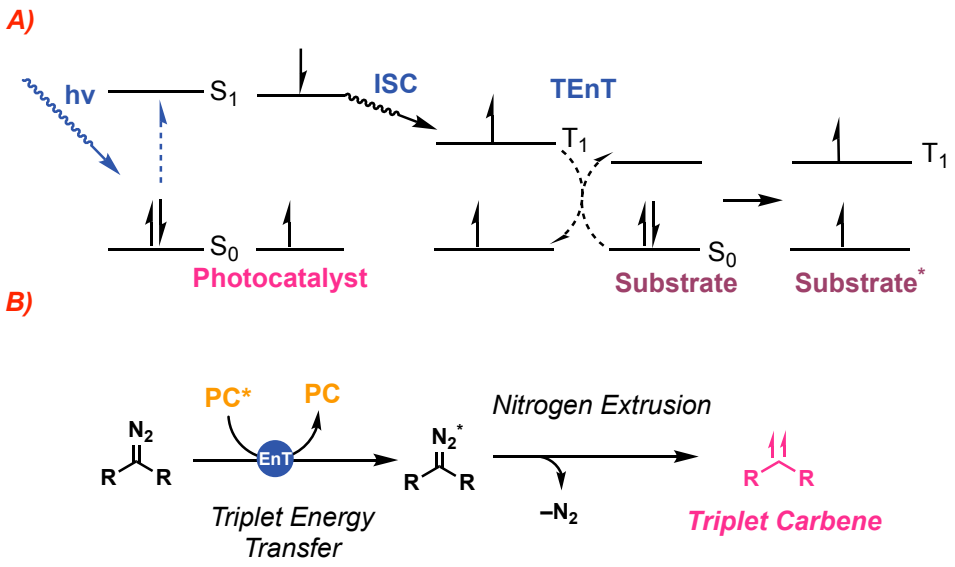

Figure 5.3 A) mechanism for TEnT of diazo compound to form triplet carbene, B) General mechanism of photosensitization TEnT.

Only in recent years have their synthetic utility become realized. In 2016, the Gryko, Kadish, and Zawada groups published the photosensitization of ethyldiazoacetate (EDA) to furnish functionalized aldehyde derivatives (Scheme 5.3A).[33] They used a porphyrin photocatalyst and propose both an energy and electron transfer event as the operational mechanism. In 2022, Koenigs reported a gem-difluoroolefination reaction in which a triplet

carbene adds into a gem-disubstituted olefin, showing a range of diazo compounds can be photosensitized to the triplet state (Scheme 5.3B).[34] This diradical carbene can then add into an olefin, which upon two subsequent electron transfer events leads to the desired product. Koenigs followed this work up with two more examples of photosensitization of diazo compounds to afford triplet carbenes.

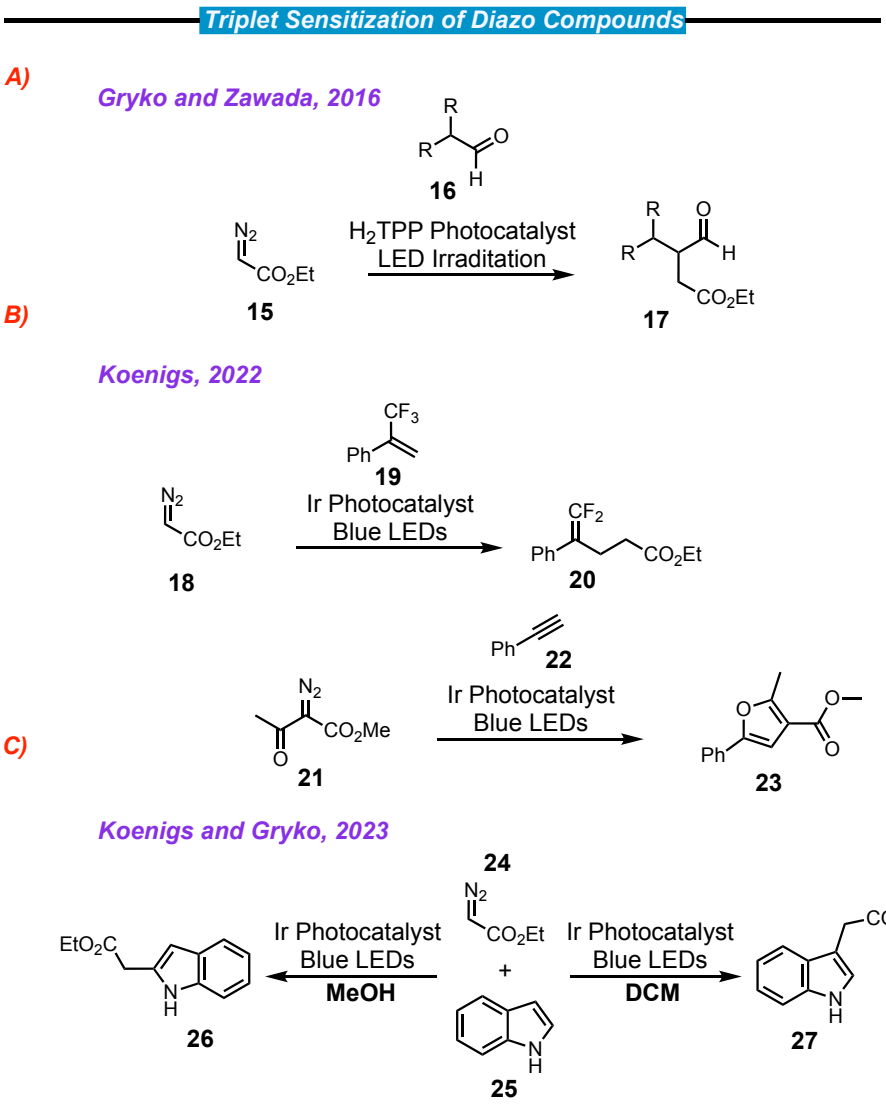

Scheme 5.3 Reactions with triplet sensitized carbene intermediates A) porphyrin catalyzed TEnT of EDA to generate alpha-substutued aldehydes, B) examples of

organic transformations using TEnT of diazo compounds, C) divergent reactivity for triplet carbenes based on solvent effects.

They show the stereoconvergent synthesis of trisubstituted cyclopropanes as well as the facile synthesis of furan derivatives.[35, 36] Most recently, the Gryko and Koenigs groups showed that triplet carbene generation is highly dependent on solvent choice, with divergent reactivity being seen in either protic or aprotic solvents (Scheme 5.3C).[37] Inspired by these recent reports photosensitization of diazo compounds, and our longstanding interest in developing novel approaches to synthetically challenging motifs, we envisioned the inherent radical character of triplet carbenes would enable the addition into the strained C–C bond of a BCB (Scheme 5.4). The resulting intermediate would then undergo intersystem crossing and radical recombination to reveal a 2-substituted BCP. This methodology would stand as a facile method to afford a valuable yet underexplored scaffold, opening new possibilities for drug discovery.

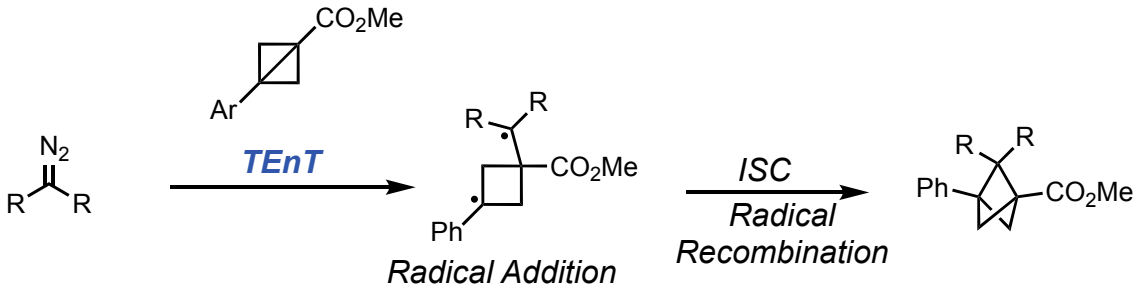

Scheme 5.4 Reaction design

5.2 Results and discussion

The study began by employing EDA (**15**) with a known triplet sensitizer catalyst[37] $Ir(ppy)_3$ with methyl 3-phenylbicyclo[1.1.0]butane-1-carboxylate (**8**) under 440 nm light

irradiation. An initial hit at room temperature gave us 13% yield of the desired BCP product **28** by NMR (Table 5.1, Entry 1). Upon cooling to 0 and – 40 °C we saw an improvement to 21% for both reactions, while the desired product was generated in 50% yield at -65°C (Entries 2-3).

Table 5.1 Optimization of reaction conditions.

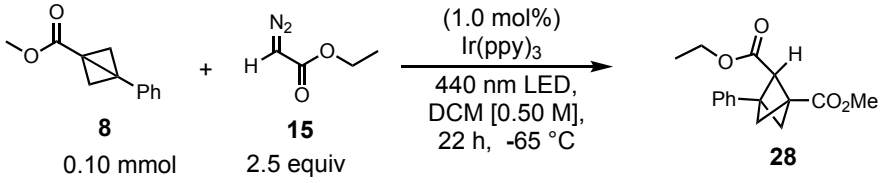

Entry	Deviations from Above	Yield (%)[a]
1	None	50 (66)[b]
2	25 °C	13
3	0 °C	36
4	-40 °C	36
5	-78	45
6	2.5 mol% Catalyst Loading	40
7	5.0 mol% Catalyst Loading	21
8	$[Ir(ppy)_2(dtbbpy)]PF_6$ as Catalyst	22
9	$[Ir[dF(CF_3)ppy]_2(dtbpy)]PF_6$ as Catalyst	34
10	4-CZIPN as Catalyst	35
11	Chloroform as solvent	6
12	THF, diethyl ether, or hexane as solvent	0
13	5 equiv of EDA	25
14	[0.10 M]	36
15	No photocatalyst or no light	0

However, the yield was slightly lower when cooling all the way to -78 °C (Entry 5). Varying the photocatalyst loading to 2.5 and 5.0 mol% proved to be suboptimal, with the loading of 1 mol% giving the best yield (Entries 6-7). Next, several known triplet sensitizers were screened, showing that $Ir(ppy)_3$ was the best catalyst for this transformation (Entries 8-

10). Performing the reaction in dichloromethane was seen to be the choice solvent, with only trace product being formed when the reaction was run in chloroform and no product when run in THF, diethyl ether, or hexanes (Entries 11-12).

Varying the equivalents of **15** and increasing the concentration showed no improvement from the standard conditions (Entries 13-14). Finally, no product was seen in the absence of 440 nm light, or photocatalyst.

With the optimized conditions in hand, the scope of this transformation was elaborated. A variety of diazo compounds were amenable to this methodology (Table 5.2).

Table 5.2 Scope of reaction.

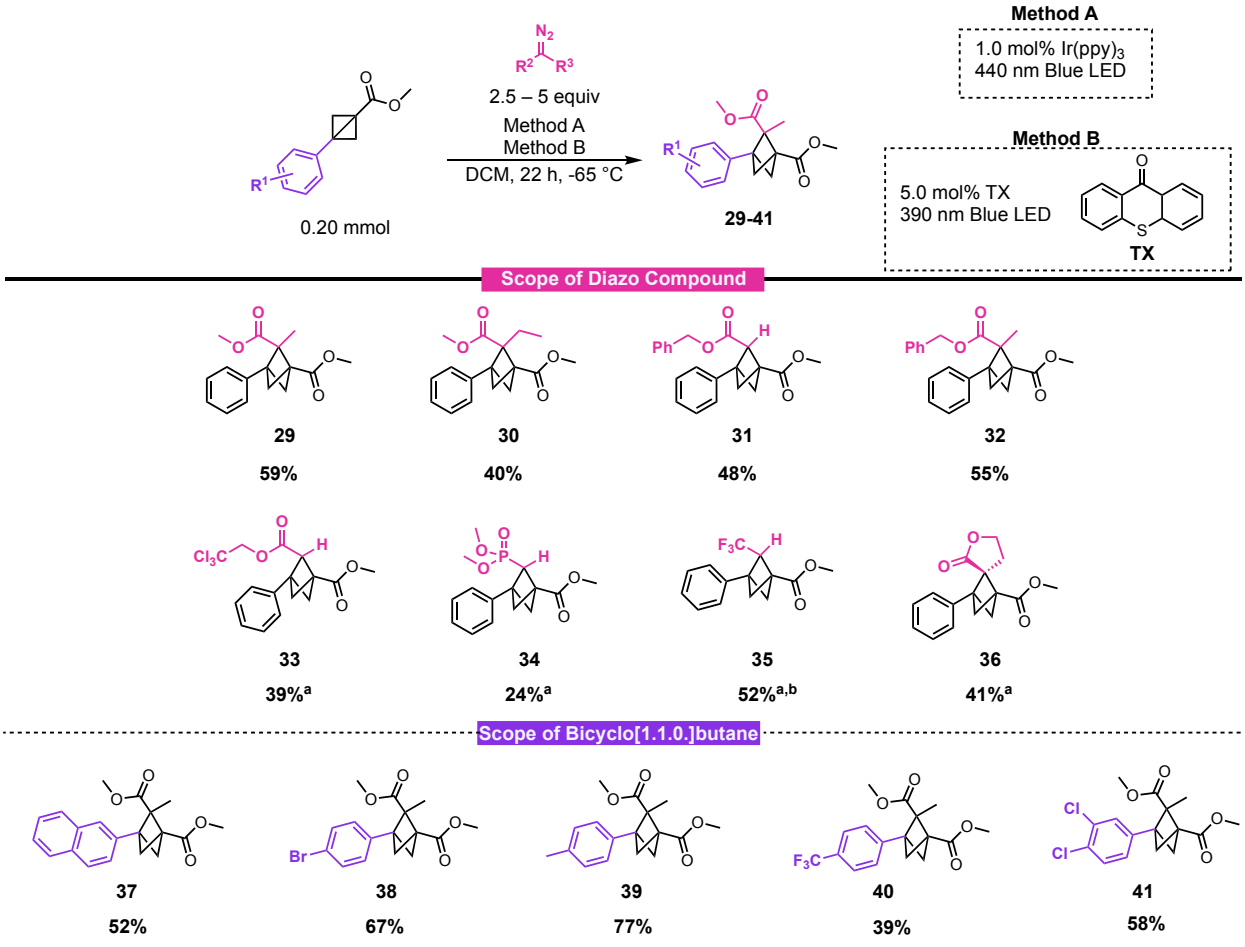

[a]Reaction run using method B. [b]5.0 equiv of diazo compound

Alkyl diazoester compounds were found to work nicely, with both methyl-2-diazopropionate and -butanoate yielding products **29** and **30**, respectively. These results were somewhat surprising due to the fact that alkyl diazoesters are highly prone to undergo a 1,2-shift from the corresponding singlet carbene resulting in the acrylate (Scheme 5.5).[38]

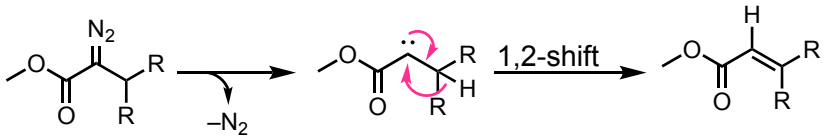

Scheme 5.5 1,2-hydride shift for alkyldiazoacetates.

Interestingly, the major byproducts from these reactions were the cyclopropane products, formed from the cyclopropanation of the acrylate 1,2-shift byproduct. The fact that the major product is the desired BCP indicates that the carbene exists primarily in the triplet state, not known to undergo the 1,2-shift. The propensity to undergo the hydride shift increases with decreasing bond strength of the β C–H bond, thus it would be expected for the methine carbene derivative to be the most susceptible to this side reaction.[39] Indeed, when subjecting the 3-methylbutanoate diazo to the reaction conditions, the only product observed was the acrylate, with no BCP detected.

Products **31** and **32** were formed in 48% and 55% yield, respectively, giving access to orthogonal ester protecting groups for further product derivatization. When using 2,2,2-trichloroethyl 2-diazoacetate as the carbene precursor under the standard conditions, only trace product was observed. We hypothesized that using a photocatalyst with a

higher triplet energy would enable higher product formation. Gratifyingly, using thioxanthone (TX) as the photocatalyst under 390 nm irradiation gave product **33** in 39% yield, giving another orthogonal protecting group. It was found that three other diazo compounds needed the TX photocatalyst to give appreciable yields. Products **34** and **35** were formed in moderate yields, 24% and 52% respectively. These compounds provide interesting scaffolds for further drug discovery, gaining access to synthetically challenging substituents on the BCP core. Finally, the cyclic beta-lactone diazo gave the spiro-BCP **36** in 41% yield. Importantly, the control reaction with no catalysts under these new conditions gave no product, indicating the photosensitization pathway was still operational. Moving to the scope of bicylco[1.1.0]butanes, yields were generally higher when we used methyl 2-diazopropionate as the carbene precursor rather than EDA. Using the sterically bulky naphthyl group on the BCB gave product **37** in 52% yield. The methodology was compatible with several *para* substituents, with *para*-bromo, methyl, and trifluoromethyl substituents giving 67%, 77%, and 39%, respectively (**38-40**). Finally, a 3,4-dichloro substitution pattern was shown to be amenable, with product **41** being formed in 58% yield.

Next, the practicality of this methodology was tested by showcasing a one-pot sequential reaction procedure (Scheme 5.6). The dirhodium catalyzed cyclization to generate the BCB is a fast and quantitative reaction, with a high tolerance towards additives and impurities needing only 0.01 mol% catalyst loading. We hypothesized that the BCB cyclization would be tolerant of the iridium photocatalyst, allowing for both catalysts to be added at the beginning of the reaction sequence. Then, following completion of the BCB cyclization, EDA could be added to the solution followed by blue

light irradiation at -65 °C to afford the desired BCP product. Gratifyingly, when testing this dual reaction sequence, the **28** was formed in 38% yield by NMR.

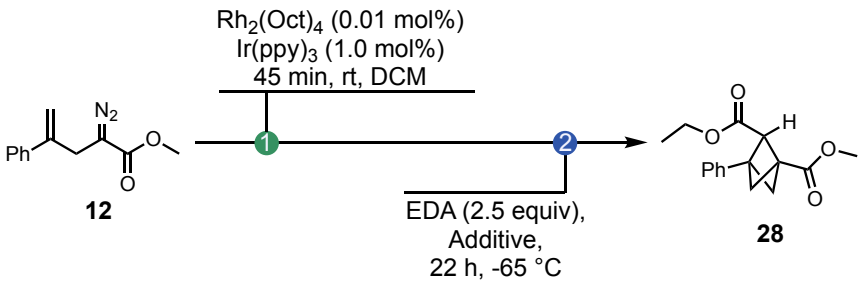

Entry	Additive	Yield (%)[a]
1	-	38
2	Pyridine (0.1 mol%)	47

[a]Yields determined using crude NMR with 1,3,5-trimethoxybenzene

Scheme 5.6 1-pot sequential reaction.

The slightly lowered yield was rationalized by the competitive decomposition of the EDA by the dirhodium catalyst in the solution. Wanting to inhibit this deleterious pathway, 0.1 mol% of pyridine was added to the solution after the first step to poison the rhodium complex through competitive binding. With these new reaction conditions, the desired product was formed in 47% yield by NMR, close to the previously optimized conditions. This showcases the power of diazo carbene chemistry, with a sequential singlet and triplet carbene reaction generating a highly challenging synthetic scaffold.

5.3 Conclusion

In summary, a facile synthesis of 2-substitued bicyclo[1.1.1.]pentanes has been disclosed using a photosensitized carbene addition into a bicyclo[1.1.0]butane. This methodology was generalizable to a variety of diazo carbene precursor, giving rise to

novel BCP scaffolds that will generate interest for drug development. Additionally, it was shown that switching the mode of carbene reactivity from singlet to triplet opened up new avenues of reactivity, which we believe will help drive the field of photosensitized carbene methodology forward. Finally, a one-pot sequential reaction setup was shown to be operational, starting from the dirhodium catalyzed BCB cyclization followed by photocatalyzed BCP formation. This methodology will not only inspire further work in the area of diazo photosensitization but enable novel scaffolds to be explored for new drug discovery.

5.4 References

1. Lovering, F.; Bikker, J.; Humblet, C., Escape from Flatland: Increasing Saturation as an Approach to Improving Clinical Success. *J. Med. Chem.* **2009,** *52* (21), 6752-6756.
2. Tsien, J.; Hu, C.; Merchant, R. R.; Qin, T., Three-dimensional saturated C(sp3)-rich bioisosteres for benzene. *Nat. Rev. Chem* **2024,** *8* (8), 605-627.
3. Stepan, A. F.; Subramanyam, C.; Efremov, I. V.; Dutra, J. K.; O'Sullivan, T. J.; DiRico, K. J.; McDonald, W. S.; Won, A.; Dorff, P. H.; Nolan, C. E.; Becker, S. L.; Pustilnik, L. R.; Riddell, D. R.; Kauffman, G. W.; Kormos, B. L.; Zhang, L.; Lu, Y.; Capetta, S. H.; Green, M. E.; Karki, K.; Sibley, E.; Atchison, K. P.; Hallgren, A. J.; Oborski, C. E.; Robshaw, A. E.; Sneed, B.; O'Donnell, C. J., Application of the Bicyclo[1.1.1]pentane Motif as a Nonclassical Phenyl Ring Bioisostere in the Design of a Potent and Orally Active γ-Secretase Inhibitor. *J. Med. Chem.* **2012,** *55* (7), 3414-3424.
4. Huang, W.; Keess, S.; Molander, G. A., A General and Practical Route to Functionalized Bicyclo[1.1.1]Pentane-Heteroaryls Enabled by Photocatalytic Multicomponent Heteroarylation of [1.1.1]Propellane. *Angew. Chem. Int. Ed.* **2023,** *62* (24), e202302223.
5. Nugent, J.; Sterling, A. J.; Frank, N.; Mousseau, J. J.; Anderson, E. A., Synthesis of α-Quaternary Bicyclo[1.1.1]pentanes through Synergistic Organophotoredox and Hydrogen Atom Transfer Catalysis. *Org. Lett.* **2021,** *23* (21), 8628-8633.
6. Wong, M. L. J.; Sterling, A. J.; Mousseau, J. J.; Duarte, F.; Anderson, E. A., Direct catalytic asymmetric synthesis of α-chiral bicyclo[1.1.1]pentanes. *Nature Communications* **2021,** *12* (1), 1644.
7. Yang, Y.; Tsien, J.; Dykstra, R.; Chen, S.-J.; Wang, J. B.; Merchant, R. R.; Hughes, J. M. E.; Peters, B. K.; Gutierrez, O.; Qin, T., Programmable late-stage functionalization of bridge-substituted bicyclo[1.1.1]pentane bis-boronates. *Nat. Chem.* **2024,** *16* (2), 285-293.
8. Wright, B. A.; Matviitsuk, A.; Black, M. J.; García-Reynaga, P.; Hanna, L. E.; Herrmann, A. T.; Ameriks, M. K.; Sarpong, R.; Lebold, T. P., Skeletal Editing Approach to Bridge-Functionalized Bicyclo[1.1.1]pentanes from Azabicyclo[2.1.1]hexanes. *J. Am. Chem. Soc.* **2023,** *145* (20), 10960-10966.
9. Anderson, J. M.; Measom, N. D.; Murphy, J. A.; Poole, D. L., Bridge Heteroarylation of Bicyclo[1.1.1]pentane Derivatives. *Org. Lett.* **2023,** *25* (12), 2053-2057.
10. Yang, Y.; Tsien, J.; Hughes, J. M. E.; Peters, B. K.; Merchant, R. R.; Qin, T., An intramolecular coupling approach to alkyl bioisosteres for the synthesis of multisubstituted bicycloalkyl boronates. *Nat. Chem.* **2021,** *13* (10), 950-955.
11. Ma, X.; Han, Y.; Bennett, D. J., Selective Synthesis of 1-Dialkylamino-2-alkylbicyclo-[1.1.1]pentanes. *Org. Lett.* **2020,** *22* (22), 9133-9138.
12. Zhao, J.-X.; Chang, Y.-X.; He, C.; Burke, B. J.; Collins, M. R.; Del Bel, M.; Elleraas, J.; Gallego, G. M.; Montgomery, T. P.; Mousseau, J. J.; Nair, S. K.; Perry, M. A.; Spangler, J. E.; Vantourout, J. C.; Baran, P. S., 1,2-Difunctionalized bicyclo[1.1.1]pentanes: Long–sought-after mimetics for ortho/meta-substituted arenes. *Proceedings of the National Academy of Sciences* **2021,** *118* (28), e2108881118.
13. Garry, O. L.; Heilmann, M.; Chen, J.; Liang, Y.; Zhang, X.; Ma, X.; Yeung, C. S.; Bennett, D. J.; MacMillan, D. W. C., Rapid Access to 2-Substituted Bicyclo[1.1.1]pentanes. *J. Am. Chem. Soc.* **2023,** *145* (5), 3092-3100.

14. Che, J.-T.; Ding, W.-Y.; Zhang, H.-B.; Wang, Y.-B.; Xiang, S.-H.; Tan, B., Enantioselective synthesis of 2-substituted bicyclo[1.1.1]pentanes via sequential asymmetric imine addition of bicyclo[1.1.0]butanes and skeletal editing. *Nat. Chem.* **2025**.
15. Sharland, J. C.; Davies, H. M. L., One-Pot Synthesis of Difluorobicyclo[1.1.1]pentanes from α-Allyldiazoacetates. *Org. Lett.* **2023,** *25* (28), 5214-5219.
16. Guo, R.; Chang, Y.-C.; Herter, L.; Salome, C.; Braley, S. E.; Fessard, T. C.; Brown, M. K., Strain-Release [2π + 2σ] Cycloadditions for the Synthesis of Bicyclo[2.1.1]hexanes Initiated by Energy Transfer. *J. Am. Chem. Soc.* **2022,** *144* (18), 7988-7994.
17. Radhoff, N.; Daniliuc, C. G.; Studer, A., Lewis Acid Catalyzed Formal (3+2)-Cycloaddition of Bicyclo[1.1.0]butanes with Ketenes. *Angew. Chem. Int. Ed.* **2023,** *62* (34), e202304771.
18. Chintawar, C. C.; Laskar, R.; Rana, D.; Schäfer, F.; Van Wyngaerden, N.; Dutta, S.; Daniliuc, C. G.; Glorius, F., Photoredox-catalysed amidyl radical insertion to bicyclo[1.1.0]butanes. *Nat. Catal.* **2024,** *7* (11), 1232-1242.
19. Hu, S.; Pan, Y.; Ni, D.; Deng, L., Facile access to bicyclo[2.1.1]hexanes by Lewis acid-catalyzed formal cycloaddition between silyl enol ethers and bicyclo[1.1.0]butanes. *Nature Communications* **2024,** *15* (1), 6128.
20. Sarkar, D.; Deswal, S.; Chandra Das, R.; Biju, A. T., Lewis acid-catalyzed (3 + 2) annulation of bicyclobutanes with ynamides: access to 2-amino-bicyclo[2.1.1]hexenes. *Chem. Sci.* **2024,** *15* (39), 16243-16249.
21. Yu, T.; Yang, J.; Wang, Z.; Ding, Z.; Xu, M.; Wen, J.; Xu, L.; Li, P., Selective [2σ + 2σ] Cycloaddition Enabled by Boronyl Radical Catalysis: Synthesis of Highly Substituted Bicyclo[3.1.1]heptanes. *J. Am. Chem. Soc.* **2023,** *145* (7), 4304-4310.
22. Dutta, S.; Daniliuc, C. G.; Mück-Lichtenfeld, C.; Studer, A., Enantioselective Synthesis of Tetrahydro-1H-1,3-methanocarbazoles by Formal (3 + 3)-Cycloaddition Using Bicyclo[1.1.0]butanes. *J. Am. Chem. Soc.* **2025**.
23. Ma, X.; Pinto, W.; Pham, L. N.; Sloman, D. L.; Han, Y., Synthetic Studies of 2,2-Difluorobicyclo[1.1.1]pentanes (BCP-F2): The Scope and Limitation of Useful Building Blocks for Medicinal Chemists. *Eur. J. Org. Chem.* **2020,** *2020* (29), 4581-4605.
24. Ma, X.; Sloman, D. L.; Han, Y.; Bennett, D. J., A Selective Synthesis of 2,2-Difluorobicyclo[1.1.1]pentane Analogues: "BCP-F2". *Org. Lett.* **2019,** *21* (18), 7199-7203.
25. Bychek, R.; Mykhailiuk, P. K., A Practical and Scalable Approach to Fluoro-Substituted Bicyclo[1.1.1]pentanes. *Angew. Chem. Int. Ed.* **2022,** *61* (29), e202205103.
26. Dutta, S.; Lu, Y.-L.; Erchinger, J. E.; Shao, H.; Studer, E.; Schäfer, F.; Wang, H.; Rana, D.; Daniliuc, C. G.; Houk, K. N.; Glorius, F., Double Strain-Release [2π+2σ]-Photocycloaddition. *J. Am. Chem. Soc.* **2024,** *146* (8), 5232-5241.
27. Kadam, G. A.; Singha, T.; Rawat, S.; Hari, D. P., Rhodium(II)-Catalyzed Strain-Enabled Stereoselective Synthesis of Skipped Dienes. *ACS Catal.* **2024,** *14* (16), 12225-12233.
28. Jurberg, I. D.; Davies, H. M. L., Blue light-promoted photolysis of aryldiazoacetates. *Chem. Sci.* **2018,** *9* (22), 5112-5118.

29. Xiao, T.; Mei, M.; He, Y.; Zhou, L., Blue light-promoted cross-coupling of aryldiazoacetates and diazocarbonyl compounds. *Chem. Commun.* **2018,** *54* (64), 8865-8868.
30. Hommelsheim, R.; Guo, Y.; Yang, Z.; Empel, C.; Koenigs, R. M., Blue-Light-Induced Carbene-Transfer Reactions of Diazoalkanes. *Angew. Chem. Int. Ed.* **2019,** *58* (4), 1203-1207.
31. Yang, Z.; Stivanin, M. L.; Jurberg, I. D.; Koenigs, R. M., Visible light-promoted reactions with diazo compounds: a mild and practical strategy towards free carbene intermediates. *Chem. Soc. Rev.* **2020,** *49* (19), 6833-6847.
32. Zhang, Z.; Gevorgyan, V., Visible Light-Induced Reactions of Diazo Compounds and Their Precursors. *Chem. Rev.* **2024,** *124* (11), 7214-7261.
33. Rybicka-Jasińska, K.; Shan, W.; Zawada, K.; Kadish, K. M.; Gryko, D., Porphyrins as Photoredox Catalysts: Experimental and Theoretical Studies. *J. Am. Chem. Soc.* **2016,** *138* (47), 15451-15458.
34. Li, F.; Pei, C.; Koenigs, R. M., Photocatalytic gem-Difluoroolefination Reactions by a Formal C−C Coupling/Defluorination Reaction with Diazoacetates. *Angew. Chem. Int. Ed.* **2022,** *61* (4), e202111892.
35. Langletz, T.; Empel, C.; Jana, S.; Koenigs, R. M., Stereoconvergent, photocatalytic cyclopropanation reactions of β-substituted styrenes with ethyl diazoacetate. *Tetrahedron Chem* **2022,** *3*.
36. Zhu, S.; Li, F.; Empel, C.; Jana, S.; Pei, C.; Koenigs, R. M., Furan Synthesis via Triplet Sensitization of Acceptor/Acceptor Diazoalkanes. *Adv. Synth. Catal.* **2022,** *364* (18), 3149-3154.
37. Empel, C.; Jana, S.; Ciszewski, Ł. W.; Zawada, K.; Pei, C.; Gryko, D.; Koenigs, R. M., C−H Functionalization of Heterocycles with Triplet Carbenes by means of an Unexpected 1,2-Alkyl Radical Migration. *Chem. Eur. J.* **2023,** *29* (29), e202300214.
38. Dkhar, P. G. S.; Lyngdoh, R. H. D., Transition states for hydride and methyl 1,2-migrations in carbene rearrangements to alkenes : An AM1 SCF-MO study. *Indian Journal of Chemistry Section B-organic Chemistry Including Medicinal Chemistry* **2005,** *44*, 2138-2148.
39. DeAngelis, A.; Panish, R.; Fox, J. M., Rh-Catalyzed Intermolecular Reactions of α-Alkyl-α-Diazo Carbonyl Compounds with Selectivity over β-Hydride Migration. *Acc. Chem. Res.* **2016,** *49* (1), 115-127.

Appendix A. Chapter 2 Supporting Information

CAUTION: Diazo compounds are high energy compounds and need to be treated with respect. Even though we experienced no energetic decomposition in this work, care should be taken in handling large quantities of diazo compounds. Large scale reactions should be conducted behind a blast shield. For a more complete analysis of the risks associated with diazo compounds see the recent review by Bull et. al.[1]

General Considerations

All experiments were carried out in flame-dried glassware under argon atmosphere unless otherwise stated. Flash column chromatography was performed on silica gel. Unless otherwise noted, all other reagents were obtained from commercial sources (Sigma Aldrich, Fisher, TCI Chemicals, AK Scientific, Combi Blocks, Oakwood Chemicals, Ambeed) and used as received without purification. ^{1}H, ^{13}C, and ^{19}F NMR spectra were recorded at either 400 MHz (^{13}C at 100 MHz) on Bruker 400 spectrometer or 600 MHz (^{13}C at 151 MHz) on INOVA 600 or Bruker 600 spectrometer. NMR spectra were run in solutions of deuterated chloroform ($CDCl_3$) with residual chloroform taken as an internal standard (7.26 ppm for ^{1}H, and 77.16 ppm for ^{13}C), and were reported in parts per million (ppm). The abbreviations for multiplicity are as follows: s = singlet, d = doublet, t = triplet, q = quartet, p = pentet, m = multiplet, dd = doublet of doublet, etc. Coupling constants (J values) are obtained from the spectra. Thin layer chromatography was performed on aluminum-back silica gel plates with UV light and cerium aluminum molybdate (CAM) stain to visualize. Mass spectra were taken on a Thermo Finnigan LTQ-FTMS spectrometer with APCI or ESI. Melting points (mp) were measured in open capillary tubes with a Mel-Temp Electrothermal melting points apparatus and are uncorrected. IR spectra were collected on a Nicolet iS10 FT-IR spectrometer from Thermo Scientific and reported in unit of cm-1. Enantiomeric excess (% ee) data were

obtained on an Agilent 1100 HPLC or an Agilent 1290 Infinity UHPLC, eluting the purified products using a mixed solution of HPLC-grade 2-propanol (i-PrOH) and n-hexane.

Preparation of Known Compounds

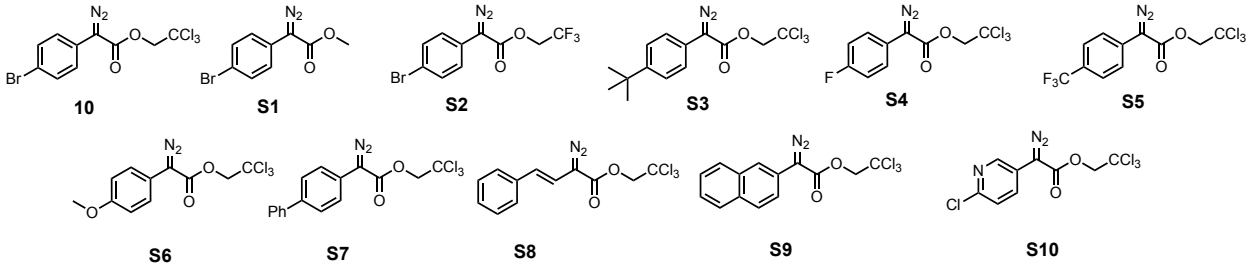

Diazo compound **10**, **S3**, **S4**, **S5**, **S10** were prepared according to the established literature and matched the reported spectra.[2]
Diazo compound **S2**, **S6**, **S8**, and **S9** were prepared according to the established literature and matched the reported spectra.[3]

Diazo compound **S1** was prepared according to the established literature and matched the reported spectra.[4]

Diazo compound **S7** was prepared according to the established literature and matched the reported spectra.[5]

Preparation of carboxylic acid ligands:

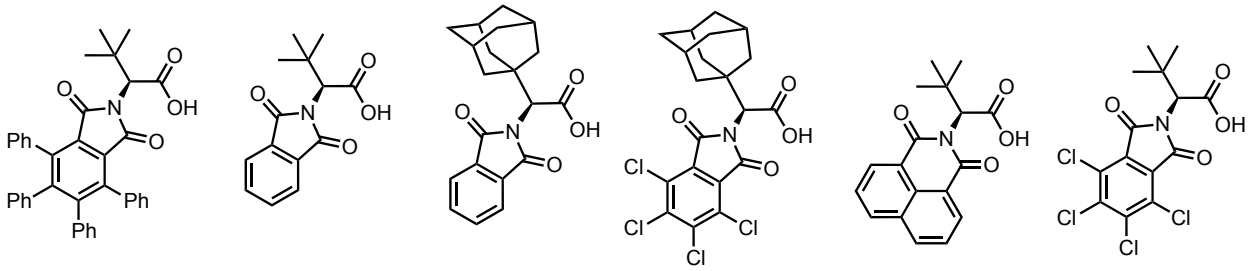

S12 **S13** **S14** **S15** **S16** **S17**

Ligand **S12**, **S13**, **S14**, **S15**, **S16**, and **S17** were prepared according to the established literature and matched the reported spectra.[6-10]

Preparation of known catalysts:

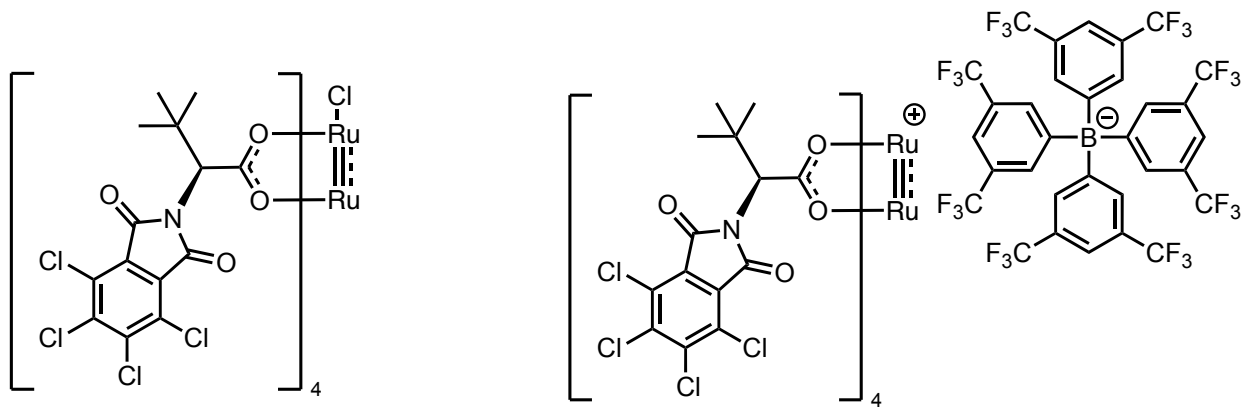

S18 **S19**

Catalyst **S18** and **S19** were prepared according to the established literature and matched the reported spectra.[10]

Preparation of Diazo Compounds

2,2,2-Trichloroethyl 2-diazo-2-(3-iodophenyl)acetate (S11)

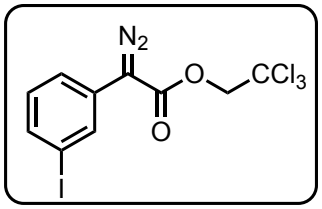

To a solution of 2-nitrobenzensulfonyl azide (2.6 g, 11 mmol, 1.5 equiv), and 2,2,2-trichloroethyl 2-(3-iodophenyl)acetate (3.0 g, 7.5 mmol, 1.0 equiv) dissolved in 50 mL of acetonitrile at 0 °C was added 2,3,4,5,6,7,8,9,10-octahydropyrido[1,2-a][1,3]diazepine (2.5 mL, 17 mmol, 2.2 equiv) slowly. Once addition was complete, the solution was allowed to stir for 1 h. Then, saturated NH_4Cl solution (50 mL) was added to the flask. The resulting solution was poured into a 250 mL separatory funnel and diluted with ether, washed with water (3x 20 mL) and brine (3x 15 mL) then dried over $MgSO_4$ and concentrated to afford a crude yellow solid. The crude material was purified through column chromatography (0% hexanes/diethyl ether, 0-2% hexanes/diethyl ether) to afford a yellow solid (2.26 g, 72%).

1H NMR (600 MHz, $CDCl_3$): δ 7.91 (t, J=1.7 Hz, 1H), 7.57 (ddd, J = 7.9, 1.7, 1.0 Hz, 1H), 7.46 (m, H), 7.15 (t, J = 7.9 Hz, 1H), 4.94 (s, 2H);

^{13}C NMR (151 MHz, $CDCl_3$): δ 162.8, 135.2, 132.5, 130.5, 127.0, 123.0, 94.9, 73.9.

HMRS (+p APCI): calcd for $C_{10}H_7O_2{}^{35}Cl_3{}^{127}I$ [-N_2] 390.8551, found 390.8548.

IR (neat): 2094, 1710, 1585, 1554, 1475, 1373, 1343, 1273, 1238, 1140, 1087, 1043, 990, 934, 826, 777, 717, 702, 678, 577 (cm^{-1}).

Cyclopropanation Reactions

General Procedure 1

To a flame dried vial equipped with a stir bar and 4Å MS (100 weight%) under inert atmosphere was added catalyst (1 mol %) and substrate (0.50 mmol, 2.5 equiv) which was subsequently dissolved in 2 mL of DCM. Then, the diazo compound (0.20 mmol, 1.0 equiv) was dissolved in 2 mL of DCM and added to the reaction vial over a period of 2 h using a syringe pump. The reaction was left to stir at room temperature for 18 h. Once completed the reaction solution was passed through a small silica plug to remove ruthenium catalyst, concentrated in vacuo, and purified through flash chromatography (0-18% hexanes/diethyl ether) to afford the desired product.

General Procedure 2

To a flame dried vial equipped with a stir bar and 4Å MS (100 weight%) under inert atmosphere was added catalyst (1 mol %) and substrate (2.0 mmol, 10 equiv) which was subsequently dissolved in 2 mL of DCM. Then, the diazo compound (0.20 mmol, 1.0 equiv) was dissolved in 2 mL of DCM and added to the reaction vial over a period of 2 h using a syringe pump. The reaction was run at room temperature for 18 h. Once completed the reaction solution was passed through a small silica plug to remove ruthenium catalyst, concentrated in vacuo, and purified through flash chromatography (0-18% hexanes/diethyl ether) to afford the desired product.

2,2,2-Trichloroethyl (1S,2R)-1-(4-bromophenyl)-2-phenylcyclopropane-1-carboxylate (12)

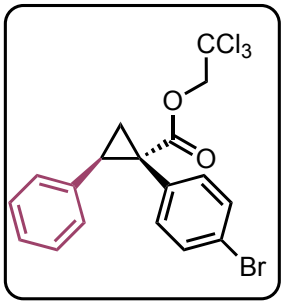

General procedure 1 was employed for the cyclopropanation of styrene (57.5 µL, 0.5 mmol, 2.5 equiv) with 2,2,2-trichloroethyl 2-(4-bromophenyl)-2-diazoacetate (0.2 mmol, 74.5 mg, 1.0 equiv) using Ru_2(*S*-TPPTTL)$_4$BAr^F (6.6 mg, 1 mol %) as catalyst. Purification by column chromatography afforded an amorphous solid (63 mg, 70%). Spectra matched literature precedent.[3]

^{1}H NMR (400 MHz, $CDCl_3$) δ 7.31 (d, J = 8.5 Hz, 2H), δ 7.15 (dd, J = 5.0, 1.9 Hz, 3H), δ 6.98 (d, J = 8.5 Hz, 2H), δ 6.85 (m, 2H), 4.88 (d, J = 11.9 Hz, 1H), δ 4.69 (d, J = 11.9 Hz, 1H), δ 3.27 (dd, J = 9.4, 7.5 Hz, 1H), δ 2.33 (dd, J = 9.4, 5.2 Hz, 1H), δ 2.02 (dd, J = 7.5, 5.2 Hz, 1H).

Chiral HPLC: The enantiopurity was determined to be 92:8 er by chiral HPLC analysis (Chiracel AD-H, 1.0% IPA/Hexanes, 1.0 mL/min, λ=230 nm, RT: Major: 6.7 min, Minor: 8.5 min).

2,2,2-Trichloroethyl (1S,2R)-1-(4-bromophenyl)-2-(4-(tert-butyl)phenyl)cyclopropane-1-carboxylate (20)

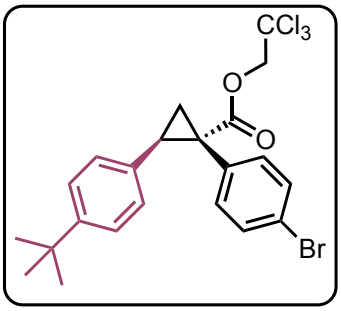

General procedure 1 was employed for the cyclopropanation of 1-(*tert*-butyl)-4-vinylbenzene (91.6 µL, 0.5 mmol, 2.5 equiv) with 2,2,2-trichloroethyl 2-(4-bromophenyl)-2-diazoacetate (0.2 mmol, 74.5 mg, 1.0 equiv) using Ru_2(S-TPPTTL)$_4$BAr^F (6.6 mg, 1 mol %) as catalyst. Purification by column chromatography afforded an oil (66 mg, 65%)

^{1}H NMR (600 MHz, $CDCl_3$): δ 7.27 (d, J = 8.5 Hz, 2H), δ 7.13 (d, J = 8.5 Hz, 2H), δ 6.96 (d, J = 8.5 Hz, 2H), δ 6.73 (d, J = 8.5 Hz, 2H), δ 4.84 (d, J = 11.9 Hz, 1H), δ 4.64 (d, J = 11.9 Hz, 1H), δ 3.18 (dd, J = 9.4, 7.5, 1H), δ 2.28 (dd, J = 9.4, 5.1 Hz, 1H), δ 1.93 (dd, J = 7.5, 5.1 Hz, 1H), δ 1.24 (s, 1H);

^{13}C NMR (151 MHz, $CDCl_3$): δ 171.7, 149.9, 133.8, 133.1, 132.2, 130.9, 127.8, 124.9, 121.5, 95.0, 74.4, 65.9, 36.5, 34.4, 33.8, 31.3, 20.5, 15.3.

HRMS (+p APCI): calcd for C22H23BrCl3O2 (M+H)+ 502.9942 found 502.9945.

Chiral HPLC: The enantiopurity was determined to be 90:10 er by chiral HPLC analysis (Chiracel OD-H, 1.0% IPA/Hexanes, 1.0 mL/min, λ=230 nm, RT: Major: 7.2 min, Minor: 4.7 min).

2,2,2-Trichloroethyl (1*S*,2*R*)-1-(4-bromophenyl)-2-(4-fluorophenyl)cyclopropane-1-carboxylate (21)

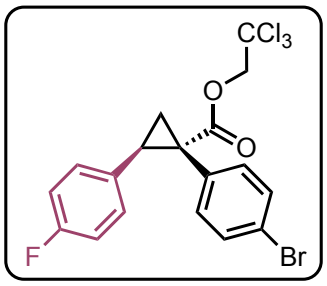

General procedure 1 was employed for the cyclopropanation of 1-fluoro-4-vinylbenzene (91.6 µL, 0.5 mmol, 2.5 equiv) with 2,2,2-trichloroethyl 2-(4-bromophenyl)-2-diazoacetate (0.2 mmol, 74.48 mg, 1.0 equiv) using Ru_2(*S*-TPPTTL)$_4$BAr^F (6.6 mg, 1 mol %) as catalyst. Purification by column chromatography afforded an amorphous solid (64 mg, 68%). Spectrum matched literature precedent.[3]

^{1}H NMR(400 MHz, $CDCl_3$) δ 7.28 (d, J = 8.4 Hz, 2H), δ 6.93 (d, J = 8.4 Hz, 2H), δ 6.78 (m, 4H), δ 4.83 (d, J = 11.9 Hz, 1H), δ 4.64 (d, J = 11.9 Hz, 1H), δ 3.20 (dd, J = 9.4, 7.4 Hz, 1H), δ 2.28 (dd, J = 9.4, 5.3 Hz, 1H), δ 1.92 (dd, J = 7.4, 5.3 Hz, 1H).

Chiral HPLC: The enantiopurity was determined to be 89:11 er by chiral HPLC analysis (Chiracel AD-H, 1.0% IPA/Hexanes, 1.0 mL/min, λ=230 nm, RT: Major: 6.9 min, Minor: 9.2 min).

2,2,2-Trichloroethyl (1*S*,2*R*)-1-(4-bromophenyl)-2-(naphthalen-2-yl)cyclopropane-1-carboxylate (22)

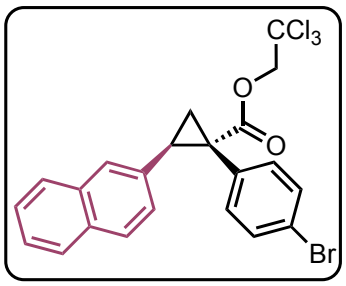

This structure was synthesized through general procedure 1. 2-Vinylnaphthalene (77.1 mg, 0.5 mmol, 2.5 equiv), 2,2,2-trichloroethyl 2-(4-bromophenyl)-2-diazoacetate (0.2 mmol, 74.5 mg, 1.0 equiv), and Ru_2(*S*-TPPTTL)$_4$BAr^F (6.6 mg, 1 mol %) were added to the reaction. The reaction was run overnight in 4 mL of DCM. Purification by column chromatography afforded an amorphous solid (66 mg, 66%). Spectra matched literature precedent.[11]

^{1}H NMR (400 MHz, $CDCl_3$) δ 7.75 (m, 1H), δ 7.68 (m, 1H), δ 7.60 (d, J = 8.5 Hz, 1H), δ 7.44 (m, 2H), δ 7.40 (m, 1H), δ 7.25 (d, J = 8.5 Hz, 2H), δ 7.02 (d, J = 8.5 Hz, 2H), δ 6.88 (dd, J = 8.5, 1.8 Hz, 1H), δ 4.89 (d, J = 11.9 Hz, 1H), δ 4.71 (d, J = 11.9 Hz, 1H), δ 3.43 (dd, J = 9.4, 7.4 Hz, 1H), δ 2.40 (dd, J = 9.4, 5.2, 1H), δ 2.14 (dd, J = 7.5, 5.2 Hz, 1H).

Chiral HPLC: The enantiopurity was determined to be 88:12 er by chiral HPLC analysis (Chiracel OD-H, 1.0% IPA/Hexanes, 1.0 mL/min, λ=230 nm, RT: Major: 13.0 min, Minor: 11.9 min).

2,2,2-Trichloroethyl (1*S*,2*R*)-1-(4-bromophenyl)-2-(*p*-tolyl)cyclopropane-1-carboxylate (23)

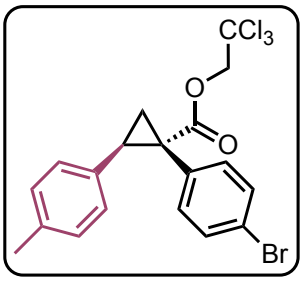

This structure was synthesized through general procedure 1. 1-Methyl-4-vinylbenzene (65.9 µL, 0.5 mmol, 2.5 equiv), 2,2,2-trichloroethyl 2-(4-bromophenyl)-2-diazoacetate (0.2 mmol, 74.5 mg, 1.0 equiv), and Ru_2(*S*-TPPTTL)$_4$BAr^F (6.6 mg, 1 mol %) were added to the reaction. The reaction was run overnight in 4 mL of DCM. Purification by column chromatography afforded a crystalline solid (69 mg, 75%):

MP: 95-98 °C

^{1}H NMR (600 MHz, $CDCl_3$) δ 7.30 (d, J = 8.5 Hz, 2H), δ 6.97 (d, J = 8.5 Hz, 2H), δ 6.94 (d, J = 8.2 Hz, 2H), δ 6.71 (d, J = 8.2 Hz, 2H), δ 4.85 (d, J = 11.9 Hz, 1H), δ 4.66 (d, J = 11.9 Hz, 1H), δ 3.21 (dd, J = 9.4, 7.45Hz, 1H), δ 2.29 (dd, J = 9.4, 5.1 Hz, 1H), δ 2.26 (s, 3H), δ 1.96 (dd, J = 7.5, 5.1 Hz, 1H).

^{13}C NMR (151 MHz, $CDCl_3$) δ 171.7, 136.5, 133.7. 133.1. 132.2, 130.9, 128.8, 121.5, 95.0, 74.4, 36.5, 33.9, 21.0, 20.3.

HRMS (+p APCI) calcd for $C_{19}H_{17}BrCl_3O_2$ (M+H) 460.9472 found 460.9471.

Chiral HPLC: Enantiopurity was determined to be 96:4 er by chiral HPLC analysis (Chiracel AD-H, 1.0% IPA/Hexanes, 1.0 mL/min, λ=230 nm, RT: Major: 6.9 min, Minor: 5.9 min)

2,2,2-Trichloroethyl (1*S*,2*R*)-1-(4-bromophenyl)-2-(4-chlorophenyl)cyclopropane-1-carboxylate (24)

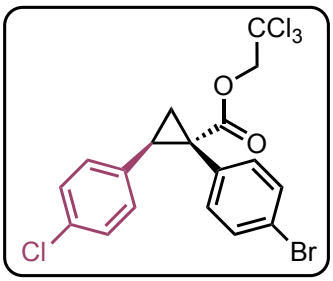

General procedure 1 was employed for the cyclopropanation of 1-methyl-4-vinylbenzene (60.0 µL, 0.5 mmol, 2.5 equiv) with 2,2,2-trichloroethyl 2-(4-bromophenyl)-2-diazoacetate (0.2 mmol, 74.5 mg, 1.0 equiv) using Ru_2(*S*-TPPTTL)$_4$BAr^F (6.6 mg, 1 mol %) as catalyst. Purification by column chromatography afforded an amorphous solid (73.6 mg, 76%). Spectra matched literature precedent.[3]

^{1}H NMR (400 MHz, $CDCl_3$) δ 7.29 (d, J = 8.5 Hz, 2H), δ 7.08 (d, J = 8.5 Hz, 2H), δ 6.93 (d, J = 8.5 Hz, 2H), δ 6.73 (d, J = 8.5 Hz, 2H), 4.82 (d, J = 11.9 Hz, 1H), δ 4.64 (d, J = 11.9 Hz, 1H), δ 3.18 (dd, J = 9.4, 7.4 Hz, 1H), δ 2.29 (dd, J = 9.4, 5.3 Hz, 1H), δ 1.92 (dd, J = 7.4, 5.3 Hz, 1H).

Chiral HPLC: Enantiopurity was determined to be 91:9 by chiral HPLC analysis (Chiracel AD-H, 1.0% IPA/Hexanes, 1.0 mL/min, λ=230 nm, RT: Major: 10.1 min, Minor: 7.5 min)

2,2,2-Trichloroethyl (1*S*,2*R*)-2-([1,1'-biphenyl]-4-yl)-1-(4-bromophenyl)cyclopropane-1-carboxylate (25)

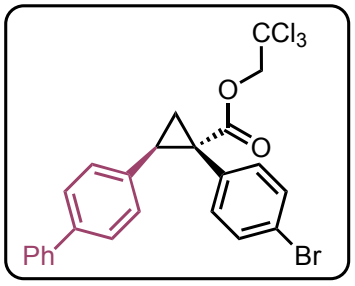

General procedure 1 was employed for the cyclopropanation of 4-vinyl-1,1'-biphenyl (0.5 mmol, 90.1 mg, 2.5 equiv) with 2,2,2-trichloroethyl 2-(4-bromophenyl)-2-diazoacetate (0.2 mmol, 74.5 mg, 1.0 equiv) using Ru_2(*S*-TPPTTL)$_4$BAr^F (6.6 mg, 1 mol %) as catalyst. Purification by column chromatography afforded a crystalline solid (49.3 mg, 47%):

MP: 145-147 °C

^{1}H NMR (600 MHz, $CDCl_3$) δ 7.53 (d, J = 8.3 Hz, 2H), δ 7.41 (dd, J = 8.5, 7.0 Hz, 2H), δ 7.37 (d, J = 8.3 Hz, 2H), δ 7.33 (m, 1H), δ 7.29 (d, J = 8.5, 2H), δ 6.99 (d, J = 8.5 Hz, 2H), δ 6.87 (d, J = 8.3 Hz, 2H) δ 4.85 (d, J = 11.9, 1H), δ 4.67 (d, J = 11.9 Hz, 1H), δ 3.26 (dd, J = 9.4, 7.5 Hz, 1H), δ 2.33 (dd, J = 9.4, 5.2 Hz, 1H), δ 2.00 (dd, 7.5, 5.2 Hz, 1H).

^{13}C NMR (151 MHz, $CDCl_3$) δ 171.6, 140.4, 139.6, 134.4, 133.7, 132.9, 131.1, 128.8, 127.3, 126.9, 126.7, 121.7, 94.9, 74.4, 36.8, 33.7, 20.6.

HRMS (+p APCI) calcd for $C_{24}H_{19}BrCl_3O_2$ (M+H) 522.9628 found 522.9631.

Chiral HPLC: Enantiopurity was determined to be 90:10 er by chiral HPLC analysis (Chiracel AD-H, 1.0% IPA/Hexanes, 1.0 mL/min, λ=254 nm, RT: Major: 8.5 min, Minor: 12.7 min).

2,2,2-Trichloroethyl (1*S*,2*R*)-2-(4-acetoxyphenyl)-1-(4-bromophenyl)cyclopropane-1-carboxylate (26)

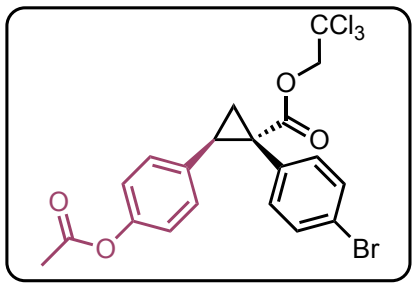

General procedure 1 was used for the cyclopropanation of 4-vinylphenyl acetate (77.5 µL, 0.5 mmol, 2.5 equiv), with 2,2,2-trichloroethyl 2-(4-bromophenyl)-2-diazoacetate (0.2 mmol, 74.5 mg, 1.0 equiv) using Ru_2(*S*-TPPTTL)$_4$BAr^F (6.6 mg, 1 mol %). The reaction was run overnight in 4 mL of DCM. Purification by column chromatography afforded a crystalline solid (55.7 mg, 55%). Spectra matched literature precedent.[3]

^{1}H NMR (400 MHz, $CDCl_3$) δ 7.07 (m, 3H), δ 6.98 (d, J = 8.1 Hz, 2H), δ 6.89 (d, J = 8.3 Hz, 2H), δ 6.83 (d, J = 8.3 Hz, 2H), δ 4.86 (d, J = 11.9 Hz, 1H), δ 4.67 (d, J = 11.9 Hz, 1H), δ 3.24 (dd, J = 9.4, 7.4 Hz, 1H), δ 1.95 (s, 3H), δ 1.95 (dd, J = 7.43, 5.29 Hz, 1H). Other cyclopropane proton signal falls under the methyl singlet at δ 1.95.

Chiral HPLC: Enantiopurity was determined to be 91:9 er by chiral HPLC analysis (Chiracel AD-H, 1.0% IPA/Hexanes, 1.0 mL/min, λ=230 nm, RT: Major: 15.4 min, Minor: 29.9 min).

2,2,2-Trichloroethyl (1*S*,2*S*)-1-(4-bromophenyl)-2-butylcyclopropane-1-carboxylate (27)

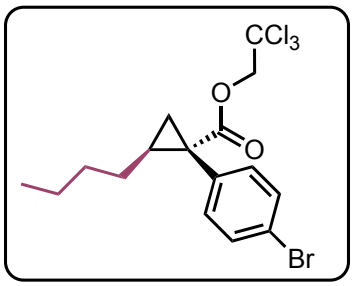

General procedure 2 was employed for the cyclopropanation of hex-1-ene (250 µL, 2.0 mmol, 10 equiv) with 2,2,2-trichloroethyl 2-(4-bromophenyl)-2-diazoacetate (0.2 mmol, 74.5 mg, 1.0 equiv) using Ru_2(*S*-TPPTTL)$_4$BAr^F (6.6 mg, 1 mol %) as catalyst. Purification by column chromatography afforded an oil (68.4 mg, 80%). Spectra matched literature precedent.[12]

^{1}H NMR (400 MHz, $CDCl_3$): δ 7.48 (d, 8.4 Hz, 2H), δ 7.21 (d, 8.4 Hz, 2H), δ 4.81 (d, J = 12.0 Hz, 1H), δ 4.56 (d, J = 12.0 Hz, 1H), δ 1.95 (m, 1H), δ 1.88 (dd, J = 9.2, 4.2 Hz, 1H), δ 1.39 (m, 3H), δ 1.28 (m, 2H), δ 1.20 (dd, J = 6.9, 4.3 Hz, 1H), δ 0.85 (t, J = 7.3 Hz, 3H), δ 0.60 (ddd, J = 11.9, 9.7, 7.1 Hz, 1H).

Chiral HPLC: Enantiopurity was determined to be 96:3 er by chiral HPLC analysis (R,R-Whelk, 0.0% IPA/Hexanes, 1.0 mL/min, λ=230 nm, RT: Major: xx min, Minor: xx min).

2,2,2-Trichloroethyl (1*S*,2*S*)-1-(4-bromophenyl)-2-isobutylcyclopropane-1-carboxylate (28)

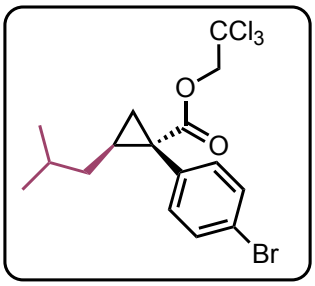

General procedure 2 was employed for the cyclopropanation of 4-methylpent-1-ene (257 µL, 2.0 mmol, 10 equiv) with 2,2,2-trichloroethyl 2-(4-bromophenyl)-2-diazoacetate (0.2 mmol, 74.5 mg, 1.0 equiv) using Ru_2(*S*-TPPTTL)$_4$BAr^F (6.6 mg, 1 mol %) as catalyst. Purification by column chromatography afforded an oil (67.8 mg, 79%). Spectra matched literature precedent.[12]

^{1}H NMR (400 MHz, $CDCl_3$): δ 7.48 (d, J = 8.5 Hz, 2H), δ 7.20 (d, J = 8.5 Hz, 2H), δ 4.81 (d, J = 11.9 Hz, 1H), δ 4.6 (d, J = 11.9 Hz, 1H), δ 1.99 (m, 1H), δ 1.92 (dd, J = 9.2, 4.2 Hz, 1H), δ 1.70 (dq, J = 13.4, 6.7 Hz, 1H), δ 1.40 (ddd, 13.8, 6.5, 4.3 Hz, 1H), δ 1.22 (dd, 6.9, 4.2 Hz, 1H), δ 0.90 (dd, J = 6.7, 2.7 Hz, 6H), δ 0.36 (ddd, J = 13.8, 9.7, 7.2 Hz, 1H).

HPLC Chiral: Enantiopurity was determined to be 97:3 er by chiral HPLC analysis (R,R-Whelk, 0.0% IPA/Hexanes, 1.0 mL/min, λ=230 nm, RT: Major: 14.4 min, Minor: 27.4 min).

2,2,2-Trichloroethyl (1*S*,2*S*)-1-(4-bromophenyl)-2-((triMethylsilyl)Methyl)cyclopropane-1-carboxylate (29)

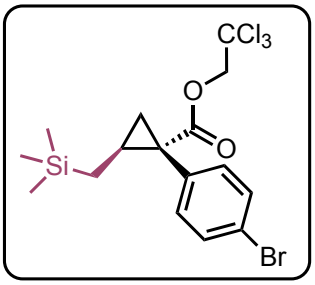

General procedure 2 was employed for the cyclopropanation of allyltrimethylsilane (320 µL, 2.0 mmol, 10 equiv) with 2,2,2-trichloroethyl 2-(4-bromophenyl)-2-diazoacetate (0.2 mmol, 74.5 mg, 1.0 equiv) using Ru_2(*S*-TPPTTL)$_4$BAr^F (6.6 mg, 1 mol %) as catalyst. Purification by column chromatography afforded an oil (71.6 mg, 88%). Spectra matched literature precedent.[12]

^{1}H NMR (400 MHz, $CDCl_3$) δ 7.49 (d, J = 8.4 Hz, 2H), δ 7.19 (d, J = 8.4 Hz, 2H), δ 4.80 (d, J = 11.9 Hz, 1H), δ 4.58 (d, J = 11.9 Hz, 1H), δ 1.97 (m, 2H), δ 1.12 (q, 3.3 Hz, 1H), δ 0.86 (ddd, J = 14.4, 2.7, 1.3 Hz, 1H), δ 0.04 (s, 9H), δ -0.44 (m, 1H).

Chiral HPLC: Enantiopurity was determined to be 96:4 er by chiral HPLC analysis (R,R-Whelk, 0.0% IPA/Hexanes, 1.0 mL/min, λ=230 nm, RT: Major: 14.0 min, Minor: 27.7 min).

2,2,2-Trichloroethyl (1*S*,2*S*)-1-(4-bromophenyl)-2-phenethylcyclopropane-1-carboxylate (30)

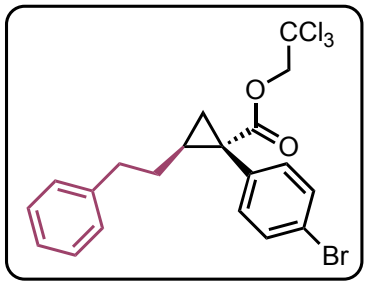

General procedure 2 was employed for the cyclopropanation of but-3-en-1-ylbenzene (300 µL, 2.0 mmol, 10 equiv) with 2,2,2-trichloroethyl 2-(4-bromophenyl)-2-diazoacetate (0.2 mmol, 74.5 mg, 1.0 equiv) using Ru_2(*S*-TPPTTL)$_4$BAr^F (6.6 mg, 1 mol %) as catalyst. Purification by column chromatography afforded an oil (51.6 mg, 60%). Spectra matched literature precedent.[12]

^{1}H NMR (400 MHz, $CDCl_3$): δ 7.48 (d, J = 8.5 Hz, 2H), δ 7.28 (m, 2H), δ 7.21 (d, J = 8.5 Hz, 3H), δ 7.11 (m, 2H), δ 4.81 (d, J = 11.9 Hz, 1H), δ 4.59 (d, J = 11.9 Hz, 1H), δ 2.71 (m, 2H), δ 2.03 (tdd, J = 9.0, 7.0, 5.2 Hz, 1H), δ 1.89 (ddd, J = 9.0, 4.5, 0.70 Hz, 1H), δ 1.70 (m, 1H), δ 1.21 (dd, J = 7.0, 4.5 Hz, 1H), δ 0.97 (dtd, J = 13.9, 9.0, 6.4 Hz, 1H).

Chiral HPLC The enantiopurity was determined to be 88:12 er by chiral HPLC analysis (Chiracel AD-H, 1.0% IPA/Hexanes, 1.0 mL/min, λ=230 nm, RT: Major: 6.6 min, Minor: 7.6 min).

2,2,2-Trichloroethyl (1*S*,2*R*)-1-(4-bromophenyl)-2-(2-(*tert*-butoxy)-2-oxoethyl)cyclopropane-1-carboxylate (31)

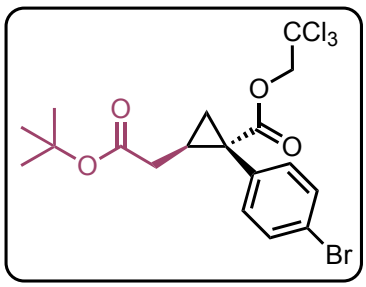

General procedure 2 was employed for the cyclopropanation of *tert*-butyl but-3-enoate (324 µL, 2.0 mmol, 10 equiv) with 2,2,2-trichloroethyl 2-(4-bromophenyl)-2-diazoacetate (0.2 mmol, 74.5 mg, 1.0 equiv) using Ru_2(*S*-TPPTTL)$_4$BAr^F (6.6 mg, 1 mol %) as catalyst. Purification by column chromatography afforded an oil (20.5 mg, 21%):

^{1}H NMR (400 MHz, $CDCl_3$) δ 7.46 (d, J = 8.4 Hz, 2H), 7.18 (d, J = 8.4 Hz, 2H), 4.80 (d, J = 11.9 Hz, 1H), 4.57 (d, J = 11.9 Hz, 1H), 2.31 (dq, J = 9.0, 7.0 Hz, 1H), 2.05-1.86 (m, 3H), 1.42 (s, 9H), 1.28 (dd, J = 7.0, 4.9 Hz, 1H).

^{13}C NMR (101 MHz, $CDCl_3$) δ 171.9, 170.9, 133.7, 133.1, 131.4, 121.9, 94.9, 80.9, 74.4, 36.1, 32.7, 28.1, 24.6, 20.6.

HRMS (+p APCI): calcd for $C_{18}H_{21}BrCl_3O_4$ [M+H] 484.9600 found 484.9497.

Chiral HPLC The enantiopurity was determined to be 96:4 er by chiral HPLC analysis (Chiracel AD-H, 1.0% IPA/Hexanes, 1.0 mL/min, λ=230 nm, RT: Major: 9.0 min, Minor: 9.6 min).

Methyl (1*S*,2*R*)-1-(4-bromophenyl)-2-phenylcyclopropane-1-carboxylate (32)

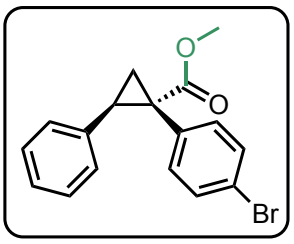

General procedure 1 was employed for the cyclopropanation of styrene (57.5 µL, 0.5 mmol, 2.5 equiv) with methyl 2-(4-bromophenyl)-2-diazoacetate (0.2 mmol, 51.0 mg, 1.0 equiv) using Ru_2(*S*-TPPTTL)$_4$BAr^F (6.6 mg, 1 mol %) as catalyst. Purification by column chromatography afforded an amorphous solid (39.6 mg, 60%). Spectra matched literature precedent.[4]

^{1}H NMR (400 MHz, $CDCl_3$) δ 7.29 (m, 2H), δ 7.12 (m, 3H), δ 6.92 (d, J = 8.0 Hz, 2H), δ 6.81 (dd, J = 6.5, 3.0 Hz, 2H), δ 3.69 (s, 3H), δ 3.15 (dd, J = 9.4, 7.3 Hz, 1H), δ 2.17 (dd, J = 9.4, 5.0 Hz, 1H), 1.87 (dd, J = 7.3, 5.0 Hz, 1H).

Chiral HPLC: The enantiopurity was determined to be 83:17 er by chiral HPLC analysis (Chiracel OD-H, 1.0% IPA/Hexanes, 0.5 mL/min, λ=230 nm, RT: Major: 15.7 min, Minor: 18.7 min).

2,2,2-Trifluoroethyl (1*S*,2*R*)-1-(4-bromophenyl)-2-phenylcyclopropane-1-carboxylate (33)

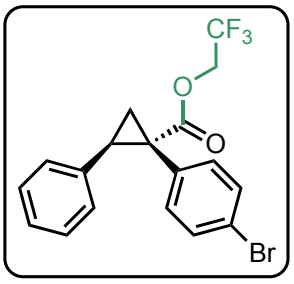

General procedure 1 was employed for the cyclopropanation of styrene (57.5 µL, 0.5 mmol, 2.5 equiv) with 2,2,2-trifluoroethyl 2-(4-bromophenyl)-2-diazoacetate (0.2 mmol, 64.6 mg, 1.0 equiv) using Ru_2(*S*-TPPTTL)$_4$BAr^F (6.6 mg, 1 mol %) as catalyst. Purification by column chromatography afforded an amorphous solid (51.8 mg, 65%). Spectra matched literature precedent.[3]

^{1}H NMR (400 MHz, $CDCl_3$) δ 7.46 (d, J = 8.5 Hz, 2H), δ 7.14 (d, J = 8.5 Hz, 2H), δ 4.50 (dq, J = 12.7, 8.4 Hz, 1H), δ 4.32 (dq, J = 12.7, 8.4 Hz, 1H), δ 1.89 (tdd, J = 9.0, 6.8, 4.3 Hz, 1H), δ 1.80 (dd, J = 9.0, 4.3 Hz, 1H), δ 1.36 (m, 3H), δ 1.24 (m, 2H), δ 1.17 (dd, J = 6.8, 4.3 Hz, 1H), δ 0.83 (t, J = 7.2 Hz, 3H), δ 0.53 (m, 1H).

Chiral HPLC: The enantiopurity was determined to be 90:10 er by chiral HPLC analysis (Chiracel AD-H, 1.0% IPA/Hexanes, 1.0 mL/min, λ=230 nm, RT: Major: 5.8 min, Minor: 6.6 min).

2,2,2-Trichloroethyl (1*S*,2*R*)-2-phenyl-1-(4-(trifluoroMethyl)phenyl)cyclopropane-1-carboxylate (34)

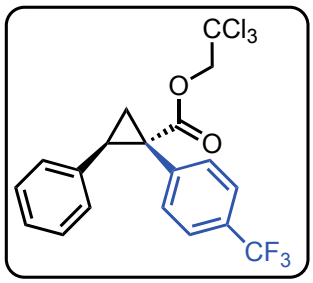

General procedure 1 was employed for the cyclopropanation of styrene (57.5 µL, 0.5 mmol, 2.5 equiv) with 2,2,2-trichloroethyl 2-diazo-2-(4-(trifluoromethyl)phenyl)acetate (0.2 mmol, 72.3 mg, 1.0 equiv) using Ru_2(*S*-TPPTTL)$_4$BAr^F (6.6 mg, 1 mol %) as catalyst. Purification by column chromatography afforded an amorphous solid (74.6 mg, 85%):

^{1}H NMR (400 MHz, $CDCl_3$) δ 7.43 (d, J = 8.0 Hz, 2H), 7.22 (d, J = 8.0 Hz, 2H), 7.15-7.11 (m, 3H), 6.83 (dd, J = 6.4, 3.1 Hz, 2H), 4.87 (d, J = 11.8 Hz, 1H), 4.69 (d, J = 11.8 Hz, 1H), 3.31 (dd, J = 9.4, 7.5 Hz, 1H), 2.37 (dd, J = 9.4, 5.2 Hz, 1H), 2.07 (dd, J = 7.5, 5.2 Hz, 1H).

^{13}C NMR (101 MHz, $CDCl_3$) δ 171.4, 138.0 (d, J = 1.2 Hz), 135.0, 132.4, 128.1, 128.0, 127.02, 124.7 (q, J = 3.7 Hz), 121.4 (q, J = 272.2 Hz), 94.9, 74.4, 36.9, 34.1, 20.1.

^{19}F NMR (376 MHz, $CDCl_3$) δ -62.54.

HRMS (+p APCI) calcd for $C_{19}H_{15}O_2Cl_3F_3$ (M+H) 437.0084 found 437.0084.

Chiral HPLC: The enantiopurity was determined to be 88:12 er by chiral HPLC analysis (Chiracel AD-H, 1.0% IPA/Hexanes, 1.0 mL/min, λ=230 nm, RT: Major: 5.5 min, Minor: 7.2 min).

2,2,2-Trichloroethyl (1*S*,2*R*)-1-(4-(*tert*-butyl)phenyl)-2-phenylcyclopropane-1-carboxylate (35)

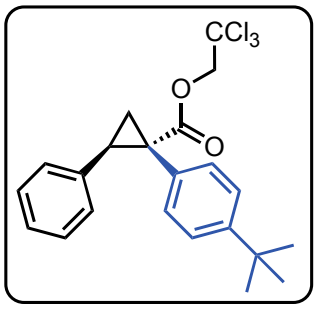

General procedure 1 was employed for the cyclopropanation of styrene (57.5 µL, 0.5 mmol, 2.5 equiv) with 2,2,2-trichloroethyl 2-(4-(*tert*-butyl)phenyl)-2-diazoacetate (0.2 mmol, 69.9 mg, 1.0 equiv) using Ru_2(*S*-TPPTTL)$_4$BAr^F (6.6 mg, 1 mol %) as catalyst. Purification by column chromatography afforded an amorphous solid (41.3 mg, 49%). Spectra matched literature precedent.[3]

^{1}H NMR (400 MHz, CDC_3) δ 7.17 (d, J = 8.4 Hz, 2H), δ 7.09 (m, 3H), δ 7.01 (d, J = 8.4 Hz, 2H), δ 6.81 (m, 2H), δ 4.86 (d, J = 11.9 Hz, 1H), δ 4.68 (d, J = 11.9 Hz, 1H), δ 3.22 (dd, J = 9.4, 7.4 Hz, 1H), δ 2.31 (dd, J = 7.4, 5.1 Hz, 1H), δ 2.00 (dd, J = 9.4, 5.1 Hz, 1H).

Chiral HPLC: The enantiopurity was determined to be 84:16 er by chiral HPLC analysis (Chiracel AD-H, 1.0% IPA/Hexanes, 0.5 mL/min, λ=230 nm, RT: Major: 8.5 min, Minor: 9.9 min).

2,2,2-Trichloroethyl (1*S*,2*R*)-1-(4-fluorophenyl)-2-phenylcyclopropane-1-carboxylate (36)

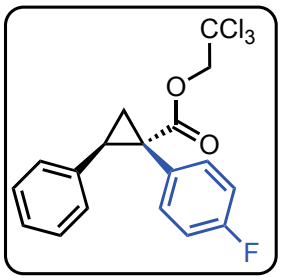

General procedure 1 was employed for the cyclopropanation of styrene (57.5 µL, 0.5 mmol, 2.5 equiv) with 2,2,2-trichloroethyl 2-diazo-2-(4-fluorophenyl)acetate (0.2 mmol, 62.3 mg, 1.0 equiv) using Ru_2(*S*-TPPTTL)$_4$BAr^F (6.6 mg, 1 mol %) as catalyst. Purification by column chromatography afforded an amorphous solid (35 mg, 45%). Spectra matched literature precedent.[3]

^{1}H NMR (400 MHz, $CDCl_3$) δ 7.13 (m, 3H), δ 7.06 (dd, J = 8.8, 5.3 2H), δ 6.83 (m, 4H), δ 4.83 (d, J = 11.9 Hz, 1H), δ 4.68 (d, J = 11.9 Hz, 1H), δ 3.24 (dd, J = 9.4, 7.4 Hz, 1H), δ 2.31 (dd, J = 9.4, 5.2 Hz, 1H), δ 2.00 (dd, J = 7.4, 5.2 Hz, 1H).

Chiral HPLC: The enantiopurity was determined to be 91:9 er by chiral HPLC analysis (Chiracel AD-H, 1.0% IPA/Hexanes, 1.0 mL/min, λ=230 nm, RT: Major: 6.0 min, Minor: 6.5 min).

2,2,2-Trichloroethyl (1*S*,2*R*)-1-(4-methoxyphenyl)-2-phenylcyclopropane-1-carboxylate (37)

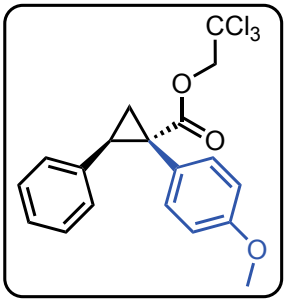

General procedure 1 was employed for the cyclopropanation of styrene (57.5 µL, 0.5 mmol, 2.5 equiv) with 2,2,2-trichloroethyl 2-diazo-2-(4-methoxyphenyl)acetate (0.2 mmol, 64.7 mg, 1.0 equiv) using Ru_2(*S*-TPPTTL)$_4$BAr^F (6.6 mg, 1 mol %) as catalyst. Purification by column chromatography afforded an oil (48.4 mg, 61%). Spectra matched literature precedent.[3]

^{1}H NMR (400 MHz, $CDCl_3$) δ 7.10 (dd, J = 5.2, 1.9 Hz, 3H), δ 6.99 (d, J = 8.2 Hz, 2H), δ 6.82 (m, 2H), δ 6.67 (d, J = 8.2 Hz, 2H), δ 4.85 (d, J = 11.9 Hz, 1H), δ 4.66 (d, J = 11.9 Hz, 1H), δ 3.72 (s, 3H), δ 3.20 (dd, J = 9.5, 7.4 Hz, 1H), δ 2.28 (dd, J = 9.5, 5.1 Hz, 1H), δ 1.97 (dd, J = 7.4, 5.1 Hz, 1H).

Chiral HPLC: The enantiopurity was determined to be 90:10 er by chiral HPLC analysis (Chiracel AD-H, 1.0% IPA/Hexanes, 1.0 mL/min, λ=254 nm, RT: Major: 8.3 min, Minor: 9.3 min).

2,2,2-Trichloroethyl (1*S*,2*R*)-1-([1,1'-biphenyl]-4-yl)-2-phenylcyclopropane-1-carboxylate (38)

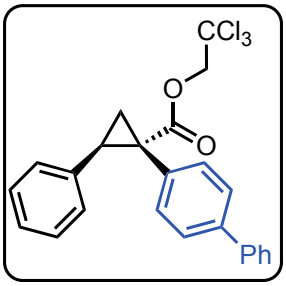

General procedure 1 was employed for the cyclopropanation of styrene (57.5 µL, 0.5 mmol, 2.5 equiv) with 2,2,2-trichloroethyl 2-([1,1'-biphenyl]-4-yl)-2-diazoacetate (0.2 mmol, 73.9 mg, 1.0 equiv) using Ru_2(*S*-TPPTTL)$_4$BAr^F (6.6 mg, 1 mol %) as catalyst. Purification by column chromatography afforded an amorphous solid (79.2 mg, 89%)

^{1}H NMR (400 MHz, $CDCl_3$) δ 7.53 (d, J = 7.0 Hz, 2H), 7.40 (m, 4H), 7.32 (m, 1H), 7.15 (d, J = 8.3 Hz, 2H), 7.09 (dd, J = 5.2, 1.9, 2H), 6.85 (m, 2H), 4.87 (d, J = 11.9, 1H), 4.68 (d, J = 11.9, 1H), 3.26 (dd, J = 9.4, 7.4, 1H), 2.33 (dd, J = 9.4, 5.1, 1H), 2.05 (dd, J = 7.4, 5.1, 1H).

^{13}C NMR (101 MHz, $CDCl_3$): δ 172.1, 140.7, 139.9, 135.7, 132.8, 132.4, 128.7, 128.2, 127.9, 127.3, 127.0, 126.7, 126.4 95.1, 74.4, 36.9, 34.0, 20.3.

HRMS (+p APCI) calcd for $C_{24}H_{20}O_2Cl_3$ (M+H) 445.0523 found 445.0518.

Chiral HPLC: The enantiopurity was determined to be 89:11 er by chiral HPLC analysis (Chiracel AD-H, 1.0% IPA/Hexanes, 1.0 mL/min, λ=230 nm, RT: Major: 7.9 min, Minor: 8.8 min).

2,2,2-Trichloroethyl (1*S*,2*R*)-1-(naphthalen-2-yl)-2-phenylcyclopropane-1-carboxylate (39)

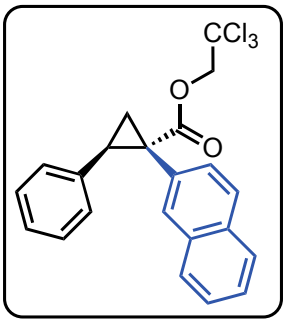

General procedure 1 was employed for the cyclopropanation of styrene (57.5 µL, 0.5 mmol, 2.5 equiv) with 2,2,2-trichloroethyl 2-diazo-2-(naphthalen-2-yl)acetate (0.2 mmol, 68.7 mg, 1.0 equiv) using Ru_2(*S*-TPPTTL)$_4$BAr^F (6.6 mg, 1 mol %) as catalyst. Purification by column chromatography afforded a crystalline solid (43.1 mg, 51%). Spectra matched literature precedent.[3]

^{1}H NMR (400 MHz, 400 $CDCl_3$) δ 7.75 (dt, J = 7.0, 3.9 Hz, 2H), δ 7.69 (s, 1H), δ 7.59 (d, J = 8.5 Hz, 1H), δ 7.46 (m, 2H), δ 7.15 (d, J = 8.5 Hz, 1H), δ 7.06 (m, 3H), δ 6.88 (m, 2H), δ 4.92 (d, J = 11.9 Hz, 1H), δ 4.67 (d, J = 11.9 Hz, 1H), δ 3.34 (dd, J = 9.5, 7.4 Hz, 1H), δ 2.41 (dd, J = 9.5, 5.1 Hz, 1H), δ 2.20 (dd, J = 7.4, 5.1 Hz, 1H).
Chiral HPLC: The enantiopurity was determined to be 94:6 er by chiral HPLC analysis (Chiracel AD-H, 1.0% IPA/Hexanes, 1.0 mL/min, λ=230 nm, RT: Major: 7.7 min, Minor: 8.9 min).

2,2,2-Trichloroethyl (1*S*,2*R*)-1-(3-iodophenyl)-2-phenylcyclopropane-1-carboxylate (40)

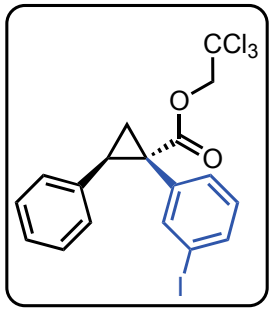

General procedure 1 was employed for the cyclopropanation of styrene (57.5 μL, 0.5 mmol, 2.5 equiv) with 2,2,2-trichloroethyl 2-diazo-2-(3-iodophenyl)acetate (0.2 mmol, 83.9 mg, 1.0 equiv) using Ru_2(*S*-TPPTTL)$_4$$BAr^F$ (6.6 mg, 1 mol %) as catalyst. Purification by column chromatography afforded an oil (79.1 mg, 80%):

^{1}H NMR (400 MHz, $CDCl_3$) δ 7.46 (m, 2H), 7.12 (dd, J = 5.2, 2.0 Hz, 3H), 6.98 (dt, J = 5.2, 2.0 Hz, 1H), 6.83 (m, 3H), 4.85 (d, J = 11.9 Hz, 1H), 4.63 (d, J = 11.9 Hz, 1H), 3.22 (dd, J = 9.4, 7.5 Hz, 1H), 2.27 (dd, J = 9.4, 5.2 Hz, 1H), 2.00 (dd, J = 7.5, 5.2 Hz, 1H).
^{13}C NMR (101 MHz, $CDCl_3$): δ 171.5, 140.9, 136.4, 136.2, 135.1, 131.4, 129.9, 129.3, 128.1, 128.0, 94.9, 93.3, 74.5, 36.6, 34.0, 20.1.
HRMS (+p APCI) calcd for $C_{18}H_{15}O_2Cl_3I$ (M+H) 494.9177 found 494.9176.
Chiral HPLC: The enantiopurity was determined to be 72:27 er by chiral HPLC analysis (Chiracel OD-H, 0.5% IPA/Hexanes, 1.0 mL/min, λ=230 nm, RT: Major: 14.9 min, Minor: 13.7 min)

2,2,2-Trichloroethyl (1*R*,2*R*)-2-phenyl-1-((*E*)-styryl)cyclopropane-1-carboxylate (41)

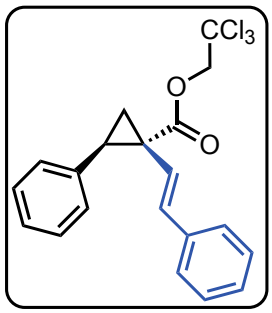

General procedure 1 was employed for the cyclopropanation of styrene (57.5 µL, 0.5 mmol, 2.5 equiv) with 2,2,2-trichloroethyl (*E*)-2-diazo-4-phenylbut-3-enoate (0.2 mmol, 63.9 mg, 1.0 equiv) using Ru_2(*S*-TPPTTL)$_4$BAr^F (6.6 mg, 1 mol %) as catalyst. Purification by column chromatography afforded an amorphous solid (47.5 mg, 50%). Spectra matched literature precedent.[3]

^{1}H NMR (400 MHz, $CDCl_3$) δ 7.29 (m, 2H), δ 7.25 (m, 2H), δ 7.22 (m, 1H), δ 7.20 (td, J = 6.7, 3.4 Hz, 4H), δ 4.91 (d, J = 11.9 Hz, 1H), δ 4.85 (d, J = 11.9 Hz, 1H), δ 3.21 (dd, J = 9.3, 7.4 Hz, 1H), δ 2.23 (dd, J = 9.3, 5.3 Hz, 1H), δ 1.97 (dd, J = 7.4, 5.3 Hz, 1H).

Chiral HPLC: The enantiopurity was determined to be 72:28 er by chiral HPLC analysis (Chiracel AD-H, 1.0% IPA/Hexanes, 1.0 mL/min, λ=230 nm, RT: Major: 6.8 min, Minor: 7.6 min).

2,2,2-Trichloroethyl (1*S*,2*R*)-1-(2-chloropyridin-4-yl)-2-phenylcyclopropane-1-carboxylate (42)

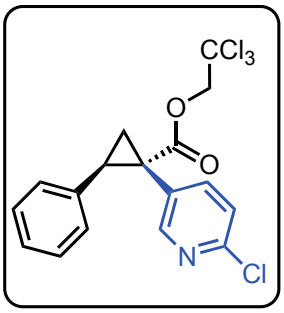

General procedure 1 was employed for the cyclopropanation of styrene (57.5 µL, 0.5 mmol, 2.5 equiv) with 2,2,2-trichloroethyl 2-(6-chloropyridin-3-yl)-2-diazoacetate (0.2 mmol, 65.8 mg, 1.0 equiv) using Ru_2(*S*-TPPTTL)$_4$BAr^F (6.6 mg, 1 mol %) as catalyst. Purification by column chromatography afforded an amorphous solid (31.3 mg, 39%). Spectra matched literature precedent.[3]

^{1}H NMR (400 MHz, $CDCl_3$) δ 8.16 (d, J = 2.5 Hz, 1H), δ 7.29 (m, 1H), δ 7.16 (dq, J = 4.7, 2.2 Hz, 3H), δ 7.08 (d, J = 8.0 Hz, 1H), 6.86 (dd, J = 7.4, 2.2 Hz, 2H), δ 4.86 (d, J = 11.9 Hz, 1H), δ 4.68 (d, J = 11.9 Hz, 1H), δ 3.30 (dd, J = 9.4, 7.5 Hz, 1H), δ 2.37 (dd, J = 9.4, 5.4 Hz, 1H), δ 2.07 (dd, J = 7.5, 5.4 Hz, 1H).

Chiral HPLC: The enantiopurity was determined to be 82:18 er by chiral HPLC analysis (Chiracel OD-H, 1.0% IPA/Hexanes, 1.0 mL/min, λ=230 nm, RT: Major: 14.8 min, Minor: 19.2 min).

2,2,2-Trichloroethyl (1*S*,2*R*)-1-(3-methoxyphenyl)-2-phenylcyclopropane-1-carboxylate (43)

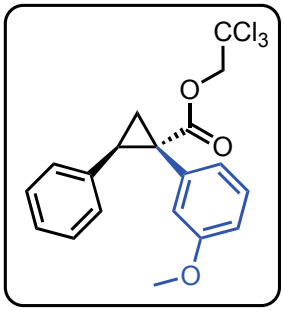

General procedure 1 was employed for the cyclopropanation of styrene (57.5 µL, 0.5 mmol, 2.5 equiv) with 2,2,2-trichloroethyl 2-diazo-2-(3-methoxyphenyl)acetate (0.2 mmol, 64.7 mg, 1.0 equiv) using Ru_2(*S*-TPPTTL)$_4$BAr^F (6.6 mg, 1 mol %) as catalyst. Purification by column chromatography afforded an oil (61.3 mg, 77%). Spectra matched literature precedent.[13]

^{1}H NMR (400 MHz, $CDCl_3$) δ 7.10 (dd, J = 5.1, 1.9 Hz, 3H), δ 7.05 (t, J = 7.9 Hz, 1H), δ 6.83 (m, 2H), δ 6.69 (t, 6.3 Hz, 2H), δ 6.56 (m, 1H), δ 4.87 (d, J = 11.8 Hz, 1H), δ 4.65 (d, J = 11.8 Hz, 1H), δ 3.59 (s, 3H), δ 3.21 (dd, J = 9.4, 7.5 Hz, 1H), δ 2.27 (d, J = 9.4, 5.2 Hz, 1H), δ 2.00 (dd, J = 7.5, 5.1 Hz, 1H).

Chiral HPLC: The enantiopurity was determined to be 79:21 er by chiral HPLC analysis (Chiracel AD-H, 1.0% IPA/Hexanes, 1.0 mL/min, λ=230 nm, RT: Major: 8.0 min, Minor: 7.1 min).

Methyl (1*S*,2*S*)-1-(4-bromophenyl)-2-butylcyclopropane-1-carboxylate (44)

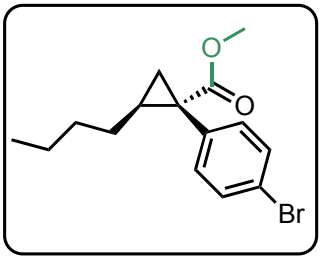

General procedure 2 was employed for the cyclopropanation of hex-1-ene (250 µL, 2.0 mmol, 10 equiv) with methyl 2-(4-bromophenyl)-2-diazoacetate (0.2 mmol, 74.5 mg, 1.0 equiv) using Ru_2(*S*-TPPTTL)$_4$BAr^F (6.6 mg, 1 mol %) as catalyst. Purification by column chromatography afforded a clear colorless oil (51.0 mg, 41%).

^{1}H NMR (400 MHz, $CDCl_3$) δ 7.46 (d, J = 8.5 Hz, 2H), 7.16 (d, J = 8.5 Hz, 2H), 3.63 (s, 3H), 1.84 (tdd, J = 9.0, 6.7, 4.3 Hz, 1H), 1.73 (dd, J = 9.0, 4.1 Hz, 1H), 1.42-1.32 (m, 3H), 1.31-1.19 (m, 2H), 1.07 (dd, J = 6.7, 4.1 Hz, 1H), 0.84 (t, J = 7.2 Hz, 3H), 0.51 (ddd, J = 11.9, 9.7, 7.8 Hz, 1H).

^{13}C NMR (101 MHz, $CDCl_3$): δ 174.7, 135.5, 133.1, 132.1, 131.2, 121.1, 52.4, 33.1, 31.3, 30.0, 28.8, 22.4, 21.8, 14.0.

HRMS (+p APCI) calcd for $C_{15}H_{20}O_2Br$ (M+H) 311.0641 found 311.0638.

Chiral HPLC: The enantiopurity was determined to be 79:21 er by chiral HPLC analysis (S,S, Whelk, 1.0% IPA/Hexanes, 1.0 mL/min, λ=230 nm, RT: Major: 24.2 min, Minor: 14.7 min).

2,2,2-Trifluoroethyl (1*S*,2*S*)-1-(4-bromophenyl)-2-butylcyclopropane-1-carboxylate (45)

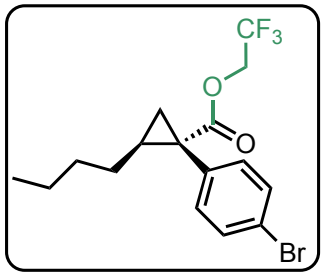

General procedure 2 was employed for the cyclopropanation of hex-1-ene (250 µL, 2.0 mmol, 10 equiv) with 2,2,2-trifluoroethyl 2-(4-bromophenyl)-2-diazoacetate (0.2 mmol, 64.6 mg, 1.0 equiv) using Ru_2(*S*-TPPTTL)$_4$BAr^F (6.6 mg, 1 mol %) as catalyst. Purification by column chromatography afforded an oil (53.8 mg, 71%).

^{1}H NMR (400 MHz, $CDCl_3$) δ 7.46 (d, J = 8.5 Hz, 2H), 7.14 (d, J = 8.5 Hz, 2H), 4.50 (dq, J = 12.7, 8.4 Hz, 1H), 4.32 (dq, J = 12.7, 8.4 Hz, 1H), 1.89 (tdd, J = 9.0, 6.8, 4.3 Hz, 1H), 1.80 (dd, J = 9.0, 4.3 Hz, 1H), 1.42-1.31 (m, 3H), 1.29-1.20 (m, 2H), 1.17 (dd, J = 6.8, 4.3 Hz, 1H), 0.83 (t, J = 7.2 Hz, 3H), 0.53 (m, 1H).

^{13}C NMR (101 MHz, $CDCl_3$) δ 172.6, 134.3, 133.0, 131.3, 122.7 (q, J = 277.4 Hz), 121.5, 60.7 (q, J = 36.6 Hz), 32.8, 31.2, 30.0, 29.7, 22.4, 22.1, 14.0.

^{19}F NMR (376 MHz, $CDCl_3$) δ -73.93.

HRMS (+p APCI) calcd for $C_{16}H_{19}O_2BrF_3$ (M+H) 379.0515 found 379.0511.

Chiral HPLC: The enantiopurity was determined to be 95:5 er by chiral HPLC analysis (Chiracel OD-H, 1.0% IPA/Hexanes, 1.0 mL/min, λ=230 nm, RT: Major: 5.4 min, Minor: 4.3 min).

2,2,2-Trichloroethyl (1*S*,2*S*)-2-butyl-1-(4-(trifluoroMethyl)phenyl)cyclopropane-1-carboxylate (46)

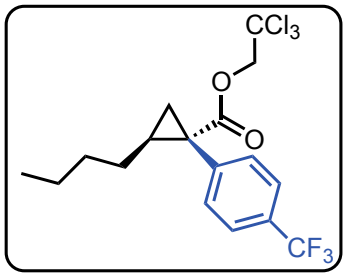

General procedure 2 was employed for the cyclopropanation of hex-1-ene (250 µL, 2.0 mmol, 10 equiv) with 2,2,2-trichloroethyl 2-diazo-2-(4-(trifluoromethyl)phenyl)acetate (0.2 mmol, 72.3 mg, 1.0 equiv) using Ru_2(*S*-TPPTTL)$_4$BAr^F (6.648 mg, 1 mol %) as catalyst. Purification by column chromatography afforded a clear colorless oil (59.9 mg, 74%).

^{1}H NMR (400 MHz, $CDCl_3$): δ 7.62 (d, J = 8.0 Hz, 2H), 7.46 (d, J = 8.0 Hz, 2H), 4.82 (d, J = 11.9 Hz, 1H), 4.59 (d, J = 11.9 Hz, 1H), 2.00 (ddd, J = 9.0, 6.5, 4.2 Hz, 1H), 1.94 (dd, J = 9.0, 4.2 Hz, 1H), 1.47-1.35 (m, 3H), 1.27 (dt, J = 10.0, 6.2 Hz, 3H), 0.85 (t, J = 7.3 Hz, 3H), 0.56 (dt, J = 11.5, 7.3 Hz, 1H).

^{13}C NMR (101 MHz, $CDCl_3$): δ 172.3, 139.4 (d, J = 1.1 Hz), 131.8, 125.0 (q, J = 3.9 Hz), 124.0 (q, J = 270.5 Hz), 94.9, 74.3, 33.4, 31.2, 30.0, 29.7, 22.4, 22.0, 14.0.

^{19}F NMR (376 MHz, $CDCl_3$) δ -62.49.

HRMS (+p APCI) calcd for $C_{17}H_{19}O_2Cl_3F_3$ (M+H) 417.0397 found 417.0392.

Chiral HPLC: The enantiopurity was determined to be 90:10 er by chiral HPLC analysis (Chiracel AD-H, 1.0% IPA/Hexanes, 1.0 mL/min, λ=210 nm, RT: Major: 3.8 min, Minor: 4.3 min).

2,2,2-Trichloroethyl (1*S*,2*S*)-2-butyl-1-(4-(*tert*-butyl)phenyl)cyclopropane-1-carboxylate (47)

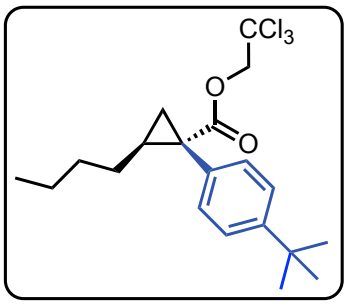

General procedure 2 was employed for the cyclopropanation of hex-1-ene (250 µL, 2.0 mmol, 10 equiv) with 2,2,2-trichloroethyl 2-(4-(tert-butyl)phenyl)-2-diazoacetate (0.2 mmol, 69.9 mg, 1.0 equiv) using Ru_2(*S*-TPPTTL)$_4$BAr^F (6.6 mg, 1 mol %) as catalyst. Purification by column chromatography afforded a clear colorless oil (63.3 mg, 87%).

^{1}H NMR (400 MHz, $CDCl_3$) δ 7.34 (d, J = 8.4 Hz, 2H), 7.23 (d, J = 8.4 Hz, 2H), 4.79 (d, J = 12.0 Hz, 1H), 4.56 (d, J = 12.0 Hz, 1H), 1.93 (tdd, J = 8.9, 6.7, 4.5 Hz, 1H), 1.85 (dd, J = 9.1, 4.1 Hz, 1H), 1.47-1.35 (m, 3H), 1.32 (s, 9H), 1.21 (dd, J = 6.7, 4.1 Hz, 1H), 0.83 (J = 7.2 Hz, 3H), 0.71-0.59 (m, 1H).

^{13}C NMR (101 MHZ, $CDCl_3$) δ 173.2, 150.1, 132.1, 131.0, 124.9, 95.2, 74.2, 34.5, 33.1, 31.3, 29.9, 29.5, 22.4, 21.7, 14.0.

HRMS (+p ACPI) calcd for $C_{20}H_{28}O_2Cl_3$ (M+H) 405.1149 found 405.1151.

Chiral HPLC: The enantiopurity was determined to be 88:12 er by chiral HPLC analysis (Chiracel AD-H, 0.5% IPA/Hexanes, 1.0 mL/min, λ=210 nm, RT: Major: 7.1 min, Minor: 7.6 min).

2,2,2-Trichloroethyl (1*S*,2*S*)-2-butyl-1-(4-fluorophenyl)cyclopropane-1-carboxylate (48)

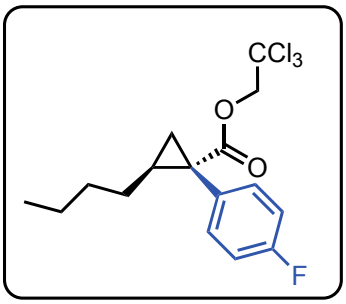

General procedure 2 was employed for the cyclopropanation of hex-1-ene (250 µL, 2.0 mmol, 10 equiv) with 2,2,2-trichloroethyl 2-diazo-2-(4-fluorophenyl)acetate (0.2 mmol, 62.3 mg, 1.0 equiv) using Ru_2(*S*-TPPTTL)$_4$BAr^F (6.6 mg, 1 mol %) as catalyst. Purification by column chromatography afforded an oil (40.9 mg, 56%).

^{1}H NMR (400 MHz, $CDCl_3$) δ 7.35-7.25 (m, 2H), 7.04 (t, J = 8.7 Hz, 2H), 4.80 (d, J = 11.9 H, 1H), 4.58 (d, J = 11.9 Hz, 1H), 1.95 (tdd, J = 11.0, 4.8, 3.2 Hz, 1H), 1.88 (dd, J = 9.0, 4.0 Hz, 1H), 1.48-1.33 (m, 3H), 1.33-1.23 (m, 2H), 1.21 (dd, J = 6.7, 4.0 Hz, 1H), 0.85 (t, J = 7.2 Hz, 3H), 0.67-0.56 (m, 1H).

^{13}C NMR (101 MHz, $CDCl_3$) δ 172.9, 161.0 (d, J = 249.8 Hz) 133.0 (d, J = 8.2 Hz), 131.1 (d, J = 3.3 Hz), 114.9 (d, J = 21.5 Hz), 95.1, 74.3, 32.8, 31.2, 30.0, 29.6, 22.4, 22.1, 14.0.

^{19}F NMR (376 MHz, $CDCl_3$) δ -115.05.

HRMS (+p APCI): calcd for $C_{16}H_{19}O_2Cl_3F$ (M+H) 367.0429 found 367.0430.

Chiral HPLC: The enantiopurity was determined to be 96:4 er by chiral HPLC analysis (Chiracel AD-H, 1.0% IPA/Hexanes, 1.0 mL/min, λ=210 nm, RT: Major: 4.1 min, Minor: 4.5 min).

2,2,2-Trichloroethyl (1*S*,2*S*)-2-butyl-1-(4-methoxyphenyl)cyclopropane-1-carboxylate (49)

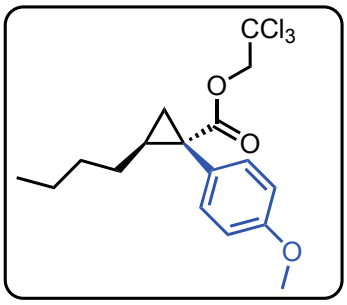

General procedure 2 was employed for the cyclopropanation of hex-1-ene (250 μL, 2.0 mmol, 10 equiv) with 2,2,2-trichloroethyl 2-diazo-2-(3-methoxyphenyl)acetate (0.2 mmol, 64.7 mg, 1.0 equiv) using Ru_2(*S*-TPPTTL)$_4$BAr^F (6.6 mg, 1 mol %) as catalyst. Purification by column chromatography afforded an oil (43.5 mg, 57%)

^{1}H NMR (400 MHz, $CDCl_3$) δ 7.22 (d, J = 8.7 Hz, 2H), 6.86 (d, J = 8.7 Hz, 2H), 4.79 (d, J = 12.0 Hz, 1H), 4.55 (d, J = 12.0 Hz, 1H) 3.81 (s, 3H), 1.95-1.86 (m, 1H), 1.83 (dd, J = 9.1, 3.9 Hz, 1H), 1.44-1.32 (m, 3H), 1.25 (pd, J = 7.8, 3.2 Hz, 2H), 1.17 (dd, J = 6.7, 4.0 Hz, 1H), 0.83 (t, J = 7.3 Hz, 3H), 0.67-0.56 (m, 1H).

^{13}C NMR (101 MHz, $CDCl_3$) δ 173.4, 158.7, 132.5, 127.4, 113.4, 95.2, 74.2, 55.2, 32.8, 31.3, 29.9, 29.6, 22.4, 22.0, 14.0.

HRMS (+p APCI) calcdd for $C_{17}H_{21}Cl_3O_3$ (M+H) 379.0629 found 379.0629.

Chiral HPLC The enantiopurity was determined to be 76:24 er by chiral HPLC analysis (Chiracel AD-H, 1.0% IPA/Hexanes, 1.0 mL/min, λ=280 nm, RT: Major: 5.3 min, Minor: 5.9 min).

2,2,2-Trichloroethyl (1*S*,2*S*)-1-([1,1'-biphenyl]-4-yl)-2-butylcyclopropane-1-carboxylate (50)

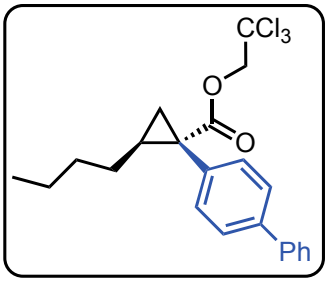

General procedure 2 was employed for the cyclopropanation of hex-1-ene (250 µL, 2.000 mmol, 10 equiv) with 2,2,2-trichloroethyl 2-diazo-2-(4-fluorophenyl)acetate (0.2 mmol, 73.9 mg, 1.0 equiv) using Ru_2(*S*-TPPTTL)$_4$BAr^F (6.6 mg, 1 mol %) as catalyst. Purification by column chromatography afforded a clear colorless oil (42.6 mg, 50%).

^{1}H NMR (400 MHz, $CDCl_3$) δ 7.62 (d, J = 8.3 Hz, 2H), 7.60 (d, J = 8.6 Hz, 2H) 7.48 (d, J = 7.6 Hz, 2H), 7.43-7.33 (m, 3H), 4.85 (d, J = 12.0 Hz, 1H), 4.61 (d, J = 12.0 Hz, 1H), 2.00 (m, 1H), 1.92 (dd, J = 9.1, 4.1 Hz, 1H), 1.51-1.37 (m, 3H), 1.29 (pd, J = 8.5, 5.8 Hz, 3H), 0.86 (t, J = 7.2 Hz, 3H), 0.74-0.64 (m, 1H).

^{13}C NMR (101, $CDCl_3$) δ 173.1, 140.8, 140.1, 134.4, 131.8, 128.8, 127.3, 127.1, 126.7, 95.2, 74.2, 33.3, 31.3, 30.0, 29.7, 22.4, 21.9, 14.0.

HRMS (+p APCI) calcdd for $C_{22}H_{24}Cl_3O_2$ (M+H) 425.0836 found 425.0830.

Chiral HPLC: The enantiopurity was determined to be 90:10 er by chiral HPLC analysis (Chiracel OD-H, 1.0% IPA/Hexanes, 1.0 mL/min, λ=230 nm, RT: Major: 6.6 min, Minor: 5.3 min).

2,2,2-Trichloroethyl (1*S*,2*S*)-2-butyl-1-(naphthalen-2-yl)cyclopropane-1-carboxylate (51)

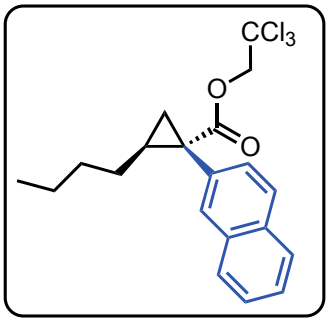

General procedure 2 was employed for the cyclopropanation of hex-1-ene (250 µL, 2.0 mmol, 10 equiv) with 2,2,2-trichloroethyl 2-diazo-2-(naphthalen-2-yl)acetate (0.2 mmol, 68.7 mg, 1.0 equiv) using Ru_2(*S*-TPPTTL)$_4$BAr^F (6.6 mg, 1 mol %) as catalyst. Purification by column chromatography afforded an oil (46.3 mg, 58%). Spectra matched literature precedent.[13]

^{1}H NMR (400 MHz, $CDCl_3$) δ 7.83 (m, 3H), δ 7.75 (d, J = 1.7 Hz, 1H), δ 7.48 (m, 3H), δ 4.86 (d, J = 11.9 Hz, 1H), δ 4.55 (d, J = 11.9 Hz, 1H), δ 2.03 (tdd, J = 9.0, 6.4, 4.3 Hz, 1H), δ 1.95 (dd, J = 9.0, 4.3 Hz, 1H), δ 1.40 (ddt, J = 14.7, 9.0, 6.4 Hz, 4H), δ 1.22 (tdd, J = 14.7, 7.3, 1.3 Hz, 2H), δ 0.81 (t, J = 7.3, 3H), δ 0.62 (m, 1H).

Chiral HPLC: The enantiopurity was determined to be 97:3 er by chiral HPLC analysis (Chiracel AD-H, 1.0% IPA/Hexanes, 1.0 mL/min, λ=280 nm, RT: Major: 4.9 min, Minor: 5.4 min).

2,2,2-Trichloroethyl (1*S*,2*S*)-2-butyl-1-(3-iodophenyl)cyclopropane-1-carboxylate (52)

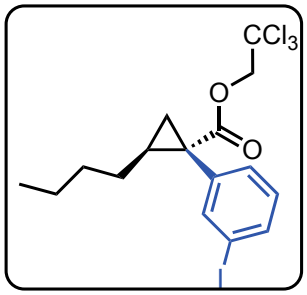

General procedure 2 was employed for the cyclopropanation of hex-1-ene (250 µL, 2.0 mmol, 10 equiv) with 2,2,2-trichloroethyl 2-diazo-2-(3-iodophenyl)acetate (0.2 mmol, 83.9 mg, 1.0 equiv) using Ru_2(*S*-TPPTTL)$_4$BAr^F (6.6 mg, 1 mol %) as catalyst. Purification by column chromatography afforded an oil (62.8 mg, 63%).

^{1}H NMR (400 MHz, $CDCl_3$) δ 7.70 (t, J = 1.7 Hz, 1H), 7.64 (ddd, J = 7.8, 1.7, 1.0 Hz, 1H), 7.35-7.27 (m, 1H), 7.09 (t, J = 7.8 Hz, 1H), 4.84 (d, J = 11.9 Hz, 1H), 4.55 (d, J = 11.90 Hz, 1H), 1.94 (ddt, J = 8.9, 6.7, 4.6 Hz, 1H), 1.87 (dd, J = 9.0, 4.2 Hz, 1H), 1.40 (ttd, J = 8.9, 4.4, 1.9 Hz, 3H), 1.33-1.25 (m, 2H), 1.22 (dd, J = 6.8, 4.2 Hz, 1H), 0.86 (t, J = 7.3 Hz, 3H), 0.68-0.56 (m, 1H).

^{13}C NMR (101 MHz, $CDCl_3$) δ 172.4, 140.5, 137.7, 136.4, 130.8, 129.6, 95.0, 93.7, 74.3, 33.2, 31.2, 29.9, 29.8, 22.4, 21.9, 14.0.

HRMS (+p APCI) calcdd for $C_{16}H_{19}Cl_3IO_2$ (M+H) 474.9490 found 474.9486.

Chiral HPLC: The enantiopurity was determined to be 89:11 er by chiral HPLC analysis (Chiracel OD-H, 1.0% IPA/Hexanes, 0.25 mL/min, λ=230 nm, RT: Major: 19.0 min, Minor: 17.0 min).

2,2,2-Trichloroethyl (1*S*,2*S*)-2-butyl-1-((*E*)-styryl)cyclopropane-1-carboxylate (53)

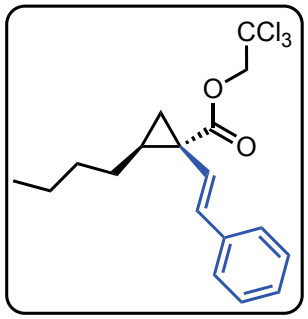

General procedure 2 was employed for the cyclopropanation of hex-1-ene (250 µL, 2.0 mmol, 10 equiv) with 2,2,2-trichloroethyl (*E*)-2-diazo-4-phenylbut-3-enoate (0.2 mmol, 63.9 mg, 1.0 equiv) using Ru_2(*S*-TPPTTL)$_4$BAr^F (6.6 mg, 1 mol %) as catalyst. Purification by column chromatography afforded an oil (50.2 mg, 67%).

^{1}H NMR (400 MHz, $CDCl_3$) δ 7.40 (dd, J = 8.32, 1.40 Hz, 2H), 7.36-7.30 (m, 2H), 7.26-7.21 (m, 2H), 6.67 (d, J = 16.0 Hz, 1H), 6.40 (d, J = 16.0 Hz, 1H), 4.80 (d, J = 11.9 Hz, 1H), 4.71 (d, J = 11.9 Hz, 1H), 1.84-1.72 (m, 2H), 1.38-1.27 (m, 6H), 1.27-1.19 (m, 2H), 0.86 (t, J = 7.1 Hz, 3H).

^{13}C NMR (101 MHz, $CDCl_3$) δ 172.1, 137.0, 132.4, 128.6, 127.5, 126.3, 123.6, 95.2, 74.2, 32.6, 31.5, 30.4, 27.8, 22.3, 19.9, 14.0.

HRMS (+p ACPI) clac for $C_{18}H_{22}O_2Cl_3$ (M+H) 375.0680 found 375.0678.

Chiral HPLC: The enantiopurity was determined to be 92:8 er by chiral HPLC analysis (Chiracel OD-H, 1.0% IPA/Hexanes, 1.0 mL/min, λ=230 nm, RT: Major: 15.6 min, Minor: 7.0 min).

2,2,2-Trichloroethyl (1*S*,2*S*)-2-butyl-1-(2-chloropyridin-4-yl)cyclopropane-1-carboxylate (54)

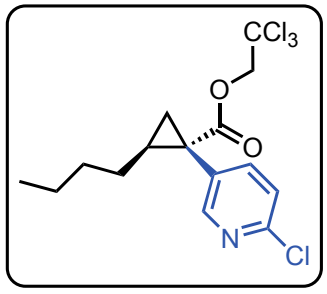

A modified General procedure 2 was employed with the temperature set to 40 °C for the cyclopropanation of Hex-1-ene (250 µL, 2.0 mmol, 10 equiv) with 2,2,2-trichloroethyl 2-(6-chloropyridin-3-yl)-2-diazoacetate (0.2 mmol, 65.8 mg, 1.0 equiv) using Ru_2(*S*-TPPTTL)$_4$BAr^F (6.6 mg, 1 mol %) as

catalyst. Purification by column chromatography afforded a clear colorless oil (54.4 mg, 67%). Spectra matched literature precedent.[13]

^{1}H NMR (400 MHz, $CDCl_3$): δ 8.35 (m, 1H), δ 7.64 (dd, J = 8.2, 2.5 Hz, 1H), δ 7.33 (dd, J = 8.2, 0.7 Hz, 1H), δ 4.80 (d, J = 11.9 Hz, 1H), δ 4.59 (d, J = 11.9 Hz, 1H), δ 1.97 (m, 2H), δ 1.40 (m, 3H), δ 1.26 (m, 3H), δ 0.85 (t, J = 7.31 Hz, 3H), δ 0.60 (m, 1H).

Chiral HPLC The enantiopurity was determined to be 89:11 er by chiral HPLC analysis (Chiracel OD-H, 1.0% IPA/Hexanes, 1.0 mL/min, λ=254 nm, RT: Major: 6.5 min, Minor: 4.0 min).

2,2,2-Trichloroethyl (1*S*,2*S*)-2-butyl-1-(3-methoxyphenyl)cyclopropane-1-carboxylate (55)

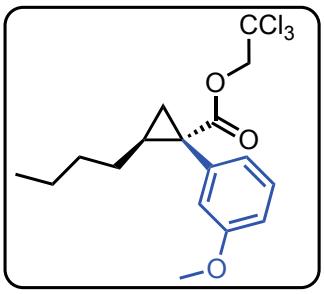

General procedure 2 was employed for the cyclopropanation of hex-1-ene (250 µL, 2.0 mmol, 10 equiv) 2,2,2-trichloroethyl 2-diazo-2-(4-methoxyphenyl)acetate (0.2 mmol, 64.7 mg, 1.0 equiv) using Ru_2(*S*-TPPTTL)$_4$BAr^F (6.6 mg, 1 mol %) as catalyst. Purification by column chromatography afforded a clear colorless oil (48.8 mg, 54%):

^{1}H NMR (400 MHz, $CDCl_3$) δ 7.29 (d, J = 8.8 Hz, 1H), δ 6.94 (m, 1H), δ 6.89 (m, 1H), δ 6.87 (m, 1H), δ 4.86 (d, J = 11.9 Hz, 1H), δ 4.59 (d, J = 11.9 Hz, 1H), δ 3.85 (s, 3H), δ 1.97 (tdd, J = 9.1, 6.8, 4.3 Hz, 1H), δ 1.87 (dd, J = 9.1, 4.3 Hz, 1H), δ 1.43 (m, 3H), δ 1.30 (m, 2H), δ 1.25 (m, 1H), δ 0.87 (t, J = 7.3 Hz, 3H), 0.67 (m, 1H).

^{13}C NMR (101 MHz, $CDCl_3$) δ 173.0, 159.2, 136.8, 128.9, 123.9, 117.2, 112.9, 95.2, 74.2, 55.2, 33.6, 31.3, 29.9, 29.6, 22.0, 22.4, 14.0.

HRMS (+p APCI) calcd for $C_{17}H_{21}Cl_3O_3$ (M+H) 378.0551 found 378.0549.

Chiral HPLC The enantiopurity was determined to be 88:12 er by chiral HPLC analysis (R,R, Whelk 1.0% IPA/Hexanes, 1.0 mL/min, λ=230 nm, RT: Major: 6.5 min, Minor: 9.6 min).

Catalyst Synthesis

Synthesis of Co_2(*S*-TPPTTL)$_4$

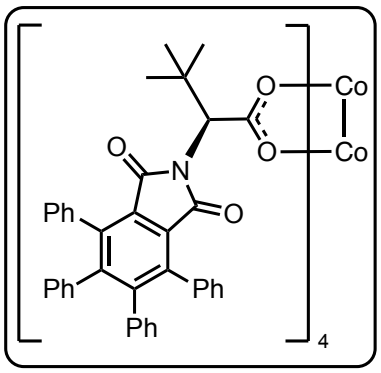

In a nitrogen-filled glovebox, a solution of KHMDS (200 mg, 1.00 mmol) in THF (6 mL) was added dropwise to a solution of *S*-TPPTTL (566 mg, 1.00 mmol) in THF (6 mL) and stirred for 5 mins. To this mixture, a partially dissolved suspension of $CoCl_2$ (64.9 mg, 0.50 mmol) in THF (10 mL) was transferred dropwise over 5 mins, resulting in a deep purple colored mixture that was stirred for 16h at r.t. At this time, all volatiles were removed *in vacuo* and resulting powder was reconstituted in DCM (25 mL), then filtered. All volatiles were removed from the filtrate *in vacuo,* affording a magenta-colored power (532 mg).

HRMS (+p ESI): Calcd for $C_{152}H_{121}O_{16}N_4{}^{59}Co_2$ 2375.7436, found 2375.7428.

Ru_2(*S*-TPPTTL)$_4$Cl (17-Cl)

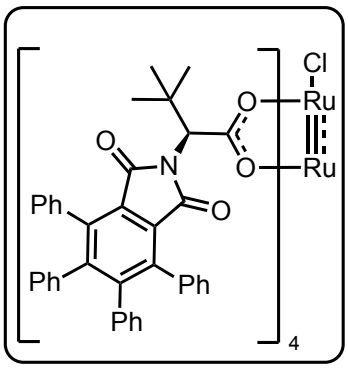

Into a 25 mL round bottom flask equipped with a stir bar was added TPPTTL ligand (0.955 g, 1.74 mmol, 8 equiv) and $Ru_2(OAc)_4Cl$ (0.100 g, 0.218 mmol, 1 equiv). Then 20 mL of chlorobenzene was added. The flask was fitted to a Soxhlet extractor, and the thimble was charged with glass wool, K_2CO_3, and a small layer of sand. The reaction was heated to 168 °C and a rigorous reflux was observed. The reaction was left for 24 h. The reaction was monitored by TLC. Once a brown moving spot was seen on TLC, the reaction was stopped, the solvent removed, and the product was dry loaded onto silica gel and subjected to flash chromatography (0-13% EtOAc/Hex). The

product eluted as a brown band to afford a brown solid upon concentration (0.391 mg, 83% yield). Crystals suitable for X-ray crystallography were grown from the slow evaporation of layered hexane over toluene. No NMR data are available for this compound due to its paramagnetic character. The key data for the structural characterization were obtained by HRMS and X-ray crystallography.

HRMS (+p ESI): Calcd for $C_{152}H_{120}O_{16}N_4{}^{96}Ru_2$ (M-Cl) 2448.6846 found 2448.6907

Ru_2(*S*-TPPTTL)$_4$BAr^F (17-BAr^F)

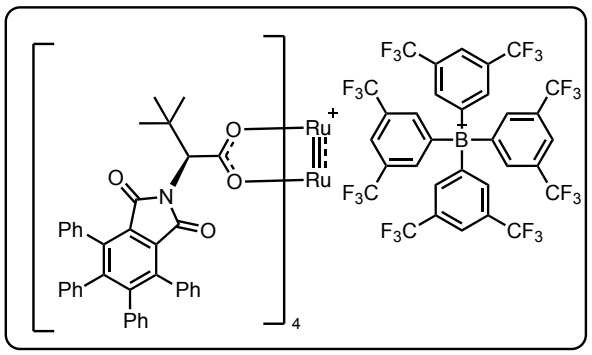

To a 20 mL vial was equipped with a stir bar was added Ru_2(*S*-TPPTTL)$_4$Cl (250 mg, 0.10 mmol, 1.0 equiv) which was subsequently dissolved in 1.00 mL of DCM. Then, NaBAr^F (88.8 mg, 0.10 mmol, 1.0 equiv) was added in one portion. The reaction was left to stir for 24 h, at which point the resulting solution was passed through a short silica plug (1:1 DCM/EtOAc eluent), the solution was concentrated and dried to afford a brown/orange solid (308 mg, 93% yield).

HRMS (+p ESI): Calcd for $C_{152}H_{120}N_4O_{16}Ru_2^+$ (M^+) 2448.6846 found 2448.6870

HRMS (-p ESI): Calcd for $C_{32}H_{12}BF_{24}^-$ (M^-) 862.0691 found 863.0716.

Ru_2(*S*-PTTL)$_4$Cl (18-Cl)

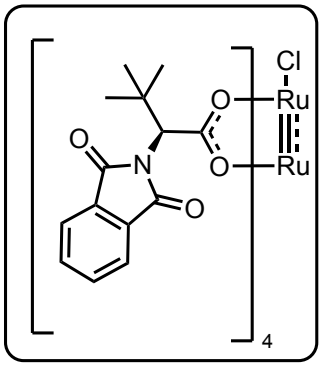

Into a 25 mL round bottom flask equipped with a stir bar was added PTTL ligand (0.441 g, 1.69 mmol, 8 equiv) and $Ru_2(OAc)_4Cl$ (0.100 g, 0.211 mmol, 1 equiv). Then 16 mL of chlorobenzene was added. The flask was fitted to a Soxhlet extractor, and the thimble was charged with glass wool, K_2CO_3, and a small layer of sand. The reaction was heated to 168 °C and a rigorous reflux was observed. The reaction was left for 24 hrs. The reaction was monitored by TLC. Once a brown moving spot was seen on TLC, the reaction was stopped, the solvent removed, and the product was dry loaded onto silica gel and subjected to flash chromatography (0-3% Methanol/DCM). The product eluted as a brown band and afforded a brown solid upon concentration (71.4 mg, Yield 27%). Crystals suitable for X-ray crystallography were grown from the vapor diffusion of acetonitrile into a solution of toluene.

HR-MS: Calcd for $C_{56}H_{56}O_{16}N_4{}^{96}Ru_2$ (M-Cl) 1232.1838 found 1232.1866.

Ru_2(*S*-PTTL)$_4$BAr^F (18-BAr^F)

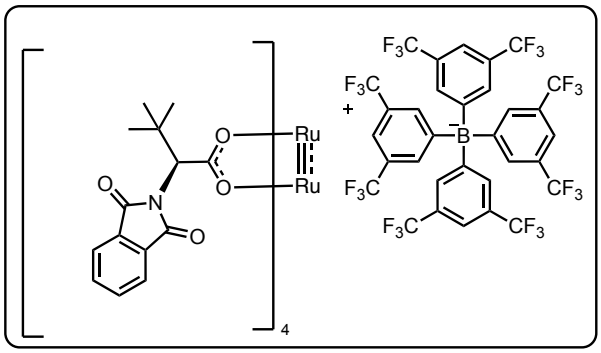

To a 20 mL vial was equipped with a stir bar was added Ru_2(S-PTTL)$_4$Cl (165.5 mg, 0.129 mmol, 1.0 equiv) which was subsequently dissolved in 0.50 mL of DCM. Then, NaBAr^F (120.4 mg, 0.1359 mmol, 1 equiv) was added in one portion. The reaction was left to stir for 24 h, at which point the resulting solution was passed through a short silica plug (1:1 DCM/EtOAc eluent), the solution was concentrated and dried to afford a brown/orange solid (265 mg, 97% yield)

HRMS (+p ESI): Calcd for $C_{56}H_{56}O_{16}N_4{}^{96}Ru_2$ (M^+) 1232.1838 found 1232.1859

HRMS (-p ESI): Calcd for $C_{32}H_{12}BF_{24}^-$ (M^-) 862.0691 found 862.0707.

Ru_2(*S*-PTAD)$_4$Cl (19-Cl)

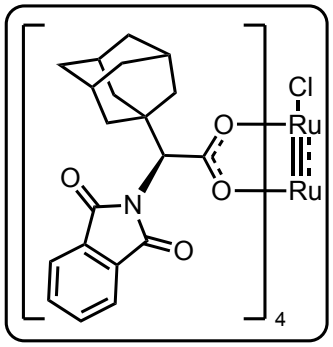

Into a 25 mL round bottom flask equipped with a stir bar was added PTAD ligand (0.344 g, 1.01 mmol, 8 equiv) and $Ru_2(OAc)_4Cl$ (60.0 mg, 0.126 mmol, 1 equiv). Then 16 mL of chlorobenzene was added. The flask was fitted to a Soxhlet extractor, and the thimble was charged with glass wool, K_2CO_3, and a small layer of sand. The reaction was heated to 168 °C and a rigorous reflux was observed. The reaction was left for 24 hrs. The reaction was monitored by TLC. Once a brown moving spot was seen on TLC, the reaction was stopped, the solvent removed, and the product was dry loaded onto silica gel and subjected to flash chromatography (0-3% DCM/Methanol). The product eluted as a brown band and afforded a brown solid upon concentration (90.0 mg, Yield 45%). Crystals suitable for X-ray crystallography were grown from the vapor diffusion of acetonitrile into a solution of toluene.

HRMS (+p ESI): Calcd for $C_{80}H_{80}O_{16}N_4{}^{96}Ru_2$ (M-Cl) 1544.3716 found 1544.3709.

Ru_2(*S*-PTAD)$_4$BAr^F (19-BAr^F)

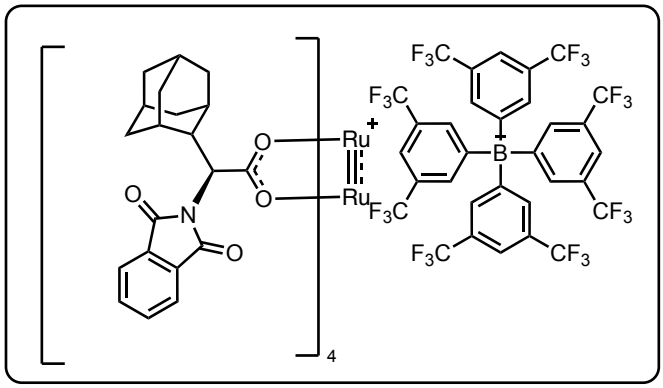

To a 20 mL vial was equipped with a stir bar was added Ru_2(*S*-PTAD)$_4$Cl (66.3 mg, 0.041 mmol, 1.0 equiv) which was subsequently dissolved in 0.50 mL of DCM. Then, NaBAr^F (38.8 mg, 0.0438 mmol, 1.05 equiv) was added in one portion. The reaction was left to stir for 24 h, at which point the resulting solution was passed through a short silica plug (1:1 DCM/EtOAc eluent), the solution was concentrated and dried to afford a brown/orange solid (76 mg, 75% Yield)

HRMS (+p ESI): Calcd for $C_{80}H_{80}O_{16}N_4{}^{96}Ru_2$ (M^+) 1544.3716 found 1544.3717.
HRMS (-p ESI): Calcd for $C_{32}H_{12}BF_{24}^-$ (M^-) 862.0691 found 862.0709

Ru_2(*S*-TCPTAD)$_4$Cl (20-Cl)

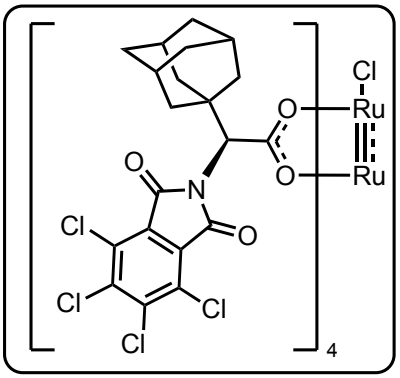

Into a 25 mL round bottom flask equipped with a stir bar was added TCPTAD ligand (0.379 g, 0.794 mmol, 8 equiv) and $Ru_2(OAc)_4Cl$ (47.0 mg, 0.099 mmol, 1 equiv). Then 16 mL of chlorobenzene was added. The flask was fitted to a Soxhlet extractor, and the thimble was charged with glass wool, K_2CO_3, and a small layer of sand. The reaction was heated to 168 °C and a rigorous reflux was observed. The reaction was left for 24 hrs. The reaction was monitored by TLC. Once a brown moving spot was seen on TLC, the reaction was stopped, the solvent removed, and the product was dry loaded onto silica gel and subjected to flash chromatography (0-14% Hexanes/Ethyl Acetate). The product eluted as a brown band and afforded a brown solid upon concentration (115.0 mg, Yield 54%). Crystals suitable for X-ray crystallography were grown from the vapor diffusion of acetonitrile into a solution of toluene.
HRMS (+p ESI): Calcd for $C_{100}H_{80}Cl_{20}N_5O_{20}Ru_2$ (M-Cl+TCPTAD Ligand) 2561.7310 found 2561.7453

Ru_2(*S*-TCPTAD)$_4$BAr^F (20-BAr^F)

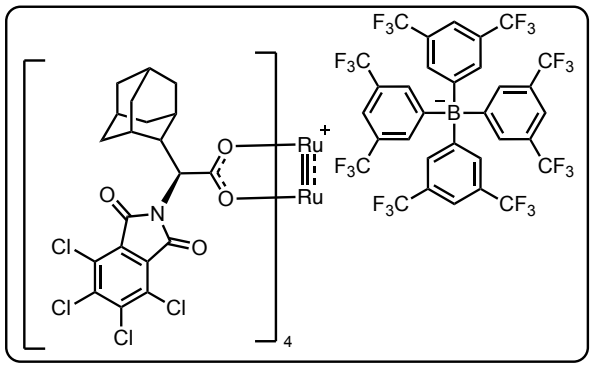

To a 20 mL vial was equipped with a stir bar was added Ru_2(S-TCPTAD)$_4$Cl (227 mg, 0.106 mmol, 1.0 equiv) which was subsequently dissolved in 1.00 mL of DCM. Then, $NaBAr^F$ (98.6 mg, 0.111 mmol, 1.05 equiv) was added in one portion. The reaction was left to stir for 24 h, at which point the resulting solution was passed through a short silica plug (1:1 DCM/EtOAc eluent), the solution was concentrated and dried to afford a brown/orange solid (237 mg, 87% Yield)

HRMS (+p ESI): Calcd for $C_{80}H_{64}Cl_{16}N_4O_{16}{}^{96}Ru_2$ (M^+) 2087.7480 found 2087.7690

HRMS (-p ESI): Calcd for $C_{32}H_{12}BF_{24}^-$ (M^-) 862.0691 found 862.0689

Ru_2(*S*-NTTL)$_4$Cl (21-Cl)

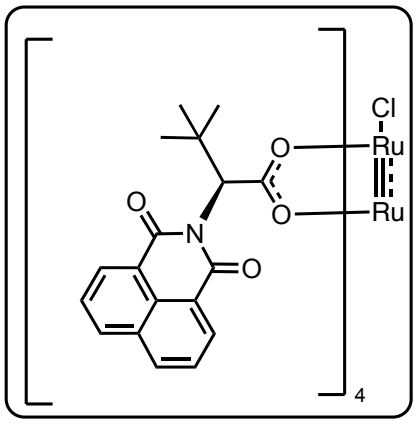

Into a 25 mL round bottom flask equipped with a stir bar was added NTTL ligand (1.04 g, 3.35 mmol, 8 equiv) and $Ru_2(OAc)_4Cl$ (200.0 mg, 0.419 mmol, 1 equiv). Then 16 mL of chlorobenzene was added. The flask was fitted to a Soxhlet extractor, and the thimble was charged with glass wool, K_2CO_3, and a small layer of sand. The reaction was heated to 168 °C and a rigorous reflux was observed. The reaction was left for 24 hrs. The reaction was monitored by TLC. Once a brown moving spot was seen on TLC, the reaction was stopped, the solvent removed, and the product was dry loaded onto silica gel and subjected to flash chromatography (0-4% DCM/Methanol). The product eluted as a brown band and afforded a brown solid upon concentration (268.3 mg, Yield 43%). Crystals suitable for X-ray crystallography were grown from slow evaporation of HFIP.

HRMS (+p ESI): Calcd for $C_{72}H_{64}O_{16}N_4{}^{96}Ru_2$ (M-Cl) 1432.2464 found 1432.2525.

Ru_2(*S*-NTTL)$_4$BAr^F (21-BAr^F)

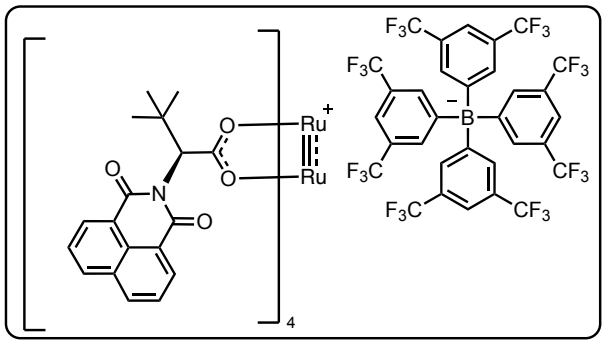

To a 20 mL vial was equipped with a stir bar was added Ru_2(S-NTTL)$_4$Cl (100 mg, 0.067 mmol, 1.0 equiv) to which 0.50 mL of DCM was added. This resulted in a cloudy brown/red solution. Then, NaBAr^F (65.8 mg, 0.074 mmol, 1.1 equiv) was added in one portion, and an immediately the soltuoin went to a clear, dark orange color. The reaction was left to stir for 24 h, at which point the resulting solution was passed through a short silica plug (1:1 DCM/EtOAc eluent), the solution was concentrated and dried to afford a brown/orange solid (153.6 mg, 99% Yield)

HRMS (+p ESI): Calcd for $C_{72}H_{64}O_{16}N_4{}^{96}Ru_2$ (M^+) 1432.2460 found 1432.2488.

HRMS (-p ESI): Calcd for $C_{32}H_{12}BF_{24}^-$ (M^-) 862.0691 found 862.0704.

All reported HR-MS values fall below the 5 ppm delta threshold except for $Ru_2(TCPTAD)_4Cl$ (Δ = 5.45 ppm) and $Ru_2(TCPTAD)_4BAr^F$ (Δ = 9.99 ppm). Reported masses were taken from the lowest isotopic peak which could be the cause for the error observed in these two complexes. When taking the average isotopic peak, the calculated Δ value is significantly lowered to below the 5 ppm threshold.

Co_2(*S*-TPPTTL)$_4$ (Top, observed. Bottom, simulated)

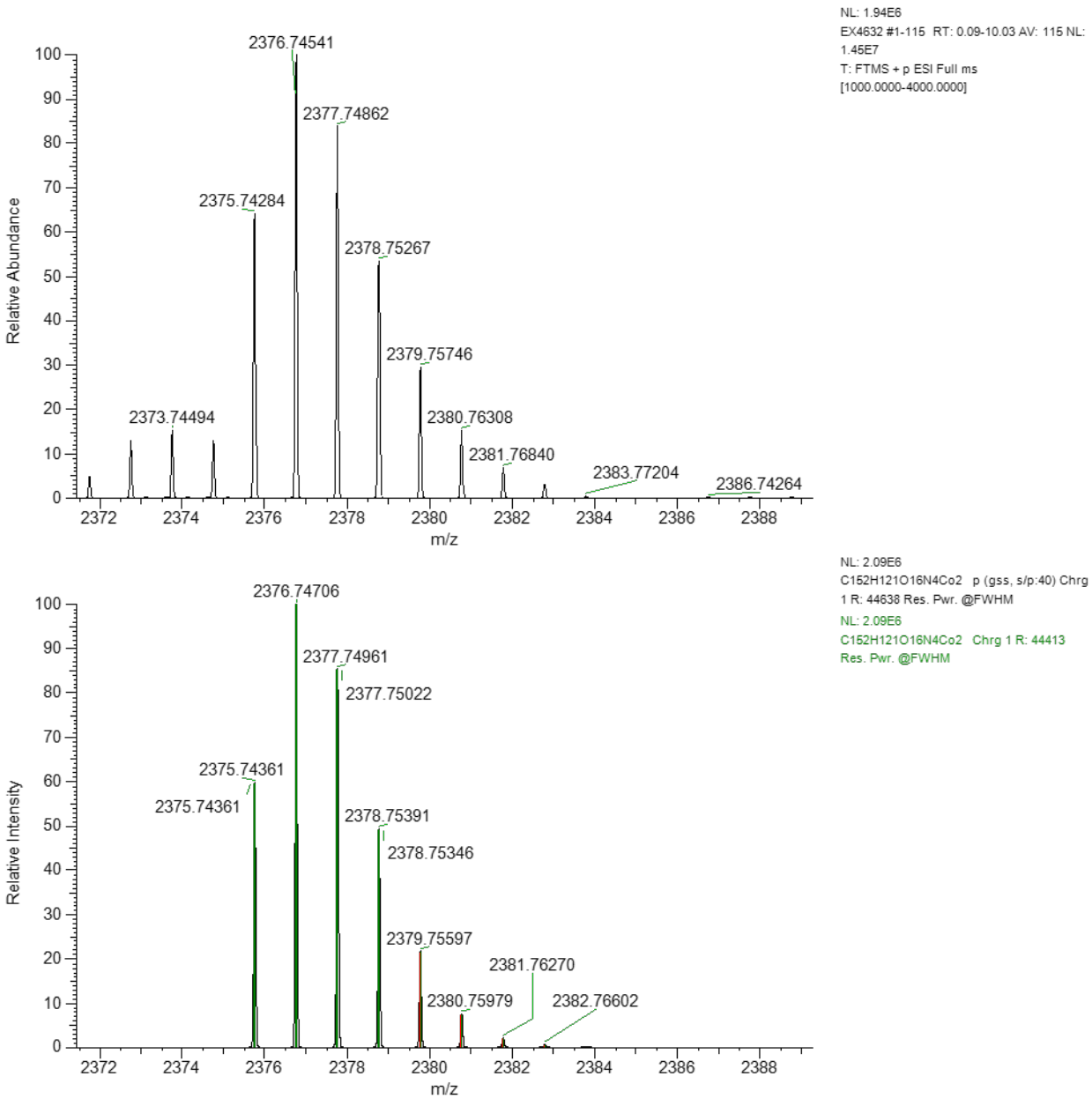

Ru_2(*S*-TPPTTL)$_4$Cl (17-Cl) (Top, observed. Bottom, simulated)

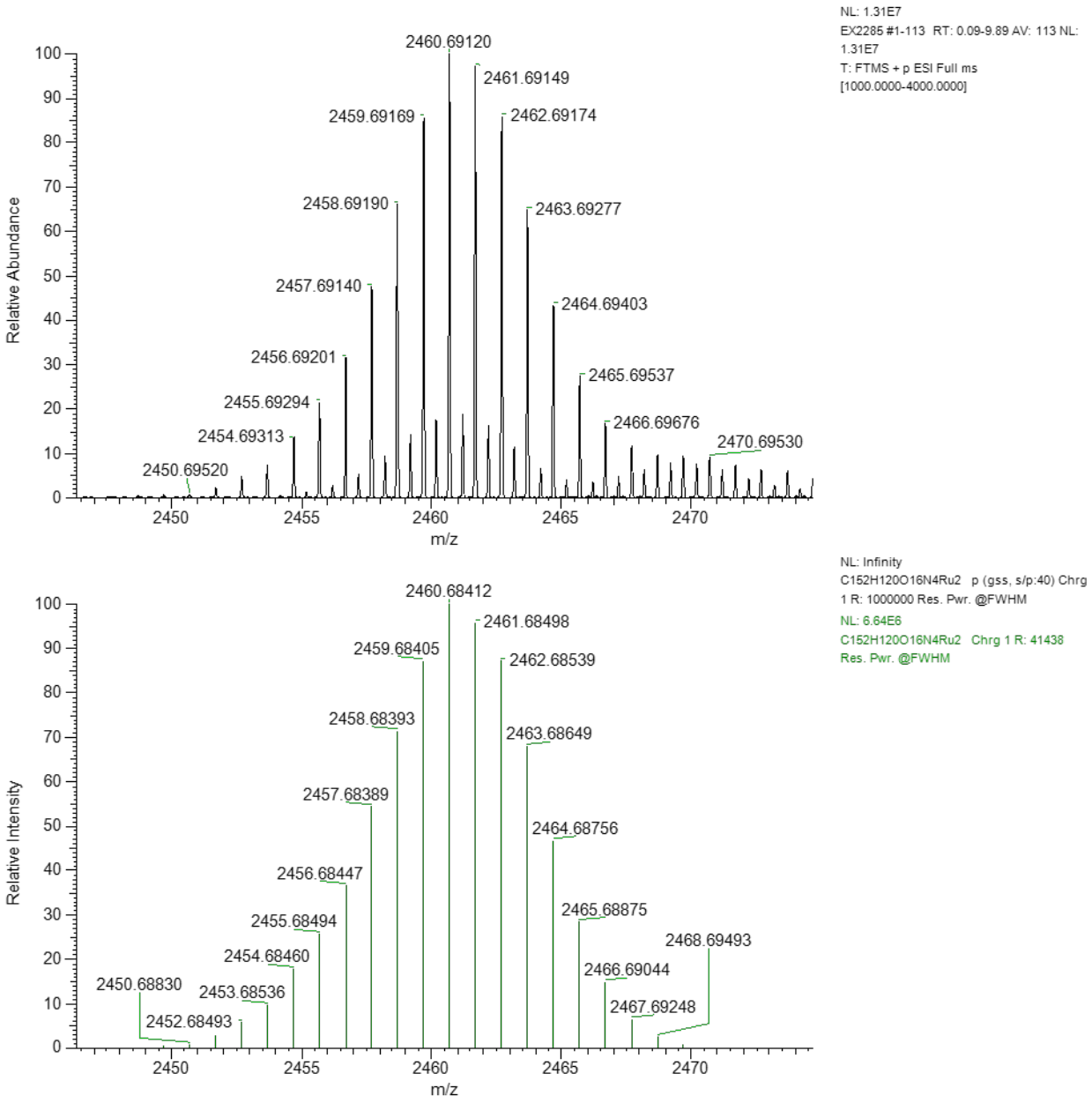

Ru_2(*S*-TPPTTL)$_4$BAr^F (17-BAr^F) (Top, observed. Bottom, simulated)

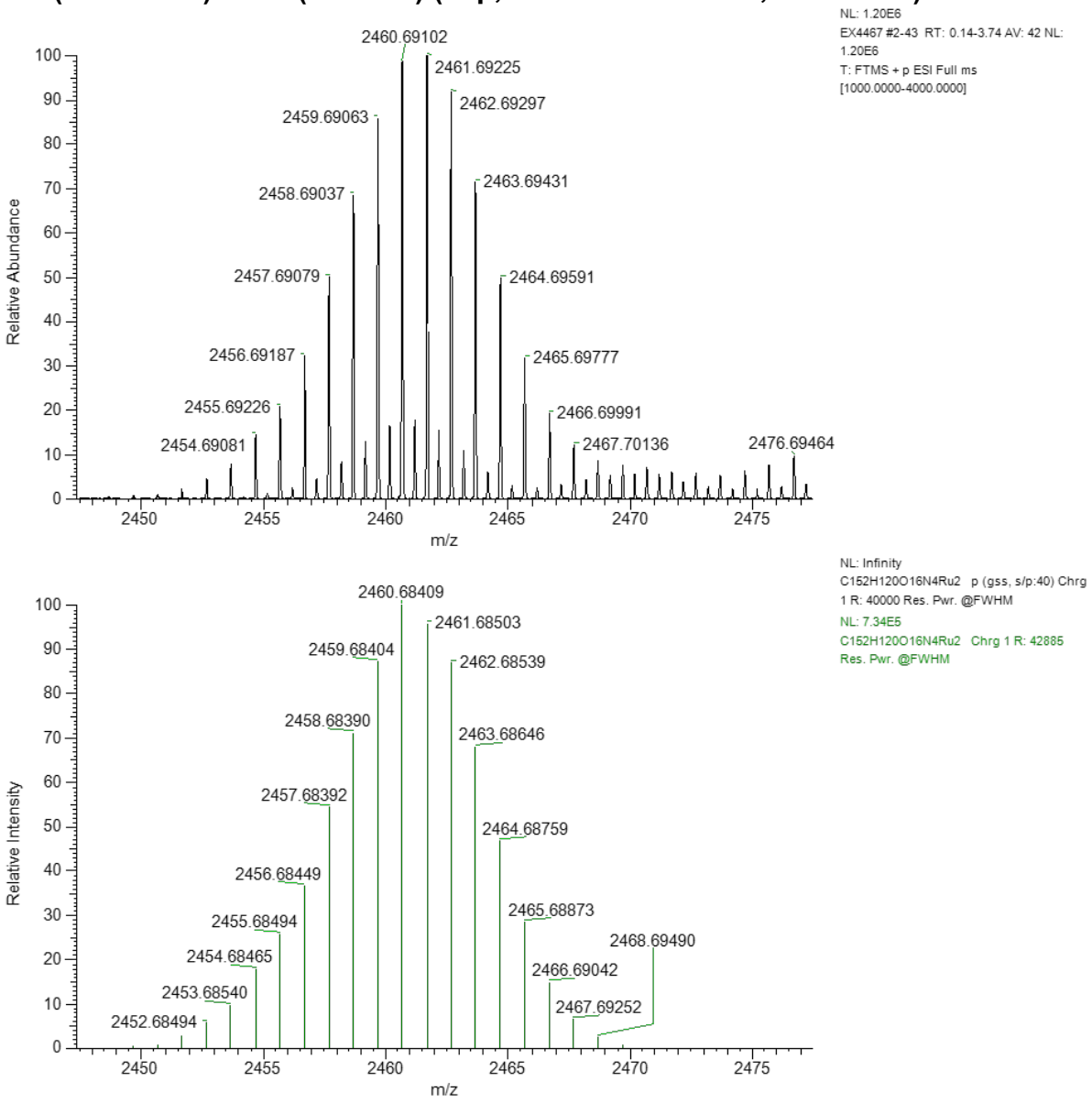

BAr^F Counter Ion (Top, observed. Bottom, simulated)

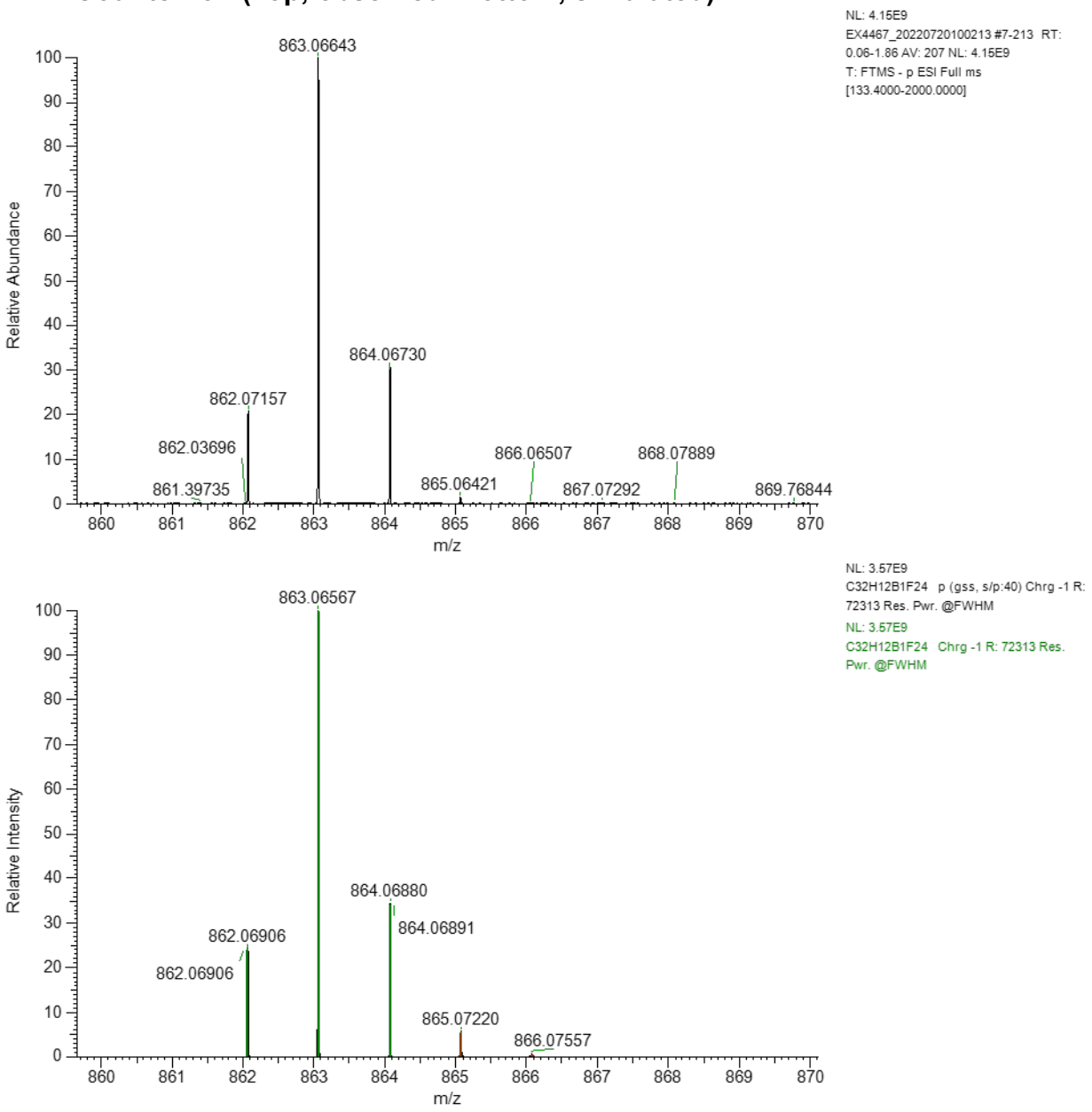

Ru_2(*S*-PTTL)$_4$Cl (18-Cl) (Top, observed. Bottom, simulated)

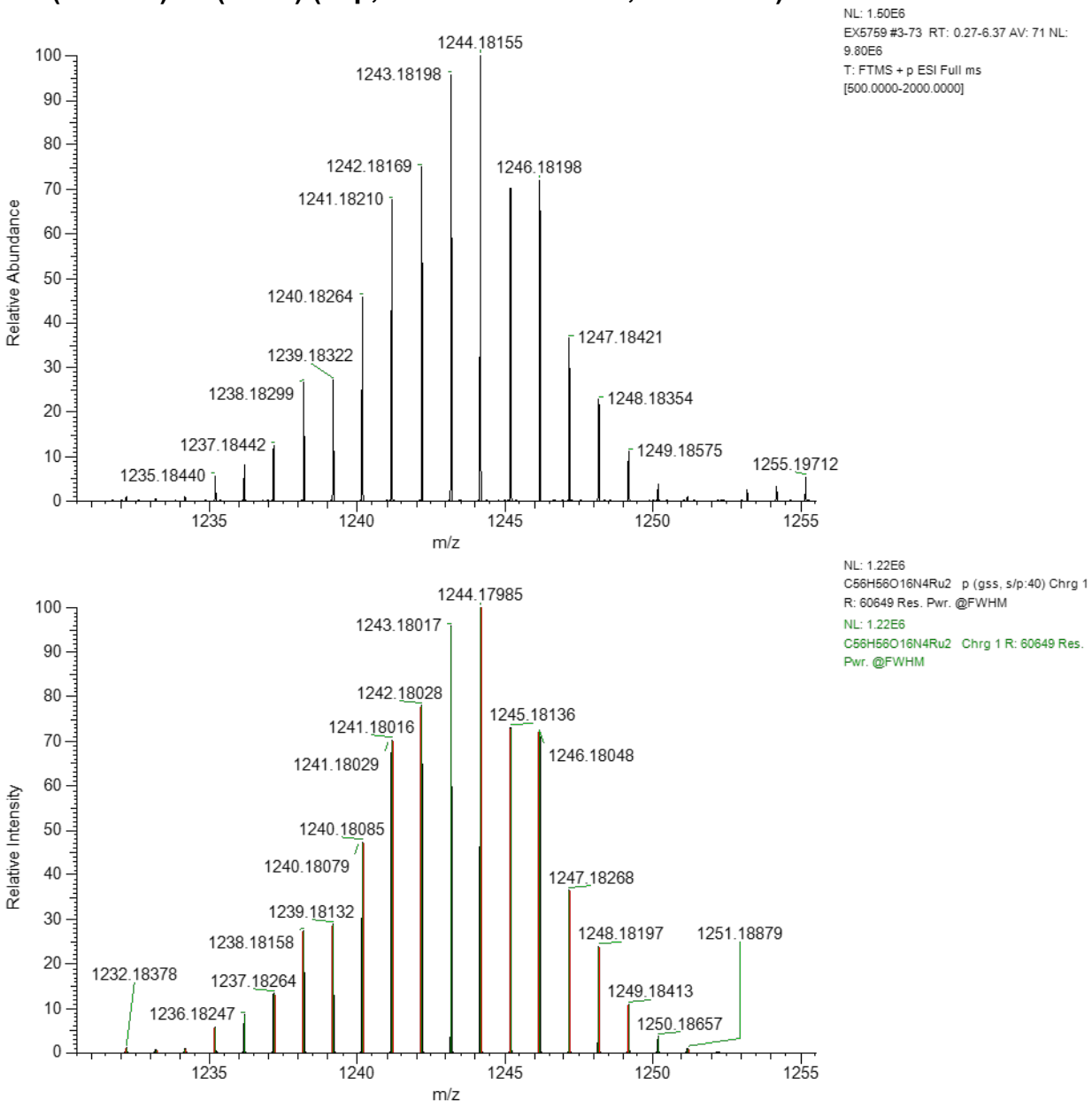

Ru_2(*S*-PTTL)$_4$BAr^F (18-BAr^F) (Top, observed. Bottom, simulated)

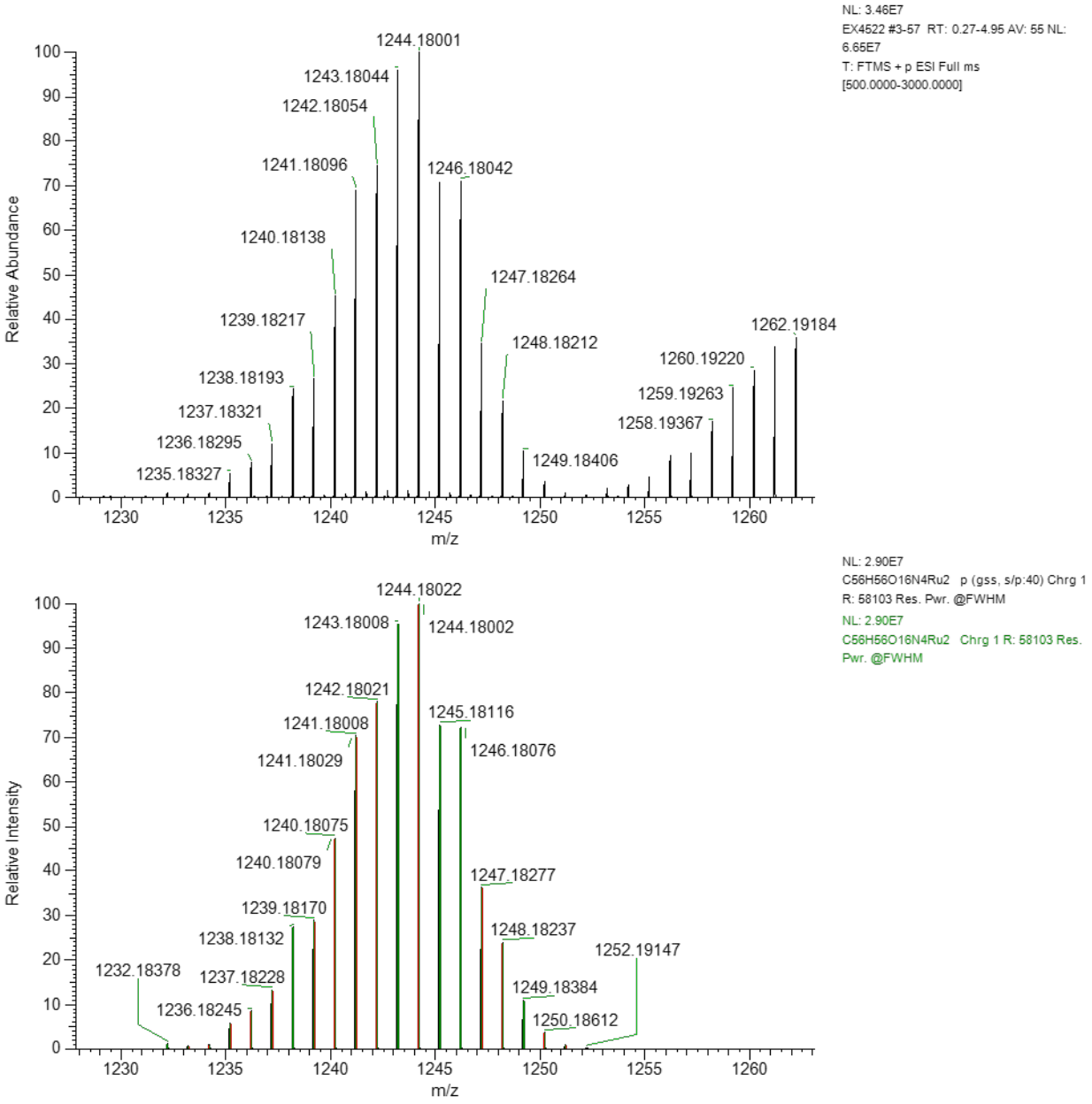

BAr^F Counterion (Top, observed. Bottom, simulated)

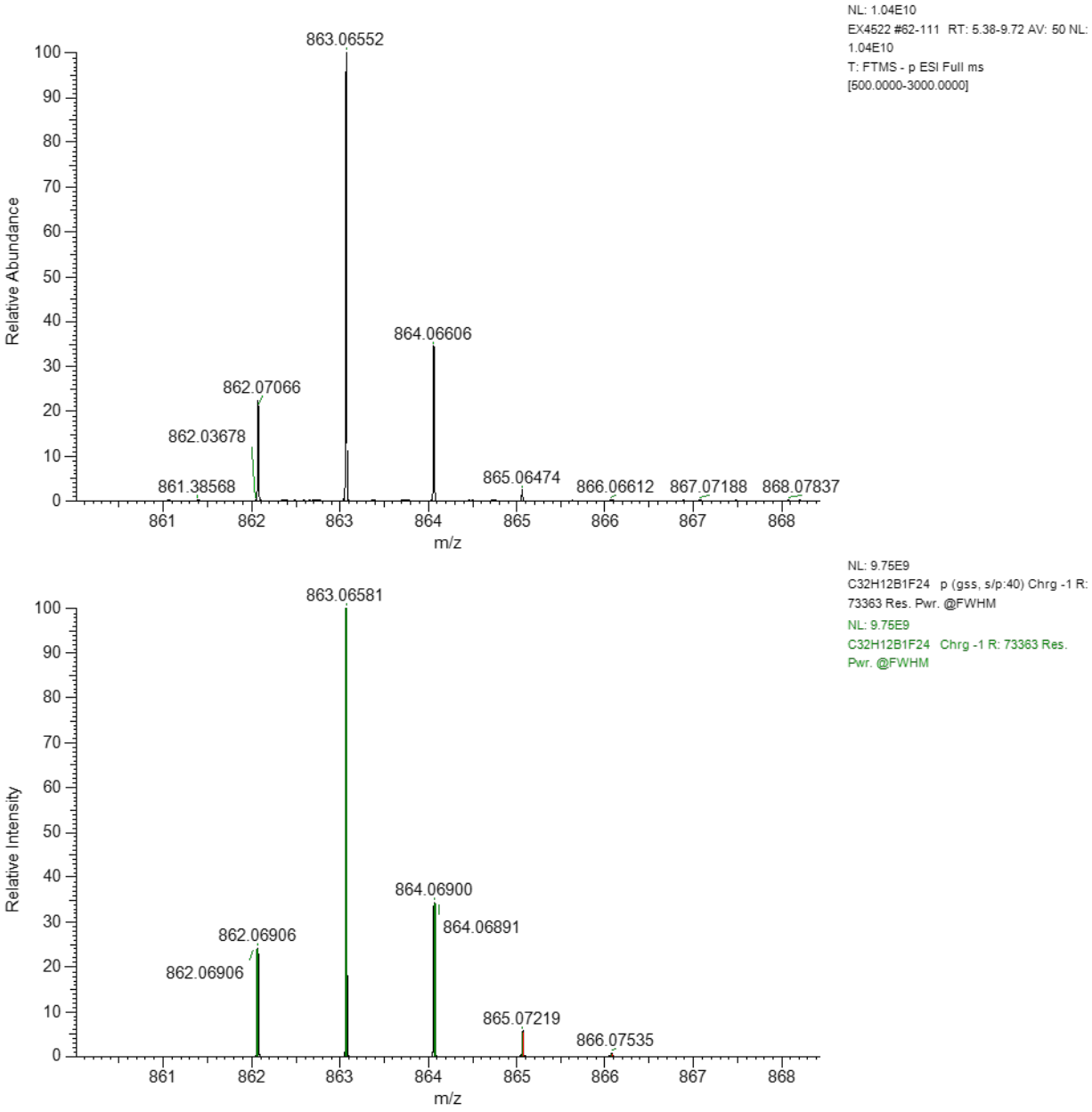

Ru_2(*S*-PTAD)$_4$Cl (19-Cl) (Top, observed. Bottom, simulated)

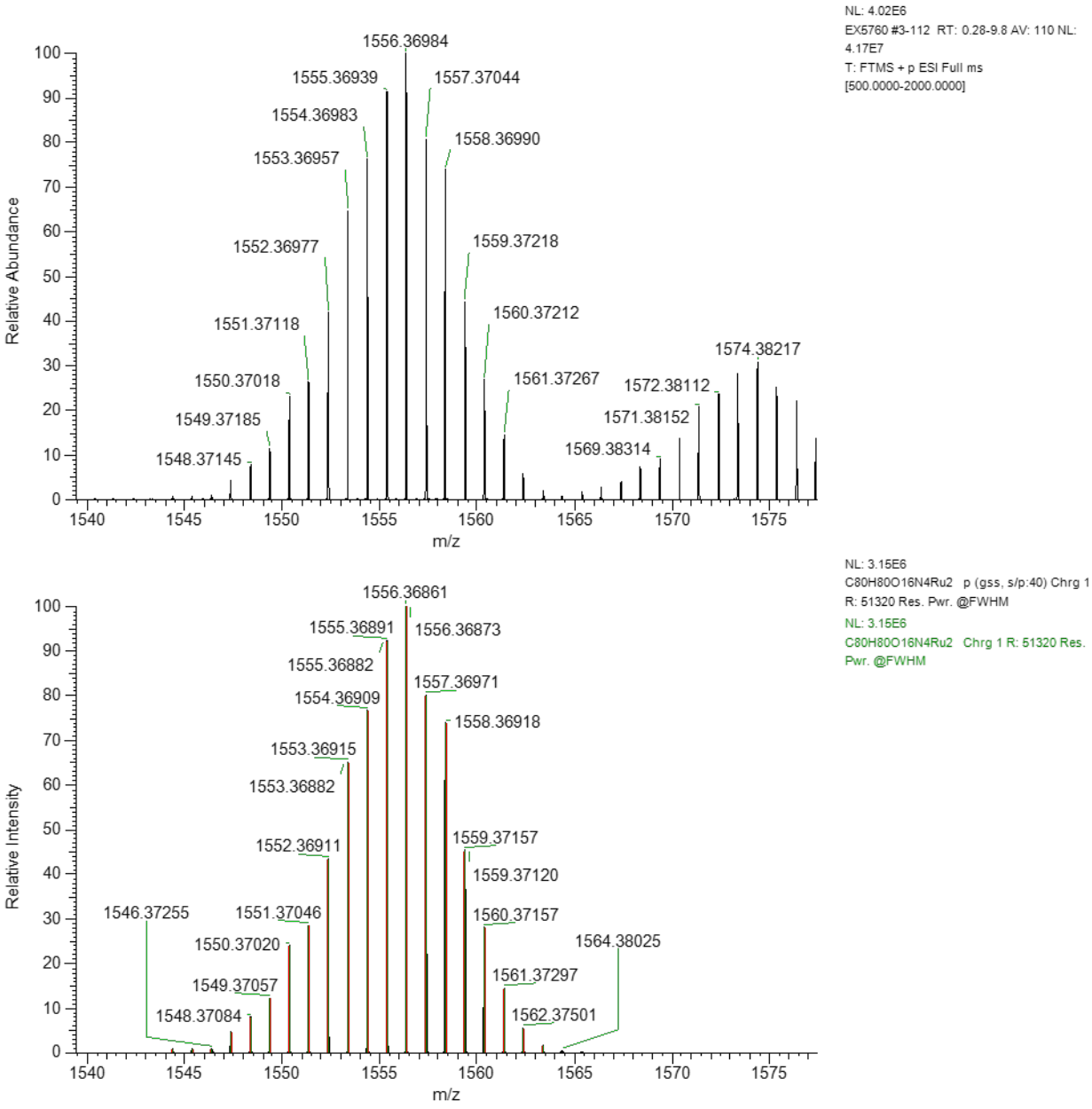

Ru_2(*S*-PTAD)$_4$BAr^F (19-BAr^F) (Top, observed. Bottom, simulated)

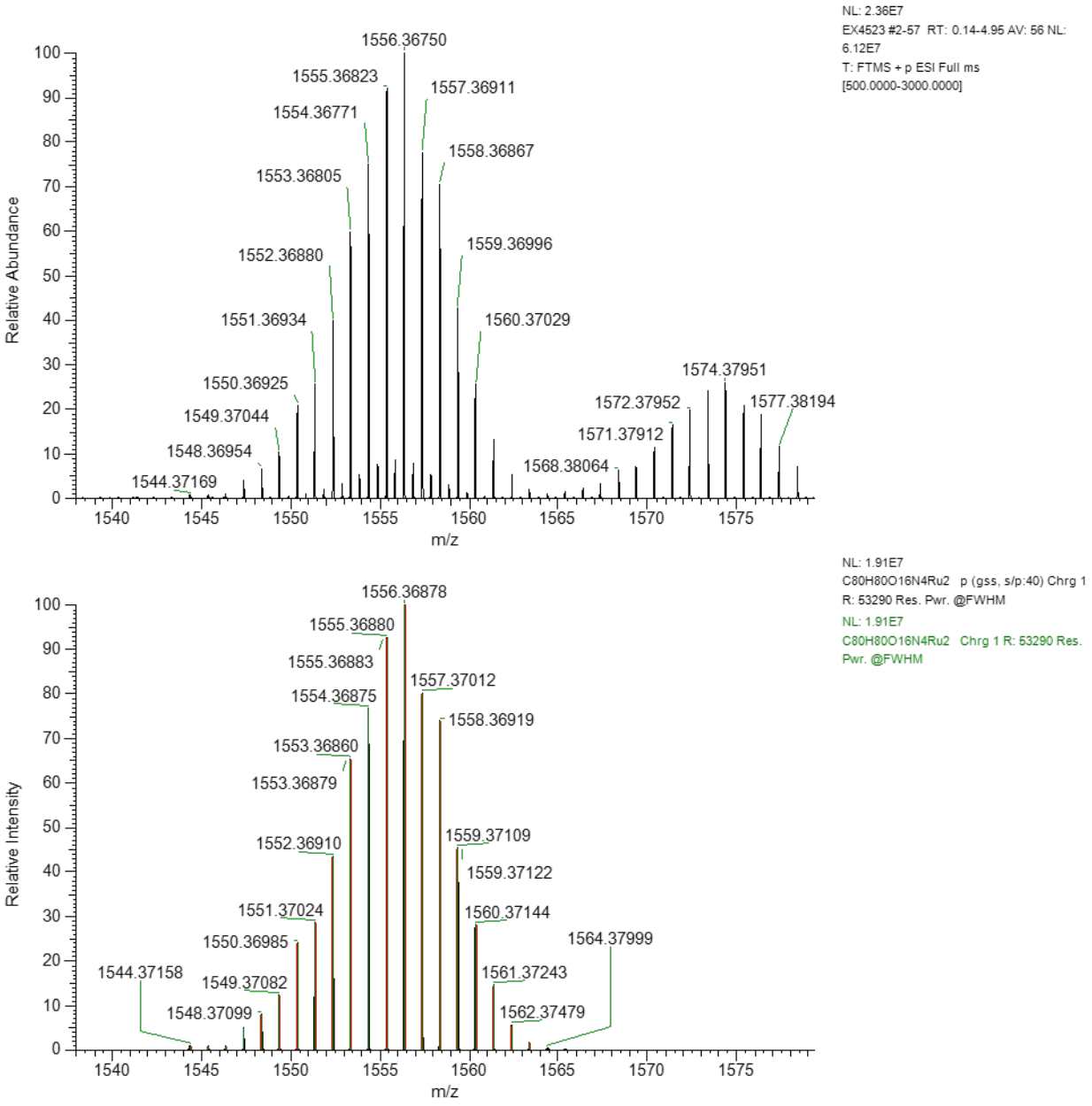

BAr^F Counterion (Top, observed. Bottom, simulated)

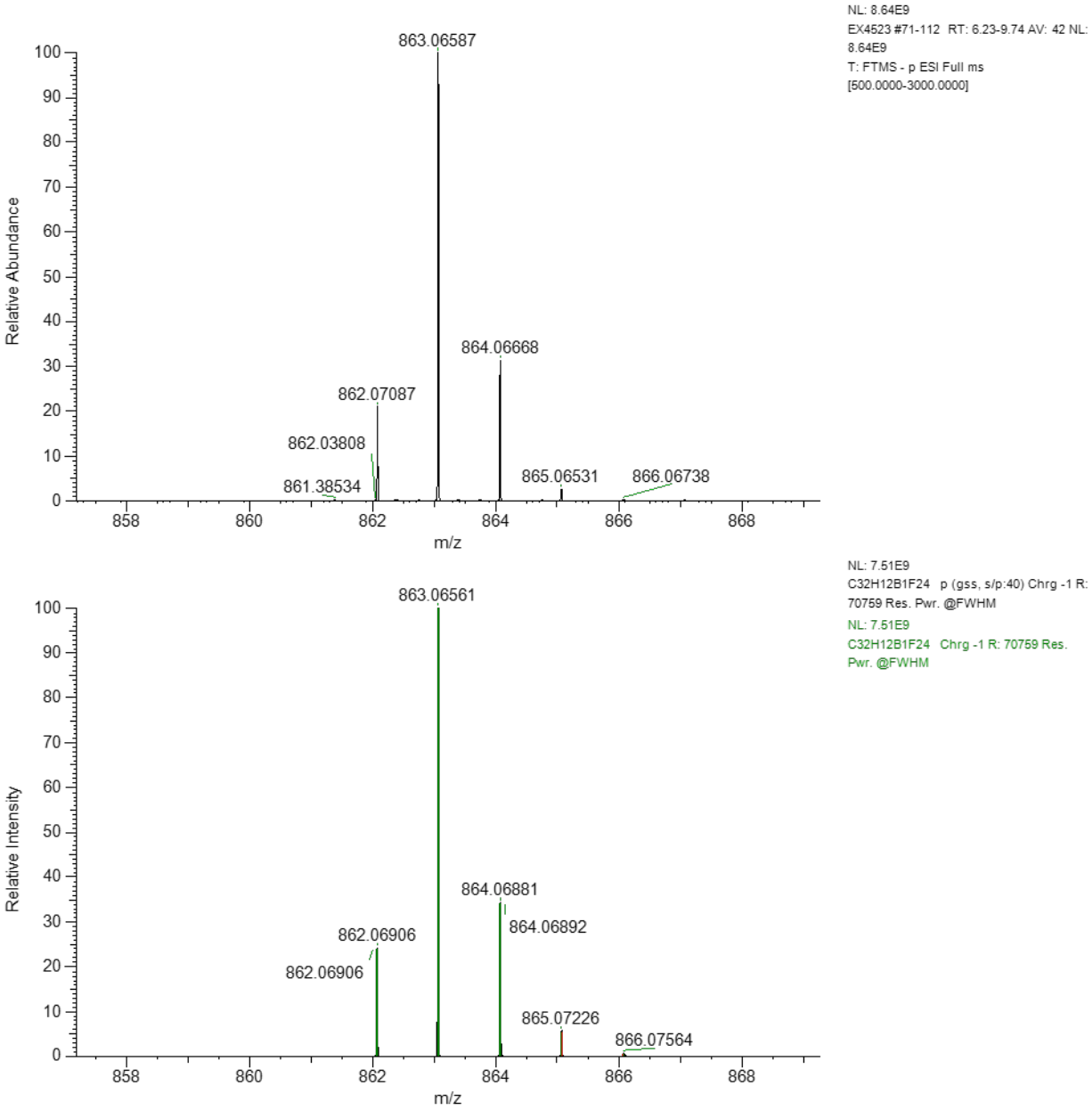

Ru_2(*S*-TCPTAD)$_4$Cl (20-Cl) (Top, observed. Bottom, simulated)

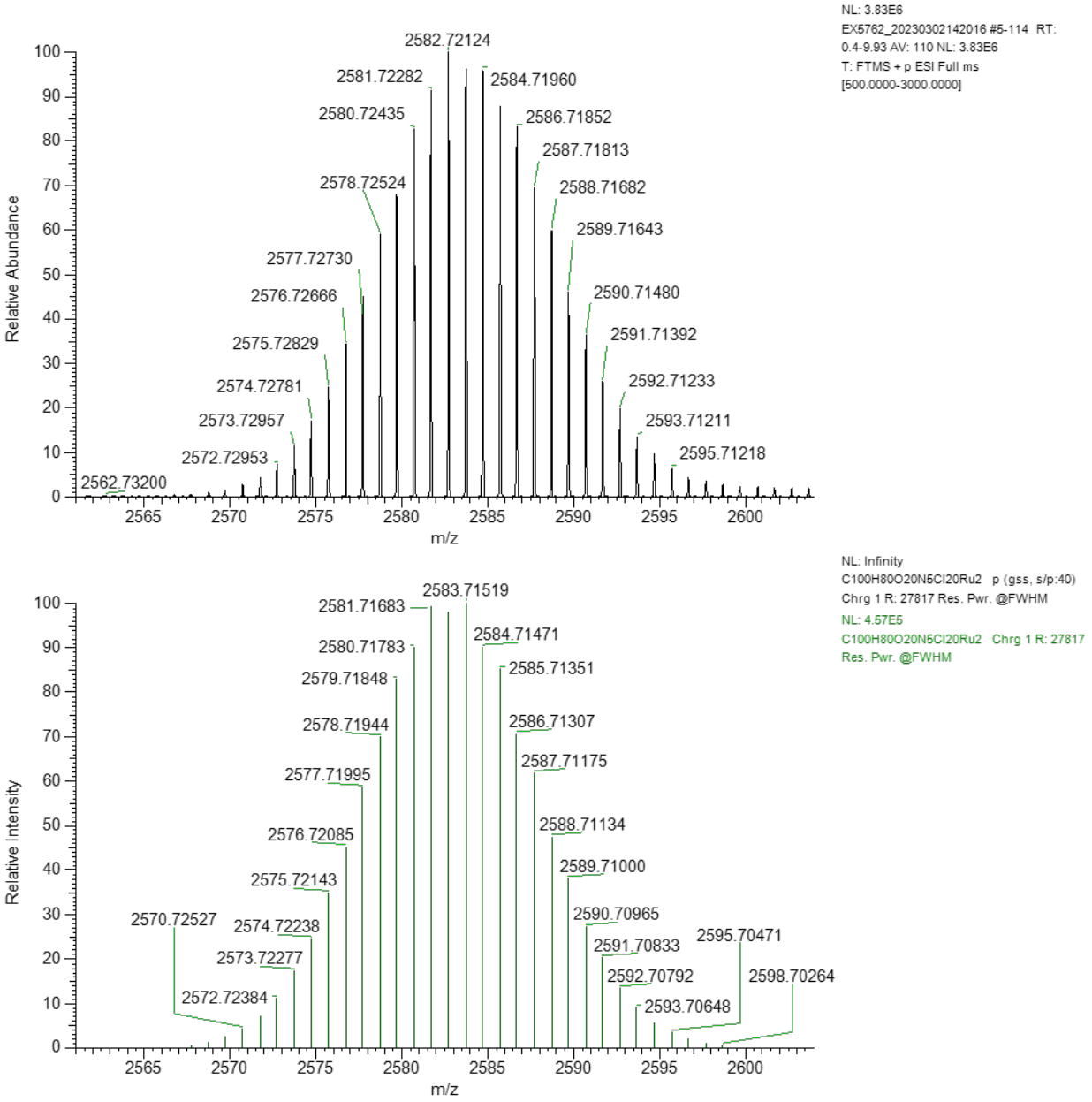

Ru_2(*S*-TCPTAD)$_4$BAr^F (20-BAr^F) (Top, observed. Bottom, simulated)

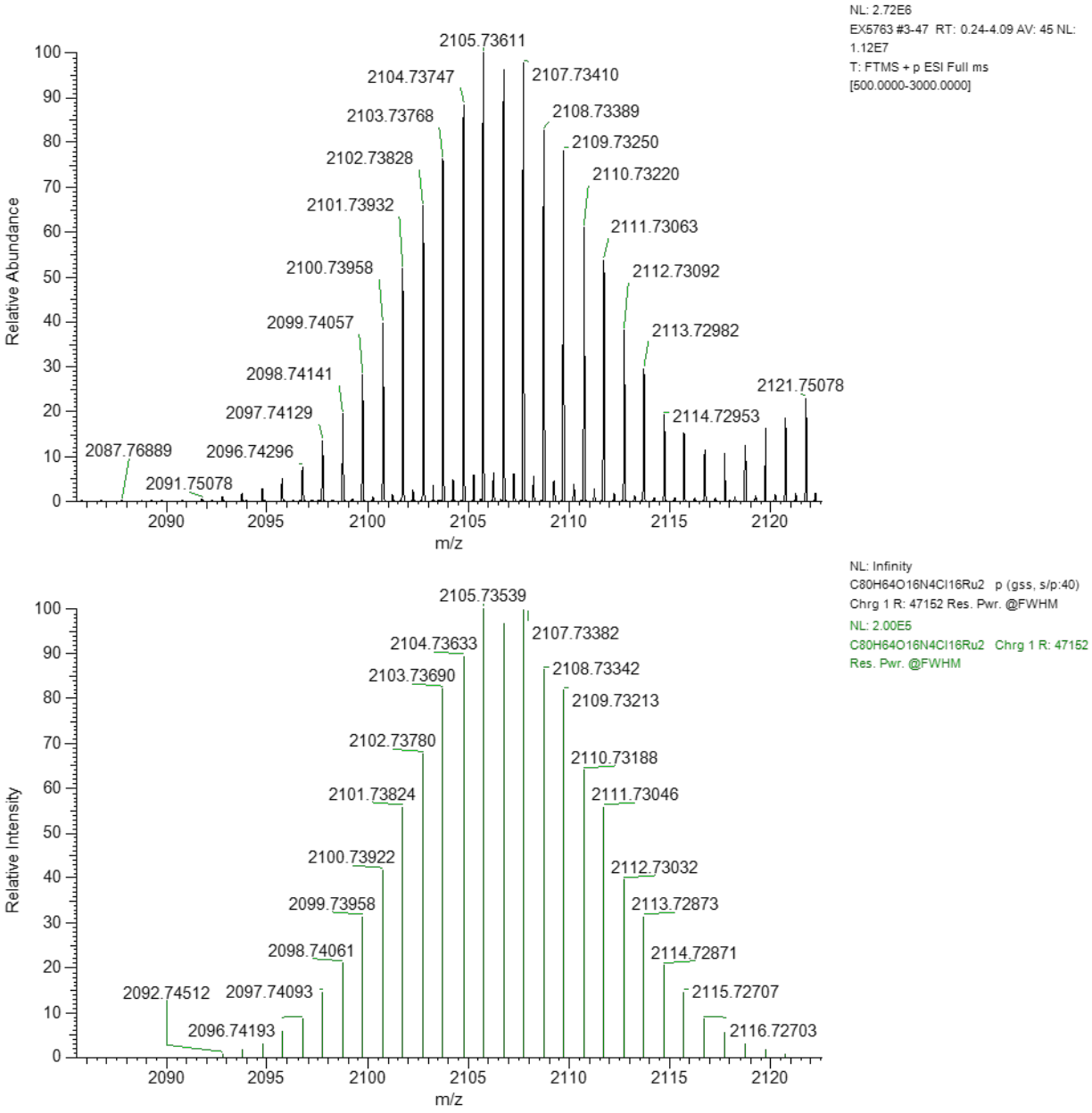

BAr^F Counterion (Top, observed. Bottom, simulated)

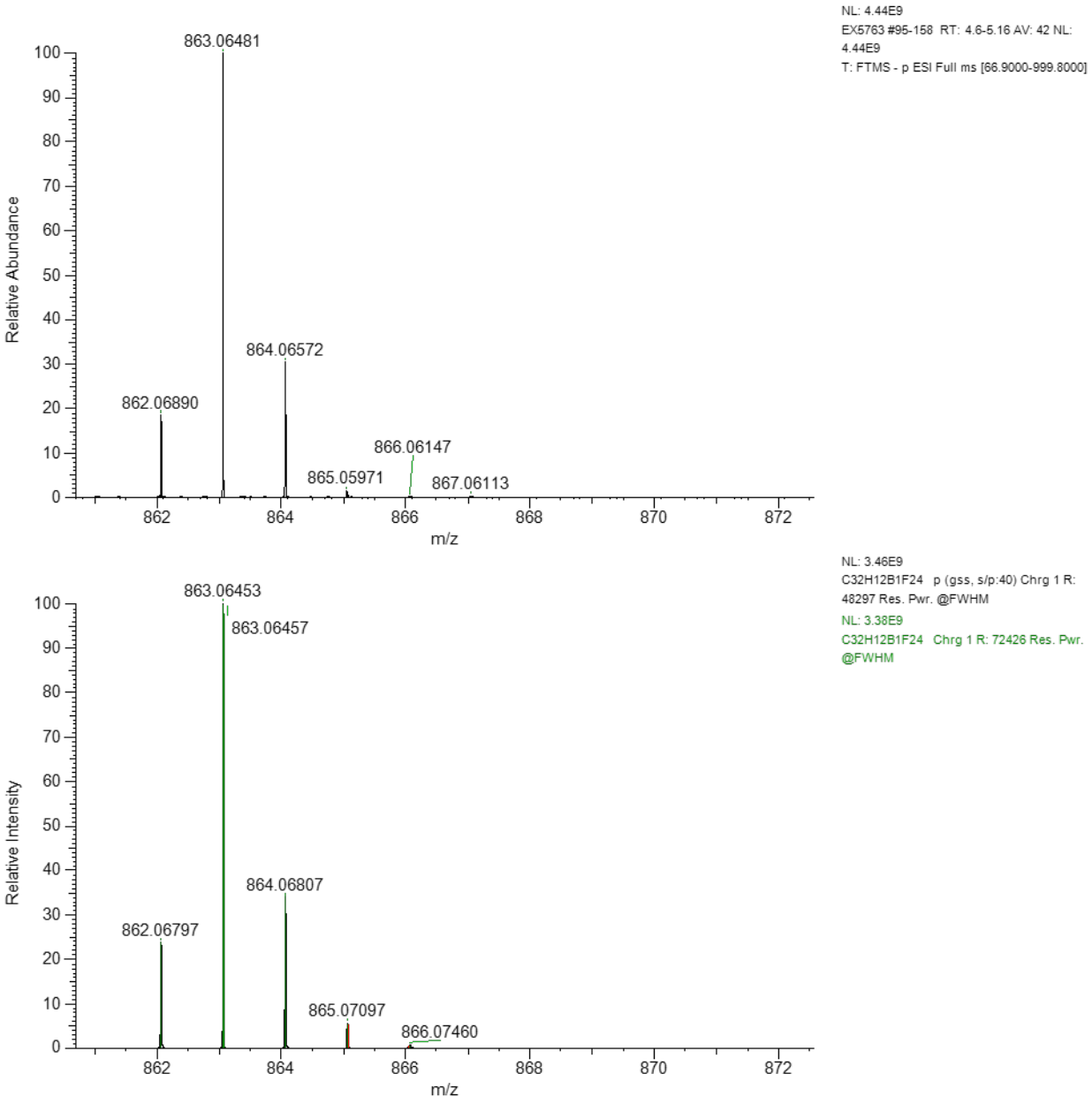

Ru_2(*S*-NTTL)$_4$Cl (21-Cl) (Top, observed. Bottom, simulated)

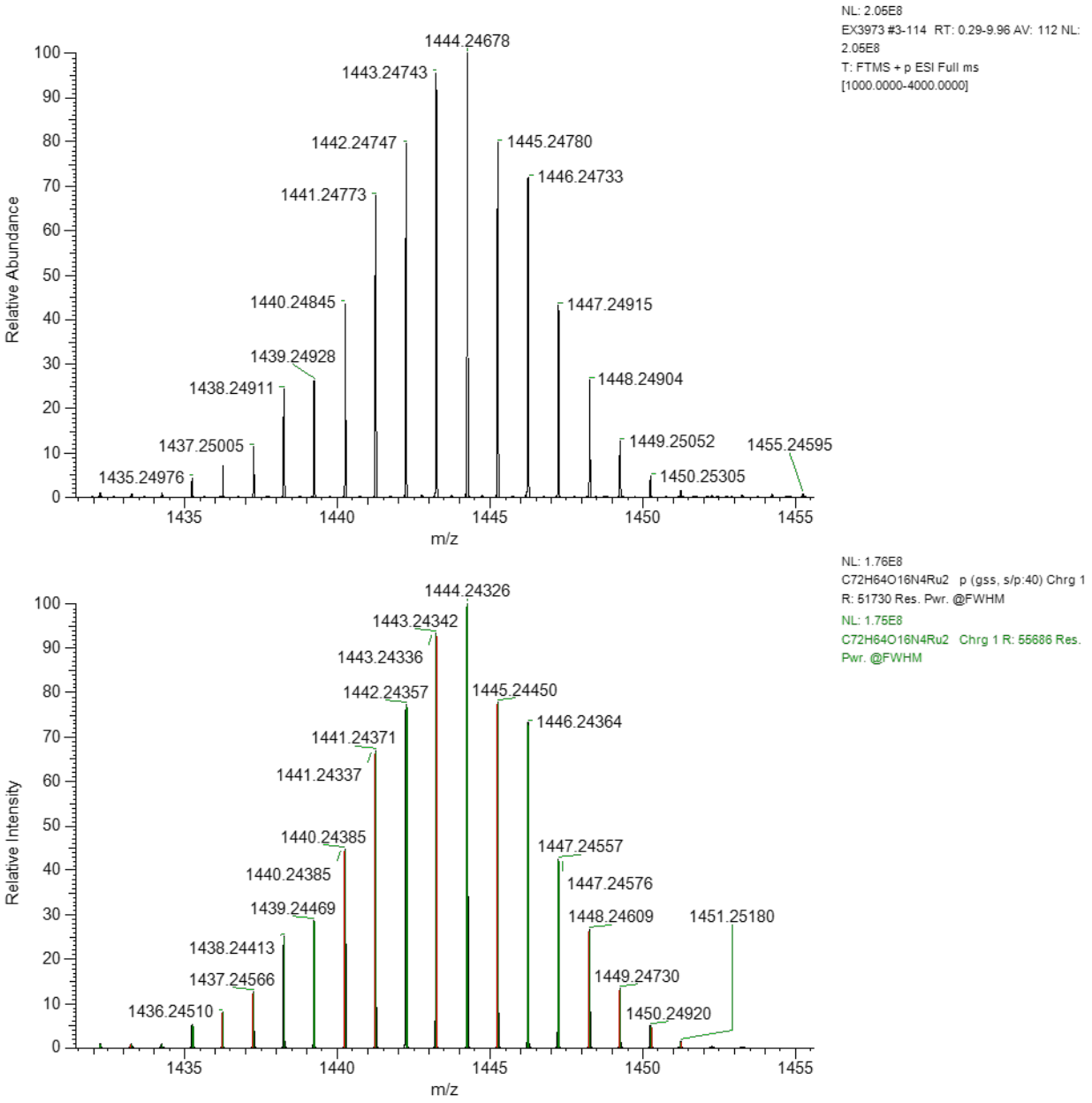

Ru_2(*S*-NTTL)$_4$BAr^F (21-BAr^F) (Top, observed. Bottom, simulated)

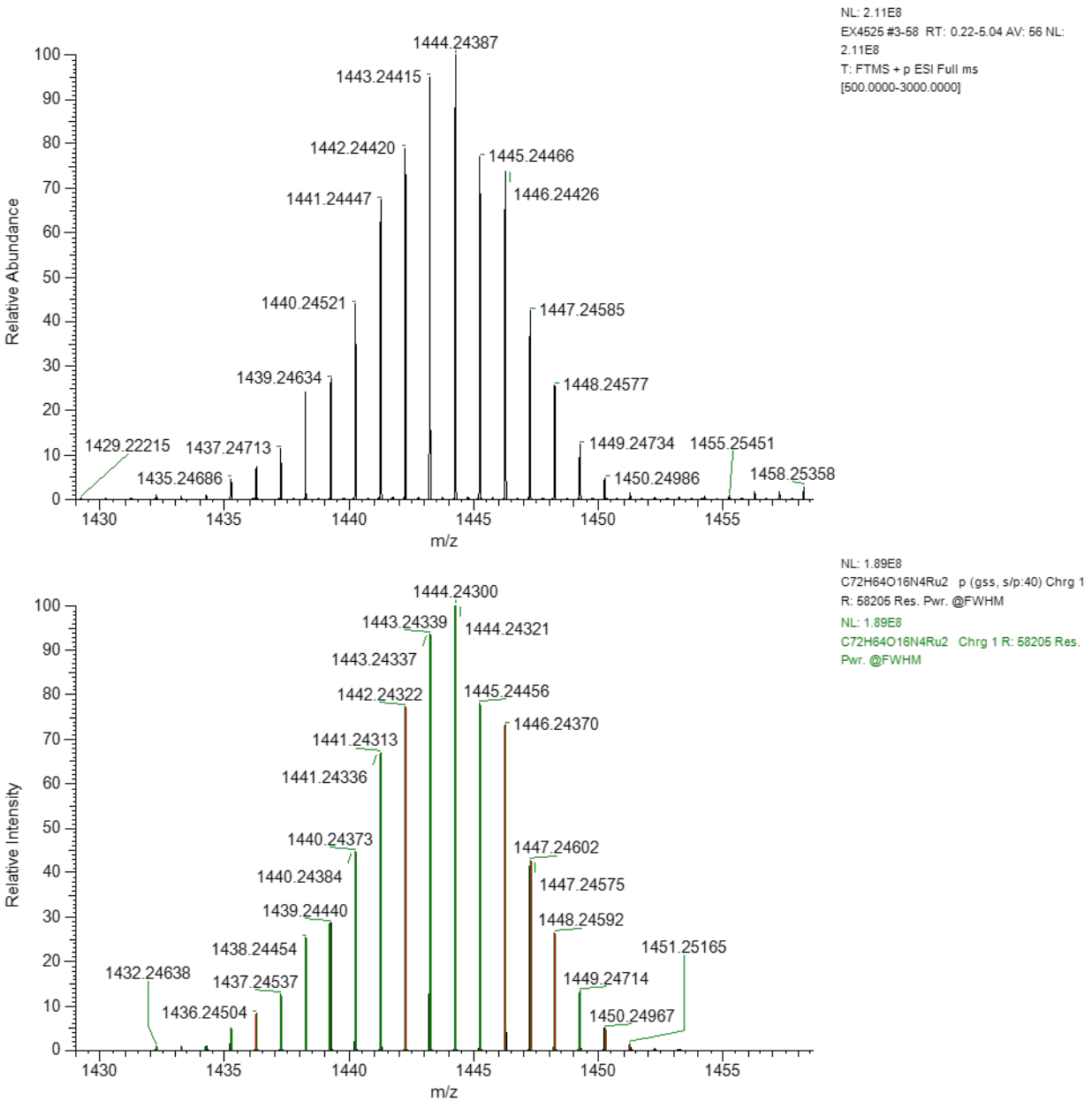

BAr^F Counterion (Top, observed. Bottom, simulated)

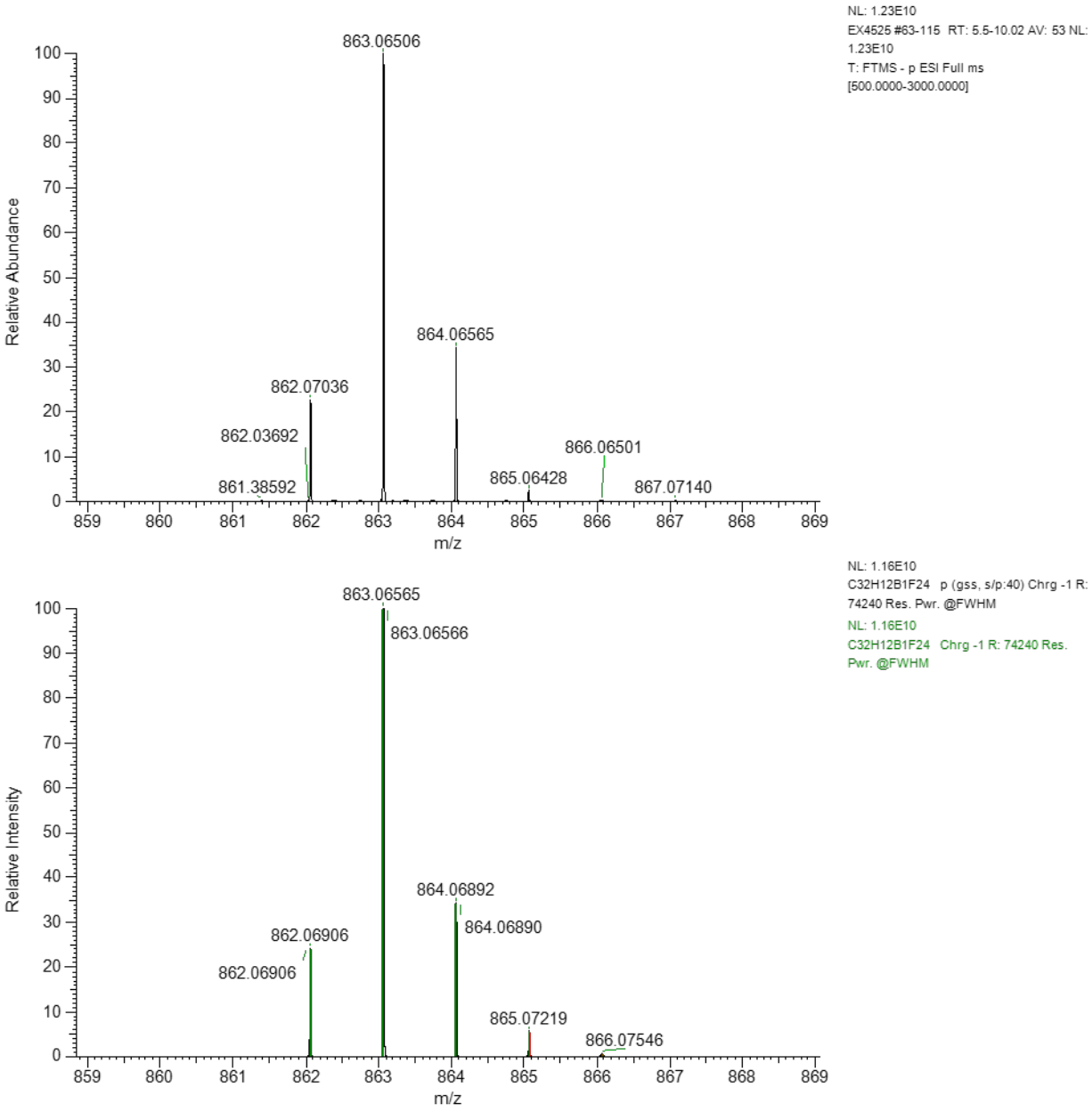

General Procedure for cobalt-catalyzed cyclopropanation:

To a flame dried vial equipped with a stir bar and 4Å MS under inert atmosphere was added catalyst (10mol %) and substrate (0.5 mmol, 2.5 equiv) which was subsequently dissolved in 2 mL of DCM. Then, the diazo compound (0.20 mmol, 1.0 equiv) was dissolved in 2 mL of DCM and added to the reaction vial over a period of 2 h using a syringe pump. The reaction was run at room temperature or 40 °C for 18 h. Once completed the reaction solution was passed through a small silica plug to remove cobalt catalyst, concentrated in vacuo, and purified through flash chromatography (0-18% Hexanes/diethyl ether) to afford the desired product.

React IR Experiments

General Procedure for react IR Experiments:

An oven dried three-neck round bottom flask equipped with a stir bar and 4Å MS was fitted to the React IR 45m probe and backfilled with nitrogen 3 times. Then, DCM (11 mL) was added to the flask and was equilibrated for 15 minutes. Styrene (xx equiv) and aryldiazoacetate (0.600 mmol) were added to the flask sequentially and the flask was left to equilibrate for 15 min. The React IR was set to monitor the diazo stretching vibration at 2300 cm^{-1}. After the equilibration, the catalysts (xxmol %) was dissolved in 1 mL of DCM and added to the reaction flask in one portion. After completion of reaction (monitored by the disappearance of the peak at 2300 cm^{-1}), the reaction was concentrated and purified through flash chromatography (0% hexanes/diethyl ether, 0-18% hexanes/diethyl ether) to afford a crystalline solid.

HPLC Chromatographs

HPLC chromatographs for cobalt-catalyzed cyclopropanation

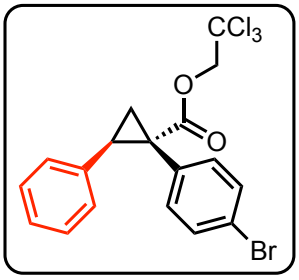

Compound **12**
Cobalt-catalyzed reaction at 25 °C

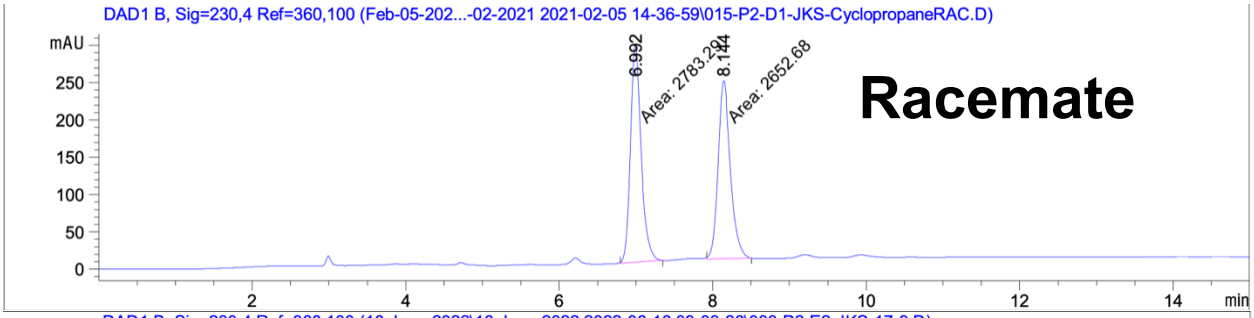

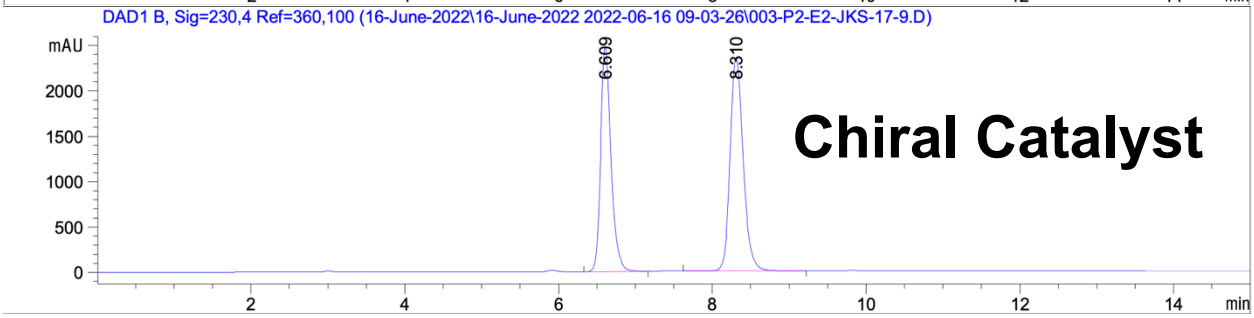

Signal 2: DAD1 B, Sig=230,4 Ref=360,100

Peak #	RetTime [min]	Type	Width [min]	Area [mAU*s]	Height [mAU]	Area %
1	6.609	BB	0.1436	2.32320e4	2472.58936	45.7450
2	8.310	BB	0.1808	2.75539e4	2350.05371	54.2550
Totals :				5.07859e4	4822.64307	

Cobalt-catalyzed reaction at 40 °C

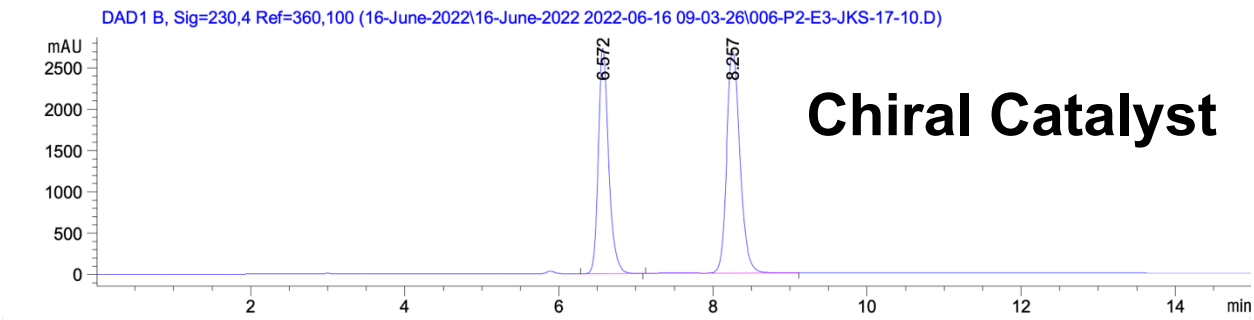

Signal 2: DAD1 B, Sig=230,4 Ref=360,100

Peak #	RetTime [min]	Type	Width [min]	Area [mAU*s]	Height [mAU]	Area %
1	6.572	BB	0.1462	2.57793e4	2729.63623	44.4686
2	8.257	VB R	0.1831	3.21926e4	2686.88770	55.5314
Totals :				5.79720e4	5416.52393	

Chromatographs for catalyst screen of cyclopropanation of styrene

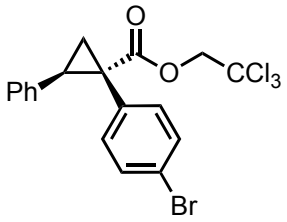

Racemate **12**

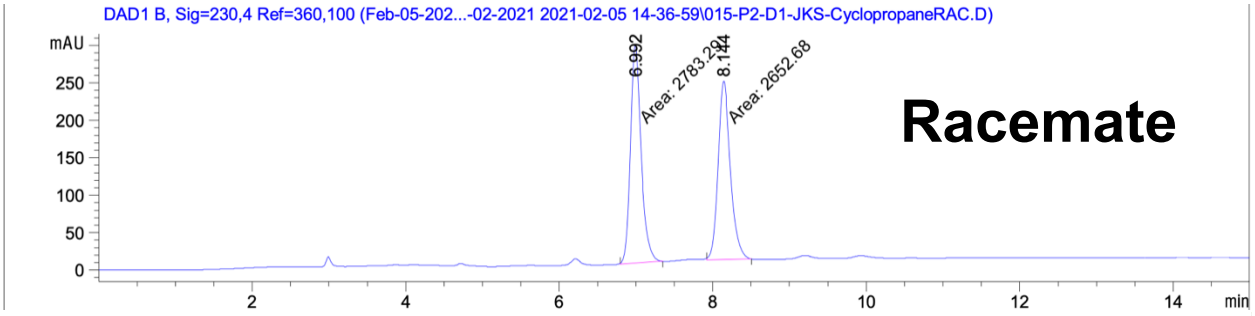

Signal 2: DAD1 B, Sig=230,4 Ref=360,100

Peak #	RetTime [min]	Type	Width [min]	Area [mAU*s]	Height [mAU]	Area %
1	6.992	MM	0.1590	2783.28638	291.76401	51.2013
2	8.144	MM	0.1852	2652.68018	238.66949	48.7987

Reaction with **17-Cl**

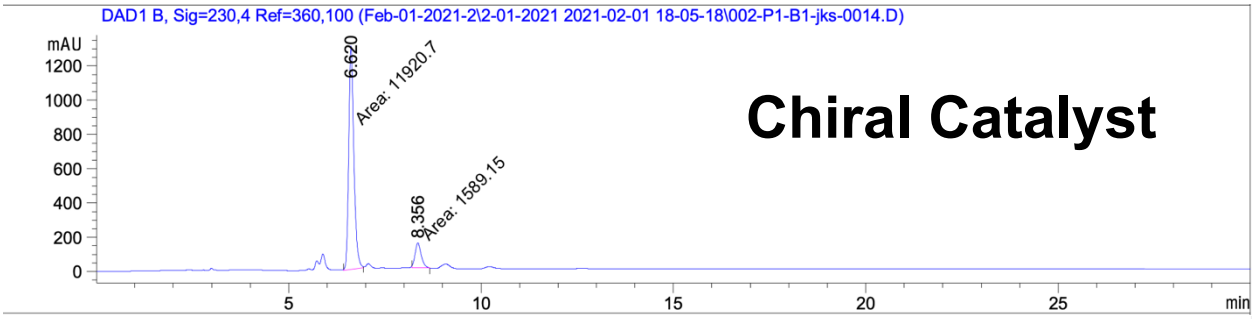

Signal 2: DAD1 B, Sig=230,4 Ref=360,100

Peak #	RetTime [min]	Type	Width [min]	Area [mAU*s]	Height [mAU]	Area %
1	6.620	MM	0.1522	1.19207e4	1305.00964	88.2371
2	8.356	MM	0.1831	1589.15454	144.62219	11.7629
Totals :				1.35099e4	1449.63184	

Reaction with **17-BAr^F**

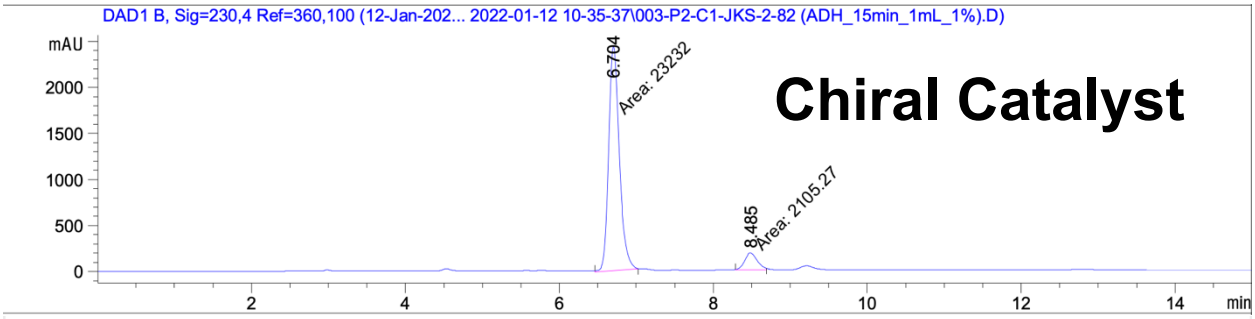

Signal 2: DAD1 B, Sig=230,4 Ref=360,100

Peak #	RetTime [min]	Type	Width [min]	Area [mAU*s]	Height [mAU]	Area %
1	6.704	MM	0.1586	2.32320e4	2441.86987	91.6910
2	8.485	MM	0.1902	2105.26636	184.43390	8.3090
Totals :				2.53373e4	2626.30377	

Reaction with **18-Cl**

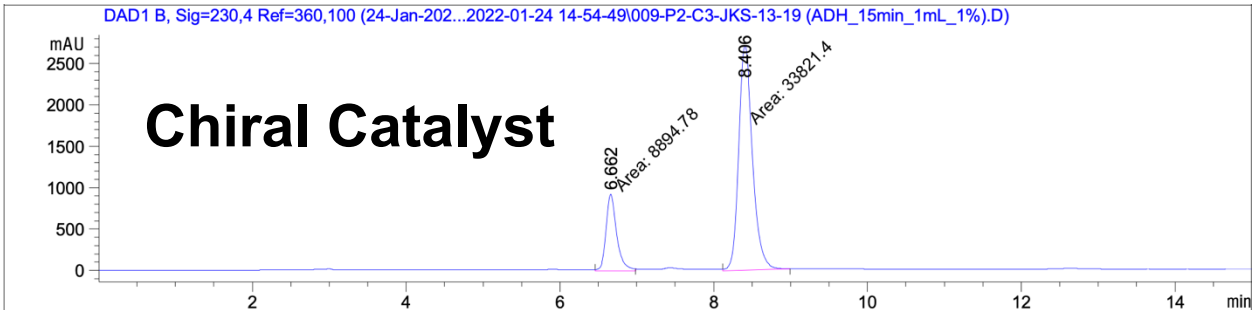

Signal 2: DAD1 B, Sig=230,4 Ref=360,100

Peak #	RetTime [min]	Type	Width [min]	Area [mAU*s]	Height [mAU]	Area %
1	6.662	MM	0.1601	8894.77539	925.95435	20.8230
2	8.406	MM	0.2079	3.38214e4	2711.37109	79.1770
Totals :				4.27162e4	3637.32544	

Reaction with **18-BAr^F**

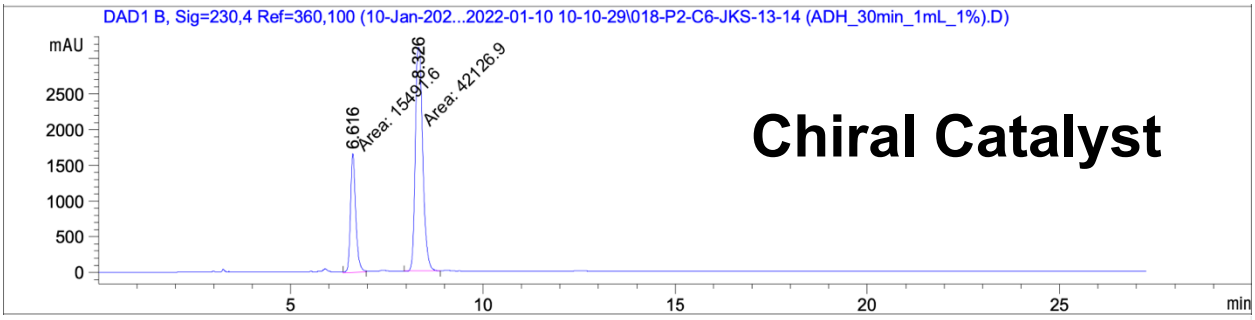

Signal 2: DAD1 B, Sig=230,4 Ref=360,100

Peak #	RetTime [min]	Type	Width [min]	Area [mAU*s]	Height [mAU]	Area %
1	6.616	MM	0.1553	1.54916e4	1662.19495	26.8865
2	8.326	MM	0.2245	4.21269e4	3128.14209	73.1135
Totals :				5.76185e4	4790.33704	

Reaction with **19-Cl**

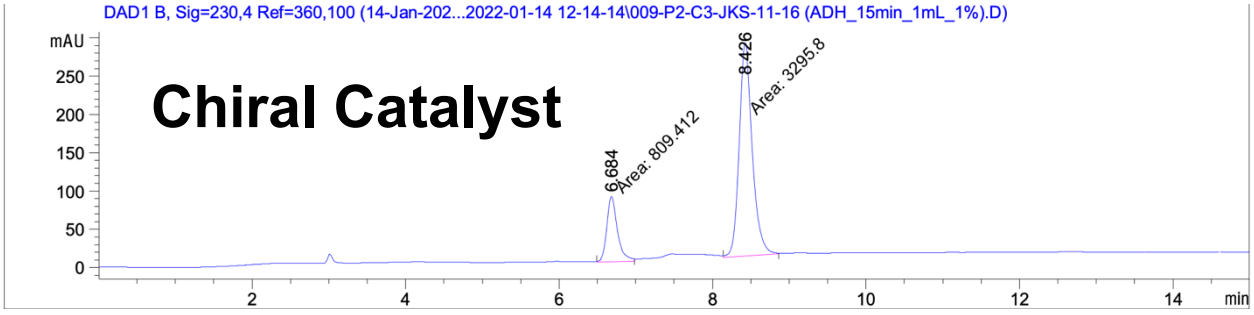

Signal 2: DAD1 B, Sig=230,4 Ref=360,100

Peak #	RetTime [min]	Type	Width [min]	Area [mAU*s]	Height [mAU]	Area %
1	6.684	MM	0.1585	809.41248	85.12662	19.7167
2	8.426	MM	0.1973	3295.80225	278.45493	80.2833
Totals :				4105.21472	363.58154	

Reaction with **19-BAr^F**

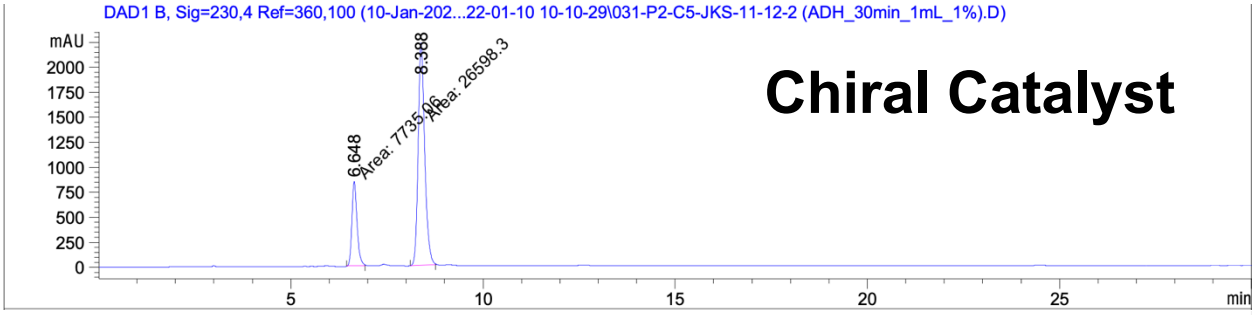

Signal 2: DAD1 B, Sig=230,4 Ref=360,100

Peak #	RetTime [min]	Type	Width [min]	Area [mAU*s]	Height [mAU]	Area %
1	6.648	MM	0.1527	7735.06250	844.47351	22.5293
2	8.388	MM	0.1992	2.65983e4	2225.34326	77.4707
Totals :				3.43334e4	3069.81677	

Reaction with **20-Cl**

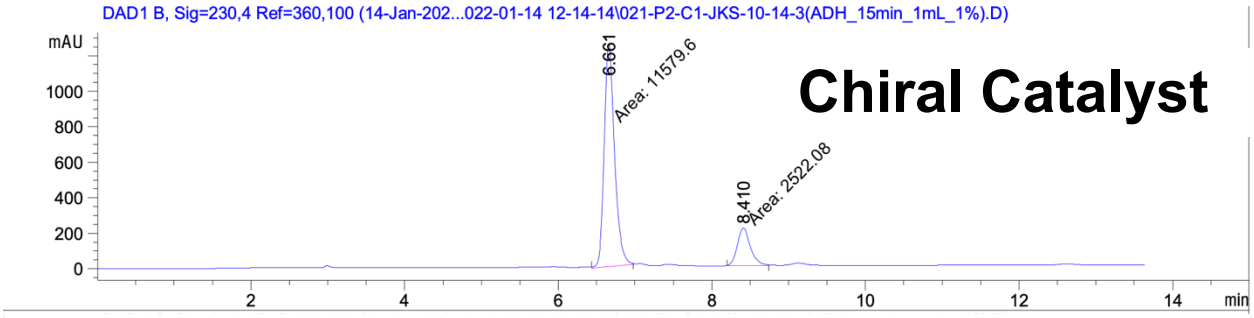

Signal 2: DAD1 B, Sig=230,4 Ref=360,100

Peak #	RetTime [min]	Type	Width [min]	Area [mAU*s]	Height [mAU]	Area %
1	6.661	MM	0.1535	1.15796e4	1257.49841	82.1150
2	8.410	MM	0.1975	2522.08228	212.81627	17.8850

Reaction with **20-BAr^{F}**

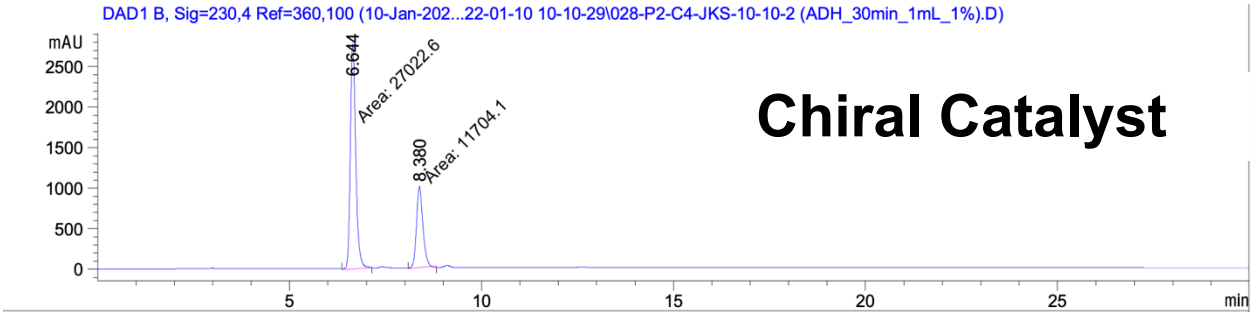

Signal 2: DAD1 B, Sig=230,4 Ref=360,100

Peak #	RetTime [min]	Type	Width [min]	Area [mAU*s]	Height [mAU]	Area %
1	6.644	MM	0.1621	2.70226e4	2777.73608	69.7776
2	8.380	MM	0.1940	1.17041e4	1005.47302	30.2224
Totals :				3.87267e4	3783.20911	

Reaction with **21-Cl**

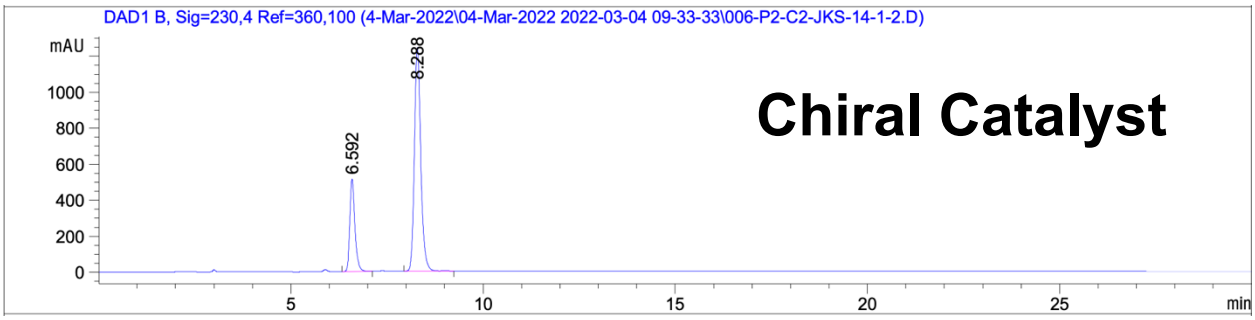

Signal 2: DAD1 B, Sig=230,4 Ref=360,100

Peak #	RetTime [min]	Type	Width [min]	Area [mAU*s]	Height [mAU]	Area %
1	6.592	BB	0.1364	4692.95605	514.33899	24.6941
2	8.288	BV R	0.1741	1.43114e4	1243.37061	75.3059
Totals :				1.90044e4	1757.70959	

Reaction with **21-BAr^F**

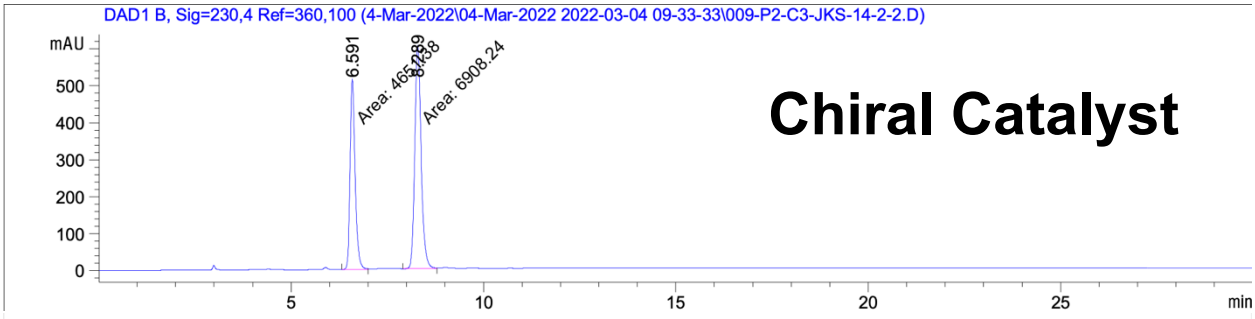

Signal 2: DAD1 B, Sig=230,4 Ref=360,100

Peak #	RetTime [min]	Type	Width [min]	Area [mAU*s]	Height [mAU]	Area %
1	6.591	MM	0.1507	4651.38281	514.31866	40.2382
2	8.289	MM	0.1907	6908.24219	603.70685	59.7618
Totals :				1.15596e4	1118.02551	

Reaction with **S18**

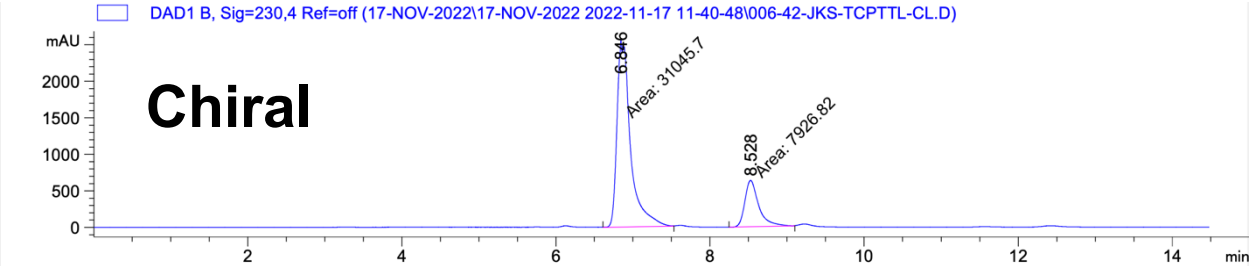

Signal 2: DAD1 B, Sig=230,4 Ref=off

Peak #	RetTime [min]	Type	Width [min]	Area [mAU*s]	Height [mAU]	Area %
1	6.846	MM	0.2024	3.10457e4	2555.91040	79.6605
2	8.528	MM	0.2077	7926.82373	636.00977	20.3395
Totals :				3.89725e4	3191.92017	

Reaction with **S19**

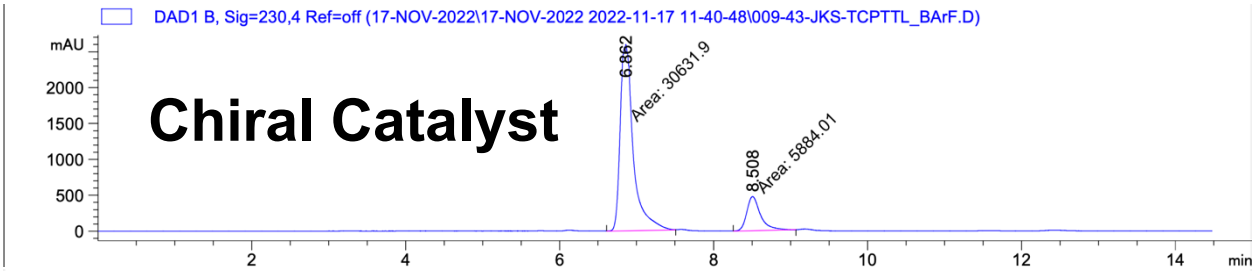

Signal 2: DAD1 B, Sig=230,4 Ref=off

Peak #	RetTime [min]	Type	Width [min]	Area [mAU*s]	Height [mAU]	Area %
1	6.862	MM	0.1965	3.06319e4	2598.30859	83.8864
2	8.508	MM	0.2059	5884.01465	476.25830	16.1136
Totals :				3.65159e4	3074.56689	

HPLC Chromatographs for substrate scope

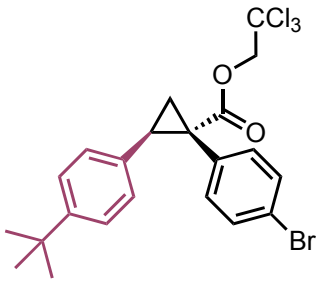

Compound **22**

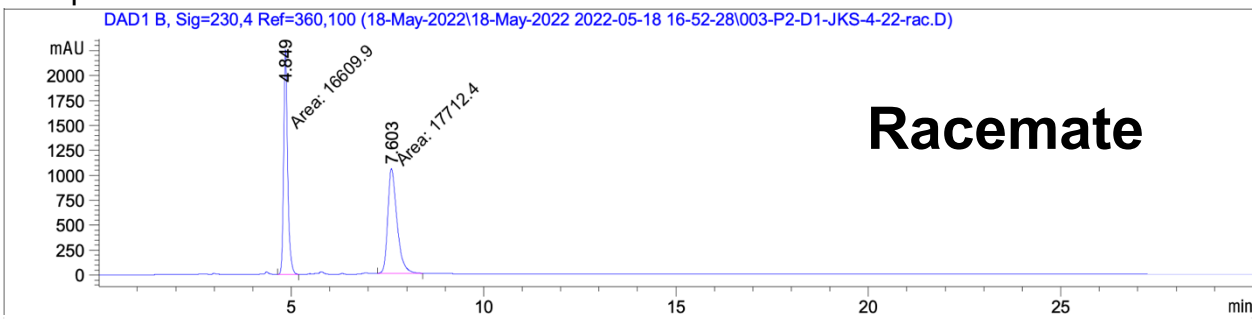

Signal 2: DAD1 B, Sig=230,4 Ref=360,100

Peak #	RetTime [min]	Type	Width [min]	Area [mAU*s]	Height [mAU]	Area %
1	4.849	MM	0.1230	1.66099e4	2250.49829	48.3940
2	7.603	MM	0.2808	1.77124e4	1051.24963	51.6060

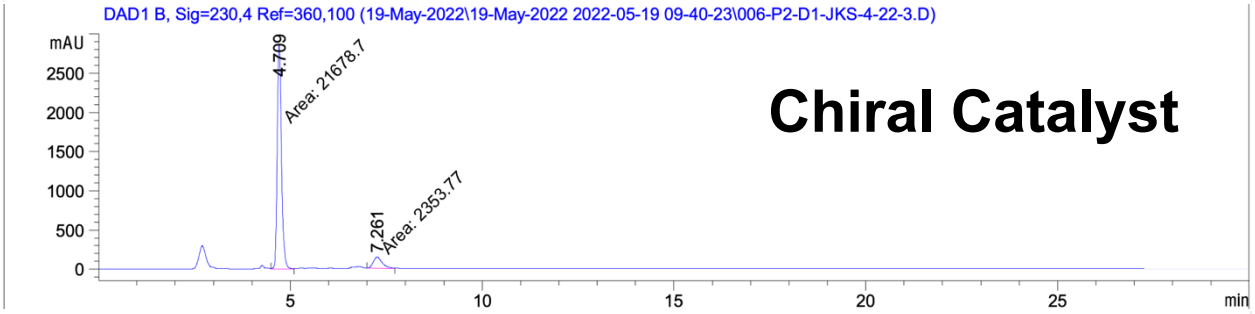

Signal 2: DAD1 B, Sig=230,4 Ref=360,100

Peak #	RetTime [min]	Type	Width [min]	Area [mAU*s]	Height [mAU]	Area %
1	4.709	MM	0.1262	2.16787e4	2863.48511	90.2059
2	7.261	MM	0.2738	2353.76660	143.26881	9.7941
Totals :				2.40325e4	3006.75392	

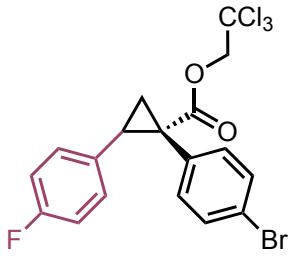

Compound **23**

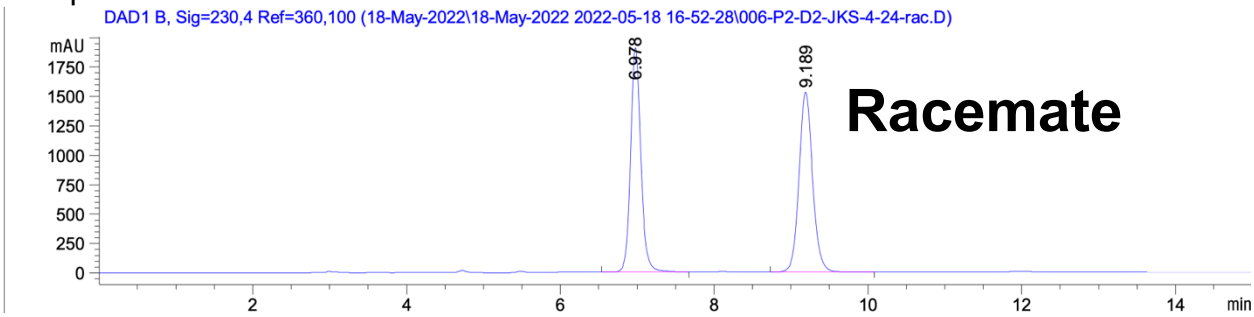

Signal 2: DAD1 B, Sig=230,4 Ref=360,100

Peak #	RetTime [min]	Type	Width [min]	Area [mAU*s]	Height [mAU]	Area %
1	6.978	VB R	0.1389	1.74849e4	1906.98328	48.2823
2	9.189	BB	0.1890	1.87290e4	1527.97461	51.7177

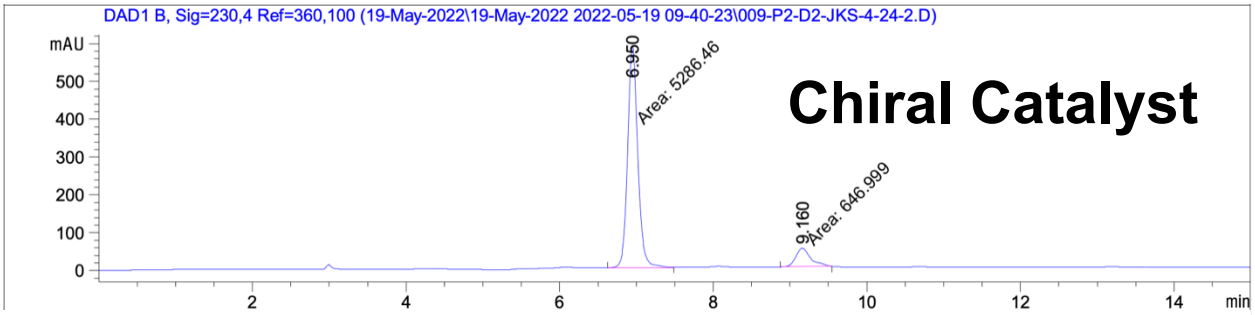

Signal 2: DAD1 B, Sig=230,4 Ref=360,100

Peak #	RetTime [min]	Type	Width [min]	Area [mAU*s]	Height [mAU]	Area %
1	6.950	MM	0.1502	5286.46191	586.70062	89.0958
2	9.160	MM	0.2222	646.99884	48.54053	10.9042
Totals :				5933.46075	635.24115	

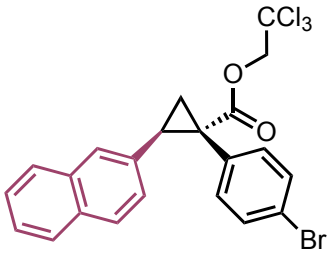

Compound **24**

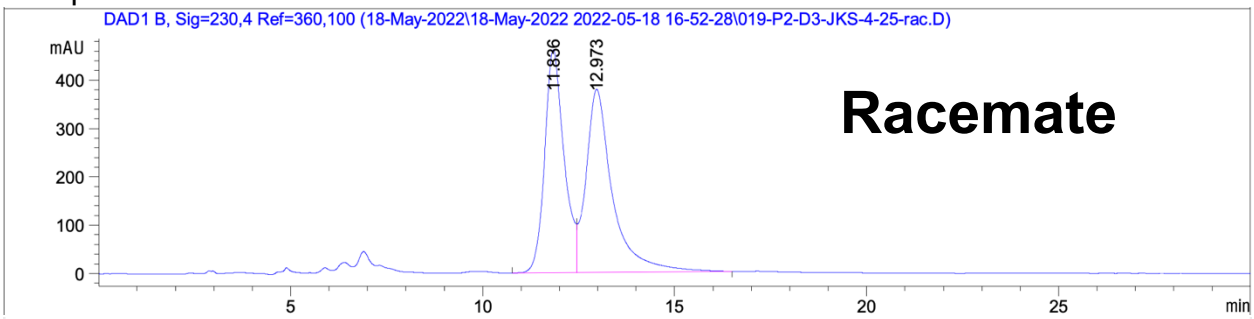

Signal 2: DAD1 B, Sig=230,4 Ref=360,100

Peak #	RetTime [min]	Type	Width [min]	Area [mAU*s]	Height [mAU]	Area %
1	11.836	BV	0.5196	1.61937e4	461.28143	47.0500
2	12.973	VB	0.6888	1.82244e4	379.11612	52.9500
Totals :				3.44181e4	840.39755	

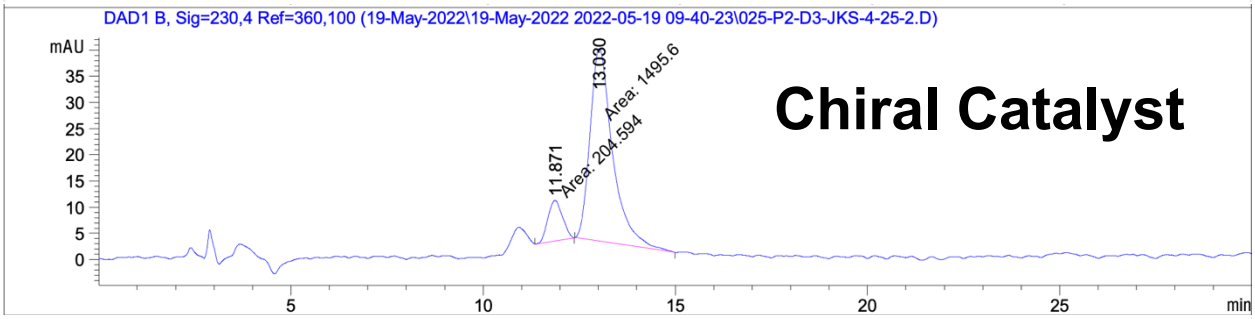

Signal 2: DAD1 B, Sig=230,4 Ref=360,100

Peak #	RetTime [min]	Type	Width [min]	Area [mAU*s]	Height [mAU]	Area %
1	11.871	MM	0.4387	204.59421	7.77239	12.0336
2	13.030	MM	0.6782	1495.59827	36.75165	87.9664
Totals :				1700.19247	44.52404	

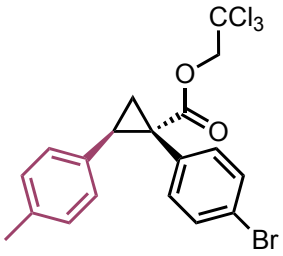

Compound **25**

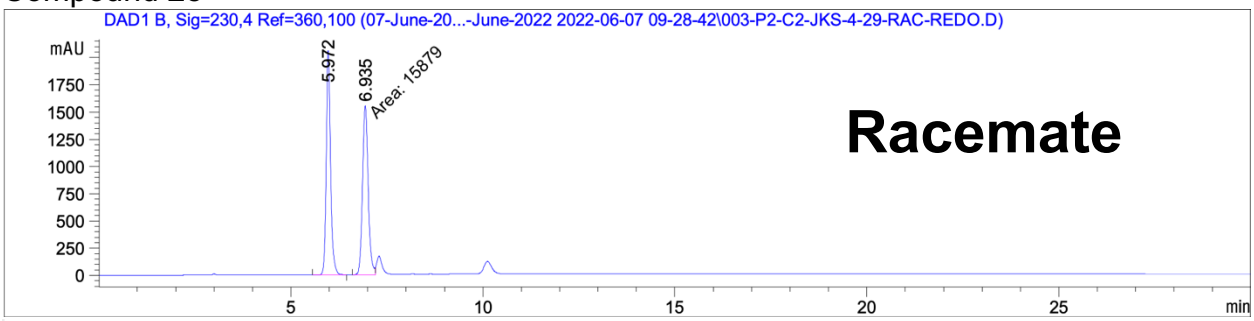

Signal 2: DAD1 B, Sig=230,4 Ref=360,100

Peak #	RetTime [min]	Type	Width [min]	Area [mAU*s]	Height [mAU]	Area %
1	5.972	BB	0.1201	1.62831e4	2062.40088	50.6283
2	6.935	MM	0.1705	1.58790e4	1552.09851	49.3717
Totals :				3.21621e4	3614.49939	

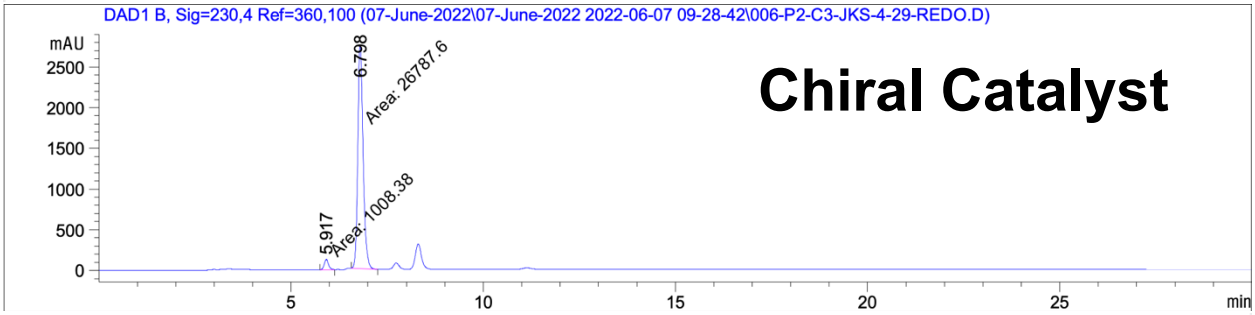

Signal 2: DAD1 B, Sig=230,4 Ref=360,100

Peak #	RetTime [min]	Type	Width [min]	Area [mAU*s]	Height [mAU]	Area %
1	5.917	MM	0.1319	1008.38159	127.42646	3.6278
2	6.798	MM	0.1625	2.67876e4	2747.04321	96.3722
Totals :				2.77960e4	2874.46967	

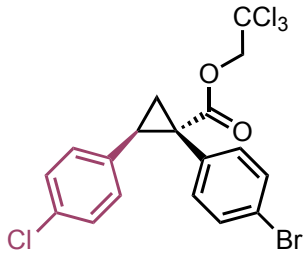

Compound **26**

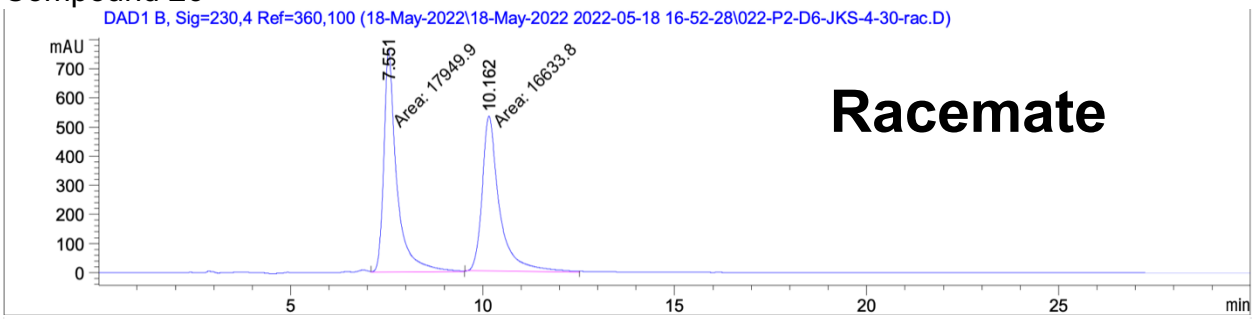

Signal 2: DAD1 B, Sig=230,4 Ref=360,100

Peak #	RetTime [min]	Type	Width [min]	Area [mAU*s]	Height [mAU]	Area %
1	7.551	MM	0.3896	1.79499e4	767.80005	51.9028
2	10.162	MM	0.5212	1.66338e4	531.93866	48.0972
Totals :				3.45837e4	1299.73871	

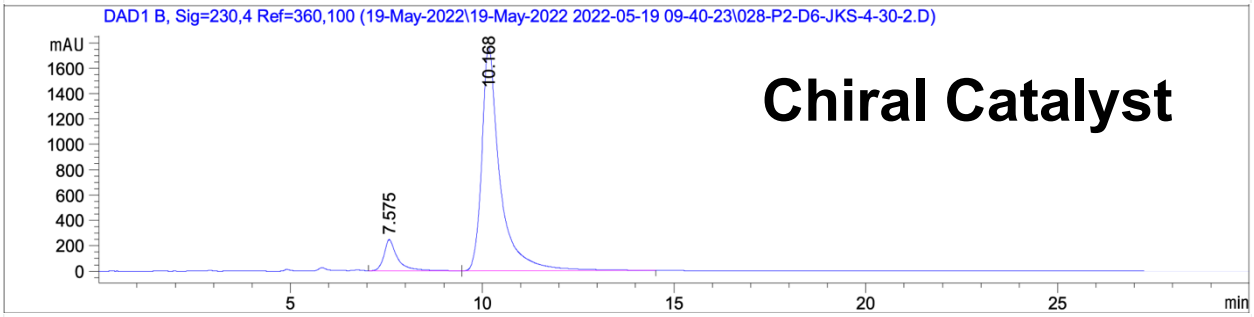

Signal 2: DAD1 B, Sig=230,4 Ref=360,100

Peak #	RetTime [min]	Type	Width [min]	Area [mAU*s]	Height [mAU]	Area %
1	7.575	BB	0.3460	6058.09277	247.13155	9.3882
2	10.168	BB	0.4721	5.84707e4	1766.87756	90.6118
Totals :				6.45288e4	2014.00911	

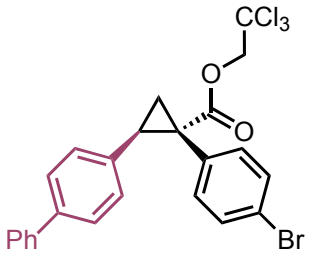

Compound **27**

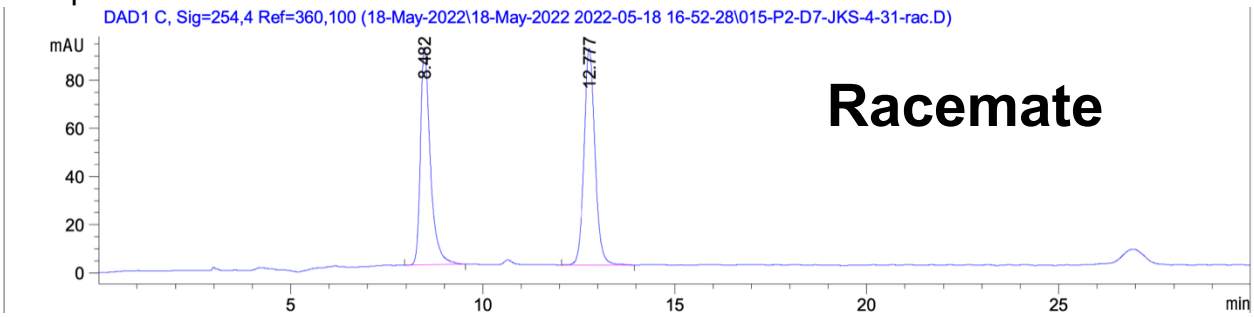

Signal 3: DAD1 C, Sig=254,4 Ref=360,100

Peak #	RetTime [min]	Type	Width [min]	Area [mAU*s]	Height [mAU]	Area %
1	8.482	BB	0.2667	1614.15369	90.24125	47.4621
2	12.777	BB	0.3039	1786.77844	89.89777	52.5379
Totals :				3400.93213	180.13902	

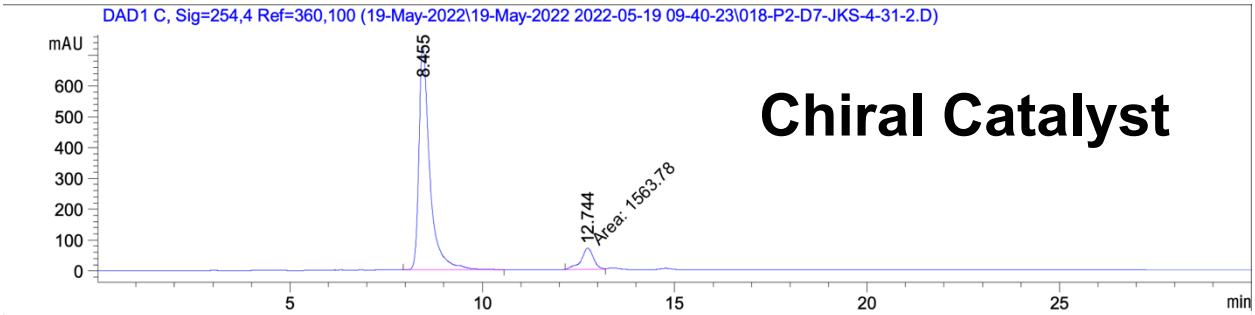

Signal 3: DAD1 C, Sig=254,4 Ref=360,100

Peak #	RetTime [min]	Type	Width [min]	Area [mAU*s]	Height [mAU]	Area %
1	8.455	BB	0.2869	1.42714e4	727.39502	90.1246
2	12.744	MM	0.3777	1563.77612	69.00871	9.8754
Totals :				1.58351e4	796.40372	

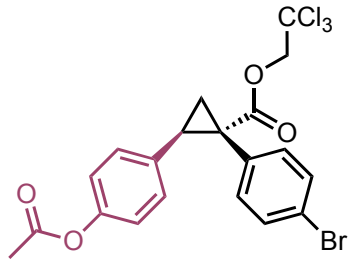

Compound **28**

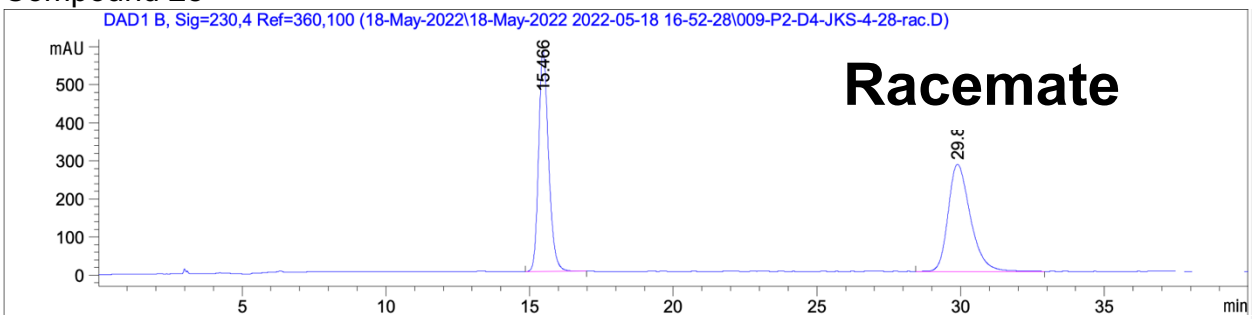

Signal 2: DAD1 B, Sig=230,4 Ref=360,100

Peak #	RetTime [min]	Type	Width [min]	Area [mAU*s]	Height [mAU]	Area %
1	15.466	BB	0.3694	1.40169e4	581.17523	48.0877
2	29.889	BB	0.8214	1.51317e4	281.38800	51.9123
Totals :				2.91486e4	862.56323	

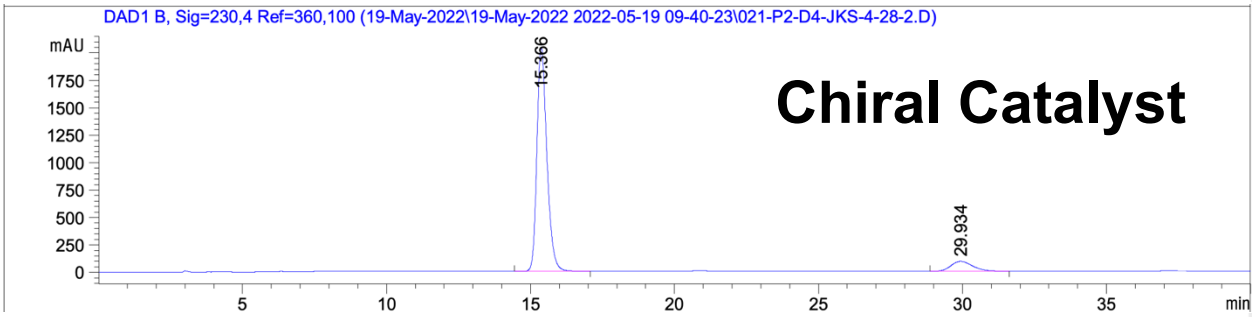

Signal 2: DAD1 B, Sig=230,4 Ref=360,100

Peak #	RetTime [min]	Type	Width [min]	Area [mAU*s]	Height [mAU]	Area %
1	15.366	BB	0.3690	4.91710e4	2041.31836	91.0851
2	29.934	BB	0.8177	4812.54932	90.60869	8.9149

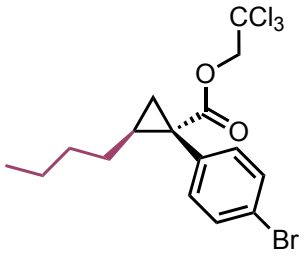

Compound **29**

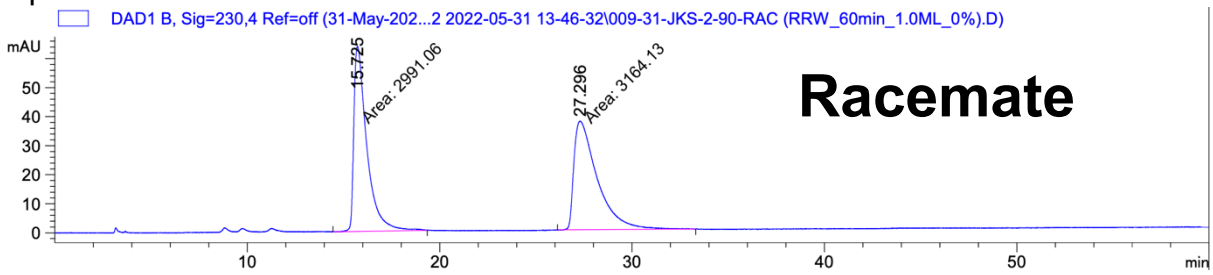

Signal 2: DAD1 B, Sig=230,4 Ref=off

Peak #	RetTime [min]	Type	Width [min]	Area [mAU*s]	Height [mAU]	Area %
1	15.725	MM	0.7814	2991.06396	63.79838	48.5941
2	27.296	MM	1.4065	3164.13354	37.49349	51.4059
Totals :				6155.19751	101.29187	

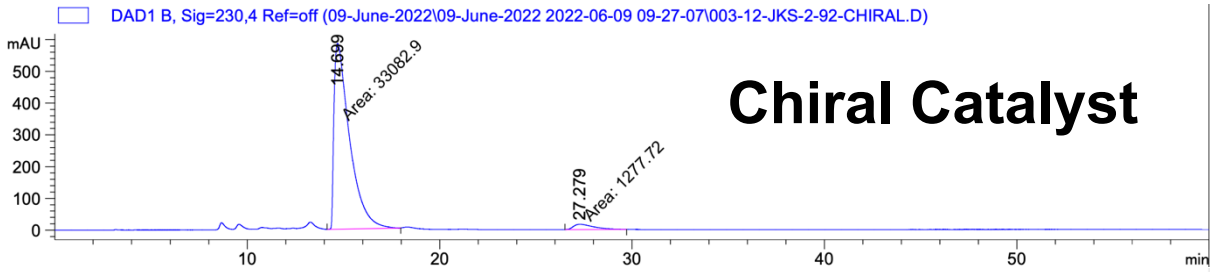

Signal 2: DAD1 B, Sig=230,4 Ref=off

Peak #	RetTime [min]	Type	Width [min]	Area [mAU*s]	Height [mAU]	Area %
1	14.699	MM	0.9411	3.30829e4	585.92126	96.2814
2	27.279	MM	1.2558	1277.71973	16.95697	3.7186
Totals :				3.43607e4	602.87823	

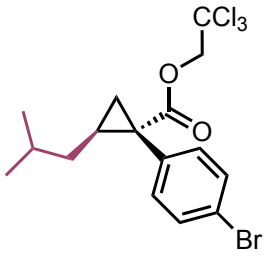

Compound **30**

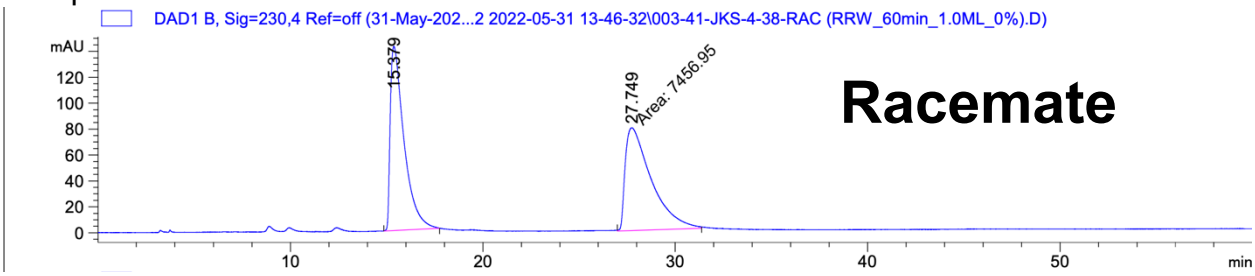

Signal 2: DAD1 B, Sig=230,4 Ref=off

Peak #	RetTime [min]	Type	Width [min]	Area [mAU*s]	Height [mAU]	Area %
1	15.379	BV R	0.5819	7056.59131	142.20984	48.6207
2	27.749	MM	1.5673	7456.95361	79.29698	51.3793
Totals :				1.45135e4	221.50682	

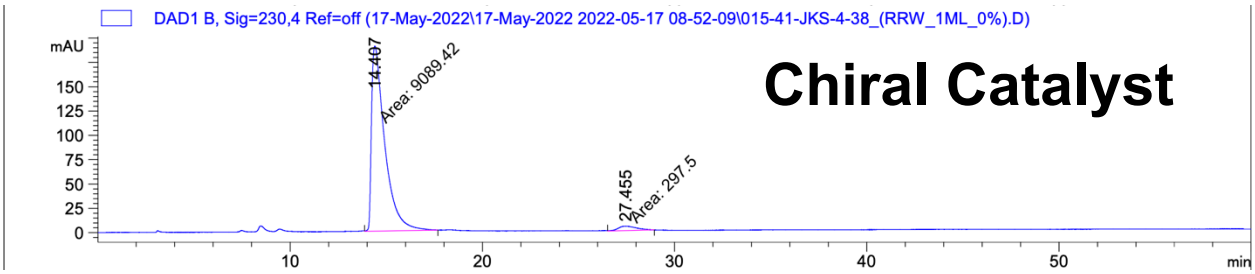

Signal 2: DAD1 B, Sig=230,4 Ref=off

Peak #	RetTime [min]	Type	Width [min]	Area [mAU*s]	Height [mAU]	Area %
1	14.407	MM	0.7962	9089.41895	190.27261	96.8307
2	27.455	MM	1.0848	297.49957	4.57061	3.1693
Totals :				9386.91852	194.84322	

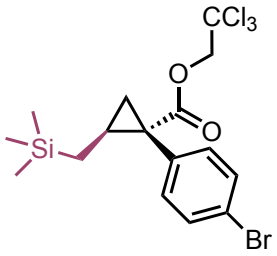

Compound **31**

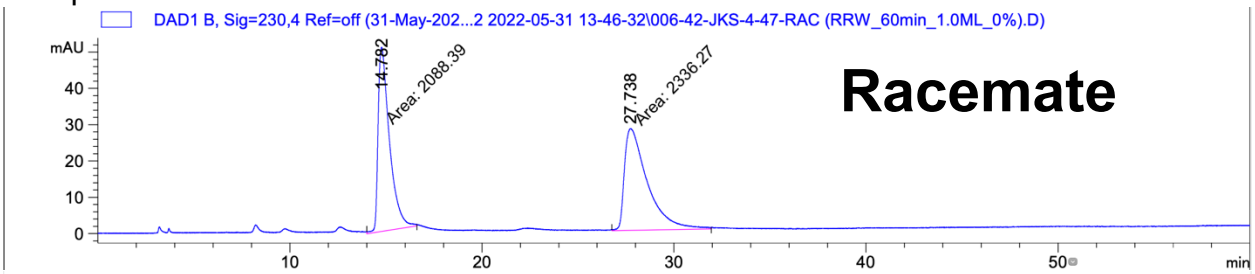

Signal 2: DAD1 B, Sig=230,4 Ref=off

Peak #	RetTime [min]	Type	Width [min]	Area [mAU*s]	Height [mAU]	Area %
1	14.782	MM	0.6861	2088.39307	50.73406	47.1990
2	27.738	MM	1.3863	2336.26611	28.08833	52.8010
Totals :				4424.65918	78.82239	

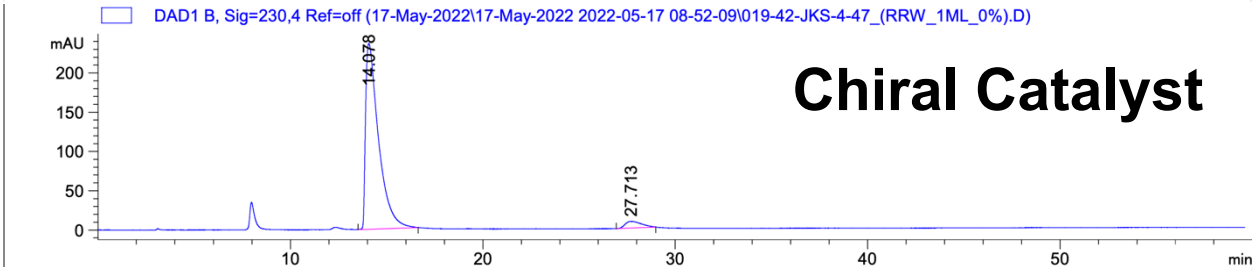

Signal 2: DAD1 B, Sig=230,4 Ref=off

Peak #	RetTime [min]	Type	Width [min]	Area [mAU*s]	Height [mAU]	Area %
1	14.078	VV R	0.5502	1.10325e4	236.72404	95.6580
2	27.713	BV R	0.6836	500.77664	8.58471	4.3420
Totals :				1.15332e4	245.30875	

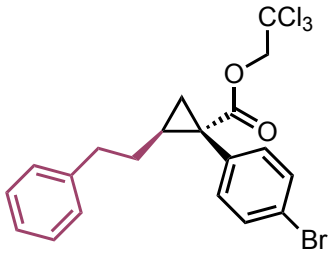

Compound **32**

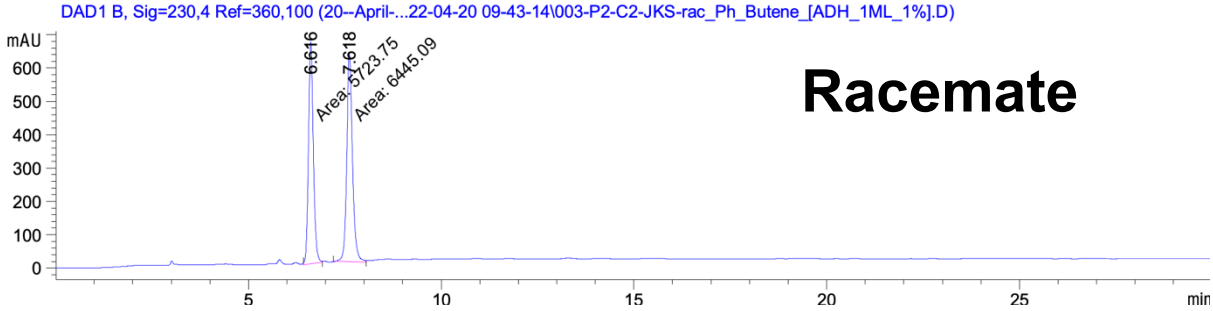

Racemate

Peak #	RetTime [min]	Type	Width [min]	Area [mAU*s]	Height [mAU]	Area %
1	6.616	MM	0.1433	5723.75439	665.78522	47.0362
2	7.618	MM	0.1730	6445.08643	620.92499	52.9638
Totals :				1.21688e4	1286.71021	

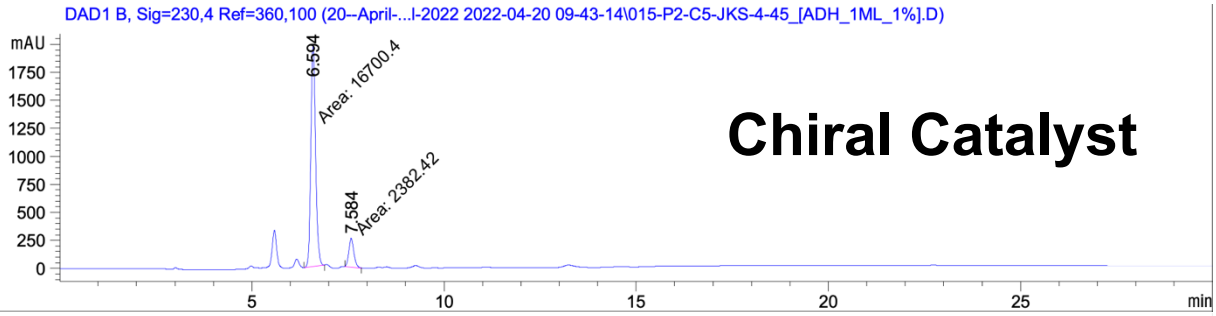

Chiral Catalyst

Signal 2: DAD1 B, Sig=230,4 Ref=360,100

Peak #	RetTime [min]	Type	Width [min]	Area [mAU*s]	Height [mAU]	Area %
1	6.594	MM	0.1404	1.67004e4	1982.03979	87.5154
2	7.584	MM	0.1542	2382.41650	257.46539	12.4846
Totals :				1.90829e4	2239.50519	

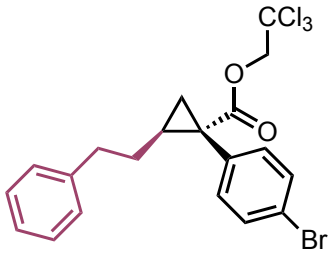

Compound **33**

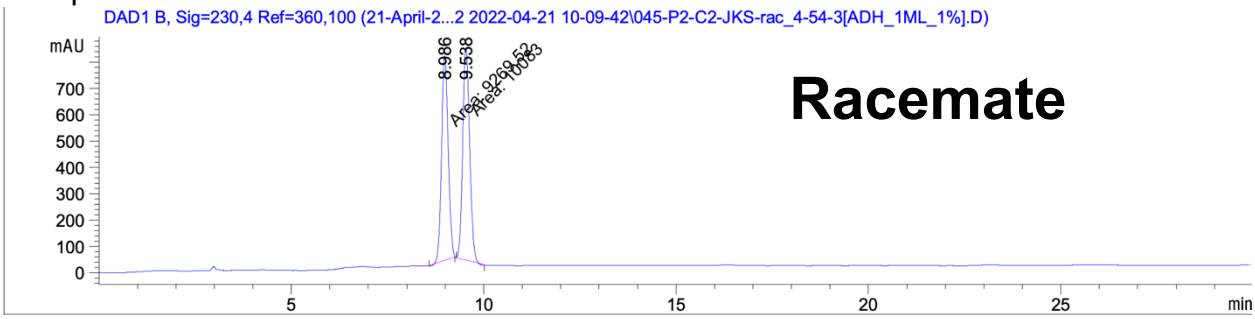

Signal 2: DAD1 B, Sig=230,4 Ref=360,100

Peak #	RetTime [min]	Type	Width [min]	Area [mAU*s]	Height [mAU]	Area %
1	8.986	MM	0.1992	9269.52246	775.65826	47.8982
2	9.538	MM	0.2084	1.00830e4	806.36584	52.1018
Totals :				1.93525e4	1582.02411	

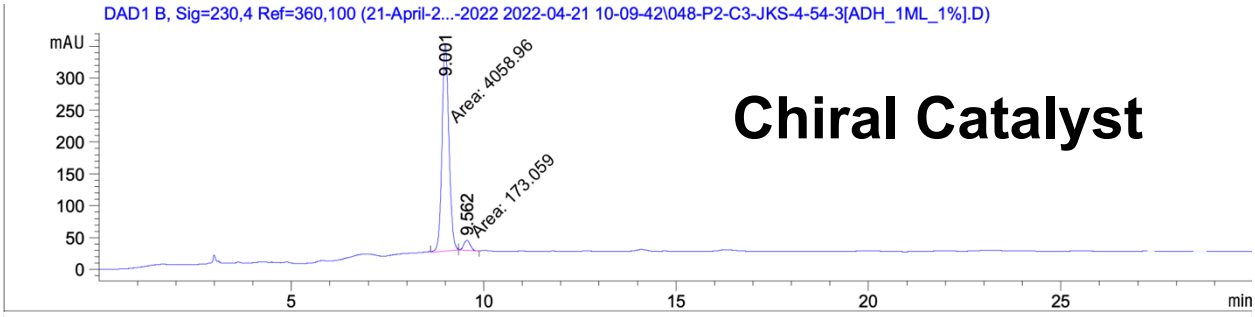

Peak #	RetTime [min]	Type	Width [min]	Area [mAU*s]	Height [mAU]	Area %
1	9.001	MM	0.2083	4058.95850	324.79349	95.9107
2	9.562	MM	0.1856	173.05934	15.53821	4.0893
Totals :				4232.01784	340.33170	

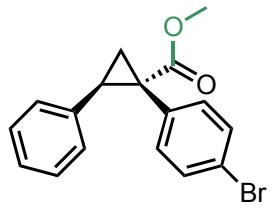

Compound **34**

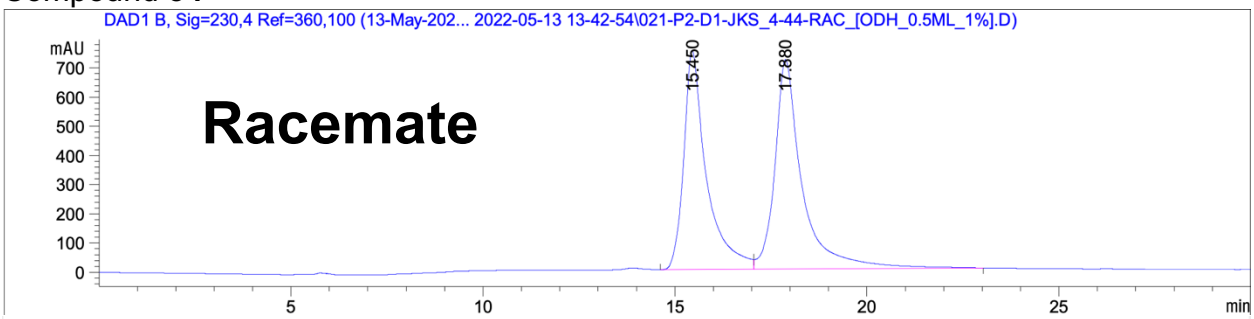

Signal 2: DAD1 B, Sig=230,4 Ref=360,100

Peak #	RetTime [min]	Type	Width [min]	Area [mAU*s]	Height [mAU]	Area %
1	15.450	BV	0.5793	3.08433e4	750.74835	46.4418
2	17.880	VB	0.6983	3.55696e4	717.59296	53.5582

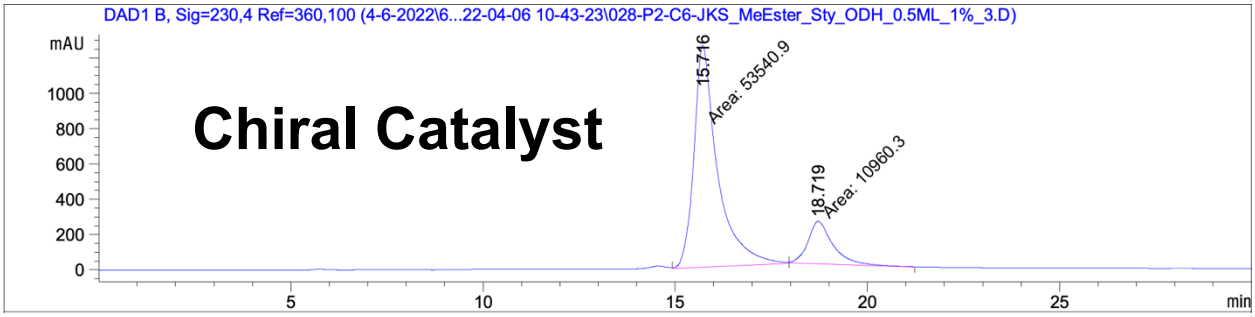

Signal 2: DAD1 B, Sig=230,4 Ref=360,100

Peak #	RetTime [min]	Type	Width [min]	Area [mAU*s]	Height [mAU]	Area %
1	15.716	MM	0.7105	5.35409e4	1255.95544	83.0076
2	18.719	MM	0.7607	1.09603e4	240.13960	16.9924
Totals :				6.45013e4	1496.09505	

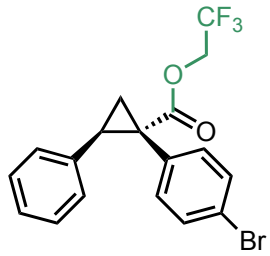

Compound **35**

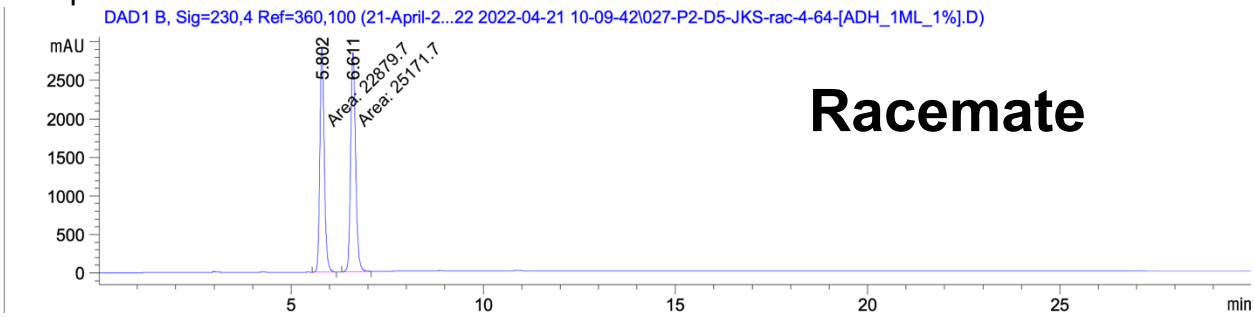

Racemate

Signal 2: DAD1 B, Sig=230,4 Ref=360,100

Peak #	RetTime [min]	Type	Width [min]	Area [mAU*s]	Height [mAU]	Area %
1	5.802	MM	0.1308	2.28797e4	2914.32568	47.6151
2	6.611	MM	0.1476	2.51717e4	2842.84131	52.3849
Totals :				4.80514e4	5757.16699	

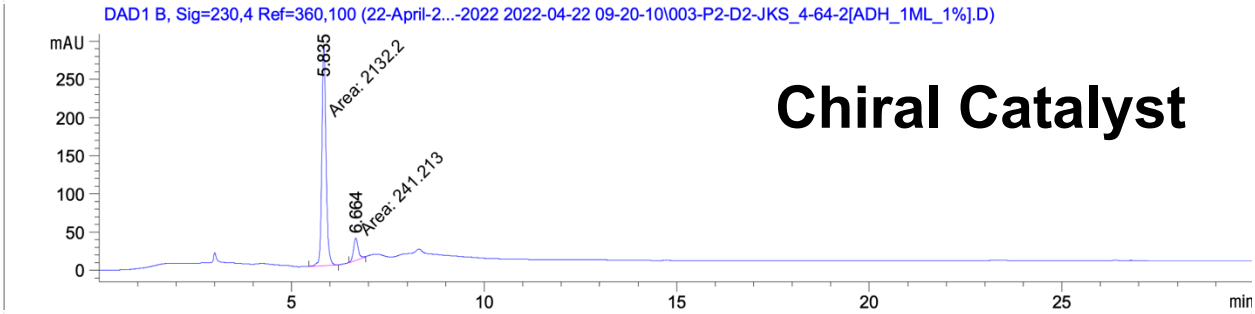

Chiral Catalyst

Signal 2: DAD1 B, Sig=230,4 Ref=360,100

Peak #	RetTime [min]	Type	Width [min]	Area [mAU*s]	Height [mAU]	Area %
1	5.835	MM	0.1228	2132.19556	289.37891	89.8369
2	6.664	MM	0.1378	241.21251	29.17617	10.1631
Totals :				2373.40807	318.55508	

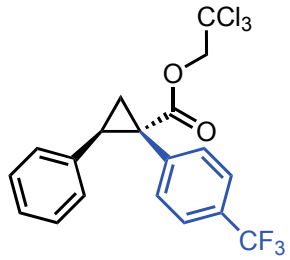

Compound **36**

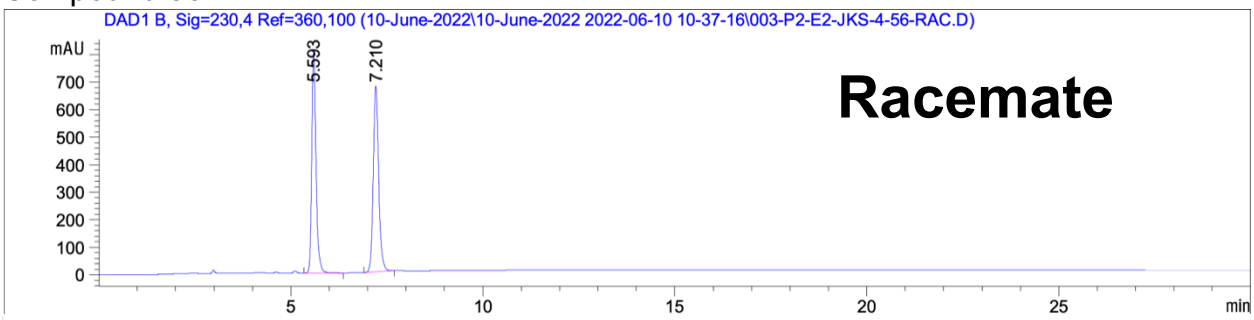

Signal 2: DAD1 B, Sig=230,4 Ref=360,100

Peak #	RetTime [min]	Type	Width [min]	Area [mAU*s]	Height [mAU]	Area %
1	5.593	BB	0.1148	6162.12988	809.81104	48.3796
2	7.210	BB	0.1475	6574.90234	675.65918	51.6204
Totals :				1.27370e4	1485.47021	

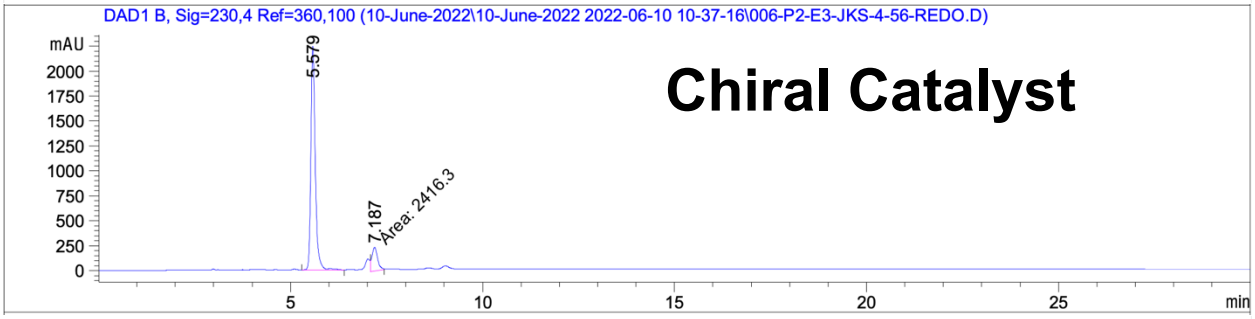

Signal 2: DAD1 B, Sig=230,4 Ref=360,100

Peak #	RetTime [min]	Type	Width [min]	Area [mAU*s]	Height [mAU]	Area %
1	5.579	BV R	0.1166	1.76200e4	2244.50024	87.9404
2	7.187	MM	0.1683	2416.29834	239.29219	12.0596
Totals :				2.00363e4	2483.79243	

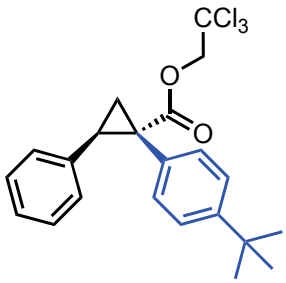

Compound **37**

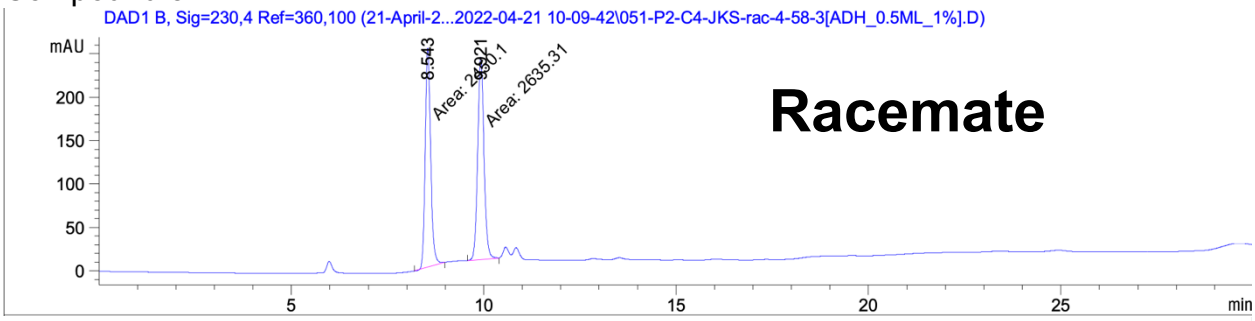

Signal 2: DAD1 B, Sig=230,4 Ref=360,100

Peak #	RetTime [min]	Type	Width [min]	Area [mAU*s]	Height [mAU]	Area %
1	8.543	MM	0.1619	2450.09912	252.23808	48.1790
2	9.921	MM	0.1888	2635.30811	232.61414	51.8210
Totals :				5085.40723	484.85222	

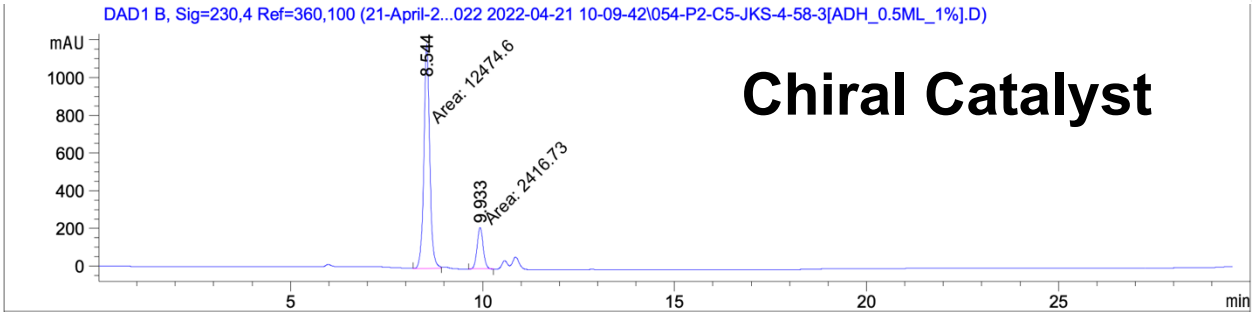

Signal 2: DAD1 B, Sig=230,4 Ref=360,100

Peak #	RetTime [min]	Type	Width [min]	Area [mAU*s]	Height [mAU]	Area %
1	8.544	MM	0.1751	1.24746e4	1187.05261	83.7709
2	9.933	MM	0.1828	2416.72705	220.29327	16.2291
Totals :				1.48913e4	1407.34589	

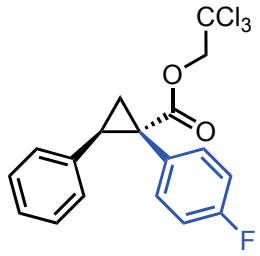

Compound **38**

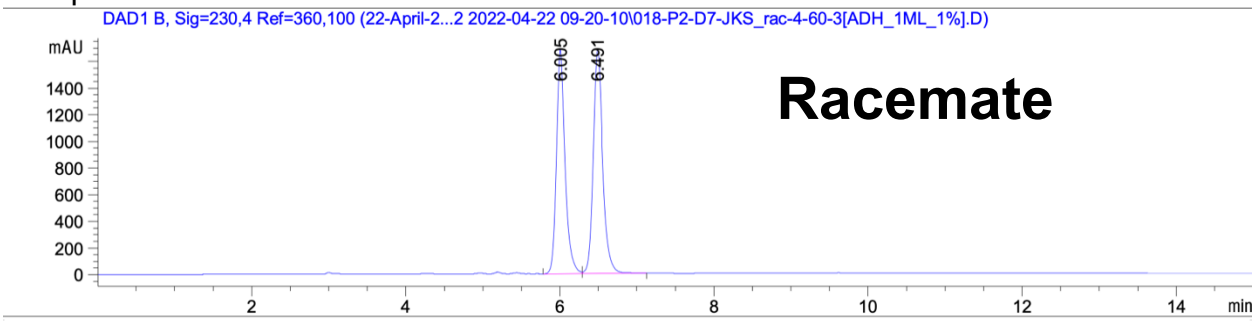

Racemate

Signal 2: DAD1 B, Sig=230,4 Ref=360,100

Peak #	RetTime [min]	Type	Width [min]	Area [mAU*s]	Height [mAU]	Area %
1	6.005	BV	0.1183	1.33428e4	1686.38867	48.0813
2	6.491	VB	0.1299	1.44078e4	1683.29883	51.9187
Totals :				2.77506e4	3369.68750	

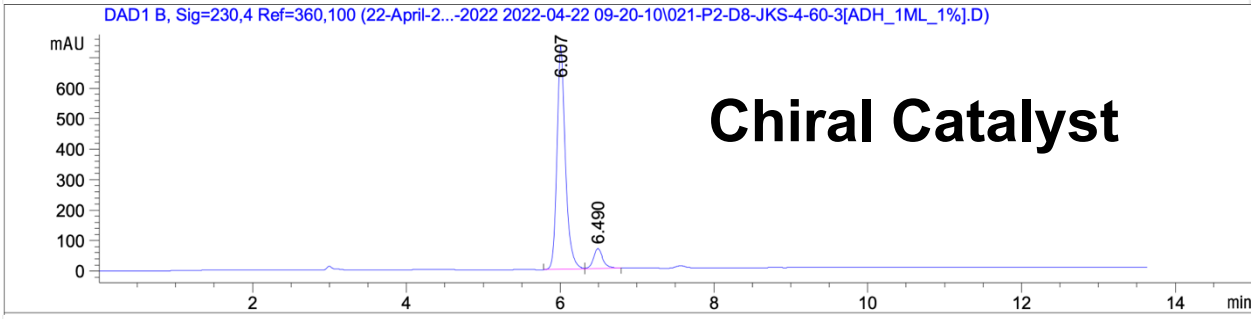

Chiral Catalyst

Signal 2: DAD1 B, Sig=230,4 Ref=360,100

Peak #	RetTime [min]	Type	Width [min]	Area [mAU*s]	Height [mAU]	Area %
1	6.007	BV	0.1168	5722.35840	735.22961	91.2220
2	6.490	VB	0.1282	550.64423	65.43978	8.7780
Totals :				6273.00262	800.66940	

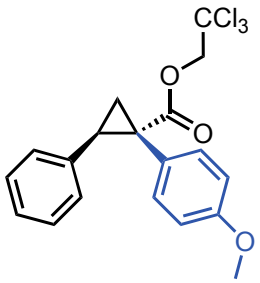

Compound **39**

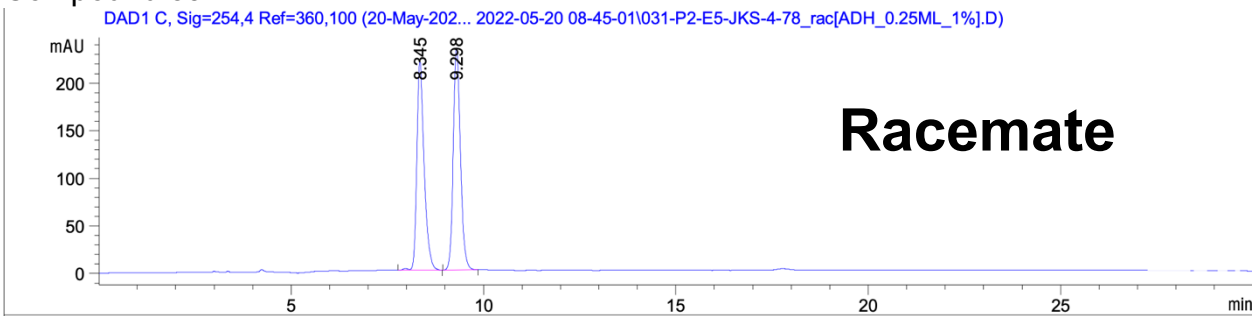

Signal 3: DAD1 C, Sig=254,4 Ref=360,100

Peak #	RetTime [min]	Type	Width [min]	Area [mAU*s]	Height [mAU]	Area %
1	8.345	VB R	0.1994	2910.02563	219.93542	49.0378
2	9.298	BB	0.1976	3024.21924	232.75323	50.9622
Totals :				5934.24487	452.68866	

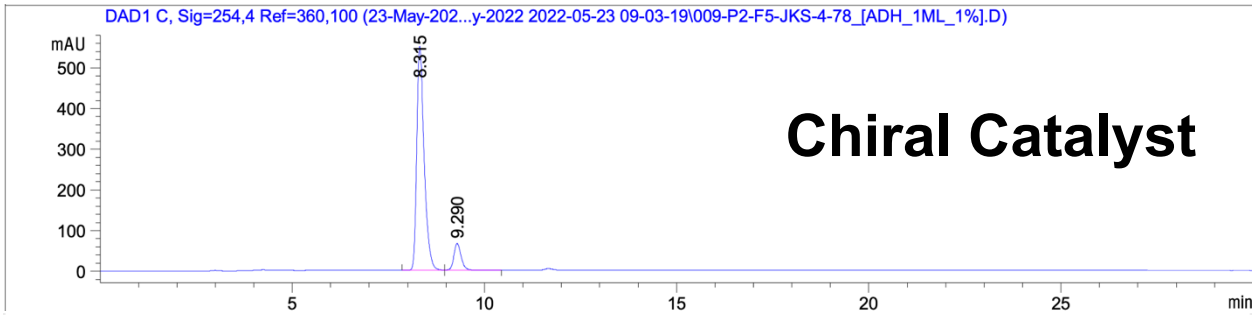

Signal 3: DAD1 C, Sig=254,4 Ref=360,100

Peak #	RetTime [min]	Type	Width [min]	Area [mAU*s]	Height [mAU]	Area %
1	8.315	BB	0.2015	7328.62402	549.76813	89.6529
2	9.290	BB	0.1972	845.81879	65.27042	10.3471
Totals :				8174.44281	615.03855	

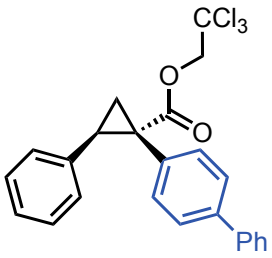

Compound **40**

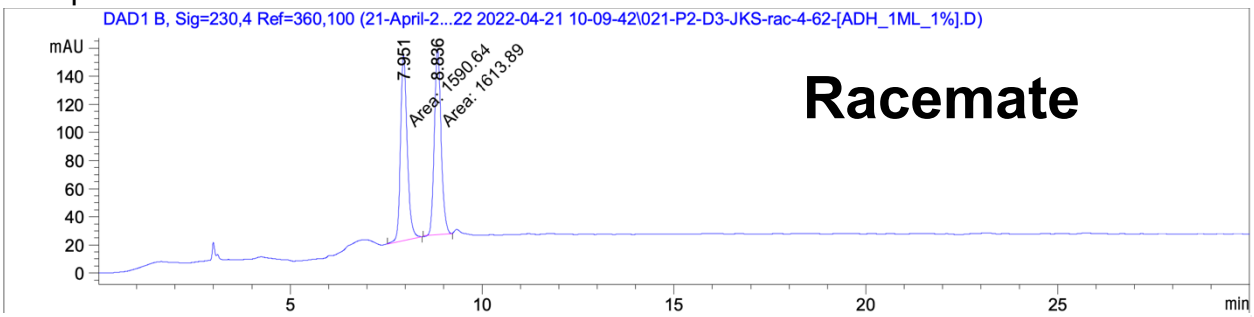

Signal 2: DAD1 B, Sig=230,4 Ref=360,100

Peak #	RetTime [min]	Type	Width [min]	Area [mAU*s]	Height [mAU]	Area %
1	7.951	MM	0.2007	1590.64087	132.11815	49.6373
2	8.836	MM	0.2031	1613.88806	132.43649	50.3627

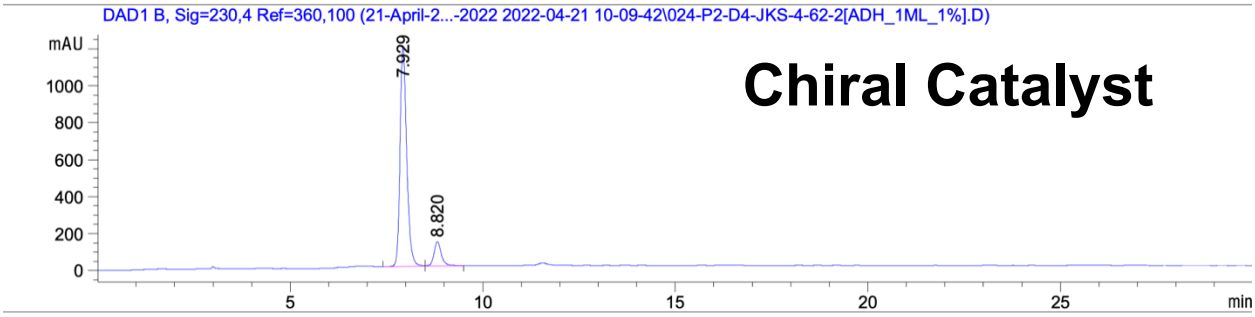

Signal 2: DAD1 B, Sig=230,4 Ref=360,100

Peak #	RetTime [min]	Type	Width [min]	Area [mAU*s]	Height [mAU]	Area %
1	7.929	BV	0.1817	1.43243e4	1196.35999	89.1717
2	8.820	VB	0.1989	1739.42395	131.02821	10.8283

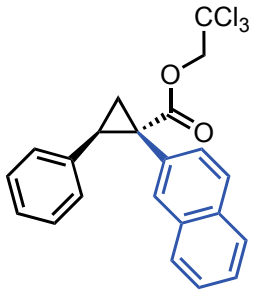

Compound **41**

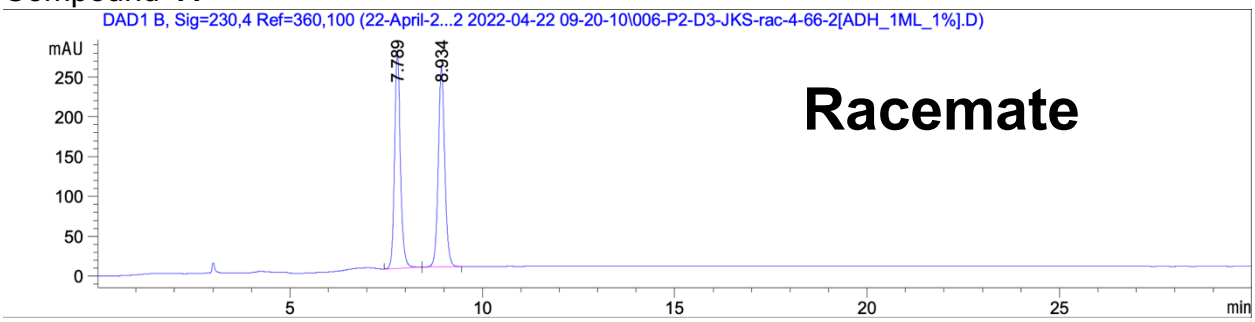

Signal 2: DAD1 B, Sig=230,4 Ref=360,100

Peak #	RetTime [min]	Type	Width [min]	Area [mAU*s]	Height [mAU]	Area %
1	7.789	BB	0.1586	2872.49951	273.36664	49.1969
2	8.934	BB	0.1808	2966.28003	252.93414	50.8031
Totals :				5838.77954	526.30078	

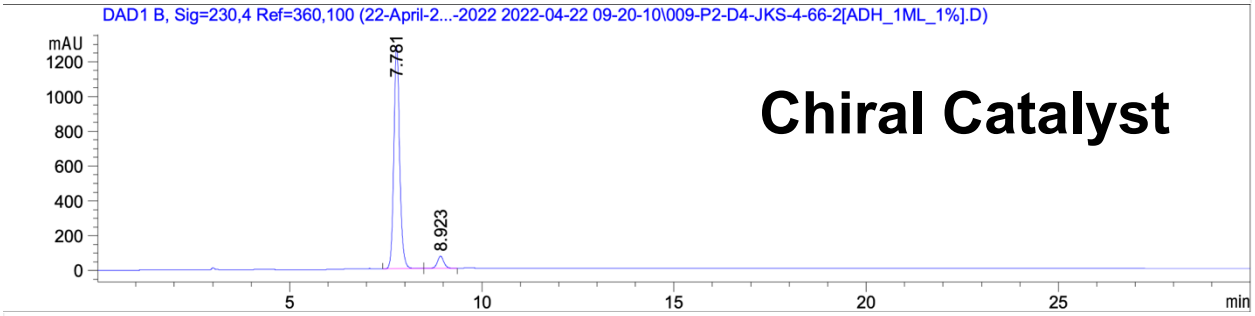

Signal 2: DAD1 B, Sig=230,4 Ref=360,100

Peak #	RetTime [min]	Type	Width [min]	Area [mAU*s]	Height [mAU]	Area %
1	7.781	BB	0.1607	1.35192e4	1285.34973	94.1376
2	8.923	BB	0.1790	841.90424	71.71494	5.8624
Totals :				1.43611e4	1357.06467	

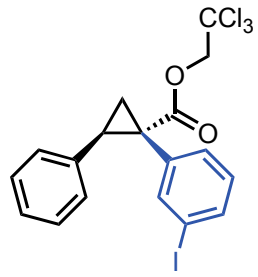

Compound **42**

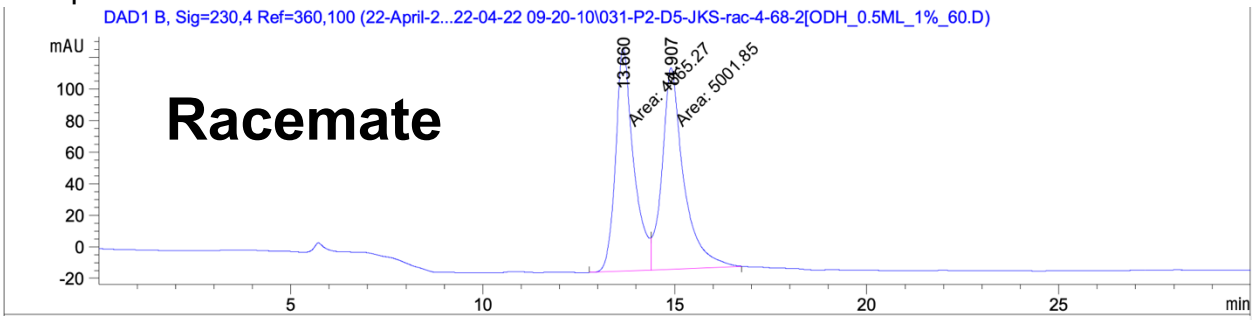

Signal 2: DAD1 B, Sig=230,4 Ref=360,100

Peak #	RetTime [min]	Type	Width [min]	Area [mAU*s]	Height [mAU]	Area %
1	13.660	MF	0.5490	4665.26953	141.61685	48.2591
2	14.907	FM	0.6527	5001.85059	127.72429	51.7409
Totals :				9667.12012	269.34114	

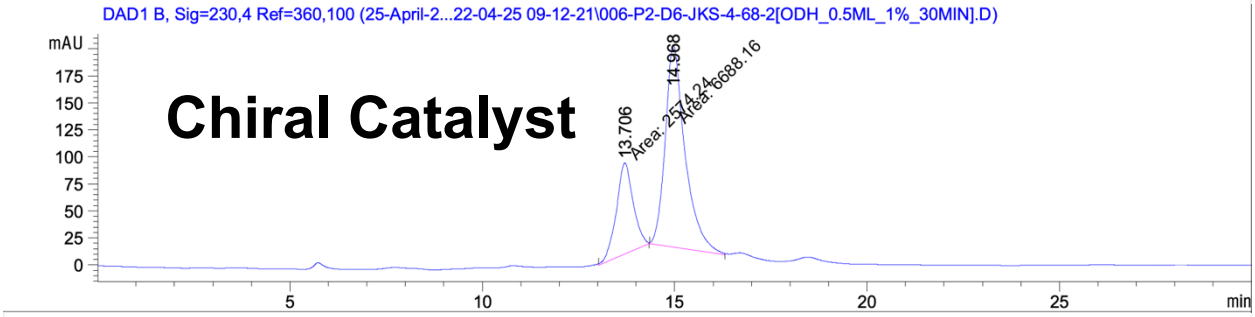

Signal 2: DAD1 B, Sig=230,4 Ref=360,100

Peak #	RetTime [min]	Type	Width [min]	Area [mAU*s]	Height [mAU]	Area %
1	13.706	MM	0.5089	2574.24121	84.30233	27.7924
2	14.968	MM	0.5958	6688.15820	187.10114	72.2076
Totals :				9262.39941	271.40347	

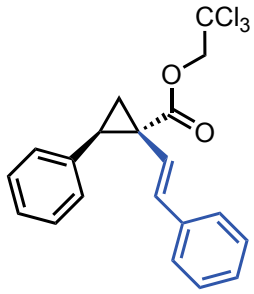

Compound **43**

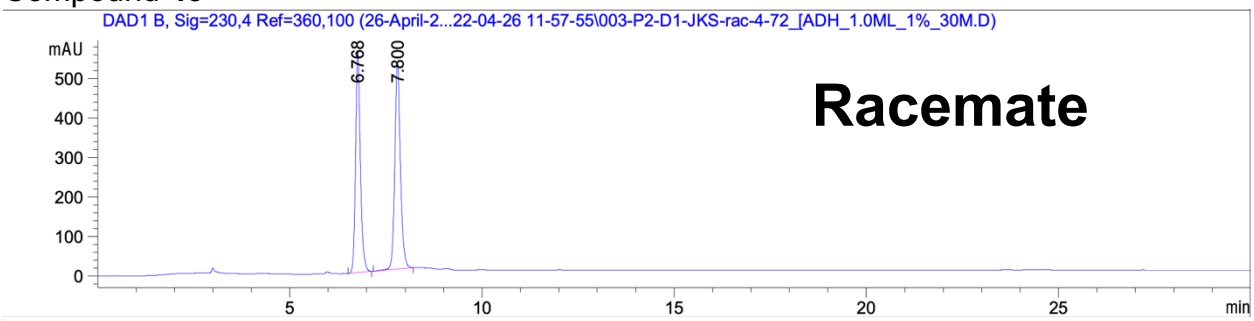

Signal 2: DAD1 B, Sig=230,4 Ref=360,100

Peak #	RetTime [min]	Type	Width [min]	Area [mAU*s]	Height [mAU]	Area %
1	6.768	BB	0.1328	4944.46826	561.41315	47.9950
2	7.800	BB	0.1558	5357.57715	521.66431	52.0050
Totals :				1.03020e4	1083.07745	

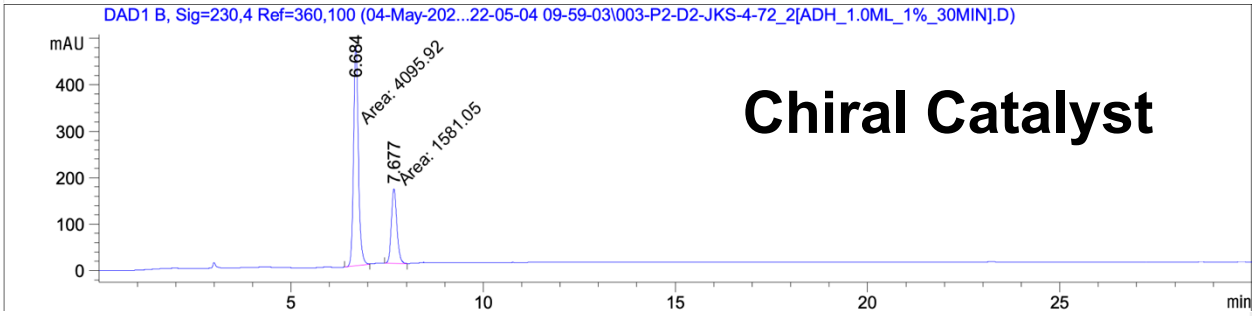

Signal 2: DAD1 B, Sig=230,4 Ref=360,100

Peak #	RetTime [min]	Type	Width [min]	Area [mAU*s]	Height [mAU]	Area %
1	6.684	MM	0.1437	4095.92334	475.20187	72.1497
2	7.677	MM	0.1634	1581.05249	161.25577	27.8503
Totals :				5676.97583	636.45764	

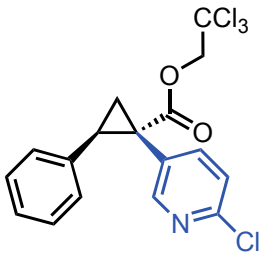

Compound **44**

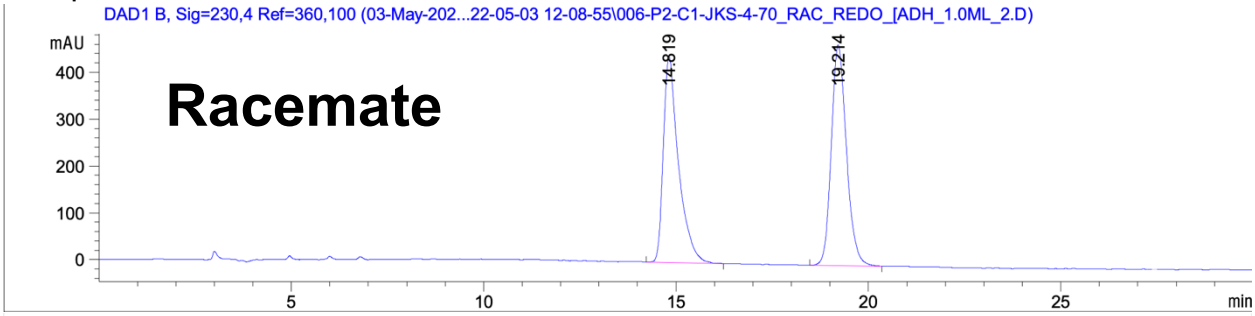

Signal 2: DAD1 B, Sig=230,4 Ref=360,100

Peak #	RetTime [min]	Type	Width [min]	Area [mAU*s]	Height [mAU]	Area %
1	14.819	BV R	0.4017	1.20413e4	439.43500	48.3026
2	19.214	BB	0.4192	1.28876e4	471.10703	51.6974

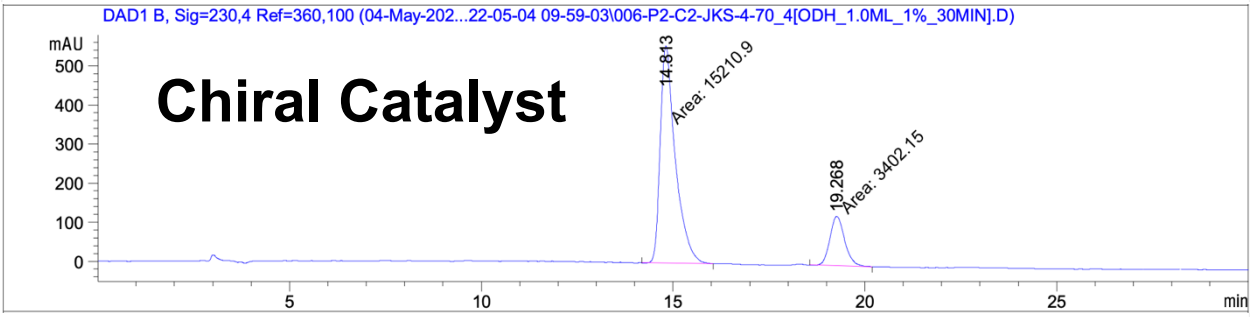

Signal 2: DAD1 B, Sig=230,4 Ref=360,100

Peak #	RetTime [min]	Type	Width [min]	Area [mAU*s]	Height [mAU]	Area %
1	14.813	MM	0.4559	1.52109e4	556.06555	81.7217
2	19.268	MM	0.4493	3402.15479	126.20539	18.2783
Totals :				1.86131e4	682.27094	

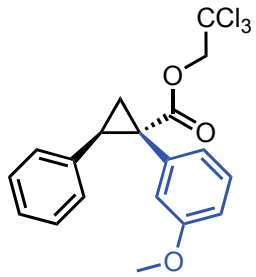

Compound **45**

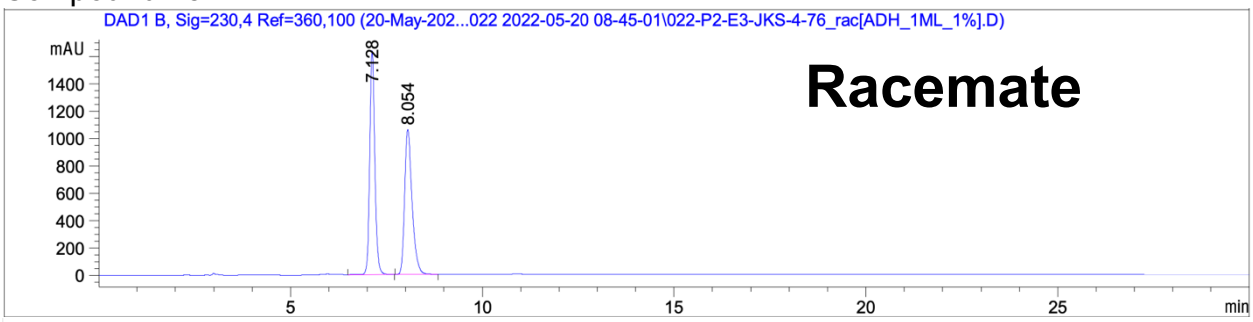

Signal 2: DAD1 B, Sig=230,4 Ref=360,100

Peak #	RetTime [min]	Type	Width [min]	Area [mAU*s]	Height [mAU]	Area %
1	7.128	VB R	0.1376	1.48454e4	1637.45007	51.0205
2	8.054	BB	0.2050	1.42515e4	1058.95117	48.9795
Totals :				2.90968e4	2696.40125	

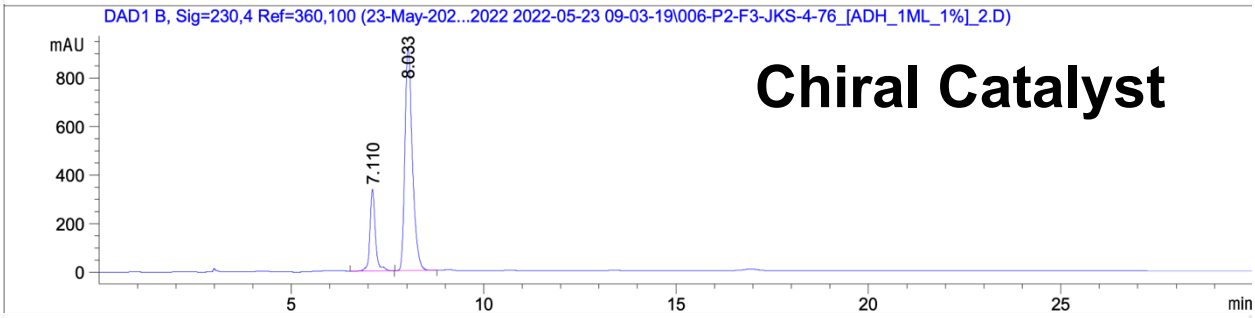

Signal 2: DAD1 B, Sig=230,4 Ref=360,100

Peak #	RetTime [min]	Type	Width [min]	Area [mAU*s]	Height [mAU]	Area %
1	7.110	BV R	0.1417	3231.21802	336.11502	20.6020
2	8.033	BB	0.2057	1.24528e4	921.41992	79.3980
Totals :				1.56840e4	1257.53494	

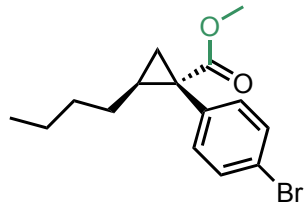

Compound **46**

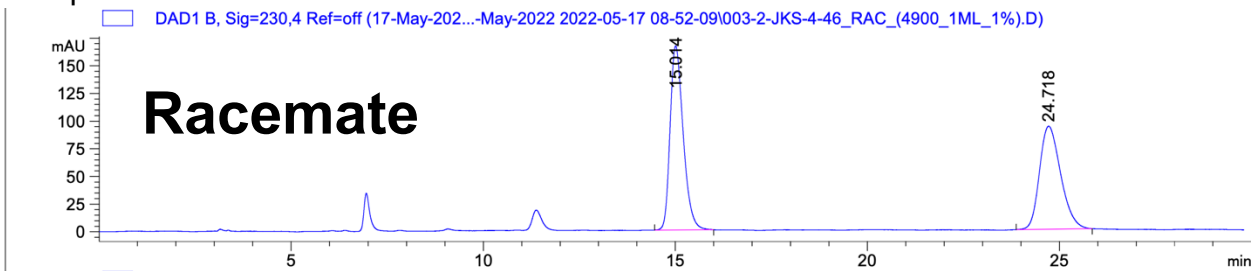

Signal 2: DAD1 B, Sig=230,4 Ref=off

Peak #	RetTime [min]	Type	Width [min]	Area [mAU*s]	Height [mAU]	Area %
1	15.014	BV R	0.3357	3931.14502	166.36209	52.4483
2	24.718	BV R	0.4530	3564.13403	93.13728	47.5517
Totals :				7495.27905	259.49937	

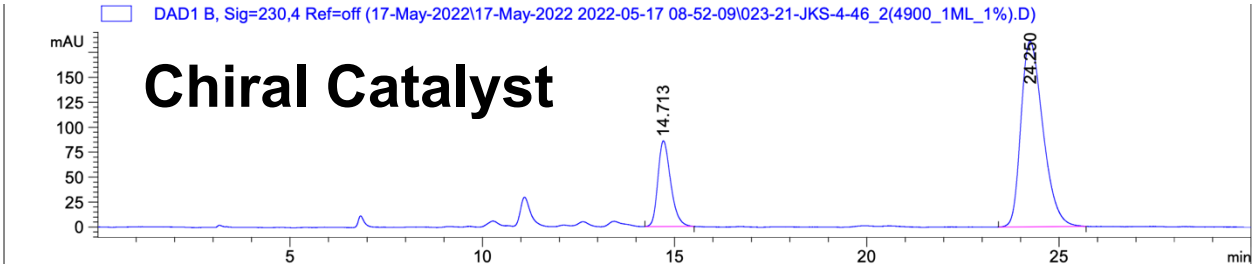

Signal 2: DAD1 B, Sig=230,4 Ref=off

Peak #	RetTime [min]	Type	Width [min]	Area [mAU*s]	Height [mAU]	Area %
1	14.713	BV R	0.3004	1986.03662	85.83268	21.1844
2	24.250	VV R	0.4685	7388.94775	185.78978	78.8156
Totals :				9374.98438	271.62246	

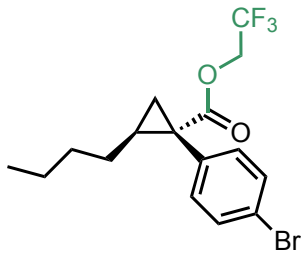

Compound **47**

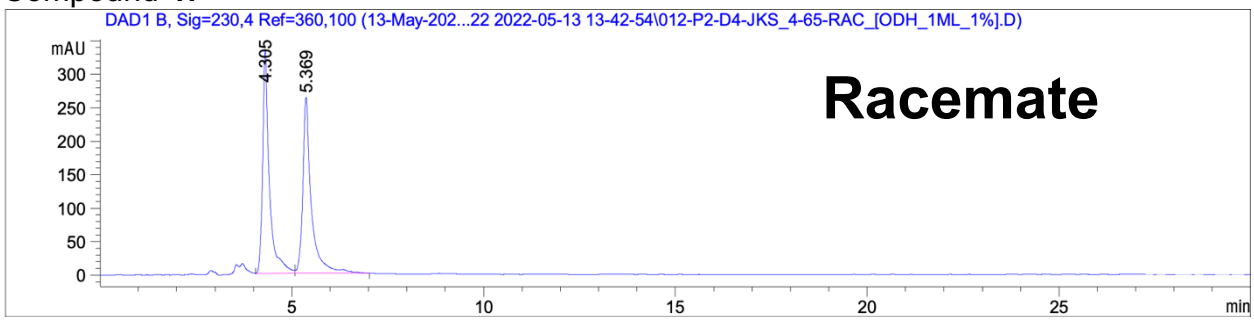

Signal 2: DAD1 B, Sig=230,4 Ref=360,100

Peak #	RetTime [min]	Type	Width [min]	Area [mAU*s]	Height [mAU]	Area %
1	4.305	BV	0.1713	4091.61035	333.14453	50.0894
2	5.369	VV R	0.2130	4076.99976	263.24207	49.9106
Totals :				8168.61011	596.38660	

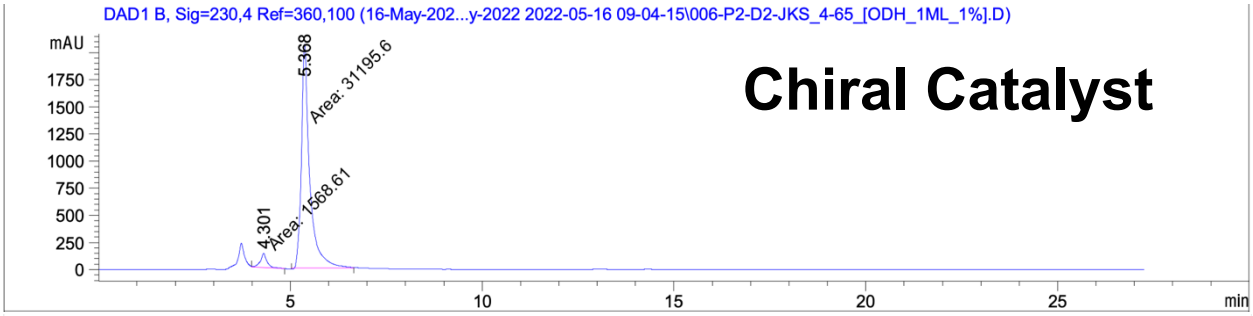

Signal 2: DAD1 B, Sig=230,4 Ref=360,100

Peak #	RetTime [min]	Type	Width [min]	Area [mAU*s]	Height [mAU]	Area %
1	4.301	MM	0.2002	1568.60901	130.61334	4.7876
2	5.368	MM	0.2526	3.11956e4	2058.07764	95.2124
Totals :				3.27642e4	2188.69098	

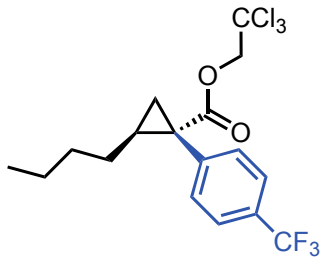

Compound **48**

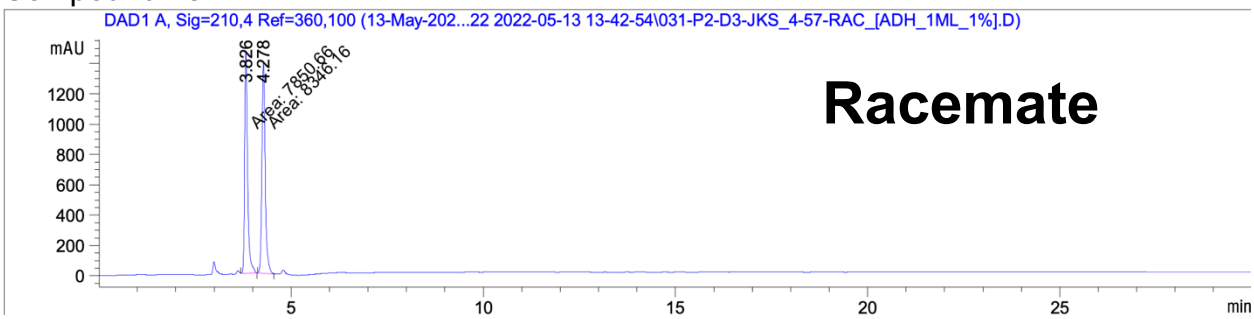

Signal 1: DAD1 A, Sig=210,4 Ref=360,100

Peak #	RetTime [min]	Type	Width [min]	Area [mAU*s]	Height [mAU]	Area %
1	3.826	MM	0.0889	7850.65771	1472.00183	48.4704
2	4.278	MM	0.1001	8346.16016	1389.61646	51.5296
Totals :				1.61968e4	2861.61829	

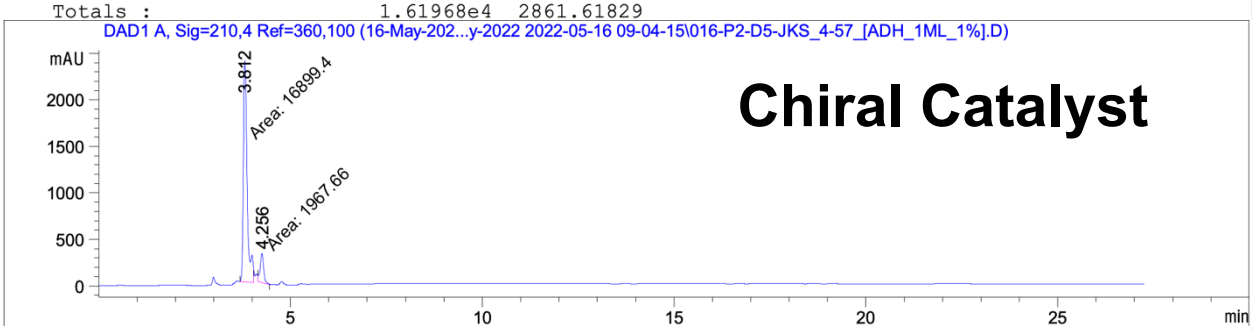

Signal 1: DAD1 A, Sig=210,4 Ref=360,100

Peak #	RetTime [min]	Type	Width [min]	Area [mAU*s]	Height [mAU]	Area %
1	3.812	MM	0.1187	1.68994e4	2372.62671	89.5709
2	4.256	MM	0.1060	1967.66187	309.25751	10.4291
Totals :				1.88671e4	2681.88422	

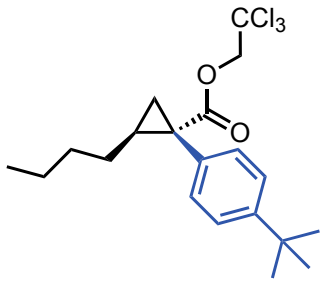

Compound **49**

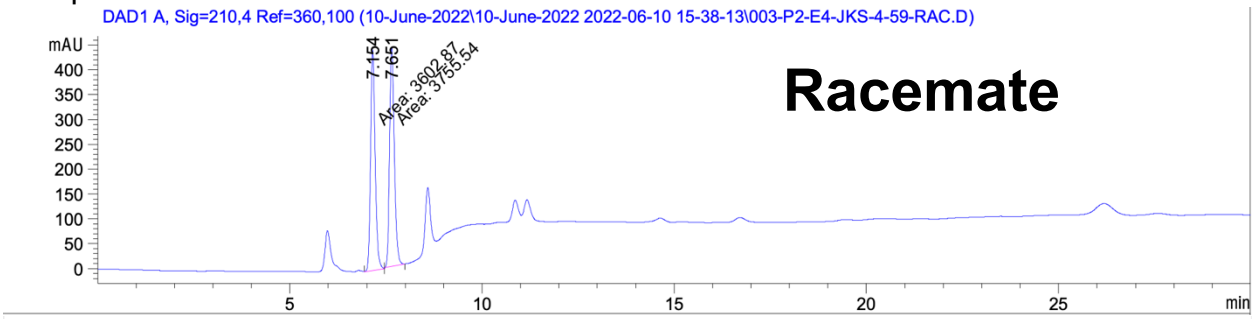

Signal 1: DAD1 A, Sig=210,4 Ref=360,100

Peak #	RetTime [min]	Type	Width [min]	Area [mAU*s]	Height [mAU]	Area %
1	7.154	MM	0.1355	3602.86768	443.24615	48.9626
2	7.651	MM	0.1414	3755.54053	442.57819	51.0374
Totals :				7358.40820	885.82434	

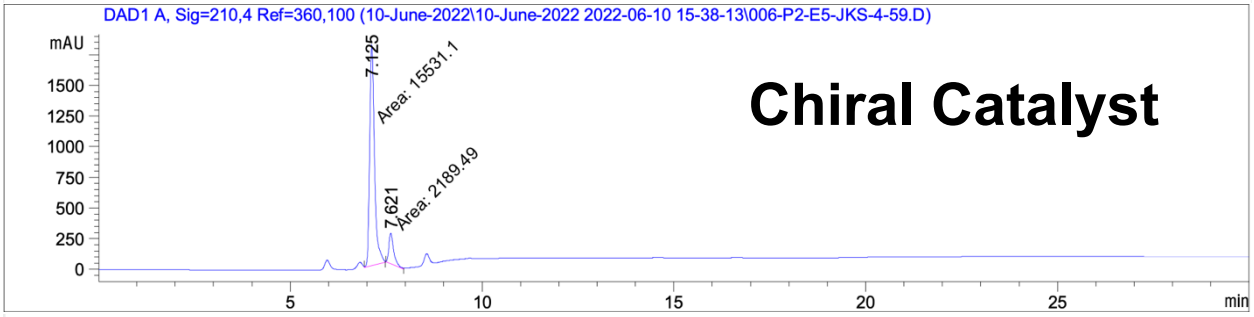

Signal 1: DAD1 A, Sig=210,4 Ref=360,100

Peak #	RetTime [min]	Type	Width [min]	Area [mAU*s]	Height [mAU]	Area %
1	7.125	MM	0.1439	1.55311e4	1798.51465	87.6444
2	7.621	MM	0.1465	2189.48853	249.00909	12.3556
Totals :				1.77206e4	2047.52374	

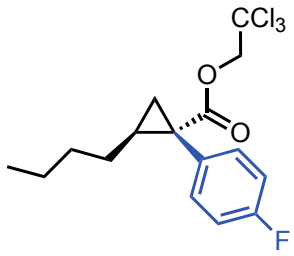

Compound **50**

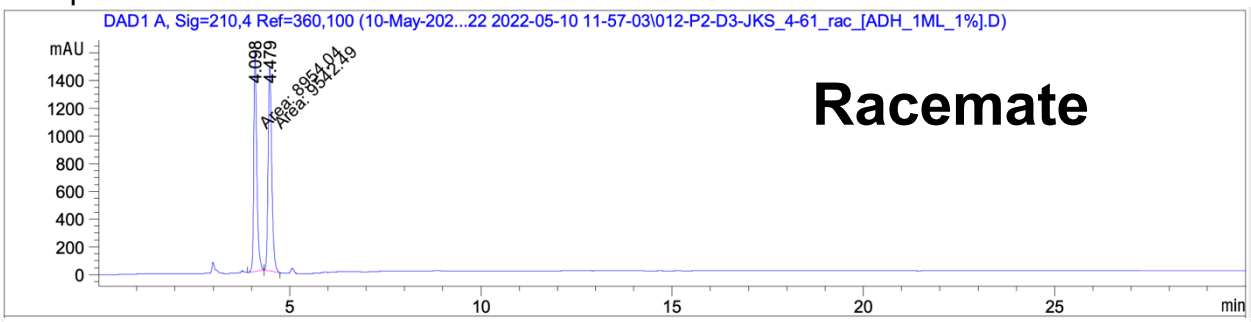

Signal 1: DAD1 A, Sig=210,4 Ref=360,100

Peak #	RetTime [min]	Type	Width [min]	Area [mAU*s]	Height [mAU]	Area %
1	4.098	MM	0.0938	8954.04492	1590.51208	48.4093
2	4.479	MM	0.1076	9542.48633	1477.88611	51.5907
Totals :				1.84965e4	3068.39819	

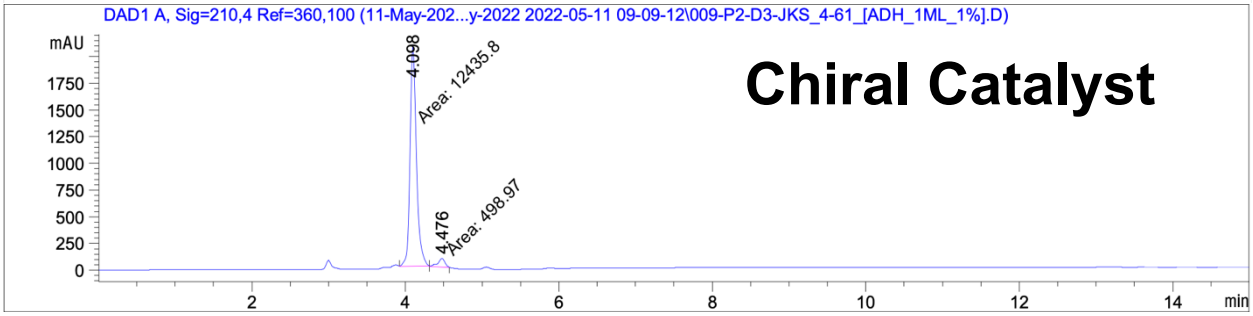

Peak #	RetTime [min]	Type	Width [min]	Area [mAU*s]	Height [mAU]	Area %
1	4.098	MM	0.1001	1.24358e4	2070.53101	96.1424
2	4.476	MM	0.1041	498.96985	79.91113	3.8576
Totals :				1.29348e4	2150.44214	

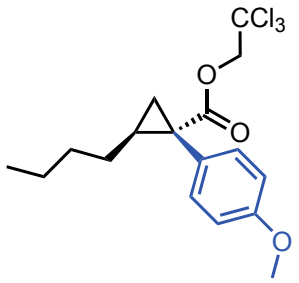

Compound **51**

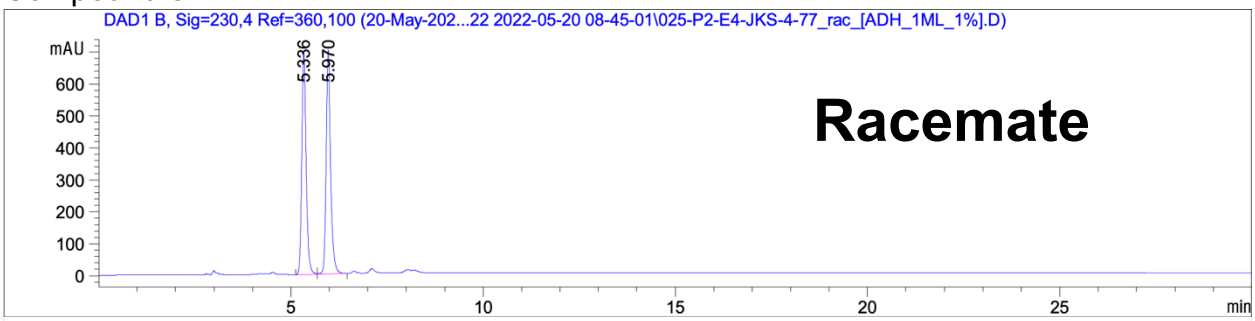

Signal 2: DAD1 B, Sig=230,4 Ref=360,100

Peak #	RetTime [min]	Type	Width [min]	Area [mAU*s]	Height [mAU]	Area %
1	5.336	BV	0.1160	5351.30273	693.85547	48.3801
2	5.970	VV	0.1230	5709.66260	701.35504	51.6199
Totals :				1.10610e4	1395.21051	

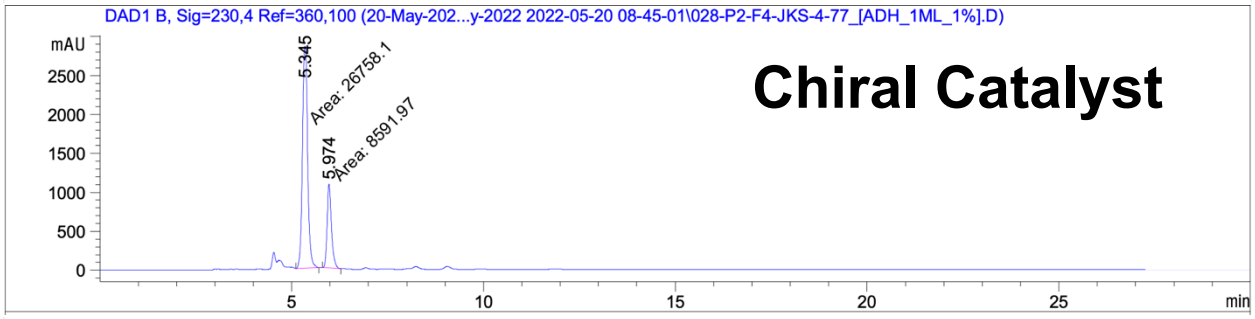

Signal 2: DAD1 B, Sig=230,4 Ref=360,100

Peak #	RetTime [min]	Type	Width [min]	Area [mAU*s]	Height [mAU]	Area %
1	5.345	MM	0.1563	2.67581e4	2853.75342	75.6946
2	5.974	MM	0.1326	8591.97461	1080.03687	24.3054
Totals :				3.53501e4	3933.79028	

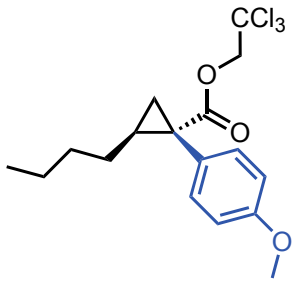

Compound **52**

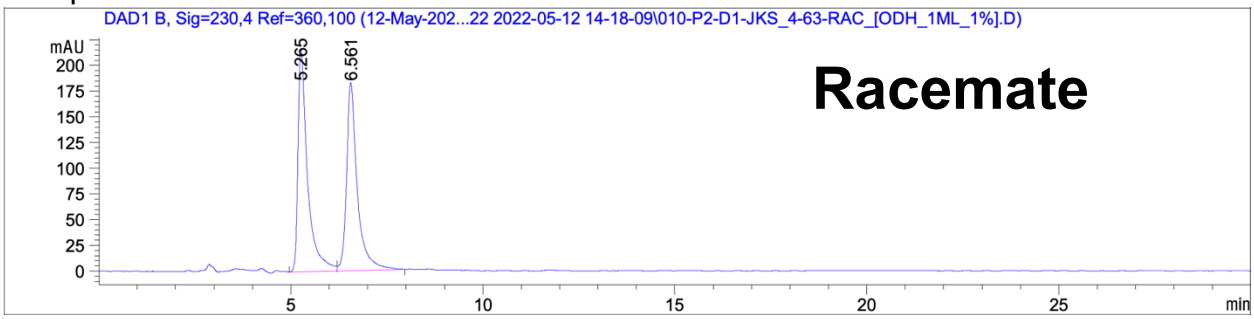

Signal 2: DAD1 B, Sig=230,4 Ref=360,100

Peak #	RetTime [min]	Type	Width [min]	Area [mAU*s]	Height [mAU]	Area %
1	5.265	BV	0.2455	3705.11035	216.69075	51.0951
2	6.561	VB	0.2801	3546.28491	183.00114	48.9049
Totals :				7251.39526	399.69189	

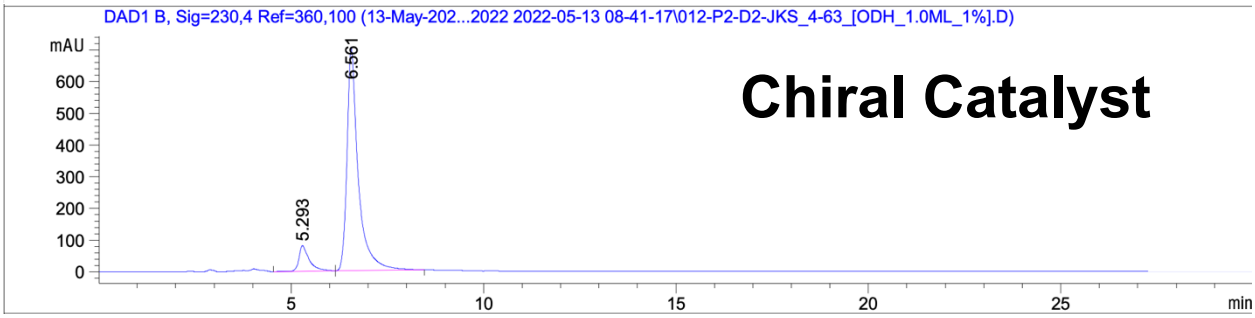

Signal 2: DAD1 B, Sig=230,4 Ref=360,100

Peak #	RetTime [min]	Type	Width [min]	Area [mAU*s]	Height [mAU]	Area %
1	5.293	BV	0.2642	1563.71777	81.38562	9.8170
2	6.561	VB	0.2916	1.43649e4	705.43890	90.1830
Totals :				1.59286e4	786.82452	

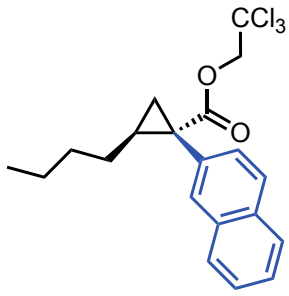

Compound **53**

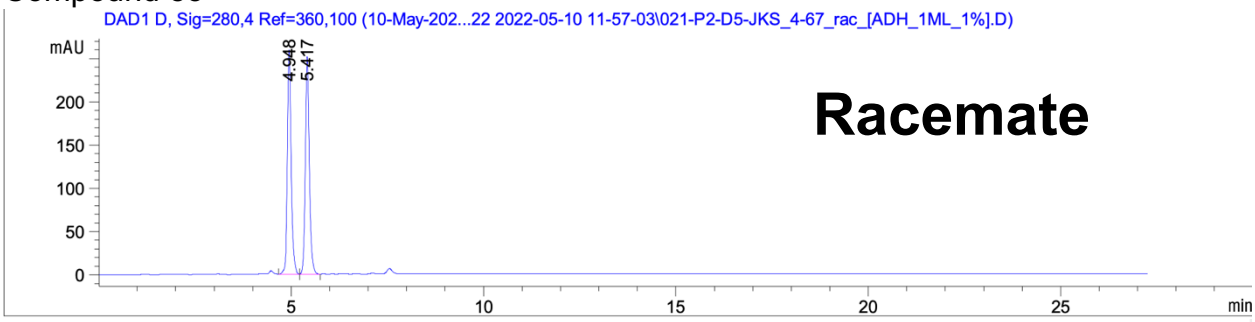

Signal 4: DAD1 D, Sig=280,4 Ref=360,100

Peak #	RetTime [min]	Type	Width [min]	Area [mAU*s]	Height [mAU]	Area %
1	4.948	BB	0.1040	1782.91492	260.08020	48.9374
2	5.417	BB	0.1123	1860.34387	251.58144	51.0626
Totals :				3643.25879	511.66164	

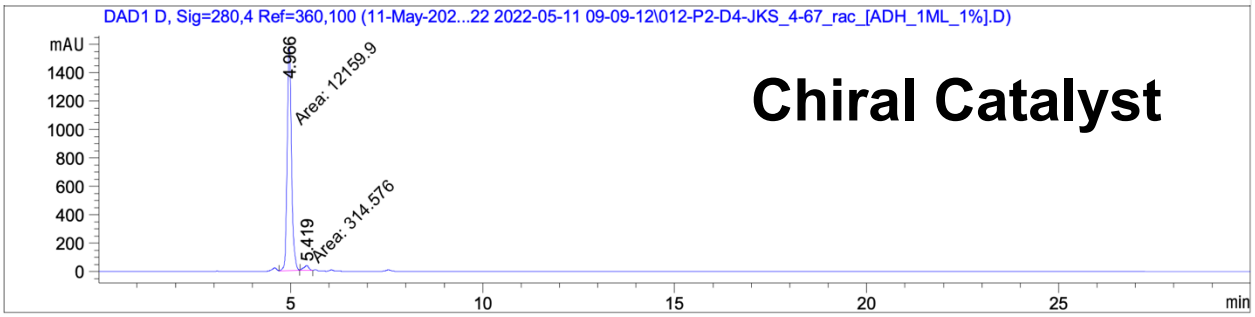

Signal 4: DAD1 D, Sig=280,4 Ref=360,100

Peak #	RetTime [min]	Type	Width [min]	Area [mAU*s]	Height [mAU]	Area %
1	4.966	MM	0.1282	1.21599e4	1580.68201	97.4782
2	5.419	MM	0.1499	314.57635	34.97344	2.5218
Totals :				1.24744e4	1615.65545	

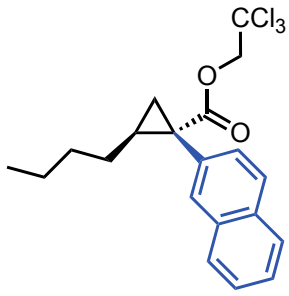

Compound **54**

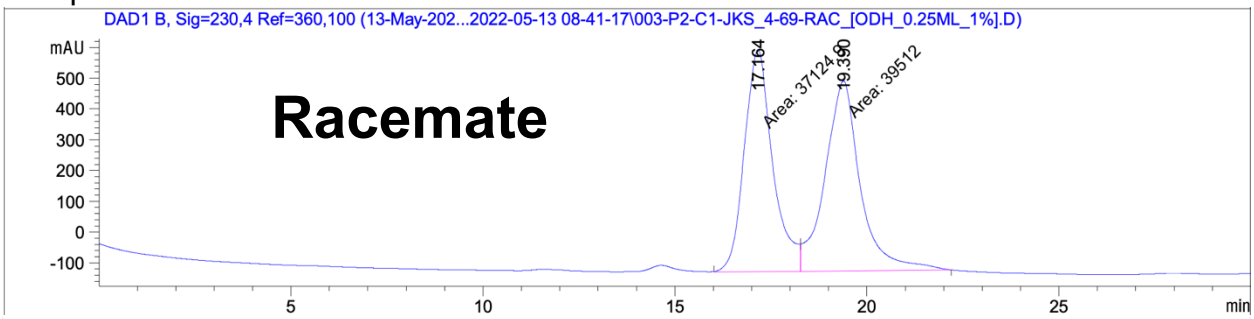

Signal 2: DAD1 B, Sig=230,4 Ref=360,100

Peak #	RetTime [min]	Type	Width [min]	Area [mAU*s]	Height [mAU]	Area %
1	17.164	MF	0.8576	3.71249e4	721.49799	48.4426
2	19.390	FM	1.0662	3.95120e4	617.63428	51.5574
Totals :				7.66369e4	1339.13226	

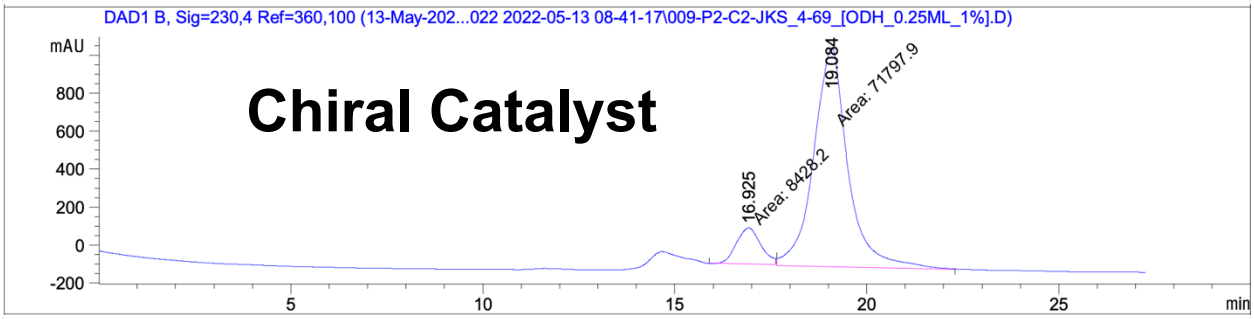

Signal 2: DAD1 B, Sig=230,4 Ref=360,100

Peak #	RetTime [min]	Type	Width [min]	Area [mAU*s]	Height [mAU]	Area %
1	16.925	MM	0.7379	8428.19922	190.36365	10.5056
2	19.084	MM	1.0385	7.17979e4	1152.28149	89.4944
Totals :				8.02261e4	1342.64514	

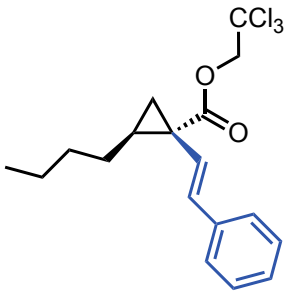

Compound **55**

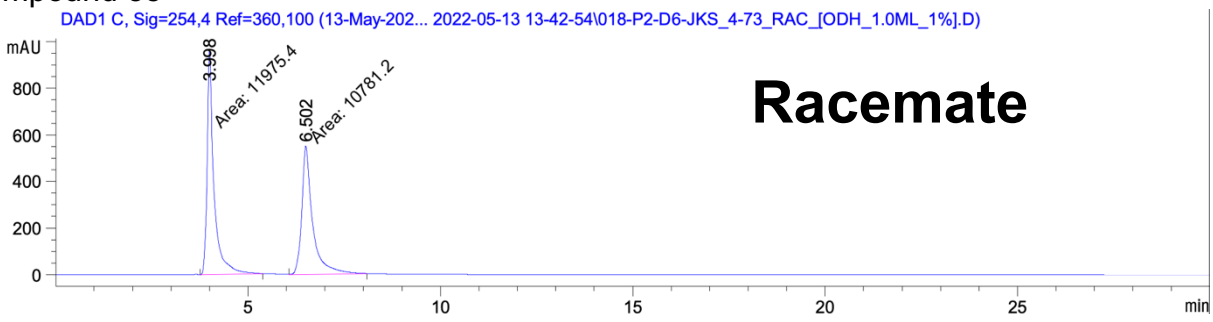

Signal 3: DAD1 C, Sig=254,4 Ref=360,100

Peak #	RetTime [min]	Type	Width [min]	Area [mAU*s]	Height [mAU]	Area %
1	3.998	MM	0.2064	1.19754e4	966.92511	52.6238
2	6.502	MM	0.3262	1.07812e4	550.84894	47.3762
Totals :				2.27565e4	1517.77405	

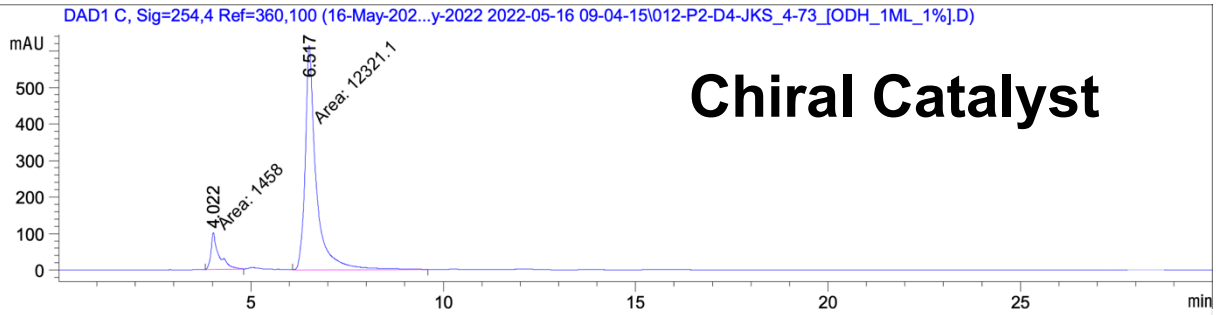

Signal 3: DAD1 C, Sig=254,4 Ref=360,100

Peak #	RetTime [min]	Type	Width [min]	Area [mAU*s]	Height [mAU]	Area %
1	4.022	MM	0.2419	1457.99976	100.45798	10.5812
2	6.517	MM	0.3345	1.23211e4	613.97955	89.4188
Totals :				1.37791e4	714.43753	

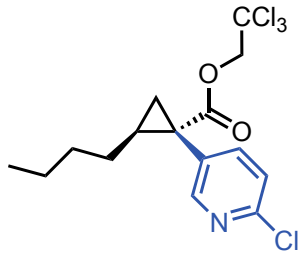

Compound **56**

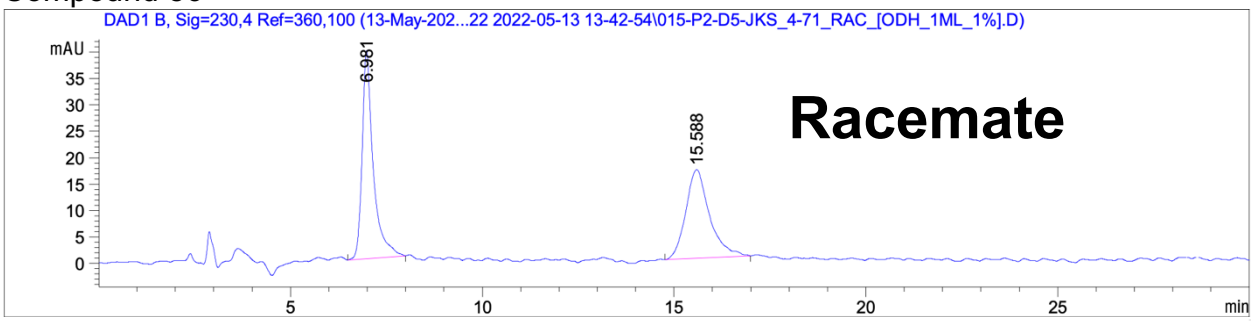

Signal 2: DAD1 B, Sig=230,4 Ref=360,100

Peak #	RetTime [min]	Type	Width [min]	Area [mAU*s]	Height [mAU]	Area %
1	6.981	BB	0.2864	791.49957	39.40199	52.2334
2	15.588	BB	0.6274	723.81415	16.77467	47.7666
Totals :				1515.31372	56.17666	

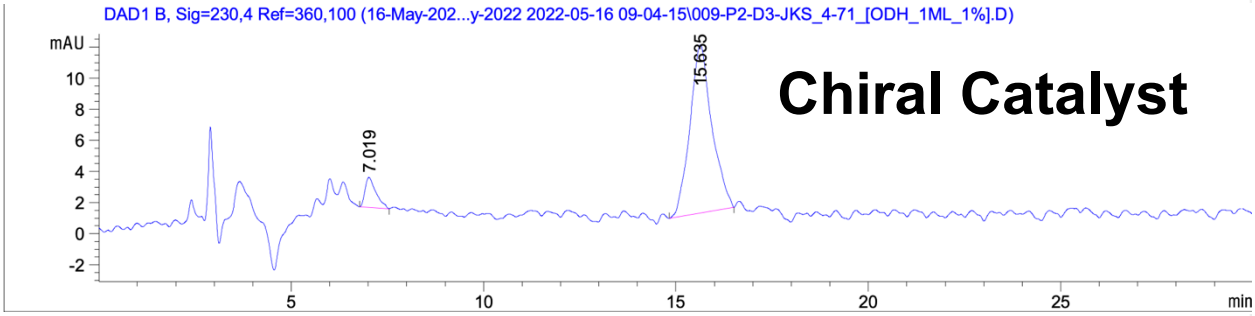

Signal 2: DAD1 B, Sig=230,4 Ref=360,100

Peak #	RetTime [min]	Type	Width [min]	Area [mAU*s]	Height [mAU]	Area %
1	7.019	BB	0.2797	38.09735	1.93466	8.1562
2	15.635	BB	0.5507	428.99942	10.81679	91.8438
Totals :				467.09677	12.75145	

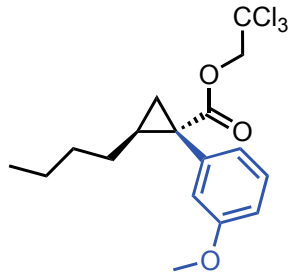

Compound **57**

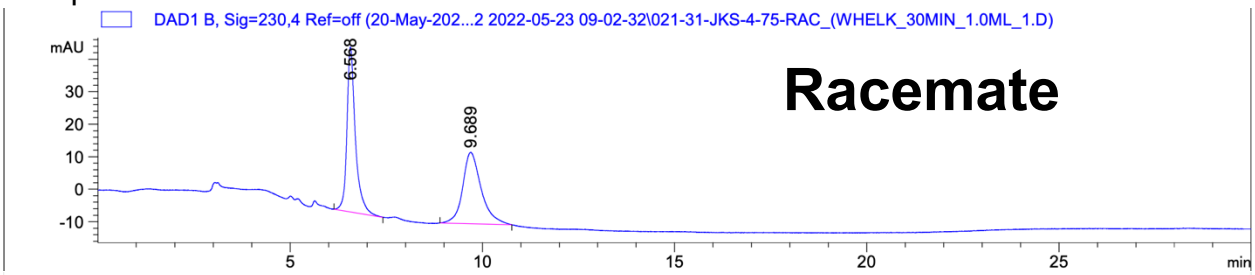

Signal 2: DAD1 B, Sig=230,4 Ref=off

Peak #	RetTime [min]	Type	Width [min]	Area [mAU*s]	Height [mAU]	Area %
1	6.568	BV R	0.2142	777.20831	50.73787	51.2671
2	9.689	VB R	0.3941	738.78949	21.95587	48.7329
Totals :				1515.99780	72.69374	

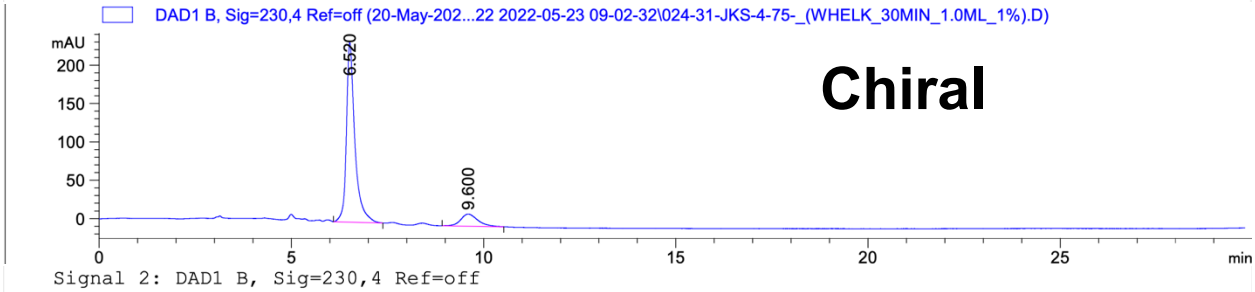

Signal 2: DAD1 B, Sig=230,4 Ref=off

Peak #	RetTime [min]	Type	Width [min]	Area [mAU*s]	Height [mAU]	Area %
1	6.520	BB	0.2230	3580.29175	234.00452	87.8815
2	9.600	VV R	0.3647	493.70880	15.92250	12.1185
Totals :				4074.00055	249.92702	

HPLC Chromatographs for React IR Experiments

React IR experiments varying the equivalents of styrene:

5.0 equivalents of styrene, 1.0mol % catalyst loading.

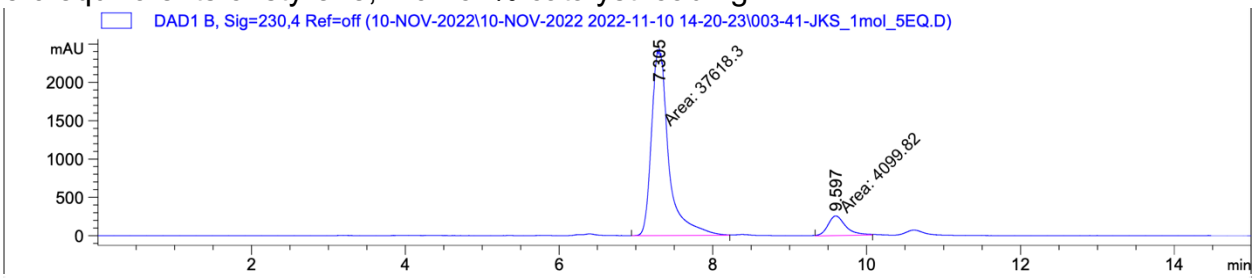

Signal 2: DAD1 B, Sig=230,4 Ref=off

Peak #	RetTime [min]	Type	Width [min]	Area [mAU*s]	Height [mAU]	Area %
1	7.305	MM	0.2570	3.76183e4	2440.00342	90.1726
2	9.597	MM	0.2671	4099.82324	255.80693	9.8274
Totals :				4.17181e4	2695.81035	

3.0 equivalents of styrene, 1.0mol % catalyst loading.

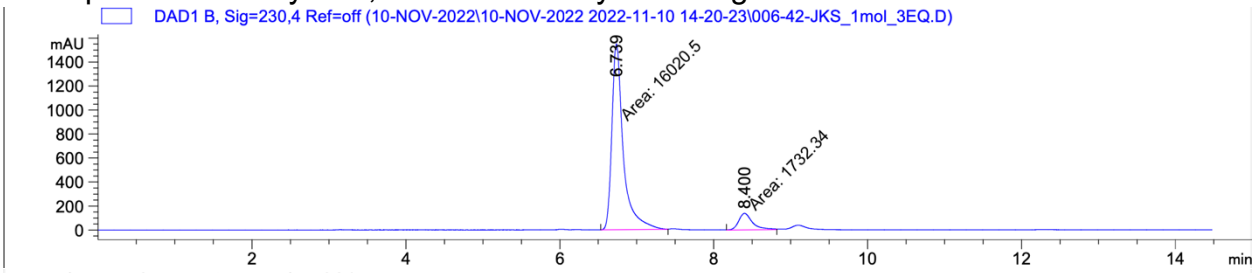

Signal 2: DAD1 B, Sig=230,4 Ref=off

Peak #	RetTime [min]	Type	Width [min]	Area [mAU*s]	Height [mAU]	Area %
1	6.739	MM	0.1722	1.60205e4	1550.22693	90.2419
2	8.400	MM	0.2082	1732.33948	138.68996	9.7581
Totals :				1.77528e4	1688.91689	

1.5 equivalents of styrene, 1.0mol % catalyst loading.

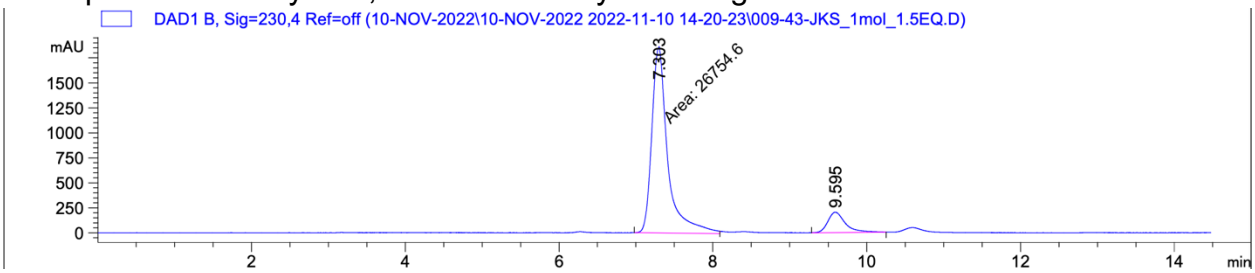

Signal 2: DAD1 B, Sig=230,4 Ref=off

Peak #	RetTime [min]	Type	Width [min]	Area [mAU*s]	Height [mAU]	Area %
1	7.303	MM	0.2392	2.67546e4	1864.29041	89.2488
2	9.595	BV R	0.1873	3222.95435	203.96759	10.7512
Totals :				2.99775e4	2068.25800	

React IR experiments varying the catalyst loading

3.0 equivalents of styrene, **0.5mol %** catalyst loading.

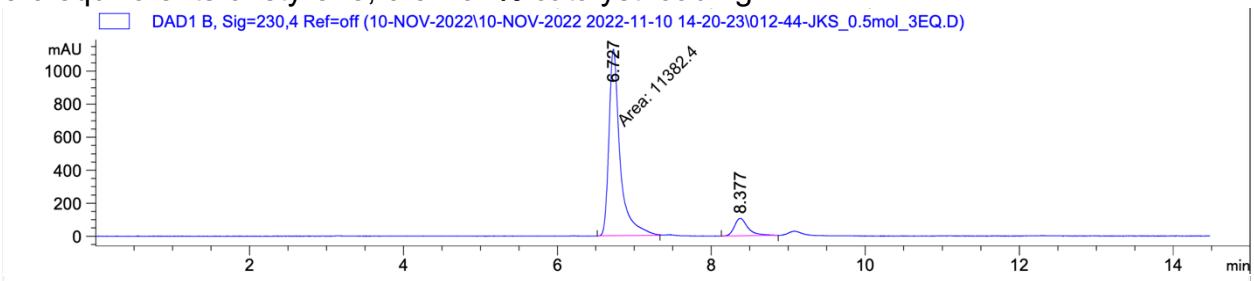

Signal 2: DAD1 B, Sig=230,4 Ref=off

Peak #	RetTime [min]	Type	Width [min]	Area [mAU*s]	Height [mAU]	Area %
1	6.727	MM	0.1678	1.13824e4	1130.75708	89.8516
2	8.377	BV R	0.1437	1285.59961	105.85095	10.1484
Totals :				1.26680e4	1236.60803	

3.0 equivalents of styrene, **0.1 mol %** catalyst loading.

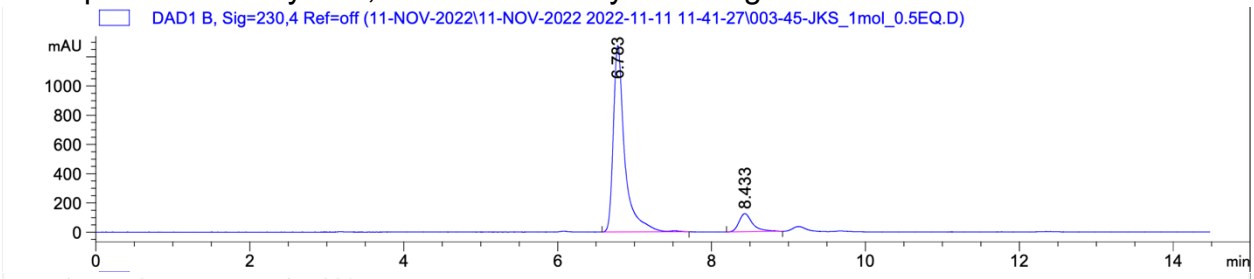

Signal 2: DAD1 B, Sig=230,4 Ref=off

Peak #	RetTime [min]	Type	Width [min]	Area [mAU*s]	Height [mAU]	Area %
1	6.783	BV R	0.1393	1.32190e4	1275.17456	89.6836
2	8.433	VV R	0.1499	1520.59167	124.54695	10.3164
Totals :				1.47396e4	1399.72151	

NMR Spectra for Novel Compounds

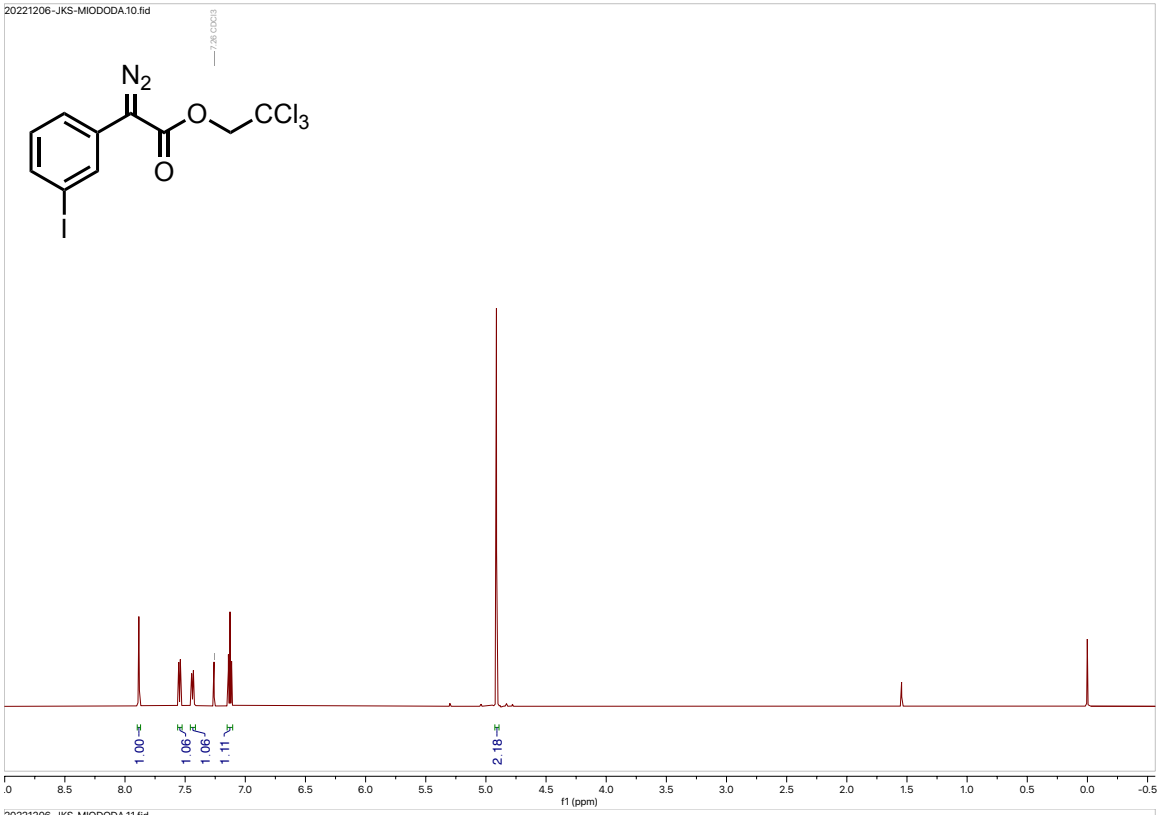

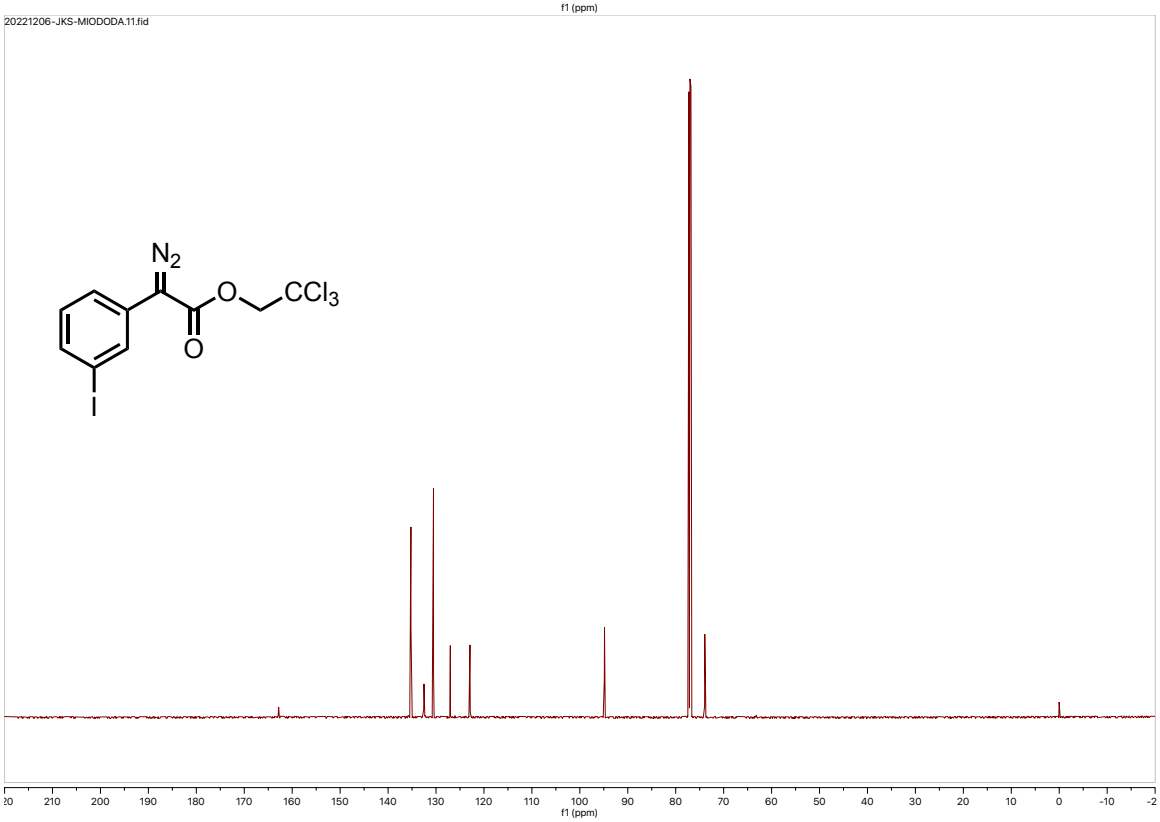

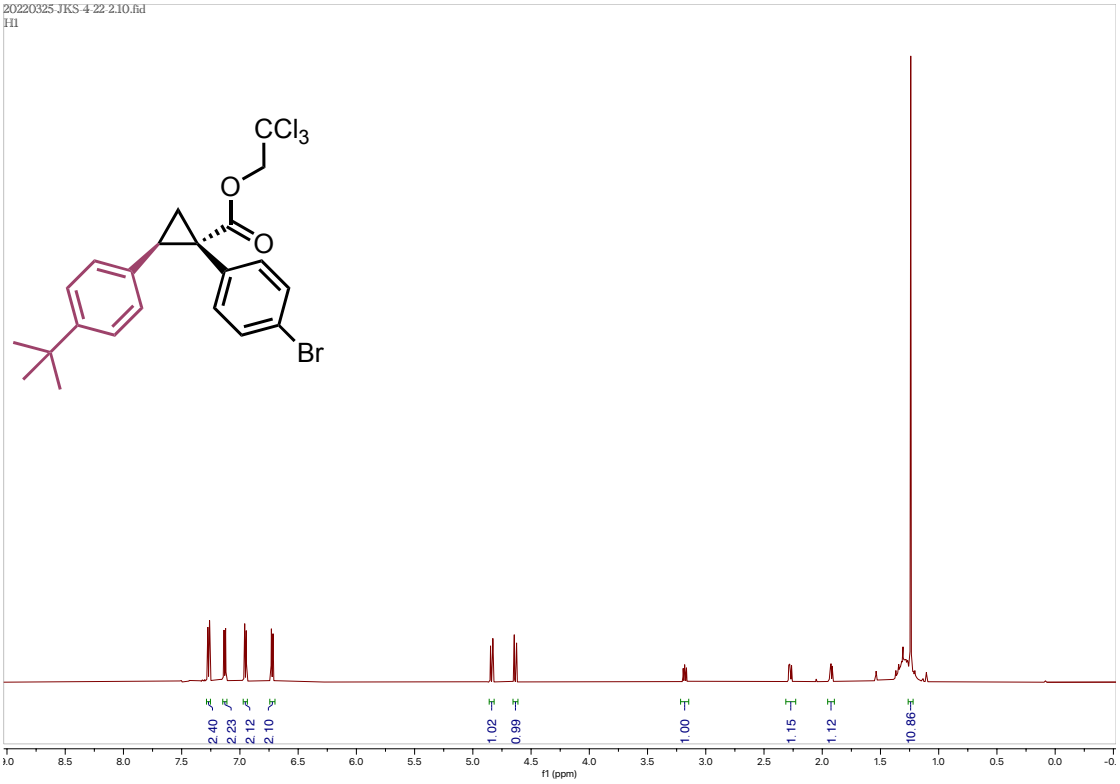
20220325 JKS 4 22 2.10.fid
H1
CCl3
O
O
Br
2.40
2.23
2.12
2.10
1.02
0.99
1.00
1.15
1.12
10.86
f1 (ppm)

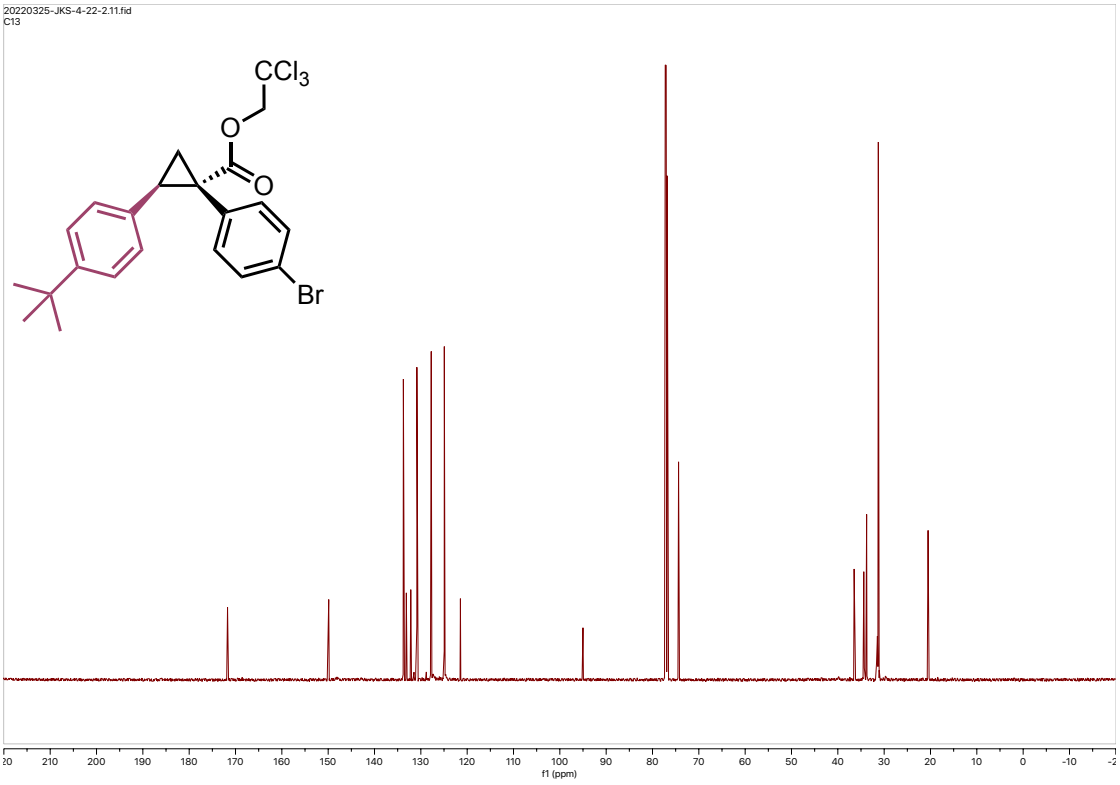
20220325-JKS-4-22-2.11.fid
C13
CCl3
O
O
Br
f1 (ppm)

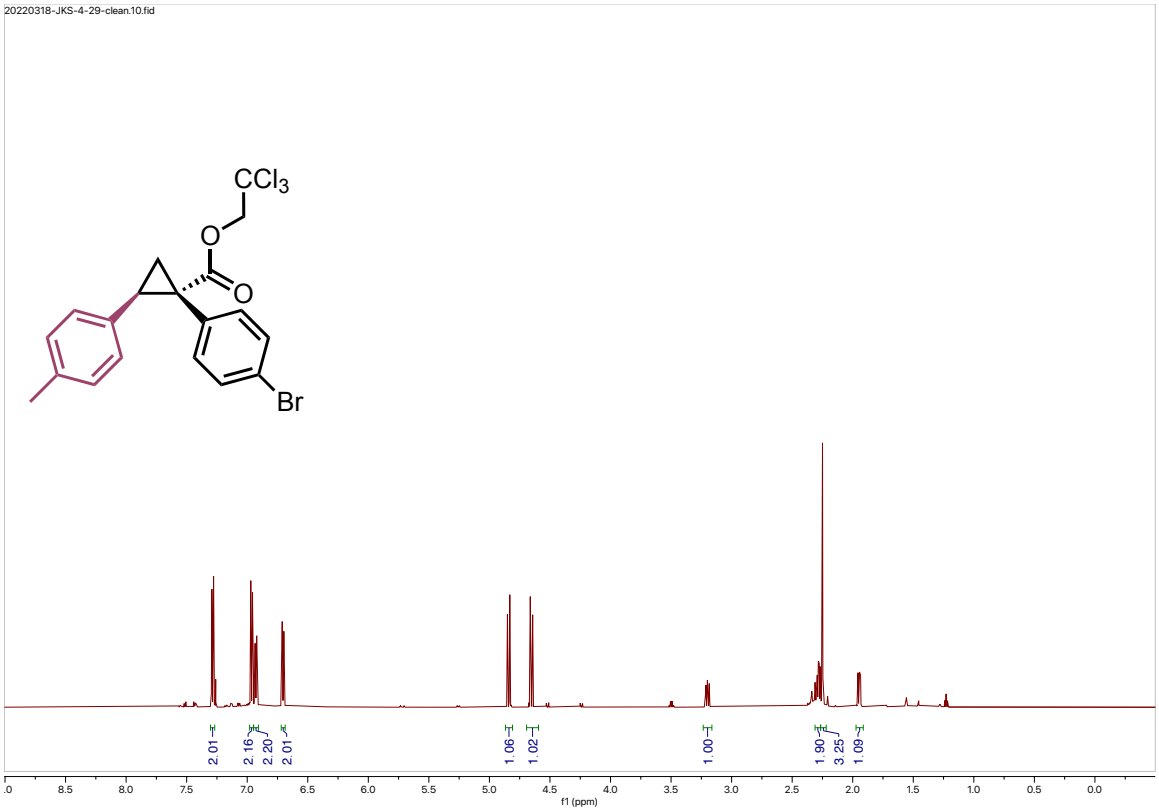
20220318-JKS-4-29-clean.10.fid
CCl3
O
O
Br
2.01
2.16
2.20
2.01
1.06
1.02
1.00
1.90
3.25
1.09
f1 (ppm)

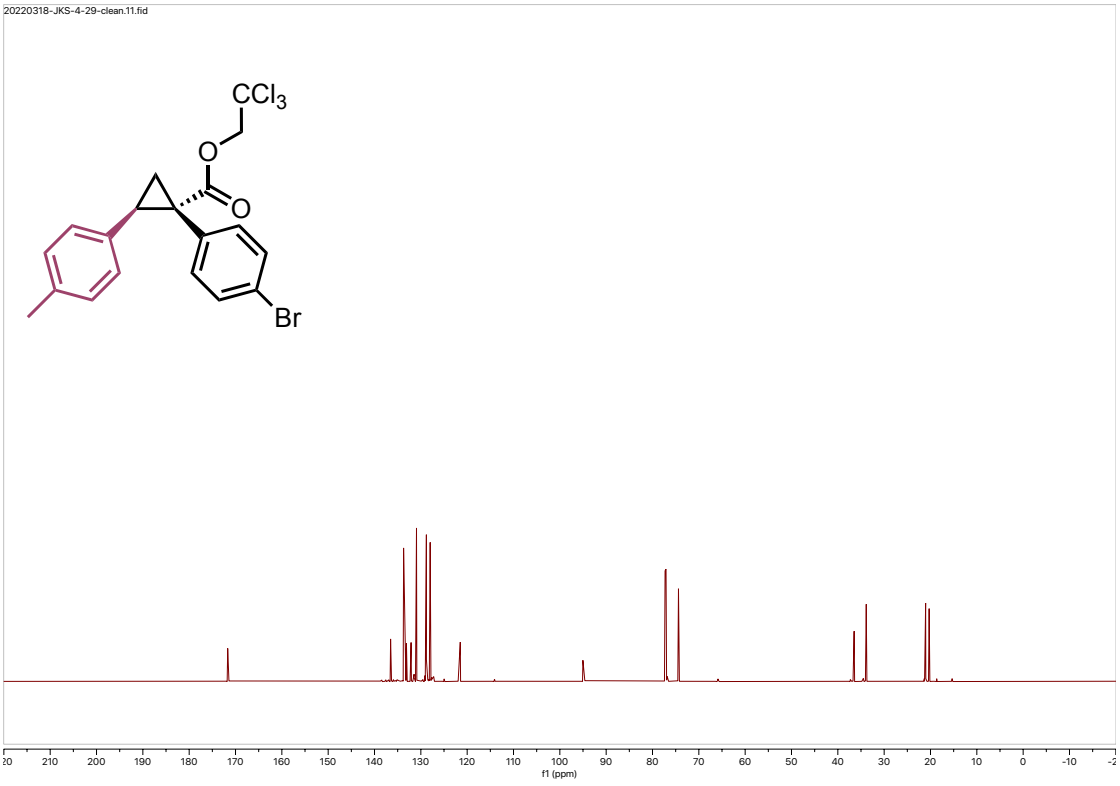
20220318-JKS-4-29-clean.11.fid
CCl3
O
O
Br
f1 (ppm)

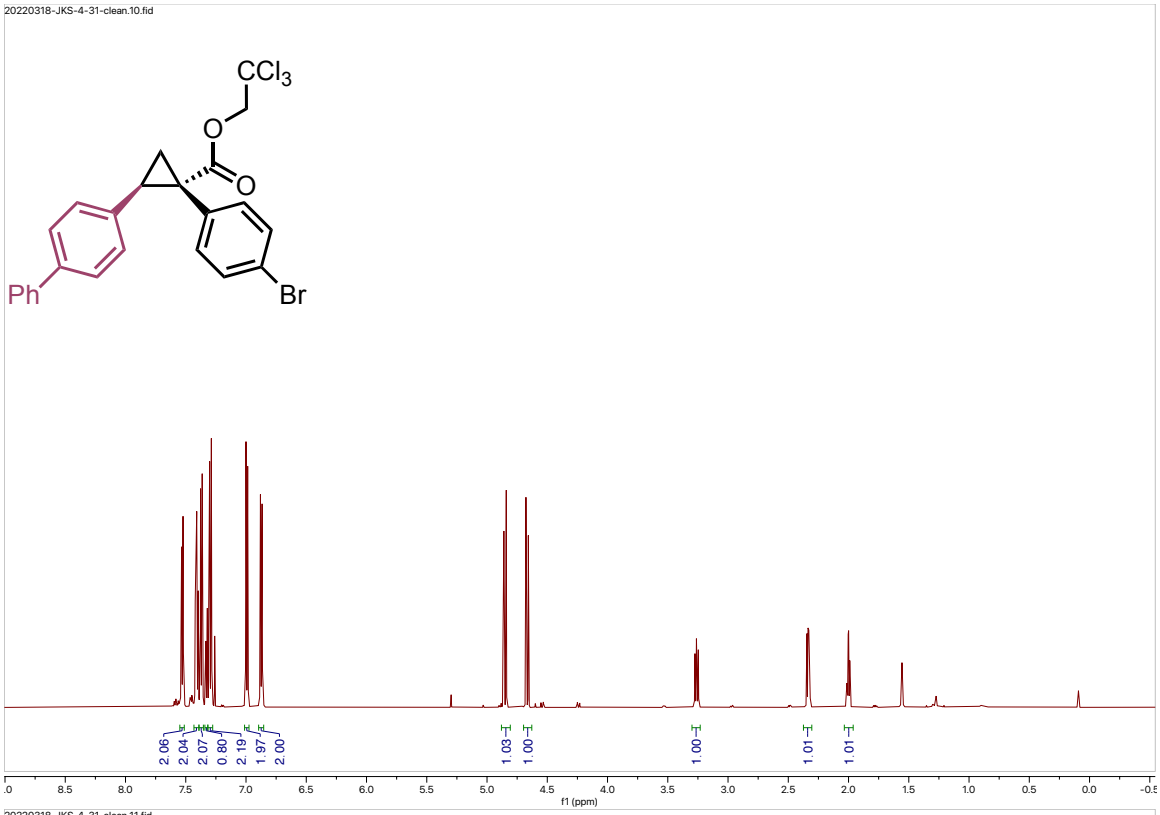
20220318-JKS-4-31-clean.10.fid
CCl3
O
O
Ph
Br
2.06
2.04
2.07
0.80
2.19
1.97
2.00
1.03
1.00
1.00
1.01
1.01
f1 (ppm)

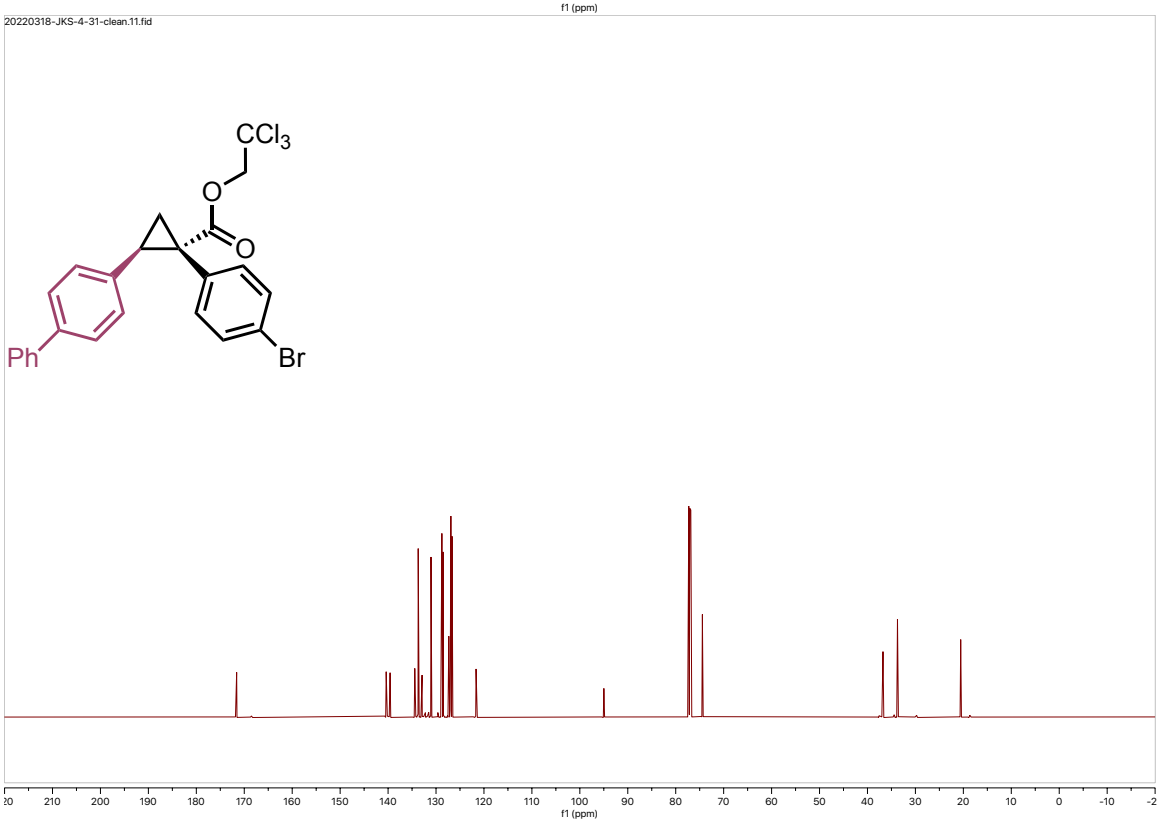
20220318-JKS-4-31-clean.11.fid
CCl3
O
O
Ph
Br
f1 (ppm)

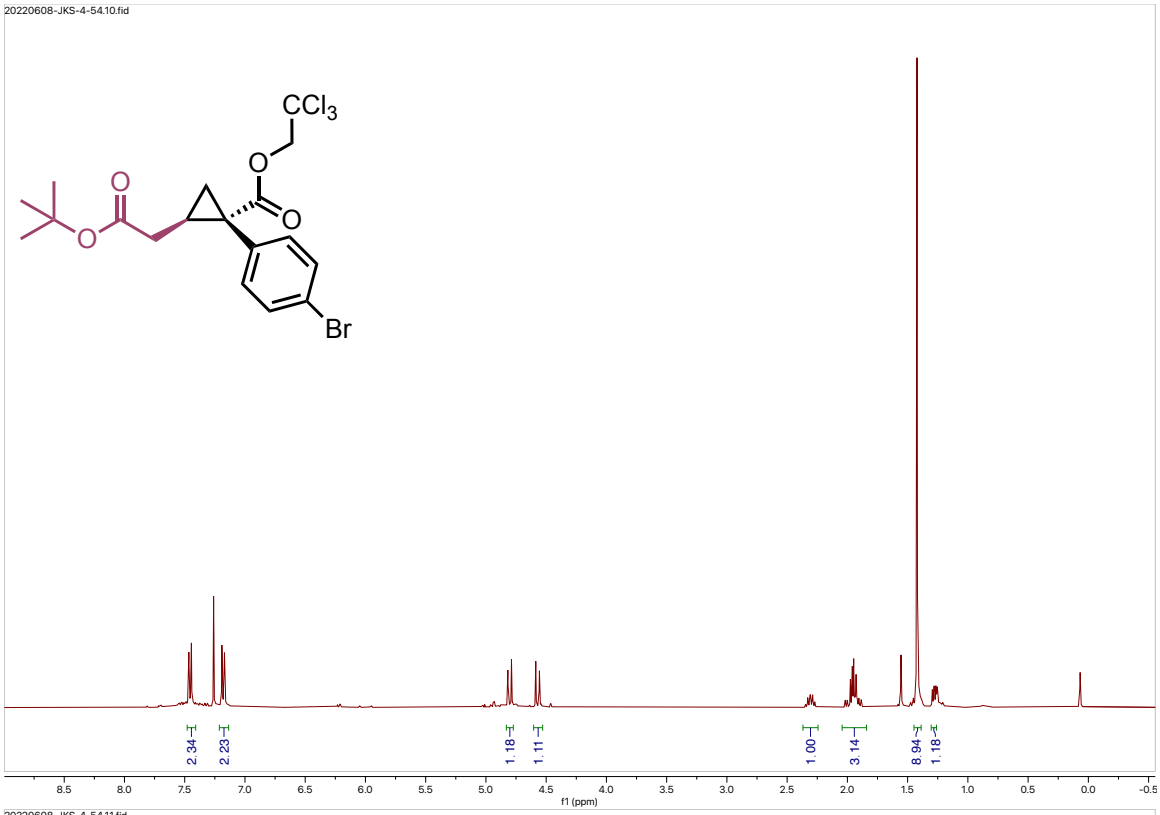
20220608-JKS-4-54.10.fid
CCl3
O
O
O
O
Br
2.34
2.23
1.18
1.11
1.00
3.14
8.94
1.18
f1 (ppm)

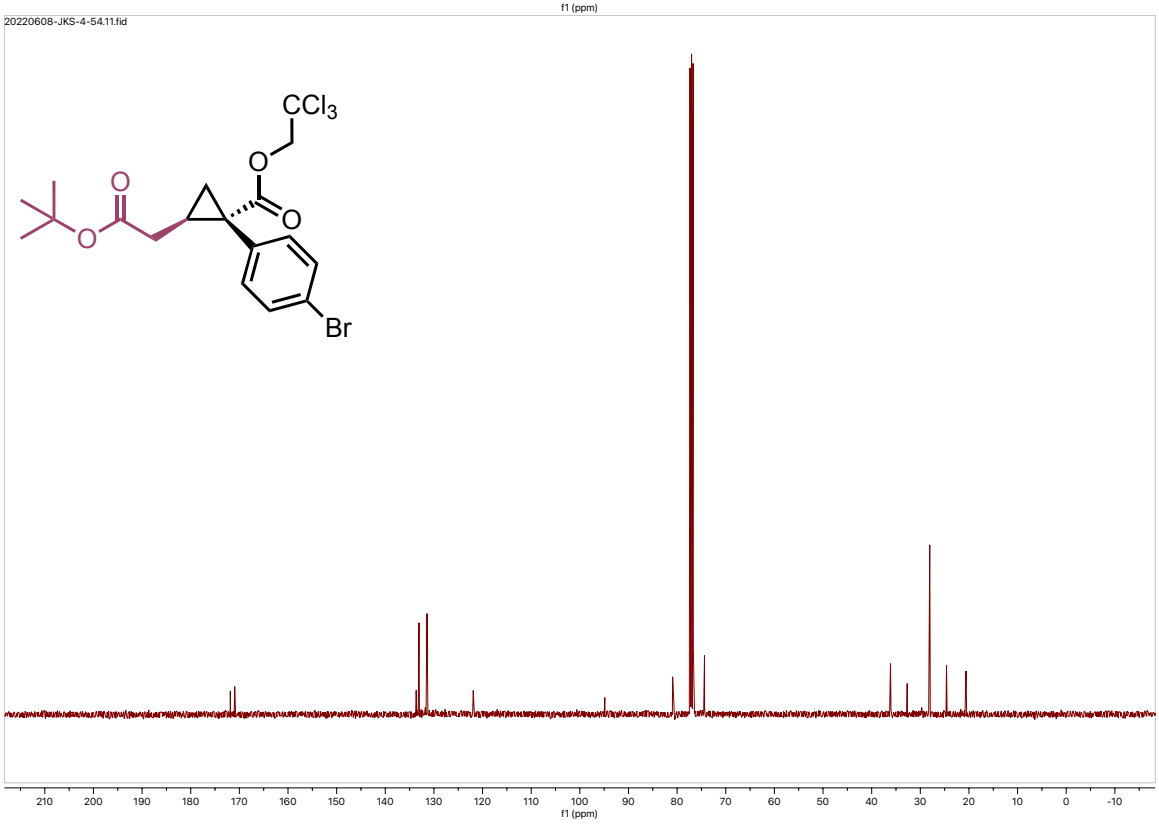
20220608-JKS-4-54.11.fid
CCl3
O
O
O
O
Br
f1 (ppm)

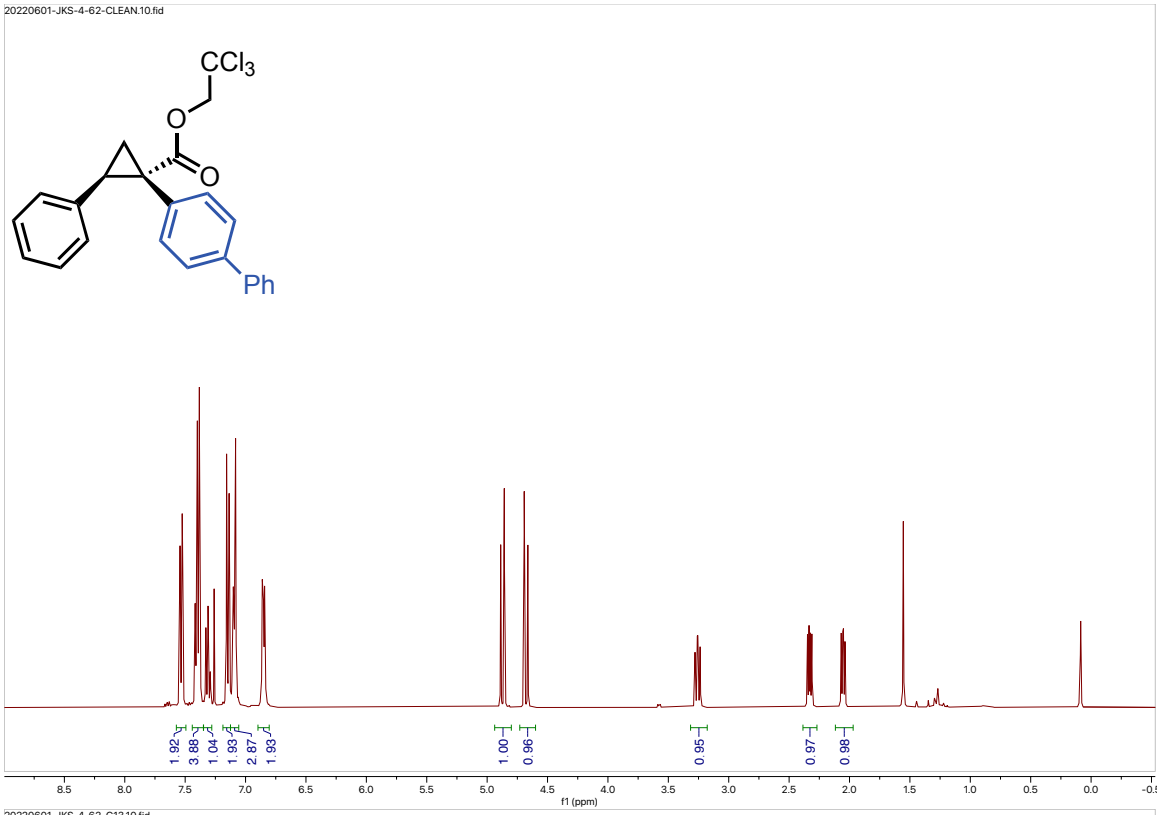
20220601-JKS-4-62-CLEAN.10.fid
CCl3
O
O
Ph
1.92
3.88
1.04
1.93
2.87
1.93
1.00
0.96
0.95
0.97
0.98
f1 (ppm)

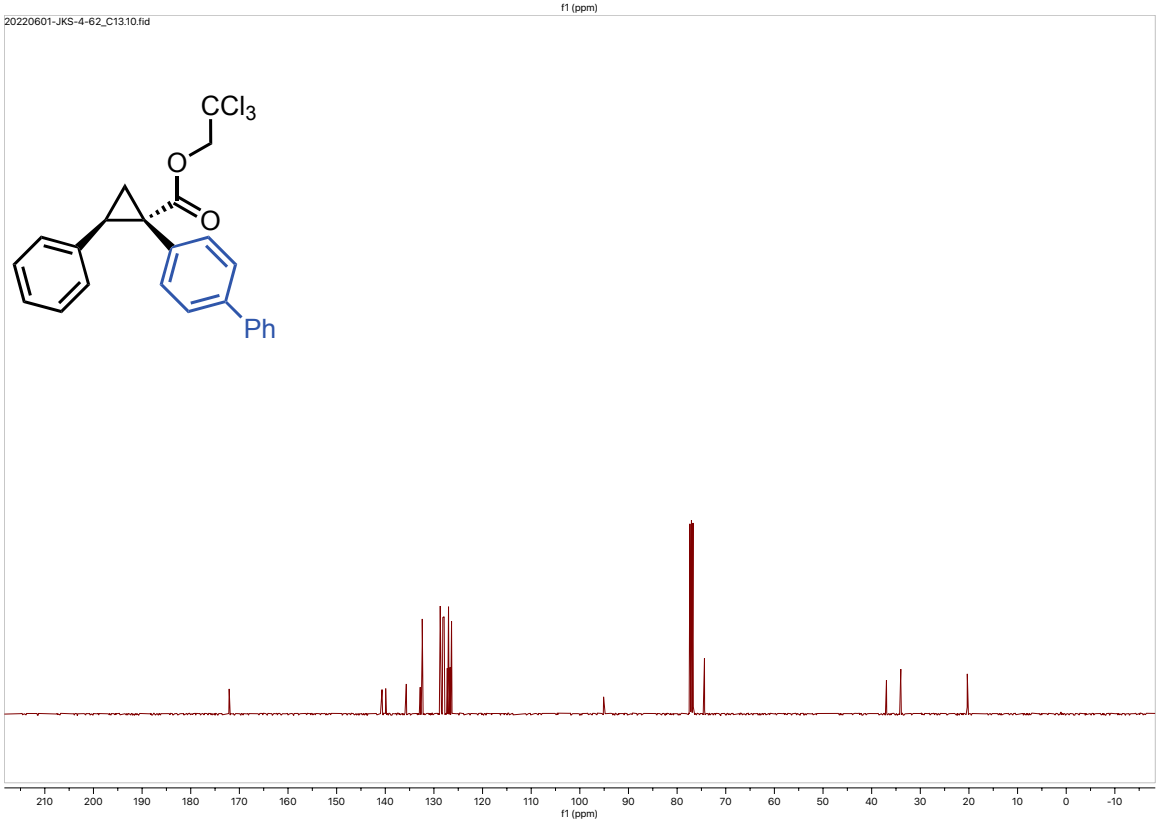
20220601-JKS-4-62_C13.10.fid
CCl3
O
O
Ph
f1 (ppm)

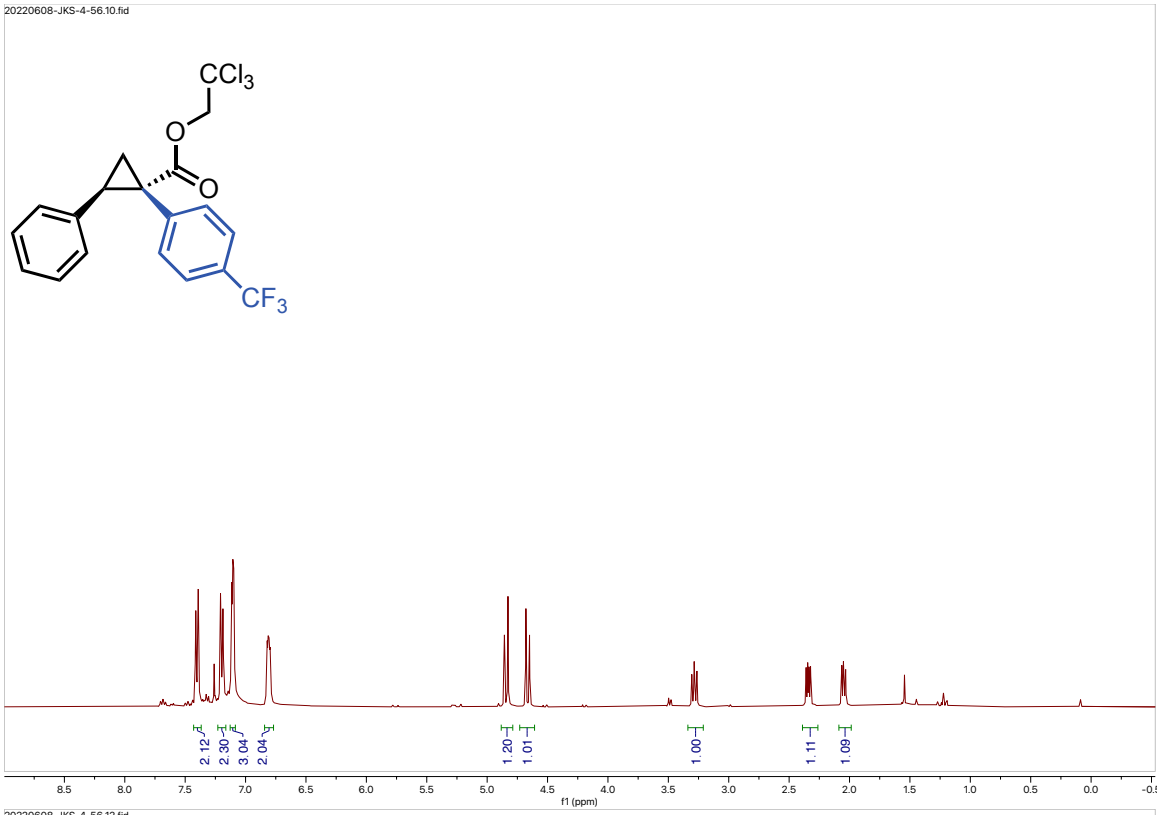
20220608-JKS-4-56.10.fid
CCl3
O
O
CF3
2.12
2.30
3.04
2.04
1.20
1.01
1.00
1.11
1.09
f1 (ppm)

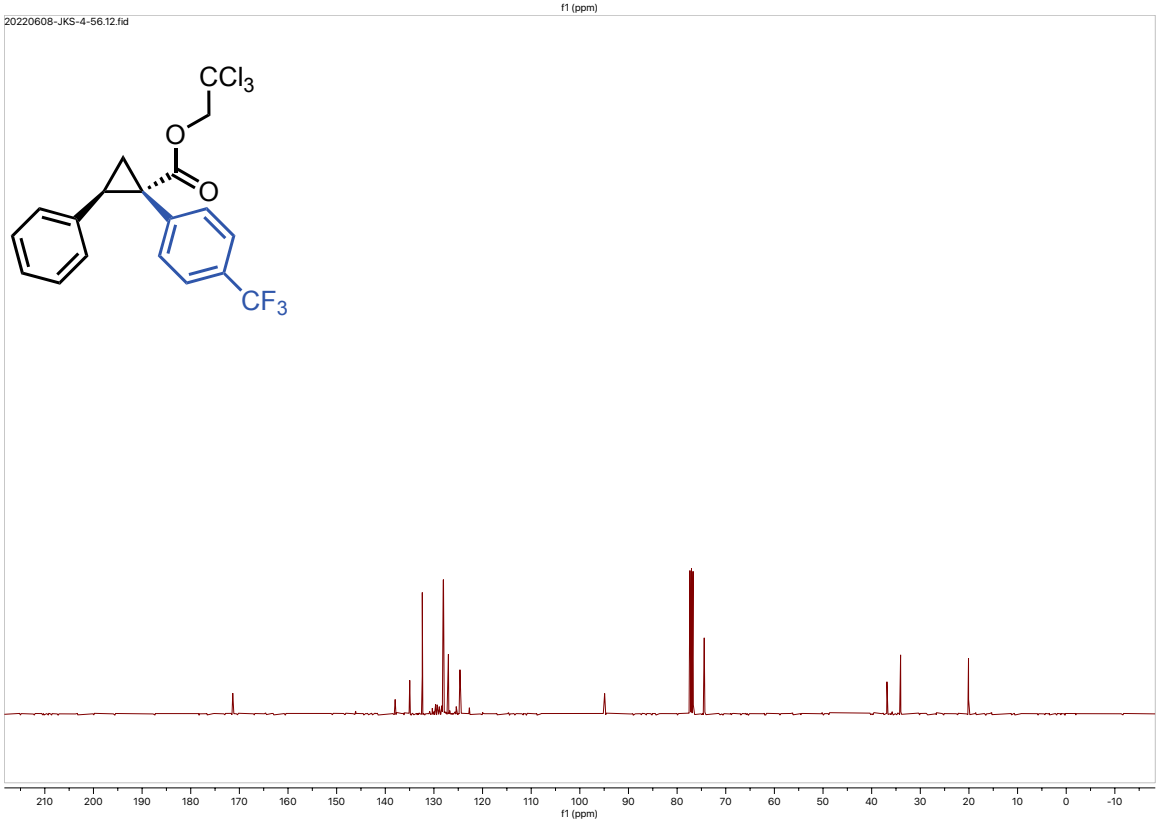
20220608-JKS-4-56.12.fid
CCl3
O
O
CF3
f1 (ppm)

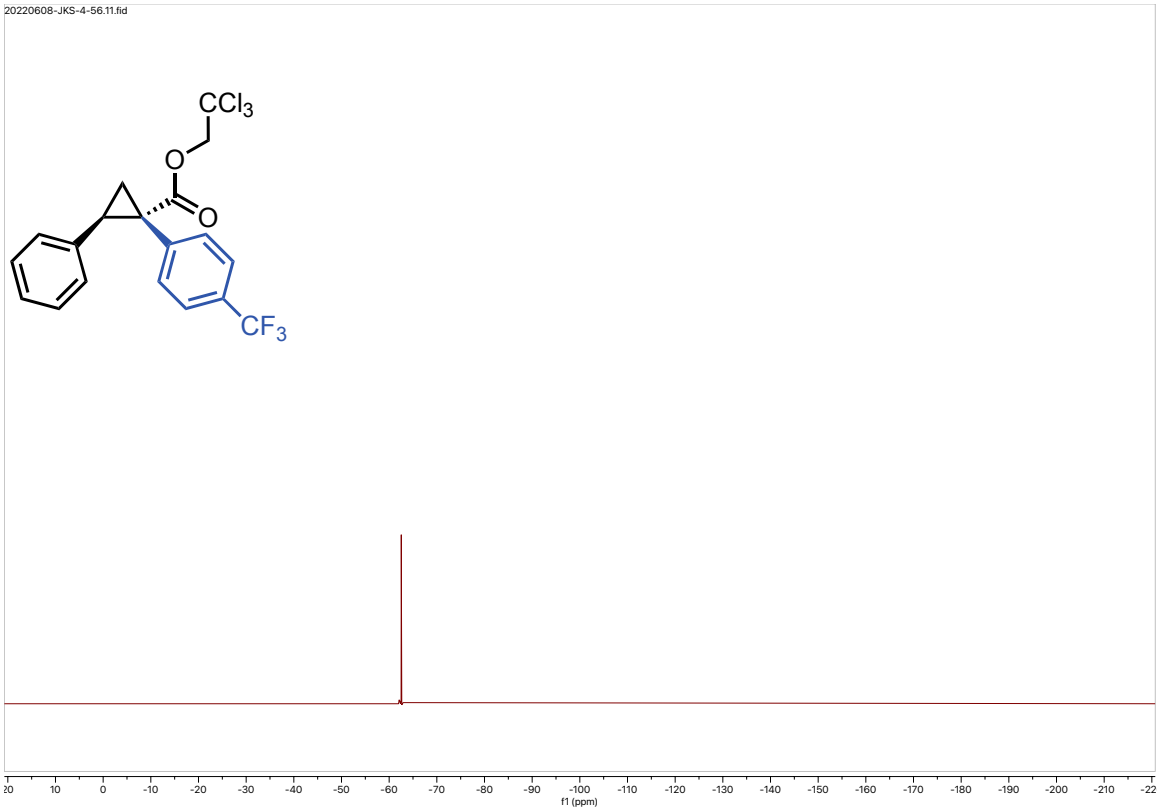
20220608-JKS-4-56.11.fid
CCl3
O
O
CF3
20
10
0
-10
-20
-30
-40
-50
-60
-70
-80
-90
-100
-110
-120
-130
-140
-150
-160
-170
-180
-190
-200
-210
-22
f1 (ppm)

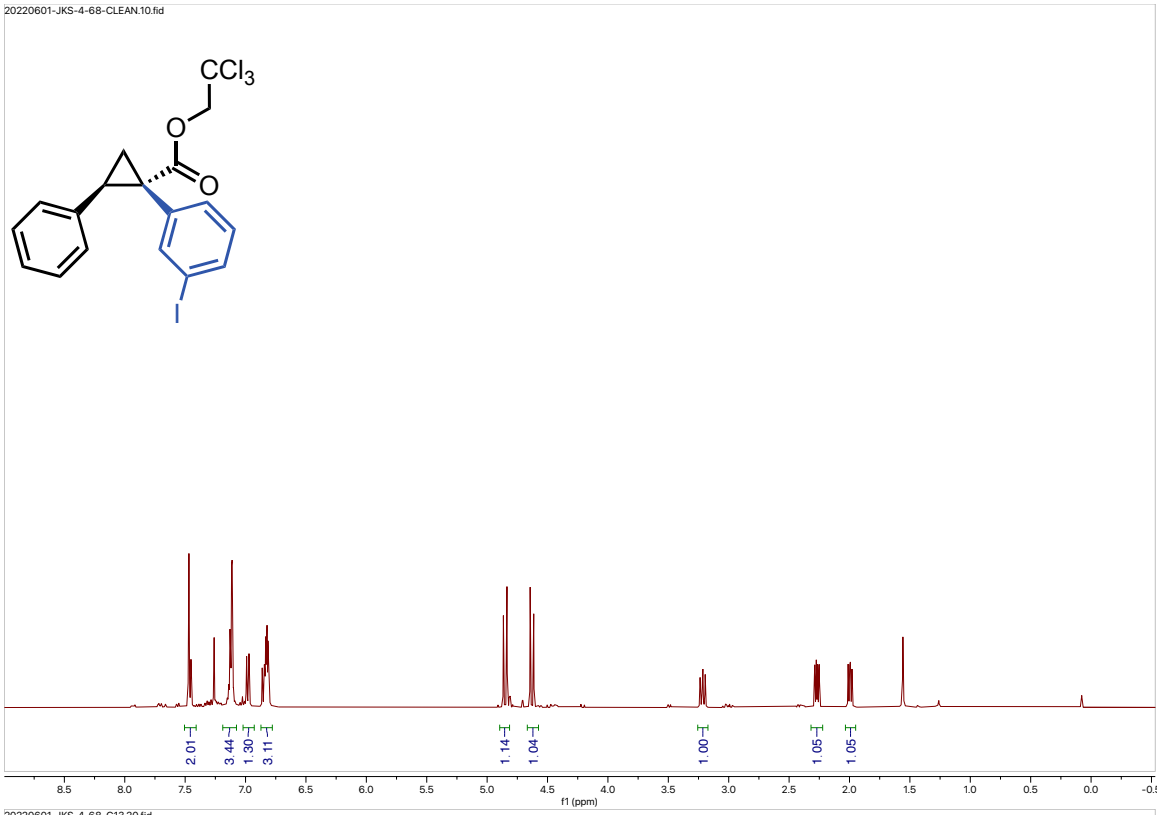
20220601-JKS-4-68-CLEAN.10.fid
CCl3
O
O
I
2.01
3.44
1.30
3.11
1.14
1.04
1.00
1.05
1.05
f1 (ppm)

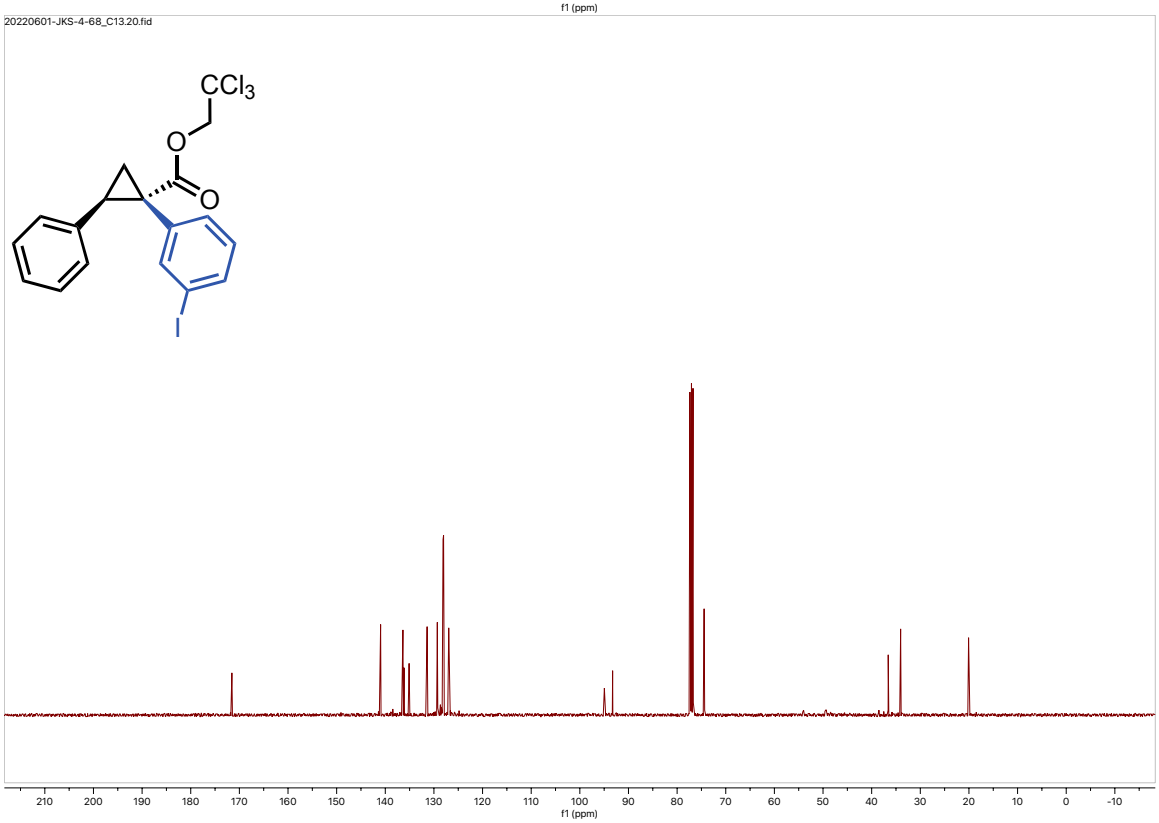
20220601-JKS-4-68_C13.20.fid
CCl3
O
O
I
f1 (ppm)

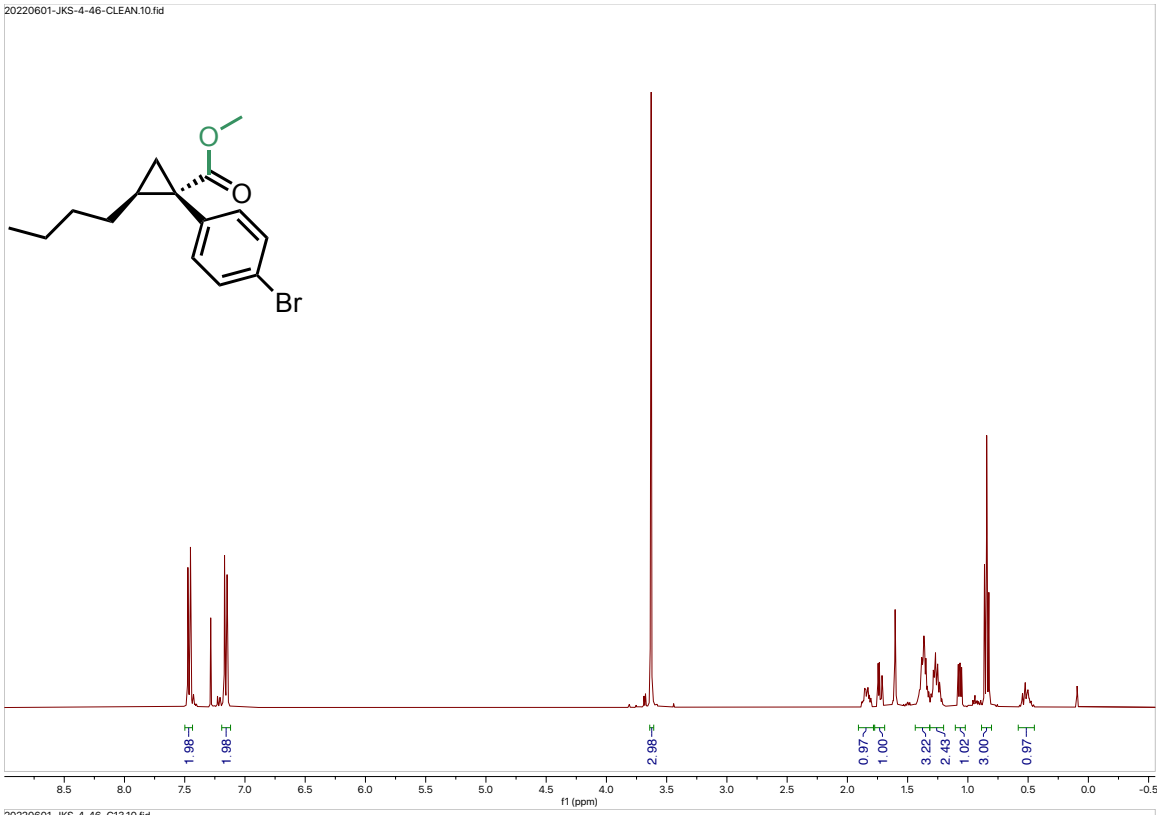
20220601-JKS-4-46-CLEAN.10.fid
O
O
Br
1.98
1.98
2.98
0.97
1.00
3.22
2.43
1.02
3.00
0.97
f1 (ppm)

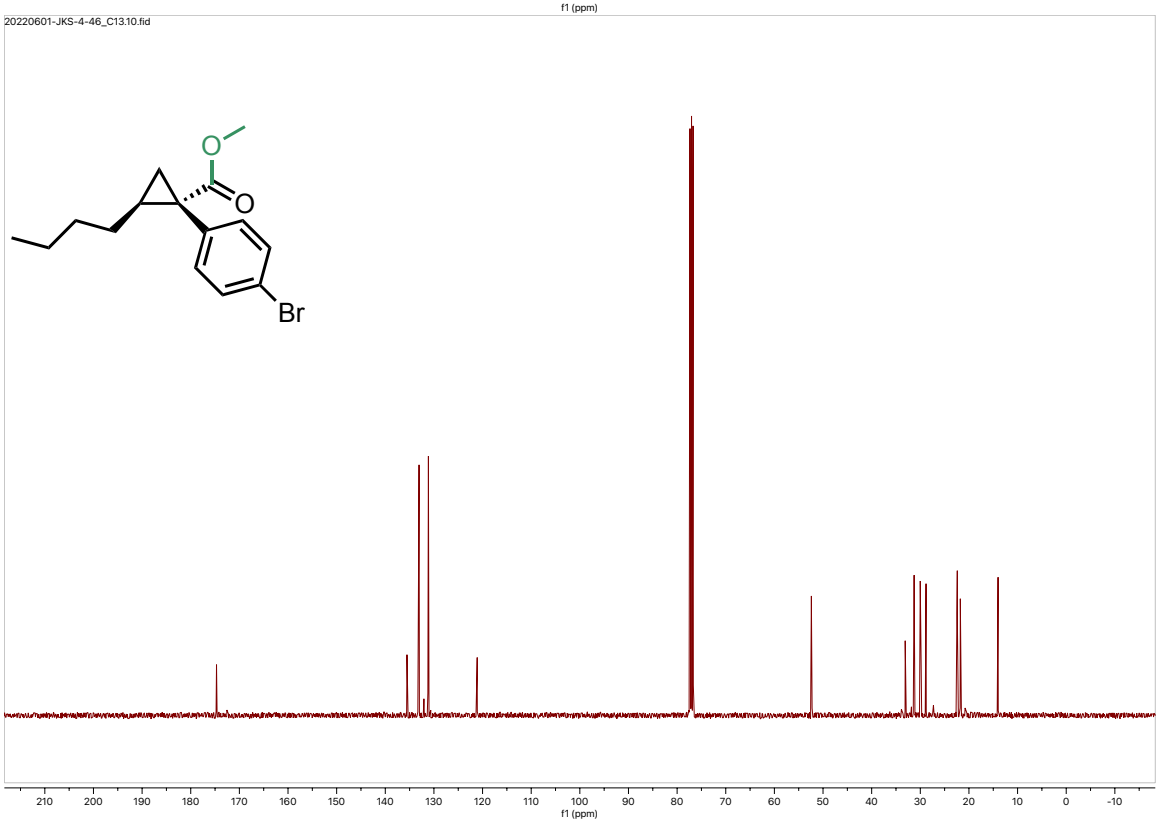
20220601-JKS-4-46_C13.10.fid
O
O
Br
f1 (ppm)

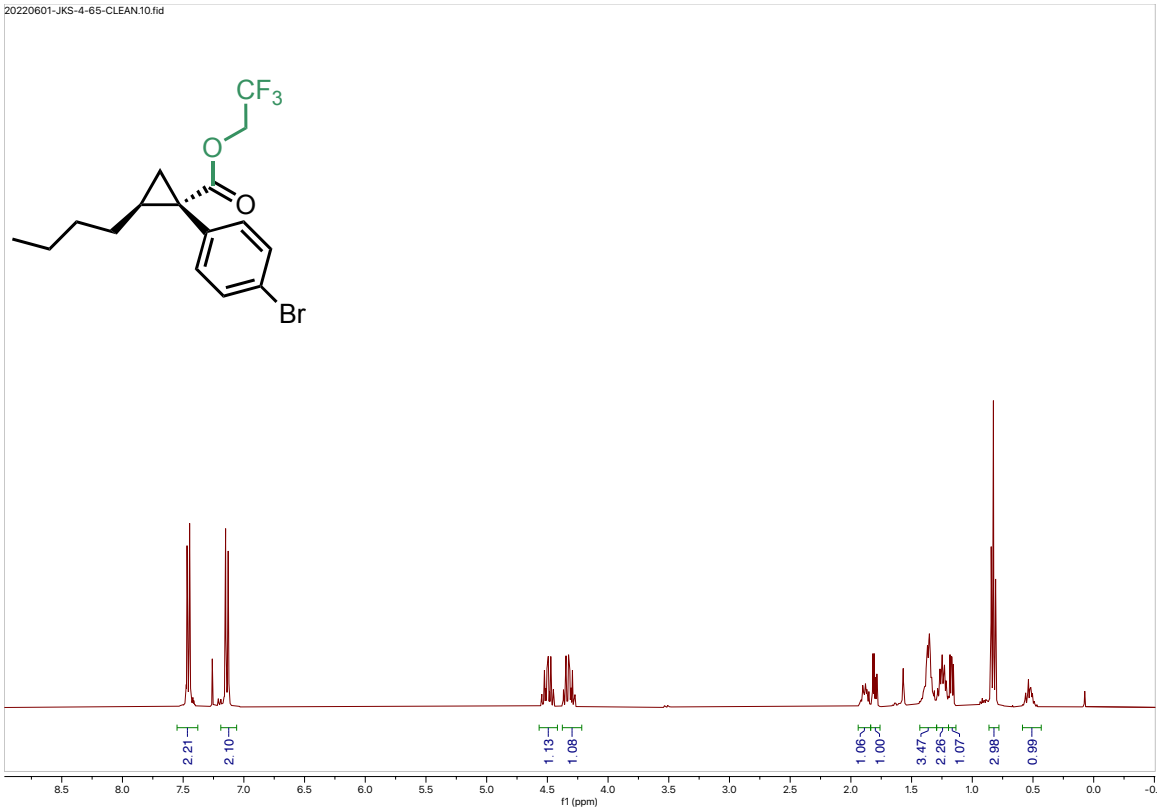
20220601-JKS-4-65-CLEAN.10.fid
CF3
O
O
Br
2.21
2.10
1.13
1.08
1.06
1.00
3.47
2.26
1.07
2.98
0.99
f1 (ppm)

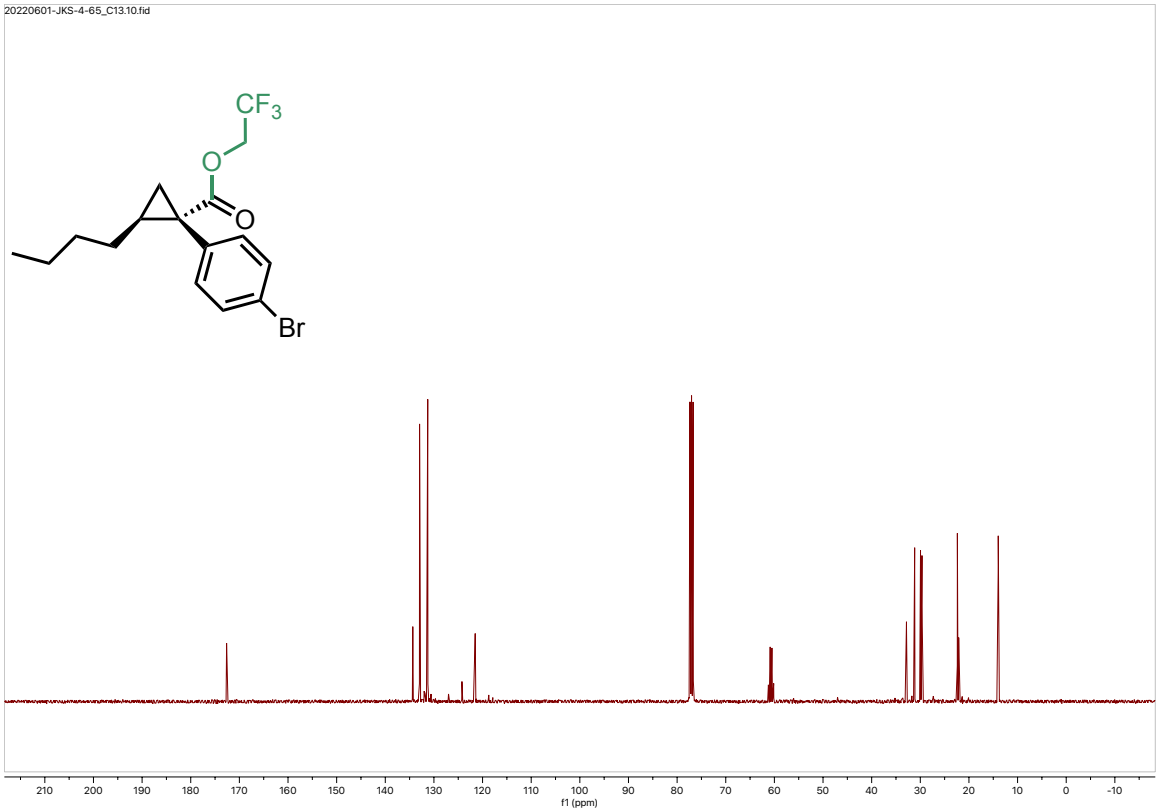
20220601-JKS-4-65_C13.10.fid
CF3
O
O
Br
f1 (ppm)

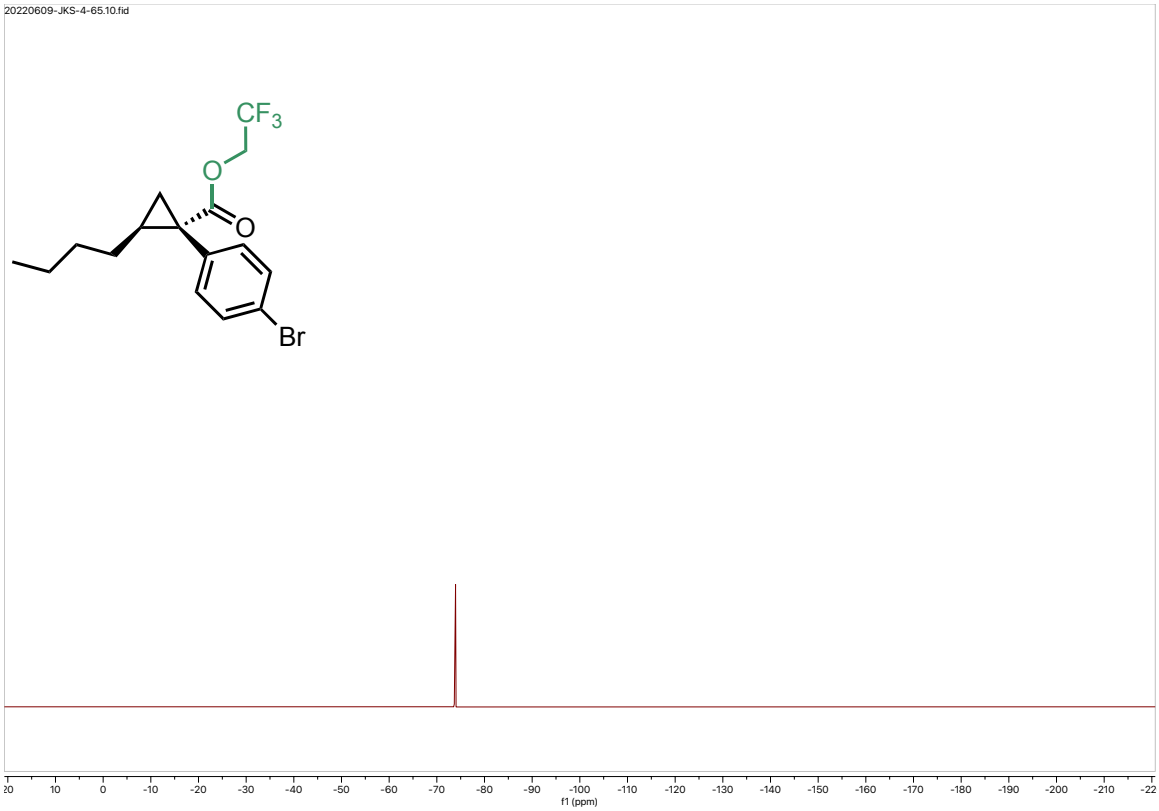
20220609-JKS-4-65.10.fid
CF3
O
O
Br
10
0
-10
-20
-30
-40
-50
-60
-70
-80
-90
-100
-110
-120
-130
-140
-150
-160
-170
-180
-190
-200
-210
f1 (ppm)

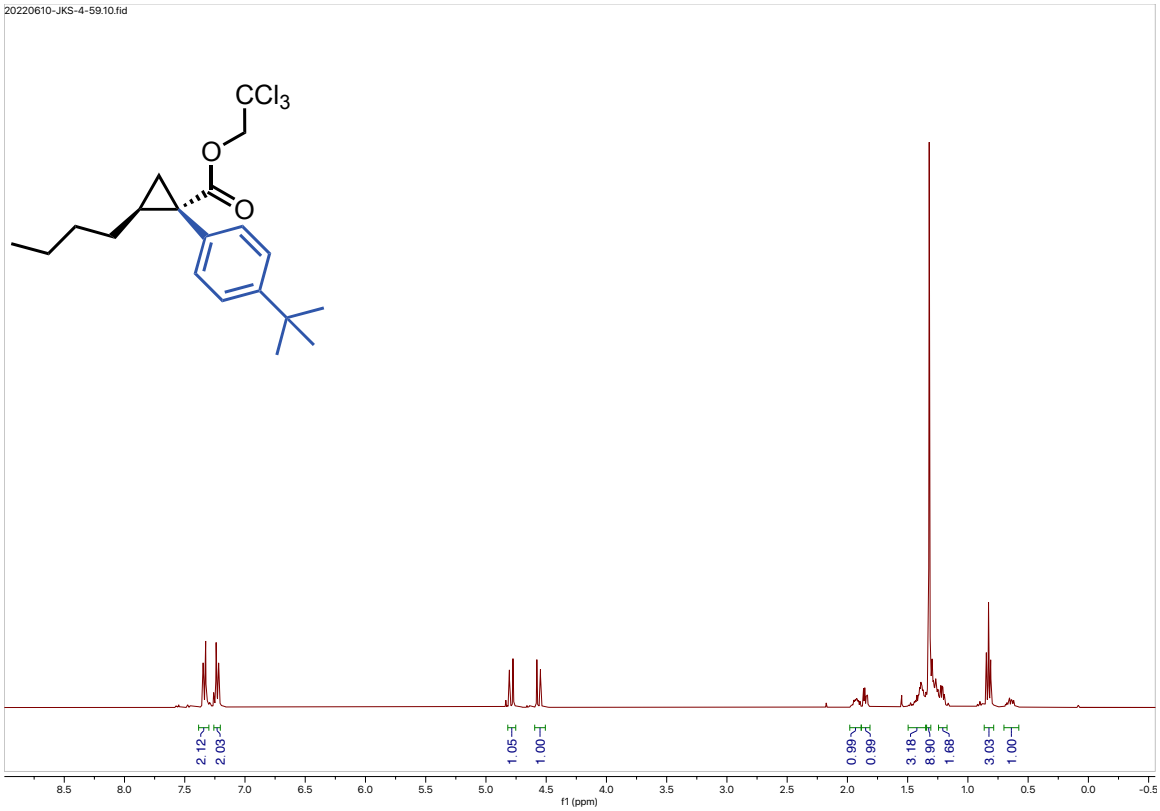
20220610-JKS-4-59.10.fid
CCl3
O
O
2.12
2.03
1.05
1.00
0.99
0.99
3.18
8.90
1.68
3.03
1.00
f1 (ppm)

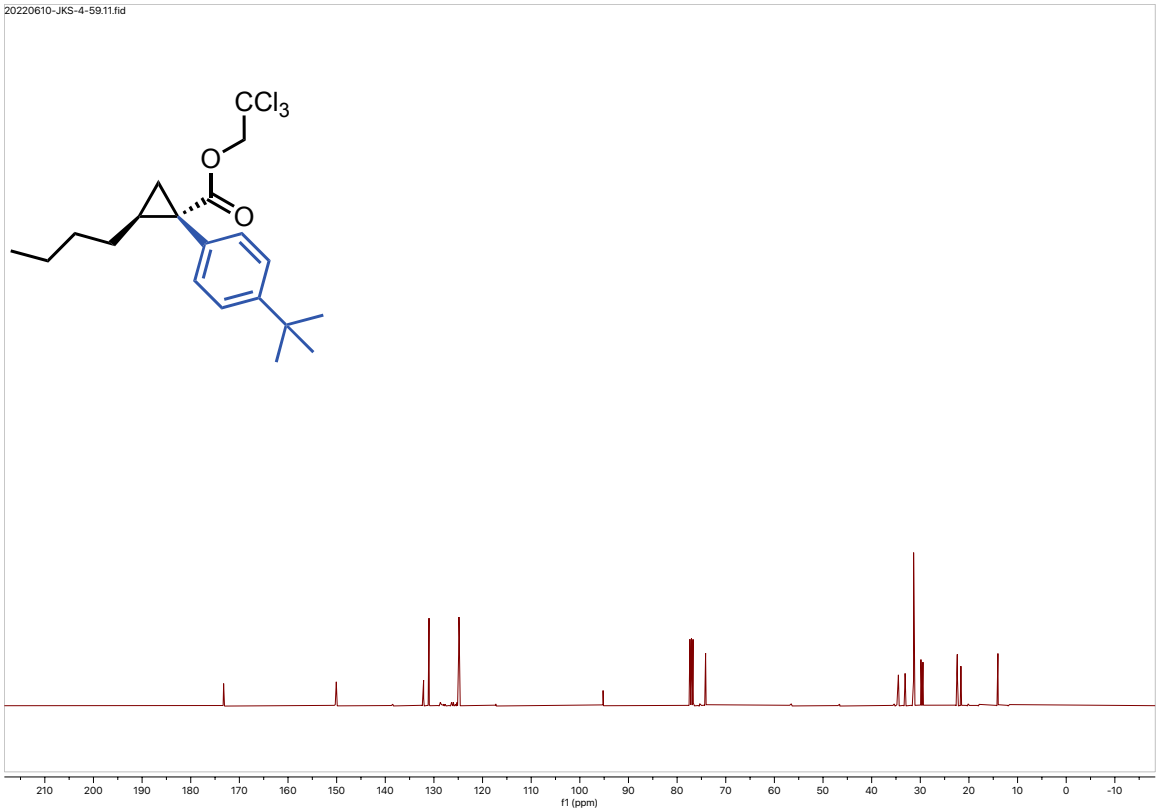
20220610-JKS-4-59.11.fid
CCl3
O
O
f1 (ppm)

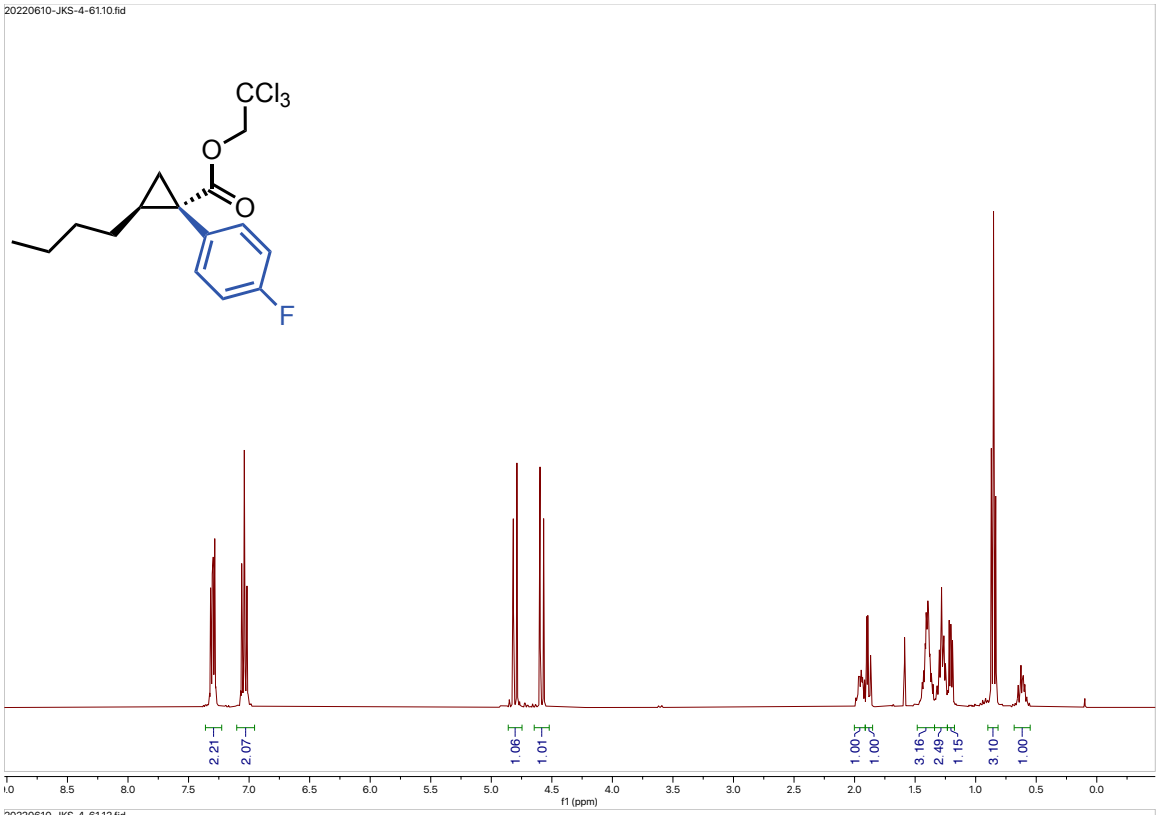
20220610-JKS-4-61.10.fid
CCl3
O
O
F
2.21
2.07
1.06
1.01
1.00
1.00
3.16
2.49
1.15
3.10
1.00
f1 (ppm)

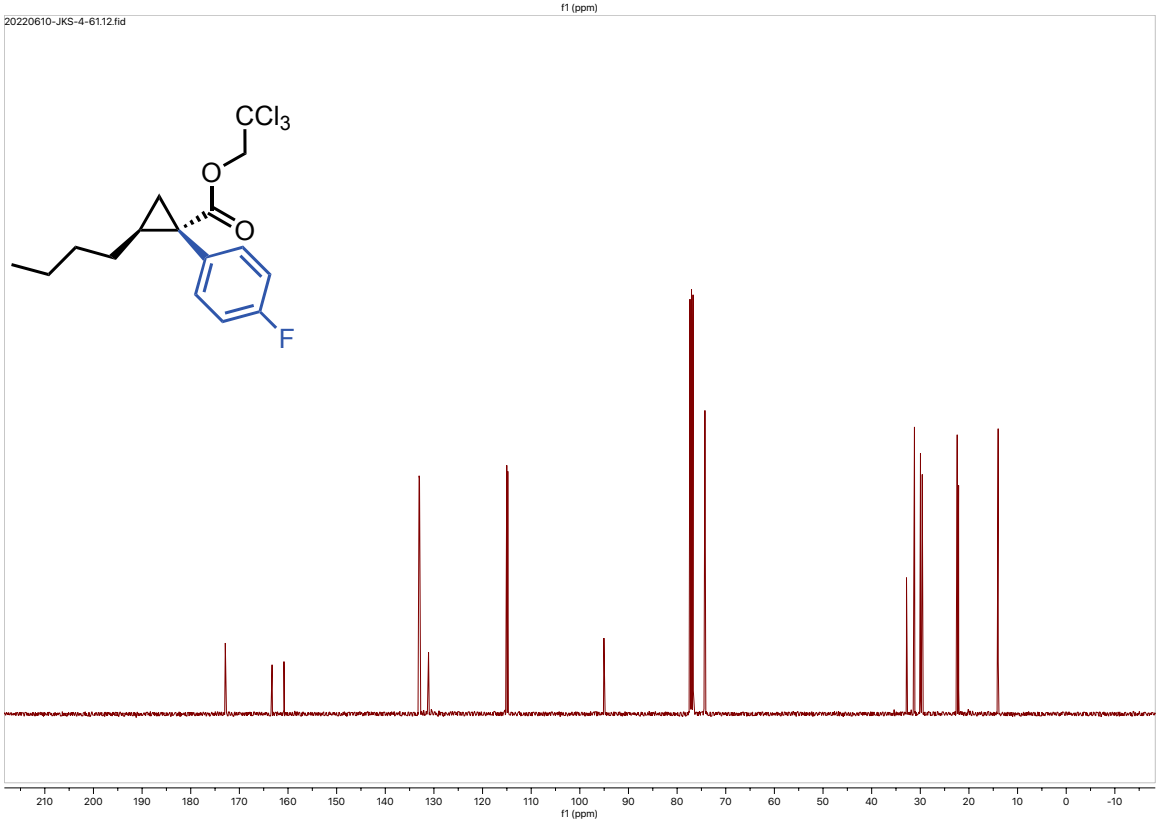
20220610-JKS-4-61.12.fid
CCl3
O
O
F
f1 (ppm)

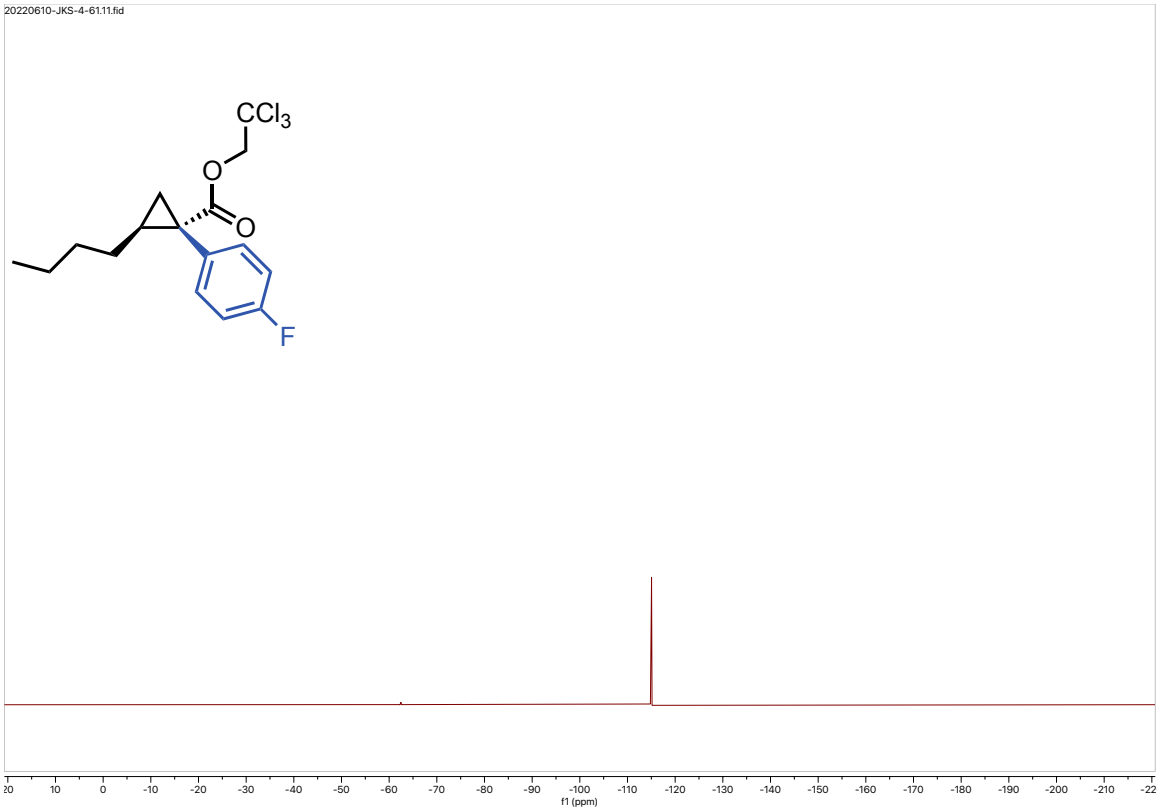
20220610-JKS-4-61.11.fid
CCl3
O
O
F
20
10
0
-10
-20
-30
-40
-50
-60
-70
-80
-90
-100
-110
-120
-130
-140
-150
-160
-170
-180
-190
-200
-210
-22
f1 (ppm)

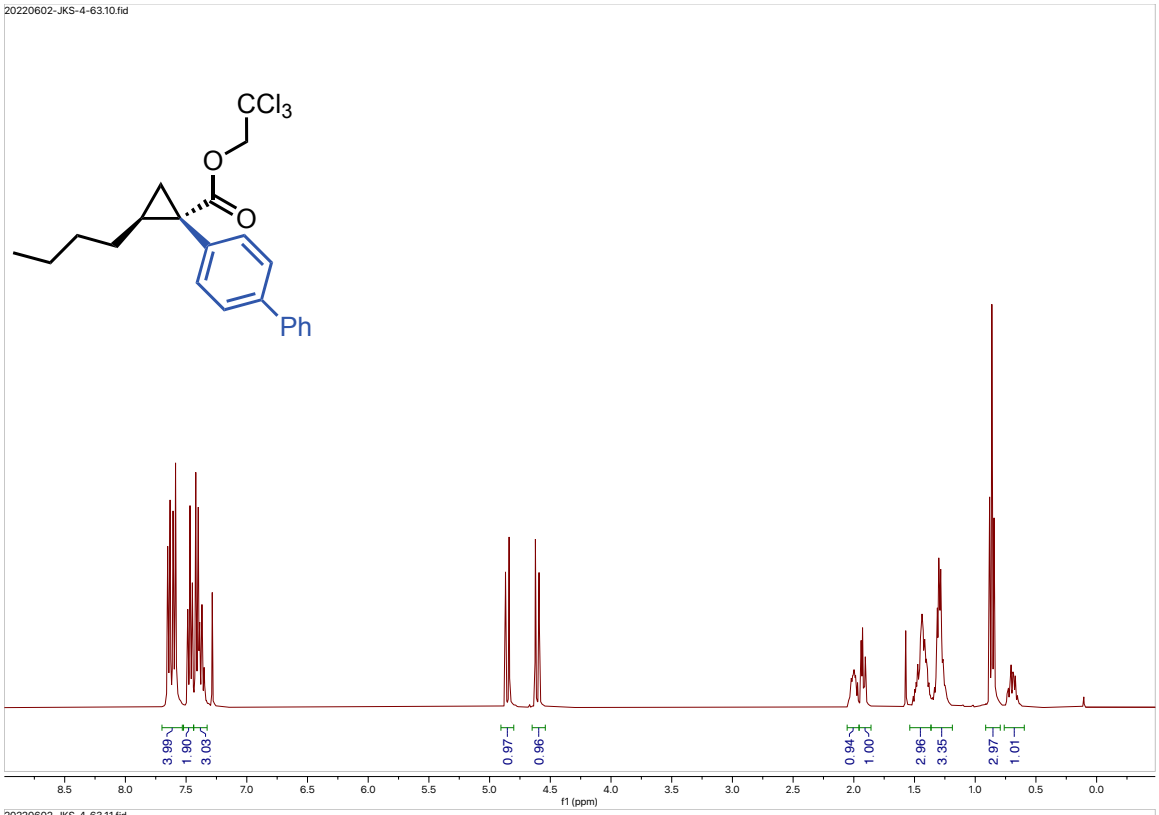
20220602-JKS-4-63.10.fid
CCl3
O
O
Ph
3.99
1.90
3.03
0.97
0.96
0.94
1.00
2.96
3.35
2.97
1.01
8.5
8.0
7.5
7.0
6.5
6.0
5.5
5.0
4.5
4.0
3.5
3.0
2.5
2.0
1.5
1.0
0.5
0.0
f1 (ppm)

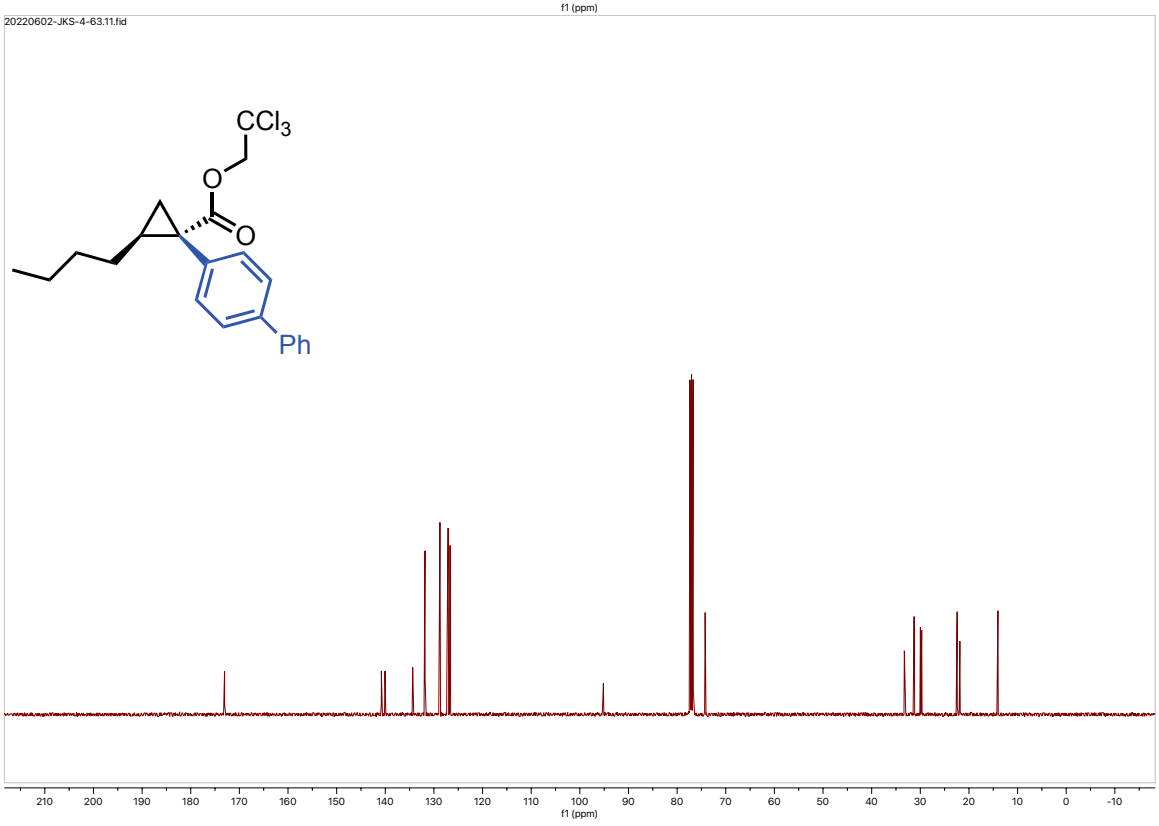
20220602-JKS-4-63.11.fid
CCl3
O
O
Ph
210
200
190
180
170
160
150
140
130
120
110
100
90
80
70
60
50
40
30
20
10
0
-10
f1 (ppm)

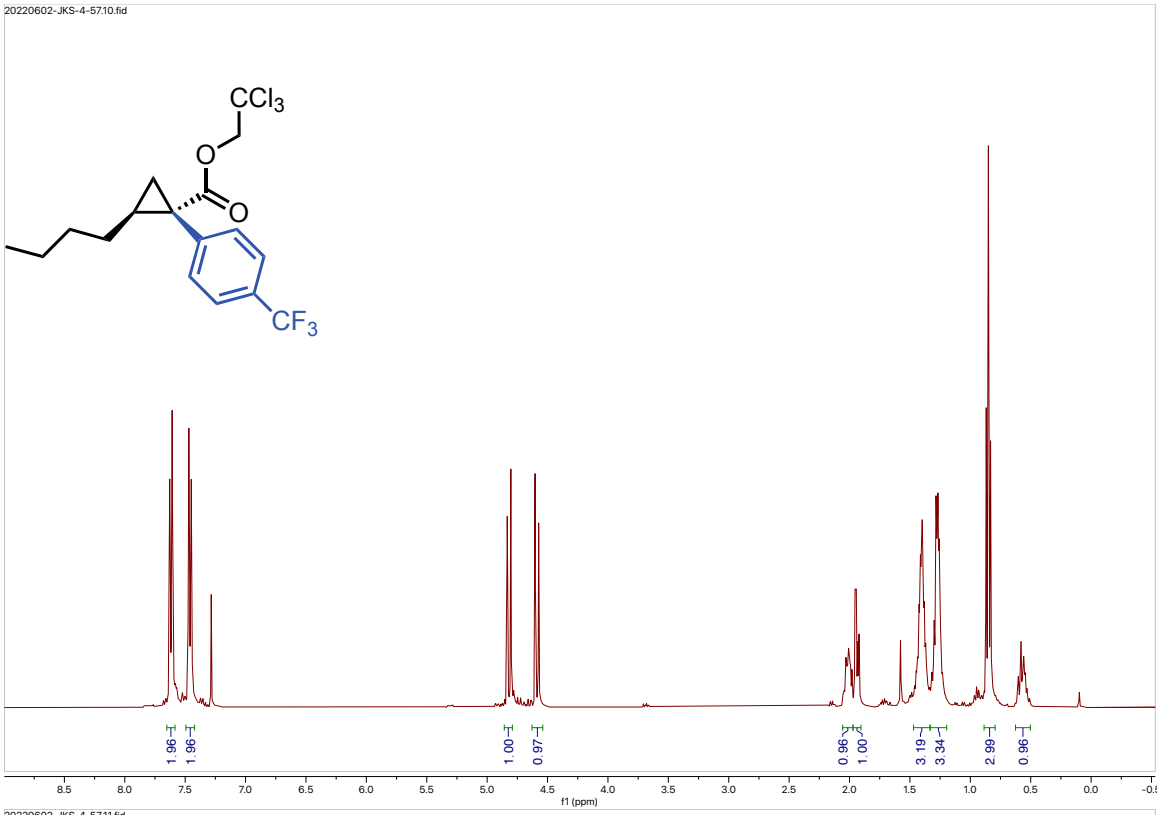
20220602-JKS-4-57.10.fid
CCl3
O
O
CF3
1.96
1.96
1.00
0.97
0.96
1.00
3.19
3.34
2.99
0.96
f1 (ppm)

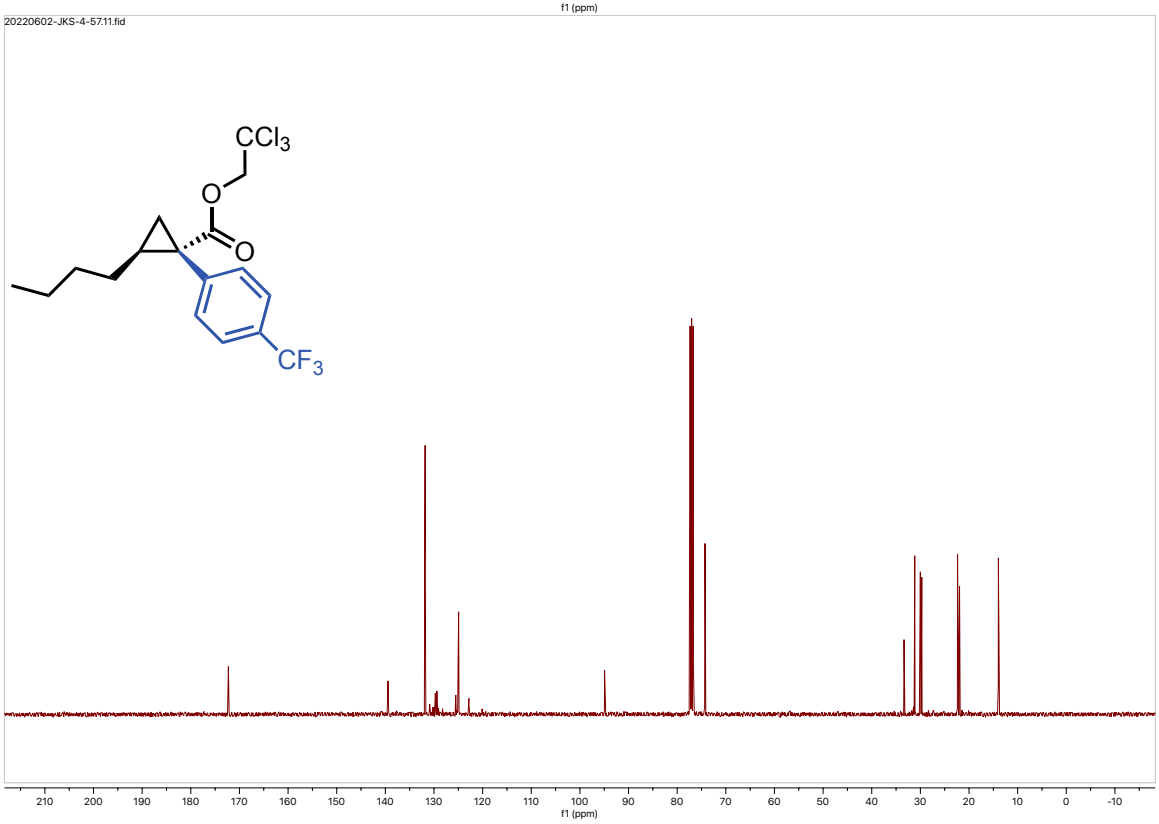
20220602-JKS-4-57.11.fid
CCl3
O
O
CF3
f1 (ppm)

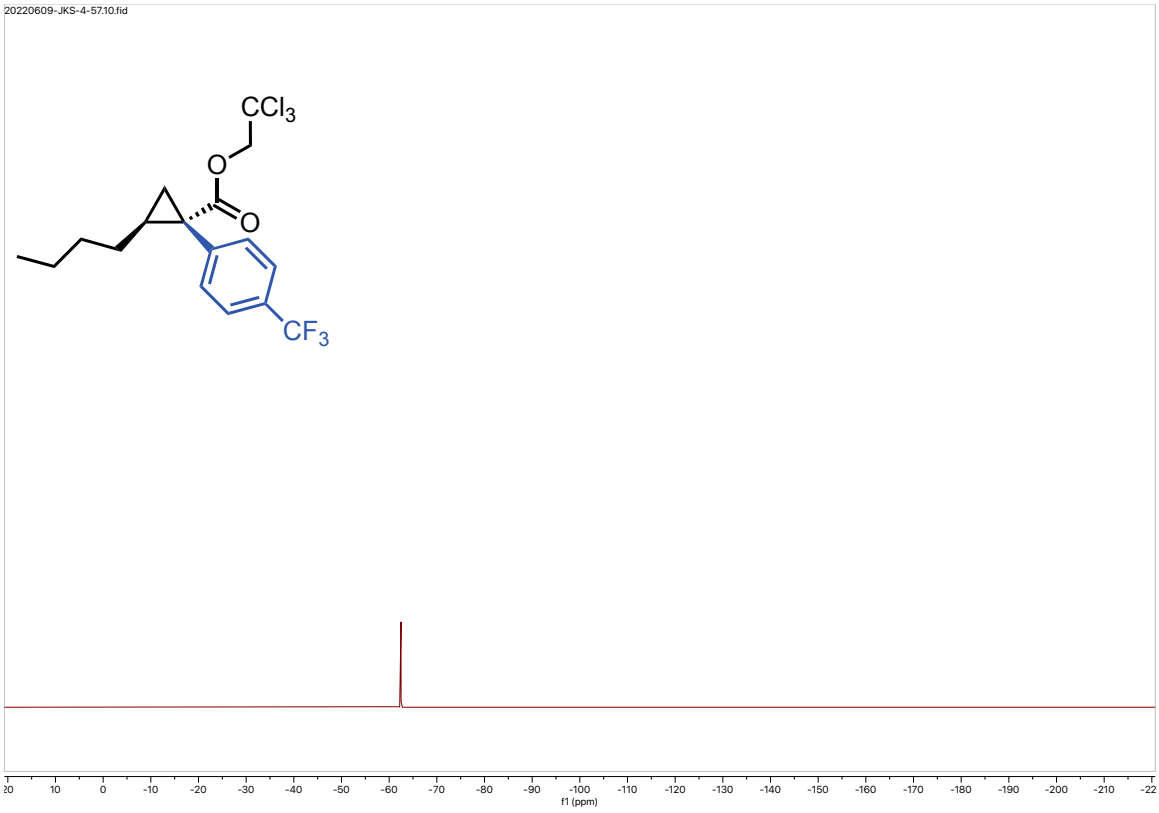
20220609-JKS-4-57.10.fid
CCl3
O
O
CF3
20
10
0
-10
-20
-30
-40
-50
-60
-70
-80
-90
-100
-110
-120
-130
-140
-150
-160
-170
-180
-190
-200
-210
-22
f1 (ppm)

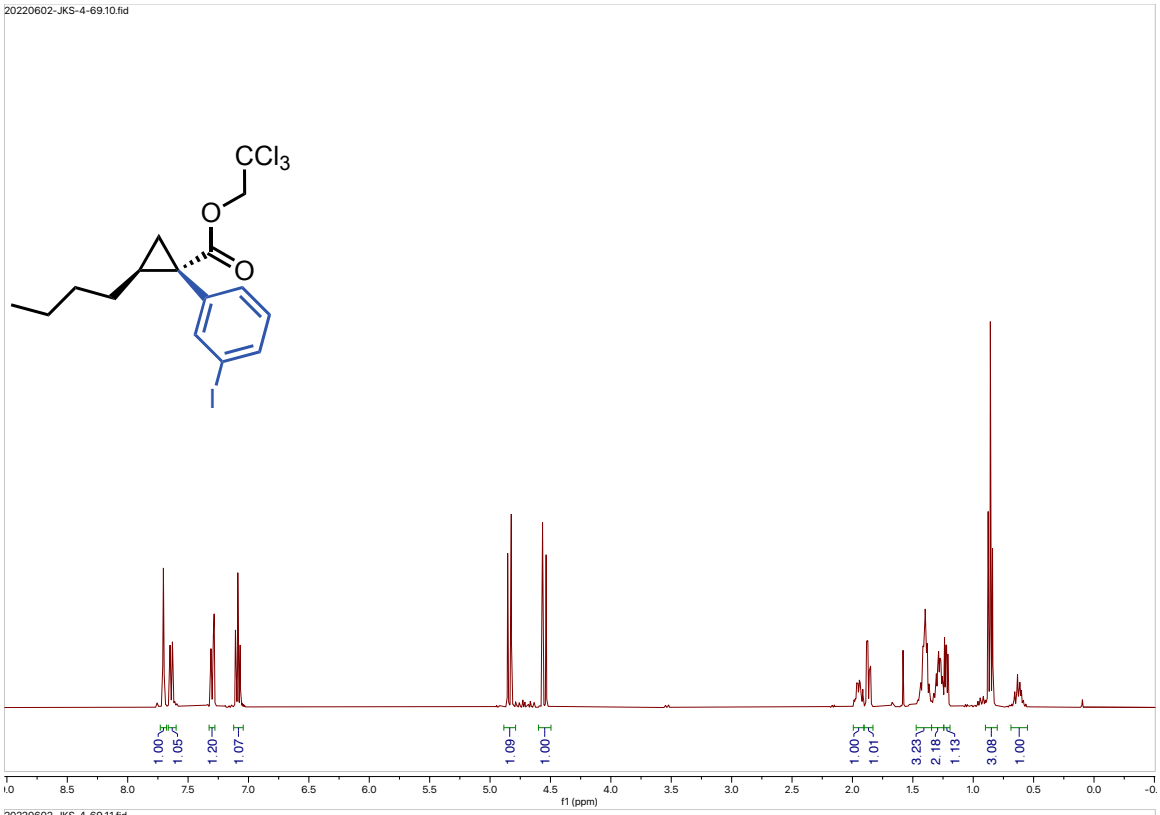
20220602-JKS-4-69.10.fid
CCl3
O
O
I
1.00
1.05
1.20
1.07
1.09
1.00
1.00
1.01
3.23
2.18
1.13
3.08
1.00
f1 (ppm)

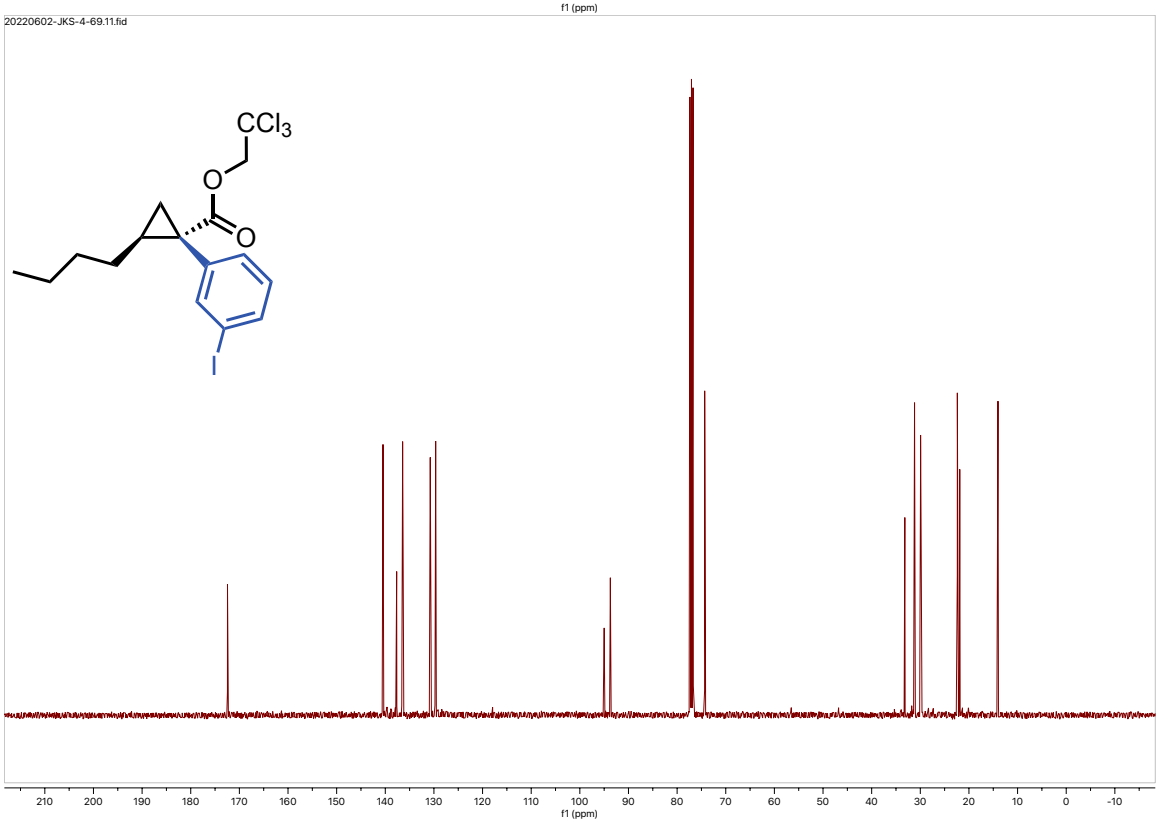
20220602-JKS-4-69.11.fid
CCl3
O
O
I
f1 (ppm)

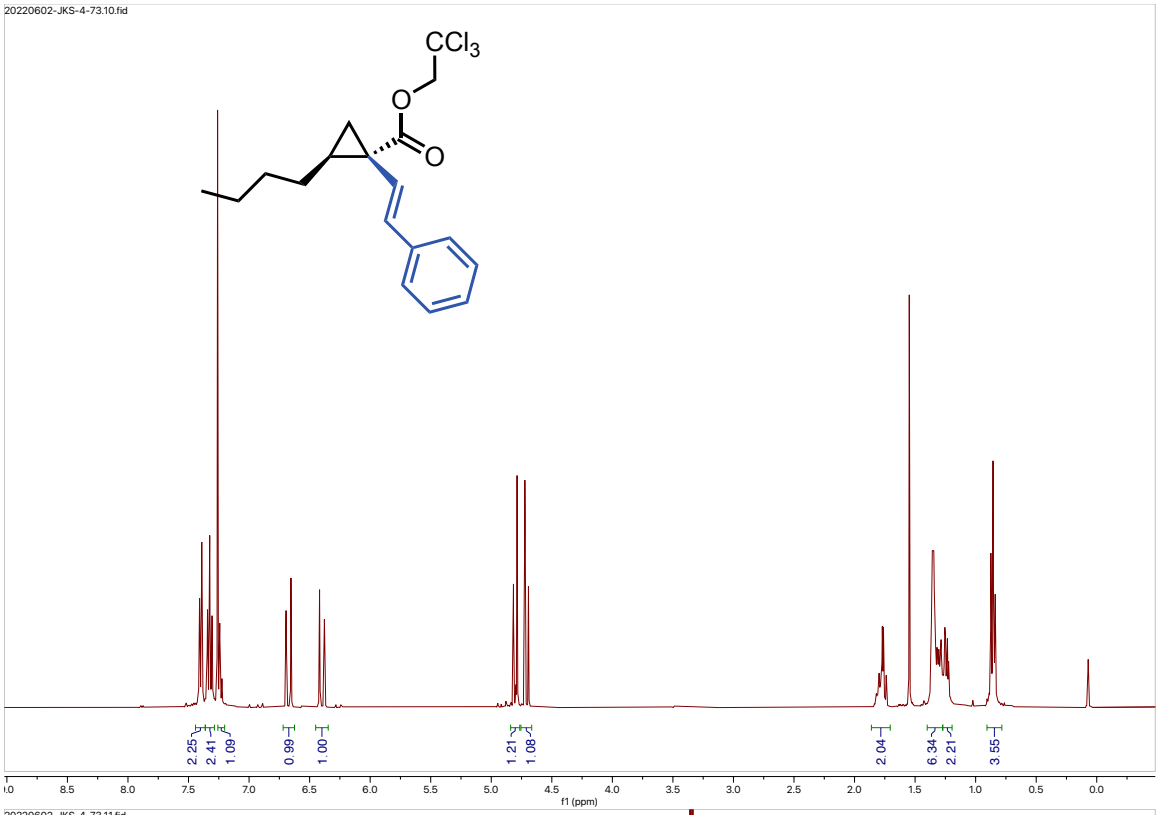
20220602-JKS-4-73.10.fid
CCl3
O
O
2.25
2.41
1.09
0.99
1.00
1.21
1.08
2.04
6.34
2.21
3.55
f1 (ppm)

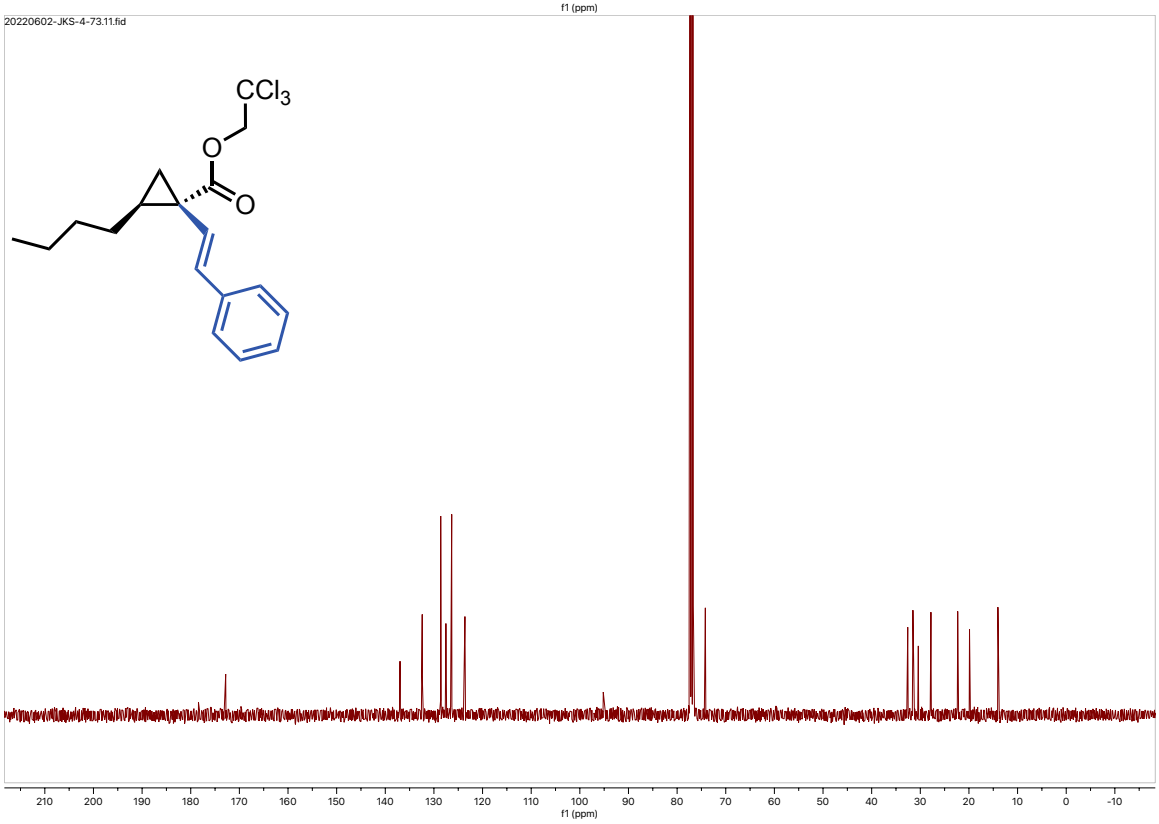
20220602-JKS-4-73.11.fid
CCl3
O
O
f1 (ppm)

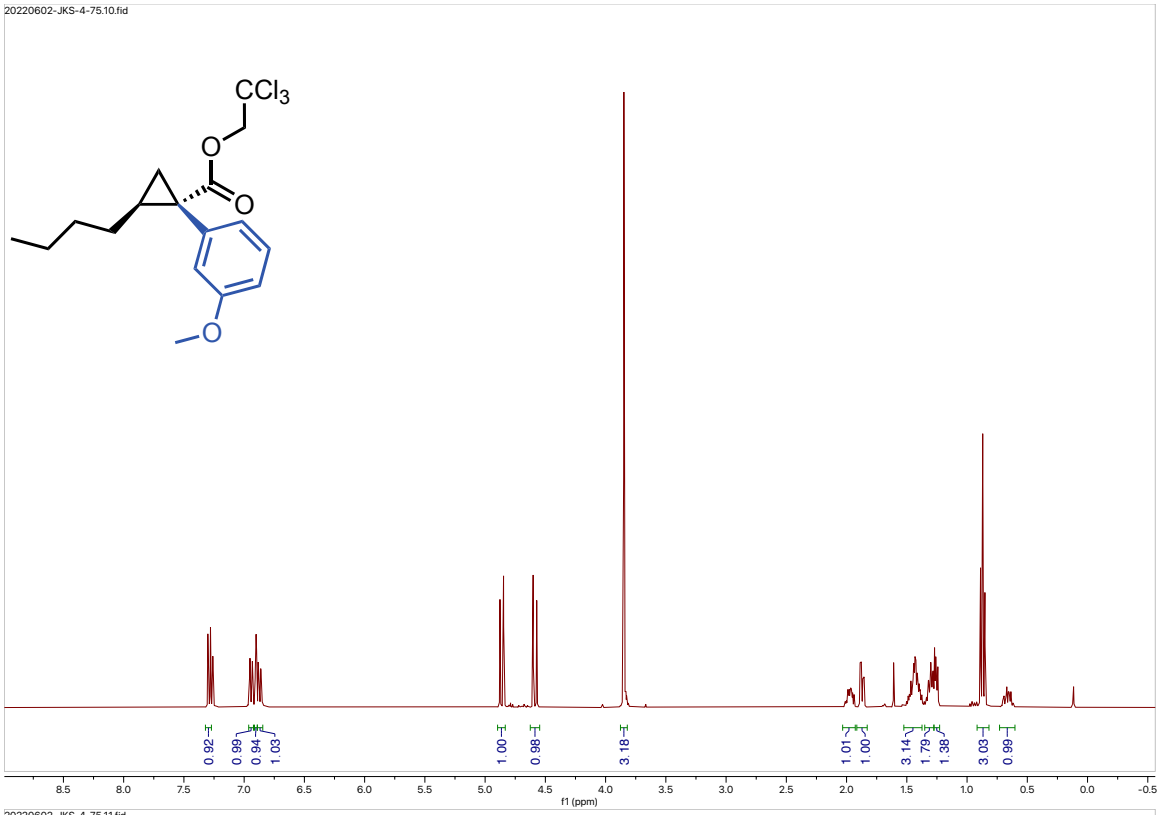
20220602-JKS-4-75.10.fid
CCl3
O
O
O
0.92
0.99
0.94
1.03
1.00
0.98
3.18
1.01
1.00
3.14
1.79
1.38
3.03
0.99
8.5 8.0 7.5 7.0 6.5 6.0 5.5 5.0 4.5 4.0 3.5 3.0 2.5 2.0 1.5 1.0 0.5 0.0 -0.5
f1 (ppm)

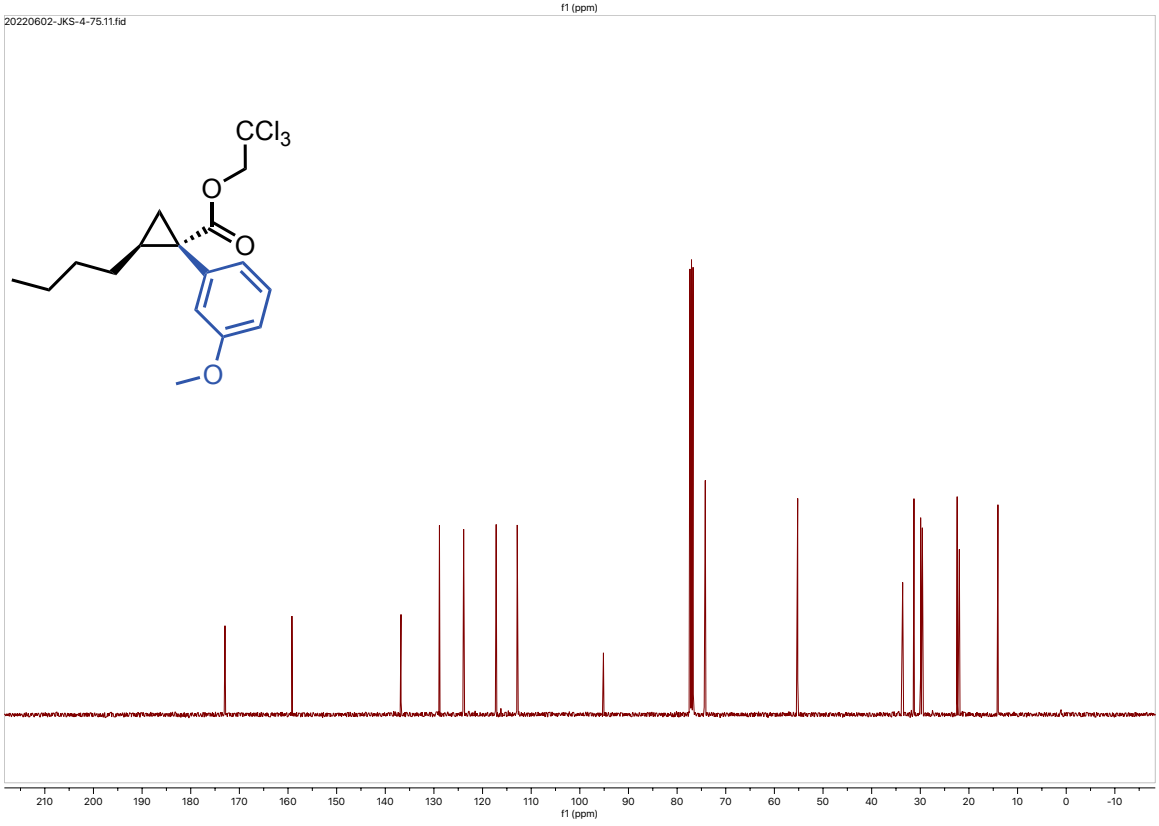
20220602-JKS-4-75.11.fid
CCl3
O
O
O
210 200 190 180 170 160 150 140 130 120 110 100 90 80 70 60 50 40 30 20 10 0 -10
f1 (ppm)

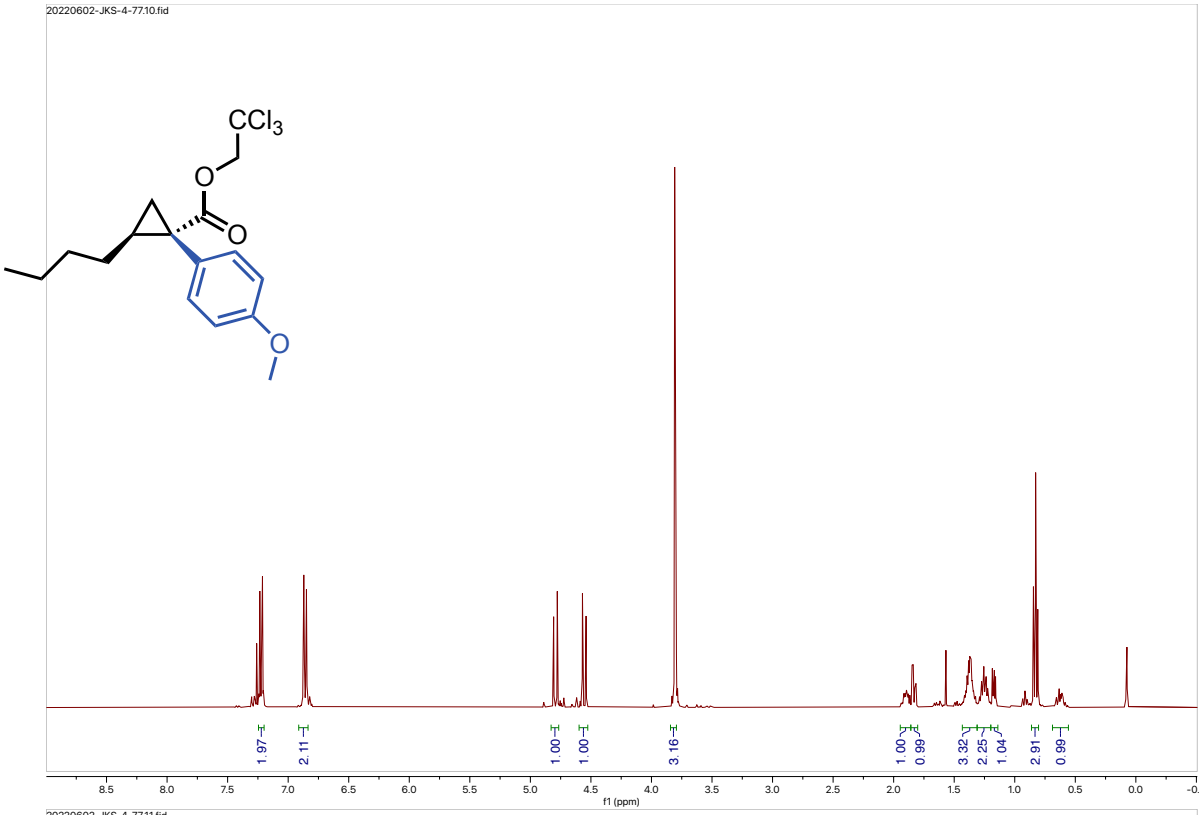
20220602-JKS-4-77.10.fid
CCl3
O
O
O
1.97
2.11
1.00
1.00
3.16
1.00
0.99
3.32
2.25
1.04
2.91
0.99
8.5 8.0 7.5 7.0 6.5 6.0 5.5 5.0 4.5 4.0 3.5 3.0 2.5 2.0 1.5 1.0 0.5 0.0
f1 (ppm)

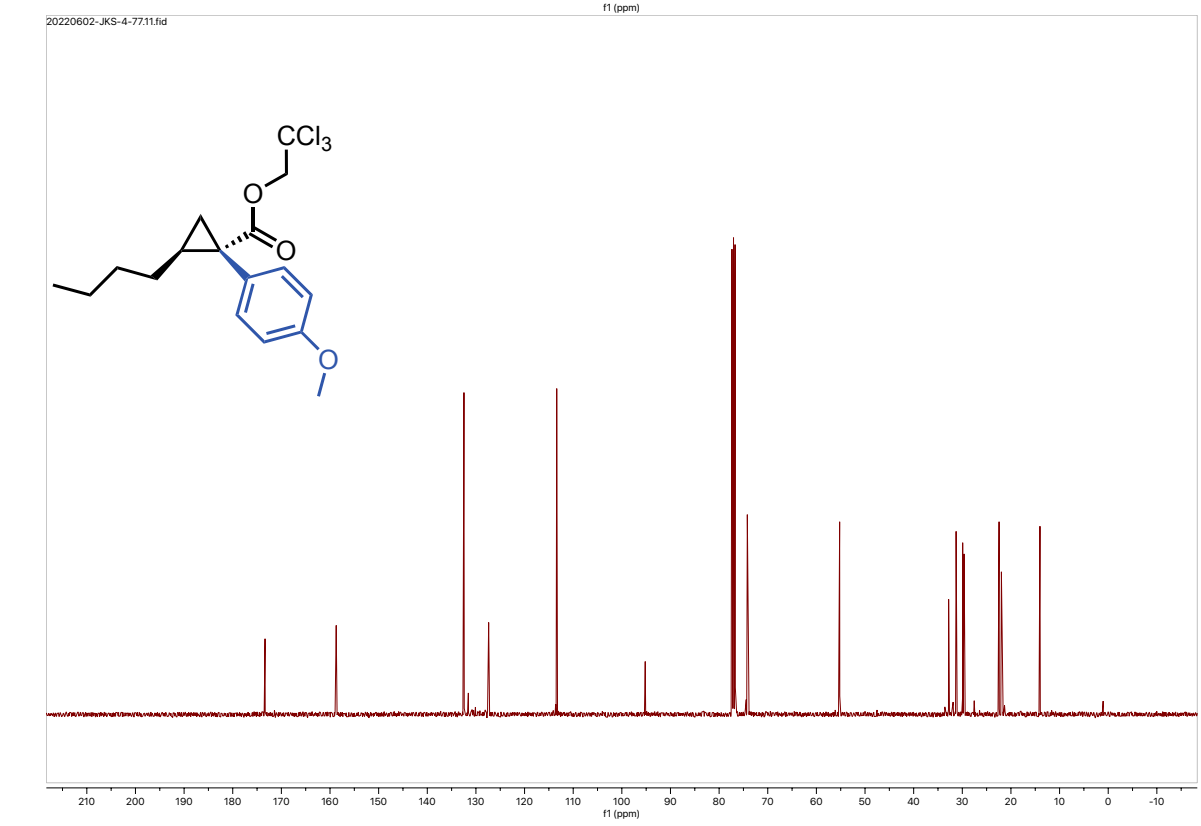
20220602-JKS-4-77.11.fid
CCl3
O
O
O
210 200 190 180 170 160 150 140 130 120 110 100 90 80 70 60 50 40 30 20 10 0 -10
f1 (ppm)

Computational Details

All calculations were carried out by utilizing the Gaussian-16 quantum chemistry software package.[14] Geometries, frequencies, and thermodynamic parameters of these species were calculated at the B3LYP density functional,[15-17] in conjunction with Grimme's empirical dispersion-correction (D3)[18], and Becke and Becke-Johnson (BJ) damping-corrections,[19-21] In these calculations we utilized the 6-31G(d,p) basis sets for all atoms, except of transition metals (Cu, Co, Rh and Ru) and bromine. For later atoms we use LANL2DZ basis sets and associated effective core potentials (ECP).[22, 23] Bulk solvent effects were incorporated into all calculations (including geometry optimizations and frequency calculations) using the self-consistent reaction field polarizable continuum model (IEF-PCM).[24, 25] We chose dichloromethane as solvent. Below, we labeled this approximation as a [B3LYP-D3(BJ)]+PCM/[6-31G(d,p) + Lanl2dz] approximation. The reported thermodynamic data were computed at a temperature of 298.15K and at 1atm of pressure. Unless otherwise stated, energies are given as ΔH/ΔG in kcal/mol.

To validate the [B3LYP-D3(BJ)]+PCM/[6-31G(d,p) + Lanl2dz] calculated energetics of the reported structures we have also re-calculated their energetics at the [wB97xd[26] + PCM]/[6-311+G(d,p)] + SDD[27] (for Cu, Co, Rh, Ru, and Br) level of theory by utilizing their [B3LYP-D3(BJ)]+PCM/[6-31G(d,p) + Lanl2dz] optimized geometries. The calculated energetics of these structures at the [B3LYP-D3(BJ)]+PCM/[6-31G(d,p) + Lanl2dz] and [wB97xd + PCM]/[6-311+G(d,p)] + SDD levels of theory are given in Table 1S. As seen from this Table, both the [B3LYP-D3(BJ)]+PCM/[6-31G(d,p) + Lanl2dz] and [B3LYP-D3(BJ)]+PCM/[6-31G(d,p) + Lanl2dz] and [wB97xd + PCM]/[6-311+G(d,p)] + SDD calculated energies lead to the same conclusions, while the calculated values of each structure at these two levels of theory differ by a few kcal/mol. Since, we have complete sets of the [B3LYP-D3(BJ)]+PCM/[6-31G(d,p) + Lanl2dz] calculated energies and geometries, for sake of simplicity, in this paper we discuss only the [B3LYP-D3(BJ)]+PCM/[6-31G(d,p) + Lanl2dz] calculated data.

Table 1S. The Gibbs free energies (in kcal/mol) of various reported reactions calculated at the [B3LYP-D3(BJ)]+PCM/[6-31G(d,p) + Lanl2dz] and [wB97xd + PCM]/[6-311+G(d,p)] + SDD levels of theory. The [wB97xd + PCM]/[6-311+G(d,p)] + SDD reported energies include the Gibbs free corrections from the [B3LYP-D3(BJ)]+PCM/[6-31G(d,p) + Lanl2dz} level calculations.

Reaction	B3LYP-D3(BJ)	wB97XD
Diazo + $Co_2(OAc)_4$ → (Carbene)–$Co_2(OAc)_4$ + N_2		
(Diazo)–$Co_2(OAc)_4$	-4.8	-0.7
TS(N_2-ext.)	19.1	20.9
(Carbene)–$Co_2(OAc)_4$ + N_2	4.5	7.3
Diazo + $[Ru_2(OAc)_4]^+$ → (Carbene)–$[Ru_2(OAc)_4]^+$ + N_2		
(Diazo)–$[Ru_2(OAc)_4]^+$	3.0	3.0

TS(N_2-ext)	12.0	10.1
(Carbene)–[$Ru_2(OAc)_4]^+$ + N_2	-15.3	-21.5

Diazo + Cl[$Ru_2(OAc)_4$] → (Carbene)–Cl[$Ru_2(OAc)_4$] + N_2

(Diazo)–$Ru_2(OAc)_4Cl$	-5.1	-13.8
TS(N_2-ext.)	19.4	7.9
(Carbene)–[$Ru_2(OAc)_4Cl$] + N_2	-5.9	-9.6

Cl[$Ru_2(OAc)_4$] → Cl^- + $[Ru_2(OAc)_4]^+$

-19.3 -20.3

Diazo + [$Rh_2(OAc)_4$] → (Carbene)–[$Rh_2(OAc)_4$] + N_2

(Diazo)–$Rh_2(OAc)_4$	-4.3	0.8
TS(N_2-ext)	7.2	11.4
(Carbene)–$Rh_2(OAc)_4$ + N_2	-15.3	-13.1

References:

1. Green, S. P.; Wheelhouse, K. M.; Payne, A. D.; Hallett, J. P.; Miller, P. W.; Bull, J. A., Thermal Stability and Explosive Hazard Assessment of Diazo Compounds and Diazo Transfer Reagents. *Org. Process Res. Dev.* **2020,** *24* (1), 67-84.
2. Guptill, D. M.; Davies, H. M. L., 2,2,2-Trichloroethyl Aryldiazoacetates as Robust Reagents for the Enantioselective C–H Functionalization of Methyl Ethers. *J. Am. Chem. Soc.* **2014,** *136* (51), 17718-17721.
3. Wei, B.; Sharland, J. C.; Lin, P.; Wilkerson-Hill, S. M.; Fullilove, F. A.; McKinnon, S.; Blackmond, D. G.; Davies, H. M. L., In Situ Kinetic Studies of Rh(II)-Catalyzed Asymmetric Cyclopropanation with Low Catalyst Loadings. *ACS Catal.* **2020,** *10* (2), 1161-1170.
4. Davies, H. M. L.; Venkataramani, C., Dirhodium Tetraprolinate-Catalyzed Asymmetric Cyclopropanations with High Turnover Numbers. *Org. Lett.* **2003,** *5* (9), 1403-1406.
5. Garlets, Z. J.; Hicks, E. F.; Fu, J.; Voight, E. A.; Davies, H. M. L., Regio- and Stereoselective Rhodium(II)-Catalyzed C–H Functionalization of Organosilanes by Donor/Acceptor Carbenes Derived from Aryldiazoacetates. *Org. Lett.* **2019,** *21* (12), 4910-4914.
6. Fu, J.; Ren, Z.; Bacsa, J.; Musaev, D. G.; Davies, H. M. L., Desymmetrization of cyclohexanes by site- and stereoselective C–H functionalization. *Nature* **2018,** *564* (7736), 395-399.
7. Tsutsui, H.; Abe, T.; Nakamura, S.; Anada, M.; Hashimoto, S., Practical Synthesis of Dirhodium(II) Tetrakis[N-phthaloyl-(S)-tert-leucinate]. *Chem. Pharm. Bull.* **2005,** *53* (10), 1366-1368.
8. Reddy, R. P.; Lee, G. H.; Davies, H. M. L., Dirhodium Tetracarboxylate Derived from Adamantylglycine as a Chiral Catalyst for Carbenoid Reactions. *Org. Lett.* **2006,** *8* (16), 3437-3440.
9. Hoshino, Y.; Yamamoto, H., Novel α-Amino Acid-Based Hydroxamic Acid Ligands for Vanadium-Catalyzed Asymmetric Epoxidation of Allylic Alcohols. *J. Am. Chem. Soc.* **2000,** *122* (42), 10452-10453.
10. Miyazawa, T.; Suzuki, T.; Kumagai, Y.; Takizawa, K.; Kikuchi, T.; Kato, S.; Onoda, A.; Hayashi, T.; Kamei, Y.; Kamiyama, F.; Anada, M.; Kojima, M.; Yoshino, T.; Matsunaga, S., Chiral paddle-wheel diruthenium complexes for asymmetric catalysis. *Nat. Catal.* **2020,** *3* (10), 851-858.
11. Wei, B.; Hatridge, T. A.; Jones, C. W.; Davies, H. M. L., Copper(II) Acetate-Induced Oxidation of Hydrazones to Diazo Compounds under Flow Conditions Followed by Dirhodium-Catalyzed Enantioselective Cyclopropanation Reactions. *Org. Lett.* **2021,** *23* (14), 5363-5367.
12. Sharland, J. C.; Dunstan, D.; Majumdar, D.; Gao, J.; Tan, K.; Malik, H. A.; Davies, H. M. L., Hexafluoroisopropanol for the Selective Deactivation of Poisonous Nucleophiles Enabling Catalytic Asymmetric Cyclopropanation of Complex Molecules. *ACS Catal.* **2022,** *12* (20), 12530-12542.
13. Singha, S.; Buchsteiner, M.; Bistoni, G.; Goddard, R.; Fürstner, A., A New Ligand Design Based on London Dispersion Empowers Chiral Bismuth–Rhodium Paddlewheel Catalysts. *J. Am. Chem. Soc.* **2021,** *143* (15), 5666-5673.

14. Frisch, M. J.; Trucks, G. W.; Schlegel, H. B.; Scuseria, G. E.; Robb, M. A.; Cheeseman, J. R.; Scalmani, G.; Barone, V.; Petersson, G. A.; Nakatsuji, H.; Li, X.; Caricato, M.; Marenich, A. V.; Bloino, J.; Janesko, B. G.; Gomperts, R.; Mennucci, B.; Hratchian, H. P.; Ortiz, J. V.; Izmaylov, A. F.; Sonnenberg, J. L.; Williams; Ding, F.; Lipparini, F.; Egidi, F.; Goings, J.; Peng, B.; Petrone, A.; Henderson, T.; Ranasinghe, D.; Zakrzewski, V. G.; Gao, J.; Rega, N.; Zheng, G.; Liang, W.; Hada, M.; Ehara, M.; Toyota, K.; Fukuda, R.; Hasegawa, J.; Ishida, M.; Nakajima, T.; Honda, Y.; Kitao, O.; Nakai, H.; Vreven, T.; Throssell, K.; Montgomery Jr., J. A.; Peralta, J. E.; Ogliaro, F.; Bearpark, M. J.; Heyd, J. J.; Brothers, E. N.; Kudin, K. N.; Staroverov, V. N.; Keith, T. A.; Kobayashi, R.; Normand, J.; Raghavachari, K.; Rendell, A. P.; Burant, J. C.; Iyengar, S. S.; Tomasi, J.; Cossi, M.; Millam, J. M.; Klene, M.; Adamo, C.; Cammi, R.; Ochterski, J. W.; Martin, R. L.; Morokuma, K.; Farkas, O.; Foresman, J. B.; Fox, D. J. *Gaussian 16 Rev. C.01*, Wallingford, CT, 2016.
15. Becke, A. D., Density-functional exchange-energy approximation with correct asymptotic behavior. *Physical Review A* **1988,** *38* (6), 3098-3100.
16. Lee, C.; Yang, W.; Parr, R. G., Development of the Colle-Salvetti correlation-energy formula into a functional of the electron density. *Physical Review B* **1988,** *37* (2), 785-789.
17. Becke, A. D., A new mixing of Hartree–Fock and local density-functional theories. *The Journal of Chemical Physics* **1993,** *98* (2), 1372-1377.
18. Grimme, S.; Antony, J.; Ehrlich, S.; Krieg, H., A consistent and accurate ab initio parametrization of density functional dispersion correction (DFT-D) for the 94 elements H-Pu. *J. Chem. Phys.* **2010,** *132* (15), 154104.
19. Becke, A. D.; Johnson, E. R., A density-functional model of the dispersion interaction. *J. Chem. Phys.* **2005,** *123* (15), 154101.
20. Becke, A. D.; Johnson, E. R., Exchange-hole dipole moment and the dispersion interaction: high-order dispersion coefficients. *J. Chem. Phys.* **2006,** *124* (1), 14104.
21. Johnson, E. R.; Becke, A. D., A post-Hartree-Fock model of intermolecular interactions: inclusion of higher-order corrections. *J. Chem. Phys.* **2006,** *124* (17), 174104.
22. Wadt, W. R.; Hay, P. J., Ab initio effective core potentials for molecular calculations. Potentials for main group elements Na to Bi. *The Journal of Chemical Physics* **1985,** *82* (1), 284-298.
23. Hay, P. J.; Wadt, W. R., Ab initio effective core potentials for molecular calculations. Potentials for K to Au including the outermost core orbitals. *The Journal of Chemical Physics* **1985,** *82* (1), 299-310.
24. Barone, V.; Cossi, M., Quantum Calculation of Molecular Energies and Energy Gradients in Solution by a Conductor Solvent Model. *The Journal of Physical Chemistry A* **1998,** *102* (11), 1995-2001.
25. Cossi, M.; Rega, N.; Scalmani, G.; Barone, V., Energies, structures, and electronic properties of molecules in solution with the C-PCM solvation model. *J. Comput. Chem.* **2003,** *24* (6), 669-681.
26. Chai, J.-D.; Head-Gordon, M., Long-range corrected hybrid density functionals with damped atom–atom dispersion corrections. *Physical Chemistry Chemical Physics* **2008,** *10* (44), 6615-6620.

27. Küchle, W.; Dolg, M.; Stoll, H.; Preuss, H., Energy-adjusted pseudopotentials for the actinides. Parameter sets and test calculations for thorium and thorium monoxide. *The Journal of Chemical Physics* **1994,** *100* (10), 7535-7542.

Appendix B. Chapter 3 Supporting Information

CAUTION: Diazo compounds are high energy compounds and need to be treated with respect. Even though we experienced no energetic decomposition in this work, care should be taken in handling large quantities of diazo compounds. Large scale reactions should be conducted behind a blast shield. For a more complete analysis of the risks associated with diazo compounds see the recent review by Bull et. al.[1]

General Considerations

All experiments were carried out in flame-dried glassware under argon atmosphere unless otherwise stated. Flash column chromatography was performed on silica gel. Unless otherwise noted, all other reagents were obtained from commercial sources (Sigma Aldrich, Fisher, TCI Chemicals, AK Scientific, Combi Blocks, Oakwood Chemicals, Ambeed) and used as received without purification. ^{1}H, ^{13}C, and ^{19}F NMR spectra were recorded at either 400 MHz (^{13}C at 100 MHz) on Bruker 400 spectrometer or 600 MHz (^{13}C at 151 MHz) on INOVA 600 or Bruker 600 spectrometer. NMR spectra were run in solutions of deuterated chloroform ($CDCl_3$) with residual chloroform taken as an internal standard (7.26 ppm for ^{1}H, and 77.16 ppm for ^{13}C), and were reported in parts per million (ppm). The abbreviations for multiplicity are as follows: s = singlet, d = doublet, t = triplet, q = quartet, p = pentet, m = multiplet, dd = doublet of doublet, etc. Coupling constants (J values) are obtained from the spectra. Thin layer chromatography was performed on aluminum-back silica gel plates with UV light and cerium aluminum molybdate (CAM) stain to visualize. Mass spectra were taken on a Thermo Finnigan LTQ-FTMS spectrometer with APCI or ESI. Enantiomeric excess (% ee) data were obtained on an Agilent 1100 HPLC or an Agilent 1290 Infinity UHPLC, eluting the purified products using a mixed solution of HPLC-grade 2-propanol (i-PrOH) and n-hexane. Waters SFC eluting with supercritical CO_2 and a 1:1 mixtures of HPLC grade methanol:isopropanol with 0.2% formic acid.

Preparation of Known Compounds

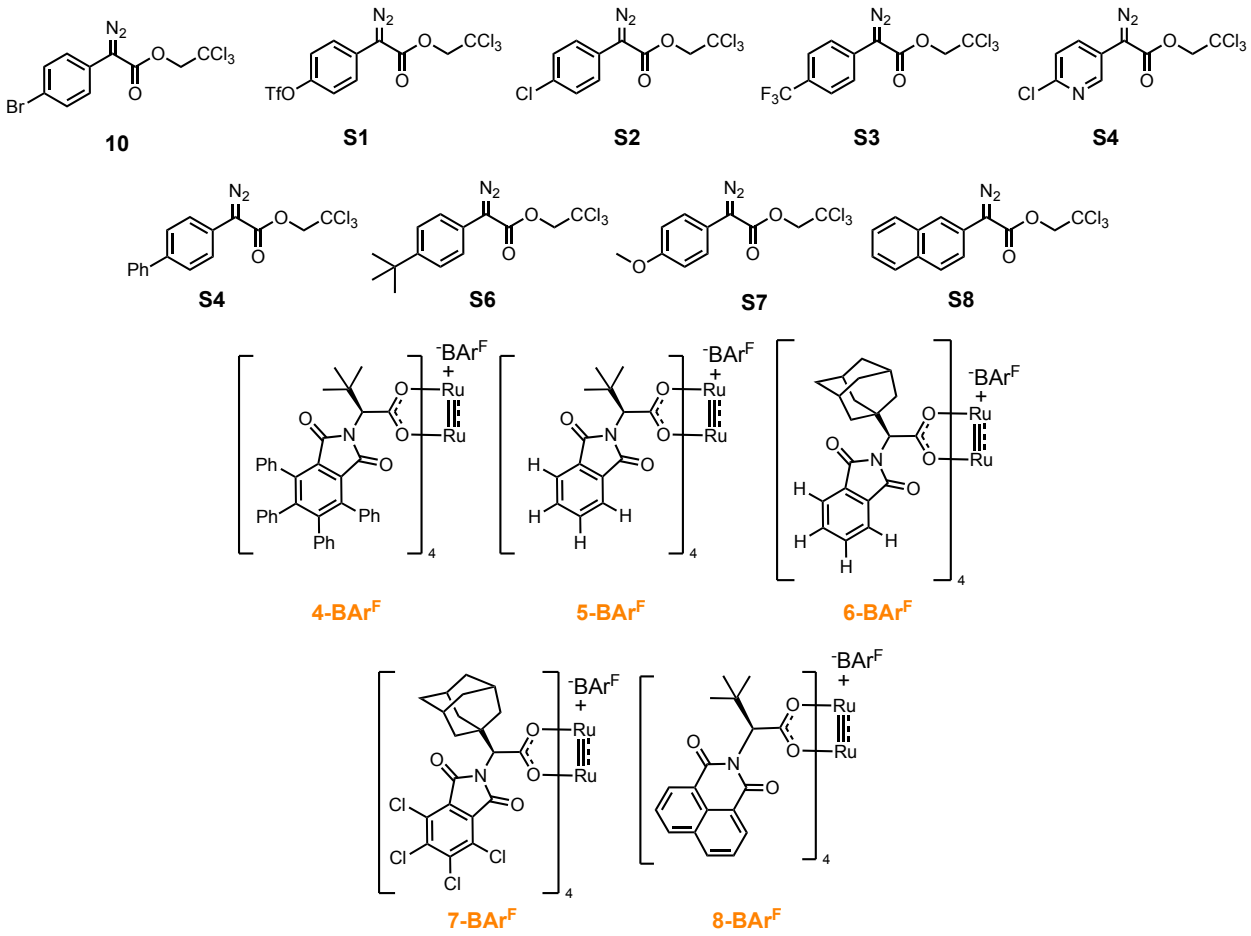

Figure S1: Known compounds synthesized.

Diazo Compounds **7** and **S1-S8** were prepared according to the established literature and matched the reported spectra.[2]

1-Ru-5-Ru were prepared according to the established literature and matched the reported spectra.[3]

Catalyst Synthesis

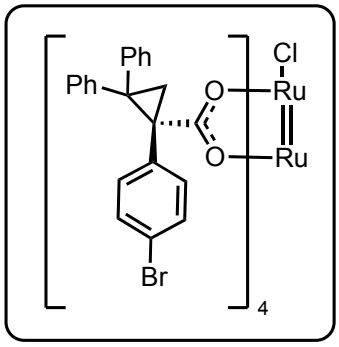

Ru_2(*S*-*p*Br-TPCP)$_4$Cl (3)

To a 25 mL RBF equipped with a stir bar was added 1-(4-bromophenyl)-2,2-diphenylcyclopropane-1-carboxylic acid (205 mg, 8 equiv, 521 μmol) and $Ru_2(OAc)_4Cl$ (50.0 mg, 1 equiv, 65.2 μmol). The solids were subsequently dissolved in *tert*-butylacetate (12.5 mL) and the RBF was fitted to a Soxlhet extractor fitted with K_2CO_3 and a small layer of sand. The reaction was heated to a vigorous reflux (~122 °C) and left for 18 h. After this time the reaction was cooled, and the crude material was concentrated and loaded onto silica. The material was purified using column chromatography (1% MeOH/DCM). The brown fractions were collected and recrystallized from chloroform and hexanes (1:3 ratio) to afford brown needle-like crystals which were collected to afford the title compound (30.1 mg, 16%).

NMR data are available for this compound due to its paramagnetic character. The key data for the structural characterization were obtained by HRMS and X-ray crystallography.

HRMS (+p ESI): Calcd for $C_{88}H_{64}O_8{}^{79}Br_2{}^{81}Br_2{}^{101}Ru{}^{102}Ru$ [M–Cl] 1770.9388 found 1770.9466

Ru_2(*S*-*p*Br-TPCP)$_4$Cl (9-Ru)

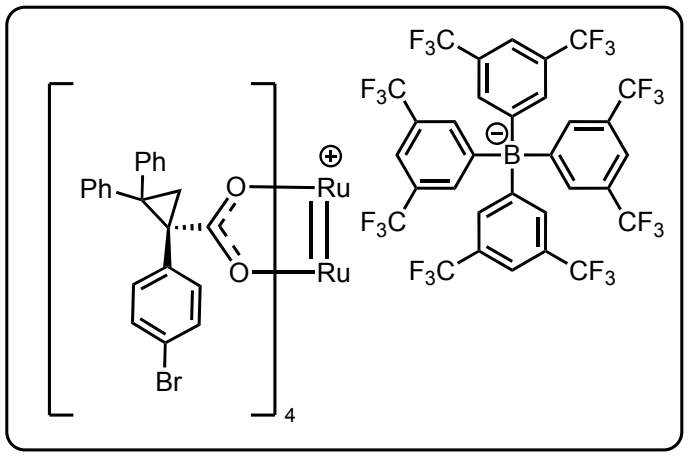

To a 4 mL vial equipped with a stir bar was added **7-Ru** (10 mg, 5.6 μmol, 1 equiv) which was subsequently dissolved in 1 mL of DCM. Then, $NaBAr^F$ (5.3 mg, 5.9 μmol, 1.05 equiv) was added in one portion and the reaction was left to stir overnight. After 16 h, the solution

was passed over a small pad of silica and concentrated down to afford an orange/brown powder (14.3 mg, 96%).

NMR data are available for this compound due to its paramagnetic character. The key data for the structural characterization were obtained by HRMS.

HRMS (+p ESI): Calcd for $C_{88}H_{64}O_8{}^{79}Br_2{}^{81}Br_2{}^{101}Ru{}^{102}Ru$ [M–Cl] 1770.9388 found 1770.9408.

HRMS (-p ESI): Calcd for $C_{32}H_{12}{}^{10}B^-F_{24}$ [M^-] 862.0691, found 862.0693.

Regioselectivity Determination

Regioselectivity determination for reactions with p-Cymene

Regioselectivity was determined through the integration of the TCE peaks comparing the 1° and 3° insertion. One of the 3° insertion TCE peak is located at 4.47 ppm and one of the 1° insertion TCE peaks is located at 4.71 ppm.

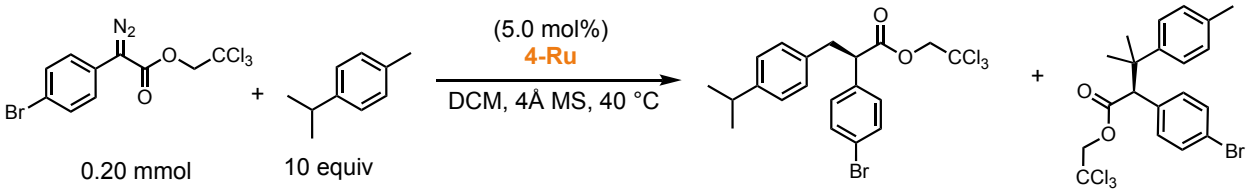

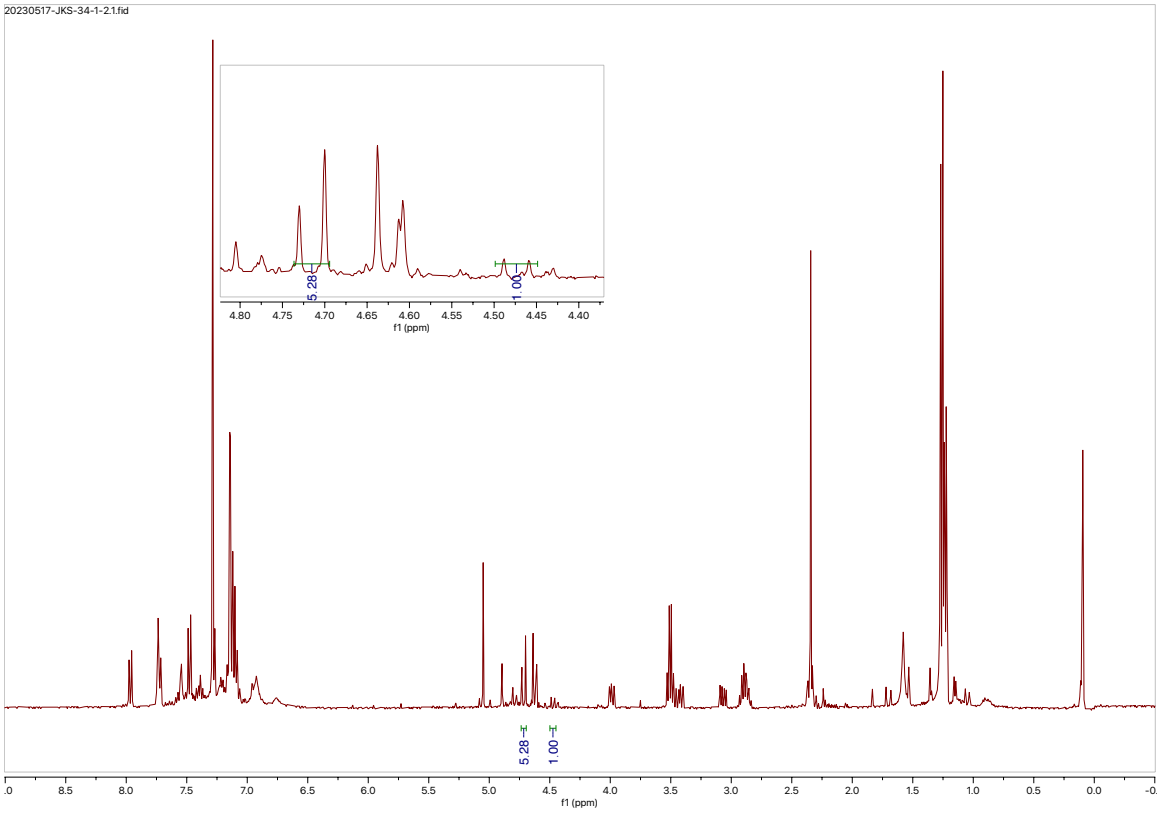

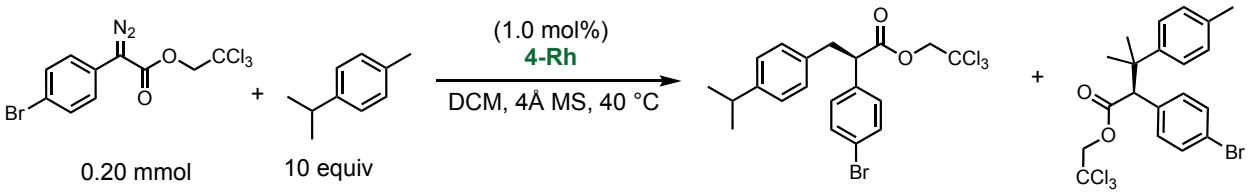

0.20 mmol

10 equiv

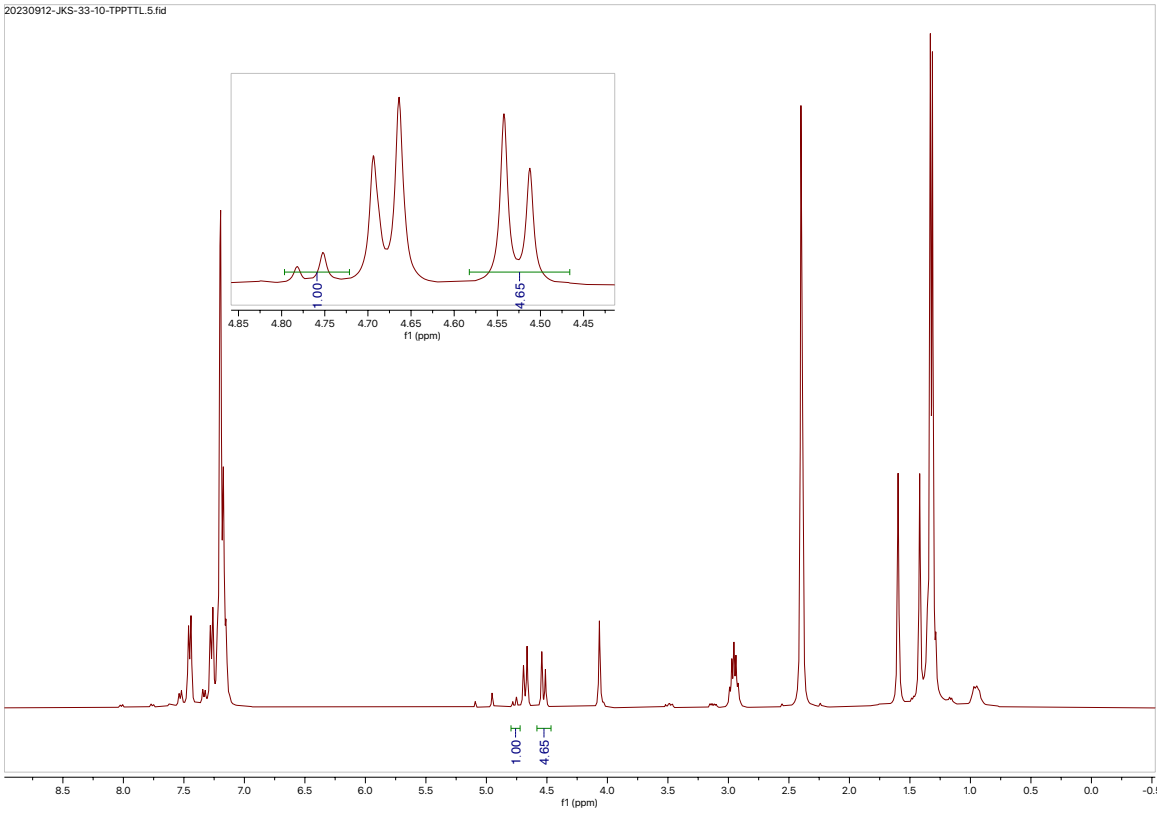

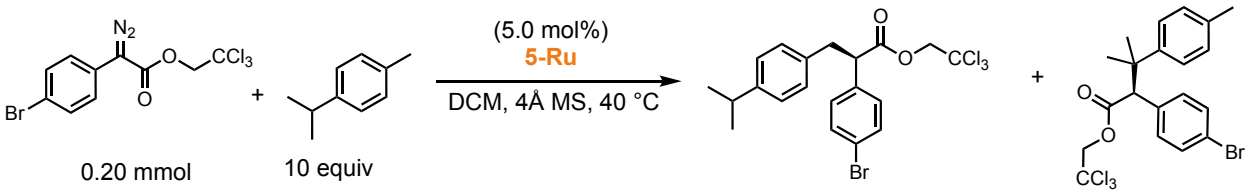

0.20 mmol

10 equiv

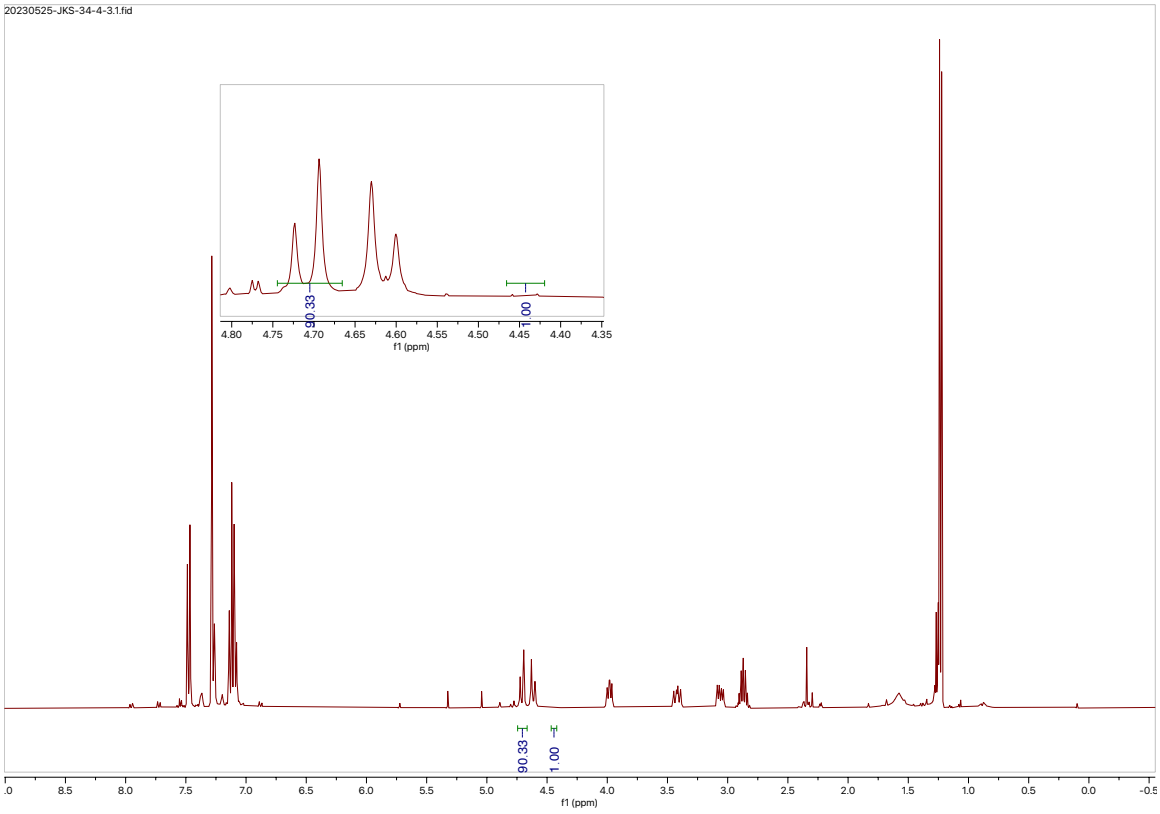

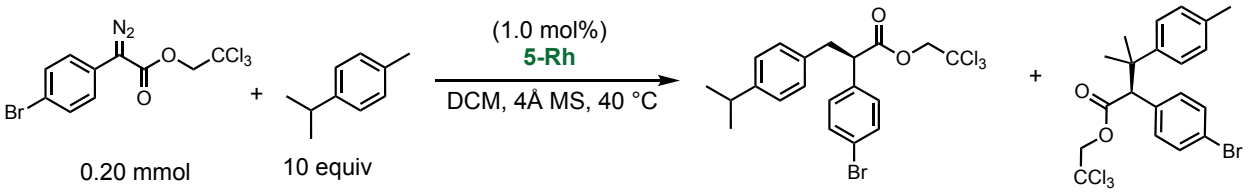
(1.0 mol%)
5-Rh
DCM, 4Å MS, 40 °C
0.20 mmol
10 equiv

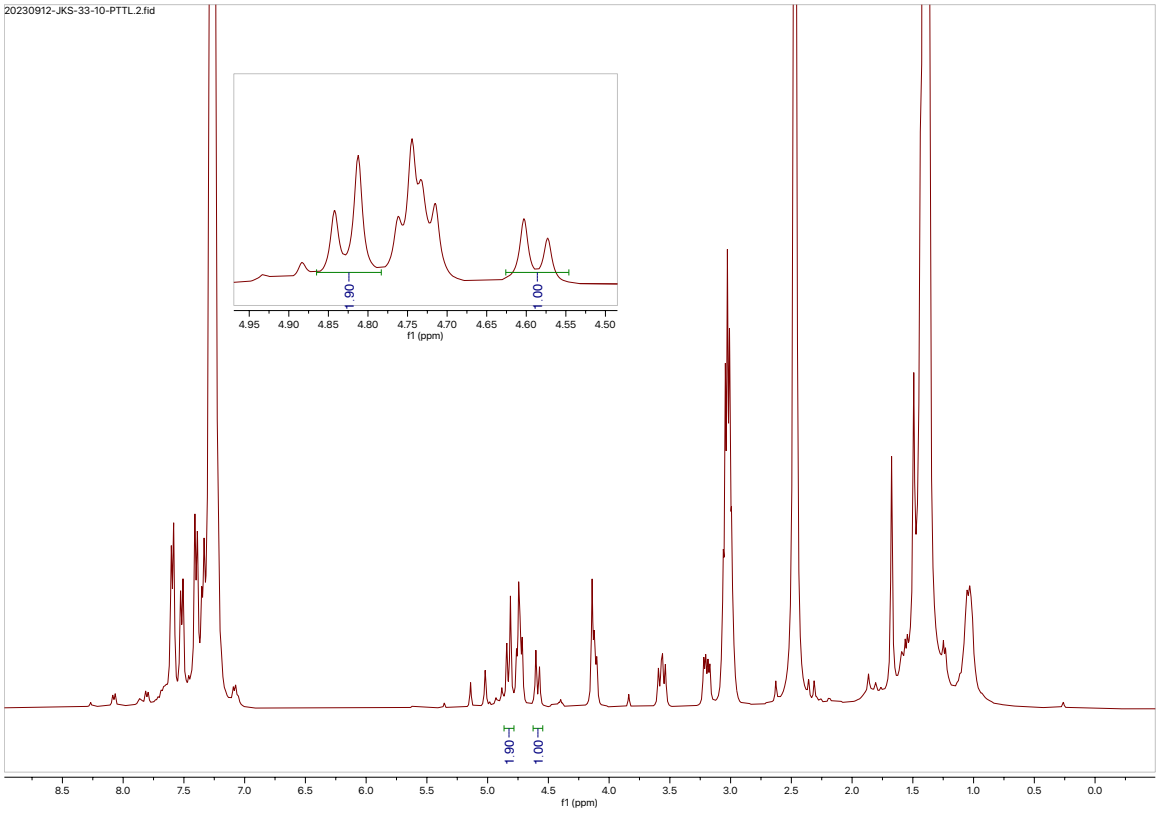
20230912-JKS-33-10-PTTL.2.fid
1.90
1.00
f1 (ppm)

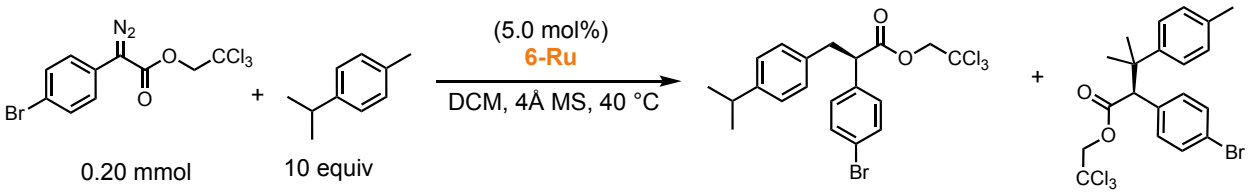

0.20 mmol

10 equiv

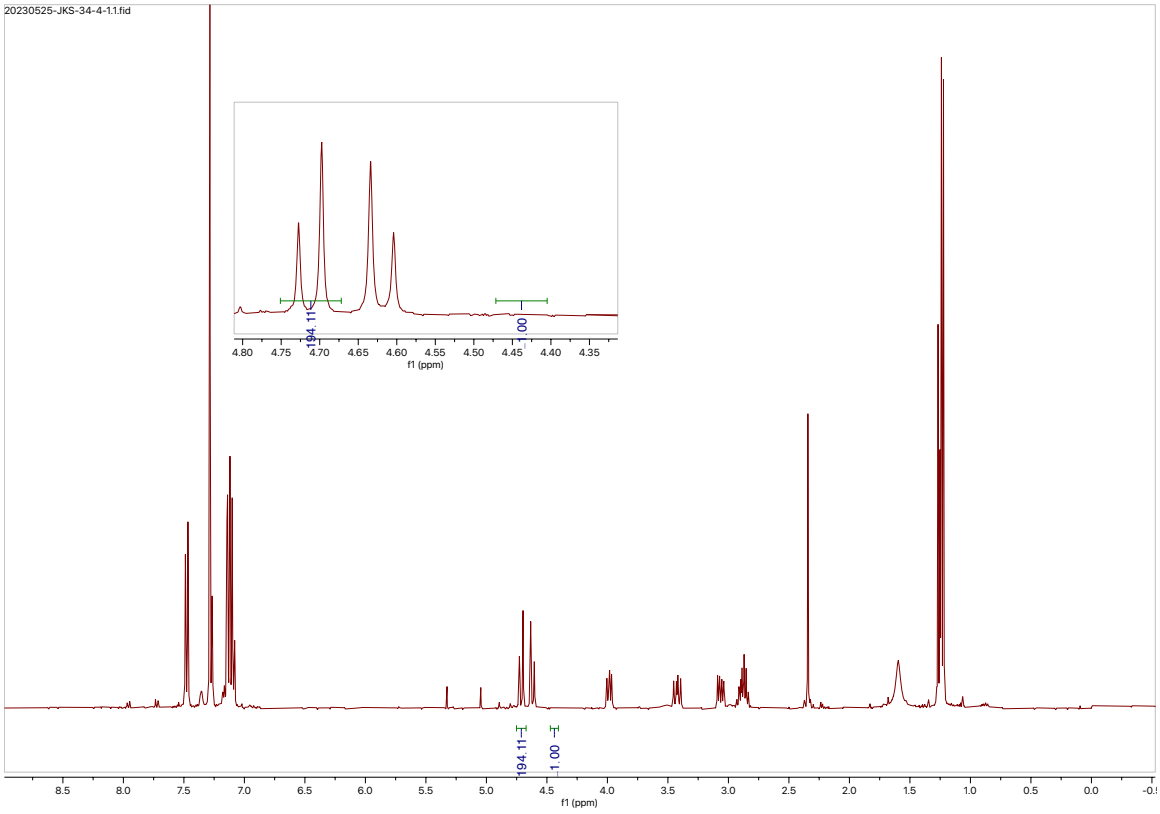

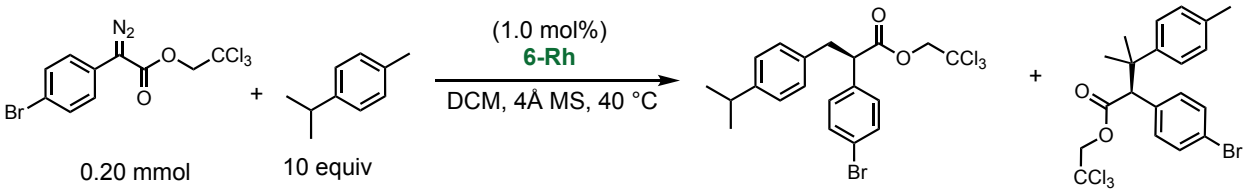
N2
O
CCl3
O
Br
+
0.20 mmol
10 equiv
(1.0 mol%)
6-Rh
DCM, 4Å MS, 40 °C
O
O
CCl3
Br
+
O
O
Br
CCl3

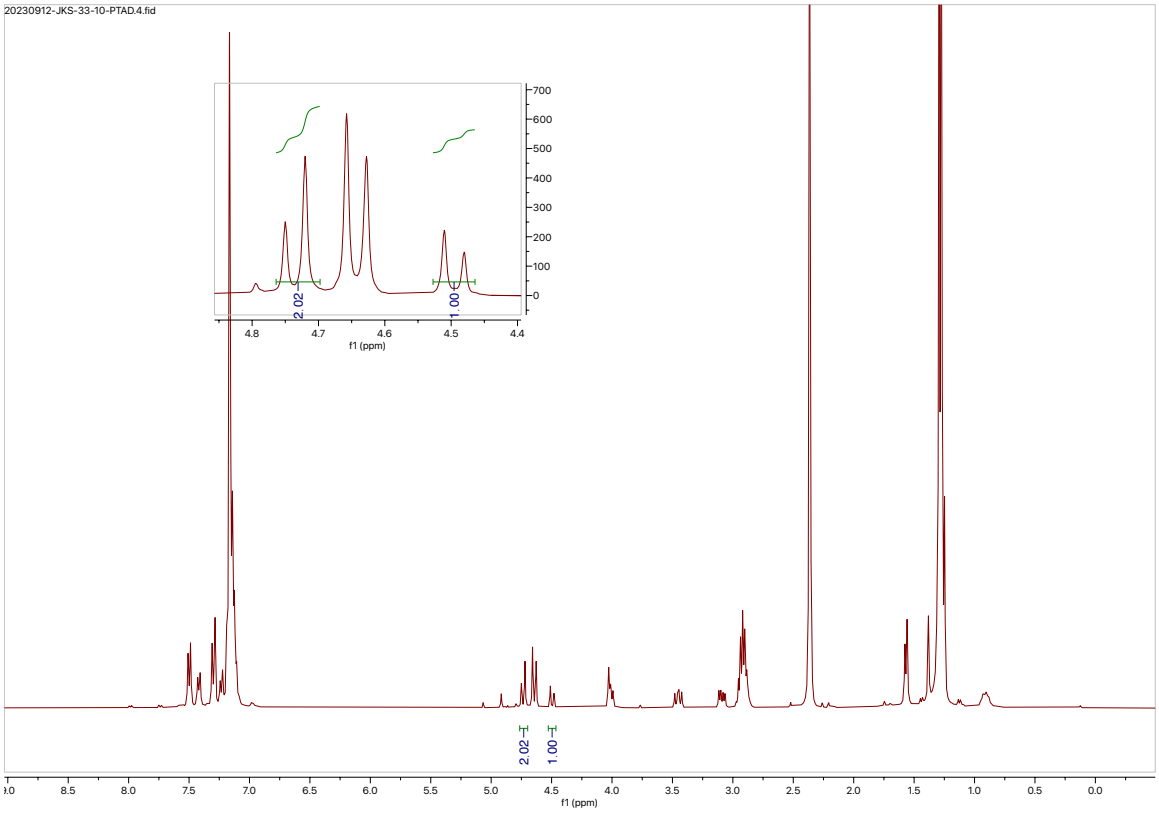
20230912-JKS-33-10-PTAD.4.fid
2.02
1.00
f1 (ppm)
2.02
1.00
f1 (ppm)

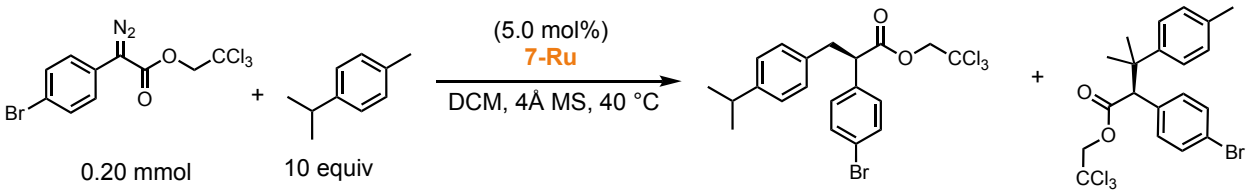
(5.0 mol%)
7-Ru
DCM, 4Å MS, 40 °C
0.20 mmol
10 equiv

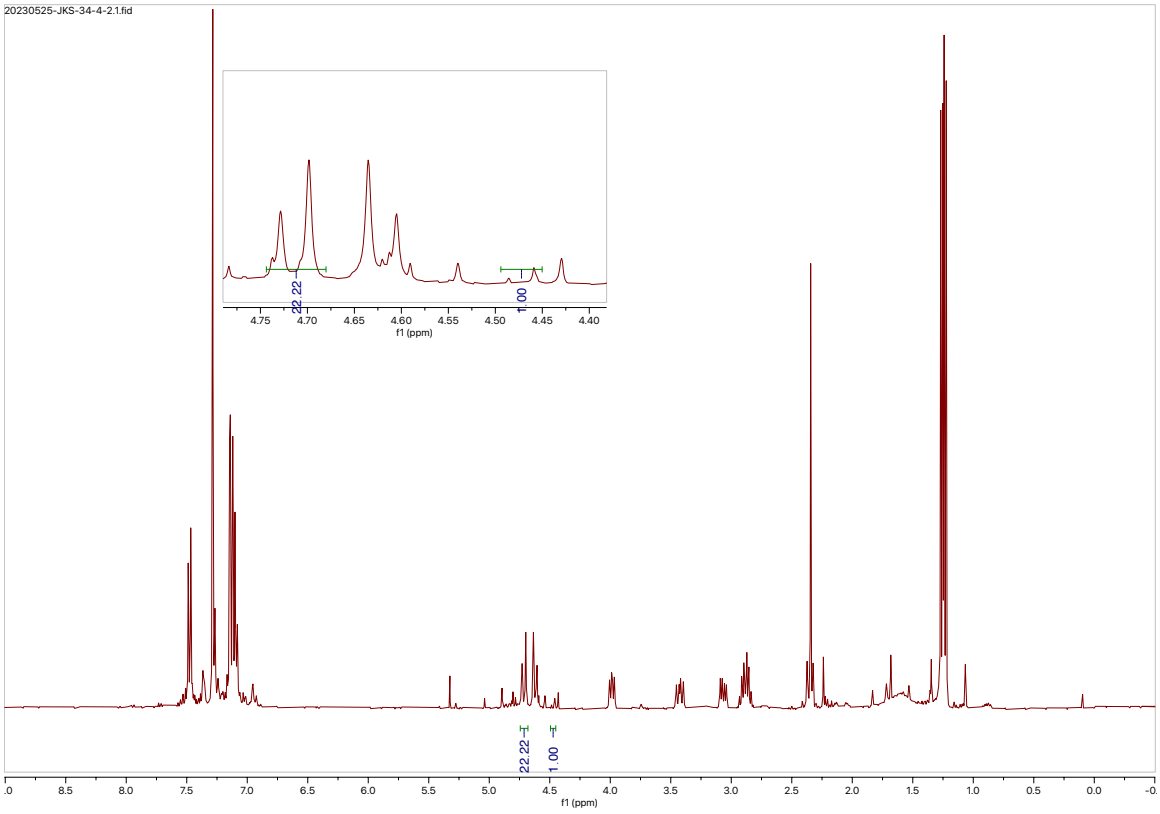
20230525-JKS-34-4-2.1.fid
22.22
1.00
f1 (ppm)

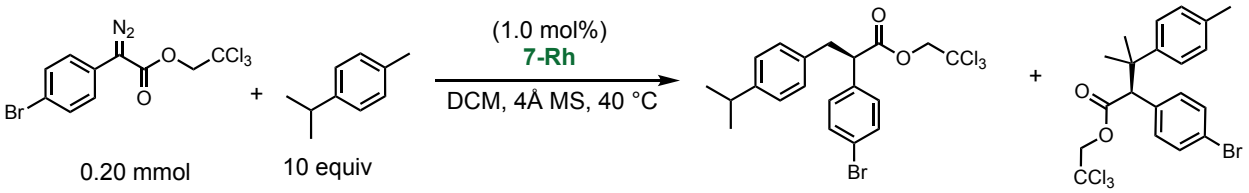
(1.0 mol%)
7-Rh
DCM, 4Å MS, 40 °C
0.20 mmol
10 equiv

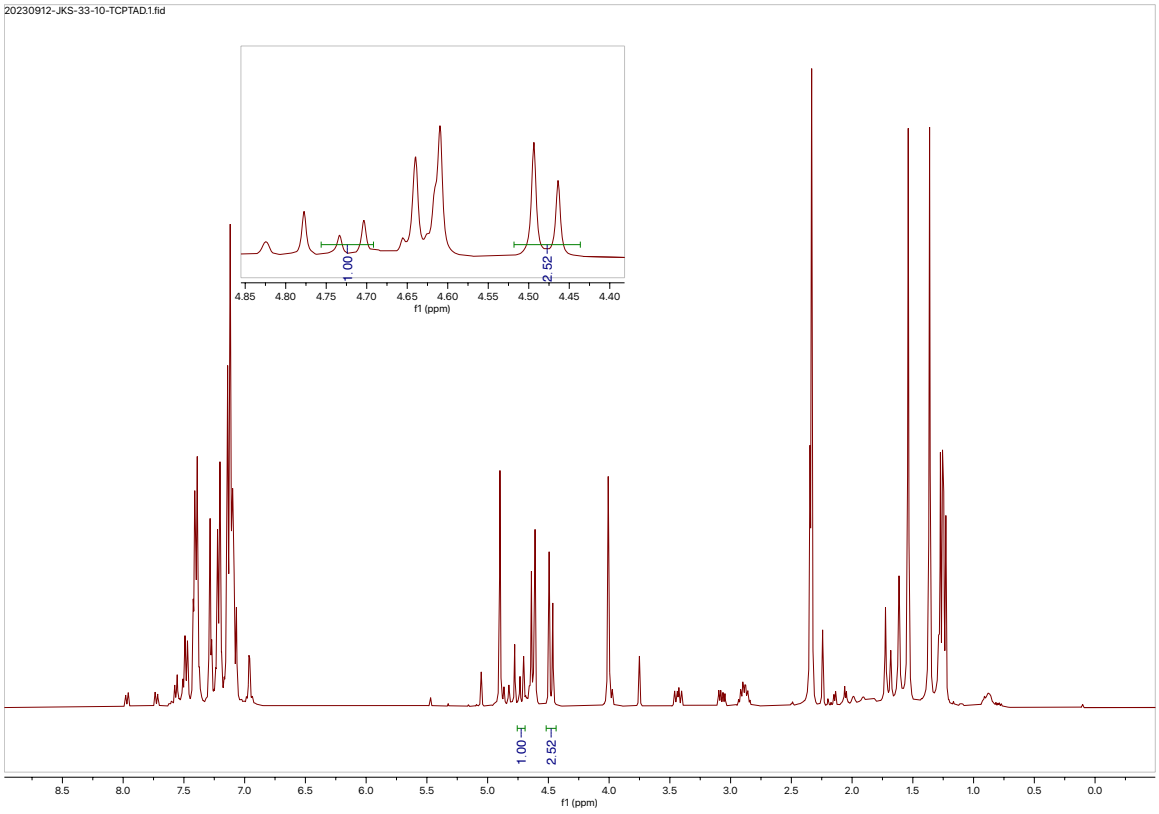
20230912-JKS-33-10-TCPTAD.1.fid
1.00
2.52
f1 (ppm)

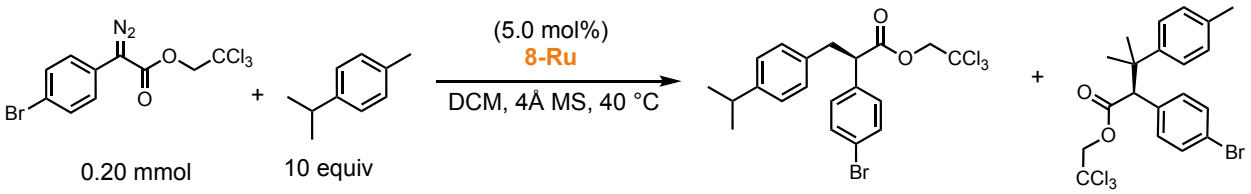
N2
O
CCl3
O
Br
+
0.20 mmol
10 equiv
(5.0 mol%)
8-Ru
DCM, 4Å MS, 40 °C
O
O
CCl3
Br
+
O
O
CCl3
Br

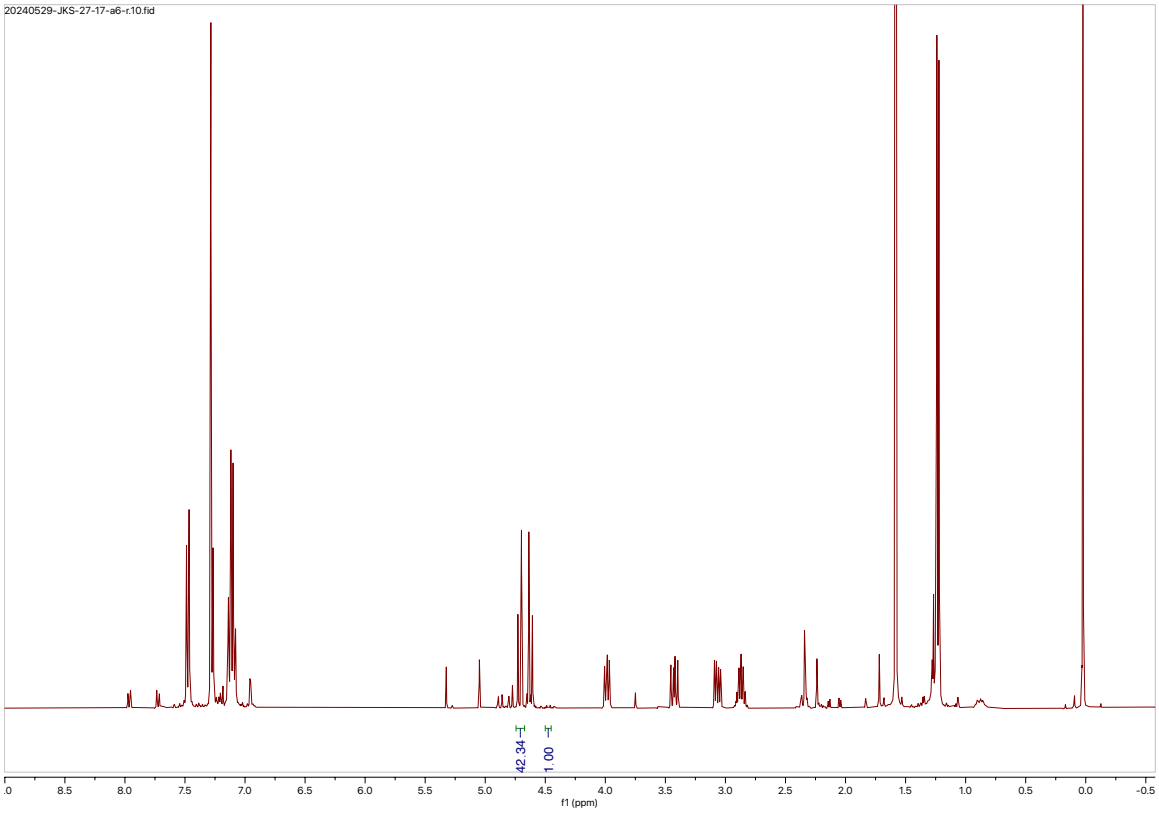
20240529-JKS-27-17-a6-r.10.fid
42.34
1.00
f1 (ppm)

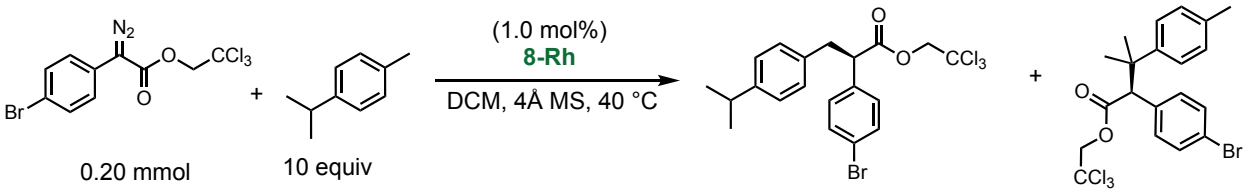
(1.0 mol%)
8-Rh
DCM, 4Å MS, 40 °C
0.20 mmol
10 equiv

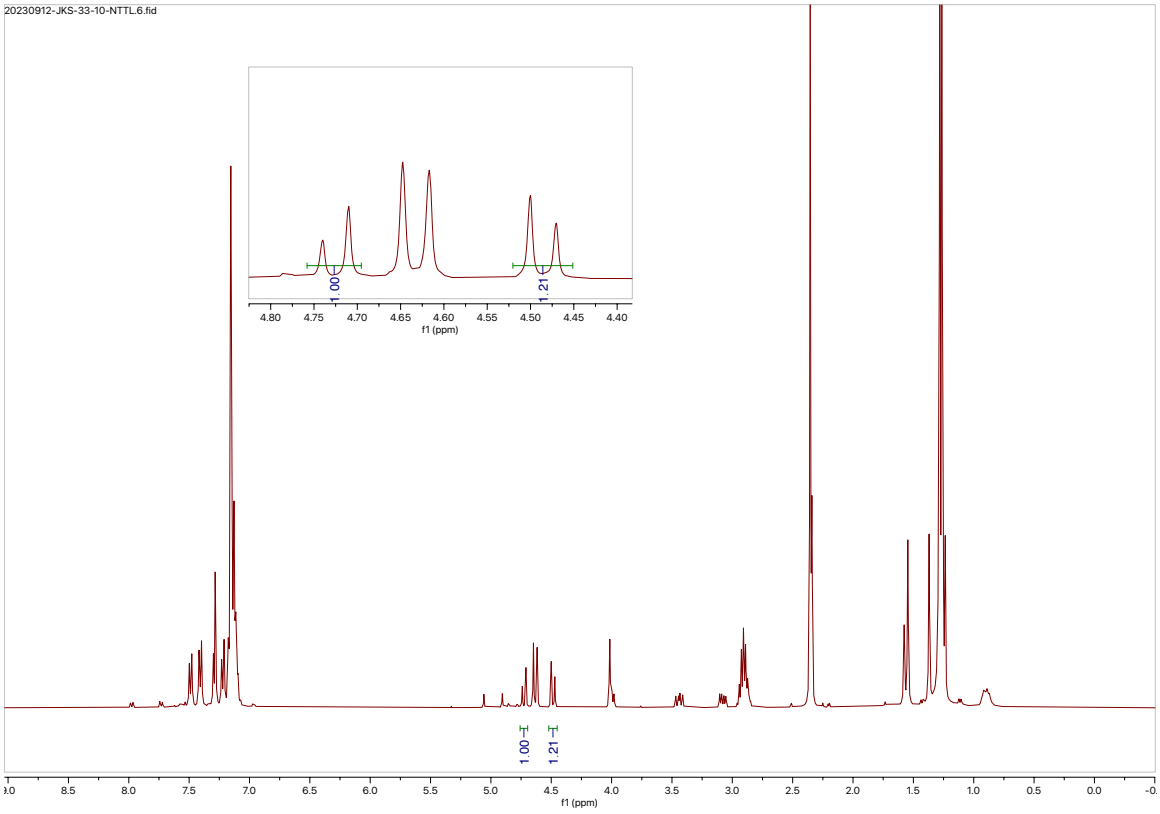
20230912-JKS-33-10-NTTL.6.fid
1.00
1.21
f1 (ppm)

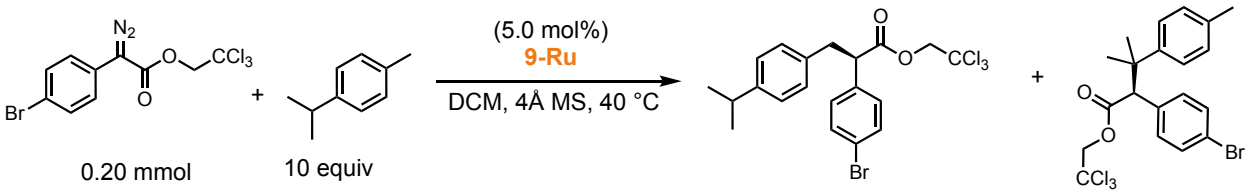
N2
CCl3
O
O
Br
+
0.20 mmol
10 equiv
(5.0 mol%)
9-Ru
DCM, 4Å MS, 40 °C
O
O
CCl3
Br
+
O
O
Br
CCl3

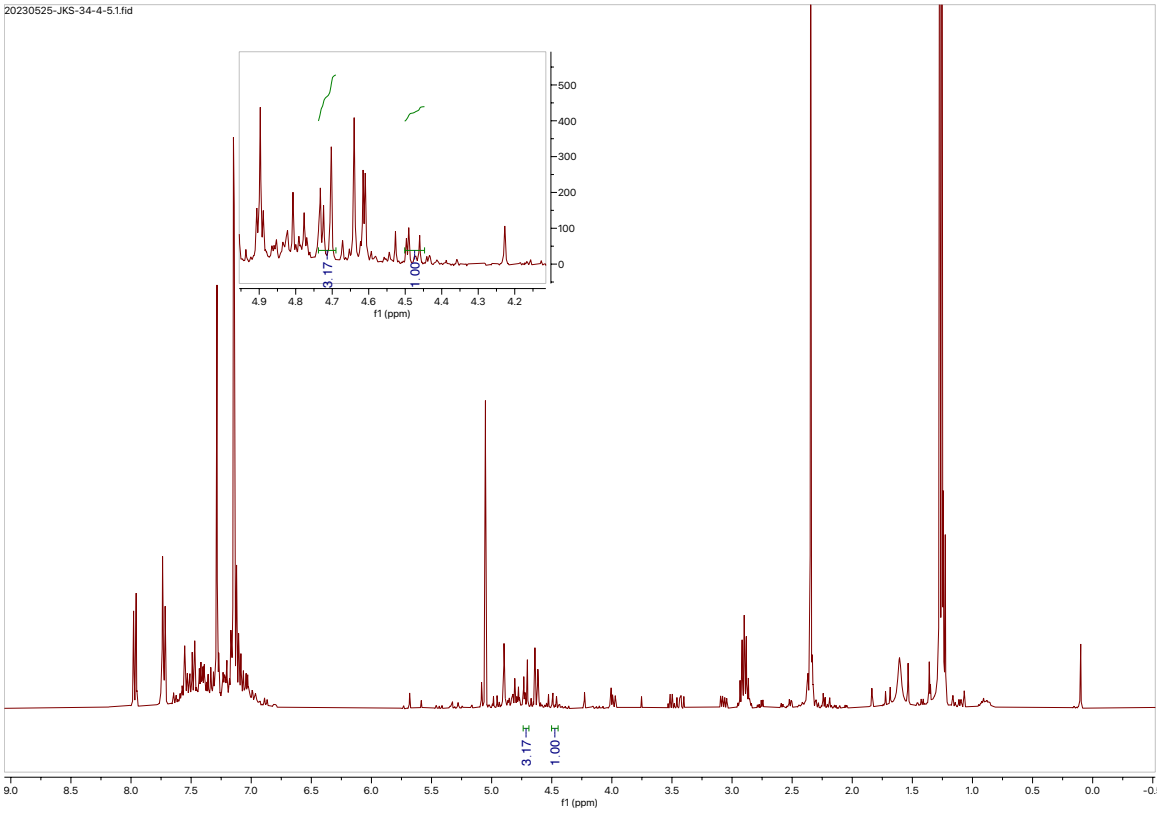
20230525-JKS-34-4-5.1.fid
3.17
1.00
f1 (ppm)

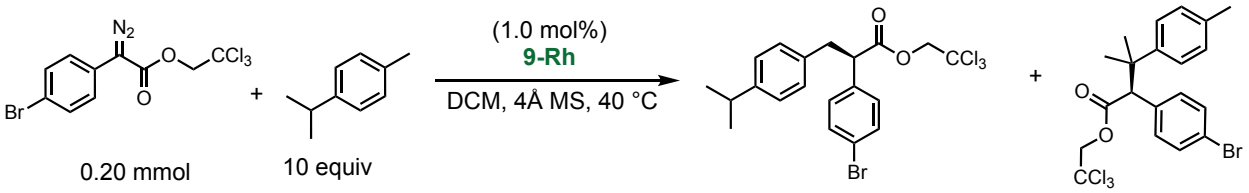
N2
O
CCl3
O
Br
+
0.20 mmol
10 equiv
(1.0 mol%)
9-Rh
DCM, 4Å MS, 40 °C
O
O
CCl3
Br
+
O
O
CCl3
Br

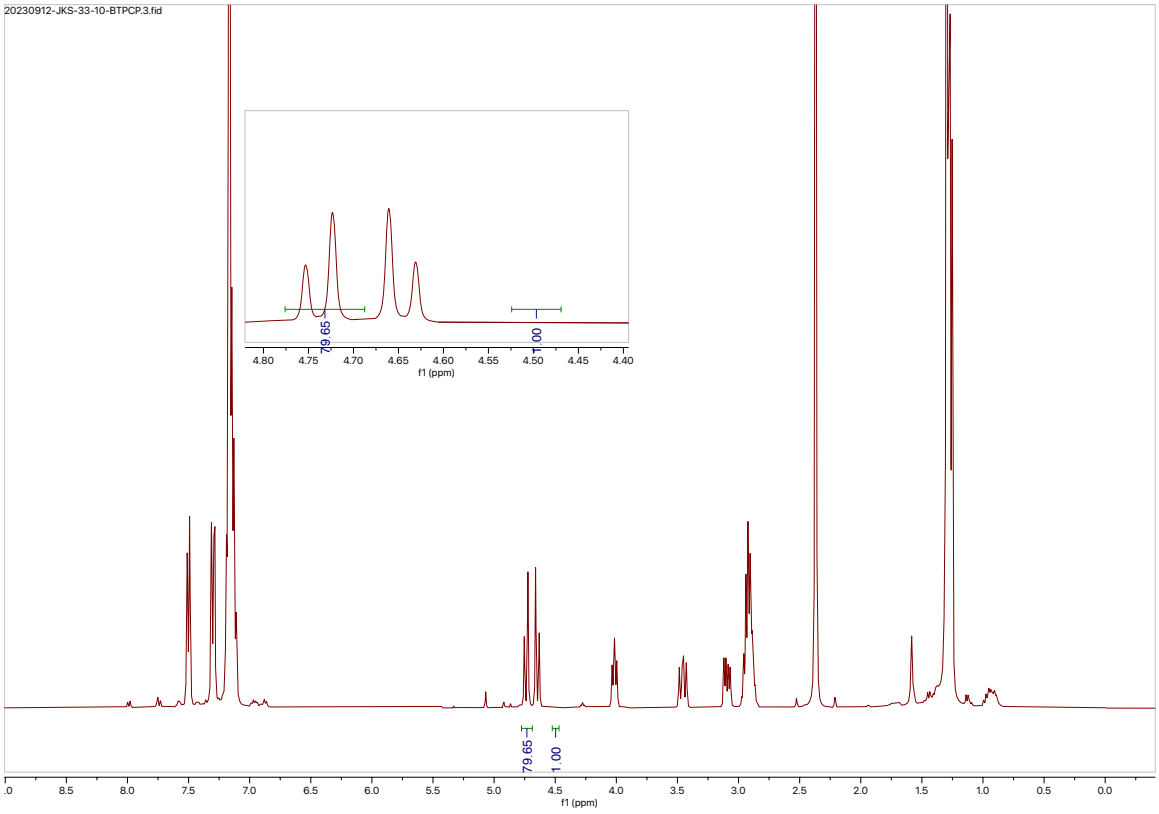
20230912-JKS-33-10-BTPCP.3.fid
79.65
1.00
4.80 4.75 4.70 4.65 4.60 4.55 4.50 4.45 4.40
f1 (ppm)
79.65
1.00
.0 8.5 8.0 7.5 7.0 6.5 6.0 5.5 5.0 4.5 4.0 3.5 3.0 2.5 2.0 1.5 1.0 0.5 0.0
f1 (ppm)

Regioselectivity and diastereoselectivity determination for reactions with 4-isopropylethylbenzene

Regioselectivity was determined through the integration of the benzylic alpha-carbonyl hydrogen comparing the 2° and 3° insertion. The 3° insertion peak is located at 3.98 ppm and one of the 2° insertion peak is located at 3.81 ppm. The diastereoselectivity is determined through comparing the methyl peak on the ethyl group. The minor diastereomer is cis with the bromo-substituted phenyl ring, shielding farther up-field.

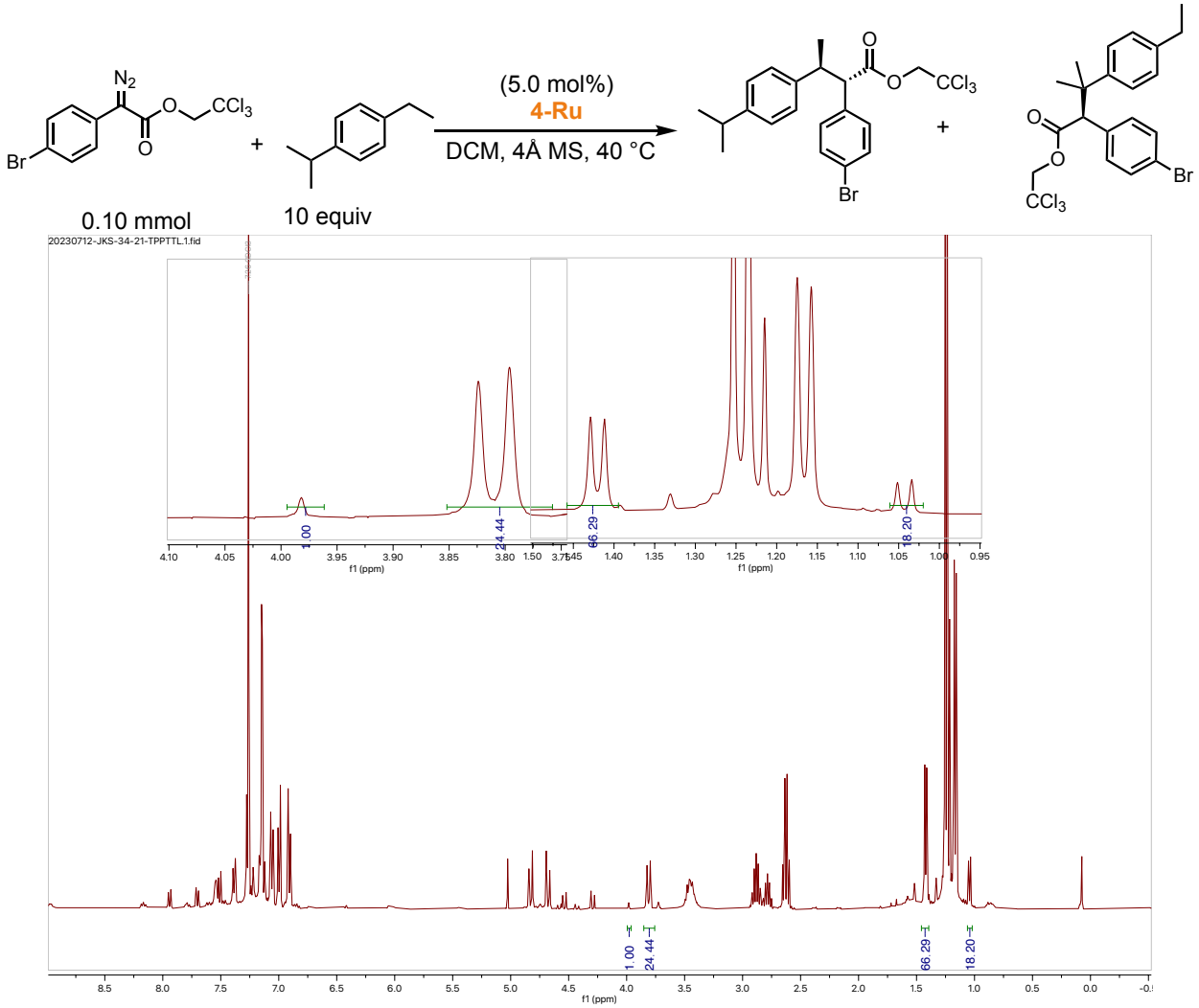

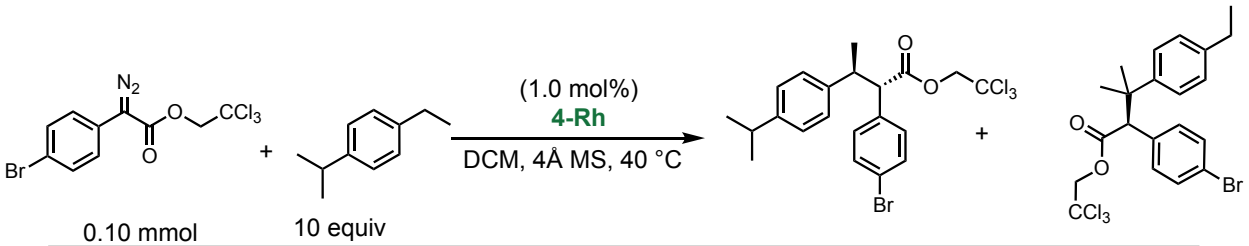

0.10 mmol

10 equiv

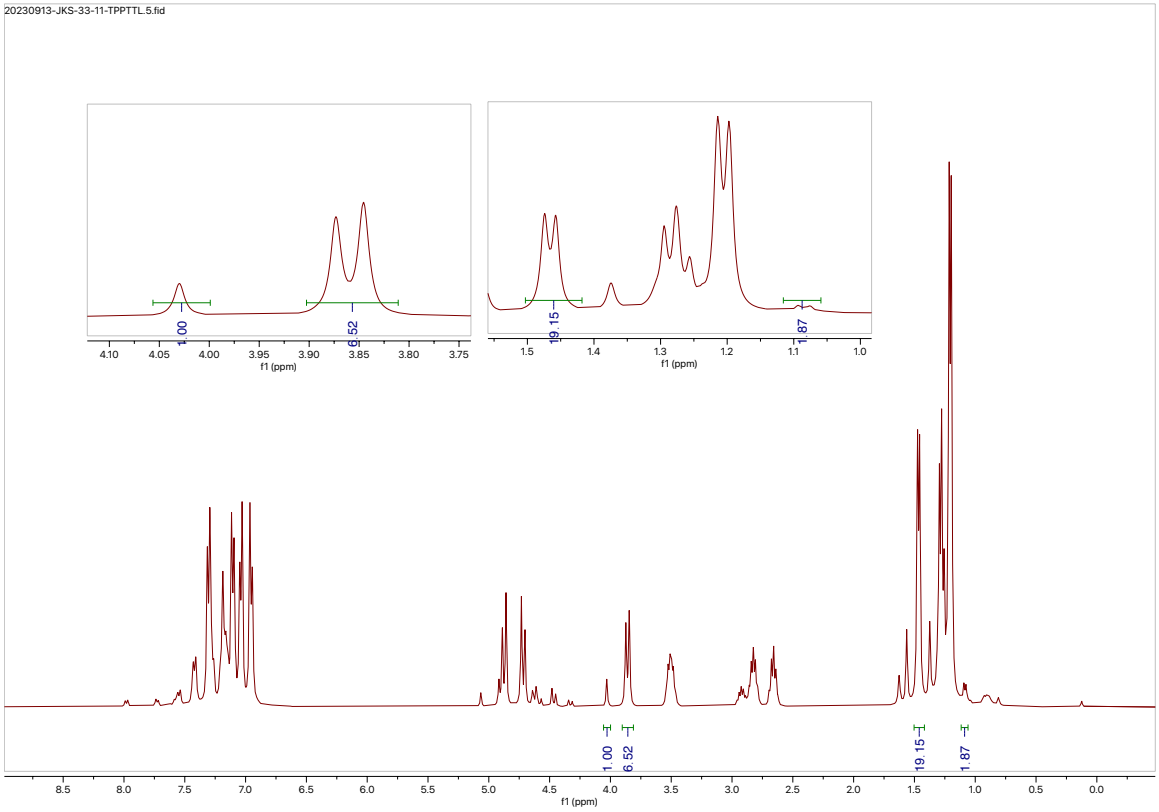

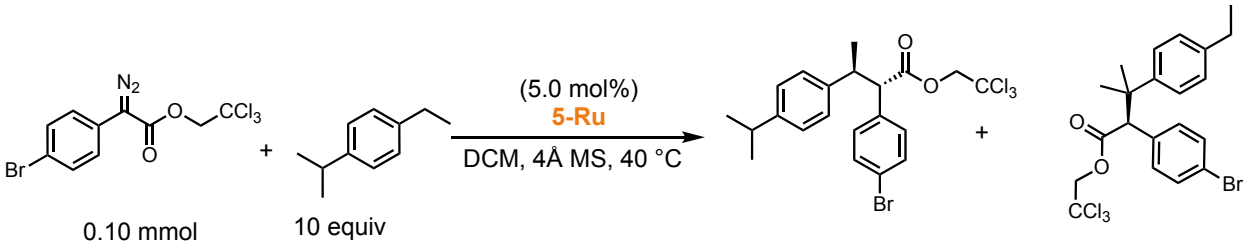
N2
O
CCl3
O
Br
+
0.10 mmol
10 equiv
(5.0 mol%)
5-Ru
DCM, 4Å MS, 40 °C
O
O
CCl3
Br
+
O
O
Br
CCl3

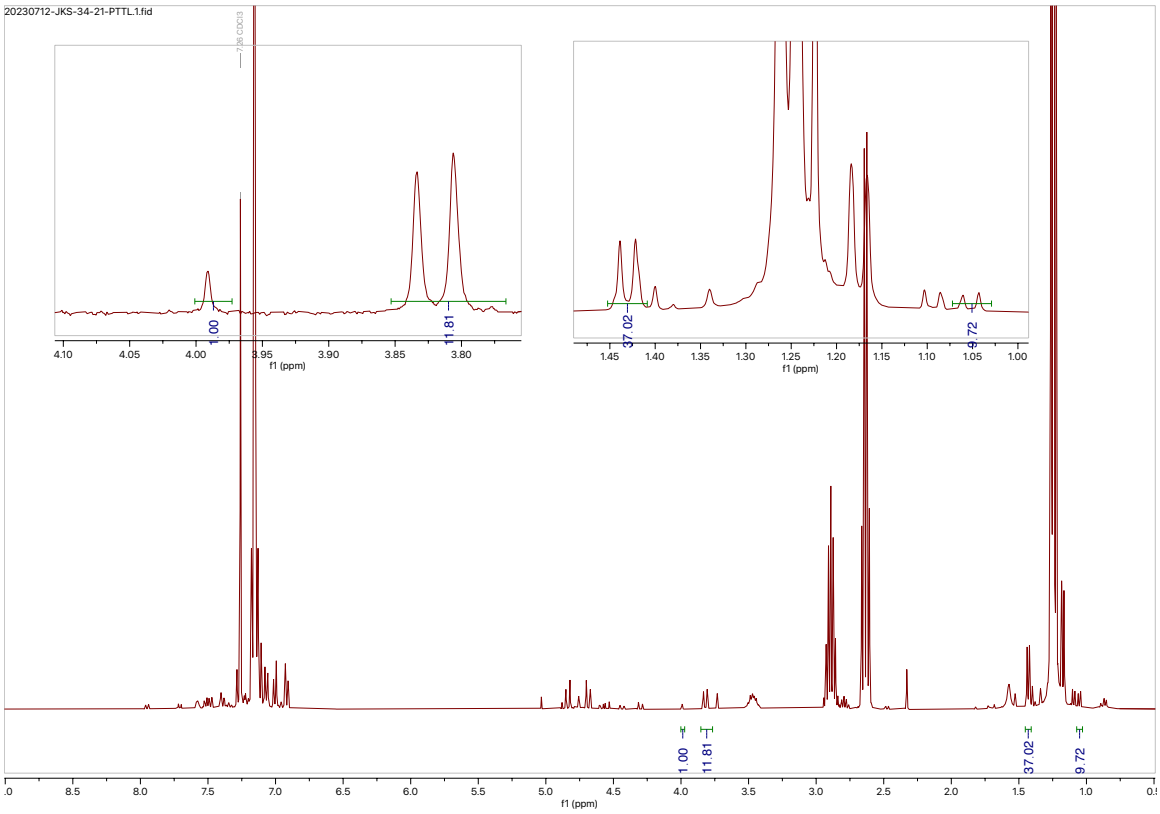
20230712-JKS-34-21-PTTL1.fid
1.00
11.81
37.02
9.72
f1 (ppm)

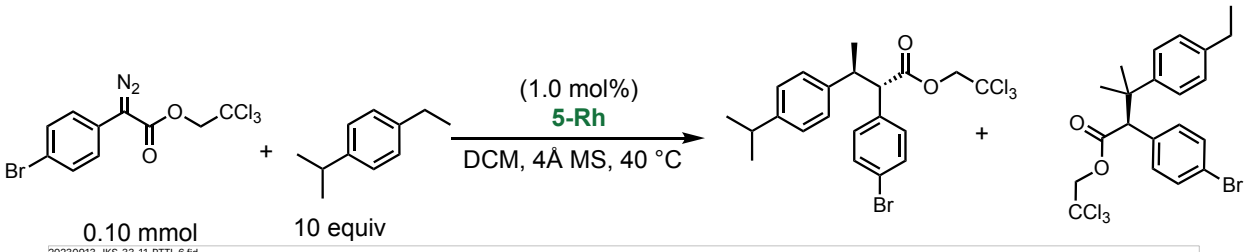

0.10 mmol 10 equiv

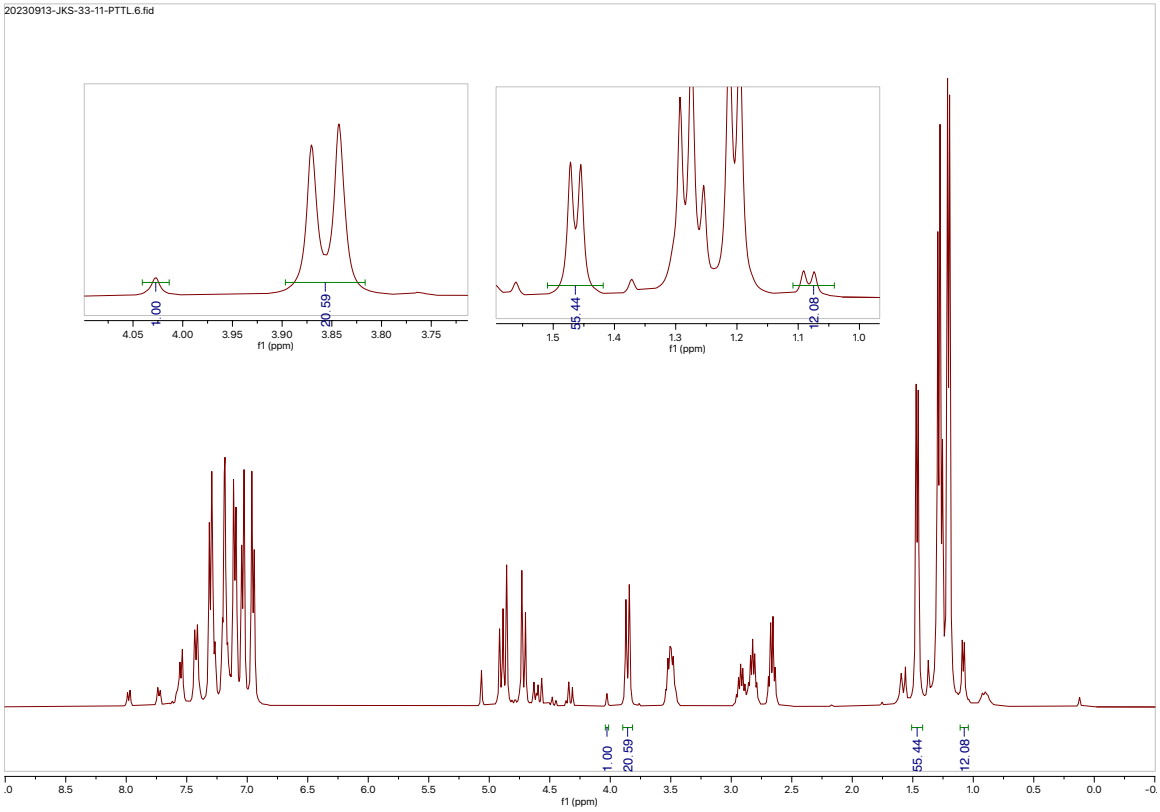

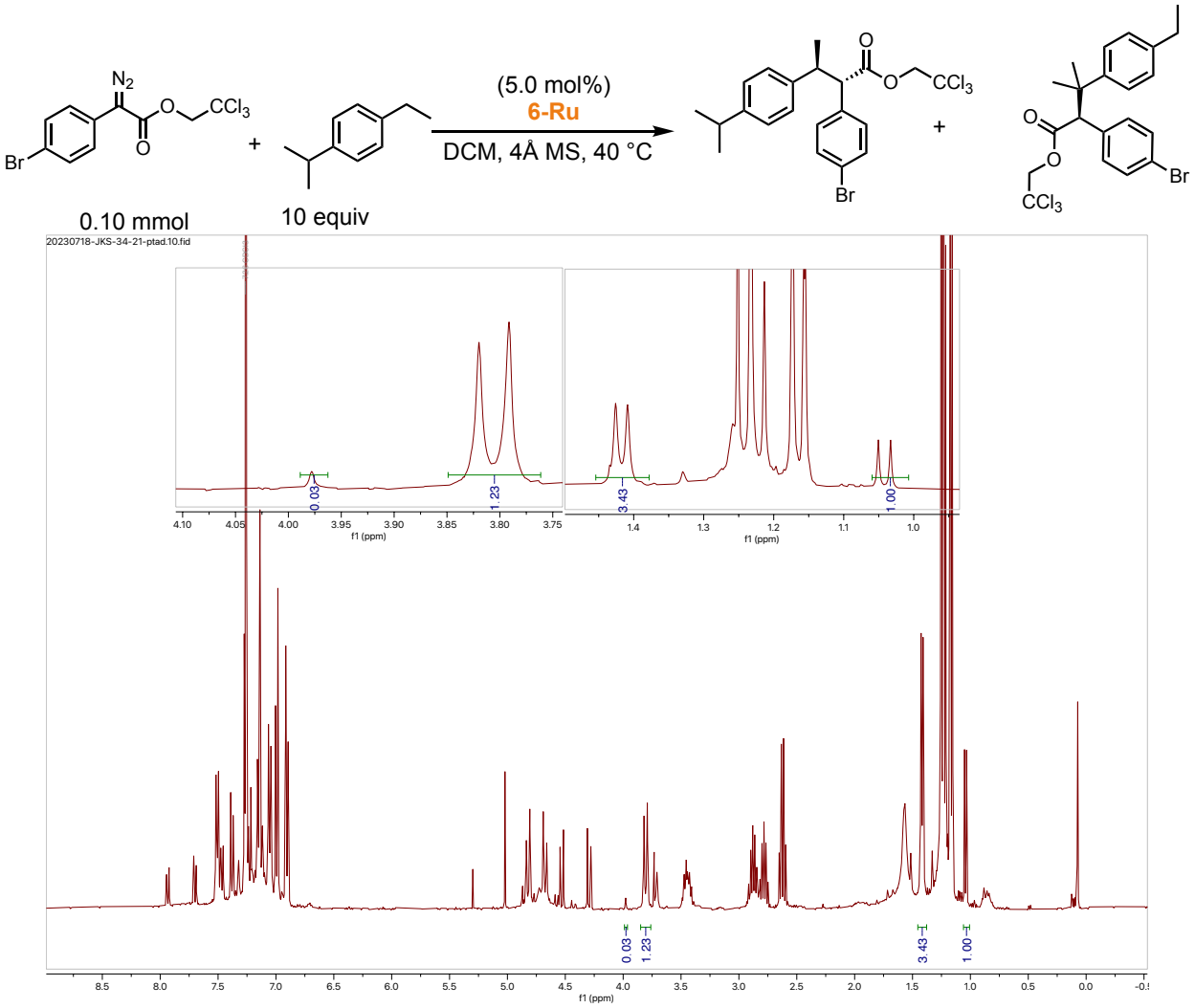
N2
O
CCl3
O
Br
+
(5.0 mol%)
6-Ru
DCM, 4Å MS, 40 °C
O
O
CCl3
Br
+
O
O
CCl3
Br
0.10 mmol
10 equiv
20230718-JKS-34-21-ptad.10.fid
0.03
1.23
3.43
1.00
f1 (ppm)

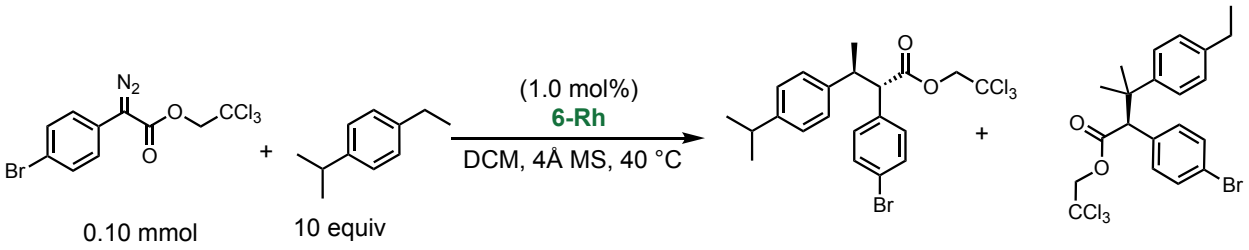
N2
O
CCl3
O
Br
+
0.10 mmol
10 equiv
(1.0 mol%)
6-Rh
DCM, 4Å MS, 40 °C
O
O
CCl3
Br
+
O
O
Br
CCl3

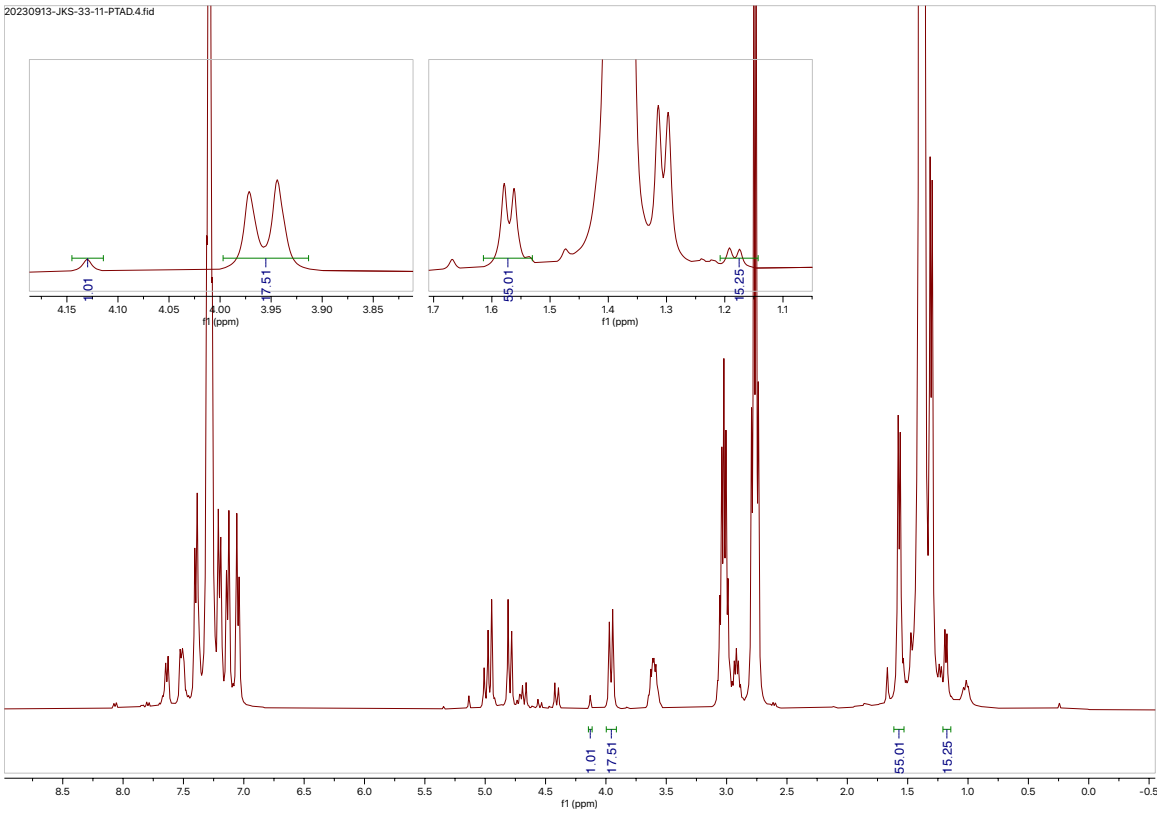
20230913-JKS-33-11-PTAD.4.fid
1.01
17.51
55.01
15.25
f1 (ppm)

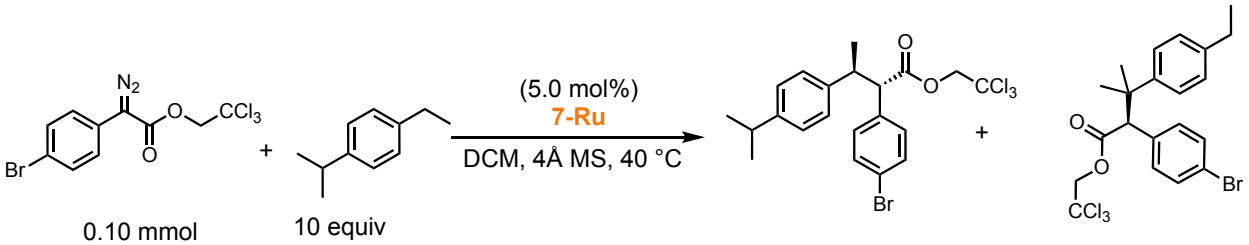

0.10 mmol

10 equiv

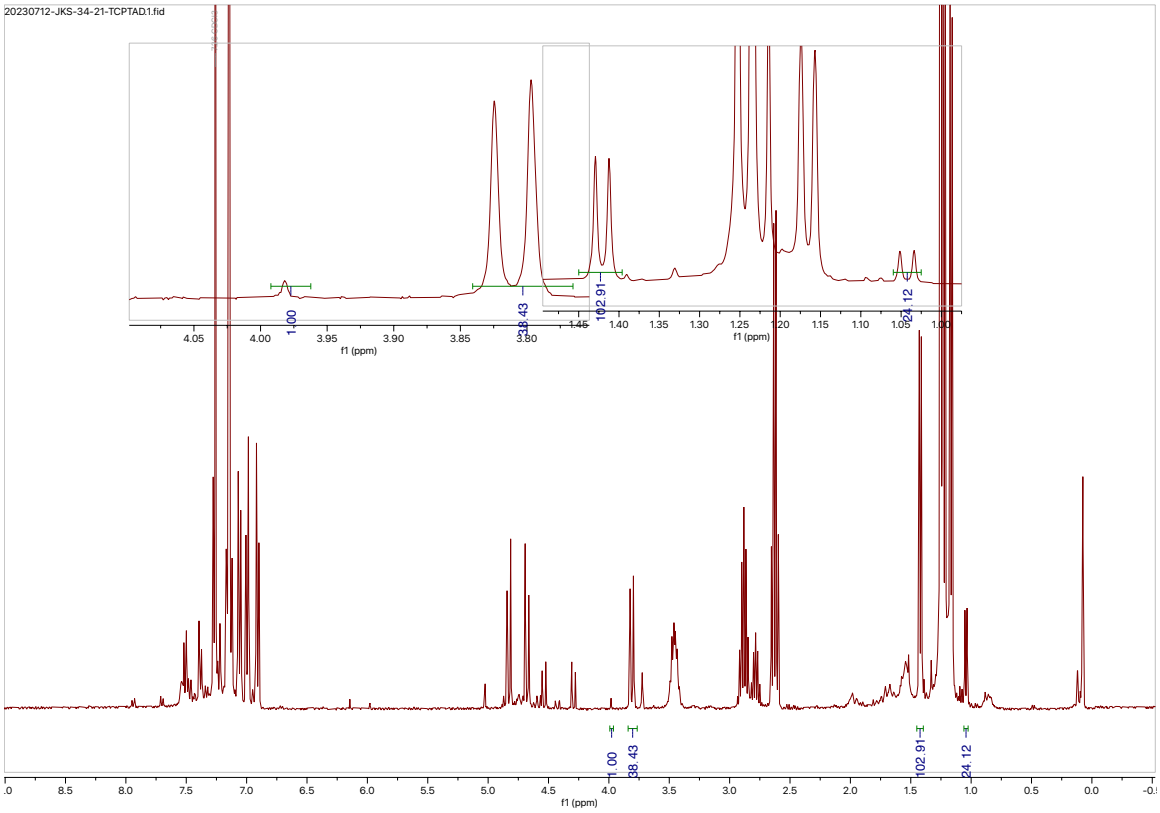

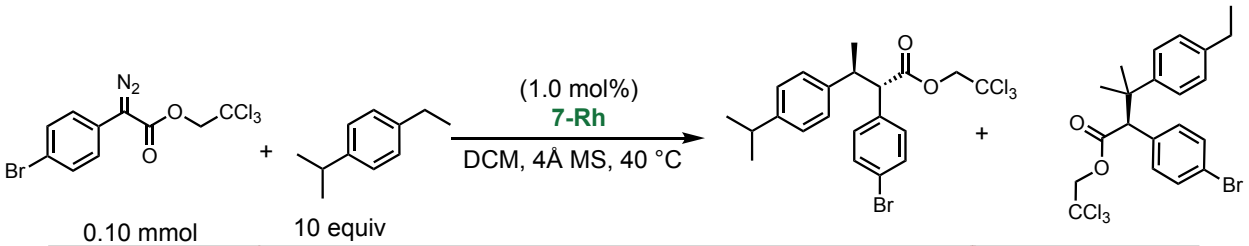

0.10 mmol 10 equiv

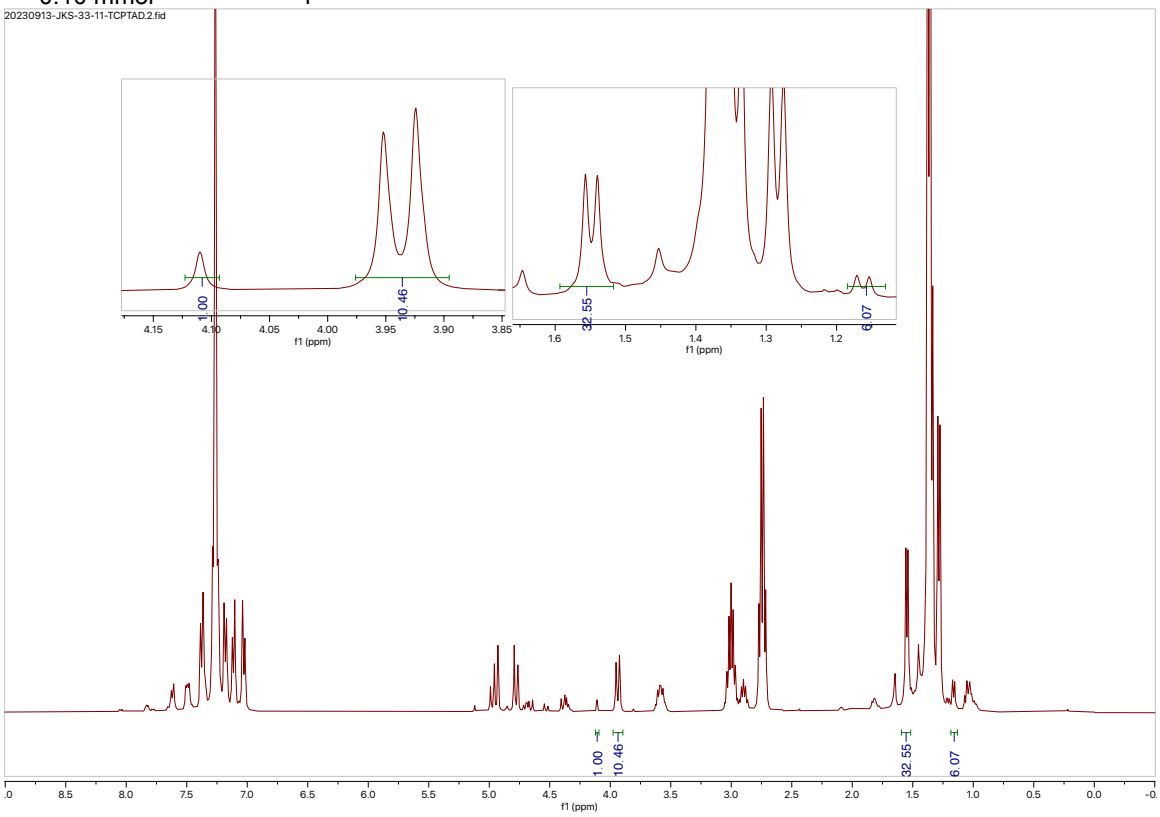

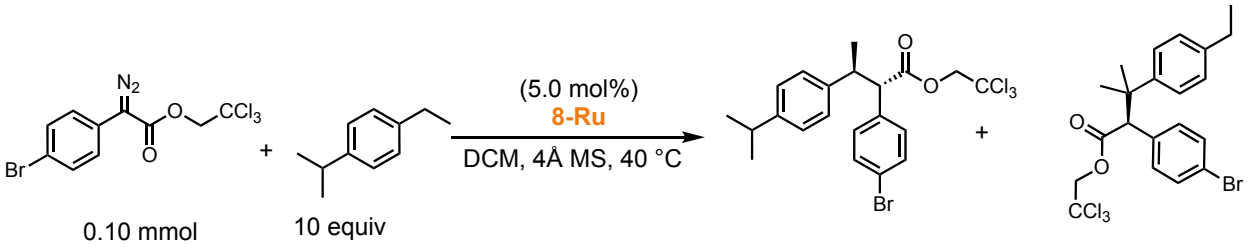
N2
O
CCl3
O
Br
+
0.10 mmol
10 equiv
(5.0 mol%)
8-Ru
DCM, 4Å MS, 40 °C
O
O
CCl3
Br
+
O
O
Br
CCl3

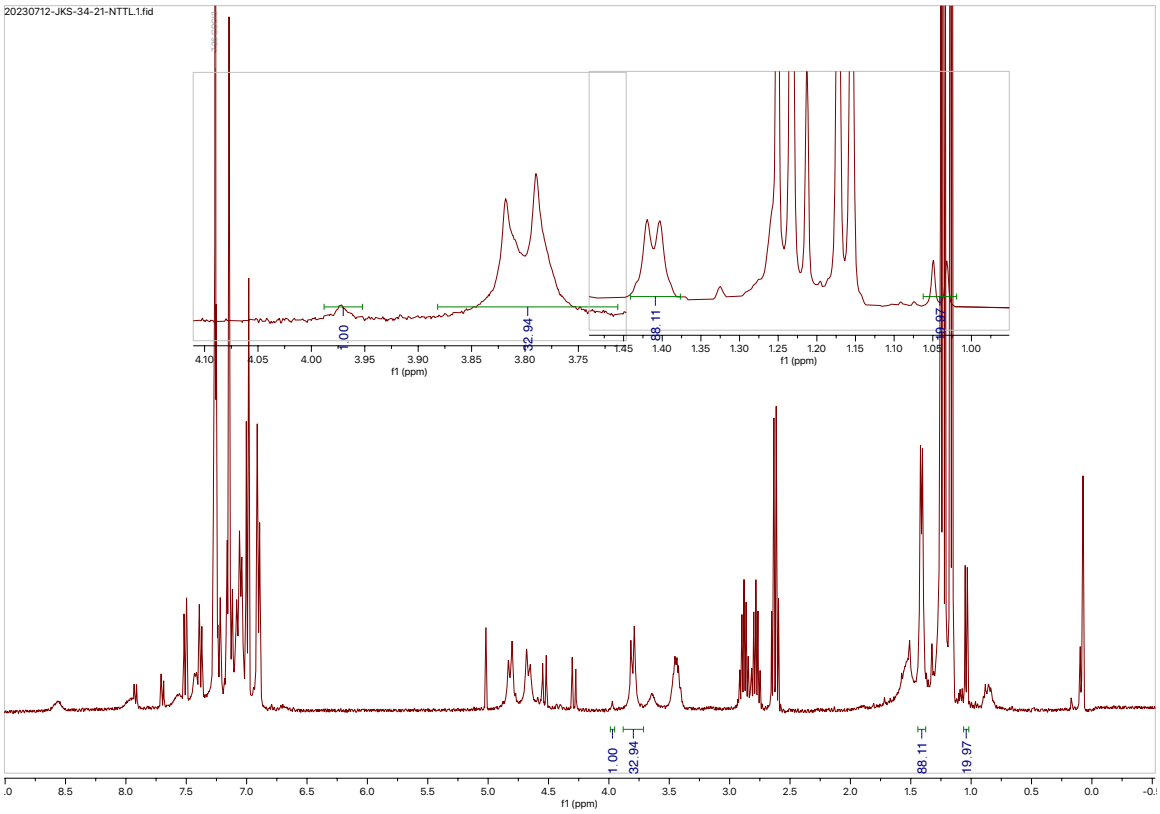
20230712-JKS-34-21-NTTL.1.fid
1.00
32.94
88.11
19.97
f1 (ppm)

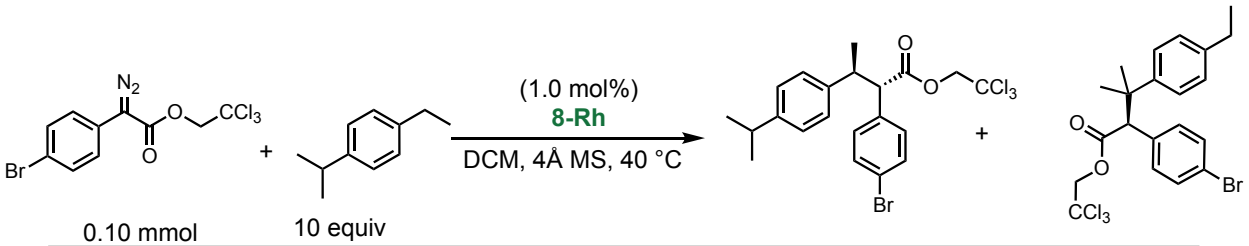

0.10 mmol 10 equiv

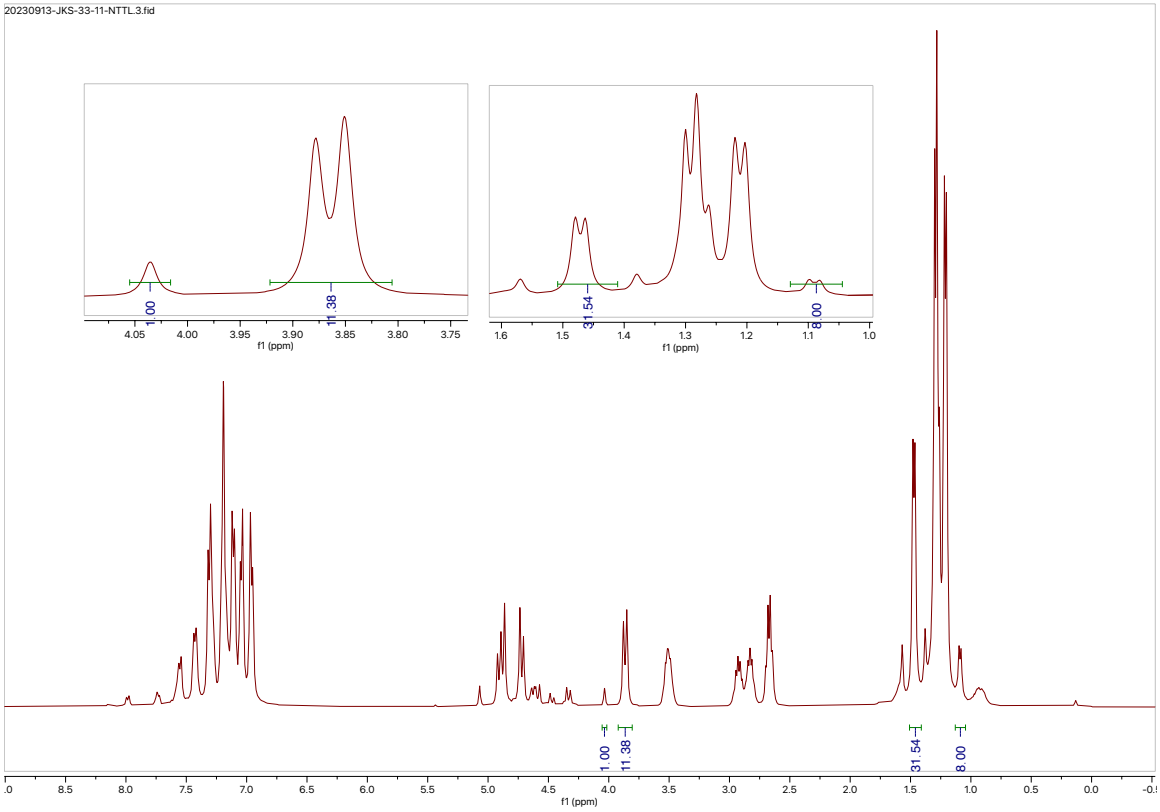

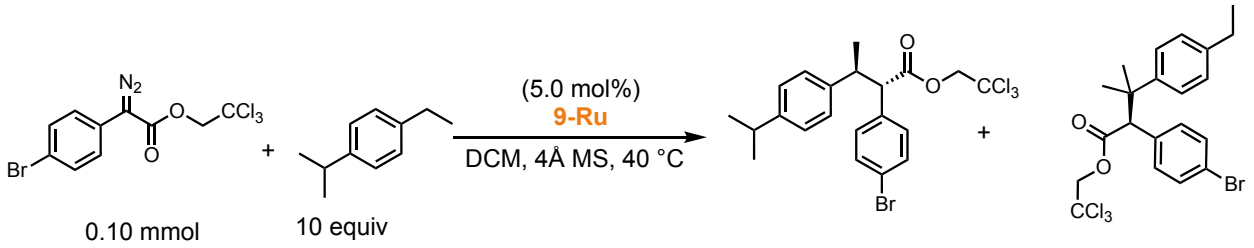
N2
O
CCl3
O
Br
+
0.10 mmol
10 equiv
(5.0 mol%)
9-Ru
DCM, 4Å MS, 40 °C
O
O
CCl3
Br
+
O
O
CCl3
Br

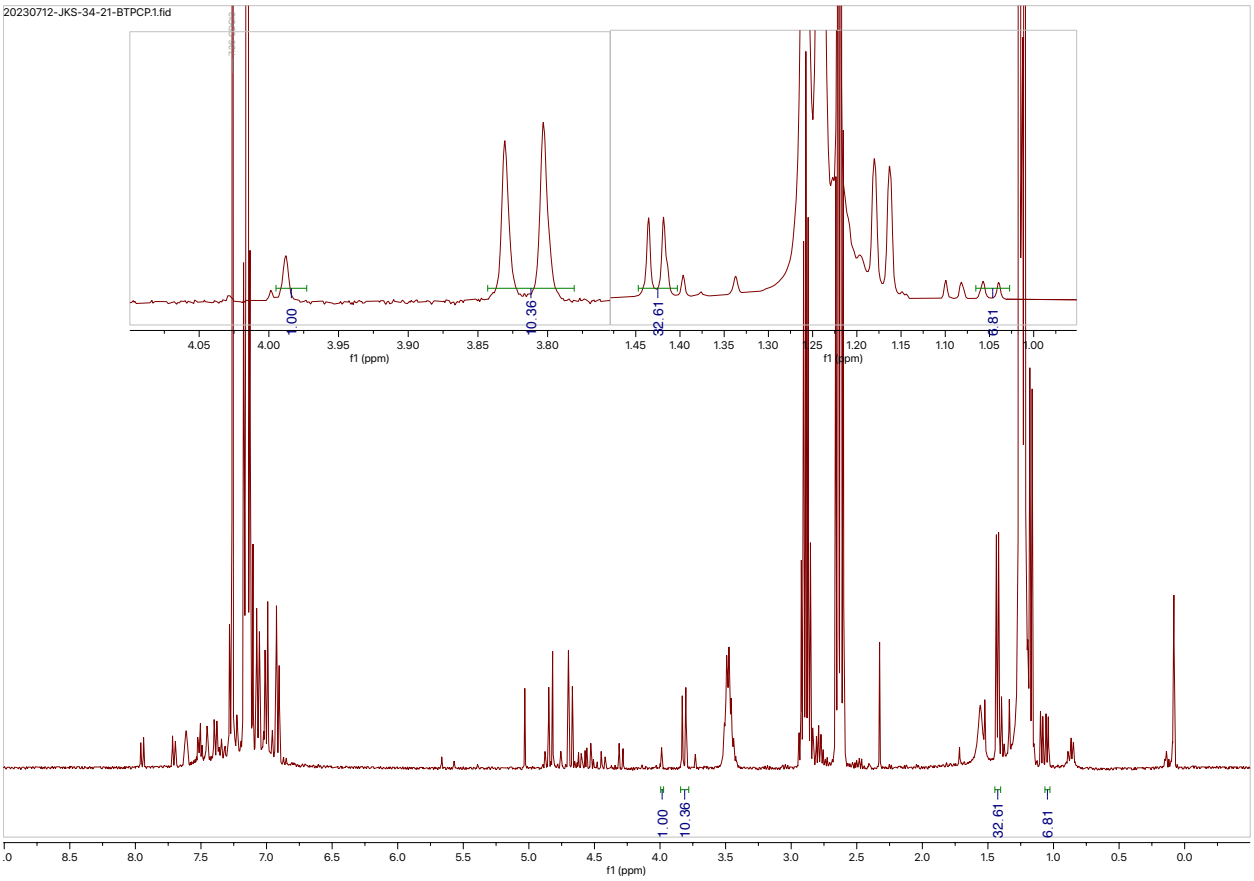
20230712-JKS-34-21-BTPCP1.fid
1.00
10.36
32.61
6.81
f1 (ppm)

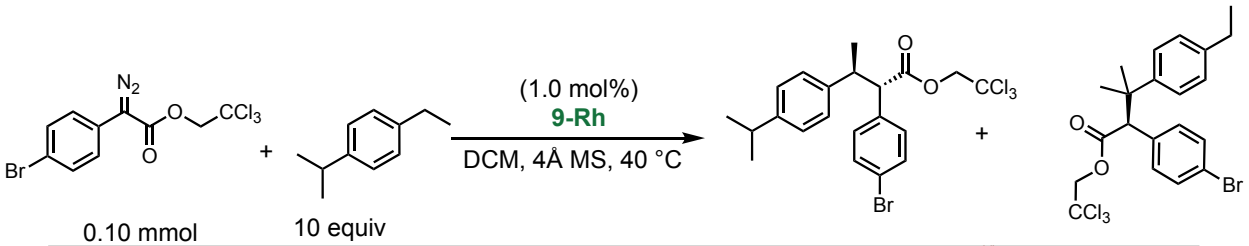

0.10 mmol 10 equiv

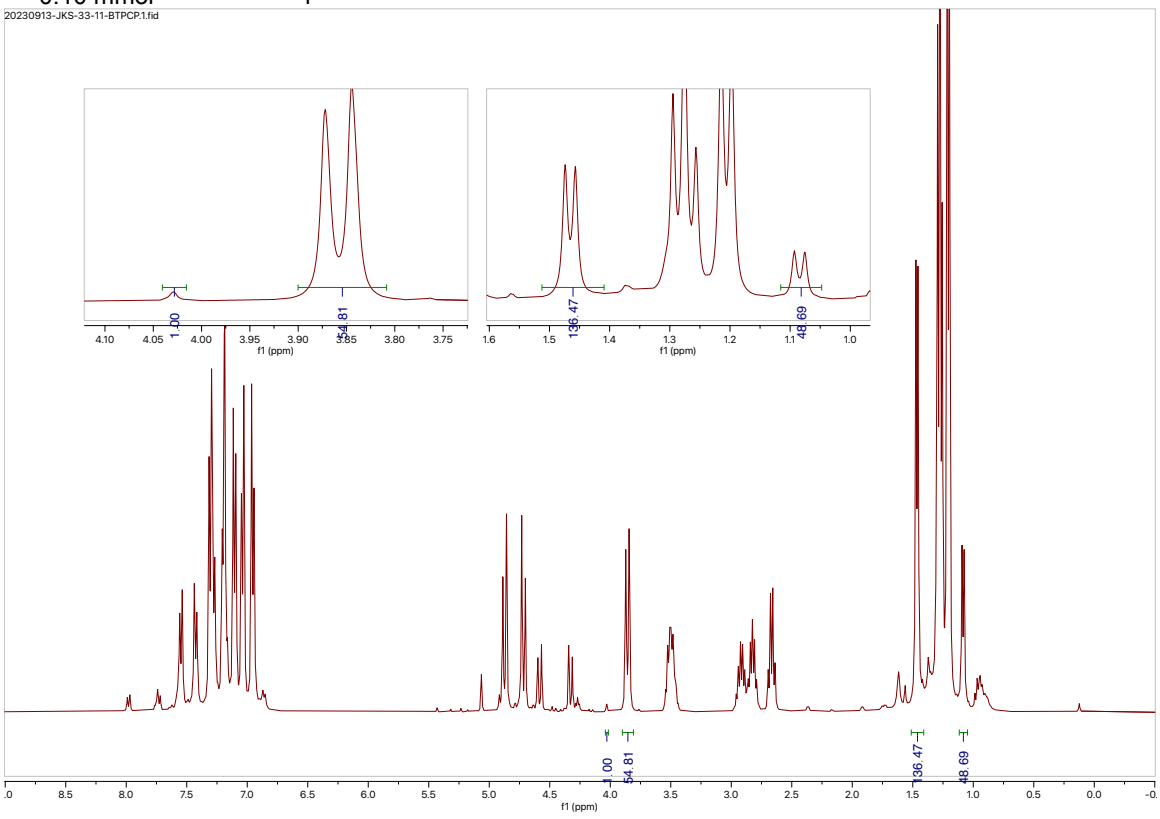

Regioselectivity and diastereoselectivity determination for reactions with tert-butylcyclohexane

Regioselectivity and diastereoselectivity were determined through previously reported analysis.[4]

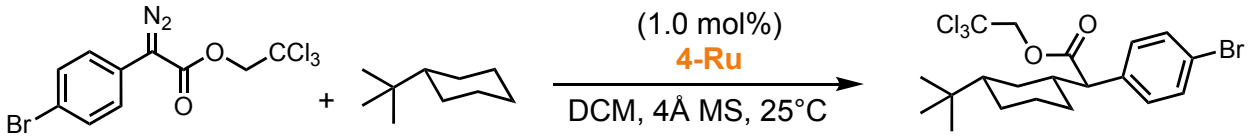

0.20 mmol 5 equiv

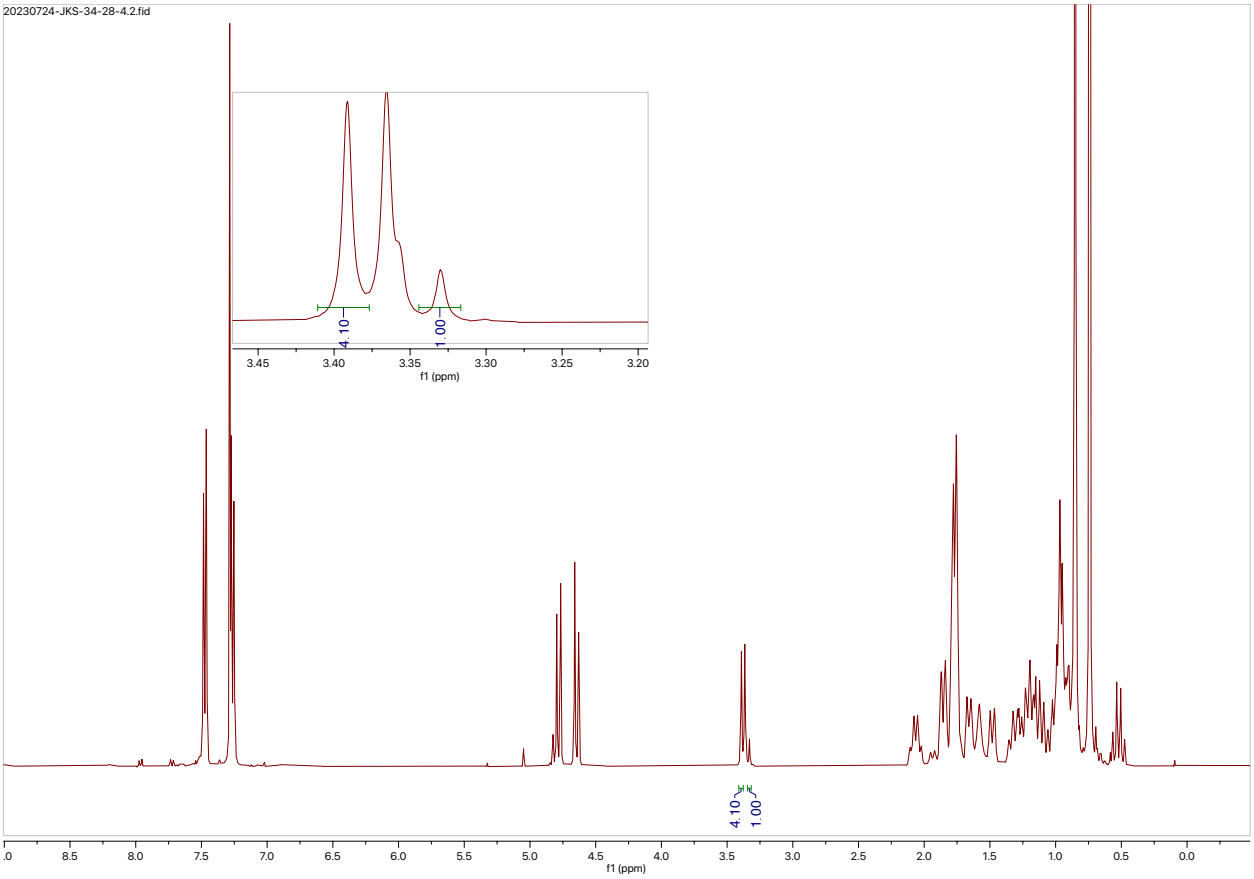

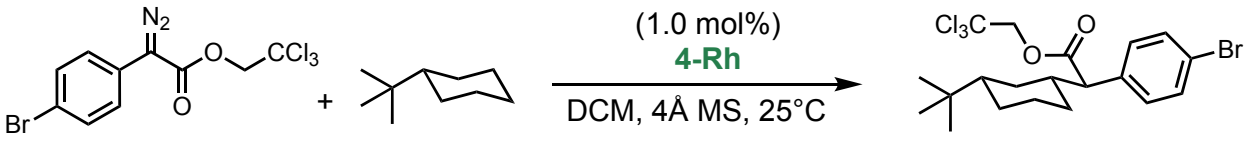

0.20 mmol

5 equiv

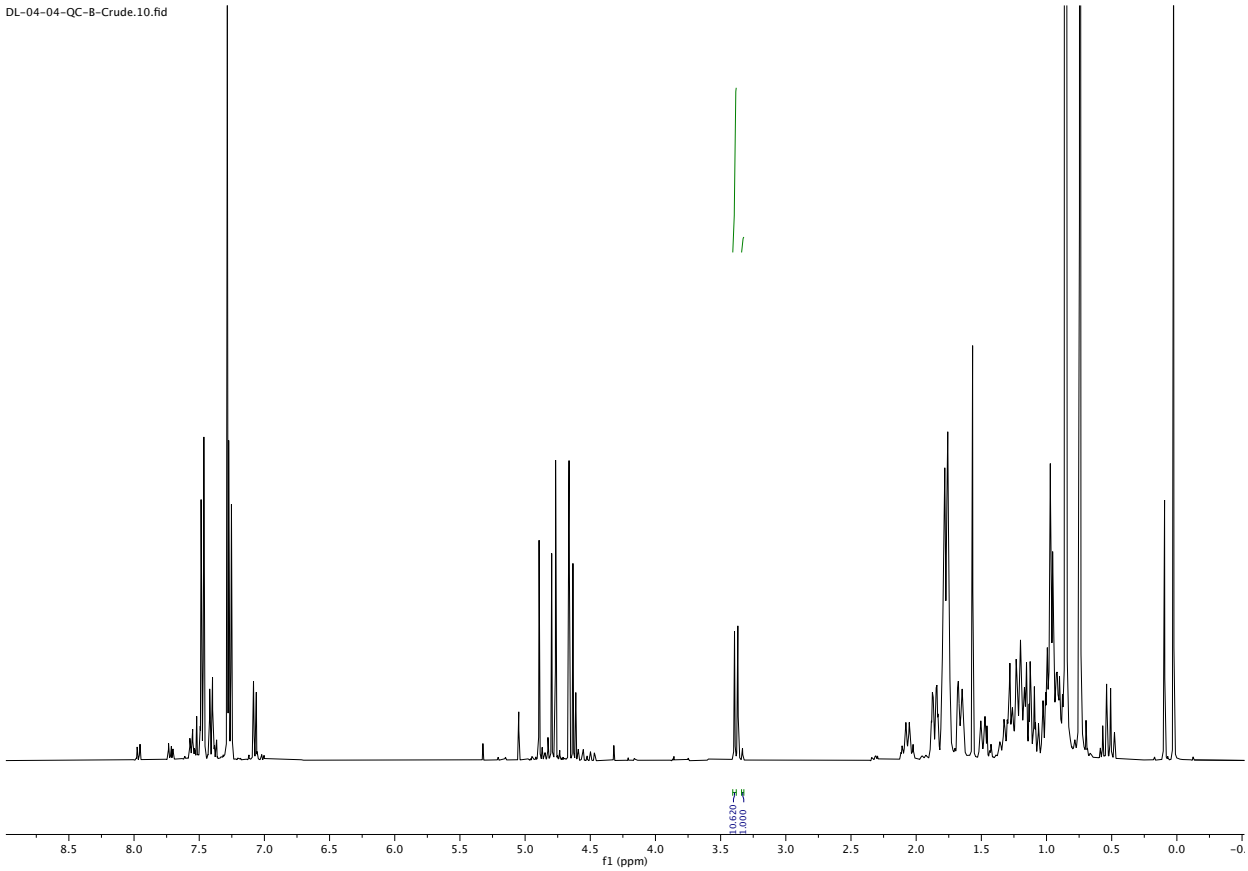

Regioselectivity and diastereoselectivity determination for reactions with pentane.

Regioselectivity and diastereoselectivity were determined through previously reported analysis.[5]

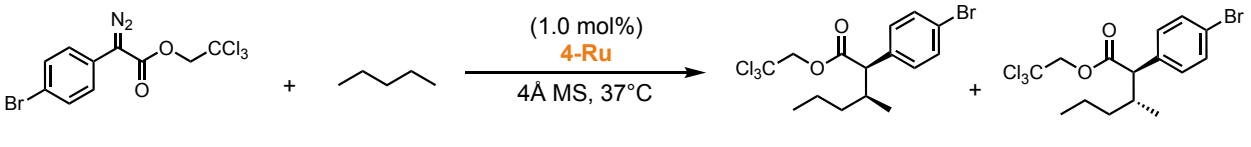

0.20 mmol solvent

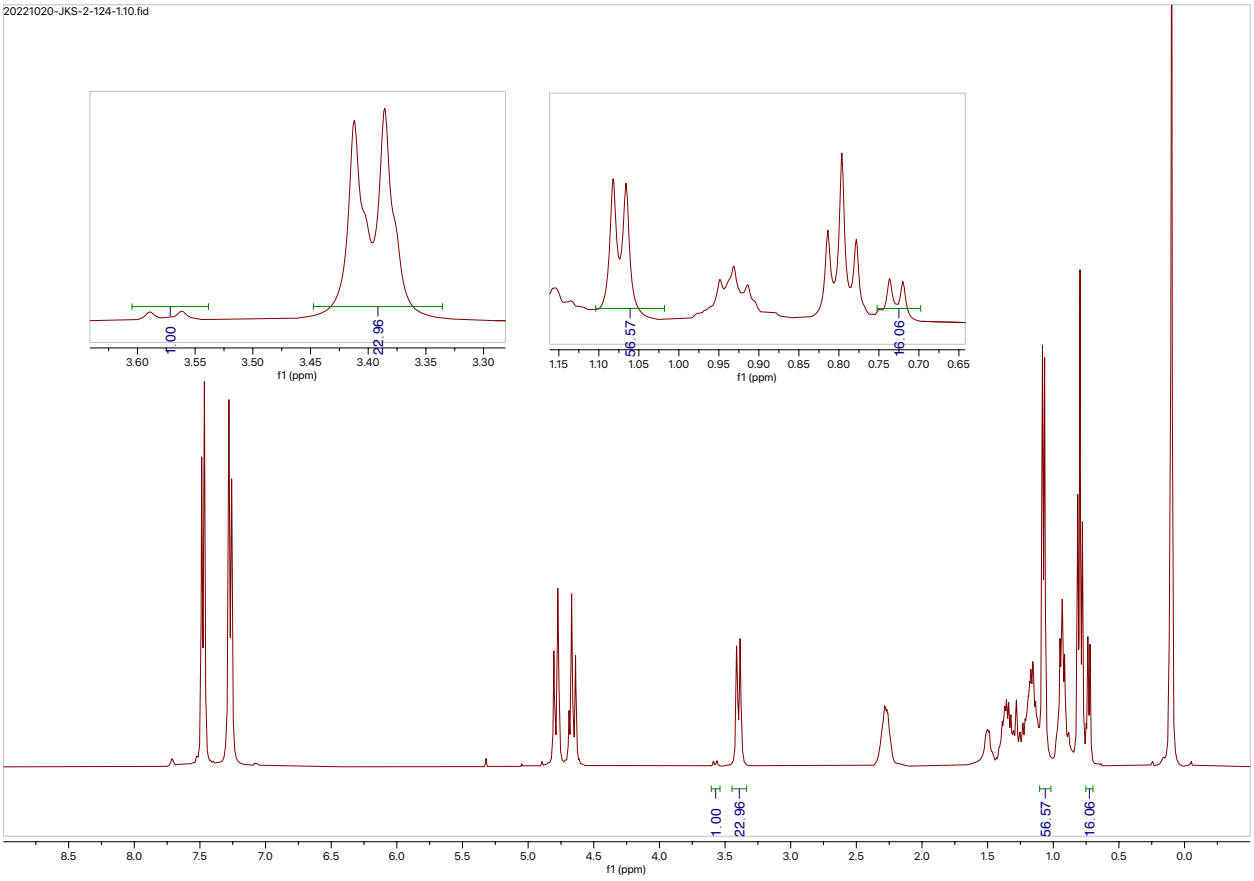

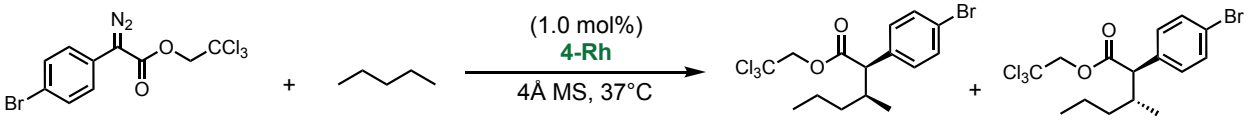

0.20 mmol solvent

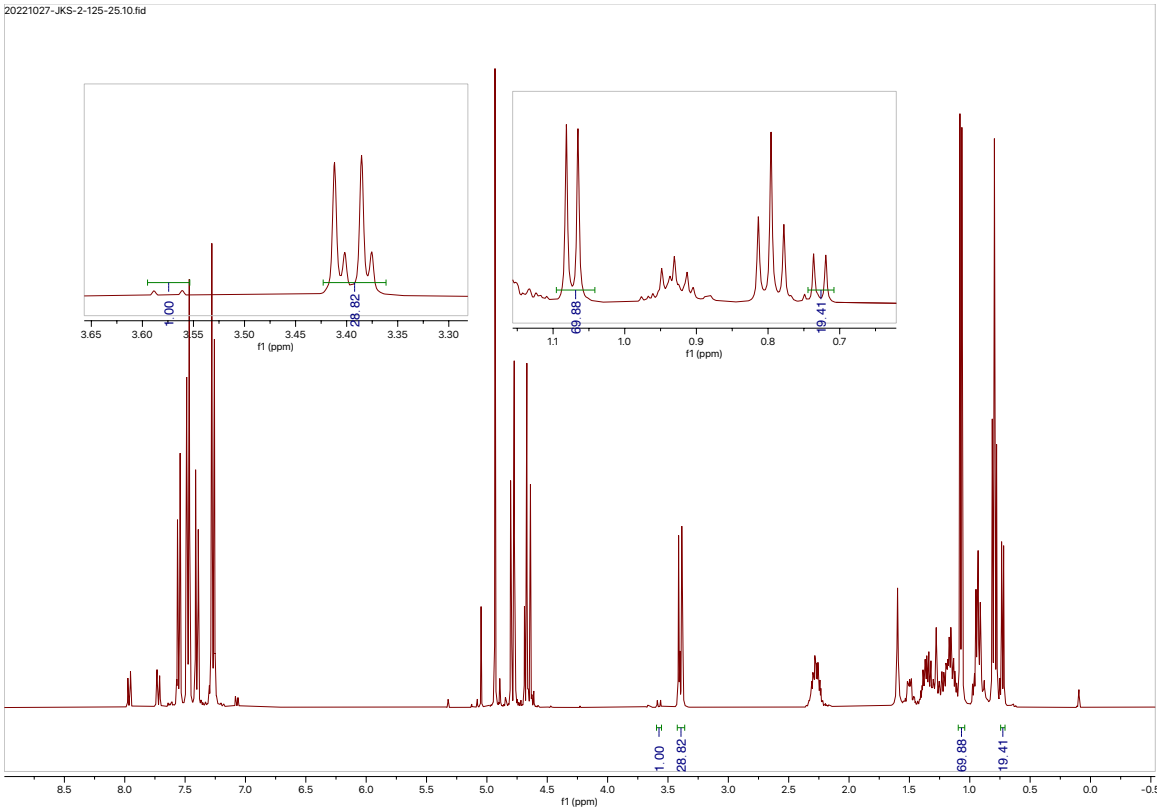

Regioselectivity and diastereoselectivity determination for reactions with 2-hexene.

The regioselectivity was determined through integration between dd at 3.72 ppm (primary insertion) and two doublets at 3.54 ppm (secondary insertion with diastereomer). Diastereomers of secondary insertion product was determined through integration of triplet at 0.77 ppm and triplet at 0.91 ppm.

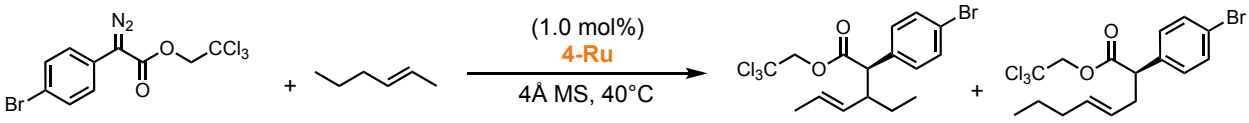

0.20 mmol 10 equiv

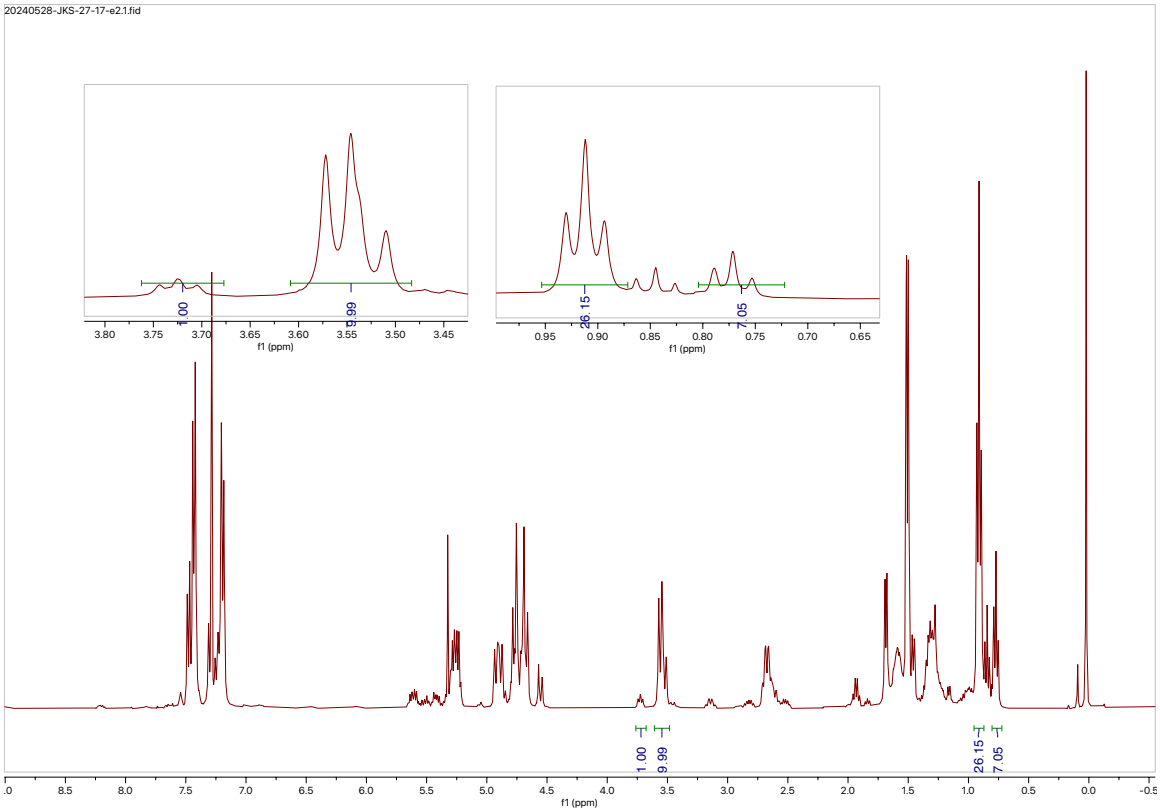

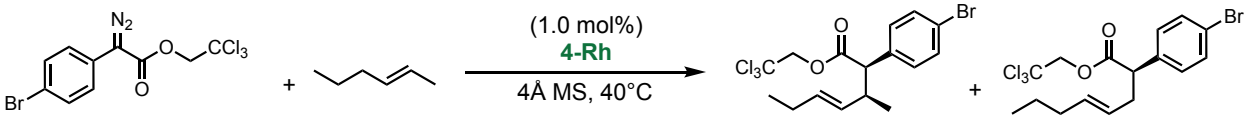

0.20 mmol

10 equiv

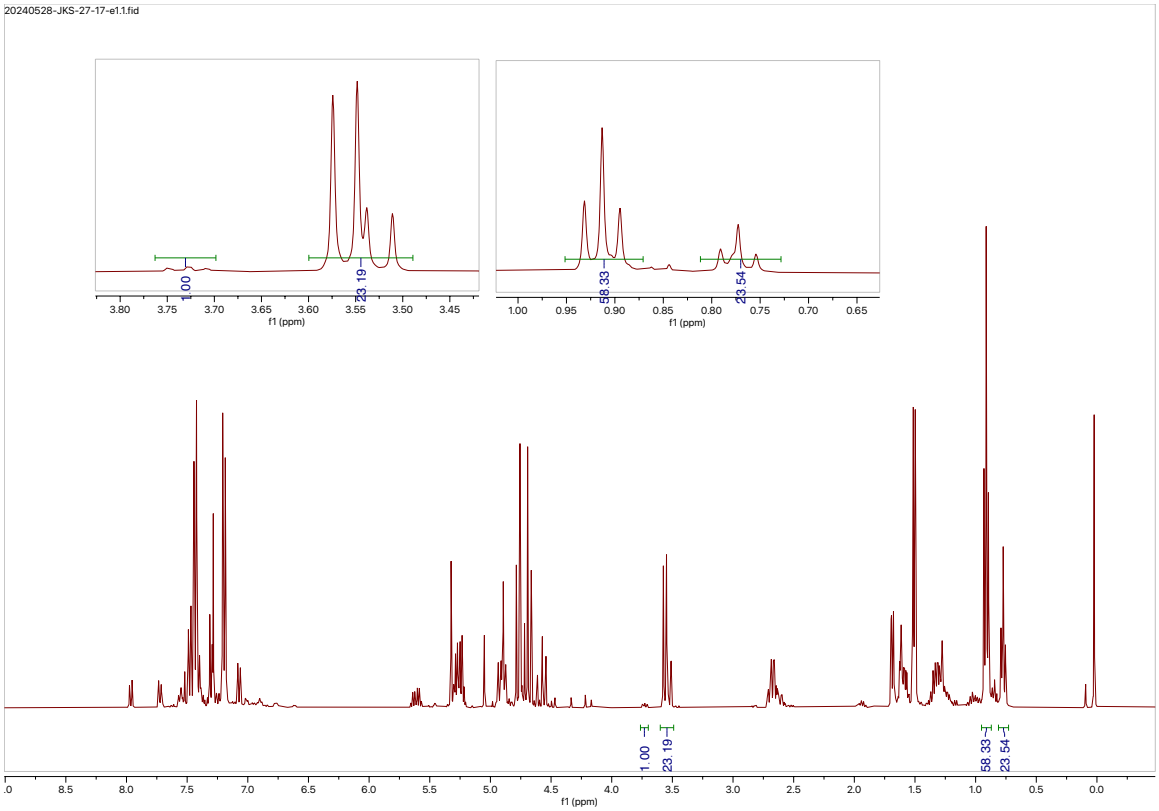

Regioselectivity and diastereoselectivity determination for reactions with tetrahydrofuran.

The regioselectivity was determined through comparing integration of the multiplets at 4.75 ppm and 4.52 ppm.

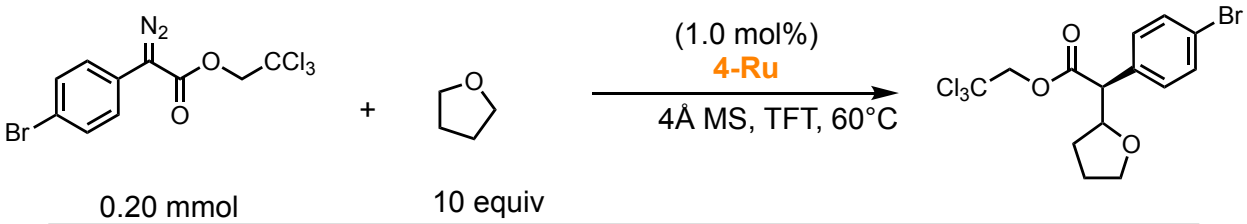

0.20 mmol 10 equiv

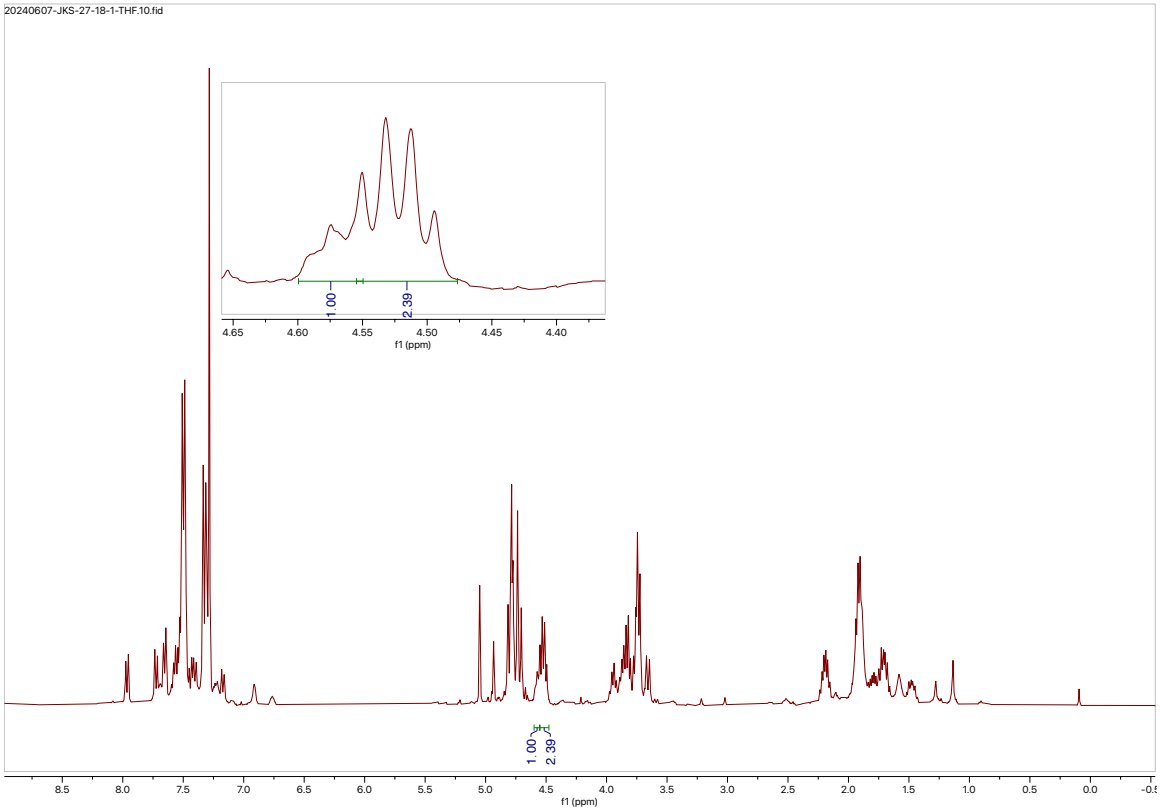

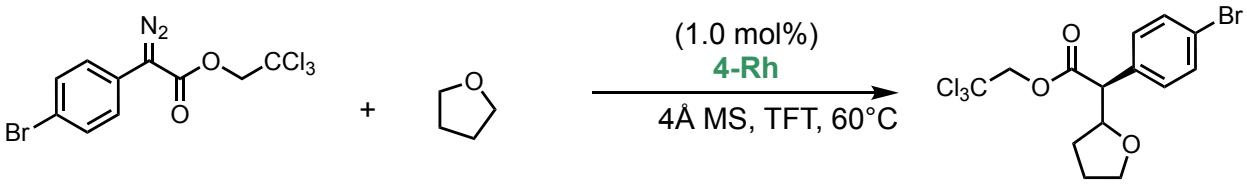

0.20 mmol

10 equiv

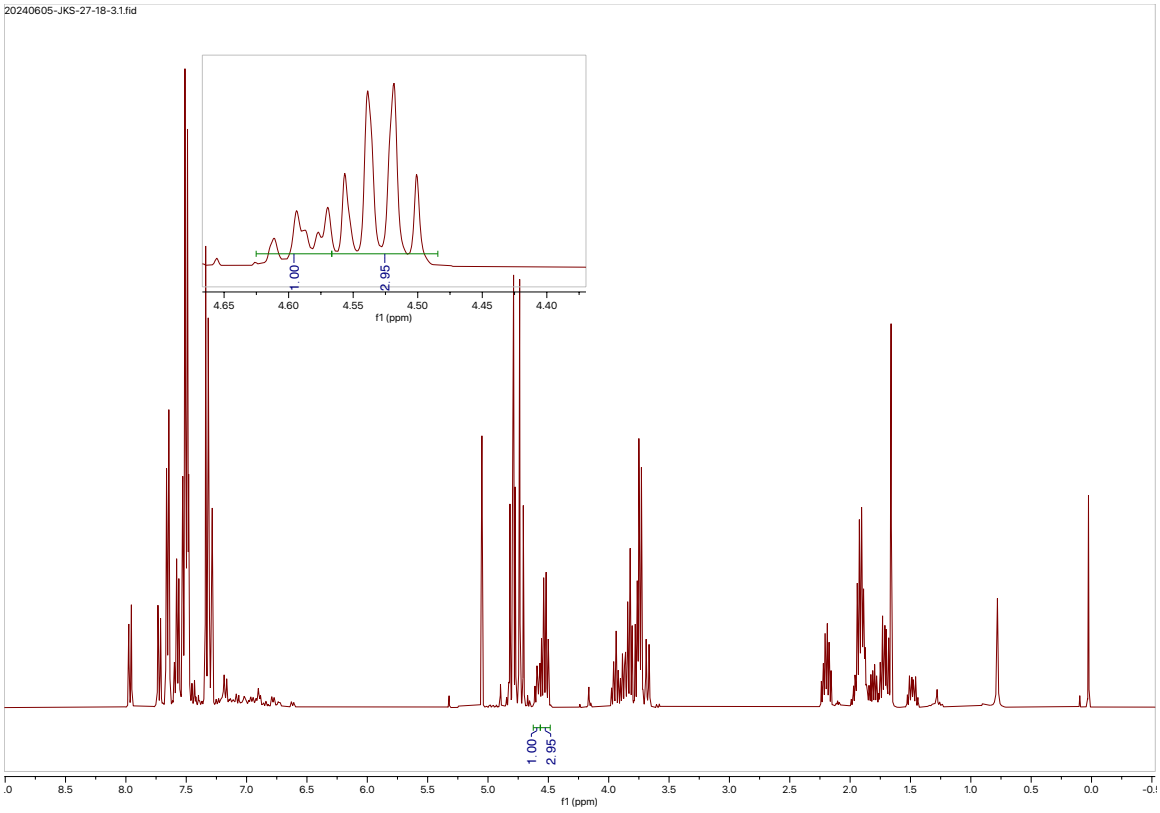

Regioselectivity Determination for Competition Reactions:

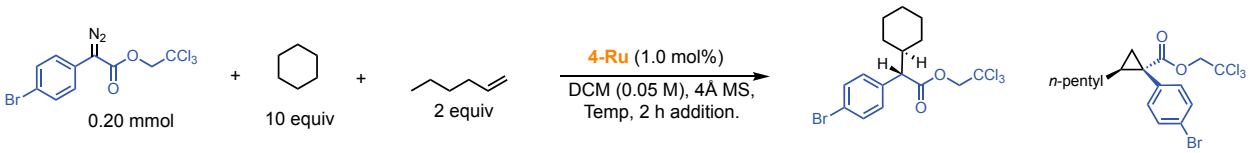

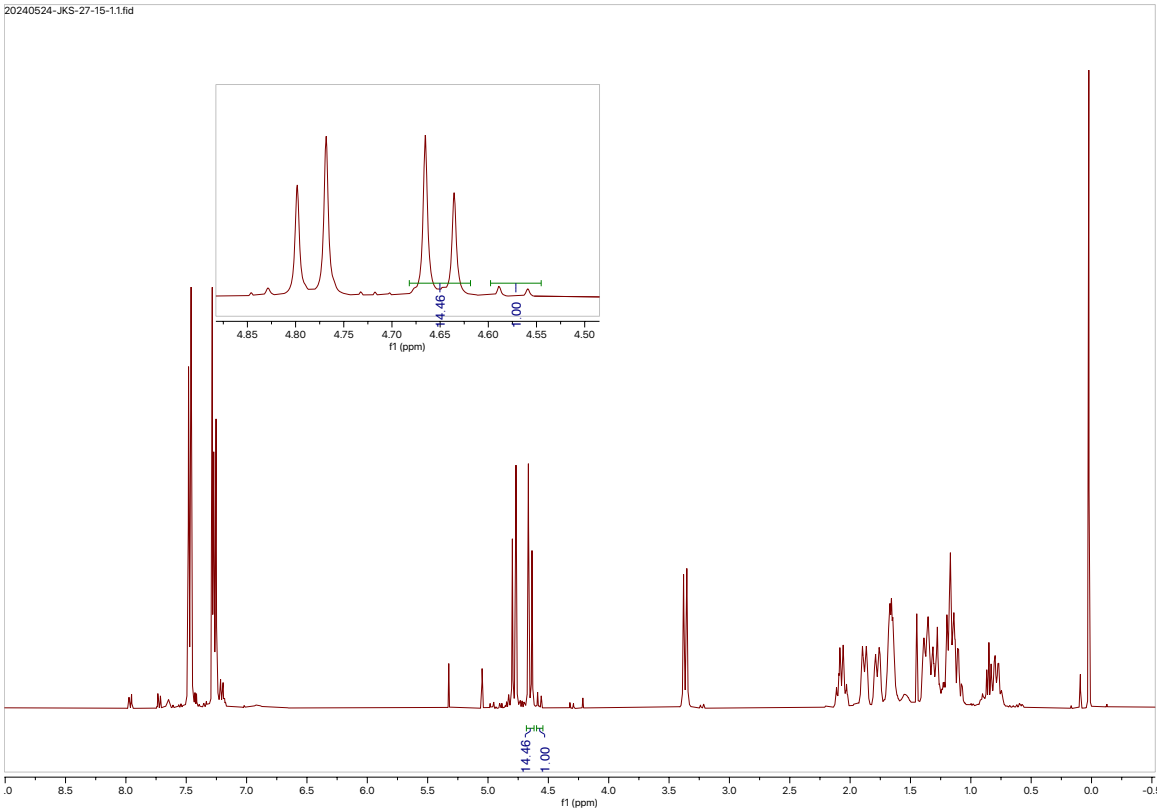

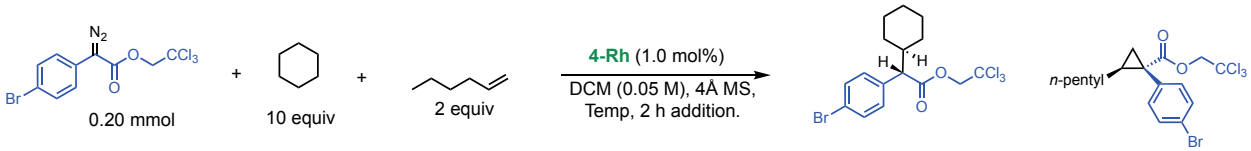
0.20 mmol
10 equiv
2 equiv
4-Rh (1.0 mol%)
DCM (0.05 M), 4Å MS,
Temp, 2 h addition.
n-pentyl

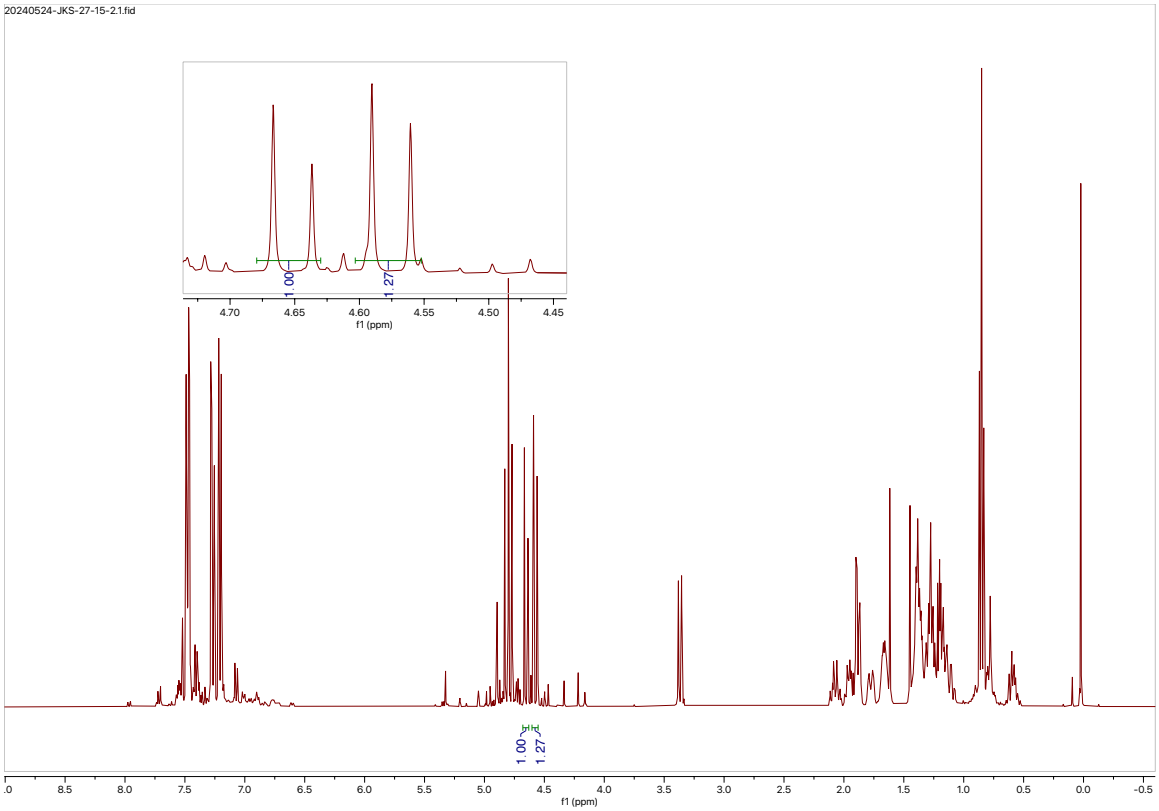
20240524-JKS-27-15-2.1.fid
1.00
1.27
f1 (ppm)

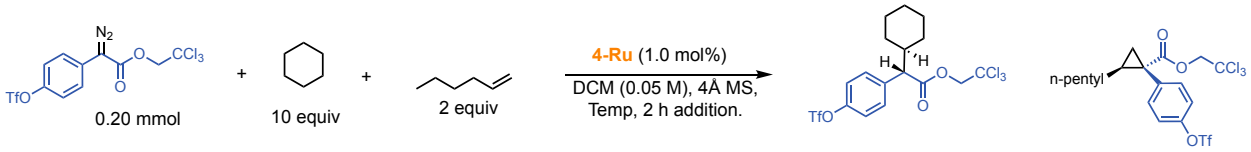
N2
CCl3
TfO
0.20 mmol
10 equiv
2 equiv
4-Ru (1.0 mol%)
DCM (0.05 M), 4Å MS,
Temp, 2 h addition.
H
H
n-pentyl
OTf

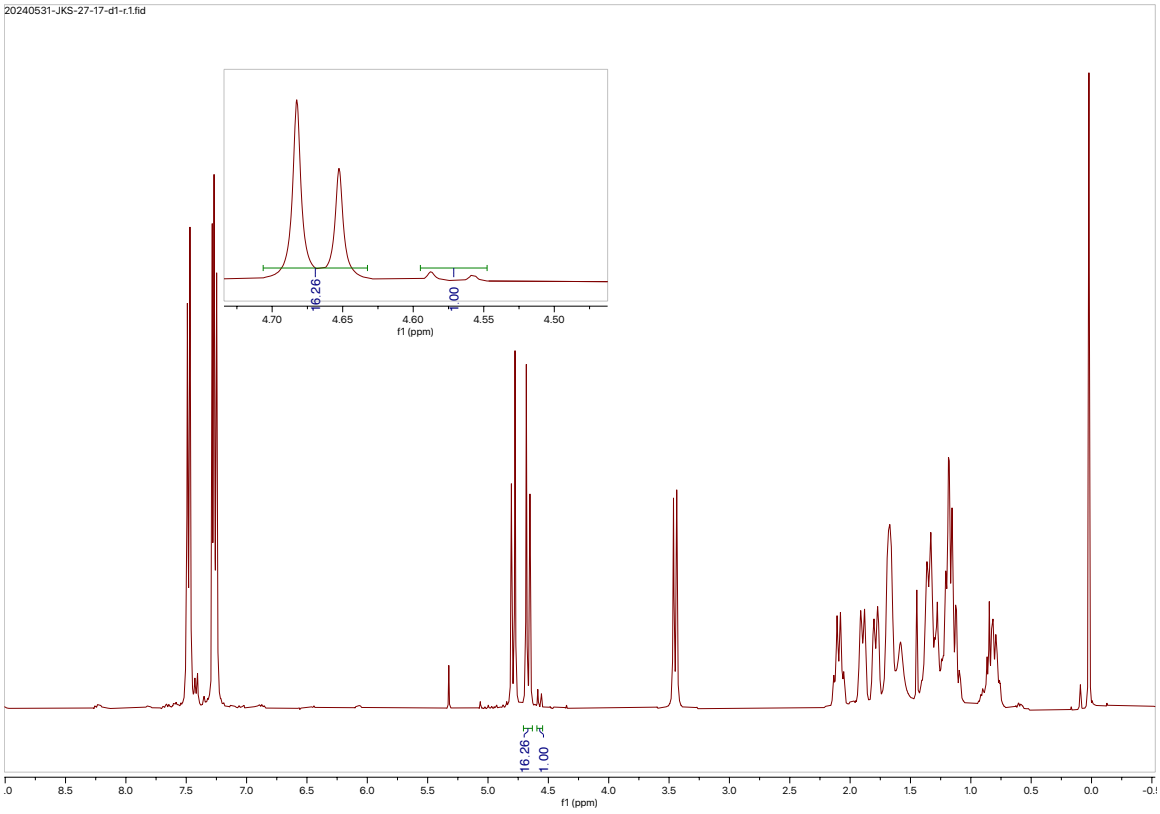
20240531-JKS-27-17-d1-r.1.fid
16.26
1.00
4.70
4.65
4.60
4.55
4.50
f1 (ppm)
16.26
1.00
8.5
8.0
7.5
7.0
6.5
6.0
5.5
5.0
4.5
4.0
3.5
3.0
2.5
2.0
1.5
1.0
0.5
0.0
f1 (ppm)

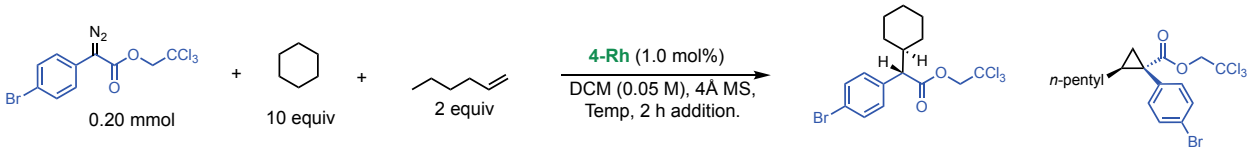
0.20 mmol
10 equiv
2 equiv
4-Rh (1.0 mol%)
DCM (0.05 M), 4Å MS,
Temp, 2 h addition.
n-pentyl

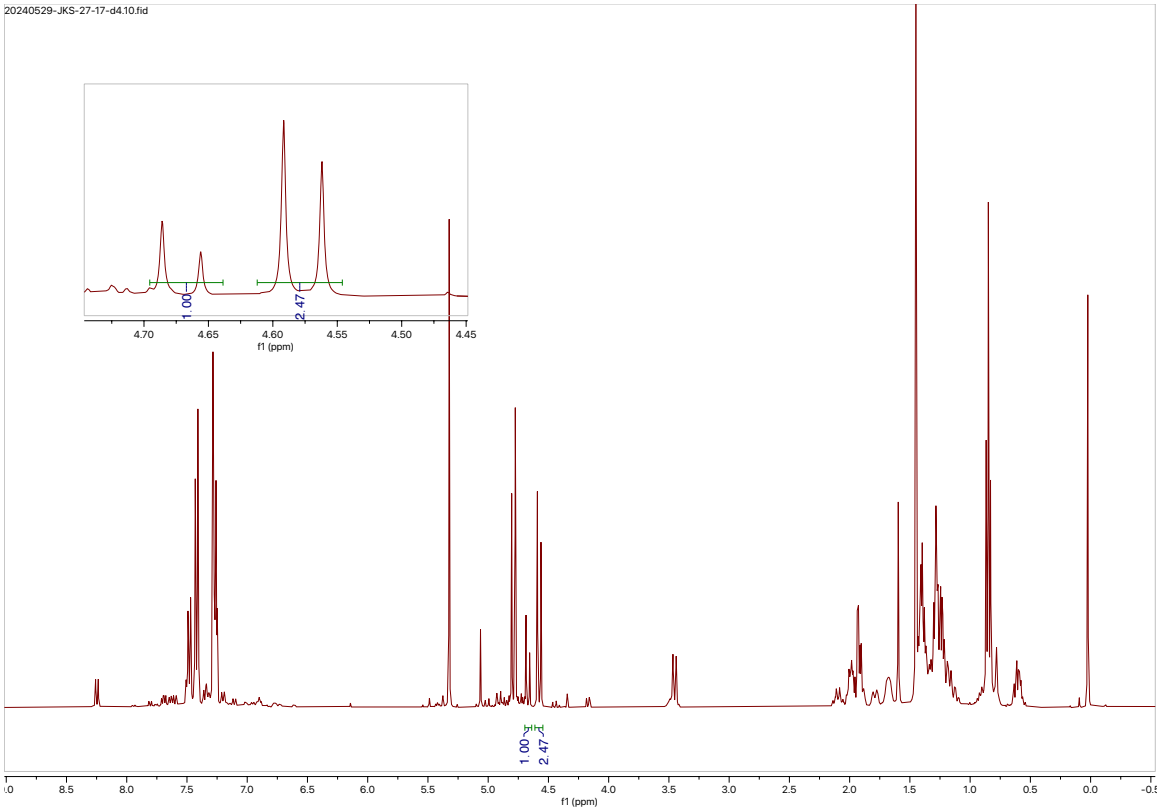
20240529-JKS-27-17-d4.10.fid
1.00
2.47
f1 (ppm)

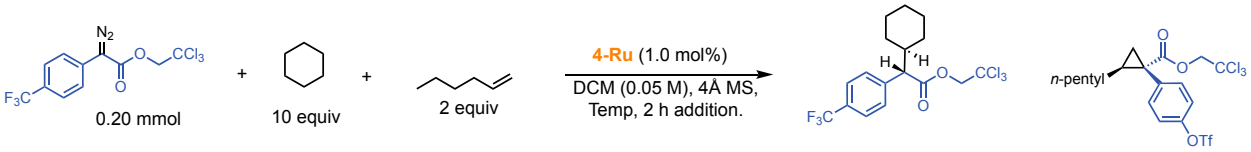
0.20 mmol
10 equiv
2 equiv
4-Ru (1.0 mol%)
DCM (0.05 M), 4Å MS,
Temp, 2 h addition.
n-pentyl
OTf

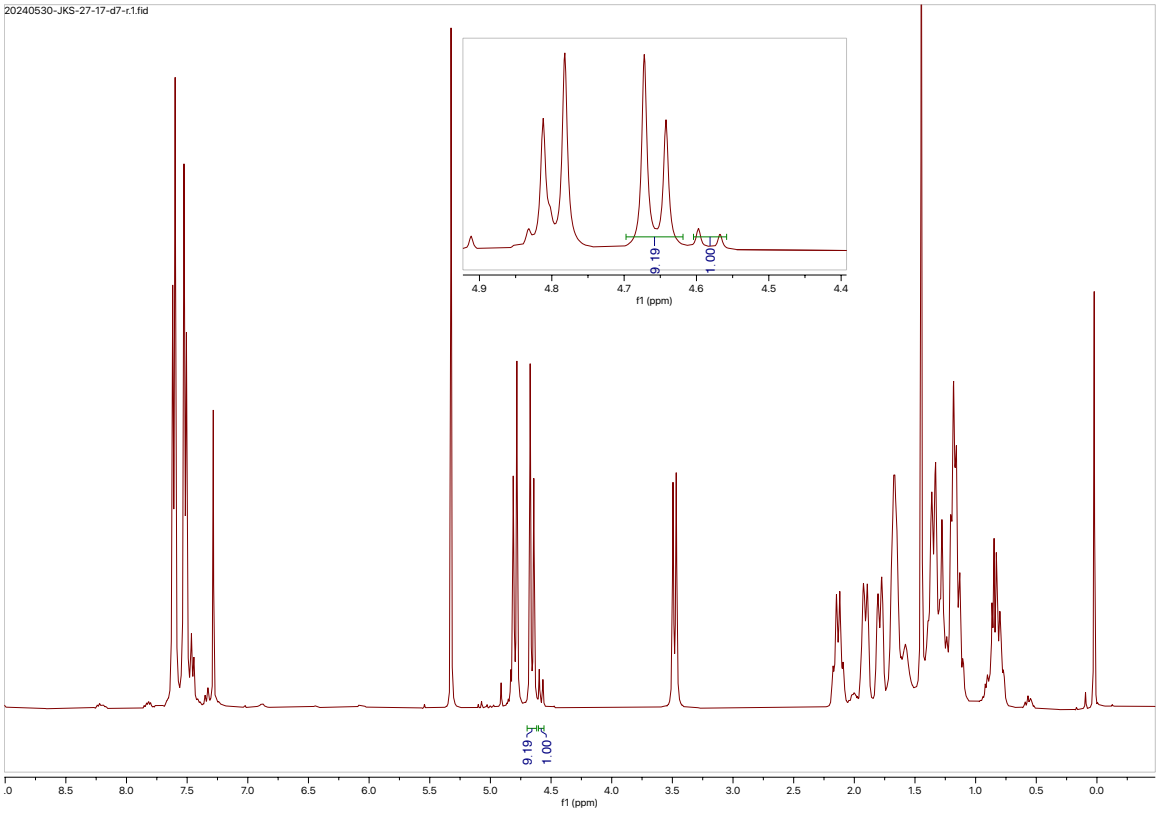
20240530-JKS-27-17-d7-r.1.fid
9.19
1.00
f1 (ppm)

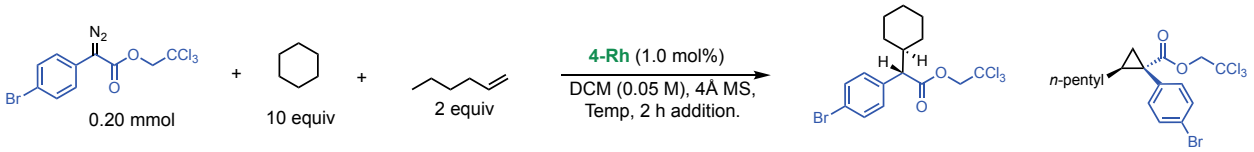
0.20 mmol
10 equiv
2 equiv
4-Rh (1.0 mol%)
DCM (0.05 M), 4Å MS,
Temp, 2 h addition.
n-pentyl

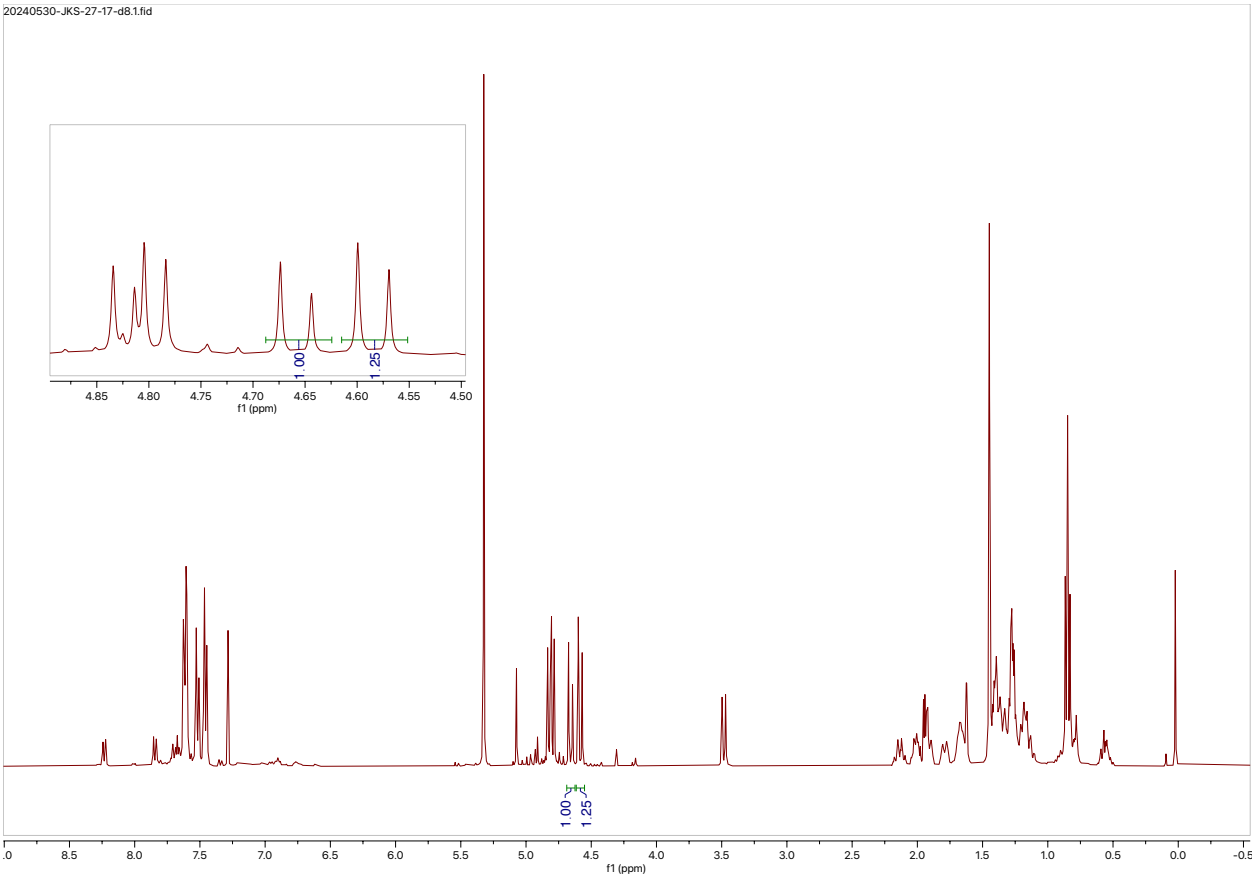
20240530-JKS-27-17-d8.1.fid
1.00
1.25
f1 (ppm)

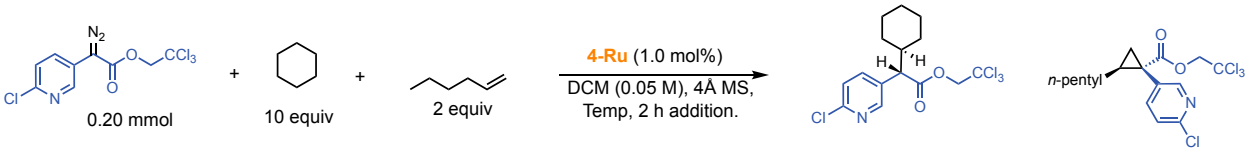
0.20 mmol
10 equiv
2 equiv
4-Ru (1.0 mol%)
DCM (0.05 M), 4Å MS,
Temp, 2 h addition.
n-pentyl

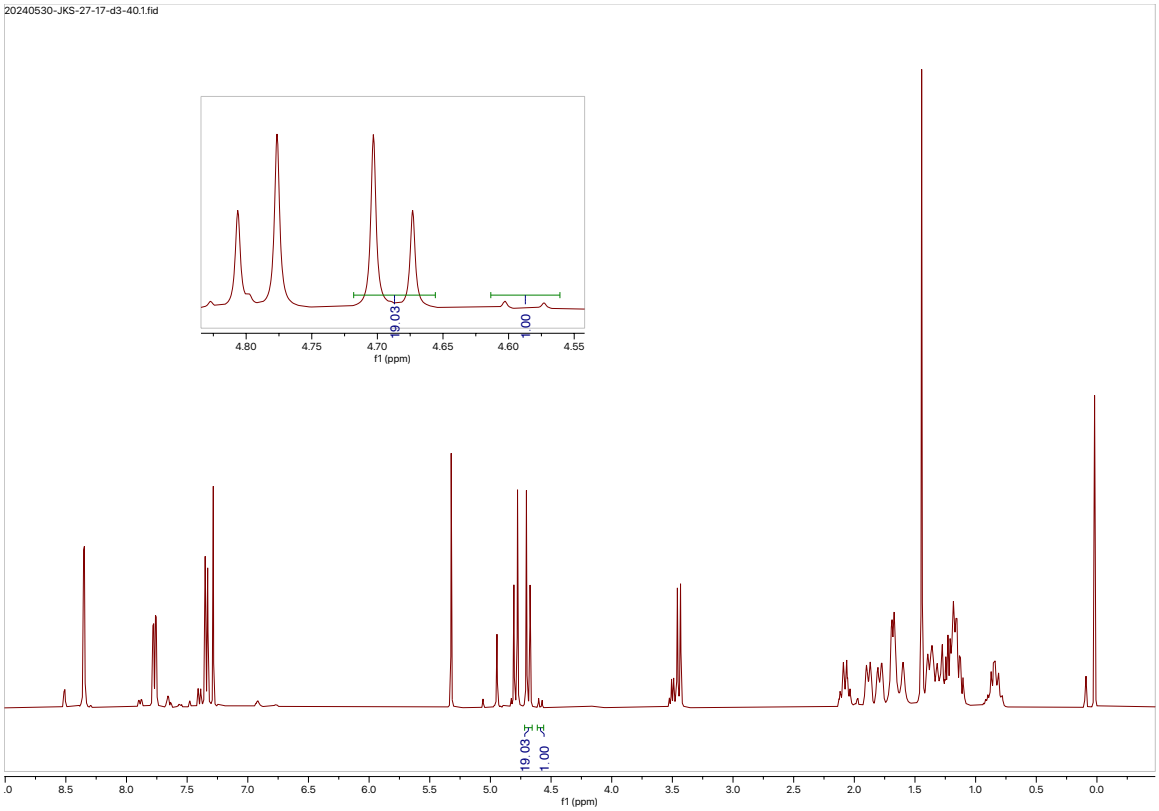
20240530-JKS-27-17-d3-40.1.fid
19.03
1.00
f1 (ppm)

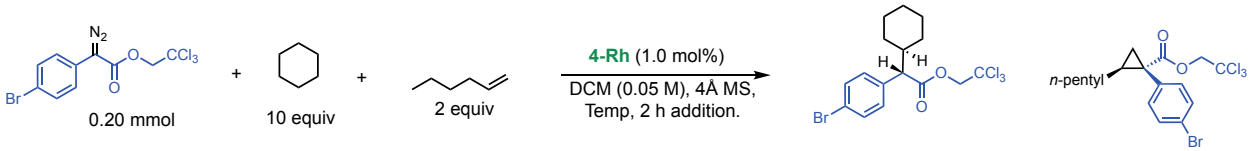
0.20 mmol
10 equiv
2 equiv
4-Rh (1.0 mol%)
DCM (0.05 M), 4Å MS,
Temp, 2 h addition.
n-pentyl

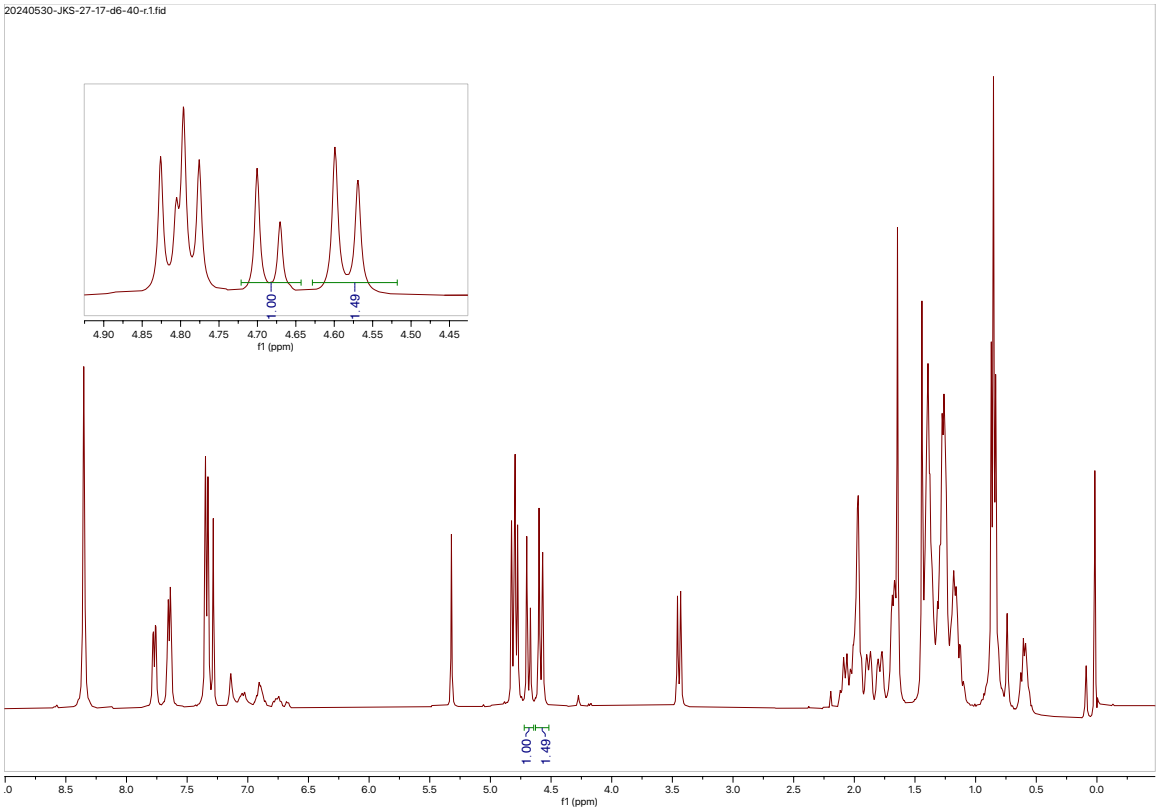
20240530-JKS-27-17-d6-40-r.1.fid
1.00
1.49
f1 (ppm)

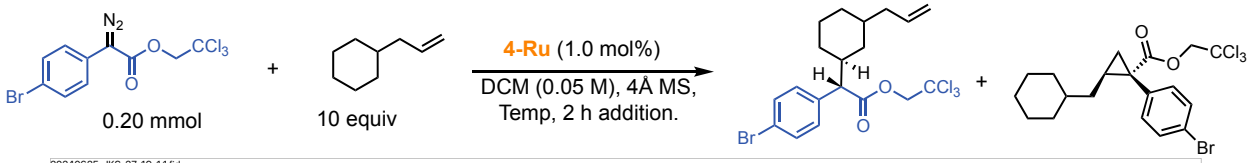
0.20 mmol
10 equiv
4-Ru (1.0 mol%)
DCM (0.05 M), 4Å MS,
Temp, 2 h addition.

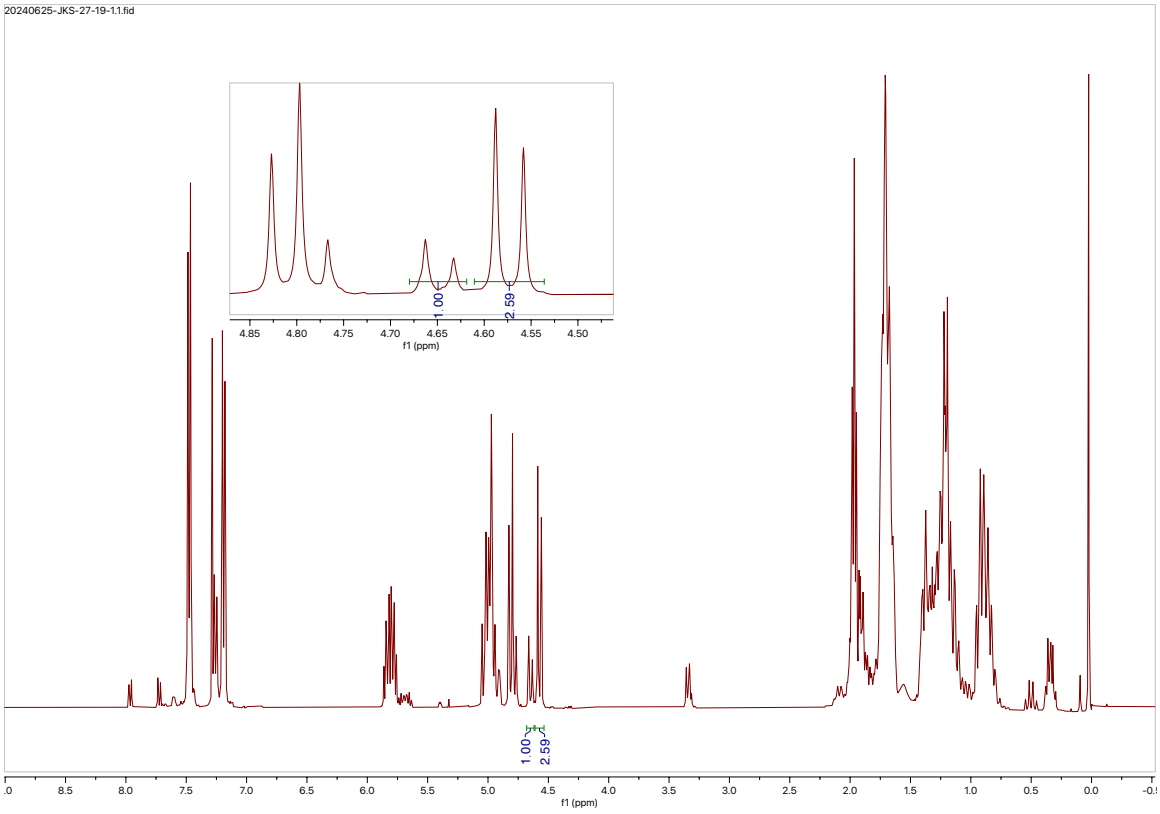
20240625-JKS-27-19-1.1.fid
f1 (ppm)

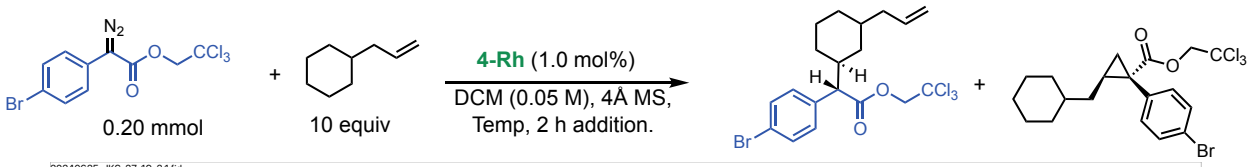
0.20 mmol
10 equiv
4-Rh (1.0 mol%)
DCM (0.05 M), 4Å MS,
Temp, 2 h addition.

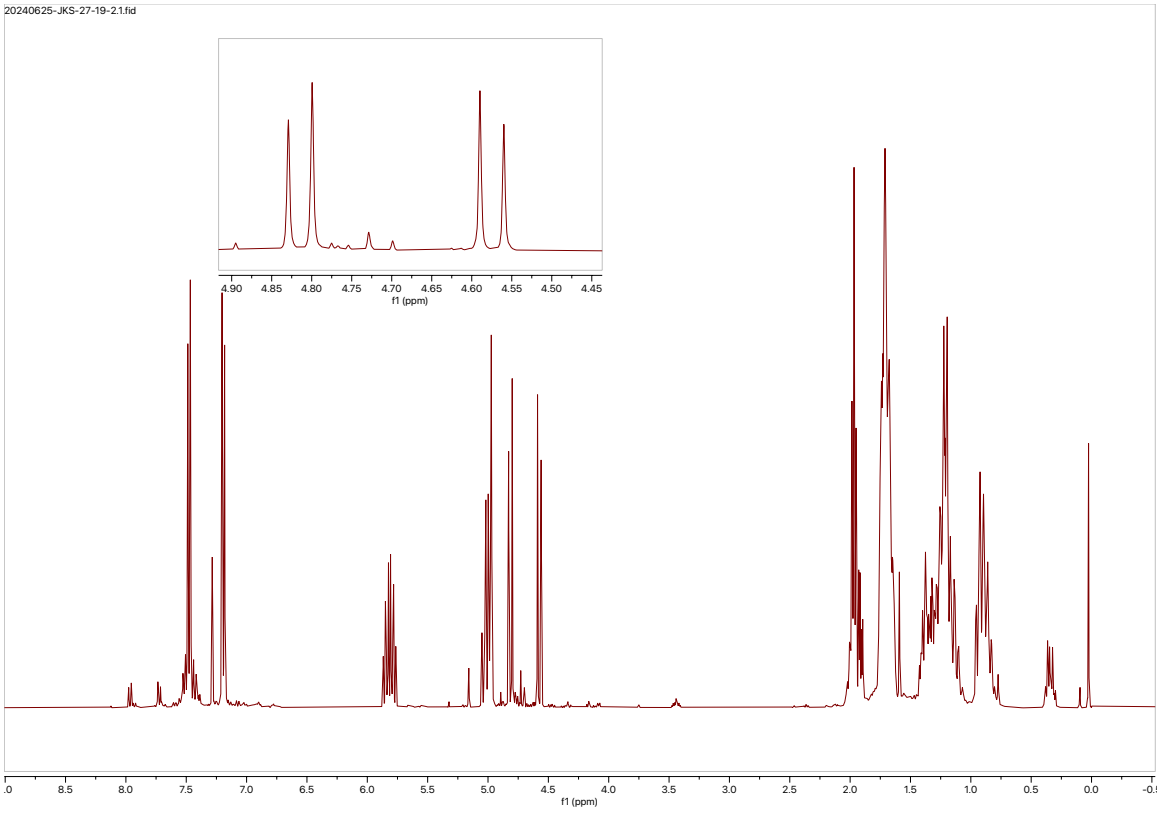
20240625-JKS-27-19-2.1.fid
f1 (ppm)

C–H Insertion Reactions

General Procedure 1

To a flame-dried 16 mL vial equipped with a stir bar and 4 Å MS (1.0 g for 100 mg of diazo) was added catalyst (xx mol %, xx μmol) and substrate (10 equiv, 2.0 mmol). DCM (2 mL) was added to dissolve the sample, and the solution was heated to 40 °C. Then, diazo (1 equiv, 0.200 mmol) was dissolved in DCM (2 mL) and added via syringe pump over the course of 2 h. The solution was left to stir overnight at which point it was stopped, passed over a small plug of celite to remove the mol sieve dust, and concentrated in vacuo for crude NMR analysis.

General Procedure 2

To a flame-dried 16 mL vial equipped with a stir bar and 4 Å MS (1.0 g for 100 mg of diazo) was added catalyst (1.0 mol %, 2.0 μmol) and substrate (5 equiv, 2.0 mmol). DCM (2 mL) was added to dissolve the sample, and the solution was set to stir at 25 °C. Then, diazo (1 equiv, 0.200 mmol) was dissolved in DCM (2 mL) and added via syringe pump over the course of 2 h. The solution was left to stir overnight at which point it was stopped, passed over a small plug of celite to remove the mol sieve dust, and concentrated in vacuo for crude NMR analysis.

General Procedure 3

To a flame-dried 16 mL vial equipped with a stir bar and 4 Å MS (1.0 g for 100 mg of diazo) was added catalyst (1.0 mol%, 2.00 μmol) and substrate (solvent equiv, 2.0 mL). The solution was heated to reflux. Then, diazo (1 equiv, 0.200 mmol) was dissolved in the substrate (2 mL) and added via syringe pump over the course of 2 h. The solution was left to stir overnight at which point it was stopped, passed over a small plug of celite to remove the mol sieve dust, and concentrated in vacuo for crude NMR analysis.

General Procedure 4

To a flame-dried 16 mL vial equipped with a stir bar and 4 Å MS (1.0 g for 100 mg of diazo) was added catalyst (1.0 mol%, 2.00 μmol) and substrate (10 equiv, 2.0 mmol)

Trifluorotoluene (TFT) (2 mL) was added to dissolve the sample, and the solution was set to stir at 60 °C. Then, diazo (1 equiv, 0.200 mmol) was dissolved in TFT (2 mL) and added via syringe pump over the course of 2 h. The solution was left to stir overnight at which point it was stopped, passed over a small plug of celite to remove the mol sieve dust, and concentrated in vacuo for crude NMR analysis.

trichloro-η^6-methyl (*S*)-2-(4-bromophenyl)-3-(4-isopropylphenyl)propanoate (12)

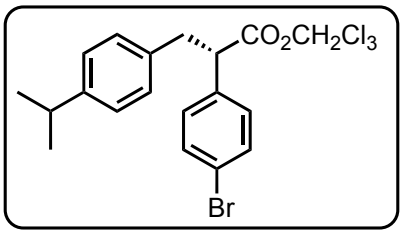

General procedure 1 was employed for the C–H insertion into *p*-cymene (313 µL, 10 equiv, 2.0 mmol), with 2,2,2-trichloroethyl 2-(4-bromophenyl)-2-diazoacetate (74.5 mg, 0.20 mmol, 1.0 equiv) using Ru_2(*S*-PTAD)$_4$BArF (24.2 mg, 5.0 mol%) as catalyst. The crude material was purified via column chromatography (2% diethyl ether/hexanes) to afford the title compound at white amorphous solid (70.1 mg, 73%). Spectra matched literature precedent.[6]

^{1}H NMR (400 MHz, $CDCl_3$): δ 7.45 (d, J = 8.4 Hz, 2H), 7.25 (d, J = 8.5 Hz, 2H), 7.09 (q, J = 8.3 Hz, 4H), 4.69 (d, J = 12.0 Hz, 1H), 4.60 (d, J = 12.0 Hz, 1H), 3.96 (dd, J = 9.1, 6.5 Hz, 1H), 3.40 (dd, J = 13.9, 9.1 Hz, 1H), 3.04 (dd, J = 13.9, 6.6 Hz, 1H), 2.85 (p, J = 6.8 Hz, 1H), 1.21 (d, J = 6.9 Hz, 6H).

Chiral HPLC: The enantiopurity was determined to be 93:7 er by chiral HPLC analysis. (Chiracel AD-H, 1.0% IPA/Hexane, 1.0 mL/min, λ=230 nm, RT: Major: 6.0 min, Minor: 6.6 min.).

trichloro-η^6-methyl (2*S*,3*S*)-2-(4-bromophenyl)-3-(4-isopropylphenyl)butanoate (15a, 15b)

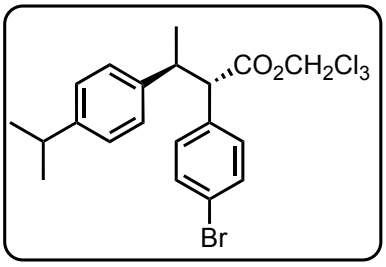

General procedure 1 was employed in the C–H insertion into 1-ethyl-4-isopropylbenzene (148.3 mg, 1.0 mmol, 10 equiv) with 2,2,2-trichloroethyl 2-(4-bromophenyl)-2-diazoacetate (37.2 mg, 0.10 mmol, 1.0 equiv) using Ru_2(*S*-TPPTTL)$_4$BAr^F (16.6 mg, 5.0 mol%) as catalyst. The crude material was purified via prep-TLC (2.5% diethyl ether in hexanes) to afford the title compound as a clear oil (25.5 mg, 52%).

Reported as a 4:1 mixture of diastereomers. Major diastereomer:

^{1}H NMR (400 MHz, $CDCl_3$): δ 7.27 (d, J = 8.5 Hz, 2H), 7.06 (d, J = 8.5 Hz, 2H), 7.00 (d, J = 8.0 Hz, 2H), 6.91 (d, J = 8.0 Hz, 2H), 4.83 (d, J = 12.0 Hz, 1H), 4.68 (d, J = 11.9 Hz, 1H), 3.81 (d, J = 11.0 Hz, 1H), 3.54 – 3.39 (m, 1H), 2.78 (p, J = 6.9 Hz, 1H), 1.42 (d, J = 6.8 Hz, 3H), 1.17 (dd, J = 6.9, 1.1 Hz, 6H).

Minor diastereomer:

^{1}H NMR (400 MHz, $CDCl_3$): δ 7.51 (d, J = 8.4 Hz, 2H), 7.38 (d, J = 8.4 Hz, 2H), 7.23 (d, J = 8.2 Hz, 2H), 7.15 (d, J = 8.0 Hz, 2H), 4.54 (d, J = 11.9 Hz, 1H), 4.29 (d, J = 12.0 Hz, 1H), 3.81 (d, J = 11.0 Hz, 1H), 3.54 – 3.36 (m, 1H), 2.86 (p, J = 7.1 Hz, 1H), 1.22 (d, J = 7.1 Hz, 6H), 1.04 (d, J = 7.0 Hz, 3H).

^{13}C NMR (101 MHz, $CDCl_3$): δ 171.6, 171.1, 147.5, 141.1, 139.9, 135.9, 131.9, 131.3, 130.4, 127.3, 126.7, 126.4, 121.9, 121.3, 94.7, 74.3, 74.0, 58.9, 43.1, 33.7, 33.5, 30.3, 23.9, 21.1, 20.0.

HMRS (-n APCI): calcd for $C_{21}H_{21}O_2{}^{79}Br^{35}Cl_3$ (M–H) 488.9796, found 488.9797.

Chiral HPLC: The enantiopurity for the major diastereomer was determined to be 97:3 er and for the minor diastereomer determined to be 97:3 er by chiral HPLC analysis (Chiracel AD-H, 1.0% IPA/Hexane, 0.50 mL/min. , λ=230 nm, Major diastereomer: RT: 12.3 min. Major, 11.4 min. Minor. Minor diastereomer: RT: 14.0 min, Major. 13.3 min, Minor.).

2,2,2-trichloroethyl (*R*)-2-(4-bromophenyl)-2-cyclohexylacetate (18)

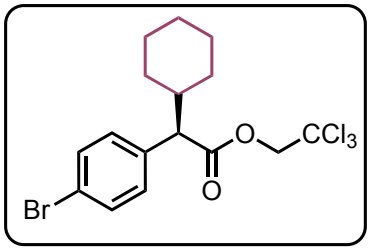

General procedure 2 was used in the C–H insertion into cyclohexane (110 µL, 5 equiv, 1.0 mmol) with 2,2,2-trichloroethyl 2-(4-bromophenyl)-2-diazoacetate (78.5 mg, 1.0 equiv, 0.20 mmol) using Ru_2(*S*-TPPTTL)$_4$BAr^F (6.6 mg, 1.0 mol %) as catalyst. The crude material was then subjected to column chromatography using a 0-2% diethyl ether/hexanes solvent system to afford the title compound as a clear colorless oil. Characterization matched literature reported value.[4]

^{1}H NMR (600 MHz, $CDCl_3$): δ 7.45 (d, J = 8.4 Hz, 2H), 7.24 (d, J = 8.4 Hz, 2H), 4.76 (d, J = 12.0 Hz, 1H), 4.63 (d, J = 12.0 Hz, 1H), 3.35 (d, J = 10.6 Hz, 1H), 2.05 (qt, J = 11.1, 3.4 Hz, 1H), 1.92 – 1.82 (m, 1H), 1.75 (ddt, J = 11.6, 3.6, 1.8 Hz, 1H), 1.64 (dddd, J = 9.2, 7.6, 3.5, 2.1 Hz, 2H), 1.38 – 1.34 (m, 1H), 1.34 – 1.26 (m, 1H), 1.19 – 1.06 (m, 3H), 0.83 – 0.73 (m, 1H).

Chiral HPLC: The enantiopurity was determined to be 97.5:2.5 er by chiral HPLC analysis (Chiracel AD-H, 0.1% IPA/Hexane, 1.0 mL/min., λ=230 nm, RT: Major: 15.6 min., Minor: 8.9 min.)

2,2,2-trichloroethyl (R)-2-(4-bromophenyl)-2-cyclopentylacetate (19)

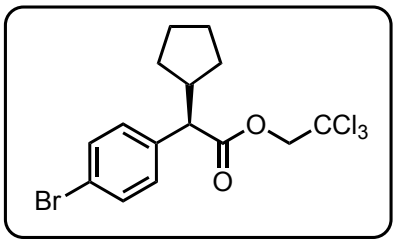

General procedure 2 was used for the C–H insertion into cyclopentane (90 µL, 1.0 mmol, 5.0 equiv) with 2,2,2-trichloroethyl 2-(4-bromophenyl)-2-diazoacetate (74.5 mg, 0.20 mmol, 1.0 equiv) using Ru_2(*S*-TPPTTL)$_4$BAr^F (6.6 mg, 1.0 mol%) as catalyst. Purification by column chromatography (2% diethyl ether/hexanes) afforded an oil (58 mg, 70%). Spectrum matched literature precedent.[4]

^{1}H NMR (400 MHz, $CDCl_3$): δ 7.47 (d, J = 8.0 Hz, 2H), 7.29 (d, J = 7.9 Hz, 2H), 4.79 (d, J = 11.9 Hz, 1H), 4.67 (d, J = 12.0 Hz, 1H), 3.41 (d, J = 11.2 Hz, 1H), 2.62 (q, J = 8.7 Hz, 1H), 1.98 (tt, J = 12.9, 5.4 Hz, 1H), 1.75 – 1.57 (m, 3H), 1.51 (dq, J = 12.3, 6.4 Hz, 2H), 1.40 – 1.23 (m, 1H), 1.10 – 0.94 (m, 1H).

Chiral HPLC: The enantiopurity was determined to be 96% ee by chiral HPLC analysis (Chiracel AD-H, 0.5% IPA/Hexane, 1.0 mL/min., λ=230 nm, RT: Major: 7.5 min., Minor: 6.7)

2,2,2-trichloroethyl (*R*)-2-(4-bromophenyl)-2-cycloheptylacetate (20)

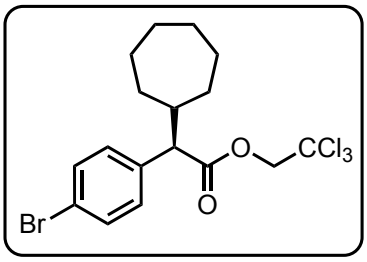

General procedure 2 was used for the C–H insertion into cycloheptane (120 μL, 1.0 mmol, 5.0 equiv) with 2,2,2-trichloroethyl 2-(4-bromophenyl)-2-diazoacetate (74.5 mg, 0.20 mmol, 1.0 equiv) using Ru_2(*S*-TPPTTL)$_4$BAr^F (6.6 mg, 1.0 mol%) as catalyst. Purification by column chromatography (2% diethyl ether/hexanes) afforded an oil (66 mg, 75%). Spectrum matched literature precedent.[4]

^{1}H NMR (400 MHz, $CDCl_3$): δ 7.47 (d, J = 8.5 Hz, 2H), 7.27 (d, J = 8.4 Hz, 2H), 4.76 (d, J = 12.0 Hz, 1H), 4.66 (d, J = 12.0 Hz, 1H), 3.45 (d, J = 11.0 Hz, 1H), 2.32 (dtt, J = 11.0, 9.4, 3.8 Hz, 1H), 1.91 – 1.79 (m, 1H), 1.72 (ddt, J = 13.1, 9.4, 4.9 Hz, 1H), 1.67 – 1.46 (m, 6H), 1.46 – 1.27 (m, 3H), 1.03 (dtd, J = 13.6, 9.5, 2.6 Hz, 1H).

Chiral HPLC: The enantiopurity was determined to be 92% ee by HPLC analysis (S,S-Whelk 0.5% IPA/Hexane, 0.50 mL/min, λ=230 nm, RT: Major: 19.9 min., Minor: 23.0 min.).

2,2,2-trichloroethyl (*R*)-2-(4-bromophenyl)-2-cyclooctylacetate (21)

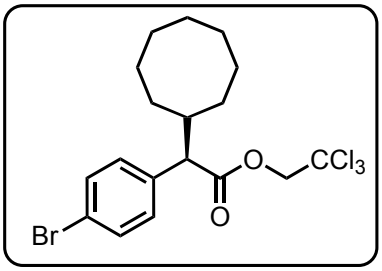

General procedure 2 was used for the C–H insertion into cyclooctane (135 μL, 1.0 mmol, 5.0 equiv) with 2,2,2-trichloroethyl 2-(4-bromophenyl)-2-diazoacetate (74.5 mg, 0.20 mmol, 1.0 equiv) using Ru_2(*S*-TPPTTL)$_4$BAr^F (6.6 mg, 1.0 mol%) as catalyst. Purification by column chromatography (2% diethyl ether/hexanes) afforded the product as an amorphous solid (66 mg, 75%).

^{1}H NMR (400 MHz, $CDCl_3$): δ 7.45 (d, J = 8.4 Hz, 2H), 7.26 (d, J = 8.4 Hz, 2H), 4.75 (d, J = 12.0 Hz, 1H), 4.62 (d, J = 12.0 Hz, 1H), 3.41 (d, J = 11.1 Hz, 1H), 2.37 (tdd, J = 11.6, 6.8, 2.5 Hz, 1H), 1.73 (d, J = 10.8 Hz, 2H), 1.67 – 1.38 (m, 9H), 1.36 – 1.21 (m, 2H), 1.09 (dtd, J = 15.7, 9.4, 3.6 Hz, 1H).

^{13}C NMR (101 MHz, $CDCl_3$): δ 172.0, 136.5, 131.7, 130.6, 121.6, 94.8, 74.2, 58.5, 40.1, 31.1, 29.1, 26.9, 26.9, 26.4, 25.4, 25.1.

HRMS (+p APCI): calcd for $C_{18}H_{23}O_2BrCl_3$ (M+H) 454.9941, found 454.9940.

Chiral HPLC: The enantiopurity was determined to be 90% ee by HPLC analysis (Chiracel AD-H 1.0 IPA/Hexane, 1.0 mL/min, λ=230 nm, RT: Major: 19.9 min., Minor: 23.0 min.).

2,2,2-trichloroethyl (*R*)-2-((3*R*,5*R*,7*R*)-adamantan-1-yl)-2-(4-bromophenyl)acetate (22)

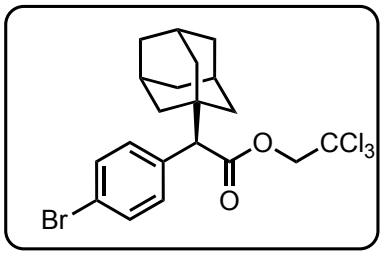

General procedure 2 was used for the C–H insertion into adamantane (136 mg, 1.0 mmol, 5.0 equiv) with 2,2,2-trichloroethyl 2-(4-bromophenyl)-2-diazoacetate (74.5 mg, 0.20 mmol, 1.0 equiv) using Ru_2(*S*-TPPTTL)$_4$BAr^F (6.6 mg, 1.0 mol%) as catalyst. Purification by column chromatography (2% diethyl ether/hexanes) afforded a clear colorless oil (64 mg, 66%).Spectrum matched literature precedent.[4]

^{1}H NMR (400 MHz, $CDCl_3$): δ 7.46 (d, J = 8.5 Hz, 2H), 7.30 (d, J = 8.5 Hz, 2H), 4.83 (d, J = 12.0 Hz, 1H), 4.64 (d, J = 12.0 Hz, 1H), 3.41 (s, 1H), 1.99 (t, J = 3.2 Hz, 3H), 1.77 – 1.64 (m, 6H), 1.62 – 1.53 (m, 6H).

Chiral HPLC: The enantiopurity was determined to be 92% ee by HPLC analysis (S,S-Whelk, 1.0% IPA/Hexane, 1.0 mL/min, λ=230 nm, RT: Major: 6.4 min., Minor: 7.1 min.).

2,2,2-trichloroethyl (*R*)-2-(4-bromophenyl)-2-((1*R*,3*S*)-3-(*tert*-butyl)cyclohexyl)acetate (23)

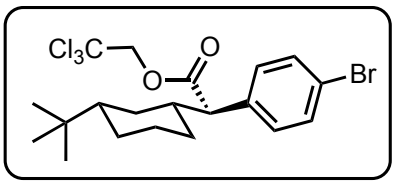

General procedure 2 was used for the C–H insertion of *t*-butylcyclohexane (169 µL, 1.0 mmol, 5 equiv) with 2,2,2-trichloroethyl 2-(4-bromophenyl)-2-diazoacetate (74.5 mg, 0.20 mmol, 1.0 equiv) using Ru_2(*S*-TPPTTL)$_4$BAr^F (6.6 mg, 1.0 mol%) as catalyst. Purification by column chromatography (2% diethyl ether/hexanes) afforded an oil (87 mg, 90%). Spectra matched literature precedent.[4]

^{1}H NMR (400 MHz, $CDCl_3$): δ 7.45 (d, J = 8.4 Hz, 2H), 7.24 (d, J = 8.5 Hz, 2H), 4.76 (d, J = 11.9 Hz, 1H), 4.62 (d, J = 12.0 Hz, 1H), 3.36 (d, J = 10.3 Hz, 1H), 2.12 – 1.99 (m, 1H), 1.94 – 1.79 (m, 2H), 1.79 – 1.68 (m, 1H), 1.46 (dt, J = 12.6, 2.7 Hz, 1H), 1.28 (tdd, J = 12.7, 9.2, 3.5 Hz, 1H), 1.06 – 0.90 (m, 2H), 0.90 – 0.78 (m, 1H), 0.72 (s, 9H), 0.50 (q, J = 12.0 Hz, 1H).

Chiral HPLC: The enantiopurity for the major diastereomer was determined to be 94% ee by HPLC analysis (Chiracel AD-H, 2.0% IPA/Hexane, 1.0 mL/min, λ=230 nm, RT Major Diastereomer: Major: 16.5 min, Minor: 14.5 min. Minor Diastereomer: Major: 18.8 min. Minor: 21.1 min.

2,2,2-trichloroethyl (2*R*,3*S*)-2-(4-bromophenyl)-3-methylhexanoate (24)

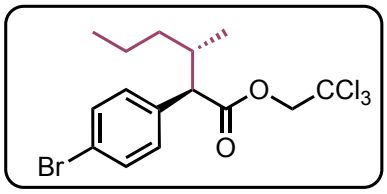

General procedure 3 was used for the C–H functionalization of pentane (2.0 mL) with 2,2,2-trichloroethyl 2-(4-bromophenyl)-2-diazoacetate (74.5 mg, 0.20 mmol, 1.0 equiv) using Ru_2(*S*-TPPTTL)$_4$BAr^F (6.6 mg, 1.0 mol%) as catalyst. Purification by column chromatography (2% diethyl ether/hexanes) afforded the title compound as a mixture of diastereomers (73 mg, 88%). Spectra matched literature precedent.[5]

^{1}H NMR (400 MHz, $CDCl_3$): δ 7.45 (d, J = 8.5 Hz, 2H), 7.24 (d, J = 8.5 Hz, 2H), 4.77 (d, J = 12.0 Hz, 1H), 4.63 (d, J = 12.0 Hz, 1H), 3.37 (d, J = 10.6 Hz, 1H), 2.24 (dddd, J =

17.2, 13.1, 6.4, 3.0 Hz, 1H), 1.51 – 1.45 (m, 1H), 1.41 – 1.27 (m, 1H), 1.25 – 1.07 (m, 1H), 1.05 (d, J = 6.5 Hz, 3H), 0.96 – 0.82 (m, 1H), 0.77 (t, J = 7.2 Hz, 3H).

Chiral HPLC: The enantiopurity of the major diastereomer was determined to be 95:5 er, and the minor diastereomer to be 90% er by chiral HPLC analysis. (S,S-Whelk, 1.0% IPA/Hexane, 1.0 mL/min, λ=230 nm, Major diastereomer: Major: 69.5 min., Minor: 40.1 min. Minor diastereomer: Major: 75.4 min., Minor: 44.6 min.).

2,2,2-trichloroethyl (2R,3R,E)-2-(4-bromophenyl)-3-methylhex-4-enoate (25)

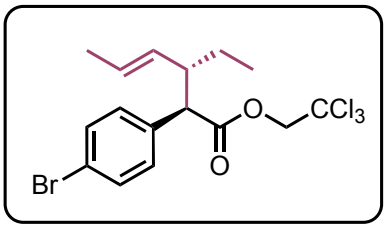

General procedure 1 was used for the C–H functionalization of (*E*)-hex-2-ene (0.25 mL, 2.0 mmol, 10 equiv) with 2,2,2-trichloroethyl 2-(4-bromophenyl)-2-diazoacetate (74.5 mg, 0.20 mmol, 1.0 equiv) using Ru_2(*S*-TPPTTL)$_4$BAr^F (6.6 mg, 1.0 mol%). Purification using 0-3% diethyl ether/hexanes column afforded the title compound as a mixture of diastereomers as a clear, colorless oil (71 mg, 83%).

Reported as a mixture of diastereomers.

^{1}H NMR (400 MHz, $CDCl_3$): δ 7.45 (d, J = 8.5 Hz, 0.75H), 7.43 – 7.38 (m, 2H), 7.28 (d, J = 8.5 Hz, 0.62H), 7.17 (d, J = 8.5 Hz, 2H), 5.59 (dq, J = 15.3, 6.4 Hz, 0.3H), 5.35 – 5.14 (m, 1.4H), 4.88 (ddd, J = 15.2, 9.3, 1.7 Hz, 1H), 4.75 (d, J = 12.0 Hz, 1H), 4.71 (d, J = 11.9 Hz, 0.4H), 4.65 (d, J = 12.0 Hz, 1H), 4.53 (d, J = 12.0 Hz, 0.3H), 3.54 (d, J = 10.3 Hz, 1H), 3.50 (d, J = 11.0 Hz, 0.4H), 2.63 (tdd, J = 15.8, 10.0, 3.2 Hz, 1.4H), 1.66 (dd, J = 6.4, 1.7 Hz, 1H), 1.63 – 1.50 (m, 1.8H), 1.48 (dd, J = 6.4, 1.7 Hz, 3H), 1.39 – 1.12 (m, 2H), 0.89 (t, J = 7.3 Hz, 3H), 0.75 (t, J = 7.3 Hz, 1H).

^{13}C NMR (101 MHz, $CDCl_3$): δ 171.6, 171.2, 135.9, 135.7, 131.7, 131.4, 131.3, 130.8, 130.6, 130.3, 128.7, 128.6, 121.7, 121.4, 94.7, 74.3, 74.2, 56.8, 47.9, 26.5, 24.8, 18.1, 17.9, 11.6, 11.3.

HRMS (-n APCI): calcd for $C_{16}H_{17}O_2{}^{79}Br^{35}Cl_3$ [M–H] 424.9483, found 424.9479.

Chiral HPLC: The enantiopurity of the major diastereomer was determined to be 46% ee by chiral HPLC analysis.. (Chiracel AD-H, 0.5% IPA/Hexane, 1.0 mL/min, λ=230 nm, Major diastereomer: Major: 5.6 min., Minor: 4.8 min. Minor diastereomer: Major: 6.5 min., Minor: 5.2 min.).

2,2,2-trichloroethyl (R)-2-(4-bromophenyl)-2-((R)-tetrahydrofuran-2-yl)acetate (26)

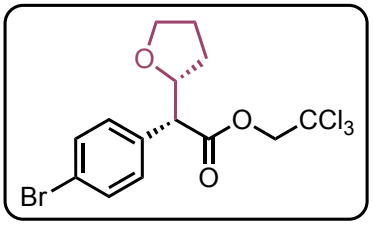

General procedure 4 was used for the C–H functionalization of tetrhydrofuran (0.16 mL, 2.0 mmol, 10 equiv) with 2,2,2-trichloroethyl 2-(4-bromophenyl)-2-diazoacetate (74.5 mg, 0.20 mmol, 1.0 equiv) using Ru_2(*S*-TPPTTL)$_4$BAr^F (6.6 mg, 1.0 mol%). Purification using 0-10% diethyl ether/hexanes afforded the title compound as a mixture of diastereomers as a clear colorless oil (47 mg, 56%).

Reported as a mixture of diastereomers:

^{1}H NMR (400 MHz, $CDCl_3$): δ 7.49 (dd, J = 8.5, 3.6 Hz, 2.8H), 7.36 – 7.26 (m, 3.1H), 4.83 – 4.77 (m, 1.8H), 4.72 (d, J = 12.0 Hz, 1.3H), 4.54 (ddt, J = 15.5, 8.5, 6.9 Hz, 1.5H), 3.95 (dt, J = 8.4, 6.8 Hz, 0.5H), 3.91 – 3.79 (m, 1.5H), 3.79 – 3.70 (m, 2H), 3.66 (d, J = 9.9 Hz, 0.5H), 2.25 – 2.13 (m, 1H), 1.92 (dddd, J = 12.8, 8.2, 6.4, 4.6 Hz, 2.8H), 1.84 – 1.75 (m, 0.6H), 1.64 – 1.58 (m, 1H), 1.56 – 1.41 (m, 0.5H).

^{13}C NMR (101 MHz, $CDCl_3$): δ 170.4, 170.0, 134.6, 134.0, 132.0, 131.7, 131.5, 130.9, 130.6, 130.3, 122.2, 122.0, 94.7, 94.7, 80.1, 79.4, 74.2, 74.1, 68.6, 68.5, 56.9, 56.3, 30.3, 29.5, 25.7, 25.4.

HRMS (+p APCI): calcd for $C_{14}H_{13}O_3{}^{79}Br^{35}Cl_3$ [M–H] 412.9119, found 412.9117.

Chiral HPLC: The enantiopurity of the major diastereomer was determined to be 94% ee, and the minor diastereomer to be 94% ee by chiral HPLC analysis. (Chiracel AD-H, 0.5% IPA/Hexane, 1.0 mL/min, λ=230 nm, Major diastereomer: Major: 16.9 min., Minor: 15.1 min. Minor diastereomer: Major: 26.7 min., Minor: 21.6 min.).

2,2,2-trichloroethyl (*R*)-2-(4-bromophenyl)-2-((*R*)-1-tosylpyrrolidin-2-yl)acetate (27)

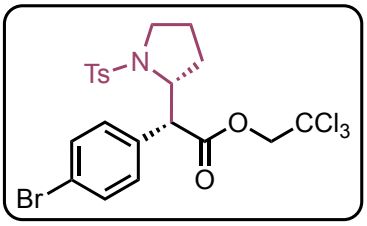

General procedure 2 was used for the C–H functionalization of N-tosyl-pyrrolidine (67 mg, 0.3 mmol, 1.5 equiv) with 2,2-trichloroethyl 2-(4-bromophenyl)-2-diazoacetate (74.5 mg, 0.20 mmol, 1.0 equiv) using Rh_2(*S*-TPPTTL)$_4$ (4.9 mg, 1.0 mol%) as catalyst. The crude material was purified using 20% diethyl ether/hexanes column to afford a white powder (72.5 mg, 64%)

^{1}H NMR (400 MHz, $CDCl_3$): δ 7.62 (d, J = 8.3 Hz, 2H), 7.46 (d, J = 8.4 Hz, 2H), 7.28 (dd, J = 8.6, 6.8 Hz, 4H), 4.84 (d, J = 12.0 Hz, 1H), 4.75 (d, J = 12.0 Hz, 1H), 4.34 – 4.24 (m, 1H), 4.16 (d, J = 6.0 Hz, 1H), 3.40 (ddd, J = 12.2, 7.5, 5.1 Hz, 1H), 3.27 – 3.14 (m, 1H), 2.42 (s, 3H), 2.10 – 1.93 (m, 1H), 1.71 – 1.55 (m, 2H), 1.33 (dt, J = 12.3, 7.4 Hz, 1H).

^{13}C NMR (101 MHz, $CDCl_3$): δ 169.9, 143.7, 134.8, 133.6, 131.7, 131.1, 129.8, 127.6, 122.2, 94.7, 74.4, 62.7, 55.0, 49.3, 29.3, 24.2, 21.6.

HRMS (+p APCI): calcd for $C_{21}H_{22}O_4N^{79}Br^{35}Cl_3{}^{32}S$ [M+H] 567.9513, found 567.9507.

Chiral SFC: The enantiopurity was determined to be 90% ee by chiral SFC analysis. (OJ-3, 5% MeOH/IPA + 0.2% Formic Acid. 5 min, 2.5 mL/min. λ=230 nm, RT: Major: 3.55 min. Minor: 3.83 min.)

2,2,2-trichloroethyl (*R*)-2-cyclohexyl-2-(4-(((trifluoromethyl)sulfonyl)oxy)phenyl)acetate (28)

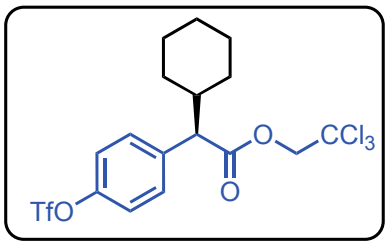

General procedure 2 was used in the C–H functionalization of cyclohexane (0.11 mL, 1.0 mmol, 5.0 equiv) with 2,2,2-trichloroethyl 2-diazo-2-(4-(((trifluoromethyl)sulfonyl)oxy)phenyl)acetate (88.3 mg, 0.20 mmol, 1.0 equiv) with Ru_2(*S*-TPPTTL)$_4$BAr^F (6.6 mg,

1.0 mol%) as catalyst. The product was purified via column chromatography (5% diethyl ether/hexanes) to afford an amorphous solid (81.5 mg, 82%). Spectra matched literature precedent.[2]

^{1}H NMR (400 MHz, $CDCl_3$): δ 7.46 (d, J = 8.8 Hz, 2H), 7.24 (d, J = 8.8 Hz, 2H), 4.77 (d, J = 11.9 Hz, 1H), 4.65 (d, J = 12.0 Hz, 1H), 3.43 (d, J = 10.6 Hz, 1H), 2.07 (qt, J = 11.0, 3.4 Hz, 1H), 1.87 (dt, J = 12.5, 3.3 Hz, 1H), 1.81 – 1.71 (m, 1H), 1.71 – 1.62 (m, 2H), 1.37 – 1.25 (m, 2H), 1.21 – 1.05 (m, 3H), 0.85 – 0.70 (m, 1H).

Chiral HPLC: The enantiopurity was determined to be 86% ee by chiral HPLC analysis (Chiracel AD-H, 1.0% IPA/Hexanes, 1.0 mL/min, λ=230 nm, RT: 6.5 Major, 5.6 Minor).

2,2,2-trichloroethyl (*R*)-2-cyclohexyl-2-(4-fluorophenyl)acetate (29)

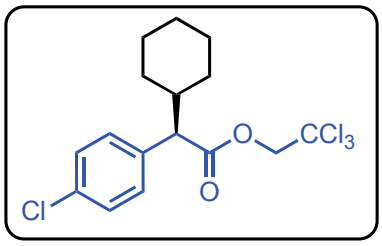

General procedure 2 was used for the C–H functionalization of cyclohexane (0.11 mL, 1.0 mmol, 5.0 equiv) with 2,2,2-trichloroethyl 2-(4-chlorophenyl)-2-diazoacetate (65.8 mg, 0.20 mmol, 1.0 equiv) using Ru_2(*S*-TPPTTL)$_4BAr^F$ (6.6 mg, 1.0 mol%) as catalyst. Purification by column chromatography (2% diethyl ether/hexanes) afforded an oil (61 mg, 79%). Spectra matched literature precedent.[2]

^{1}H NMR (400 MHz, $CDCl_3$): δ 7.32 (s, 4H), 4.78 (d, J = 12.0 Hz, 1H), 4.65 (d, J = 12.0 Hz, 1H), 3.38 (d, J = 10.7 Hz, 1H), 2.07 (qt, J = 11.0, 3.4 Hz, 1H), 1.88 (dt, J = 12.6, 3.5 Hz, 1H), 1.84 – 1.74 (m, 1H), 1.74 – 1.59 (m, 2H), 1.47 – 1.25 (m, 2H), 1.25 – 1.03 (m, 3H), 0.79 (qd, J = 12.1, 3.5 Hz, 1H).

Chiral HPLC: The enantiopurity was determined to be 96% ee by chiral HPLC analysis (Chiracel AD-H, 0.5% IPA/Hexane, 0.5 mL/min, , λ=230 nm, RT: Major: 16.7 min, Minor: 11.7 min)

2,2,2-trichloroethyl (*R*)-2-cyclohexyl-2-(4-(trifluoromethyl)phenyl)acetate (30)

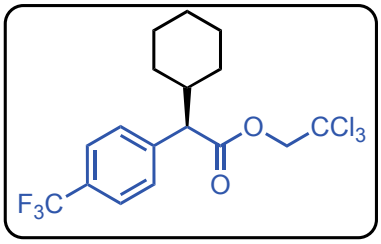

General procedure 2 was used for the C–H functionalization of cyclohexane (0.11 mL, 1.0 mmol, 5.0 equiv) with 2,2,2-trichloroethyl 2-diazo-2-(4-(trifluoromethyl)phenyl)acetate (72.3 mg, 0.20 mmol, 1.0 equiv) using Ru_2(*S*-TPPTTL)$_4$BAr^F (6.6 mg, 1.0 mol%) as catalyst. Purification by column chromatography (2% diethyl ether/hexanes) afforded an oil (59 mg, 70%). Spectra matched literature precedent.[2]

^{1}H NMR (400 MHz, $CDCl_3$): δ 7.61 (d, J = 8.0 Hz, 2H), 7.52 (d, J = 8.1 Hz, 2H), 4.80 (d, J = 12.0 Hz, 1H), 4.66 (d, J = 12.0 Hz, 1H), 3.49 (d, J = 10.7 Hz, 1H), 2.14 (qt, J = 11.0, 3.4 Hz, 1H), 1.95 – 1.87 (m, 1H), 1.83 – 1.74 (m, 1H), 1.71 – 1.60 (m, 2H), 1.39 – 1.27 (m, 2H), 1.25 – 1.08 (m, 3H), 0.81 (qd, J = 12.1, 3.5 Hz, 1H).

Chiral HPLC: The enantiopurity was determined to be 90% ee by chiral HPLC analysis (Chiracel AD-H, 0.1% IPA/Hexanes, 1.0 mL/min, λ=210 nm, RT: Major: 11.5 min, Minor: 6.8 min)

2,2,2-trichloroethyl (R)-2-(6-chloropyridin-3-yl)-2-cyclohexylacetate (31)

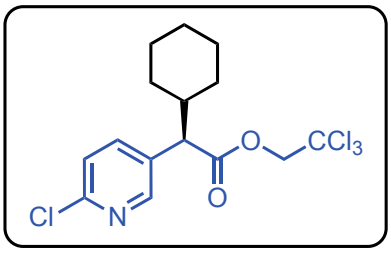

General procedure 3 was used for the C–H functionalization of cycloehxane (0.11 mL, 1.0 mmol, 5.0 equiv) with 2,2,2-trichloroethyl 2-(6-chloropyridin-3-yl)-2-diazoacetate (66 mg, 0.20 mmol, 1.0 equiv) using Ru_2(*S*-TPPTTL)$_4$BAr^F (6.6 mg, 1.0 mol%) as catalyst. Purification by column chromatography (10% diethyl ether/hexanes) afforded an oil (43.7 mg, 58%). Spectra matched literature precedent.[7]

^{1}H NMR (400 MHz, $CDCl_3$): δ 8.32 (d, J = 2.5 Hz, 1H), 7.74 (dd, J = 8.3, 2.5 Hz, 1H), 7.31 (d, J = 8.3 Hz, 1H), 4.76 (d, J = 12.0 Hz, 1H), 4.66 (d, J = 12.0 Hz, 1H), 3.42 (d, J = 10.4 Hz, 1H), 2.14 – 1.94 (m, 1H), 1.92 – 1.72 (m, 1H), 1.71 – 1.57 (m, 2H), 1.39 – 1.22 (m, 2H), 1.14 (ddt, J = 15.0, 11.3, 4.7 Hz, 2H), 0.81 (dt, J = 12.8, 5.0 Hz, 1H).

Chiral HPLC: The enantiopurity was determined to be 96% ee by chiral HPLC analysis (R,R-Whelk, 1% IPA/Hexanes, 0.5 mL/min, λ=230 nm, RT: Major: 21.9 min, Minor: 19.7 min)

2,2,2-trichloroethyl (*R*)-2-([1,1'-biphenyl]-4-yl)-2-cyclohexylacetate (32)

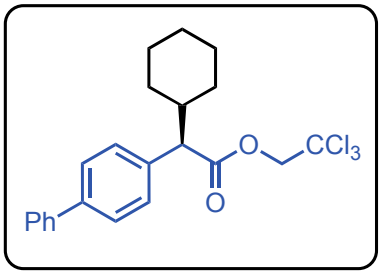

General procedure 3 was used for the C–H functionalization of cyclohexane (4.0 mL) with 2,2,2-trichloroethyl 2-diazo-2-(4-fluorophenyl)acetate (62.3 mg, 0.20 mmol, 1.0 equiv) using Ru_2(*S*-TPPTTL)$_4$BAr^F (6.6 mg, 1.0 mol%) as catalyst. Purification by column chromatography (2% diethyl ether/hexanes) afforded a white solid (63 mg, 74%). Spectra matched literature precedent.[2]

^{1}H NMR (400 MHz, $CDCl_3$) δ 7.63 – 7.53 (m, 2H), 7.50 – 7.41 (m, 2H), 7.40 – 7.31 (m, 1H), 4.82 (d, J = 12.0 Hz, 1H), 4.64 (d, J = 12.0 Hz, 1H), 3.45 (d, J = 10.7 Hz, 1H), 2.16 (qt, J = 11.1, 3.4 Hz, 1H), 1.93 (dt, J = 12.5, 3.2 Hz, 1H), 1.82 – 1.73 (m, 1H), 1.71 – 1.62 (m, 2H), 1.47 (dt, J = 11.5, 2.7 Hz, 1H), 1.40 – 1.30 (m, 1H), 1.23 – 1.13 (m, 3H), 0.85 (pd, J = 10.7, 3.9 Hz, 1H).

Chiral HPLC: The enantiopurity was determined to be 92% ee by chiral HPLC analysis (S,S-Whelk, 1.0% IPA/Hexanes, 1.0 mL/min, Major: 13.0 min. Minor: 14.5 min.).

2,2,2-trichloroethyl (*R*)-2-(4-(*tert*-butyl)phenyl)-2-cyclohexylacetate (33)

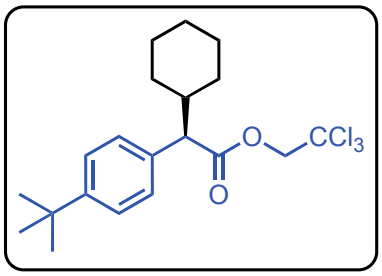

General procedure 3 was used for the C–H functionalization of cyclohexane (4.0 mL) with 2,2,2-trichloroethyl 2-diazo-2-(4-fluorophenyl)acetate (62.3 mg, 0.20 mmol, 1.0 equiv) using Ru_2(*S*-TPPTTL)$_4$BAr^F (6.6 mg, 1.0 mol%) as catalyst. Purification by column

chromatography (2% diethyl ether/hexanes) afforded an oil (53 mg, 73%). Spectra matched literature precedent.[7]

^{1}H NMR (400 MHz, $CDCl_3$) δ 7.37 – 7.33 (m, 2H), 7.30 (d, J = 9.2 Hz, 2H), 4.81 (d, J = 12.0 Hz, 1H), 4.60 (d, J = 12.0 Hz, 1H), 3.38 (d, J = 10.8 Hz, 1H), 2.10 (qt, J = 11.0, 3.4 Hz, 1H), 1.90 (d, J = 12.7 Hz, 1H), 1.81 – 1.72 (m, 1H), 1.66 (dd, J = 9.7, 5.0 Hz, 2H), 1.45 (m, 2H), 1.33 (s, 9H), 1.24 – 1.08 (m, 3H), 0.85 – 0.74 (m, 1H).

Chiral HPLC: The enantiopurity was determined to be 90% ee by chiral HPLC analysis (S,S-Whelk, 0.1% IPA/ Hexane, 0.5 mL/min. Major: 21.7 min., Minor: 18.5 min.).

2,2,2-trichloroethyl (*R*)-2-cyclohexyl-2-(4-methoxyphenyl)acetate (34)

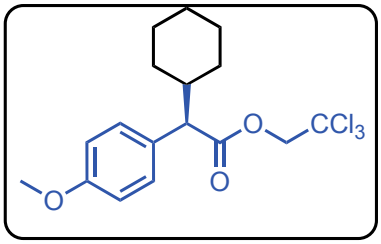

General procedure 3 was used for the C–H functionalization of cyclohexane (4.0 mL) with 2,2,2-trichloroethyl 2-diazo-2-(4-methoxyphenyl)acetate (64.7 mg, 0.200 mmol, 1.0 equiv) using Ru_2(*S*-TPPTTL)$_4$BAr^F (6.6 mg, 1.0 mol%) as catalyst. Purification by column chromatography (2% diethyl ether/hexanes) afforded a white solid (38.1 mg, 51%). Spectra matched literature precedent.[7]

^{1}H NMR (400 MHz, $CDCl_3$): δ 7.26 (d, J = 8.7 Hz, 2H), 6.85 (d, J = 8.7 Hz, 2H), 4.76 (d, J = 12.0 Hz, 1H), 4.61 (d, J = 12.0 Hz, 1H), 3.79 (s, 3H), 3.32 (d, J = 10.7 Hz, 1H), 2.04 (dddd, J = 14.4, 11.1, 7.3, 3.4 Hz, 1H), 1.86 (d, J = 12.7 Hz, 1H), 1.75 (d, J = 13.5 Hz, 1H), 1.67 – 1.57 (m, 2H), 1.39 (d, J = 15.0 Hz, 1H), 1.34 – 1.24 (m, 1H), 1.21 – 1.02 (m, 3H), 0.82 – 0.69 (m, 1H).

Chiral HPLC: The enantiopurity was determined to be 28% ee by chiral HPLC analysis (Chiracel AD-H, 1.0% IPA/Hexane, 1.0 mL/min., λ=230 nm, RT: Major: 13.2 min., Minor: 14.4 min.).

2,2,2-trichloroethyl (R)-2-cyclohexyl-2-(naphthalen-2-yl)acetate (35)

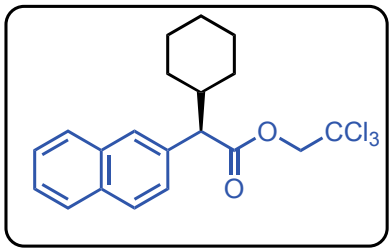

General procedure 3 was used for the reaction of cyclohexene (200 µL, 5 equiv, 2.0 mmol) with, 2,2,2-trichloroethyl (R)-2-cyclohexyl-2-(naphthalen-2-yl)acetate (69 mg, 0.20 mmol, 1.0 equiv) using Ru_2(*S*-TPPTTL)$_4$BAr^F (6.6 mg, 1.0 mol%) as catalyst. Purification by column chormatogarphy (2% diethyl ether/hexanes) afforded a clear colorless oil (60.2 mg). Spectra matched literature precedent.[2]

^{1}H NMR (400 MHz, $CDCl_3$) δ 7.84 – 7.79 (m, 4H), 7.53 (dd, J = 8.7, 1.7 Hz, 1H), 7.50 – 7.43 (m, 2H), 4.81 (d, J = 12.0 Hz, 1H), 4.62 (d, J = 12.0 Hz, 1H), 3.56 (d, J = 10.7 Hz, 1H), 2.31 – 2.15 (m, 1H), 1.95 (ddd, J = 12.7, 4.5, 2.2 Hz, 1H), 1.82 – 1.74 (m, 1H), 1.71 – 1.57 (m, 2H), 1.41 – 1.30 (m, 2H), 1.24 – 1.09 (m, 3H), 0.94 – 0.74 (m, 1H).

Chiral SFC: The enantiopurity was determined to be 99% ee by chiral SFC analysis. (OJ-3, 3% MeOH/IPA + 0.2% Formic Acid. 5 min, 2.5 mL/min. λ=230 nm, RT: Major: 1.81 min. Minor: 2.01 min.

2,2,2-trichloroethyl (1*S*,2*S*)-1-(4-bromophenyl)-2-(cyclohexylmethyl)cyclopropane-1-carboxylate (37)

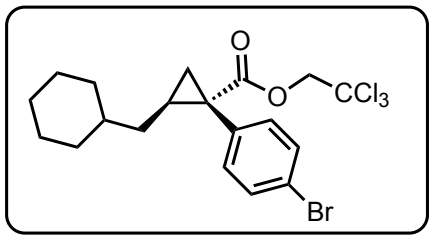

^{1}H NMR (400 MHz, $CDCl_3$): δ 7.45 (d, J = 8.4 Hz, 2H), 7.17 (d, J = 8.4 Hz, 2H), 4.79 (d, J = 11.9 Hz, 1H), 4.55 (d, J = 11.9 Hz, 1H), 1.97 (tdd, J = 10.1, 6.6, 3.6 Hz, 1H), 1.89 (dd, J = 9.0, 4.1 Hz, 1H), 1.76 – 1.59 (m, 5H), 1.42 – 1.28 (m, 2H), 1.27 – 1.06 (m, 4H), 0.92 – 0.76 (m, 2H), 0.38 – 0.27 (m, 1H).

^{13}C NMR (101 MHz, $CDCl_3$): δ 172.7, 134.4, 133.2, 131.2, 121.4, 95.0, 74.3, 38.0, 37.9, 33.3, 33.3, 32.4, 27.9, 26.5, 26.31, 26.29, 22.7.

HRMS (+p APCI): calcd for $C_{19}H_{23}O_2{}^{79}Br^{35}Cl_3$ [M+H] 466.9942 found 466.9944.

2,2,2-trichloroethyl (*S*)-2-((1*R*,3*R*)-3-allylcyclohexyl)-2-(4-bromophenyl)acetate (38)

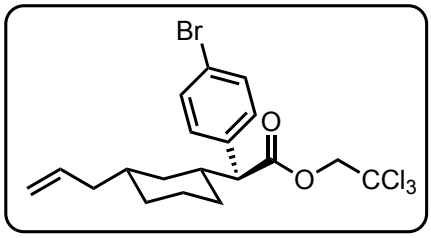

Reported as a 2:1 mixture of diastereomers:

^{1}H NMR (400 MHz, $CDCl_3$): δ 7.45 (dd, J = 8.5, 2.7 Hz, 2H), 7.23 (d, J = 8.4 Hz, 3H), 5.81 – 5.72 (m, 0.2H), 5.73 – 5.59 (m, 1H), 5.01 – 4.93 (m, 0.5H), 4.92 (s, 1H), 4.88 (q, J = 1.9 Hz, 1H), 4.76 (d, J = 12.0 Hz, 1H), 4.63 (d, J = 12.0 Hz, 1H), 3.32 (d, J = 10.4 Hz, 1H), 2.13 – 1.99 (m, 1H), 1.93 (dt, J = 13.8, 6.5 Hz, 1H), 1.86 (dd, J = 12.6, 6.2 Hz, 2H) 1.83 – 1.61 (m, 3H), 1.37 (d, J = 12.7 Hz, 1H), 1.34 – 1.17 (m, 3H), 1.00 (qd, J = 12.6, 3.6 Hz, 1H), 0.88 – 0.70 (m, 1.5H), 0.48 (q, J = 12.1 Hz, 1H).

^{13}C NMR (101 MHz, $CDCl_3$): δ 135.7, 131.7, 130.4, 121.6, 115.7, 94.8, 74.1, 58.3, 41.7, 40.8, 37.3, 36.8, 32.2, 31.7, 25.7.

HRMS (+p APCI): calcd for $C_{19}H_{23}O_2{}^{79}Br^{35}Cl_3$ [M+H] 466.9942 found 466.9941.

HPLC Traces

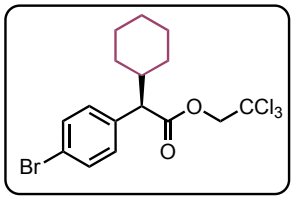

Compound **18**

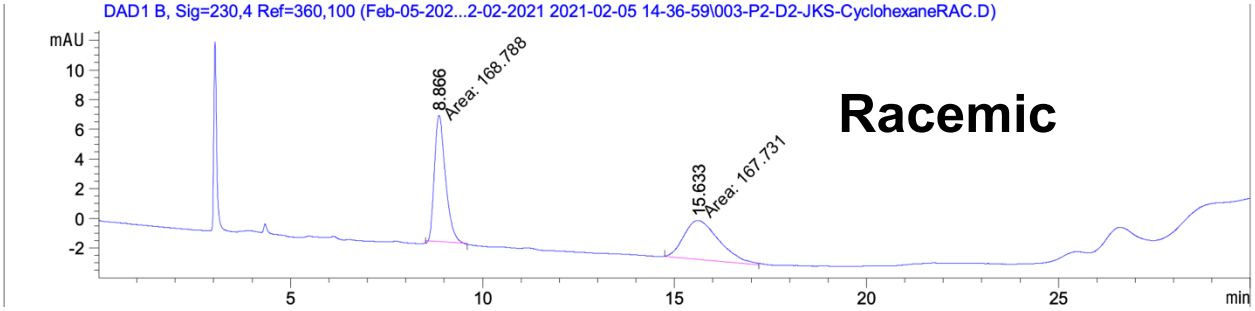

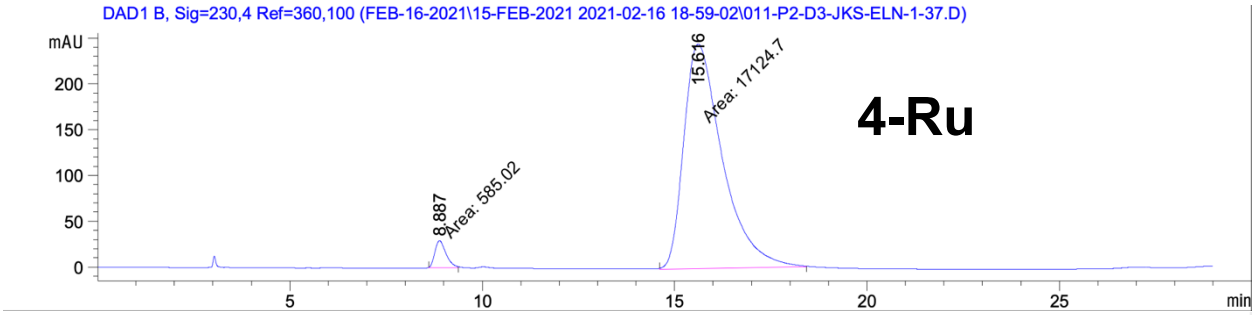

Signal 2: DAD1 B, Sig=230,4 Ref=360,100

Peak #	RetTime [min]	Type	Width [min]	Area [mAU*s]	Height [mAU]	Area %
1	8.887	MM	0.3316	585.01965	29.40377	3.3034
2	15.616	MM	1.1627	1.71247e4	245.47913	96.6966
Totals :				1.77097e4	274.88289	

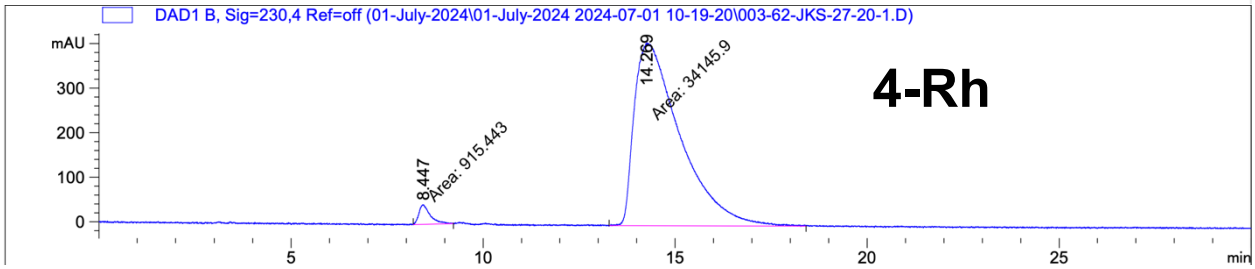

Signal 2: DAD1 B, Sig=230,4 Ref=off

Peak #	RetTime [min]	Type	Width [min]	Area [mAU*s]	Height [mAU]	Area %
1	8.447	MM	0.3431	915.44293	44.47035	2.6110
2	14.269	MM	1.3859	3.41459e4	410.64337	97.3890
Totals :				3.50613e4	455.11372	

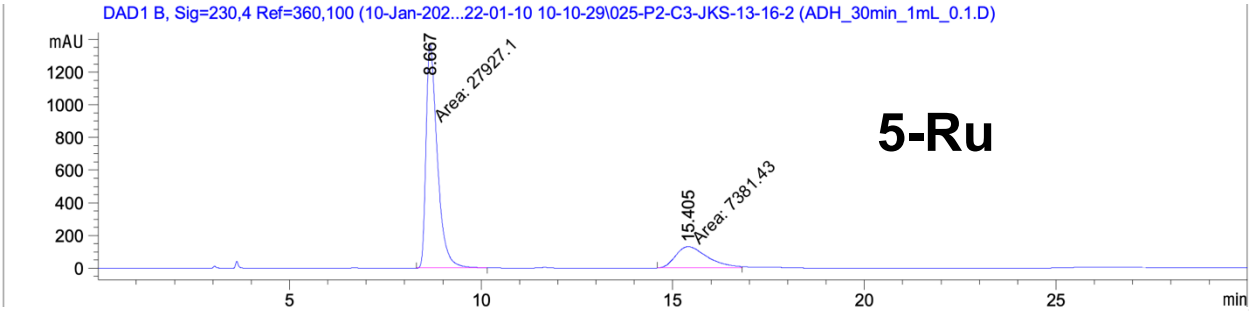

Signal 2: DAD1 B, Sig=230,4 Ref=360,100

Peak #	RetTime [min]	Type	Width [min]	Area [mAU*s]	Height [mAU]	Area %
1	8.667	MM	0.3393	2.79271e4	1371.97913	79.0945
2	15.405	MM	0.9555	7381.43066	128.74814	20.9055
Totals :				3.53086e4	1500.72726	

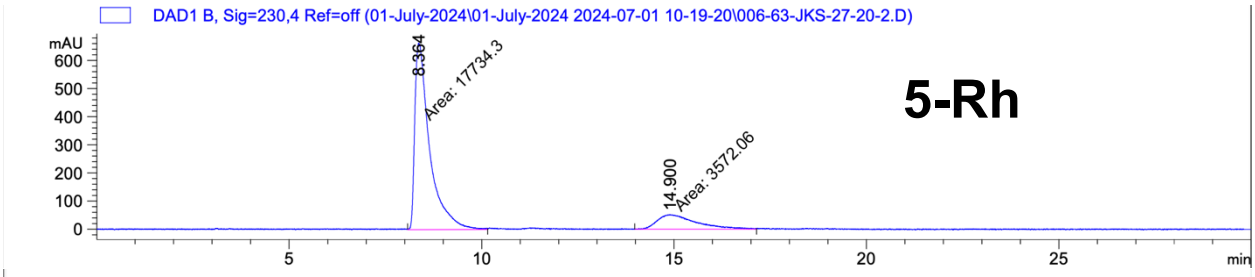

Signal 2: DAD1 B, Sig=230,4 Ref=off

Peak #	RetTime [min]	Type	Width [min]	Area [mAU*s]	Height [mAU]	Area %
1	8.364	MM	0.4456	1.77343e4	663.34113	83.2348
2	14.900	MM	1.1611	3572.06177	51.27624	16.7652
Totals :				2.13064e4	714.61736	

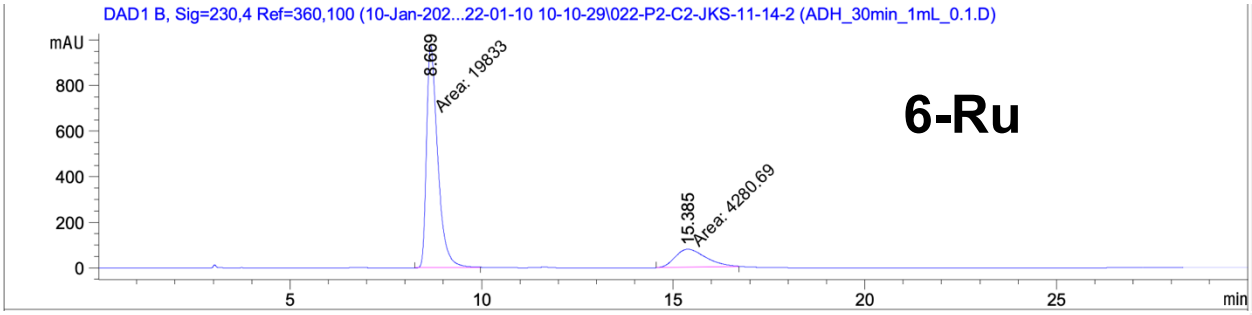

Signal 2: DAD1 B, Sig=230,4 Ref=360,100

Peak #	RetTime [min]	Type	Width [min]	Area [mAU*s]	Height [mAU]	Area %
1	8.669	MM	0.3376	1.98330e4	979.10876	82.2479
2	15.385	MM	0.9136	4280.68750	78.09247	17.7521
Totals :				2.41137e4	1057.20123	

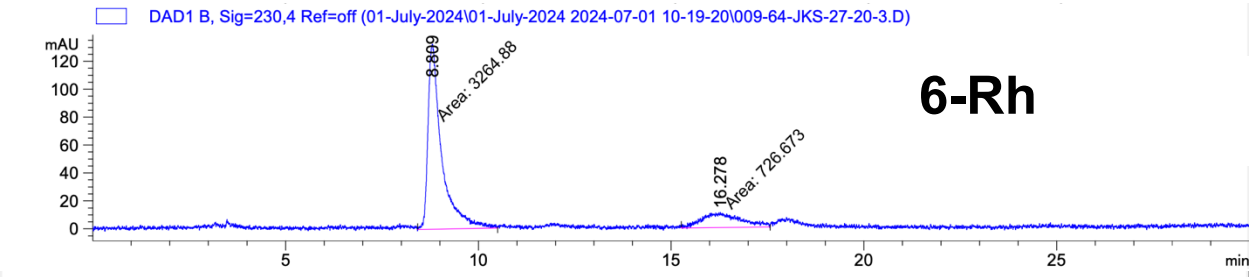

Signal 2: DAD1 B, Sig=230,4 Ref=off

Peak #	RetTime [min]	Type	Width [min]	Area [mAU*s]	Height [mAU]	Area %
1	8.809	MM	0.4103	3264.87573	132.62936	81.7947
2	16.278	MM	1.1151	726.67279	10.86073	18.2053
Totals :				3991.54852	143.49010	

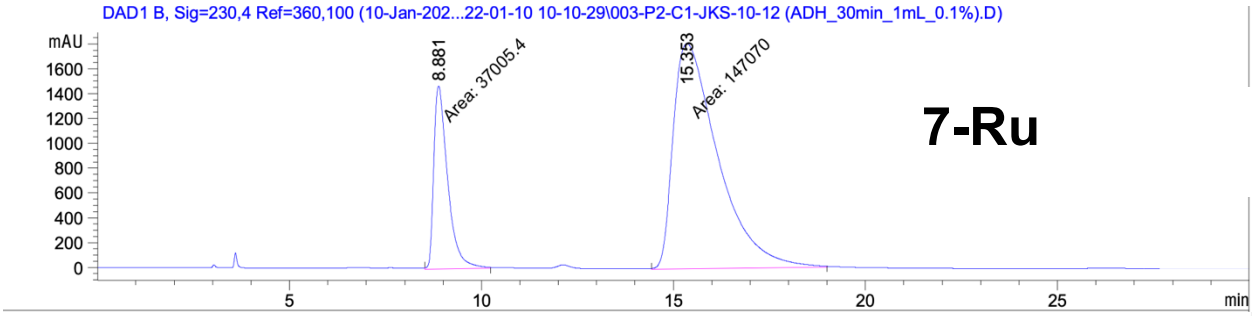

Signal 2: DAD1 B, Sig=230,4 Ref=360,100

Peak #	RetTime [min]	Type	Width [min]	Area [mAU*s]	Height [mAU]	Area %
1	8.881	MM	0.4183	3.70054e4	1474.28943	20.1034
2	15.353	MM	1.3506	1.47070e5	1814.82178	79.8966
Totals :				1.84075e5	3289.11121	

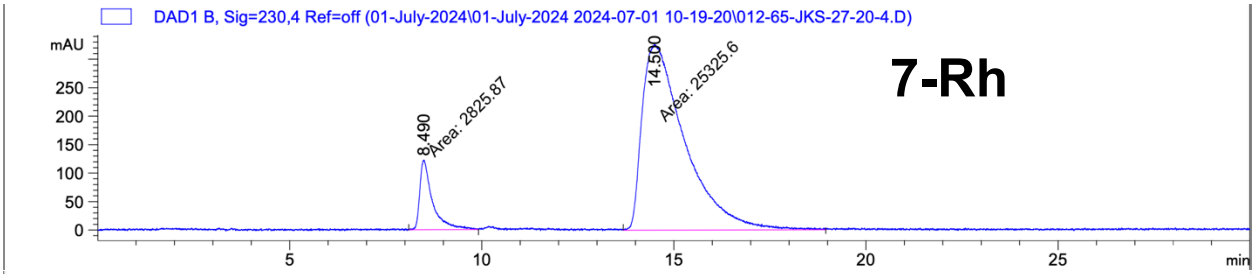

Peak #	RetTime [min]	Type	Width [min]	Area [mAU*s]	Height [mAU]	Area %
1	8.490	MM	0.3841	2825.86792	122.63290	10.0381
2	14.500	MM	1.2933	2.53256e4	326.35834	89.9619
Totals :				2.81514e4	448.99123	

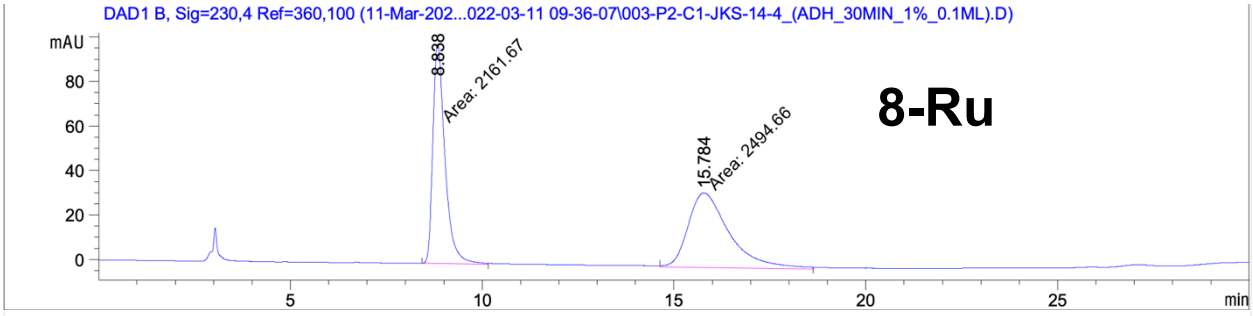

Signal 2: DAD1 B, Sig=230,4 Ref=360,100

Peak #	RetTime [min]	Type	Width [min]	Area [mAU*s]	Height [mAU]	Area %
1	8.838	MM	0.3653	2161.67261	98.62448	46.4244
2	15.784	MM	1.2428	2494.65674	33.45412	53.5756
Totals :				4656.32935	132.07861	

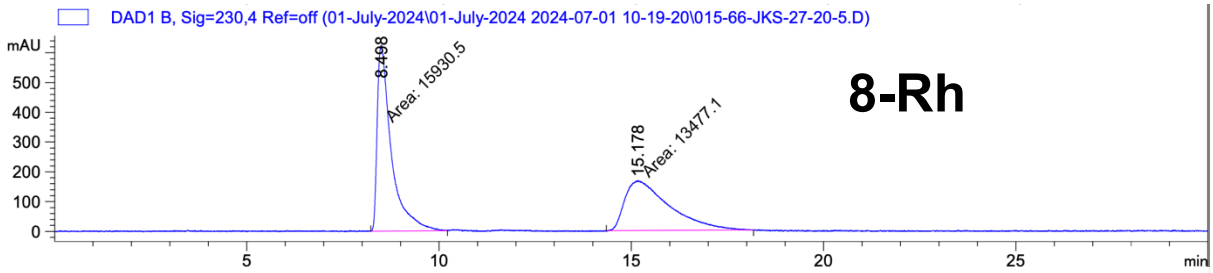

Signal 2: DAD1 B, Sig=230,4 Ref=off

Peak #	RetTime [min]	Type	Width [min]	Area [mAU*s]	Height [mAU]	Area %
1	8.498	MM	0.4245	1.59305e4	625.40485	54.1714
2	15.178	MM	1.3357	1.34771e4	168.16658	45.8286

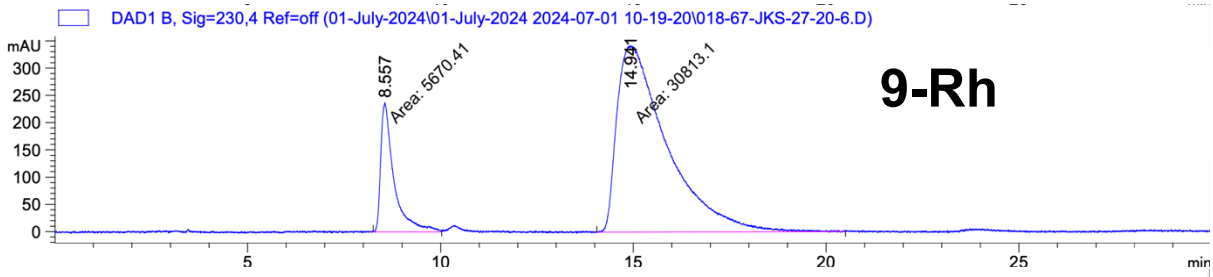

Signal 2: DAD1 B, Sig=230,4 Ref=off

Peak #	RetTime [min]	Type	Width [min]	Area [mAU*s]	Height [mAU]	Area %
1	8.557	MM	0.3972	5670.40527	237.92604	15.5424
2	14.941	MM	1.5018	3.08131e4	341.96072	84.4576
Totals :				3.64835e4	579.88676	

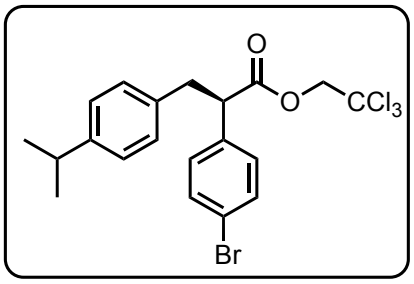

Compound **12**

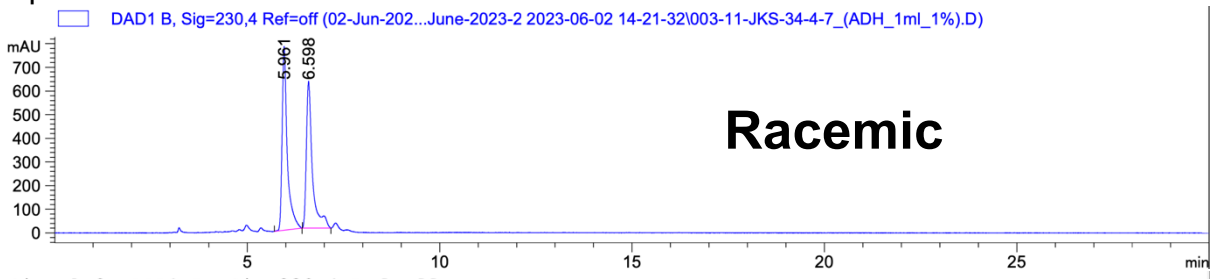

Signal 2: DAD1 B, Sig=230,4 Ref=off

Peak #	RetTime [min]	Type	Width [min]	Area [mAU*s]	Height [mAU]	Area %
1	5.961	VV R	0.1315	7262.04541	777.55066	51.6840
2	6.598	BV R	0.1303	6788.81104	621.82666	48.3160
Totals :				1.40509e4	1399.37732	

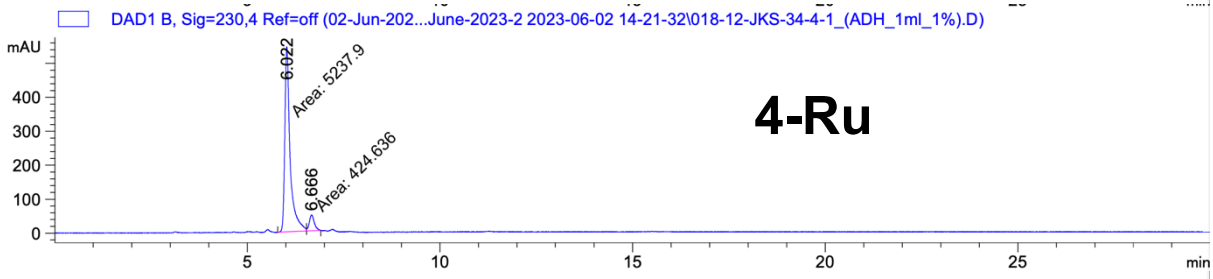

Signal 2: DAD1 B, Sig=230,4 Ref=off

Peak #	RetTime [min]	Type	Width [min]	Area [mAU*s]	Height [mAU]	Area %
1	6.022	MF	0.1601	5237.90234	545.31964	92.5010
2	6.666	FM	0.1499	424.63586	47.20139	7.4990
Totals :				5662.53821	592.52103	

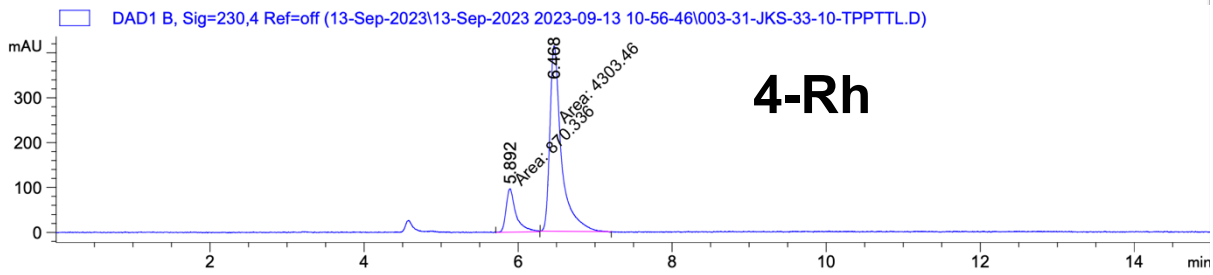

Signal 2: DAD1 B, Sig=230,4 Ref=off

Peak #	RetTime [min]	Type	Width [min]	Area [mAU*s]	Height [mAU]	Area %
1	5.892	MM	0.1501	870.33575	96.65264	16.8220
2	6.468	MM	0.1735	4303.46338	413.30762	83.1780
Totals :				5173.79913	509.96026	

Signal 3: DAD1 C, Sig=254,4 Ref=off

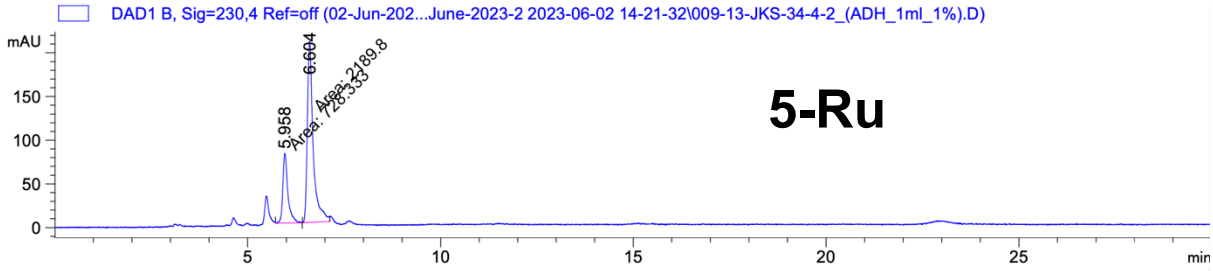

Signal 2: DAD1 B, Sig=230,4 Ref=off

Peak #	RetTime [min]	Type	Width [min]	Area [mAU*s]	Height [mAU]	Area %
1	5.958	MM	0.1521	728.33270	79.78551	24.9589
2	6.604	MM	0.1758	2189.79541	207.56432	75.0411
Totals :				2918.12811	287.34982	

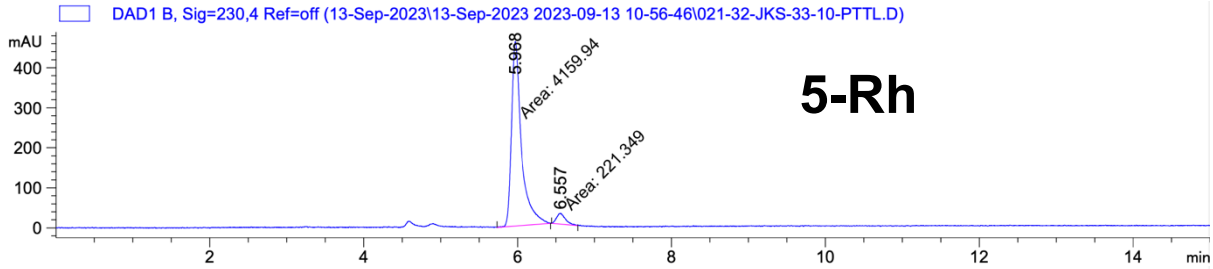

Signal 2: DAD1 B, Sig=230,4 Ref=off

Peak #	RetTime [min]	Type	Width [min]	Area [mAU*s]	Height [mAU]	Area %
1	5.968	MM	0.1503	4159.93652	461.19974	94.9478
2	6.557	MM	0.1373	221.34937	26.87223	5.0522
Totals :				4381.28589	488.07197	

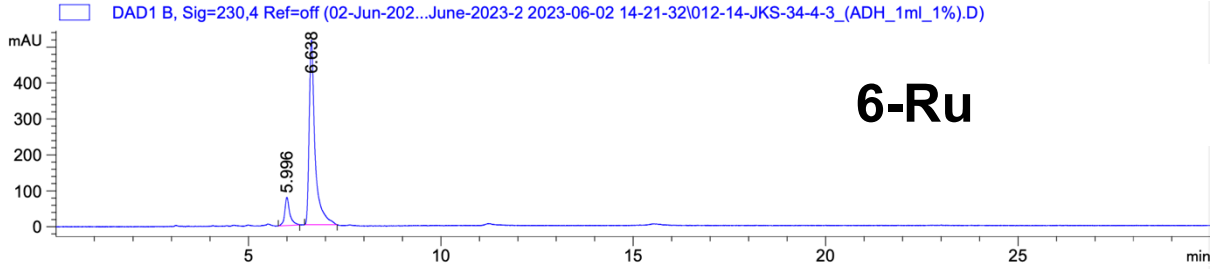

Signal 2: DAD1 B, Sig=230,4 Ref=off

Peak #	RetTime [min]	Type	Width [min]	Area [mAU*s]	Height [mAU]	Area %
1	5.996	BV R	0.1112	717.43719	78.40846	11.6098
2	6.638	BV R	0.1477	5462.13477	513.43555	88.3902
Totals :				6179.57196	591.84401	

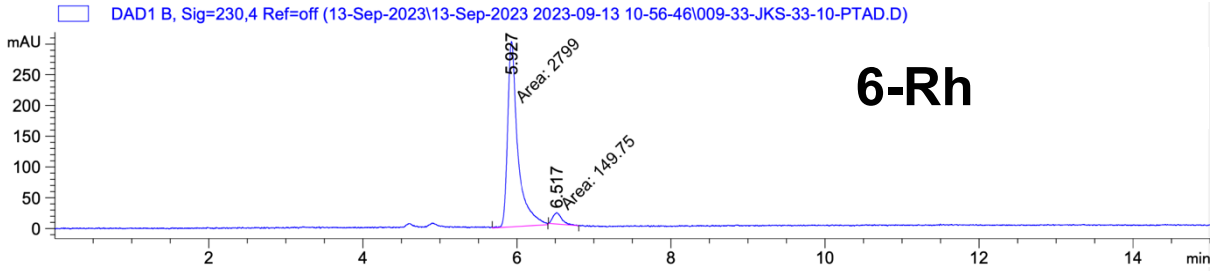

6-Rh

Signal 2: DAD1 B, Sig=230,4 Ref=off

Peak #	RetTime [min]	Type	Width [min]	Area [mAU*s]	Height [mAU]	Area %
1	5.927	MM	0.1547	2799.00171	301.45557	94.9216
2	6.517	MM	0.1351	149.75041	18.47223	5.0784
Totals :				2948.75212	319.92779	

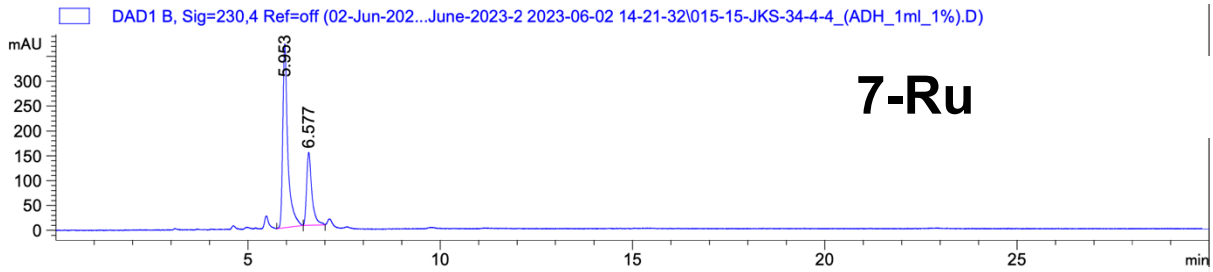

7-Ru

Signal 2: DAD1 B, Sig=230,4 Ref=off

Peak #	RetTime [min]	Type	Width [min]	Area [mAU*s]	Height [mAU]	Area %
1	5.953	VV R	0.1295	3358.67822	369.78372	70.7545
2	6.577	BV R	0.1230	1388.26697	146.45894	29.2455
Totals :				4746.94519	516.24266	

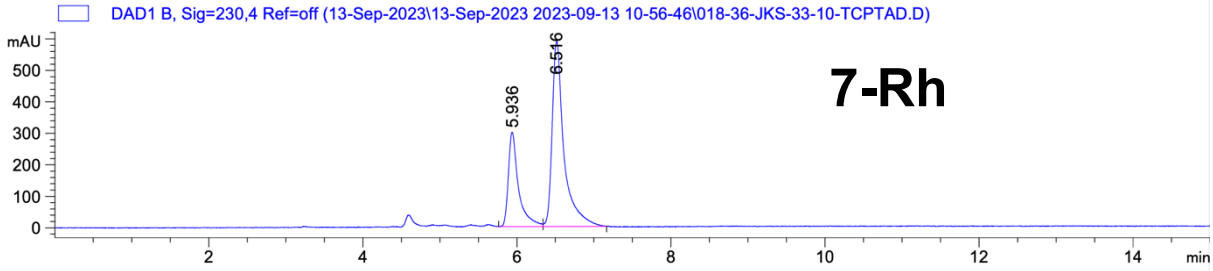

7-Rh

Signal 2: DAD1 B, Sig=230,4 Ref=off

Peak #	RetTime [min]	Type	Width [min]	Area [mAU*s]	Height [mAU]	Area %
1	5.936	BV R	0.1269	2756.40015	299.46103	30.6598
2	6.516	VV R	0.1404	6233.86621	588.56726	69.3402
Totals :				8990.26636	888.02829	

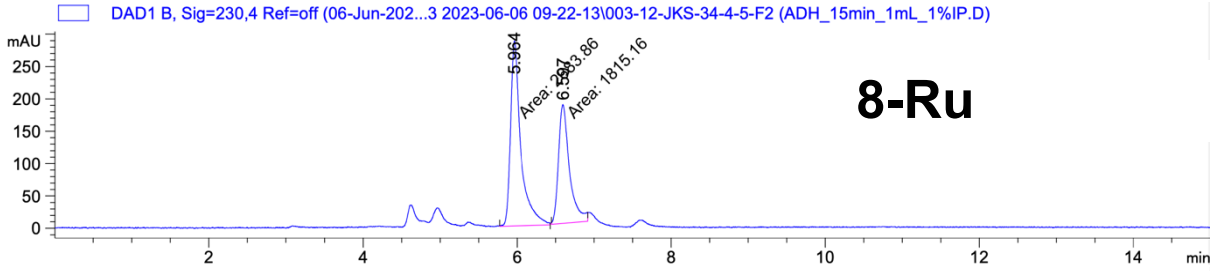

Signal 2: DAD1 B, Sig=230,4 Ref=off

Peak #	RetTime [min]	Type	Width [min]	Area [mAU*s]	Height [mAU]	Area %
1	5.964	MM	0.1565	2683.85938	285.83459	59.6543
2	6.597	MM	0.1650	1815.15979	183.32645	40.3457
Totals :				4499.01917	469.16104	

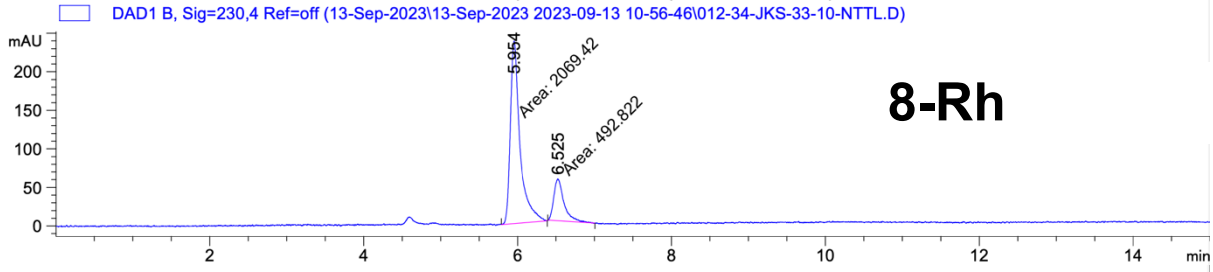

Signal 2: DAD1 B, Sig=230,4 Ref=off

Peak #	RetTime [min]	Type	Width [min]	Area [mAU*s]	Height [mAU]	Area %
1	5.954	MM	0.1455	2069.42065	237.00862	80.7660
2	6.525	MM	0.1508	492.82181	54.46803	19.2340
Totals :				2562.24246	291.47665	

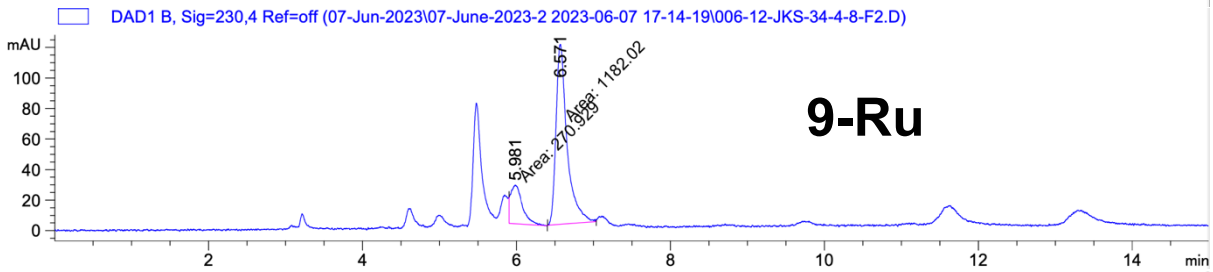

Signal 2: DAD1 B, Sig=230,4 Ref=off

Peak #	RetTime [min]	Type	Width [min]	Area [mAU*s]	Height [mAU]	Area %
1	5.981	MM	0.1777	270.92871	25.41737	18.6468
2	6.571	MM	0.1671	1182.02234	117.91237	81.3532
Totals :				1452.95105	143.32974	

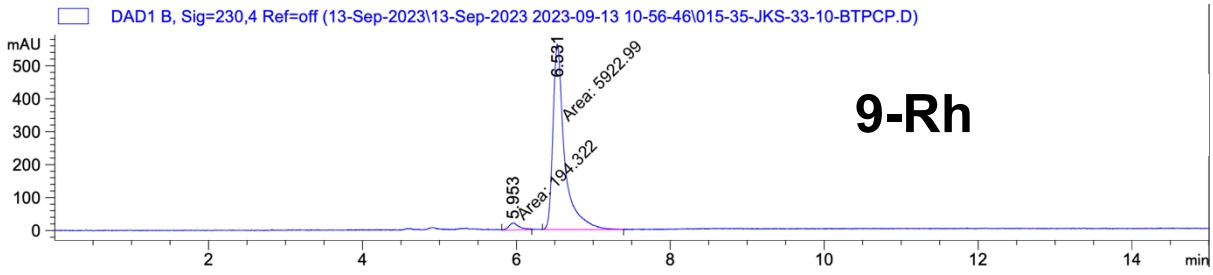

9-Rh

Signal 2: DAD1 B, Sig=230,4 Ref=off

Peak #	RetTime [min]	Type	Width [min]	Area [mAU*s]	Height [mAU]	Area %
1	5.953	MM	0.1543	194.32161	20.98520	3.1766
2	6.531	MM	0.1753	5922.98779	563.09705	96.8234
Totals :				6117.30940	584.08224	

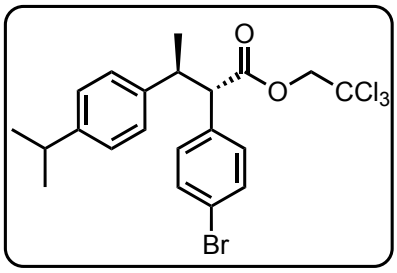

Compound **15a, 15b**

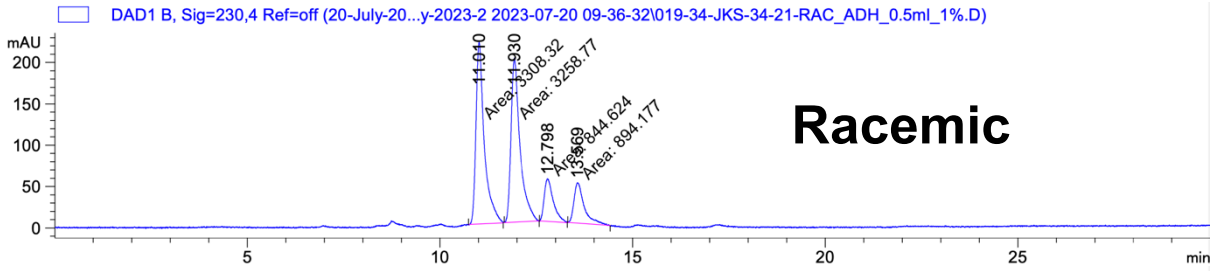

Racemic

Signal 2: DAD1 B, Sig=230,4 Ref=off

Peak #	RetTime [min]	Type	Width [min]	Area [mAU*s]	Height [mAU]	Area %
1	11.010	MM	0.2512	3308.32300	219.51834	39.8310
2	11.930	MM	0.2740	3258.77319	198.24152	39.2344
3	12.798	MM	0.2725	844.62445	51.66417	10.1690
4	13.569	MM	0.3061	894.17694	48.68564	10.7656
Totals :				8305.89758	518.10967	

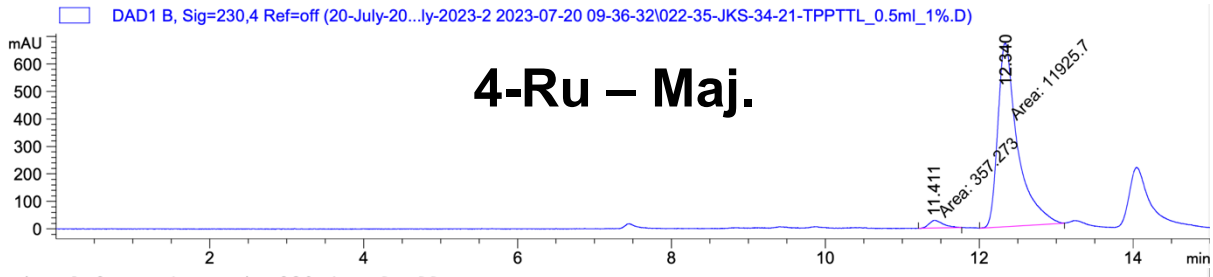

Signal 2: DAD1 B, Sig=230,4 Ref=off

Peak #	RetTime [min]	Type	Width [min]	Area [mAU*s]	Height [mAU]	Area %
1	11.411	MM	0.2128	357.27301	27.97917	2.9087
2	12.340	MM	0.2978	1.19257e4	667.49274	97.0913
Totals :				1.22830e4	695.47190	

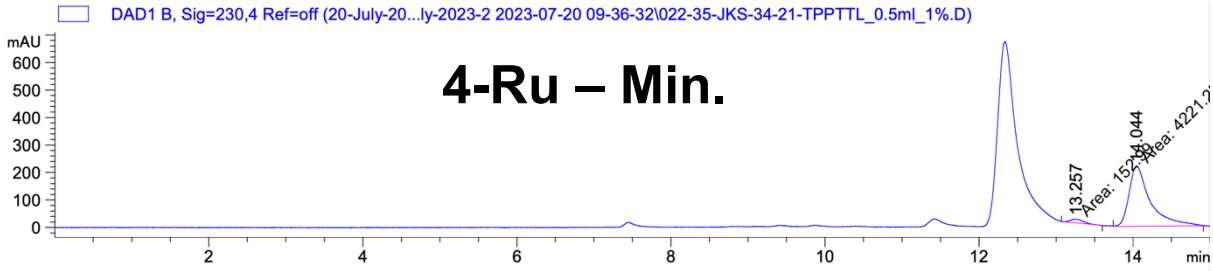

Signal 2: DAD1 B, Sig=230,4 Ref=off

Peak #	RetTime [min]	Type	Width [min]	Area [mAU*s]	Height [mAU]	Area %
1	13.257	MM	0.1941	152.98984	13.13601	3.4975
2	14.044	MM	0.3217	4221.24756	218.68088	96.5025
Totals :				4374.23740	231.81688	

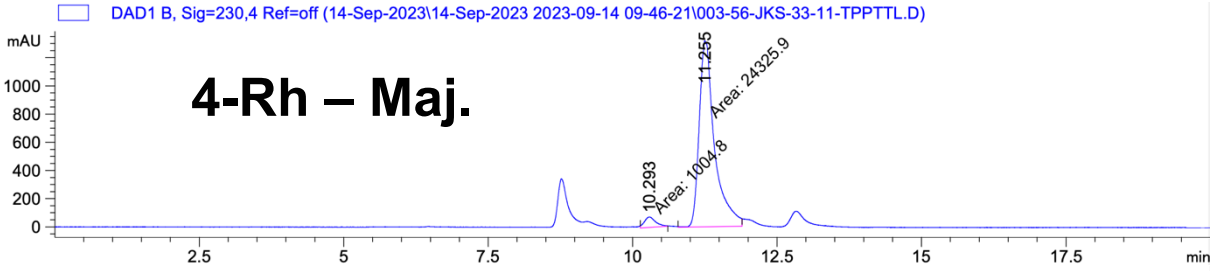

Signal 2: DAD1 B, Sig=230,4 Ref=off

Peak #	RetTime [min]	Type	Width [min]	Area [mAU*s]	Height [mAU]	Area %
1	10.293	MM	0.2242	1004.79926	74.69434	3.9667
2	11.255	MM	0.3072	2.43259e4	1319.77820	96.0333
Totals :				2.53307e4	1394.47254	

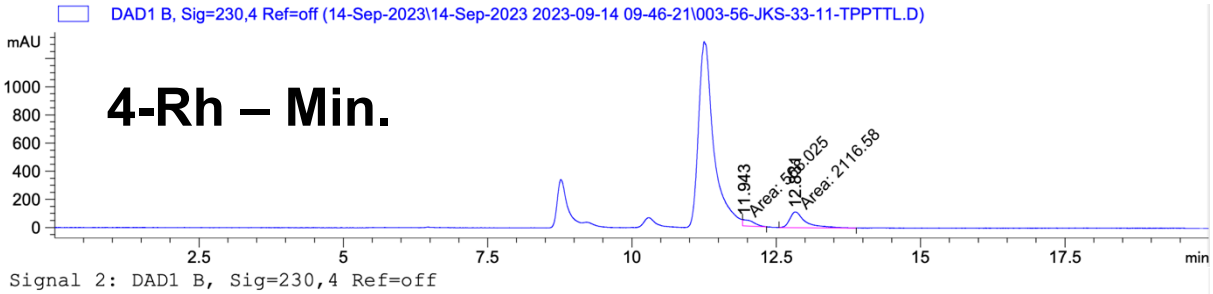

Signal 2: DAD1 B, Sig=230,4 Ref=off

Peak #	RetTime [min]	Type	Width [min]	Area [mAU*s]	Height [mAU]	Area %
1	11.943	MM	0.2211	568.02496	42.81692	21.1586
2	12.831	MM	0.3151	2116.58374	111.95480	78.8414
Totals :				2684.60870	154.77172	

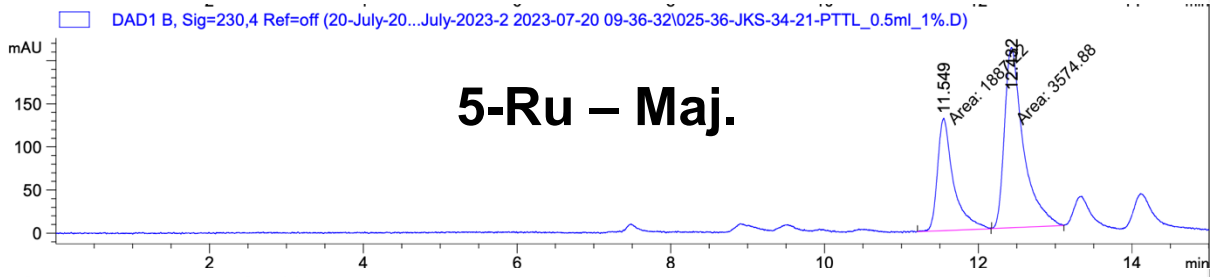

Signal 2: DAD1 B, Sig=230,4 Ref=off

Peak #	RetTime [min]	Type	Width [min]	Area [mAU*s]	Height [mAU]	Area %
1	11.549	MM	0.2411	1887.22473	130.47174	34.5513
2	12.432	MM	0.2849	3574.87720	209.15363	65.4487
Totals :				5462.10193	339.62537	

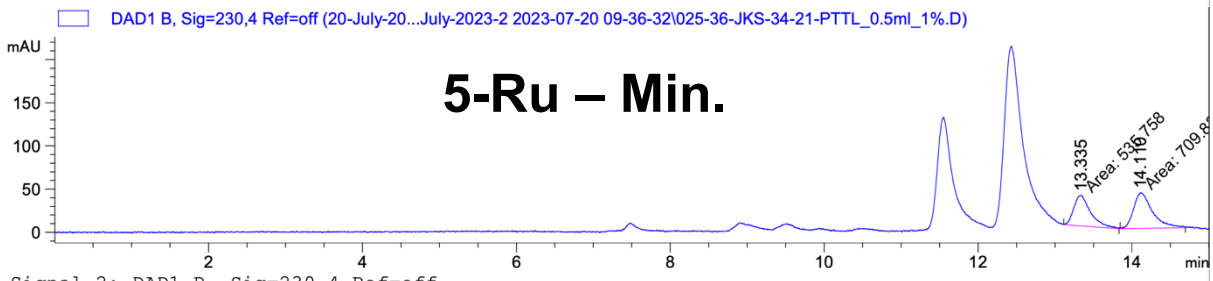

Signal 2: DAD1 B, Sig=230,4 Ref=off

Peak #	RetTime [min]	Type	Width [min]	Area [mAU*s]	Height [mAU]	Area %
1	13.335	MM	0.2533	535.75818	35.24865	43.0128
2	14.110	MM	0.2860	709.82086	41.35924	56.9872
Totals :				1245.57904	76.60789	

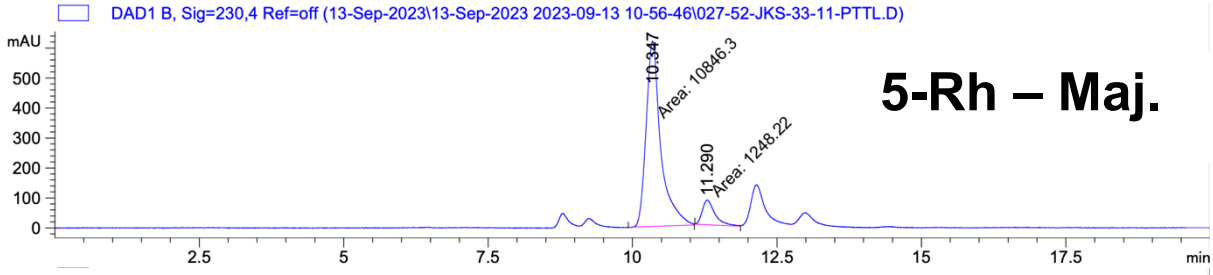

5-Rh – Maj.

Signal 2: DAD1 B, Sig=230,4 Ref=off

Peak #	RetTime [min]	Type	Width [min]	Area [mAU*s]	Height [mAU]	Area %
1	10.347	MM	0.2923	1.08463e4	618.37231	89.6795
2	11.290	MM	0.2525	1248.21838	82.39369	10.3205
Totals :				1.20946e4	700.76601	

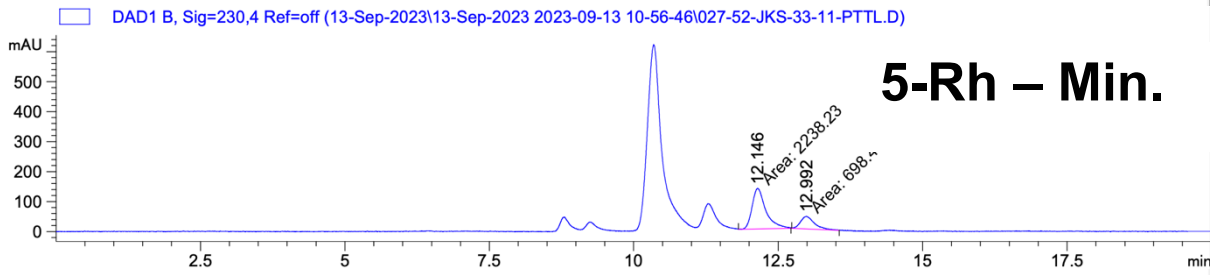

5-Rh – Min.

Signal 2: DAD1 B, Sig=230,4 Ref=off

Peak #	RetTime [min]	Type	Width [min]	Area [mAU*s]	Height [mAU]	Area %
1	12.146	MM	0.2755	2238.23438	135.38463	76.2155
2	12.992	MM	0.2756	698.48236	42.23464	23.7845
Totals :				2936.71674	177.61927	

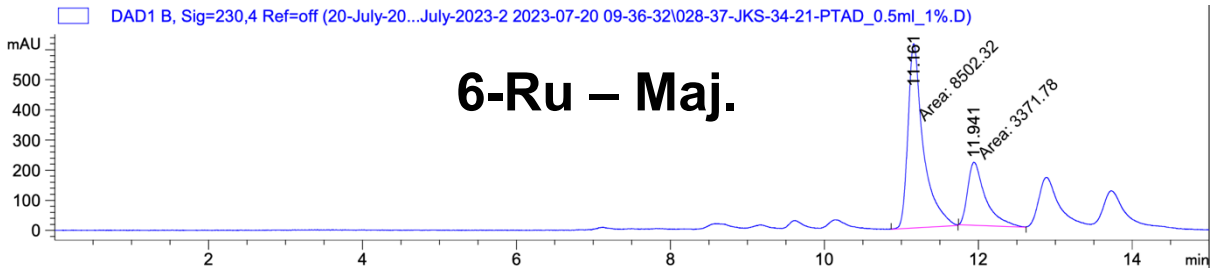

6-Ru – Maj.

Signal 2: DAD1 B, Sig=230,4 Ref=off

Peak #	RetTime [min]	Type	Width [min]	Area [mAU*s]	Height [mAU]	Area %
1	11.161	MM	0.2315	8502.32324	612.02429	71.6039
2	11.941	MM	0.2677	3371.78076	209.95772	28.3961
Totals :				1.18741e4	821.98201	

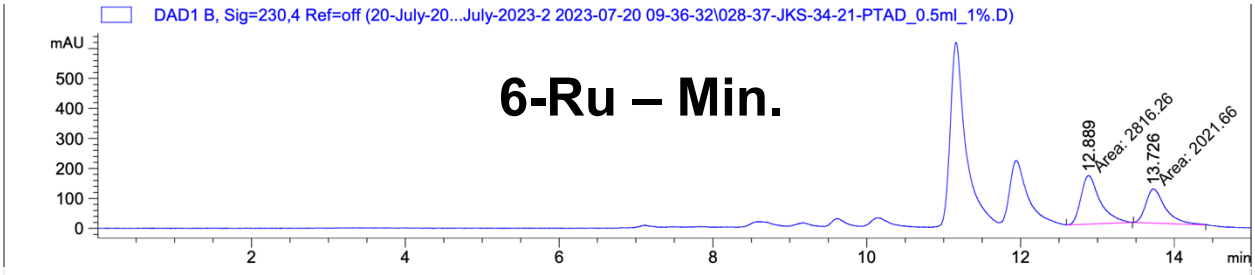

Signal 2: DAD1 B, Sig=230,4 Ref=off

Peak #	RetTime [min]	Type	Width [min]	Area [mAU*s]	Height [mAU]	Area %
1	12.889	MM	0.2895	2816.26245	162.15532	58.2123
2	13.726	MM	0.2946	2021.65747	114.37710	41.7877
Totals :				4837.91992	276.53242	

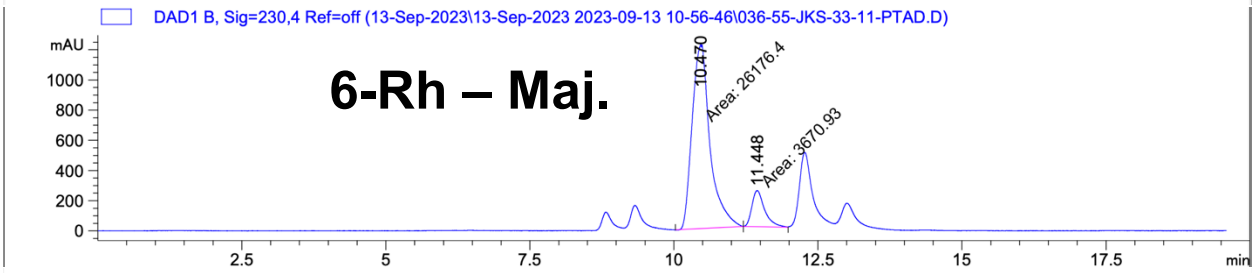

Signal 2: DAD1 B, Sig=230,4 Ref=off

Peak #	RetTime [min]	Type	Width [min]	Area [mAU*s]	Height [mAU]	Area %
1	10.470	MM	0.3581	2.61764e4	1218.39026	87.7010
2	11.448	MM	0.2545	3670.92578	240.37245	12.2990

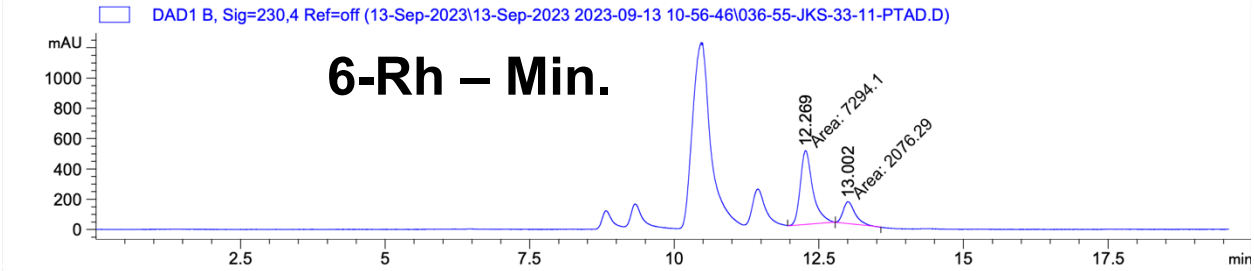

Signal 2: DAD1 B, Sig=230,4 Ref=off

Peak #	RetTime [min]	Type	Width [min]	Area [mAU*s]	Height [mAU]	Area %
1	12.269	MM	0.2496	7294.10254	486.96356	77.8420
2	13.002	MM	0.2400	2076.28882	144.18231	22.1580

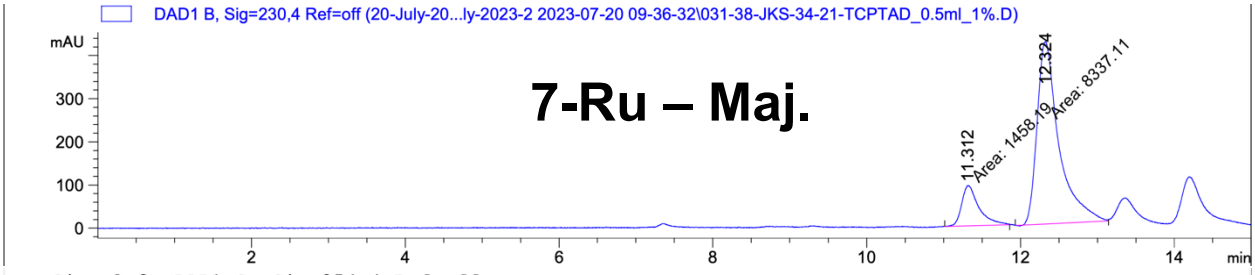

Signal 3: DAD1 C, Sig=254,4 Ref=off

Peak #	RetTime [min]	Type	Width [min]	Area [mAU*s]	Height [mAU]	Area %
1	12.237	BV	0.0355	25.27437	8.92675	15.8721
2	12.305	VV	0.0911	102.95455	13.55901	64.6546
3	12.397	VV	0.0386	31.00882	10.14883	19.4733
Totals :				159.23774	32.63458	

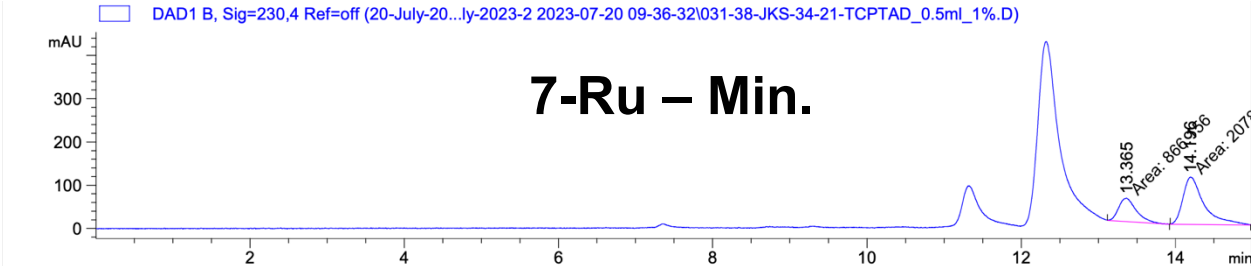

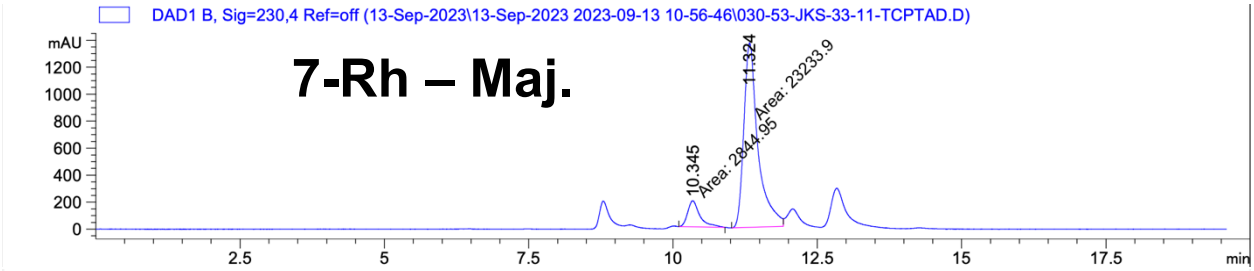

Signal 2: DAD1 B, Sig=230,4 Ref=off

Peak #	RetTime [min]	Type	Width [min]	Area [mAU*s]	Height [mAU]	Area %
1	10.345	MM	0.2450	2844.94897	193.52136	10.9090
2	11.324	MM	0.2828	2.32339e4	1369.13428	89.0910
Totals :				2.60788e4	1562.65564	

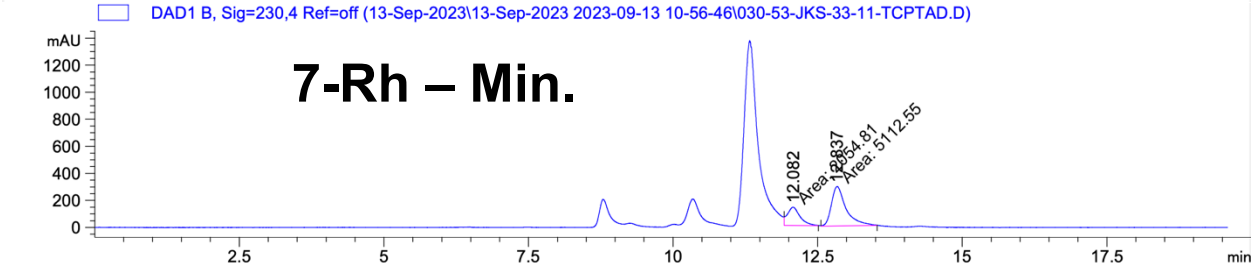

Signal 2: DAD1 B, Sig=230,4 Ref=off

Peak #	RetTime [min]	Type	Width [min]	Area [mAU*s]	Height [mAU]	Area %
1	12.082	MM	0.2547	2054.81299	134.45419	28.6690
2	12.837	MM	0.2925	5112.55029	291.32901	71.3310
Totals :				7167.36328	425.78320	

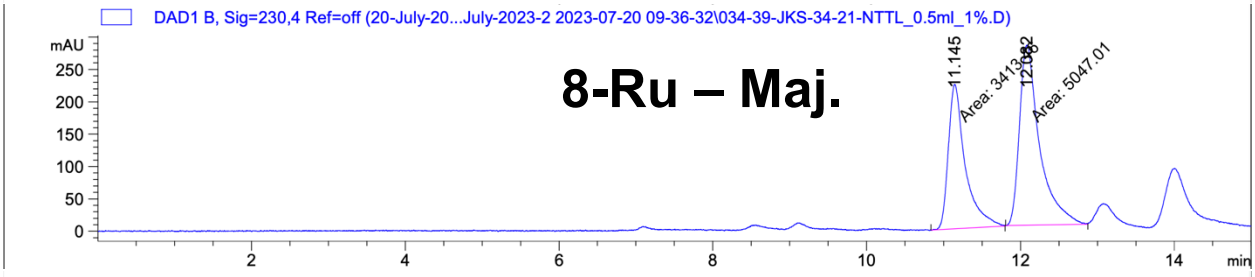

Signal 2: DAD1 B, Sig=230,4 Ref=off

Peak #	RetTime [min]	Type	Width [min]	Area [mAU*s]	Height [mAU]	Area %
1	11.145	MM	0.2548	3413.45874	223.31889	40.3460
2	12.082	MM	0.3022	5047.00635	278.37375	59.6540
Totals :				8460.46509	501.69264	

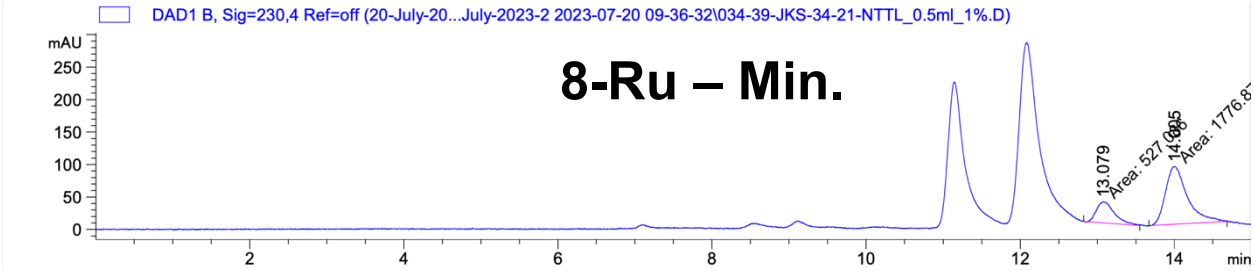

Signal 2: DAD1 B, Sig=230,4 Ref=off

Peak #	RetTime [min]	Type	Width [min]	Area [mAU*s]	Height [mAU]	Area %
1	13.079	MM	0.2686	527.08643	32.70362	22.8775
2	14.005	MM	0.3334	1776.86951	88.83726	77.1225
Totals :				2303.95593	121.54088	

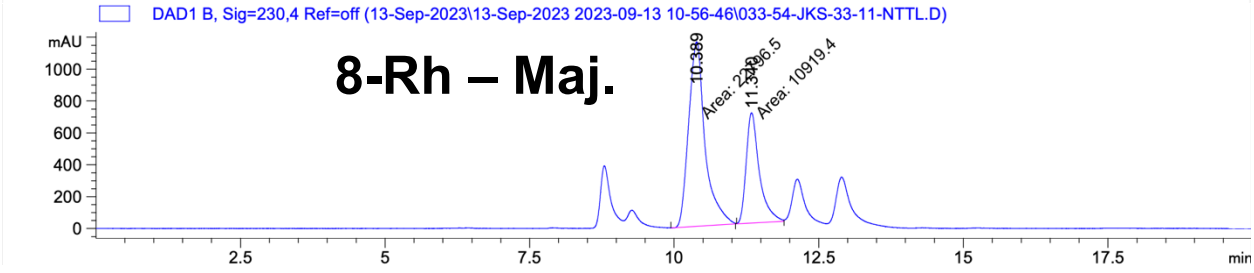

Signal 2: DAD1 B, Sig=230,4 Ref=off

Peak #	RetTime [min]	Type	Width [min]	Area [mAU*s]	Height [mAU]	Area %
1	10.389	MM	0.3279	2.27965e4	1158.75464	67.6135
2	11.340	MM	0.2631	1.09194e4	691.66125	32.3865
Totals :				3.37159e4	1850.41589	

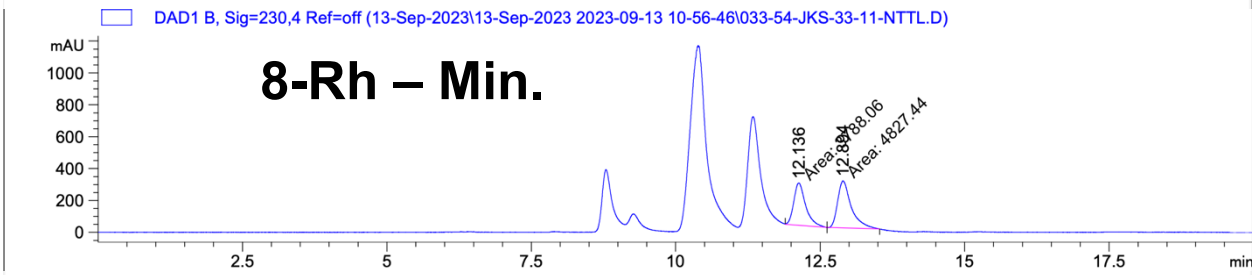

Signal 2: DAD1 B, Sig=230,4 Ref=off

Peak #	RetTime [min]	Type	Width [min]	Area [mAU*s]	Height [mAU]	Area %
1	12.136	MM	0.2381	3788.06030	265.18704	43.9679
2	12.894	MM	0.2719	4827.44482	295.86142	56.0321
Totals :				8615.50513	561.04846	

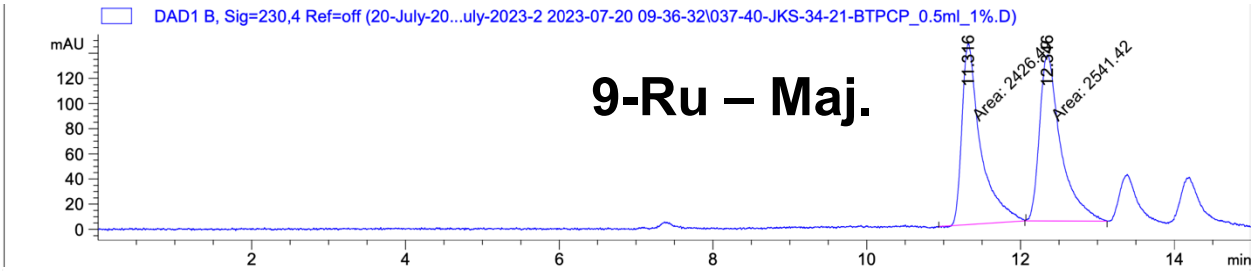

Signal 2: DAD1 B, Sig=230,4 Ref=off

Peak #	RetTime [min]	Type	Width [min]	Area [mAU*s]	Height [mAU]	Area %
1	11.316	MM	0.2815	2426.48779	143.65936	48.8432
2	12.346	MM	0.3211	2541.42163	131.92711	51.1568
Totals :				4967.90942	275.58647	

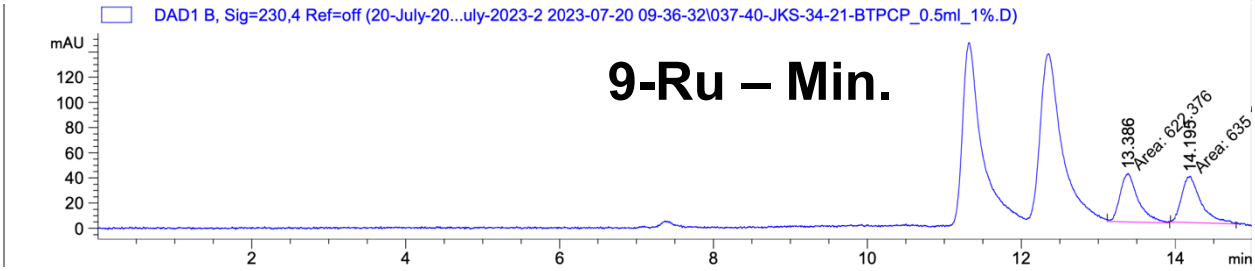

Signal 2: DAD1 B, Sig=230,4 Ref=off

Peak #	RetTime [min]	Type	Width [min]	Area [mAU*s]	Height [mAU]	Area %
1	13.386	MM	0.2699	622.37555	38.43711	49.4927
2	14.195	MM	0.2874	635.13385	36.83137	50.5073

Totals : 1257.50940 75.26849

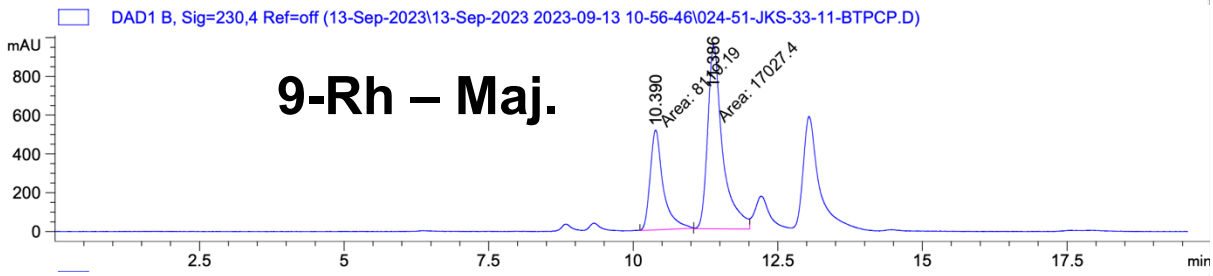

Signal 2: DAD1 B, Sig=230,4 Ref=off

Peak #	RetTime [min]	Type	Width [min]	Area [mAU*s]	Height [mAU]	Area %
1	10.390	MM	0.2626	8119.18652	515.23315	32.2875
2	11.386	MM	0.2996	1.70274e4	947.23621	67.7125

Totals : 2.51466e4 1462.46936

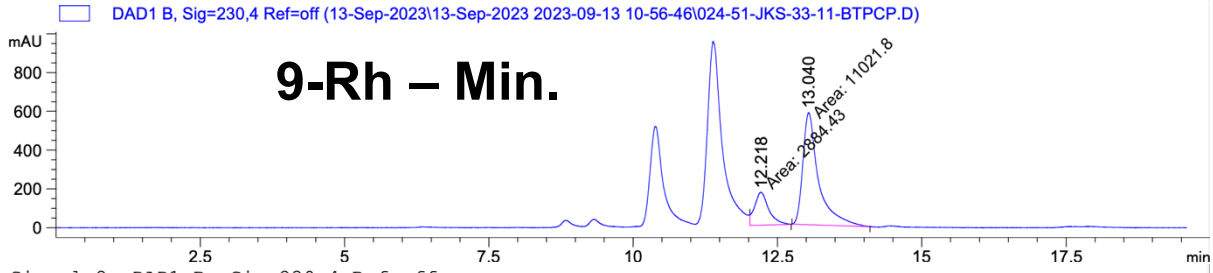

Signal 2: DAD1 B, Sig=230,4 Ref=off

Peak #	RetTime [min]	Type	Width [min]	Area [mAU*s]	Height [mAU]	Area %
1	12.218	MM	0.2829	2884.42603	169.90578	20.7420
2	13.040	MM	0.3171	1.10218e4	579.37549	79.2580

Totals : 1.39062e4 749.28127

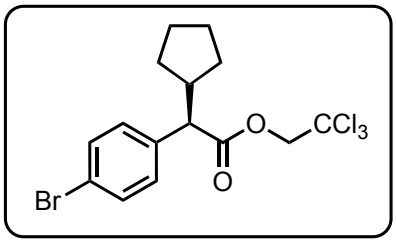

Compound **19**

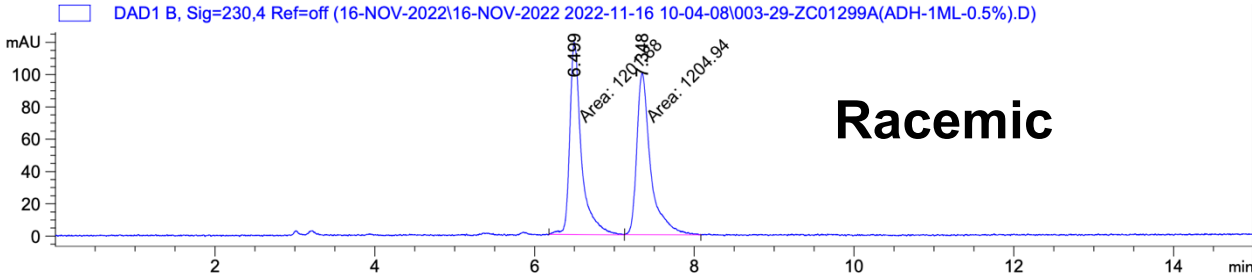

Signal 2: DAD1 B, Sig=230,4 Ref=off

Peak #	RetTime [min]	Type	Width [min]	Area [mAU*s]	Height [mAU]	Area %
1	6.499	MM	0.1682	1201.87817	119.10645	49.9364
2	7.348	MM	0.2007	1204.93994	100.07652	50.0636
Totals :				2406.81812	219.18298	

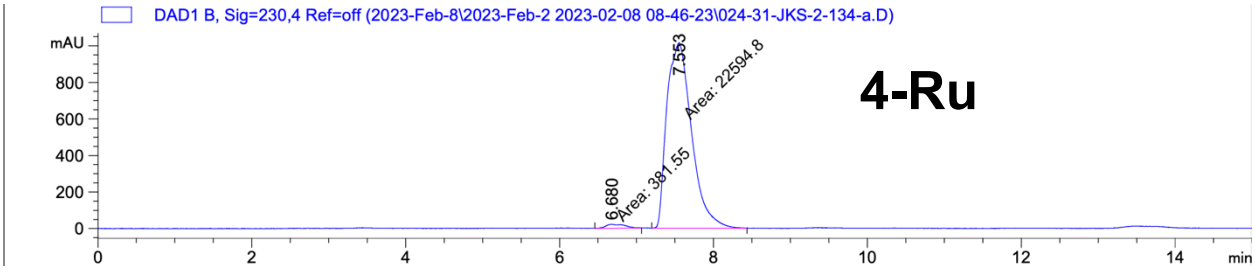

Signal 2: DAD1 B, Sig=230,4 Ref=off

Peak #	RetTime [min]	Type	Width [min]	Area [mAU*s]	Height [mAU]	Area %
1	6.680	MM	0.2961	381.54971	21.47387	1.6606
2	7.553	MM	0.3706	2.25948e4	1016.03406	98.3394
Totals :				2.29764e4	1037.50793	

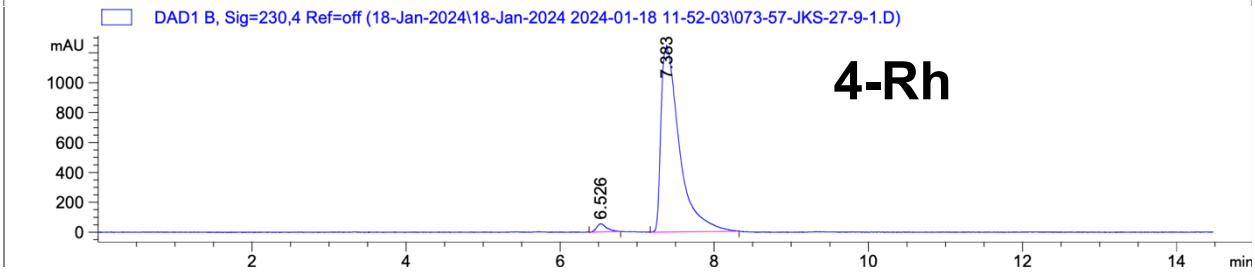

Signal 2: DAD1 B, Sig=230,4 Ref=off

Peak #	RetTime [min]	Type	Width [min]	Area [mAU*s]	Height [mAU]	Area %
1	6.526	VV R	0.1147	496.69824	53.80212	2.3631
2	7.383	VV R	0.1950	2.05225e4	1249.94275	97.6369
Totals :				2.10192e4	1303.74487	

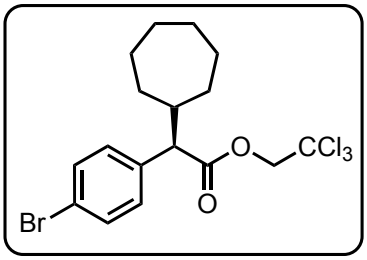

Compound **20**

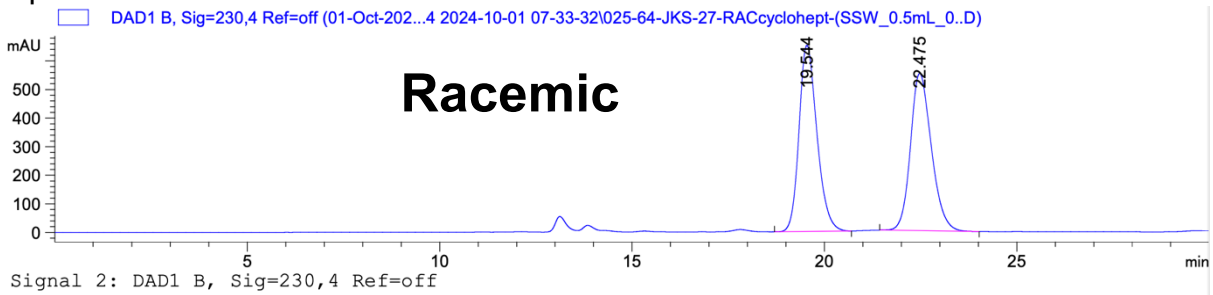

Signal 2: DAD1 B, Sig=230,4 Ref=off

Peak #	RetTime [min]	Type	Width [min]	Area [mAU*s]	Height [mAU]	Area %
1	19.544	BB	0.4846	2.10776e4	651.31793	50.3942
2	22.475	BB	0.5466	2.07478e4	550.01404	49.6058
Totals :				4.18255e4	1201.33197	

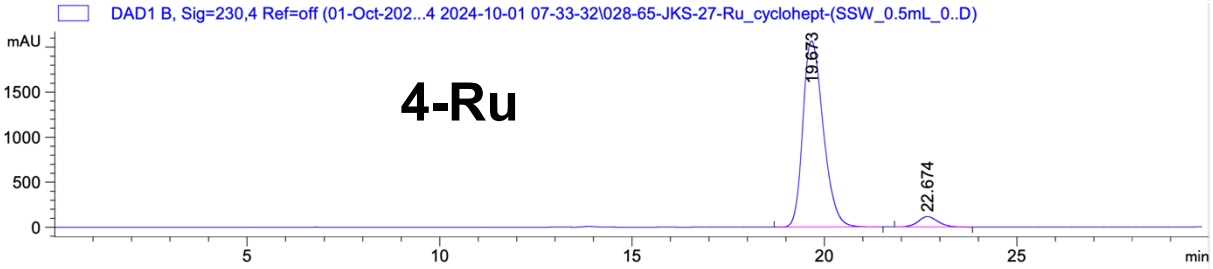

Signal 2: DAD1 B, Sig=230,4 Ref=off

Peak #	RetTime [min]	Type	Width [min]	Area [mAU*s]	Height [mAU]	Area %
1	19.673	BB	0.4343	7.60302e4	2066.04028	94.9019
2	22.674	BB	0.4722	4084.35864	114.90491	5.0981
Totals :				8.01145e4	2180.94520	

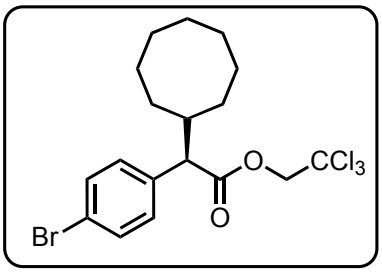

Compound **21**

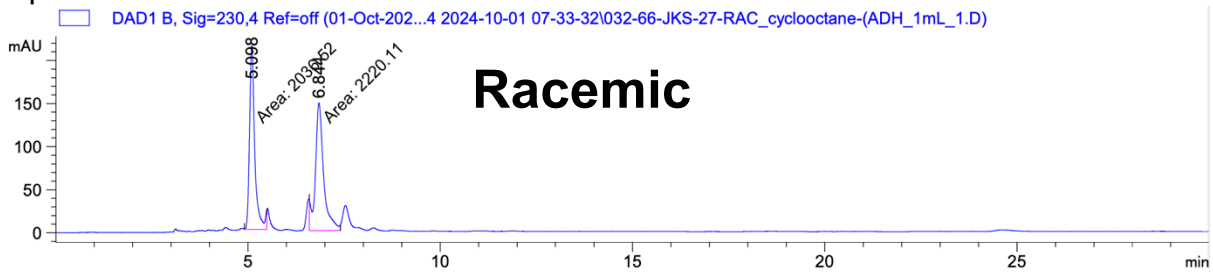

Signal 2: DAD1 B, Sig=230,4 Ref=off

Peak #	RetTime [min]	Type	Width [min]	Area [mAU*s]	Height [mAU]	Area %
1	5.098	MM	0.1593	2036.51501	213.05951	47.8434
2	6.844	MM	0.2498	2220.10986	148.14349	52.1566
Totals :				4256.62488	361.20300	

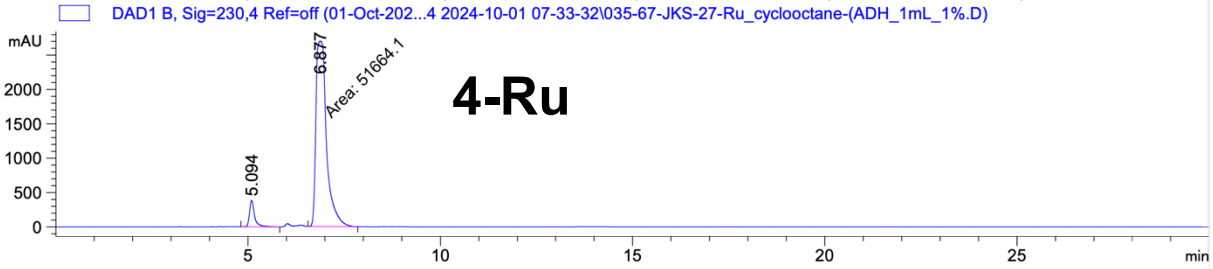

Signal 2: DAD1 B, Sig=230,4 Ref=off

Peak #	RetTime [min]	Type	Width [min]	Area [mAU*s]	Height [mAU]	Area %
1	5.094	BB	0.1365	3498.30005	383.29721	6.3418
2	6.877	MM	0.3184	5.16641e4	2704.20752	93.6582
Totals :				5.51624e4	3087.50473	

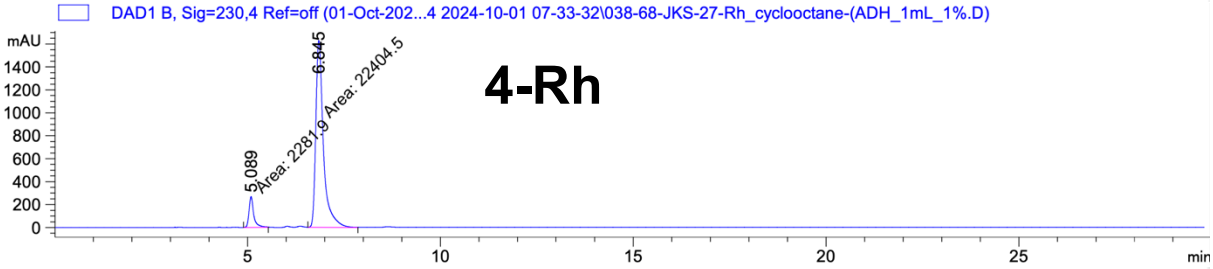

Signal 2: DAD1 B, Sig=230,4 Ref=off

Peak #	RetTime [min]	Type	Width [min]	Area [mAU*s]	Height [mAU]	Area %
1	5.089	MM	0.1416	2281.90063	268.63290	9.2436
2	6.845	MM	0.2291	2.24045e4	1629.59851	90.7564
Totals :				2.46864e4	1898.23141	

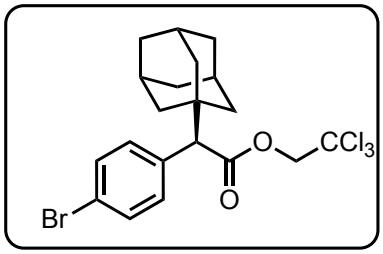

Compound **22**

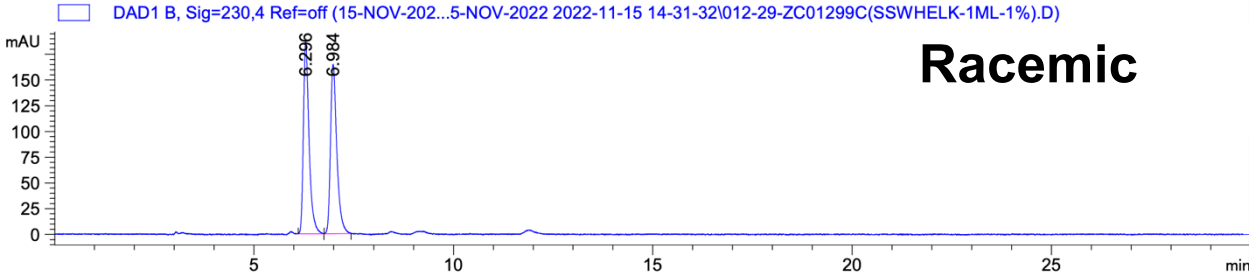

Signal 2: DAD1 B, Sig=230,4 Ref=off

Peak #	RetTime [min]	Type	Width [min]	Area [mAU*s]	Height [mAU]	Area %
1	6.296	BV R	0.1340	1842.88098	186.89391	50.3686
2	6.984	VV R	0.1352	1815.90515	164.64194	49.6314
Totals :				3658.78613	351.53584	

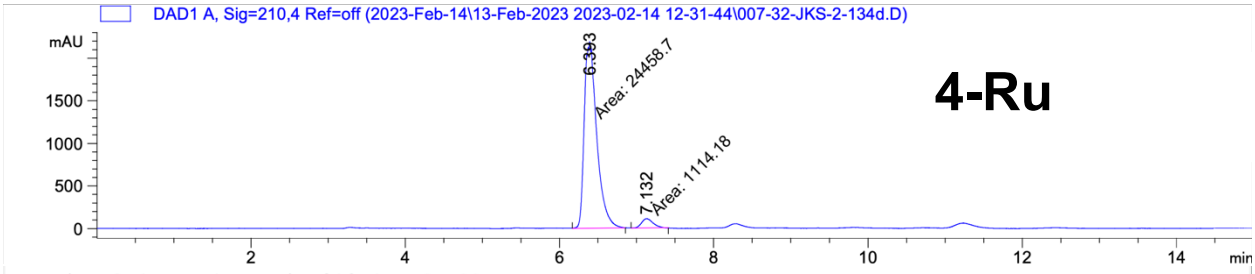

Signal 1: DAD1 A, Sig=210,4 Ref=off

Peak #	RetTime [min]	Type	Width [min]	Area [mAU*s]	Height [mAU]	Area %
1	6.393	MM	0.1859	2.44587e4	2192.61743	95.6431
2	7.132	MM	0.1712	1114.18347	108.44734	4.3569
Totals :				2.55729e4	2301.06477	

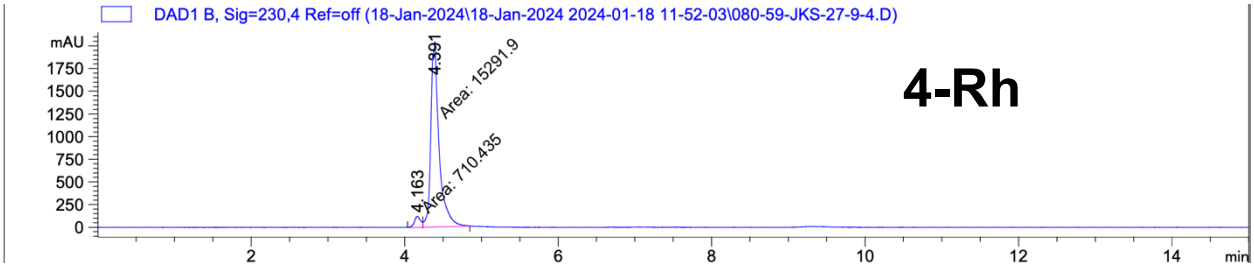

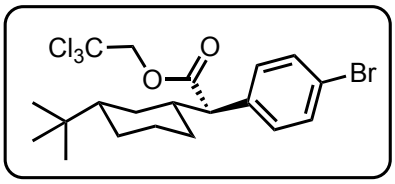

Compound **23**

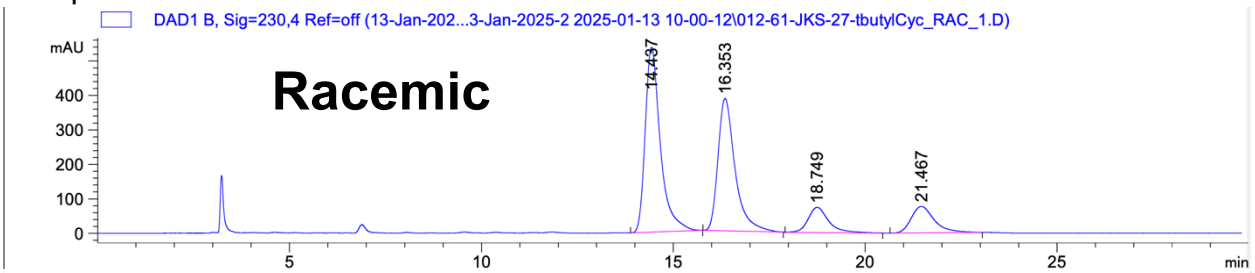

Signal 2: DAD1 B, Sig=230,4 Ref=off

Peak #	RetTime [min]	Type	Width [min]	Area [mAU*s]	Height [mAU]	Area %
1	14.437	BB	0.4059	1.46971e4	536.03296	45.2817
2	16.353	BB	0.4497	1.18732e4	383.55173	36.5815
3	18.749	BB	0.4545	2692.45996	72.88506	8.2955
4	21.467	BB	0.4931	3194.18481	76.34607	9.8413
Totals :				3.24570e4	1068.81582	

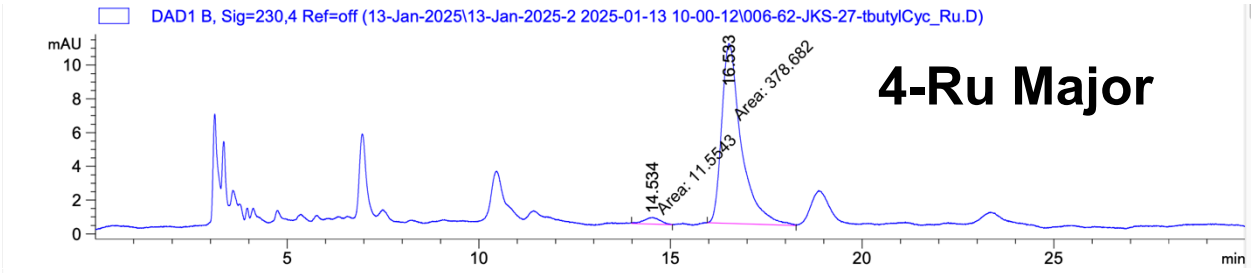

Signal 2: DAD1 B, Sig=230,4 Ref=off

Peak #	RetTime [min]	Type	Width [min]	Area [mAU*s]	Height [mAU]	Area %
1	14.534	MM	0.4844	11.55427	3.97575e-1	2.9608
2	16.533	MM	0.5925	378.68228	10.65221	97.0392
Totals :				390.23655	11.04978	

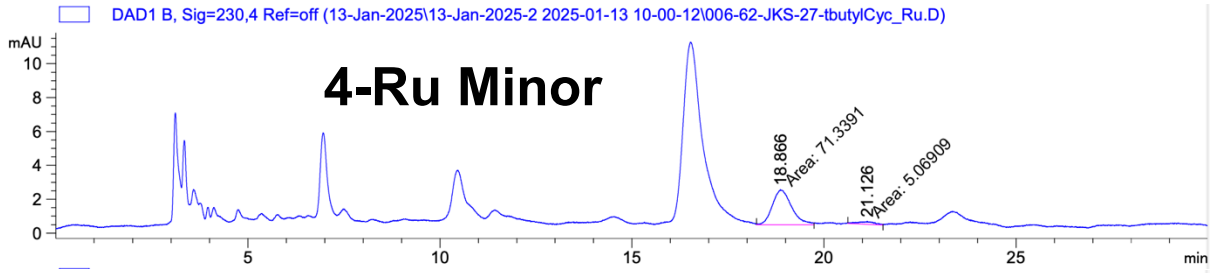

Signal 2: DAD1 B, Sig=230,4 Ref=off

Peak #	RetTime [min]	Type	Width [min]	Area [mAU*s]	Height [mAU]	Area %
1	18.866	MM	0.5742	71.33913	2.07054	93.3658
2	21.126	MM	0.4515	5.06909	1.87129e-1	6.6342
Totals :				76.40821	2.25767	

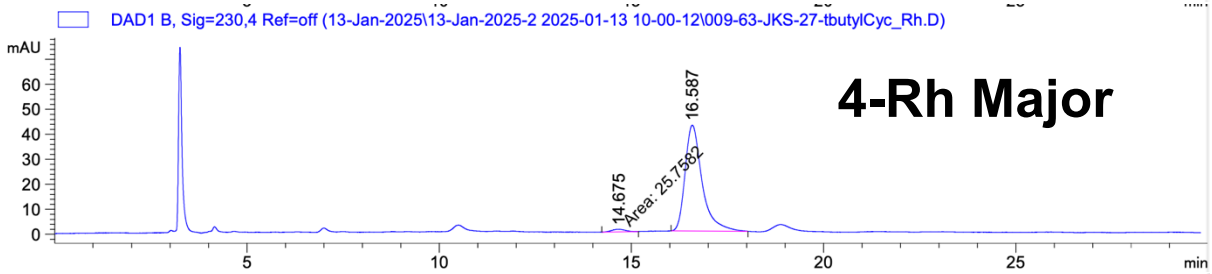

Signal 2: DAD1 B, Sig=230,4 Ref=off

Peak #	RetTime [min]	Type	Width [min]	Area [mAU*s]	Height [mAU]	Area %
1	14.675	MM	0.4057	25.75818	1.05826	1.9406
2	16.587	BB	0.3676	1301.54248	42.34519	98.0594
Totals :				1327.30066	43.40345	

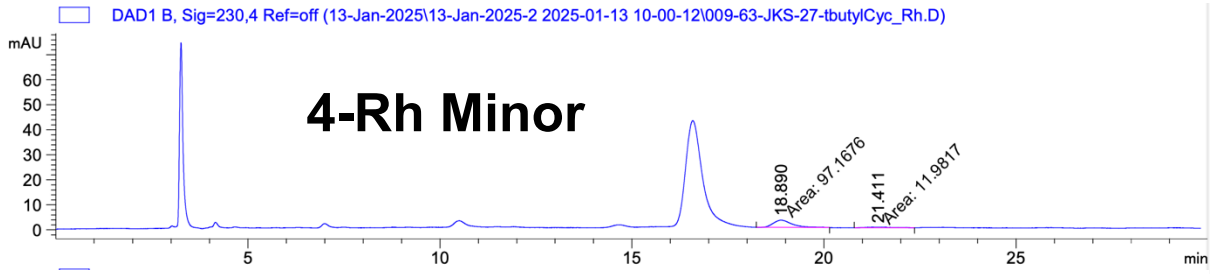

Signal 2: DAD1 B, Sig=230,4 Ref=off

Peak #	RetTime [min]	Type	Width [min]	Area [mAU*s]	Height [mAU]	Area %
1	18.890	MM	0.5588	97.16756	2.89803	89.0227
2	21.411	MM	0.8451	11.98167	2.36291e-1	10.9773
Totals :				109.14924	3.13432	

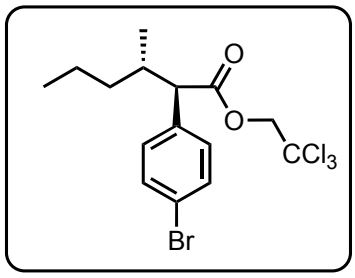

Compound **24**

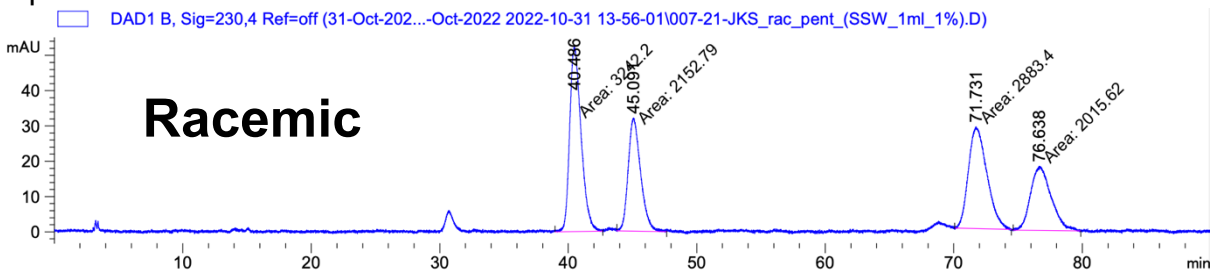

Signal 2: DAD1 B, Sig=230,4 Ref=off

Peak #	RetTime [min]	Type	Width [min]	Area [mAU*s]	Height [mAU]	Area %
1	40.486	MM	1.0320	3242.19922	52.36084	31.4960
2	45.091	MM	1.1185	2152.78516	32.07850	20.9130
3	71.731	MM	1.6665	2883.39941	28.83657	28.0105
4	76.638	MM	1.8445	2015.61963	18.21255	19.5805
Totals :				1.02940e4	131.48845	

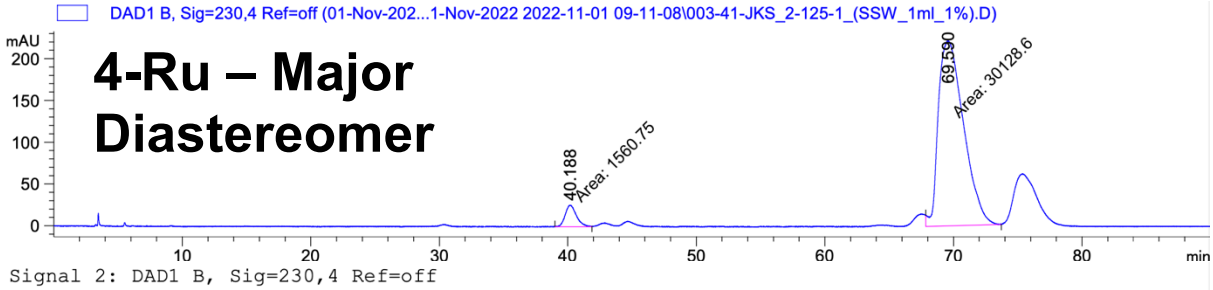

Signal 2: DAD1 B, Sig=230,4 Ref=off

Peak #	RetTime [min]	Type	Width [min]	Area [mAU*s]	Height [mAU]	Area %
1	40.188	MM	1.0053	1560.75403	25.87547	4.9252
2	69.590	MM	2.2661	3.01286e4	221.58920	95.0748
Totals :				3.16893e4	247.46467	

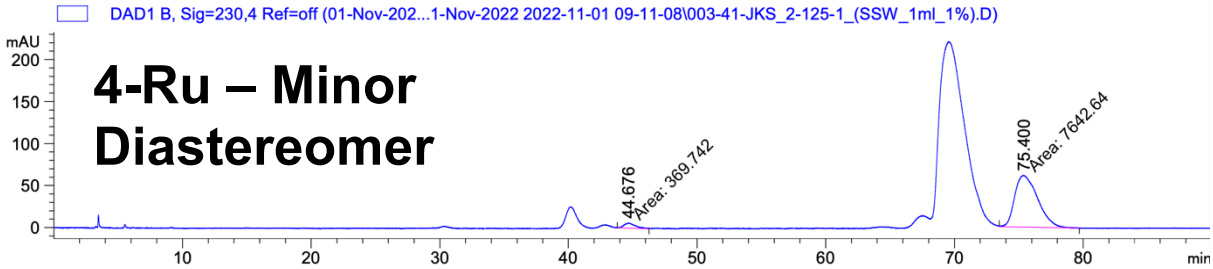

Signal 2: DAD1 B, Sig=230,4 Ref=off

Peak #	RetTime [min]	Type	Width [min]	Area [mAU*s]	Height [mAU]	Area %
1	44.676	MM	0.9953	369.74167	6.19154	4.6146
2	75.400	MM	2.0623	7642.63623	61.76421	95.3854
Totals :				8012.37790	67.95575	

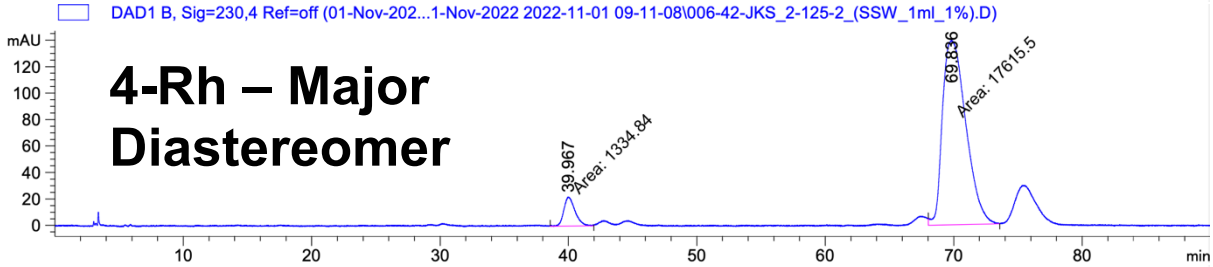

Signal 2: DAD1 B, Sig=230,4 Ref=off

Peak #	RetTime [min]	Type	Width [min]	Area [mAU*s]	Height [mAU]	Area %
1	39.967	MM	1.0087	1334.83838	22.05637	7.0439
2	69.836	MM	2.1043	1.76155e4	139.51675	92.9561
Totals :				1.89503e4	161.57313	

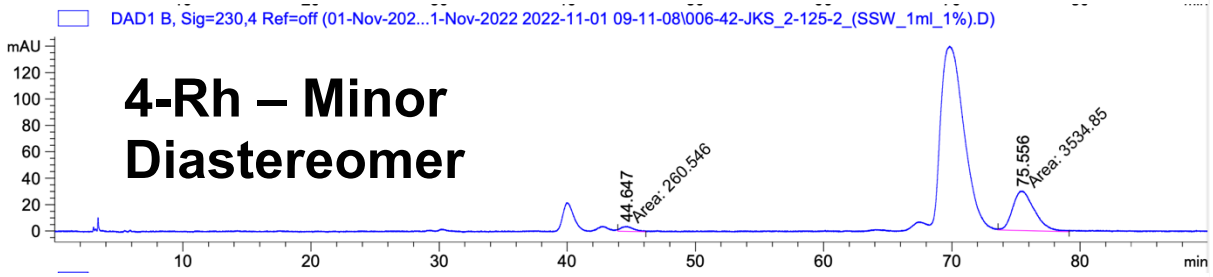

Signal 2: DAD1 B, Sig=230,4 Ref=off

Peak #	RetTime [min]	Type	Width [min]	Area [mAU*s]	Height [mAU]	Area %
1	44.647	MM	1.1142	260.54562	3.89733	6.8648
2	75.556	MM	1.9682	3534.85034	29.93359	93.1352
Totals :				3795.39597	33.83093	

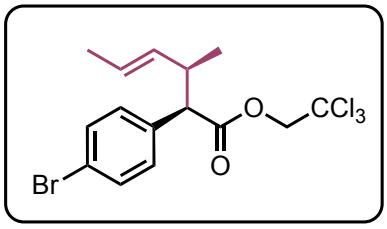

Compound **22**

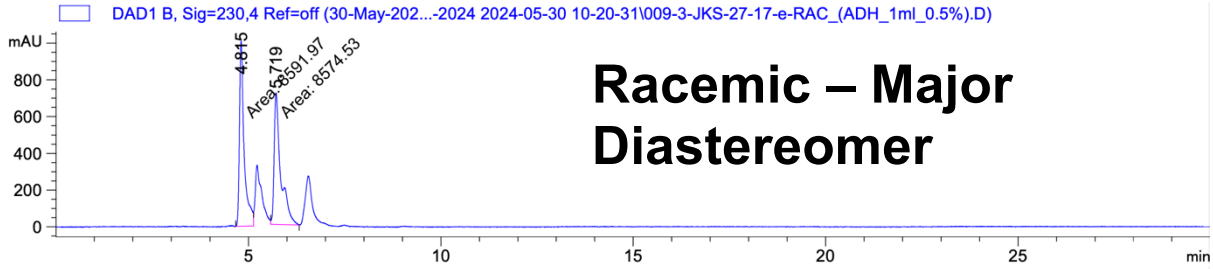

Racemic – Major Diastereomer

Signal 2: DAD1 B, Sig=230,4 Ref=off

Peak #	RetTime [min]	Type	Width [min]	Area [mAU*s]	Height [mAU]	Area %
1	4.815	MM	0.1422	8591.96875	1007.25586	50.0508
2	5.719	MM	0.1995	8574.52637	716.43311	49.9492
Totals :				1.71665e4	1723.68896	

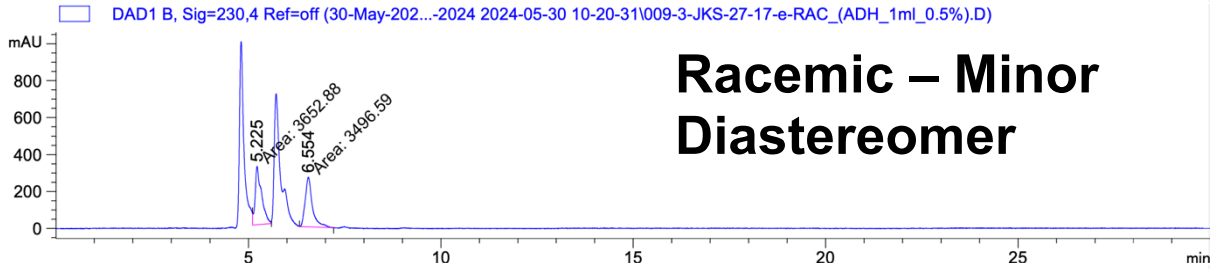

Racemic – Minor Diastereomer

Signal 2: DAD1 B, Sig=230,4 Ref=off

Peak #	RetTime [min]	Type	Width [min]	Area [mAU*s]	Height [mAU]	Area %
1	5.225	MM	0.1929	3652.88403	315.57245	51.0931
2	6.554	MM	0.2168	3496.58521	268.85019	48.9069
Totals :				7149.46924	584.42264	

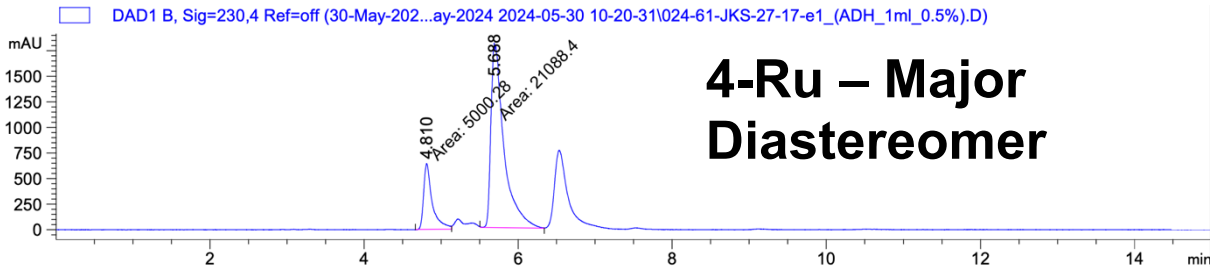

4-Ru – Major Diastereomer

Signal 2: DAD1 B, Sig=230,4 Ref=off

Peak #	RetTime [min]	Type	Width [min]	Area [mAU*s]	Height [mAU]	Area %
1	4.810	MM	0.1295	5000.28125	643.57147	19.1665
2	5.688	MM	0.1947	2.10884e4	1805.57666	80.8335
Totals :				2.60887e4	2449.14813	

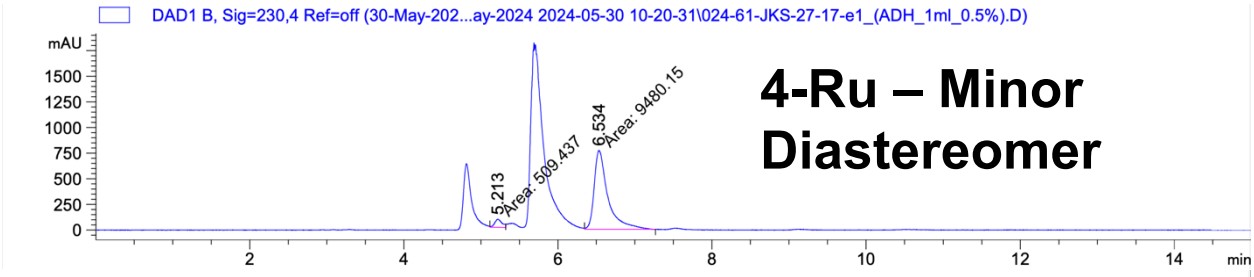

4-Ru – Minor Diastereomer

Signal 2: DAD1 B, Sig=230,4 Ref=off

Peak #	RetTime [min]	Type	Width [min]	Area [mAU*s]	Height [mAU]	Area %
1	5.213	MM	0.1101	509.43701	77.09387	5.0997
2	6.534	MM	0.2052	9480.14844	770.14447	94.9003
Totals :				9989.58545	847.23834	

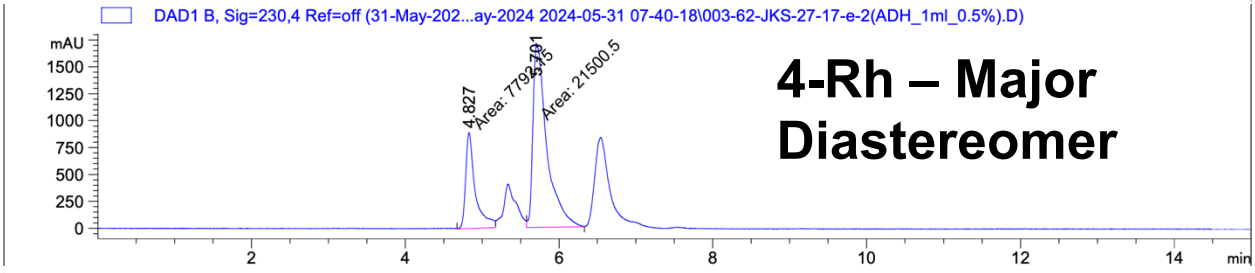

4-Rh – Major Diastereomer

Signal 2: DAD1 B, Sig=230,4 Ref=off

Peak #	RetTime [min]	Type	Width [min]	Area [mAU*s]	Height [mAU]	Area %
1	4.827	MM	0.1451	7792.15430	894.80145	26.6010
2	5.701	MM	0.2091	2.15005e4	1714.09851	73.3990
Totals :				2.92927e4	2608.89996	

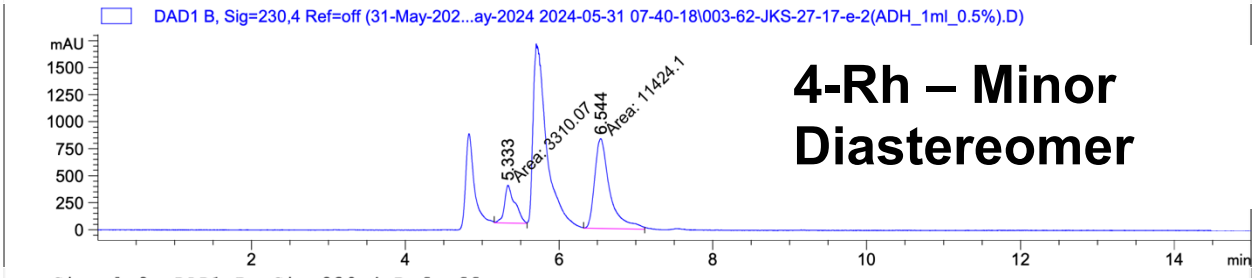

4-Rh – Minor Diastereomer

Signal 2: DAD1 B, Sig=230,4 Ref=off

Peak #	RetTime [min]	Type	Width [min]	Area [mAU*s]	Height [mAU]	Area %
1	5.333	MM	0.1571	3310.06958	351.16541	22.4653
2	6.544	MM	0.2290	1.14241e4	831.31274	77.5347
Totals :				1.47342e4	1182.47815	

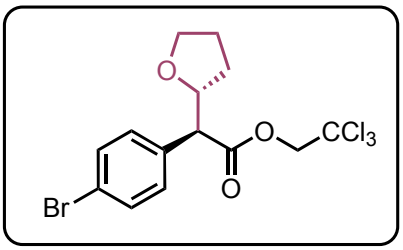

Compound **26**

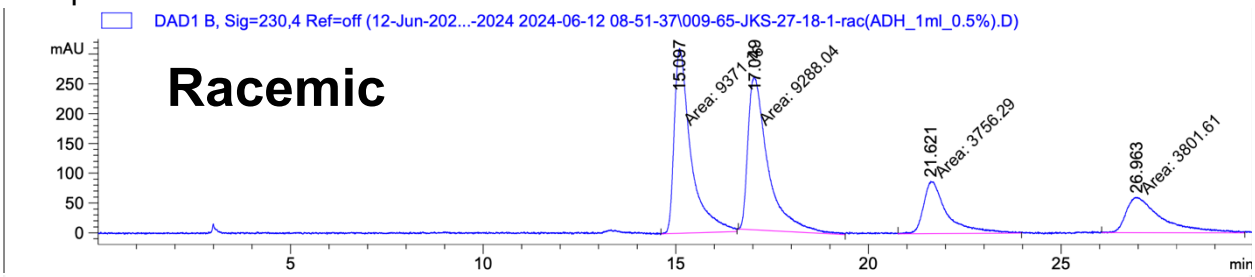

Signal 2: DAD1 B, Sig=230,4 Ref=off

Peak #	RetTime [min]	Type	Width [min]	Area [mAU*s]	Height [mAU]	Area %
1	15.097	MM	0.5031	9371.16113	310.42740	35.7444
2	17.049	MM	0.6026	9288.04492	256.87198	35.4274
3	21.621	MM	0.7109	3756.29053	88.06490	14.3276
4	26.963	MM	1.0703	3801.61182	59.19608	14.5005
Totals :				2.62171e4	714.56035	

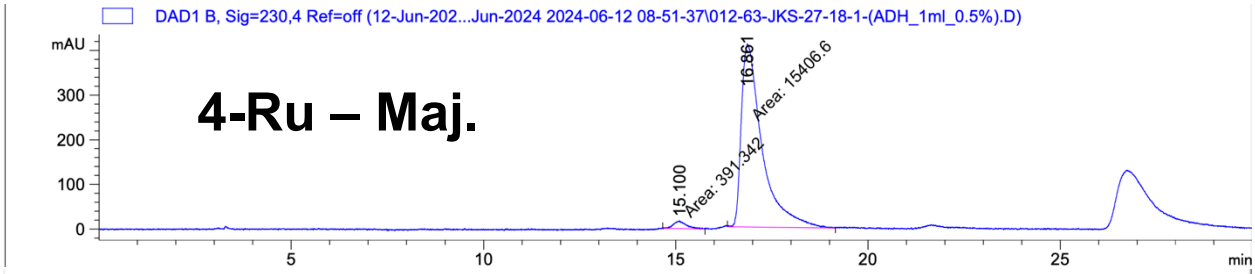

Signal 2: DAD1 B, Sig=230,4 Ref=off

Peak #	RetTime [min]	Type	Width [min]	Area [mAU*s]	Height [mAU]	Area %
1	15.100	MM	0.3686	391.34244	17.69704	2.4772
2	16.861	MM	0.6254	1.54066e4	410.60364	97.5228
Totals :				1.57980e4	428.30068	

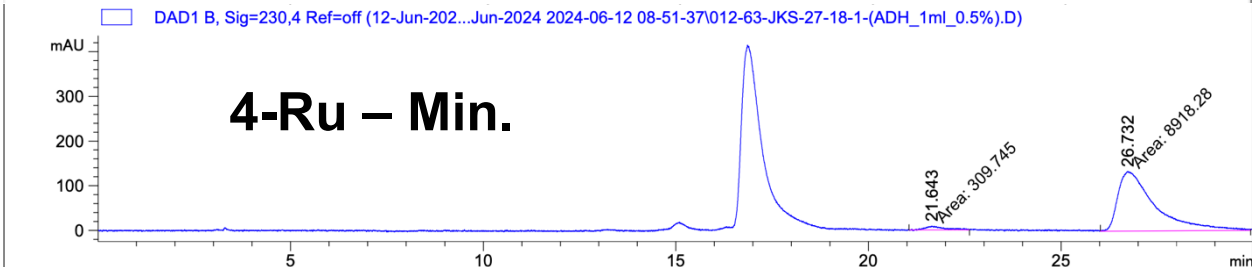

Signal 2: DAD1 B, Sig=230,4 Ref=off

Peak #	RetTime [min]	Type	Width [min]	Area [mAU*s]	Height [mAU]	Area %
1	21.643	MM	0.5684	309.74539	9.08172	3.3566
2	26.732	MM	1.1137	8918.27930	133.45743	96.6434
Totals :				9228.02469	142.53915	

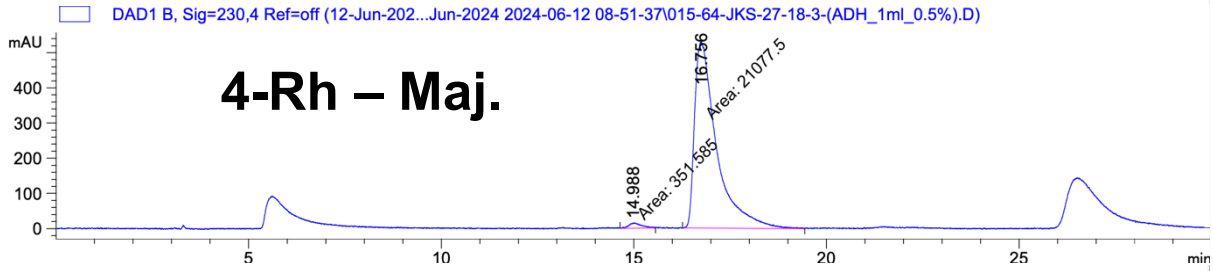

Signal 2: DAD1 B, Sig=230,4 Ref=off

Peak #	RetTime [min]	Type	Width [min]	Area [mAU*s]	Height [mAU]	Area %
1	14.988	MM	0.3787	351.58496	15.47485	1.6407
2	16.756	MM	0.6635	2.10775e4	529.42053	98.3593
Totals :				2.14291e4	544.89539	

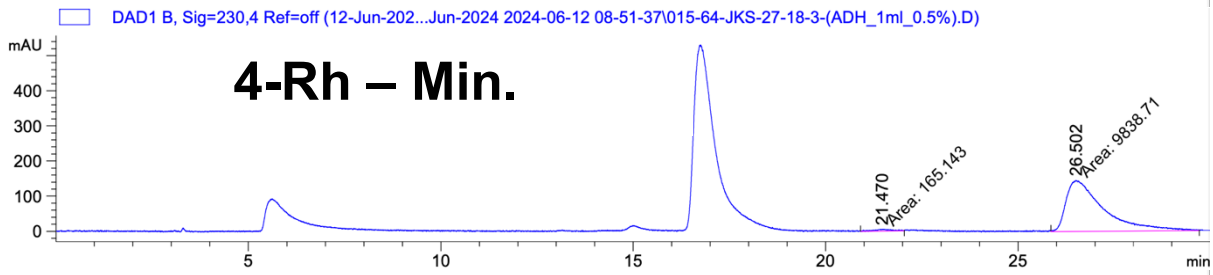

Signal 2: DAD1 B, Sig=230,4 Ref=off

Peak #	RetTime [min]	Type	Width [min]	Area [mAU*s]	Height [mAU]	Area %
1	21.470	MM	0.5203	165.14310	5.29025	1.6508
2	26.502	MM	1.1258	9838.71289	145.65511	98.3492
Totals :				1.00039e4	150.94535	

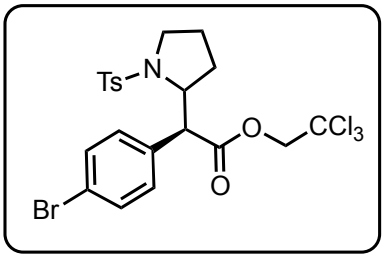

Compound **27**

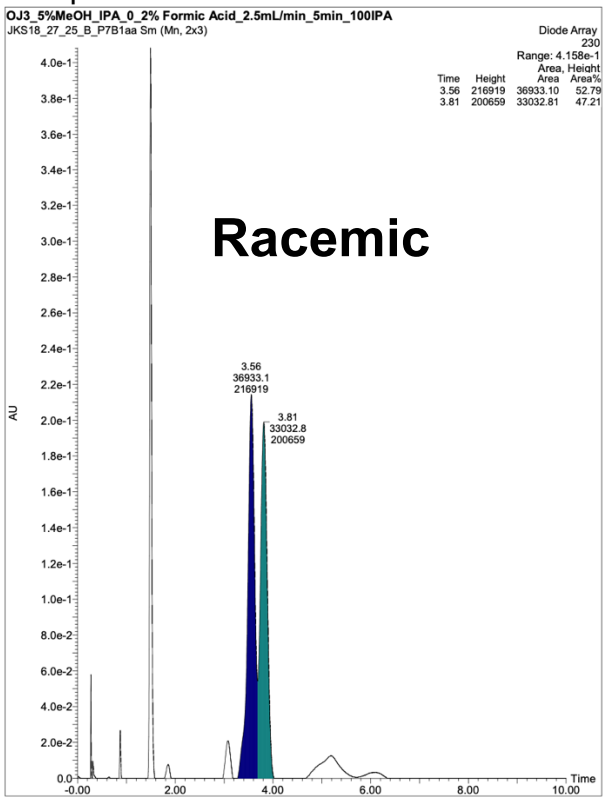

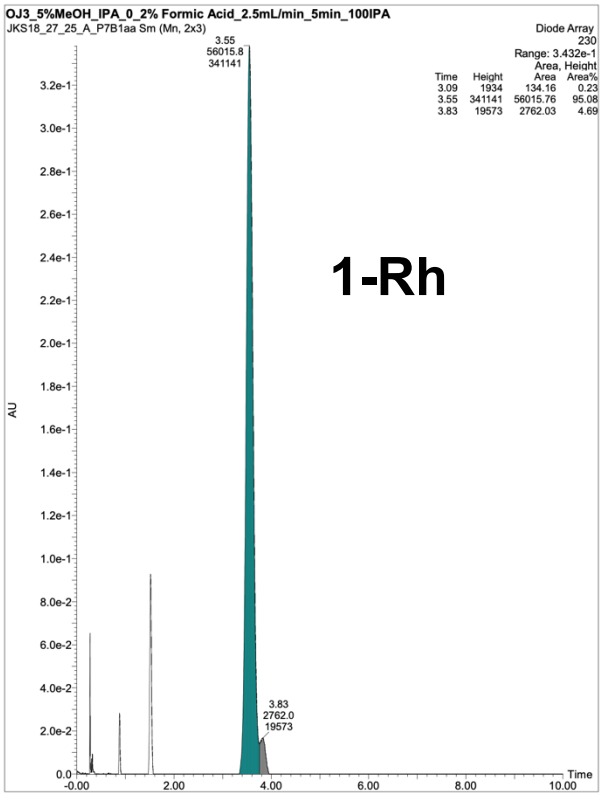

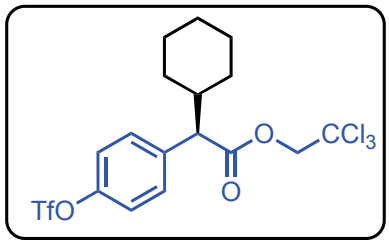

Compound **28**

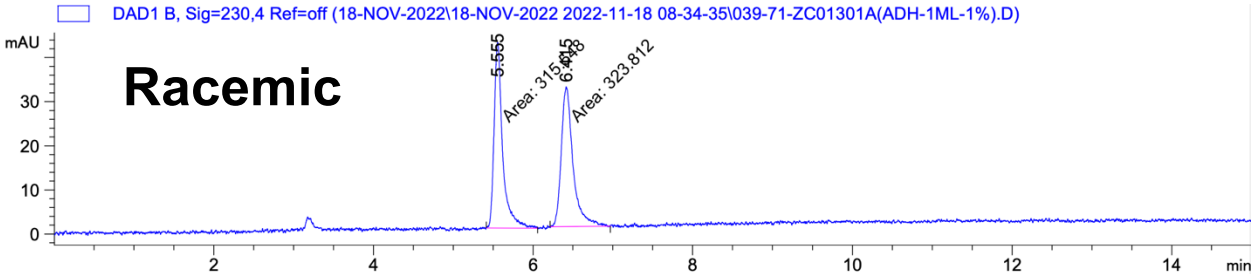

Signal 2: DAD1 B, Sig=230,4 Ref=off

Peak #	RetTime [min]	Type	Width [min]	Area [mAU*s]	Height [mAU]	Area %
1	5.555	MM	0.1249	315.54758	42.11271	49.3537
2	6.415	MM	0.1702	323.81174	31.70454	50.6463
Totals :				639.35931	73.81725	

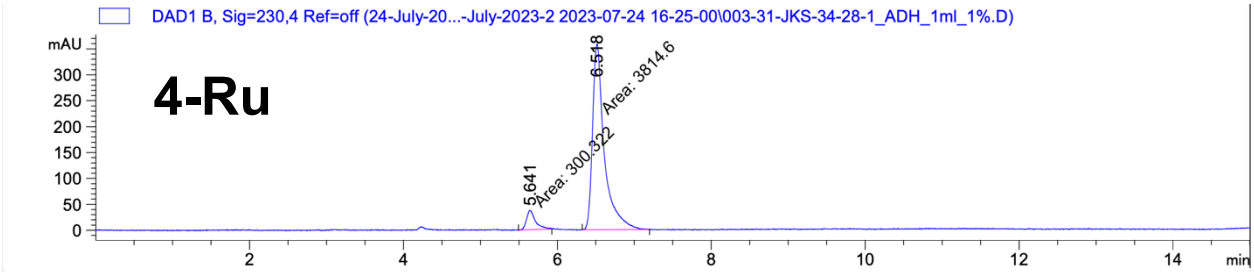

Signal 2: DAD1 B, Sig=230,4 Ref=off

Peak #	RetTime [min]	Type	Width [min]	Area [mAU*s]	Height [mAU]	Area %
1	5.641	MM	0.1346	300.32205	37.19786	7.2984
2	6.518	MM	0.1773	3814.59692	358.64355	92.7016
Totals :				4114.91898	395.84142	

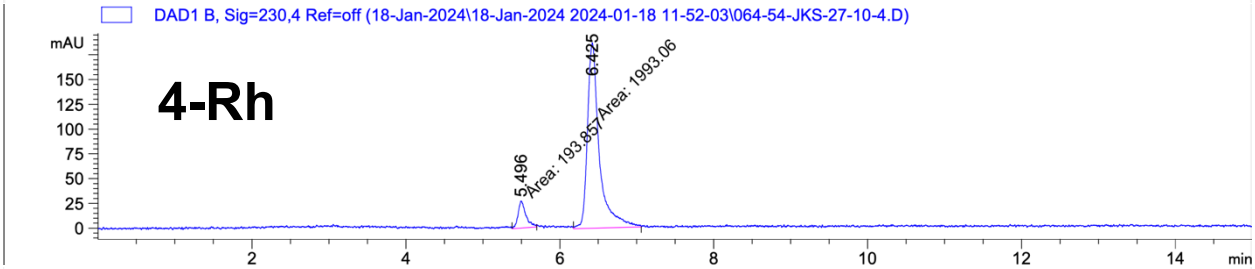

Signal 2: DAD1 B, Sig=230,4 Ref=off

Peak #	RetTime [min]	Type	Width [min]	Area [mAU*s]	Height [mAU]	Area %
1	5.496	MM	0.1186	193.85712	27.25322	8.8644
2	6.425	MM	0.1774	1993.05518	187.23053	91.1356
Totals :				2186.91229	214.48375	

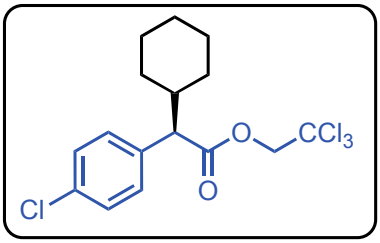

Compound **29**

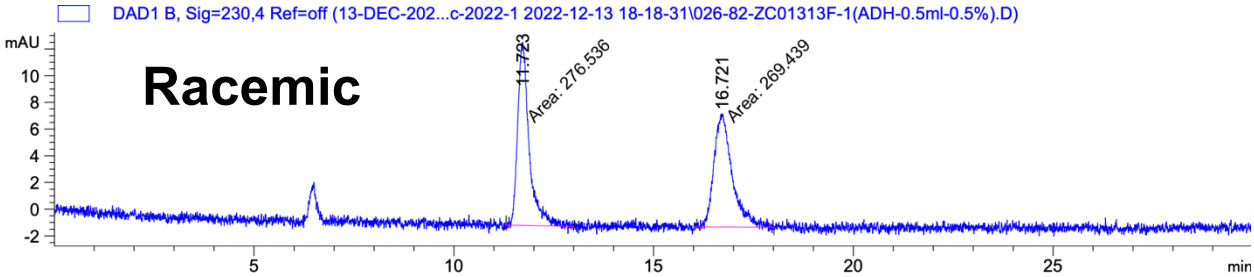

Signal 2: DAD1 B, Sig=230,4 Ref=off

Peak #	RetTime [min]	Type	Width [min]	Area [mAU*s]	Height [mAU]	Area %
1	11.723	MM	0.3359	276.53616	13.72200	50.6499
2	16.721	MM	0.5299	269.43939	8.47415	49.3501
Totals :				545.97556	22.19615	

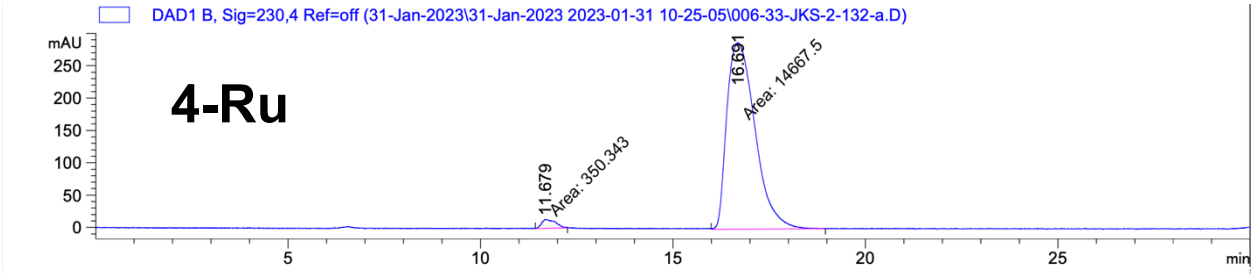

Signal 2: DAD1 B, Sig=230,4 Ref=off

Peak #	RetTime [min]	Type	Width [min]	Area [mAU*s]	Height [mAU]	Area %
1	11.679	MM	0.4140	350.34320	14.10548	2.3328
2	16.691	MM	0.8474	1.46675e4	288.48712	97.6672
Totals :				1.50179e4	302.59260	

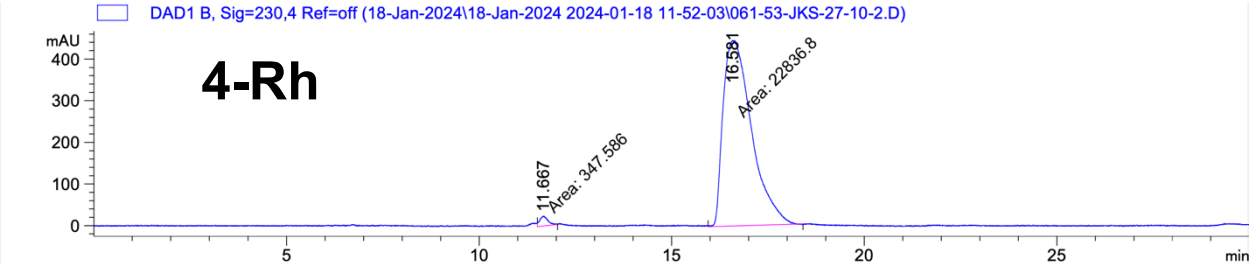

Signal 2: DAD1 B, Sig=230,4 Ref=off

Peak #	RetTime [min]	Type	Width [min]	Area [mAU*s]	Height [mAU]	Area %
1	11.667	MM	0.2409	347.58630	24.05255	1.4992
2	16.581	MM	0.8543	2.28368e4	445.53268	98.5008
Totals :				2.31844e4	469.58524	

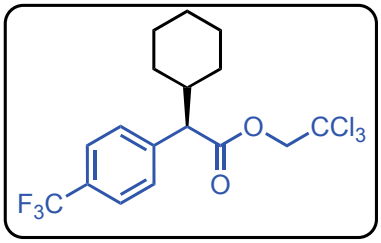

Compound **30**

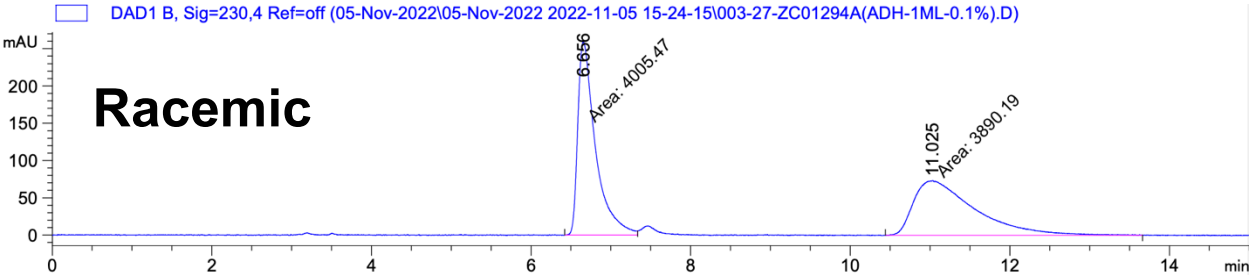

Signal 2: DAD1 B, Sig=230,4 Ref=off

Peak #	RetTime [min]	Type	Width [min]	Area [mAU*s]	Height [mAU]	Area %
1	6.656	MF	0.2576	4005.46729	259.15402	50.7300
2	11.025	MM	0.8841	3890.19043	73.33485	49.2700
Totals :				7895.65771	332.48887	

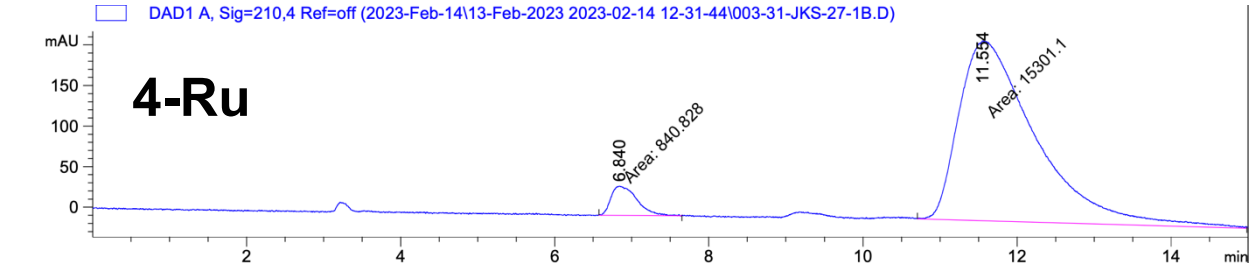

Signal 1: DAD1 A, Sig=210,4 Ref=off

Peak #	RetTime [min]	Type	Width [min]	Area [mAU*s]	Height [mAU]	Area %
1	6.840	MM	0.3892	840.82751	36.00511	5.2090
2	11.554	MM	1.1493	1.53011e4	221.90002	94.7910
Totals :				1.61419e4	257.90513	

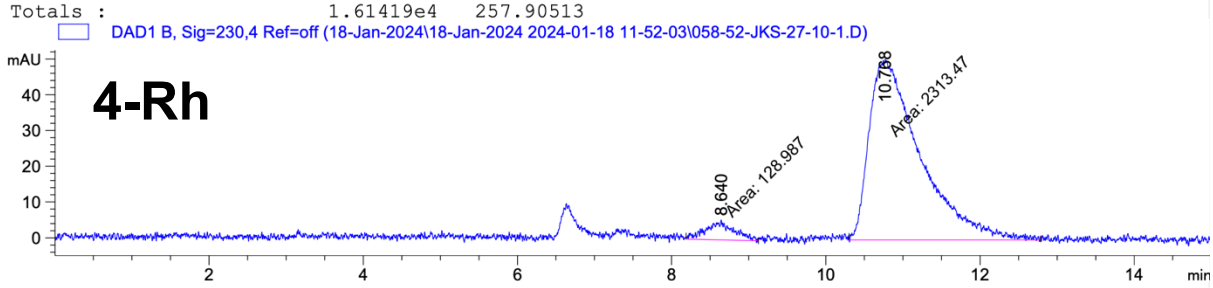

Signal 2: DAD1 B, Sig=230,4 Ref=off

Peak #	RetTime [min]	Type	Width [min]	Area [mAU*s]	Height [mAU]	Area %
1	8.640	MM	0.3882	128.98727	5.53717	5.2811
2	10.768	MM	0.7639	2313.46753	50.47333	94.7189
Totals :				2442.45480	56.01050	

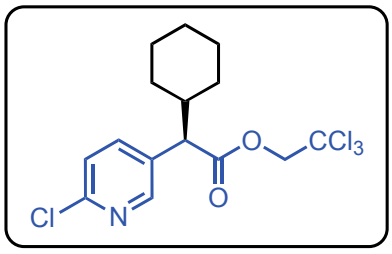

Compound **31**

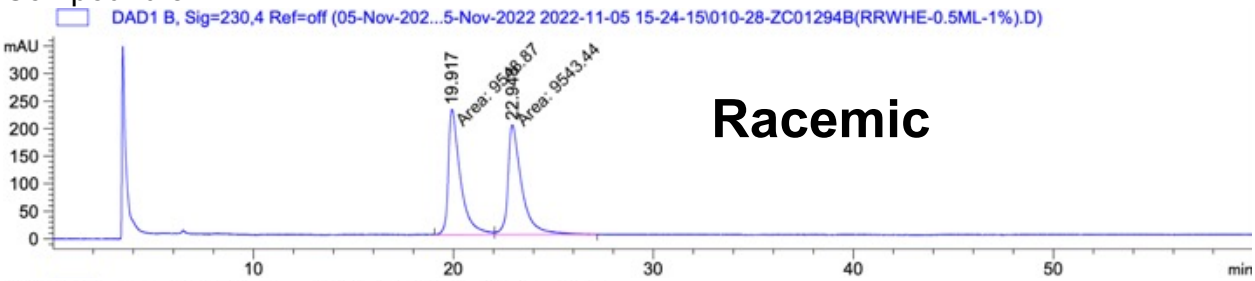

Signal 2: DAD1 B, Sig=230,4 Ref=off

Peak #	RetTime [min]	Type	Width [min]	Area [mAU*s]	Height [mAU]	Area %
1	19.917	MF	0.6999	9548.87305	227.39455	50.0142
2	22.943	FM	0.7978	9543.44238	199.35765	49.9858
Totals :				1.90923e4	426.75220	

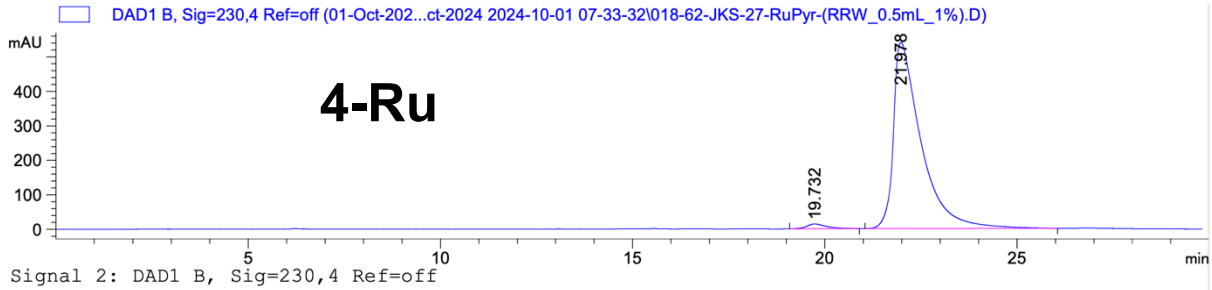

Signal 2: DAD1 B, Sig=230,4 Ref=off

Peak #	RetTime [min]	Type	Width [min]	Area [mAU*s]	Height [mAU]	Area %
1	19.732	BB	0.4238	501.34375	13.93367	1.8219
2	21.978	BB	0.6558	2.70161e4	539.90717	98.1781
Totals :				2.75174e4	553.84084	

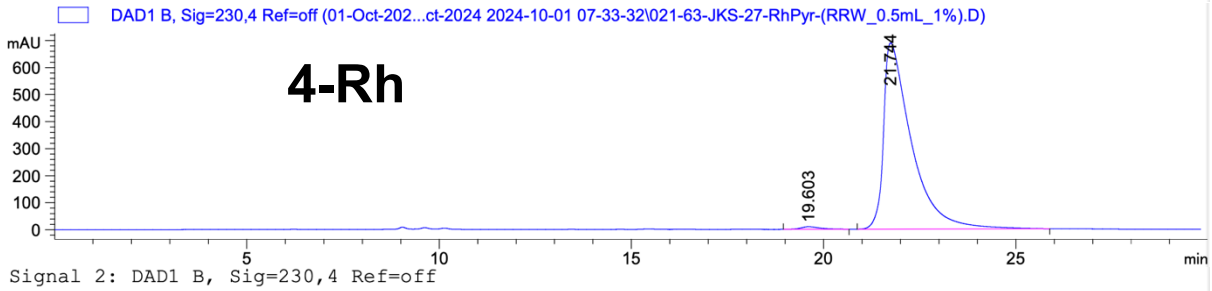

Signal 2: DAD1 B, Sig=230,4 Ref=off

Peak #	RetTime [min]	Type	Width [min]	Area [mAU*s]	Height [mAU]	Area %
1	19.603	BB	0.4089	332.29840	9.52656	0.9472
2	21.744	BB	0.6580	3.47506e4	688.86749	99.0528
Totals :				3.50829e4	698.39406	

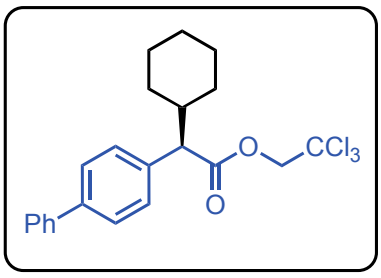

Compound **32**

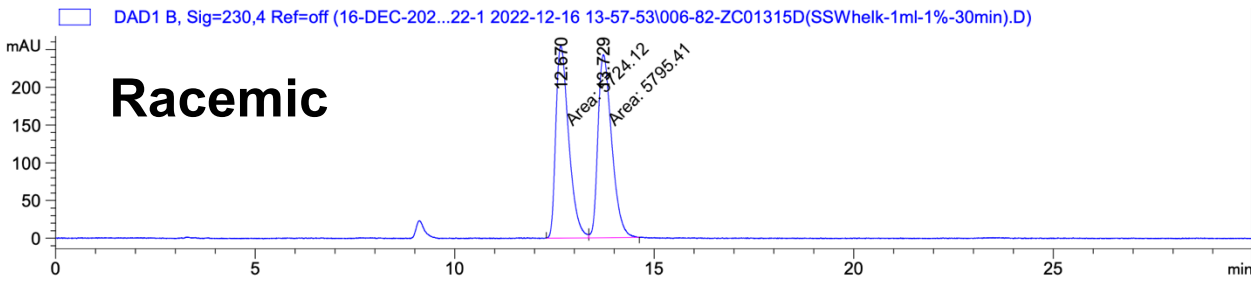

Signal 2: DAD1 B, Sig=230,4 Ref=off

Peak #	RetTime [min]	Type	Width [min]	Area [mAU*s]	Height [mAU]	Area %
1	12.670	MF	0.3746	5724.11621	254.69371	49.6905
2	13.729	FM	0.3983	5795.41357	242.49443	50.3095
Totals :				1.15195e4	497.18814	

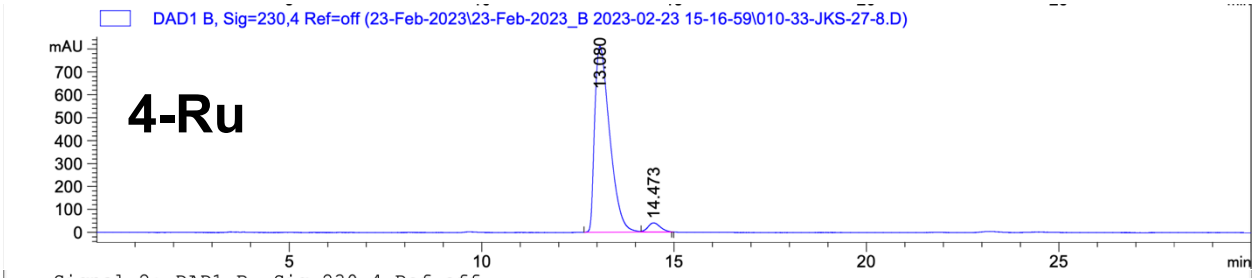

Signal 2: DAD1 B, Sig=230,4 Ref=off

Peak #	RetTime [min]	Type	Width [min]	Area [mAU*s]	Height [mAU]	Area %
1	13.080	VV R	0.3216	2.19960e4	811.79053	96.0871
2	14.473	VV E	0.2610	895.71912	40.27641	3.9129
Totals :				2.28917e4	852.06694	

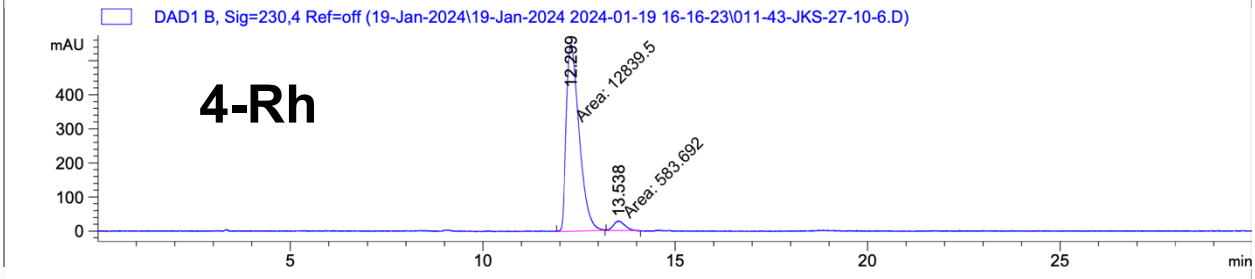

Signal 2: DAD1 B, Sig=230,4 Ref=off

Peak #	RetTime [min]	Type	Width [min]	Area [mAU*s]	Height [mAU]	Area %
1	12.299	MM	0.3906	1.28395e4	547.84998	95.6516
2	13.538	MM	0.3431	583.69165	28.35273	4.3484
Totals :				1.34232e4	576.20271	

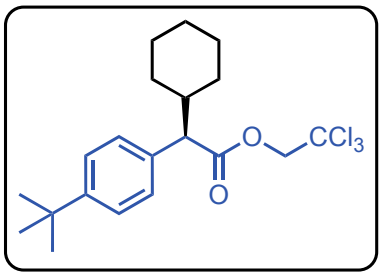

Compound **33**

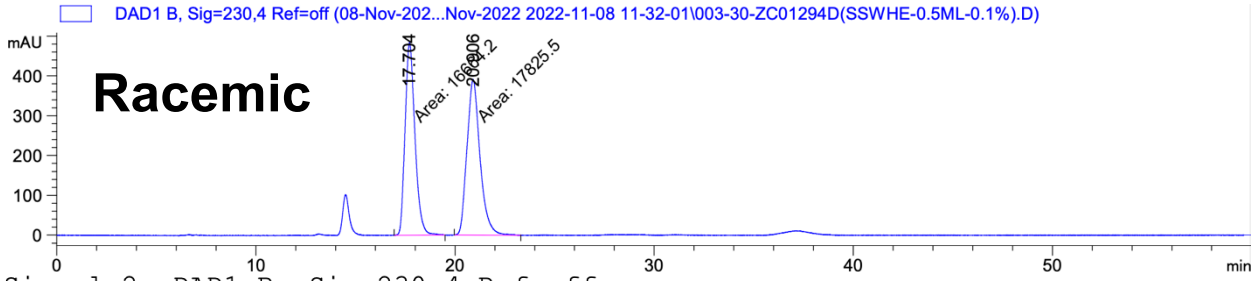

Signal 2: DAD1 B, Sig=230,4 Ref=off

Peak #	RetTime [min]	Type	Width [min]	Area [mAU*s]	Height [mAU]	Area %
1	17.704	MM	0.5737	1.66642e4	484.12158	48.3165
2	20.906	MM	0.7584	1.78255e4	391.71411	51.6835
Totals :				3.44897e4	875.83569	

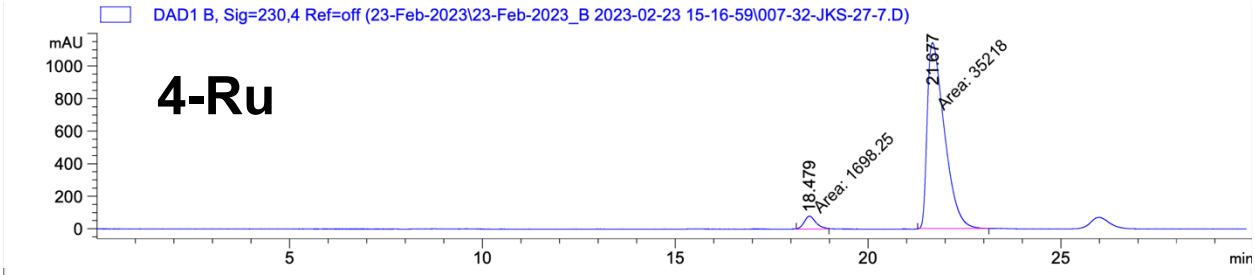

Signal 2: DAD1 B, Sig=230,4 Ref=off

Peak #	RetTime [min]	Type	Width [min]	Area [mAU*s]	Height [mAU]	Area %
1	18.479	MM	0.3558	1698.25134	79.55709	4.6003
2	21.677	MM	0.5137	3.52180e4	1142.72937	95.3997
Totals :				3.69163e4	1222.28646	

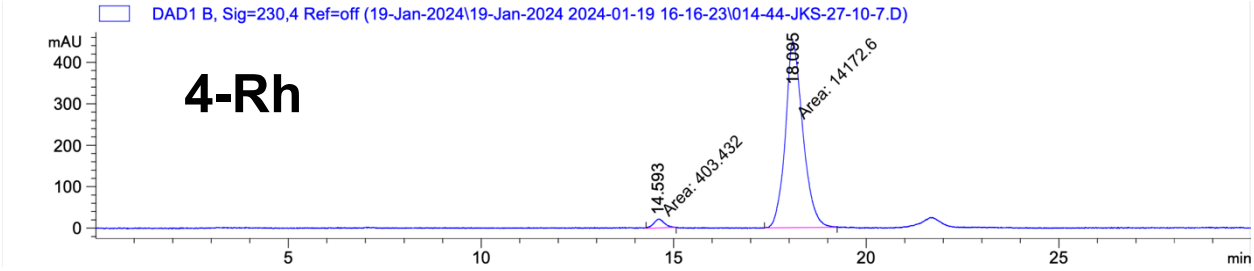

Signal 2: DAD1 B, Sig=230,4 Ref=off

Peak #	RetTime [min]	Type	Width [min]	Area [mAU*s]	Height [mAU]	Area %
1	14.593	MM	0.3174	403.43231	21.18424	2.7678
2	18.095	MM	0.5265	1.41726e4	448.67700	97.2322
Totals :				1.45760e4	469.86124	

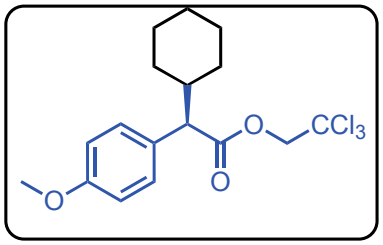

Compound **34**

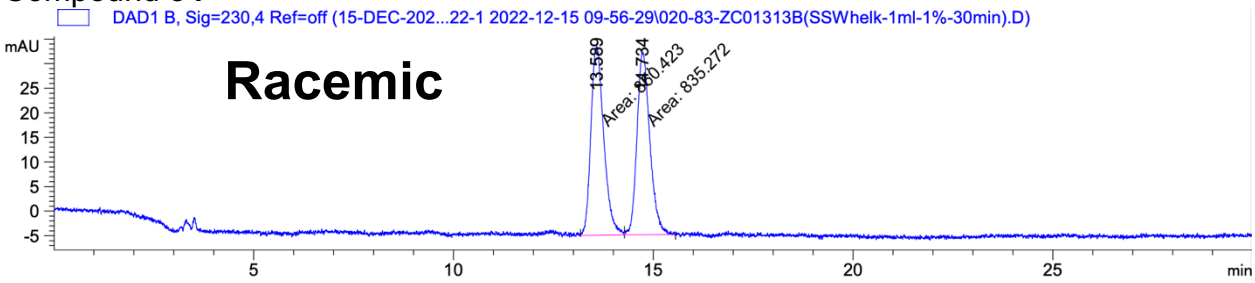

Signal 2: DAD1 B, Sig=230,4 Ref=off

Peak #	RetTime [min]	Type	Width [min]	Area [mAU*s]	Height [mAU]	Area %
1	13.589	MF	0.3730	860.42310	38.44910	50.7416
2	14.734	FM	0.3748	835.27246	37.14481	49.2584
Totals :				1695.69556	75.59391	

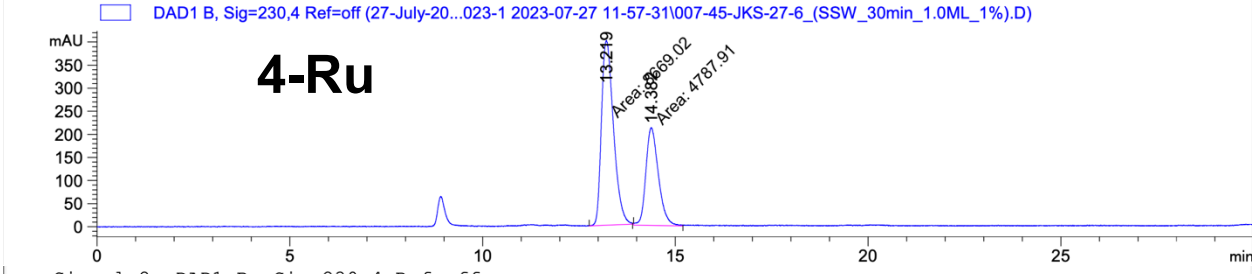

Signal 2: DAD1 B, Sig=230,4 Ref=off

Peak #	RetTime [min]	Type	Width [min]	Area [mAU*s]	Height [mAU]	Area %
1	13.219	MM	0.3608	8669.02051	400.43625	64.4205
2	14.382	MM	0.3765	4787.91064	211.92868	35.5795
Totals :				1.34569e4	612.36493	

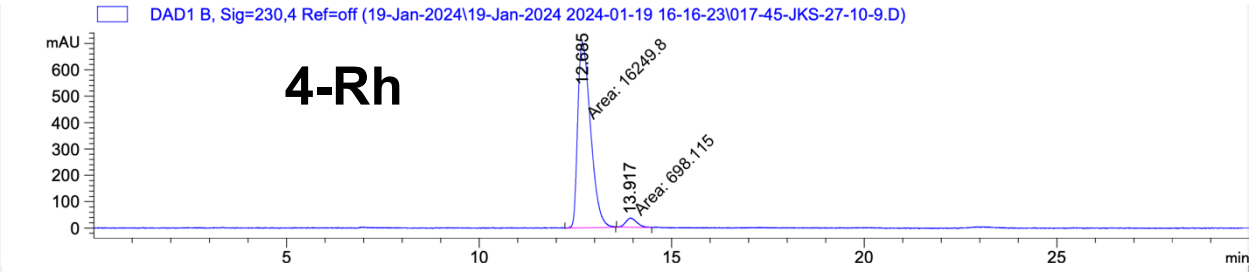

Signal 2: DAD1 B, Sig=230,4 Ref=off

Peak #	RetTime [min]	Type	Width [min]	Area [mAU*s]	Height [mAU]	Area %
1	12.685	MM	0.3842	1.62498e4	704.88867	95.8808
2	13.917	MM	0.3353	698.11475	34.69977	4.1192
Totals :				1.69479e4	739.58844	

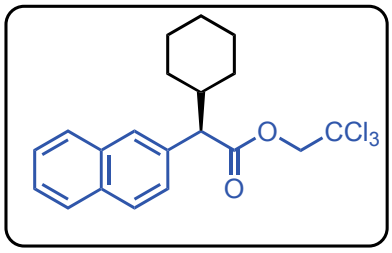

Compound **35**

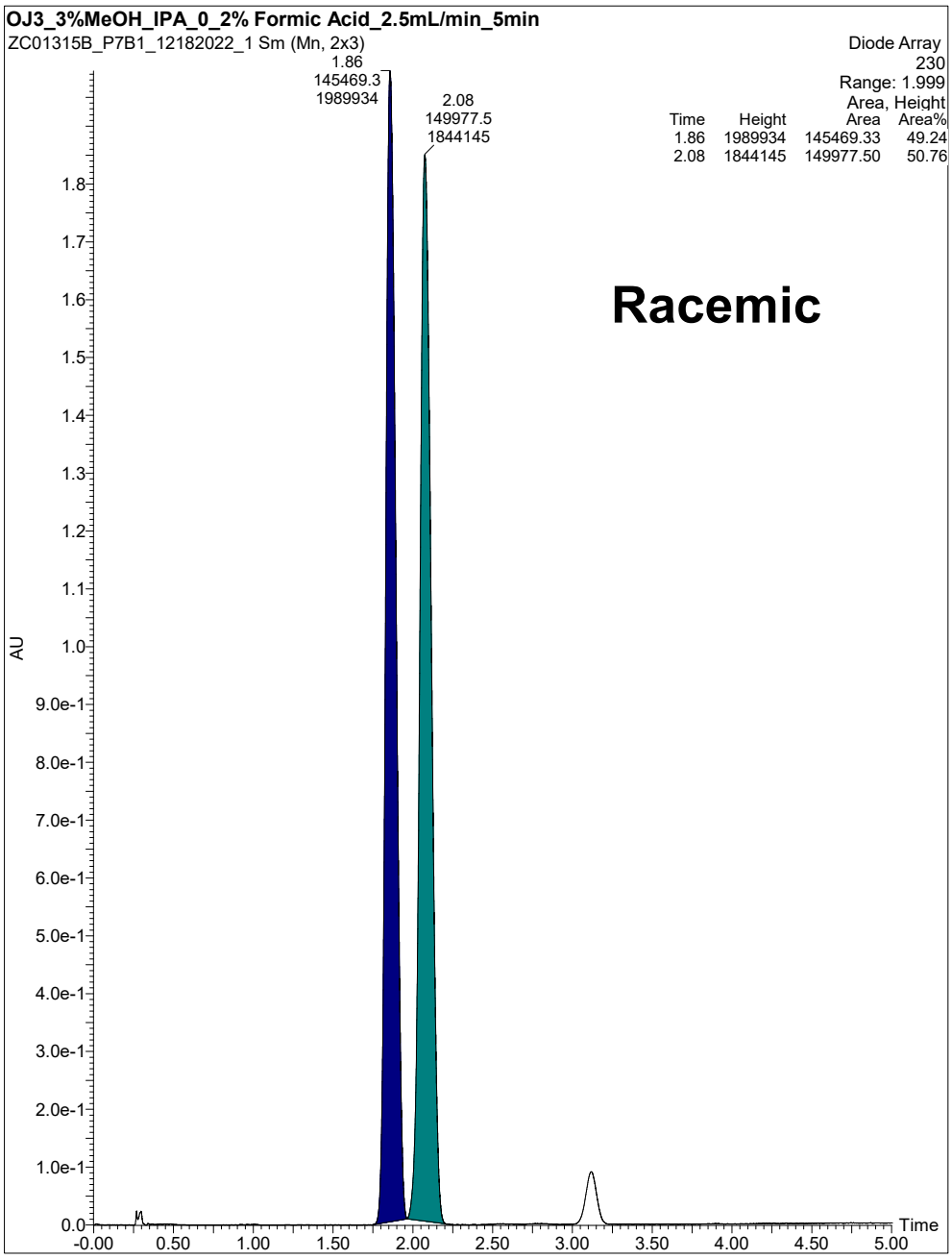
OJ3_3%MeOH_IPA_0_2% Formic Acid_2.5mL/min_5min
ZC01315B_P7B1_12182022_1 Sm (Mn, 2x3)
Diode Array
230
Range: 1.999
Area, Height
Time Height Area Area%
1.86 1989934 145469.33 49.24
2.08 1844145 149977.50 50.76
1.86
145469.3
1989934
2.08
149977.5
1844145
Racemic
AU
Time

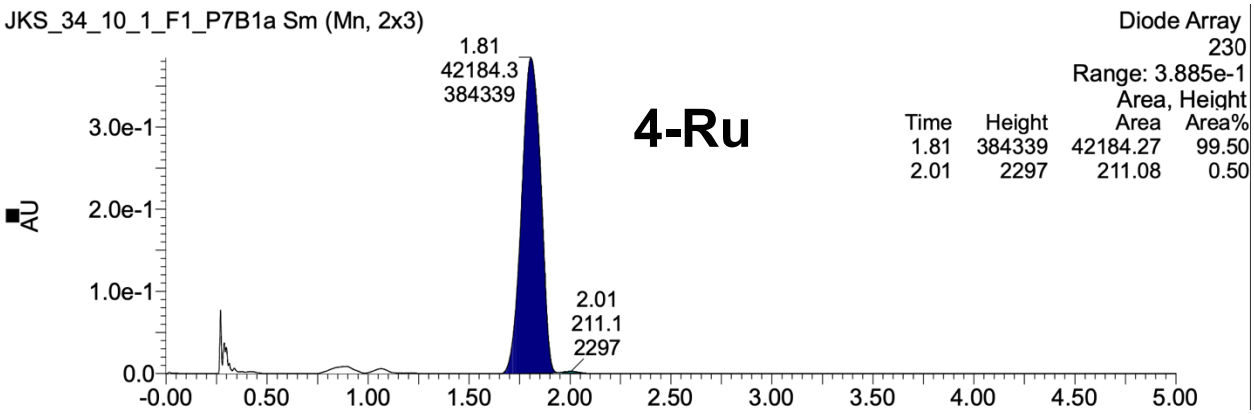
JKS_34_10_1_F1_P7B1a Sm (Mn, 2x3)
Diode Array
230
Range: 3.885e-1
Area, Height
1.81
42184.3
384339
4-Ru
2.01
211.1
2297
Time Height Area Area%
1.81 384339 42184.27 99.50
2.01 2297 211.08 0.50
AU
3.0e-1
2.0e-1
1.0e-1
0.0
-0.00 0.50 1.00 1.50 2.00 2.50 3.00 3.50 4.00 4.50 5.00

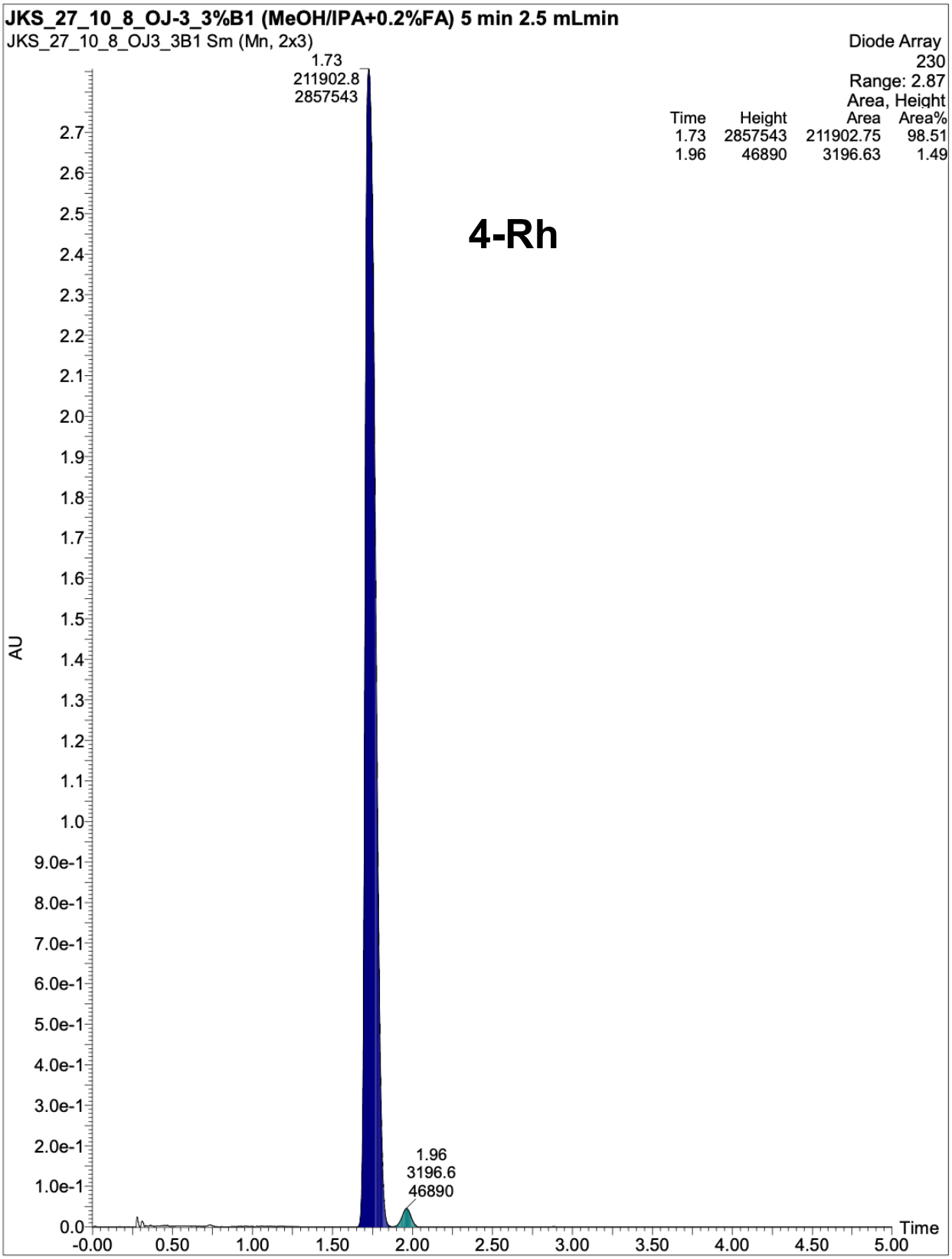
JKS_27_10_8_OJ-3_3%B1 (MeOH/IPA+0.2%FA) 5 min 2.5 mLmin
JKS_27_10_8_OJ3_3B1 Sm (Mn, 2x3)
Diode Array
230
Range: 2.87
Area, Height
Time Height Area Area%
1.73 2857543 211902.75 98.51
1.96 46890 3196.63 1.49
4-Rh
1.73
211902.8
2857543
1.96
3196.6
46890
AU
Time
2.7
2.6
2.5
2.4
2.3
2.2
2.1
2.0
1.9
1.8
1.7
1.6
1.5
1.4
1.3
1.2
1.1
1.0
9.0e-1
8.0e-1
7.0e-1
6.0e-1
5.0e-1
4.0e-1
3.0e-1
2.0e-1
1.0e-1
0.0
-0.00
0.50
1.00
1.50
2.00
2.50
3.00
3.50
4.00
4.50
5.00

NMR Spectra for Novel Compounds

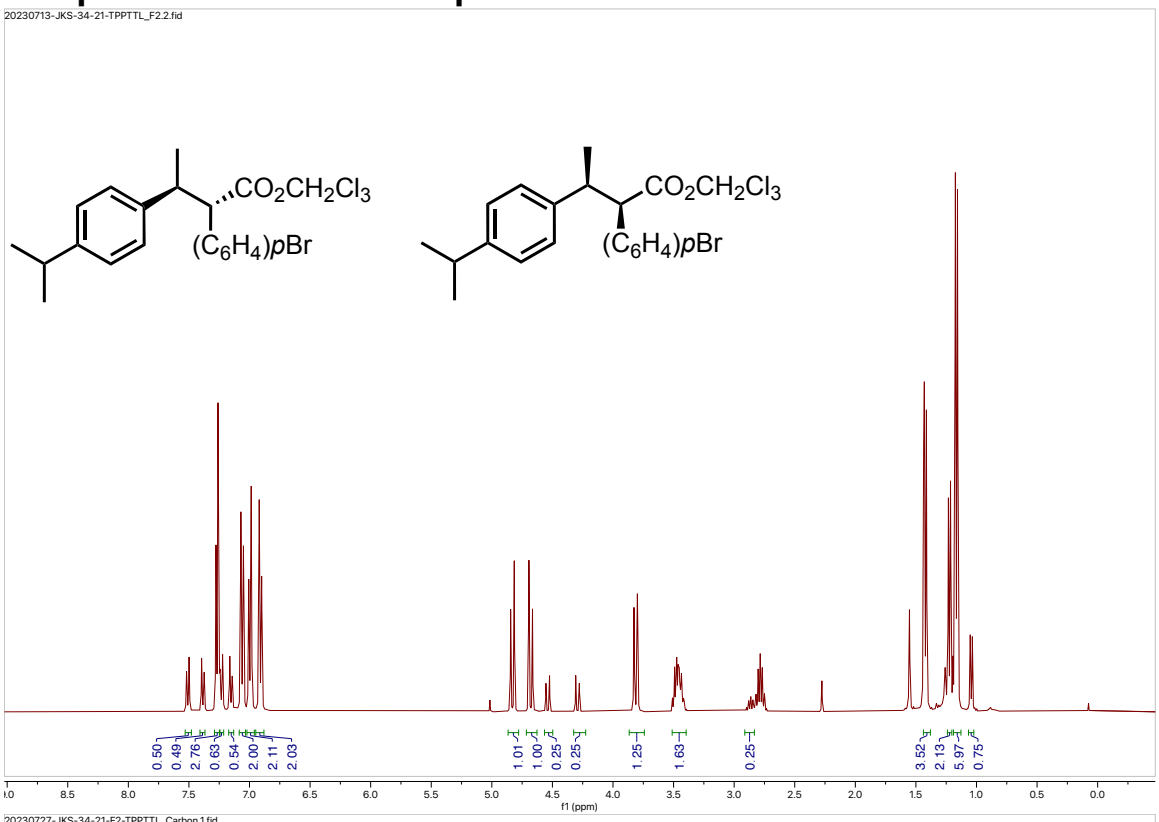

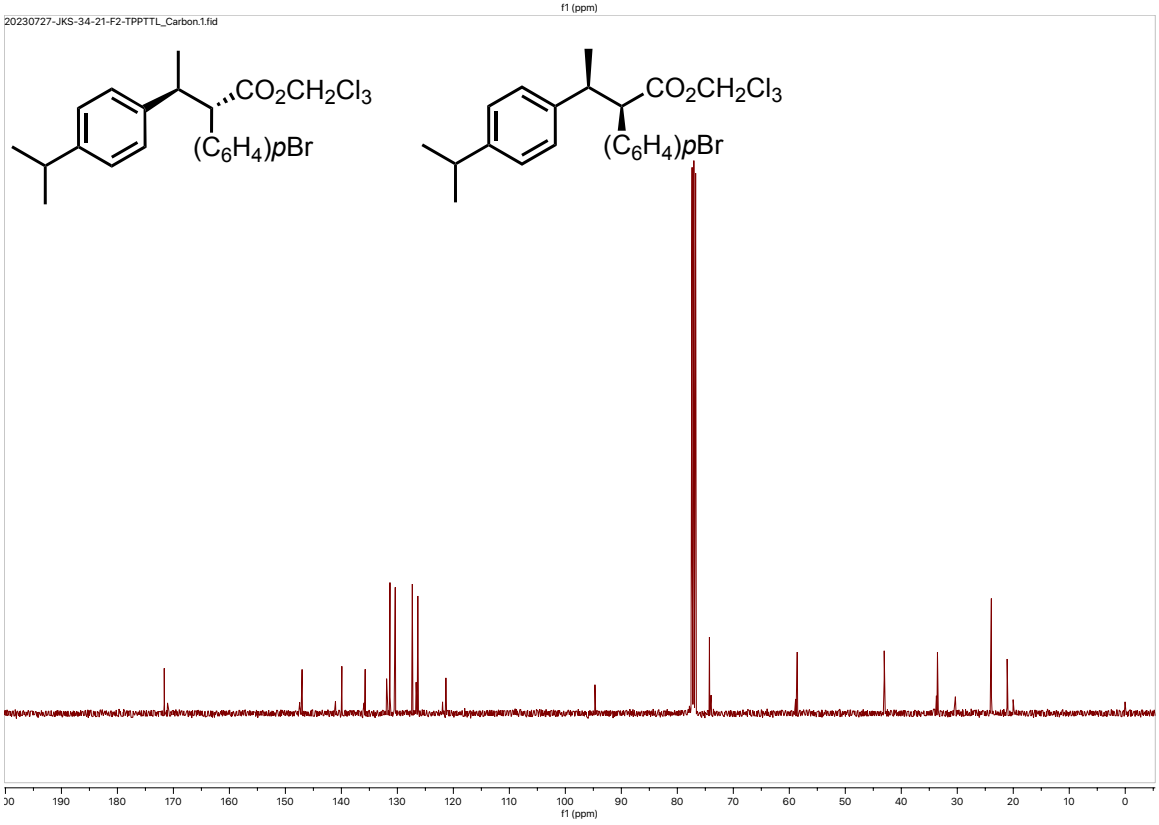

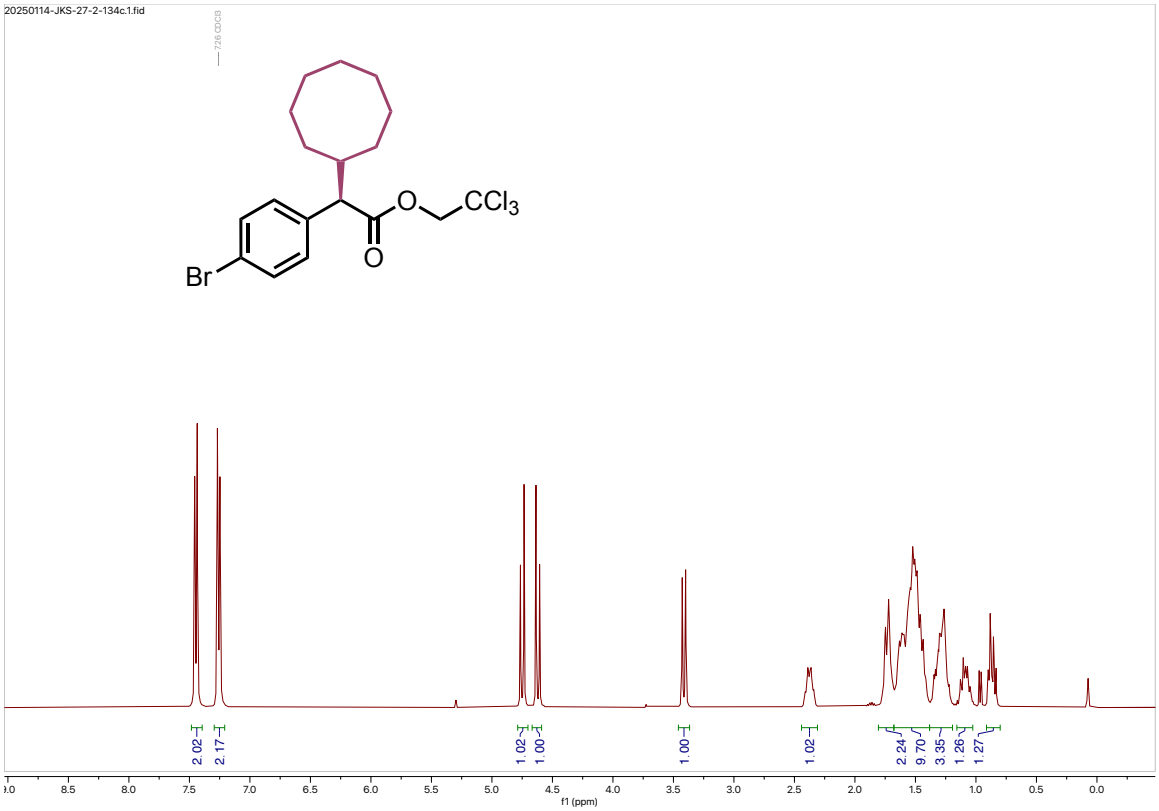
20250114-JKS-27-2-134c.1.fid
726 CDCl3
Br
O
O
CCl3
2.02
2.17
1.02
1.00
1.00
1.02
2.24
9.70
3.35
1.26
1.27
f1 (ppm)

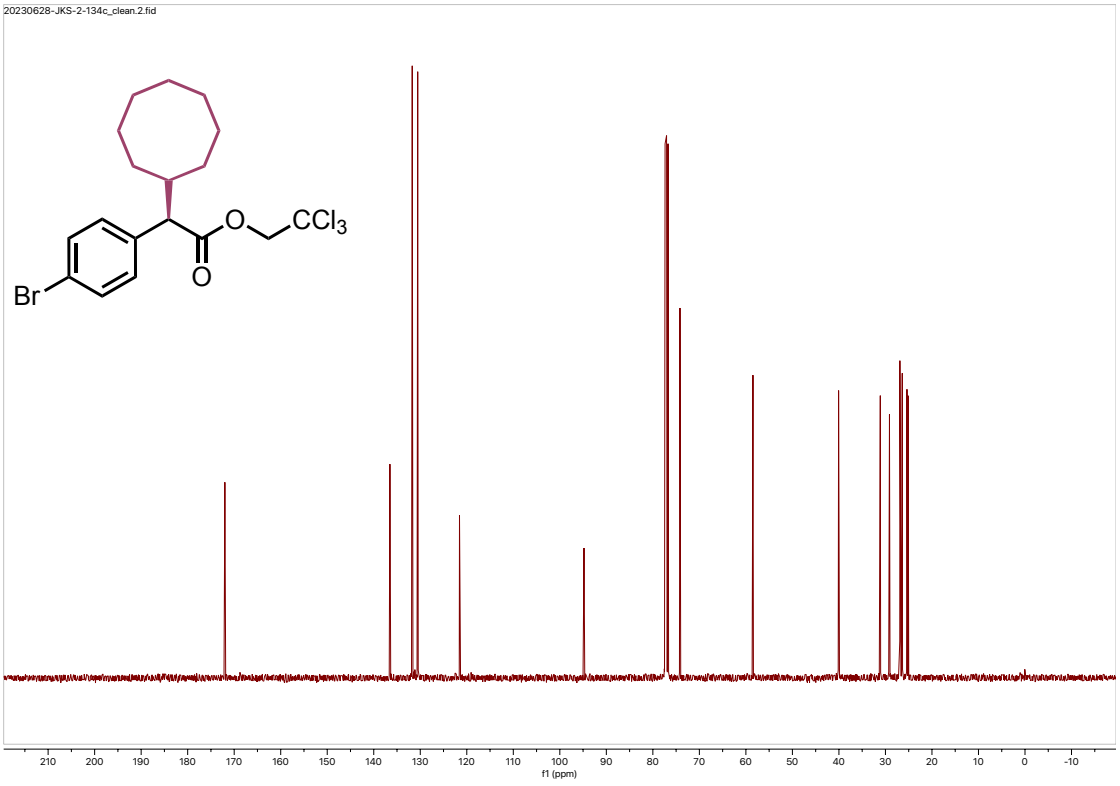
20230628-JKS-2-134c_clean.2.fid
Br
O
O
CCl3
f1 (ppm)

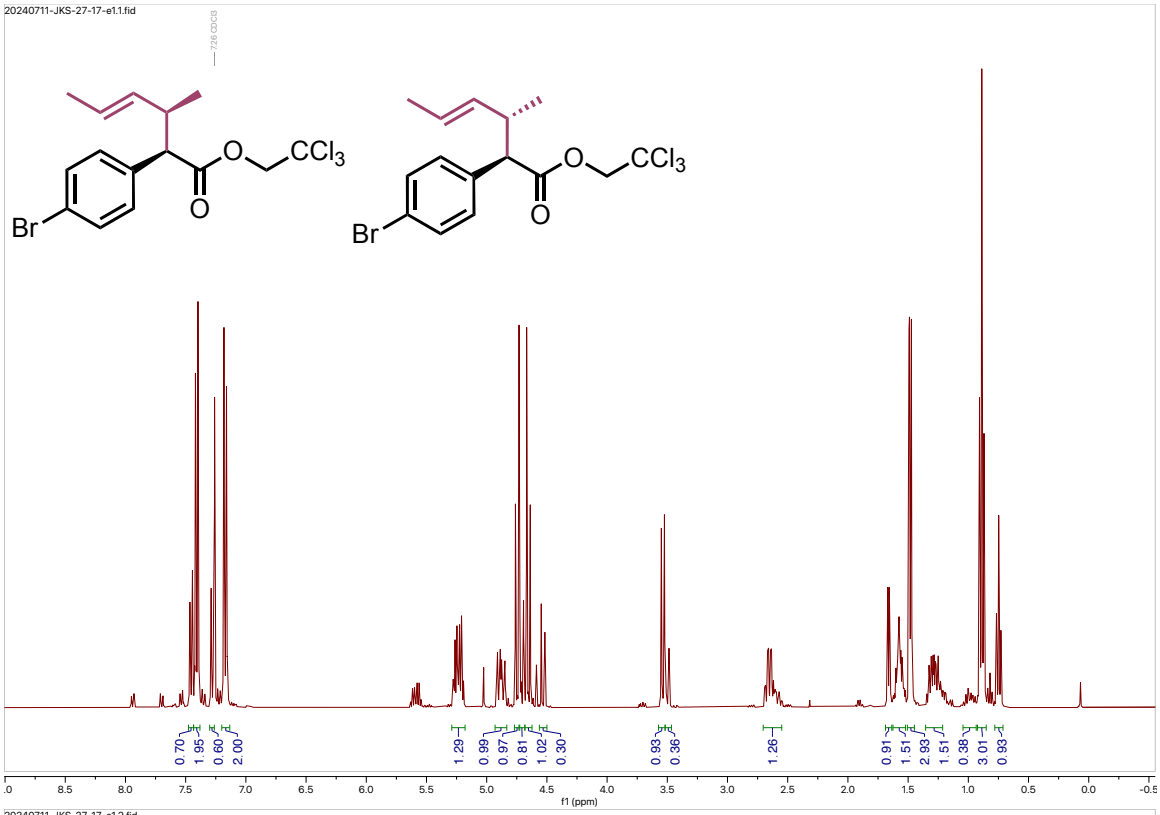
20240711-JKS-27-17-e1.1.fid
Br
O
O
CCl3
Br
O
O
CCl3
0.70
1.95
0.60
2.00
1.29
0.99
0.97
0.81
1.02
0.30
0.93
0.36
1.26
0.91
1.51
2.93
1.51
0.38
3.01
0.93
f1 (ppm)

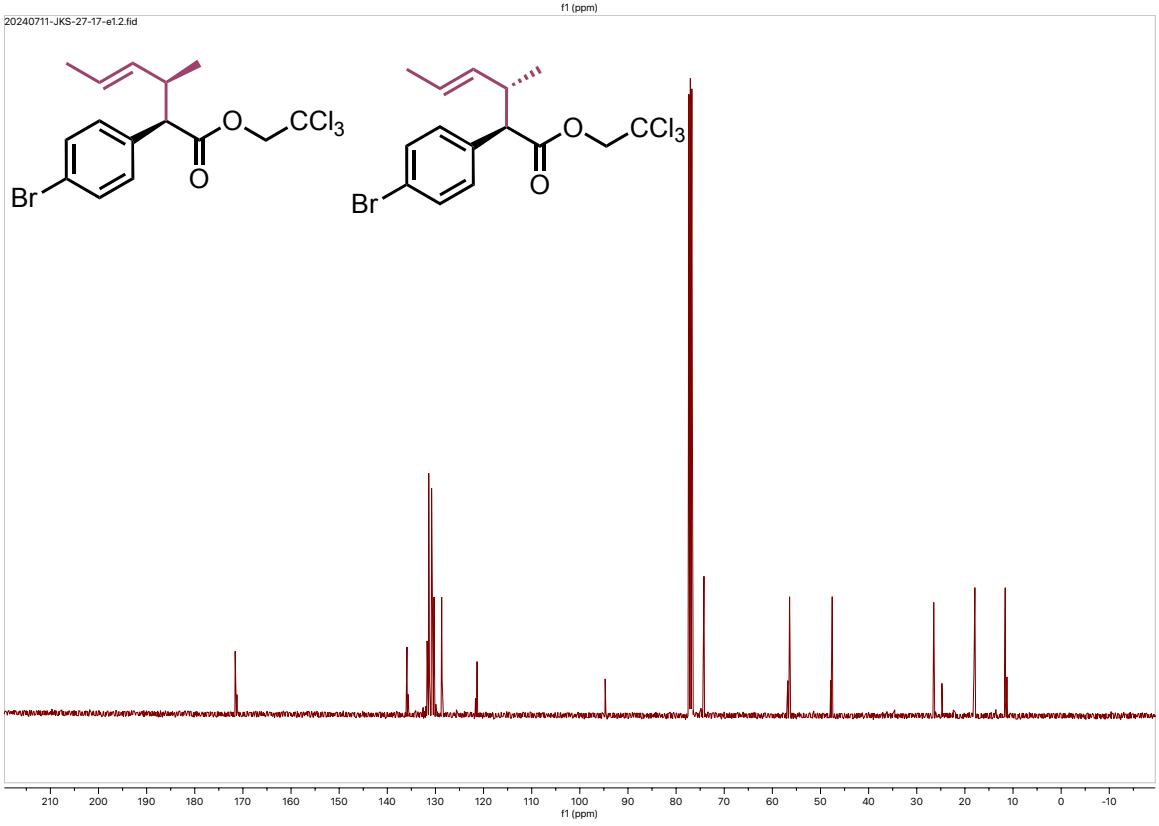
20240711-JKS-27-17-e1.2.fid
Br
O
O
CCl3
Br
O
O
CCl3
f1 (ppm)

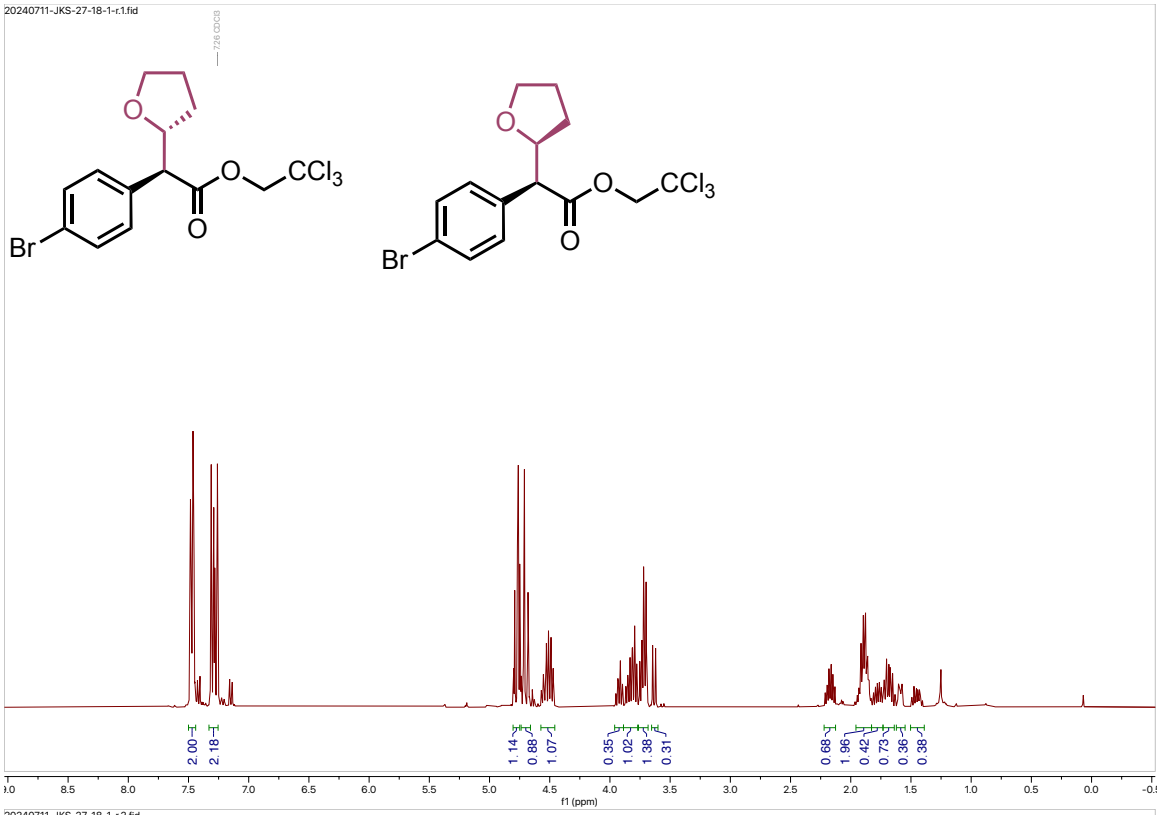
20240711-JKS-27-18-1-r.1.fid
Br
O
O
O
CCl3
2.00
2.18
1.14
0.88
1.07
0.35
1.02
1.38
0.31
0.68
1.96
0.42
0.73
0.36
0.38
f1 (ppm)

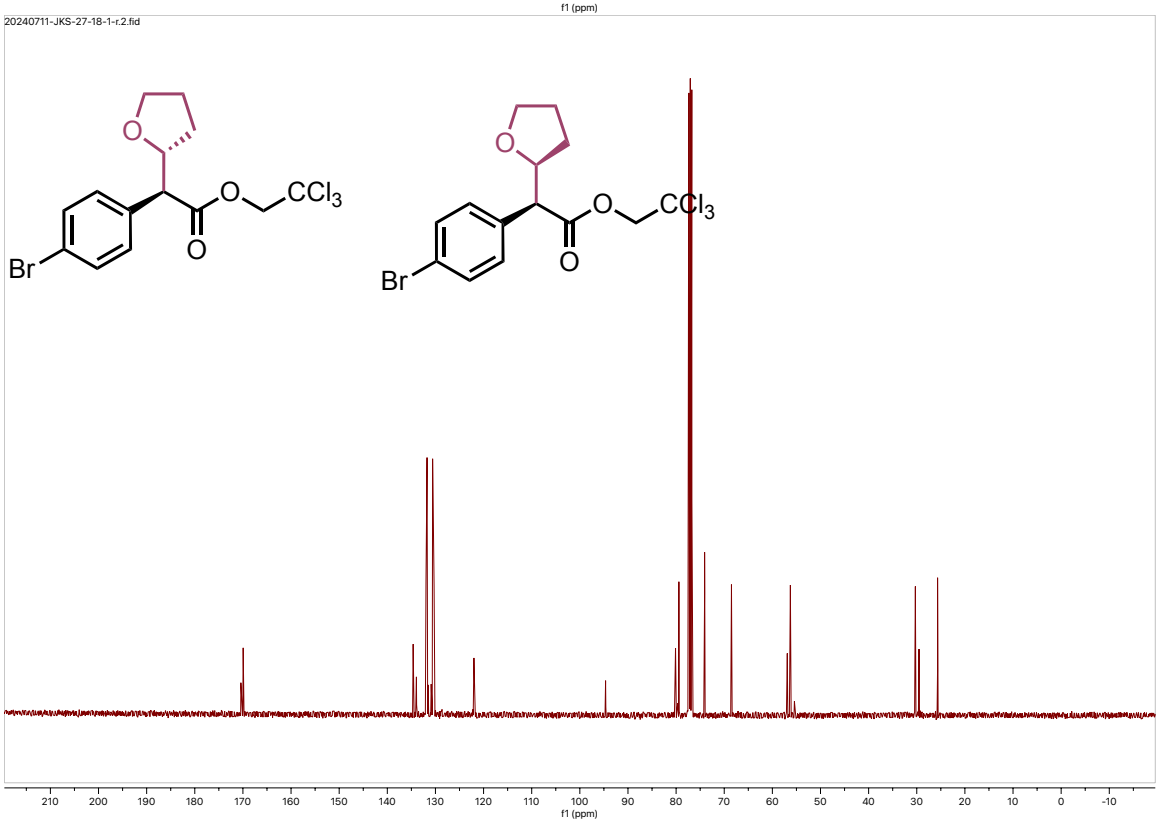
20240711-JKS-27-18-1-r.2.fid
Br
O
O
O
CCl3
f1 (ppm)

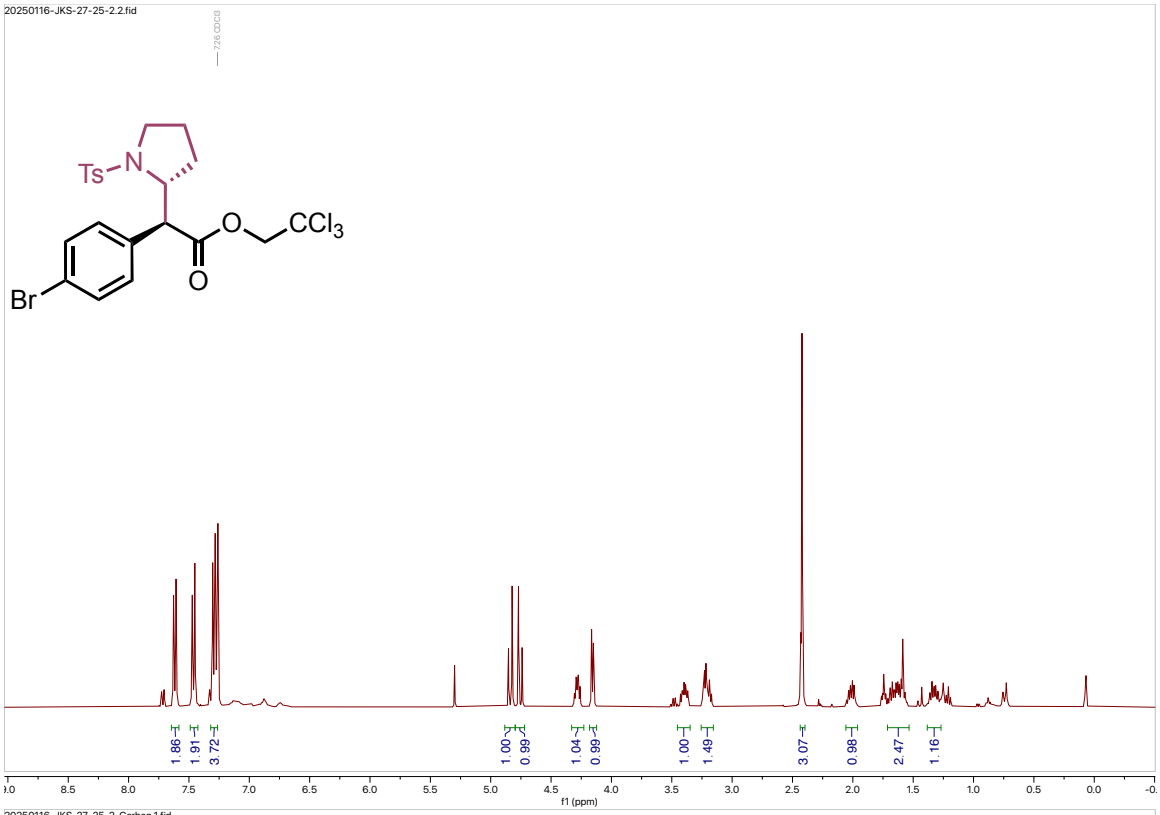
20250116-JKS-27-25-2.2.fid
Ts
N
O
O
CCl3
Br
1.86
1.91
3.72
1.00
0.99
1.04
0.99
1.00
1.49
3.07
0.98
2.47
1.16
f1 (ppm)

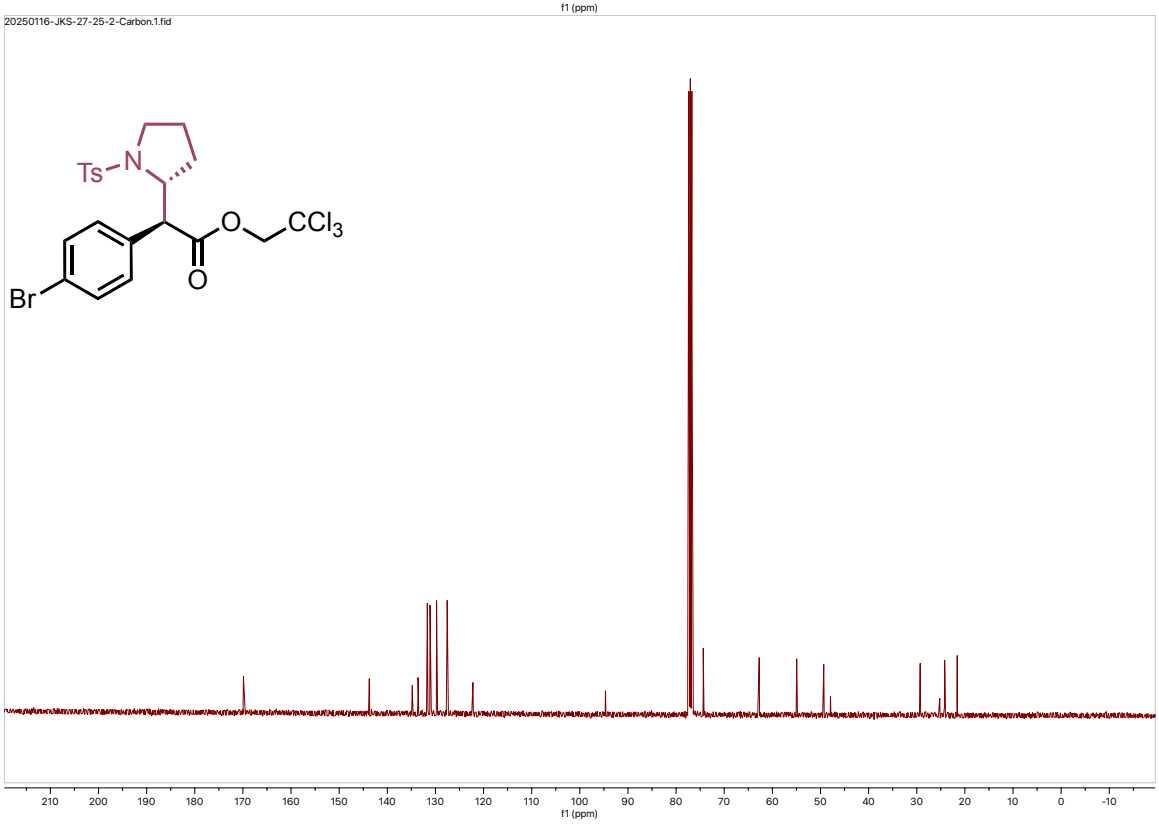
20250116-JKS-27-25-2-Carbon.1.fid
Ts
N
O
O
CCl3
Br
f1 (ppm)

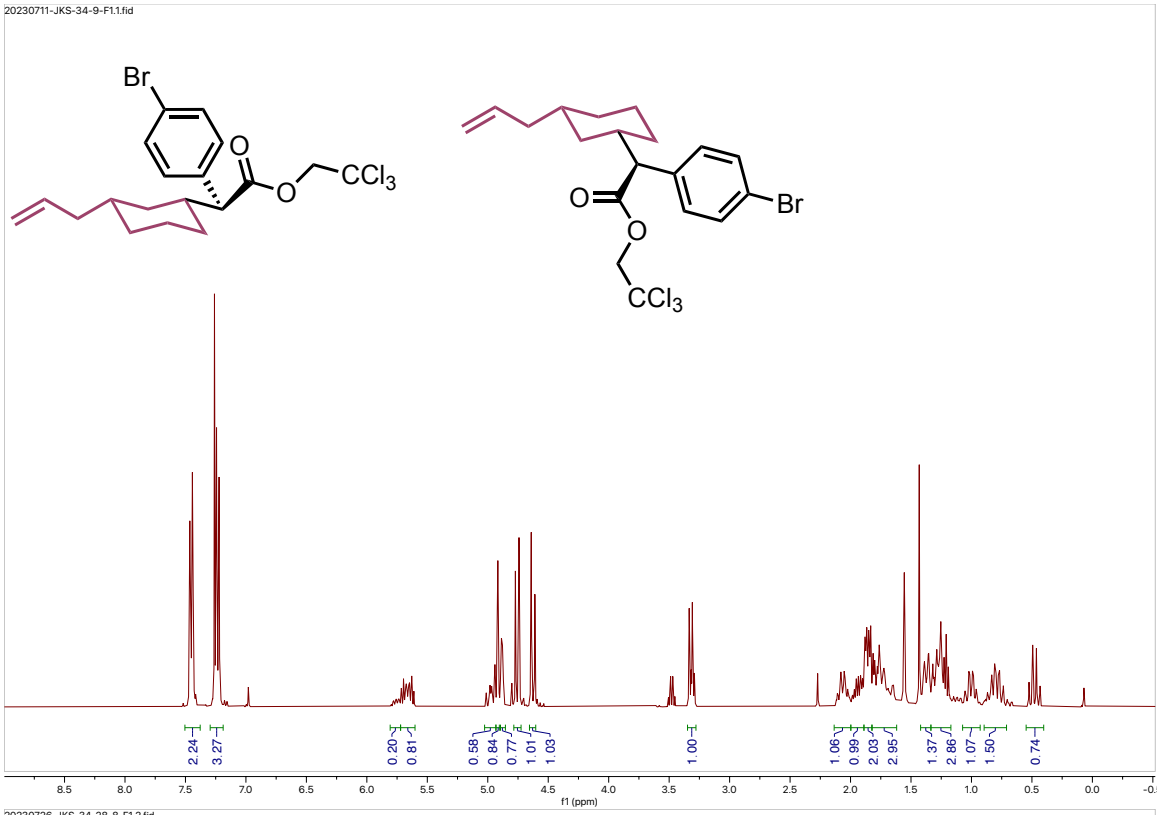
20230711-JKS-34-9-F1.1.fid
Br
O
O
CCl3
O
O
CCl3
Br
2.24
3.27
0.20
0.81
0.58
0.84
0.77
1.01
1.03
1.00
1.06
0.99
2.03
2.95
1.37
2.86
1.07
1.50
0.74
f1 (ppm)

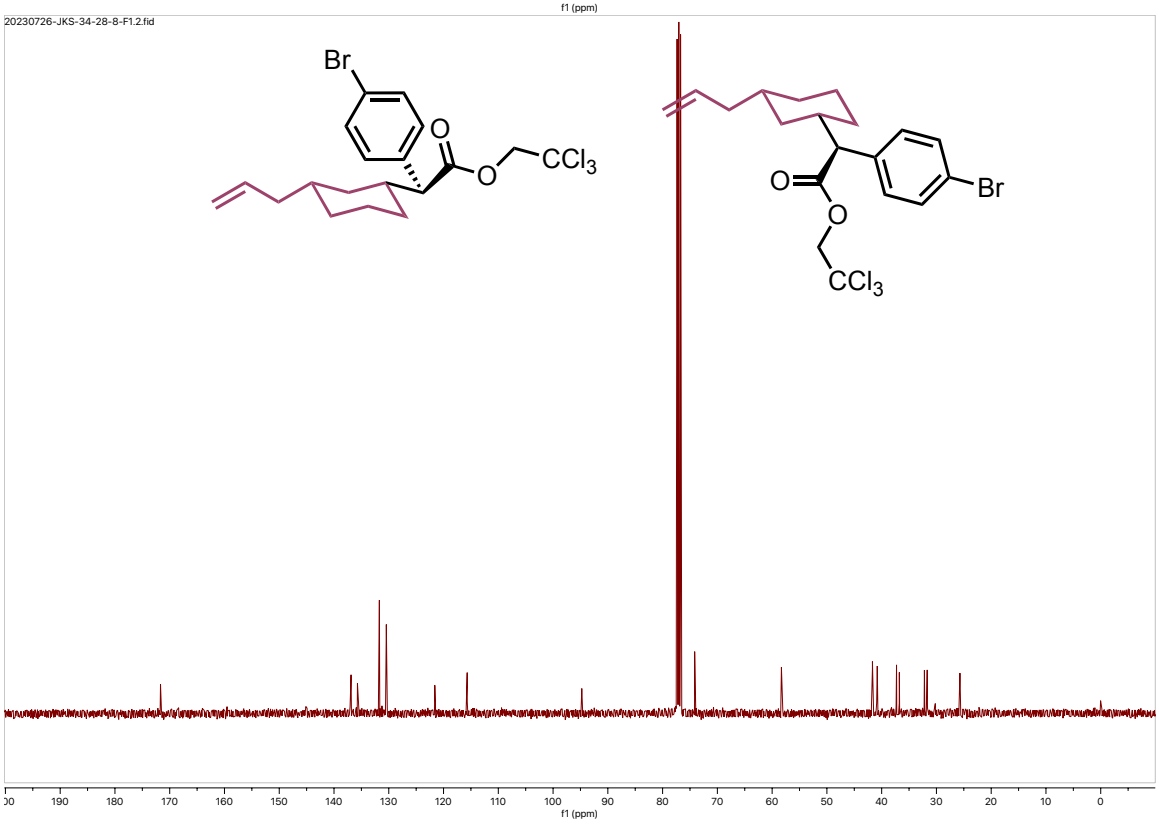
20230726-JKS-34-28-8-F1.2.fid
Br
O
O
CCl3
O
O
CCl3
Br
f1 (ppm)

References

1. Green, S. P.; Wheelhouse, K. M.; Payne, A. D.; Hallett, J. P.; Miller, P. W.; Bull, J. A., Thermal Stability and Explosive Hazard Assessment of Diazo Compounds and Diazo Transfer Reagents. *Org. Process Res. Dev.* **2020,** *24* (1), 67-84.
2. Chen, Z.; Shimabukuro, K.; Bacsa, J.; Musaev, D. G.; Davies, H. M. L., D4-Symmetric Dirhodium Tetrakis(binaphthylphosphate) Catalysts for Enantioselective Functionalization of Unactivated C–H Bonds. *J. Am. Chem. Soc.* **2024,** *146* (28), 19460-19473.
3. Sailer, J. K.; Sharland, J. C.; Bacsa, J.; Harris, C. F.; Berry, J. F.; Musaev, D. G.; Davies, H. M. L., Diruthenium Tetracarboxylate-Catalyzed Enantioselective Cyclopropanation with Aryldiazoacetates. *Organometallics* **2023,** *42* (15), 2122-2133.
4. Fu, J.; Ren, Z.; Bacsa, J.; Musaev, D. G.; Davies, H. M. L., Desymmetrization of cyclohexanes by site- and stereoselective C–H functionalization. *Nature* **2018,** *564* (7736), 395-399.
5. Liao, K.; Negretti, S.; Musaev, D. G.; Bacsa, J.; Davies, H. M. L., Site-selective and stereoselective functionalization of unactivated C–H bonds. *Nature* **2016,** *533* (7602), 230-234.
6. Wertz, B.; Ren, Z.; Bacsa, J.; Musaev, D. G.; Davies, H. M. L., Comparison of 1,2-Diarylcyclopropanecarboxylates with 1,2,2-Triarylcyclopropanecarboxylates as Chiral Ligands for Dirhodium-Catalyzed Cyclopropanation and C–H Functionalization. *J. Org. Chem.* **2020,** *85* (19), 12199-12211.
7. Tortoreto, C.; Rackl, D.; Davies, H. M. L., Metal-Free C–H Functionalization of Alkanes by Aryldiazoacetates. *Org. Lett.* **2017,** *19* (4), 770-773.

Appendix C. Chapter 4 Supporting Information

General Considerations

All experiments were carried out in flame-dried glassware under argon atmosphere unless otherwise stated. Flash column chromatography was performed on silica gel. Unless otherwise noted, all other reagents were obtained from commercial sources (Sigma Aldrich, Fisher, TCI Chemicals, AK Scientific, Combi Blocks, Oakwood Chemicals, Ambeed) and used as received without purification. ^{1}H, ^{13}C, and ^{19}F NMR spectra were recorded at either 400 MHz (^{13}C at 100 MHz) on Bruker 400 spectrometer or 600 MHz (^{13}C at 151 MHz) on INOVA 600 or Bruker 600 spectrometer. NMR spectra were run in solutions of deuterated chloroform ($CDCl_3$) with residual chloroform taken as an internal standard (7.26 ppm for ^{1}H, and 77.16 ppm for ^{13}C), and were reported in parts per million (ppm). The abbreviations for multiplicity are as follows: s = singlet, d = doublet, t = triplet, q = quartet, p = pentet, m = multiplet, dd = doublet of doublet, etc. Coupling constants (J values) are obtained from the spectra. Thin layer chromatography was performed on aluminum-back silica gel plates with UV light and cerium aluminum molybdate (CAM) stain to visualize. Mass spectra were taken on a Thermo Finnigan LTQ-FTMS spectrometer with APCI or ESI. Enantiomeric excess (% ee) data were obtained on an Agilent 1100 HPLC eluting the purified products using a mixed solution of HPLC-grade 2-propanol (i-PrOH) and n-hexane or a Waters SFC eluting with supercritical CO2 and a 1:1 mixtures of HPLC grade methanol:isopropanol with 0.2% formic acid.

Known Compounds

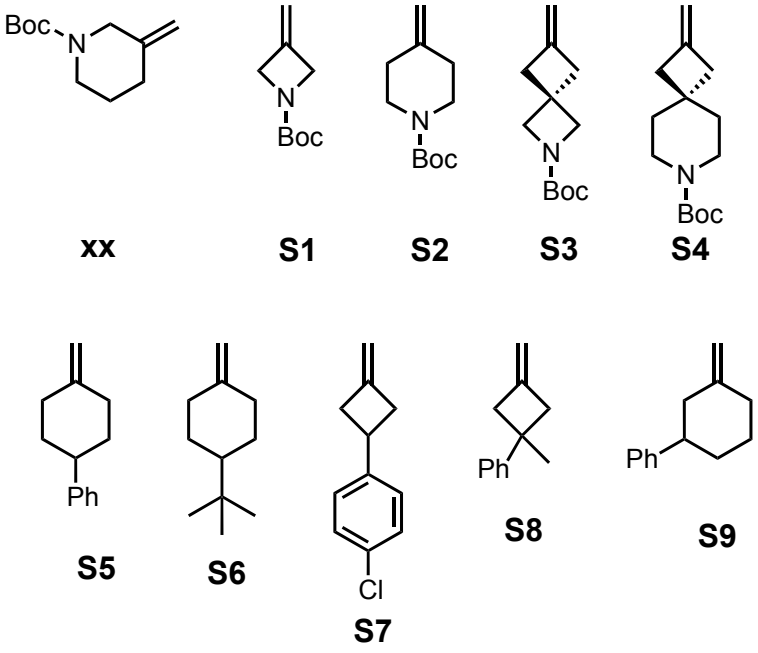

Compound **xx,**[1] **S1** and **S2**,[2] **S3**,[3] **S4**,[4] **S5**,[5] **S6**,[6] **S7**,[7] **S8**,[8] and **S9**[9] were synthesized according to known methods and spectra matched literature procedure.

Substrate Synthesis
3-methylene-1-tosylpiperidine (S10)

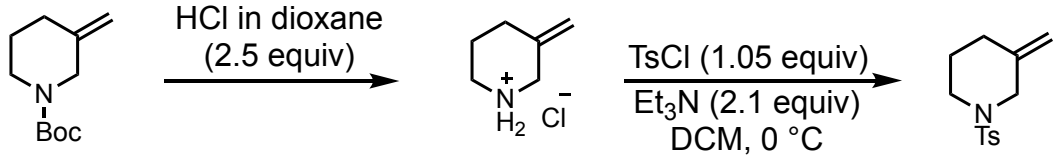

1-Boc-3-methylenepiperidine (5.0 g, 25.3 mmol) and diethyl ether (10 mL) were added into a single-necked flask. Then, hydrogen chloride in dioxane solution (15.8 ml, 63.4 mmol, 4.0 M, 2.5 equiv) was added dropwise, and the reaction was stired at room temperature for 0.5 h. At this time, the solution was suction filtered, and the filter cake was rinsed with 20 mL of diethyl ether to obtain 3-methylenepiperidine hydrochloride as a white solid, which was directly used in the next reaction without further purification.

To a mixture of 3-methylenepiperidine hydrochloride (802 mg, 6.0 mmol) and Et_3N (1.76 mL, 12.6 mmol, 2.1 equiv) in DCM (20 mL) was added tosyl chloride (1.20 g, 6.3 mmol, 1.05 equiv) at 0 °C. This solution was stirred for 4 h at room temperature. Then, HCl (5

ml, 1 M) and H_2O (10 ml) were added and the organic layer was separated, washed with brine (10 ml), dried over Na2SO4, filtered and concentrated under reduced pressure. The residue was purified by flash column chromatography (SiO_2, 0-30% Et_2O in hexane) to afford 3-methylene-1-tosylpiperidine as a white solid (1.30 g, 86% yield)

^{1}H NMR (400 MHz, $CDCl_3$) δ 7.66 (d, J = 8.0 Hz, 2H), 7.32 (d, J = 8.0 Hz, 2H), 4.90 (s, 1H), 4.82 (s, 1H), 3.50 (s, 2H), 3.08 – 3.04 (m, 2H), 2.43 (s, 2H), 2.10 (t, J = 6.3 Hz, 2H), 1.75 – 1.63 (m, 2H).

^{13}C NMR (101 MHz, $CDCl_3$) δ 143.5, 140.6, 133.2, 129.6, 127.9, 111.8, 52.5, 46.4, 32.0, 25.7, 21.6.

HRMS (+p APCI) calcd for $C_{13}H_{18}O_2N^{32}S$ (M+H) 252.1053, found 252.1054

3-methylene-1-((4-nitrophenyl)sulfonyl)piperidine (S11)

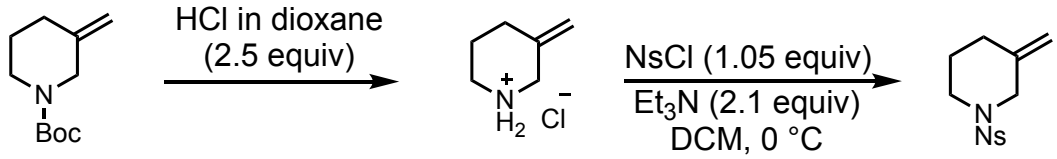

First step analogous to above.

To a mixture of 3-methylenepiperidine hydrochloride (267 mg, 2.0 mmol) and Et_3N (0.73 mL, 5.2 mmol, 2.6 equiv) in DCM (6.7 mL) was added nosyl chloride (465 mg, 2.1 mmol, 1.05 equiv) at 0 °C. This solution was stirred for 4 h at room temperature. Then, HCl (5 ml, 1 M) and H_2O (10 ml) were added and the organic layer was separated, washed with brine (10 ml), dried over Na2SO4, filtered and concentrated under reduced pressure. The residue was purified by flash column chromatography (SiO_2, 0-13% ethyl acetate in hexane) to afford the title compound as an off-white solid (462 mg, 92% yield)

^{1}H NMR (400 MHz, $CDCl_3$) δ 8.37 (d, J = 8.9 Hz, 2H), 7.97 (d, J = 8.8 Hz, 2H), 4.91 (d, J = 1.7 Hz, 1H), 4.84 (d, J = 1.5 Hz, 1H), 3.62 (s, 2H), 3.25 – 3.11 (m, 2H), 2.14 (t, J = 6.3 Hz, 2H), 1.77 – 1.62 (m, 2H).

^{13}C NMR (101 MHz, $CDCl_3$) δ 150.1, 143.0, 139.8, 128.9, 124.3, 112.4, 52.3, 46.3, 31.8, 25.7.

HRMS (+p APCI) calcd for $C_{12}H_{15}O_4N_2{}^{32}S$ (M+H) 283.0747, found 283.0745

2-methylene-1-tosylpyrrolidine (S12)

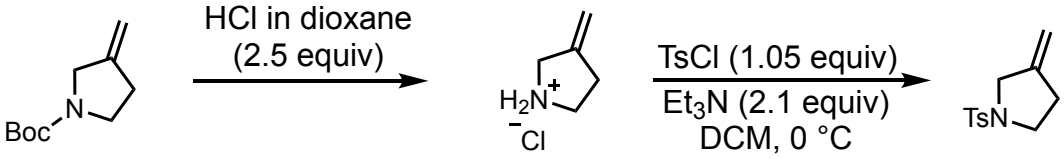

Tert-butyl 3-methylenepyrrolidine-1-carboxylate (2.5 g, 13.6 mmol) and diethyl ether (7.0 mL) were added into a single-necked. Then, hydrogen chloride in dioxane solution (8.53 ml, 34.1 mmol, 4.0 M, 2.5 equiv) was added dropwise, and the solution was stirred at room temperature. After 2.0 hour, the reaction mixture was cooled to 0 °C with an ice bath. Then, 20 ml of DCM and Et_3N (5.89 mL, 42.3 mmol, 2.1 equiv) were added. Finally, tosyl chloride (2.73 g, 14.3 mmol, 1.05 equiv) was added and the mixture was stirred for 4 h at room temperature. HCl (5 ml, 1 M) and H_2O (10 ml) were added and the organic layer was separated, washed with brine (10 ml), dried over Na2SO4, filtered and concentrated under reduced pressure. The residue was purified by flash column chromatography (SiO_2, 0-30% Et_2O in hexane) to afford 3-methylene-1-tosylpyrrolidine as a white solid (2.50 g, 77% yield)

^{1}H NMR (400 MHz, $CDCl_3$) δ 7.71 (d, J = 8.3 Hz, 2H), 7.33 (d, J = 8.0 Hz, 2H), 4.91 (dt, J = 7.4, 2.2 Hz, 2H), 3.79 – 3.74 (m, 2H), 3.28 (t, J = 7.1 Hz, 2H), 2.51 – 2.44 (m, 2H), 2.43 (s, 3H).

^{13}C NMR (101 MHz, $CDCl_3$) δ 144.1, 143.7, 132.7, 129.7, 127.9, 107.4, 51.9, 48.1, 31.8, 21.6.

HRMS (+p APCI) calcd for $C_{12}H_{16}O_2N^{32}S$ (M+H) 238.0896, found 238.0898

1-chloro-4-(3-methylenecyclohexyl)benzene (S13)

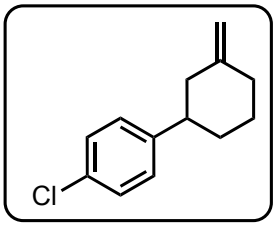

To a flame dried round bottom flask equipped with a stir bar was added methyltriphenylphosphonium bromide (7.27 g, 20.3 mmol, 1.5 equiv) which was dissolved in 20 mL of THF. Then potassium tert-butoxide (2.28 g, 20.3 mmol, 1.5 equiv) was added portion wise at 0 °C and the resulting yellow solution was let to stir for 1 h. Then, the 3-(4-chlorophenyl)cyclohexan-1-one (2.83 g, 13.6 mmol, 1.0 equiv) was

added to the flask and the solution was heated to 50 °C overnight in an aluminum pieblock. In the morning, the reaction was cooled, diluted with water, and extracted with diethyl ether and washed with brine. The crude reaction was purified using column chromatography with hexanes as eluent, affording the title compound as a clear, colorless oil (1.5 g, 53%)

^{1}H NMR (400 MHz, $CDCl_3$) δ 7.28 (d, J = 8.5 Hz, 2H), 7.17 (d, J = 8.5 Hz, 2H), 4.71 (dd, J = 10.6, 2.0 Hz, 2H), 2.59 (tt, J = 12.0, 3.5 Hz, 1H), 2.51 – 2.42 (m, 1H), 2.37 (dq, J = 13.1, 2.2 Hz, 1H), 2.16 (td, J = 12.5, 1.5 Hz, 1H), 2.11 – 1.99 (m, 1H), 1.99 – 1.87 (m, 2H), 1.61 – 1.37 (m, 2H).

^{13}C NMR (101 MHz, $CDCl_3$) δ 148.6, 145.3, 131.7, 128.5, 128.2, 108.0, 45.2, 42.8, 34.6, 33.9, 27.6.

HRMS (+p APCI) calcd for $C_{13}H_{16}{}^{35}Cl$ (M+H) 207.0935, found 207.0939.

1,3-di-tert-butyl-5-(3-methylenecyclohexyl)benzene (S14)

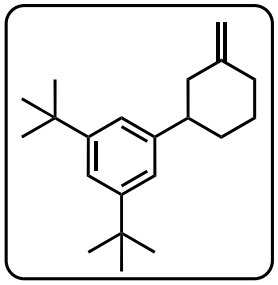

To a flame dried round bottom flask equipped with a stir bar was added methyltriphenylphosphonium bromide (4.75 g, 13.3 mmol, 1.5 equiv) which was dissolved in 20 mL of THF. Then potassium tert-butoxide (1.49 g, 20.3 mmol, 1.5 equiv) was added portion wise at 0 °C and the resulting yellow solution was let to stir for 1 h. Then, the 3-(3,5-di-tert-butylphenyl)cyclohexan-1-one (2.54 g, 8.7 mmol, 1.0 equiv) was added to the flask and the solution was heated to 50 °C overnight in an aluminum pieblock. In the morning, the reaction was cooled, diluted with water, and extracted with diethyl ether and washed with brine. The crude reaction was purified using column chromatography with hexanes as eluent, affording the title compound as a clear, colorless oil (1.4 g, 56%)

^{1}H NMR (400 MHz, $CDCl_3$) δ 7.28 (t, J = 1.8 Hz, 1H), 7.08 (d, J = 1.9 Hz, 2H), 4.69 (dt, J = 7.2, 2.0 Hz, 2H), 2.61 (tt, J = 12.1, 3.5 Hz, 1H), 2.56 – 2.45 (m, 1H), 2.40 – 2.31 (m, 1H), 2.29 – 2.17 (m, 1H), 2.13 – 2.02 (m, 1H),

^{13}C NMR (101 MHz, $CDCl_3$) δ 150.5, 149.5, 145.9, 121.0, 120.2, 107.4, 46.4, 43.0, 34.9, 34.7, 34.1, 31.6, 27.8.

HRMS (+p APCI) calcd for $C_{21}H_{33}$ (M+H) 285.2577, found 285.2578.

Product Characterization

General Procedure 1: To a flame dried vial equipped with a stir bar and 4Å MS (1000 w%) was added catalyst (1.0 mol% or 0.5 mol%). The reaction was then purged and backfilled three times with nitrogen and capped with an argon balloon. Then, the substrate and 2 mL of DCM was added to the vial and it was set to stir (200 RPM) at 25 °C. At this time, the aryldiazoacetate compound (1.0 equiv) was dissolved in 2 mL of DCM and added to the reaction vial over a period of 1 h via syringe pump. The reaction was left either for an additional 2 h or overnight. At this time, the reaction was stopped, concentrated to dryness, and taken for crude NMR analysis. Following this, the reaction was purified via column chromatography to afford the desired product.

5-(*tert*-butyl) 1-(2,2,2-trichloroethyl) (*S*)-1-(4-bromophenyl)-5-azaspiro[2.3]hexane-1,5-dicarboxylate (2)

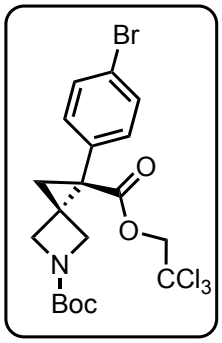

General procedure 1 was used for the cyclopropanation of *tert*-butyl 3-methyleneazetidine-1-carboxylate (34 µL, 0.20 mmol, 2 equiv) with 2,2,2-trichloroethyl 2-(4-bromophenyl)-2-diazoacetate (37.1 mg, 0.10 mmol, 1.0 equiv) using Rh_2(*S*-TPPTTL)$_4$ (2.54 mg, 1.0 mol%) as catalyst. Purification by column chromatography (0-40% diethyl ether/hexanes) afforded the product as a white solid (39.5 mg, 77%).

^{1}H NMR (400 MHz, $CDCl_3$) δ 7.50 (d, J = 8.4 Hz, 2H), 7.24 – 7.18 (m, 2H), 4.89 (d, J = 11.9 Hz, 1H), 4.50 (d, J = 11.9 Hz, 1H), 4.23 – 4.13 (m, 2H), 3.73 (d, J = 9.2 Hz, 1H), 3.62 (d, J = 9.2 Hz, 1H), 2.05 (d, J = 5.6 Hz, 1H), 1.67 (d, J = 5.6 Hz, 1H), 1.43 (s, 9H).

^{13}C NMR (101 MHz, $CDCl_3$) δ 169.8, 156.0, 133.0, 132.4, 131.7, 128.3, 122.2, 94.5, 80.0, 74.5, 35.1, 31.0, 28.4, 24.3.

HRMS (+p APCI) calcd for $C_{19}H_{21}O_4N^{79}Br^{35}Cl_3$ (M+) 510.9714, found 510.9725.

Chiral SFC: The enantiopurity was determined to be 97:3 er by SFC analysis (SS-Whelk, 10% MeOH/IPA 0.2% Formic Acid, 2.5 mL/min, λ=230 nm, RT: Major: 3.53 min., Minor: 2.29 min.)

6-(tert-butyl) 1-(2,2,2-trichloroethyl) (S)-1-(4-bromophenyl)-6-azaspiro[2.5]octane-1,6-dicarboxylate (3)

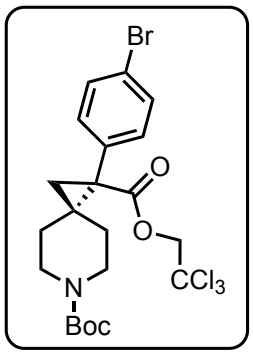

General procedure 1 was used for the cyclopropanation of *tert*-butyl 4-methylenepiperidine-1-carboxylate (40 µL, 0.20 mmol, 2.0 equiv) with 2,2,2-trichloroethyl 2-(4-bromophenyl)-2-diazoacetate (37.2 mg, 0.10 mmol, 1.0 equiv) using Rh_2(*S*-pPhTPCP)$_4$ (1.76 mg, 1.0 mol%) as catalyst. Purification by column chromatography (0-40% diethyl ether/hexanes) afforded the product as a a white solid (41.9 mg, 77%).

^{1}H NMR (400 MHz, $CDCl_3$) δ 7.44 (d, J = 8.5 Hz, 1H), 7.27 (d, J = 8.0 Hz, 2H), 4.84 (d, J = 12.0 Hz, 1H), 4.50 (d, J = 11.9 Hz, 1H), 3.98 (s, 1H), 3.86 (s, 1H), 3.03 (t, J = 12.0 Hz, 1H), 2.86 (t, J = 11.9 Hz, 1H), 1.89 – 1.77 (m, 1H), 1.81 – 1.74 (m, 1H), 1.65 (d, J = 13.6 Hz, 1H), 1.45 (s, 9H), 1.29 (d, J = 5.1 Hz, 1H), 0.64 (d, J = 13.5 Hz, 1H).

^{13}C NMR (101 MHz, $CDCl_3$) δ 169.4 154.7, 134.7, 133.2, 131.2, 121.7, 94.7, 79.7, 74.6, 38.9, 33.2, 30.2, 28.5, 23.9, 14.2.

HRMS (+p APCI) calcd for $C_{21}H_{25}O_4N^{79}Br^{35}Cl_3$ (M+) 539.0027, found 539.0029.

Chiral SFC: The enantiopurity was determined to be 98:2 er by SFC analysis (SS-Whelk, 10% MeOH/IPA 0.2% Formic Acid, 2.5 mL/min, λ=230 nm, RT: Major: 2.88 min., Minor: 2.49 min.)

7-(tert-butyl) 1-(2,2,2-trichloroethyl) (S)-1-(4-bromophenyl)-7-azadispiro[2.1.35.13]nonane-1,7-dicarboxylate (4)

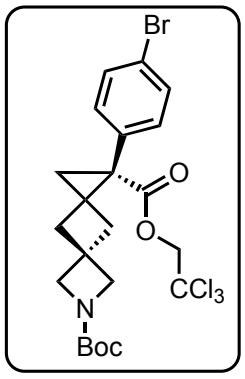

General procedure xx was used for the cyclopropanation of *tert*-butyl 6-methylene-2-azaspiro[3.3]heptane-2-carboxylate (52.3 mg, 0.25 mmol, 2 equiv) with 2,2,2-trichloroethyl 2-(4-bromophenyl)-2-diazoacetate (37.2 mg, 0.10 mmol, 1.0 equiv) using Rh_2(*S*-TPPTTL) (2.5 mg, 1.0 mol%) as catalyst. Purification by column chromatography (0-40% diethyl ether/hexanes) afforded the product as a white solid (44 mg, 79%).

^{1}H NMR (400 MHz, $CDCl_3$) δ 7.47 (d, J = 8.4 Hz, 2H), 7.15 (d, J = 8.5 Hz, 2H), 4.88 (d, J = 12.0 Hz, 1H), 4.49 (d, J = 12.0 Hz, 1H), 4.03 (d, J = 8.7 Hz, 1H), 3.98 – 3.87 (m, 3H), 2.65 – 2.43 (m, 2H), 2.18 (d, J = 12.8 Hz, 1H), 1.96 (d, J = 5.1 Hz, 1H), 1.81 (d, J = 13.3 Hz, 1H), 1.53 (d, J = 5.1 Hz, 1H), 1.42 (s, 9H).

^{13}C NMR (101 MHz, $CDCl_3$) δ 170.1, 156.2, 134.3, 132.5, 131.5, 121.6, 94.8, 79.5, 74.3, 40.6, 39.3, 35.8, 32.4, 32.1, 28.4, 26.4.

HRMS (+p APCI) calcd for $C_{22}H_{25}O_4N^{79}Br^{35}Cl_3$ (M+) 551.0027, found. 551.0032.

Chiral HPLC: The enantiopurity was determined to be 99:1 er by HPLC analysis (AD-H, 1 mL/min, 2% IPA/Hexane, λ=230 nm, RT: Major: 29.7 min., Minor: 26.4 min.)

8-(tert-butyl) 1-(2,2,2-trichloroethyl) (S)-1-phenyl-8-azadispiro[2.1.55.13]undecane-1,8-dicarboxylate (5)

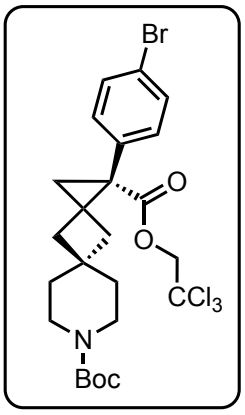

General procedure 1 was used for the cyclopropanation of *tert*-butyl 2-methylene-7-azaspiro[3.5]nonane-7-carboxylate (71.2 mg, 0.30 mmol, 1.5 equiv) with 2,2,2-trichloroethyl 2-(4-bromophenyl)-2-diazoacetate (74.5 mg, 0.20 mmol, 1.0 equiv) using Rh_2(*S*-TPPTTL)$_4$ (5.0 mg, 1.0 mol%) as catalyst. Purification by column chromatography (0-40% diethyl ether/hexanes) afforded the product as a clear oil (82.9 mg, 71% yield).

^{1}H NMR (400 MHz, $CDCl_3$) δ 7.47 (d, *J* = 8.4 Hz, 2H), 7.19 (d, *J* = 8.5 Hz, 2H), 4.93 (d, *J* = 11.9 Hz, 1H), 4.47 (d, *J* = 12.0 Hz, 1H), 3.43 – 3.16 (m, 4H), 2.25 – 2.08 (m, 2H), 1.98 (d, *J* = 4.9 Hz, 1H), 1.77 (d, *J* = 12.3 Hz, 1H), 1.68 – 1.52 (m, 5H), 1.44 (s, 9H).

^{13}C NMR (101 MHz, $CDCl_3$) δ 170.4, 155.0, 134.8, 132.8, 131.5, 121.6, 95.0, 79.5, 74.4, 39.8, 38.6, 35.9, 33.1, 32.5, 28.6, 27.7.

HRMS (+p APCI) calcd for $C_{24}H_{29}O_4N^{79}Br^{35}Cl_3$ (M+) 579.0340, found 579.0356.

Chiral SFC: The enantiopurity was determined to be 90% ee by SFC analysis (SSWhelk, 2.5 mL/min, 10% (50% methanol in isopropanol with 0.2% Formic Acid) in CO2, 1.0 mg/ml), λ=230 nm, RT: Major: 4.48 min., Minor: 3.52 min.)

5-(tert-butyl) 1-(2,2,2-trichloroethyl) (1S,3S)-1-(4-bromophenyl)-5-azaspiro[2.5]octane-1,5-dicarboxylate (8)

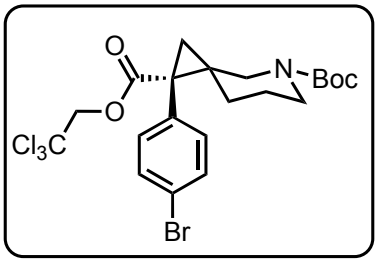

General procedure 1 was used for the cyclopropanation of *tert*-butyl 3-methylenepiperidine-1-carboxylate (29.6 mg, 0.15 mmol, 1.5 equiv) with 2,2,2-trichloroethyl 2-(4-bromophenyl)-2-diazoacetate (37.2 mg, 0.10 mmol, 1.0 equiv) using Rh_2(*S*-*p*PhTPCP)$_4$ (1.7 mg, 1.0 mol%) as catalyst. Purification by column chromatography (0-40% diethyl ether/hexanes) afforded the product as an amorphous white solid 36.7 mg, 86% yield).

^{1}H NMR (400 MHz, $CDCl_3$) δ 7.43 (d, J = 8.5 Hz, 2H), 7.28 (s, 2H), 4.79 (bs, 1H), 4.66 – 4.44 (m, 1H), 3.88 (s, 1H), 3.49 (s, 2H), 2.94 (s, 1H), 1.95 (d, J = 5.0 Hz, 1H), 1.65 – 1.55 (m, 1H), 1.48 (s, 9H), 1.21 (d, J = 5.0 Hz, 1H), 1.09 – 0.75 (m, 1H).

^{13}C NMR (101 MHz, $CDCl_3$) δ 169.4, 169.1, 154.8, 134.6, 133.1, 131.8, 131.1, 128.3, 121.6, 94.8, 79.7, 74.7, 49.8, 48.2, 43.9, 38.9, 33.3, 28.5, 24.6.

HRMS (+p APCI) calcd for $C_{21}H_{25}O_4N^{79}Br^{35}Cl_3$ (M+) 539.0027, found 539.0028.

Chiral SFC: The enantiopurity was determined to be 99% ee by SFC analysis (OJ3, 2.5 mL/min, 3% (50% methanol in isopropanol with 0.2% Formic Acid) in CO2, 1.0 mg/ml), λ=230 nm, RT: Major: 2.51 min., Minor: 4.19 min.)

2,2,2-trichloroethyl (1S,3S)-1-(4-bromophenyl)-5-tosyl-5-azaspiro[2.5]octane-1-carboxylate (9)

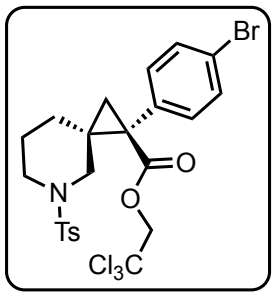

General procedure 1 was used for the cyclopropanation of *tert*-butyl 3-methylenepiperidine-1-carboxylate (50.3 mg, 0.20 mmol, 2 equiv) with 2,2,2-trichloroethyl 2-(4-bromophenyl)-2-diazoacetate (37.2 mg, 0.10 mmol, 1.0 equiv) using Rh_2(*S*-pPhTPCP)$_4$ (3.4 mg, 1.0 mol%) as catalyst. Purification by column chromatography (0-25%

diethyl ether/hexanes) afforded the product as a white solid (48 mg, 80%).

^{1}H NMR (400 MHz, $CDCl_3$) δ 7.62 (d, J = 8.3 Hz, 2H), 7.44 (d, J = 8.5 Hz, 2H), 7.31 (dd, J = 8.1, 5.4 Hz, 4H), 4.90 (d, J = 12.0 Hz, 1H), 4.65 (d, J = 12.0 Hz, 1H), 3.13 (s, 2H), 3.11 – 2.98 (m, 2H), 2.44 (s, 3zH), 1.95 (d, J = 5.4 Hz, 1H), 1.75 (ddd, J = 14.4, 6.9, 3.3 Hz, 1H), 1.60 (tt, J = 9.4, 5.1 Hz, 1H), 1.30 (d, J = 5.4 Hz, 1H), 1.11 (ddd, J = 12.6, 7.9, 4.2 Hz, 1H), 1.05 – 0.94 (m, 1H).

^{13}C NMR (101 MHz, $CDCl_3$) δ 169.1, 143.6, 134.1, 133.3, 133.0, 131.1, 129.7, 127.7, 121.8, 94.8, 74.9, 50.1, 46.6, 39.1, 32.4, 30.6, 23.8, 23.4, 21.6.

HRMS (+p APCI) calcd for (M+) $C_{23}H_{24}O_4N^{79}Br^{35}Cl_3{}^{32}S$ 593.9670, found 593.9674.

Chiral HPLC: The enantiopurity was determined to be 98% ee by HPLC analysis (AD-H, 1 mL/min, 10% IPA/Hexane, λ=230 nm, RT: Major: 29.1 min., Minor: 24.4 min.)

2,2,2-trichloroethyl (1*S*,3*S*)-5-tosyl-1-(4-(trifluoromethyl)phenyl)-5-azaspiro[2.5]octane-1-carboxylate (10)

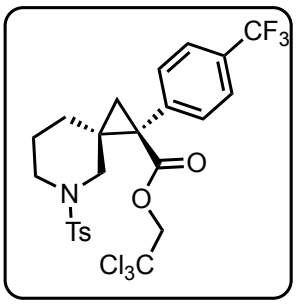

General procedure 1 was used for the cyclopropanation of *tert*-butyl 3-methylenepiperidine-1-carboxylate (75.4 mg, 0.30 mmol, 1.5 equiv) with 2,2,2-trichloroethyl 2-diazo-2-(4-(trifluoromethyl)phenyl)acetate (73.2 mg, 0.20 mmol, 1.0 equiv) using Rh_2(*S*-pPhTPCP)$_4$ (3.4 mg, 1.0 mol%) as catalyst. Purification by column chromatography (0-40%% diethyl ether/hexanes) afforded the product as a white solid (93 mg, 83%).

^{1}H NMR (400 MHz, $CDCl_3$) δ 7.60 (d, J = 8.2 Hz, 2H), 7.32 (d, J = 8.1 Hz, 2H), 6.50 (s, 1H), 4.95 (d, J = 12.0 Hz, 1H), 4.87 (d, J = 12.1 Hz, 1H), 3.53 – 3.39 (m, 2H), 2.78 (d, J = 12.5 Hz, 1H), 2.60 – 2.51 (m, 1H), 2.43 (s, 3H), 2.29 (s, 3H), 2.02 (d, J = 5.8 Hz, 1H), 1.86 (d, J = 5.8 Hz, 1H), 1.78 – 1.64 (m, 1H), 1.57 (dt, J = 13.7, 4.2 Hz, 1H), 1.43 – 1.34 (m, 1H), 1.13 (dt, J = 14.4, 4.6 Hz, 1H).

^{13}C NMR (101 MHz, $CDCl_3$) δ 168.83, 143.63, 139.10 (d, J = 1.2 Hz), 133.29, 131.75, 129.71, 127.65, 124.91 (q, J = 3.8 Hz), 124.0 (q, J = 271.5 Hz), 94.68, 74.87, 49.98, 46.56, 39.33, 32.64, 30.74, 23.76, 23.57, 21.58.

^{19}F NMR (376 MHz, $CDCl_3$) δ -62.5.

HRMS (+p APCI) calcd for (M+H) $C_{24}H_{24}O_4N^{35}Cl_3F_3{}^{32}S$ 584.0438, found 584.0429

Chiral HPLC: The enantiopurity was determined to be 99.5:0.5 er by HPLC analysis (AD-H, 1 mL/min, 10% IPA/Hexane, λ=230 nm, RT: Major: 19.5 min., Minor: 25.7 min.)

2,2,2-trichloroethyl (1*S*,3*S*)-1-(4-(methoxycarbonyl)phenyl)-5-tosyl-5-azaspiro[2.5]octane-1-carboxylate (11)

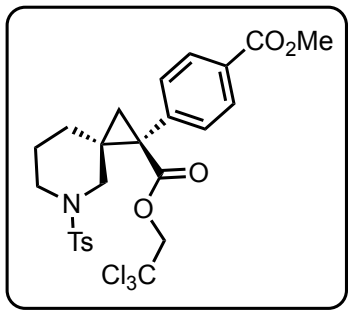

General procedure xx was used for the cyclopropanation of *tert*-butyl 3-methylenepiperidine-1-carboxylate (100.5 mg, 0.30 mmol, 2 equiv) with methyl 4-(1-diazo-2-oxo-2-(2,2,2-trichloroethoxy)ethyl)benzoate (70.3 mg, 0.20 mmol, 1.0 equiv) using Rh_2(*S*-pPhTPCP)$_4$ (3.4 mg, 1.0 mol%) as catalyst. Purification by column chromatography (0-30% diethyl ether/hexanes) afforded the product as a white solid (91 mg, 81%).

^{1}H NMR (400 MHz, $CDCl_3$) δ 8.00 (d, J = 8.2 Hz, 2H), 7.64 (d, J = 8.3 Hz, 2H), 7.53 (d, J = 8.1 Hz, 2H), 7.34 (d, J = 8.0 Hz, 2H), 4.91 (d, J = 11.9 Hz, 1H), 4.68 (d, J = 12.0 Hz, 1H), 3.93 (s, 3H), 3.19 (s, 2H), 3.11 (td, J = 7.3, 3.4 Hz, 1H), 3.08 – 2.99 (m, 1H), 2.46 (s, 3H), 2.01 (d, J = 5.4 Hz, 1H), 1.84 – 1.73 (m, 1H), 1.60 (dtt, J = 15.7, 7.7, 4.2 Hz, 1H), 1.40 (d, J = 5.5 Hz, 1H), 1.12 (ddd, J = 12.5, 7.8, 4.2 Hz, 1H), 0.98 (ddd, J = 13.3, 7.9, 4.2 Hz, 1H).

^{13}C NMR (101 MHz, $CDCl_3$) δ 168.9, 166.8, 143.6, 140.2, 133.3, 131.4, 129.7, 129.5, 129.2, 127.7, 94.7, 74.9, 52.2, 50.0, 46.6, 39.5, 32.7, 30.7, 23.8, 23.6, 21.6.

HRMS (+p APCI) calcd for (M+H) $C_{25}H_{27}O_6N^{35}Cl_3{}^{32}S$ 574.0619, found 574.0609.

Chiral HPLC: The enantiopurity was determined to be 99:1 er by HPLC analysis (AD-H, 1 mL/min, 10% IPA/Hexane, λ=230 nm, RT: Major: 41.4 min., Minor: 35.7 min.)

2,2,2-trichloroethyl (1*S*,3*S*)-1-(4-nitrophenyl)-5-tosyl-5-azaspiro[2.5]octane-1-carboxylate (12)

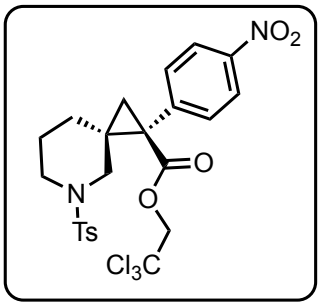

General procedure 1 was used for the cyclopropanation of 3-methylene-1-tosylpiperidine (75.4 mg, 0.30 mmol, 1.5 equiv) with 2,2,2-trichloroethyl 2-diazo-2-(4-nitrophenyl)acetate (67.7 mg, 0.20 mmol, 1.0 equiv) using Rh_2(*S*-*p*-PhTPCP)$_4$ (3.4 mg, 1.0 mol%) as catalyst. Purification by column chromatography (0-40% diethyl ether/hexanes) afforded the product as a white solid (81 mg, 72% yield).

^{1}H NMR (400 MHz, $CDCl_3$) δ 8.18 (d, J = 8.8 Hz, 2H), 7.63 (dd, J = 8.6, 2.1 Hz, 4H), 7.33 (d, J = 8.1 Hz, 2H), 4.89 (d, J = 12.0 Hz, 1H), 4.69 (d, J = 12.0 Hz, 1H), 3.24 (d, J = 12.4 Hz, 1H), 3.15 (d, J = 12.3 Hz, 1H), 3.12 – 3.00 (m, 2H), 2.44 (s, 3H), 2.07 (d, J = 5.5 Hz, 1H), 1.75 (ddt, J = 12.2, 8.0, 4.9 Hz, 1H), 1.66 – 1.58 (m, 1H), 1.41 (d, J = 5.6 Hz, 1H), 1.05 (dt, J = 7.8, 4.9 Hz, 2H).

^{13}C NMR (101 MHz, $CDCl_3$) δ 168.3, 147.3, 143.7, 142.5, 133.3, 132.4, 129.7, 127.6, 123.1, 94.6, 75.0, 49.7, 46.5, 39.3, 33.2, 30.8, 23.8, 23.7, 21.6.

HRMS (+p APCI) calcd for $C_{23}H_{24}O_6N_2{}^{35}Cl_3{}^{32}S$ (M+H) 561.0415, found 561.0407.

Chiral HPLC: The enantiopurity was determined to be 99% ee by HPLC analysis (AD-H, 1 mL/min, 10% IPA/Hexane, λ=230 nm, RT: Major: 26.8 min., Minor: 37.5 min.)

2,2,2-trichloroethyl (1S,3S)-1-([1,1'-biphenyl]-4-yl)-5-tosyl-5-azaspiro[2.5]octane-1-carboxylate (13)

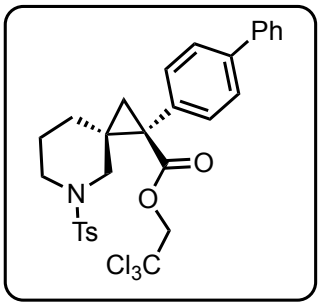

General procedure 1 was used for the cyclopropanation of 3-methylene-1-tosylpiperidine (75.4 mg, 0.30 mmol, 1.5 equiv) with 2,2,2-trichloroethyl 2-([1,1'-biphenyl]-4-yl)-2-diazoacetate (73.9 mg, 0.20 mmol, 1.0 equiv) using Rh_2(*S*-*p*-PhTPCP)$_4$ (3.4 mg, 1.0 mol%) as catalyst. Purification by column chromatography (0-40% diethyl ether/hexanes) afforded the product as a white solid (102.8 mg, 87% yield).

^{1}H NMR (400 MHz, $CDCl_3$) δ 7.64 (d, *J* = 8.3 Hz, 2H), 7.59 (d, *J* = 7.0 Hz, 2H), 7.53 (s, 2H), 7.49 (d, *J* = 8.4 Hz, 2H), 7.46 – 7.40 (m, 2H), 7.38 – 7.30 (m, 3H), 4.93 (d, *J* = 12.0 Hz, 1H), 4.66 (d, *J* = 11.9 Hz, 1H), 3.26 – 3.11 (m, 3H), 2.98 (ddd, *J* = 11.6, 8.2, 3.6 Hz, 1H), 2.45 (s, 3H), 1.97 (d, *J* = 5.4 Hz, 1H), 1.89 – 1.74 (m, 1H), 1.69 – 1.58 (m, 1H), 1.38 (d, *J* = 5.4 Hz, 1H), 1.22 (ddd, *J* = 13.0, 8.6, 4.4 Hz, 1H), 1.00 (ddd, *J* = 13.8, 7.5, 4.1 Hz, 1H).

^{13}C NMR (101 MHz, $CDCl_3$) δ 169.7, 143.6, 140.6, 140.5, 134.1, 133.5, 131.8, 129.8, 128.9, 127.8, 127.6, 127.2, 126.7, 95.0, 74.9, 50.5, 46.8, 39.5, 32.3, 30.8, 24.0, 23.5, 21.7.

HRMS (+p APCI) calcd for $C_{29}H_{29}O_4N^{35}Cl_3{}^{32}S$ (M+H) 592.0877, found 592.0871.

Chiral HPLC: The enantiopurity was determined to be 99% ee by HPLC analysis (AD-H, 1 mL/min, 10% IPA/Hexane, λ=230 nm, RT: Major: 26.8 min., Minor: 37.5 min.)

2,2,2-trichloroethyl (1S,3S)-1-(4-methoxyphenyl)-5-tosyl-5-azaspiro[2.5]octane-1-carboxylate (14)

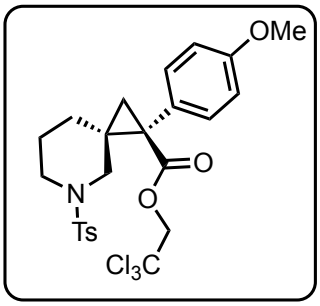

General procedure 1 was used for the cyclopropanation of 3-methylene-1-tosylpiperidine (75.4 mg, 0.30 mmol, 1.5 equiv) with 2,2,2-trichloroethyl 2-diazo-2-(4-methoxyphenyl)acetate (64.7 mg, 0.20 mmol, 1.0 equiv) using Rh_2(*S*-*p*-PhTPCP)$_4$ (3.4 mg, 1.0 mol%) as catalyst. Purification by column chromatography (0-40% diethyl ether/hexanes) afforded the product as a white solid (97.8 mg, 89% yield).

^{1}H NMR (400 MHz, $CDCl_3$) δ 7.62 (d, *J* = 8.3 Hz, 2H), 7.38 – 7.28 (m, 4H), 6.83 (d, *J* = 8.8 Hz, 2H), 4.89 (d, *J* = 12.0 Hz, 1H), 4.64 (d, *J* = 12.0 Hz, 1H), 3.79 (s, 3H), 3.19 – 3.06 (m, 3H), 3.01 – 2.91 (m, 1H), 2.44 (s, 3H), 1.89 (d, *J* = 5.3 Hz, 1H), 1.81 – 1.69 (m, 1H), 1.64 – 1.52 (m, 1H), 1.28 (d, *J* = 5.3 Hz, 1H), 1.16 (ddd, *J* = 13.0, 8.3, 4.1 Hz, 1H), 0.96 (ddd, *J* = 13.7, 7.6, 4.2 Hz, 1H).

^{13}C NMR (101 MHz, $CDCl_3$) δ 169.9, 159.1, 143.6, 133.5, 132.4, 129.8, 127.8, 127.1, 113.4, 95.0, 74.9, 55.4, 50.5, 46.8, 39.0, 32.1, 30.7, 24.0, 23.5, 21.7.

HRMS (+p APCI) calcd for $C_{24}H_{27}O_5N^{35}Cl_3{}^{32}S$ ($M+H^+$) 546.0670, found 546.0665.

Chiral SFC: The enantiopurity was determined to be 99% ee by SFC analysis (OJ3, 2.5 mL/min, 10% (50% methanol in isopropanol with 0.2% Formic Acid) in CO2, 1.0 mg/ml), λ=230 nm, RT: Major: 4.08 min., Minor: 5.21 min.)

2,2,2-trichloroethyl (1*S*,3*S*)-1-phenyl-5-tosyl-5-azaspiro[2.5]octane-1-carboxylate (15)

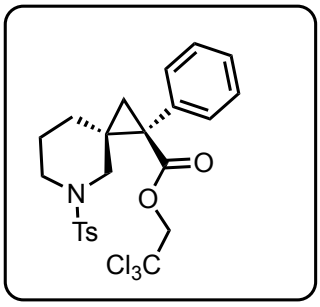

General procedure 1 was used for the cyclopropanation of 3-methylene-1-tosylpiperidine (75.4 mg, 0.30 mmol, 1.5 equiv) with 2,2,2-trichloroethyl 2-diazo-2-phenylacetate (58.7 mg, 0.20 mmol, 1.0 equiv) using Rh_2(*S*-*p*-PhTPCP)$_4$ (3.4 mg, 1.0 mol%) as catalyst. Purification by column chromatography (0-40% diethyl ether/hexanes) afforded the product as a white solid (97.8 mg, 89% yield).

^{1}H NMR (400 MHz, $CDCl_3$) δ 7.63 (d, J = 8.2 Hz, 2H), 7.44 – 7.39 (m, 2H), 7.35 – 7.27 (m, 5H), 4.89 (d, J = 12.0 Hz, 1H), 4.64 (d, J = 12.0 Hz, 1H), 3.25 – 3.06 (m, 3H), 2.94 (ddd, J = 11.6, 8.1, 3.5 Hz, 1H), 2.44 (s, 3H), 1.93 (d, J = 5.3 Hz, 1H), 1.77 (dtt, J = 14.8, 7.5, 3.9 Hz, 1H), 1.67 – 1.52 (m, 1H), 1.33 (d, J = 5.3 Hz, 1H), 1.15 (dd, J = 8.7, 4.4 Hz, 1H), 0.93 (ddd, J = 13.8, 7.4, 4.1 Hz, 1H).

^{13}C NMR (101 MHz, $CDCl_3$) δ 169.6, 143.5, 135.0, 133.4, 131.3, 129.7, 128.0, 127.7, 127.6, 94.9, 74.8, 65.9, 50.4, 46.6, 39.6, 32.1, 30.7, 23.9, 23.4, 21.6, 15.3.

HRMS (+p APCI) calcd for $C_{23}H_{25}O_4N^{35}Cl_3{}^{32}S$ (M+H) 516.0564, found 516.0555.

Chiral HPLC: The enantiopurity was determined to be 99% ee by HPLC analysis (AD-H, 1 mL/min, 10% IPA/Hexane, λ=230 nm, RT: Major: 27.4 min., Minor: 20.1 min.)

2,2,2-trichloroethyl (1S,3S)-1-(m-tolyl)-5-tosyl-5-azaspiro[2.5]octane-1-carboxylate (16)

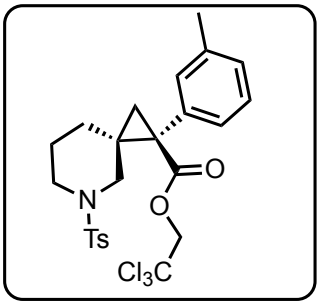

General procedure 1 was used for the cyclopropanation of 3-methylene-1-tosylpiperidine (75.4 mg, 0.30 mmol, 1.5 equiv) with 2,2,2-trichloroethyl 2-diazo-2-(m-tolyl)acetate (61.5 mg, 0.20 mmol, 1.0 equiv) using Rh_2(*S*-*p*-PhTPCP)$_4$ (1.7 mg, 1.0 mol%) as catalyst. Purification by column chromatography (0-20% diethyl ether/hexanes) afforded the product as a white solid (95.6 mg, 90% yield).

^{1}H NMR (400 MHz, $CDCl_3$) δ 7.62 (d, *J* = 8.0 Hz, 2H), 7.32 (d, *J* = 8.0 Hz, 2H), 7.26 (s, 1H), 7.19 (d, *J* = 1.4 Hz, 2H), 7.12 – 7.04 (m, 1H), 4.91 (d, *J* = 11.9 Hz, 1H), 4.62 (d, *J* = 11.9 Hz, 1H), 3.25 – 3.02 (m, 3H), 3.00 – 2.85 (m, 1H), 2.44 (s, 3H), 2.32 (s, 3H), 1.91 (d, *J* = 5.3 Hz, 1H), 1.76 (ddt, *J* = 14.4, 7.6, 3.7 Hz, 1H), 1.60 (ddt, *J* = 13.4, 8.8, 4.4 Hz, 1H), 1.33 (d, *J* = 5.3 Hz, 1H), 1.17 (ddd, *J* = 13.3, 8.6, 4.1 Hz, 1H), 0.92 (ddd, *J* = 13.9, 7.4, 4.2 Hz, 1H).

^{13}C NMR (101 MHz, $CDCl_3$) δ 169.7, 143.6, 137.6, 134.9, 133.4, 132.3, 129.8, 128.5, 128.3, 127.9, 127.8, 95.0, 74.8, 50.5, 46.8, 39.7, 32.0, 30.8, 24.0, 23.4, 21.7, 21.5.

HRMS (+p APCI) calcd for $C_{24}H_{27}O_4N^{35}Cl_3{}^{32}S$ (M+H) 530.0721, found 530.0707.

Chiral HPLC: The enantiopurity was determined to be 98% ee by HPLC analysis (AD-H, 1 mL/min, 10% IPA/Hexane, λ=230 nm, RT: Major: 28.98 min., Minor: 13.86 min.)

2,2,2-trichloroethyl (1S,3S)-1-(3-bromophenyl)-5-tosyl-5-azaspiro[2.5]octane-1-carboxylate (17)

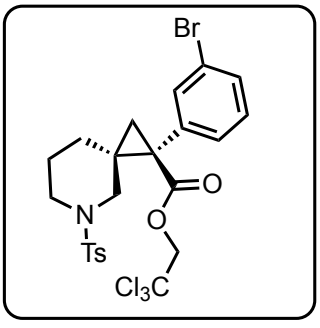

General procedure 1 was used for the cyclopropanation of 3-methylene-1-tosylpiperidine (75.4 mg, 0.30 mmol, 1.5 equiv) with 2,2,2-trichloroethyl 2-(3-bromophenyl)-2-diazoacetate (74.5 mg, 0.20 mmol, 1.0 equiv) using Rh_2(*S*-*p*-PhTPCP)$_4$ (1.7 mg, 1.0 mol%) as catalyst. Purification by column chromatography (0-30% diethyl ether/hexanes) afforded the product as a white solid (108.9 mg, 91% yield).

^{1}H NMR (400 MHz, $CDCl_3$) δ 7.66 – 7.56 (m, 3H), 7.41 (d, *J* = 7.9 Hz, 1H), 7.35 (d, *J* = 8.0 Hz, 1H), 7.32 (d, *J* = 8.0 Hz, 2H), 7.18 (t, *J* = 7.9 Hz, 1H), 4.89 (d, *J* = 11.9 Hz, 1H), 4.65 (d, *J* = 11.9 Hz, 1H), 3.22 – 3.06 (m, 3H), 2.99 (ddd, *J* = 11.4, 7.9, 3.6 Hz, 1H), 2.44

(s, 3H), 1.95 (d, *J* = 5.4 Hz, 1H), 1.83 – 1.70 (m, 1H), 1.66 – 1.56 (m, 1H), 1.33 (d, *J* = 5.5 Hz, 1H), 1.16 (ddd, *J* = 12.9, 8.2, 4.2 Hz, 1H), 0.98 (ddd, *J* = 13.8, 7.7, 4.2 Hz, 1H).

^{13}C NMR (101 MHz, $CDCl_3$) δ 169.0, 143.7, 137.4, 134.6, 133.5, 131.0, 130.0, 129.8, 129.6, 127.8, 122.0, 94.9, 75.0, 50.2, 46.7, 39.4, 32.6, 30.8, 23.9, 23.6, 21.7.

HRMS (+p APCI) calcd for $C_{23}H_{24}O_4N^{79}Br^{35}Cl_3{}^{32}S$ ($M+H^+$) 593.9670, found 593.9661.

Chiral HPLC: The enantiopurity was determined to be 96% ee by HPLC analysis (AD-H, 1 mL/min, 10% IPA/Hexane, λ=230 nm, RT: Major: 31.7 min., Minor: 19.8 min.)

2,2,2-trichloroethyl (1S,3S)-1-(3,5-dibromophenyl)-5-tosyl-5-azaspiro[2.5]octane-1-carboxylate (18)

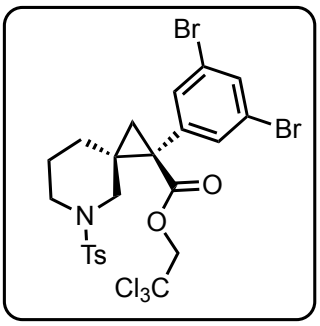

General procedure 1 was used for the cyclopropanation of 3-methylene-1-tosylpiperidine (75.4 mg, 0.30 mmol, 1.5 equiv) with 2,2,2-trichloroethyl 2-diazo-2-(3,5-dibromophenyl)acetate (90.3 mg, 0.20 mmol, 1.0 equiv) using Rh_2(*S*-*p*-PhTPCP)$_4$ (1.7 mg, 1.0 mol%) as catalyst. Purification by column chromatography (0-20% diethyl ether/hexanes) afforded the product as a white solid (94.4 mg, 73% yield, 7:1 dr).

^{1}H NMR (400 MHz, $CDCl_3$) δ 7.66 – 7.57 (m, 3H), 7.52 (d, *J* = 1.8 Hz, 2H), 7.32 (d, *J* = 8.1 Hz, 2H), 4.90 (d, *J* = 11.9 Hz, 1H), 4.66 (d, *J* = 11.9 Hz, 1H), 3.20 – 3.06 (m, 3H), 3.06 – 2.94 (m, 1H), 2.44 (s, 3H), 1.96 (d, *J* = 5.6 Hz, 1H), 1.79 – 1.70 (m, 1H), 1.69 – 1.59 (m, 1H), 1.33 (d, *J* = 5.6 Hz, 1H), 1.16 (ddd, *J* = 12.6, 7.9, 4.3 Hz, 1H), 1.02 (ddd, *J* = 13.4, 7.7, 4.2 Hz, 1H). *For clarity, only the major diastereomer is reported.*

^{13}C NMR (101 MHz, $CDCl_3$) δ 168.4, 143.8, 139.0, 133.6, 133.4, 133.3, 129.8, 127.8, 122.5, 94.8, 75.1, 49.9, 46.7, 39.1, 33.0, 30.9, 23.9, 23.6, 21.7. *For clarity, only the major diastereomer is reported.*

HRMS (+p APCI) calcd for $C_{23}H_{23}O_4N^{79}Br_2{}^{35}Cl_3{}^{32}S$ (M+H) 671.8775, found 671.8776.

Chiral SFC: The enantiopurity was determined to be 97% ee by SFC analysis (SSWhelk, 2.5 mL/min, 10% (50% methanol in isopropanol with 0.2% Formic Acid) in CO2, 1.0 mg/ml), λ=230 nm, RT: Major: 9.98 min., Minor: 10.82 min.)

2,2,2-trichloroethyl (1*S*,3*S*)-1-((*E*)-styryl)-5-tosyl-5-azaspiro[2.5]octane-1-carboxylate (19)

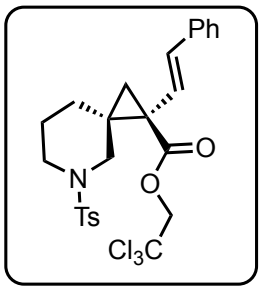

General procedure 1 was used for the cyclopropanation of 3-methylene-1-tosylpiperidine (75.4 mg, 0.30 mmol, 1.5 equiv) with 2,2,2-trichloroethyl (E)-2-diazo-4-phenylbut-3-enoate (63.9 mg, 0.20 mmol, 1.0 equiv) using Rh_2(*S*-TPPTTL)$_4$ (5.0 mg, 1.0 mol%) as catalyst. Purification by column chromatography (0-40% diethyl ether/hexanes) afforded the product as a white solid (65.3 mg, 60% yield).

^{1}H NMR (400 MHz, $CDCl_3$) δ 7.52 (d, J = 8.3 Hz, 2H), 7.34 – 7.27 (m, 2H), 7.23 (d, J = 7.8 Hz, 3H), 7.20 – 7.15 (m, 2H), 6.71 (d, J = 16.0 Hz, 1H), 6.35 (d, J = 15.9 Hz, 1H), 4.91 (d, J = 12.0 Hz, 1H), 4.74 (d, J = 12.0 Hz, 1H), 3.49 – 3.38 (m, 1H), 3.31 (d, J = 12.3 Hz, 1H), 2.66 (d, J = 12.3 Hz, 1H), 2.51 (ddd, J = 11.3, 8.4, 4.8 Hz, 1H), 2.35 (s, 3H), 1.68 (d, J = 5.6 Hz, 1H), 1.64 – 1.55 (m, 2H), 1.43 – 1.33 (m, 2H), 1.22 (d, J = 5.7 Hz, 1H).

^{13}C NMR (101 MHz, $CDCl_3$) δ 169.6, 143.5, 136.5, 133.5, 133.3, 129.7, 128.7, 127.9, 127.6, 126.4, 123.6, 95.1, 74.9, 49.9, 46.7, 36.4, 33.6, 28.7, 24.6, 21.5, 21.1.

HRMS (+p APCI) calcd for $C_{25}H_{27}O_4N^{35}Cl_3{}^{32}S$ (M+H) 542.0721, 542.0717 found.

Chiral HPLC: The enantiopurity was determined to be 78% ee by HPLC analysis (R,R-Whelk, 1 mL/min, 10% IPA/Hexane, λ=230 nm, RT: Major: 30.3 min., Minor: 25.8 min.)

2,2,2-trichloroethyl (1S,3S)-1-(benzo[d][1,3]dioxol-5-yl)-5-tosyl-5-azaspiro[2.5]octane-1-carboxylate (20)

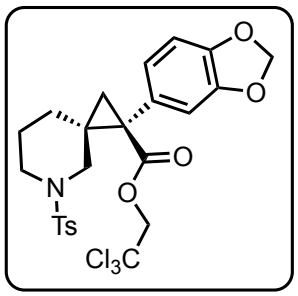

General procedure 1 was used for the cyclopropanation of *tert*-butyl 3-methylenepiperidine-1-carboxylate (75.4 mg, 0.30 mmol, 1.5 equiv) with 2,2,2-trichloroethyl 2-(benzo[d][1,3]dioxol-5-yl)-2-diazoacetate (67.5 mg, 0.20 mmol, 1.0 equiv) using Rh_2(*S*-pPhTPCP)$_4$ (1.76 mg, 0.5 mol%) as catalyst. Purification by

column chromatography (0-30% diethyl ether/hexanes) afforded the product as a white solid (82.1 mg, 73%).

^{1}H NMR (400 MHz, $CDCl_3$) δ 7.61 (d, J = 8.3 Hz,2H), 7.31 (d, J = 8.0 Hz, 2H), 6.93 (d, J = 1.8 Hz, 1H), 6.84 (dd, J = 8.1, 1.8 Hz, 1H), 6.73 (d, J = 8.0 Hz, 1H), 5.94 (s, 2H), 4.89 (d, J = 11.9 Hz, 1H), 4.65 (d, J = 11.9 Hz, 1H), 3.16 (dd, J = 13.5, 7.2 Hz, 2H), 3.06 (d, J = 12.1 Hz, 1H), 2.92 (ddd, J = 11.7, 8.1, 3.4 Hz, 1H), 2.44 (s, 3H), 1.89 (d, J = 5.3 Hz, 1H), 1.77 (ddq, J = 14.5, 7.4, 3.6 Hz, 1H), 1.68 – 1.54 (m, 2H), 1.26 (d, J = 5.4 Hz, 1H), 1.21 (tt, J = 8.5, 4.2 Hz, 1H), 1.03 – 0.94 (m, 1H).
^{13}C NMR (101 MHz, $CDCl_3$) δ 169.6, 147.2, 147.1, 143.5, 133.3, 129.7, 128.6, 127.7, 124.5, 111.9, 107.7, 101.2, 94.9, 74.8, 50.4, 46.6, 39.4, 32.1, 30.6, 23.9, 23.7, 21.6.
HRMS (+p APCI) calcd for $C_{24}H_{25}O_6N^{35}Cl_3{}^{32}S$ (M+) 560.0463, found 560.0456.
Chiral HPLC: The enantiopurity was determined to be 99.5:0.5 er by HPLC analysis (AD-H, 1 mL/min, 10% IPA/Hexane, λ=230 nm, RT: Major: 49.6 min., Minor: 28.4 min.)

2,2,2-trichloroethyl (1S,3S)-1-(2,3-dihydrobenzofuran-5-yl)-5-tosyl-5-azaspiro[2.5]octane-1-carboxylate (21)

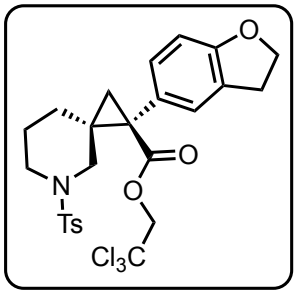

General procedure 1 was used for the cyclopropanation of *tert*-butyl 3-methylenepiperidine-1-carboxylate (75.4 mg, 0.30 mmol, 1.5 equiv) with 2 2,2,2-trichloroethyl 2-diazo-2-(2,3-dihydrobenzofuran-6-yl)acetate (67.1 mg, 0.20 mmol, 1.0 equiv) using Rh_2(*S*-pPhTPCP)$_4$ (1.75 mg, 0.50 mol%) as catalyst. Purification by column chromatography (0-30% diethyl ether/hexanes) afforded the product as a white solid (77 mg, 69%).

^{1}H NMR (400 MHz, $CDCl_3$) δ 7.61 (d, J = 8.3 Hz, 2H), 7.31 (d, J = 8.1 Hz, 2H), 7.28 (d, J = 1.9 Hz, 1H), 7.11 (dd, J = 8.4, 2.0 Hz, 1H), 6.69 (d, J = 8.3 Hz, 1H), 4.90 (d, J = 12.0 Hz, 1H), 4.63 (d, J = 12.0 Hz, 1H), 4.56 (t, J = 8.7 Hz, 2H), 3.25 – 3.03 (m, 5H), 2.95 (ddd, J = 11.5, 8.2, 3.5 Hz, 1H), 2.44 (s, 3H), 1.88 (d, J = 5.3 Hz, 1H), 1.76 (ddq, J = 14.5, 7.4,

3.6 Hz, 1H), 1.67 – 1.53 (m, 1H), 1.26 (d, J = 5.3 Hz, 1H), 1.24 – 1.13 (m, 1H), 0.98 (ddd, J = 14.0, 7.6, 4.0 Hz, 1H).

^{13}C NMR (101 MHz, $CDCl_3$) δ 169.9, 159.6, 143.5, 133.3, 130.9, 129.7, 128.0, 127.7, 126.8, 126.7, 108.6, 95.0, 74.8, 71.4, 50.5, 46.7, 39.2, 31.9, 30.6, 29.6, 23.9, 23.4, 21.6.

HRMS (+p APCI) calcd for $C_{25}H_{27}O_5N^{35}Cl_3{}^{32}S$ (M+) 558.0670, found 558.0659.

Chiral HPLC: The enantiopurity was determined to be 99.5:0.5 er by HPLC analysis (AD-H, 1 mL/min, 10% IPA/Hexane, λ=230 nm, RT: Major: 50.3 min., Minor: 21.3 min.)

2,2,2-trichloroethyl (1*R*,3*S*)-1-(3-methylisoxazol-5-yl)-5-tosyl-5-azaspiro[2.5]octane-1-carboxylate (22)

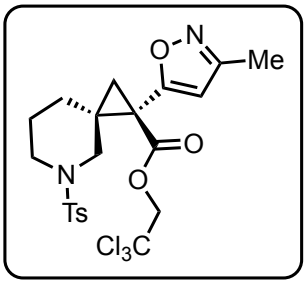

General procedure 1 was used for the cyclopropanation of *tert*-butyl 3-methylenepiperidine-1-carboxylate (75.4 mg, 0.30 mmol, 1.5 equiv) with 2,2,2-trichloroethyl 2-diazo-2-(3-methylisoxazol-5-yl)acetate (60 mg, 0.20 mmol, 1.0 equiv) using Rh_2(*S*-pPhTPCP)$_4$ (1.8 mg, 0.50 mol%) as catalyst. Purification by column chromatography (0-35% diethyl ether/hexanes) afforded the product as a white solid (81.4 mg, 78%).

^{1}H NMR (400 MHz, $CDCl_3$) δ 7.60 (d, J = 8.2 Hz, 2H), 7.32 (d, J = 8.1 Hz, 2H), 6.50 (s, 1H), 4.95 (d, J = 12.0 Hz, 1H), 4.87 (d, J = 12.1 Hz, 1H), 3.53 – 3.39 (m, 2H), 2.78 (d, J = 12.5 Hz, 1H), 2.60 – 2.51 (m, 1H), 2.43 (s, 3H), 2.29 (s, 3H), 2.02 (d, J = 5.8 Hz, 1H), 1.86 (d, J = 5.8 Hz, 1H), 1.78 – 1.64 (m, 1H), 1.57 (dt, J = 13.7, 4.2 Hz, 1H), 1.43 – 1.34 (m, 1H), 1.13 (dt, J = 14.4, 4.6 Hz, 1H).

^{13}C NMR (101 MHz, $CDCl_3$) δ 166.7, 165.9, 160.5, 143.7, 133.1, 129.8, 127.6, 106.9, 94.6, 75.4, 49.4, 46.6, 36.0, 32.0, 29.3, 23.6, 23.1, 21.6, 11.6.

HRMS (+p APCI) calcd for $C_{21}H_{24}O_5N_2{}^{35}Cl_3{}^{32}S$ (M+) 521.0466, 521.0460 found.

Chiral HPLC: The enantiopurity was determined to be 97:3 er by HPLC analysis (AD-H, 1 mL/min, 10% IPA/Hexane, λ=230 nm, RT: Major: 39.7 min., Minor: 22.1 min.)

2,2,2-trichloroethyl (1*R*,3*S*)-1-(6-chloropyridin-3-yl)-5-tosyl-5-azaspiro[2.5]octane-1-carboxylate (23)

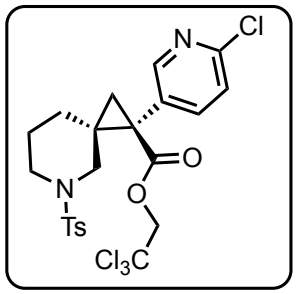

General procedure 1 was used for the cyclopropanation of *tert*-butyl 3-methylenepiperidine-1-carboxylate (75.4 mg, 0.30 mmol, 1.5 equiv) with 2,2,2-trichloroethyl 2-(6-chloropyridin-3-yl)-2-diazoacetate (65.8 mg, 0.20 mmol, 1.0 equiv) using Rh_2(*S*-pPhTPCP)$_4$ (1.8 mg, 0.50 mol%) as catalyst. Purification by column chromatography (0-35% diethyl ether/hexanes) afforded the product as a white solid (57.8 mg, 50%).

^{1}H NMR (400 MHz, $CDCl_3$) δ 8.39 (d, J = 2.5 Hz, 1H), 7.82 (dd, J = 8.3, 2.6 Hz, 1H), 7.62 (d, J = 8.2 Hz, 2H), 7.31 (dd, J = 8.3, 6.4 Hz, 3H), 4.89 (d, J = 11.9 Hz, 1H), 4.70 (d, J = 11.9 Hz, 1H), 3.23 (d, J = 12.4 Hz, 1H), 3.17 – 3.07 (m, 2H), 3.01 (td, J = 8.0, 4.1 Hz, 1H), 2.04 (d, J = 5.6 Hz, 1H), 1.72 (tt, J = 6.7, 3.6 Hz, 1H), 1.66 – 1.55 (m, 2H), 1.37 (d, J = 5.6 Hz, 1H), 1.08 (t, J = 6.1 Hz, 2H).

^{13}C NMR (101 MHz, $CDCl_3$) δ 168.3, 151.8, 150.8, 143.7, 142.0, 133.3, 130.1, 129.8, 127.6, 123.6, 94.6, 75.0, 49.6, 46.5, 36.5, 32.8, 30.6, 23.7, 23.2, 21.6.

HRMS (+p APCI) calcd for $C_{22}H_{23}O_4N_2{}^{35}Cl_4{}^{32}S$ (M+H) 551.0127, found 551.0120.

Chiral HPLC: The enantiopurity was determined to be 98% ee by HPLC analysis (AD-H, 1 mL/min, 10% IPA/Hexane, λ=230 nm, RT: Major: 38.2 min., Minor: 33.3 min.)

2,2,2-trichloroethyl (1*S*,3*S*)-1-(4-bromophenyl)-5-((4-nitrophenyl)sulfonyl)-5-azaspiro[2.5]octane-1-carboxylate--ethyne (24)

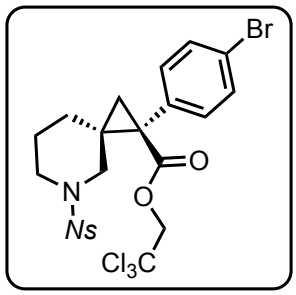

General procedure 1 with some slight modifcations used for the cyclopropanation of *tert*-butyl 3-methylenepiperidine-1-carboxylate (339 mg, 1.20 mmol, 1.2 equiv) with 2,2,2-trichloroethyl 2-(4-bromophenyl)-2-diazoacetate (372 mg, 1.0 mmol, 1.0 equiv) using Rh_2(*S*-pPhTPCP)$_4$ (17.6 mg, 1.0 mol%) as

catalyst. Purification by column chromatography (0-35% diethyl ether/hexanes) afforded the product as a white solid (461 mg, 78%).

^{1}H NMR (400 MHz, $CDCl_3$) δ 8.05 – 7.96 (m, 1H), 7.76 – 7.66 (m, 2H), 7.66 – 7.59 (m, 1H), 7.45 (d, J = 8.6 Hz, 2H), 7.30 (d, J = 8.5 Hz, 2H), 4.79 (d, J = 11.9 Hz, 1H), 4.66 (d, J = 11.9 Hz, 1H), 3.55 – 3.45 (m, 2H), 3.48 – 3.39 (m, 1H), 3.26 (ddd, J = 12.3, 8.1, 3.6 Hz, 1H), 1.95 (d, J = 5.4 Hz, 1H), 1.76 (dtd, J = 14.3, 7.3, 3.7 Hz, 1H), 1.63 (dtt, J = 12.7, 8.4, 4.0 Hz, 1H), 1.32 (d, J = 5.5 Hz, 1H), 1.30 – 1.24 (m, 1H), 1.07 (ddd, J = 13.1, 7.4, 4.1 Hz, 1H).

^{13}C NMR (101 MHz, $CDCl_3$) δ 169.1, 148.2, 134.1, 133.6, 133.0, 132.0, 131.6, 131.2, 131.1, 124.1, 121.9, 94.7, 74.9, 49.4, 46.4, 39.2, 32.6, 31.0, 24.3, 23.8.

HRMS (+p APCI) calcd for $C_{22}H_{21}O_6N_2{}^{79}Br^{35}Cl_3{}^{32}S$ (M+H) 624.9364, found 624.9362.

Chiral SFC: The enantiopurity was determined to be 99% ee by chiral SFC analysis (CEL-1, 2.5 mL/min, 10% methanol in isopropanol with 0.2% Formic Acid in CO2, 1.0 mg/ml, λ=230 nm, RT: Major: 6.13 min., Minor: 6.72 min.)

2,2,2-trichloroethyl (1S,3S)-1-(4-bromophenyl)-5-tosyl-5-azaspiro[2.4]heptane-1-carboxylate (25)

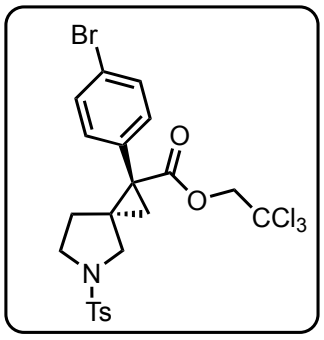

General procedure 1 was used for the cyclopropanation of 3-methylene-1-tosylpyrrolidine (71.2 mg, 0.30 mmol, 1.5 equiv) with 2,2,2-trichloroethyl 2-(4-bromophenyl)-2-diazoacetate (74.5 mg, 0.20 mmol, 1.0 equiv) using Rh_2(*S*-*p*-PhTPCP)$_4$ (1.7 mg, 1.0 mol%) as catalyst. Purification by column chromatography (0-40% diethyl ether/hexanes) afforded the product as a white solid (98.4 mg, 85% yield, 9:1 dr) – a mixture of 4:1 of two diastereomers which are inseparable by flash chromatography.

^{1}H NMR (400 MHz, $CDCl_3$) δ 7.72 (d, *J* = 8.3 Hz, 2H), 7.43 (d, *J* = 8.4 Hz, 2H), 7.35 (d, *J* = 7.9 Hz, 2H), 7.07 (d, *J* = 8.5 Hz, 2H), 4.82 (d, *J* = 11.9 Hz, 1H), 4.51 (d, *J* = 11.9 Hz, 1H), 3.53 (d, *J* = 11.2 Hz, 1H), 3.45 (d, *J* = 11.2 Hz, 1H), 3.42 – 3.35 (m, 1H), 3.31 – 3.20 (m, 1H), 2.46 (s, 3H), 1.85 (d, *J* = 5.2 Hz, 1H), 1.70 (dt, *J* = 13.1, 8.0 Hz, 1H), 1.43 (d, *J*

= 5.2 Hz, 1H), 1.14 (ddd, *J* = 13.1, 7.0, 4.4 Hz, 1H). *For clarity, only the major diastereomer is reported.*

^{13}C NMR (101 MHz, $CDCl_3$) δ 169.8, 143.8, 134.2, 133.3, 132.4, 131.5, 129.8, 127.8, 122.0, 94.5, 74.6, 52.3, 47.5, 37.0, 36.6, 32.7, 26.5, 21.6. *For clarity, only the major diastereomer is reported.*

HRMS (+p APCI) calcd for $C_{22}H_{22}O_4N^{79}Br^{35}Cl_3{}^{32}S$ (M+H) 579.9513, found 579.9511.

Chiral SFC: The enantiopurity was determined to be 98% ee by SFC analysis (OJ3, 2.5 mL/min, 10% (50% methanol in isopropanol with 0.2% Formic Acid) in CO2, 1.0 mg/ml), λ=230 nm, RT: Major: 3.06 min., Minor: 3.62 min.)

2,2,2-trichloroethyl (1S,3r,6S)-1-(4-bromophenyl)-6-phenylspiro[2.5]octane-1-carboxylate (27)

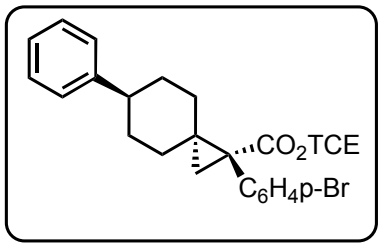

General procedure 1 was used for the cyclopropanation of (4-methylenecyclohexyl)benzene (25.6 mg, 0.15 mmol, 1.5 equiv) with 2,2,2-trichloroethyl 2-(4-bromophenyl)-2-diazoacetate (37.2 mg, 0.10 mmol, 1.0 equiv) using Rh_2(*S*-TPPTTL)$_4$ (2.5 mg, 1.0 mol%) as catalyst. Purification by column chromatography (0-10% diethyl ether/hexanes) afforded the product as a white solid (35.6 mg, 67% yield).

^{1}H NMR (400 MHz, $CDCl_3$) δ 7.46 (d, J = 8.6 Hz, 2H), 7.31 (dd, J = 8.0, 6.2 Hz, 4H), 7.24 – 7.15 (m, 3H), 4.86 (d, J = 12.0 Hz, 1H), 4.53 (d, J = 12.0 Hz, 1H), 2.59 (tt, J = 12.2, 3.5 Hz, 1H), 2.00 (dt, J = 12.7, 2.8 Hz, 1H), 1.93 – 1.79 (m, 3H), 1.81 – 1.62 (m, 3H), 1.59 – 1.46 (m, 1H), 1.27 (dd, J = 4.8, 1.3 Hz, 1H), 0.69 – 0.57 (m, 1H).

^{13}C NMR (101 MHz, $CDCl_3$) δ 169.7, 146.7, 135.6, 133.2, 131.2, 128.4, 126.8, 126.2, 121.4, 94.9, 74.6, 44.1, 39.3, 34.6, 34.2, 33.3, 33.2, 30.9, 24.8.

HRMS (+p APCI) calcd for $C_{23}H_{23}O_2{}^{79}Br^{35}Cl_3$ (M+H) 514.9942, found 514.9953.

Chiral SFC: The enantiopurity was determined to be 92% ee by SFC analysis (SSWhelk, 2.5 mL/min, 10% (50% methanol in isopropanol with 0.2% Formic Acid) in CO2, 1.0 mg/ml), λ=230 nm, RT: Major: 2.50 min., Minor: 2.09 min.)

2,2,2-trichloroethyl (1*R*,3*r*,6*R*)-1-(4-bromophenyl)-6-(*tert*-butyl)spiro[2.5]octane-1-carboxylate (28)

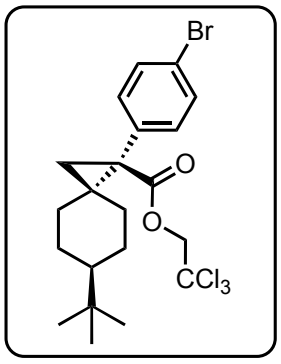

General procedure 1 was used for the cyclopropanation of 1-(tert-butyl)-4-methylenecyclohexane (45.7 mg, 0.30 mmol, 1.5 equiv) with 2,2,2-trichloroethyl 2-(4-bromophenyl)-2-diazoacetate (74.5 mg, 0.20 mmol, 1.0 equiv) using Rh_2(*S*-TPPTTL)$_4$ (5.0 mg, 1.0 mol%) as catalyst. Purification by column chromatography (0-10% diethyl ether/hexanes) afforded the product as a white solid (72.6 mg, 73% yield).

^{1}H NMR (400 MHz, $CDCl_3$) δ 7.35 (d, J = 8.4 Hz, 2H), 7.19 (d, J = 8.5 Hz, 2H), 4.75 (d, J = 11.9 Hz, 1H), 4.43 (d, J = 11.9 Hz, 1H), 1.77 (dt, J = 13.2, 2.8 Hz, 1H), 1.67 (dd, J = 4.8, 1.6 Hz, 1H), 1.66 – 1.60 (m, 1H), 1.58 (dd, J = 9.0, 3.3 Hz, 2H), 1.45 – 1.37 (m, 1H), 1.18 – 1.02 (m, 2H), 1.02 – 0.87 (m, 2H), 0.77 (s, 9H), 0.44 (d, J = 12.5 Hz, 1H).

^{13}C NMR (101 MHz, $CDCl_3$) δ 169.8, 135.8, 133.2, 130.9, 121.2, 94.9, 74.5, 47.9, 39.2, 34.9, 32.4, 31.0, 27.6, 26.6, 26.5, 24.8.

HRMS (+p APCI) calcd for $C_{21}H_{27}O_2{}^{79}Br^{35}Cl_3$ (M+H) 495.0255, found 495.0253.

Chiral HPLC: The enantiopurity was determined to be 97% ee by HPLC analysis (AD-H, 1 mL/min, 0.5% IPA/Hexane, λ=230 nm, RT: Major: 5.2 min., Minor: 5.8 min.)

2,2,2-trichloroethyl (1*R*,3*s*,5*R*)-1-(4-bromophenyl)-5-(4-chlorophenyl)spiro[2.3]hexane-1-carboxylate (29)

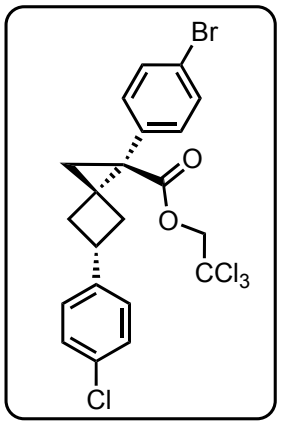

General procedure 1 was used for the cyclopropanation of 1-chloro-4-(3-methylenecyclobutyl)benzene (35.7 mg, 0.20 mmol, 2 equiv) with 2,2,2-trichloroethyl 2-(4-bromophenyl)-2-diazoacetate (37.2 mg, 0.20 mmol, 1.0 equiv) using Rh_2(*S*-TPPTTL)$_4$ (5.0 mg, 1.0 mol%) as catalyst. Purification by column chromatography (0-10% diethyl ether/hexanes) afforded the product as a colorless oil (38 mg, 72% yield).

Reported as a mixture of diastereomers

^{1}H NMR (400 MHz, $CDCl_3$) δ 7.49 (d, J = 8.4 Hz, 1H), 7.46 (d, J = 8.4 Hz, 2.6H), 7.29 – 7.22 (m, 6H), 7.19 (dd, J = 8.5, 3.5 Hz, 3.5H), 7.11 (d, J = 8.3 Hz, 1H), 4.93 (d, J = 12.0 Hz, 1H), 4.88 (d, J = 11.9 Hz, 1H), 4.50 (dd, J = 11.9, 1.8 Hz, 1H), 3.64 (p, J = 8.6 Hz, 1H), 3.59 – 3.49 (m, 1H), 2.89 – 2.71 (m, 2H), 2.58 (dd, J = 12.2, 8.9 Hz, 1H), 2.49 (dd, J = 12.9, 7.0 Hz, 1H), 2.31 (ddt, J = 10.7, 9.3, 1.7 Hz, 1H), 2.26 – 2.14 (m, 1H), 2.09 (d, J = 4.9 Hz, 1H), 1.99 (d, J = 5.2 Hz, 2H), 1.97 – 1.85 (m, 1H), 1.67 (d, J = 4.9 Hz, 1H), 1.53 (d, J = 5.2 Hz, 2H).

^{13}C NMR (101 MHz, $CDCl_3$) δ 170.4, 170.2, 143.7, 143.4, 134.6, 132.8, 132.5, 131.8, 131.8, 131.4, 131.4, 128.6, 128.5, 127.9, 127.7, 121.6, 121.5, 94.9, 74.4, 74.3, 37.2, 36.9, 36.2, 36.0, 35.8, 35.1, 34.4, 34.1, 33.6, 33.2, 31.9, 29.1, 27.4, 26.3, 22.7, 14.2.

HRMS (+p APCI) calcd for (M+H) $C_{21}H_{18}O_2{}^{79}Br^{35}Cl_4$ 520.9239, found 520.9256.

Chiral SFC: The enantiopurity was determined to be 94% ee by Chiral SFC analysis (OJ-3, 2.5 mL/min, 50% methanol in isopropanol with 0.2% Formic Acid in CO2, 1.0 mg/ml, λ=230 nm, RT: Major: 1.14 min., Minor: 4.65 min.)

2,2,2-trichloroethyl (1*R*,3*s*,5*R*)-1-(4-bromophenyl)-5-(4-chlorophenyl)spiro[2.3]hexane-1-carboxylate (30)

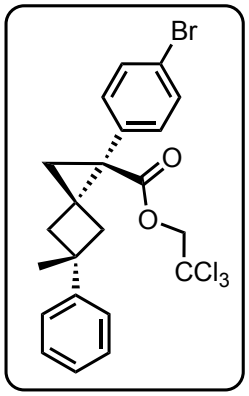

General procedure 1 was used for the cyclopropanation of (1-methyl-3-methylenecyclobutyl)benzene (39.6 mg, 0.25 mmol, 2.5 equiv) with 2,2,2-trichloroethyl 2-(4-bromophenyl)-2-diazoacetate (37.2 mg, 0.10 mmol, 1.0 equiv) using Rh_2(*S*-TPPTTL)$_4$ (2.5 mg, 1.0 mol%) as catalyst. Purification by column chromatography (0-10% diethyl ether/hexanes) afforded the product as a white solid (39.6 mg, 79% yield).

^{1}H NMR (400 MHz, $CDCl_3$) δ 7.43 (d, J = 8.4 Hz, 1H), 7.36 – 7.28 (m, 1H), 7.23 – 7.16 (m, 1H), 7.16 – 7.09 (m, 2H), 4.85 (d, J = 11.9 Hz, 1H), 4.50 (d, J = 12.0 Hz, 1H), 2.85 (d, J = 11.8 Hz, 1H), 2.44 (d, J = 11.7 Hz, 1H),

^{13}C NMR (101 MHz, $CDCl_3$) δ 170.6, 151.0, 134.8, 132.6, 131.3, 128.4, 125.7, 125.0, 121.4, 94.8, 74.3, 42.3, 41.4, 38.1, 34.6, 32.9, 31.5, 28.2.

HRMS (+p APCI) calcd for $C_{22}H_{21}O_2{}^{79}Br^{35}Cl_3$ (M+H) 500.9785, found 500.97886

Chiral HPLC: The enantiopurity was determined to be 96% ee by HPLC analysis (AD-H, 1.0 mL/min, 1% IPA/Hexane), λ=230 nm, RT: Major: 6.3 min., Minor: 5.8 min.)

2,2,2-trichloroethyl 1-(4-bromophenyl)-5-phenylspiro[2.5]octane-1-carboxylate (31)

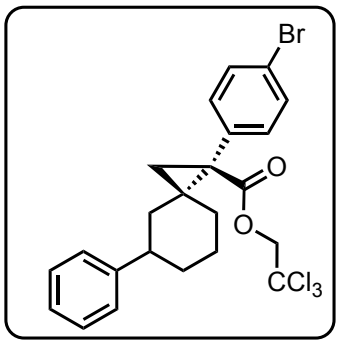

General procedure 1 was used for the cyclopropanation of (3-methylenecyclohexyl)benzene (52 mg, 0.30 mmol, 3 equiv) with 2,2,2-trichloroethyl 2-(4-bromophenyl)-2-diazoacetate (37.2 mg, 0.10 mmol, 1.0 equiv) using Rh_2(*S*-TPPTTL)$_4$ (2.5 mg, 1.0 mol%) as catalyst. Purification by column chromatography (0-5% diethyl ether/hexanes) afforded the product as a white solid (42 mg, 81% yield)

Reported as a mixture of diastereomers.

^{1}H NMR (400 MHz, $CDCl_3$) δ 7.52 – 7.45 (m, 3H), 7.44 – 7.37 (m, 0.5H), 7.36 – 7.26 (m, 5H), 7.26 – 7.15 (m, 4H), 7.15 – 7.08 (m, 0.5H), 4.86 (d, J = 11.9 Hz, 0.2H), 4.81 (d, J = 12.0 Hz, 0.2H), 4.73 (d, J = 12.0 Hz, 1H), 4.61 (d, J = 11.9 Hz, 0.2H), 4.54 (d, J = 11.9 Hz, 1H), 2.75 (ddd, J = 11.8, 8.0, 3.6 Hz, 1H), 2.62 (t, J = 12.1 Hz, 0.2H), 1.96 (td, J = 13.6, 6.3 Hz, 2H), 1.90 – 1.69 (m, 5H), 1.69 – 1.44 (m, 5H), 1.37 (d, J = 5.2 Hz, 0.3H), 1.35 – 1.21 (m, 1.5H), 0.99 (d, J = 6.6 Hz, 0.2H), 0.92 – 0.78 (m, 0.2H), 0.68 (d, J = 13.1 Hz, 0.2H), 0.61 – 0.52 (m, 1H).

^{13}C NMR (101 MHz, $CDCl_3$) δ 170.0, 169.6, 169.5, 146.4, 146.4, 135.5, 135.2, 135.0, 133.3, 133.2, 131.1, 130.9, 128.5, 126.9, 126.7, 126.2, 121.5, 121.4, 94.8, 74.9, 74.6, 44.0, 43.8, 43.0, 41.7, 40.3, 39.5, 39.4, 38.5, 38.1, 35.0, 34.6, 34.5, 34.0, 33.7, 33.5, 31.4, 30.4, 25.7, 25.6, 24.7, 24.0, 23.9.

HRMS (+p APCI) calcd for $C_{23}H_{23}O_2{}^{79}Br^{35}Cl_3$ (M+H) 514.9942, found 514.9954.

2,2,2-trichloroethyl 1-(4-bromophenyl)-5-(4-chlorophenyl)spiro[2.5]octane-1-carboxylate (32)

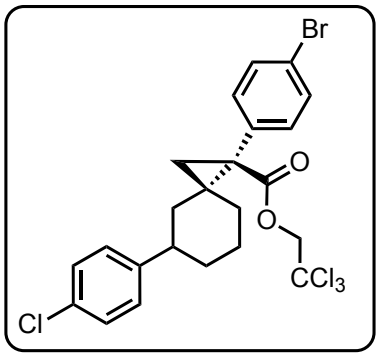

General procedure 1 was used for the cyclopropanation of 1-chloro-4-(3-methylenecyclohexyl)benzene (62 mg, 0.30 mmol, 3 equiv) with 2,2,2-trichloroethyl 2-(4-bromophenyl)-2-diazoacetate (37.2 mg, 0.10 mmol, 1.0 equiv) using Rh_2(*S*-TPPTTL)$_4$ (2.5 mg, 1.0 mol%) as catalyst. Purification by column chromatography (0-5% diethyl ether/hexanes) afforded the product as a white solid (45 mg, 82% yield)

^{1}H NMR (400 MHz, $CDCl_3$) δ 7.52 – 7.44 (m, 3H), 7.41 (d, J = 8.5 Hz, 0.5H), 7.36 – 7.25 (m, 5H), 7.21 (d, J = 8.4 Hz, 0.5H), 7.18 – 7.09 (m, 2H), 7.07 – 7.00 (m, 0.5H), 4.86 (d, J = 12.0 Hz, 0.2H), 4.81 (d, J = 12.0 Hz, 0.3H), 4.75 (d, J = 12.0 Hz, 1H), 4.59 (d, J = 11.9 Hz, 0.2H), 4.54 (d, J = 11.9 Hz, 1H), 2.73 (ddd, J = 11.8, 8.0, 3.8 Hz, 1H), 2.65 – 2.51 (m, 0.2H), 2.02 – 1.88 (m, 2H), 1.88 (m, 5H), 1.73 – 1.50 (m, 3H), 1.51 – 1.40 (m, 2H), 1.38 (d, J = 5.2 Hz, 0.5H), 1.34 – 1.25 (m, 2H), 0.95 – 0.77 (m, 0.5H), 0.68 – 0.60 (m, 0.2H), 0.61 – 0.48 (m, 1H).

^{13}C NMR (101 MHz, $CDCl_3$) δ 170.0, 169.5, 169.5, 144.8, 144.8, 144.8, 135.4, 135.1, 134.9, 133.2, 133.2, 133.1, 131.8, 131.2, 131.1, 131.0, 128.5, 128.2, 128.15, 128.0, 121.5, 121.47, 94.8, 74.8, 74.6, 43.3, 43.2, 42.3, 41.7, 40.2, 39.5, 39.3, 38.4, 37.9, 34.9, 34.5, 34.4, 33.9, 33.7, 33.5, 31.3, 30.3, 25.5, 25.4, 24.7, 24.6, 23.9.

HRMS (+p APCI) calcd for $C_{23}H_{22}O_2{}^{79}Br^{35}Cl_4$ (M+H) 548.9552, found 548.9566.

2,2,2-trichloroethyl-1-(4-bromophenyl)-5-(3,5-di-*tert* butylphenyl)spiro[2.5]octane-1-carboxylate (33)

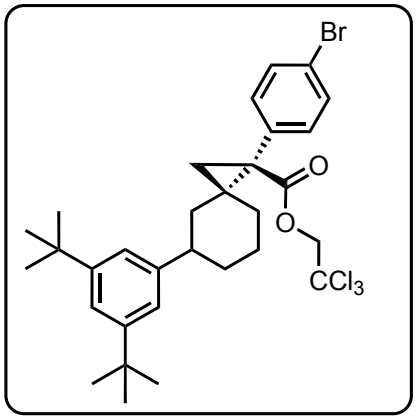

General procedure 1 was used for the cyclopropanation of 1,3-di-tert-butyl-5-(3-methylenecyclohexyl)benzene (86 mg, 0.30 mmol, 3 equiv) with 2,2,2-trichloroethyl 2-(4-bromophenyl)-2-diazoacetate (37.2 mg, 0.10 mmol, 1.0 equiv) using Rh_2(*S*-TPPTTL)$_4$ (2.5 mg, 1.0 mol%) as catalyst. Purification by column chromatography (0-10% diethyl ether/hexanes) afforded the product as a white solid (39 mg, 62% yield).

^{1}H NMR (400 MHz, $CDCl_3$) δ 7.47 (d, J = 8.3 Hz, 2H), 7.35 (d, J = 8.3 Hz, 2H), 7.29 (t, J = 1.8 Hz, 1H), 7.05 (d, J = 1.8 Hz, 2H), 4.78 (d, J = 12.0 Hz, 1H), 4.50 (d, J = 12.0 Hz, 1H), 2.74 (tt, J = 11.9, 3.5 Hz, 1H), 1.96 (dd, J = 12.1, 7.6 Hz, 2H), 1.92 – 1.85 (m, 1H), 1.85 (s, 1H), 1.79 – 1.70 (m, 1H), 1.69 – 1.55 (m, 1H), 1.57 – 1.43 (m, 2H), 1.34 (s, 18H), 1.28 (d, J = 5.1 Hz, 1H), 0.55 (d, J = 12.8 Hz, 1H).

^{13}C NMR (101 MHz, $CDCl_3$) δ 169.5, 150.6, 145.6, 135.6, 133.3, 131.1, 121.4, 121.1, 120.4, 94.9, 74.5, 44.5, 39.4, 38.5, 34.9, 34.6, 34.3, 34.0, 31.6, 25.6, 24.5.

HRMS (+p APCI) calcd for $C_{31}H_{38}O_2{}^{79}Br^{35}Cl_3$ (M+) 626.1115, found 626.1114.

Chiral HPLC: The enantiopurity was determined to be 92% ee by HPLC analysis (AD-H, 1.0 mL/min, 1% IPA/Hexane), λ=230 nm, RT: Major: 11.9 min., Minor: 10.8 min.)**Crude**

NMR for Diastereomer Determination

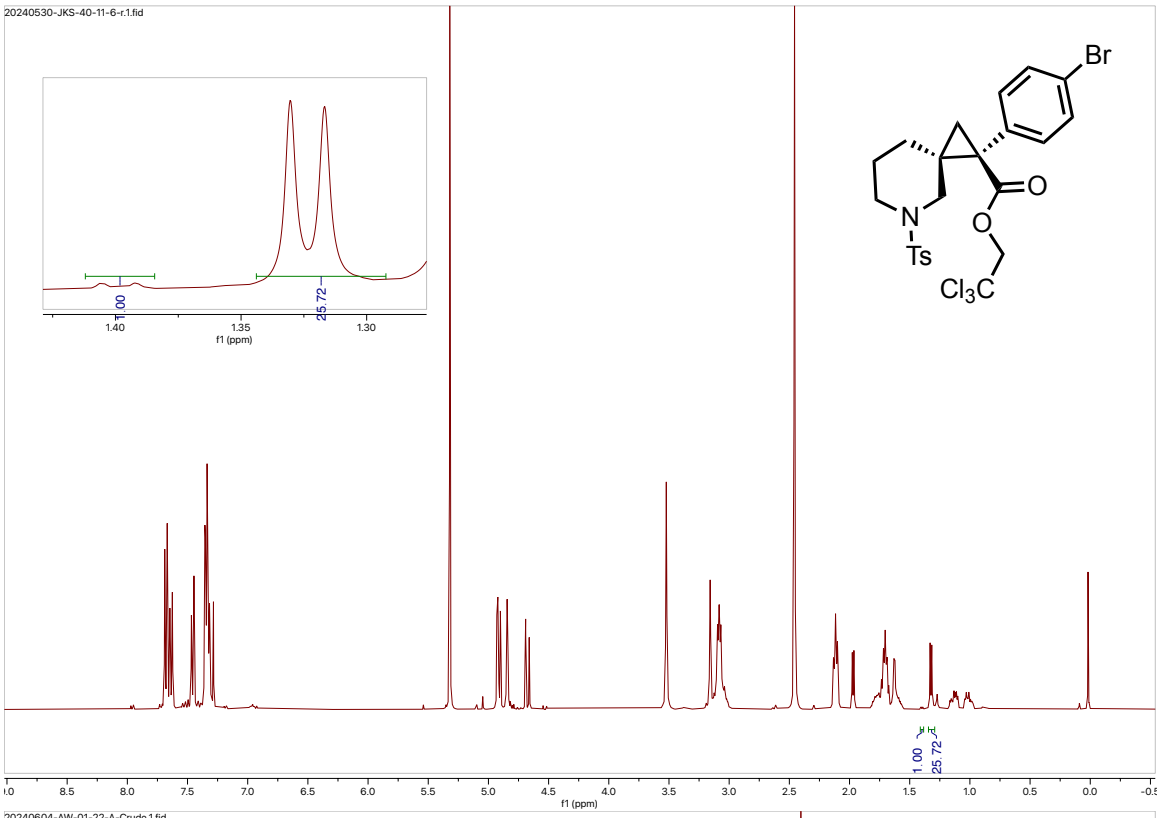

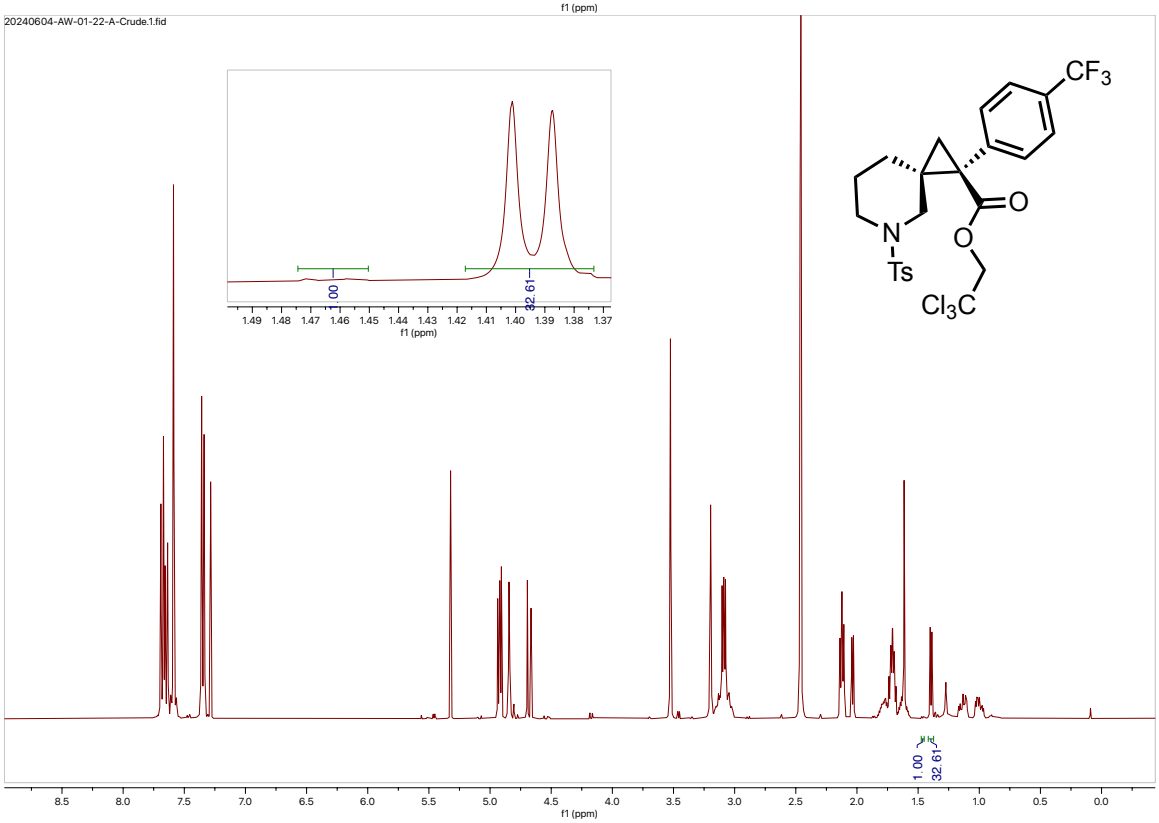

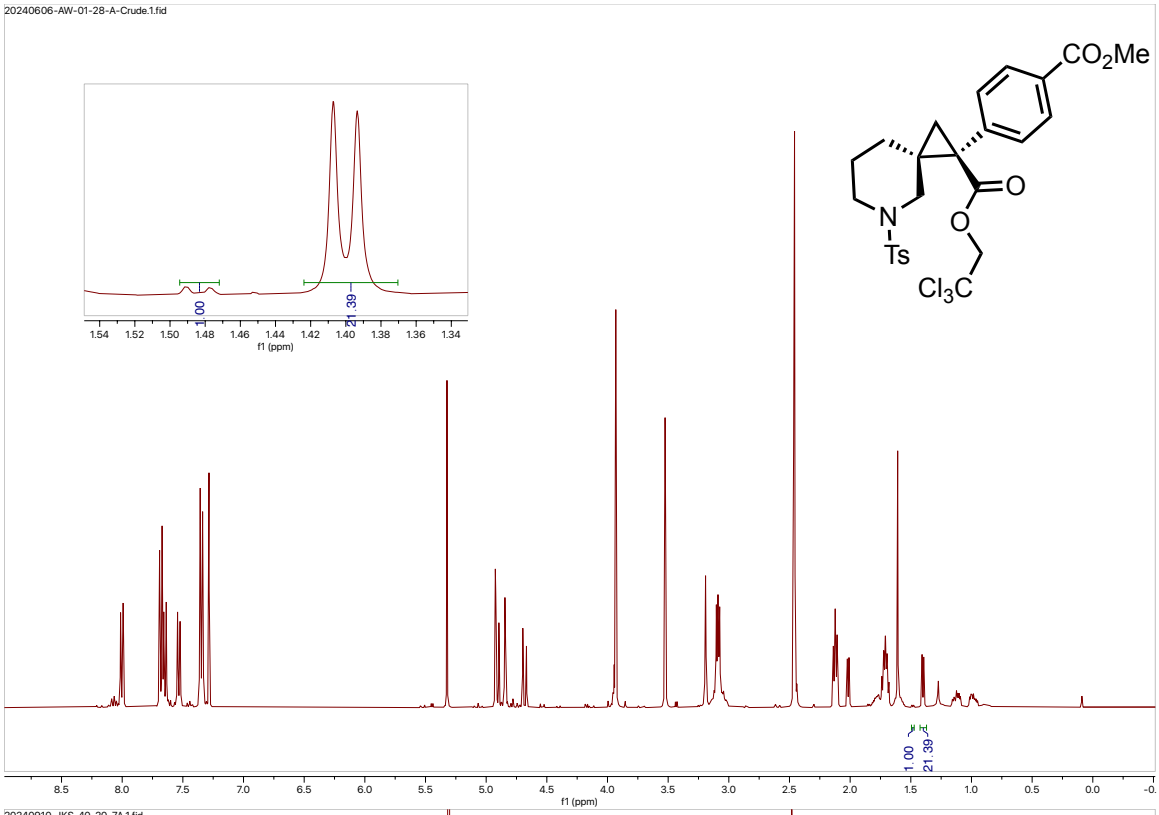
20240606-AW-01-28-A-Crude.1.fid
CO2Me
O
N
Ts
O
Cl3C
1.00
21.39
f1 (ppm)

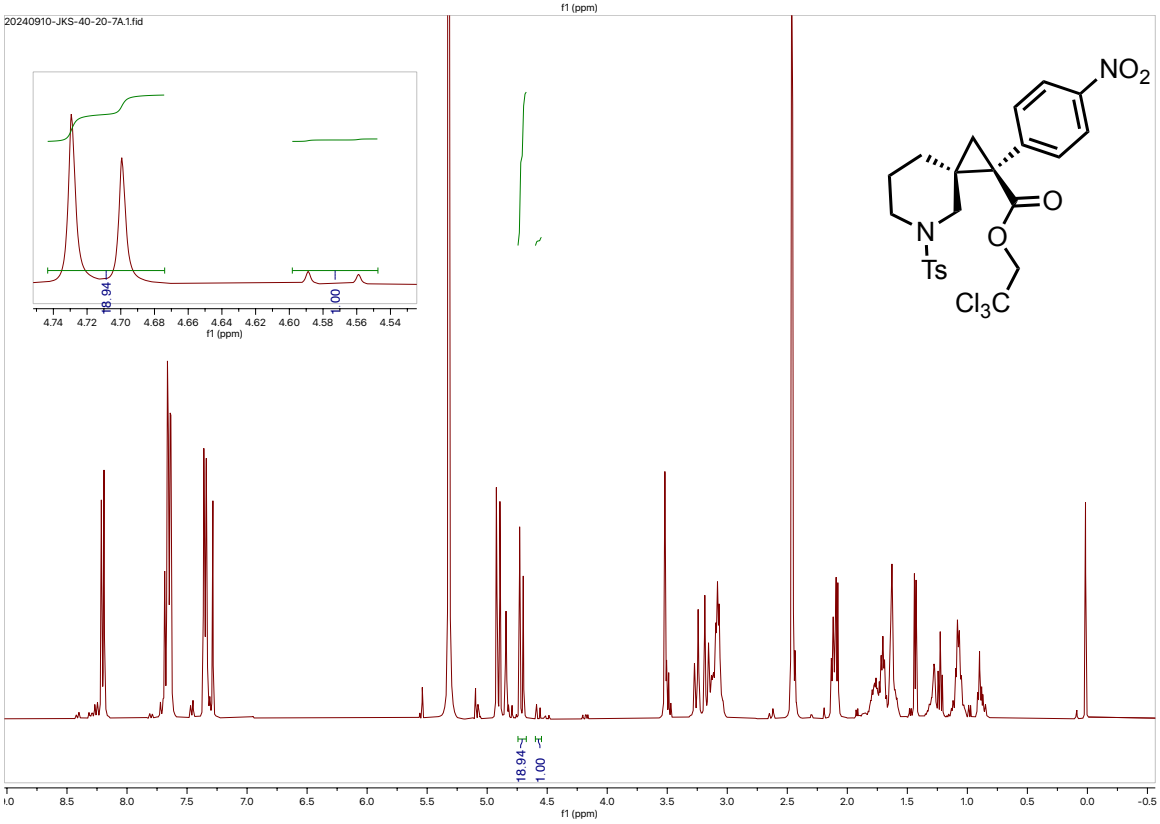
20240910-JKS-40-20-7A.1.fid
NO2
O
N
Ts
O
Cl3C
18.94
1.00
f1 (ppm)

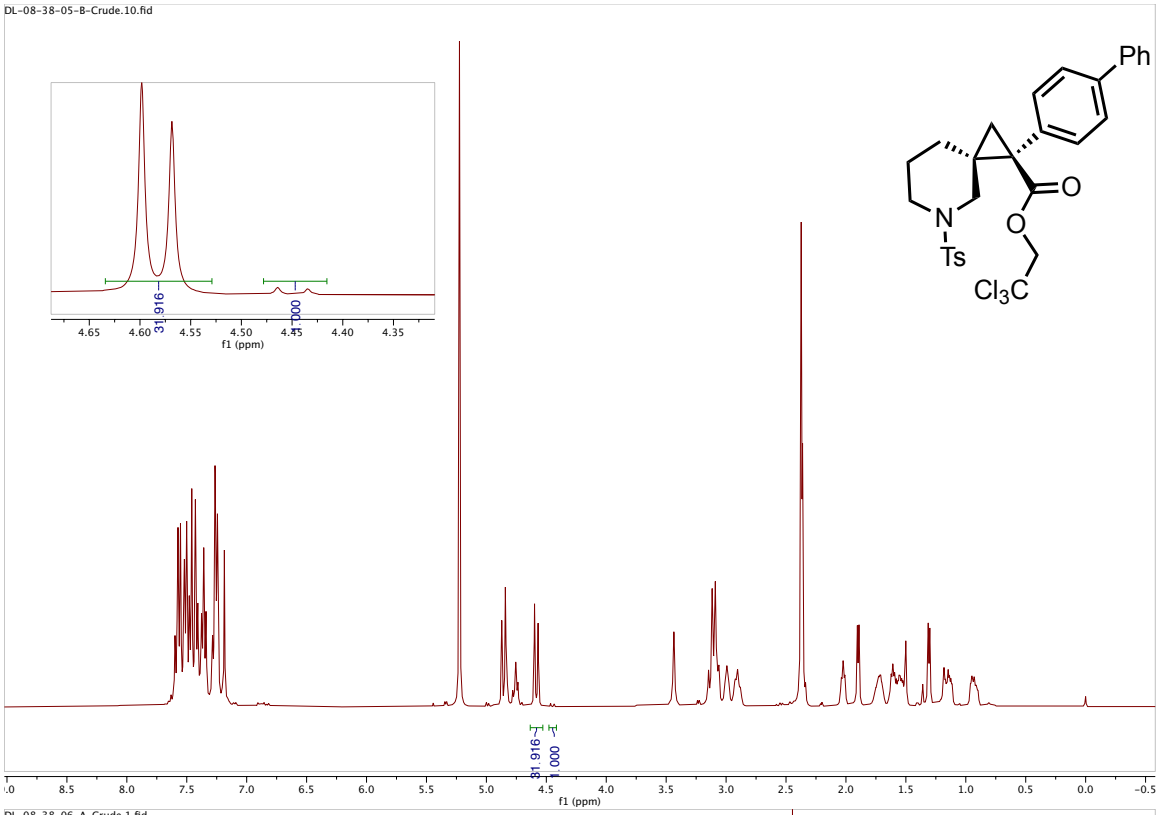
DL-08-38-05-B-Crude.10.fid
Ph
O
N
Ts
O
Cl3C
31.916
1.000
f1 (ppm)

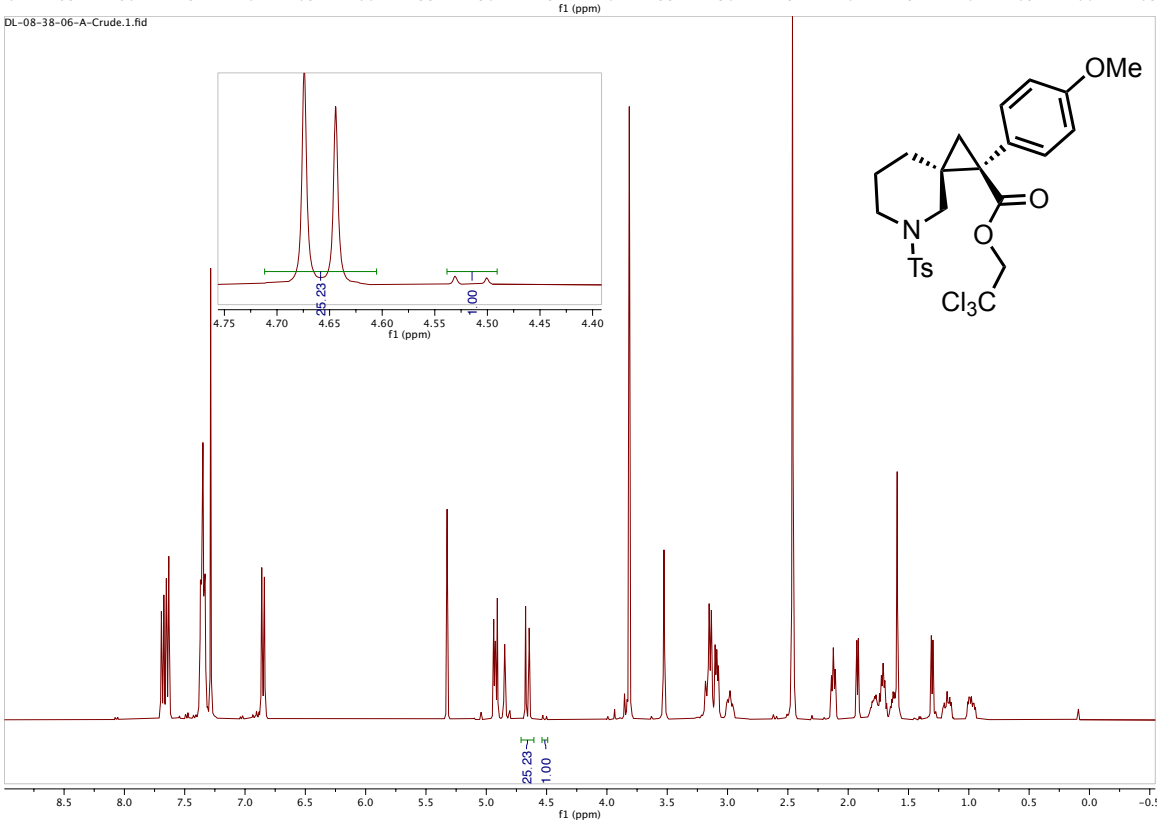
DL-08-38-06-A-Crude.1.fid
OMe
O
N
Ts
O
Cl3C
25.23
1.00
f1 (ppm)

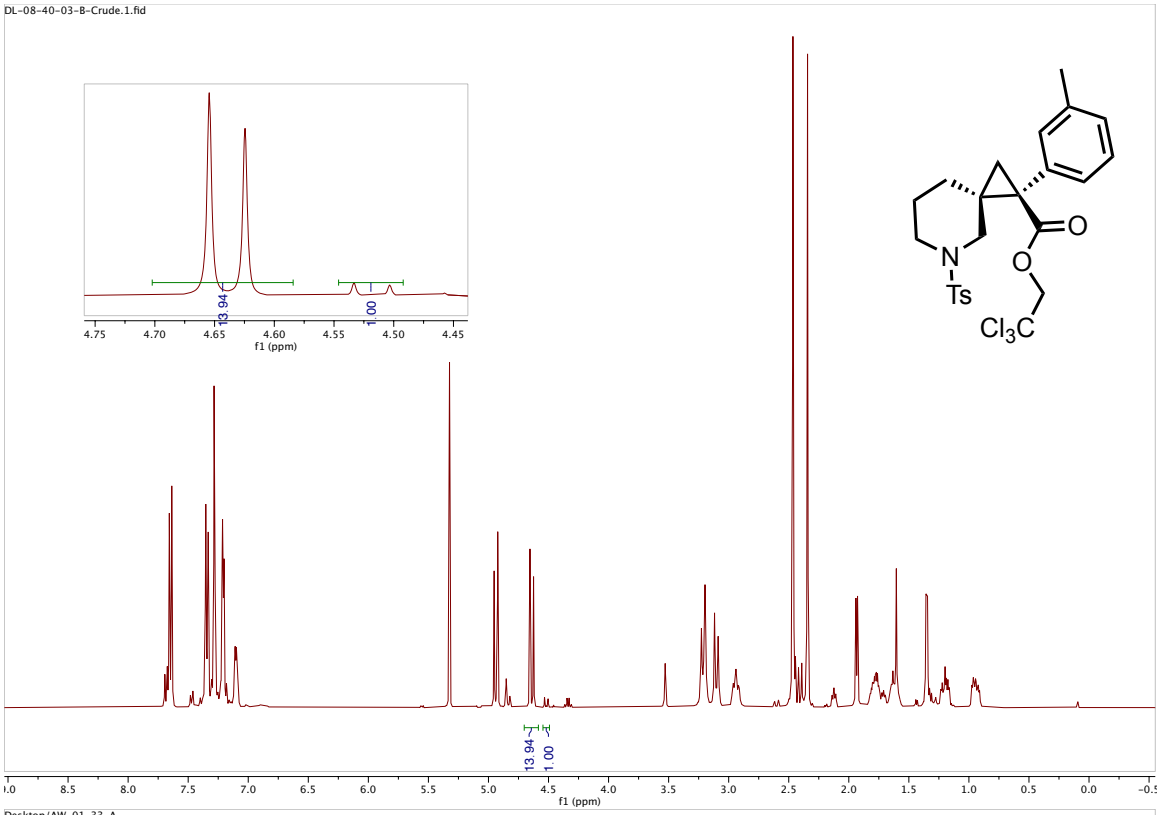
DL-08-40-03-B-Crude.1.fid
13.94
1.00
f1 (ppm)
N
Ts
O
O
Cl3C

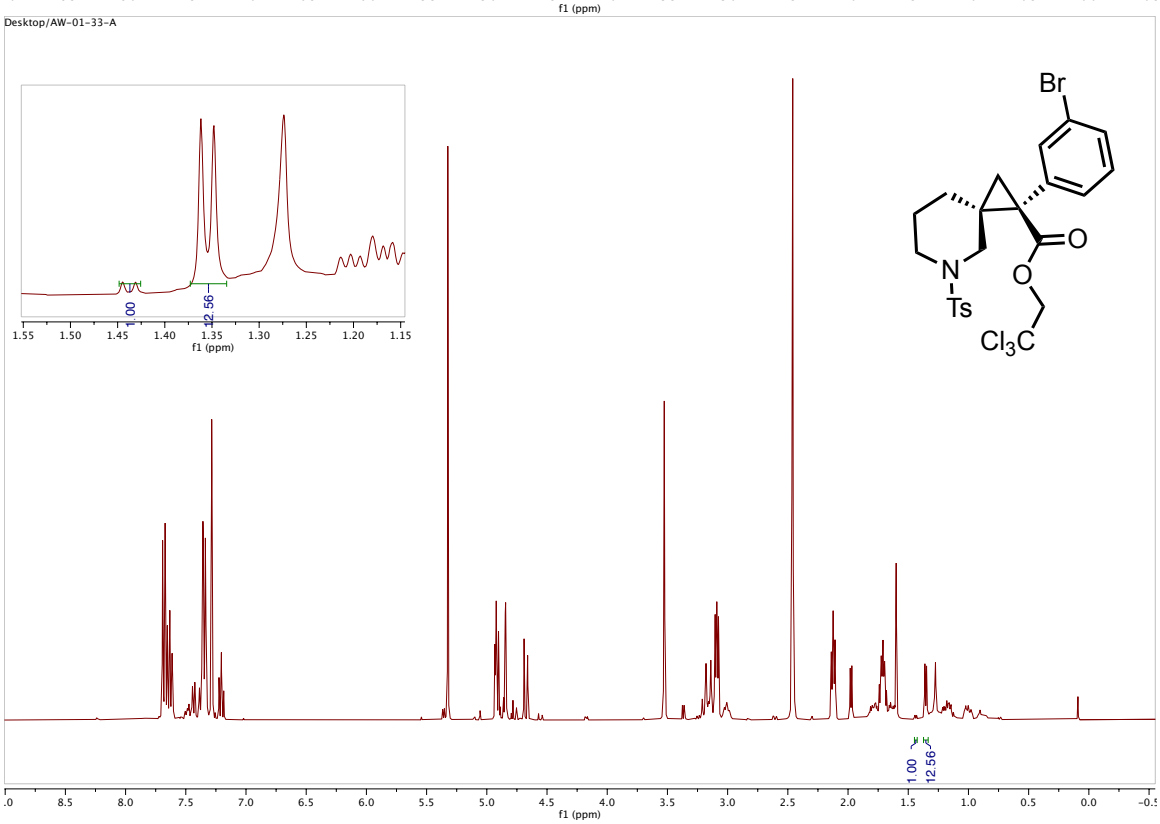
Desktop/AW-01-33-A
1.00
12.56
f1 (ppm)
Br
N
Ts
O
O
Cl3C

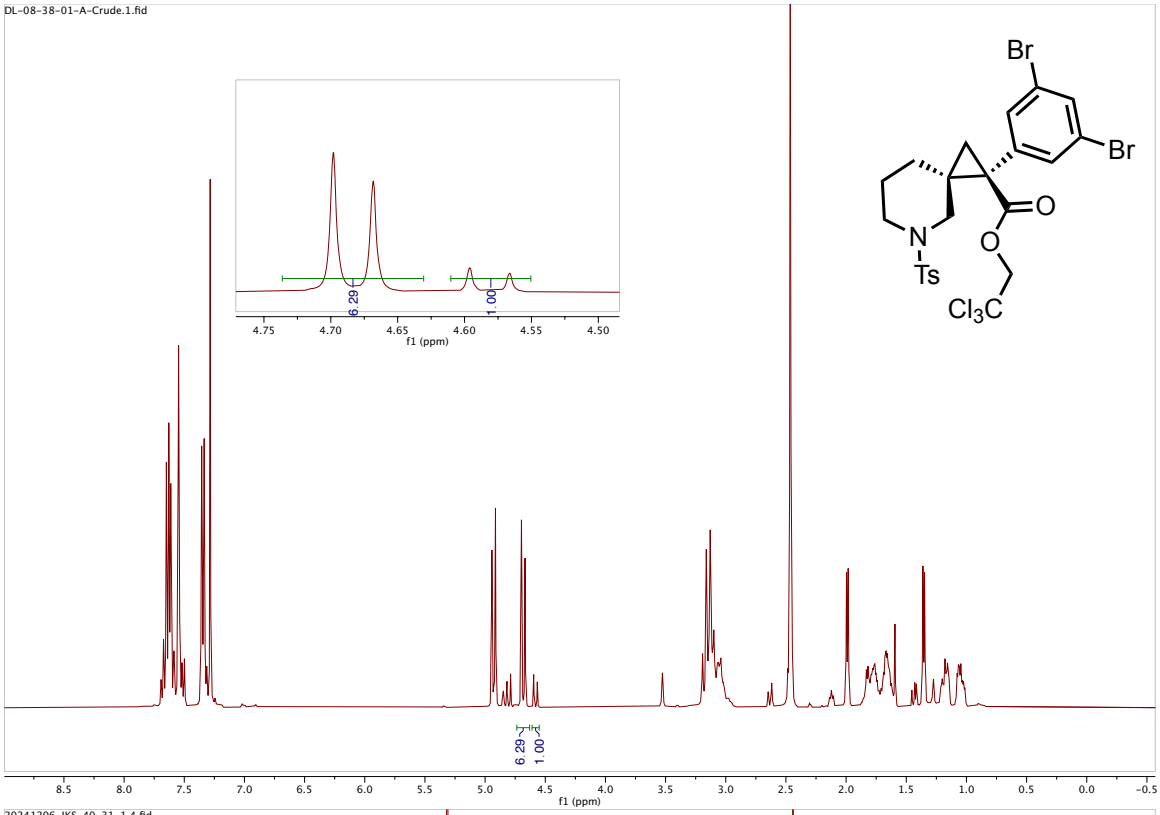
DL-08-38-01-A-Crude.1.fid
Br
Br
O
O
N
Ts
Cl3C
6.29
1.00
f1 (ppm)

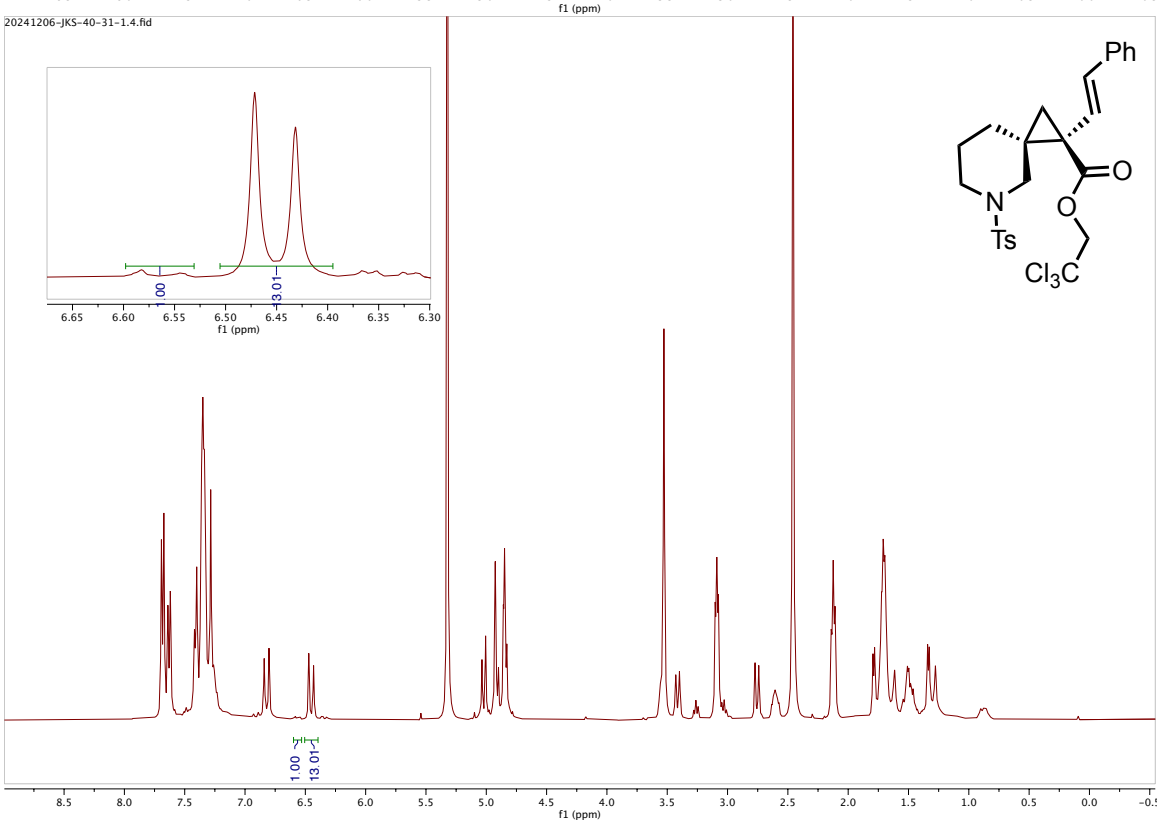
20241206-JKS-40-31-1.4.fid
Ph
O
O
N
Ts
Cl3C
1.00
3.01
f1 (ppm)

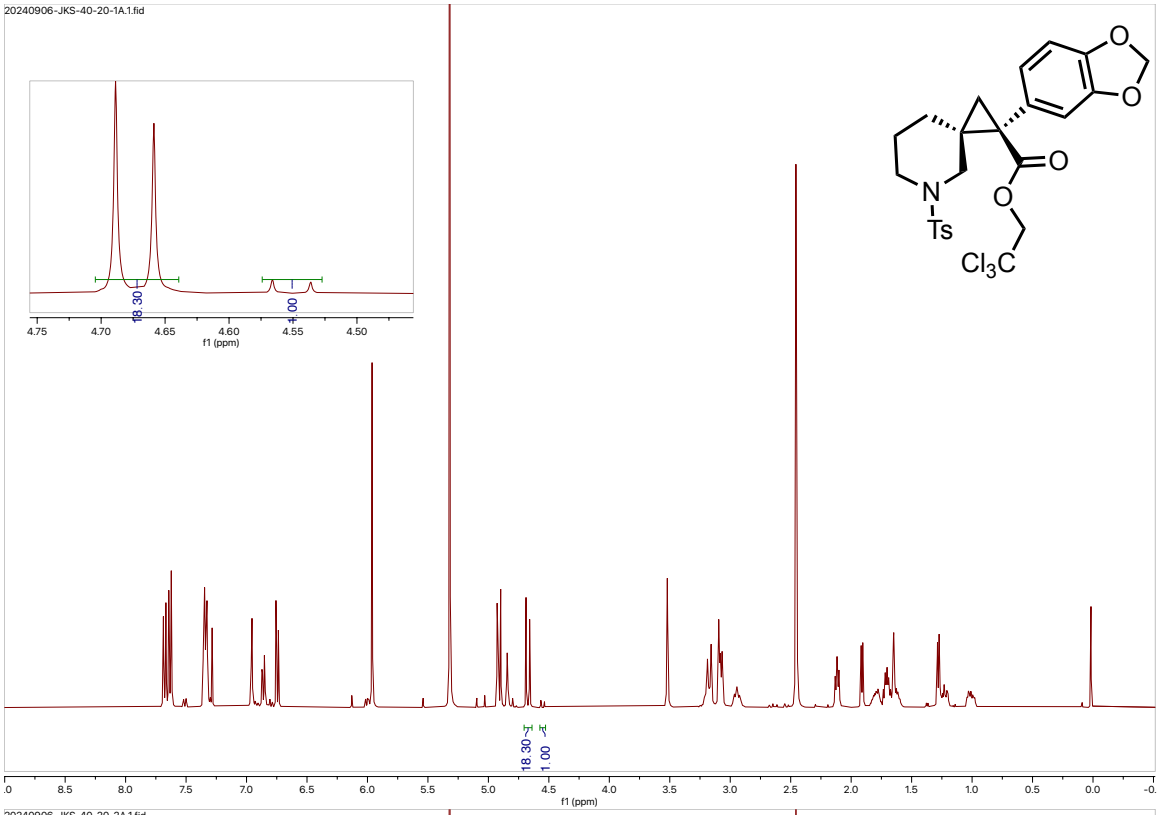
20240906-JKS-40-20-1A.1.fid
18.30
1.00
f1 (ppm)
O
O
N
Ts
O
O
Cl3C

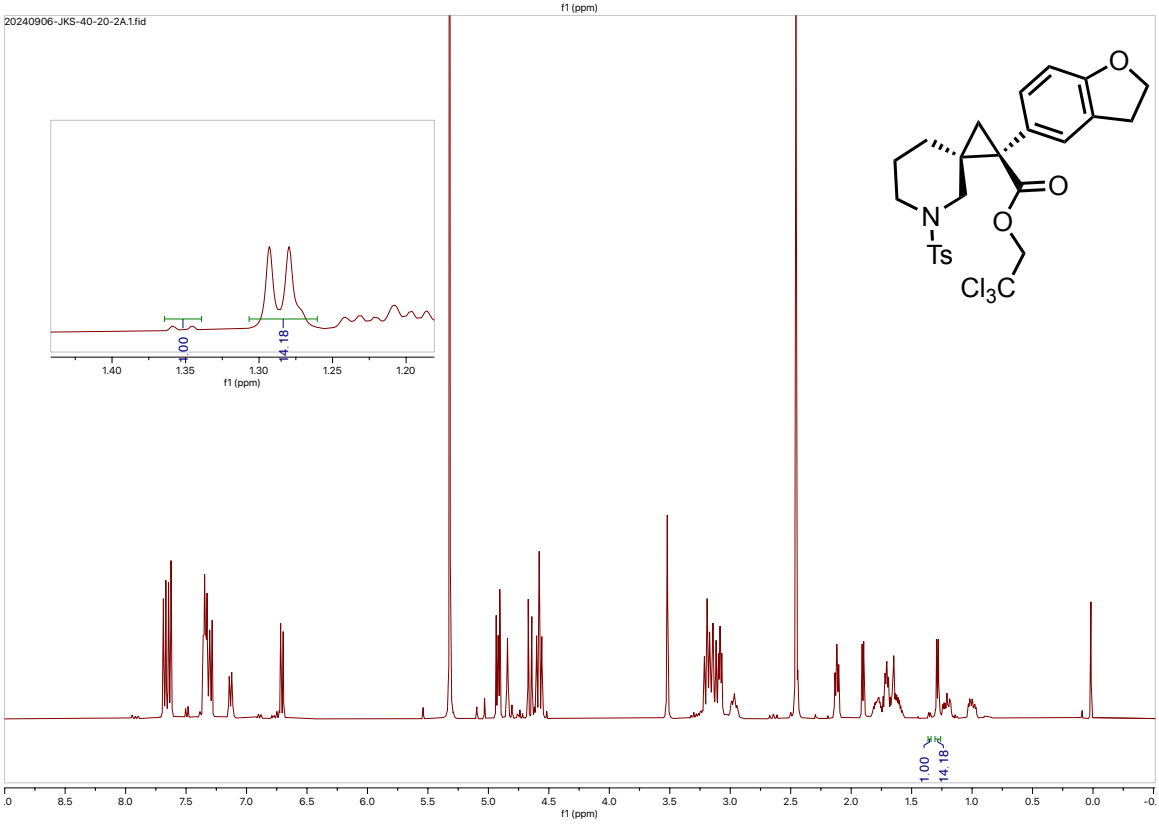
20240906-JKS-40-20-2A.1.fid
1.00
14.18
f1 (ppm)
O
N
Ts
O
O
Cl3C

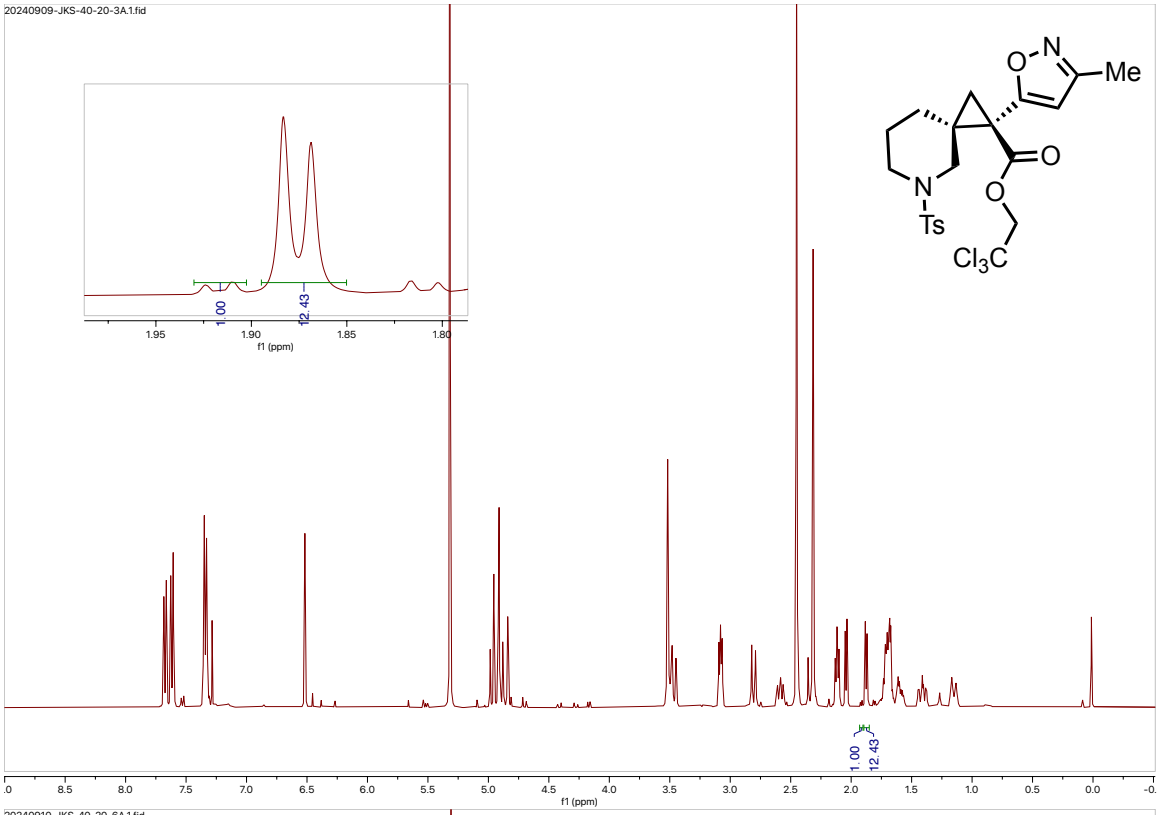
20240909-JKS-40-20-3A.1.fid
1.00
12.43
f1 (ppm)
1.00
12.43
f1 (ppm)
N
O
Me
O
N
Ts
O
O
Cl3C

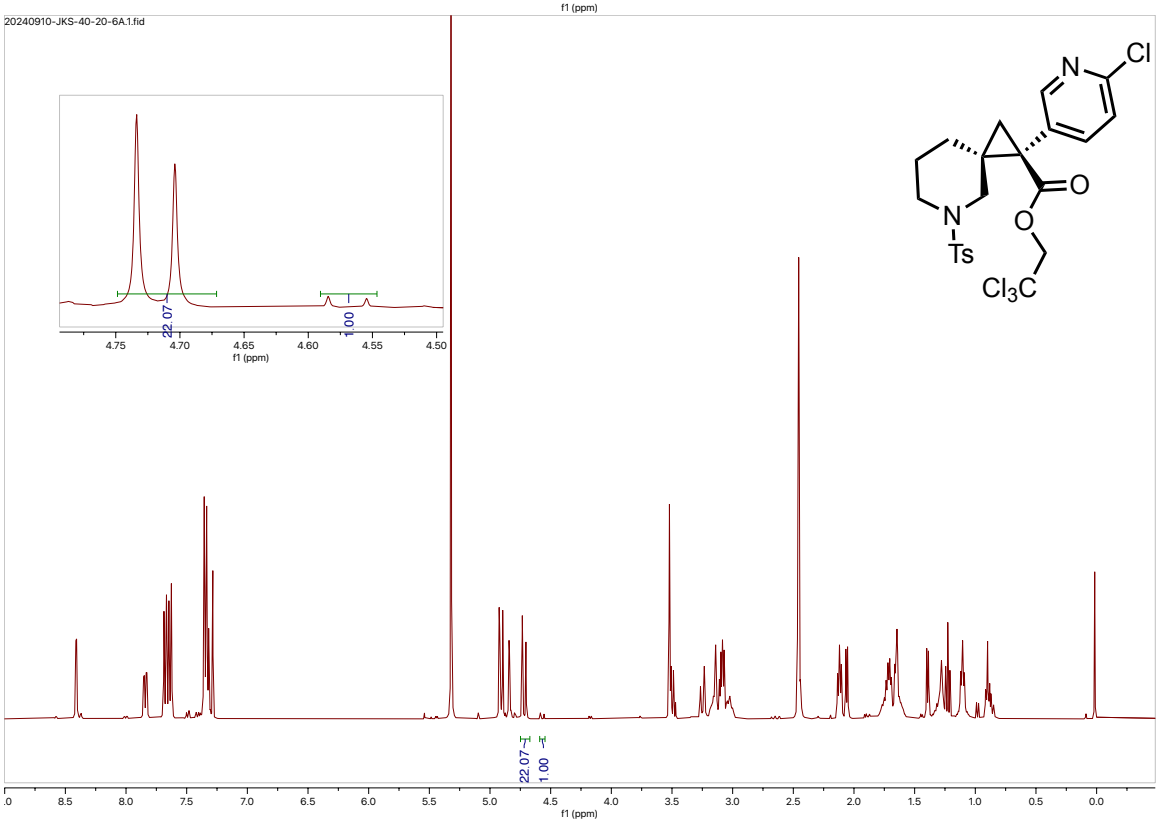
20240910-JKS-40-20-6A.1.fid
22.07
1.00
f1 (ppm)
22.07
1.00
f1 (ppm)
N
Cl
O
N
Ts
O
O
Cl3C

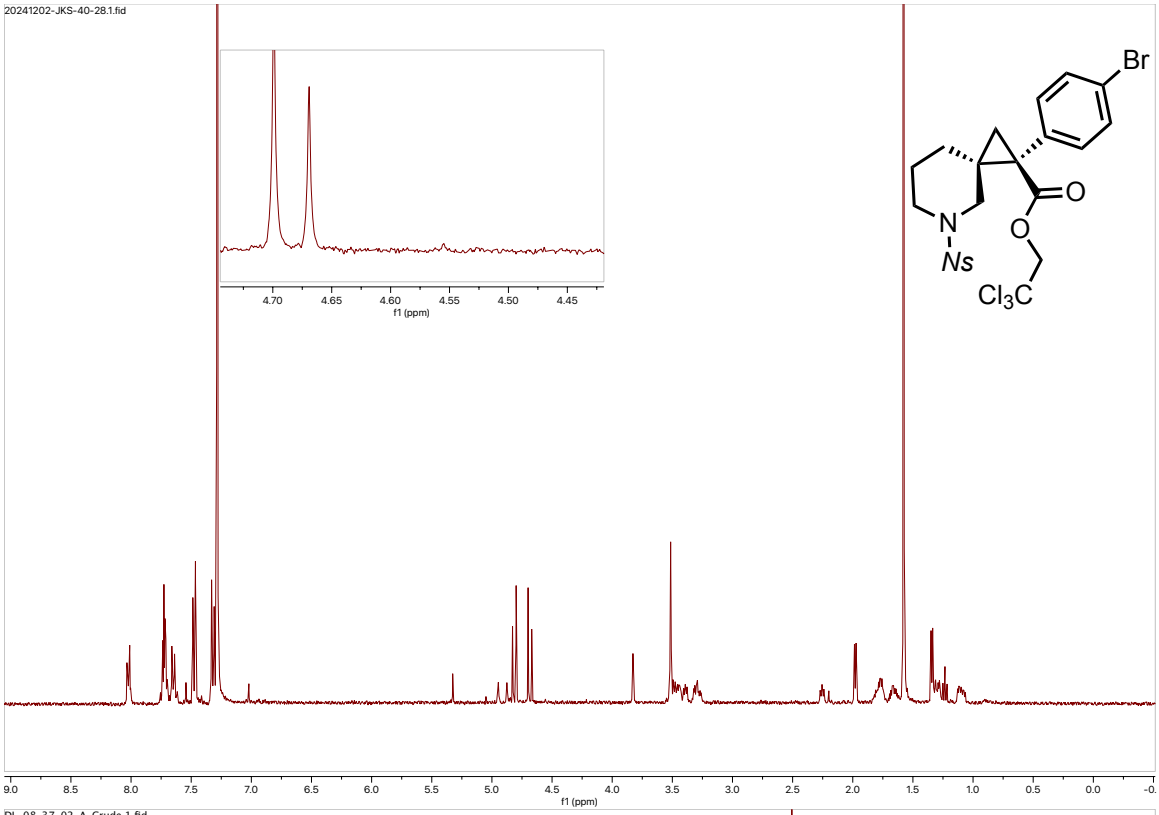
20241202-JKS-40-28.1.fid
Br
O
N
Ns
O
Cl3C
f1 (ppm)

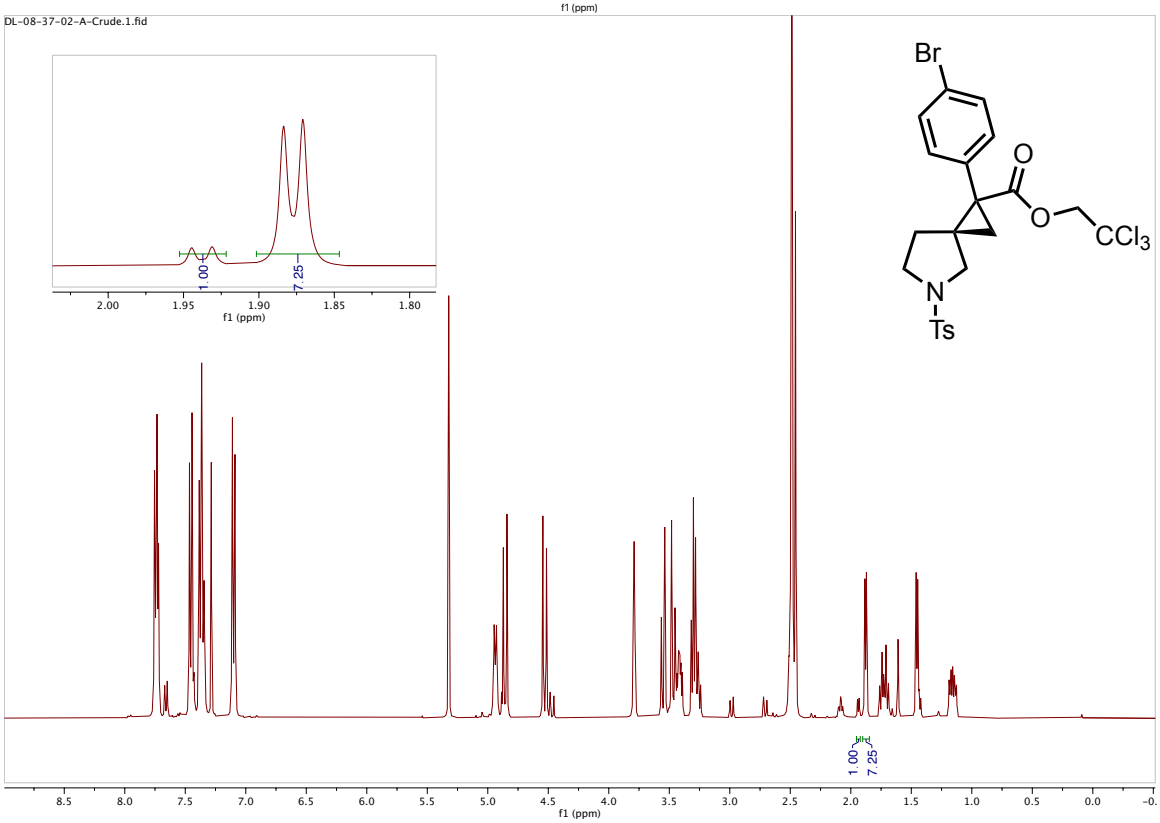
DL-08-37-02-A-Crude.1.fid
Br
O
O
CCl3
N
Ts
1.00
7.25
f1 (ppm)

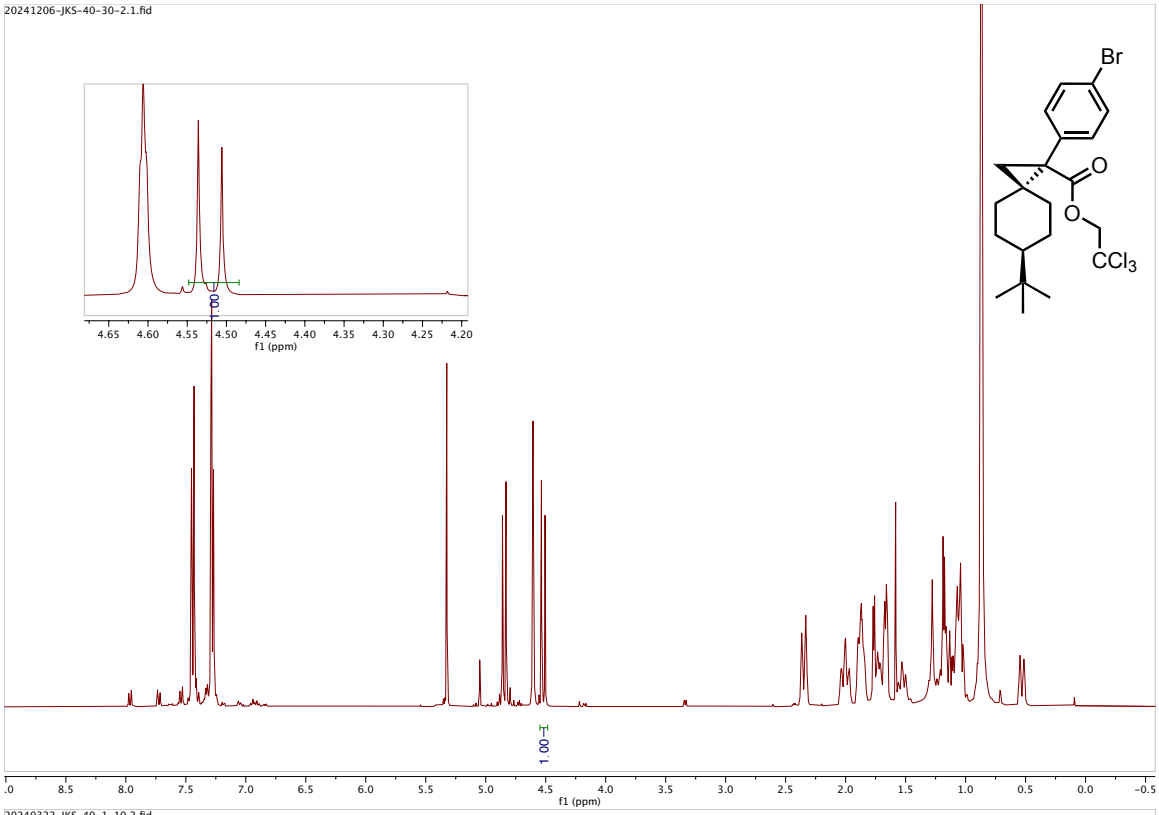
20241206-JKS-40-30-2.1.fid
Br
O
O
CCl3
1.00
4.65 4.60 4.55 4.50 4.45 4.40 4.35 4.30 4.25 4.20
f1 (ppm)
1.00
8.5 8.0 7.5 7.0 6.5 6.0 5.5 5.0 4.5 4.0 3.5 3.0 2.5 2.0 1.5 1.0 0.5 0.0
f1 (ppm)

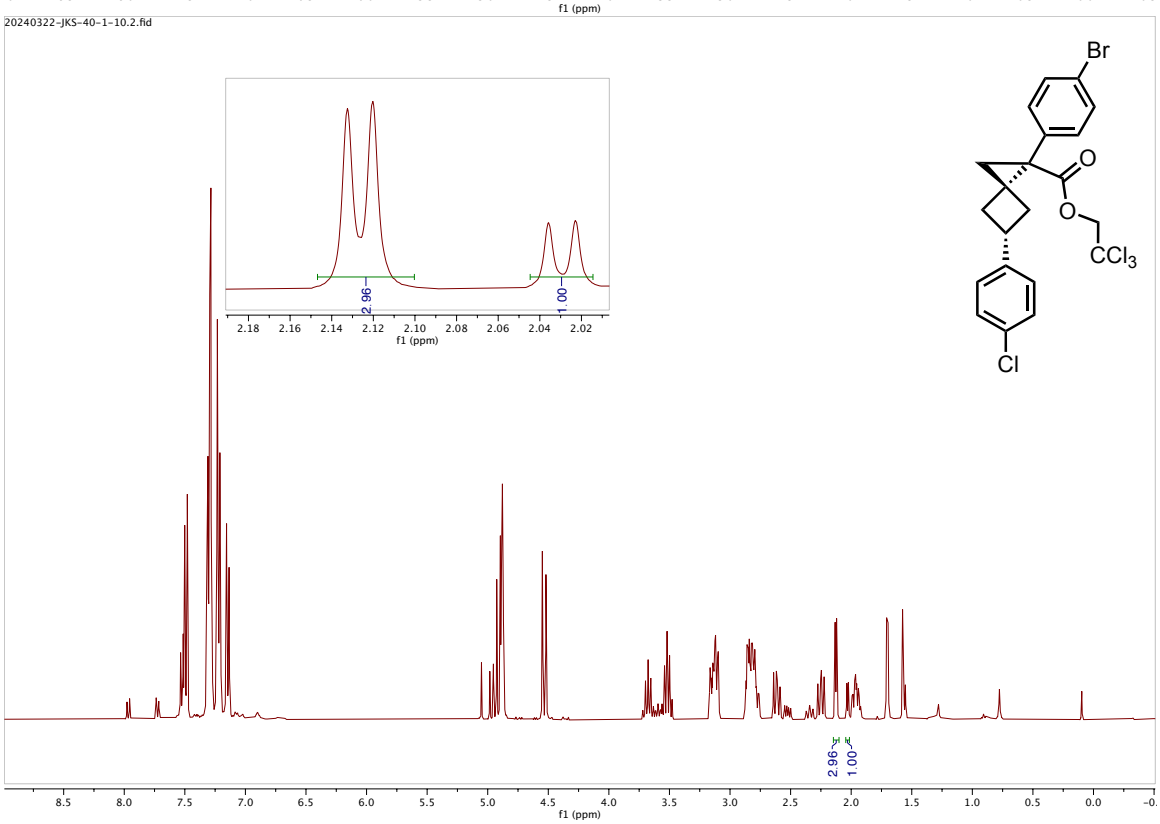
20240322-JKS-40-1-10.2.fid
Br
O
O
CCl3
Cl
2.96
1.00
2.18 2.16 2.14 2.12 2.10 2.08 2.06 2.04 2.02
f1 (ppm)
2.96
1.00
8.5 8.0 7.5 7.0 6.5 6.0 5.5 5.0 4.5 4.0 3.5 3.0 2.5 2.0 1.5 1.0 0.5 0.0
f1 (ppm)

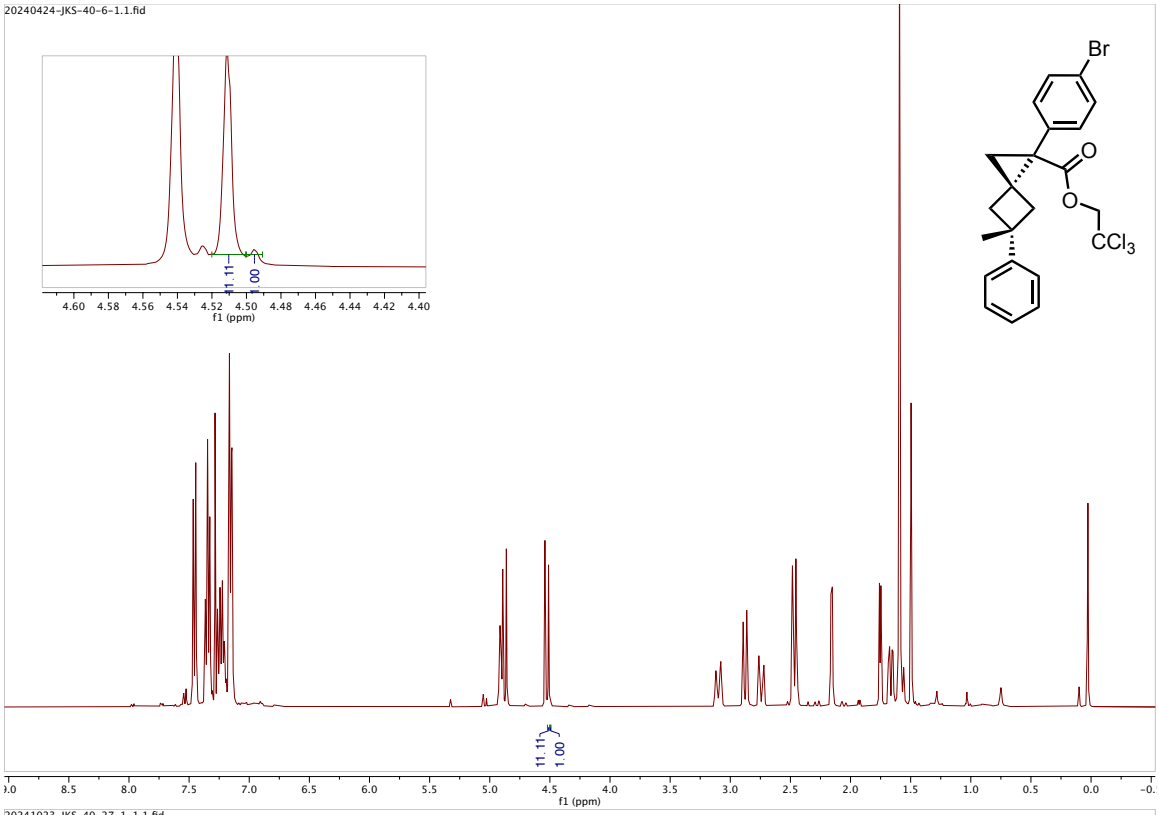
20240424-JKS-40-6-1.1.fid
Br
O
O
CCl3
11.11
1.00
f1 (ppm)

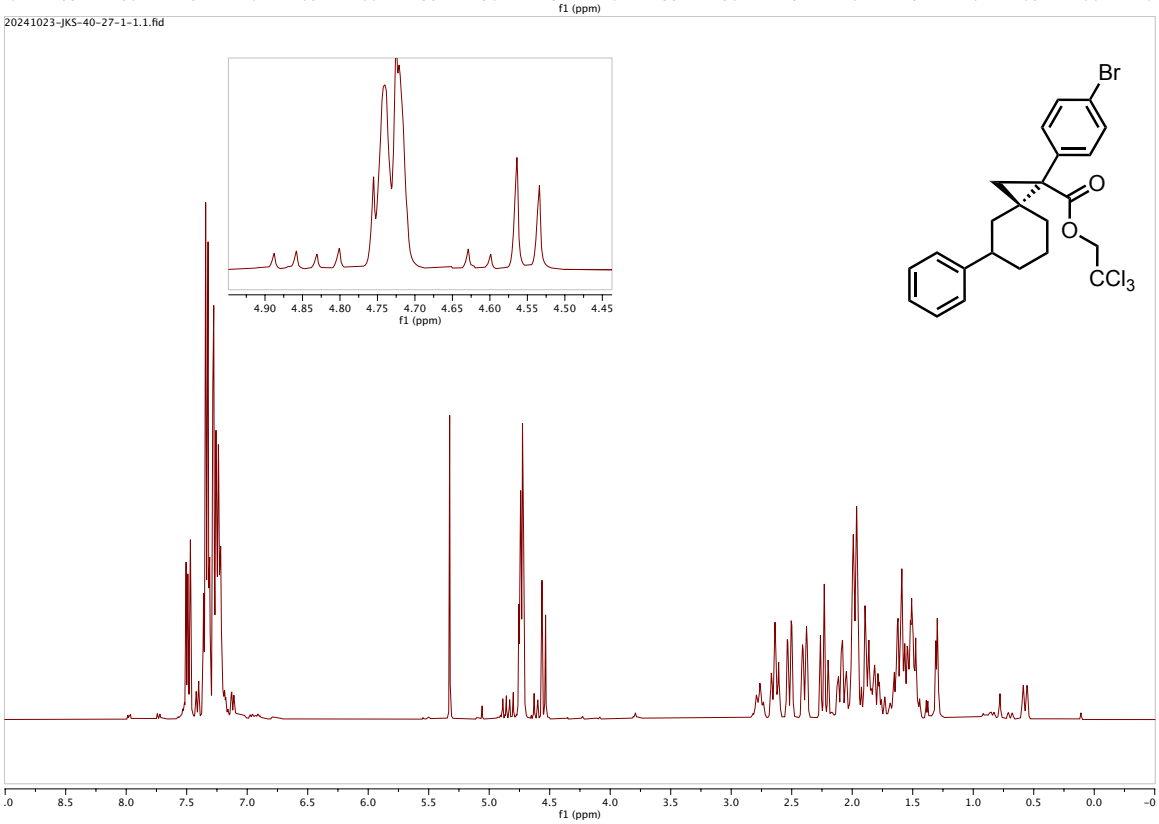
20241023-JKS-40-27-1-1.1.fid
Br
O
O
CCl3
f1 (ppm)

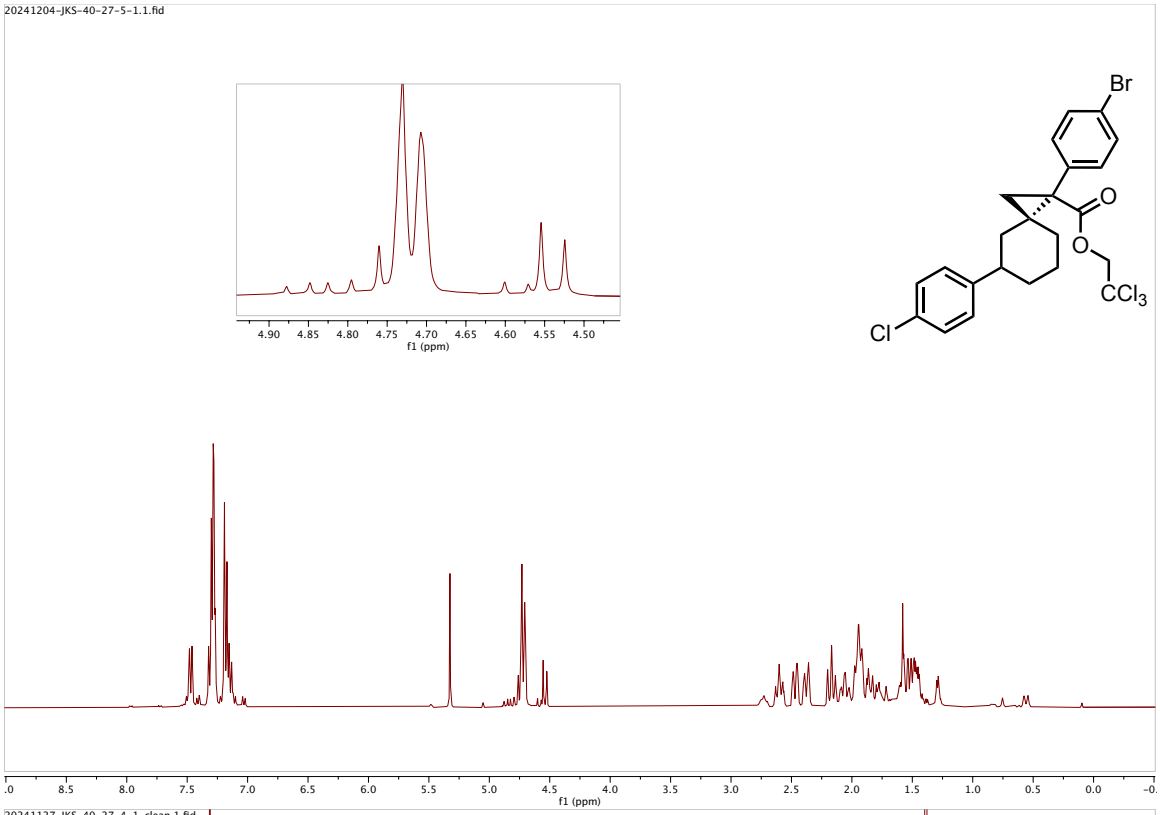
20241204-JKS-40-27-5-1.1.fid
Br
O
O
CCl3
Cl
f1 (ppm)

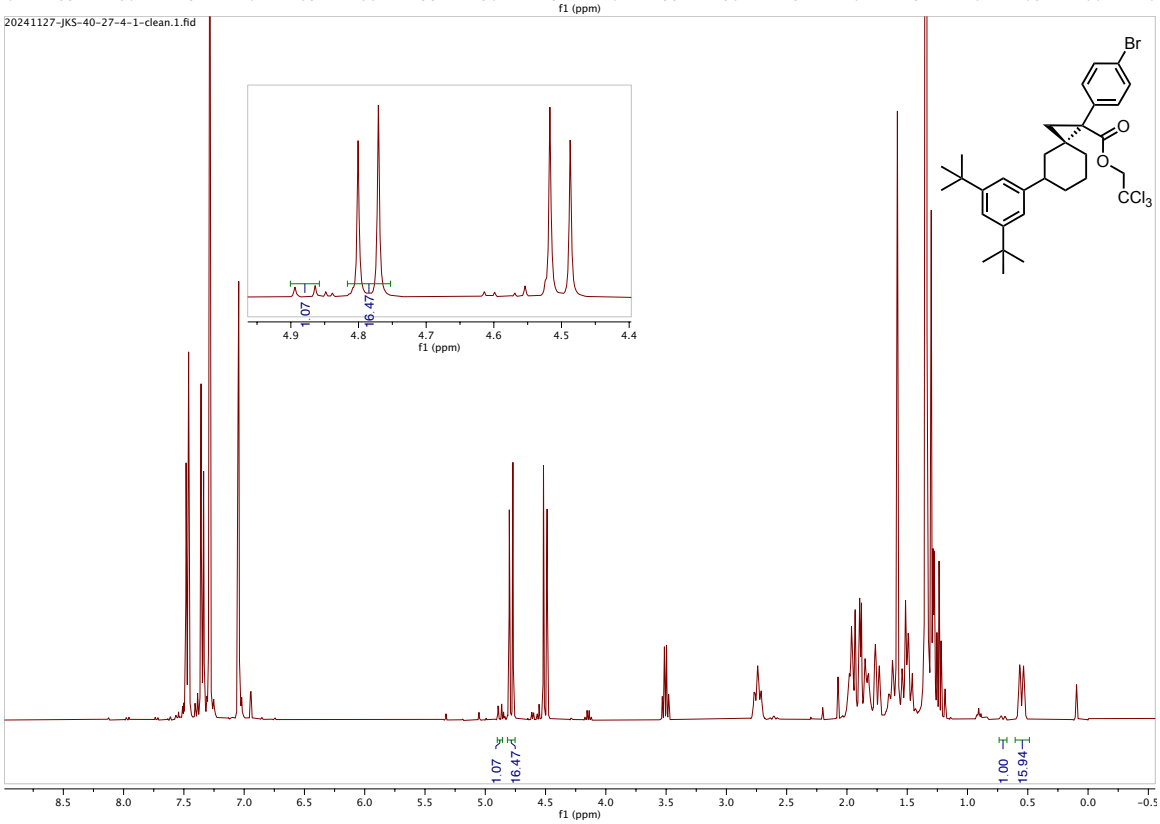
20241127-JKS-40-27-4-1-clean.1.fid
Br
O
O
CCl3
1.07
16.47
1.00
15.94
f1 (ppm)

HPLC and SFC Chiral Traces

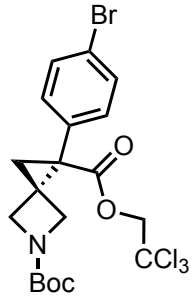

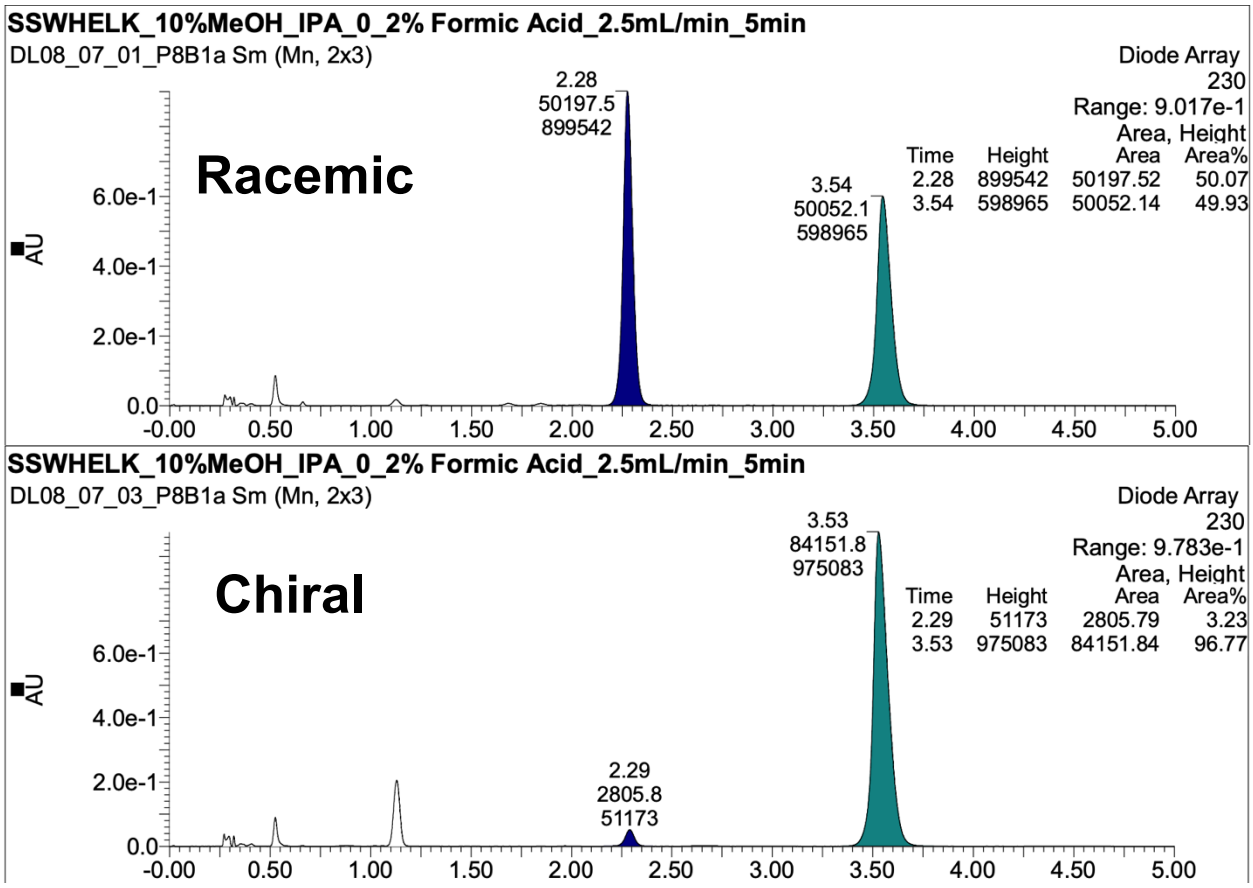

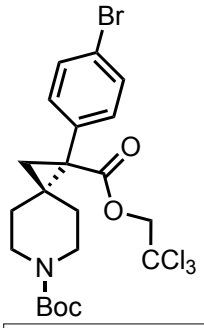
Br
O
O
CCl3
N
Boc

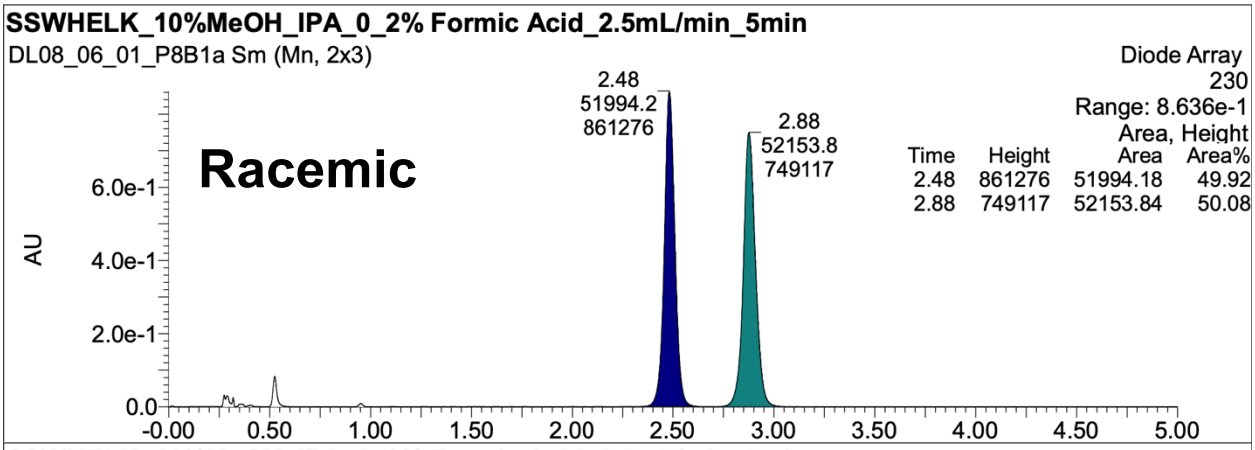
SSWHELK_10%MeOH_IPA_0_2% Formic Acid_2.5mL/min_5min
DL08_06_01_P8B1a Sm (Mn, 2x3)
Diode Array
230
Range: 8.636e-1
Area, Height
Racemic
2.48
51994.2
861276
2.88
52153.8
749117
Time Height Area Area%
2.48 861276 51994.18 49.92
2.88 749117 52153.84 50.08
AU
6.0e-1
4.0e-1
2.0e-1
0.0
-0.00 0.50 1.00 1.50 2.00 2.50 3.00 3.50 4.00 4.50 5.00

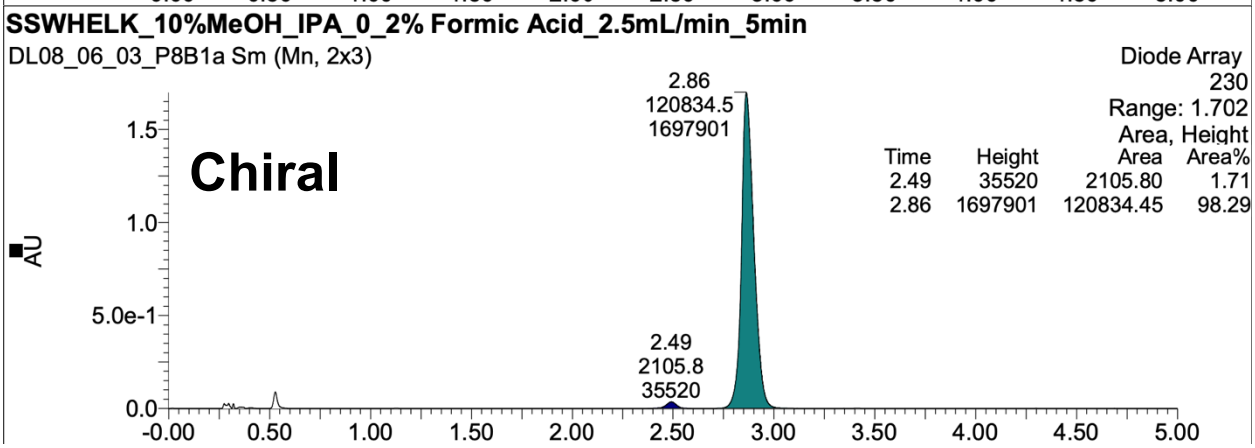
SSWHELK_10%MeOH_IPA_0_2% Formic Acid_2.5mL/min_5min
DL08_06_03_P8B1a Sm (Mn, 2x3)
Diode Array
230
Range: 1.702
Area, Height
Chiral
2.86
120834.5
1697901
2.49
2105.8
35520
Time Height Area Area%
2.49 35520 2105.80 1.71
2.86 1697901 120834.45 98.29
AU
1.5
1.0
5.0e-1
0.0
-0.00 0.50 1.00 1.50 2.00 2.50 3.00 3.50 4.00 4.50 5.00

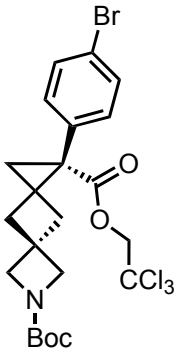

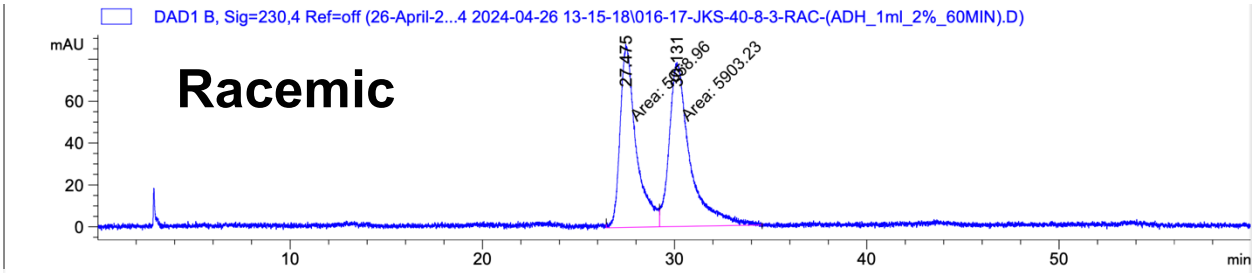

Signal 2: DAD1 B, Sig=230,4 Ref=off

Peak #	RetTime [min]	Type	Width [min]	Area [mAU*s]	Height [mAU]	Area %
1	27.475	MF	0.9633	5058.95850	87.52956	46.1492
2	30.131	FM	1.2537	5903.22852	78.47722	53.8508
Totals :				1.09622e4	166.00677	

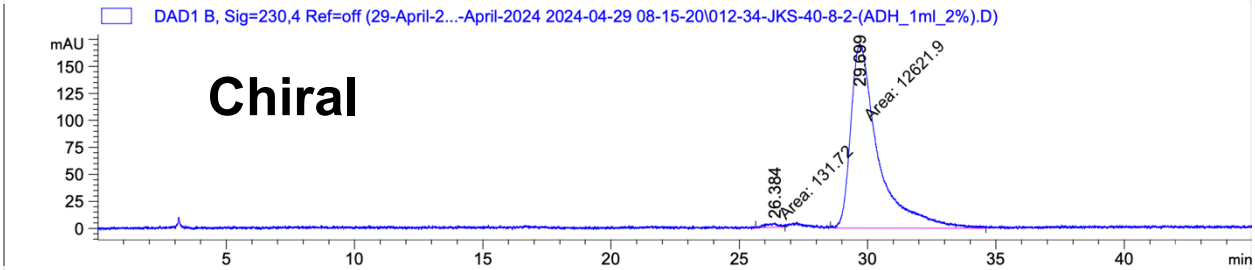

Signal 2: DAD1 B, Sig=230,4 Ref=off

Peak #	RetTime [min]	Type	Width [min]	Area [mAU*s]	Height [mAU]	Area %
1	26.384	MM	0.5105	131.71962	4.30054	1.0328
2	29.699	MM	1.2326	1.26219e4	170.67297	98.9672
Totals :				1.27536e4	174.97351	

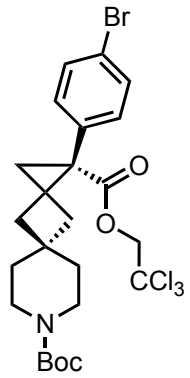
Br
O
O
CCl3
N
Boc

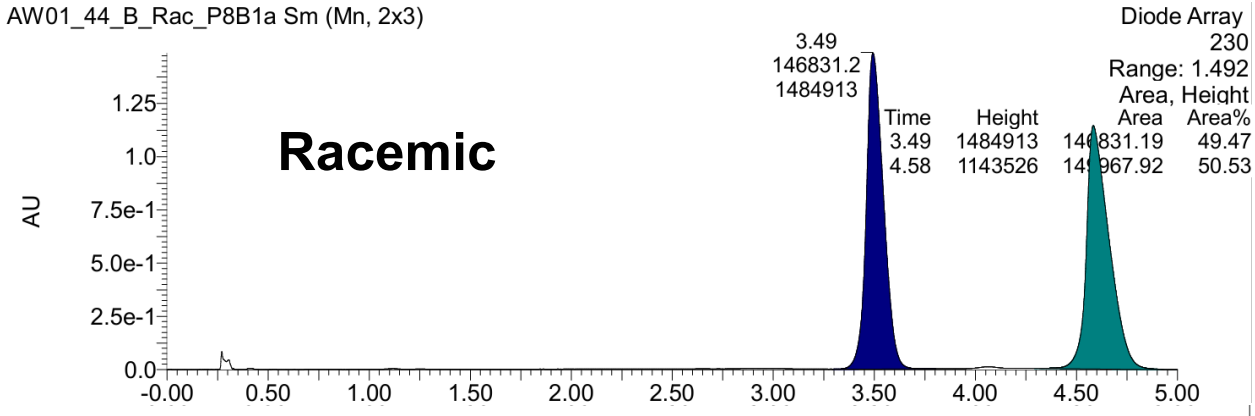
AW01_44_B_Rac_P8B1a Sm (Mn, 2x3)
Racemic
Diode Array
230
Range: 1.492
Area, Height
3.49
146831.2
1484913
Time Height Area Area%
3.49 1484913 146831.19 49.47
4.58 1143526 149967.92 50.53
AU
1.25
1.0
7.5e-1
5.0e-1
2.5e-1
0.0
-0.00 0.50 1.00 1.50 2.00 2.50 3.00 3.50 4.00 4.50 5.00

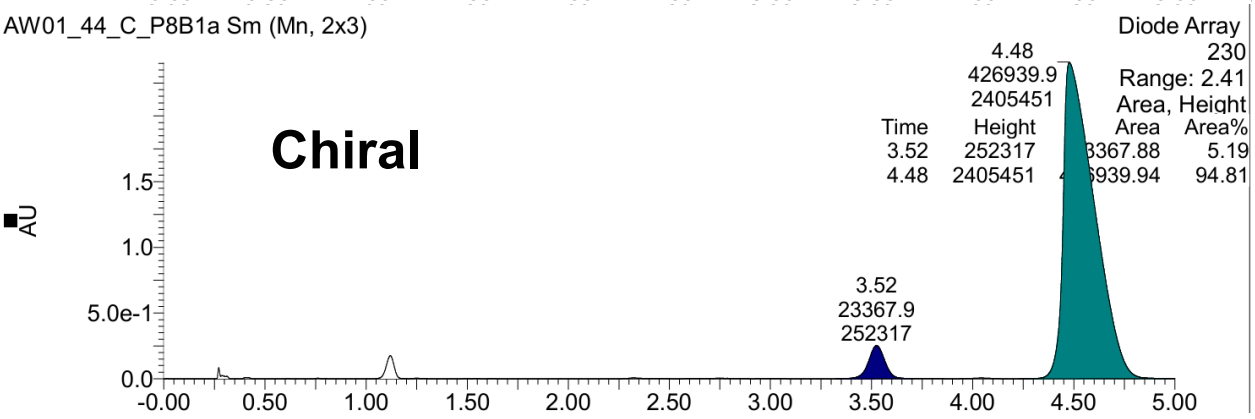
AW01_44_C_P8B1a Sm (Mn, 2x3)
Chiral
Diode Array
230
Range: 2.41
Area, Height
4.48
426939.9
2405451
Time Height Area Area%
3.52 252317 23367.88 5.19
4.48 2405451 426939.94 94.81
3.52
23367.9
252317
AU
1.5
1.0
5.0e-1
0.0
-0.00 0.50 1.00 1.50 2.00 2.50 3.00 3.50 4.00 4.50 5.00

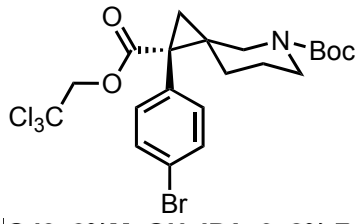

OJ3_3%MeOH_IPA_0_2% Formic Acid_2.5mL/min_5min

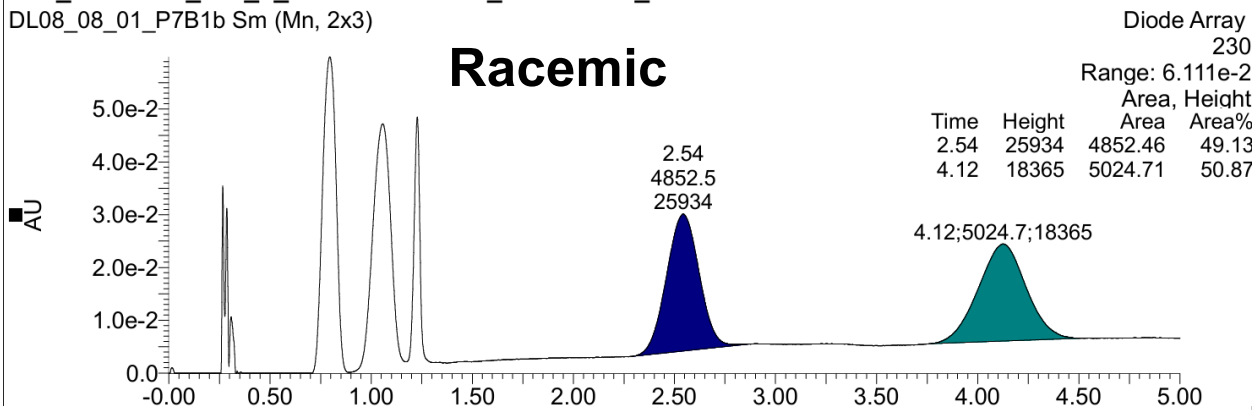

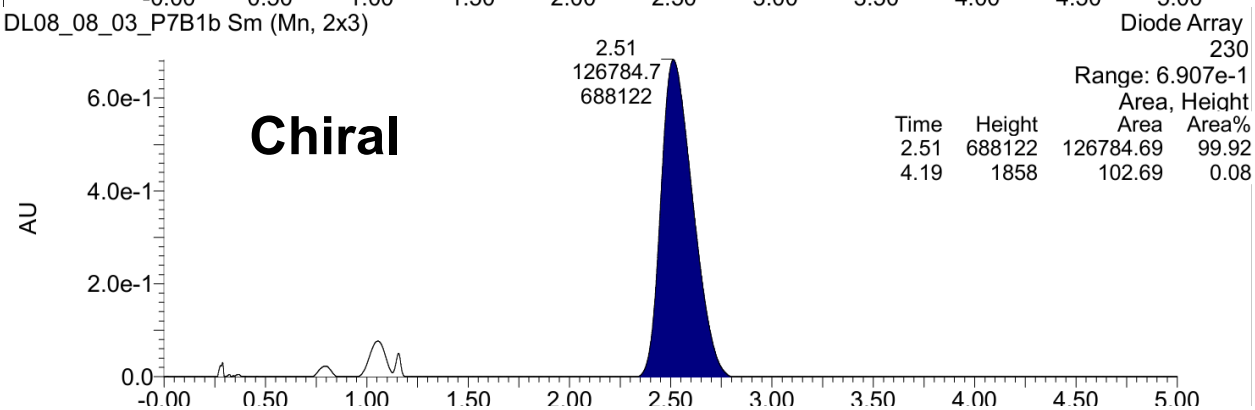

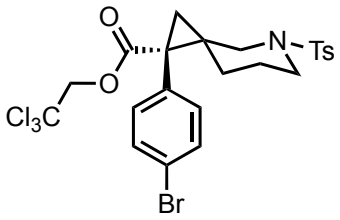

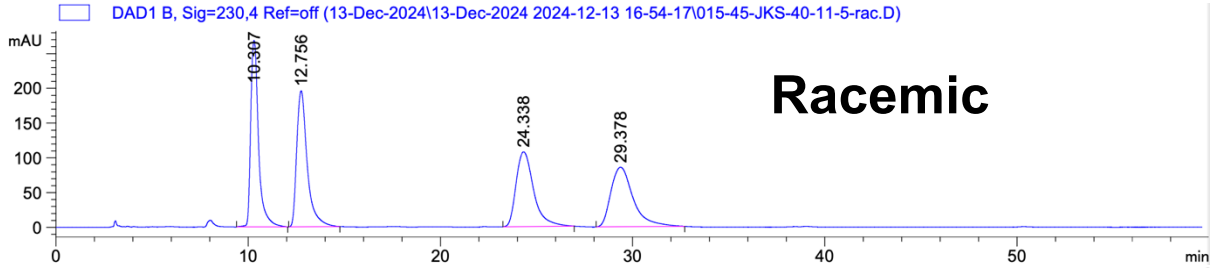

Signal 2: DAD1 B, Sig=230,4 Ref=off

Peak #	RetTime [min]	Type	Width [min]	Area [mAU*s]	Height [mAU]	Area %
1	10.307	BB	0.4240	7579.24902	268.33194	26.2699
2	12.756	BB	0.5437	7440.13916	195.83569	25.7878
3	24.338	BB	0.7523	6905.04004	107.58592	23.9331
4	29.378	BB	0.9456	6927.00830	85.73902	24.0092
Totals :				2.88514e4	657.49258	

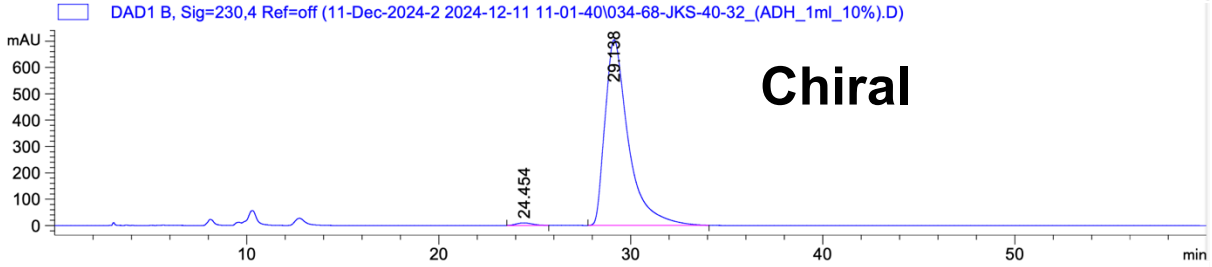

Signal 2: DAD1 B, Sig=230,4 Ref=off

Peak #	RetTime [min]	Type	Width [min]	Area [mAU*s]	Height [mAU]	Area %
1	24.454	BB	0.6733	540.69104	9.41764	0.8991
2	29.138	BB	0.9910	5.95989e4	704.82300	99.1009
Totals :				6.01396e4	714.24064	

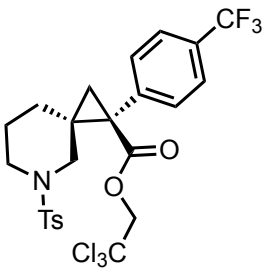

DAD1 B, Sig=230,4 Ref=off (05-Jun-202...un-2024 2024-06-05 08-32-00\006-81-AW_01_22_B_Rac(ADH_1ml_10%).D)

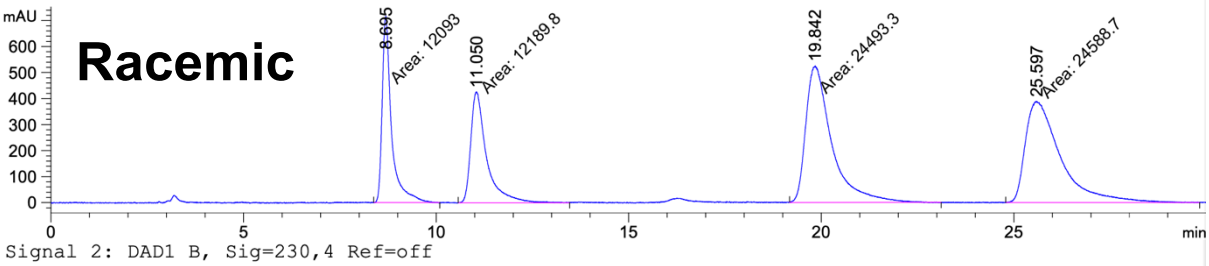

Signal 2: DAD1 B, Sig=230,4 Ref=off

Peak #	RetTime [min]	Type	Width [min]	Area [mAU*s]	Height [mAU]	Area %
1	8.695	MM	0.2811	1.20930e4	717.11755	16.4834
2	11.050	MM	0.4760	1.21898e4	426.84717	16.6153
3	19.842	MM	0.7774	2.44933e4	525.12231	33.3856
4	25.597	MM	1.0536	2.45887e4	388.97781	33.5157
Totals :				7.33649e4	2058.06485	

DAD1 B, Sig=230,4 Ref=off (05-Jun-202...2024 2024-06-05 08-32-00\025-82-AW_01_22_A_Chiral(ADH_1ml_10%).D)

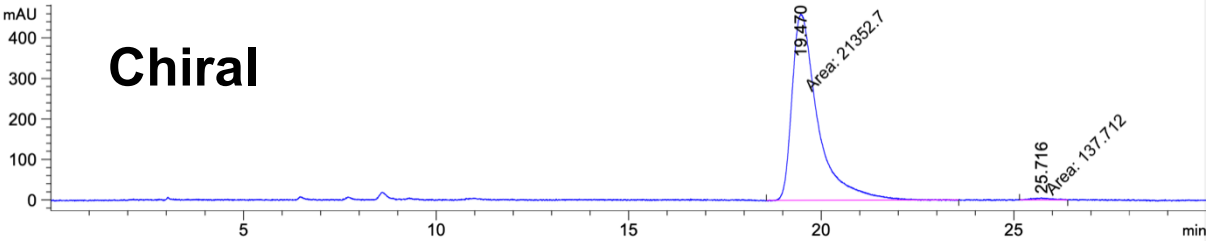

Signal 2: DAD1 B, Sig=230,4 Ref=off

Peak #	RetTime [min]	Type	Width [min]	Area [mAU*s]	Height [mAU]	Area %
1	19.470	MM	0.7735	2.13527e4	460.09781	99.3592
2	25.716	MM	0.4654	137.71191	4.93118	0.6408
Totals :				2.14904e4	465.02899	

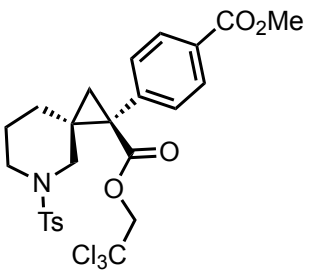

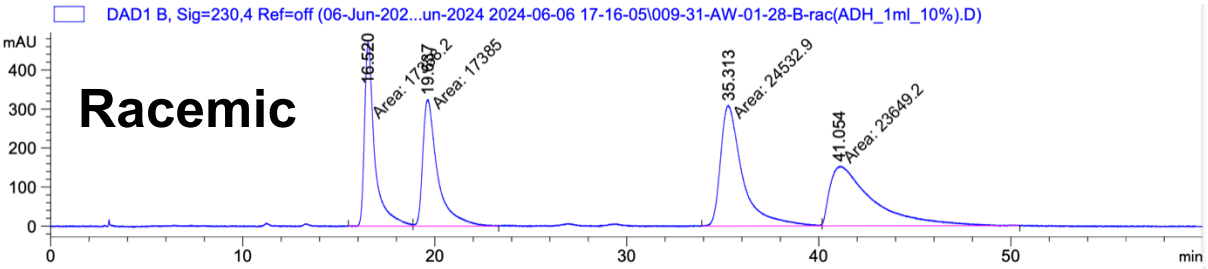

Signal 2: DAD1 B, Sig=230,4 Ref=off

Peak #	RetTime [min]	Type	Width [min]	Area [mAU*s]	Height [mAU]	Area %
1	16.520	MF	0.6129	1.73582e4	472.04211	20.9324
2	19.637	FM	0.8936	1.73850e4	324.23386	20.9646
3	35.313	MF	1.3217	2.45329e4	309.36719	29.5844
4	41.054	FM	2.5788	2.36492e4	152.84401	28.5187
Totals :				8.29253e4	1258.48717	

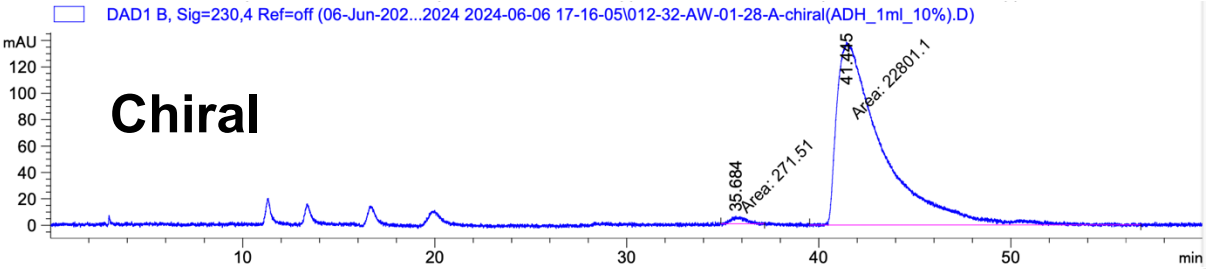

Signal 2: DAD1 B, Sig=230,4 Ref=off

Peak #	RetTime [min]	Type	Width [min]	Area [mAU*s]	Height [mAU]	Area %
1	35.684	MM	0.7741	271.50958	5.84591	1.1768
2	41.445	MM	2.7371	2.28011e4	138.84218	98.8232
Totals :				2.30726e4	144.68809	

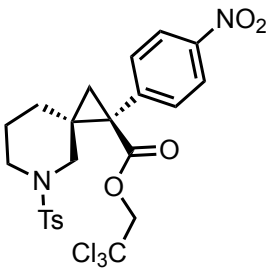
NO2
O
O
N
Ts
Cl3C

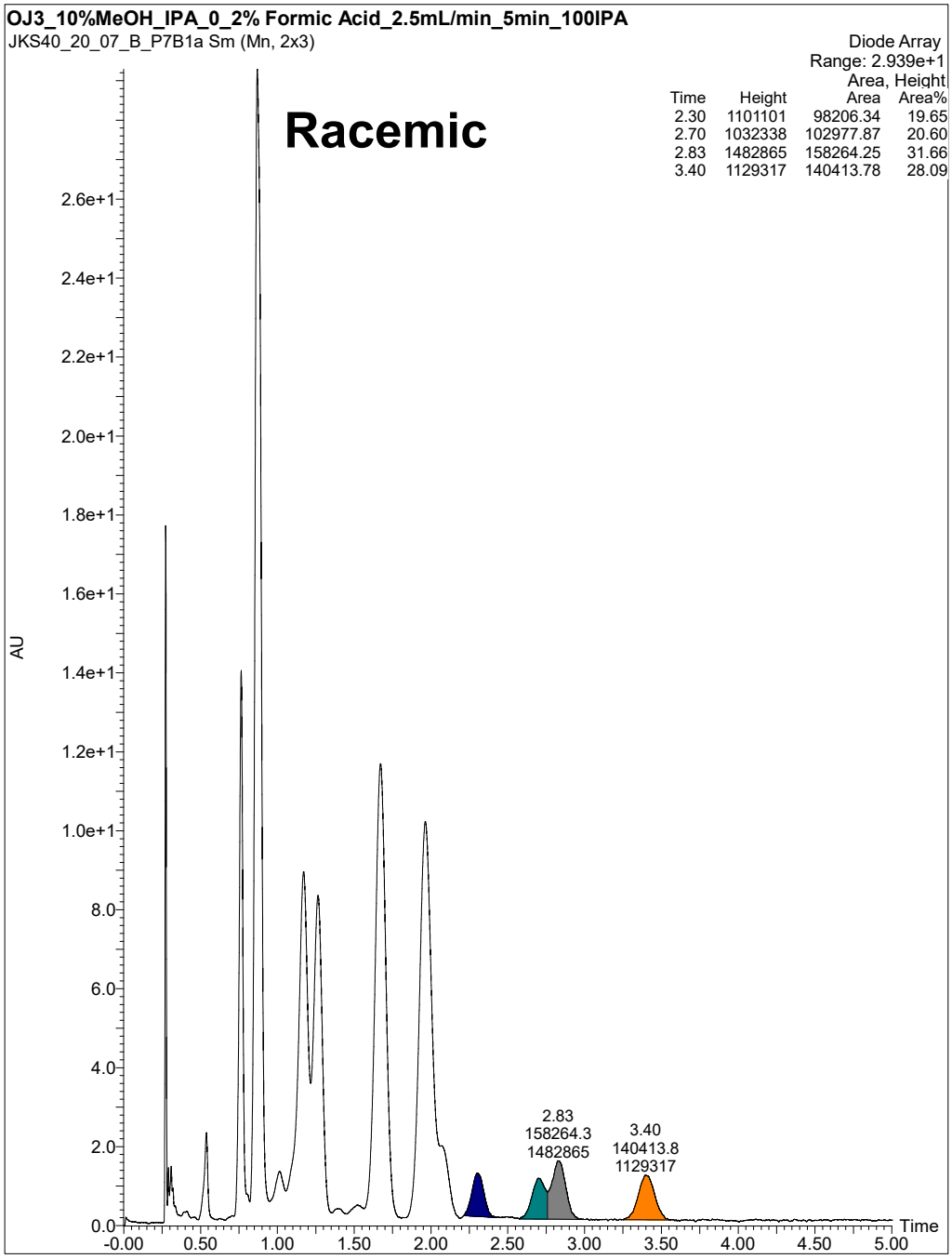
OJ3_10%MeOH_IPA_0_2% Formic Acid_2.5mL/min_5min_100IPA
JKS40_20_07_B_P7B1a Sm (Mn, 2x3)
Diode Array
Range: 2.939e+1
Area, Height
Racemic
Time Height Area Area%
2.30 1101101 98206.34 19.65
2.70 1032338 102977.87 20.60
2.83 1482865 158264.25 31.66
3.40 1129317 140413.78 28.09
AU
Time
2.83
158264.3
1482865
3.40
140413.8
1129317

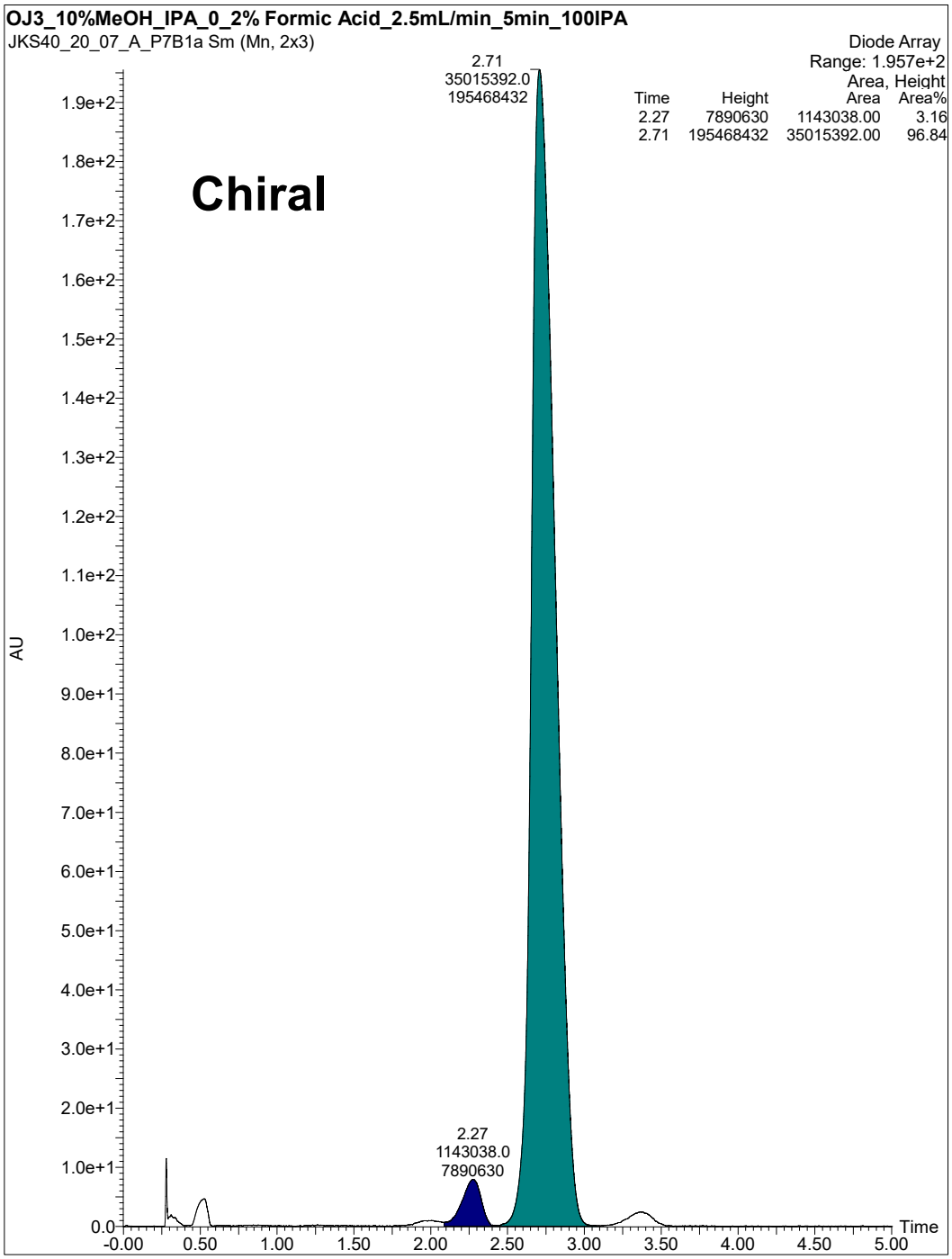
OJ3_10%MeOH_IPA_0_2% Formic Acid_2.5mL/min_5min_100IPA
JKS40_20_07_A_P7B1a Sm (Mn, 2x3)
Diode Array
Range: 1.957e+2
Area, Height
Time Height Area Area%
2.27 7890630 1143038.00 3.16
2.71 195468432 35015392.00 96.84
Chiral
2.71
35015392.0
195468432
2.27
1143038.0
7890630
AU
Time
1.9e+2
1.8e+2
1.7e+2
1.6e+2
1.5e+2
1.4e+2
1.3e+2
1.2e+2
1.1e+2
1.0e+2
9.0e+1
8.0e+1
7.0e+1
6.0e+1
5.0e+1
4.0e+1
3.0e+1
2.0e+1
1.0e+1
0.0
-0.00
0.50
1.00
1.50
2.00
2.50
3.00
3.50
4.00
4.50
5.00

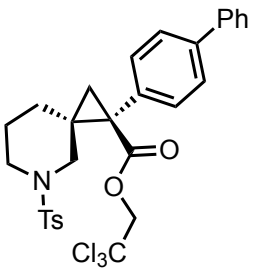

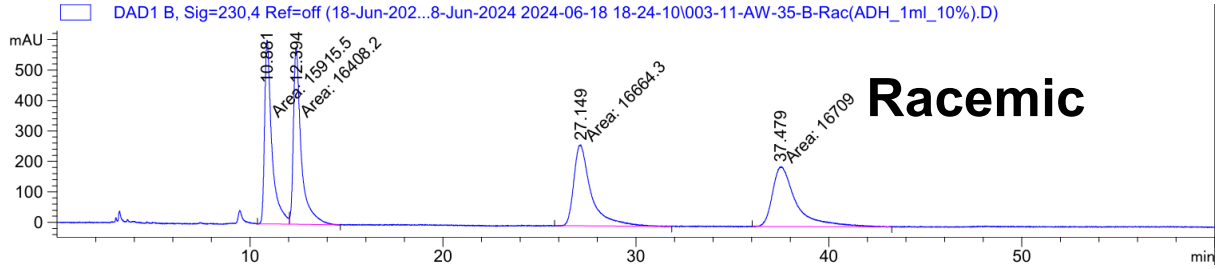

Signal 2: DAD1 B, Sig=230,4 Ref=off

Peak #	RetTime [min]	Type	Width [min]	Area [mAU*s]	Height [mAU]	Area %
1	10.881	MF	0.4399	1.59155e4	603.01996	24.2256
2	12.394	FM	0.4706	1.64082e4	581.11865	24.9756
3	27.149	MM	1.0453	1.66643e4	265.68961	25.3654
4	37.479	MM	1.4157	1.67090e4	196.70488	25.4334

Totals : 6.56970e4 1646.53310

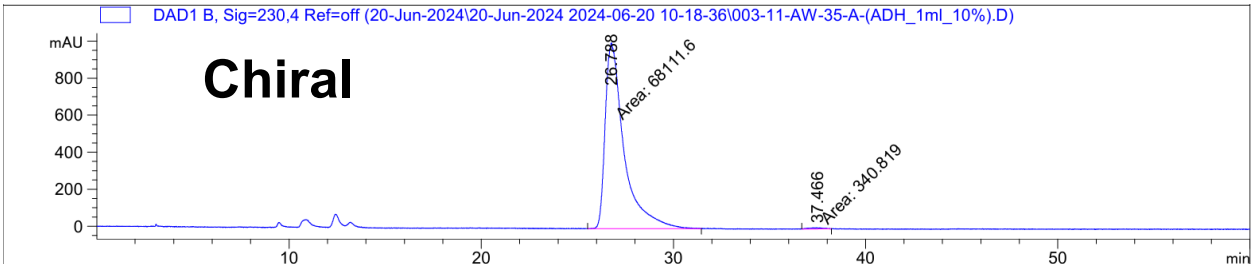

Signal 2: DAD1 B, Sig=230,4 Ref=off

Peak #	RetTime [min]	Type	Width [min]	Area [mAU*s]	Height [mAU]	Area %
1	26.788	MM	1.1299	6.81116e4	1004.72119	99.5021
2	37.466	MM	0.7474	340.81906	7.60009	0.4979

Totals : 6.84524e4 1012.32129

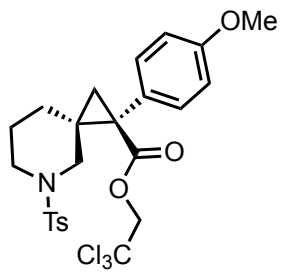
OMe
O
N
Ts
O
Cl3C

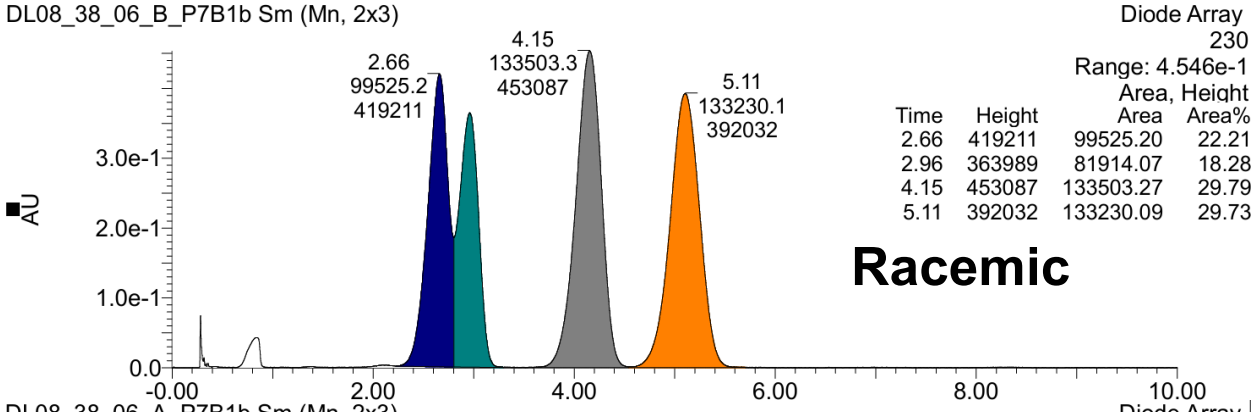
DL08_38_06_B_P7B1b Sm (Mn, 2x3)
Diode Array
230
Range: 4.546e-1
Area, Height
2.66
99525.2
419211
4.15
133503.3
453087
5.11
133230.1
392032
Time Height Area Area%
2.66 419211 99525.20 22.21
2.96 363989 81914.07 18.28
4.15 453087 133503.27 29.79
5.11 392032 133230.09 29.73
Racemic
AU
3.0e-1
2.0e-1
1.0e-1
0.0
-0.00
2.00
4.00
6.00
8.00
10.00

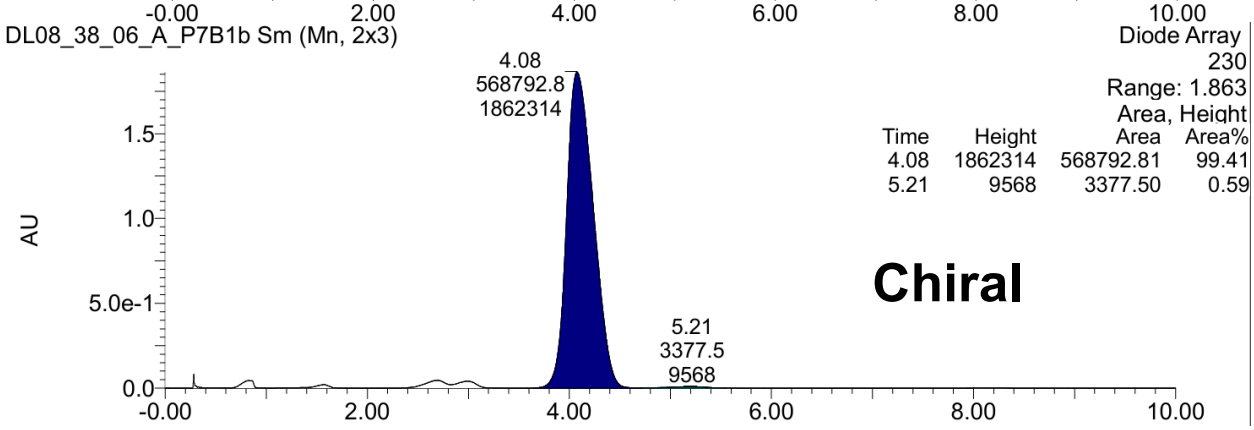
DL08_38_06_A_P7B1b Sm (Mn, 2x3)
Diode Array
230
Range: 1.863
Area, Height
4.08
568792.8
1862314
5.21
3377.5
9568
Time Height Area Area%
4.08 1862314 568792.81 99.41
5.21 9568 3377.50 0.59
Chiral
AU
1.5
1.0
5.0e-1
0.0
-0.00
2.00
4.00
6.00
8.00
10.00

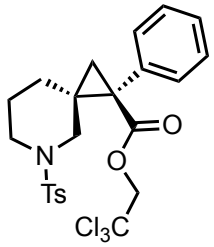

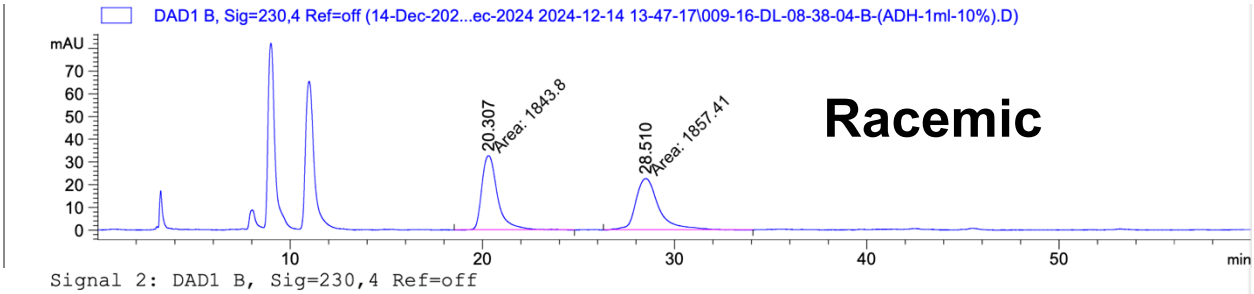

Signal 2: DAD1 B, Sig=230,4 Ref=off

Peak #	RetTime [min]	Type	Width [min]	Area [mAU*s]	Height [mAU]	Area %
1	20.307	MM	0.9422	1843.80420	32.61585	49.8162
2	28.510	MM	1.3755	1857.40833	22.50531	50.1838
Totals :				3701.21252	55.12116	

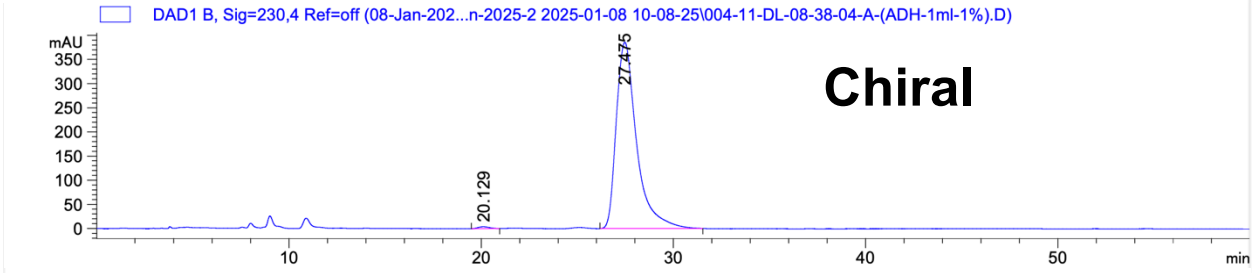

Signal 2: DAD1 B, Sig=230,4 Ref=off

Peak #	RetTime [min]	Type	Width [min]	Area [mAU*s]	Height [mAU]	Area %
1	20.129	BB	0.4672	152.31375	3.82389	0.5353
2	27.475	BB	0.8624	2.83015e4	385.79425	99.4647
Totals :				2.84538e4	389.61814	

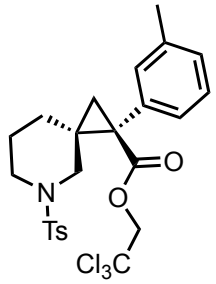

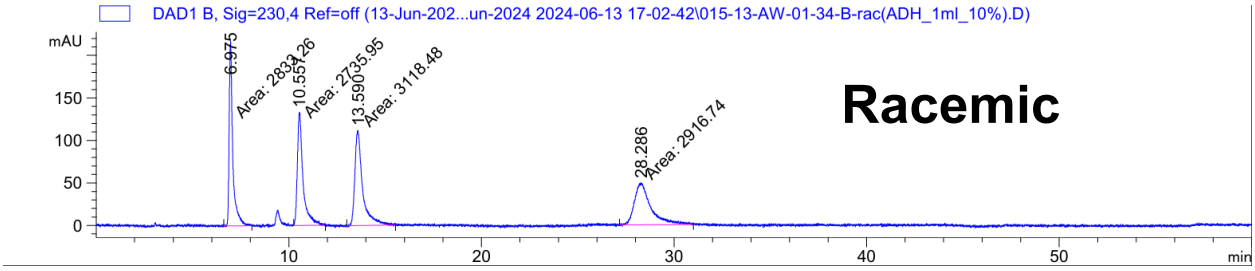

Signal 2: DAD1 B, Sig=230,4 Ref=off

Peak #	RetTime [min]	Type	Width [min]	Area [mAU*s]	Height [mAU]	Area %
1	6.975	MM	0.2174	2833.26294	217.18852	24.4153
2	10.557	MM	0.3422	2735.95483	133.24054	23.5768
3	13.590	MM	0.4632	3118.48145	112.21455	26.8732
4	28.286	MM	0.9771	2916.74219	49.75204	25.1347
Totals :				1.16044e4	512.39565	

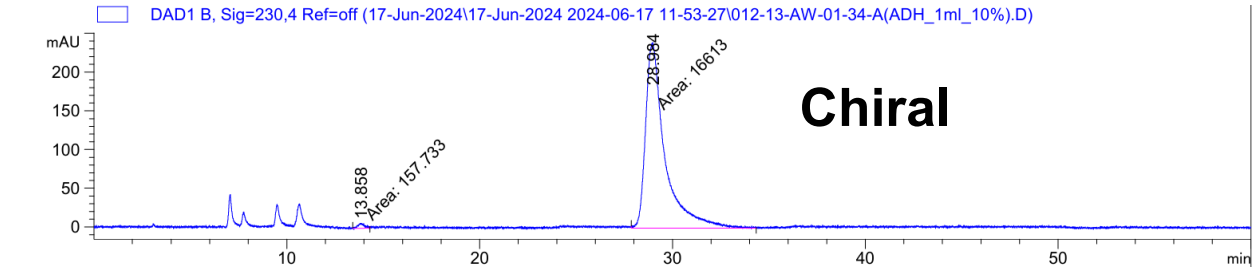

Signal 2: DAD1 B, Sig=230,4 Ref=off

Peak #	RetTime [min]	Type	Width [min]	Area [mAU*s]	Height [mAU]	Area %
1	13.858	MM	0.3966	157.73332	6.62812	0.9405
2	28.984	MM	1.1533	1.66130e4	240.07753	99.0595
Totals :				1.67708e4	246.70565	

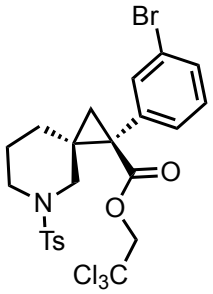

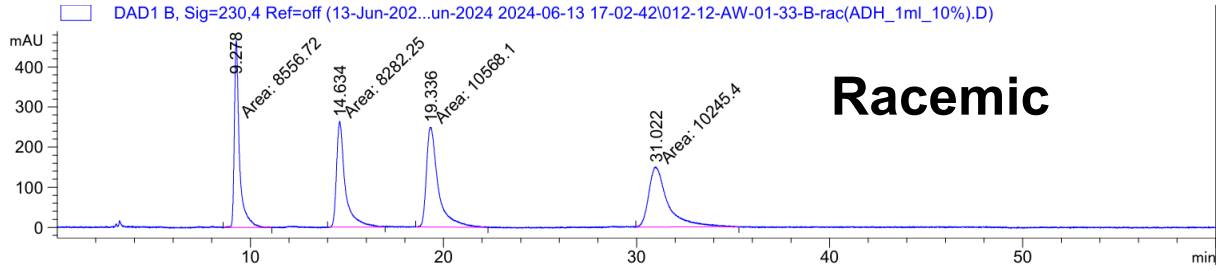

Signal 2: DAD1 B, Sig=230,4 Ref=off

Peak #	RetTime [min]	Type	Width [min]	Area [mAU*s]	Height [mAU]	Area %
1	9.278	MM	0.3065	8556.71680	465.34409	22.7255
2	14.634	MM	0.5231	8282.24707	263.89575	21.9966
3	19.336	MM	0.7058	1.05681e4	249.54501	28.0674
4	31.022	MM	1.1378	1.02454e4	150.07767	27.2105

Totals : 3.76525e4 1128.86252

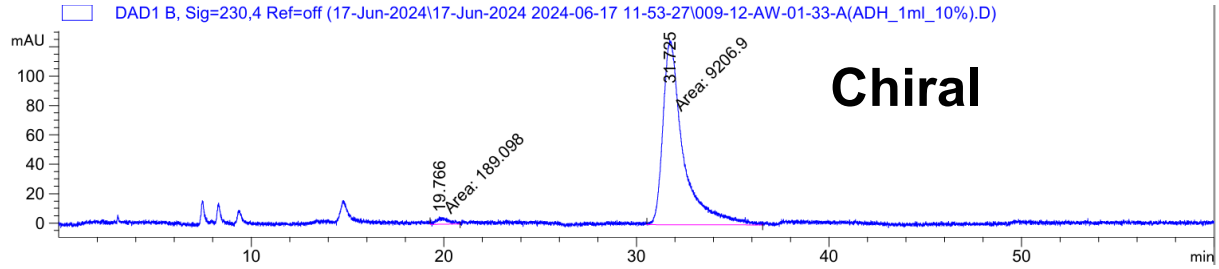

Signal 2: DAD1 B, Sig=230,4 Ref=off

Peak #	RetTime [min]	Type	Width [min]	Area [mAU*s]	Height [mAU]	Area %
1	19.766	MM	0.6149	189.09784	5.12543	2.0125
2	31.725	MM	1.2239	9206.90234	125.37157	97.9875

Totals : 9396.00018 130.49701

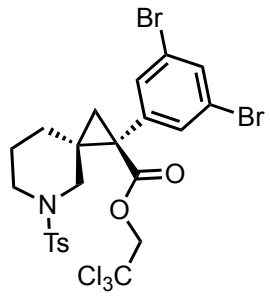
Br
Br
O
N
Ts
O
Cl3C

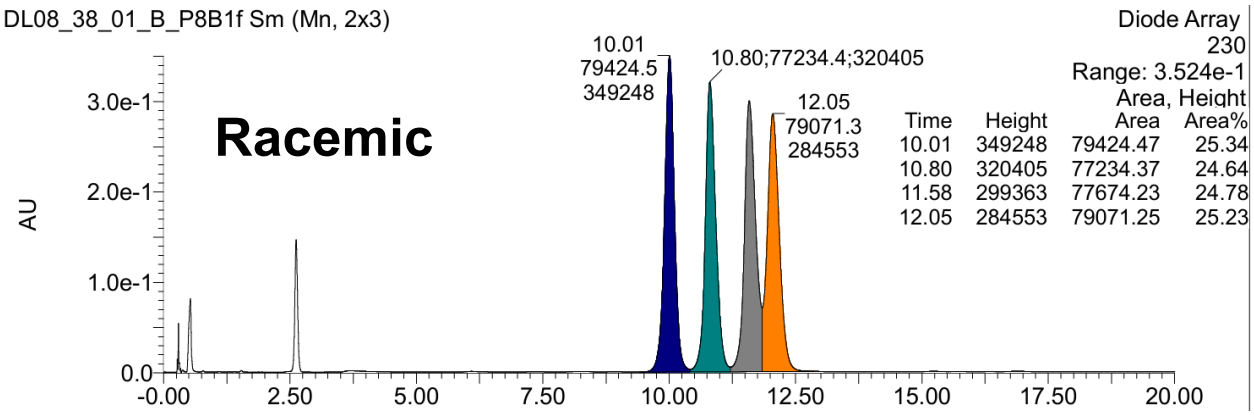
DL08_38_01_B_P8B1f Sm (Mn, 2x3)
Diode Array
230
Range: 3.524e-1
Area, Height
Racemic
10.01
79424.5
349248
10.80;77234.4;320405
12.05
79071.3
284553
Time Height Area Area%
10.01 349248 79424.47 25.34
10.80 320405 77234.37 24.64
11.58 299363 77674.23 24.78
12.05 284553 79071.25 25.23
AU
3.0e-1
2.0e-1
1.0e-1
0.0
-0.00 2.50 5.00 7.50 10.00 12.50 15.00 17.50 20.00

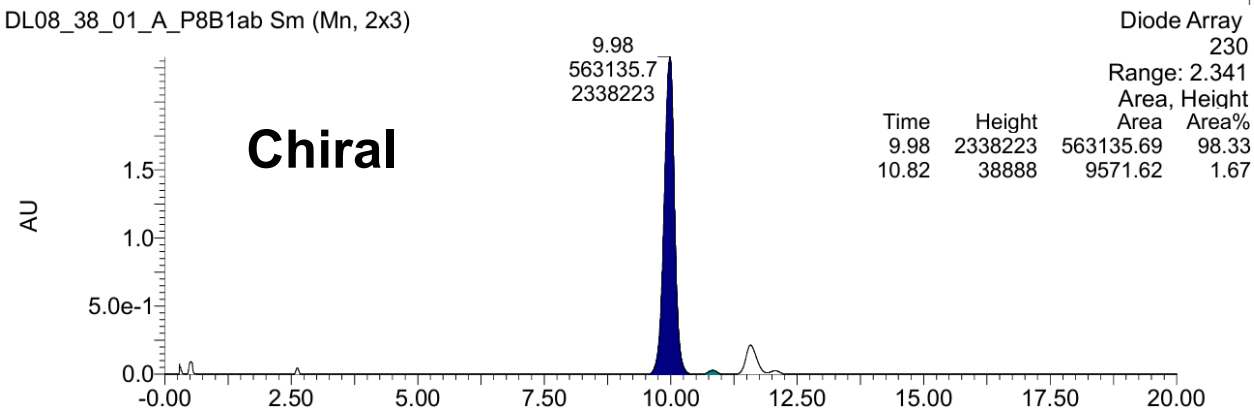
DL08_38_01_A_P8B1ab Sm (Mn, 2x3)
Diode Array
230
Range: 2.341
Area, Height
Chiral
9.98
563135.7
2338223
Time Height Area Area%
9.98 2338223 563135.69 98.33
10.82 38888 9571.62 1.67
AU
1.5
1.0
5.0e-1
0.0
-0.00 2.50 5.00 7.50 10.00 12.50 15.00 17.50 20.00

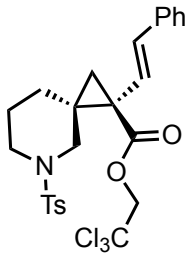

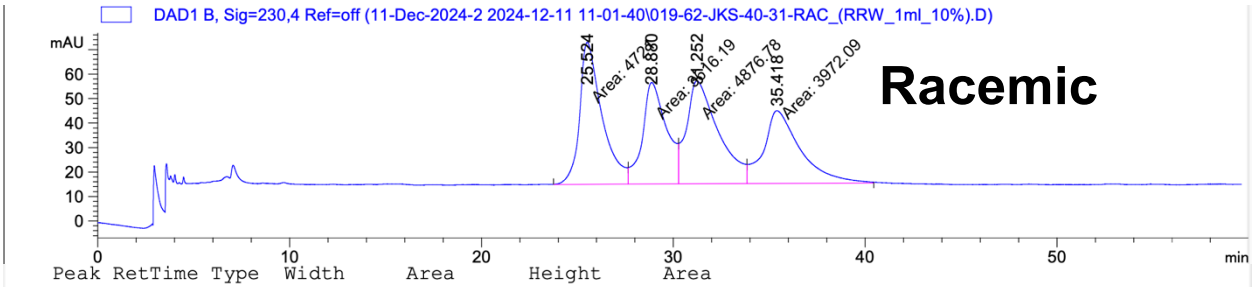

Peak #	RetTime [min]	Type	Width [min]	Area [mAU*s]	Height [mAU]	Area %
1	25.524	MF	1.3560	4721.00342	58.02432	27.4699
2	28.880	MF	1.4529	3616.19043	41.48373	21.0414
3	31.252	MF	1.9341	4876.78320	42.02508	28.3764
4	35.418	FM	2.2281	3972.08789	29.71251	23.1123
Totals :				1.71861e4	171.24564	

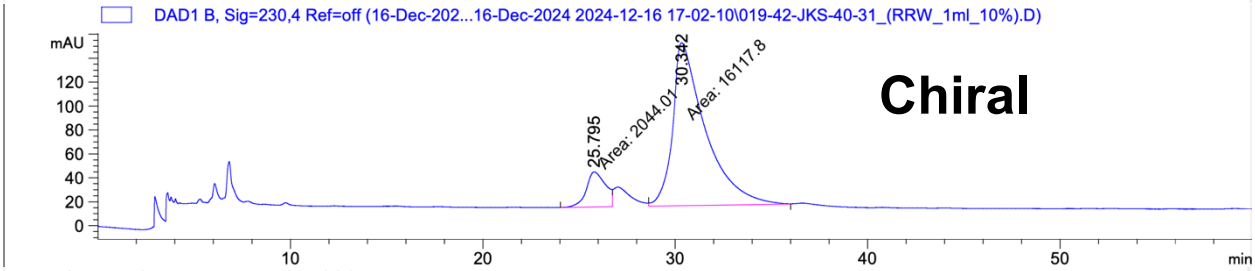

Signal 2: DAD1 B, Sig=230,4 Ref=off

Peak #	RetTime [min]	Type	Width [min]	Area [mAU*s]	Height [mAU]	Area %
1	25.795	MF	1.1652	2044.00745	29.23696	11.2544
2	30.342	FM	1.9708	1.61178e4	136.30537	88.7456
Totals :				1.81618e4	165.54234	

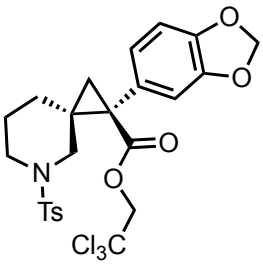

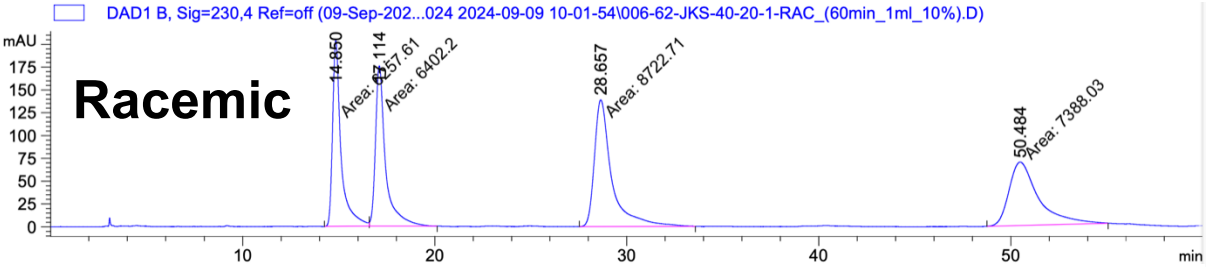

Signal 2: DAD1 B, Sig=230,4 Ref=off

Peak #	RetTime [min]	Type	Width [min]	Area [mAU*s]	Height [mAU]	Area %
1	14.850	MF	0.5124	6257.60889	203.52505	21.7500
2	17.114	FM	0.6071	6402.19727	175.76636	22.2526
3	28.657	MM	1.0460	8722.71484	138.98969	30.3182
4	50.484	MM	1.7739	7388.03027	69.41290	25.6791
Totals :				2.87706e4	587.69400	

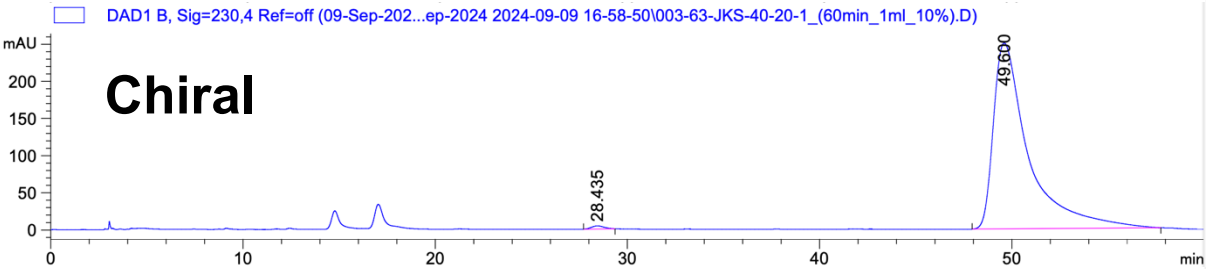

Signal 2: DAD1 B, Sig=230,4 Ref=off

Peak #	RetTime [min]	Type	Width [min]	Area [mAU*s]	Height [mAU]	Area %
1	28.435	BB	0.5279	186.83641	4.15263	0.5858
2	49.600	BB	1.4802	3.17083e4	250.16870	99.4142
Totals :				3.18951e4	254.32133	

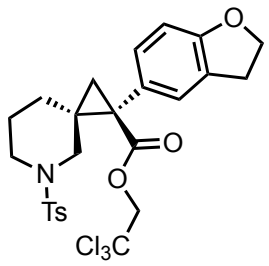

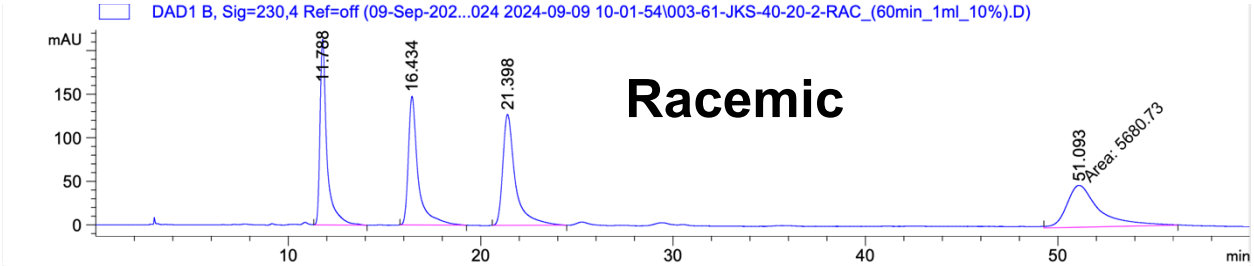

Signal 2: DAD1 B, Sig=230,4 Ref=off

Peak #	RetTime [min]	Type	Width [min]	Area [mAU*s]	Height [mAU]	Area %
1	11.788	BB	0.3573	5312.70117	212.81085	24.1626
2	16.434	BB	0.4837	5223.51416	147.66246	23.7569
3	21.398	BB	0.6140	5770.38525	127.26087	26.2441
4	51.093	MM	1.9687	5680.73047	48.09103	25.8364
Totals :				2.19873e4	535.82522	

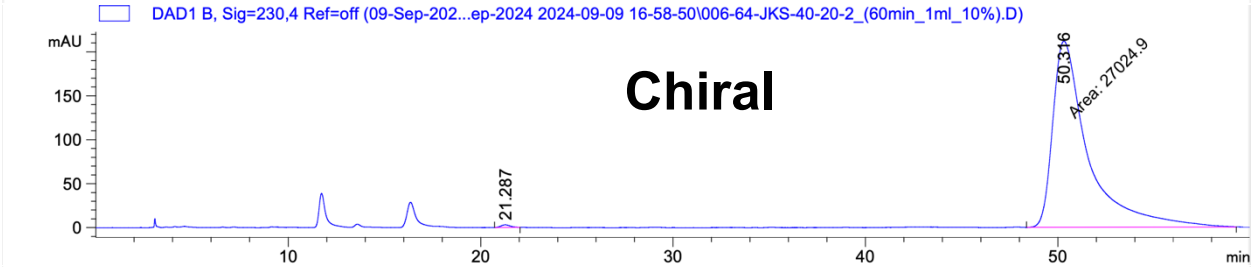

Signal 2: DAD1 B, Sig=230,4 Ref=off

Peak #	RetTime [min]	Type	Width [min]	Area [mAU*s]	Height [mAU]	Area %
1	21.287	BB	0.3950	100.09361	2.96406	0.3690
2	50.316	MM	2.1288	2.70249e4	211.58566	99.6310
Totals :				2.71250e4	214.54972	

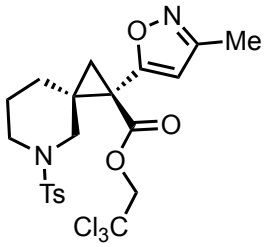

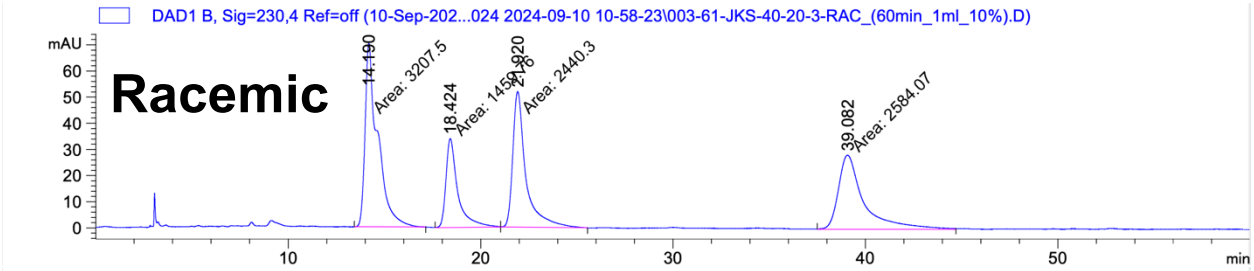

Signal 2: DAD1 B, Sig=230,4 Ref=off

Peak #	RetTime [min]	Type	Width [min]	Area [mAU*s]	Height [mAU]	Area %
1	14.190	MM	0.7616	3207.50220	70.19487	33.0956
2	18.424	MM	0.7152	1459.75647	34.01768	15.0620
3	21.920	MM	0.7842	2440.30127	51.86623	25.1795
4	39.082	MM	1.5211	2584.06812	28.31438	26.6629
Totals :				9691.62805	184.39316	

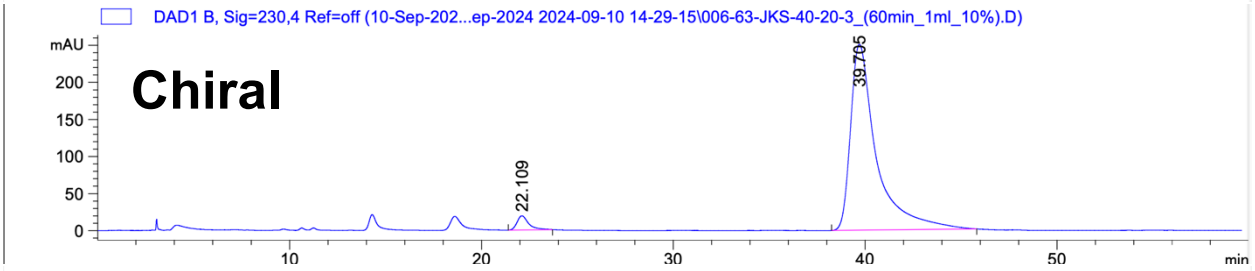

Signal 2: DAD1 B, Sig=230,4 Ref=off

Peak #	RetTime [min]	Type	Width [min]	Area [mAU*s]	Height [mAU]	Area %
1	22.109	BB	0.4918	801.14905	19.12359	3.2992
2	39.705	BB	1.0970	2.34818e4	250.76302	96.7008
Totals :				2.42829e4	269.88661	

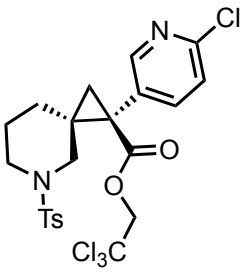

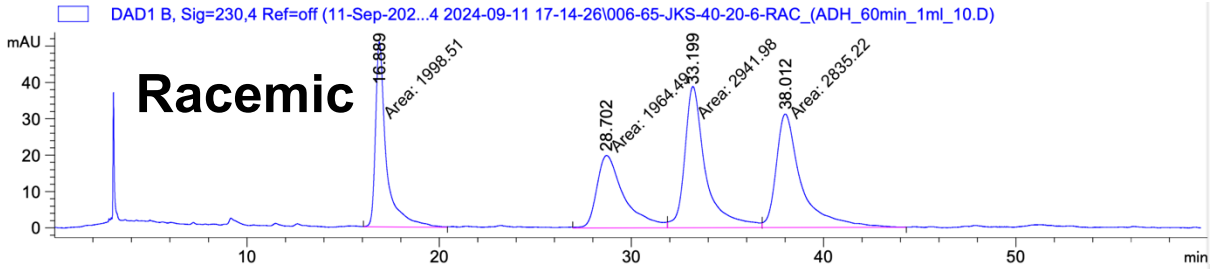

Signal 2: DAD1 B, Sig=230,4 Ref=off

Peak #	RetTime [min]	Type	Width [min]	Area [mAU*s]	Height [mAU]	Area %
1	16.889	MM	0.6540	1998.50598	50.92659	20.5181
2	28.702	MF	1.6441	1964.49316	19.91454	20.1689
3	33.199	MF	1.2619	2941.98315	38.85551	30.2045
4	38.012	FM	1.5153	2835.21680	31.18527	29.1084
Totals :				9740.19910	140.88191	

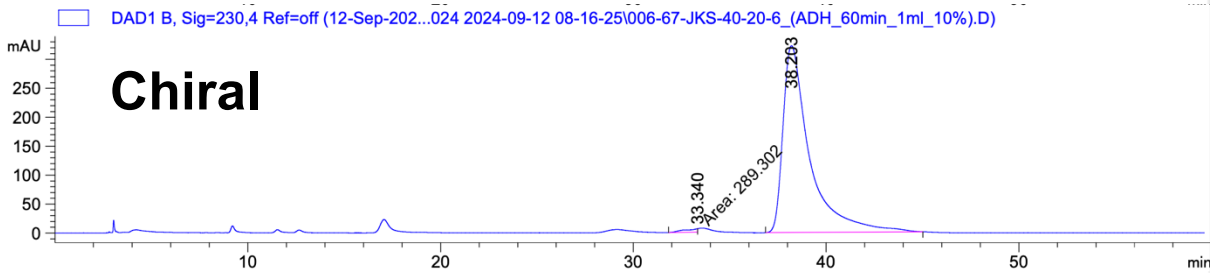

Signal 2: DAD1 B, Sig=230,4 Ref=off

Peak #	RetTime [min]	Type	Width [min]	Area [mAU*s]	Height [mAU]	Area %
1	33.340	MM	0.8001	289.30200	6.02654	0.9205
2	38.203	BB	1.1296	3.11380e4	322.58481	99.0795
Totals :				3.14273e4	328.61135	

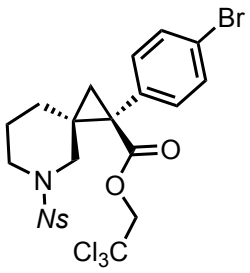
Br
O
O
N
Ns
Cl3C

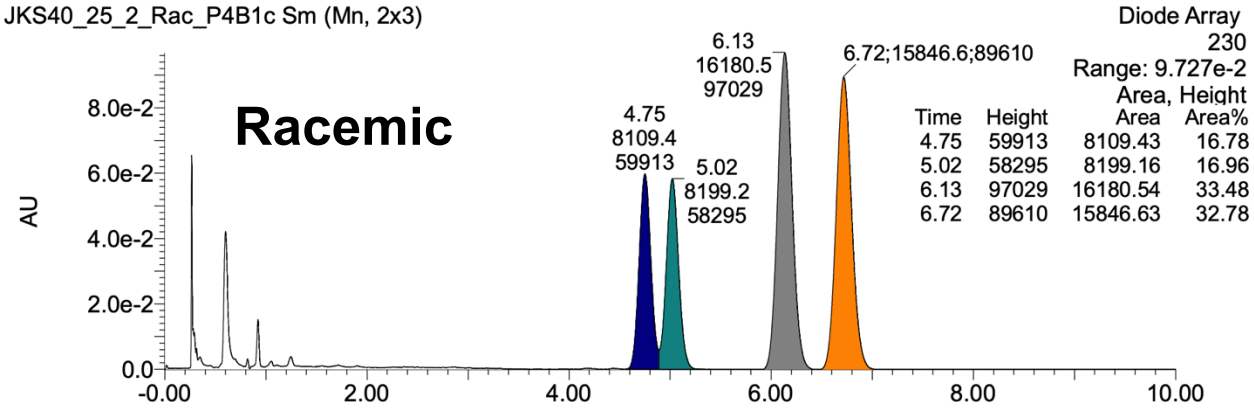
JKS40_25_2_Rac_P4B1c Sm (Mn, 2x3)
Diode Array
230
Range: 9.727e-2
Racemic
6.13
16180.5
97029
6.72;15846.6;89610
4.75
8109.4
59913
5.02
8199.2
58295
Area, Height
Time Height Area Area%
4.75 59913 8109.43 16.78
5.02 58295 8199.16 16.96
6.13 97029 16180.54 33.48
6.72 89610 15846.63 32.78
AU
8.0e-2
6.0e-2
4.0e-2
2.0e-2
0.0
-0.00
2.00
4.00
6.00
8.00
10.00

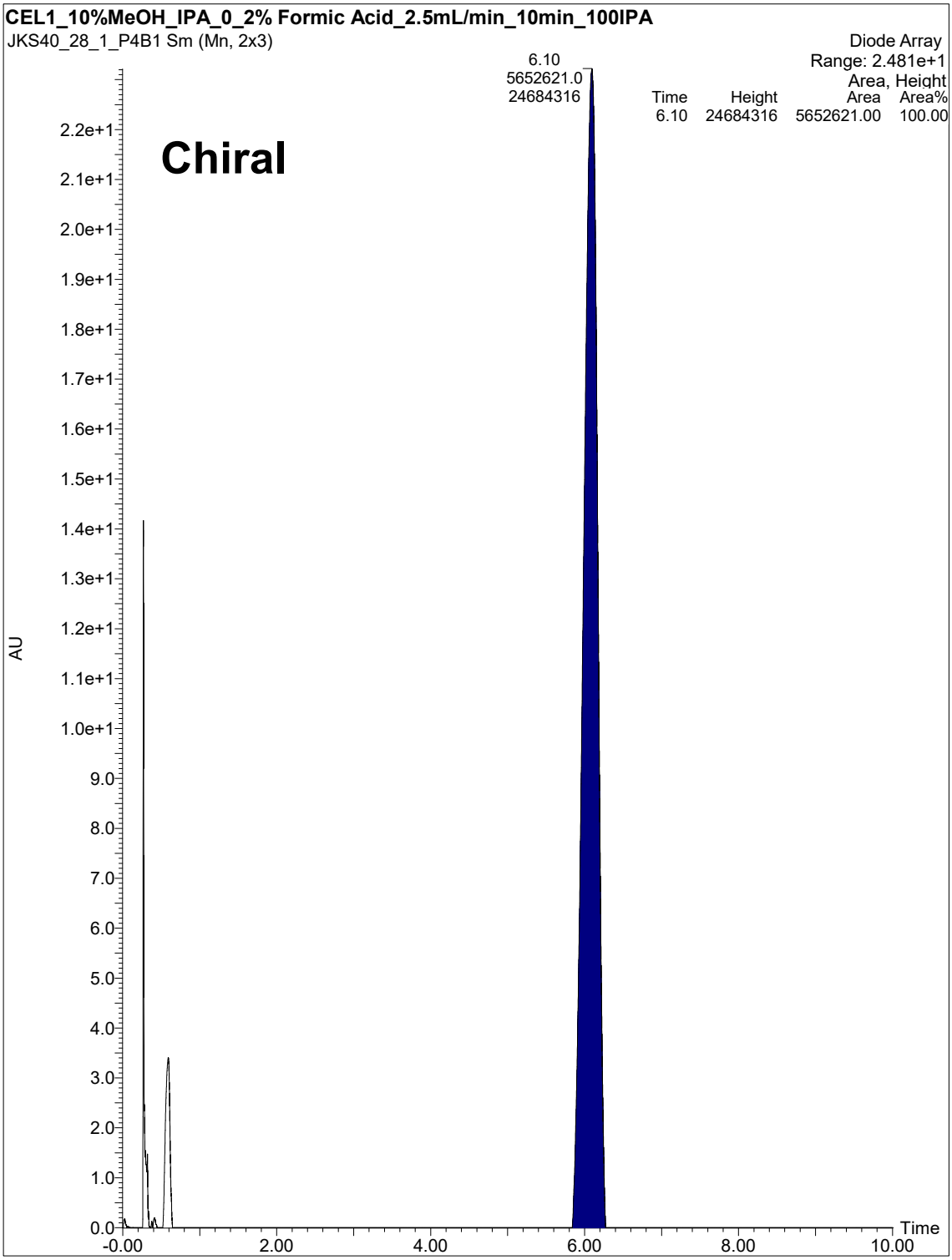
CEL1_10%MeOH_IPA_0_2% Formic Acid_2.5mL/min_10min_100IPA
JKS40_28_1_P4B1 Sm (Mn, 2x3)
Diode Array
Range: 2.481e+1
Area, Height
6.10
5652621.0
24684316
Time Height Area Area%
6.10 24684316 5652621.00 100.00
Chiral
AU
Time
2.2e+1
2.1e+1
2.0e+1
1.9e+1
1.8e+1
1.7e+1
1.6e+1
1.5e+1
1.4e+1
1.3e+1
1.2e+1
1.1e+1
1.0e+1
9.0
8.0
7.0
6.0
5.0
4.0
3.0
2.0
1.0
0.0
-0.00
2.00
4.00
6.00
8.00
10.00

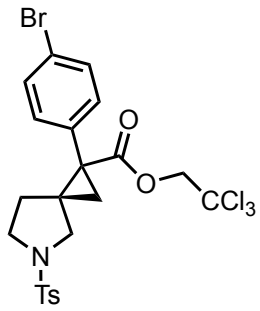
Br
O
O
CCl3
N
Ts

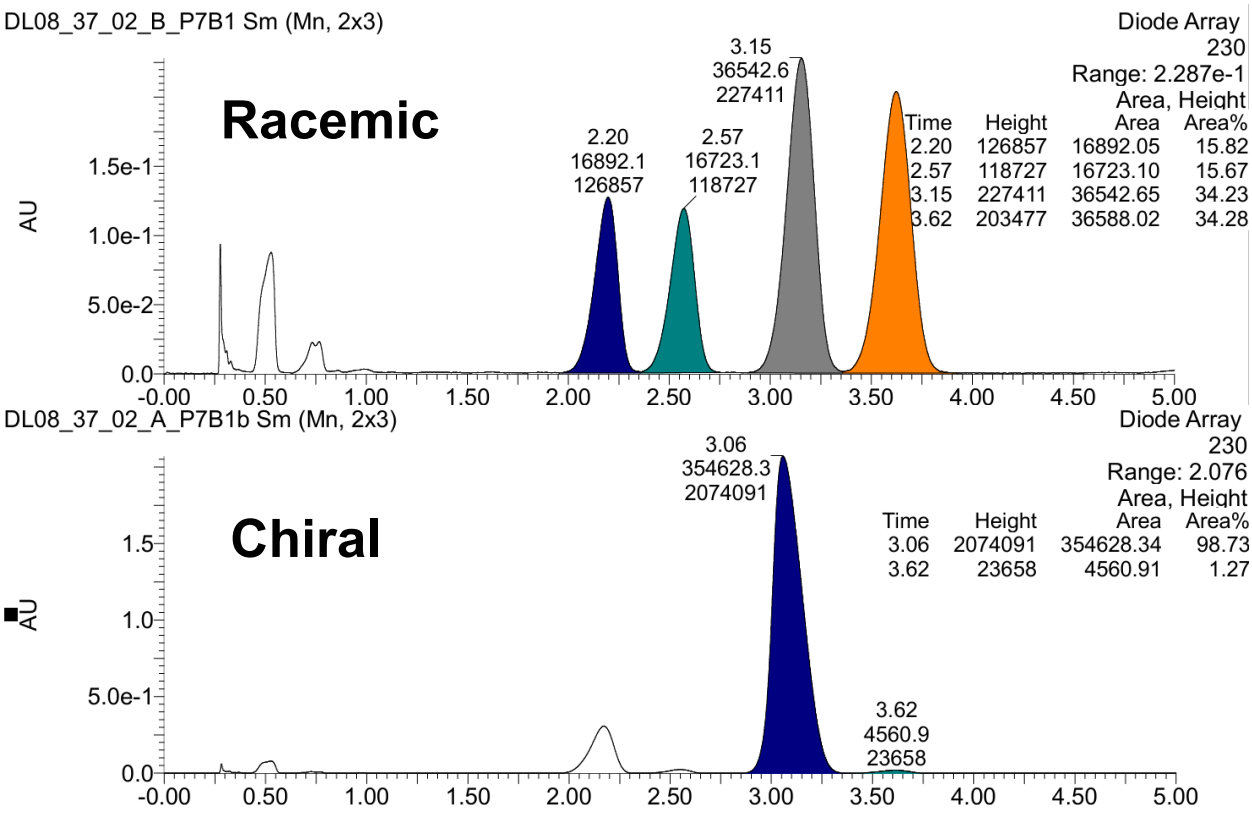
DL08_37_02_B_P7B1 Sm (Mn, 2x3)
Diode Array
230
Range: 2.287e-1
Area, Height
Racemic
3.15
36542.6
227411
2.20
16892.1
126857
2.57
16723.1
118727
Time Height Area Area%
2.20 126857 16892.05 15.82
2.57 118727 16723.10 15.67
3.15 227411 36542.65 34.23
3.62 203477 36588.02 34.28
AU
1.5e-1
1.0e-1
5.0e-2
0.0
-0.00 0.50 1.00 1.50 2.00 2.50 3.00 3.50 4.00 4.50 5.00

DL08_37_02_A_P7B1b Sm (Mn, 2x3)
Diode Array
230
Range: 2.076
Area, Height
Chiral
3.06
354628.3
2074091
3.62
4560.9
23658
Time Height Area Area%
3.06 2074091 354628.34 98.73
3.62 23658 4560.91 1.27
AU
1.5
1.0
5.0e-1
0.0
-0.00 0.50 1.00 1.50 2.00 2.50 3.00 3.50 4.00 4.50 5.00

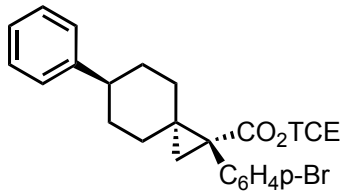
CO_2TCE
C_6H_4p-Br

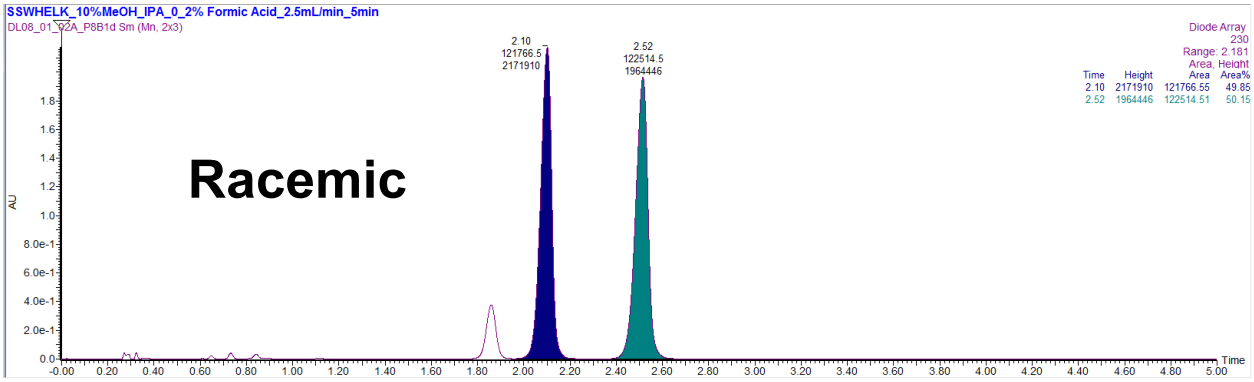
SSWHELK_10%MeOH_IPA_0_2% Formic Acid_2.5mL/min_5min
DL08_01_02A_P8B1d Sm (Mn, 2x3)
Racemic
2.10
121766.5
2171910
2.52
122514.5
1964446
Diode Array
230
Range: 2.181
Area, Height
Time Height Area Area%
2.10 2171910 121766.55 49.85
2.52 1964446 122514.51 50.15
AU
Time

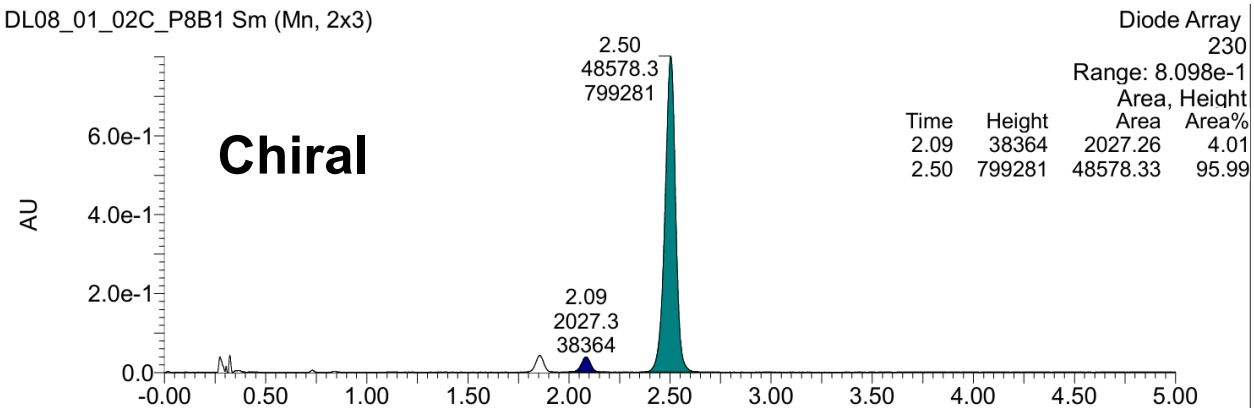
DL08_01_02C_P8B1 Sm (Mn, 2x3)
Chiral
2.50
48578.3
799281
2.09
2027.3
38364
Diode Array
230
Range: 8.098e-1
Area, Height
Time Height Area Area%
2.09 38364 2027.26 4.01
2.50 799281 48578.33 95.99
AU

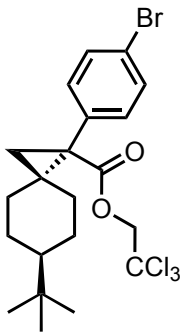

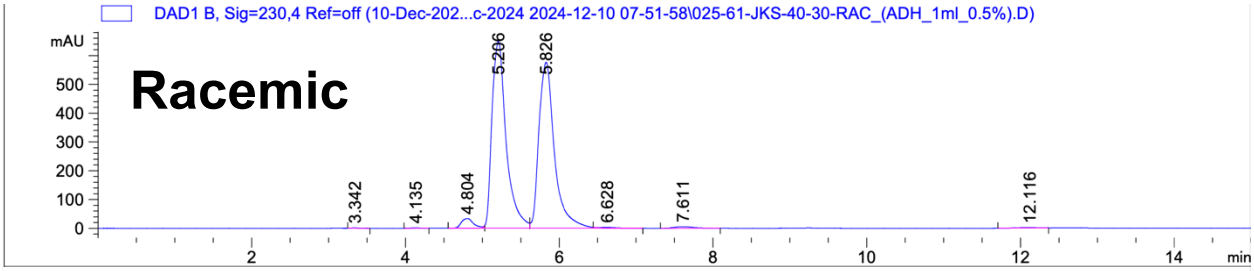

Signal 2: DAD1 B, Sig=230,4 Ref=off

Peak #	RetTime [min]	Type	Width [min]	Area [mAU*s]	Height [mAU]	Area %
1	3.342	BB	0.0842	7.88460	1.13971	0.0466
2	4.135	BB	0.1067	11.83894	1.33835	0.0699
3	4.804	BV E	0.1679	362.02682	33.55718	2.1375
4	5.206	VV R	0.1983	8304.85938	649.17322	49.0345
5	5.826	VV R	0.2181	8087.47852	576.72919	47.7510
6	6.628	VB E	0.1796	37.27687	2.45561	0.2201
7	7.611	BB	0.2088	94.15876	5.35126	0.5559
8	12.116	BB	0.2563	31.23736	1.44143	0.1844
Totals :				1.69368e4	1271.18596	

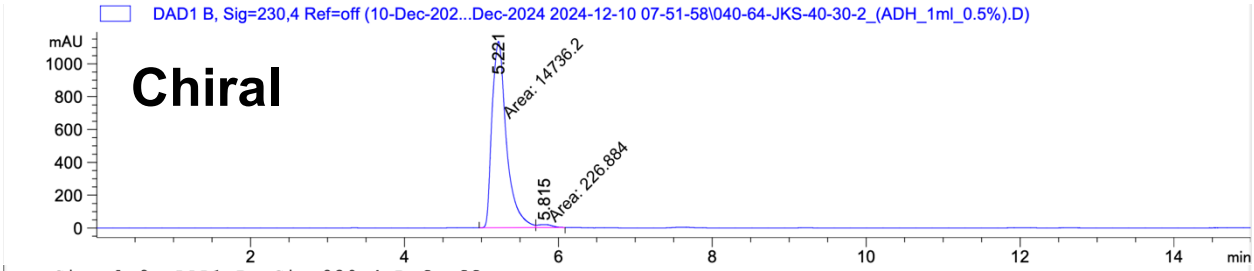

Signal 2: DAD1 B, Sig=230,4 Ref=off

Peak #	RetTime [min]	Type	Width [min]	Area [mAU*s]	Height [mAU]	Area %
1	5.221	MF	0.2164	1.47362e4	1135.07288	98.4837
2	5.815	FM	0.2159	226.88441	17.51468	1.5163
Totals :				1.49631e4	1152.58755	

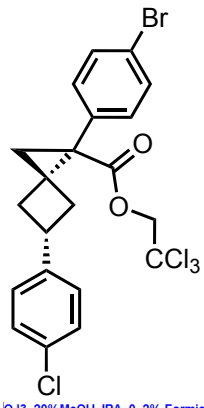
Br
O
O
CCl3
Cl

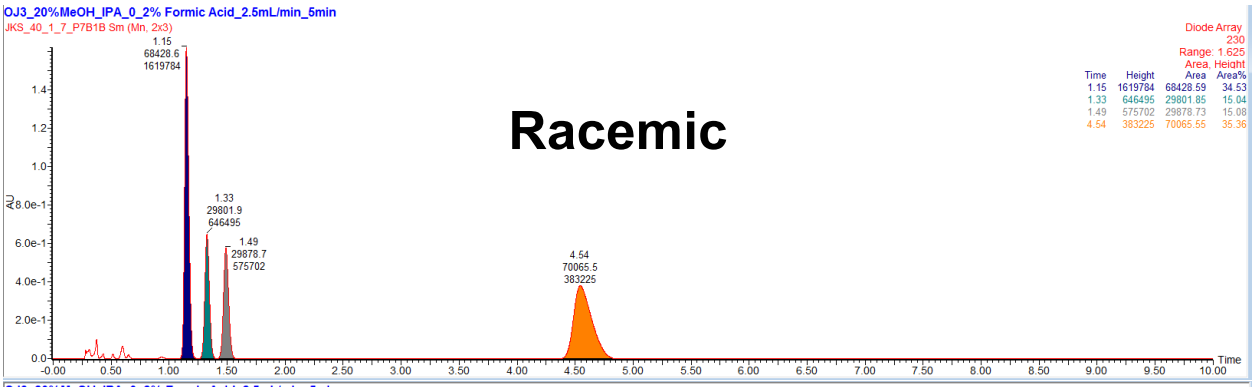
OJ3_20%MeOH_IPA_0_2% Formic Acid_2.5mL/min_5min
JKS_40_1_7_P7B1B Sm (Mn, 2x3)
Racemic
1.15
68428.6
1619784
1.33
29801.9
646495
1.49
29878.7
575702
4.54
70065.5
383225
Diode Array
230
Range: 1.625
Area, Height
Time Height Area Area%
1.15 1619784 68428.59 34.53
1.33 646495 29801.85 15.04
1.49 575702 29878.73 15.08
4.54 383225 70065.55 35.36
AU
Time

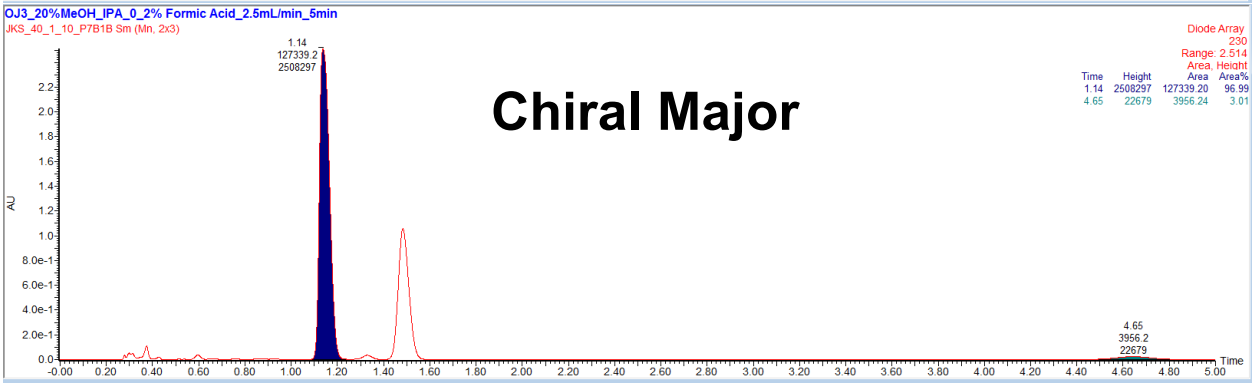
OJ3_20%MeOH_IPA_0_2% Formic Acid_2.5mL/min_5min
JKS_40_1_10_P7B1B Sm (Mn, 2x3)
Chiral Major
1.14
127339.2
2508297
4.65
3956.2
22679
Diode Array
230
Range: 2.514
Area, Height
Time Height Area Area%
1.14 2508297 127339.20 96.99
4.65 22679 3956.24 3.01
AU
Time

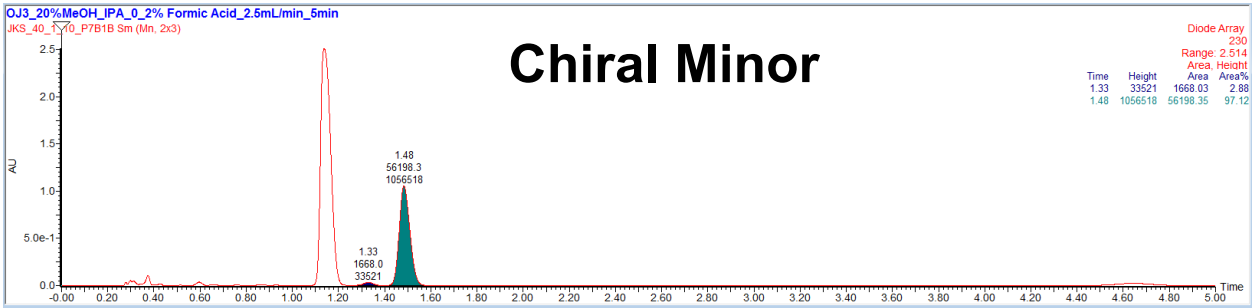
OJ3_20%MeOH_IPA_0_2% Formic Acid_2.5mL/min_5min
JKS_40_1_10_P7B1B Sm (Mn, 2x3)
Chiral Minor
1.48
56198.3
1056518
1.33
1668.0
33521
Diode Array
230
Range: 2.514
Area, Height
Time Height Area Area%
1.33 33521 1668.03 2.88
1.48 1056518 56198.35 97.12
AU
Time

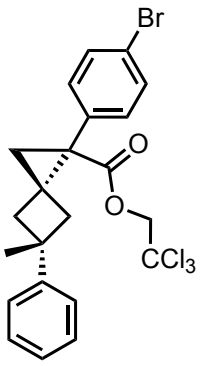

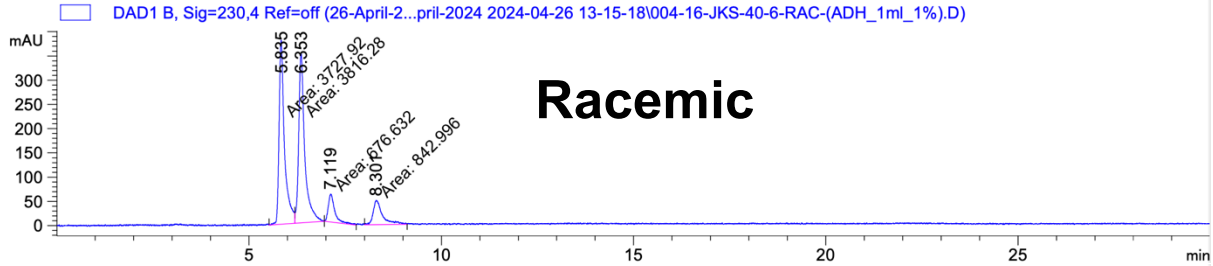

Signal 2: DAD1 B, Sig=230,4 Ref=off

Peak #	RetTime [min]	Type	Width [min]	Area [mAU*s]	Height [mAU]	Area %
1	5.835	MF	0.1637	3727.92236	379.45377	41.1297
2	6.353	FM	0.1825	3816.28076	348.45789	42.1045
3	7.119	MM	0.1944	676.63159	57.99733	7.4652
4	8.301	MM	0.2825	842.99554	49.73677	9.3007
Totals :				9063.83026	835.64576	

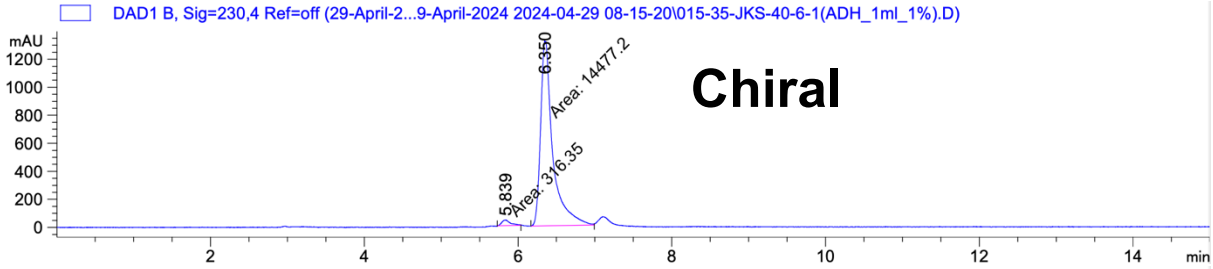

Signal 2: DAD1 B, Sig=230,4 Ref=off

Peak #	RetTime [min]	Type	Width [min]	Area [mAU*s]	Height [mAU]	Area %
1	5.839	MM	0.1314	316.35037	40.12105	2.1384
2	6.350	MM	0.1826	1.44772e4	1321.03687	97.8616
Totals :				1.47936e4	1361.15792	

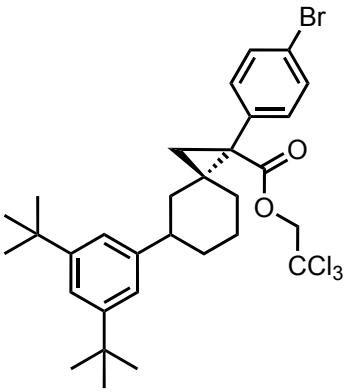

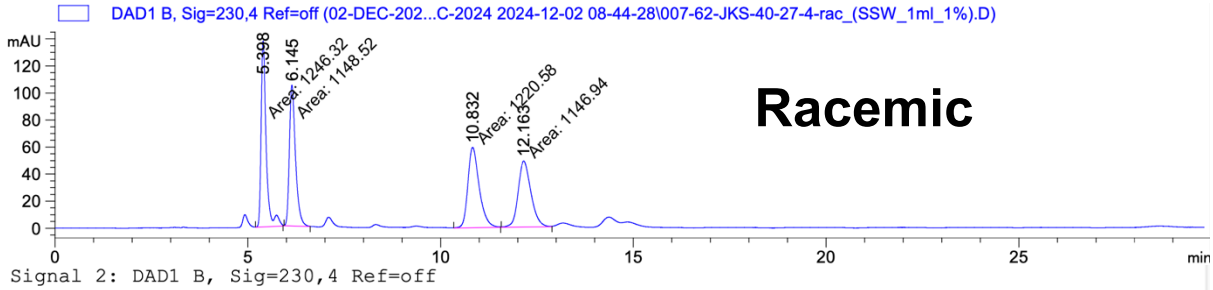

Signal 2: DAD1 B, Sig=230,4 Ref=off

Peak #	RetTime [min]	Type	Width [min]	Area [mAU*s]	Height [mAU]	Area %
1	5.398	MM	0.1512	1246.32227	137.41602	26.1702
2	6.145	MM	0.1836	1148.52039	104.23109	24.1166
3	10.832	MM	0.3421	1220.57971	59.46639	25.6297
4	12.163	MM	0.3910	1146.94080	48.88954	24.0834
Totals :				4762.36316	350.00304	

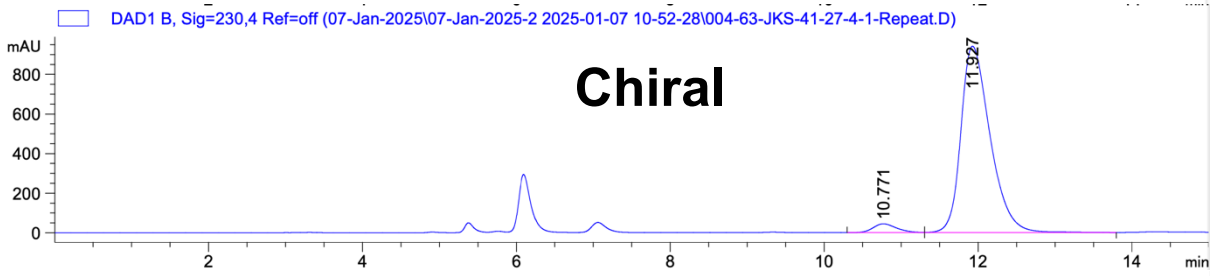

Signal 2: DAD1 B, Sig=230,4 Ref=off

Peak #	RetTime [min]	Type	Width [min]	Area [mAU*s]	Height [mAU]	Area %
1	10.771	BV	0.2829	948.20013	44.36388	3.6768
2	11.927	VB	0.3759	2.48403e4	941.16705	96.3232
Totals :				2.57885e4	985.53093	

NMR of Novel Compounds

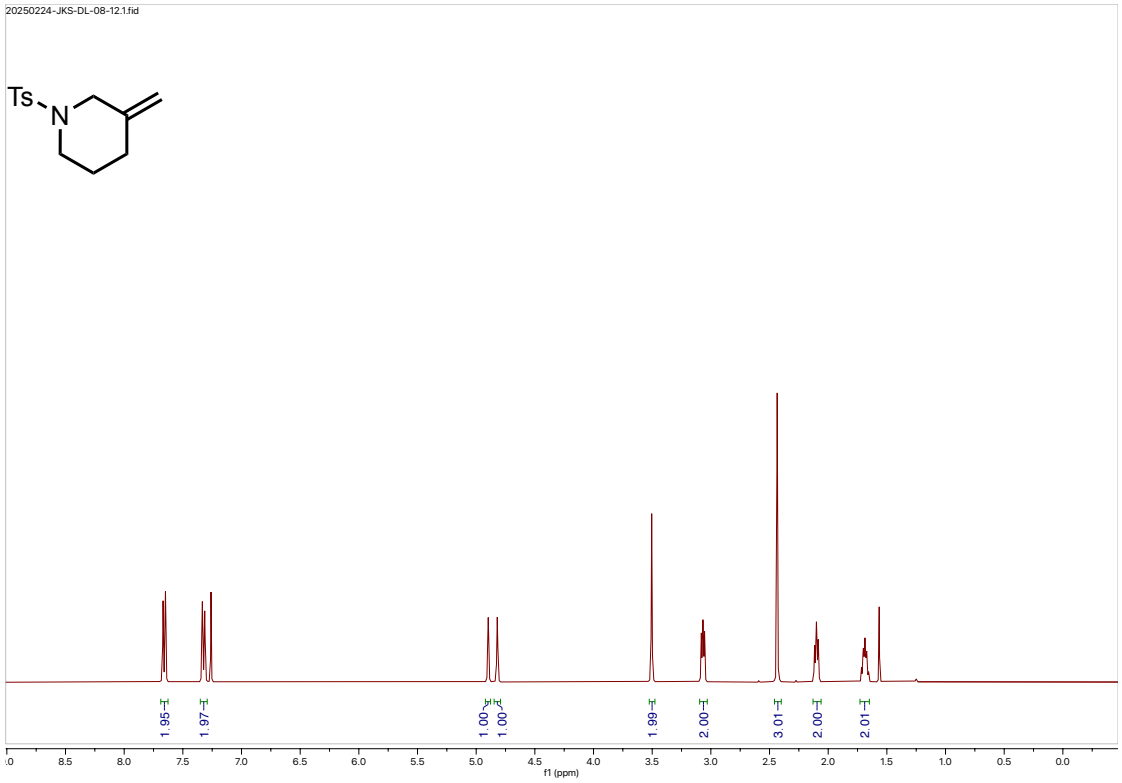

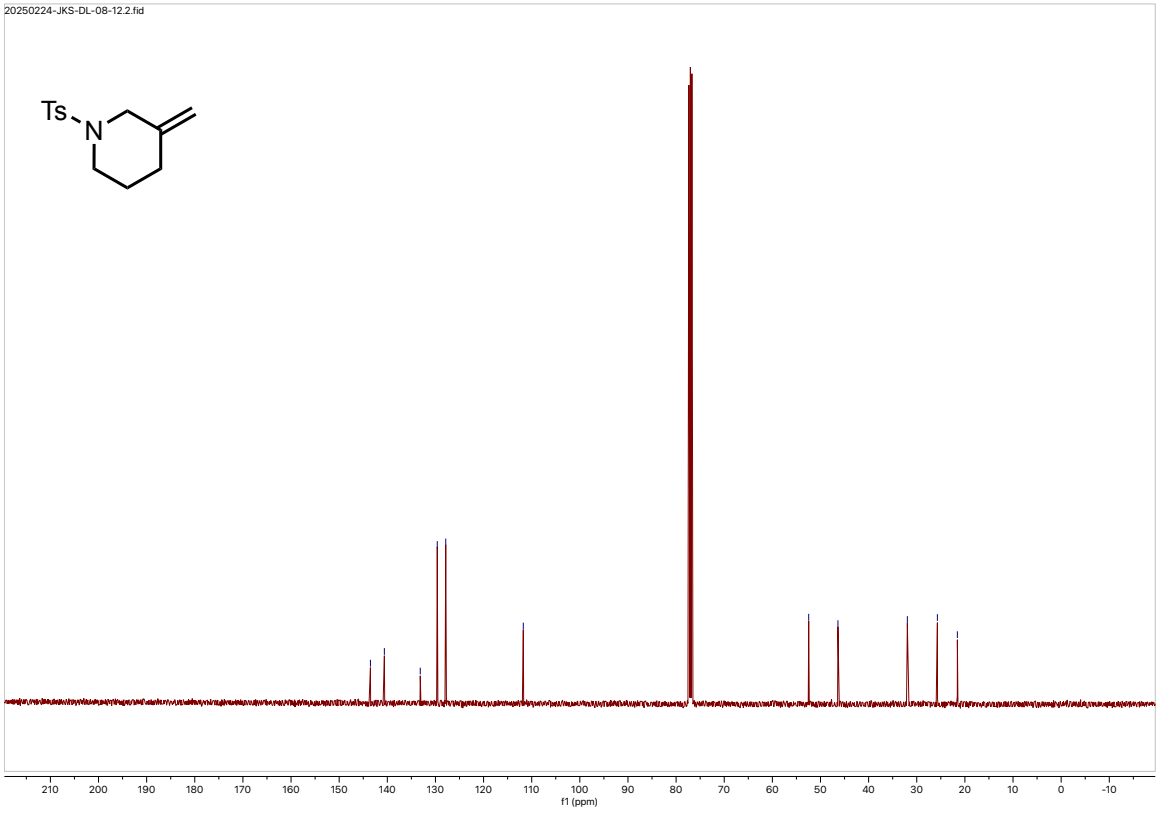

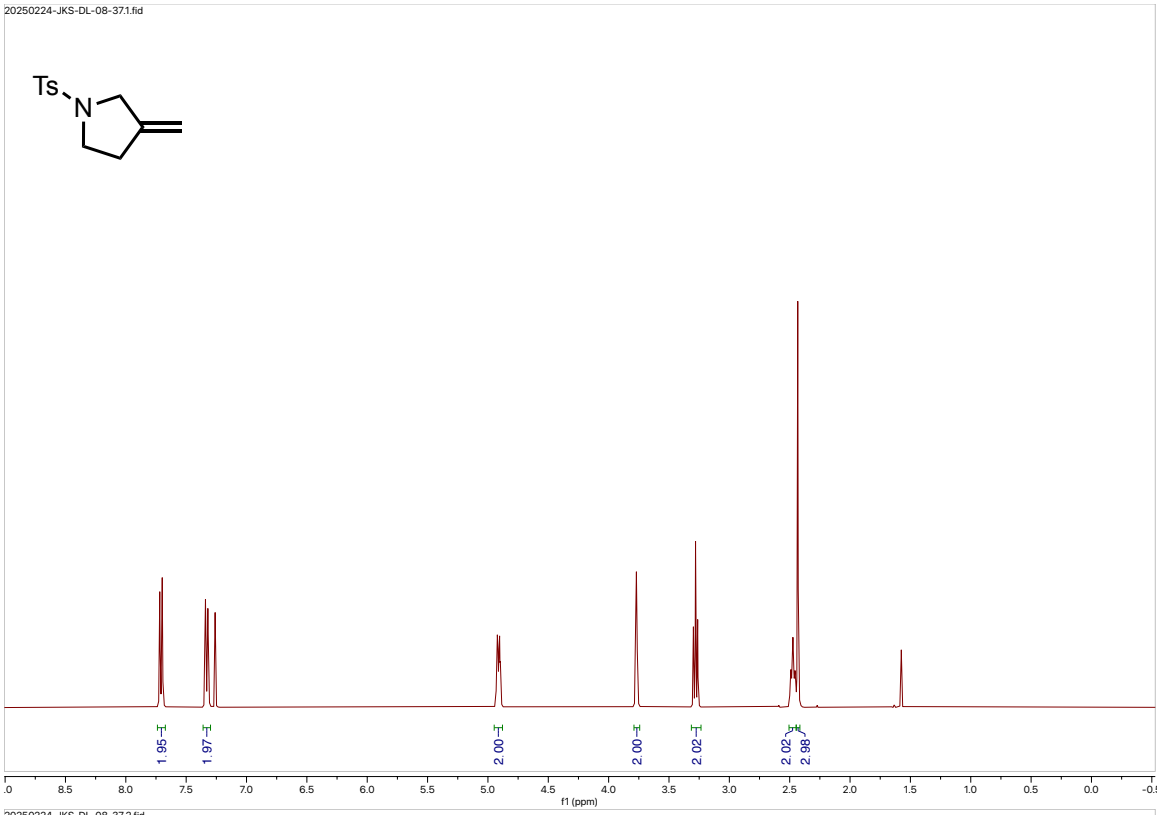
20250224-JKS-DL-08-37.1.fid
Ts
N
1.95
1.97
2.00
2.00
2.02
2.02
2.98
f1 (ppm)

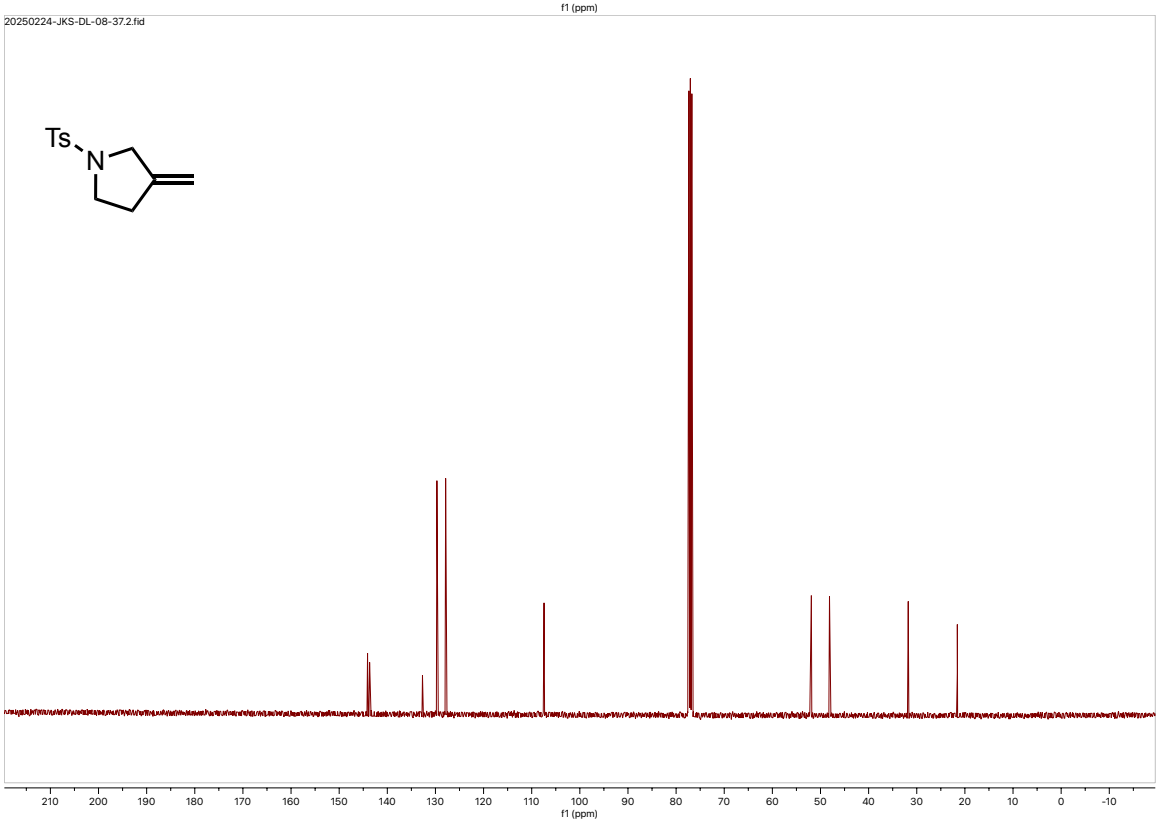
20250224-JKS-DL-08-37.2.fid
Ts
N
f1 (ppm)

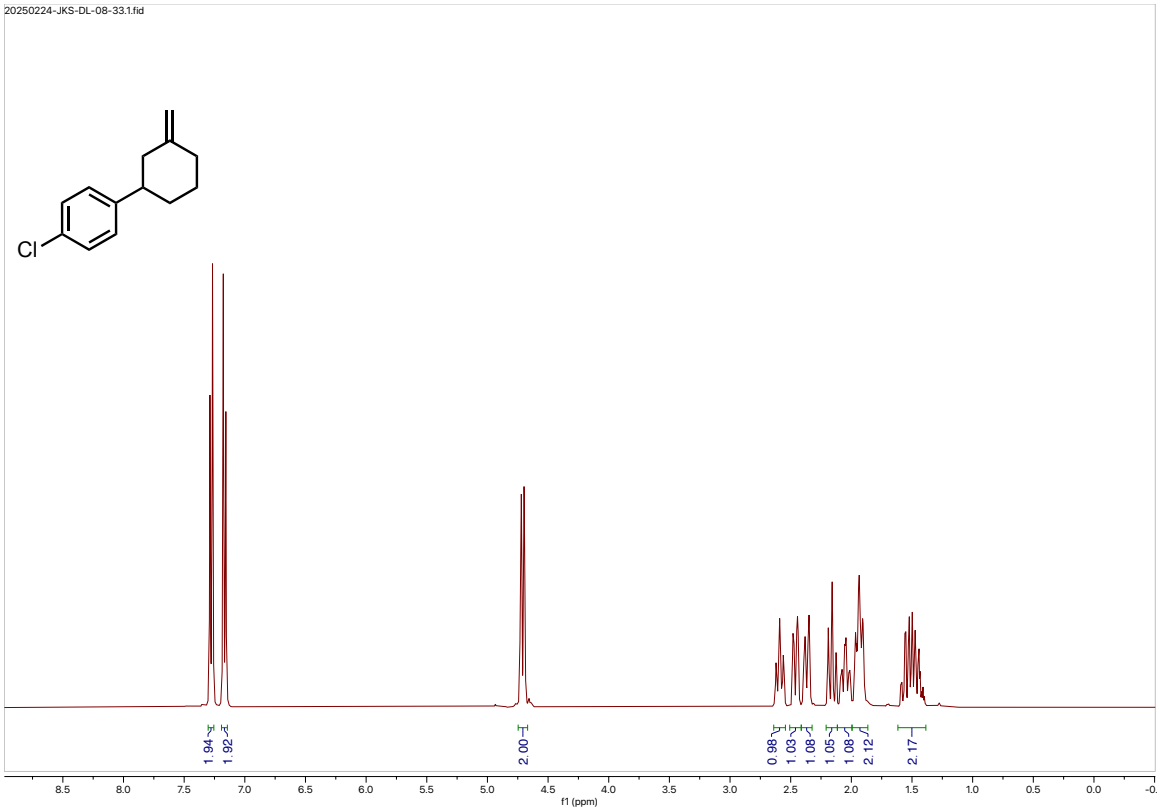
20250224-JKS-DL-08-33.1.fid
Cl
1.94
1.92
2.00
0.98
1.03
1.08
1.05
1.08
2.12
2.17
8.5 8.0 7.5 7.0 6.5 6.0 5.5 5.0 4.5 4.0 3.5 3.0 2.5 2.0 1.5 1.0 0.5 0.0
f1 (ppm)

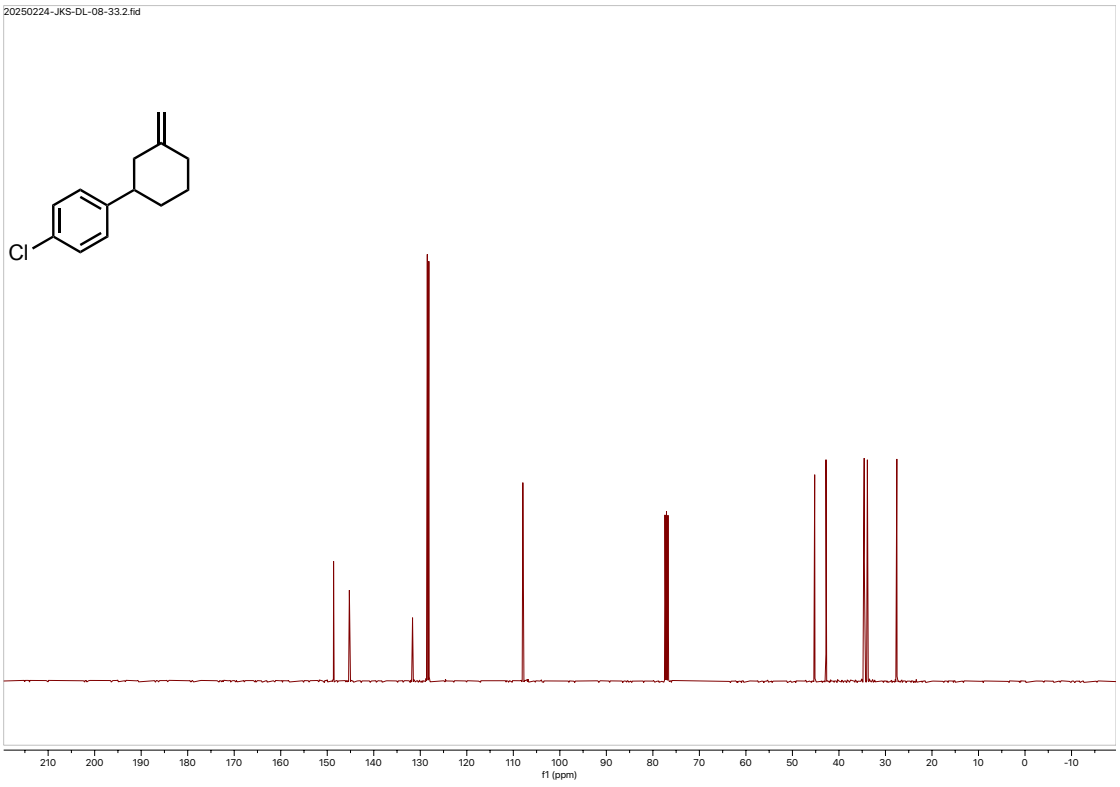
20250224-JKS-DL-08-33.2.fid
Cl
210 200 190 180 170 160 150 140 130 120 110 100 90 80 70 60 50 40 30 20 10 0 -10
f1 (ppm)

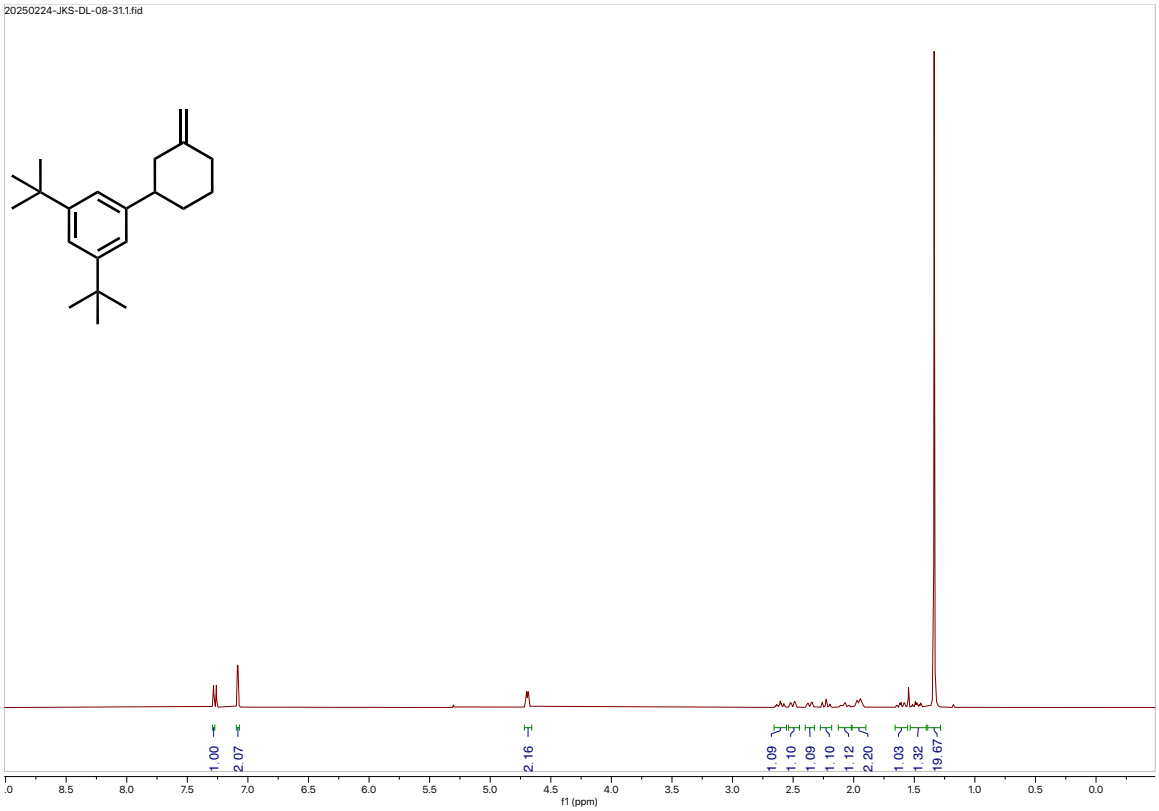
20250224-JKS-DL-08-31.1.fid
1.00
2.07
2.16
1.09
1.10
1.09
1.10
1.12
2.20
1.03
1.32
19.67
f1 (ppm)

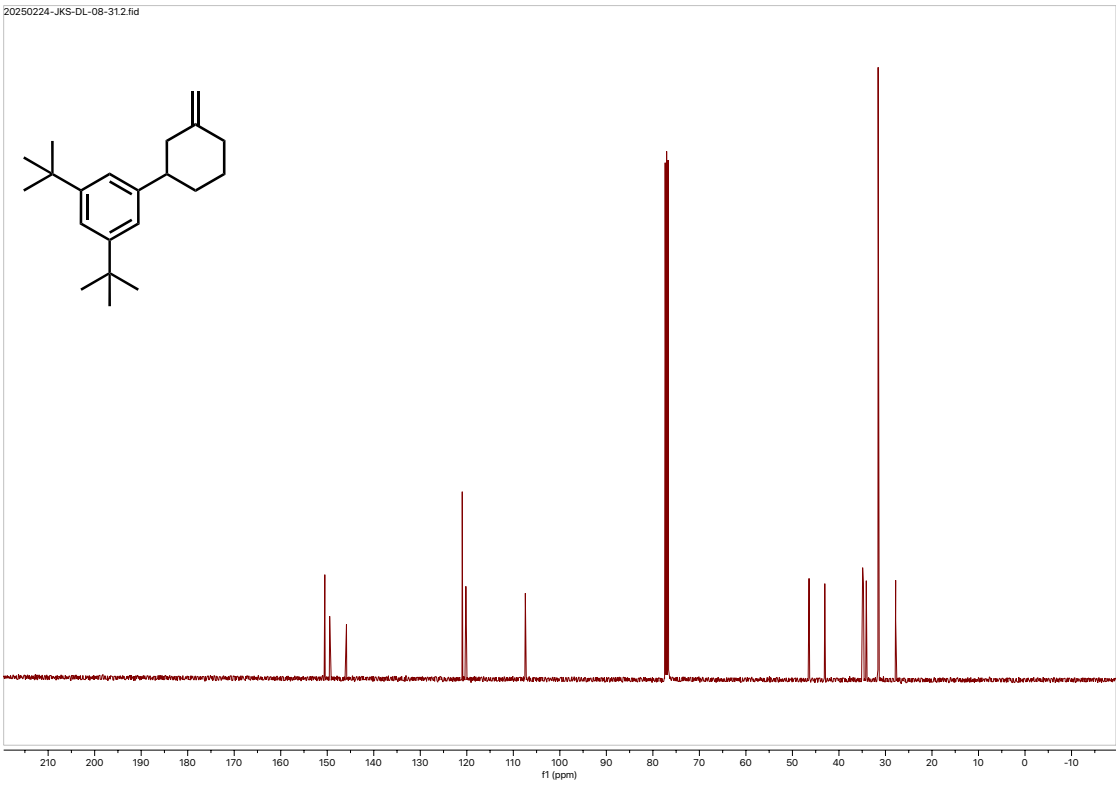
20250224-JKS-DL-08-31.2.fid
f1 (ppm)

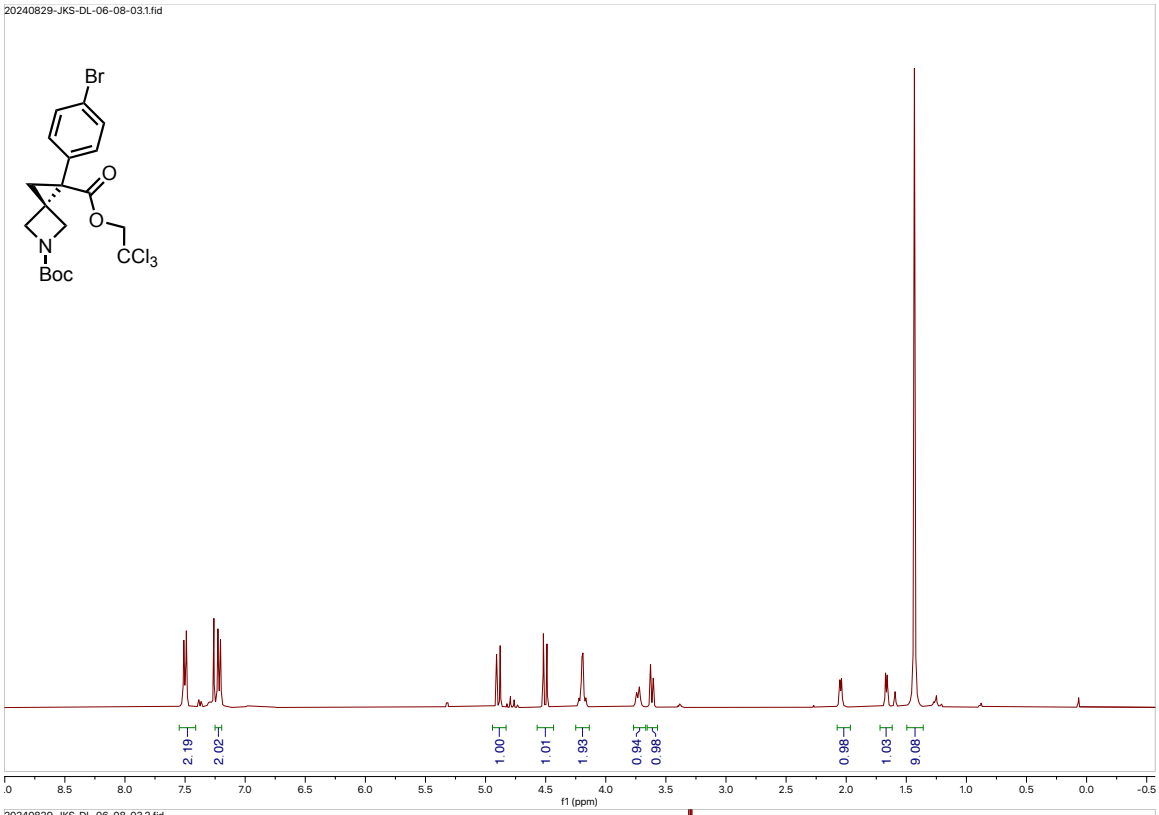
20240829-JKS-DL-06-08-03.1.fid
Br
O
O
N
Boc
CCl3
2.19
2.02
1.00
1.01
1.93
0.94
0.98
0.98
1.03
9.08
f1 (ppm)

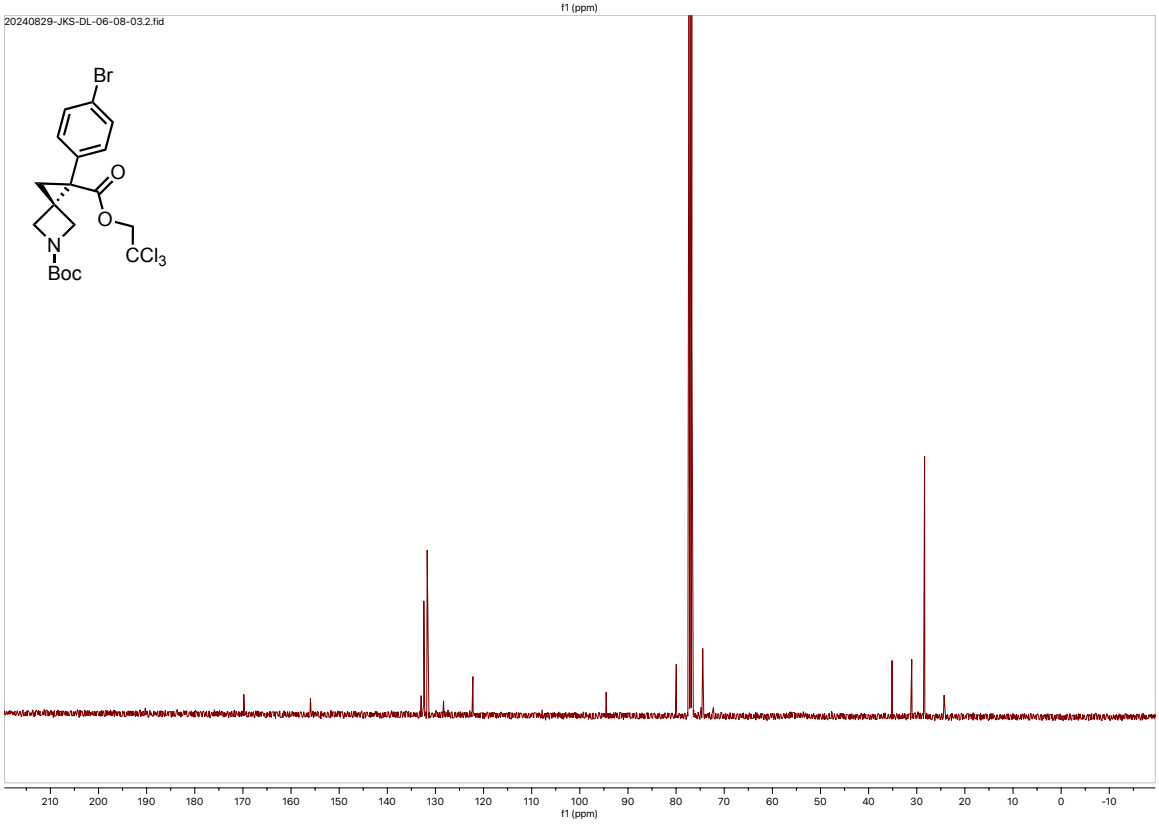
20240829-JKS-DL-06-08-03.2.fid
Br
O
O
N
Boc
CCl3
f1 (ppm)

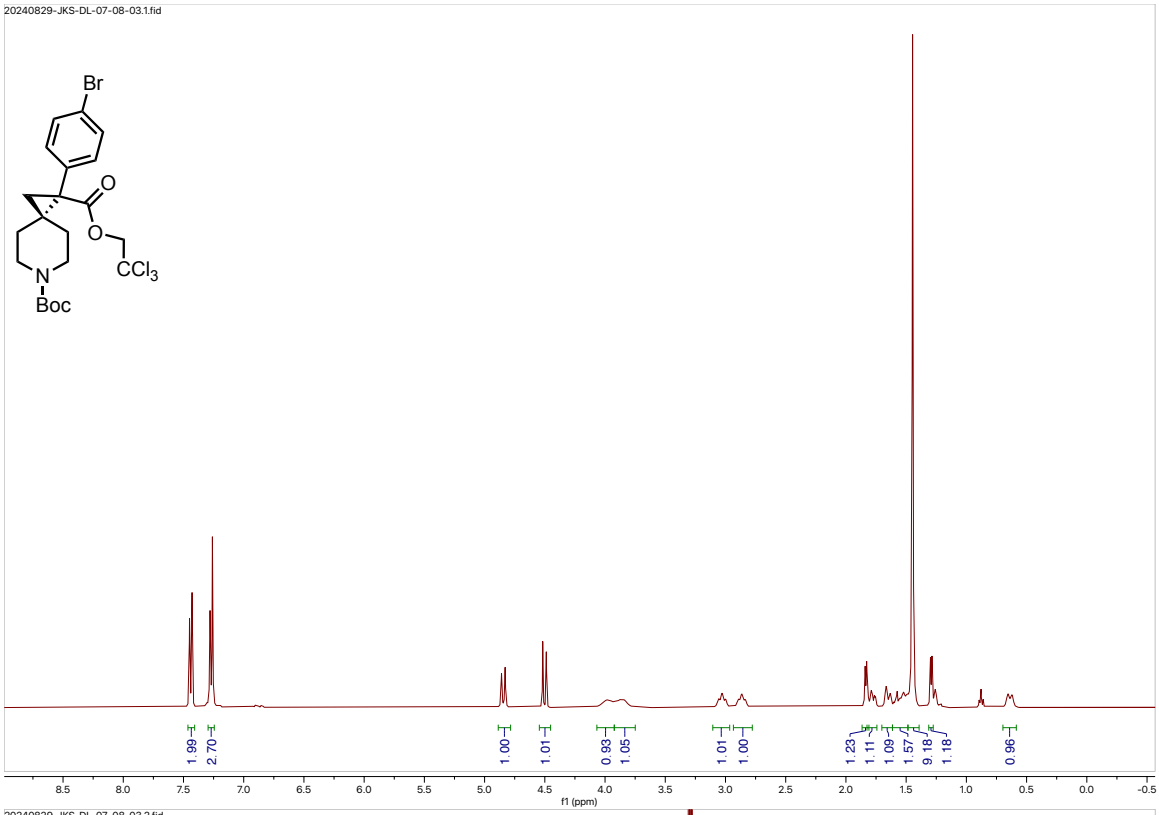
20240829-JKS-DL-07-08-03.1.fid
Br
O
O
CCl3
N
Boc
1.99
2.70
1.00
1.01
0.93
1.05
1.01
1.00
1.23
1.11
1.09
1.57
9.18
1.18
0.96
f1 (ppm)

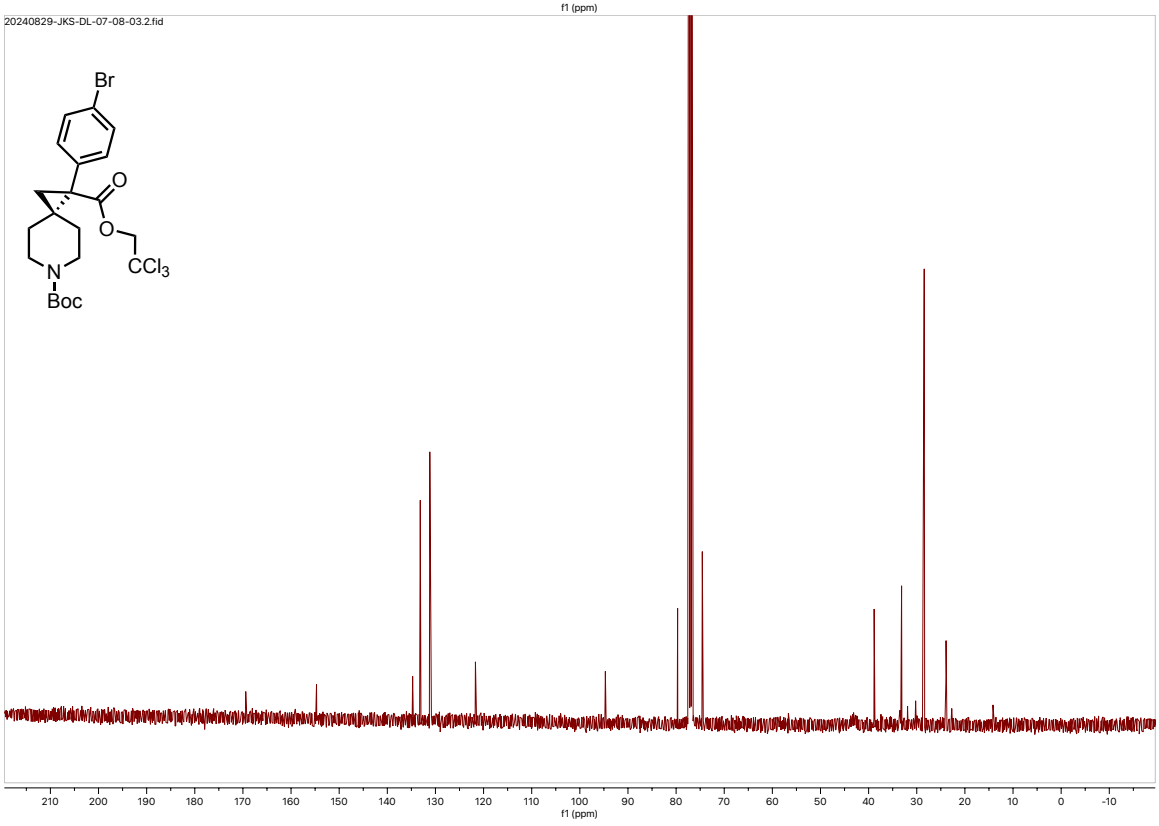
20240829-JKS-DL-07-08-03.2.fid
Br
O
O
CCl3
N
Boc
f1 (ppm)

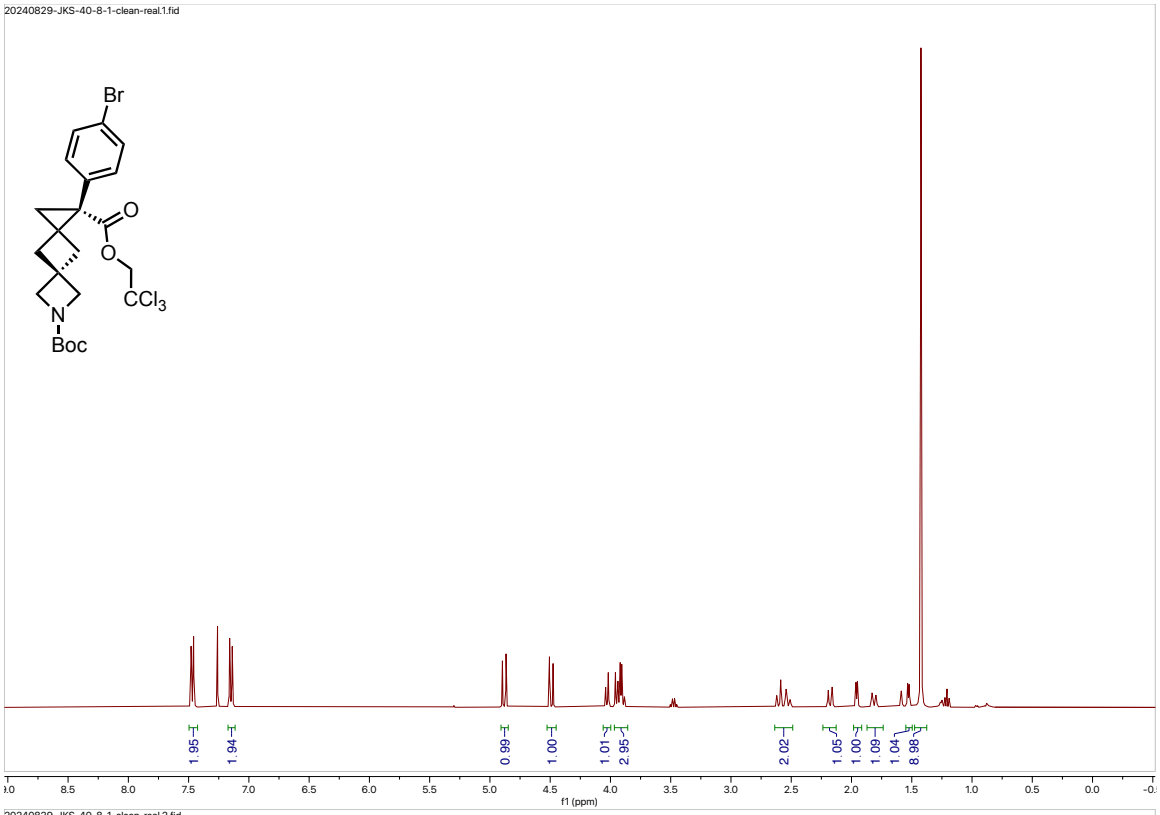
20240829-JKS-40-8-1-clean-real.1.fid
Br
O
O
CCl3
N
Boc
1.95
1.94
0.99
1.00
1.01
2.95
2.02
1.05
1.00
1.09
1.04
8.98
f1 (ppm)

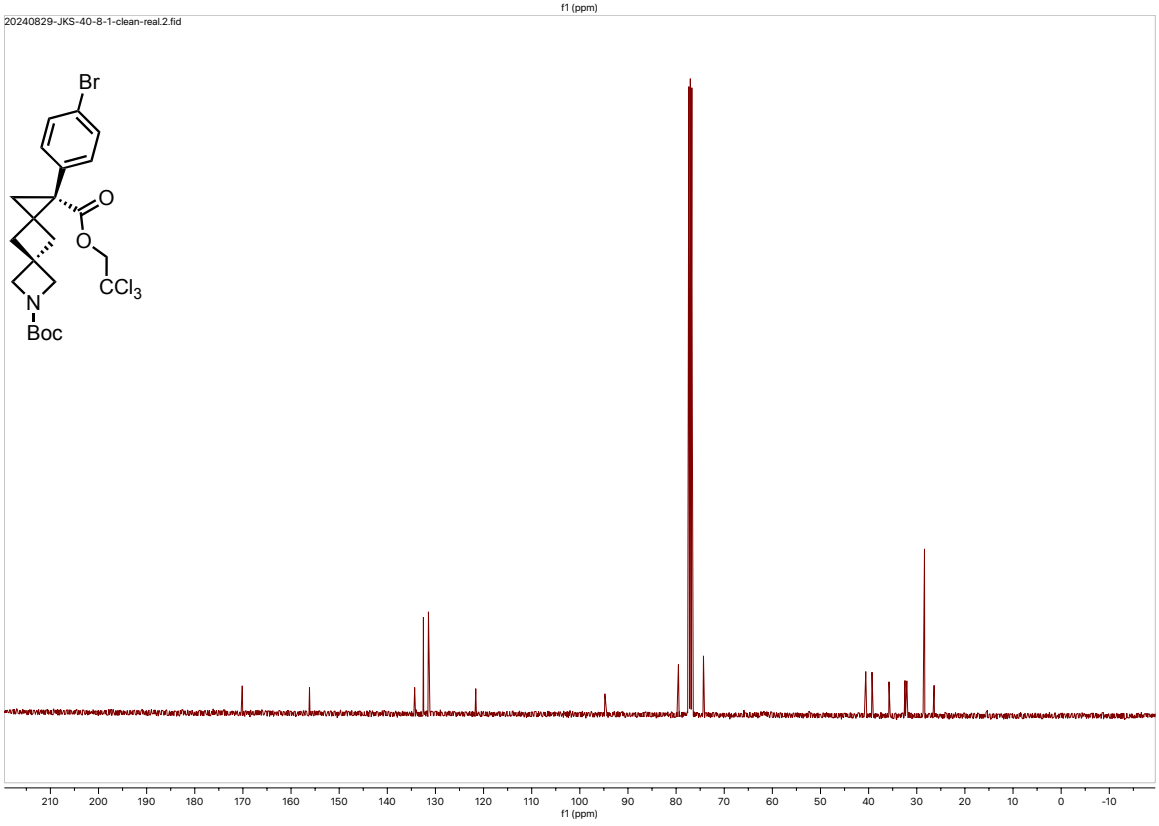
20240829-JKS-40-8-1-clean-real.2.fid
Br
O
O
CCl3
N
Boc
f1 (ppm)

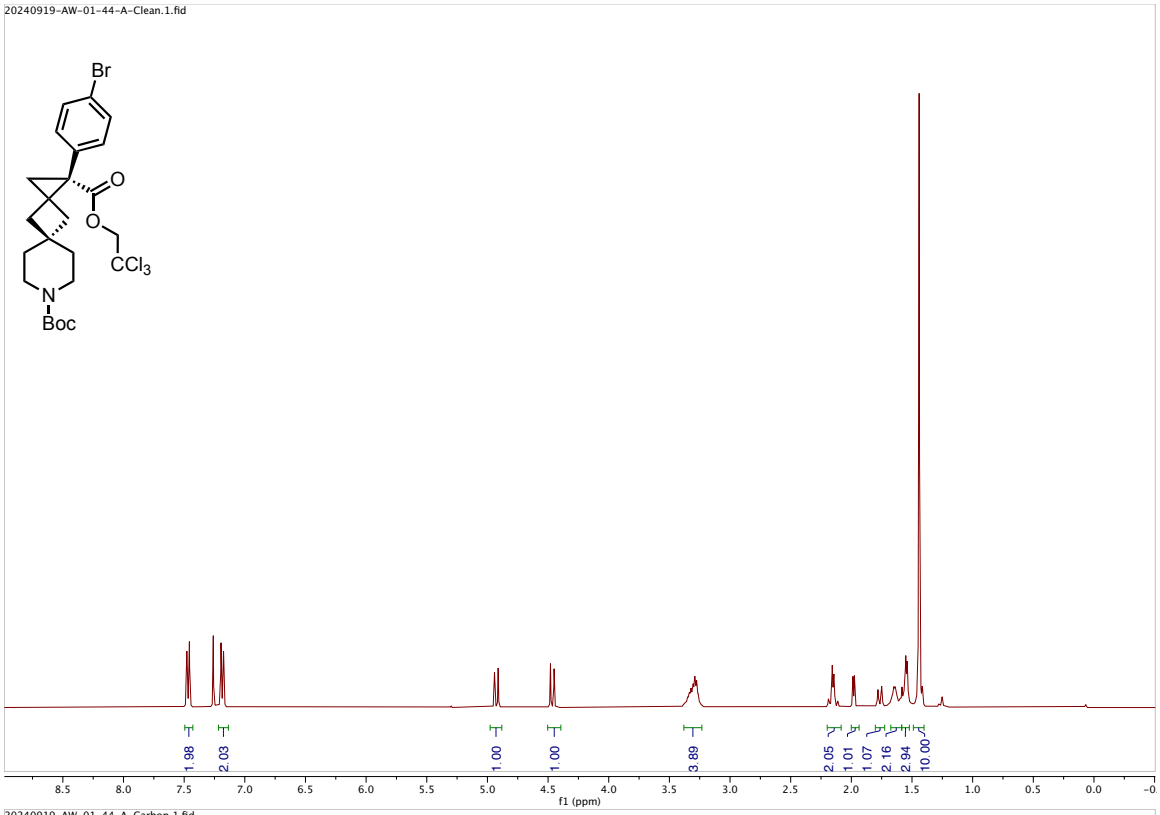
20240919-AW-01-44-A-Clean.1.fid
Br
O
O
CCl3
N
Boc
1.98
2.03
1.00
1.00
3.89
2.05
1.01
1.07
2.16
2.94
10.00
f1 (ppm)

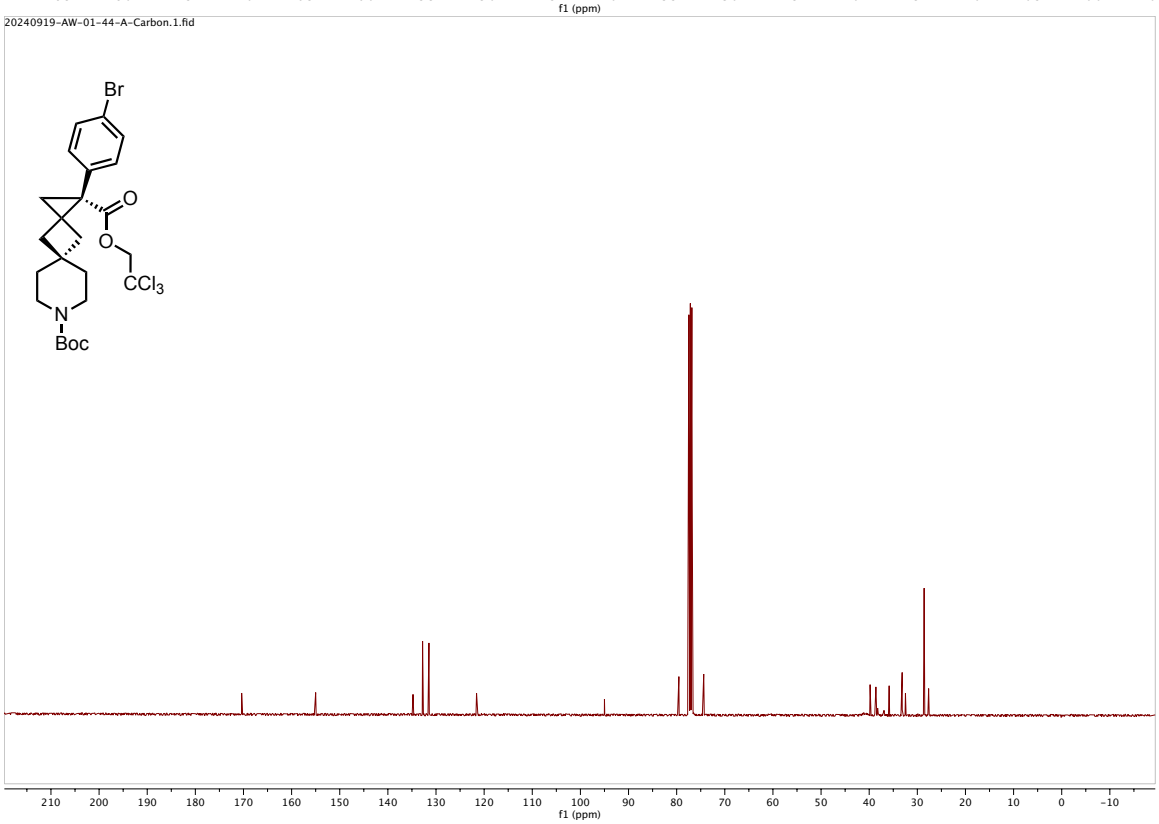
20240919-AW-01-44-A-Carbon.1.fid
Br
O
O
CCl3
N
Boc
f1 (ppm)

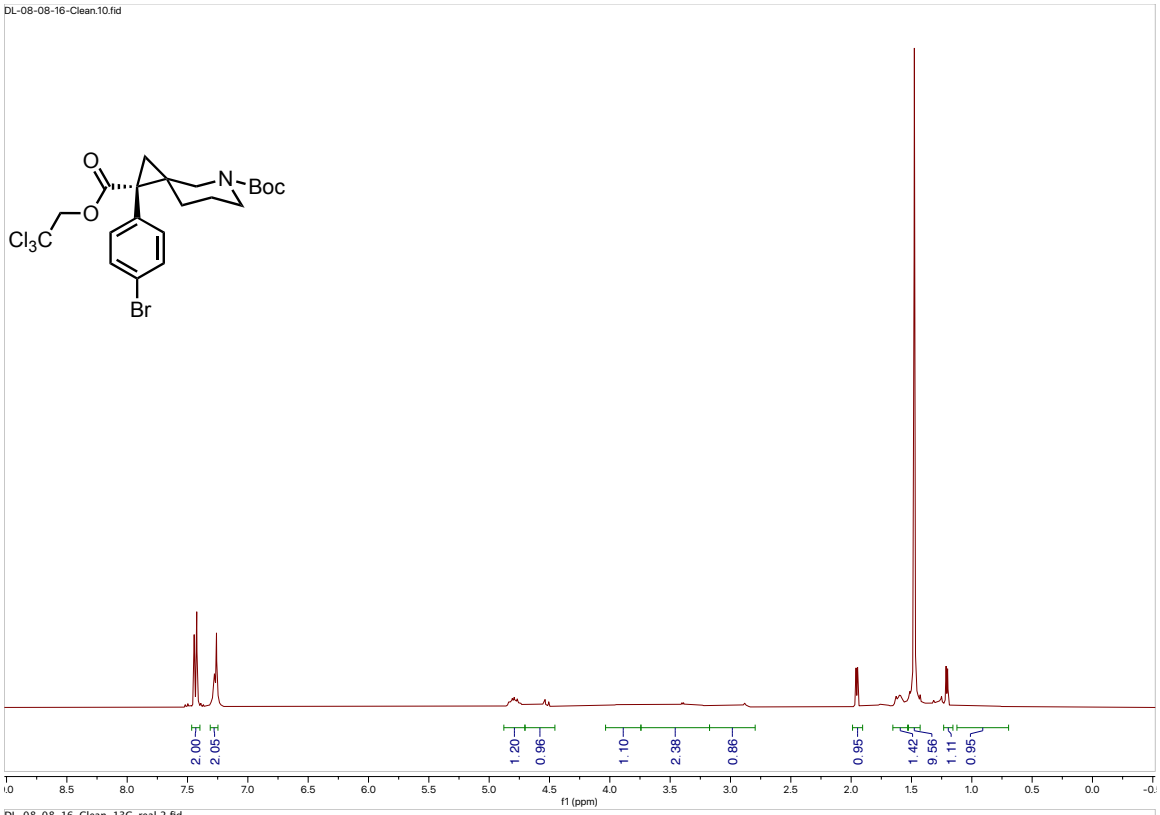
DL-08-08-16-Clean.10.fid
O
N
Boc
O
Cl3C
Br
2.00
2.05
1.20
0.96
1.10
2.38
0.86
0.95
1.42
9.56
1.11
0.95
f1 (ppm)

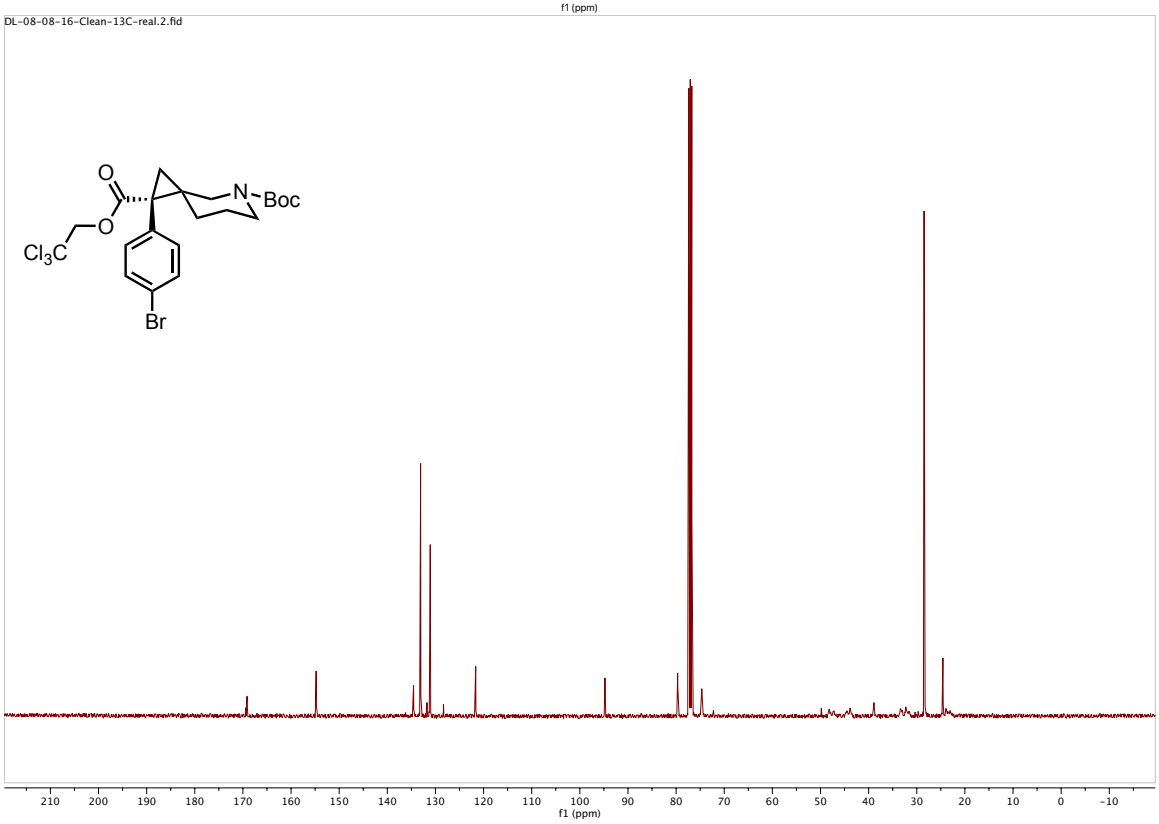
DL-08-08-16-Clean-13C-real.2.fid
O
N
Boc
O
Cl3C
Br
f1 (ppm)

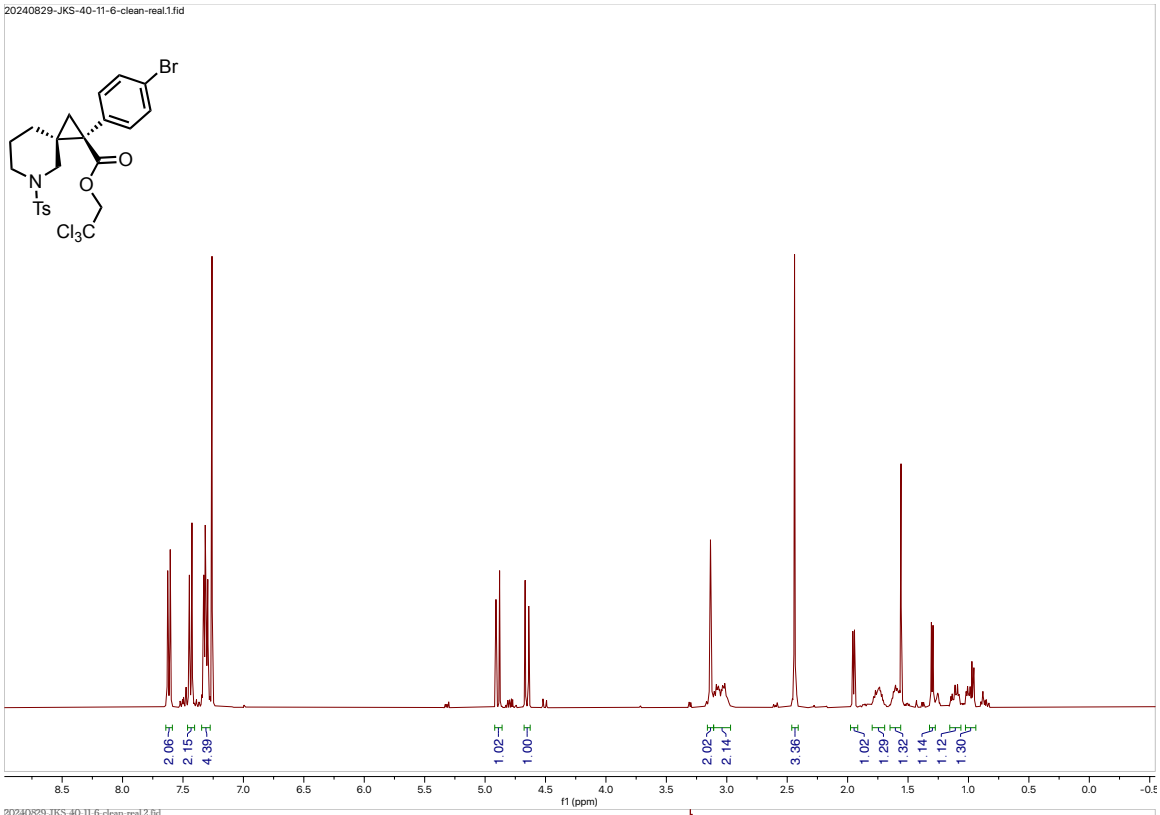
20240829-JKS-40-11-6-clean-real.1.fid
Br
O
O
N
Ts
Cl3C
2.06
2.15
4.39
1.02
1.00
2.02
2.14
3.36
1.02
1.29
1.32
1.14
1.12
1.30
f1 (ppm)

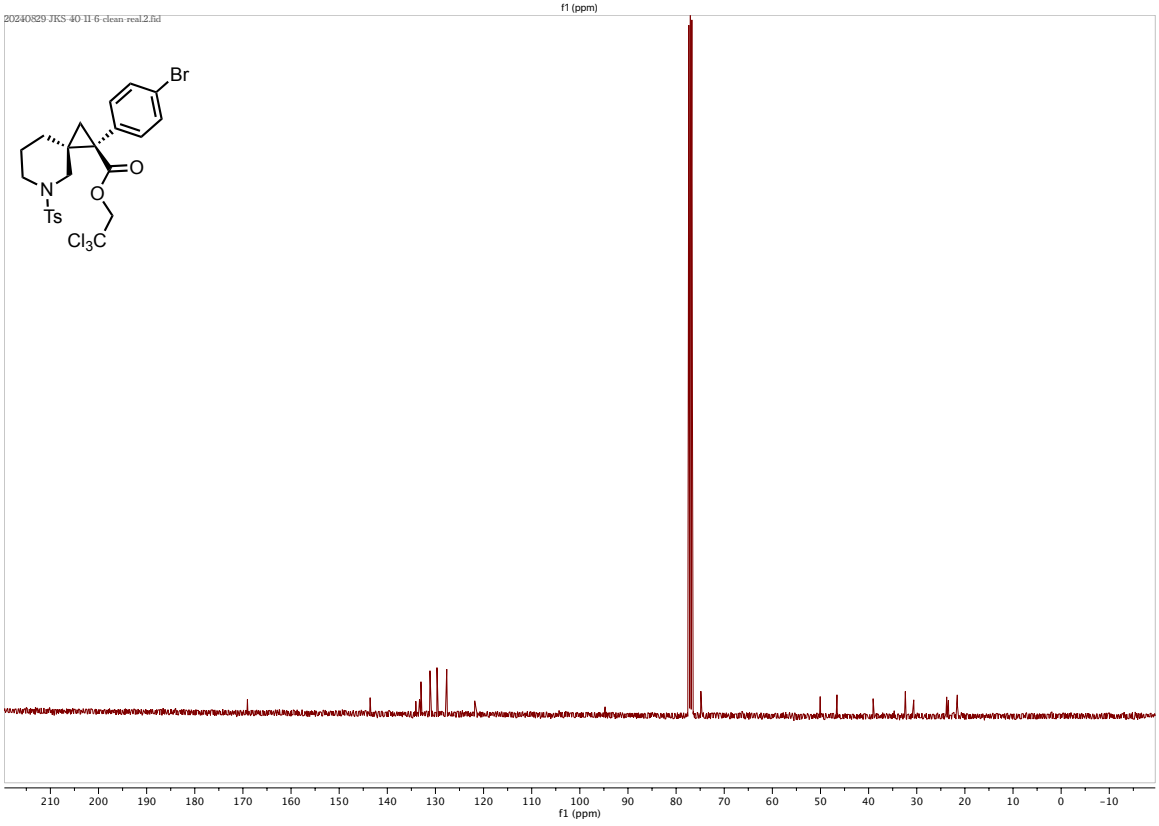
20240829-JKS-40-11-6-clean-real.2.fid
Br
O
O
N
Ts
Cl3C
f1 (ppm)

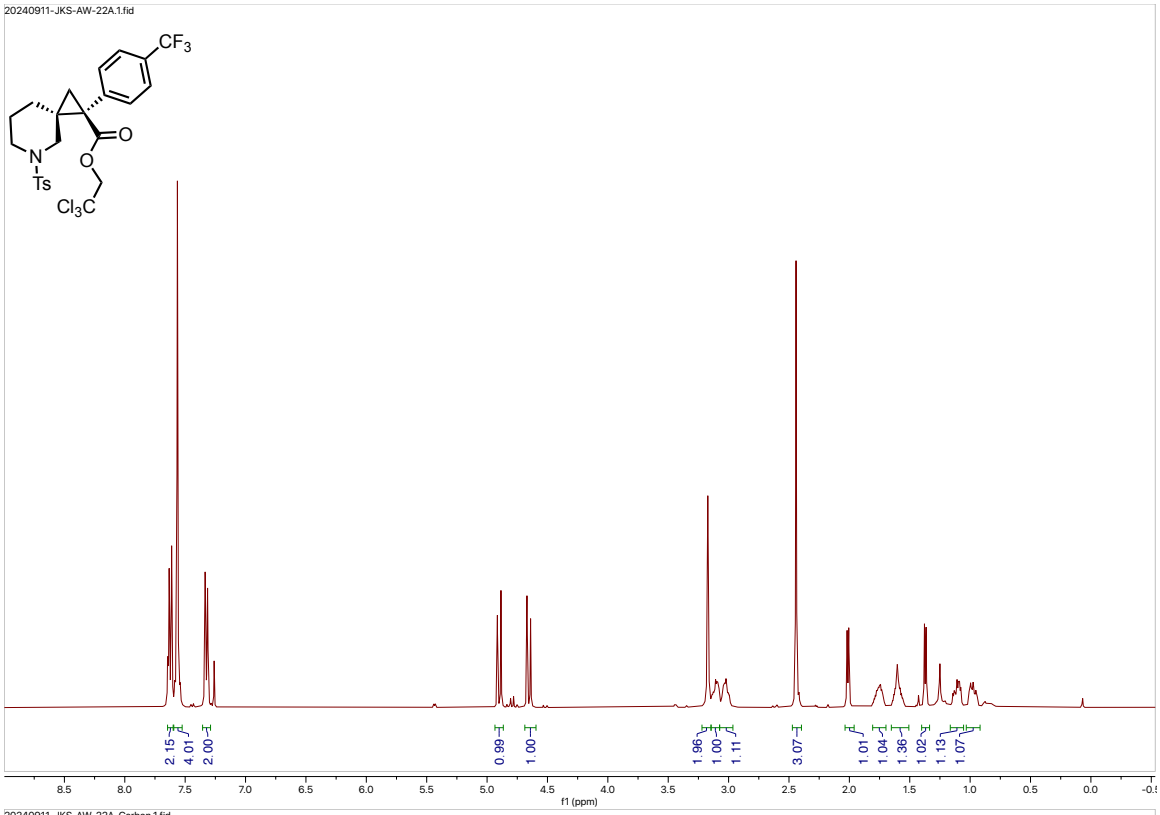
20240911-JKS-AW-22A.1.fid
CF3
O
O
N
Ts
Cl3C
2.15
4.01
2.00
0.99
1.00
1.96
1.00
1.11
3.07
1.01
1.04
1.36
1.02
1.13
1.07
f1 (ppm)

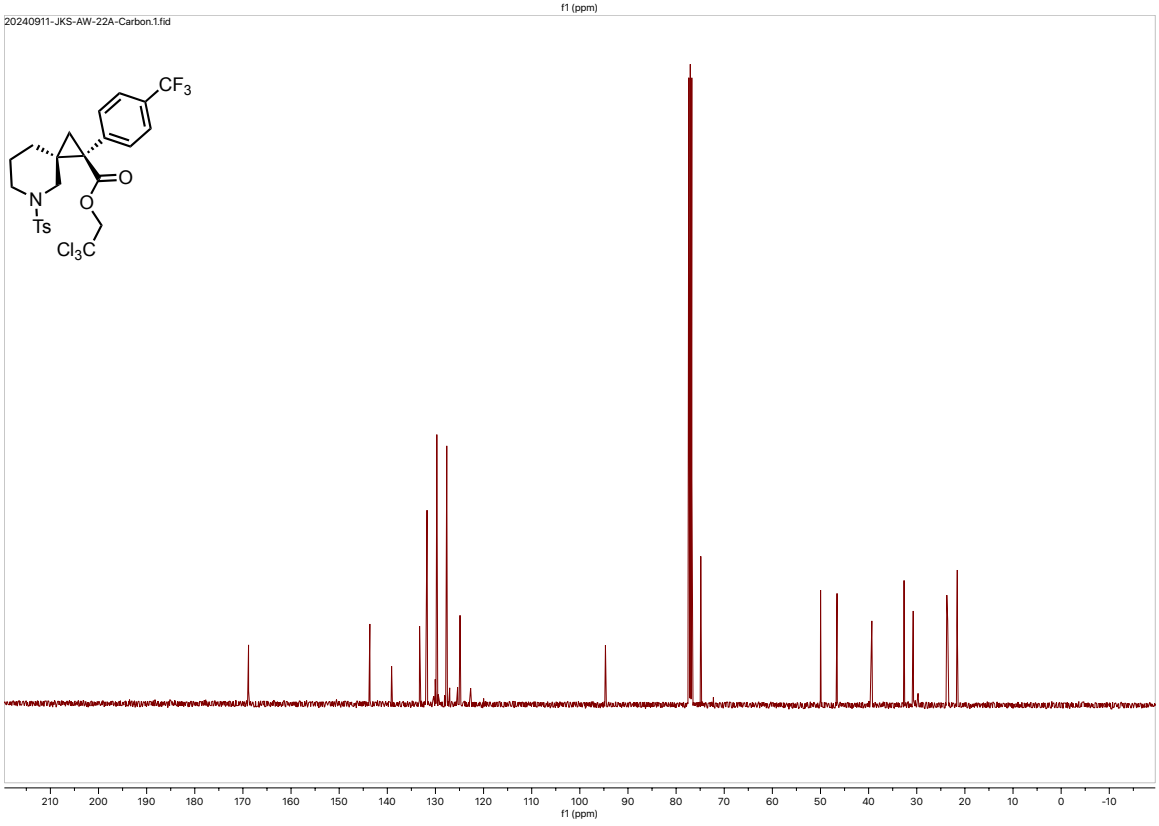
20240911-JKS-AW-22A-Carbon.1.fid
CF3
O
O
N
Ts
Cl3C
f1 (ppm)

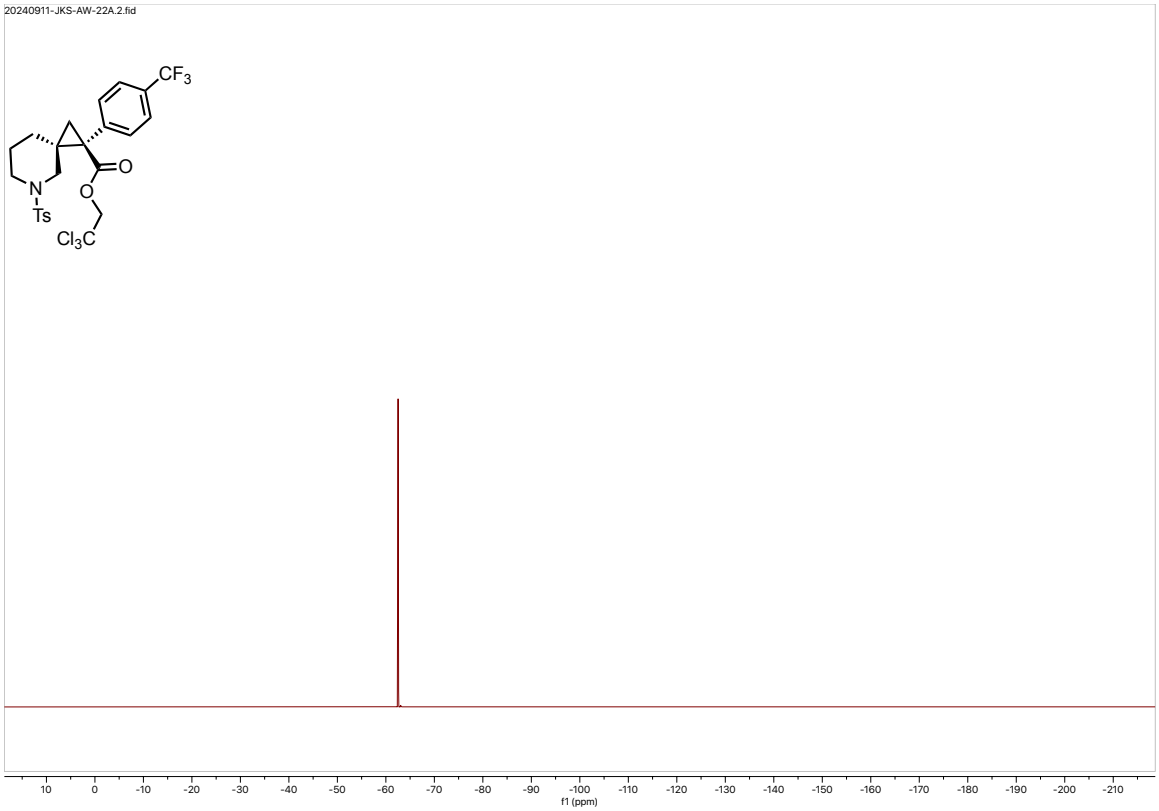
20240911-JKS-AW-22A.2.fid
CF3
O
O
N
Ts
Cl3C
10
0
-10
-20
-30
-40
-50
-60
-70
-80
-90
-100
-110
-120
-130
-140
-150
-160
-170
-180
-190
-200
-210
f1 (ppm)

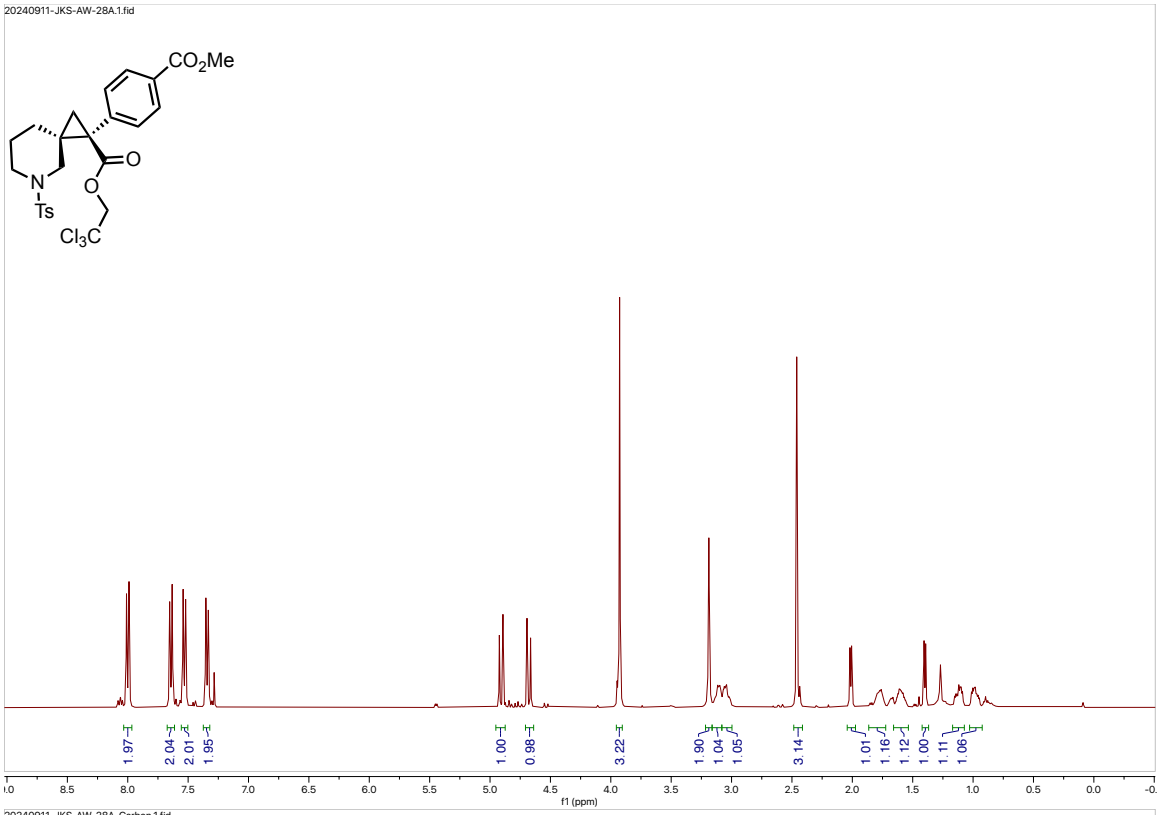
20240911-JKS-AW-28A.1.fid
CO2Me
O
O
N
Ts
Cl3C
1.97
2.04
2.01
1.95
1.00
0.98
3.22
1.90
1.04
1.05
3.14
1.01
1.16
1.12
1.00
1.11
1.06
f1 (ppm)

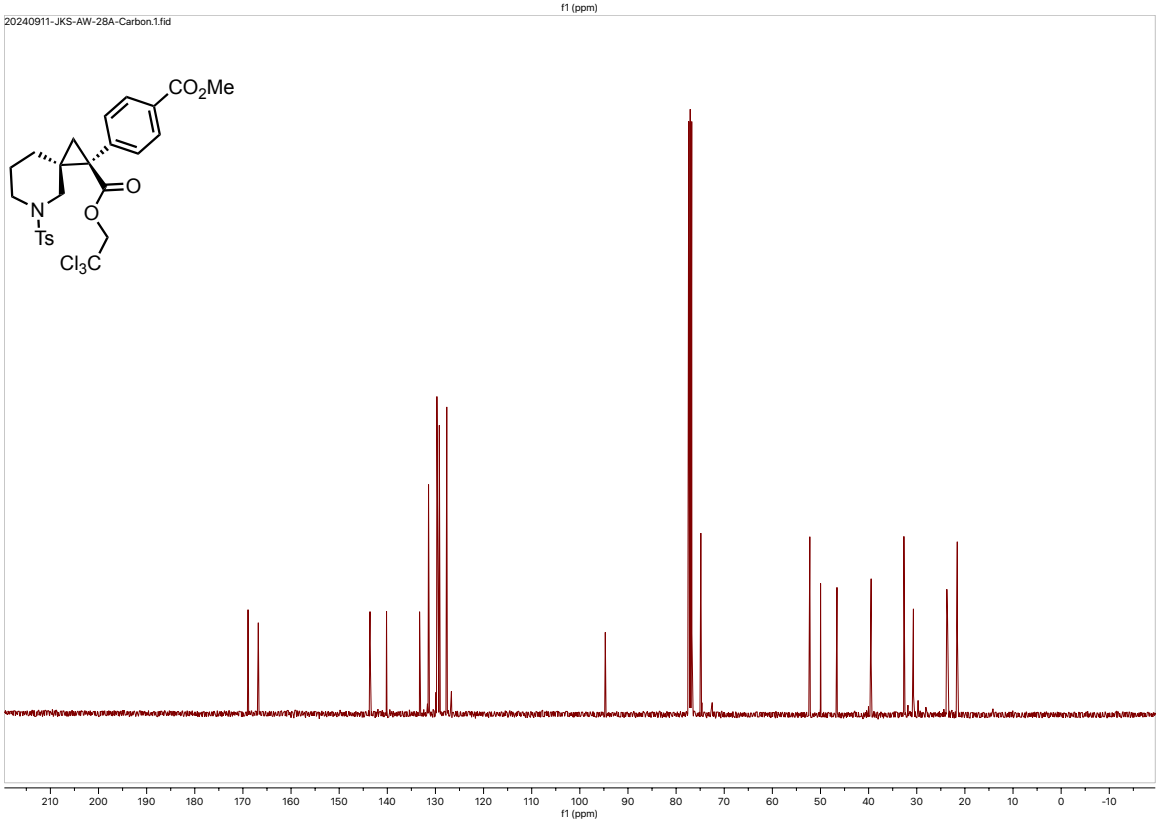
20240911-JKS-AW-28A-Carbon.1.fid
CO2Me
O
O
N
Ts
Cl3C
f1 (ppm)

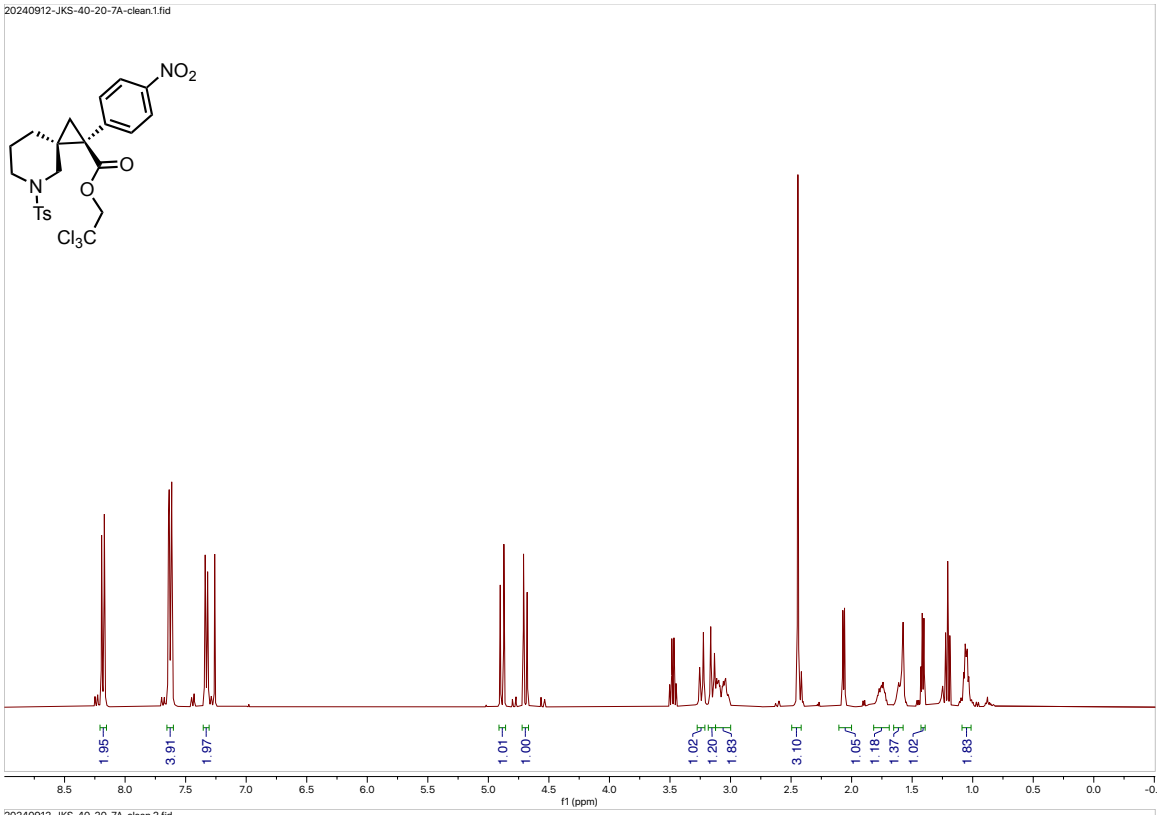
20240912-JKS-40-20-7A-clean.1.fid
NO2
O
O
N
Ts
Cl3C
1.95
3.91
1.97
1.01
1.00
1.02
1.20
1.83
3.10
1.05
1.18
1.37
1.02
1.83
f1 (ppm)

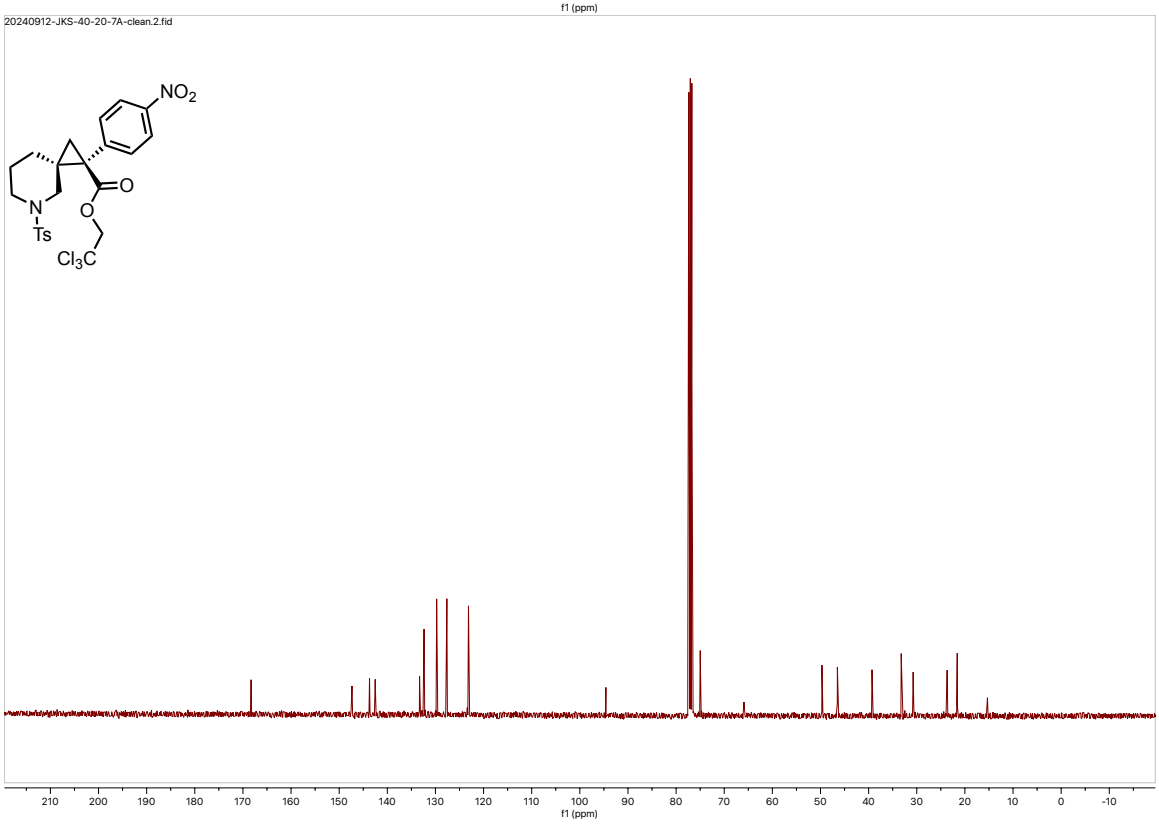
20240912-JKS-40-20-7A-clean.2.fid
NO2
O
O
N
Ts
Cl3C
f1 (ppm)

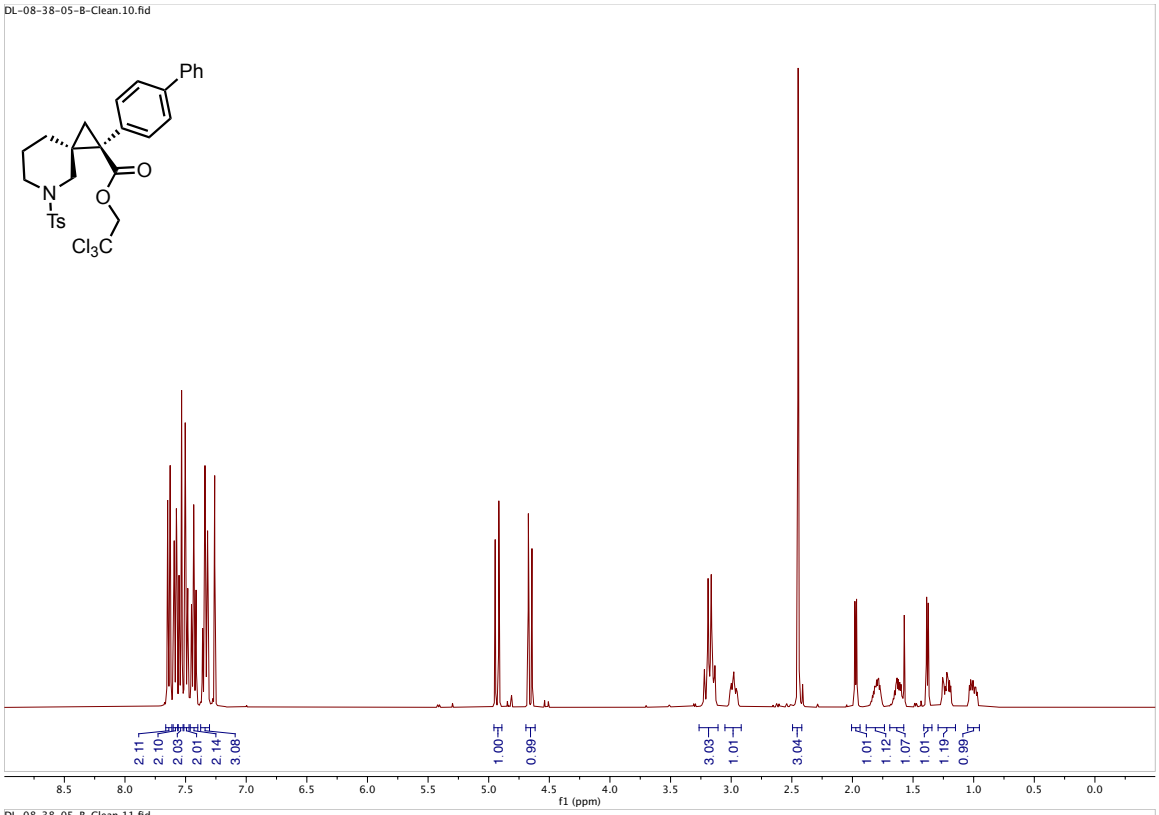
DL-08-38-05-B-Clean.10.fid
Ph
O
N
Ts
O
Cl3C
2.11
2.10
2.03
2.01
2.14
3.08
1.00
0.99
3.03
1.01
3.04
1.01
1.12
1.07
1.01
1.19
0.99
f1 (ppm)

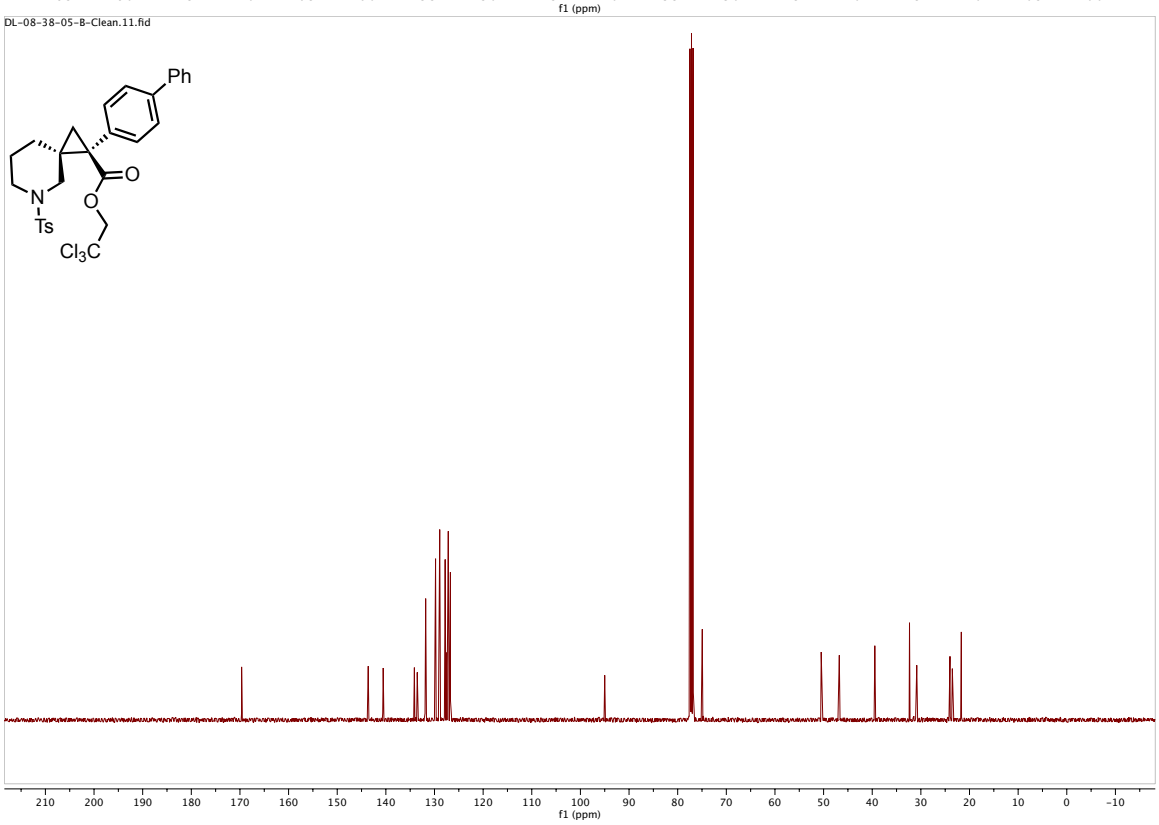
DL-08-38-05-B-Clean.11.fid
Ph
O
N
Ts
O
Cl3C
f1 (ppm)

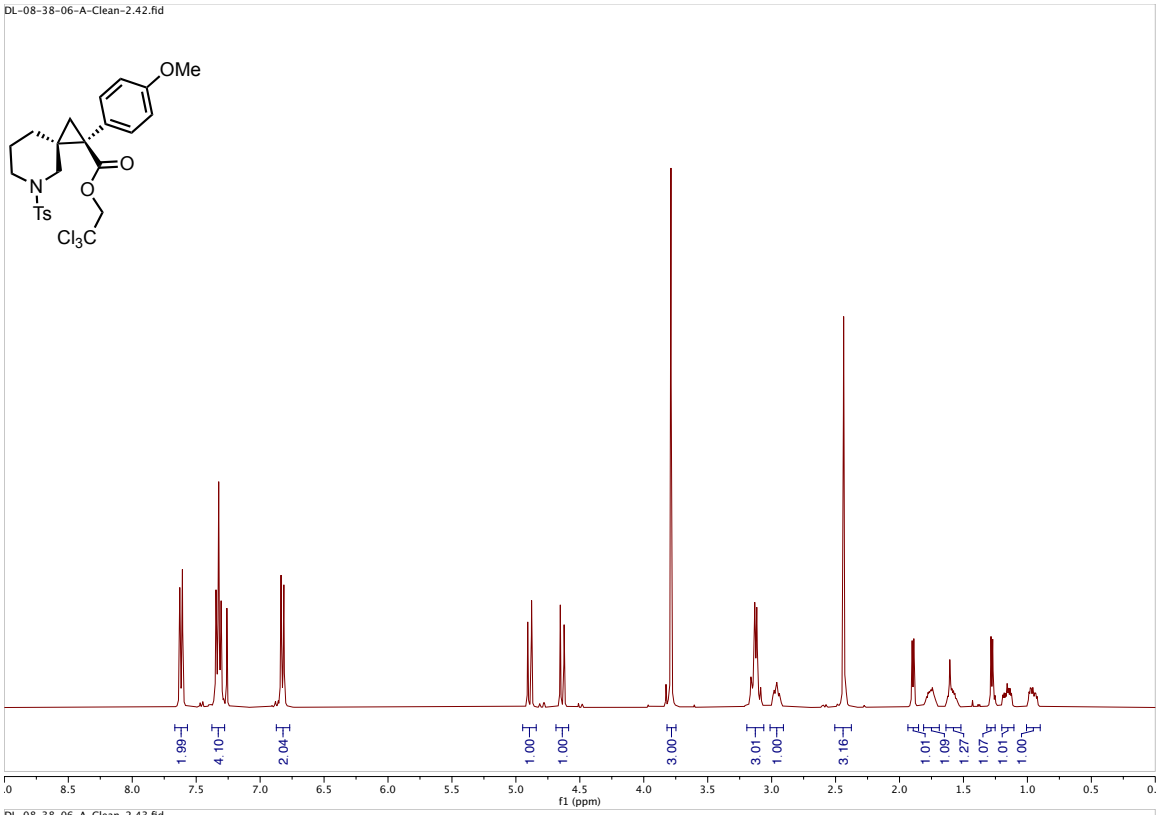
DL-08-38-06-A-Clean-2.42.fid
OMe
O
O
N
Ts
Cl3C
1.99
4.10
2.04
1.00
1.00
3.00
3.01
1.00
3.16
1.01
1.09
1.27
1.07
1.01
1.00
f1 (ppm)

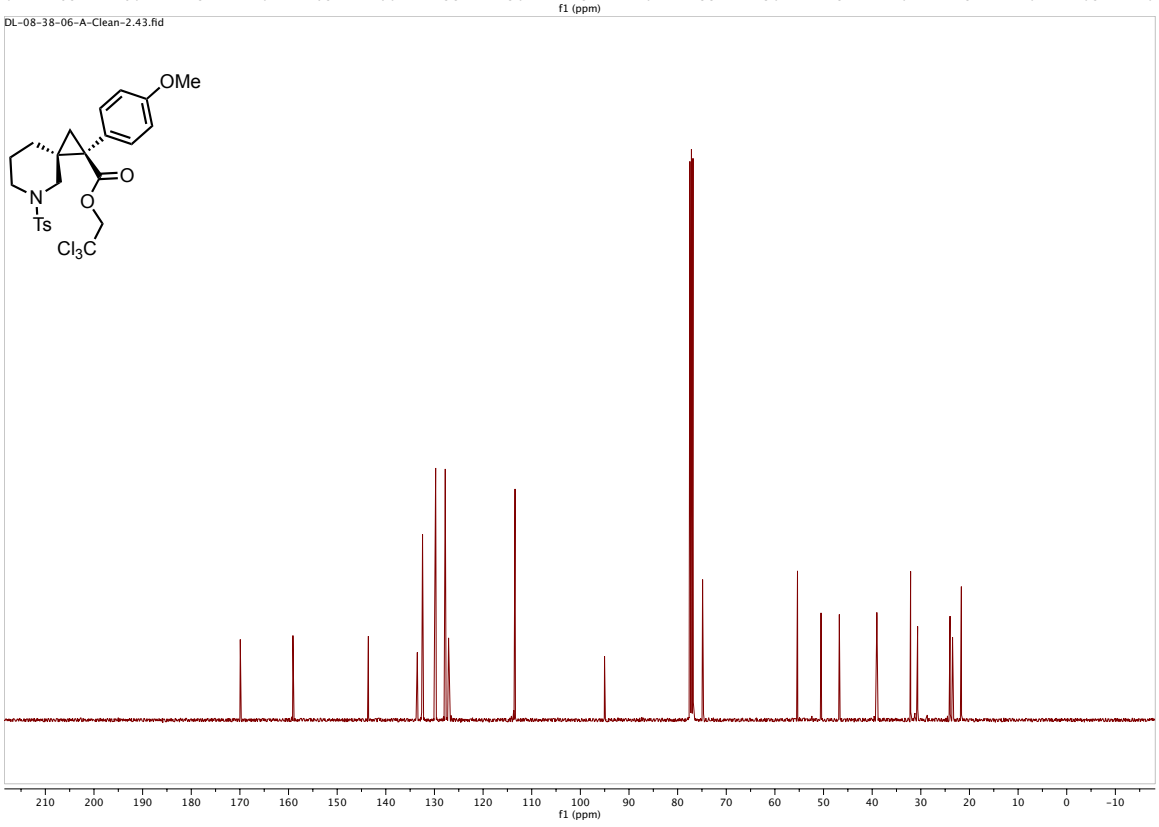
DL-08-38-06-A-Clean-2.43.fid
OMe
O
O
N
Ts
Cl3C
f1 (ppm)

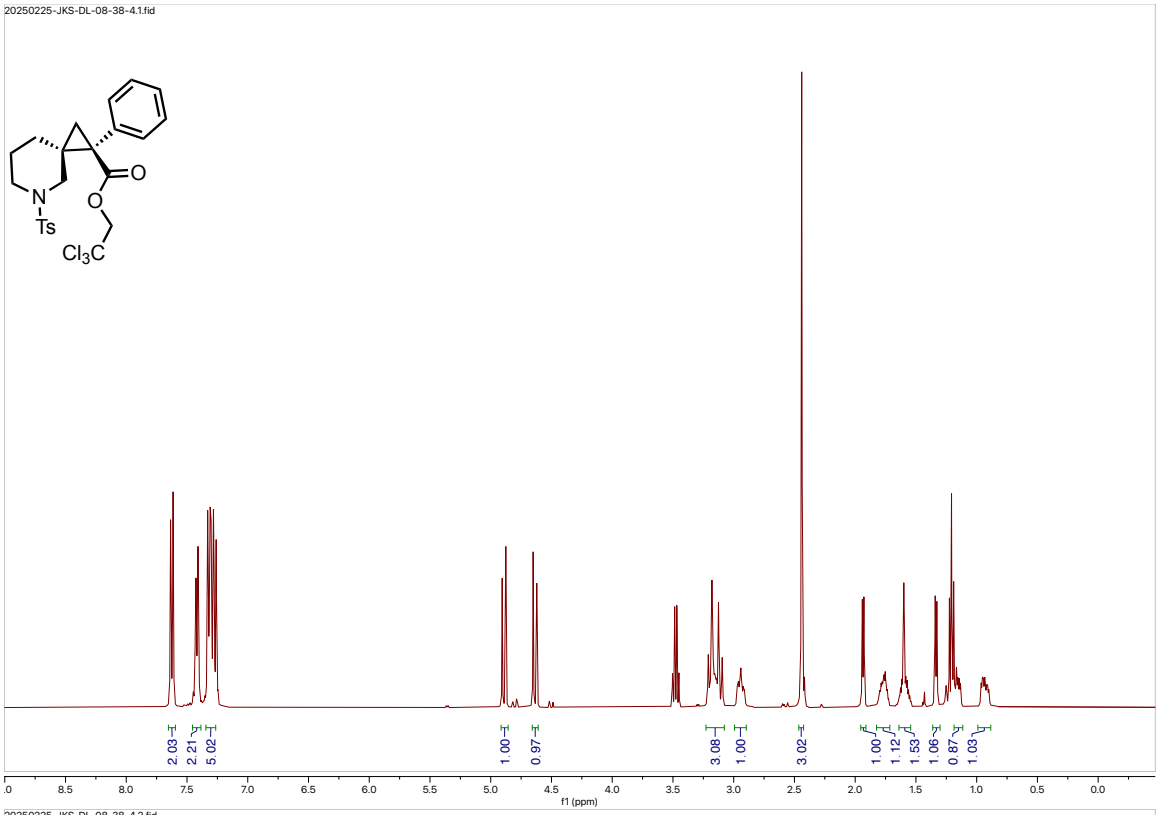
20250225-JKS-DL-08-38-4.1.fid
O
O
N
Ts
Cl3C
2.03
2.21
5.02
1.00
0.97
3.08
1.00
3.02
1.00
1.12
1.53
1.06
0.87
1.03
f1 (ppm)

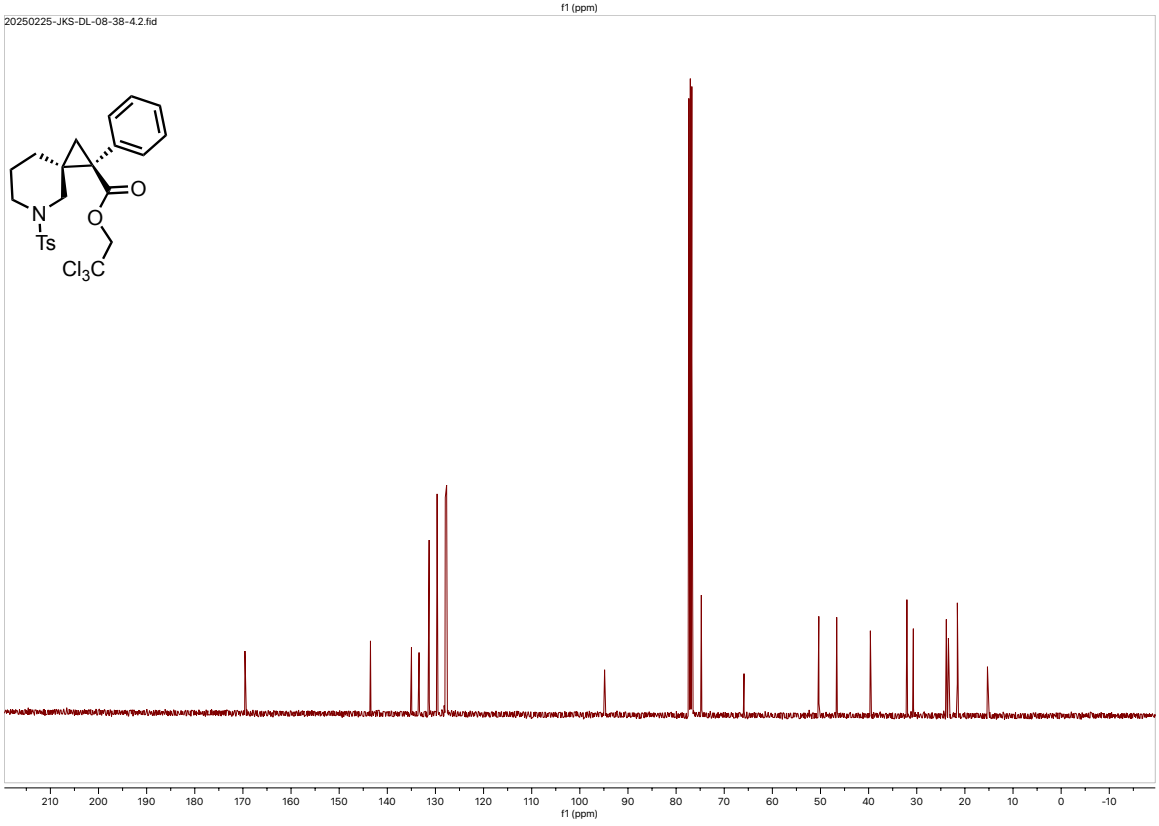
20250225-JKS-DL-08-38-4.2.fid
O
O
N
Ts
Cl3C
f1 (ppm)

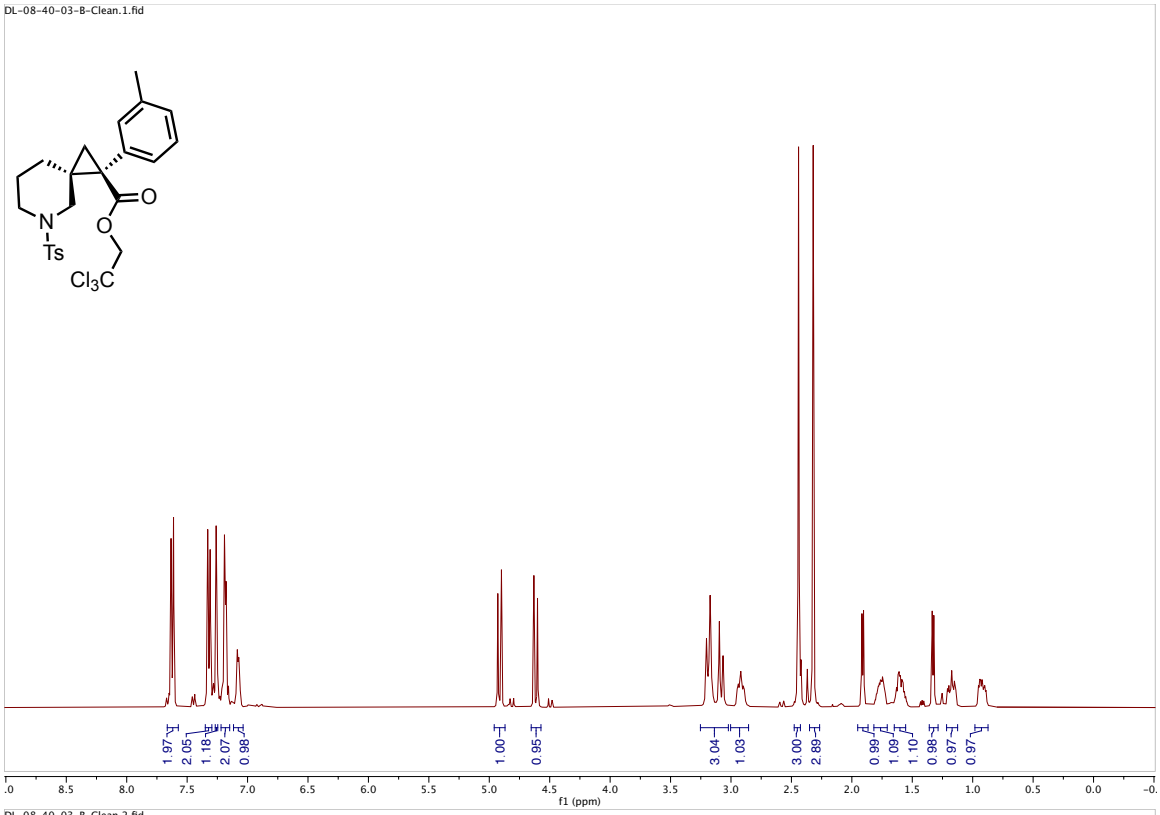
DL-08-40-03-B-Clean.1.fid
O
N
Ts
O
Cl3C
1.97
2.05
1.18
2.07
0.98
1.00
0.95
3.04
1.03
3.00
2.89
0.99
1.09
1.10
0.98
0.97
1.00
f1 (ppm)

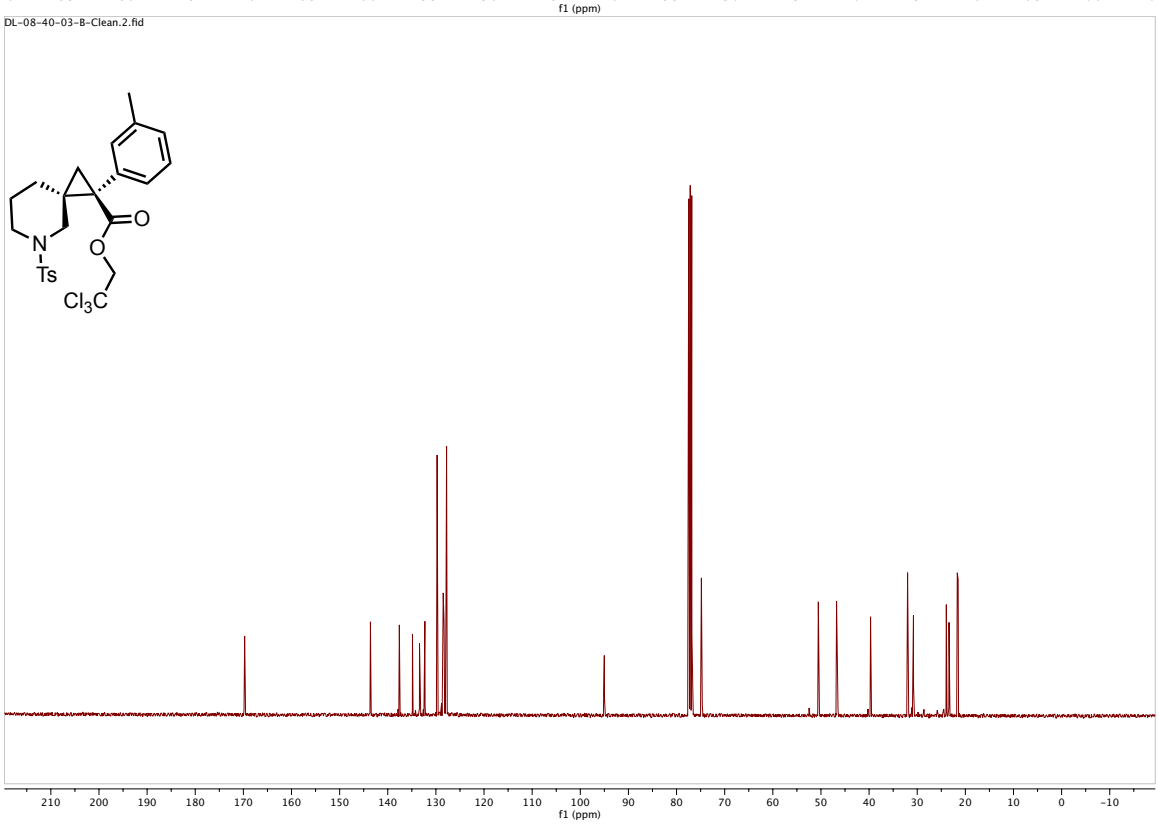
DL-08-40-03-B-Clean.2.fid
O
N
Ts
O
Cl3C
f1 (ppm)

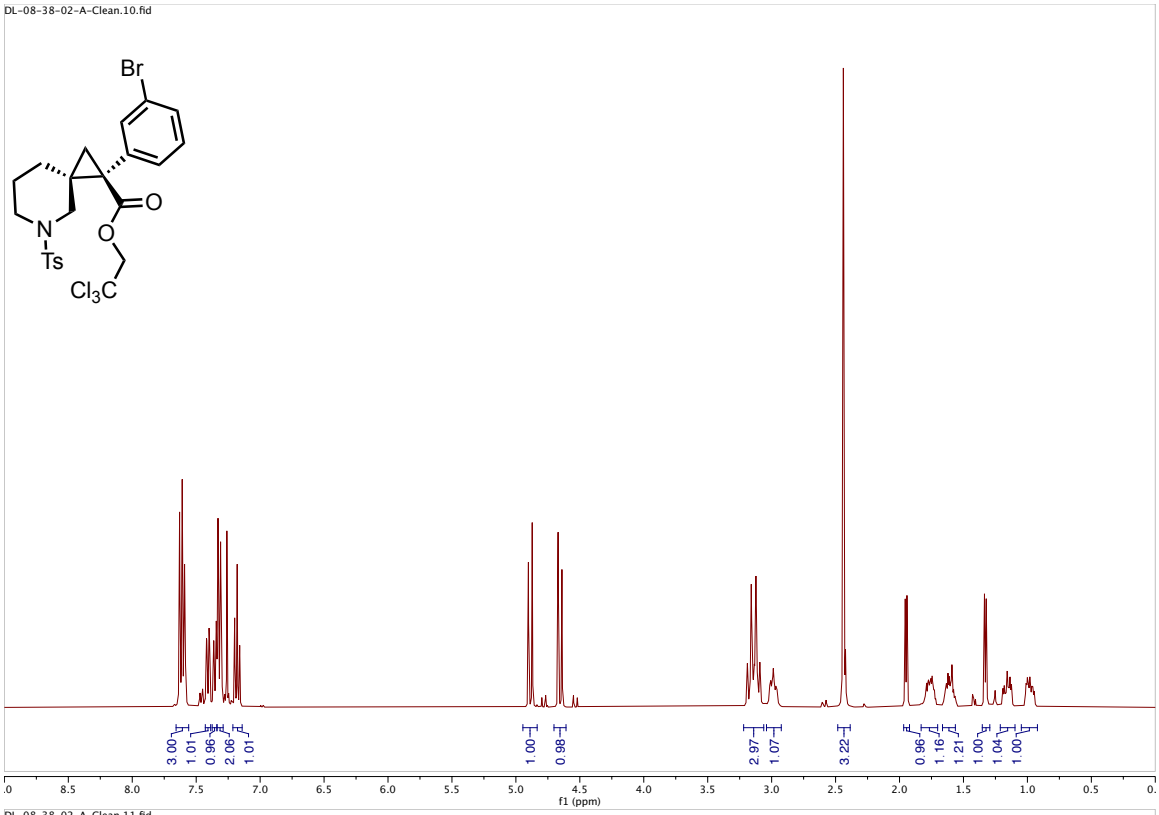
DL-08-38-02-A-Clean.10.fid
Br
O
O
N
Ts
Cl3C
3.00
1.01
0.96
2.06
1.01
1.00
0.98
2.97
1.07
3.22
0.96
1.16
1.21
1.00
1.04
1.00
f1 (ppm)

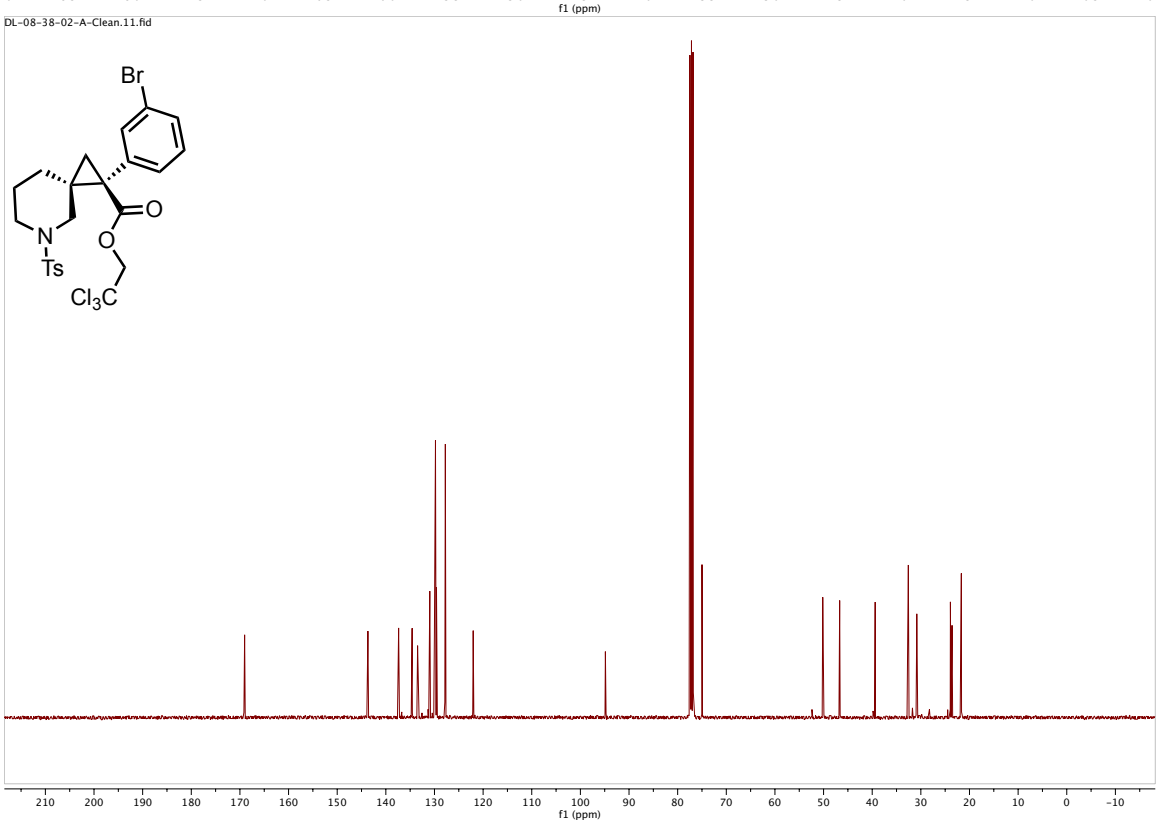
DL-08-38-02-A-Clean.11.fid
Br
O
O
N
Ts
Cl3C
f1 (ppm)

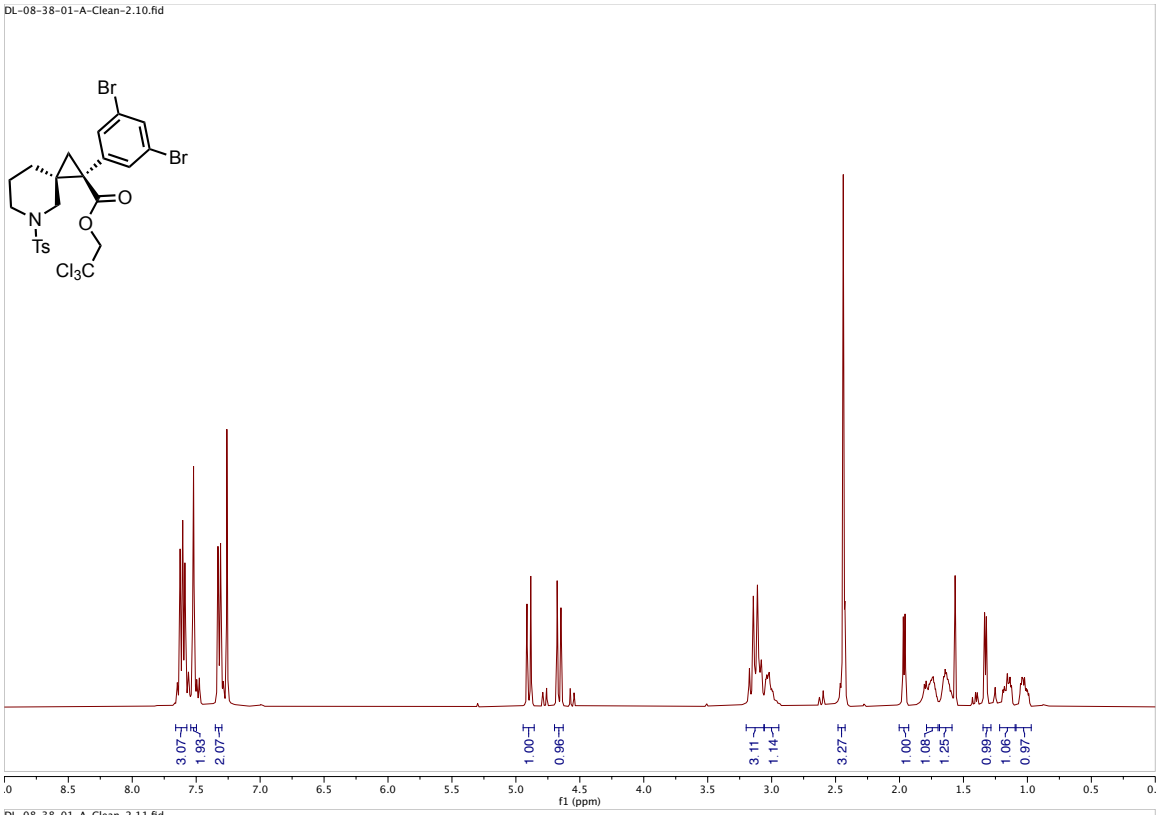
DL-08-38-01-A-Clean-2.10.fid
Br
Br
O
O
N
Ts
Cl3C
3.07
1.93
2.07
1.00
0.96
3.11
1.14
3.27
1.00
1.08
1.25
0.99
1.06
0.97
f1 (ppm)

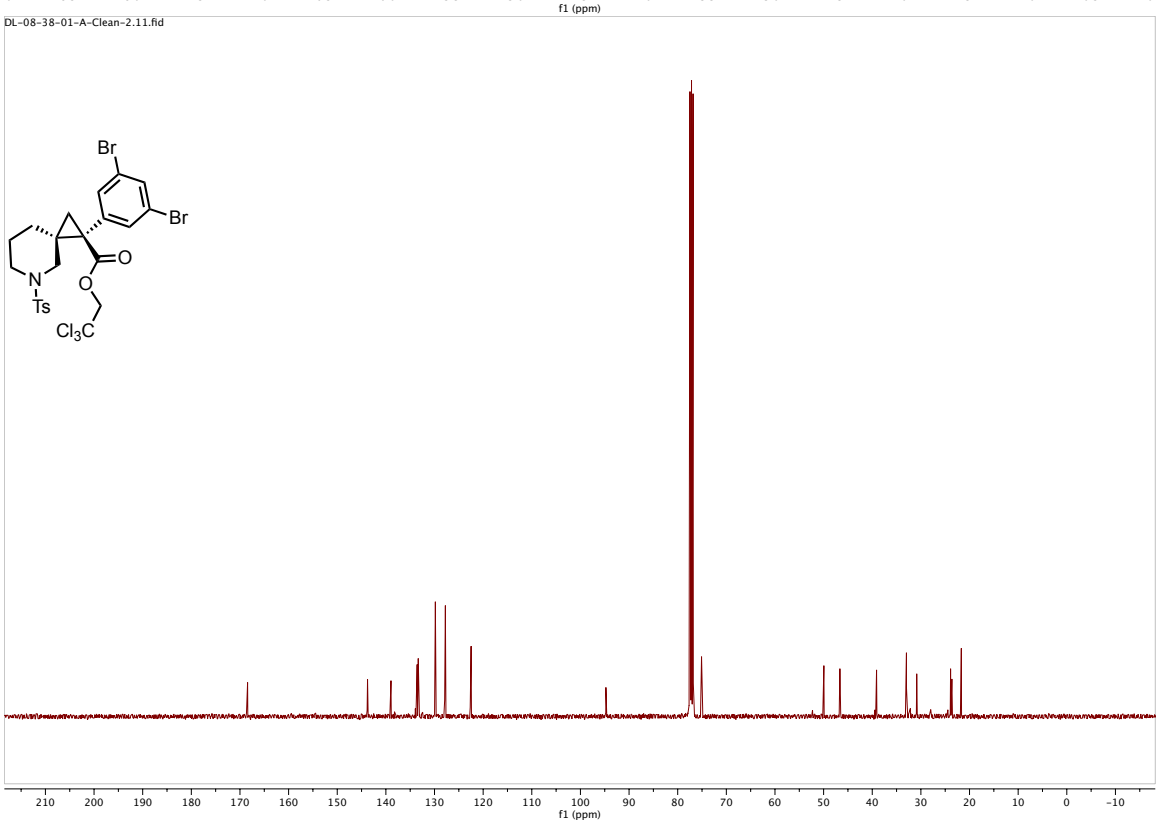
DL-08-38-01-A-Clean-2.11.fid
Br
Br
O
O
N
Ts
Cl3C
f1 (ppm)

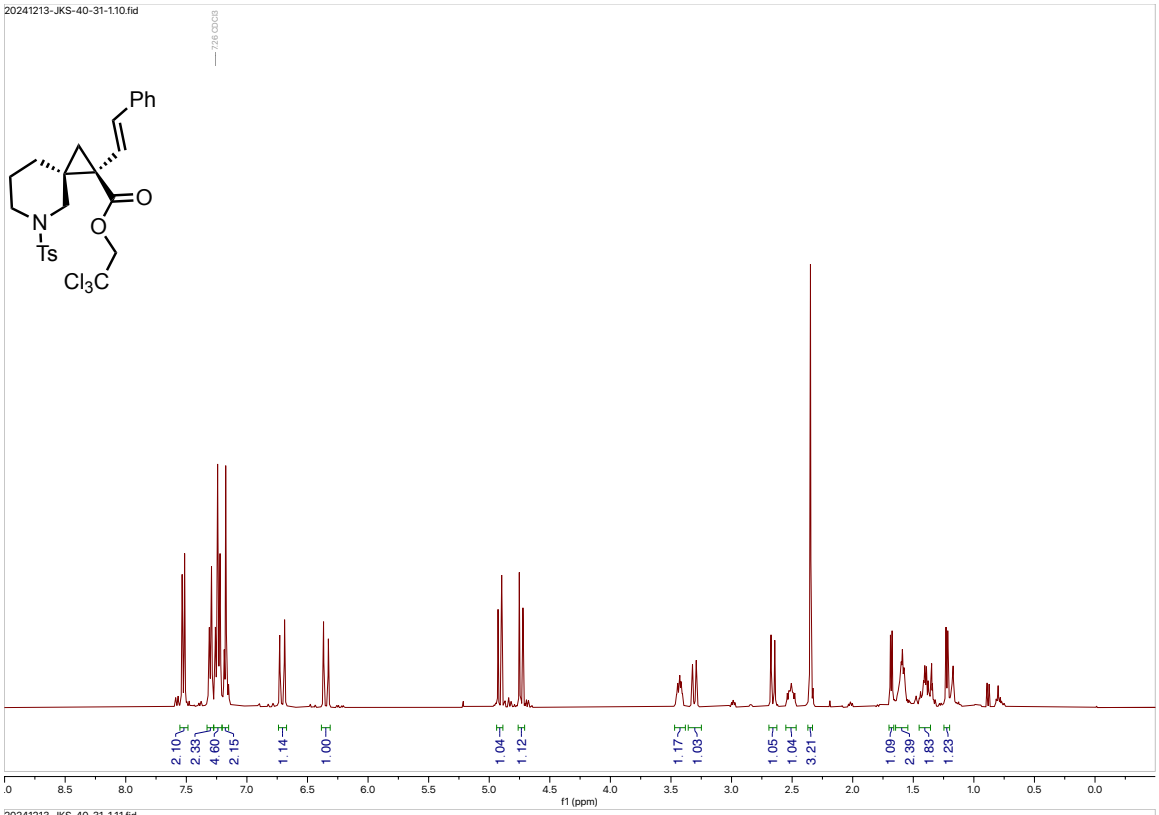
20241213-JKS-40-31-1.10.fid
Ph
O
N
Ts
O
Cl3C
2.10
2.33
4.60
2.15
1.14
1.00
1.04
1.12
1.17
1.03
1.05
1.04
3.21
1.09
2.39
1.83
1.23
f1 (ppm)

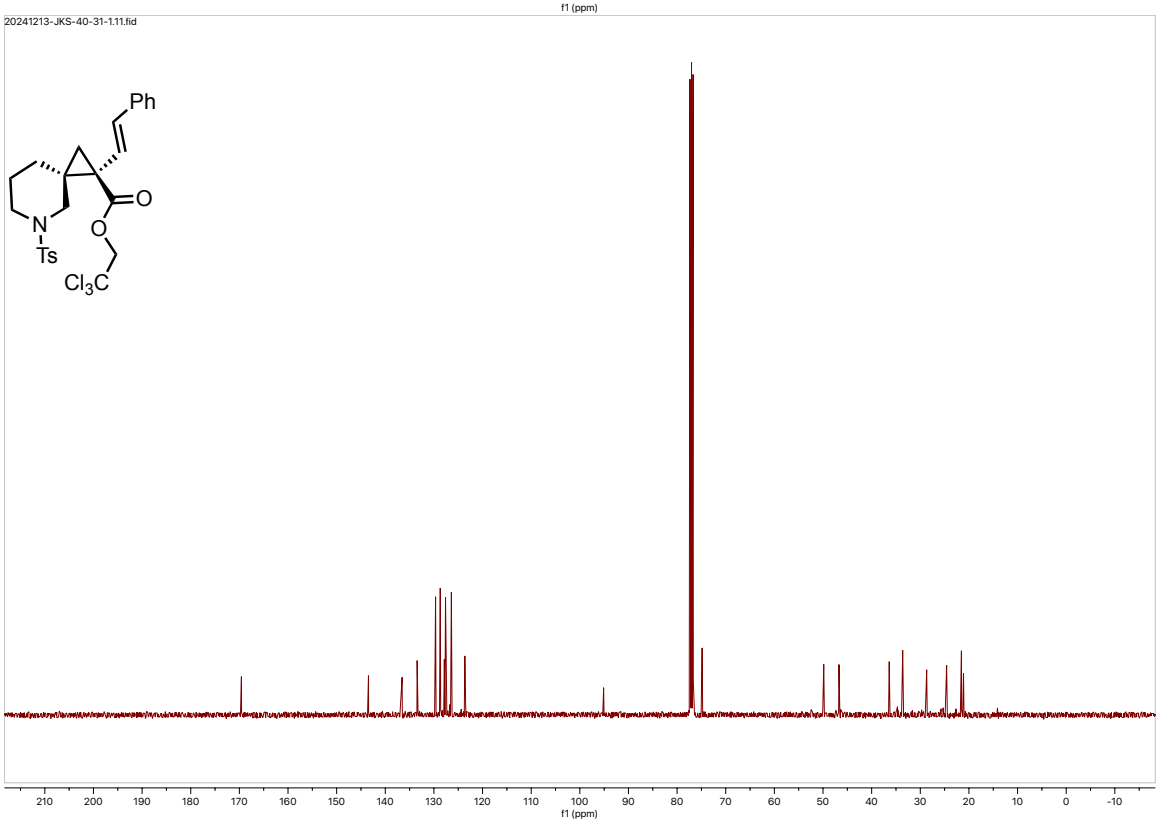
20241213-JKS-40-31-1.11.fid
Ph
O
N
Ts
O
Cl3C
f1 (ppm)

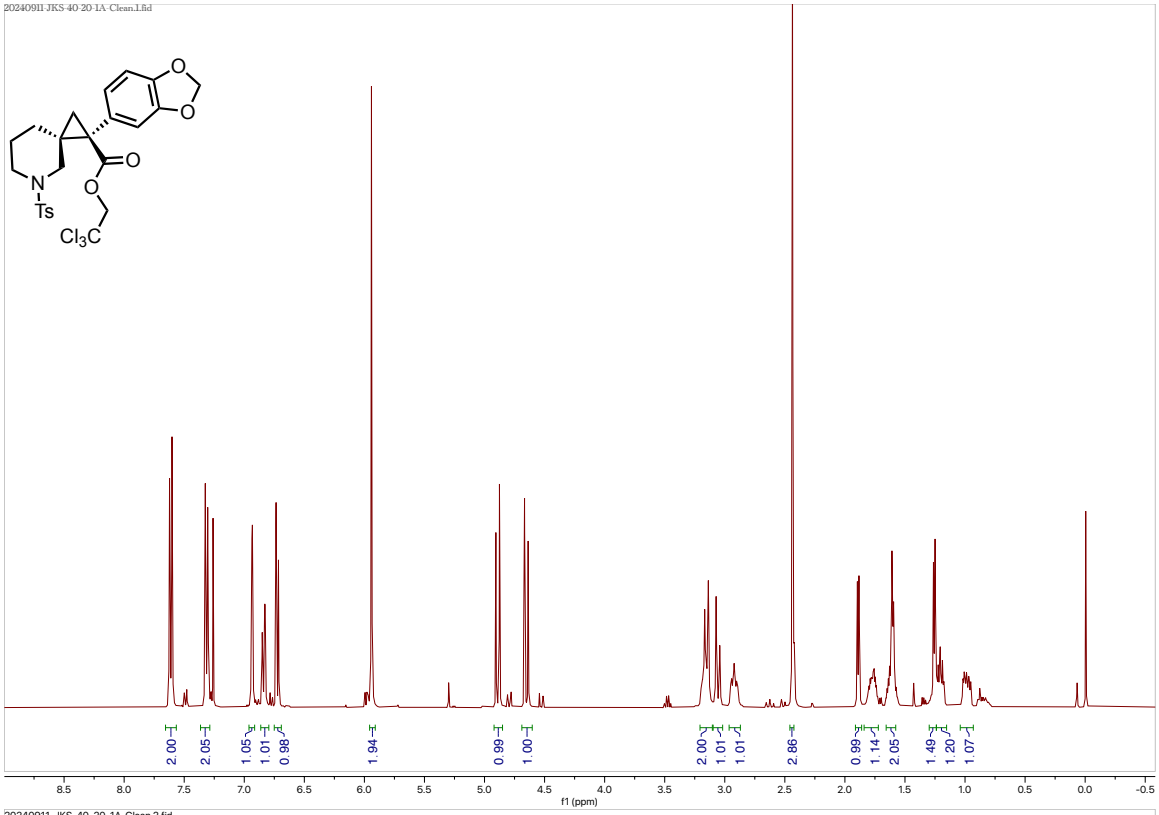
20240911-JKS-40-20-1A-Clean.1.fid
O
O
O
O
N
Ts
Cl3C
2.00
2.05
1.05
1.01
0.98
1.94
0.99
1.00
2.00
1.01
1.01
2.86
0.99
1.14
2.05
1.49
1.20
1.07
f1 (ppm)

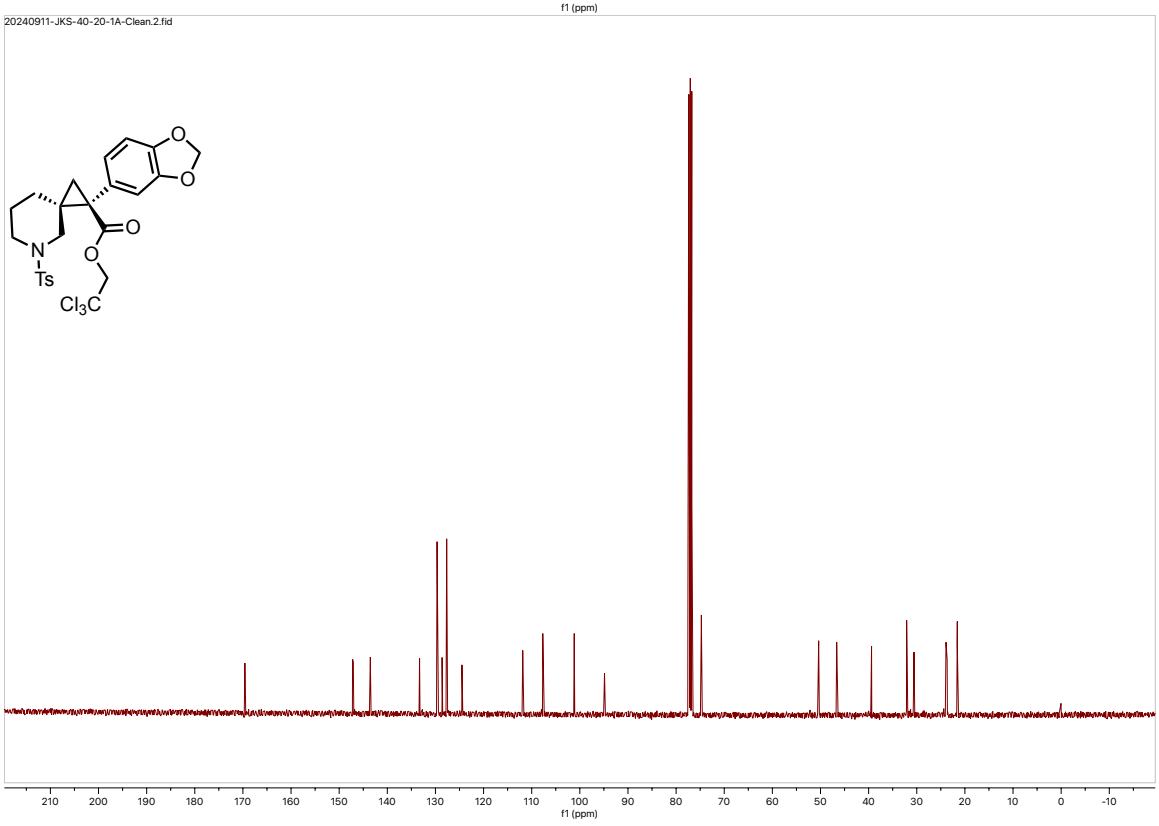
20240911-JKS-40-20-1A-Clean.2.fid
O
O
O
O
N
Ts
Cl3C
f1 (ppm)

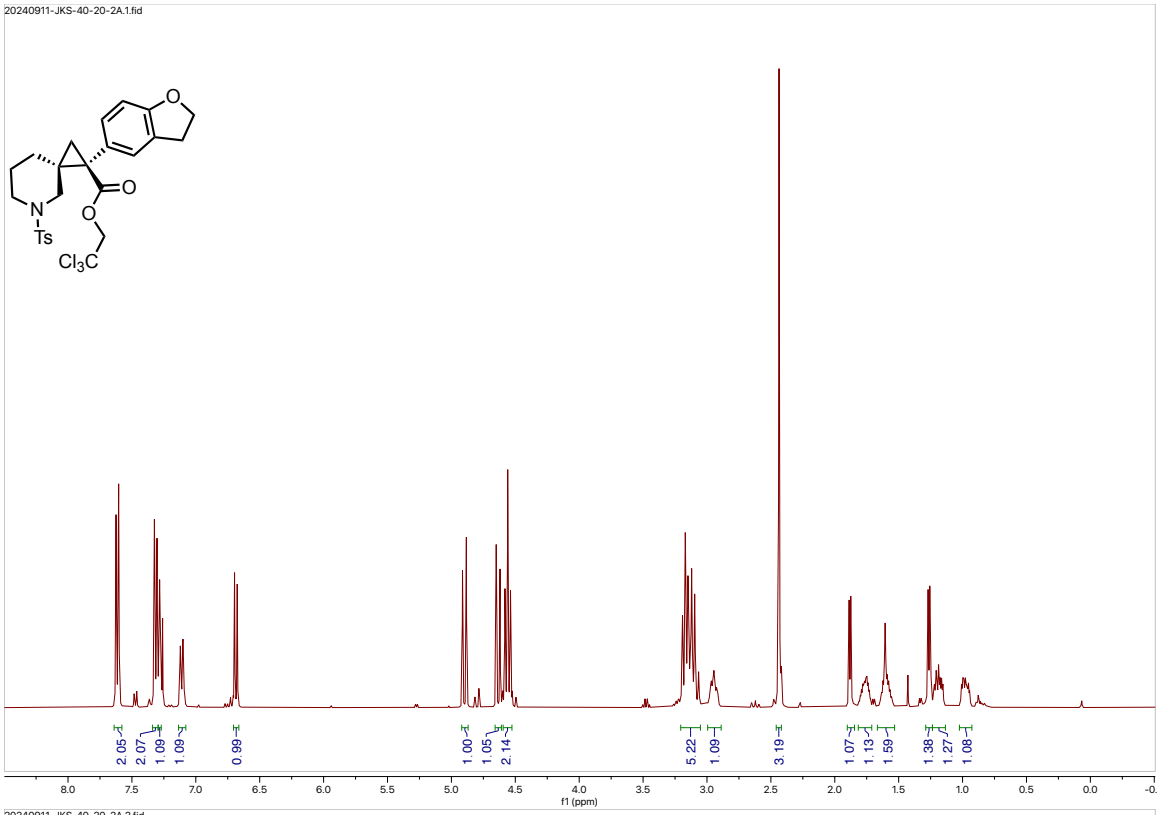
20240911-JKS-40-20-2A.1.fid
O
O
N
Ts
O
Cl3C
2.05
2.07
1.09
1.09
0.99
1.00
1.05
2.14
5.22
1.09
3.19
1.07
1.13
1.59
1.38
1.27
1.08
f1 (ppm)

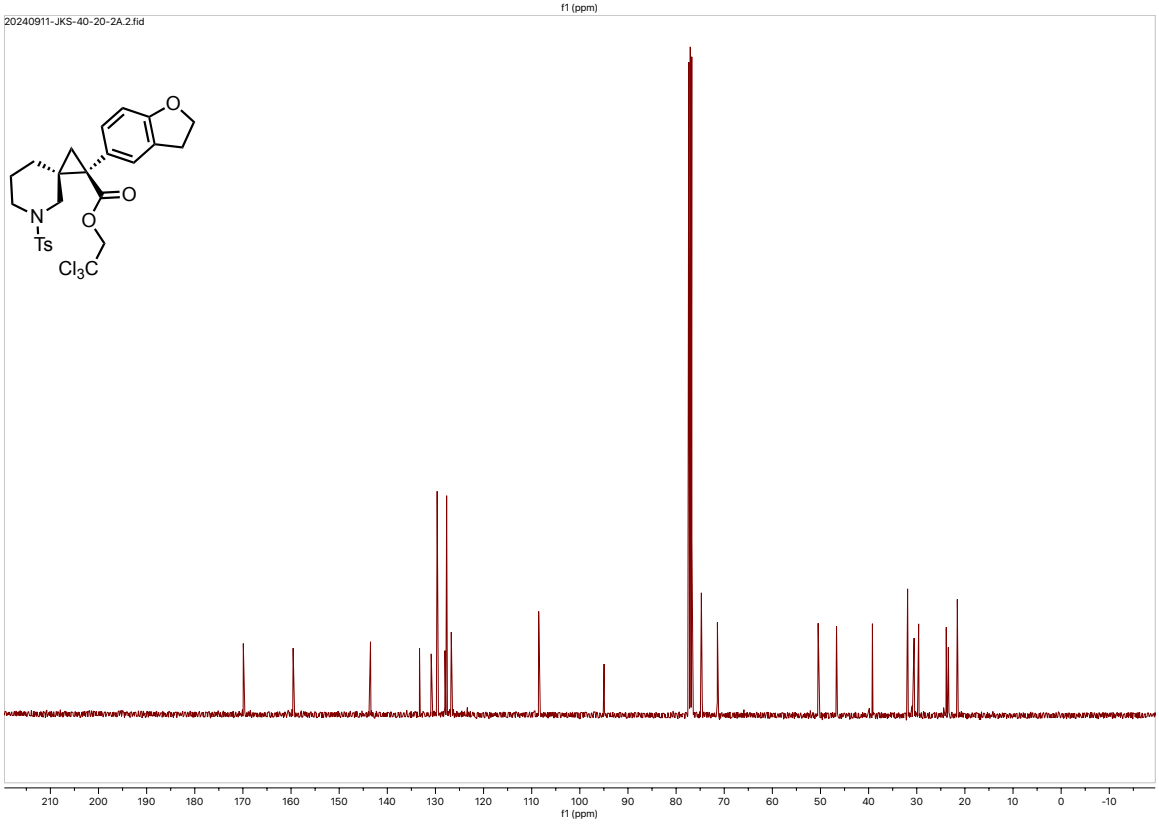
20240911-JKS-40-20-2A.2.fid
O
O
N
Ts
O
Cl3C
f1 (ppm)

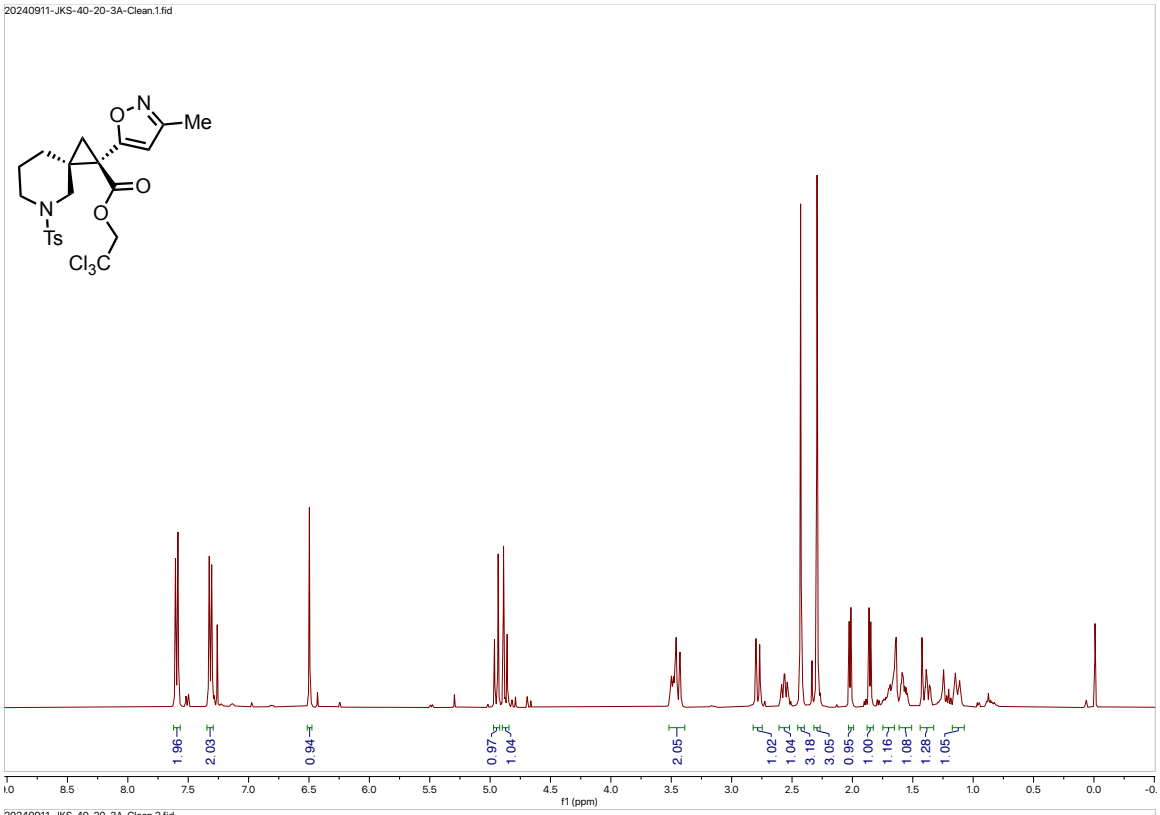
20240911-JKS-40-20-3A-Clean.1.fid
O
N
Me
O
O
N
Ts
Cl3C
1.96
2.03
0.94
0.97
1.04
2.05
1.02
1.04
3.18
3.05
0.95
1.00
1.16
1.08
1.28
1.05
f1 (ppm)

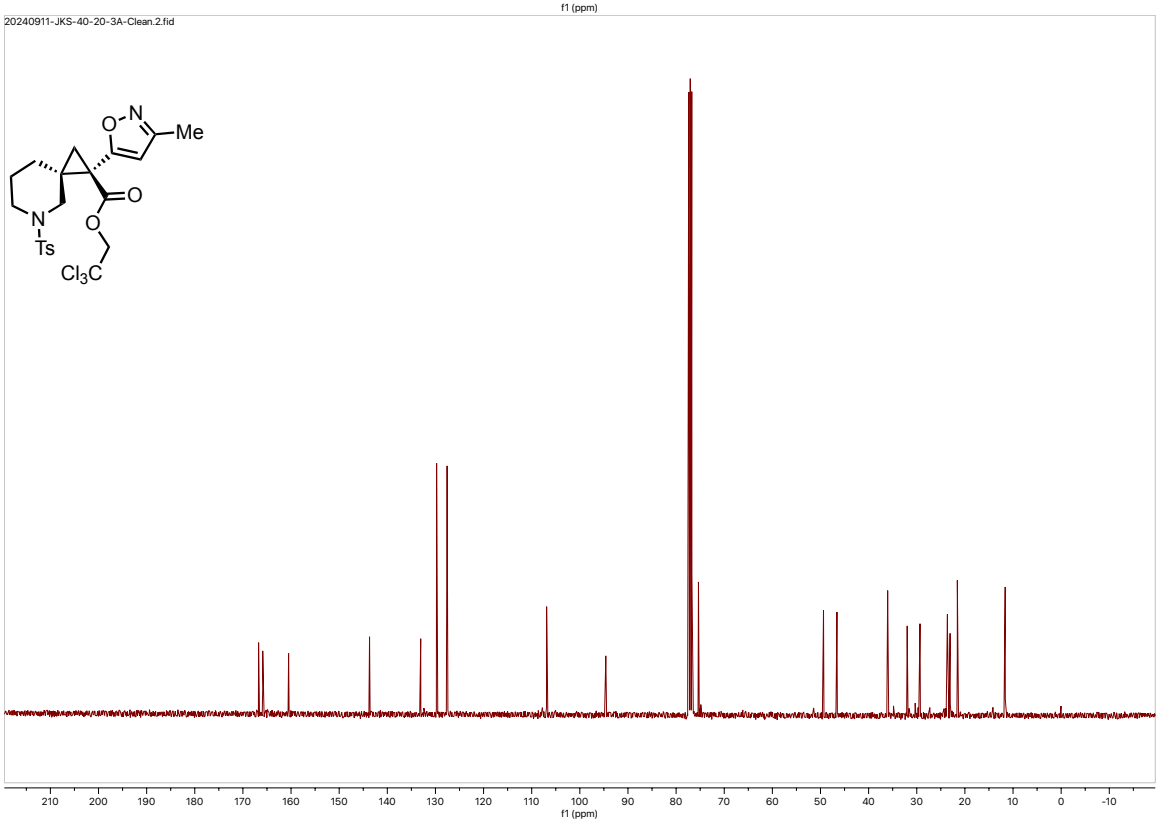
20240911-JKS-40-20-3A-Clean.2.fid
O
N
Me
O
O
N
Ts
Cl3C
f1 (ppm)

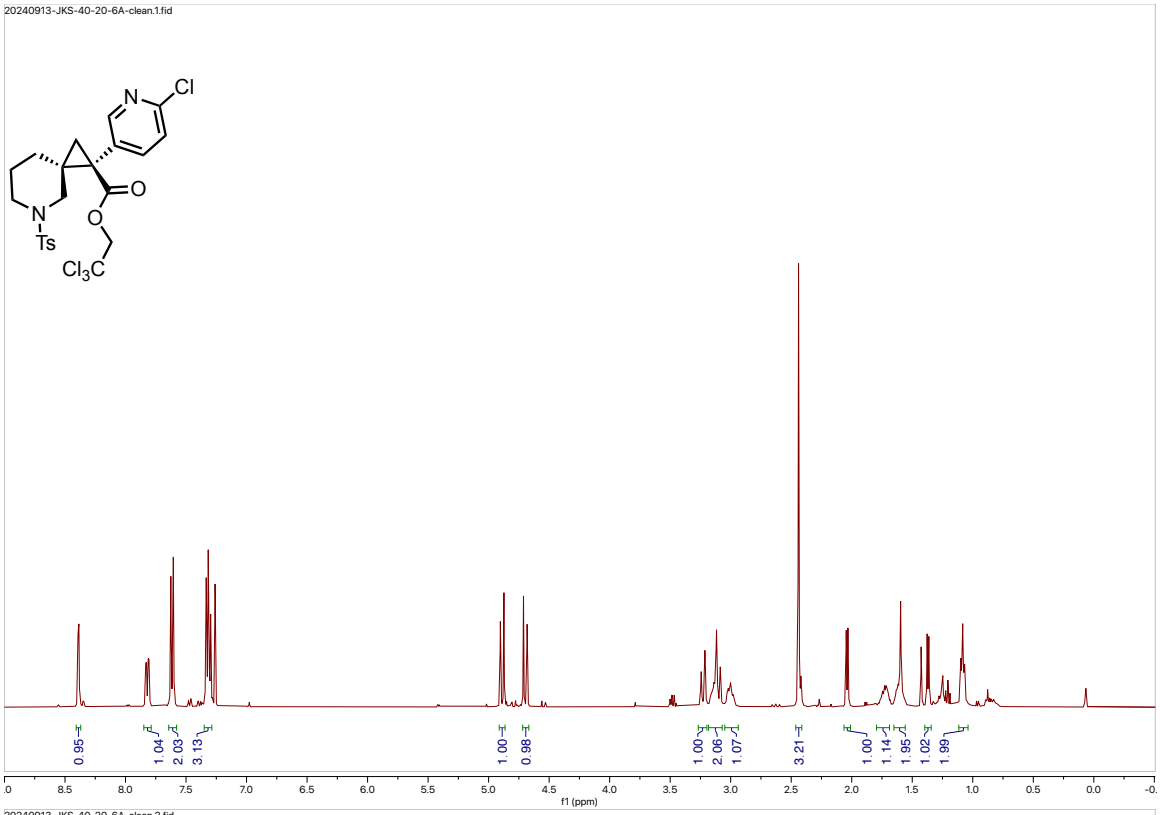
20240913-JKS-40-20-6A-clean.1.fid
N
Cl
O
O
N
Ts
Cl3C
0.95
1.04
2.03
3.13
1.00
0.98
1.00
2.06
1.07
3.21
1.00
1.14
1.95
1.02
1.99
f1 (ppm)

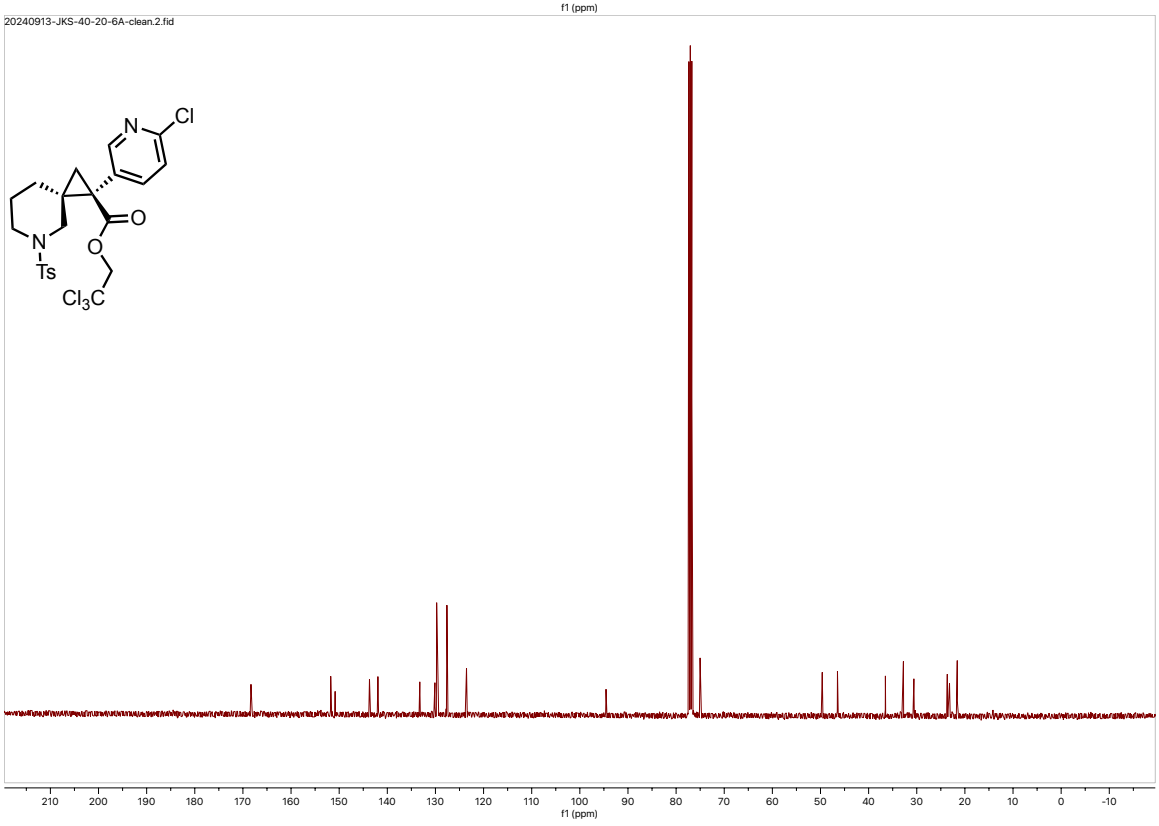
20240913-JKS-40-20-6A-clean.2.fid
N
Cl
O
O
N
Ts
Cl3C
f1 (ppm)

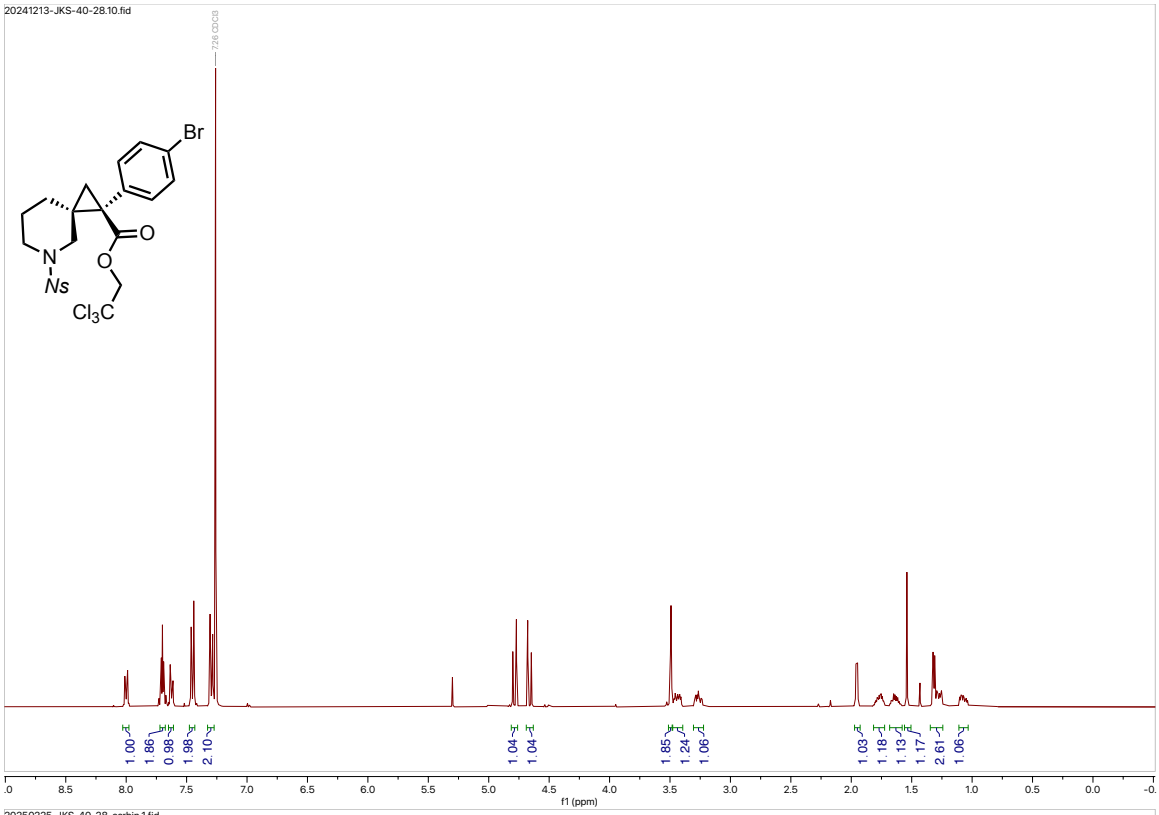
20241213-JKS-40-28.10.fid
7.26 CDCl3
Br
O
O
N
Ns
Cl3C
1.00
1.86
0.98
1.98
2.10
1.04
1.04
1.85
1.24
1.06
1.03
1.18
1.13
1.17
2.61
1.06
f1 (ppm)

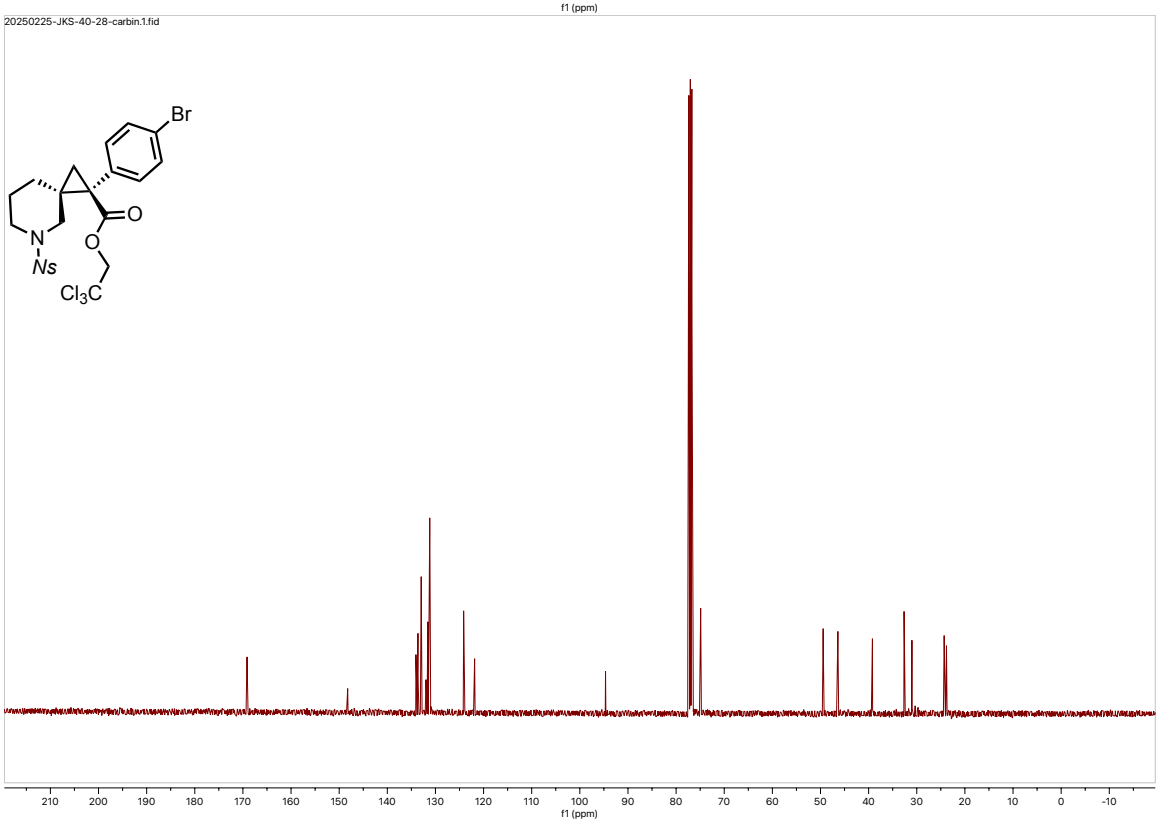
20250225-JKS-40-28-carbin.1.fid
Br
O
O
N
Ns
Cl3C
f1 (ppm)

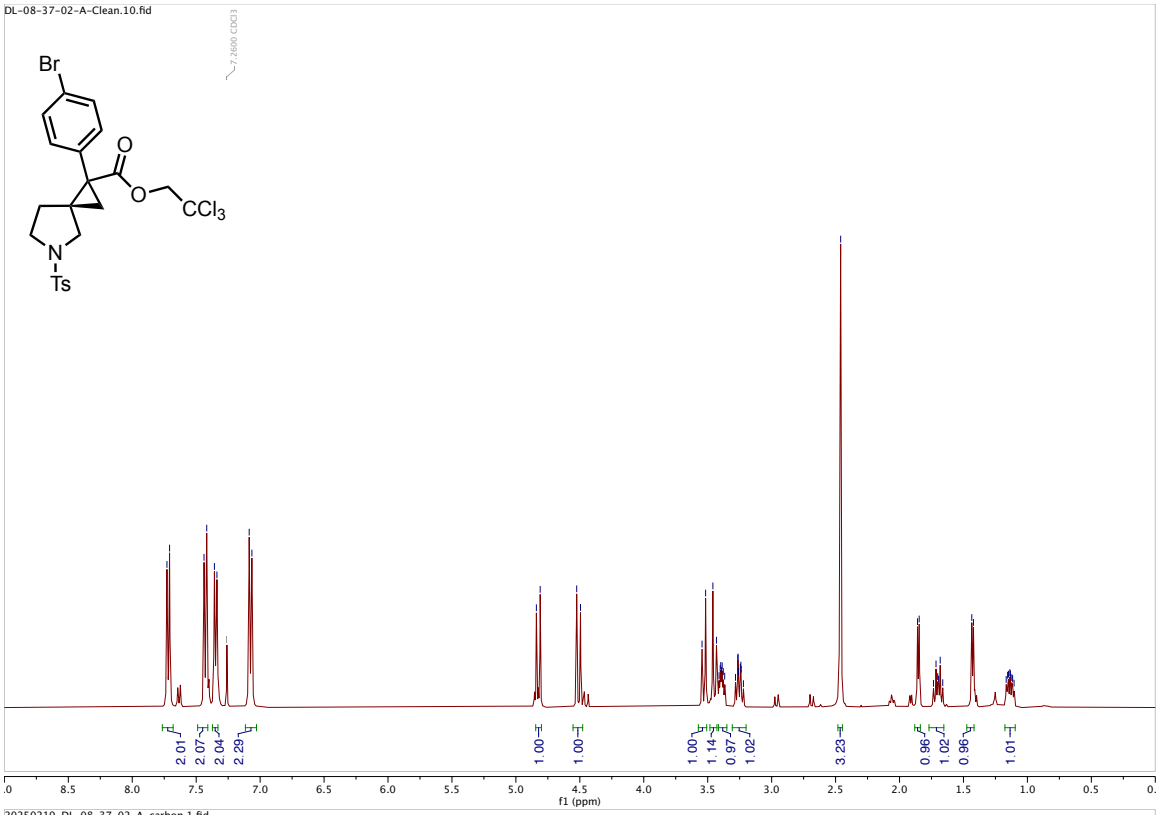
DL-08-37-02-A-Clean.10.fid
Br
O
O
CCl3
N
Ts
2.01
2.07
2.04
2.29
1.00
1.00
1.00
1.14
0.97
1.02
3.23
0.96
1.02
0.96
1.01
f1 (ppm)

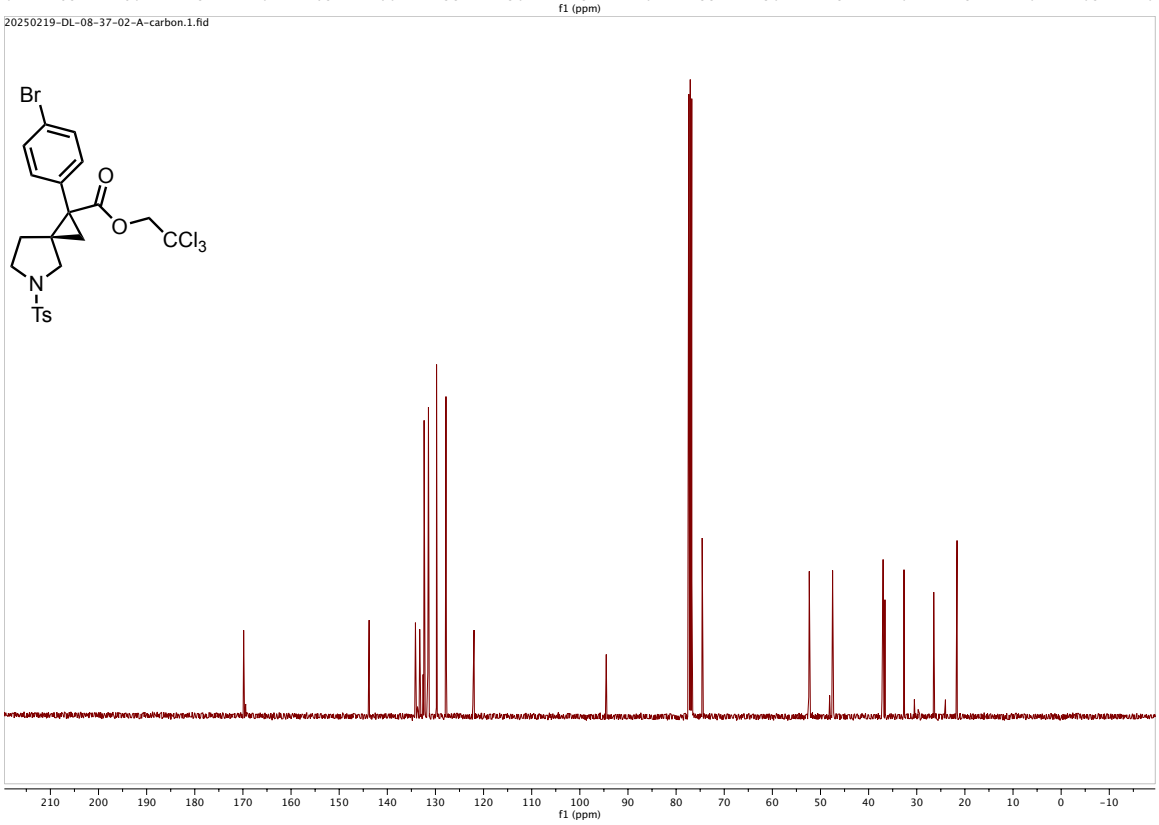
20250219-DL-08-37-02-A-carbon.1.fid
Br
O
O
CCl3
N
Ts
f1 (ppm)

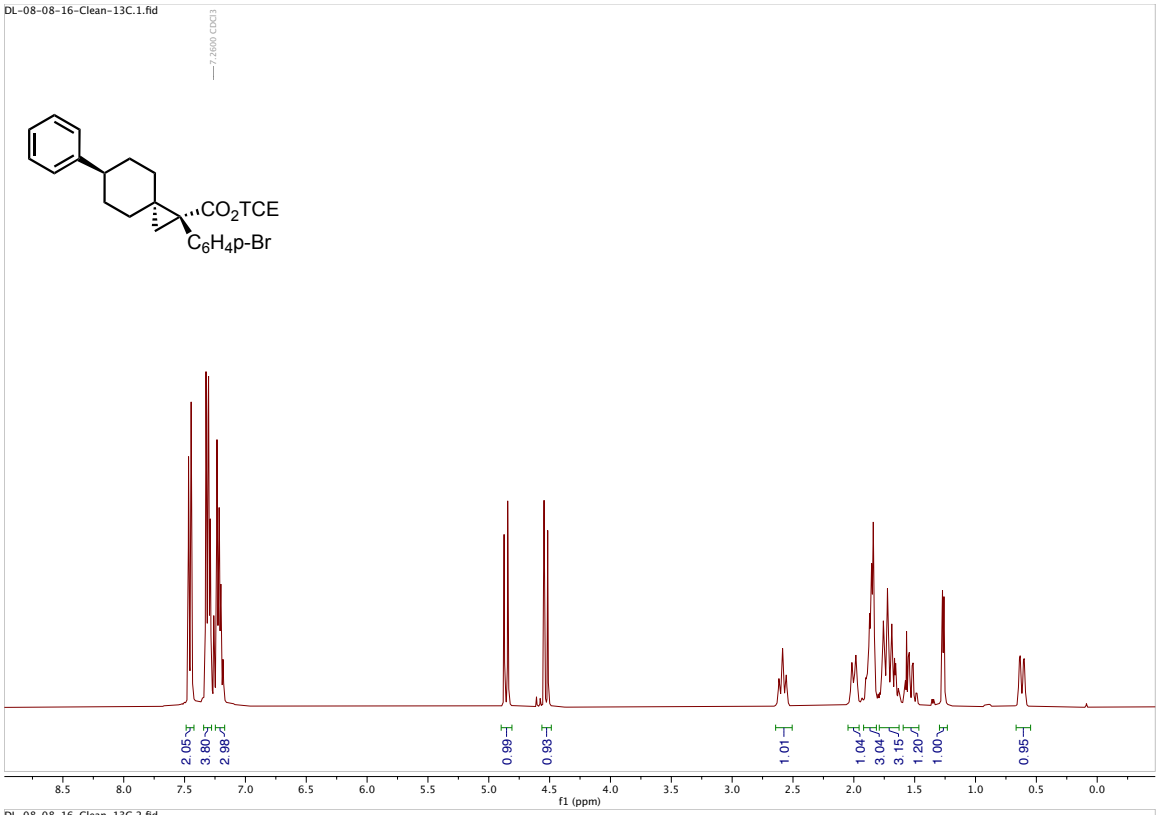
DL-08-08-16-Clean-13C.1.fid
7.2600 CDCl3
CO2TCE
C6H4p-Br
2.05
3.80
2.98
0.99
0.93
1.01
1.04
3.04
3.15
1.20
1.00
0.95
f1 (ppm)

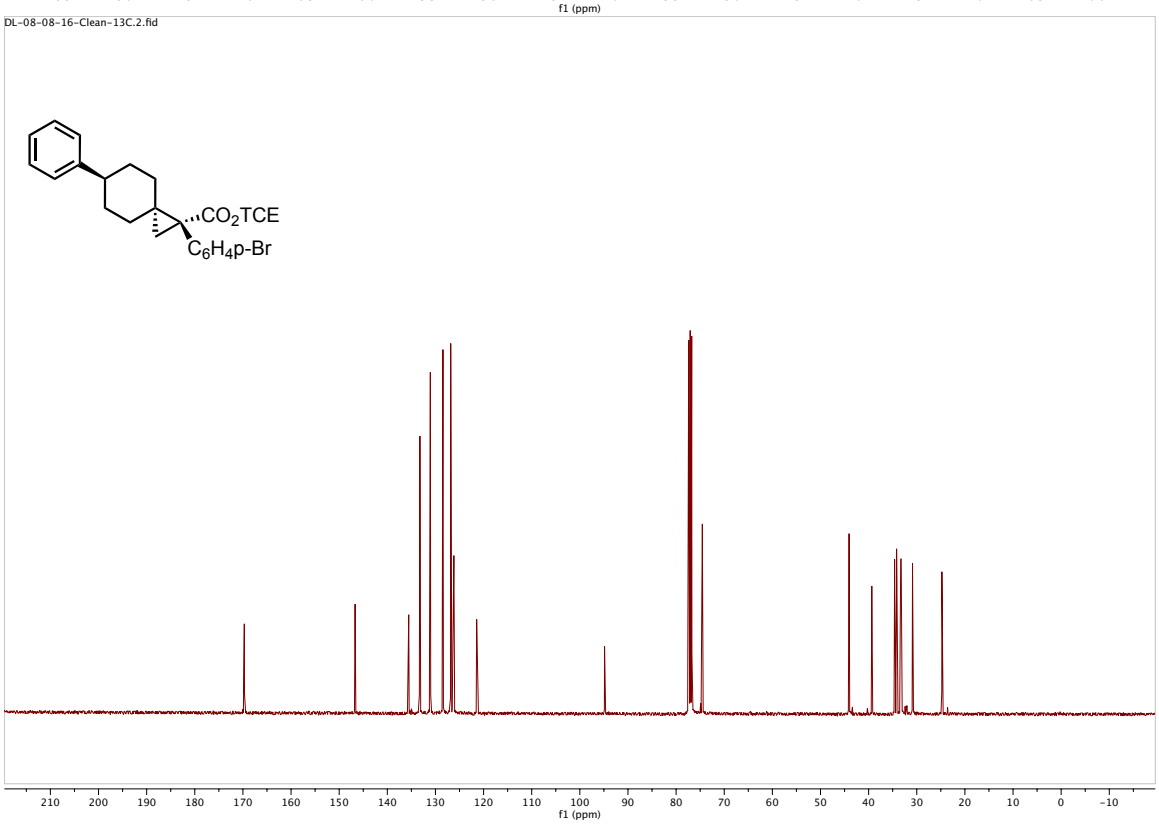
DL-08-08-16-Clean-13C.2.fid
CO2TCE
C6H4p-Br
f1 (ppm)

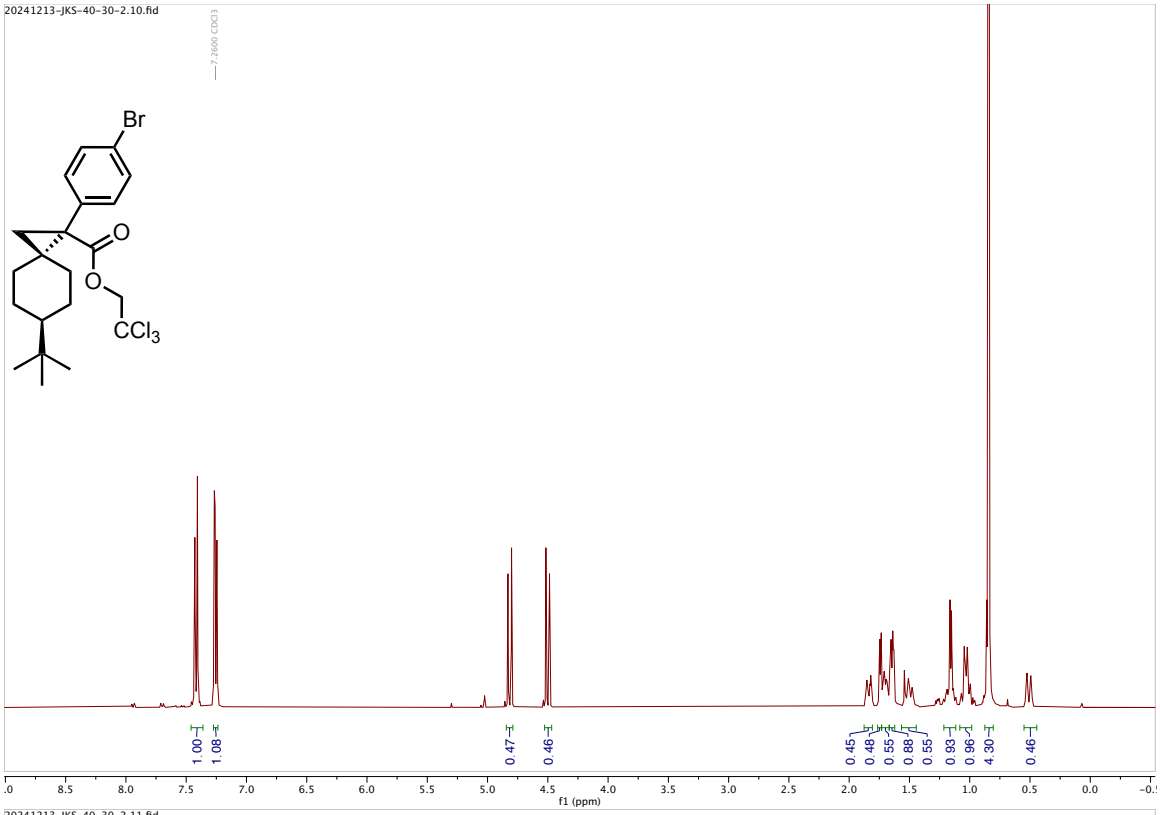
20241213-JKS-40-30-2.10.fid
Br
O
O
CCl3
1.00
1.08
0.47
0.46
0.45
0.48
0.55
0.88
0.55
0.93
0.96
4.30
0.46
f1 (ppm)

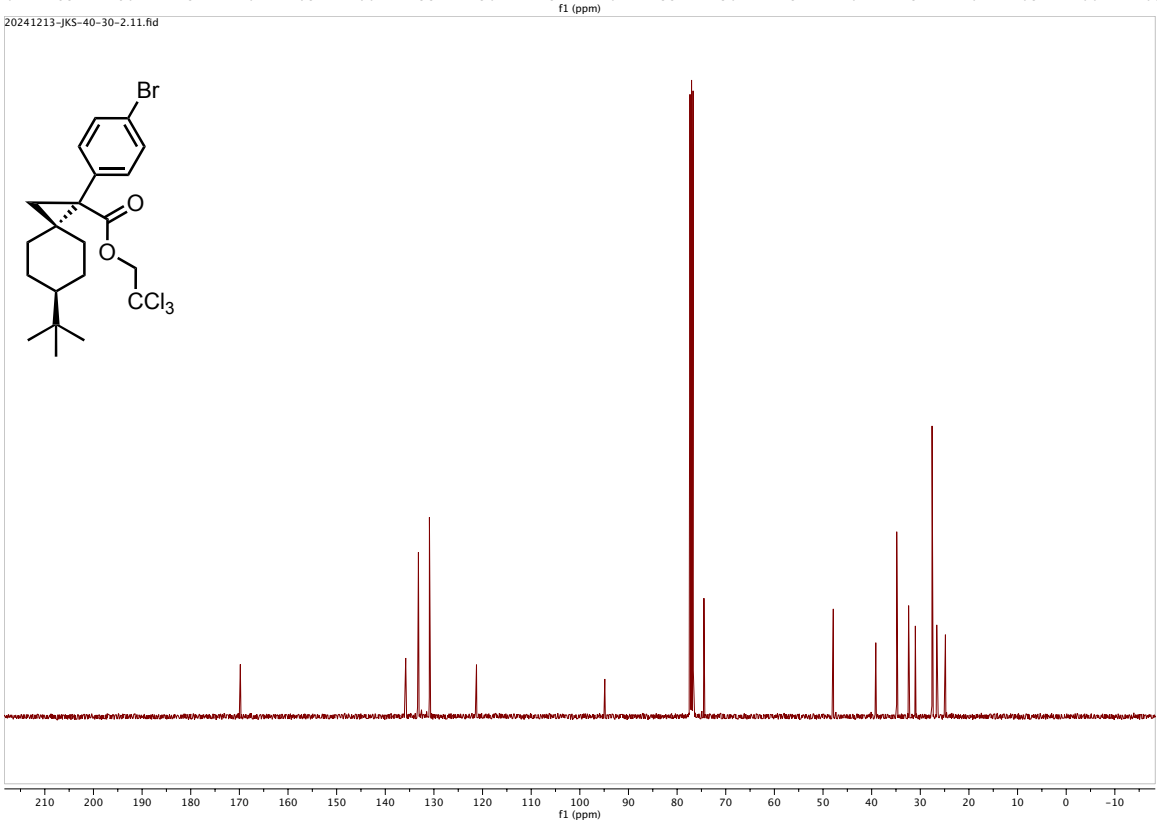
20241213-JKS-40-30-2.11.fid
Br
O
O
CCl3
f1 (ppm)

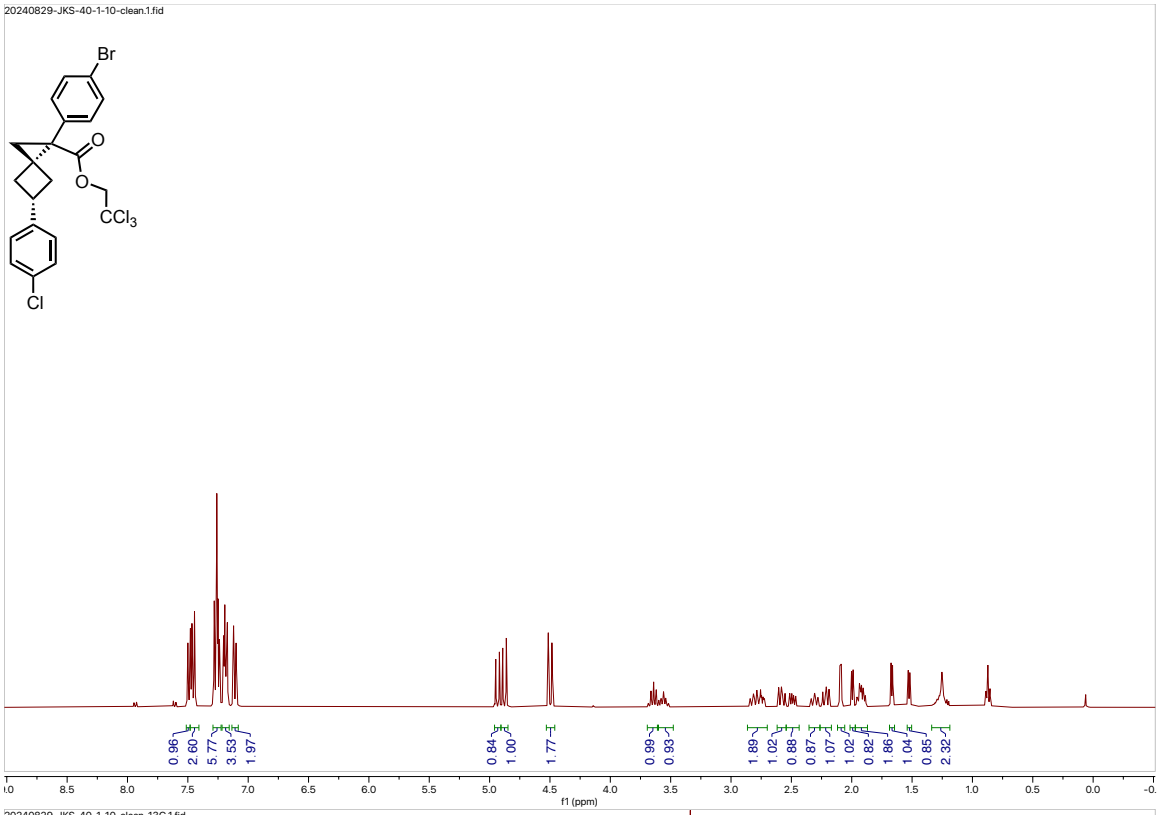
20240829-JKS-40-1-10-clean.1.fid
Br
O
O
CCl3
Cl
0.96
2.60
5.77
3.53
1.97
0.84
1.00
1.77
0.99
0.93
1.89
1.02
0.88
0.87
1.07
1.02
0.82
1.86
1.04
0.85
2.32
f1 (ppm)

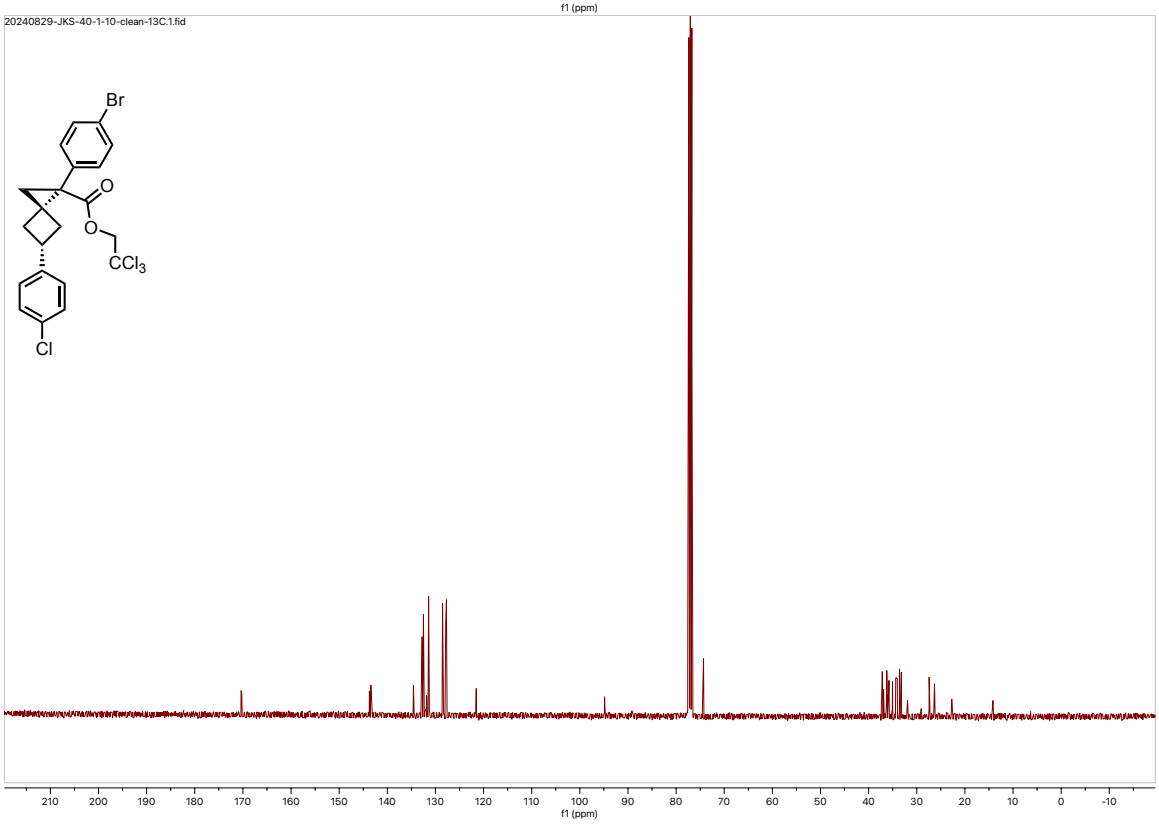
20240829-JKS-40-1-10-clean-13C.1.fid
Br
O
O
CCl3
Cl
f1 (ppm)

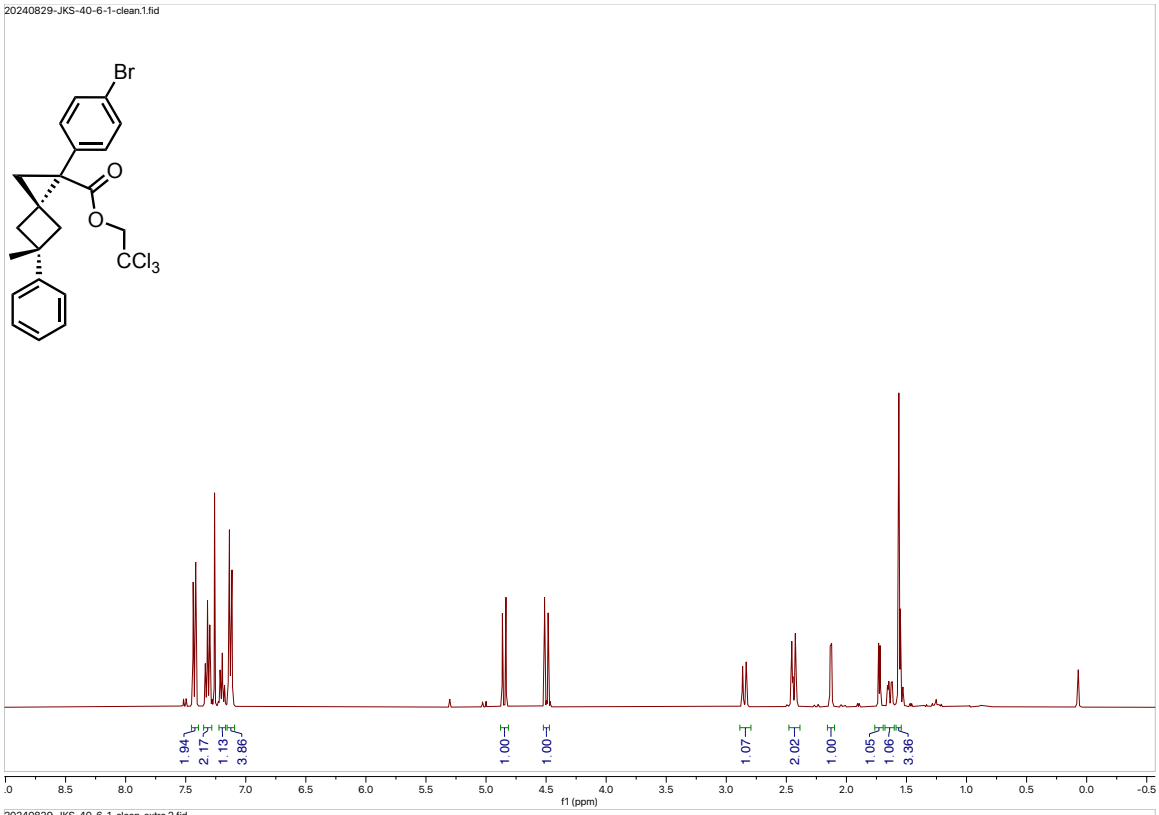
20240829-JKS-40-6-1-clean.1.fid
Br
O
O
CCl3
1.94
2.17
1.13
3.86
1.00
1.00
1.07
2.02
1.00
1.05
1.06
3.36
f1 (ppm)

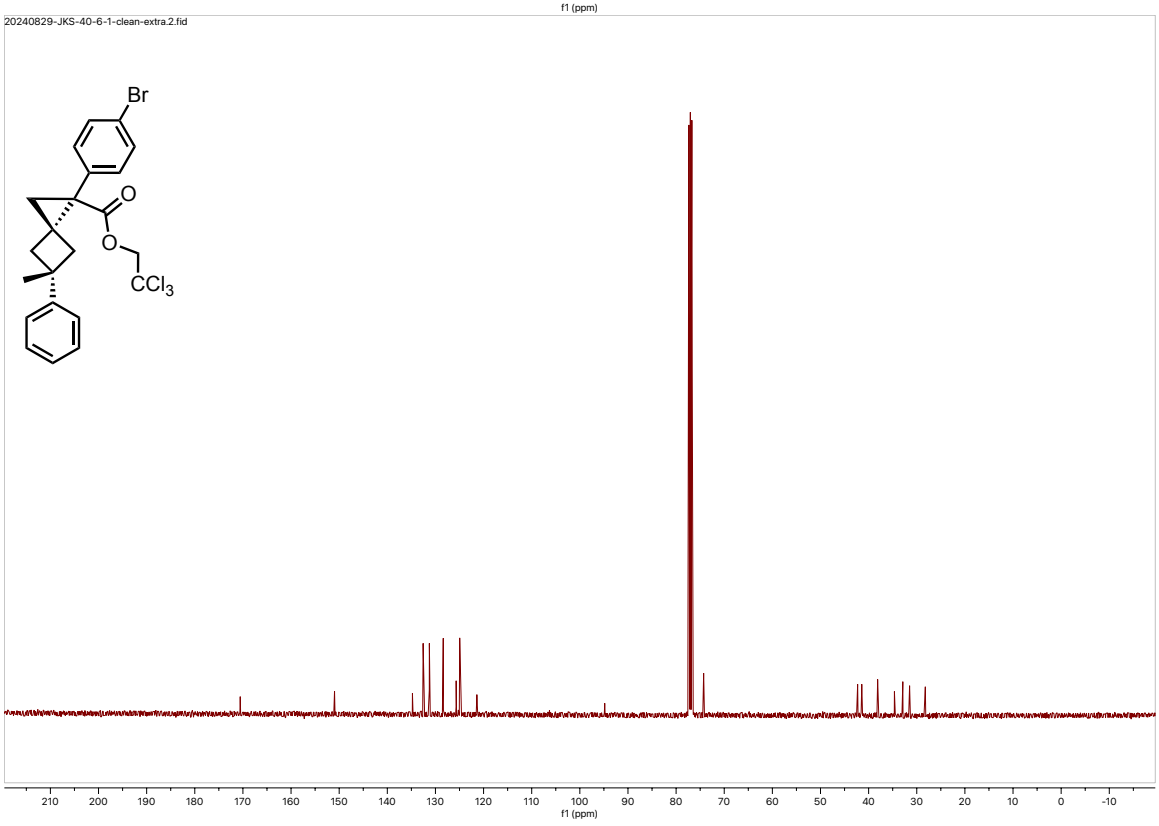
20240829-JKS-40-6-1-clean-extra.2.fid
Br
O
O
CCl3
f1 (ppm)

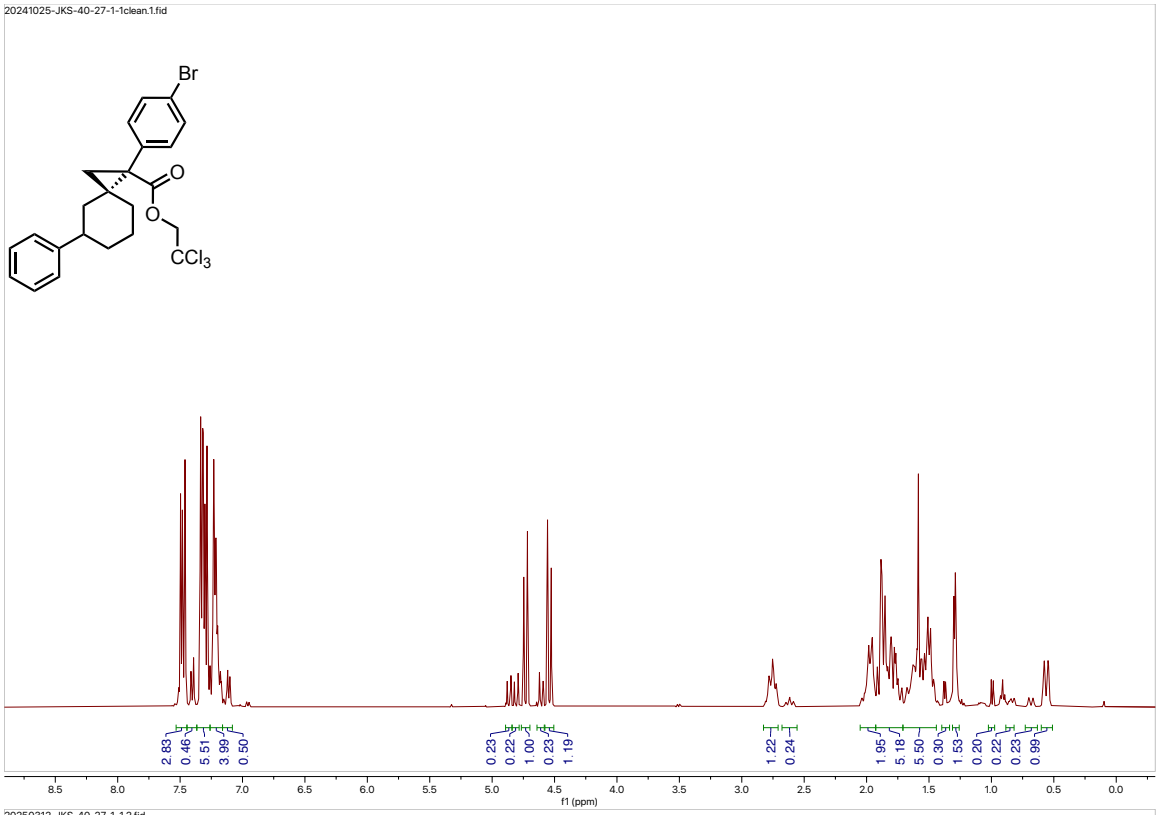
20241025-JKS-40-27-1-1clean.1.fid
Br
O
O
CCl3
2.83
0.46
5.51
3.99
0.50
0.23
0.22
1.00
0.23
1.19
1.22
0.24
1.95
5.18
5.50
0.30
1.53
0.20
0.22
0.23
0.99
8.5
8.0
7.5
7.0
6.5
6.0
5.5
5.0
4.5
4.0
3.5
3.0
2.5
2.0
1.5
1.0
0.5
0.0
f1 (ppm)

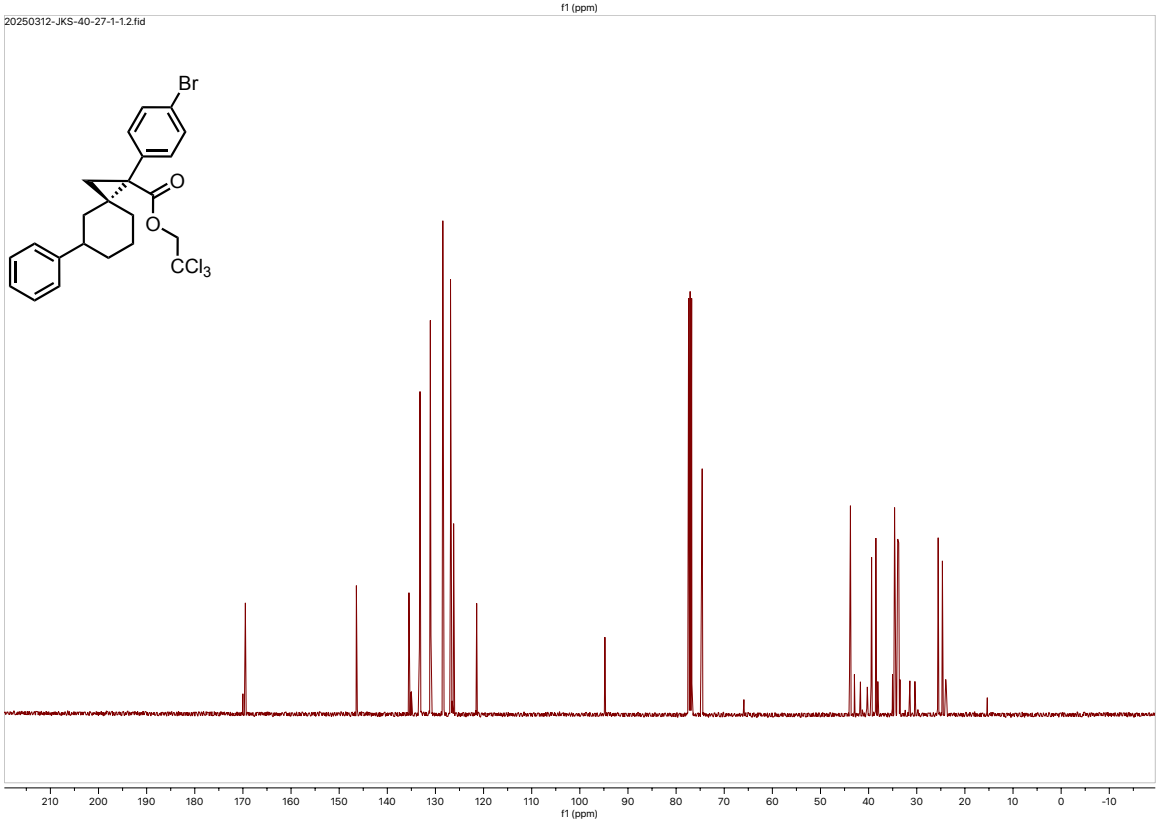
20250312-JKS-40-27-1-1.2.fid
Br
O
O
CCl3
210
200
190
180
170
160
150
140
130
120
110
100
90
80
70
60
50
40
30
20
10
0
-10
f1 (ppm)

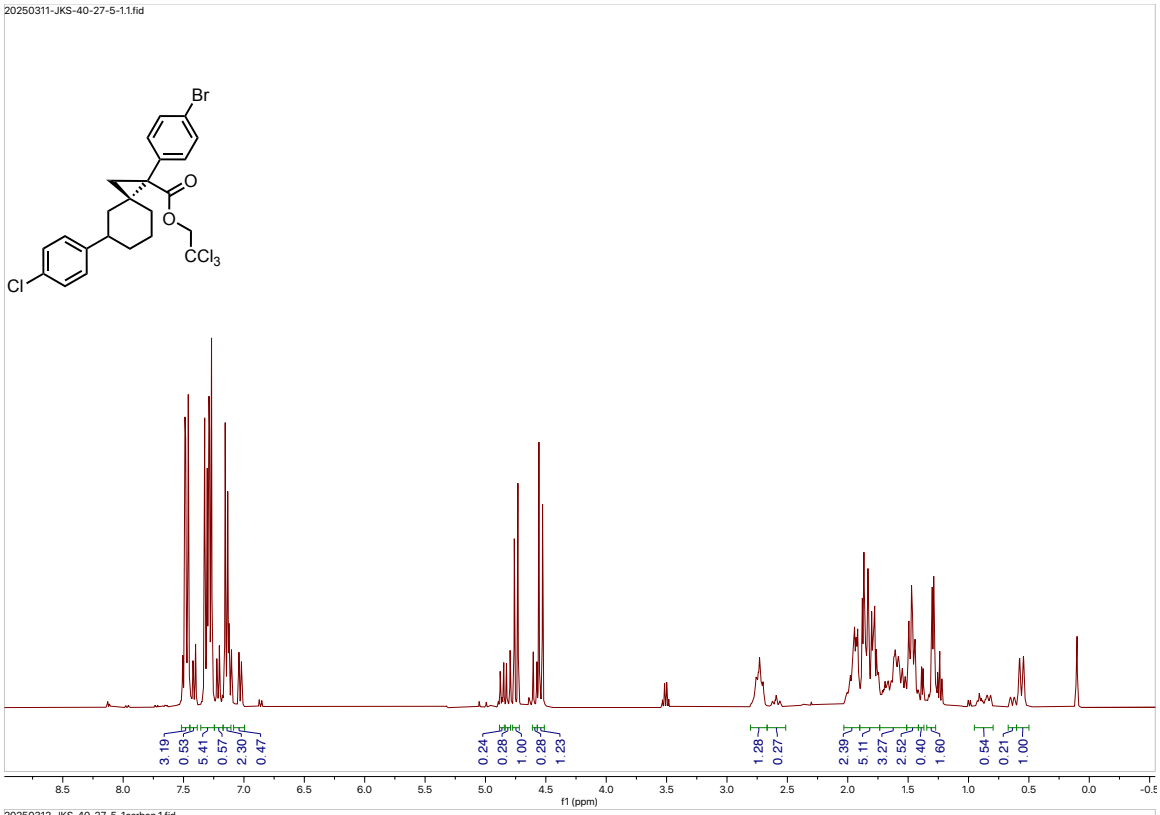
20250311-JKS-40-27-5-1.1.fid
Br
O
O
CCl3
Cl
3.19
0.53
5.41
0.57
2.30
0.47
0.24
0.28
1.00
0.28
1.23
1.28
0.27
2.39
5.11
3.27
2.52
0.40
1.60
0.54
0.21
1.00
8.5
8.0
7.5
7.0
6.5
6.0
5.5
5.0
4.5
4.0
3.5
3.0
2.5
2.0
1.5
1.0
0.5
0.0
f1 (ppm)

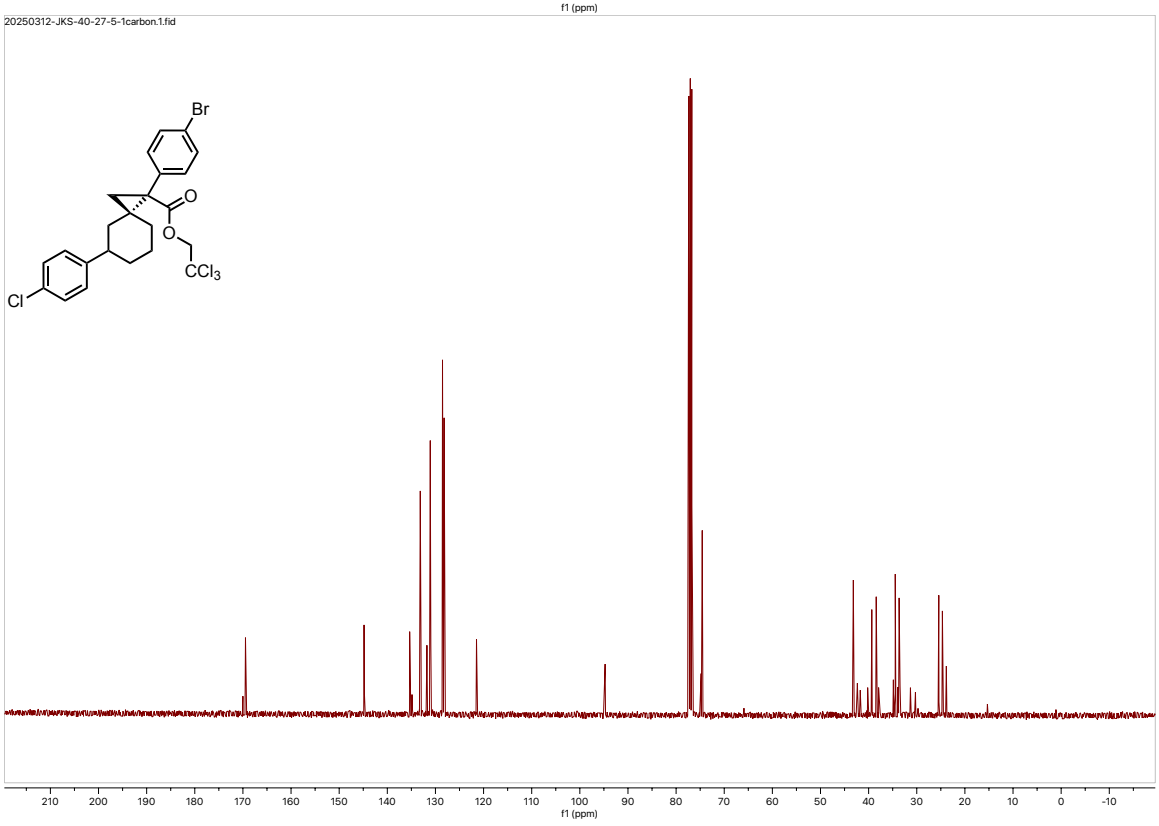
20250312-JKS-40-27-5-1carbon.1.fid
Br
O
O
CCl3
Cl
210
200
190
180
170
160
150
140
130
120
110
100
90
80
70
60
50
40
30
20
10
0
-10
f1 (ppm)

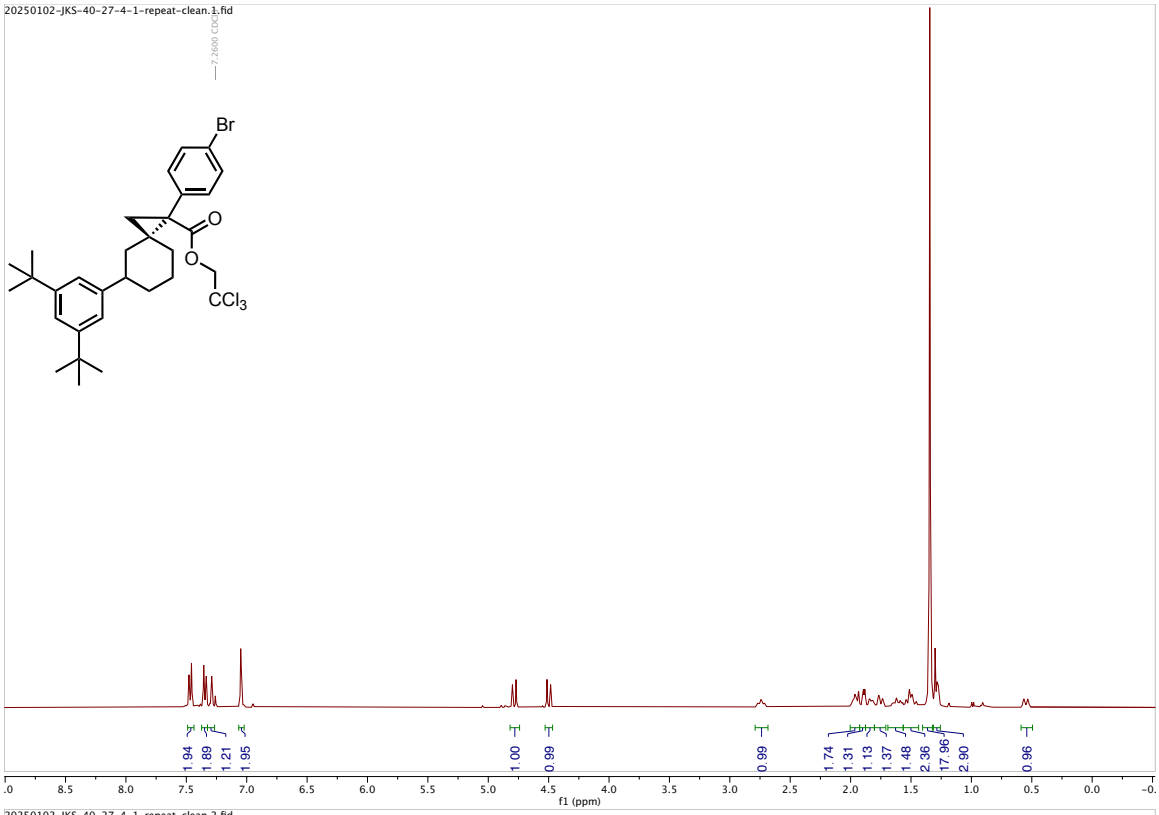
20250102-JKS-40-27-4-1-repeat-clean.1.fid
7.2600 CDCl3
Br
O
O
CCl3
1.94
1.89
1.21
1.95
1.00
0.99
0.99
1.74
1.31
1.13
1.37
1.48
2.36
17.96
2.90
0.96
f1 (ppm)

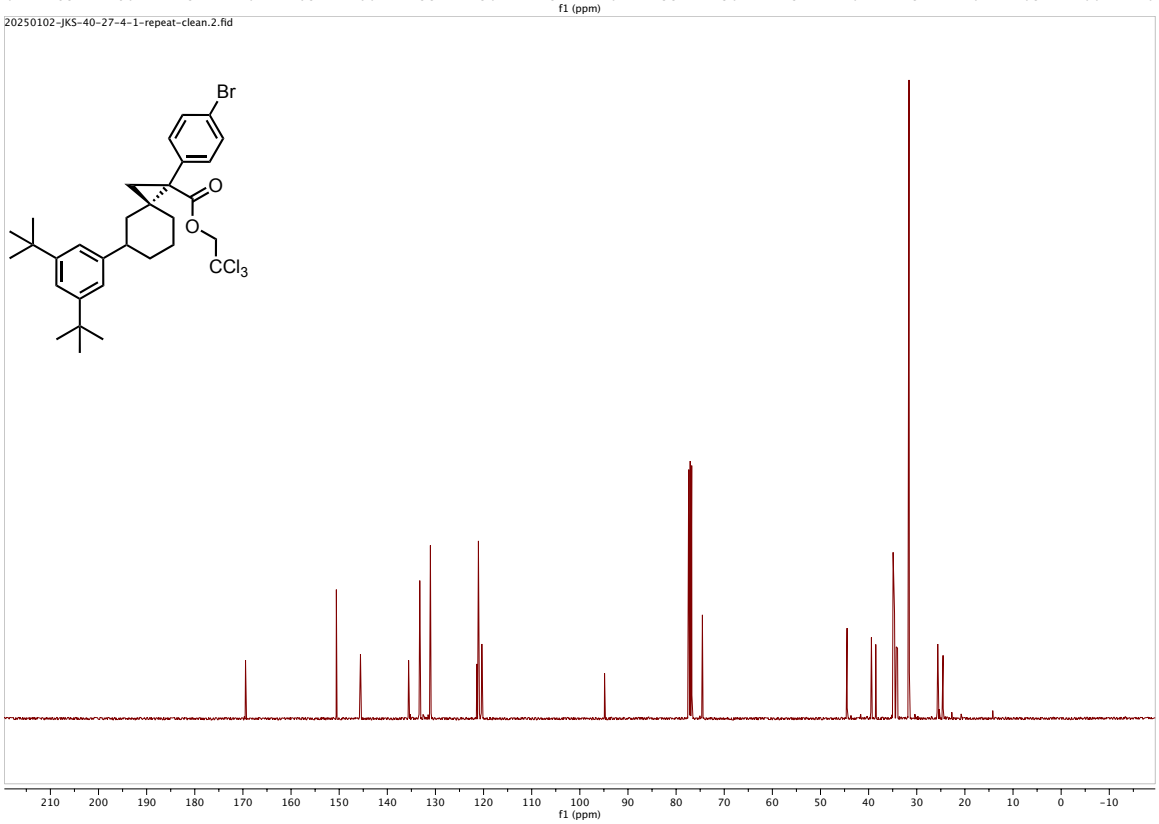
20250102-JKS-40-27-4-1-repeat-clean.2.fid
Br
O
O
CCl3
f1 (ppm)

Structural Assignment for Compound 30
We begin by assigning the alkyl protons in the ^{1}H-NMR. We see 7 distinct peaks.

- a_3 : s at 1.59 ppm integrating to 3, corresponding to the methyl group.
- b : dd at 1.66 ppm (J = 11.37, 3.64 Hz), integrating to 1
- c: d at 1.75 ppm (J = 4.84 Hz), integrating to 1
- d: d at 2.15 ppm (J = 4.83 Hz), integrating to 1
- e: An overlapping d and dd at 2.46 ppm (J = 11.67, 3.74 Hz), integrating to 2.
- f: d at 2.87 ppm (J = 11.78)

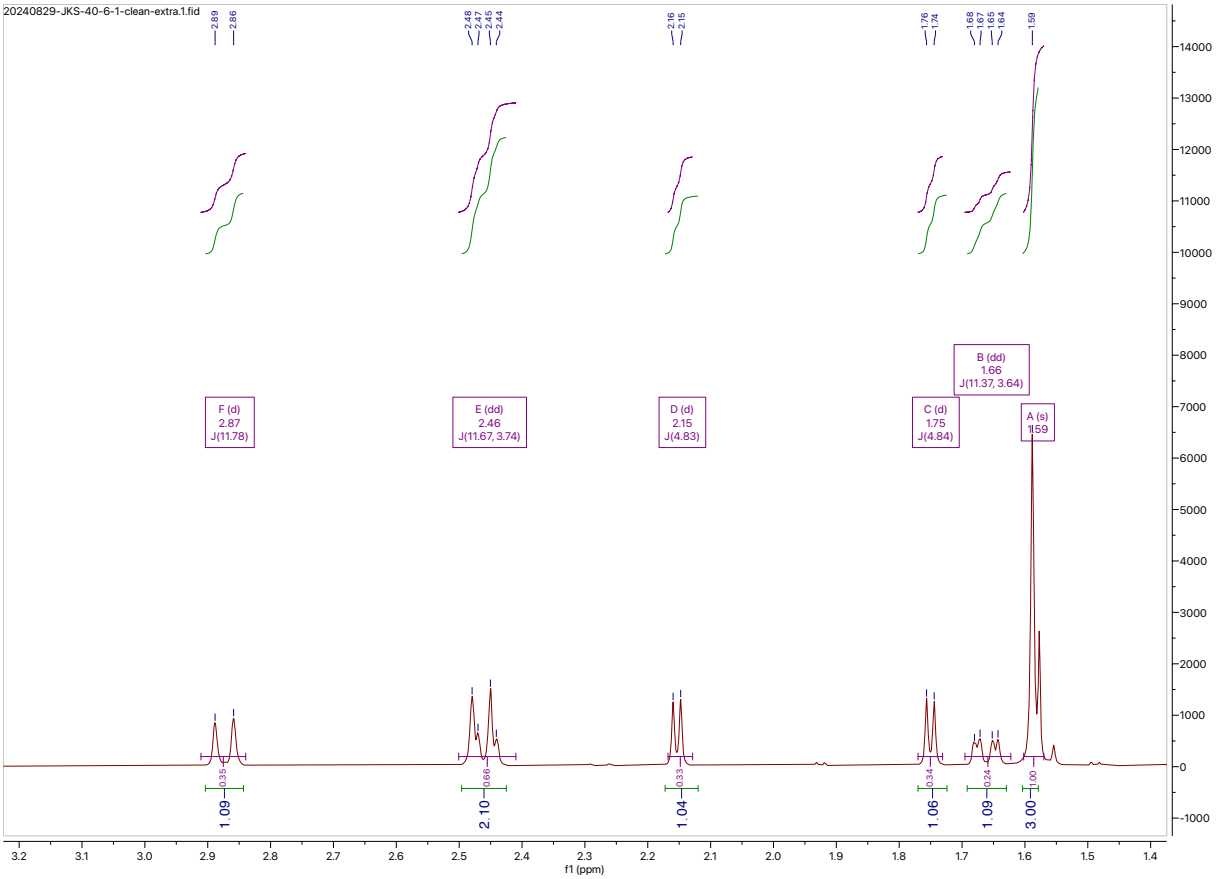

We can determine the cyclopropane peaks are signals C and D by looking at the COSY correlations:

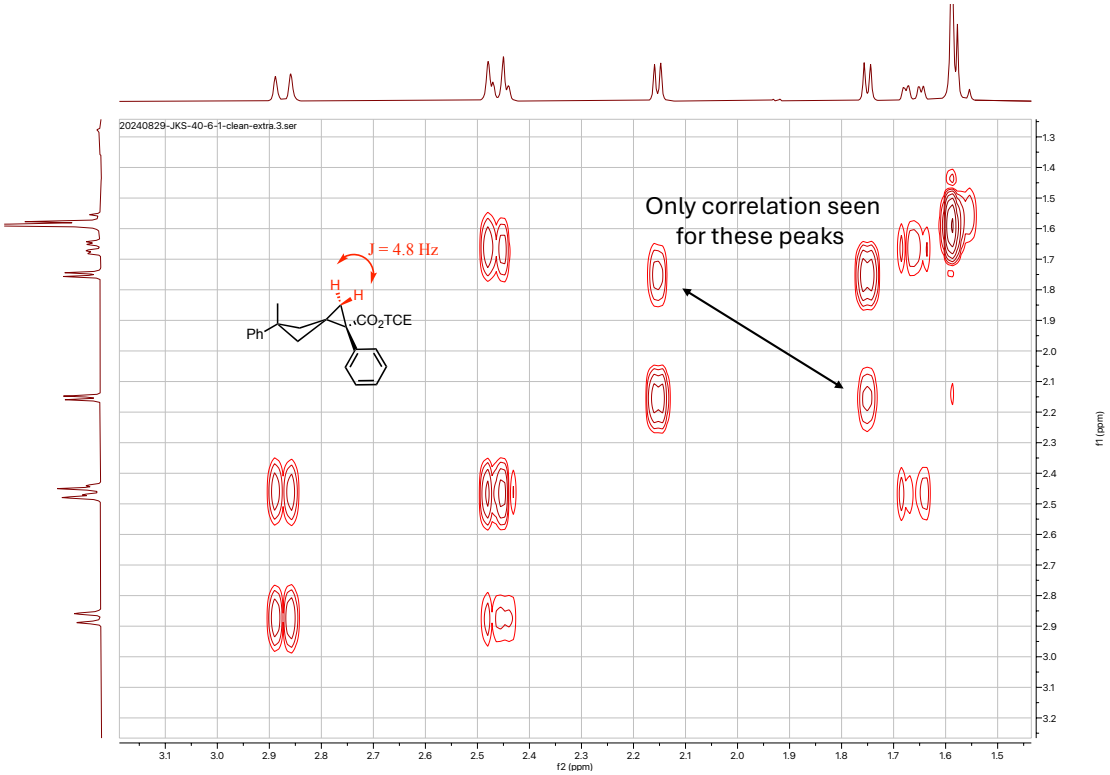

The cyclopropyl peaks should only have geminal coupling. In the COSY NMR we find that peaks C and D are the only peaks which couple only to each other. Thus, these peaks can be confidently assigned to the cyclopropyl protons.
We can then conclude that peaks B, E, and F make up the four protons on the cyclobutane ring.
We see that peak B is a dd, but there is no obvious dd which it is coupling to. Referring to the COSY, we find that there is a correlation with peak E. However, the height of the peaks looks strange. Looking at it as two separate signals, a d and a dd can deconvolute the system. Thus, two peaks are overlapping at E. The two dd peaks (B and part of E) are the equatorial protons on the cyclobutane ring, with geminal coupling to the axial proton, and w-coupling with one another (second geminal coupling not explicitly drawn in figure for clarity).

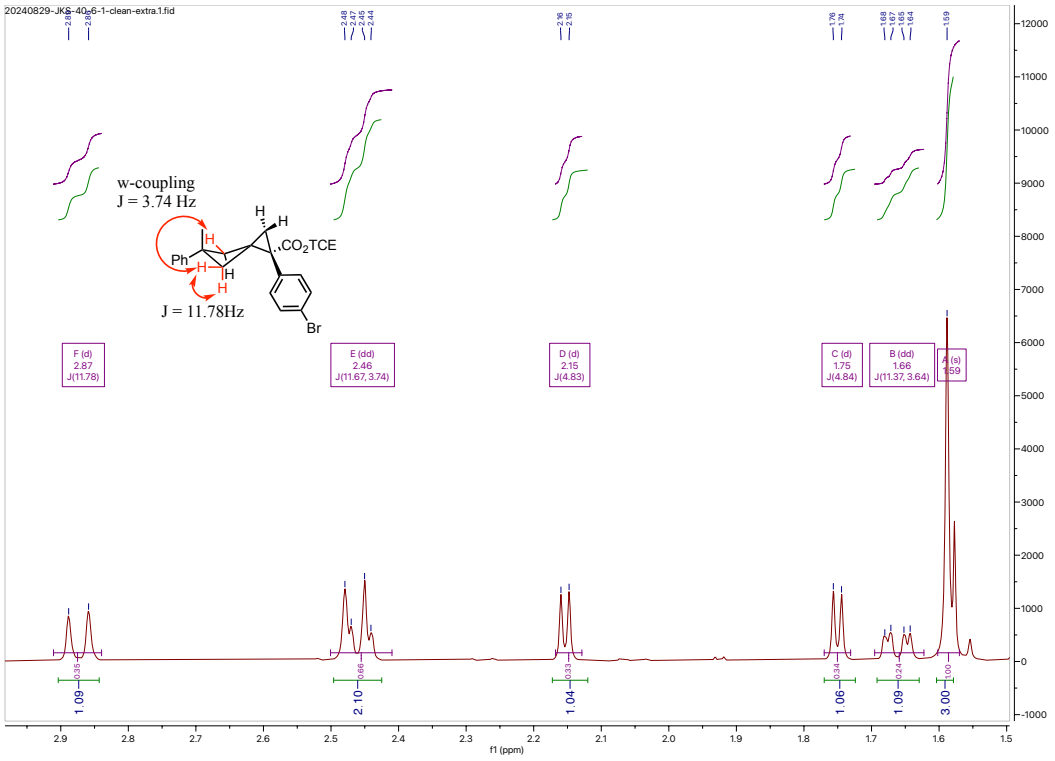

Three of the protons are distinctly shielded by the *p*-Br phenyl ring and are expected to be shifted upfield as a result of this. This can be seen with the distinct chemical shifts of B, C, and the left-half of E, which are all shifted upfield relative to their counter parts D, the right-half of E, and F. Because of this, we can conclude that B, C, and E are cis to the 4-substituted phenyl ring. This shows that the phenyl and carboxyl on the carbene carbon is down.

To determine whether the cyclopropane methylene is cis or trans to the methyl we look to the NOESY NMR. Here, we can see several through-space correlations that support our structural assignment.
First, if the methyl group is trans to the axial cyclobutane protons, we would not expect to see NOESY correlation between these two protons. We would expect to see NOESY correlation between the methyl and equatorial signals. We can observe the correlation with the methyl and the ‘right-half’ of the dd, along with the absence of a correlation between the methyl and peak F, one of the axial cyclobutane protons. This suggests that the methyl is trans to the axial protons and is cis to the equatorial protons.

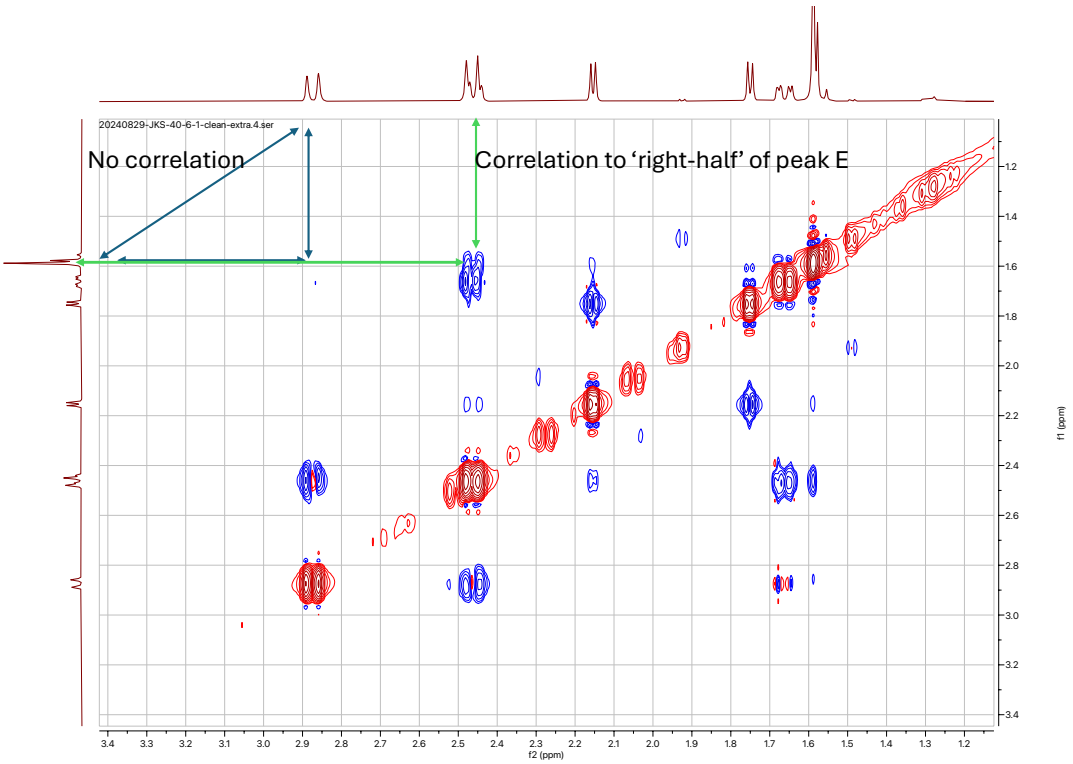

Finally, there is a weak correlation between the methyl group and the cyclopropyl peaks seen in the NOESY, indicating that these groups are cis to one another.

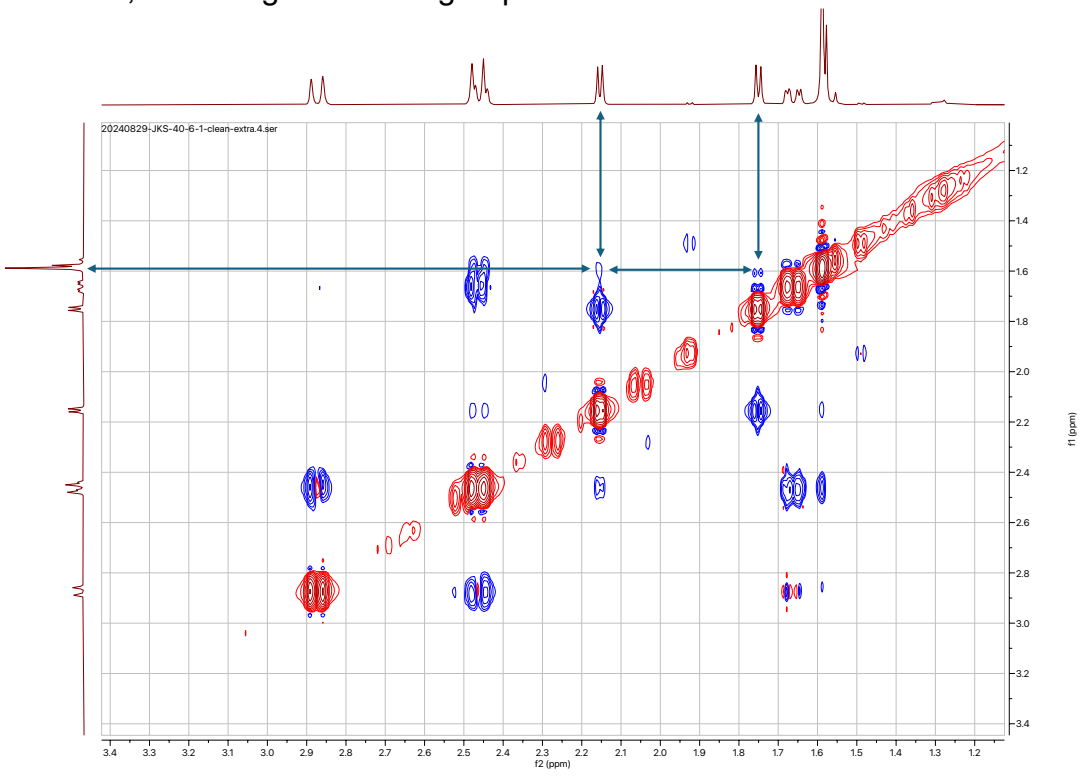

Final assigment:

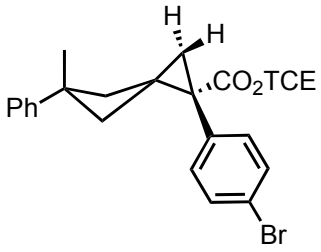
H
H
CO2TCE
Ph
Br

References

1. Noji, S.; Hara, Y.; Miura, T.; Yamanaka, H.; Maeda, K.; Hori, A.; Yamamoto, H.; Obika, S.; Inoue, M.; Hase, Y.; Orita, T.; Doi, S.; Adachi, T.; Tanimoto, A.; Oki, C.; Kimoto, Y.; Ogawa, Y.; Negoro, T.; Hashimoto, H.; Shiozaki, M., Discovery of a Janus Kinase Inhibitor Bearing a Highly Three-Dimensional Spiro Scaffold: JTE-052 (Delgocitinib) as a New Dermatological Agent to Treat Inflammatory Skin Disorders. *J. Med. Chem.* **2020,** *63* (13), 7163-7185.
2. Law, J. A.; Bartfield, N. M.; Frederich, J. H., Site-Specific Alkene Hydromethylation via Protonolysis of Titanacyclobutanes. *Angew. Chem. Int. Ed.* **2021,** *60* (26), 14360-14364.
3. Cong, F.; Sun, G.-Q.; Ye, S.-H.; Hu, R.; Rao, W.; Koh, M. J., A Bimolecular Homolytic Substitution-Enabled Platform for Multicomponent Cross-Coupling of Unactivated Alkenes. *J. Am. Chem. Soc.* **2024,** *146* (15), 10274-10280.
4. Nóvoa, L.; Trulli, L.; Parra, A.; Tortosa, M., Stereoselective Diboration of Spirocyclobutenes: A Platform for the Synthesis of Spirocycles with Orthogonal Exit Vectors. *Angew. Chem. Int. Ed.* **2021,** *60* (21), 11763-11768.
5. Soulard, V.; Villa, G.; Vollmar, D. P.; Renaud, P., Radical Deuteration with D2O: Catalysis and Mechanistic Insights. *J. Am. Chem. Soc.* **2018,** *140* (1), 155-158.
6. Liu, X.; Rong, X.; Liu, S.; Lan, Y.; Liu, Q., Cobalt-Catalyzed Desymmetric Isomerization of Exocyclic Olefins. *J. Am. Chem. Soc.* **2021,** *143* (49), 20633-20639.
7. Lei, S.-H.; Zou, Y.-F.; Qu, J.-P.; Kang, Y.-B., TBN as Organic Redox Cocatalyst for Oxidative Tiffeneau–Demjanov-Type Rearrangement Using O2 as Sole Oxidant. *Org. Lett.* **2024,** *26* (30), 6454-6458.
8. Sietmann, J.; Tenberge, M.; Wahl, J. M., Wacker Oxidation of Methylenecyclobutanes: Scope and Selectivity in an Unusual Setting. *Angew. Chem. Int. Ed.* **2023,** *62* (7), e202215381.
9. Zhang, Z.; Sun, Z.; Song, J.; Guo, H.; Wang, Y.; Hu, X., Construction of the A–B–C Ring of Simplicissin through an Oxidative Dearomatization/Iodination/[3+2] Annulation Cascade. *Org. Lett.* **2023,** *25* (48), 8645-8649.

Appendix D. Chapter 5 Supporting Information

General Considerations

All experiments were carried out in flame-dried glassware under argon atmosphere unless otherwise stated. Flash column chromatography was performed on silica gel. Unless otherwise noted, all other reagents were obtained from commercial sources (Sigma Aldrich, Fisher, TCI Chemicals, AK Scientific, Combi Blocks, Oakwood Chemicals, Ambeed) and used as received without purification. ^{1}H, ^{13}C, and ^{19}F NMR spectra were recorded at either 400 MHz (^{13}C at 100 MHz) on Bruker 400 spectrometer or 600 MHz (^{13}C at 151 MHz) on INOVA 600 or Bruker 600 spectrometer. NMR spectra were run in solutions of deuterated chloroform ($CDCl_3$) with residual chloroform taken as an internal standard (7.26 ppm for ^{1}H, and 77.16 ppm for ^{13}C), and were reported in parts per million (ppm). The abbreviations for multiplicity are as follows: s = singlet, d = doublet, t = triplet, q = quartet, p = pentet, m = multiplet, dd = doublet of doublet, etc. Coupling constants (J values) are obtained from the spectra. Thin layer chromatography was performed on aluminum-back silica gel plates with UV light and cerium aluminum molybdate (CAM) stain to visualize. Mass spectra were taken on a Thermo Finnigan LTQ-FTMS spectrometer with APCI or ESI.

Low temperature irradiation setup

The screw-cap photoreaction vials were placed in a cystalization dish in an acetone bath, completely submerging the vial in acetone up to the solvent line. The acetone bath was cooled using Thermo/Neslab CB80 Cryocool. The reactions were irradiated using a 440 nm Kessel lamp at 100% intensity. The light source was ~15 cm away from the vials. The temperature of the acetone bath was verified using a low temperature alcohol thermometer.

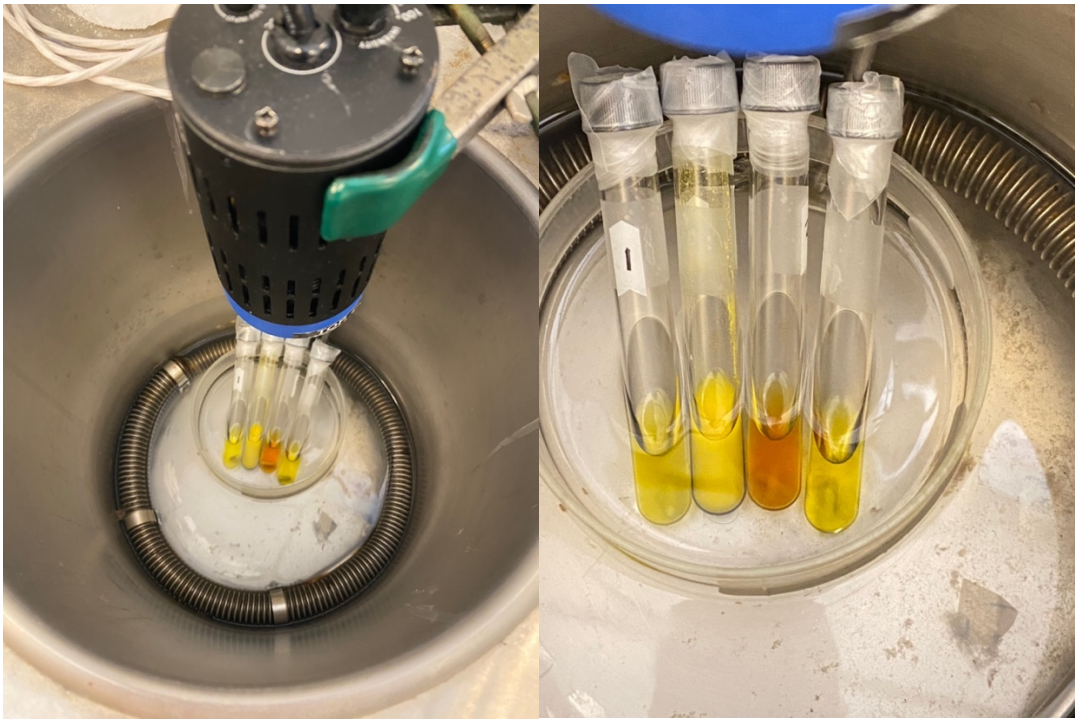

Known Compounds:

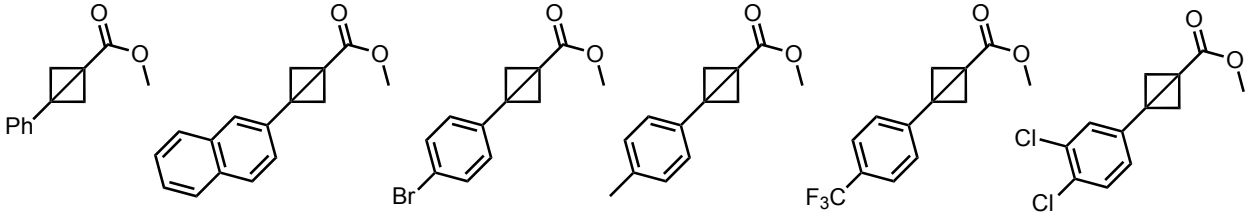

8 **S1** **S2** **S3** **S4** **S5**

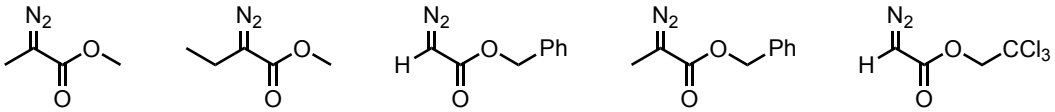

S6 **S7** **S8** **S9** **S10**

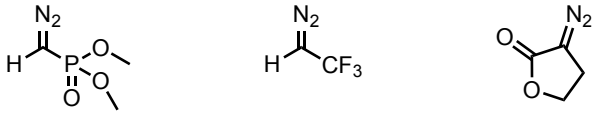

S11 **S12** **S13**

Compound **8, S1-S5** were synthesized according to known methods and specta matched the literature reported spectra.[1]

Compounds **S6** and **S7** were synthesized according to known methods and spectra matched the literature reported spectra.[2]

Compounds **S8**,[3] **S9**,[4] **S10**,[5] **S11**,[6] **S12**,[7] and **S13**[8] were synthesized according to known methods and spectra matched the literature reported spectra.

Product Characterization

General Procedure A

To an oven dried photoreaction tube under inert atmosphere was added $Ir(ppy)_3$ (1.0 mol%, 1.31 mg) and the bicyclo[1.0]butane (0.20 mmol, 1.0 equiv). This was purged and backfilled three times with nitrogen. Then, 2 mL of DCM (degassed for 20 minutes using an argon balloon) as added to the reaction vessel. The diazo was weighed out into a separate vial and was purged with nitrogen, followed by the addition of 2 mL of DCM. Then, the diazo solution was added to the reaction vessel, the septum was sealed with parafilm, and the vessel was placed in a -65 °C acetone bath using the constant chiller. The reaction was irradiated with 440 nm Kessel lamp at 100% intensity for 22 h. At this time the reaction solution was concentrated and analyzed for crude NMR before column chromatography to afford the desired product.

General Procedure B

To an oven dried photoreaction tube under inert atmosphere was added thioxanthone (5.0 mol%, 2.12 mg) and the bicyclo[1.0]butane (0.20 mmol, 1.0 equiv). This was purged and backfilled three times with nitrogen. Then, 2 mL of DCM (degassed for 20 minutes using an argon balloon) as added to the reaction vessel. The diazo (0.5-1.0 mmol, 2.5-5.0 equiv) was weighed out into a separate vial and was purged with nitrogen, followed by the addition of 2 mL of DCM. Then, the diazo solution was added to the reaction vessel, the septum was sealed with parafilm, and the vessel was placed in a -65 °C acetone bath using the constant chiller. The reaction was irradiated with 390 nm Kessel lamp at 100% intensity for 22 h. At this time the reaction solution was concentrated and analyzed for crude NMR before column chromatography to afford the desired product.

2-ethyl 1-methyl 3-phenylbicyclo[1.1.1]pentane-1,2-dicarboxylate (28)

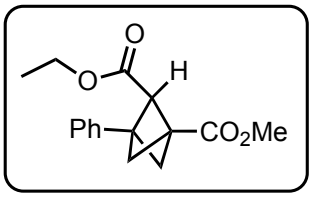

General procedure A was used for the reaction of methyl 3-phenylbicyclo[1.1.0]butane-1-carboxylate (0.20 mmol, 37.6 mg, 1 equiv) with ethyl 2-diazoacetate (0.50 mmol, 55.6 µL 83% wt in toluene, 2.5 equiv) using $Ir(ppy)_3$ (1.0 mol%, 1.31 mg) as catalyst. The reaction was purified using column chromatography (0-12% diethyl ether/hexanes gradient) affording a clear, colorless oil (28.8 mg, 55%).

^{1}H NMR (400 MHz, $CDCl_3$) δ 7.39 – 7.24 (m, 5H), 4.17 (q, J = 7.1 Hz, 2H), 3.77 (s, 3H), 3.37 (d, J = 7.0 Hz, 1H), 3.08 (dd, J = 9.8, 2.8 Hz, 1H), 2.37 (dd, J = 7.0, 2.8 Hz, 1H), 2.31 (dd, J = 9.8, 1.9 Hz, 1H), 2.25 (d, J = 1.8 Hz, 1H), 1.23 (t, J = 7.2 Hz, 3H).

^{13}C NMR (101 MHz, $CDCl_3$) δ 169.4, 169.1, 137.1, 128.3, 127.5, 126.6, 64.2, 60.5, 52.7, 52.0, 48.8, 46.3, 40.3, 14.2**.**

HRMS (+pAPCI): Calcd for $C_{16}H_{19}O_4$ [M+H] 275.1278, found 275.1280.

dimethyl 2-methyl-3-phenylbicyclo[1.1.1]pentane-1,2-dicarboxylate (29)

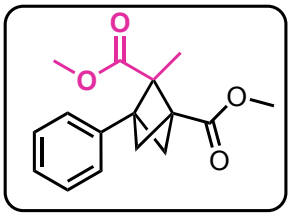

General procedure A was used for the reaction of methyl 3-phenylbicyclo[1.1.0]butane-1-carboxylate (0.20 mmol, 37.6 mg, 1 equiv) with methyl 2-diazopropanoate (0.50 mmol, 57.1 mg, 2.5 equiv) using $Ir(ppy)_3$ (1.0 mol%, 1.31 mg) as catalyst. The reaction was purified using column chromatography (0-12% diethyl ether/hexanes gradient) affording a clear, colorless oil (32.1 mg, 59%).

^{1}H NMR (400 MHz, $CDCl_3$) δ 7.40 – 7.24 (m, 5H), 3.75 (s, 3H), 3.68 (s, 3H), 2.84 (dd, J = 10.3, 3.0 Hz, 1H), 2.46 (dd, J = 10.3, 3.5 Hz, 1H), 2.24 (d, J = 3.5 Hz, 1H), 2.05 (d, J = 3.0 Hz, 1H), 1.58 (s, 3H).

^{13}C NMR (101 MHz, $CDCl_3$) δ 174.5, 169.1, 136.2, 128.2, 127.4, 127.2, 69.9, 51.8, 51.7, 49.1, 48.7, 47.2, 42.9, 13.1.

HRMS (+pAPCI): Calcd for $C_{16}H_{19}O_4$ [M+H] 275.1278, found 275.1275.

dimethyl 2-ethyl-3-phenylbicyclo[1.1.1]pentane-1,2-dicarboxylate (30)

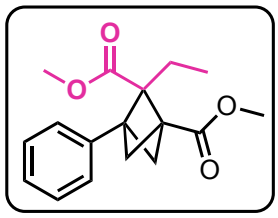

General procedure A was used for the reaction of methyl 3-phenylbicyclo[1.1.0]butane-1-carboxylate (0.20 mmol, 37.6 mg, 1 equiv) with methyl 2-diazobutanoate (0.50 mmol, 64.1 mg, 2.5 equiv) using $Ir(ppy)_3$ (1.0 mol%, 1.31 mg) as catalyst. The reaction was purified using column chromatography (0-12% diethyl ether/hexanes gradient) affording a clear, colorless oil (21.8 mg, 40%).

^{1}H NMR (400 MHz, $CDCl_3$) δ 7.36 – 7.26 (m, 4H), 3.75 (s, 3H), 3.70 (s, 3H), 2.91 (dd, J = 10.3, 3.1 Hz, 1H), 2.48 (dd, J = 10.3, 3.5 Hz, 1H), 2.21 – 2.09 (m, 2H), 2.09 – 1.94 (m, 2H), 0.86 (t, J = 7.6 Hz, 3H).

^{13}C NMR (101 MHz, $CDCl_3$) δ 173.6, 169.2, 136.6, 128.1, 127.4, 127.3, 75.7, 51.8, 51.4, 49.3, 48.6, 46.4, 43.0, 20.6, 10.3.

HRMS (+pAPCI): Calcd for $C_{17}H_{21}O_4$ [M+H] 289.1434, found 289.1432.

2-benzyl 1-methyl 3-phenylbicyclo[1.1.1]pentane-1,2-dicarboxylate (31)

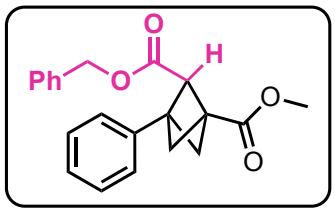

General procedure A was used for the reaction of methyl 3-phenylbicyclo[1.1.0]butane-1-carboxylate (0.20 mmol, 37.6 mg, 1 equiv) with benzyl 2-diazoacetate (0.50 mmol, 88.1 mg, 2.5 equiv) using $Ir(ppy)_3$ (1.0 mol%, 1.31 mg) as catalyst. The reaction was purified using column chromatography (0-12% diethyl ether/hexanes gradient) affording a clear, colorless oil (32.1 mg, 48%).

^{1}H NMR (400 MHz, $CDCl_3$) δ 7.39 – 7.36 (m, 1H), 7.35 – 7.31 (m, 5H), 7.30 – 7.26 (m, 2H), 7.26 – 7.21 (m, 2H), 5.19 (d, J = 12.5 Hz, 1H), 5.12 (d, J = 12.5 Hz, 1H), 3.72 (s, 3H), 3.45 (d, J = 7.0 Hz, 1H), 3.08 (dd, J = 9.8, 2.9 Hz, 1H), 2.38 (dd, J = 7.1, 2.9 Hz, 1H), 2.33 (dd, J = 9.7, 1.9 Hz, 1H), 2.26 (d, J = 1.9 Hz, 1H).

^{13}C NMR (101 MHz, $CDCl_3$) δ 169.2, 169.0, 137.0, 135.8, 128.5 , 128.3, 128.1, 128.0, 127.5, 126.7, 66.2, 64.1, 52.8, 52.0, 48.7, 40.3.

HRMS (+pAPCI): Calcd for $C_{21}H_{21}O_4$ [M+H] 337.1434, found 337.1434.

2-benzyl 1-methyl 2-methyl-3-phenylbicyclo[1.1.1]pentane-1,2-dicarboxylate (32)

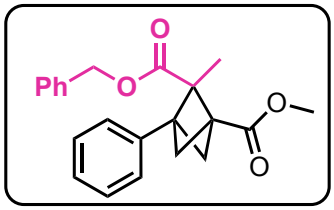

General procedure A was used for the reaction of methyl 3-phenylbicyclo[1.1.0]butane-1-carboxylate (0.20 mmol, 37.6 mg, 1 equiv) with benzyl 2-diazopropanoate (0.50 mmol, 95.1 mg, 2.5 equiv) using $Ir(ppy)_3$ (1.0 mol%, 1.31 mg) as catalyst. The reaction was purified using column chromatography (0-12% diethyl ether/hexanes gradient) affording a clear, colorless oil (38.6 mg, 55%).

^{1}H NMR (400 MHz, $CDCl_3$) δ 7.36 – 7.32 (m, 4H), 7.32 – 7.29 (m, 2H), 7.29 – 7.23 (m, 4H), 5.20 (d, J = 12.5 Hz, 1H), 5.12 (d, J = 12.5 Hz, 1H), 3.69 (s, 3H), 2.88 (dd, J = 10.3, 3.0 Hz, 1H), 2.50 (dd, J = 10.2, 3.5 Hz, 1H), 2.26 (d, J = 3.5 Hz, 1H), 2.08 (d, J = 3.0 Hz, 1H), 1.64 (s, 3H).

^{13}C NMR (101 MHz, $CDCl_3$) δ 173.8, 169.1, 136.2, 135.8, 128.5, 128.2, 128.1, 128.0, 127.4, 127.3, 69.9, 66.1, 51.7, 49.0, 48.8, 47.2, 42.9, 13.1.

HRMS (+pAPCI): Calcd for $C_{22}H_{23}O_4$ [M+H] 351.1591, found 351.1589.

1-methyl 2-(2,2,2-trichloroethyl) 3-phenylbicyclo[1.1.1]pentane-1,2-dicarboxylate (33)

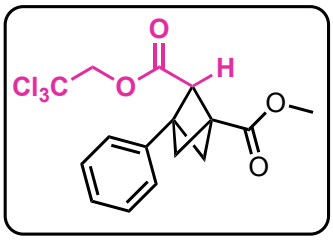

General procedure B was used for the reaction of methyl 3-phenylbicyclo[1.1.0]butane-1-carboxylate (0.20 mmol, 37.6 mg, 1 equiv) with 2,2,2-trichloroethyl 2-diazoacetate (0.50 mmol, 109 mg, 2.5 equiv) using TX (5.0 mol%, 2.12 mg) as catalyst. The reaction was purified using column chromatography (0-12% diethyl ether/hexanes gradient) affording a clear, colorless oil (29.6 mg, 39%).

^{1}H NMR (400 MHz, $CDCl_3$) δ 7.36 – 7.26 (m, 5H), 4.73 (d, J = 2.9 Hz, 2H), 3.75 (s, 3H), 3.52 (d, J = 7.0 Hz, 1H), 3.07 (dd, J = 9.8, 3.1 Hz, 1H), 2.42 (dd, J = 7.0, 3.1 Hz, 1H), 2.34 (dd, J = 9.8, 2.0 Hz, 1H), 2.27 (d, J = 2.0 Hz, 1H).

^{13}C NMR (101 MHz, CDCl3) δ 168.7, 167.8, 136.5, 128.4, 127.7, 126.7, 94.6, 74.0, 63.4, 53.3, 52.1, 48.7, 46.7, 40.4.

HRMS (+pAPCI): Calcd for $C_{16}H_{16}O_4{}^{35}Cl_3$ [M+H] 377.0109, found 377.0109.

methyl 2-(dimethoxyphosphoryl)-3-phenylbicyclo[1.1.1]pentane-1-carboxylate (34)

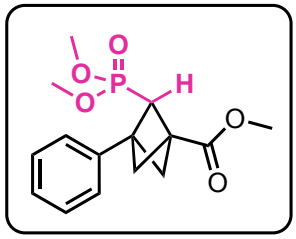

General procedure B was used for the reaction of methyl 3-phenylbicyclo[1.1.0]butane-1-carboxylate (0.20 mmol, 37.6 mg, 1 equiv) with dimethyl (diazomethyl)phosphonate (0.50 mmol, 75.0 mg, 2.5 equiv) using TX (5.0 mol%, 2.12 mg) as catalyst. The reaction was purified using column chromatography (50-75% ethyl aceate/hexanes gradient) affording a clear, colorless oil (14.8 mg, 24%)

^{1}H NMR (400 MHz, $CDCl_3$) δ 7.40 – 7.26 (m, 5H), 3.75 (s, 3H), 3.68 (d, J = 10.9 Hz, 3H), 3.56 (dd, J = 9.9, 2.8 Hz, 1H), 3.45 (d, J = 10.9 Hz, 3H), 2.94 (t, J = 7.1 Hz, 1H), 2.39 (dd, J = 9.9, 1.7 Hz, 1H), 2.35 (dd, J = 7.5, 2.7 Hz, 1H), 2.27 (dd, J = 30.1, 2.7 Hz, 1H).

^{13}C NMR (101 MHz, $CDCl_3$) δ 168.9, 137.2, 128.3, 127.6, 126.6, 60.6, 59.1, 56.5, 56.2, 52.5 (d, J = 6.5 Hz), 52.1, 52.0, 49.2 (d, J = 6.9 Hz), 46.1 (d, J = 3.4 Hz), 40.4 (d, J = 3.6 Hz).

^{31}P NMR (162 MHz, $CDCl_3$) δ 24.73 (dddd, J = 28.8, 21.9, 18.0, 11.0 Hz).

HRMS (+pAPCI): Calcd for $C_{15}H_{20}O_5P$ [M+H] 311.1043, found 311.1038.

methyl 3-phenyl-2-(trifluoromethyl)bicyclo[1.1.1]pentane-1-carboxylate (35)

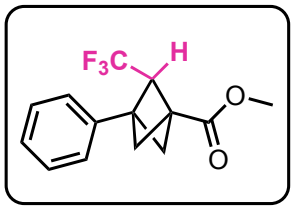

General procedure B was used for the reaction of methyl 3-phenylbicyclo[1.1.0]butane-1-carboxylate (0.20 mmol, 37.6 mg, 1 equiv) with 2-diazo-1,1,1-trifluoroethane (1.0 mmol, 1.37 mL of 0.73 M solution, 5 equiv) using TX (5.0 mol%, 2.12 mg) as catalyst. The reaction was purified using column chromatography (0-12% diethylether/hexanes gradient) affording a clear, colorless oil (28.1 mg, 52%).

^{1}H NMR (400 MHz, $CDCl_3$) δ 7.40 – 7.27 (m, 3H), 7.26 – 7.19 (m, 2H), 3.76 (s, 3H), 3.24 (qd, J = 9.1, 6.6 Hz, 1H), 3.16 (ddd, J = 10.1, 3.5, 1.6 Hz, 1H), 2.38 (ddd, J = 7.1, 3.5, 1.8 Hz, 1H), 2.26 (dd, J = 10.0, 2.0 Hz, 1H), 2.21 (d, J = 1.9 Hz, 1H).

^{13}C NMR (101 MHz, $CDCl_3$) δ 168.3, 136.1, 128.5, 127.8, 126.4, 63.2 (q, J = 29.8 Hz), 53.8, 52.2, 47.5 (q, J = 2.1 Hz), 45.7 (q, J = 2.7 Hz), 40.0 (q, J = 3.1 Hz), 35.8.

^{19}F NMR (376 MHz, $CDCl_3$) δ -59.37 (d, J = 9.3 Hz).

HRMS (+pAPCI): Calcd for $C_{14}H_{14}O_2F_3$ [M+H] 271.0940, found 271.0941.

methyl-2'-oxo-3-phenyldihydro-2'H-spiro[bicyclo[1.1.1]pentane-2,3'-furan]-1-carboxylate (36)

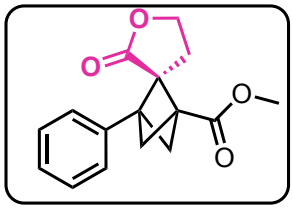

General procedure B was used for the reaction of methyl 3-phenylbicyclo[1.1.0]butane-1-carboxylate (0.20 mmol, 37.6 mg, 1 equiv) with 3-diazodihydrofuran-2(3H)-one (0.50 mmol, 56.0 mg,, 2.5 equiv) using TX (5.0 mol%, 2.12 mg) as catalyst. The reaction was purified using column chromatography (0-12% diethylether/hexanes gradient) affording a clear, colorless oil (22.1 mg, 41%).

^{1}H NMR (400 MHz, $CDCl_3$) δ 7.26 – 7.18 (m, 3H), 7.18 – 7.13 (m, 2H), 4.25 – 4.10 (m, 2H), 3.93 (td, J = 8.5, 5.4 Hz, 1H), 3.65 (s, 3H), 2.64 – 2.54 (m, 2H), 2.32 (ddd, J = 13.4, 8.4, 7.1 Hz, 1H), 2.19 (d, J = 2.5 Hz, 1H), 2.16 (d, J = 2.7 Hz, 1H).

^{13}C NMR (101 MHz, $CDCl_3$) δ 174.4, 168.5, 135.5, 128.7, 128.1, 126.7, 66.0, 64.4, 52.1, 50.8, 50.1 48.1, 45.4, 25.5.

HRMS (+pAPCI): Calcd for $C_{16}H_{17}O_4$ [M+H] 273.1121, found 273.1120.

dimethyl 2-methyl-3-(naphthalen-2-yl)bicyclo[1.1.1]pentane-1,2-dicarboxylate (37)

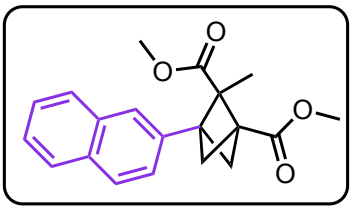

General procedure A was used for the reaction of methyl 3-(naphthalen-2-yl)bicyclo[1.1.0]butane-1-carboxylate (0.20 mmol, 47.7 mg, 1 equiv) with methyl 2-diazopropanoate (0.50 mmol, 57.1 mg, 2.5 equiv) using $Ir(ppy)_3$ (1.0 mol%, 1.31 mg) as catalyst. The reaction was purified using column chromatography (0-12% diethylether/hexanes gradient) affording a clear, colorless oil (33.8 mg, 52%).

^{1}H NMR (400 MHz, $CDCl_3$) δ 7.87 – 7.76 (m, 3H), 7.69 (d, J = 1.9 Hz, 1H), 7.50 – 7.44 (m, 2H), 7.41 (dd, J = 8.5, 1.7 Hz, 1H), 3.78 (s, 3H), 3.69 (s, 3H), 2.94 (dd, J = 10.3, 2.9 Hz, 1H), 2.56 (dd, J = 10.3, 3.4 Hz, 1H), 2.33 (d, J = 3.4 Hz, 1H), 2.13 (d, J = 2.9 Hz, 3H).

^{13}C NMR (101 MHz, $CDCl_3$) δ 174.6, 169.1, 133.8, 133.1, 132.7, 127.9, 127.8, 127.7, 126.2, 125.9, 125.2, 70.1, 51.8, 51.7, 49.2, 48.9, 47.3, 43.0, 13.2.

HRMS (+pAPCI): Calcd for $C_{20}H_{21}O_4$ [M+H] 325.1434, found 325.1435

dimethyl 3-(4-bromophenyl)-2-methylbicyclo[1.1.1]pentane-1,2-dicarboxylate (38)

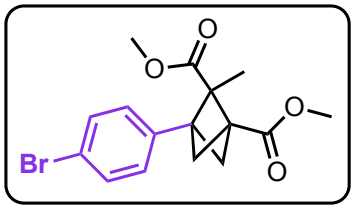

General procedure A was used for the reaction of methyl 3-(4-bromophenyl)bicyclo[1.1.0]butane-1-carboxylate (0.20 mmol, 53.4 mg, 1 equiv) with methyl 2-diazopropanoate (0.50 mmol, 57.1 mg, 2.5 equiv) using $Ir(ppy)_3$ (1.0 mol%, 1.31 mg) as catalyst. The reaction was purified using column chromatography (0-12% diethylether/hexanes gradient) affording a clear, colorless oil (47.5 mg, 67%).

^{1}H NMR (400 MHz, $CDCl_3$) δ 7.44 (d, J = 8.4 Hz, 2H), 7.14 (d, J = 8.3 Hz, 2H), 3.75 (s, 3H), 3.67 (s, 3H), 2.80 (dd, J = 10.3, 3.0 Hz, 1H), 2.43 (dd, J = 10.3, 3.5 Hz, 1H), 2.22 (d, J = 3.5 Hz, 1H), 2.03 (d, J = 3.0 Hz, 1H), 1.55 (s, 3H).

^{13}C NMR (101 MHz, $CDCl_3$) δ 174.4, 168.8, 135.2, 131.3, 129.0, 121.6, 69.9, 51.8, 51.7, 49.1, 48.2, 47.1, 42.9, 13.1.

HRMS (+pAPCI): Calcd for $C_{16}H_{18}O_4{}^{79}Br$ [M+H] 353.0383, found 353.0383.

dimethyl 2-methyl-3-(p-tolyl)bicyclo[1.1.1]pentane-1,2-dicarboxylate (39)

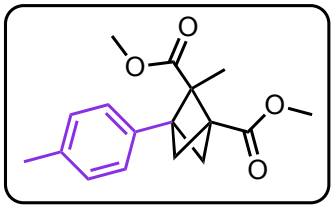

General procedure A was used for the reaction of methyl 3-(p-tolyl)bicyclo[1.1.0]butane-1-carboxylate (0.20 mmol, 40.5 mg, 1 equiv) with methyl 2-diazopropanoate (0.50 mmol, 57.1 mg, 2.5 equiv) using $Ir(ppy)_3$ (1.0 mol%, 1.31 mg) as catalyst. The reaction was purified using column chromatography (0-12% diethylether/hexanes gradient) affording a clear, colorless oil (44.4 mg, 77%).

^{1}H NMR (400 MHz, $CDCl_3$) δ 7.21 – 7.10 (m, 4H), 3.75 (s, 3H), 3.68 (s, 3H), 2.82 (dd, J = 10.2, 2.9 Hz,1H), 2.45 (dd, J = 10.3, 3.4 Hz, 1H), 2.34 (s, 3H), 2.22 (d, J = 3.5 Hz, 1H), 2.02 (d, J = 2.9 Hz, 1H), 1.57 (s, 3H).

^{13}C NMR (101 MHz, $CDCl_3$) δ 174.6, 169.2, 137.1, 133.2, 128.9, 127.1, 69.8, 51.8, 51.6, 49.1, 48.5, 47.1, 42.9, 21.2, 13.1.

HRMS (+pAPCI): Calcd for $C_{17}H_{21}O_4$ [M+H] 289.1434, found 289.1433

dimethyl 2-methyl-3-(4-(trifluoromethyl)phenyl)bicyclo[1.1.1]pentane-1,2-dicarboxylate (40)

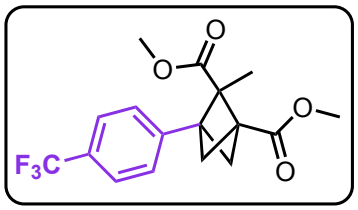

General procedure A was used for the reaction of methyl 3-(4-(trifluoromethyl)phenyl)bicyclo[1.1.0]butane-1-carboxylate (0.20 mmol, 51.2 mg, 1 equiv) with methyl 2-diazopropanoate (0.50 mmol, 57.1 mg, 2.5 equiv) using $Ir(ppy)_3$ (1.0 mol%, 1.31 mg) as catalyst. The reaction was purified using column chromatography (0-12% diethylether/hexanes gradient) affording a clear, colorless oil (26.6 mg, 39%).

^{1}H NMR (400 MHz, $CDCl_3$) δ 7.58 (d, J = 8.1 Hz, 2H), 7.38 (d, J = 7.4 Hz, 2H), 3.76 (s, 3H), 3.69 (s, 3H), 2.86 (dd, J = 10.3, 3.0 Hz, 1H), 2.48 (dd, J = 10.3, 3.5 Hz, 1H), 2.26 (s, 1H), 2.08 (d, J = 3.0 Hz, 1H), 1.59 (s, 3H).

^{13}C NMR (101 MHz, $CDCl_3$) δ 174.2, 168.6, 140.1 (d, J = 1.1 Hz), 129.6 (q, J = 32.5 Hz), 127.6, 125.1 (q, J = 3.8 Hz), 124.2 (q, J = 271.7 Hz), 70.1, 51.8, 51.8, 49.2, 48.2, 47.2, 43.0, 13.1.

^{19}F NMR (376 MHz, CDCl3) δ -62.54.

HRMS (+pAPCI): Calcd for $C_{17}H_{18}O_4F_3$ [M+H] 343.1152, found 343.1150.

dimethyl 3-(3,4-dichlorophenyl)-2-methylbicyclo[1.1.1]pentane-1,2-dicarboxylate (41)

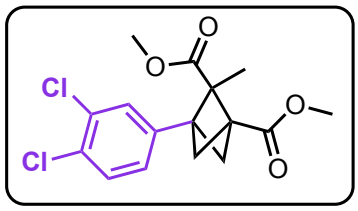

General procedure A was used for the reaction of methyl 3-(3,4-dichlorophenyl)bicyclo[1.1.0]butane-1-carboxylate (0.20 mmol, 51.4 mg, 1 equiv) with methyl 2-diazopropanoate (0.50 mmol, 57.1 mg, 2.5 equiv) using $Ir(ppy)_3$ (1.0 mol%, 1.31 mg) as catalyst. The reaction was purified using column chromatography (0-12% diethylether/hexanes gradient) affording a clear, colorless oil (39.8 mg, 58%).

^{1}H NMR (400 MHz, $CDCl_3$) δ 7.38 (d, J = 8.2 Hz, 1H), 7.34 (d, J = 2.0 Hz, 1H), 7.11 (dd, J = 8.2, 2.0 Hz, 1H), 3.75 (s, 3H), 3.69 (s, 3H), 2.80 (dd, J = 10.2, 3.0 Hz, 1H), 2.43 (dd, J = 10.3, 3.5 Hz, 1H), 2.23 (d, J = 3.5 Hz, 1H), 2.05 (d, J = 3.0 Hz, 1H), 1.56 (s, 3H).

^{13}C NMR (101 MHz, $CDCl_3$) δ 174.2, 168.5, 136.5, 132.3, 131.6, 130.2, 129.3, 126.8, 70.0, 51.83, 51.80, 49.3, 47.7, 47.1, 42.9, 13.0.

HRMS (+pAPCI): Calcd for $C_{16}H_{17}O_4{}^{35}Cl_2$ [M+H] 343.0498, found 343.0498.

NMR Spectra of Novel Compounds

20241219-JKS-41-49-8-clean.1.fid

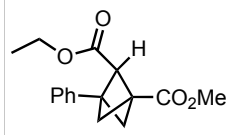

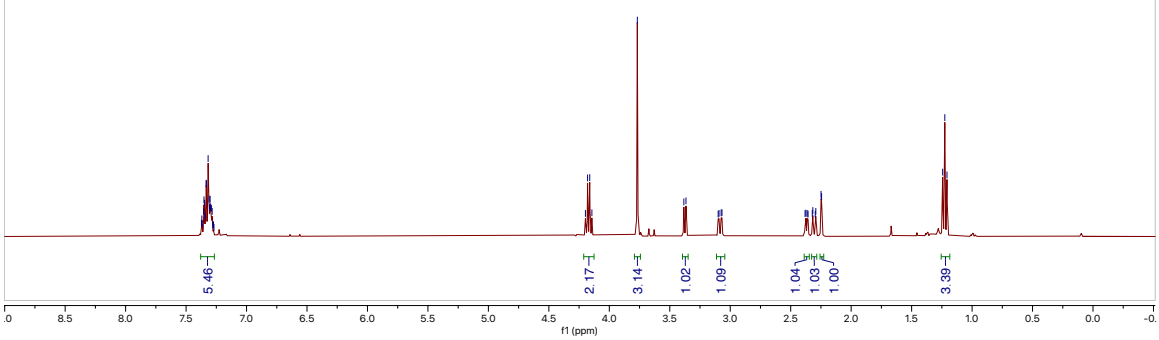

20241219-JKS-41-49-8-clean.2.fid

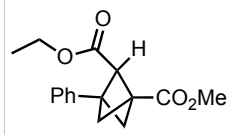

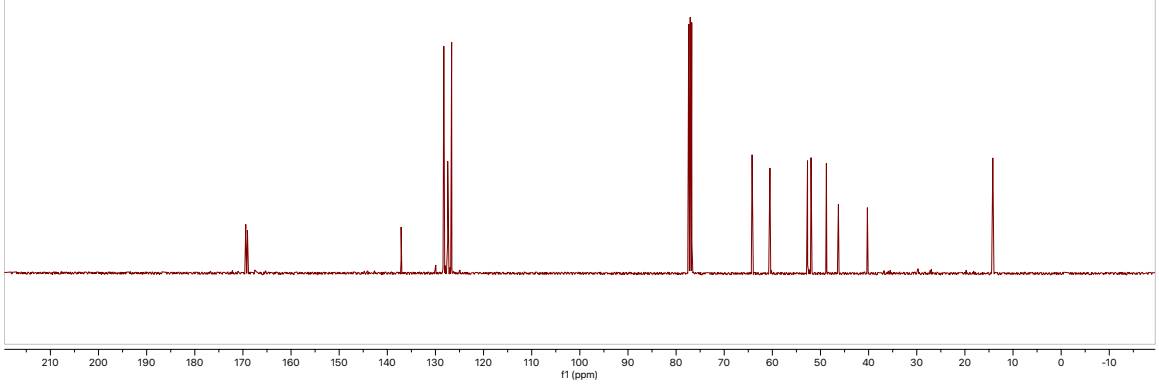

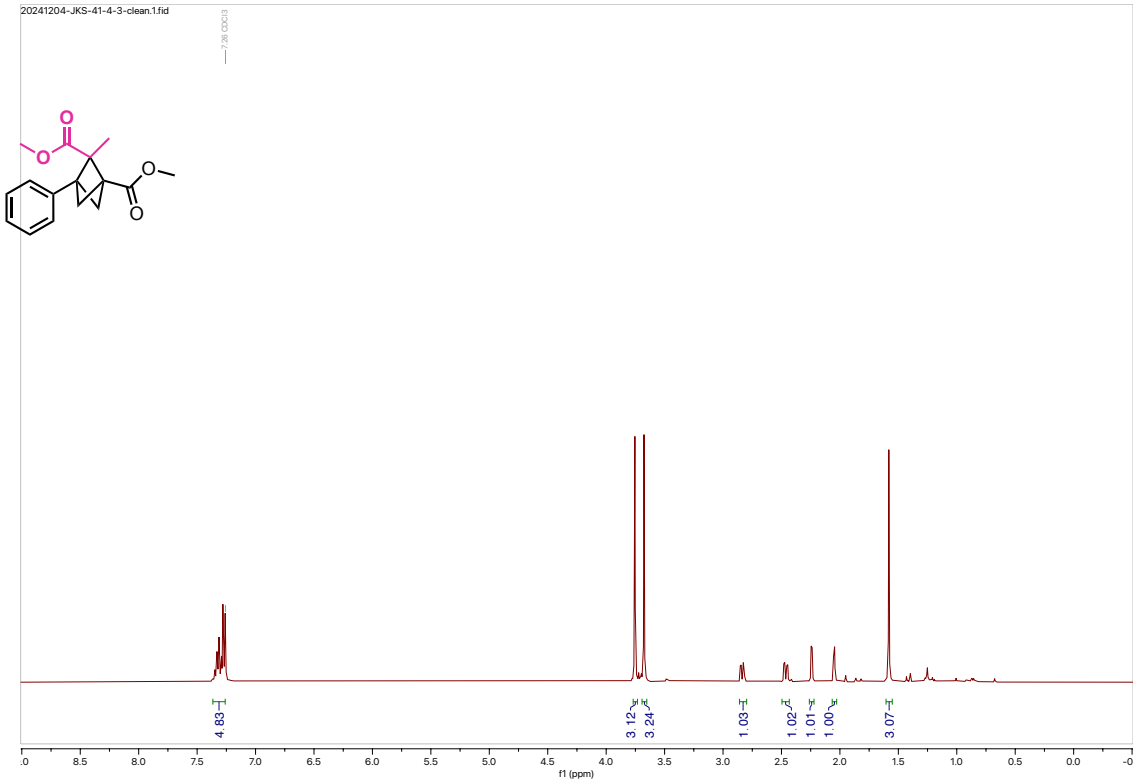
20241204-JKS-41-4-3-clean.1.fid
4.83
3.12
3.24
1.03
1.02
1.01
1.00
3.07
f1 (ppm)

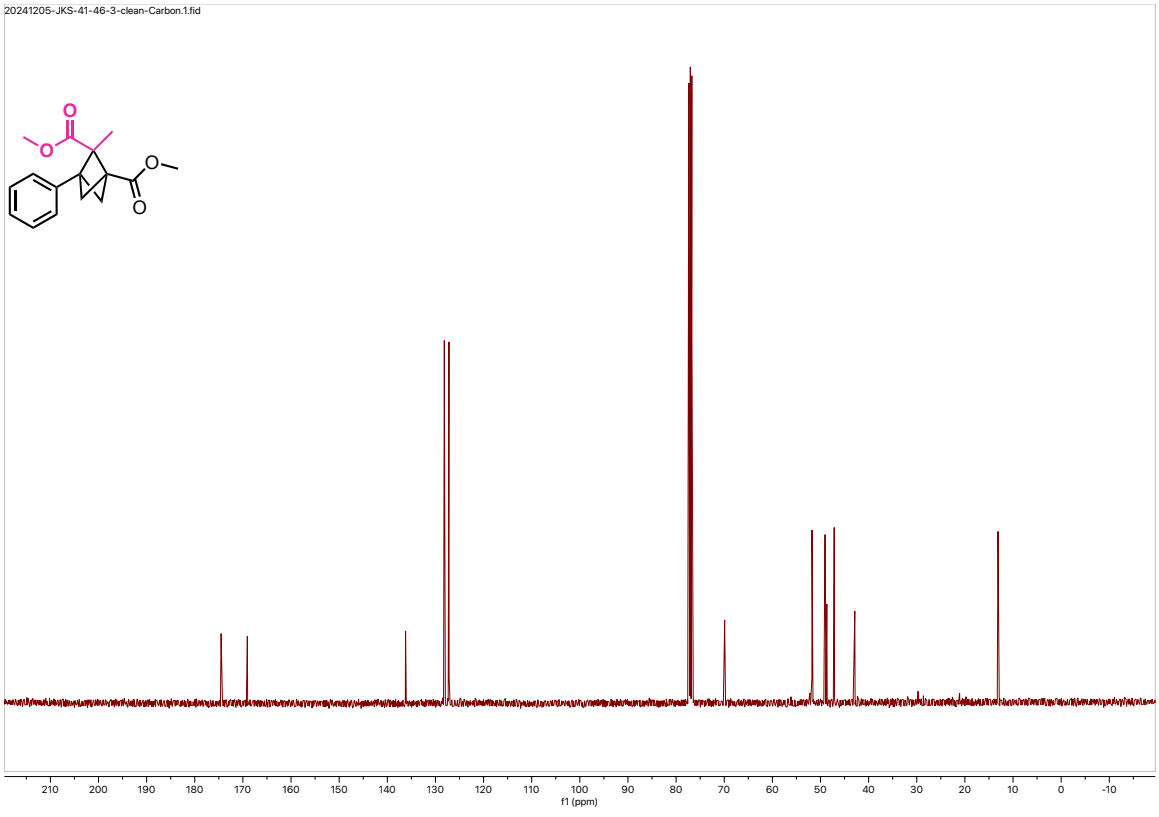
20241205-JKS-41-46-3-clean-Carbon.1.fid
f1 (ppm)

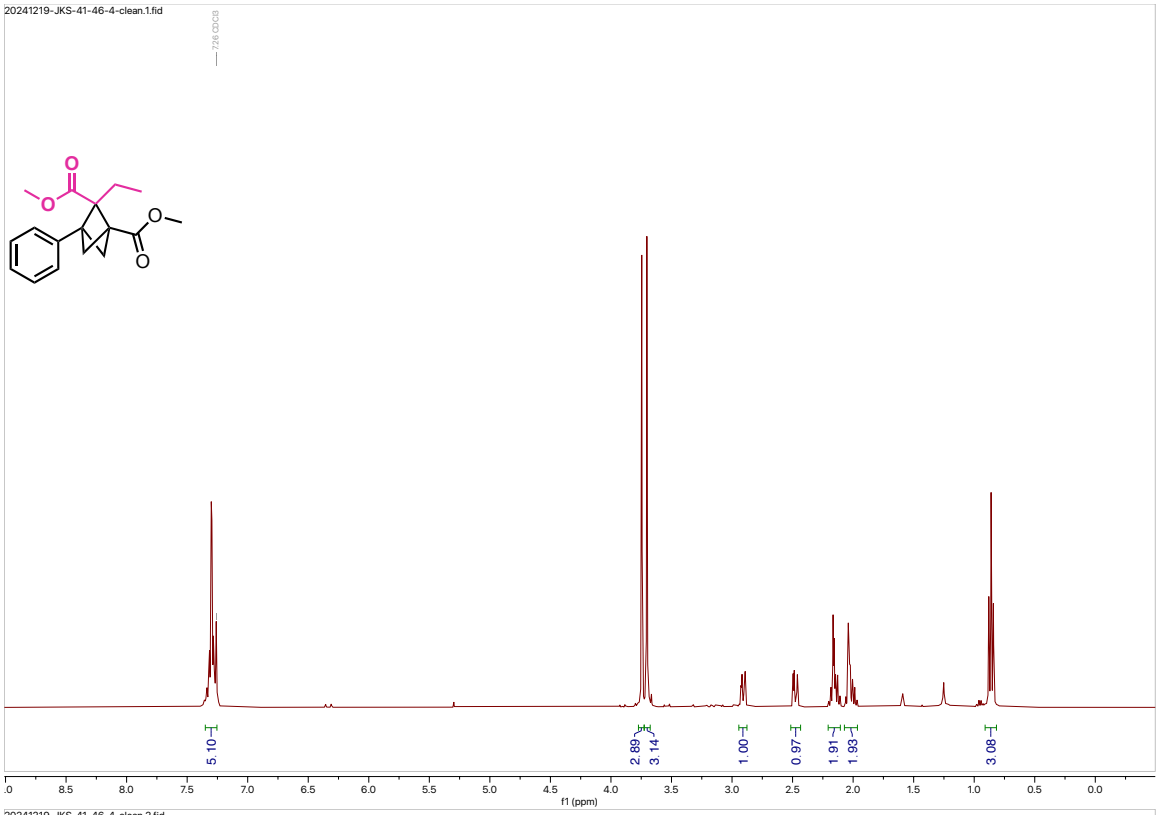
20241219-JKS-41-46-4-clean.1.fid
7.26 CDCl3
O
O
O
O
5.10
2.89
3.14
1.00
0.97
1.91
1.93
3.08
f1 (ppm)

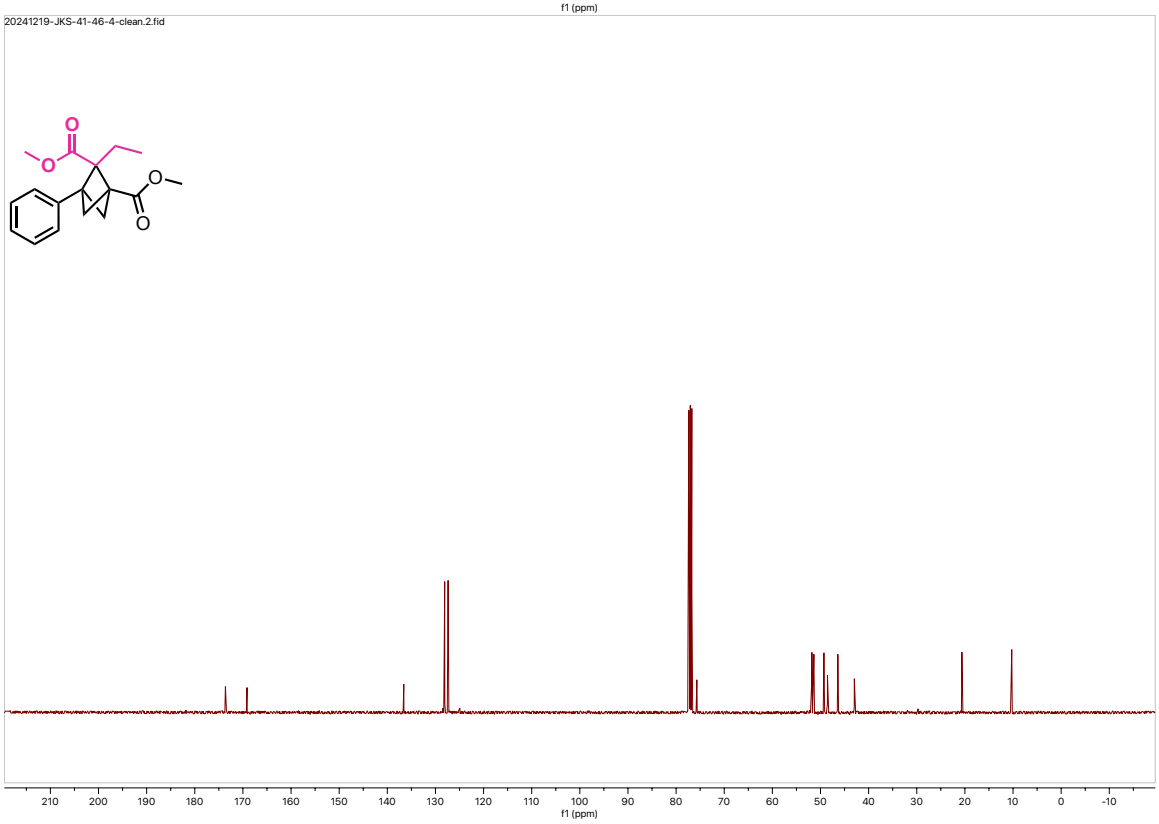
20241219-JKS-41-46-4-clean.2.fid
O
O
O
O
f1 (ppm)

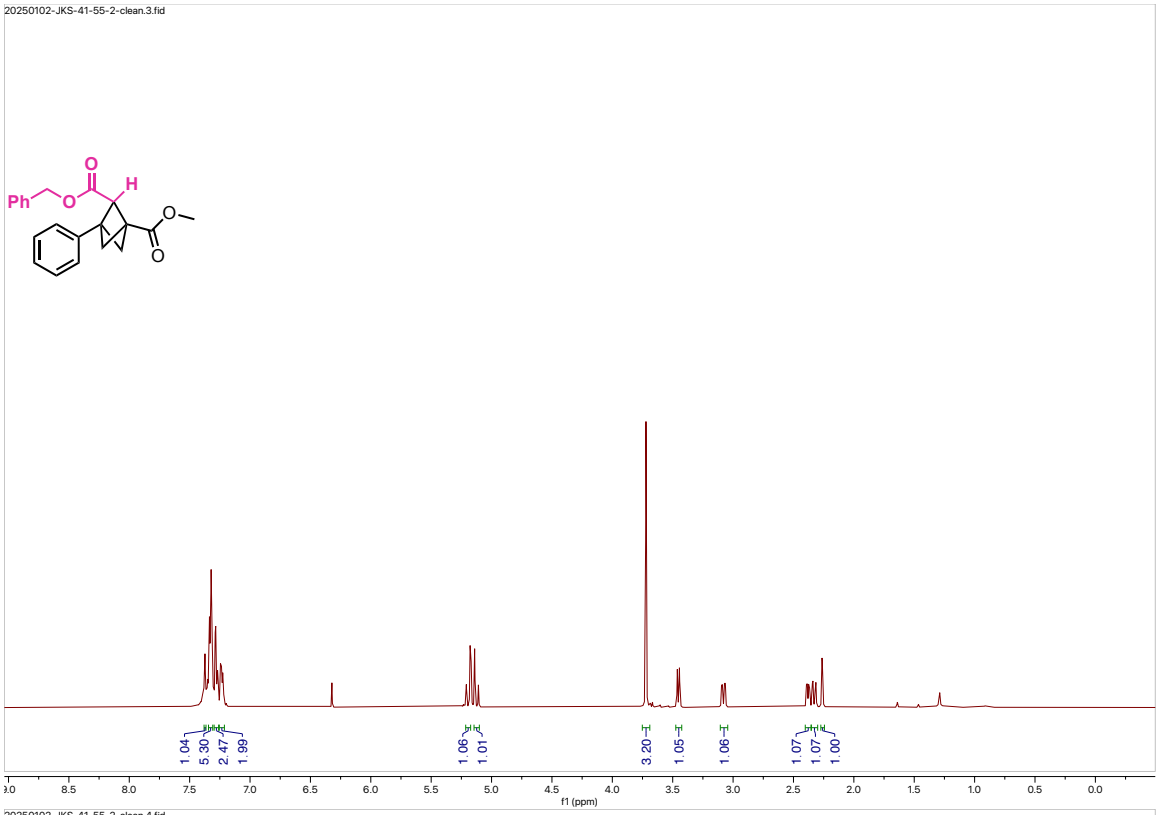
20250102-JKS-41-55-2-clean.3.fid
Ph
O
O
H
O
O
1.04
5.30
2.47
1.99
1.06
1.01
3.20
1.05
1.06
1.07
1.07
1.00
f1 (ppm)

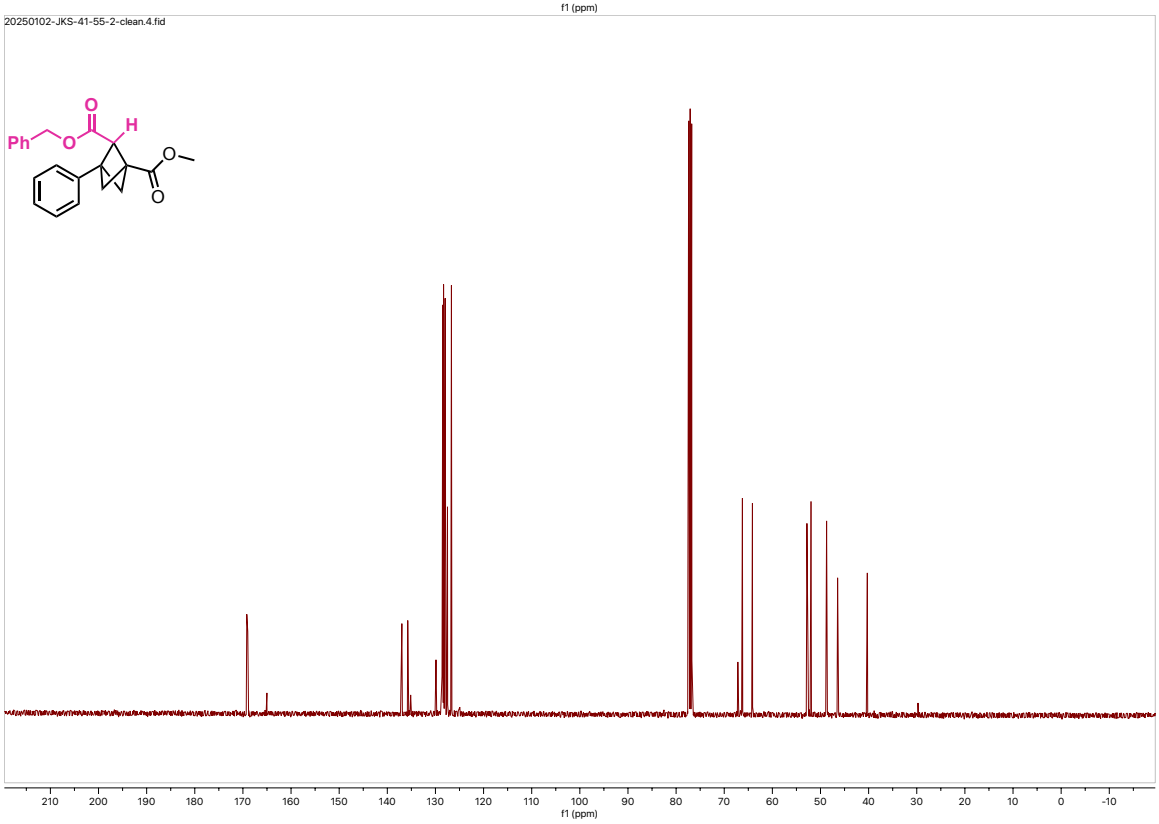
20250102-JKS-41-55-2-clean.4.fid
Ph
O
O
H
O
O
f1 (ppm)

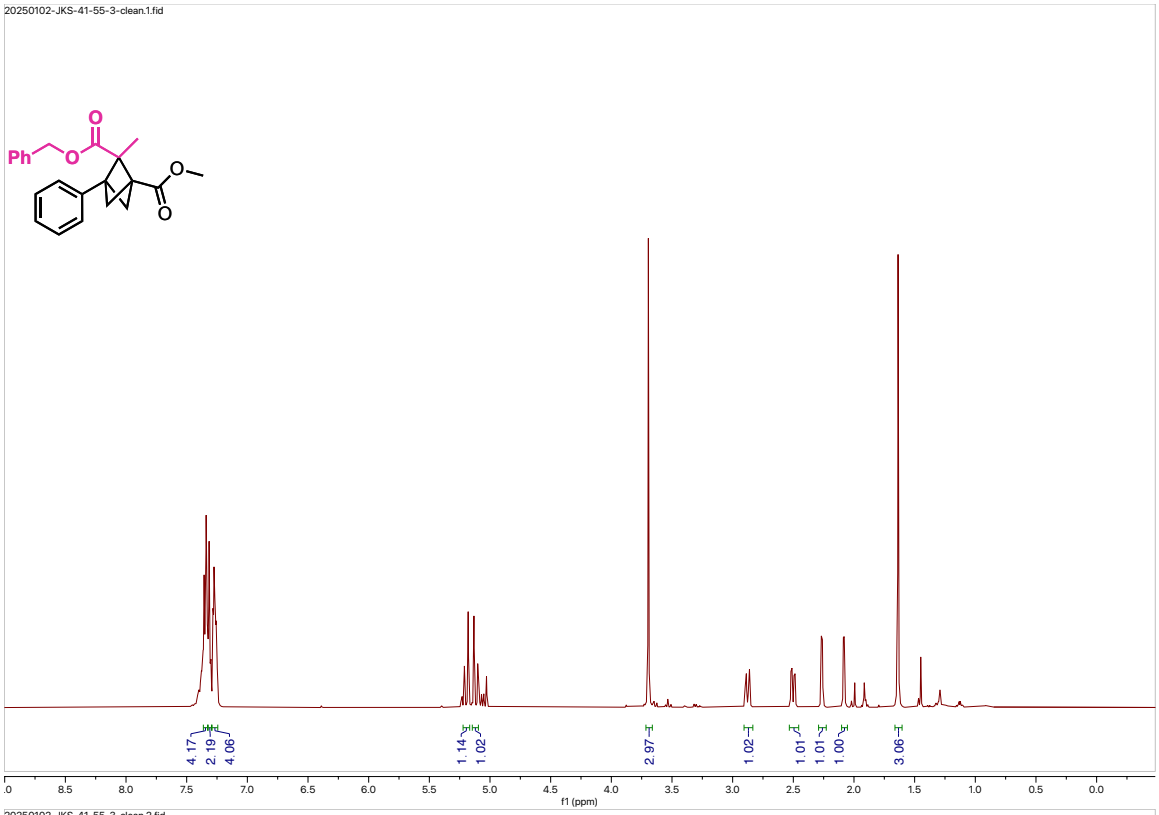
20250102-JKS-41-55-3-clean.1.fid
Ph
O
O
O
O
4.17
2.19
4.06
1.14
1.02
2.97
1.02
1.01
1.01
1.00
3.06
f1 (ppm)

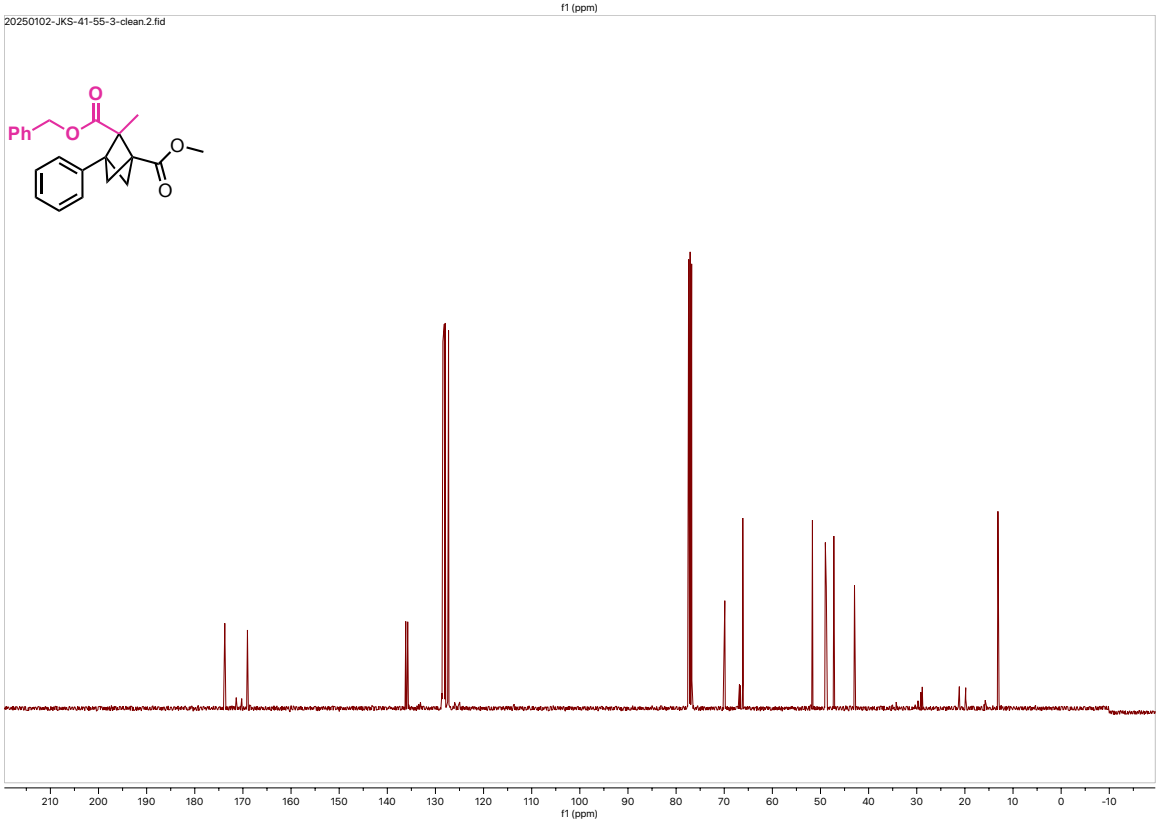
20250102-JKS-41-55-3-clean.2.fid
Ph
O
O
O
O
f1 (ppm)

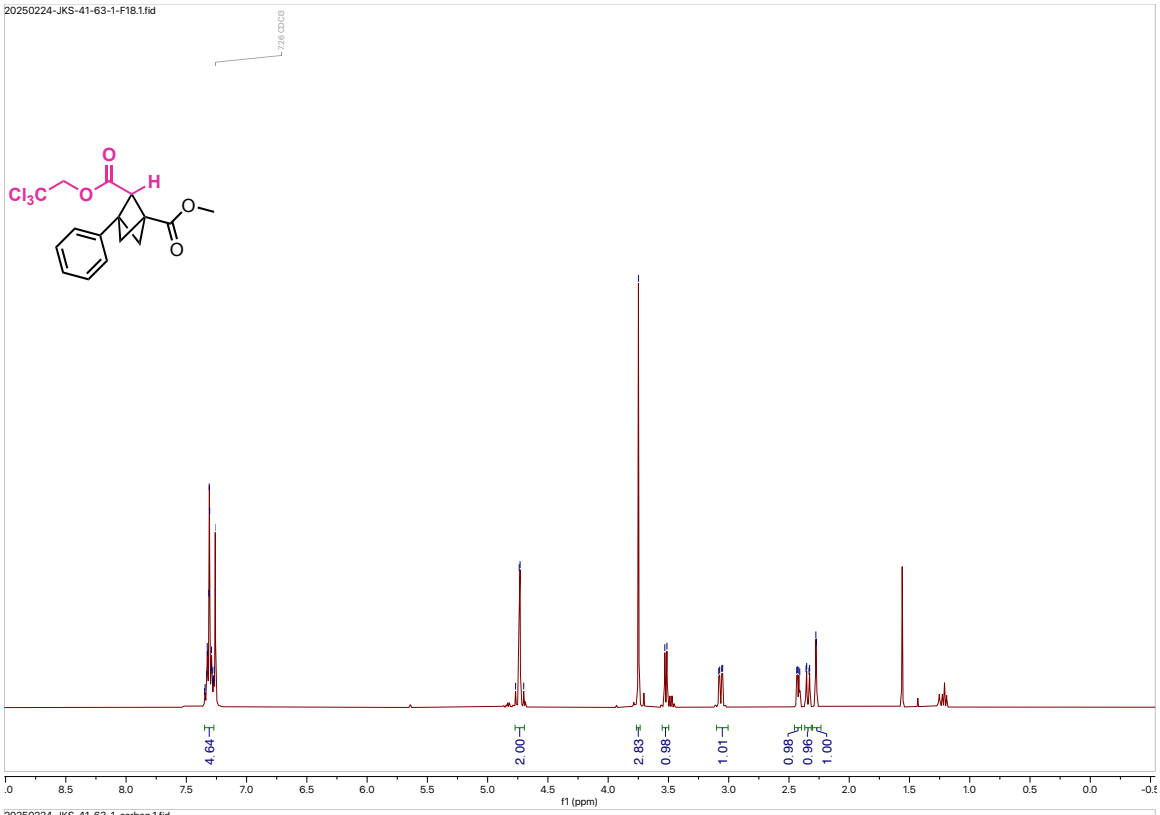
20250224-JKS-41-63-1-F18.1.fid
7.26 CDCl3
O
H
Cl3C
O
O
O
4.64
2.00
2.83
0.98
1.01
0.98
0.96
1.00
f1 (ppm)

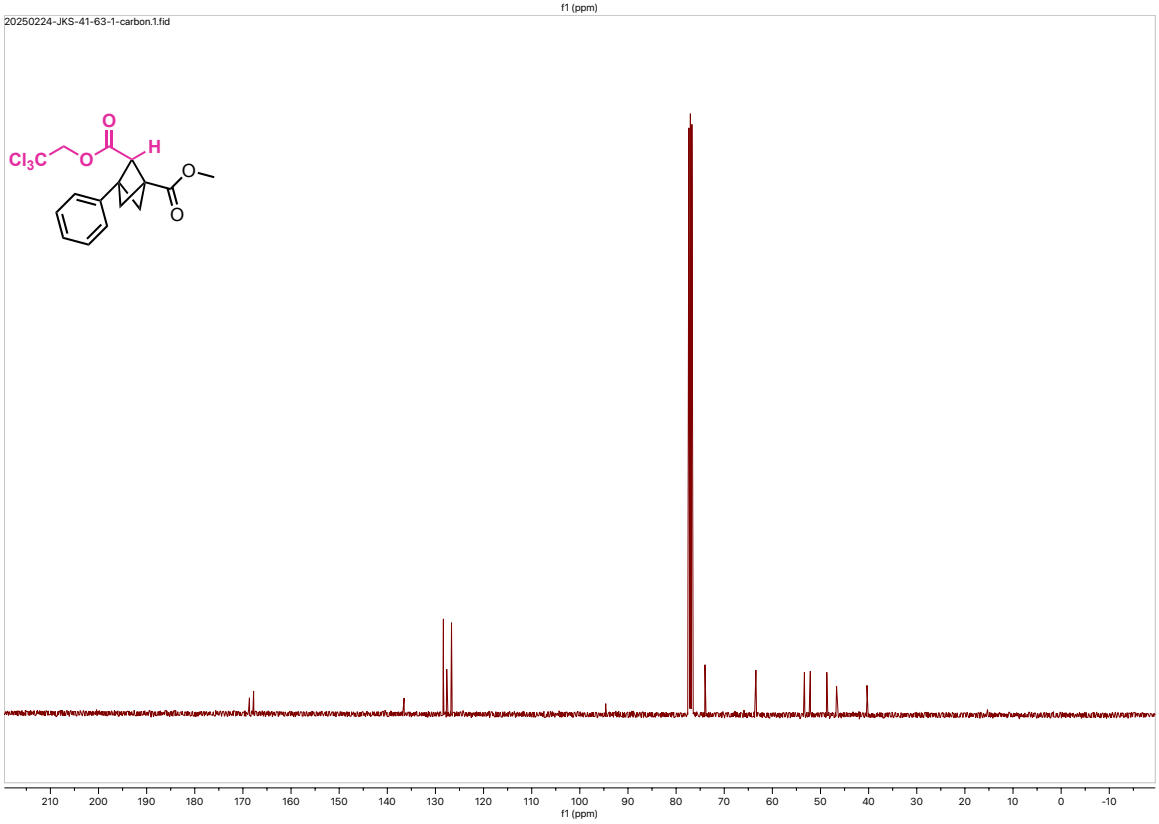
20250224-JKS-41-63-1-carbon.1.fid
O
H
Cl3C
O
O
O
f1 (ppm)

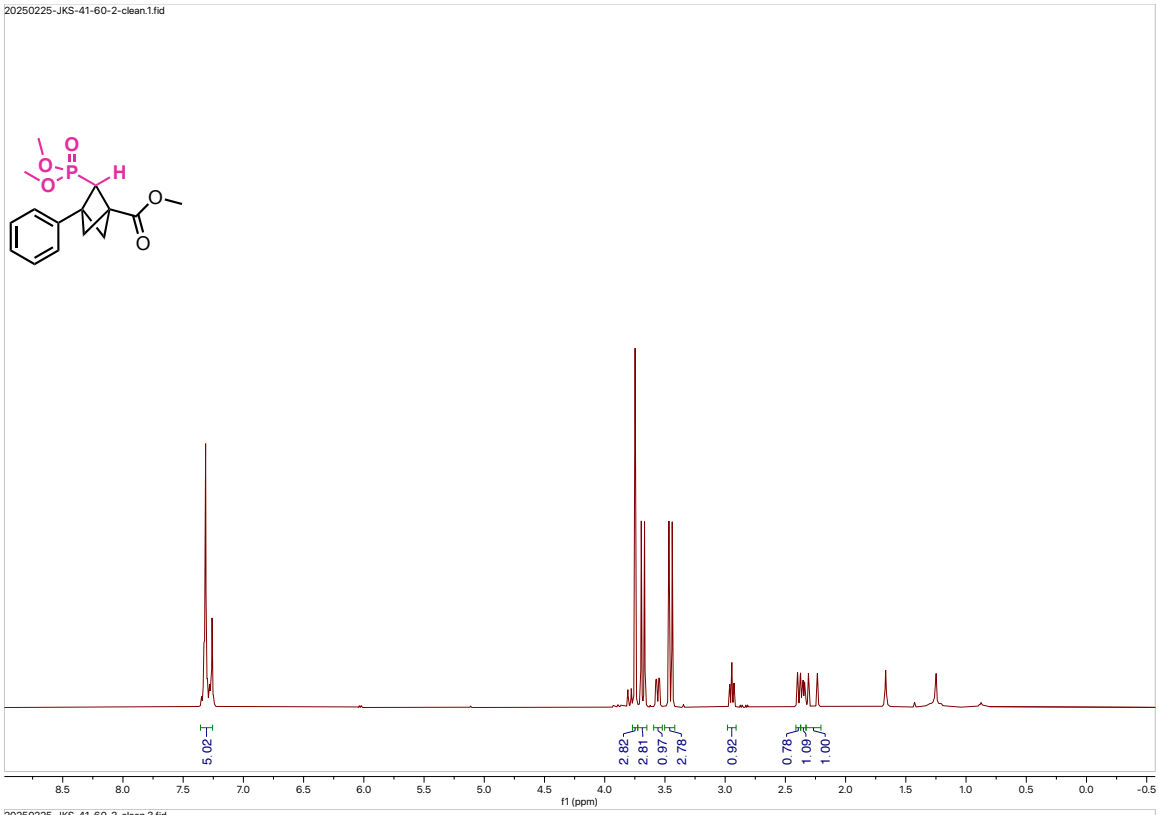
20250225-JKS-41-60-2-clean.1.fid
5.02
2.82
2.81
0.97
2.78
0.92
0.78
1.09
1.00
f1 (ppm)

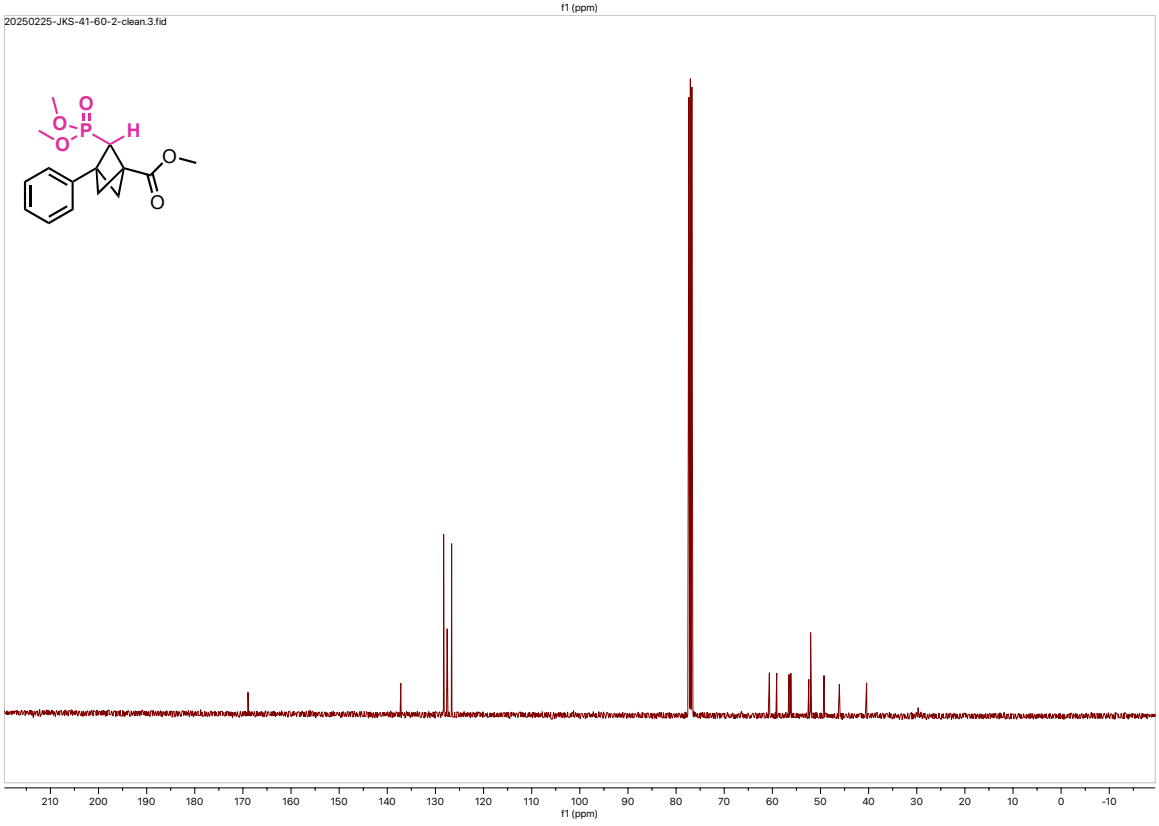
20250225-JKS-41-60-2-clean.3.fid
f1 (ppm)

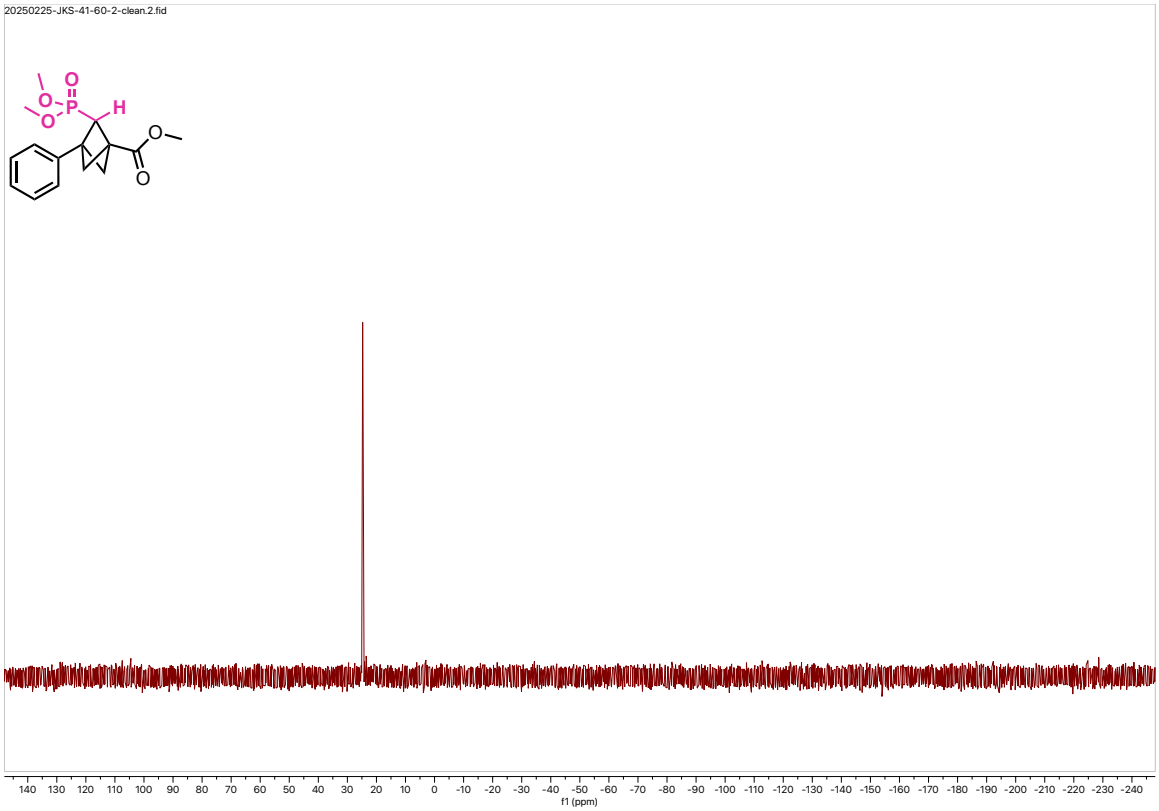
20250225-JKS-41-60-2-clean.2.fid
O
O
O
P
H
O
O
140 130 120 110 100 90 80 70 60 50 40 30 20 10 0 -10 -20 -30 -40 -50 -60 -70 -80 -90 -100 -110 -120 -130 -140 -150 -160 -170 -180 -190 -200 -210 -220 -230 -240
f1 (ppm)

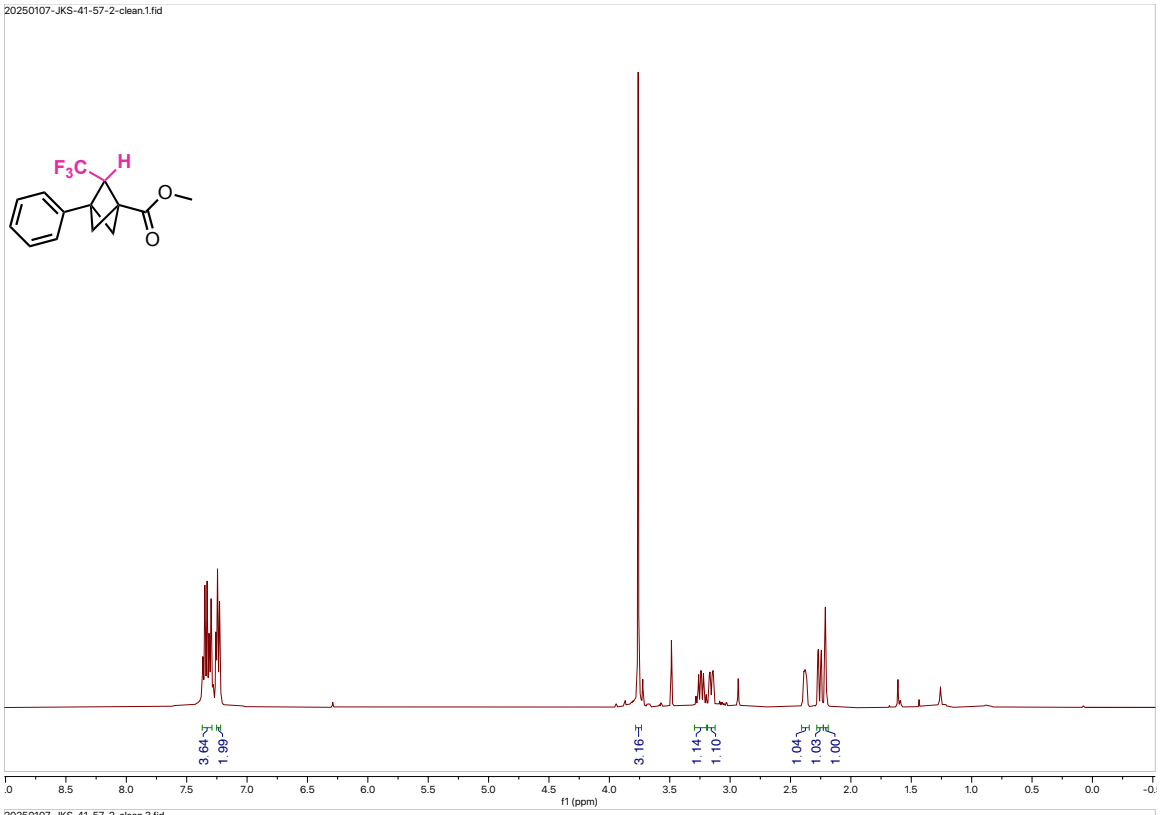
20250107-JKS-41-57-2-clean.1.fid
F3C
H
O
O
3.64
1.99
3.16
1.14
1.10
1.04
1.03
1.00
f1 (ppm)

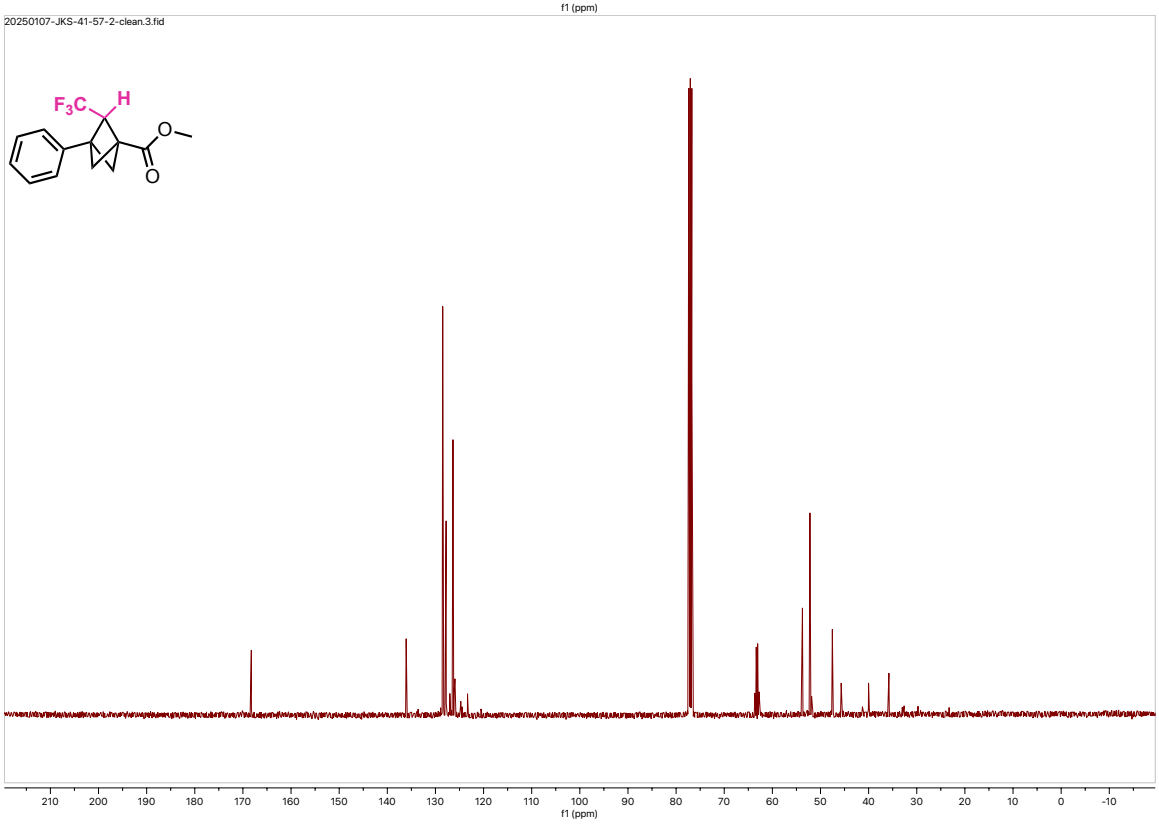
20250107-JKS-41-57-2-clean.3.fid
F3C
H
O
O
f1 (ppm)

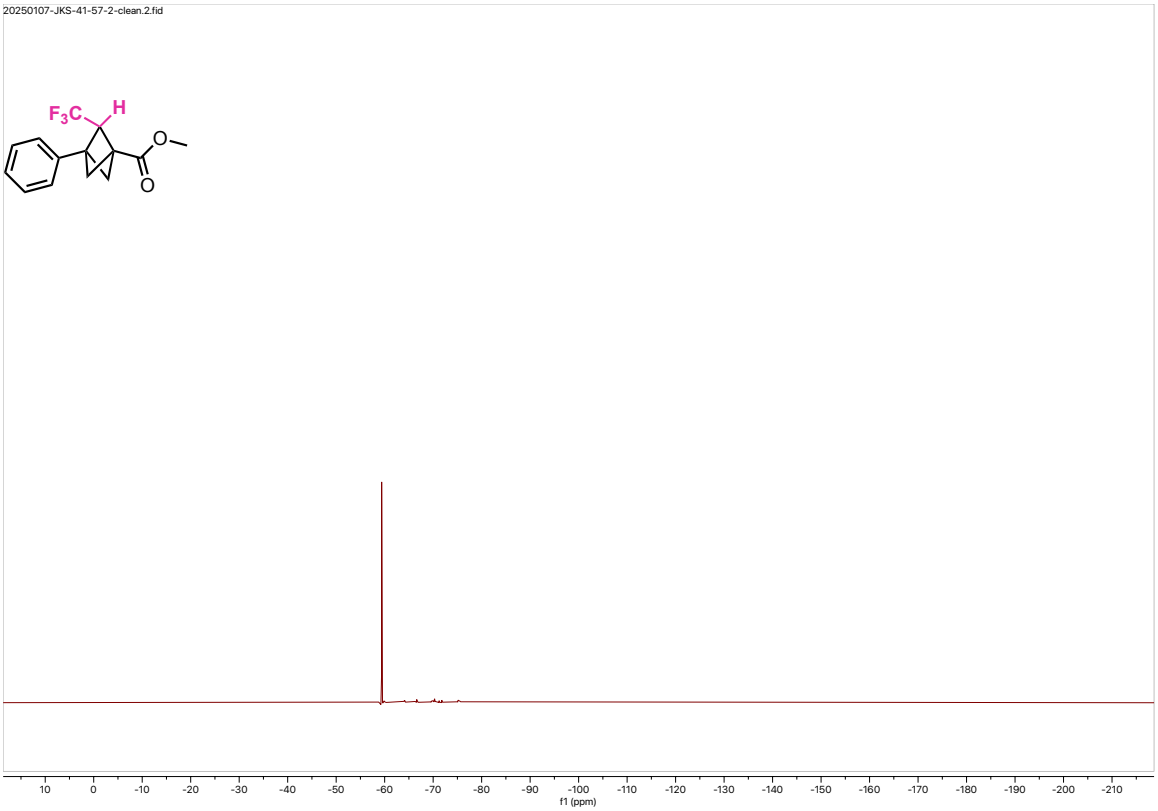
20250107-JKS-41-57-2-clean.2.fid
F3C
H
O
O
10
0
-10
-20
-30
-40
-50
-60
-70
-80
-90
-100
-110
-120
-130
-140
-150
-160
-170
-180
-190
-200
-210
f1 (ppm)

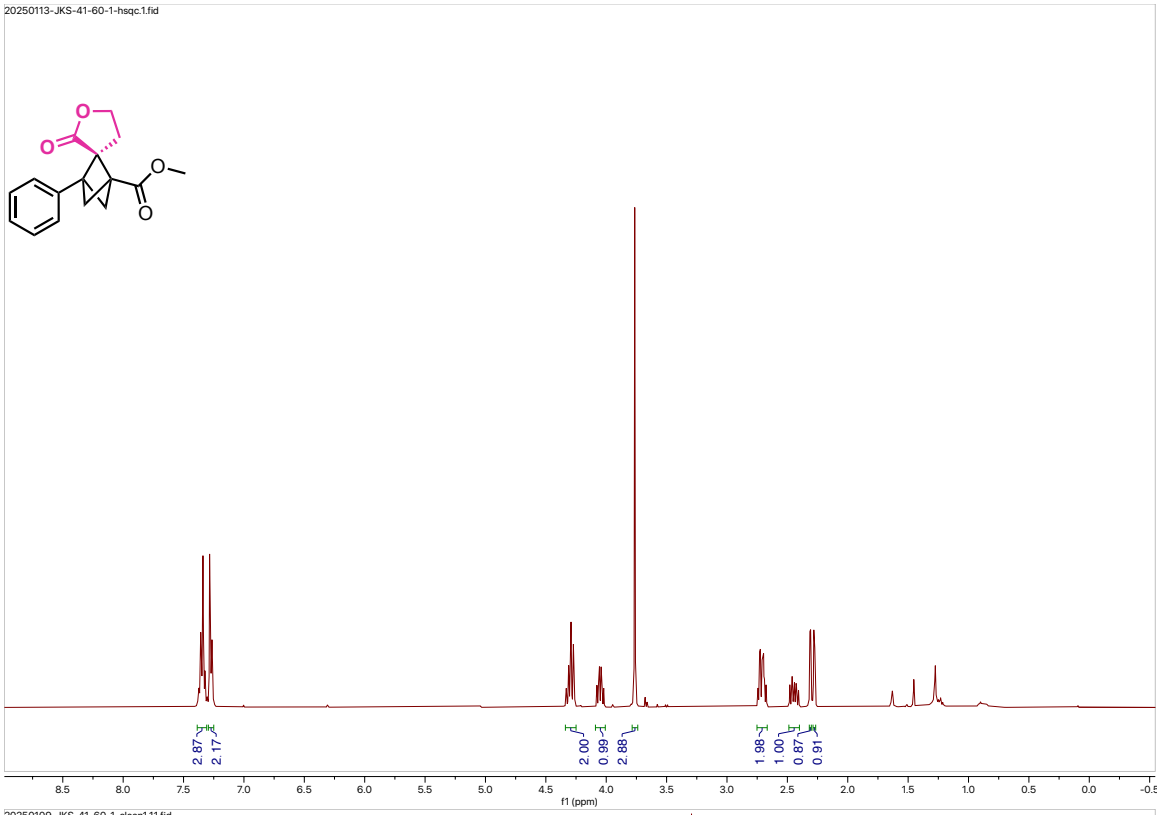
20250113-JKS-41-60-1-hsqc.1.fid
O
O
O
O
2.87
2.17
2.00
0.99
2.88
1.98
1.00
0.87
0.91
8.5
8.0
7.5
7.0
6.5
6.0
5.5
5.0
4.5
4.0
3.5
3.0
2.5
2.0
1.5
1.0
0.5
0.0
f1 (ppm)

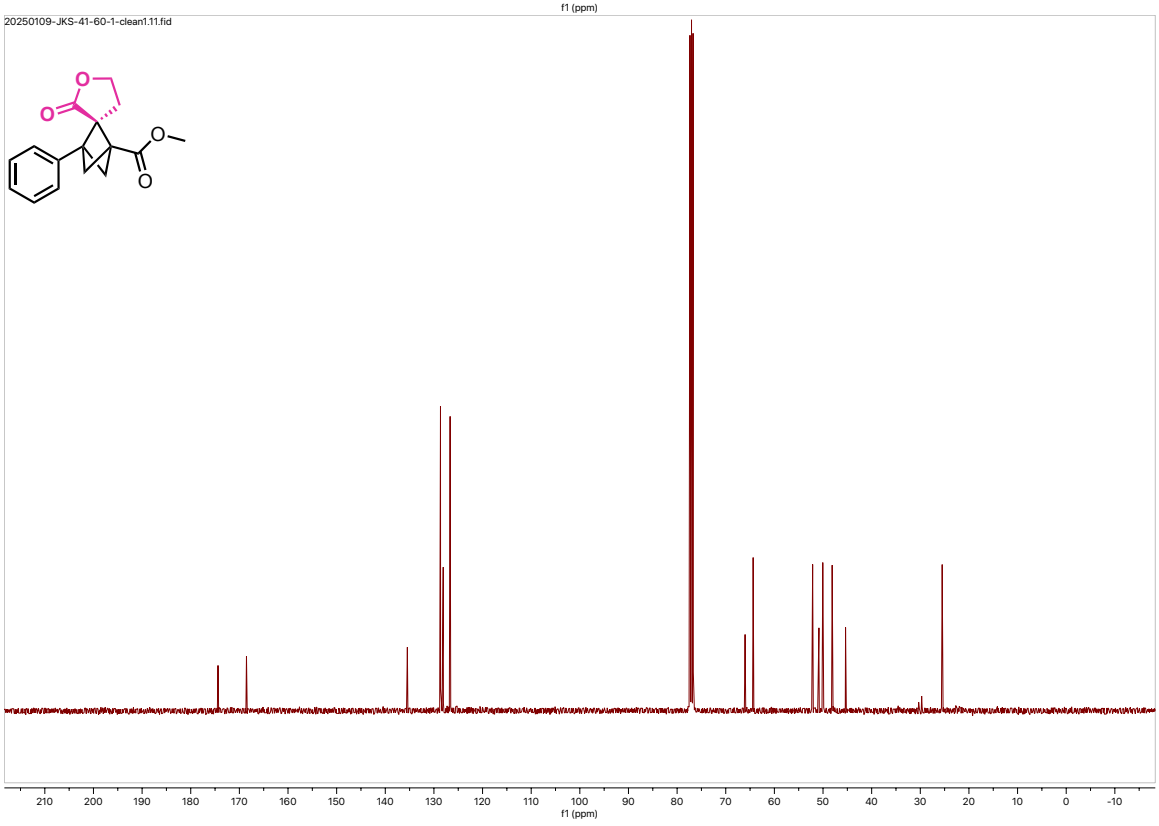
20250109-JKS-41-60-1-clean1.11.fid
O
O
O
O
210
200
190
180
170
160
150
140
130
120
110
100
90
80
70
60
50
40
30
20
10
0
-10
f1 (ppm)

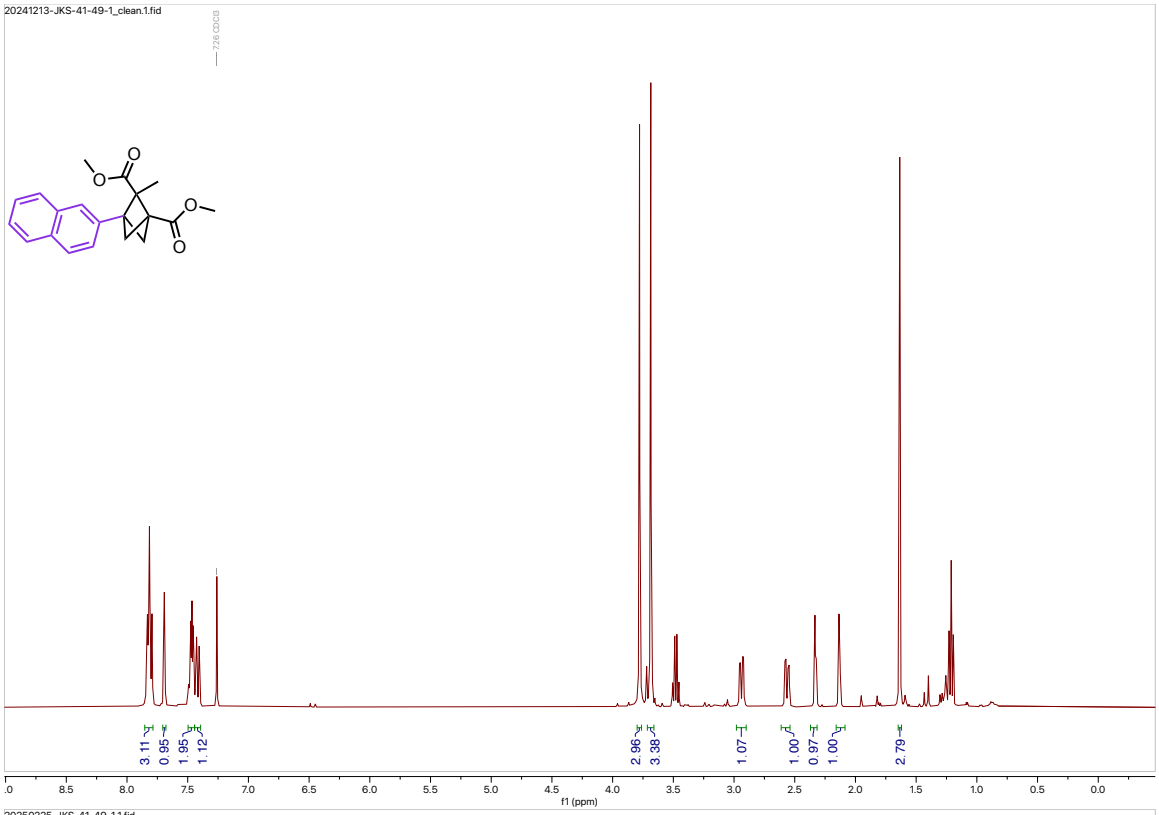
20241213-JKS-41-49-1_clean.1.fid
726 CDCl3
O
O
O
O
3.11
0.95
1.95
1.12
2.96
3.38
1.07
1.00
0.97
1.00
2.79
f1 (ppm)

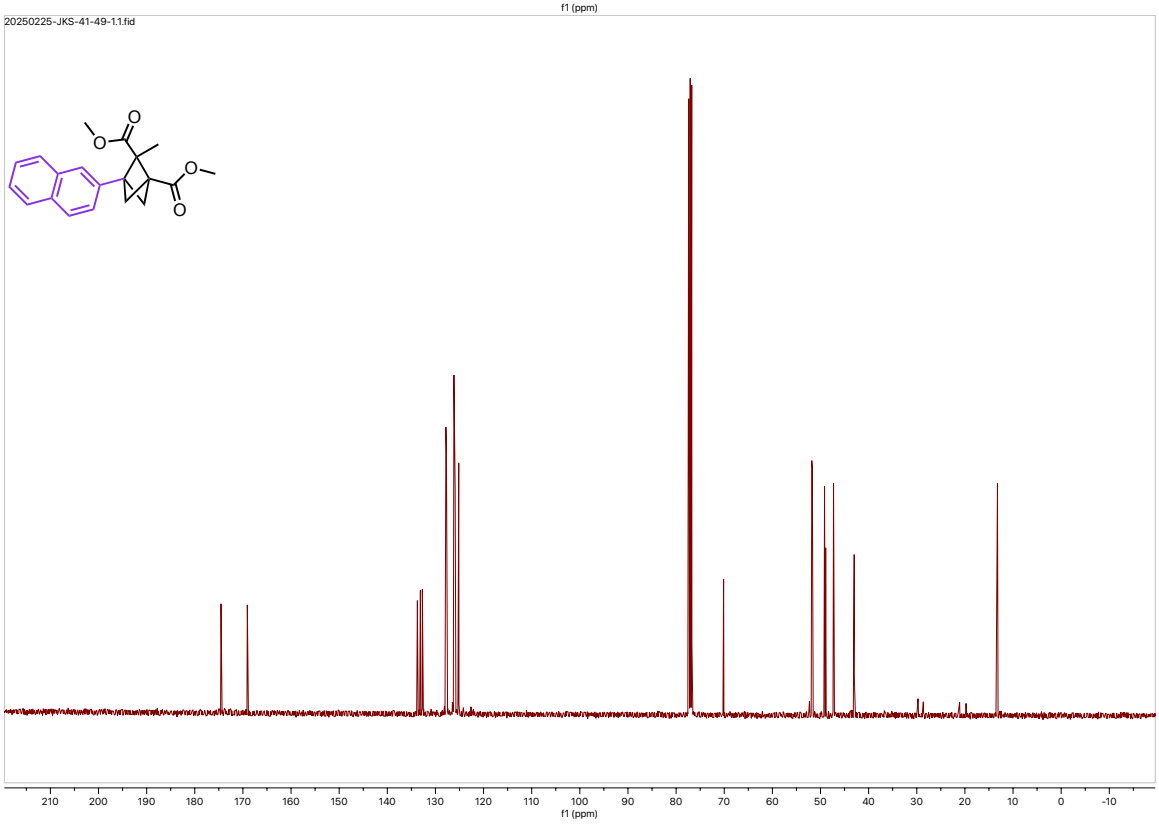
20250225-JKS-41-49-1.1.fid
O
O
O
O
f1 (ppm)

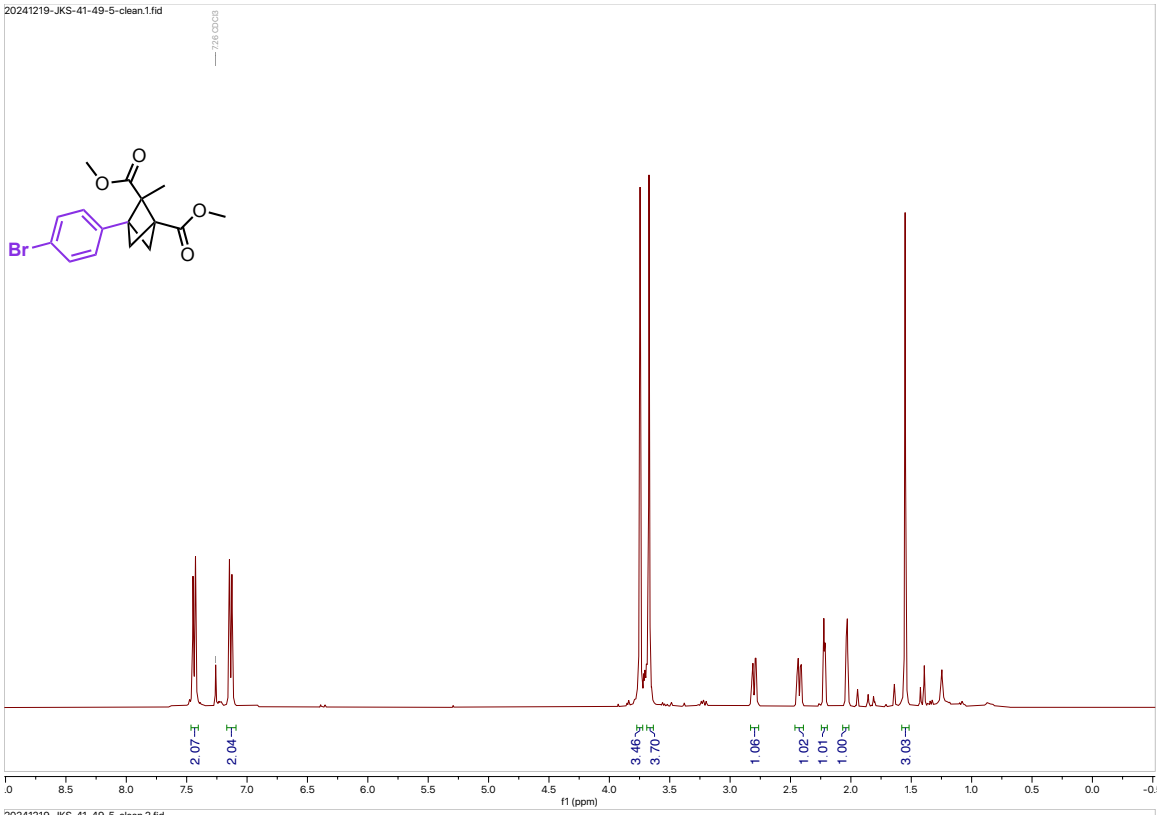
20241219-JKS-41-49-5-clean.1.fid
Br
2.07
2.04
3.46
3.70
1.06
1.02
1.01
1.00
3.03
f1 (ppm)

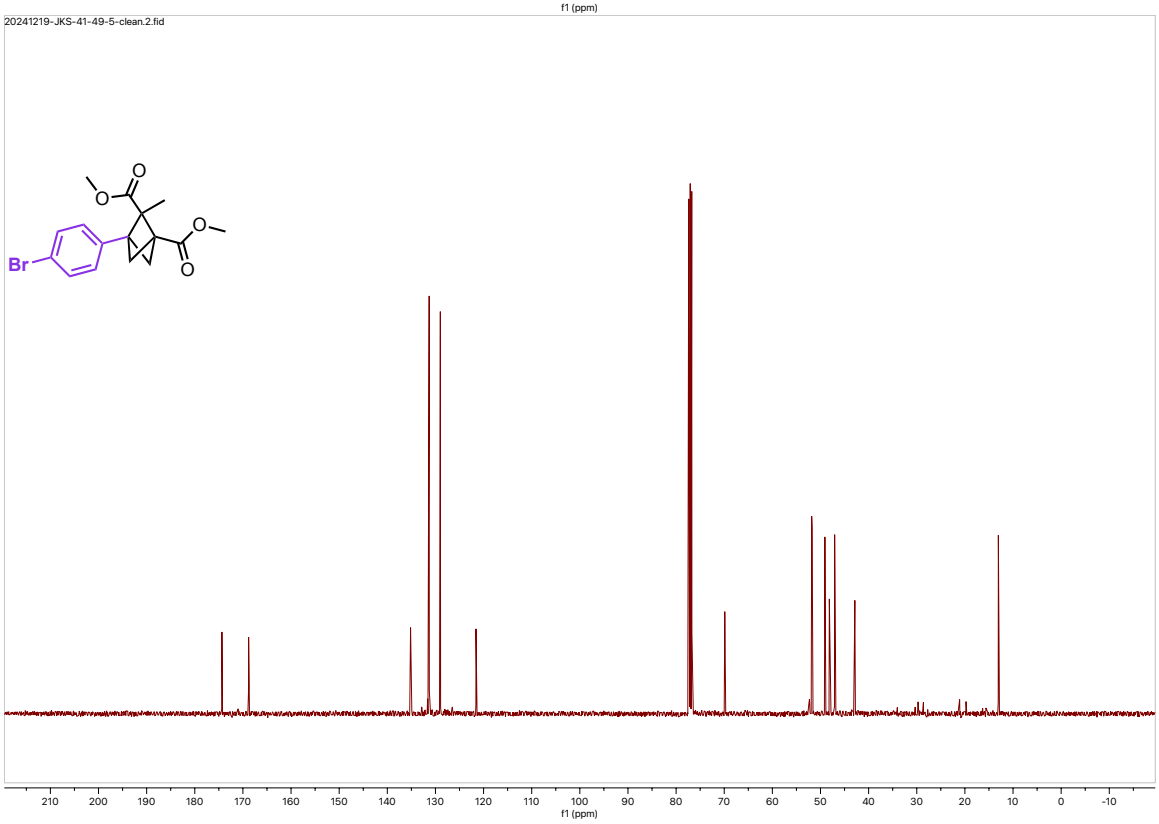
20241219-JKS-41-49-5-clean.2.fid
Br
f1 (ppm)

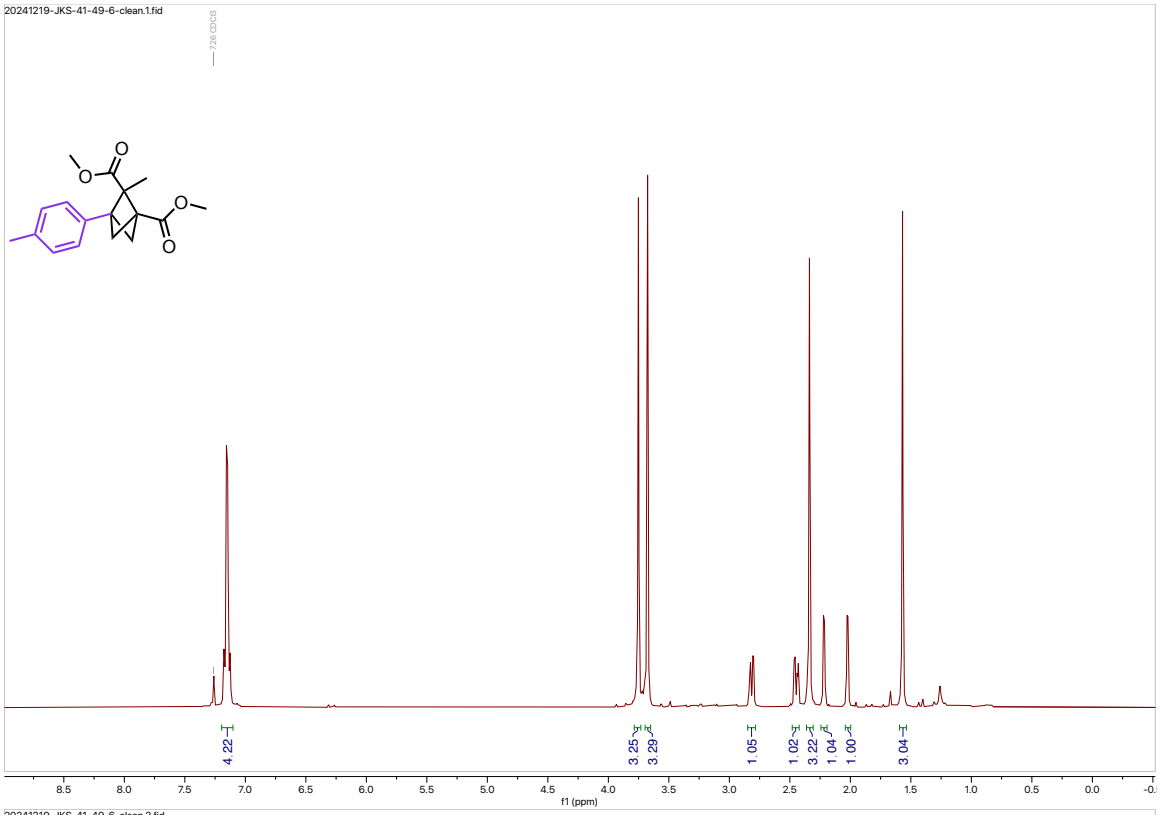
20241219-JKS-41-49-6-clean.1.fid
726 CDCl3
4.22
3.25
3.29
1.05
1.02
3.22
1.04
1.00
3.04
f1 (ppm)

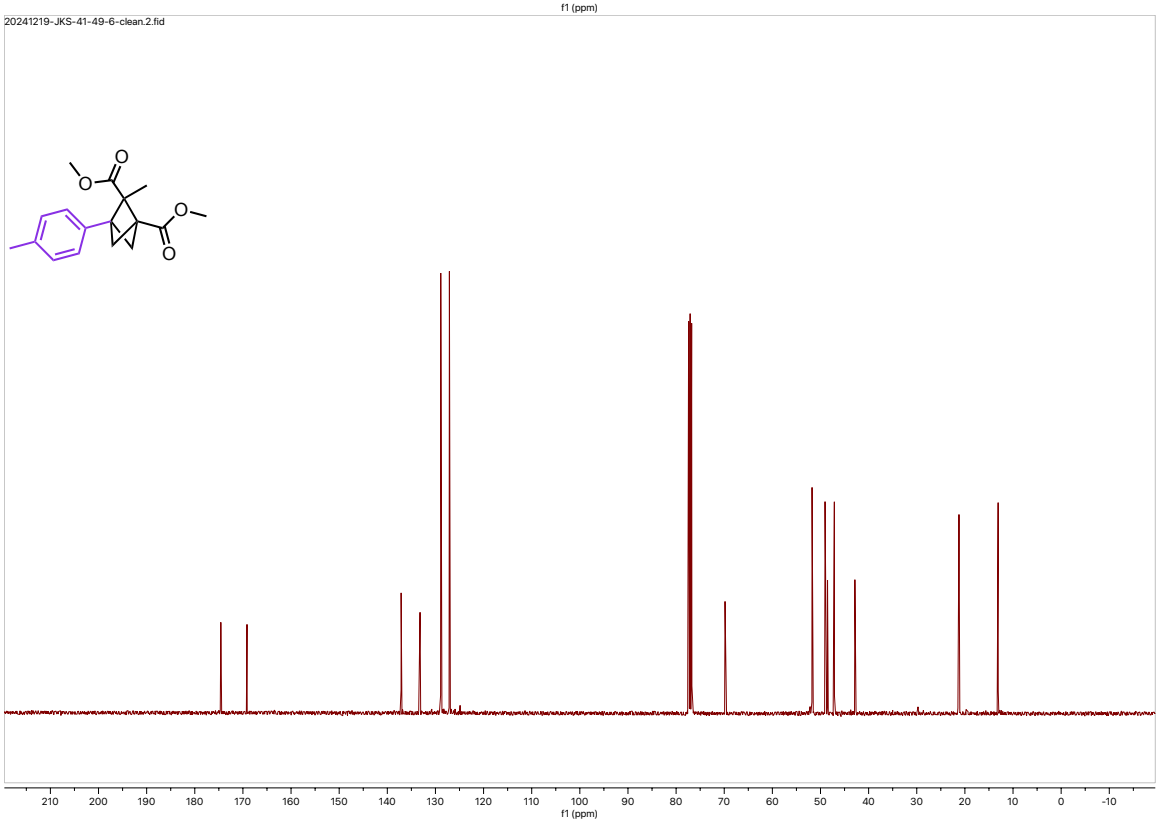
20241219-JKS-41-49-6-clean.2.fid
f1 (ppm)

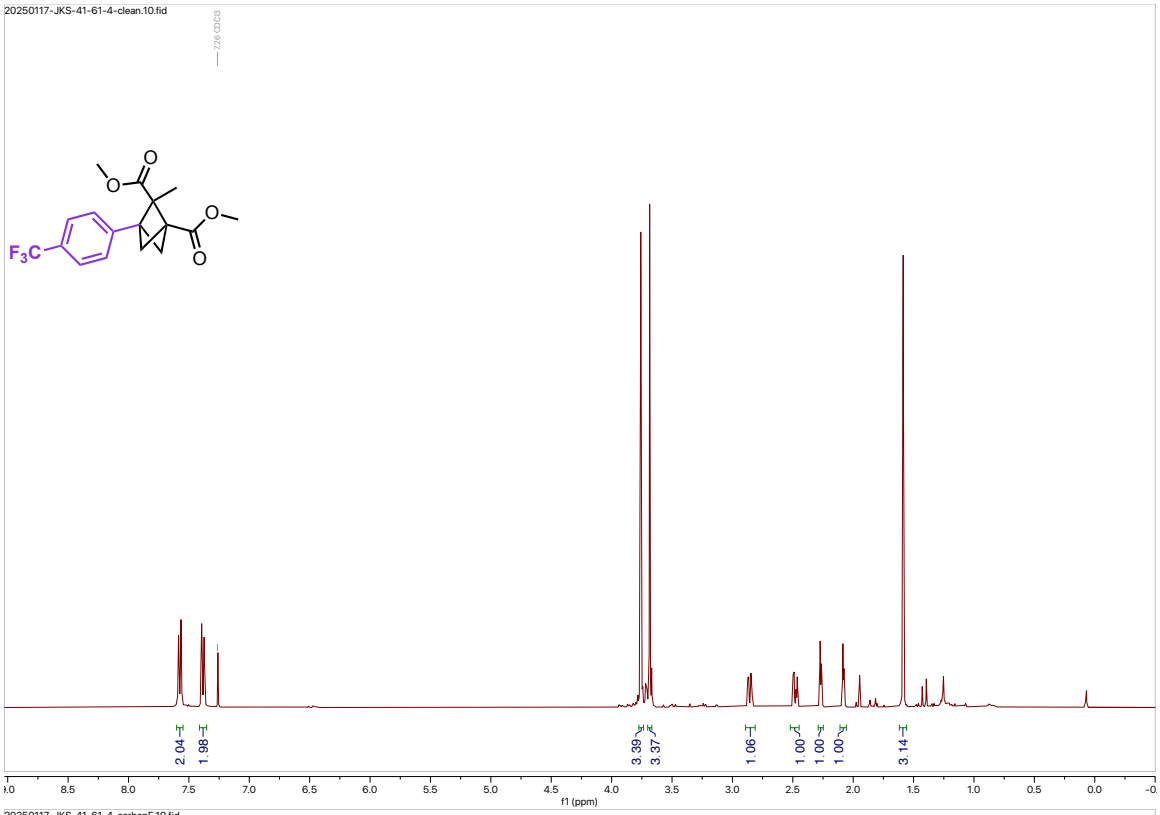
20250117-JKS-41-61-4-clean.10.fid
726 CDCl3
O
O
O
O
F3C
2.04
1.98
3.39
3.37
1.06
1.00
1.00
1.00
3.14
f1 (ppm)

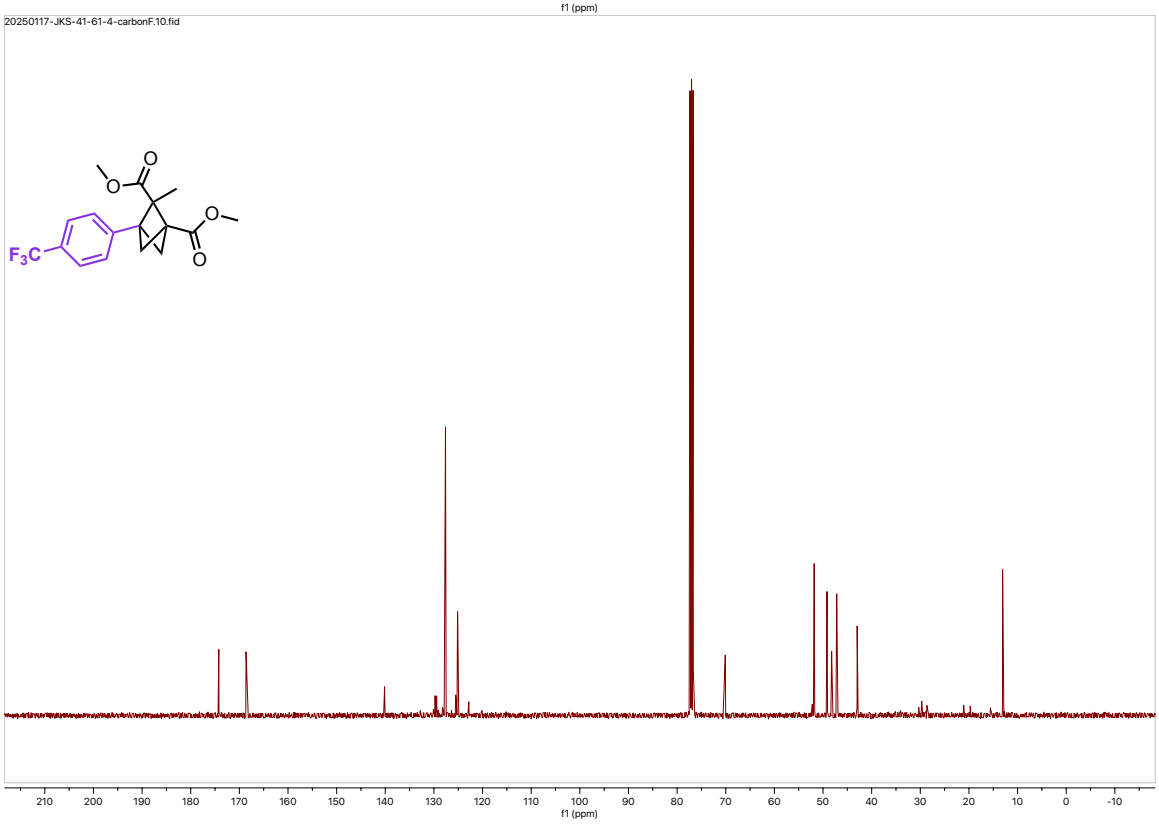
20250117-JKS-41-61-4-carbonF.10.fid
O
O
O
O
F3C
f1 (ppm)

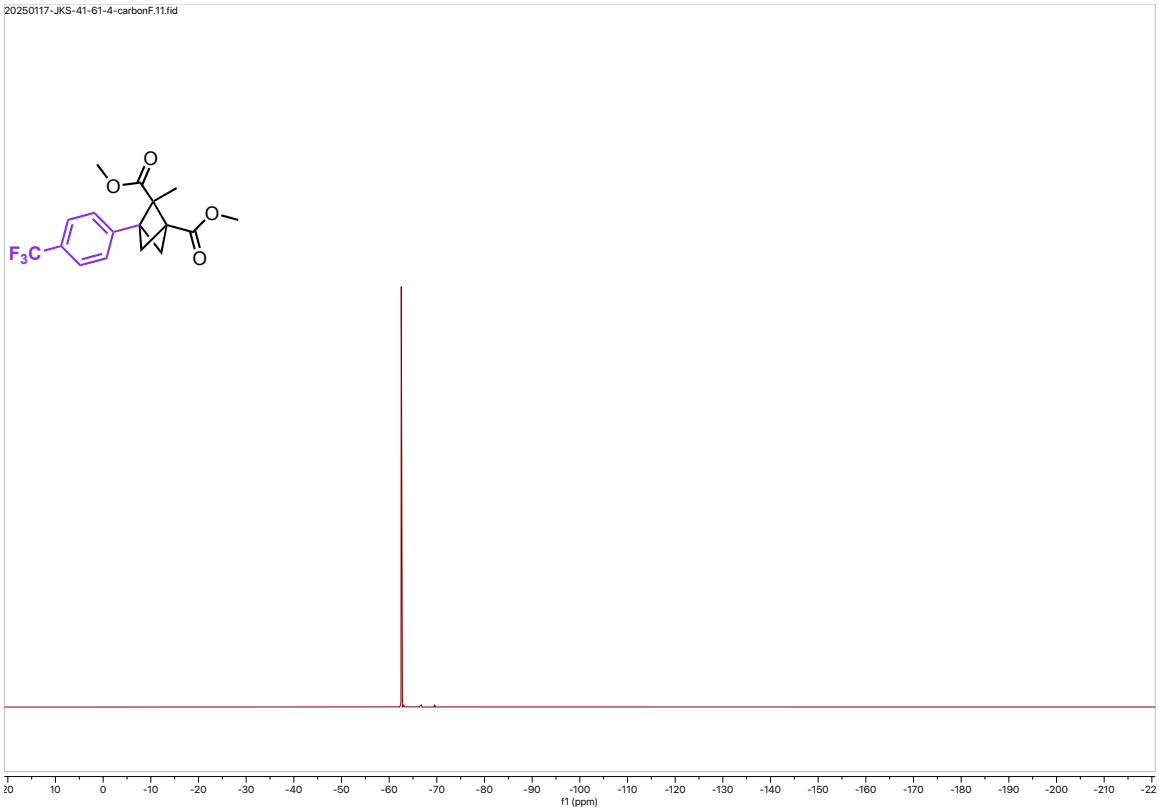
20250117-JKS-41-61-4-carbonF.11.fid
O
O
O
O
F3C
20
10
0
-10
-20
-30
-40
-50
-60
-70
-80
-90
-100
-110
-120
-130
-140
-150
-160
-170
-180
-190
-200
-210
-22
f1 (ppm)

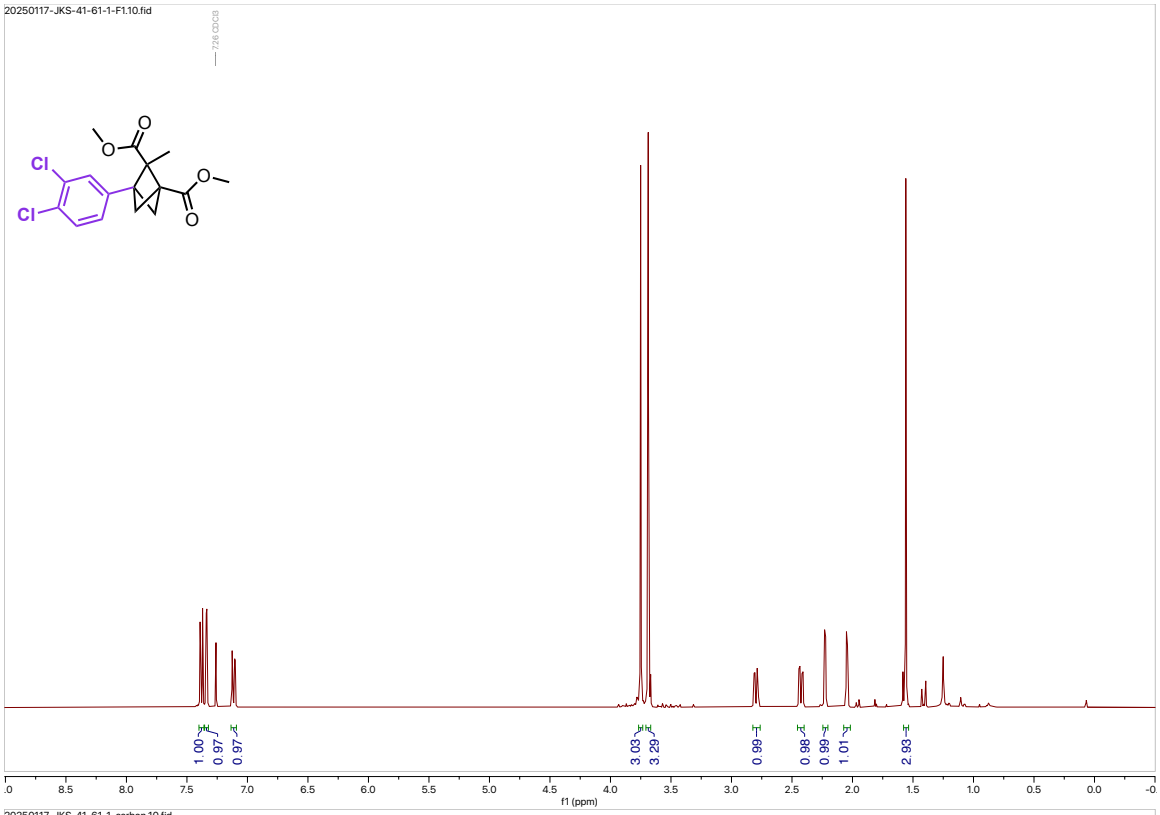
20250117-JKS-41-61-1-F1.10.fid
726 CDCl3
Cl
Cl
O
O
O
O
1.00
0.97
0.97
3.03
3.29
0.99
0.98
0.99
1.01
2.93
f1 (ppm)

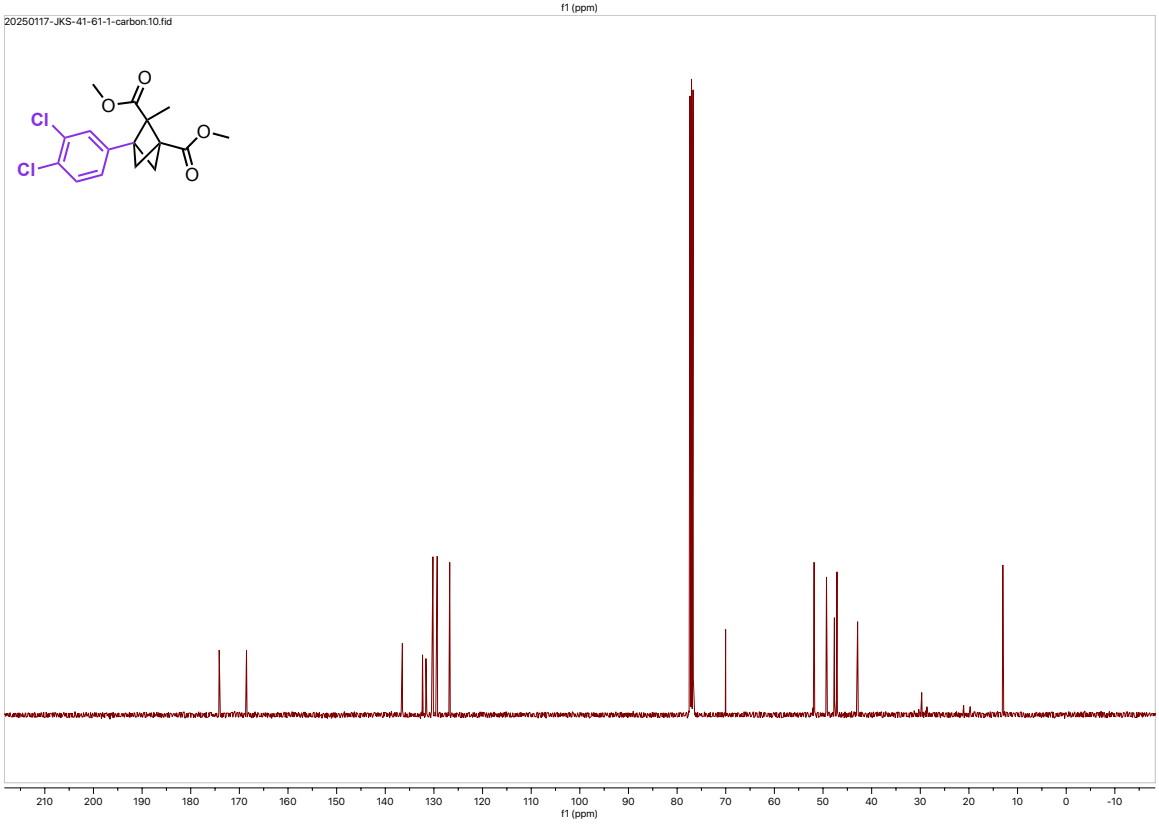
20250117-JKS-41-61-1-carbon.10.fid
Cl
Cl
O
O
O
O
f1 (ppm)

References

1. Sharland, J. C.; Davies, H. M. L., One-Pot Synthesis of Difluorobicyclo[1.1.1]pentanes from α-Allyldiazoacetates. *Org. Lett.* **2023,** *25* (28), 5214-5219.
2. Keipour, H.; Ollevier, T., Iron-Catalyzed Carbene Insertion Reactions of α-Diazoesters into Si–H Bonds. *Org. Lett.* **2017,** *19* (21), 5736-5739.
3. Toma, T.; Shimokawa, J.; Fukuyama, T., N,N'-Ditosylhydrazine: A Convenient Reagent for Facile Synthesis of Diazoacetates. *Org. Lett.* **2007,** *9* (16), 3195-3197.
4. Nakagawa, Y.; Chanthamath, S.; Fujisawa, I.; Shibatomi, K.; Iwasa, S., Ru(ii)-Pheox-catalyzed Si–H insertion reaction: construction of enantioenriched carbon and silicon centers. *Chem. Commun.* **2017,** *53* (26), 3753-3756.
5. Fu, L.; Mighion, J. D.; Voight, E. A.; Davies, H. M. L., Synthesis of 2,2,2,-Trichloroethyl Aryl- and Vinyldiazoacetates by Palladium-Catalyzed Cross-Coupling. *Chem. Eur. J.* **2017,** *23* (14), 3272-3275.
6. Chanthamath, S.; Ozaki, S.; Shibatomi, K.; Iwasa, S., Highly Stereoselective Synthesis of Cyclopropylphosphonates Catalyzed by Chiral Ru(II)-Pheox Complex. *Org. Lett.* **2014,** *16* (11), 3012-3015.
7. Le, T. V.; Romero, I.; Daugulis, O., "Sandwich" Diimine-Copper Catalyzed Trifluoroethylation and Pentafluoropropylation of Unactivated C(sp3)−H Bonds by Carbene Insertion. *Chem. Eur. J.* **2023,** *29* (48), e202301672.
8. Chen, K.; Zhang, S.-Q.; Brandenberg, O. F.; Hong, X.; Arnold, F. H., Alternate Heme Ligation Steers Activity and Selectivity in Engineered Cytochrome P450-Catalyzed Carbene-Transfer Reactions. *J. Am. Chem. Soc.* **2018,** *140* (48), 16402-16407.